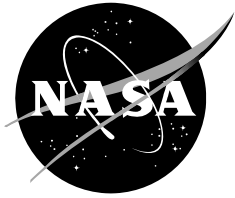


NASA/CR—2008–215370



Rotor Performance at High Advance Ratio; Theory versus Test

Franklin D. Harris

Prepared for Ames Research Center
under Contract NNA07BB01C

October 2008

The NASA STI Program Office ... in Profile

Since its founding, NASA has been dedicated to the advancement of aeronautics and space science. The NASA Scientific and Technical Information (STI) Program Office plays a key part in helping NASA maintain this important role.

The NASA STI Program Office is operated by Langley Research Center, the lead center for NASA's scientific and technical information. The NASA STI Program Office provides access to the NASA STI Database, the largest collection of aeronautical and space science STI in the world. The Program Office is also NASA's institutional mechanism for disseminating the results of its research and development activities. These results are published by NASA in the NASA STI Report Series, which includes the following report types:

- **TECHNICAL PUBLICATION.** Reports of completed research or a major significant phase of research that present the results of NASA programs and include extensive data or theoretical analysis. Includes compilations of significant scientific and technical data and information deemed to be of continuing reference value. NASA counterpart of peer-reviewed formal professional papers, but having less stringent limitations on manuscript length and extent of graphic presentations.
- **TECHNICAL MEMORANDUM.** Scientific and technical findings that are preliminary or of specialized interest, e.g., quick release reports, working papers, and bibliographies that contain minimal annotation. Does not contain extensive analysis.
- **CONTRACTOR REPORT.** Scientific and technical findings by NASA-sponsored contractors and grantees.

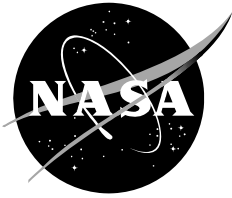
- **CONFERENCE PUBLICATION.** Collected papers from scientific and technical conferences, symposia, seminars, or other meetings sponsored or co-sponsored by NASA.
- **SPECIAL PUBLICATION.** Scientific, technical, or historical information from NASA programs, projects, and missions, often concerned with subjects having substantial public interest.
- **TECHNICAL TRANSLATION.** English-language translations of foreign scientific and technical material pertinent to NASA's mission.

Specialized services that complement the STI Program Office's diverse offerings include creating custom thesauri, building customized databases, organizing and publishing research results ... even providing videos.

For more information about the NASA STI Program Office, see the following:

- Access the NASA STI Program Home Page at <http://www.sti.nasa.gov>
- E-mail your question via the Internet to help@sti.nasa.gov
- Fax your question to the NASA STI Help Desk at (301) 621-0134
- Telephone the NASA STI Help Desk at (301) 621-0390
- Write to:
NASA STI Help Desk
NASA Center for AeroSpace Information
7121 Standard Drive
Hanover, MD 21076-1320

NASA/CR—2008–215370



Rotor Performance at High Advance Ratio; Theory versus Test

*Franklin D. Harris
F. D. Harris & Associates
Piedmont, OK 73078*

National Aeronautics and
Space Administration
Ames Research Center
Moffett Field, CA 94035

Prepared for Monterey Technology, Inc,
under NASA Contract NNA07BB01C
Subcontract 200703, Task Order 01–03

October 2008

Available from:

NASA Center for AeroSpace Information
7121 Standard Drive
Hanover, MD 21076-1320
301-621-0390

National Technical Information Service
5285 Port Royal Road
Springfield, VA 22161
703-605-6000

ABSTRACT

Five analytical tools have been used to study rotor performance at high advance ratio. One is representative of autogyro rotor theory in 1934 and four are representative of helicopter rotor theory in 2008. The five theories are measured against three sets of well documented, full-scale, isolated rotor performance experiments.

The major finding of this study is that the decades spent by many rotorcraft theoreticians to improve prediction of basic rotor aerodynamic performance has paid off. This payoff, illustrated by comparing the CAMRAD II comprehensive code and Wheatley & Bailey theory to H-34 test data, shows that rational rotor lift to drag ratios are now predictable. The 1934 theory predicted L/D ratios as high as 15. CAMRAD II predictions compared well with H-34 test data having L/D ratios more on the order of 7 to 9. However, the detailed examination of the selected codes compared to H-34 test data indicates that not one of the codes can predict – to engineering accuracy above an advance ratio of 0.62– the control positions and shaft angle of attack required for a given lift.

There is no full-scale rotor performance data available for advance ratios above 1.0 and extrapolation of currently available data to advance ratios on the order of 2.0 is unreasonable despite the needs of future rotorcraft. Therefore, it is recommended that an overly strong full-scale rotor blade set be obtained and tested in a suitable wind tunnel to at least an advance ratio of 2.5. A tail rotor from a Sikorsky CH-53 or other large single rotor helicopter should be adequate for this exploratory experiment.

ACKNOWLEDGMENTS

Dr. William Warmbrodt, Chief of the Aeromechanics Branch at the NASA Ames Research Center, has been the guiding champion behind this project. Bill initiated and has mentored this advanced research program with considerable enthusiasm.

The actual work has been done by seven volunteers and one paid scribe. Wayne Johnson, a member of NASA, provided hours of lead off computations using his well know CAMRAD II computer program. Bob Ormiston, on the U.S. Army's payroll, put his shoulder to the wheel with a raft of computations using the RCAS code. Dan Wachspress and Todd Quackenbush, leading members of Continuum Dynamics, Inc, broke new ground with their CHARM lifting surface code. On the CFD side, Roger Strawn (U.S. Army), Jan Theron (a technical consultant to the Groen Brothers) and Ethan Romander, a NASA member, began the Herculean task of applying the computational fluid dynamics code called OVERFLOW-2 to a real problem. And Ray Prouty, well known to all if for no other reason than his articles in Vertiflight, gave guiding thoughts plus output from his personal rotor performance theory.

The rotorcraft industry owes Bill, Wayne, Bob, Dan, Todd, Roger, Jan, Ethan and Ray a great deal for tackling this theory/test correlation problem in such depth and breadth. The scribe can only offer his very deeply felt thanks to these volunteers.

Contents

ABSTRACT	iii
ACKNOWLEDGMENTS	iii
1 SUMMARY	1
2 INTRODUCTION	19
2.1 Study Objective	25
2.2 Performance Fundamentals	25
2.3 Rotor Theory In The 1930s	34
3 ROTORS STUDIED	43
3.1 H-34 Untwisted Blade Set	43
3.2 UH-1 Thirty Four Foot Blade Set	48
3.3 PCA-2 Autogyro Blade Set	50
4 THEORIES EVALUATED	53
4.1 Background	53
4.2 Selected Theories	55
4.3 Wheatley & Bailey (1934)	55
4.4 CAMRAD II (2008)	55
4.5 RCAS (2008)	57
4.6 CHARM (2008)	58
4.7 OVERFLOW-2 Coupled with CAMRAD II	59
5 EXPERIMENTAL DATA	63
5.1 H-34	65
5.2 UH-1	73
5.3 PCA-2	79
5.4 Discussion	81
5.4.1 Performance at zero angles	81
5.4.2 Obtaining Lift and Controlling Flapping	86
5.4.3 Blade Stall	91
6 THEORY VERSUS TEST OVERVIEW	92
6.1 Evaluation Method	92
6.2 Major Progress	100
6.2.1 Cyclic Controls, B_{1C} and A_{1C}	100
6.2.2 Lift Coefficient, C_L/σ	102
6.2.3 Drag Coefficient, C_D/σ	103
6.2.4 Side Force Coefficient, C_Y/σ	105
6.2.5 Torque (or Power) Coefficient, C_Q/σ	106
6.2.6 Effective Drag Coefficient, C_{De}/σ	107
6.2.7 Rotor L/D_E	107
7 THEORY VERSUS TEST DETAILS	109
7.1 H-34 Test versus CAMRAD II (Appendix 11.10)	113
7.2 H-34 Test versus CHARM (Appendix 11.11)	126
7.3 H-34 Test versus RCAS (Appendix 11.12)	136
7.4 H-34 Test versus OVERFLOW-2 with CAMRAD II (Appendix 11.13)	146
7.5 H-34 Concluding Remarks	160

7.6	UH-1 Test versus CAMRAD II (Appendix 11.14).....	161
7.7	UH-1 Test versus CHARM (Appendix 11.15)	167
7.8	UH-1 Test versus RCAS (Appendix 11.16)	168
7.9	UH-1 Test versus OVERFLOW-2 with CAMRAD II (Appendix 11.17)	172
7.10	UH-1 Concluding Remarks.....	172
7.11	PCA-2 Test versus CAMRAD II (Appendix 11.18).....	173
7.12	PCA-2 Test versus CHARM (Appendix 11.19)	177
7.13	PCA-2 Test versus RCAS (Appendix 11.20)	177
7.14	PCA-2 Test versus OVERFLOW-2 with CAMRAD II (Appendix 11.21) ...	177
8	CONCLUSIONS	179
9	RECOMMENDATIONS.....	183
10	REFERENCES.....	185
11	APPENDICES	191
11.1	Minimum Profile Power, H and Y Forces, Torque and Thrust Coefficients..	191
11.2	Wheatley/ Bailey Equations with Sample Case.....	198
11.3	H-34 Blade Section Properties.....	218
11.4	UH-1 Blade Section Properties.....	219
11.5	PCA-2 Blade Section Properties.....	222
11.6	H-34 Experimental Data Set	225
11.7	UH-1 Experimental Data Set	234
11.8	PCA-2 Experimental Data Set.....	242
11.9	Göttingen 429 and N.A.C.A. 0012 Airfoil Tables.....	246
11.10	H-34 versus CAMRAD II.....	273
11.11	H-34 versus CHARM	329
11.12	H-34 versus RCAS.....	385
11.13	H-34 versus OVERFLOW-2 Coupled with CAMRAD II.....	441
11.14	UH-1 versus CAMRAD II.....	451
11.15	UH-1 versus CHARM.....	458
11.16	UH-1 versus RCAS.....	458
11.17	UH-1 versus OVERFLOW-2 Coupled with CAMRAD II	503
11.18	PCA-2 versus CAMRAD II	503
11.19	PCA-2 versus CHARM.....	513
11.20	PCA-2 versus RCAS.....	513
11.21	PCA-2 versus OVERFLOW-2 Coupled with CAMRAD II	513

Page intentionally blank

1 SUMMARY

In May of 2007, Dr. William Warmbrodt, Chief of the Aeromechanics Branch at the NASA Ames Research Center, initiated a rotorcraft program concerning High Speed Slowed Rotor Technology. A portion of this program has been devoted to rotor performance for slowed, edgewise-flying helicopter rotors operating at high advance ratios. The specific objectives of this portion of the initiative have been to (1) assess aerodynamic performance behavior of rotors up to an advance ratio of 1.0 using available experimental data, (2) see how well current analytical tools are able to predict the available experimental performance data and then (3) make recommendations that, when implemented, will improve current analytical tools.

Five analytical tools have been chosen to study rotor performance at high advance ratio. One is representative of autogyro rotor theory in 1934 and four are representative of helicopter rotor theory in 2008. Three sets of well documented, full-scale, isolated rotor performance experiments have been selected against which the five theories are measured. This 3 by 5 matrix is summarized by the following table and the progress made as of this report is noted.

Rotors	Wheatley & Bailey	CAMRAD II	CHARM	RCAS	Overflow CFD Coupled With CAMRAD II
H-34	✓	✓	✓	✓	Partial
UH-1	✓	Partial		✓	
PCA-2	✓	✓			

The Wheatley & Bailey theory has been included – not only for historical interest – but as a bench mark for the improvements achieved by the theories known as CAMRAD II, CHARM and RCAS. These relatively advanced theories, commonly referred to as comprehensive codes, have demonstrated successful prediction of many helicopter parameters and design factors in the advance ratio range between hover and 0.4. *However, it is the extension, evaluation and usability of these codes beyond their known capabilities that is under study in this report.* The application of computational fluid dynamics (CFD) to the rotating wing in forward flight has already shown considerable promise in predicting helicopter rotor airloads. Therefore one CFD solver known as OVERFLOW-2 has been included as a hint for future development.

The three rotors providing experimental data, as summarized below, were tested

Parameter	Modified H-34	Modified UH-1	Production PCA-2
Diameter (ft)	56.00	34.00	45.00
Nominal chord (ft)	1.337	1.75	1.81
Twist (deg)	0.00	-1.42	Non-linear
Number of blades	4	2	4
Nominal blade airfoil	N.A.C.A. 0012	N.A.C.A. 0012	Göttingen 429
Hub type	Articulated	Teetering (Under slung)	Articulated
Flap hinge offset (inch)	12	0	3.375
Lag hinge offset (inch)	12	No lag hinge	7.750
Reference	NASA TN D-4632	USAAVLABS TR 69-2	N.A.C.A. Rep. No. 515

in large scale wind tunnels. The PCA-2 autogyro rotor was tested to an advance ratio of 0.7 in the N.A.C.A. Langley 30 by 60 foot wind tunnel in 1934. The modified Sikorsky H-34 rotor and the modified Bell UH-1 rotor were tested in the mid-1960s in the 40 by 80 foot wind tunnel located at NASA Ames. Data from the H-34 and UH-1 rotors was obtained up to an advance ratio just above 1.0.

The three rotors under study each had well documented measurements of their aerodynamic performance. This tabulated experimental data base has been put into Microsoft EXCEL spreadsheets and examined in considerable detail. Also, graphs similar to those given in the respective reports were constructed to insure that the original impressions were reasonable. Finally, a simple regression analysis of the H-34 and UH-1 data was used to judge the overall usability of the experimental data for theory versus test correlation. The PCA-2 data was accepted at face value after confirming the graphs that Wheatley gave in N.A.C.A. TR 515 had been reproduced.

The ability of the several theories to predict the 1960s H-34 and UH-1 test data was measured in a very quantitative way. In these experiments, each test point was obtained at one combination of advance ratio (μ), 3/4 radius collective pitch ($\theta_{0.75R}$), and shaft angle of attack (α_s). The experimental rotor's cyclic controls were used to trim the rotor tip path plane normal to the shaft. This test requirement forced the once per revolution flapping to zero. Rotor lift, drag, side force, shaft torque and cyclic required to obtain zero flapping were recorded. The theory computations were made at each test point using the recorded advance ratio, collective pitch, and shaft angle of attack. Each theory was required to find the cyclic control positions that zeroed flapping. Given both data sets, test parameters were plotted versus theory calculated parameters. For example, test rotor lift coefficient was plotted versus theory lift coefficient. These graphs should appear as $y = x$ if the agreement is perfect. In fact, all test versus theory graphs appeared in the form $y = Ax + B$. Furthermore, the slope constant, A, was not generally found to be 1.0 and the intercept constant, B, was not generally found to be 0.0. A linear regression analysis, performed to find A and B, yielded the statistical confidence value, R^2 . The author defined a criteria for acceptable test/theory correlation suited to engineering accuracy. This "not good enough" criteria is:

1. Slope (A) outside of 0.95 to 1.05 is not good enough
2. Intercept (B) outside of
 - Longitudinal cyclic, $B_{1C}, \pm 0.3$ degrees
 - Lateral cyclic, $A_{1C}, \pm 0.3$ degrees
 - Lift coefficient, $C_L/\sigma, \pm 0.003$
 - Drag coefficient, $C_D/\sigma, \pm 0.0005$
 - Side Force coefficient, $C_Y/\sigma, \pm 0.0004$
 - Torque (power) coefficient, $C_Q/\sigma, \pm 0.0003$
3. R^2 less than 0.97

The most complete comparison of theory versus test was conducted with the H-34 rotor. This experiment acquired 250 data points covering a range in advance ratio from 0.3 to 1.05. An overview comparison of CAMRAD II and Wheatley/Bailey theories to

the 250 test points was first made using longitudinal cyclic prediction and rotor lift prediction as immediate barometers of progress made over 75 years. The results were very encouraging as Figures A and B show. Because advanced theories include blade deflection and non-uniform inflow when computing blade element airloads, prediction of longitudinal cyclic required to trim first harmonic flapping to zero has been significantly improved. Figure A shows this improvement as measured by both the slope and intercept values. Including blade deflection (primarily torsional) and non-uniform inflow additions to 1934 theory also significantly improved prediction of rotor lift as Figure B shows.

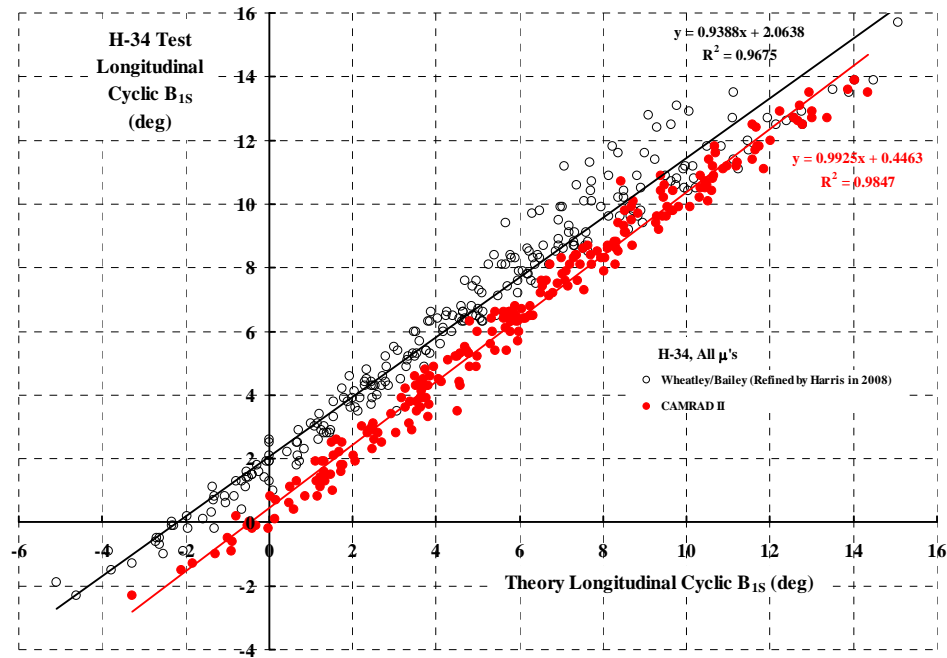


Figure A.

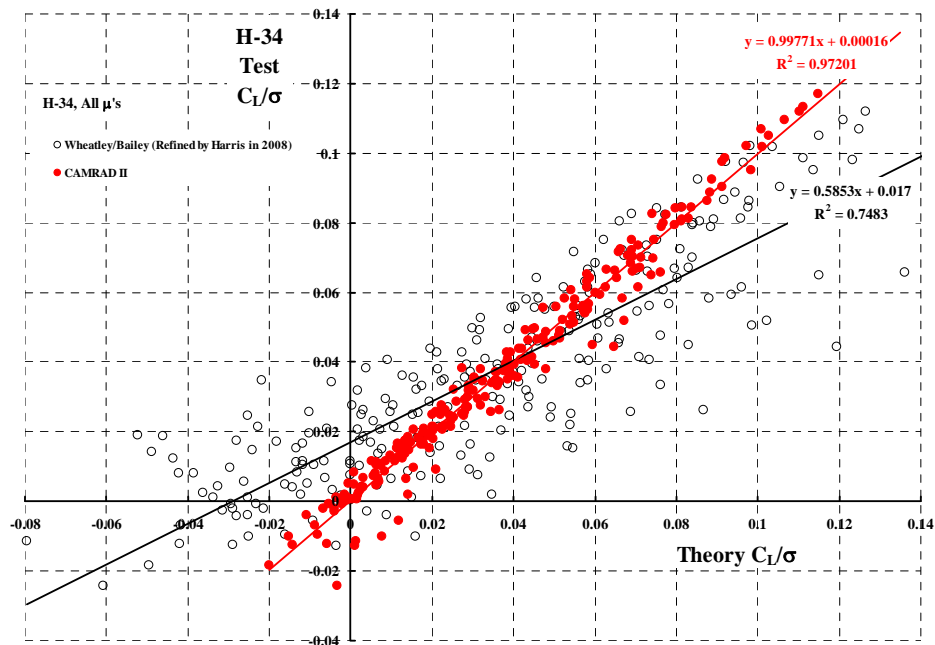


Figure B.

The overview also showed that since 1934 a giant step forward has been made in predicting a rotor's lift to effective drag ratio. This ratio is based on a denominator calculated as

$$\text{Effective drag} \equiv D_E = \frac{P_{\text{Total}}}{V} - X = \frac{P_{\text{induced}} + P_{\text{profile}}}{V}$$

where X is propulsive force and P is power. Effective drag is a measure of the induced plus profile drag of a rotating wing. In concept design, it is expeditious to assume a rough order of rotor performance by choosing a maximum rotor L/D_E . All during the 1940s, 1950s and even into the 1960s, the assumed value was more than once based on Wheatley/Bailey theory. Figure C shows just how overly optimistic rotorcraft aerodynamic performance engineers were in those decades. However, prediction of L/D_E to better than the ± 1.0 that Figure C shows is certainly necessary during preliminary design.

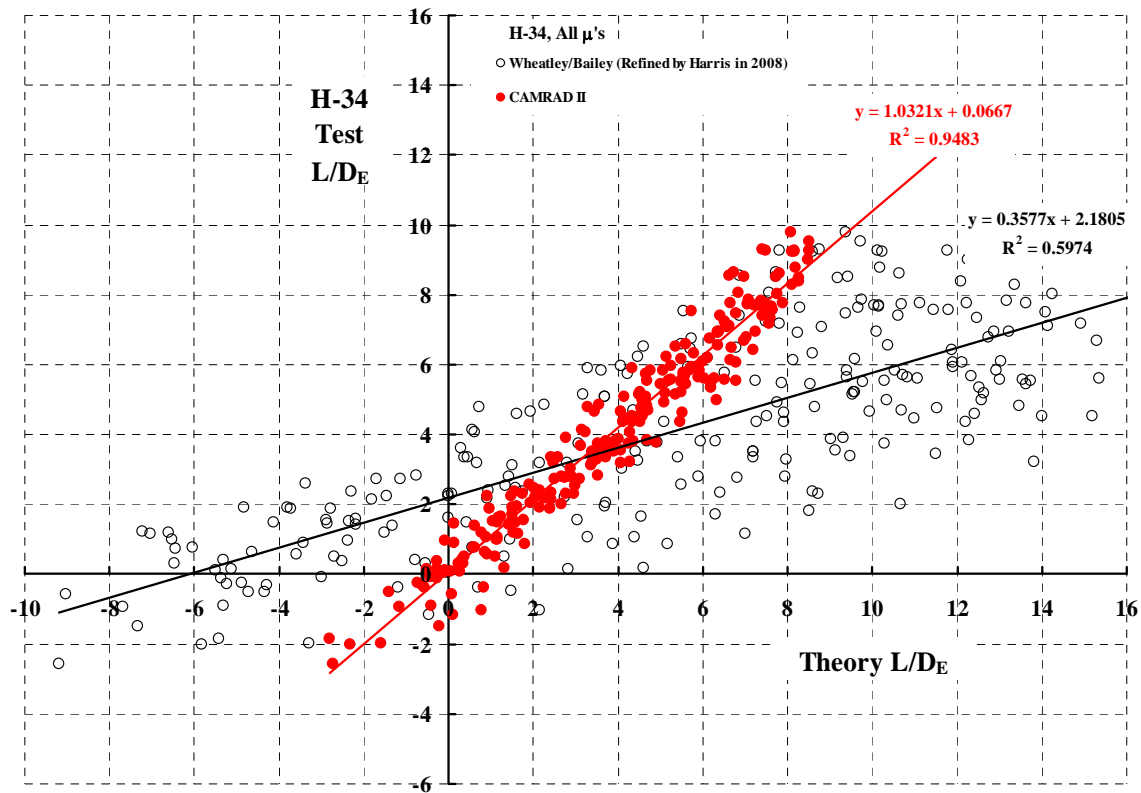


Figure C.

The positive outlook conveyed by Figures A, B and C is somewhat offset by the detailed theory versus test comparison reported herein. The negative fact is that the comprehensive codes' accuracy in predicting the rotor parameters measured at any given μ , α_S , and $\theta_{0.75R}$ deteriorates with advance ratios above 0.5 to 0.6. *Because the H-34 test data at an advance ratio of 1.05 appears unusable*, the $\mu = 0.82$ data set is used in this summary to illustrate some troublesome points.

The one H-34 performance parameter that each comprehensive code succeeded in predicting was the amount of longitudinal cyclic required to trim the rotor tip path plane normal to the shaft (i.e., zero longitudinal flapping). Figure D shows that at even this high advance ratio, predicted trim longitudinal cyclic is encouragingly close. The regression analysis' slope value indicates an over prediction by about 5 percent. Because the intercept is under predicted by about 0.75 degrees, the correlation of the three codes appears nearly perfect. While not shown, similar success was definitely not demonstrated with respect to trim lateral cyclic correlation. As discussed in the body of this report, none of the codes came remotely close to accurate prediction of the lateral axis data.

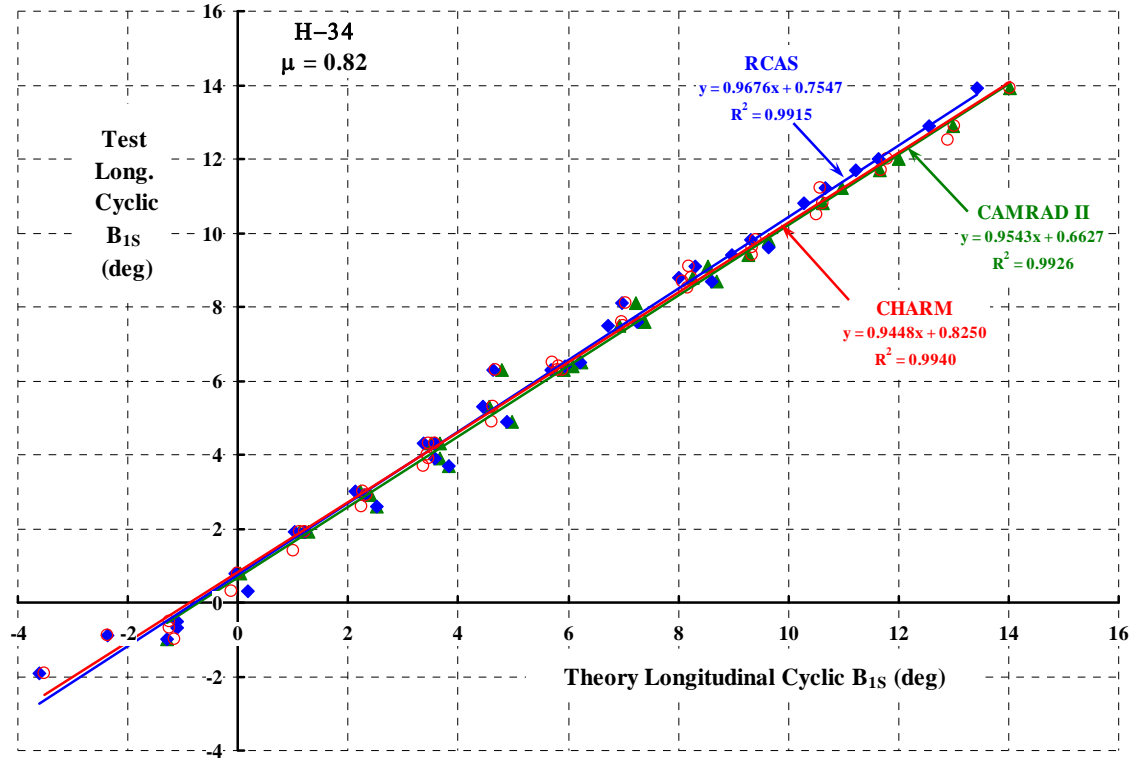


Figure D.

By an advance ratio of 0.82, the prediction accuracy of rotor lift by each code (given the test values of μ , α_s , and $\theta_{0.75R}$) has deteriorated substantially. This disturbing situation is illustrated with Figure E. A major key to coming even this close was the inclusion of blade torsion in the H-34 correlation study. It was discovered that the trailing edge of H-34 blades were bent up over the 0.8 to 0.9 radius station. This deflection acted as a trim tab so that the normal N.A.C.A. 0012 airfoil did not have a zero pitching moment over this short span. The approximate airfoil pitching moment coefficient about the 1/4 chord of + 0.03 used in the codes caused significant elastic twisting which required cyclic control to trim the rotor to zero first harmonic flapping (the test requirement). A most significant finding was that the measured lift when the shaft angle of attack and collective pitch were zero could finally be predicted. Up until this time, investigators had charged the non-zero lift as an experimental error of about 1 degree in the collective pitch records. This story is summarized with Figure F.

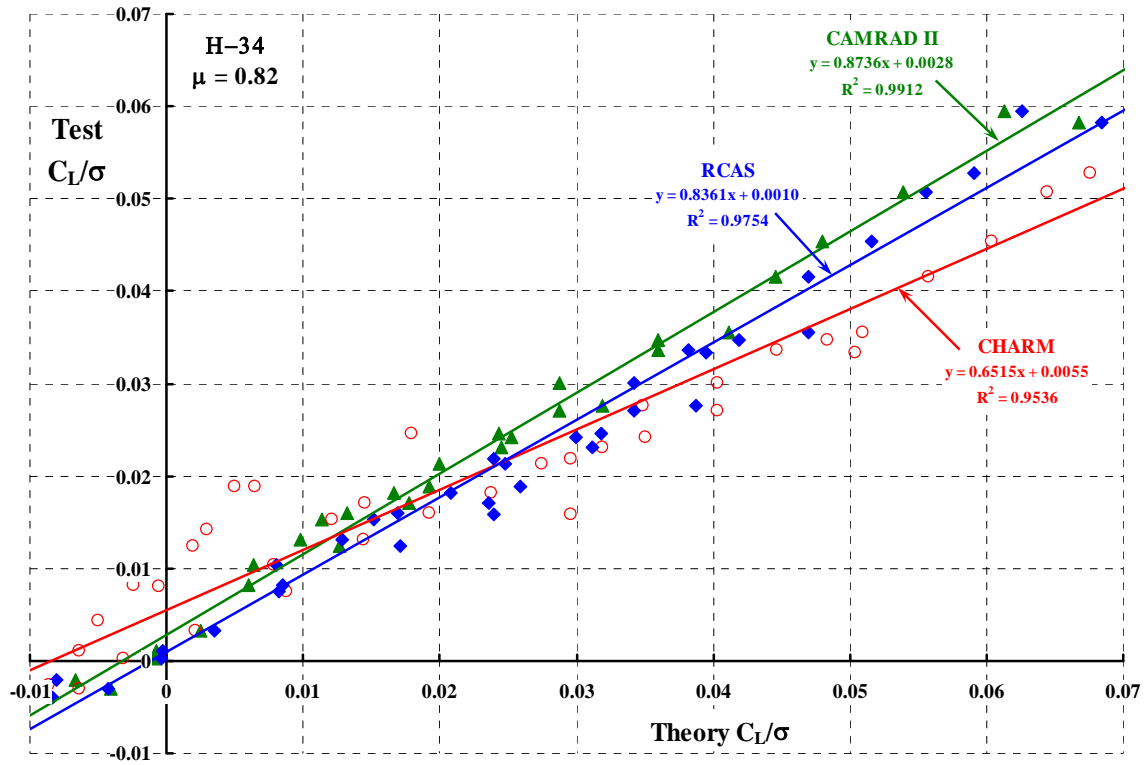


Figure E.

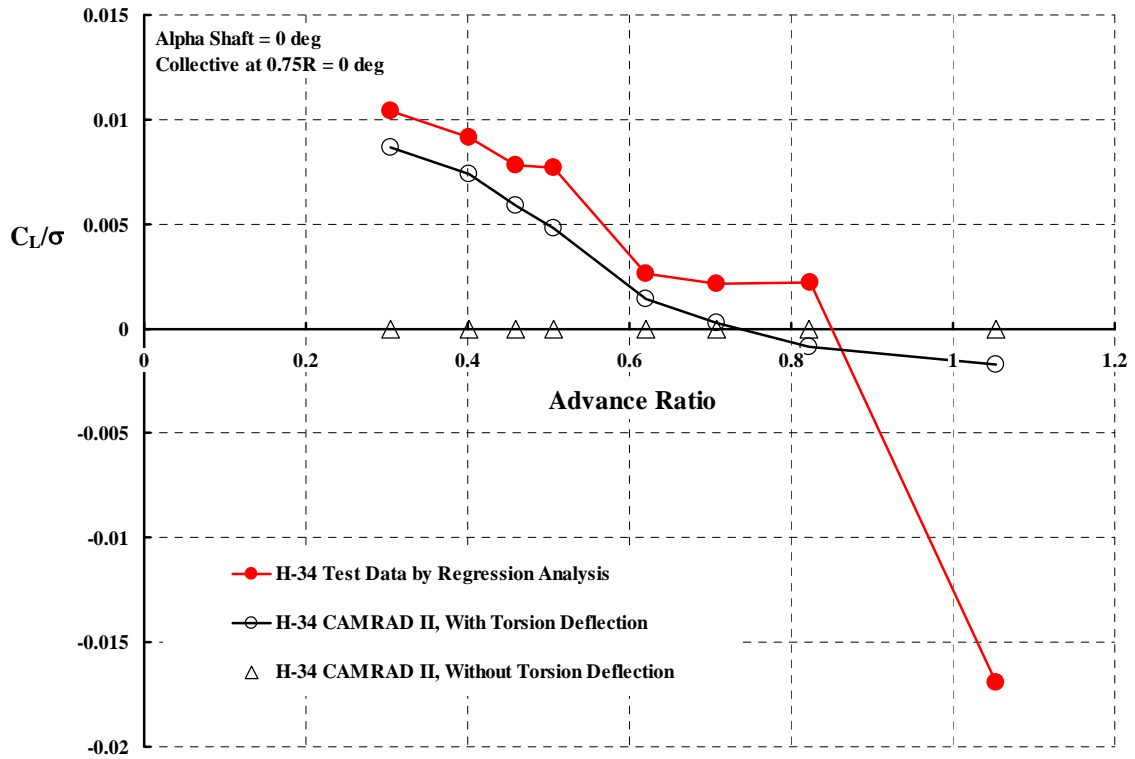


Figure F.

Predicting a rotor's lift – effective drag ratio is a serious test of any comprehensive code. In this regard, Figure G shows that neither CHARM nor RCAS have fully modeled the H-34 at high advance ratio. CAMRAD II appears as the code of choice in the near term. A key factor in the progress that Figure G shows was properly accounting for the H-34 blade root end. The N.A.C.A. 0012 airfoil of the H-34 blade extends from the tip inboard to the 57.76 inch radius station. This airfoil portion of the blade is connected to the hub/blade bolt joint with a D spar, which ends at the 28.94 inch radius station. Thus, the blade root end (called the blade shank in this report) is nearly two and one half feet long and has a very high “airfoil” minimum drag coefficient, on the order of five times the C_{d0} for the N.A.C.A. 0012. Based on the detailed correlation reported herein, the best that can be said is that comprehensive codes can not predict L/D_E to better than ± 0.5 to ± 1.0 , given a high advance ratio, a shaft angle of attack and a collective pitch setting.

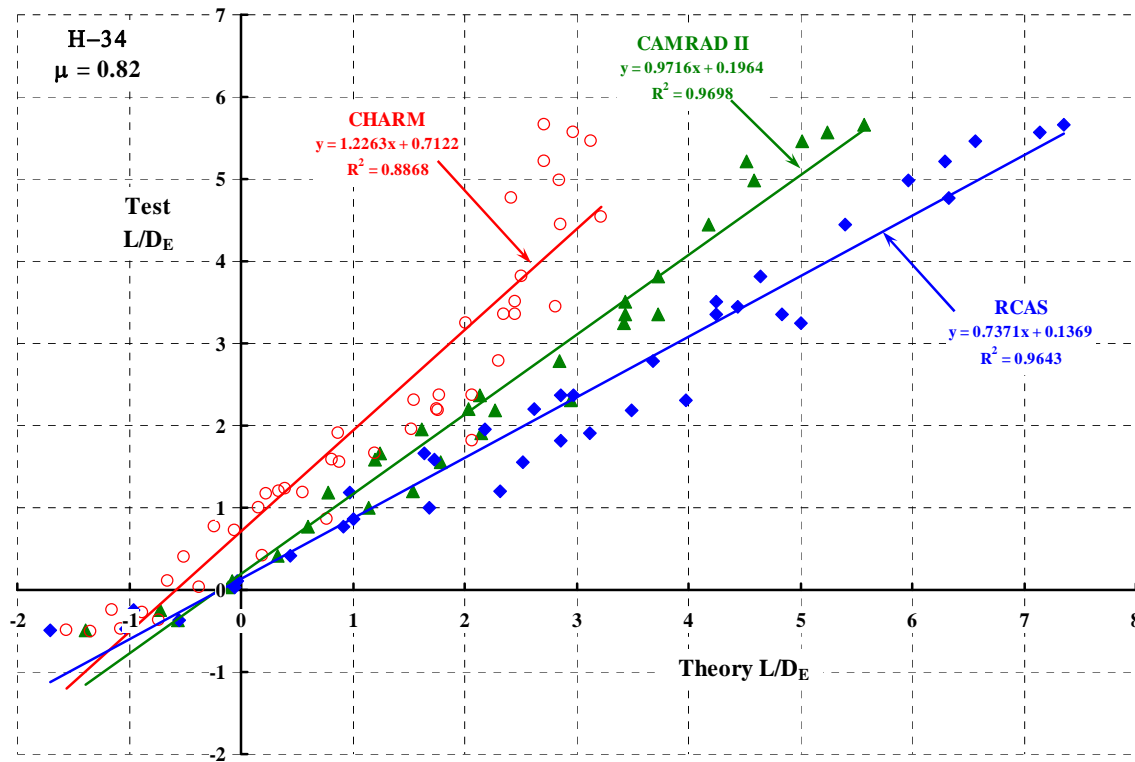


Figure G.

Figures D through G do not include results using OVERFLOW-2 or OVERFLOW-2 coupled to CAMRAD II. The reason for this very advanced theory's absence is that the fundamental baseline calculation yielded unrealistic results. The baseline case for all theories has been to calculate H-force and torque with the rectangular, untwisted H-34 blade. The calculation is made with the shaft angle of attack set to zero and the collective pitch set to zero. No cyclic feathering or structural deformation is permitted. Calculations for this idealized, non-lifting, edgewise flying rotor are made over the complete advance ratio range from zero to 1.0. Three investigators tackled this deceptively simple problem and each got different answers. The

collective results showed that OVERFLOW-2 failed to calculate measured blade element drag when the airfoil was at an angle of attack of 180 degrees. Since high advance ratio operation creates a very large portion of the rotor disc where airfoils are “flying backwards,” few calculations beyond this baseline attempt were made. The author’s further investigation disclosed that OVERFLOW-2 has – apparently – not been test against the fundamental problem of infinite circular cylinder drag variation with Reynolds number. The ability to calculate pressure drag of a bluff body is absolutely necessary because rotor blade root ends are currently far from airfoil shapes. On the positive side, OVERFLOW-2 coupled to CAMRAD II has shown very promising results in calculating airloads in the helicopter regime where the reverse flow region is quite small and blade root end drag is much less important. However, OVERFLOW-2 (coupled or not) can not – at the present time – be recommended for use beyond an advance ratio of 0.35 to 0.40.

Based on the encouraging H-34 correlation, the author, hoping that the success could be repeated with a different rotor, prevailed upon the volunteers to tackle the UH-1 rotor problem. However, the theory versus test comparison with the modified UH-1 rotor is considerably less complete at the present time. There are four reasons for the incompleteness:

- a. First and foremost, the author, acting as the scribe, simply wore out the volunteer investigators with the H-34 correlations. These volunteers are identified in the opening acknowledgement.
- b. Secondly, the UH-1 rotor system is not as intimately understood as the H-34 rotor system. In particular, the reduced radius UH-1 rotor as tested forced consideration of a very distorted airfoil over the inboard region of the blade. The distortion comes because the blade root end is reinforced with progressively thicker doublers to insure a satisfactory bolt joint of the blade to the hub. The doubler stack begins around the bolt located at the 28 inch radius station ($r/R = 28/204 = 0.137$). The stack reduces in thickness and is finally gone at the 80 inch radius station ($r/R = 0.392$). Thus the N.A.C.A. 0012 airfoil is hardly representative over an excessively long span of the modified 17 foot blade.
- c. Thirdly, the investigators using CHARM were not happy with their H-34 results and saw complications with the lifting surface model in the reverse flow region. They therefore elected to delay UH-1 computations.
- d. Finally, CAMRAD II’s (and RCAS’) prediction of UH-1 lift and longitudinal cyclic (when the shaft angle of attack equals zero and collective pitch at the 3/4 radius station equals zero) was not adequate. Therefore, only minimal points required for the complete correlation data set sought for this report were completed. Instead, CAMRAD II’s attention was turned to the PCA-2 rotor, as will be discussed shortly.

Only results using RCAS provided the nearly full 218 UH-1 data point computational data bank sought for this report. It is this author's position that correlation begins by predicting the lift and longitudinal cyclic when the shaft angle of attack equals zero and collective pitch at the 3/4 radius station equals zero. Until this fundamental is captured, there is little reason to expect other aerodynamic performance parameters will be accurately predicted. That there is a serious error in this RCAS computational set is confirmed by Figures H and I. Based on the H-34 examination, it could well be that torsional deflection is not reflected in these first RCAS predictions of UH-1 test data. Of course, the UH-1 differs from the H-34 in that the UH-1 has an under slung teetering hub. Furthermore, the blades are attached to the hub with precone and the rotor system is stiff inplane. There is a drag strut which holds the blade at a specified lead-lag angle relative to the pitch axis (see Appendix 11.4, figure 2). A pre-lag or lead angle coupled with a soft control system may be a significant factor. Of course, the UH-1 two bladed rotor with low aspect ratio blades may pose some unusual non-uniform downwash calculation problems. Clearly, there must be several configuration ingredients missing in the RCAS setup at this time.

Figures J and K show that there is very little scatter in the lift and longitudinal cyclic correlation at an advance ratio of 0.51. Interestingly, the lift regression analysis from Figure J gives a slope value of 0.8635 and this value was relatively unchanged with higher advance ratios. This suggests that RCAS is capturing a fundamental trend. No doubt, additional study will uncover what missing factor(s) about the UH-1 test data and/or RCAS is at the bottom of this current correlation problem.

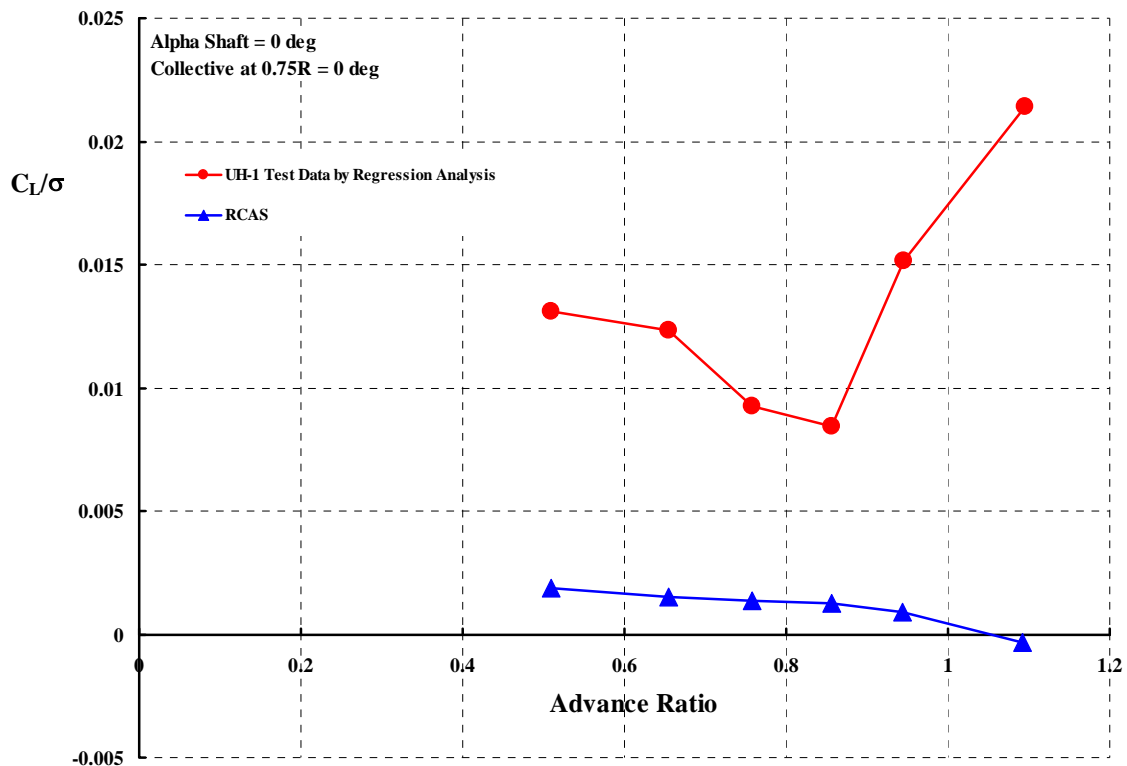


Figure H.

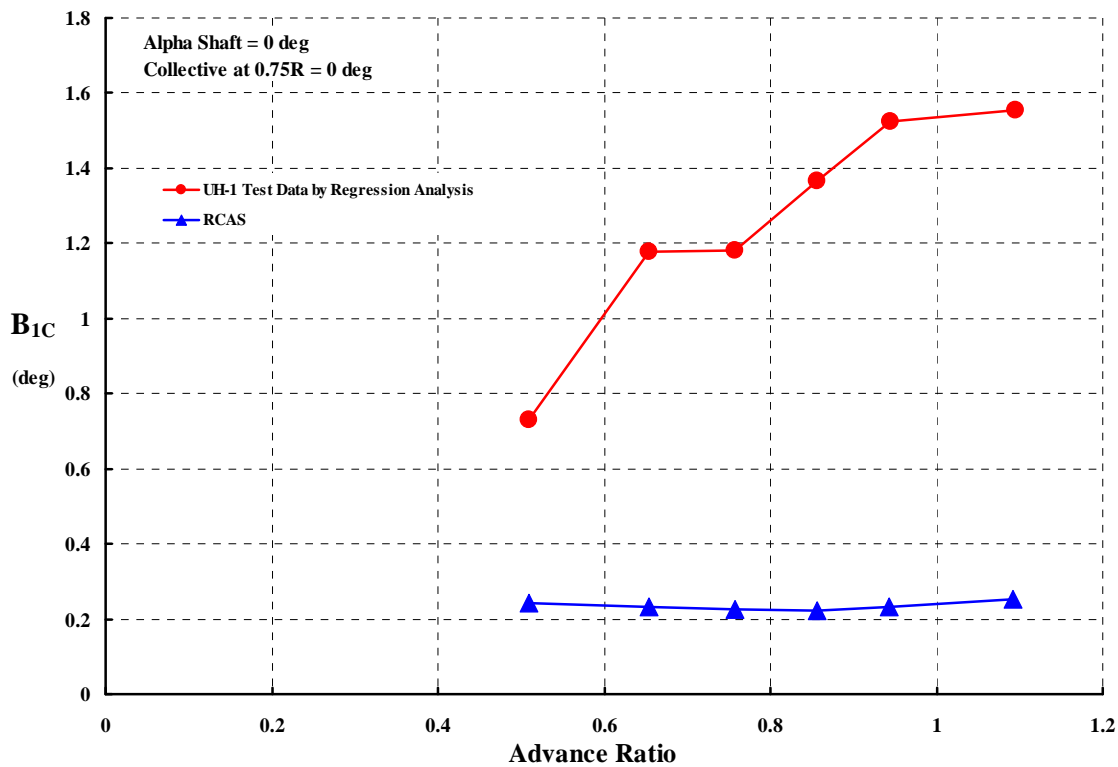


Figure I.

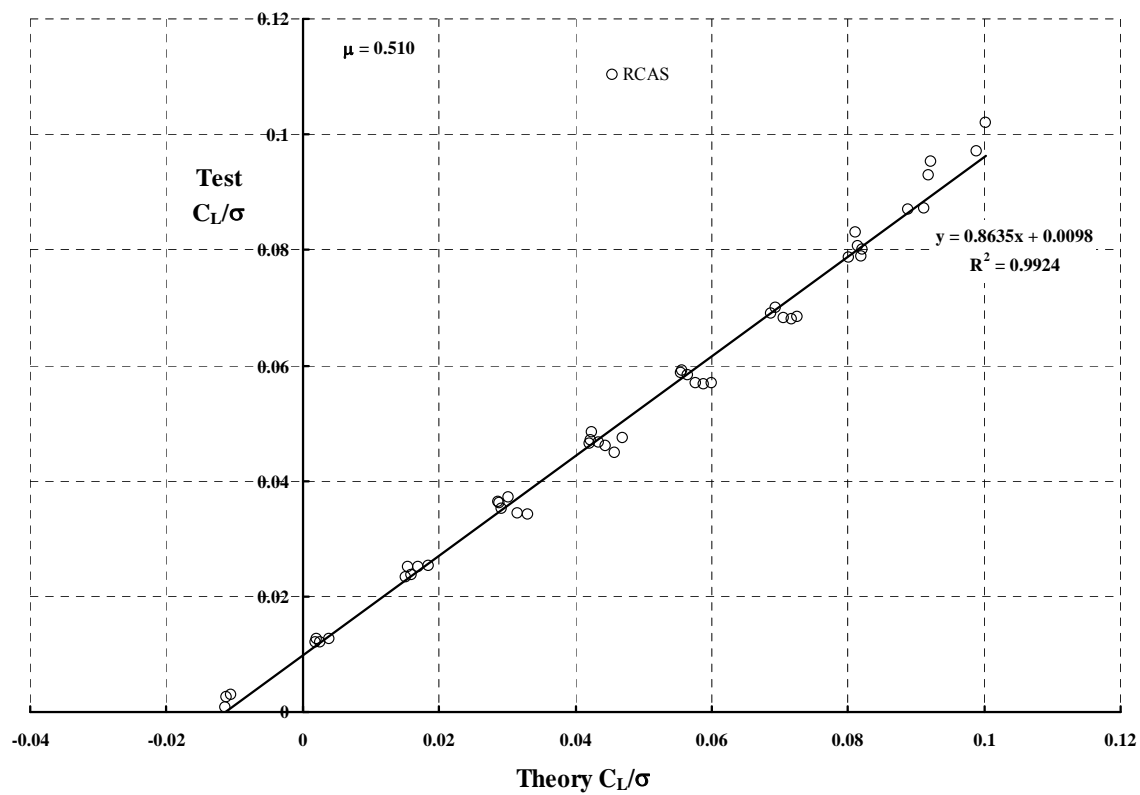


Figure J.

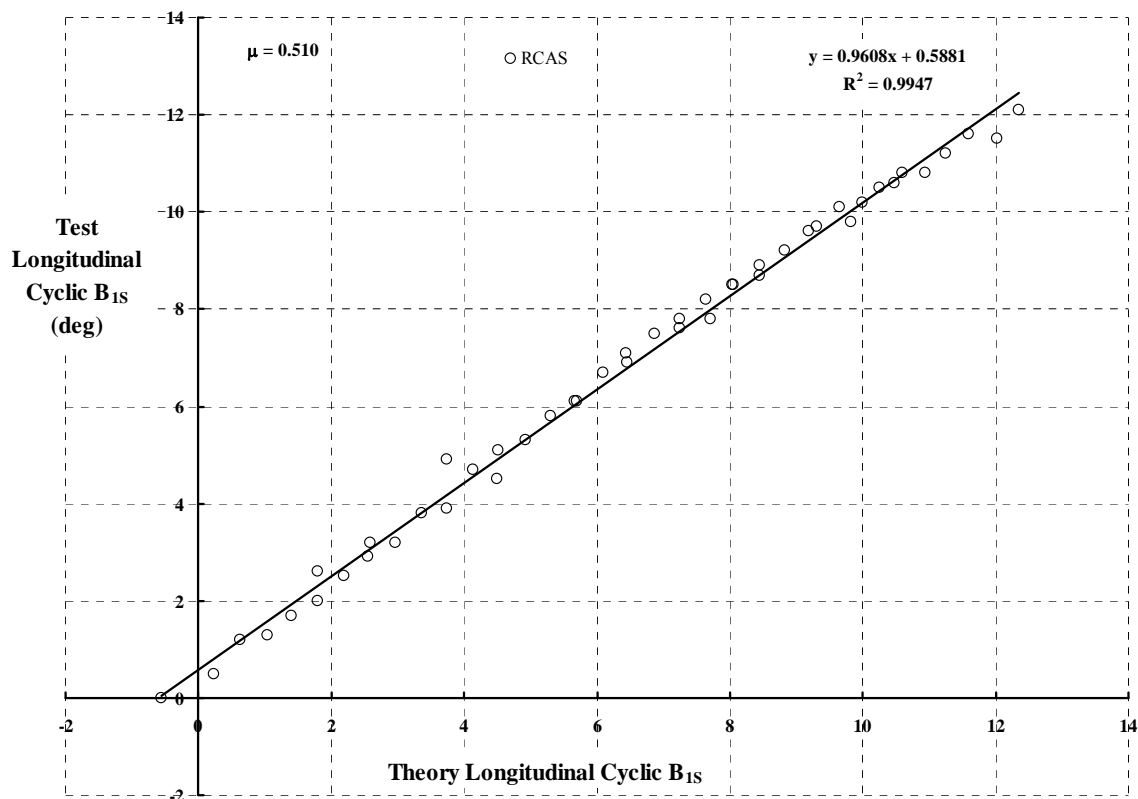


Figure K.

The final theory/test comparison discussed in this report deals with the PCA-2 isolated rotor test reported by N.A.C.A.'s John Wheatley and Manley Hood in N.A.C.A. Report No. 515. This rotor was first tested as part of the production Pitcairn PCA-2 autogyro Wheatley studied in 1932 and reported in N.A.C.A. Report No. 434. The wing and fuselage of this autogyro clouded the rotor performance aspects, so Wheatley installed the production rotor alone in the N.A.C.A. 30 by 60 foot open throat wind tunnel for more carefully controlled testing. The performance of the total hub plus blades plus droop cables and blade to blade lag damper cables as well as several fittings was measured. That is, no "hub tares" were obtained and subtracted from the total forces and moments that the wind tunnel balance recorded. Because the rotor was unpowered and had no pitch change mechanism, it is – in this author's opinion – the most rigorous baseline that modern theories can be measured against.

CAMRAD II is a modern comprehensive code that demands a great deal of detailed blade geometry and structural properties information. The necessary PCA-2 input data was provided by the author working backwards from drawings provided by Mr. Stephen Pitcairn (son of Mr. Harold Pitcairn who brought Cierva's invention to the U.S.A.) and Mr. Mike Posey who kept a PCA-2 in flight ready condition at the Pitcairn hanger in Robbinsville, Pennsylvania for many years. The author also constructed Göttingen 429 airfoil aerodynamic properties in the so called C81 format. Wayne

Johnson took on the ground breaking work of describing the PCA-2 rotor to CAMRAD II and then making calculations at 12 advance ratios covering the test range.

CAMRAD II was asked to compute the shaft angle of attack at which autorotation would occur given the input blade structural properties, blade configuration geometry and airfoil aerodynamics. At selected advance ratios (prescribe rotor RPM and wind tunnel velocity), CAMRAD II searched for the shaft angle of attack that achieved autorotation. Once this shaft angle of attack was found, the analysis calculated the three forces and two moments associated with the operating condition. (Remember the shaft torque was required to be zero.) This approach reasonably duplicated how Wheatley conducted the PCA-2, rotor alone, wind tunnel test.

Wheatley obtained data at four nominal rotor speeds by adjusting shaft angle of attack and wind tunnel speed. No ground adjustment to the fixed root end collective pitch was made to obtain the four rotor speeds. Unfortunately, blade flapping motion data was not published and, if measured, may be lost forever. An example of CAMRAD II's prediction of the Wheatley test results for three rotor performance parameters at one nominal rotor speed of 98.6 RPM is sufficient to appreciate the total correlation effort.

CAMRAD II's search for the shaft angle of attack at which autorotation occurred provided the results shown on Figure L. At this rotor speed as well as higher values, CAMRAD II generally over predicted the shaft angle of attack required for autorotation. That is the basic trend up to advance ratios somewhat above 0.5. Above this advance ratio, theory and test clearly are arriving at very different opinions. The comparison of calculated and measured thrust coefficient, Figure M, indicates that some root collective

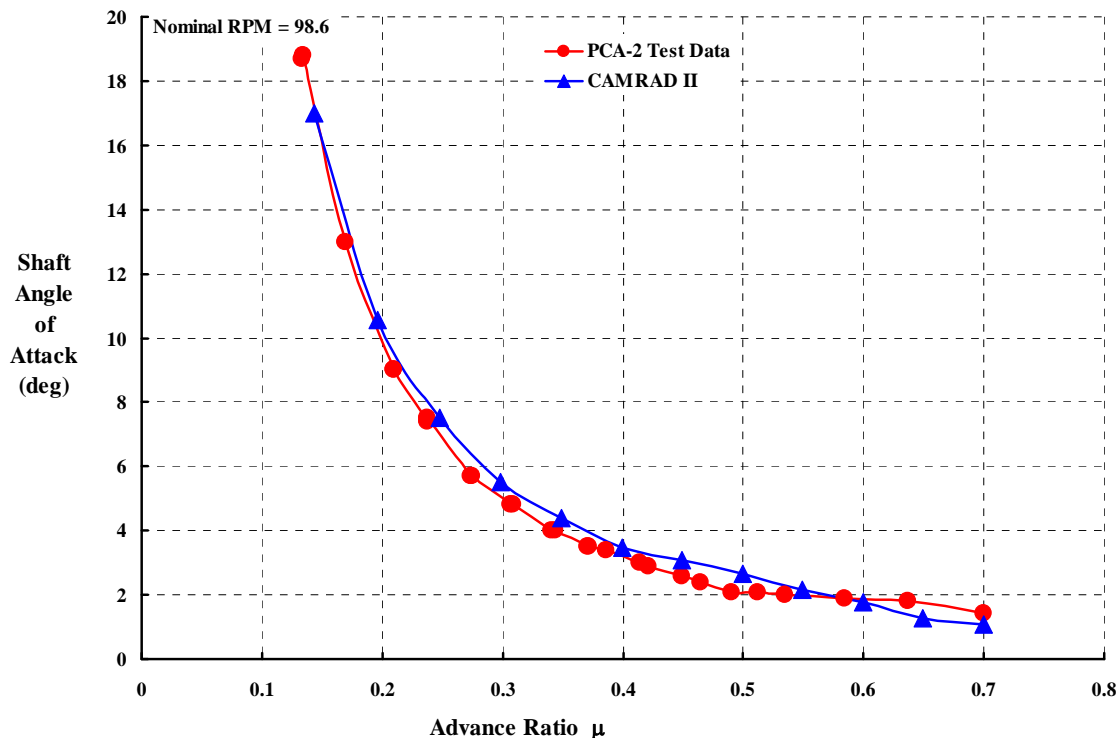


Figure L.

pitch or, more likely, some positive elastic twist must be calculated by CAMRAD II to improve the correlation. Wheatley advocated elastic twist as the missing factor in his study of autogyro rotor performance. The experimental data shows a marked sensitivity of thrust coefficient to rotor speed at equal advance ratio. CAMRAD II results do not follow the experiment in this regard.

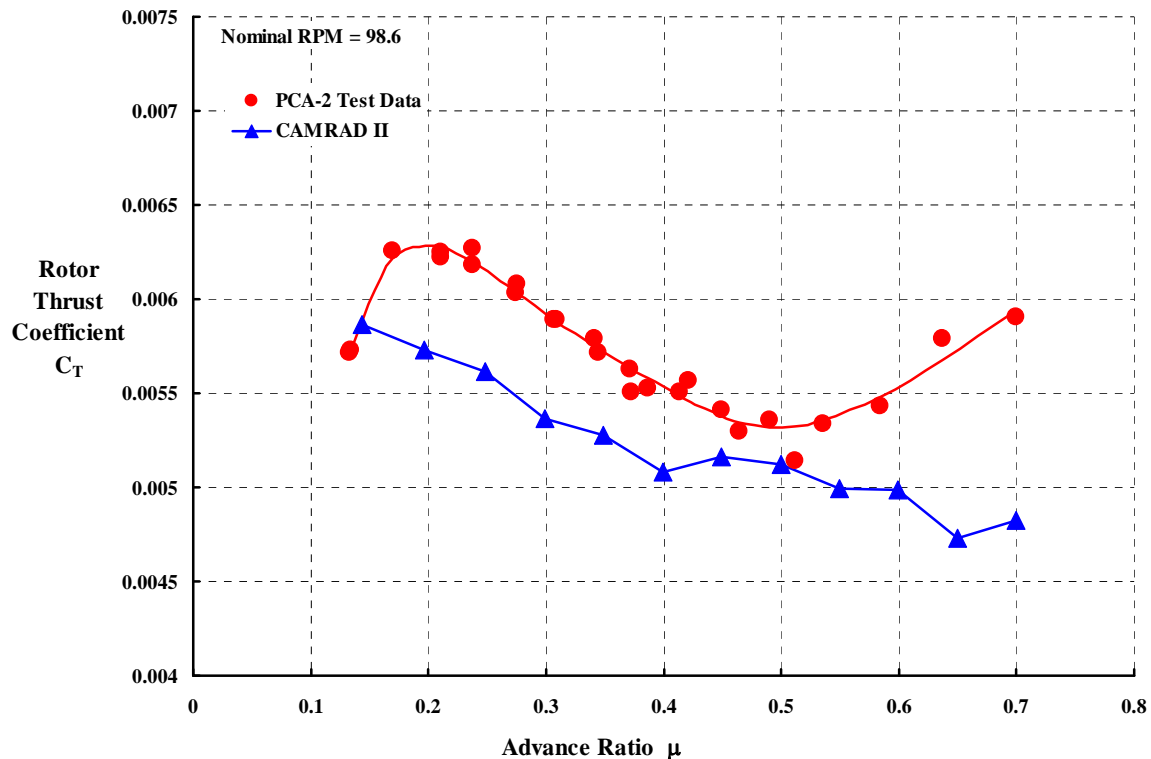


Figure M.

The third performance parameter presented in this summary of PCA-2 data versus CAMRAD II is shown with Figure N. The rotor lift to drag ratio is, of course, a fundamental measure of autogyro rotor performance. Wheatley was unable to extract this parameter from the production PCA-2 flight tests, but the wind tunnel testing of the isolated rotor left no doubt that the rotor did not compare favorably to a fixed wing of equal span. CAMRAD II calculations are rather pessimistic as Figure N shows. However, the major difference is attributable to under predicting rotor lift as illustrated with Fig. M.

This study uncovered several additional facts of note:

1. With respect to H-34 experimental data reported in NASA TN D-4632, the data set at an advance ratio of 1.05 is of very doubtful value in any theory/test comparison.
2. With respect to UH-1 experimental data reported in USAAVLABS TR 69-2, there are five (5) points at an advance ratio of 0.65 where there was insufficient longitudinal cyclic to trim the tip path plane normal to the shaft. These points were discarded in this study because all theories used zero first harmonic flapping as a trim requirement.

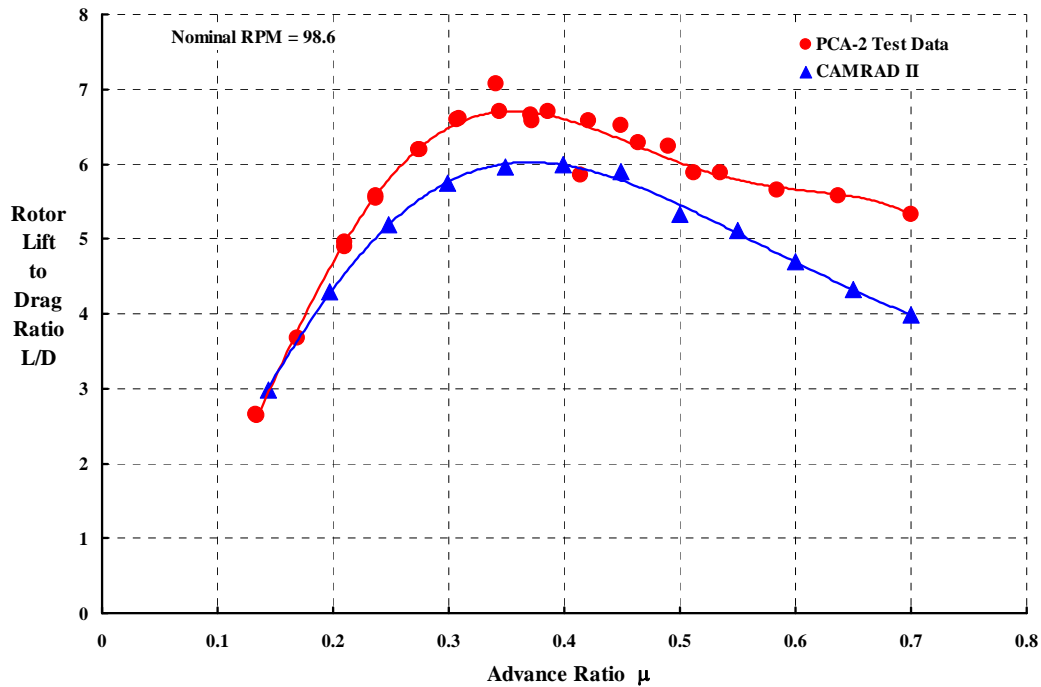


Figure N.

3. There was an expectation that a rotor with untwisted blades would produce no lift and require no cyclic control input to trim to zero flapping (at any advance ratio) if operated at zero shaft angle of attack and zero collective pitch at the 3/4 radius station. This was a very incorrect preconceived notion.

4. A speculative situation arose about the H-34/UH-1 versus CAMRAD II and RCAS codes. At an advance ratio of 0.51, CAMRAD II accurately predicted rotor lift curve slope for both rotors using a rigid wake model. RCAS accurately predicted rotor lift curve slope only for the H-34 using non-uniform downwash calculated with the Peters – He dynamic inflow model set to 8 by 8 mode. RCAS’ predicted lift curve slope was some 15 percent too high for the UH-1 at $\mu = 0.51$. The applicability of dynamic inflow models with low aspect ratio blades operating at high advance ratio is in question.

5. The lateral cyclic control required to trim lateral flapping to zero was unpredictable by the comprehensive codes examined with this report. Furthermore, not one of the comprehensive codes came close to predicting measured rotor side force. However, OVERFLOW-2 identified a side force at zero thrust, zero collective pitch and zero shaft angle of attack. Simple and advanced theories do not suggest that there would be a side force at this condition.

6. The several codes were relatively unsuccessful (compared to predicting lift) in calculating rotor H-force and rotor power given test values of μ , α_s , and $\theta_{0.75R}$. High advance ratio flight leads to many blade elements in the reverse flow region operating at large sweep angles in an unsteady flow condition. Airloads for airfoils “flying backwards” are not as well understood as for airfoils in normal flow.

7. The H-34 and UH-1 measurements of H-force and power – at the fundamental condition where of $\alpha_S = 0$ and $\theta_{0.75R} = 0$ – varied with advance ratio in approximately the same manner. This fact is conveyed with Figures O and P. Unfortunately, the advanced codes did not predict either rotor's experimental values to within engineering accuracy. The codes over predict power and under predict H-force as discussed in the theory versus test detail for each code's correlation.

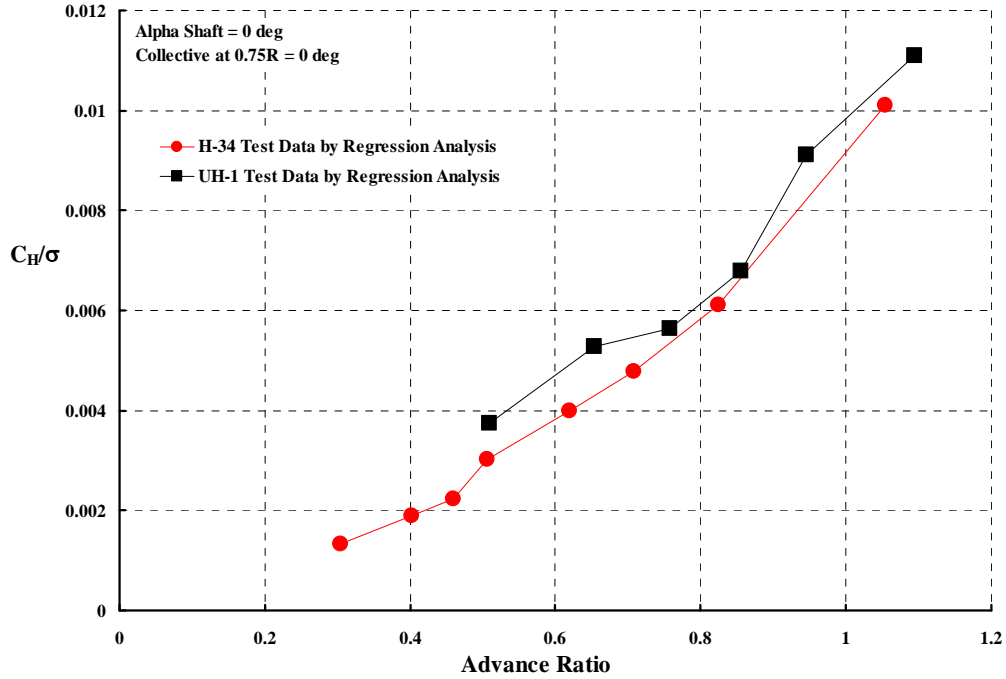


Figure O.

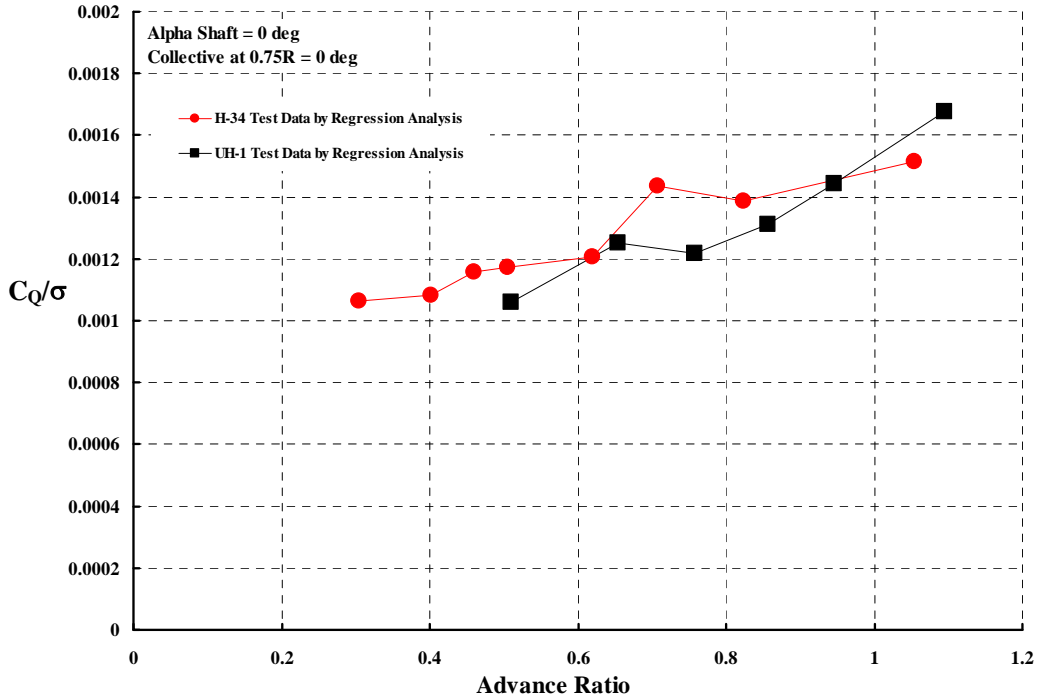


Figure P.

8. Both the H-34 and UH-1 rotors exhibited the undesirable lift coefficient sensitivity to changes in collective pitch shown with Figure Q. The rotor lift becomes non-responsive to a collective pitch input at advance ratios near 1.0 – *if the rotor blade flapping is zeroed out by cyclic control as the collective pitch is changed and the shaft angle of attack remains constant*. The data indicate that in the advance ratio range of 0.9 to 1.0 there is a control reversal. At advance ratios below 0.9 an increase in collective pitch will increase rotor lift, but at advance ratios above 1.0 an increase in collective pitch reduces lift. In contrast, there is no reversal in the rotor lift curve slope (i.e., $\Delta C_L/\sigma$ per $\Delta \alpha_s$ at fixed collective), although the sensitivity increases with advance ratio. This rotor behavior may be unfamiliar to some; however, the unfavorable trend in $\Delta C_L/\sigma$ due to a $\Delta \theta$ at constant tip path plane angle of attack was first reported by Larry Jenkins in 1965 in NASA TN D-2628. The codes are quite able to capture this undesirable behavior.

8. Because of the control reversal characteristic that Figure Q shows, future high advance ratio performance testing should acquire data by fixing collective pitch and varying shaft angle of attack while maintaining the tip path plane normal to the shaft.

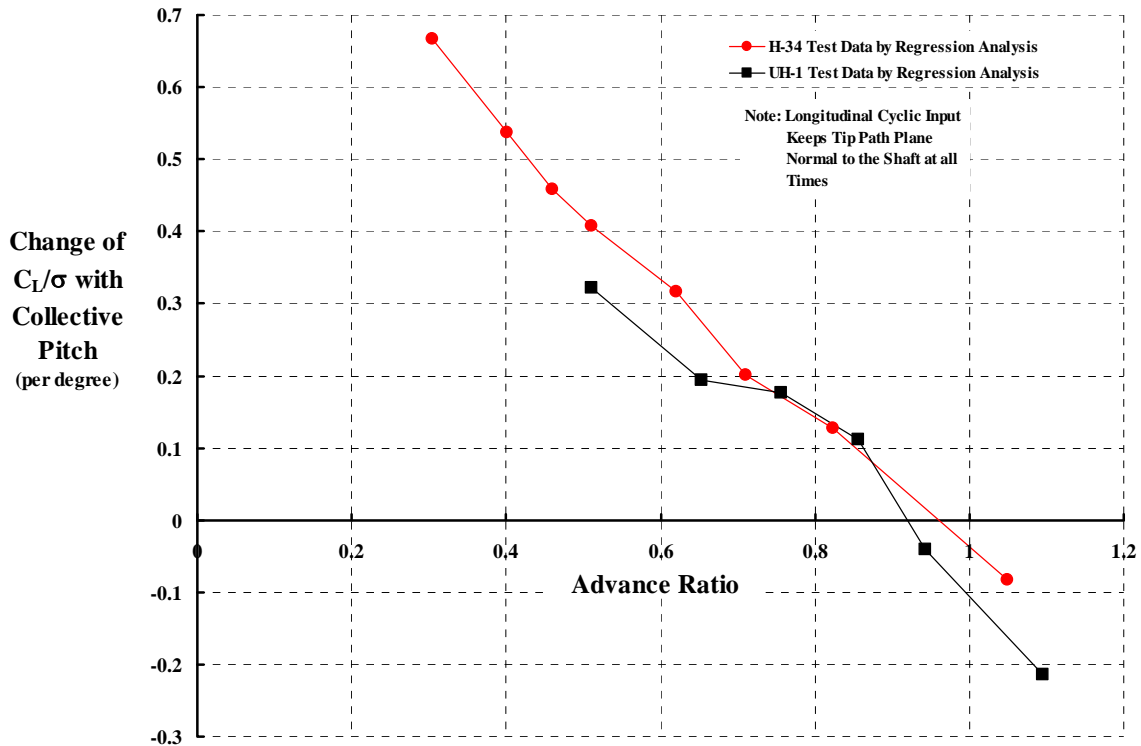


Figure Q.

9. The blade element airload modeling successfully achieved for helicopter speeds is inadequate when extrapolated to advance ratios above 0.5 to 0.6. Until this technology shortcoming is repaired, the only available experimental data will have to do. The regression analysis equations of the H-34 and UH-1 test data as given in Chapter 5 should suffice for the near term calculation of conventional rotor performance at high advance ratio – at least up to $\mu = 1.0$.

The findings uncovered by this study suggest several recommendations for future efforts. The immediate concern is that the matrix of five theories compared to three experiments was not completed during this study. Therefore, it is recommended that theory comparisons to UH-1 and PCA-2 test data be finished. In addition:

1. Computational fluid dynamic theoreticians must provide the tools to accurately compute airfoil lift, drag and pitching moment when the airfoil is operating in a rotor's reverse flow region. These CFD tools must also be able to accurately predict at least the drag of typical non-airfoil shapes used for rotor blade root ends.

2. Comprehensive code developers must incorporate airfoil tables much more representative of airfoils operating in a rotor's reverse flow region. Inclusion of Reynolds number effects is of utmost priority if these codes are to be useful at advance ratios beyond 0.5 to 0.6. Special attention to modeling blade root end geometry and associated aerodynamic characteristics can no longer be ignored. Furthermore, rotor blade trailing edge geometry and its influence on blade element aerodynamics must be examined in great detail.

3. There is no full-scale rotor performance data available for advance ratios above 1.0 and extrapolation of currently available data to advance ratios on the order of 2.0 is unreasonable despite the needs of future rotorcraft. Therefore, it is recommended that an overly strong full-scale rotor blade set be obtained and tested in a suitable wind tunnel to at least an advance ratio of 2.5. A tail rotor from a Sikorsky CH-53 or other large single rotor helicopter may be adequate for this exploratory experiment.

4. Because so little is known about the reverse flow region, at least two small scale tests of a fundamental research nature should be conducted. Both tests should reach an advance ratio of at least 3.0 and only drag and power need be measured. These two tests, of considerable benefit to the rotorcraft community in general (and CFD theoreticians in particular), are:

- a. Circular cylinders of selected diameters tested as a two bladed rotor, but without a hub (and typical blade retention hardware) and without a control system. In essence, a 6 or 7 foot pipe center mounted to a shaft so that no aerodynamic tares need be accounted for.
- b. Similarly, a very strong two bladed rotor with no hub or control system and with NACA 0012 airfoil blades should be built. The blades should be of rectangular planform and untwisted. In essence, a 6 or 7 foot carved ruler (i.e., a club), center mounted to a shaft so that no aerodynamic tares need be accounted for.

5. Because of the control reversal characteristic associated with rotor lift, future high advance ratio performance testing should acquire data by fixing collective pitch and varying shaft angle of attack while maintaining the tip path plane normal to the shaft. Additionally, the behavior of side force with lateral cyclic control should be measured.

Page intentionally blank

2 INTRODUCTION

The study of rotor performance at airplane-like forward speeds and when the rotor is turning relatively slowly began when Juan de la Cierva invented the autogyro in the mid-1920s. Since then, the rotorcraft industry has pursued both analytical and experimental studies of high speed, slowed rotor performance technology in fits and starts. This technology is keyed to the ratio of forward speed (V) to rotor blade tip speed (V_t). This ratio is referred to as advance ratio and denoted by the Greek symbol μ (μ).

The evolutionary story of high advance ratio technology is rather interesting. In brief, Cierva's early autogyros grew quickly into a configuration that combined a rotor for lift at low speed with a relatively typical airplane of the day. One popular configuration is illustrated with Fig. 2-1. The Pitcairn PCA-2 was certificated in the United States for civil aviation use on April 2, 1931 and became commercially successful. Because the PCA-2's wing carried the majority of the aircraft's weight at high speed, the rotor tip speed slowed down in high speed flight. Advance ratio frequently ranged up to $\mu = 0.7$. Slowed rotor aerodynamic technology was vigorously pursued both in England and in the United States because of these early autogyro types. In the U.S., the N.A.C.A. took a leading research role, while Harold Pitcairn and the Kellett brothers concentrated on development and manufacturing various autogyro types.



Fig. 2-1 The Pitcairn PCA-2 autogyro popular in the early 1930s. N.A.C.A. used this aircraft to pursue its slowed rotor technology. At high speed, the rotor advance ratio approached 0.7.

By the mid-1930s, Cierva's product development program evolved a rotor system that did not require the airplane's wing. The most commercially successful version of this advanced autogyro was the Cierva C.30 shown in Fig. 2-2.



Fig. 2-2 The Cierva C.30 was the most produced autogyro, even serving during World War II in Britain. Advance ratio rarely exceeded 0.4

Without the wing, the rotor had to maintain a much higher rotor tip speed in forward flight to carry the aircraft's weight. Thus the advance ratio dropped to a relatively modest maximum of $\mu = 0.4$. The effect of this wingless autogyro configuration was a cutback in slowed rotor technology studies. The cutback was reinforced by Sikorsky's R-4 helicopter (Fig. 2-3) in the early 1940s. The R-4's advance ratio rarely reached a maximum of $\mu = 0.25$, which reinforced the shift in research efforts from high advance ratios up to $\mu = 0.7$ to the helicopter's lower range of $\mu = 0$ to $\mu = 0.4$. In particular, the N.A.C.A. shifted its rotorcraft research from high advance ratio rotor performance to low advance ratio helicopter rotor problems such as blade stall and compressibility effects.

Throughout much of the 1940s, all of the 1950s and even into the early 1960s, military support for helicopter improvements drove rotorcraft research until the limitations to helicopter top speeds and maneuverability became increasingly clear. However, the 1950s did give rise to a U.S. Army and Air Force sponsored research program to find a high speed VTOL that complemented the helicopter.¹ The Services selected three concepts to pursue:

¹ The helicopter speed record as of April 1949 was 112.6 knots set by a Sikorsky S-52-1. A Piasecki YH-21 raised the record to 127 knots in September 1953. Westland's G-Lynx now holds the helicopter speed record at 216.3 knots, set on August 11, 1986. At this speed, the Lynx aircraft L/D was about 2.



Fig. 2-3. The Sikorsky R-4 was the first production helicopter in the U. S. The rotor operated at advance ratios below 0.3.

1. the XV-1 Convertiplane from McDonnell Aircraft Corp.'s Helicopter Division, which was a compound helicopter with pressure jet tip drive rotor, plus a wing and a propeller.

2. the XV-2 from Sikorsky, which had a one (1) bladed rotor that would be stopped and stowed, plus a wing and two propellers,

3. the XV-3 from Bell, which had side-by-side tilting rotors, plus a wing.

A down select was made to the XV-1 and XV-3. By the end of 1956, the XV-1 (Fig. 2-4) had demonstrated helicopter like speeds and its slowed rotor operated successfully, even up to an advance ratio of 1. (As you know, Bell Helicopter's XV-3 tilt rotor was followed up by the NASA/Army supported XV-15, which led to the V-22 for the U.S. Marines.) In Britain, the Rotodyne (Fig. 2-5) was developed based upon the tip jet principle. Unfortunately, both British government and civil support was withdrawn. The concentration of research and development on helicopters and tilt rotor aircraft caused another lull in high advance ratio studies, the lull lasting until the mid-1960s.



Fig. 2-4. The McDonnell Aircraft Corp., Helicopter Division's XV-1 Convertiplane. At maximum speed, the rotor operated at an advance ratio just below 1.



Fig. 2-5. The Fairey Rotodyne was successfully developed, but British Government and civil funding eroded in the late 1950s. This was the largest compound helicopter ever flown. Its maximum advance ratio was below 1.

A renewed interest in compound helicopters as a way around helicopter high speed limitations grew in the 1960s and by 1970 four companies participated in U.S. Army Aviation Material Laboratories sponsored programs. Sikorsky (S-61), Kaman (UH-2), Bell (UH-1) and Lockheed (XH-51A) each converted their helicopter to a compound by adding a wing and one or two jet engines. The Bell machine achieved 274 knots using two jet engines. The Lockheed very low drag compound reached 263 knots with one jet engine. The maximum advance ratio of these aircraft ranged from 0.5 to 0.7. In general, these demonstrators showed some promise, which led, in part, to the U.S. Army requesting proposals for an Advanced Aerial Fire Support System – the AAFSS – on August 1, 1964. An excellent summary of the complete program through to August 9, 1972 when the Army cancelled the program was written by Landis and Jenkins [1]. Lockheed won the competition November 3, 1965 with its AH-56 Cheyenne, a compound helicopter with pusher propeller as Fig. 2-6 and Fig. 2-7 show. First flight was made September 1967. The usual development problems – with one exception – were found as the flight envelope was expanded. The one exception was control system related and caused a half per rev, very lightly damped rotor instability. Ray Prouty and Al Yackle [2] wrote a thorough technical discussion of the AH-56 including some very important lessons learned. Several Lockheed reports [3-7] provide even more detail.

In this author's opinion, the Lockheed hingeless rotor system (without the gyro bars) was the lowest hub drag configuration the rotorcraft industry has ever devised. Given modern materials, this hub is the ideal starting point for any advanced helicopter or compound helicopter. Reducing/eliminating control system drag would be the next task.

Cancellation of the AH-56 program put a real damper on high advance ratio technology interest. This damper lasted for nearly 30 years.



Fig. 2-6. The Lockheed AH-56 had a tail rotor for hover and a pusher propeller and wing for forward flight



Fig. 2-7. The AH-56's rotor reached an advance ratio slightly over 0.52 at a flight speed of 204 knots.

In contrast to fits and starts in Government sponsored research and development, homebuilt autogyros by amateurs continues to expand. A typical example, Fig. 2-8, illustrates the movement to two place autogyros. The basic configuration started out with the Focke Achgelis Fa-330 rotary wing kite in Germany and the Hafner Rotachute in Britain. The Fa-330 was designed to be towed behind a submarine. After World War II, Igor Bensen, in the United States, experimented with the German glider concept and naturally gravitated to a powered configuration.

High advance ratio technology interest was sparked anew in the mid-2000s when DARPA, the U.S. Army and NASA suggested that perhaps advances in technology

might, if applied to an advanced compound helicopter, offer an attractive alternate to the tilt rotor. DARPA let a small contract to the Groen Brothers to investigate the possibilities further. The concept approach (Fig. 2-9) is to add a tip driven rotor to a very low drag, small commercial corporate jet, the Adams A700. DARPA has set the high speed goal at 400 miles per hour at commercial jet transport altitudes. To achieve this goal, an advance ratio of about 2 is expected. During the same period, the U.S. Army and NASA gave small contracts to the industry who studied very clean helicopters, compound helicopters and tilt rotor approaches. Several of the proposed conceptual compound helicopters were to operate their rotor above advance ratios of 1.0.



Fig. 2-8. The fleet of homebuilt autogyros continues to expand since their introduction by Igor Bensen in the early 1950s.



Fig. 2-9. The DARPA funded Groen Brothers Heliplane is expected to reach 400 mph with the rotor operating at an advance ratio near 2.

From this brief discussion, you can see that up until the end of the 20th century rotor operation was well below an advance ratio of 1.0. Furthermore, technology concentration on the helicopter has led only to adequate analytical and thorough experimental knowledge for rotor operation below an advance ratio of 0.45. In fact, very little is known today about rotor aerodynamic behavior in the advance ratio range from 0.45 up to 1.0. The advance ratio range from 1.0 to 2.0 is a complete unknown.

2.1 Study Objective

NASA has funded this high speed, slowed rotor technology initiative. Their objective is to extend our rotor knowledge (both analytical and experimental) at least up to an advance ratio of 2.0. The specific objectives of this portion of the initiative are (1) to assess aerodynamic performance behavior of rotors up to an advance ratio of 1.0 using available experimental data, (2) see how well current analytical tools are able to predict the available experimental performance data and then (3) make recommendations that, when implemented, will improve current analytical tools.

2.2 Performance Fundamentals

The various rotorcraft configurations that use a rotor for vertical or short field takeoff and landing (i.e., V/STOL) invariably lead to a calculation of power required to fly. The simple sketch shown with Fig. 2-10 helps guide this calculation for autogyros and compound helicopters. The installed power plant, say a reciprocating or turboshaft engine, is coupled to a propeller and can be coupled and uncoupled to a rotor. The propeller is directly driven by the engine. The rotor receives its power from a right angle gear box, which is driven by a separate shaft from the engine. The rotor drive train might well have a clutch to manage its portion of the engine's power. The basic question raised by Fig. 2-10 is: How much power must the engine provide so that the machine will fly?

The answer to this engine power required to fly question can be found with a very simple approach using the principle of energy per unit time, which is power. To begin with, the engine power (P_{engine}) must equal – at a minimum – the sum of power required by the propeller (P_{prop}) and power required by the rotor (P_{rotor})². That is

$$(1) \quad P_{\text{engine}} = P_{\text{prop}} + P_{\text{rotor}}$$

The propeller power required can be calculated in a relatively direct manner [8] as

$$(2) \quad P_{\text{prop}} = T_{\text{prop}} V + P_{\text{prop induced}} + P_{\text{prop profile}}$$

where T_{prop} is the propeller thrust, V is the aircraft flight speed, $P_{\text{prop induced}}$ is the propeller's induced power to produce thrust and $P_{\text{prop profile}}$ is the profile power required to overcome the propeller blade drag.

² The engine must, of course, also supply additional power to overcome transmission losses and to run accessories, but these burdens will not be included in this discussion.

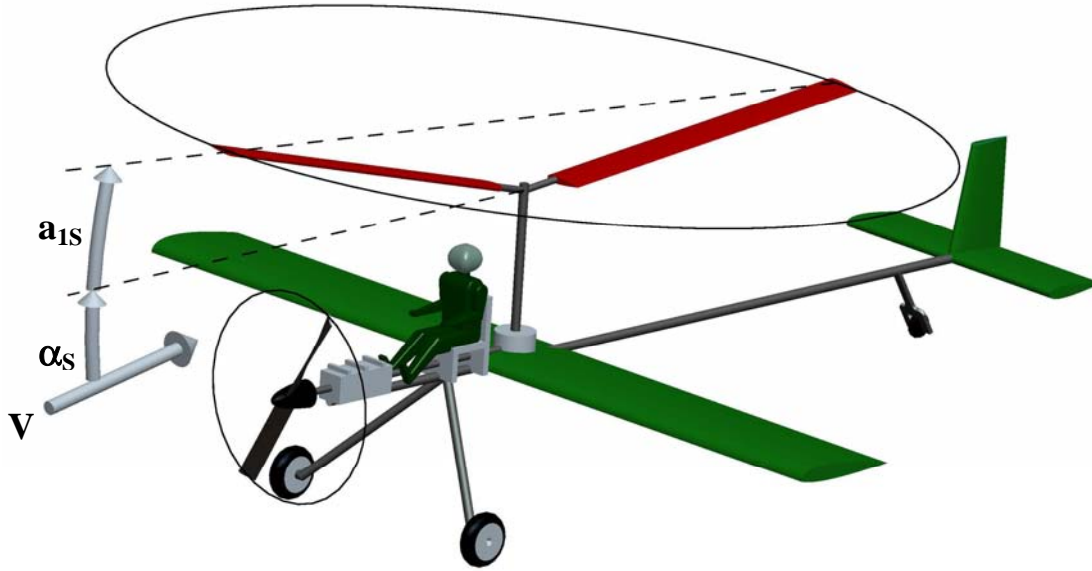


Fig. 2-10. The simple elements of autogyros and compound helicopters. Tail rotor not shown for clarity. Rendition provided by Gerardo Nunez from author's sketch.

In a similar manner, the rotor power required can be obtained [9] from

$$(3) \quad P_{\text{rotor}} = X_{\text{rotor}} V + P_{\text{rotor induced}} + P_{\text{rotor profile}}$$

where X_{rotor} is the propulsive force the rotor can add to the propeller thrust so that there is force equilibrium in the horizontal direction (i.e., $\sum F_x = 0$), $P_{\text{rotor induced}}$ is the rotor's induced power to produce thrust and $P_{\text{rotor profile}}$ is the rotor profile power required to overcome the blade drag.

Consider next the equilibrium of forces in both the horizontal and vertical directions assuming steady level flight. In the vertical direction you have

$$(4) \quad \sum F_z = 0 = L_{\text{wing}} + L_{\text{rotor}} - W$$

and in the horizontal direction

$$(5) \quad \sum F_x = 0 = T_{\text{prop}} + X_{\text{rotor}} - D_{\text{wing}} - f_e \left(\frac{1}{2} \rho V^2 \right)$$

where f_e is the equivalent parasite drag area of the aircraft and ρ is the density of air.

Now, the propeller thrust depends on the rotor's propulsive force, the wing's drag (D_{wing}) and the parasite drag. Thus, from Eq. (5)

$$(6) \quad T_{\text{prop}} = -X_{\text{rotor}} + D_{\text{wing}} + f_e \left(\frac{1}{2} \rho V^2 \right)$$

But, from Eq. (3) the rotor propulsive force is simply

$$(7) \quad X_{\text{rotor}} = \frac{P_{\text{rotor}} - P_{\text{rotor induced}} - P_{\text{rotor profile}}}{V}$$

and therefore the propeller thrust is

$$(8) \quad T_{\text{prop}} = -\left(\frac{P_{\text{rotor}} - P_{\text{rotor induced}} - P_{\text{rotor profile}}}{V}\right) + D_{\text{wing}} + f_e \left(\frac{1}{2} \rho V^2\right)$$

Suppose now that the rotor is autorotating, which means that $P_{\text{rotor}} = 0$. The propeller thrust – in this special case – then becomes

$$(9) \quad T_{\text{prop}} = \left(\frac{P_{\text{rotor induced}} + P_{\text{rotor profile}}}{V}\right) + D_{\text{wing}} + f_e \left(\frac{1}{2} \rho V^2\right)$$

and the engine is supplying all of its power to the propeller and none to the rotor. Then after substituting T_{prop} from Eq. (9) into Eq. (2), the engine power required amounts to

$$(10) \quad P_{\text{engine}} = \left[\left(\frac{P_{\text{rotor induced}} + P_{\text{rotor profile}}}{V}\right) + D_{\text{wing}} + f_e \left(\frac{1}{2} \rho V^2\right)\right] V + P_{\text{prop induced}} + P_{\text{prop profile}}$$

Before addressing the rotor induced and profile powers, the other powers in Eq. (10) must be discussed. First of all, the wing drag and parasite drag are calculated with any number of classical airplane aerodynamic approaches. Secondly, the propeller induced and profile powers have first order approximations [8] of

$$(11) \quad \begin{aligned} P_{\text{prop induced}} &= T_{\text{prop}} \left\{ \sqrt{\left(\frac{V}{2}\right)^2 + \frac{T_{\text{prop}}}{2\rho A_{\text{prop}}}} - \frac{V}{2} \right\} \\ P_{\text{prop profile}} &= \left[\frac{\rho (bcR) V_t^3 C_d}{8} \right]_{\text{prop}} \left\{ \left(1 + \frac{5}{2} \lambda^2\right) \sqrt{1 + \lambda^2} + \frac{3}{2} \lambda^4 \ln \left[\frac{1 + \sqrt{1 + \lambda^2}}{\lambda} \right] \right\} \end{aligned}$$

where the propeller advance ratio (λ) equals V/V_t .

For the rotor, equally simple and useful approximations, slightly modified with empirical corrections, are available. For example, the rotor induced power ($P_{\text{rotor induced}}$) has the first order approximation [9] of

$$(12) \quad \begin{aligned} P_{\text{rotor induced}} &= K_i \frac{L_{\text{rotor}}^2}{2\rho A_{\text{rotor}} V} \\ \text{where } K_i &= 1.075 \cosh(6.76\mu^2) \text{ for } \mu \leq 0.5 \\ \text{and } K_i &= 1 - 29.332\mu + 92.439\mu^2 - 51.746\mu^3 \text{ for } 0.5 \leq \mu \leq 1.0 \end{aligned}$$

The rotor disc area (A_{rotor}) equals πR^2 and R is the radius of a rotor blade. The rotor profile power is frequently estimated for simple rectangular blade geometry [10] as

$$(13) \quad \begin{aligned} P_{\text{rotor profile}} &= \Omega Q_{\text{rotor profile}} + V H_{\text{rotor profile}} \\ &= \left[\frac{\rho (bcR) V_t^3 C_d}{8} \right]_{\text{rotor}} \left(1 + 4.65\mu^2 + 4.15\mu^4 - \mu^6\right) \text{ for } \mu \leq 1.0 \end{aligned}$$

where b is blade number, c is blade chord and R is rotor blade radius. The blade airfoil drag coefficient is denoted by C_d and the blade tip speed by V_t .

It is important to remember that a rotor cannot autorotate if rotor lift is zero. When the rotor lift is zero, the engine must supply power ($\Omega Q_{\text{rotor profile}}$) to the rotor and the propeller must provide a thrust equal to the rotor H-force ($H_{\text{rotor profile}}$) plus any other aircraft drag. In fact, there is a threshold level for rotor lift (which depends on advance ratio) that must be reached before autorotation begins. This minimum threshold lift is crudely given by

$$(14) \quad \text{Rotor shaft power} = \Omega Q_{\text{rotor profile}} - L_{\text{rotor}} (\alpha_s + a_{1s}) V = 0$$

where $(\alpha_s + a_{1s})$ is the rotor's tip path plane angle of attack as shown in Fig. 2-10. Equation (14) says that the decelerating torque created by blade element drag (which tends to reduce rotor speed) must be offset by an accelerating torque created by blade element lift. From Eq. (14) it follows that in autorotation

$$(15) \quad L_{\text{rotor}} = \frac{\Omega Q_{\text{rotor profile}}}{(\alpha_s + a_{1s}) V} \quad \text{for autorotation} \quad (\text{Note: very crude, neglects induced drag})$$

This approximation to the rotor lift required for autorotation can be put in standard rotor coefficient form by dividing both sides of Eq. (21) by $\rho A_{\text{rotor}} V_t^2$, which yields

$$(16) \quad \text{Rotor } C_L = \frac{C_{Q_{\text{rotor profile}}}}{(\alpha_s + a_{1s}) \mu} \quad \text{for autorotation}$$

The minimum rotor profile torque coefficient ($C_{Q_{\text{rotor profile}}}$) is, from Appendix 11.1, on the order of

$$(17) \quad \text{Minimum } C_{Q_{\text{rotor profile}}} = \frac{\sigma C_d}{8} \left\{ 1 + \frac{3}{2} \mu^2 - \frac{\mu^4}{16} \left[5 + 3 \ln \left(\frac{2}{\mu} \right) \right] + \frac{7}{64} \mu^6 \right\}$$

and therefore the minimum rotor blade loading coefficient (C_L/σ) for autorotation is

$$(18) \quad \text{Minimum } \frac{C_L}{\sigma} = \frac{C_d}{8(\alpha_s + a_{1s}) \mu} \left\{ 1 + \frac{3}{2} \mu^2 - \frac{\mu^4}{16} \left[5 + 3 \ln \left(\frac{2}{\mu} \right) \right] + \frac{7}{64} \mu^6 \right\} \quad \text{for autorotation}$$

The term $\frac{P_{\text{rotor induced}} + P_{\text{rotor profile}}}{V}$ in Eqs. (9) and (10) is frequently referred to as the rotor effective drag (D_E). In the general case, this effective drag follows from Eq. (3) and is written as

$$(19) \quad D_E = \frac{P_{\text{rotor}}}{V} - X_{\text{rotor}} = \frac{P_{\text{rotor induced}} + P_{\text{rotor profile}}}{V}$$

Note that the effective drag can be obtained through experiment by dividing measured power by flight velocity and subtracting rotor propulsive force. On the other hand, only theory (so far) can separately calculate induced and profile power. Also note that when

the rotor is autorotating (i.e., $P_{\text{rotor}} = 0$), the effective drag becomes the actual rotor drag. That is

$$(20) \quad D_E = \frac{0}{V} - X_{\text{rotor}} = -X_{\text{rotor}} = D_{\text{rotor}} = \frac{P_{\text{rotor induced}} + P_{\text{rotor profile}}}{V}$$

This effective drag can be estimated from rather simple classical theory using empirical corrections. The semi-empirical relationship is

$$(21) \quad D_E = K_i \frac{L_{\text{rotor}}^2}{2\rho A_{\text{rotor}} V^2} + \frac{\rho(bcR)V_t^3}{V} \left(\frac{C_d}{8} \right) (1 + 4.65\mu^2 + 4.15\mu^4 - \mu^6)$$

The approximation can be put in the airplane form of drag divided by dynamic pressure ($1/2 \rho V^2$), which is a rotor parasite drag area. Thus,

$$(22) \quad \frac{D_E}{q} = \frac{K_i}{\pi} \left(\frac{L_{\text{rotor}}}{2Rq} \right)^2 + \frac{(bcR)C_d}{4} \left(\frac{1 + 4.65\mu^2 + 4.15\mu^4 - \mu^6}{\mu^3} \right)$$

The rotor's effective drag can also be put in standard rotor coefficient form by dividing both sides of Eq. (21) by $\rho A_{\text{rotor}} V_t^2$

$$(23) \quad C_{D_E} = K_i \frac{C_L^2}{2\mu^2} + \left(\frac{\sigma C_d}{8} \right) \left(\frac{1 + 4.65\mu^2 + 4.15\mu^4 - \mu^6}{\mu} \right)$$

It is quite common to divide Eq. (23) through by rotor solidity (σ) and apply this result universally to any rotor of differing solidity. The result of this step is

$$(24) \quad \frac{C_{D_E}}{\sigma} = \frac{K_i \sigma}{2\mu^2} \left(\frac{C_L}{\sigma} \right)^2 + \left(\frac{C_d}{8} \right) \left(\frac{1 + 4.65\mu^2 + 4.15\mu^4 - \mu^6}{\mu} \right)$$

While this step gives the familiar blade loading coefficient (C_L/σ) and can be handy for many purposes (e.g., identifying the onset of blade stall), the step can be a misleading practice because advanced theory that includes a complete model of the rotor wake shows that induced power (or induced drag) does not scale with solidity. This point is emphasized with Fig. 2-11, which was obtained with today's advance theory. One way of keeping this point in mind is to write the rotor solidity for a rotor with rectangular blades in two forms as follows:

$$(25) \quad \sigma = \frac{bc}{\pi R} = \left(\frac{b}{\pi} \right) \left(\frac{1}{R/c} \right) = \frac{b}{\pi (\text{Aspect Ratio})}$$

Of course, when theory is to be compared to test *at equal solidity* this important point is rather mute.

Simple theory – such as Eq. (23) – suggests that the rotor effective drag coefficient varies as lift coefficient squared. Experimental data [11] confirms this dependency as Fig. 2-12 shows for the H-34 rotor with untwisted blades as tested in the National Full-Scale Aerodynamics Complex 40-by-80 foot wind tunnel at NASA Ames

Research Center [11]. The divergence of the experimental data versus the simple theory occurs when blade stall becomes a factor, in this case approximately at $C_L/\sigma = 0.07$.

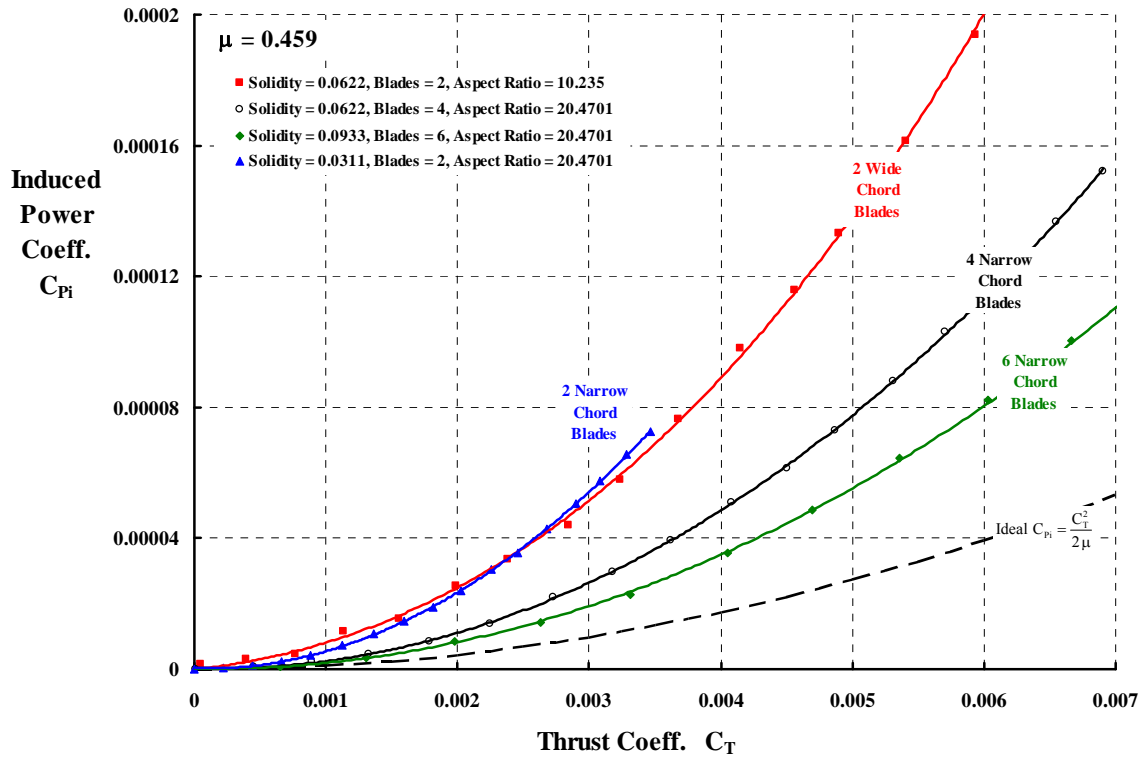


Fig. 2-11. Induced power of 4 narrow chord blades is less than 2 wide chord blades, keeping solidity constant. Rectangular, untwisted blades with N.A.C.A. 0012 airfoil. Calculated with CAMRAD II, an advanced rotor theory.

An important question can now be raised: How much does the rotor effective drag coefficient vary as the rotor propulsive force varies while rotor lift coefficient is held constant? When the rotor tip path plane is tilted aft (as shown with Fig. 2-10), the rotor can be in or near autorotation. As power is applied and the tip path plane is tilted forward, the rotor's propulsive force overcomes its own drag. A further forward tilting accompanied by an increase in power allows the rotor to provide a useable propulsive force. This behavior is illustrated with Fig. 2-13 using the full scale H-34 rotor data tabulated in NASA TN D-4632 Table IV-4 for the untwisted blade set and Table IV-1 for the -8 degree twisted blade set. Autorotation occurs somewhere along the dashed line defined by Eq. (20). Note that at this advance ratio and lift coefficient both untwisted and twisted blades autorotate with nearly equal drag. However, when required to propel, the twisted blades offer a performance advantage.

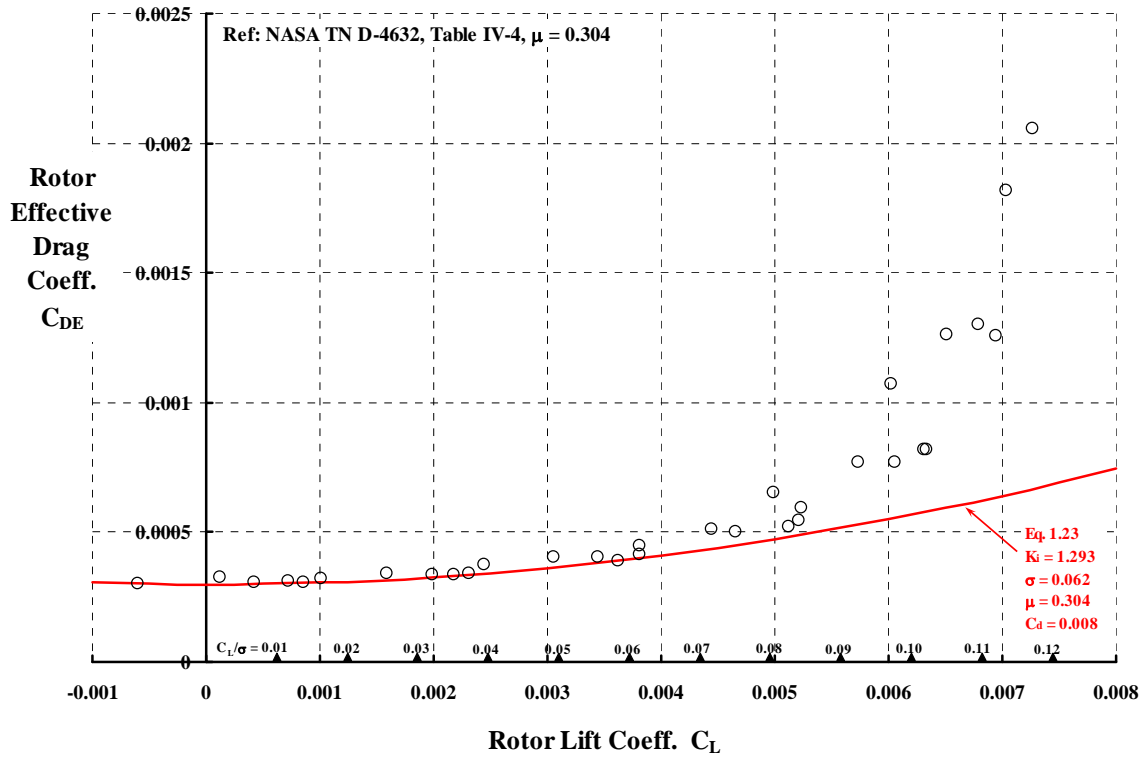


Fig. 2-12. Effective drag varies as lift squared up to the onset of blade stall.

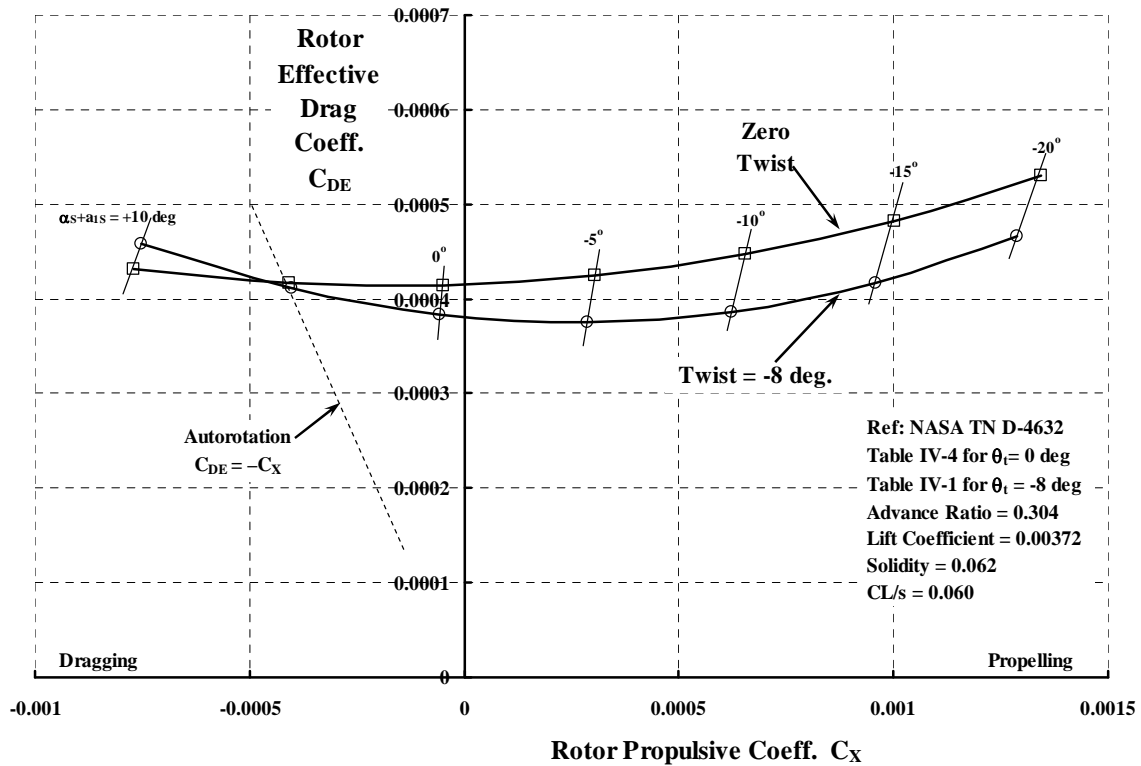


Fig. 2-13. The effect of propulsion on rotor effective drag coefficient at constant rotor lift is influenced by blade twist.

There is a considerable advantage in looking at performance in a more direct way using Eq. (3) in coefficient form. By dividing both sides by $\rho A_{\text{rotor}} V_t^3$ you have

$$(26) \quad C_P = C_X \mu + C_{P \text{ induced}} + C_{P \text{ profile}}$$

In this view, $C_X \mu$ is the ideal power to propel and the induced and profile powers are primarily required to produce lift. Therefore, it makes sense to graph total power (C_P) versus ideal power ($C_X \mu$). This graph is provided with Fig. 2-14. Ideal propulsive power is shown on this figure with the dashed line. Suppose now that the power at zero propulsive force is taken as the reference for the sum of induced and profile power. A further forward tilt of the tip path plane produces propulsive force and this increases the total power. The increase is slightly greater than ideal propulsive power for the untwisted blade set. That is, the slope of the untwisted blade total power with ideal propulsive power is nearly parallel with the dashed line in Fig. 2-14. The -8 degree twisted blade set presents an entirely different conclusion. From the reference $C_X = 0$ power, this twisted blade set requires less power than ideal with increasing propulsive power (i.e., the slope is *less* than the dashed line). However, in the range of $C_X \mu = 0.0003$ to 0.0004 the slope of power versus ideal power appears parallel to the dashed line. This indicates the advantage twisted blades have over untwisted blades for helicopters, which use the rotor to both lift and propel. Of course, the question as to whether this is the “optimum” twist for this advance ratio, lift and rotor geometry is not answered by Fig. 2-14.

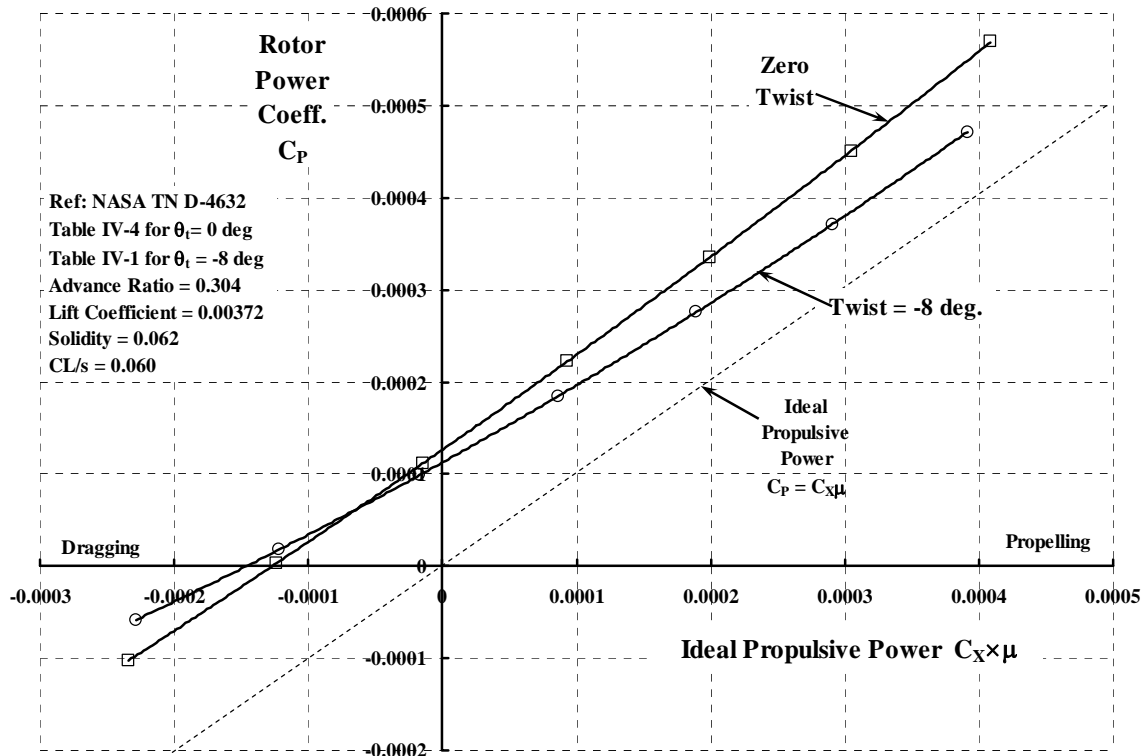


Fig. 2-14. The effect of propulsion on rotor total power.

To conclude this discussion of performance fundamentals, consider the special case of autorotation using experimental data obtained with the H-34 untwisted blade set at an advance ratio of 0.304 from NASA TN D-4632, Table IV-4 as an example. The test data was obtained by varying collective pitch holding shaft angle of attack constant and adjusting longitudinal and lateral cyclic controls so that first harmonic flapping (a_{1S} and b_{1S}) was zero (or nearly zero). The cyclic control adjustment to zero out flapping means that the rotor tip path plane angle of attack ($\alpha_S + a_{1S}$) is virtually identical to the shaft angle of attack (α_S). Data analysis is, however, generally clearer by plotting any measured parameter versus shaft angle of attack or versus rotor lift *holding collective pitch constant*.

Three key graphs are necessary to fully understand rotor performance in autorotation. The first establishes the rotor lift at which autorotation will occur and this graph is shown with Fig. 2-15. The data points at equal collective pitch are connected with solid lines. The secondary information dealing with the shaft angle of attack is noted by the dashed lines. The variation of power coefficient with lift as the tip path plane angle of attack is increased – holding collective pitch constant – defines the lift coefficient (for each collective pitch) at which autorotation is obtained. Interpolation and some extrapolation are obviously needed.

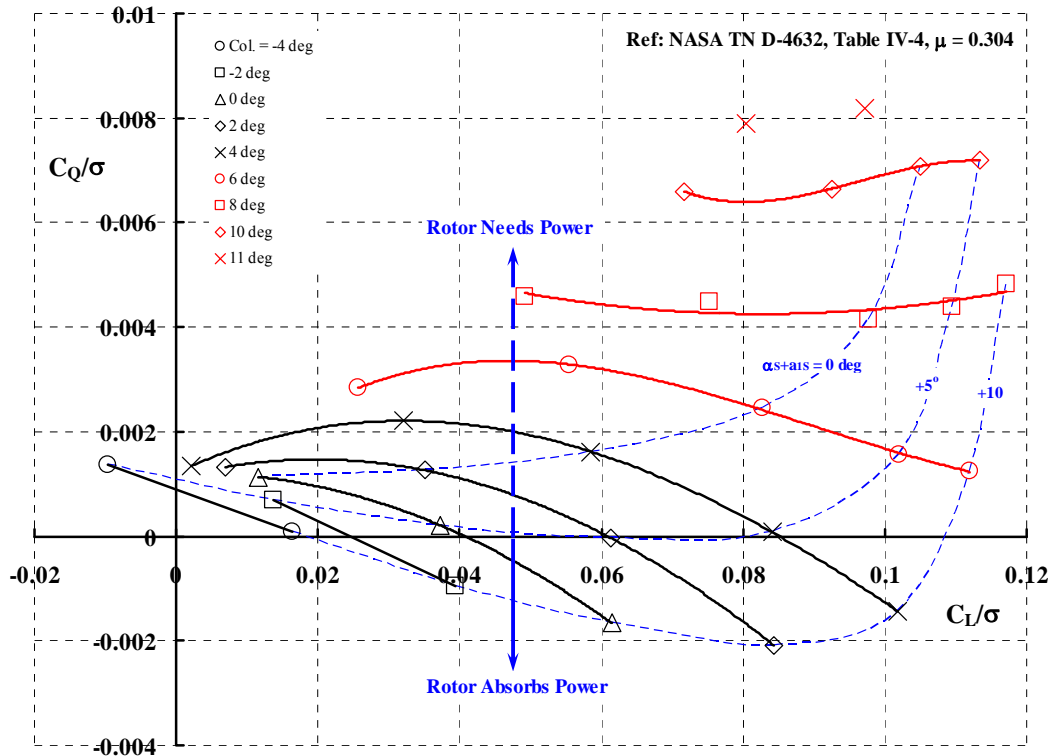


Fig. 2-15. The variation of rotor power with rotor lift holding collective pitch constant and varying shaft angle of attack. Untwisted H-34 blades.

The second key graph is shown with Fig. 2-16. On this figure, the rotor drag when power is zero can be traced out using the rotor lift points defined from Fig. 2-15. The heavy blue line on Fig. 2-16 shows the rotor drag versus lift at zero power and is, for

practical purposes, the rotor's drag polar. This rotor at this advance ratio has its maximum lift to drag ratio of 9.80 at the blade loading coefficient of 0.085.

The third key graph is shown with Fig. 2-17 and this figure establishes the lift – angle of attack behavior at constant collective pitch. The rotor has a clearly defined lift curve slope just as an airplane's wing has. Furthermore, the rotor's collective pitch acts just like a wing's flap in that the angle of attack for zero lift can be controlled by the amount of collective pitch applied. Finally, the heavy blue line traces out the combinations of angle of attack and collective pitch at which autorotation is obtained.

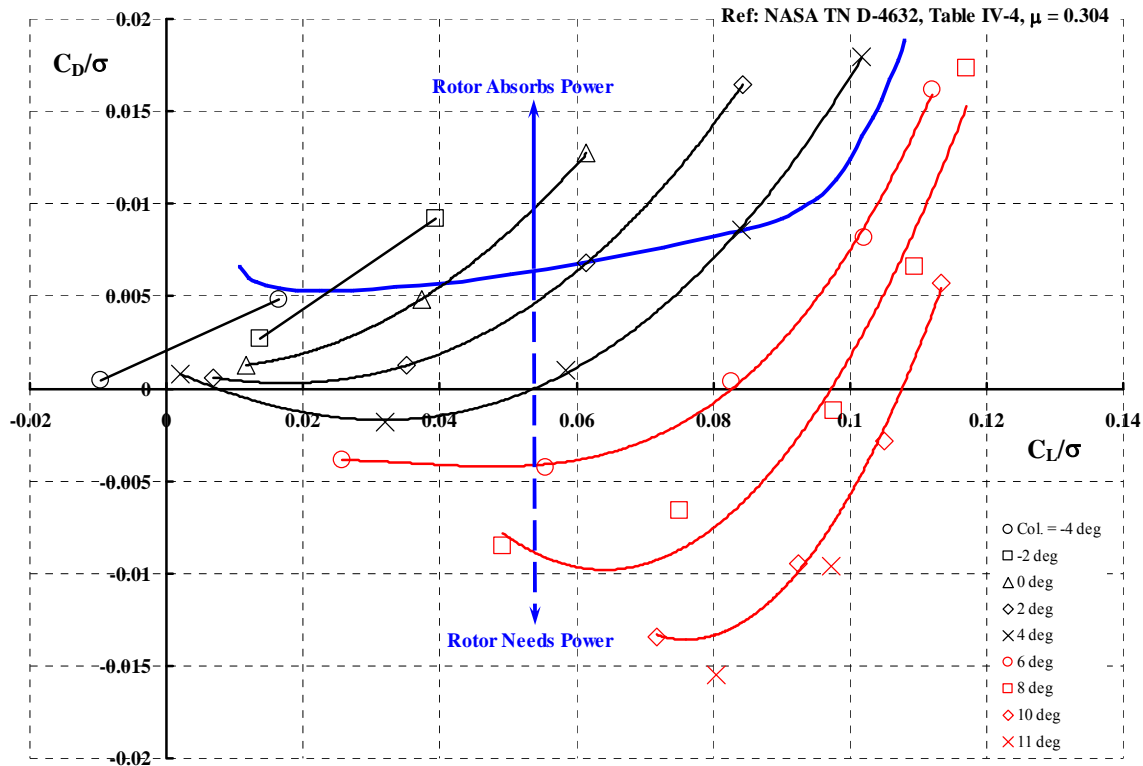


Fig. 2-16. The variation of rotor drag with rotor lift holding collective pitch constant and varying shaft angle of attack. Untwisted H-34 blades.

2.3 Rotor Theory In The 1930s

It is a well known historical fact that Juan de la Cierva invented and developed the autogyro. It is also well known that Harold Pitcairn and the Kellett brothers obtained licenses for autogyro development and manufacturing in the United States. What is not so well known is that Cierva personally applied his engineering education (obtained in Spain) to the autogyro's evolution [12, 13]. Cierva's two technology/design handbooks show that he had a commanding grasp of his invention's behavior in flight.³

³ The American Helicopter Society has copies of these two handbooks in their library.

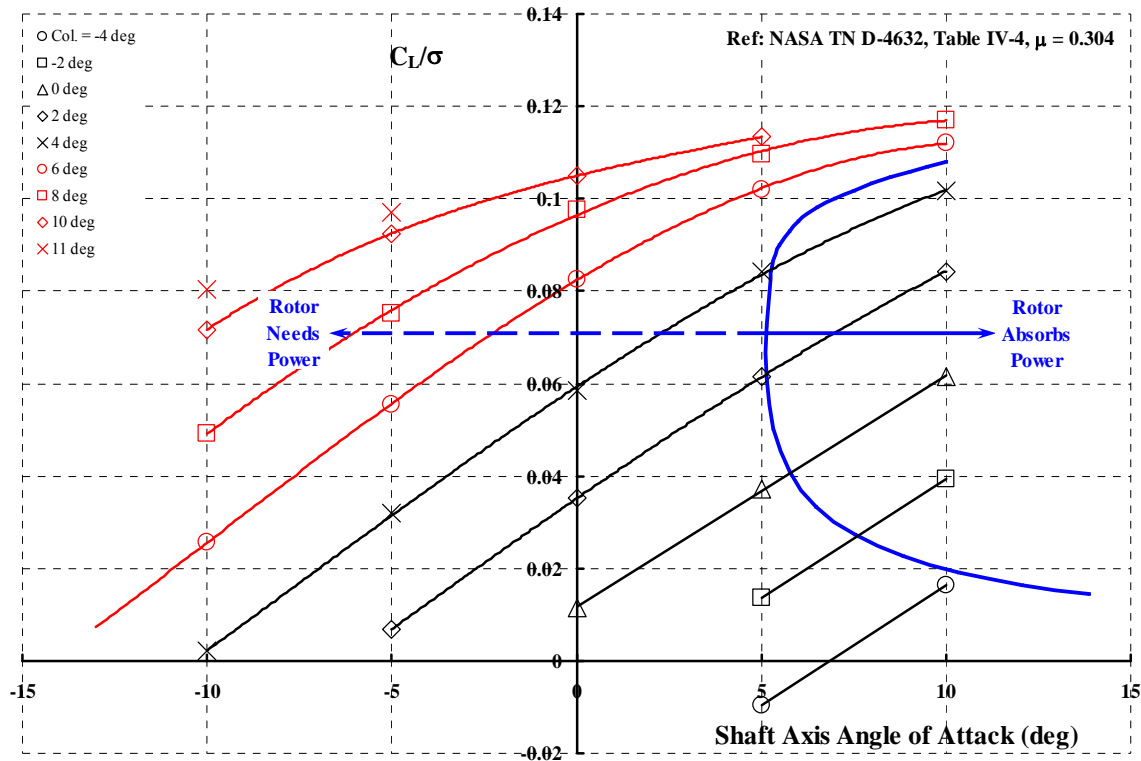


Fig. 2-17. The variation of rotor drag with rotor lift holding collective pitch constant and varying shaft angle of attack. Untwisted H-34 blades.

Cierva's, Pitcairn's and Kellett's technical progress and product development was followed closely in Britain and the United States. Britain's leading aerodynamicist, Herman Glauert, was the first to follow Cierva's foundational technology. Glauert's published work [14-16], the efforts by Lock [17-24] and Beavan [25] are frequently referred to by rotorcraft engineers. In the United States, the N.A.C.A. quickly followed Britain's lead. At the N.A.C.A., John Wheatley extended autogyro fundamental aerodynamic technology [26-36]. And Wheatley's efforts were supplemented and continued by Bailey [37-41].

Autogyro research efforts of these early pioneers reached a high point when the N.A.C.A. purchased the Pitcairn PCA-2 flight research aircraft shown in Fig. 2-1. Under Wheatley's direction, a thorough flight program was conducted during 1931-1932 and the test results, including theory versus test correlation, were published in January 1934 [26]. Wheatley quickly found that extracting the rotor behavior and performance from the complete autogyro data left something to be desired. He therefore took the PCA-2 rotor system off the aircraft and conducted a rotor alone test in the Langley 30 foot by 60 foot open throat wind tunnel in December 1933. PCA-2 rotor alone testing up to advance ratios of about 0.7 became available when Wheatley published N.A.C.A. Report No. 515 [35] October 12, 1934. This one set of test data became a bench mark for theory development.

High speed, slowed rotor technology at the end of 1939 is worth reviewing because it lays the foundation for this present 2007–2008 study. The theory, which Wheatley published in January 1934 as N.A.C.A. Report No. 487 [28], represents the very core of today's most advanced rotorcraft technology. Wheatley sums up the theoretical state of affairs in 1934 with his introduction, saying:

The aerodynamic analysis of the autogyro has been the subject of several studies, the most note-worthy being presented by Glauert and Lock in references 1 and 2 [16, 21]. The validity of the analyses made has not at the present time been established, however, so their application to the problems of design has been impossible.

Wheatley then goes on to extend Glauert's and Lock's analyses to include the variation of linear blade twist and compare his rather rigorously derived equations to flight test data obtained with the PCA-2 autogyro. Because Wheatley had no modern computer, the originally derived equations discarded several higher order terms that he felt were relatively minor. For the sake of completeness, Appendix 11.2 to this report provides the most accurate accumulation of terms involved in the rotor equations, while still retaining Wheatley's approach and assumptions.

The comparison of Appendix 11.2's refinement of Wheatley's theory to the PCA-2 rotor alone test data which follows completes this assessment of 1930s rotor aerodynamic technology. In autorotation, the rotor flies without benefit of any shaft horsepower. That is, the rotor simply glides. On the complete autogyro, a propeller powered by an engine is the forward propulsive unit and the rotor acts just like a wing flying at some positive angle of attack. The application of Wheatley's theory yields the rotor lift coefficient and drag coefficient, which are defined in *conventional fixed wing nomenclature* as

$$C_L = \frac{\text{Lift}}{\left(\frac{1}{2}\rho V^2\right)(\pi R^2)} \quad C_D = \frac{\text{Drag}}{\left(\frac{1}{2}\rho V^2\right)(\pi R^2)}$$

where V is the flight or wind tunnel speed in feet per second, density, ρ , is in slugs per cubic foot and R is the radius of the rotor.

Using Appendix 11.2 equations, one can imagine that the very first theory comparison Wheatley made to the PCA-2 rotor alone wind tunnel test data might have gone like this:

A. Input to the theoretical problem,

- (1) the shaft (or hub plane) angle of attack (α_s), positive aft in radians.
- (2) the root collective pitch (θ_o), positive airfoil nose up in radians
- (3) the rotor speed (RPM),
- (4) the wind tunnel speed (V), in feet per second
- (5) the density of air in the wind tunnel at that time (ρ) in slugs per cubic foot, nominally 0.002378 slugs/ft³,

- (6) the rotor geometry of chord (c) in feet, rotor radius (R) in feet, blade twist (θ_t) in radians and number of blades (b),
- (7) the blade flapping moment of inertia (I_f) in slug-feet²
- (8) the airfoil aerodynamic properties of lift curve slope (a) in per radian nominally 5.73 per radian and the airfoil drag polar, assumed as $C_d = C_{d_0} + \delta_1(\alpha) + \delta_2(\alpha)^2$, nominally used by Wheatley and others as $C_d = 0.012 - 0.0216(\alpha) + 0.4(\alpha)^2$. However, for the PCA-2 rotor blade airfoil, a German developed Göttingen 429 symmetrical aerofoil, $C_d = 0.012 - 0(\alpha) + 0.25(\alpha)^2$ [23]

B. Calculate the primary parameters the equations need,

- (1) the rotor tip speed, $V_t = \frac{\pi}{30}(\text{RPM})R$,
- (2) the advance ratio, $\mu = \frac{V \cos \alpha_s}{V_t}$,
- (3) the rotor solidity, $\sigma = \frac{bc}{\pi R}$
- (4) the Lock number, $\gamma = \frac{\rho a c R^4}{I_f}$ and
- (5) the tip loss factor, B , nominally $B = 0.97$.

For illustration purposes of this hypothesized discussion, PCA-2 test data given by Wheatley on Table I of N.A.C.A. Report No. 515 is quite sufficient. The pitch setting for the 89 experimental data points obtained was quoted as $\theta_0 = 1.9$ degrees. The rotor autorotated in a well behaved way at all advance ratios with the hub plane angle of attack (i.e., the shaft angle of attack) varying as Fig. 2-18 shows.

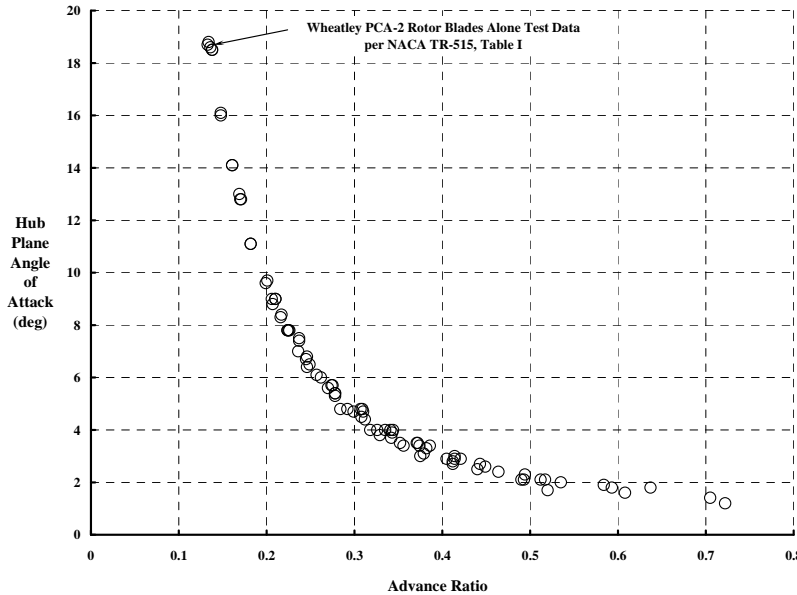


Fig. 2-18. The Pitcairn PCA-2 rotor autorotated quite reasonably during the tests Wheatley conducted in the N.A.C.A. Langley 30 foot by 60 foot wind tunnel as reported in N.A.C.A. Report No. 515.

Using the test hub plane angle of attack of Fig. 2-18, Wheatley would have arrived at the theory versus test comparison of rotor lift and drag shown with Fig. 2-19. Take care to note that the vertical axis on Fig. 2-19 is a logarithm scale and that the theory points are small, solid symbols while the large, open symbols are test data.

On the surface, the prediction of measured lift and drag shown with Fig. 2-19 might well have been quite pleasing. *But, unfortunately, the predicted torque was not zero as required by the definition of autorotation.* The magnitude of this disappointing fact about the theory is shown with Fig. 2-20.

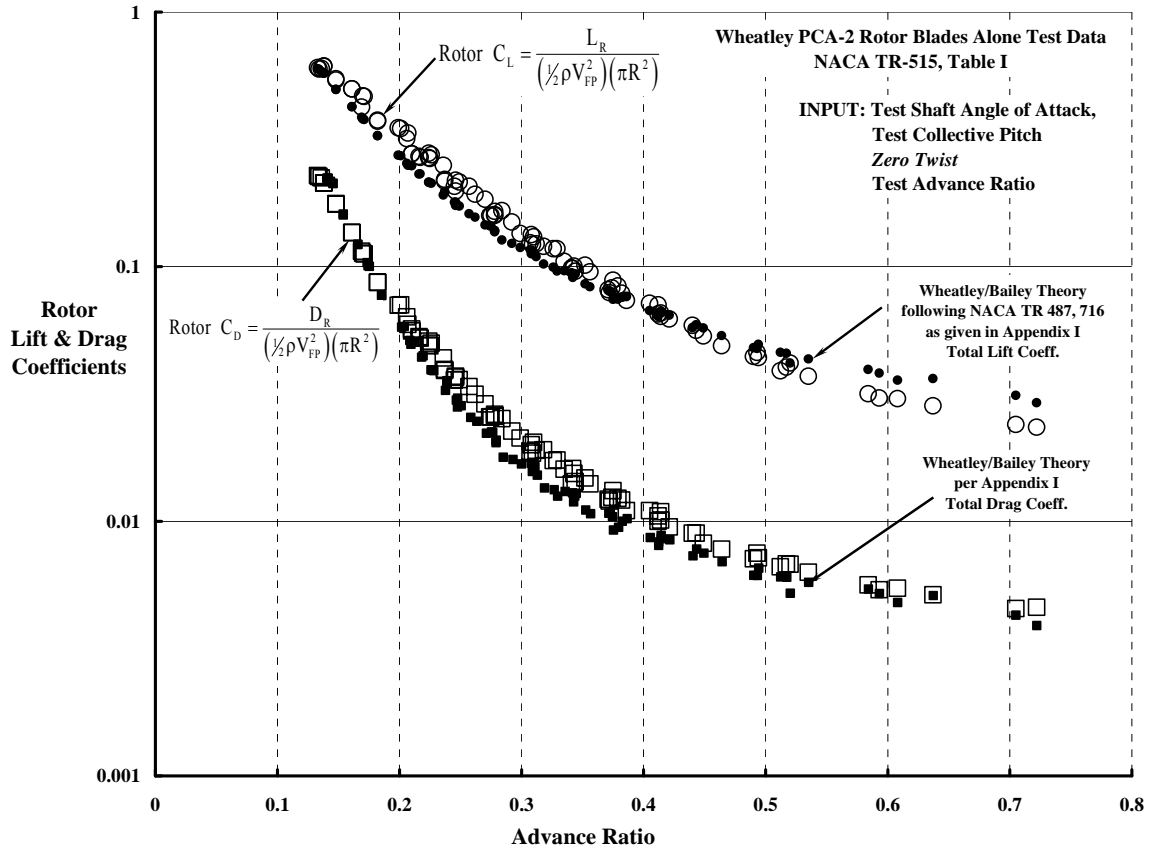


Fig. 2-19. On the surface, Wheatley's theoretical lift and drag predictions appear promising.

To obtain an accurate prediction of rotor lift and drag in autorotation when the torque is *exactly zero* is rather difficult. However, it can be done with Wheatley's and Bailey's theory by reevaluating the input. On the one hand, there is little room to question the wind tunnel speed, the air's density, the rotor RPM, hub plane angle of attack or the measured lift and drag. The accuracy of these parameters is assessed by Wheatley [35]. On the other hand, Wheatley points out that the blade pitch angle, assumed theoretically as $\theta = \theta_o + x \theta_i$, was affected by the rotor speed and thrust. Wheatley devotes a paragraph to this input variable saying:

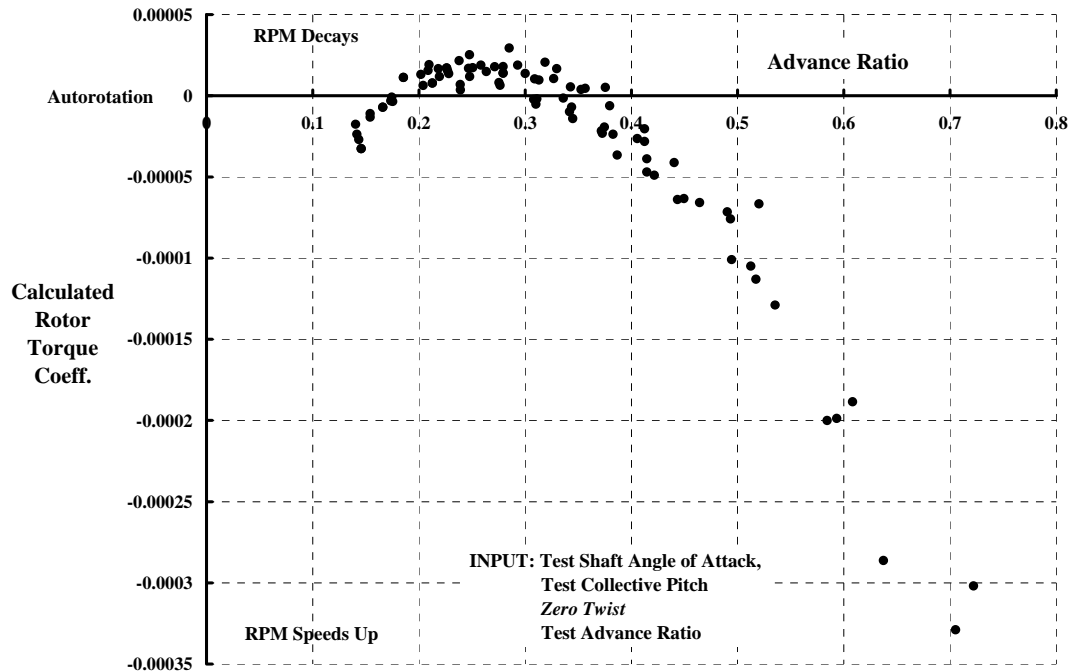


Fig. 2-20. Unfortunately, predicted torque is not zero as required by autorotation.

“It will be noted that the nominal pitch angle, represented by the symbol, θ , differs from the pitch setting noted on each figure and is not constant at a given pitch setting. The nominal pitch angle is the pitch angle of the tip of the rotor blade under operating conditions and the pitch setting is the pitch angle at the tip of the rotor blade when at rest. The difference between the two is the dynamic twist, arising because the component of centrifugal force normal to the rotor blade is applied aft of the blade center of pressure; the couple resulting from these two forces is within small limits proportional to the thrust, so the dynamic twist also varies with the thrust. Flight tests on the PCA-2 rotor [26] established the fact that the dynamic twist is about 0.89° at the tip for 1,000 pounds thrust, and the nominal pitches assigned to the different runs made in the wind-tunnel tests were determined from this relation, employing the average thrust obtained at a given rotor speed.”

Given this knowledge, the prediction of the PCA-2's autorotating rotor lift and drag can be found by maintaining the root collective pitch, θ_o , at a fixed value and varying the linear twist variable, θ_t , to zero out the torque. The logic here is that the blades are tightly fixed at the blade root which defines θ_o at some value that stays the same for a run. The “linear” twist, θ_t , on the other hand, varies in some manner with each data point. Of course, today's advanced technology, which includes “dynamic twist” calculations, could do a better job on the correlation. But, keep in mind that the current discussion is focused on the capability in the 1930s.

The lift calculated by theory can be adjusted for better agreement with the measured lift using the tip loss factor, B. This empirical factor was in common use and frequently was set at $B = 0.97$. The function of the tip loss factor was (and still is in simpler analyses) to remove a small portion of the blade's lift from the final calculated lift. The factor was initially used for static thrust calculations and seems to have been carried over to forward flight calculations.

For the following results, the Wheatley theory as given by Appendix 11.2 is compared to the PCA-2 rotor alone test data using a collective pitch of $\theta_0 = 1.9$ degrees and a tip loss factor of $B = 1.0$. The lift and drag coefficients resulting from adjusting torque to zero using the linear twist variable (see Fig. 2-23) are shown with Fig. 2-21.

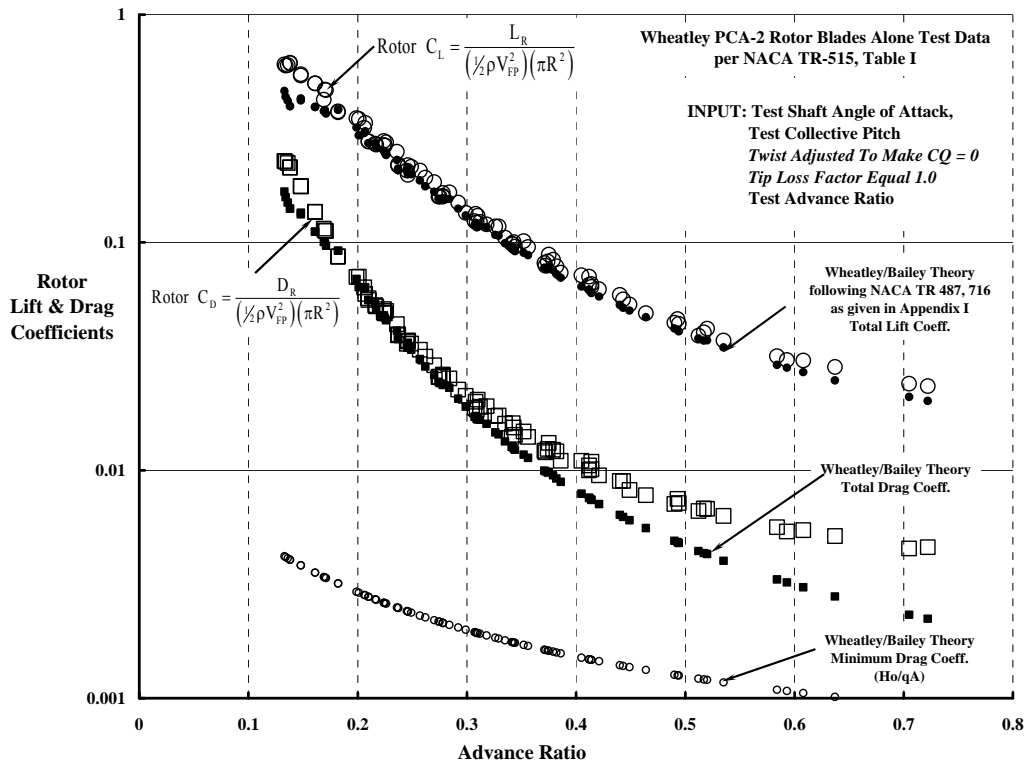


Fig. 2-21. The agreement between vintage 1930s rotor aerodynamic theory and available test data with the PCA-2 rotor blades alone using dynamic twist to insure zero torque and a tip loss factor, B, of 1.0.

Fig. 2-21 is a very direct summary of high speed, slowed aerodynamic technology (i.e., high advance ratio technology) for an autorotating rotor at the end of 1939. Very clearly, rotor lift might be estimated rather closely, but prediction of rotor drag was quite inadequate.⁴ In fact, using a logarithmic scale on the vertical axis, as Fig. 2-21 does, disguises the real error between theory and test. The error is much more apparent as Fig. 2-22 shows.

⁴ Wheatley's data in modern rotorcraft notation of coefficients based on tip speed – not airspeed – shows an entirely different and penetrating view and allows use of a linear scale as opposed to a logarithmic scale. The data in this form is shown in Fig. 5-17 through Fig. 5-20, with theory discussed later in this report.

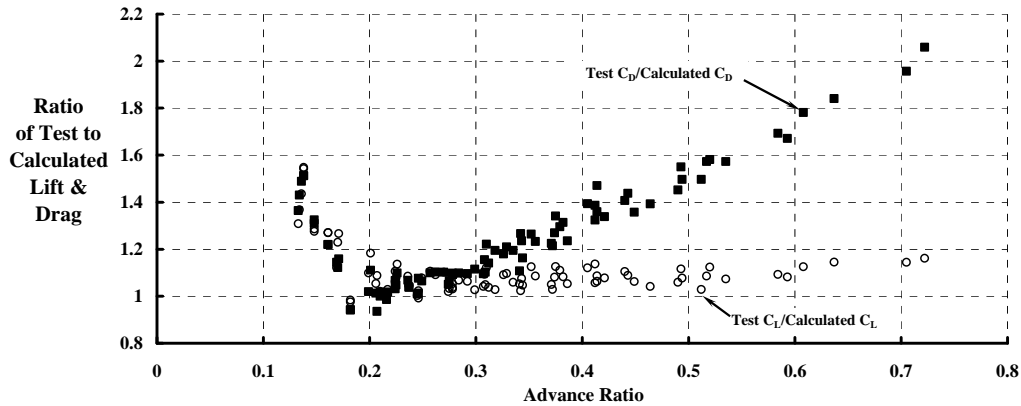


Fig. 2-22. The most advanced rotor performance theory of the late 1930s was still inadequate in predicting the PCA-2's rotor drag measured in the wind tunnel.

While not a topic under discussion in this report, the substantial error in prediction below an advance ratio of 0.2 was very important to helicopter aerodynamic engineers. This group has worked for nearly 6 decades to improve every facet of rotor technology important for advance ratios between zero and 0.4 to 0.5.

As to the dynamic twist, the Appendix 11.2 theory required to zero rotor shaft torque, Fig. 2-23, shows only 2 degrees (from + 0.5 degrees to – 1.5 degrees) is at issue. This seems very reasonable since Wheatley measured “dynamic twist” on the order of “0.89° at the tip for 1,000 pounds thrust.”

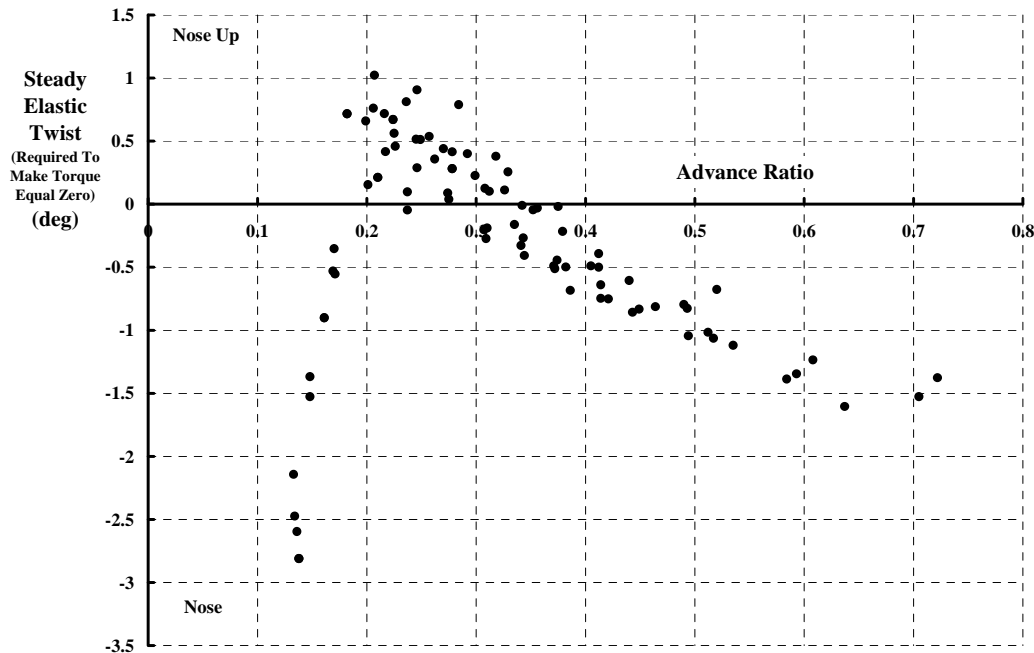


Fig. 2-23. The “dynamic twist” required to zero rotor shaft torque with Wheatley’s theory as computed by the equations in Appendix 11.2.

To conclude, it is apparent from Fig. 2-21 and Fig. 2-22 that accurate prediction, particularly of drag, was a very serious shortcoming of early autogyro aerodynamic theory. Considerable refinements to the theory over the decades since the 1930s have been incorporated. Of course, the application of digital computers has been a major factor in realizing the refinements. However, even the most advanced aerodynamic theories of today have only been measured against helicopter experimental data and only up to advance ratios approaching 0.45.

3 ROTORS STUDIED

Evaluating high speed slowed rotor technology in this study has been approached by comparing experiment to theory. Reports of three experiments with full scale isolated rotors were found that constitute a primary data bank accumulated over four decades. Two rotors were tested up to an advance ratio of 1.0 in the 1960s and the third (a PCA-2 autogyro rotor) was tested up to an advance ratio of 0.7 in the mid-1930s. No small scale, isolated rotor experiments have been included in this study.

Test data from three rotors is available in both tabulated and graphical form. The first rotor studied is a modified Sikorsky H-34 (the S-58) rotor system. The standard H-34 rotor is four bladed, the rectangular blades are twisted – 8 degrees and the hub is fully articulated. The modified H-34 rotor set has the same dimensional geometry but the blades are untwisted. The second rotor studied is a modified Bell UH-1 rotor system. The standard UH-1 is a semi-rigid two bladed system of 44 foot diameter. The modified rotor is 34 foot in diameter and the blades are twisted –1.42 degrees. The third rotor studied is a 1930s Pitcairn PCA-2 rotor system having four blades and a fully articulated hub. Each rotor, its properties and its test apparatus are discussed in the following paragraphs.

3.1 H-34 Untwisted Blade Set

Testing of this rotor is reported in NASA TN D-4632 [11] with tabulated data included on Tables IV-4 through IV-12. The more commonly quoted rotor system properties of the modified H-34 are listed on Table 1. The rotor was tested in the then NASA Ames operated⁵ 40 foot by 80 foot wind tunnel during January 1966 and the test report was published in January 1968. The 56 foot diameter rotor was mounted to the rotor test stand as shown in the wind tunnel with Fig. 3-1. The four untwisted blades were mounted to the articulated hub shown in Fig. 3-2.

Rotor shaft angle of attack was remotely controlled using an extendable tail strut. Rotor power was provided by one 1,500 horsepower, variable–frequency electric motor inside the faired body. Collective and cyclic pitch were remotely controlled and monitored from the control room. First harmonic rotor blade flapping coefficients relative to the rotor shaft were obtained from electronic flapping resolvers.

The test operating procedure was quite straight forward. Tunnel speed and rotor rotational speed were adjusted to obtain the desired advance ratio and advancing tip Mach number. At each combination of shaft angle of attack and collective pitch, the

⁵ NASA elected to close this national large scale testing facility in 2003. Fortunately, the Department of Defense recognized the wind tunnel's value. The Secretary of Defense directed the Air Force to get the facility back on line starting with a lease agreement from NASA to the Air Force signed in February 2006. And in January 2008, the Air Force had the National Full–Scale Aerodynamics Complex fully operational for rotorcraft testing.

Table 1. Properties of the Three Rotors under Study.

Parameter	H-34	UH-1	PCA-2
Diameter (ft)	56.00	34.00	45.00
Nominal chord (ft)	1.337	1.75	1.81
Twist (deg)	0.00	-1.42	See Appendix 11.5
Number of blades	4	2	4
Ref. total area for all blades (ft ²)	153.1	59.5	154.4
Swept disc area (ft ²)	2,463	908	1,588
Nominal solidity (nd)	0.062	0.0656	0.0971
Lock number (nd)	8.86	3.62	19.2
Flap moment of inertia (slug ft ²)	1,265	1,584	334
Weight moment (lb-ft)	2,265	na	2,265
Flap hinge offset (inch)	12	0	3.375
Lag hinge offset (inch)	12	No lag hinge	7.750
Nominal airfoil	N.A.C.A. 0012	N.A.C.A. 0012	Göttingen 429



Fig. 3-1. The H-34, fifty-six foot diameter rotor system installed in the NASA Ames 40 by 80 foot wind tunnel during tests in January 1966.

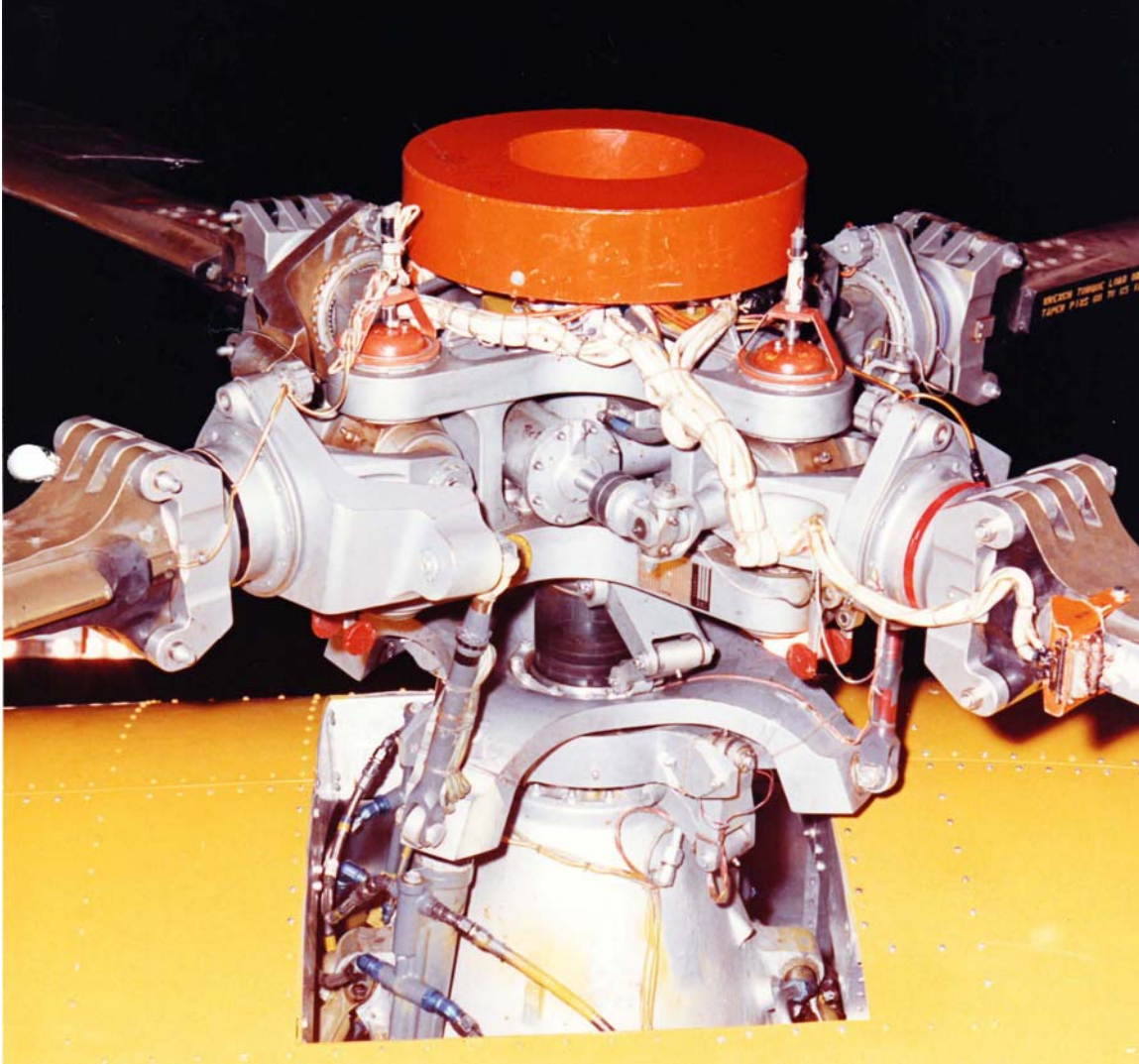


Fig. 3-2. The H-34 rotor system hub topped by a slip ring assembly.

cyclic pitch was adjusted to minimize first harmonic blade flapping, and data were then recorded. Collective pitch or shaft angle was then changed and the above procedure repeated until a limit was reached in motor power, control position, or structural loading.

Six-component forces and moments were measured by the wind tunnel balance system. Tare corrections were applied to the balance data to account for forces and moments produced by the exposed model support struts, the faired body, and the rotating hub. The rotating hub tares included all hardware inboard of the 0.0814 radius station (2.28 feet), which is at the blade attachment bolts seen with Fig. 3-2. The tares applied were based on wind-tunnel dynamic pressure and shaft angle of attack. Rotor downwash effects on the tares were neglected because of a lack of confidence in any known technique for assessing their magnitude. The tares used are those given in NASA TN D-4632 (figures 2, 3, and 4) with faired curves. The blades off tare forces and moments

were subtracted from the blades on data to obtain “blades alone” tabulated and plotted data.

Special attention was taken with regard to power measurements. Rotor torque and rotational speed were used to compute the total power coefficient C_p/σ . Torque was measured with a shaft torsion gage as well as with the wind tunnel balance. The shaft power data are considered more valid since these data are independent of rotor wake interference effects on the fuselage. Comparison of torque obtained from the rotor shaft with that obtained from the wind tunnel balance indicated that these interference effects were small. The maximum difference between these two torques corresponds to 3 percent of maximum power.

In modeling the modified H-34 rotor system, this study found that both blade aerodynamic geometry and structural properties were equally important. For example, the blade airfoil proper does not extend into the blade attachment bolts as Fig. 3-3, Fig. 3-4 and Fig. 3-5 show. Furthermore, the tip was near parabolic in planform as Fig. 3-6 shows. Structural property data used in this study of the H-34 blade is in Appendix 11.3.

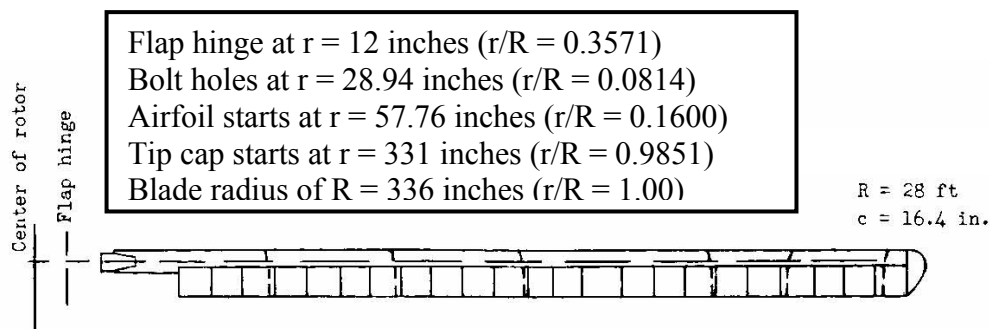


Fig. 3-3. The modified H-34 blade was untwisted and had a near parabolic tip. The root end was a D-spar.



Fig. 3-4. Edgewise view of H-34 blade root end.

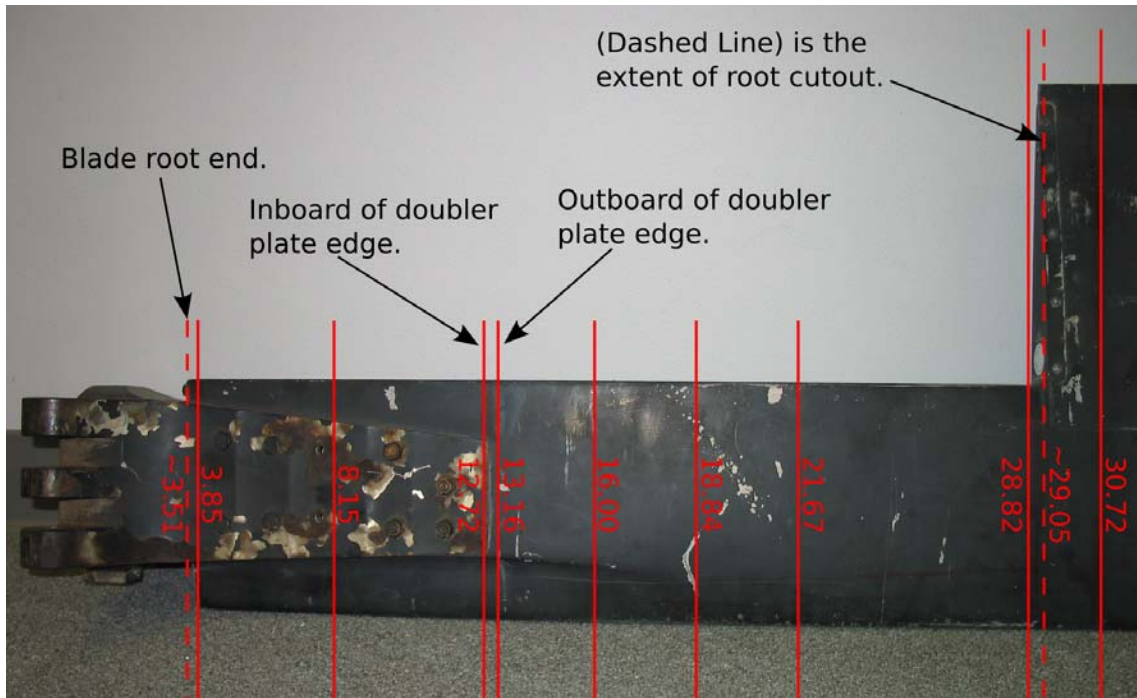


Fig. 3-5. Planform view of H-34 blade root end. Bolt holes are the reference zero for the dimensions in this photo.

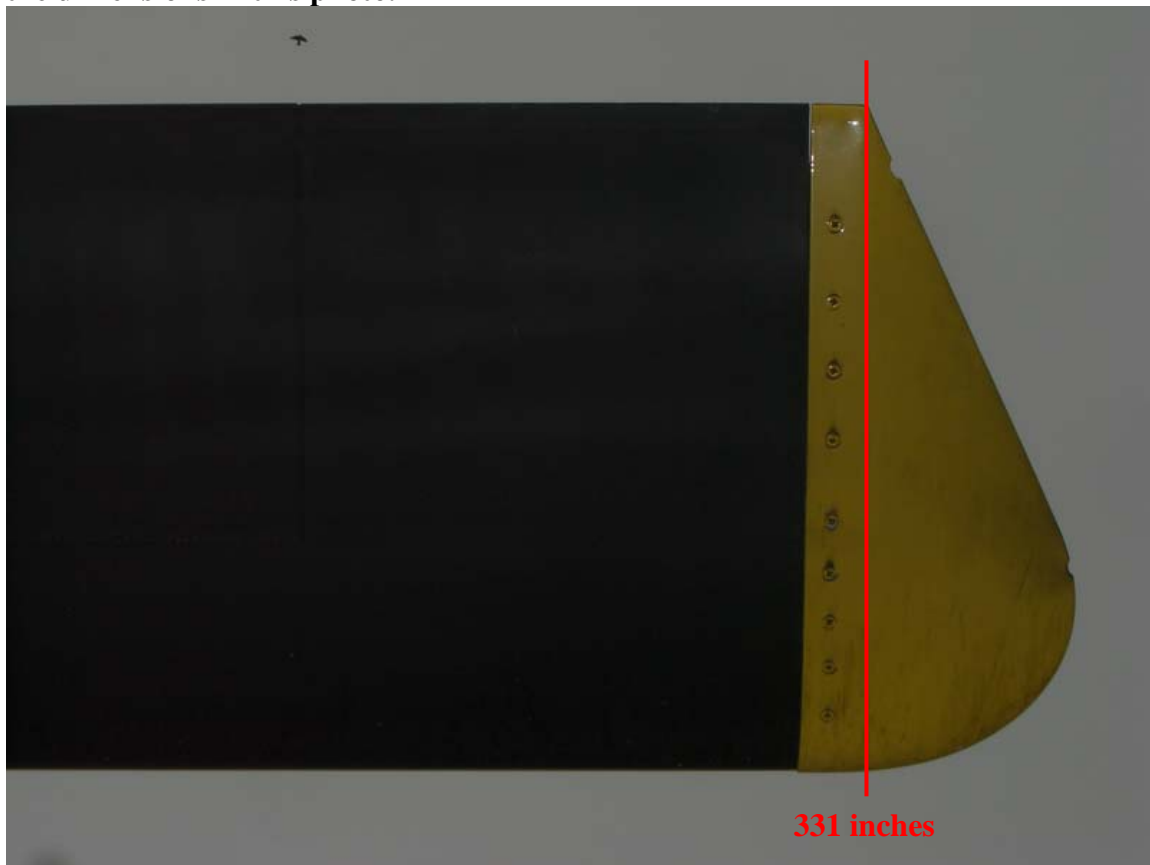


Fig. 3-6. Planform view of H-34 blade tip.

3.2 UH-1 Thirty Four Foot Blade Set

Testing of this rotor is reported in USAAVLABS TR 69-2 [42] with tabulated data included on Tables IV-11 through IV-16 of that report. The more commonly quoted rotor system properties of the cut down UH-1 rotor system are listed on Table 1. The rotor was tested in the then NASA Ames operated 40 foot by 80 foot wind tunnel during January 1968 and the test report was published in January 1969. The two bladed, 34 foot diameter rotor was mounted to the rotor test stand as shown in the wind tunnel with Fig. 3-7.

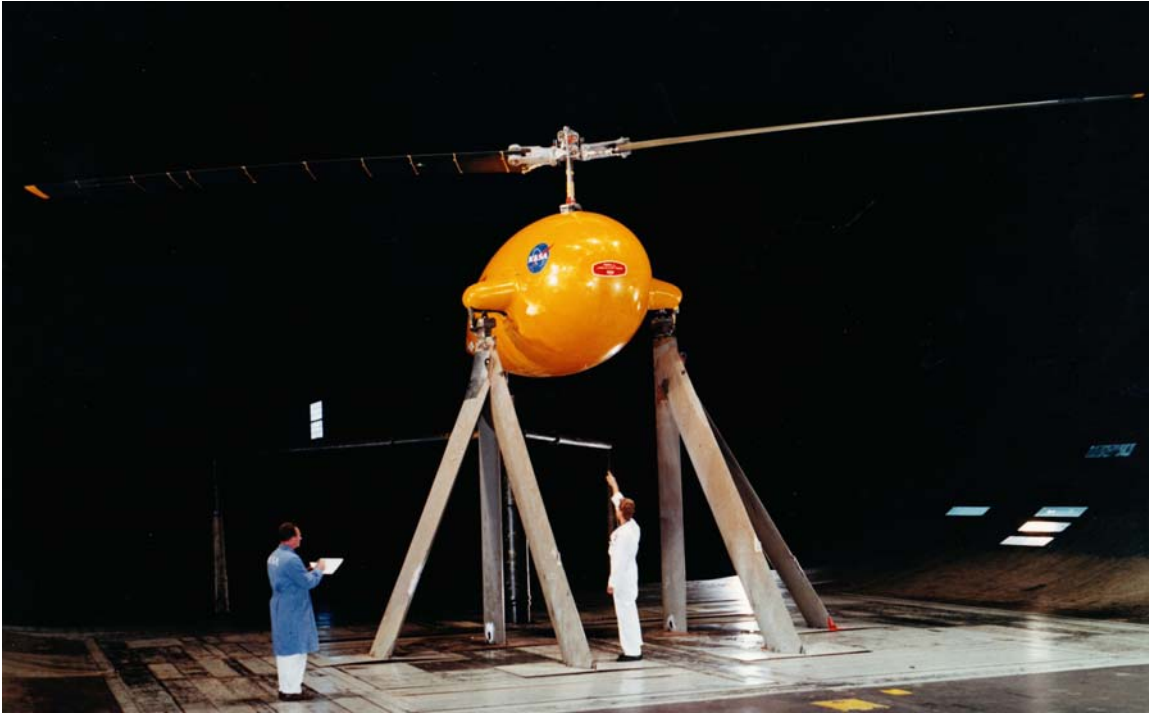


Fig. 3-7. The *unmodified* UH-1, forty-eight foot diameter rotor system installed in the NASA Ames 40 by 80 foot wind tunnel during tests in January 1968.

The test operating procedure was similar to that used for the H-34 testing. At each test point condition the cyclic pitch was adjusted to minimize first harmonic blade flapping, and data were then recorded. Collective pitch or shaft angle was then changed and the above procedure repeated until a limit was reached in motor power, control position, or structural loading. Six-component forces and moments were measured by the wind tunnel balance system. Tare corrections were applied to the balance data to account for forces and moments produced by the exposed model support struts, the faired body, and the rotating hub. The rotating hub tares included all hardware inboard of the 0.1569 radius station (2.66 feet), which is at the blade attachment bolts seen with Fig. 3-7. The tares used are those given in NASA TN D-4632 (figure 4) with faired curves. The blades off tare forces and moments were subtracted from the blades on data to obtain “blades alone” tabulated and plotted data. Unlike the H-34 test, the UH-1 shaft was not instrumented for torque. Torque was measured with the wind tunnel balance forces transferred to a yawing moment about the shaft.

In modeling the 34 foot diameter UH-1 rotor system, this study found that both blade aerodynamic geometry and structural properties were equally important. For example, the blade airfoil proper (basically an N.A.C.A. 0012) only exists from the rectangular tip into about the 80 inch radius station (0.392 R). Further inboard the airfoil is distorted by a growing stack of metal doublers used to strengthen the blade root end. A cross-section through the blade bolt holes radius station (about 32 inches radius station or 0.1565 R), Fig. 3-9, shows just how much the N.A.C.A. 0012 airfoil has been distorted. Structural property data used in this study of the UH-1 blade is in Appendix 11.4. This appendix also includes the complete drawing for the root end, which can be enlarged to show more detail.⁶

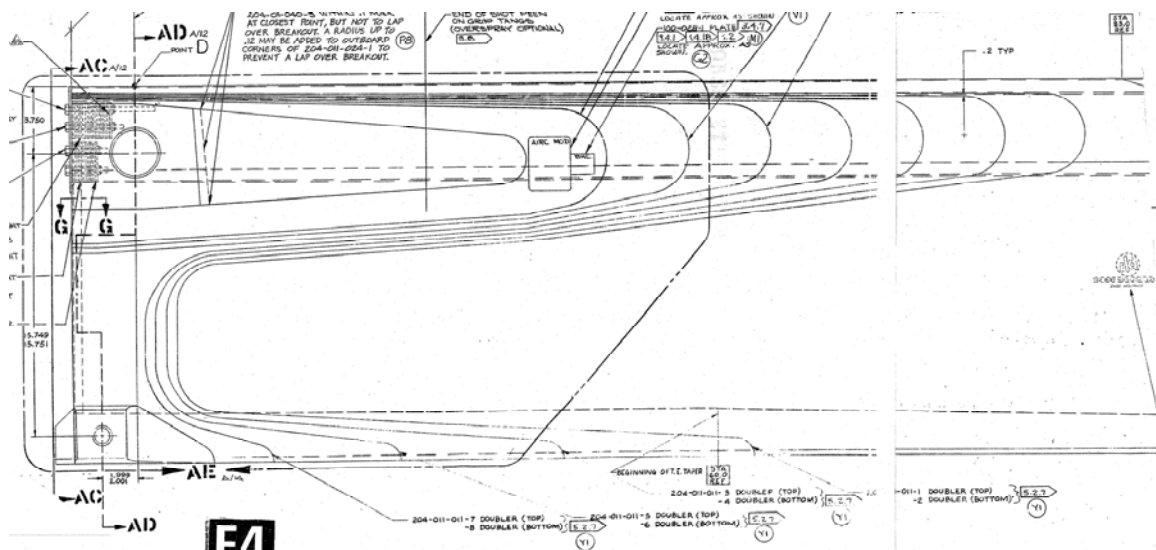


Fig. 3-8. The UH-1 root end doubler build up,

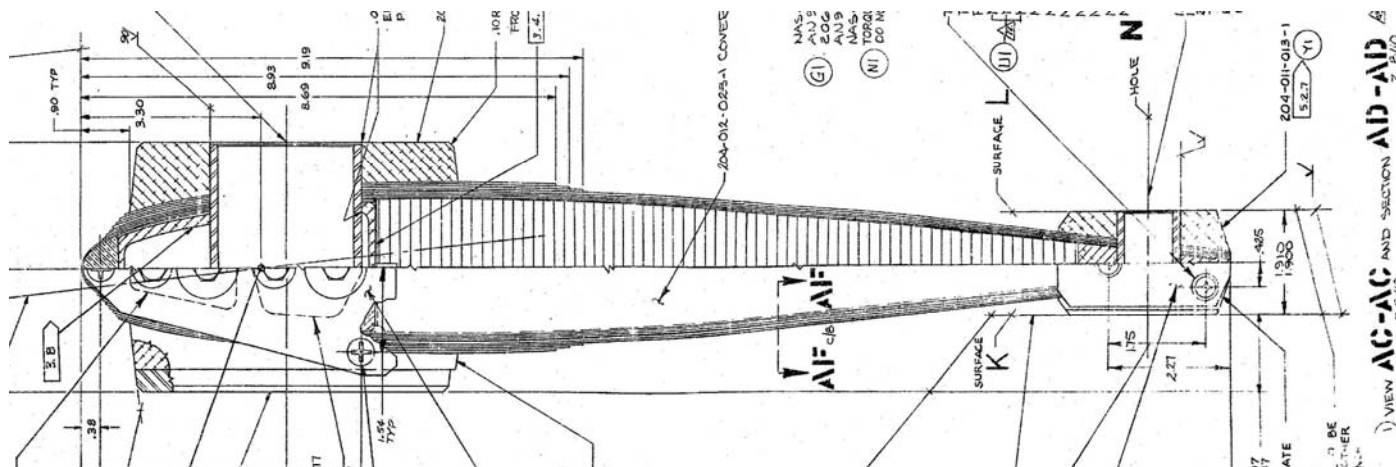


Fig. 3-9. The UH-1 "airfoil" at the blade bolt attachment radius.

⁶ The UH-1 drawing was provided by Tom Wood of Bell Helicopter Textron and I thank him very much.

3.3 PCA-2 Autogyro Blade Set

Testing of this rotor is reported in N.A.C.A. Report No. 515 [35] with tabulated data included on tables I through IV of that report. The more commonly quoted rotor system properties of the PCA-2 are listed on Table 1. The rotor was tested in the then N.A.C.A. Langley 30 foot by 60 foot wind tunnel during 1934 and the test report was published in October 1934. The 45 foot diameter rotor was mounted to the rotor test stand as shown in the wind tunnel with Fig. 3-10. The four, twisted blades were mounted to an articulated hub. The flapping hinge was located at 3.375 inches from the shaft centerline. The lead-lag hinge was 7.75 inches from the shaft centerline. The blade structure, shown with Fig. 3-11 before covering, was built around a steel tube.

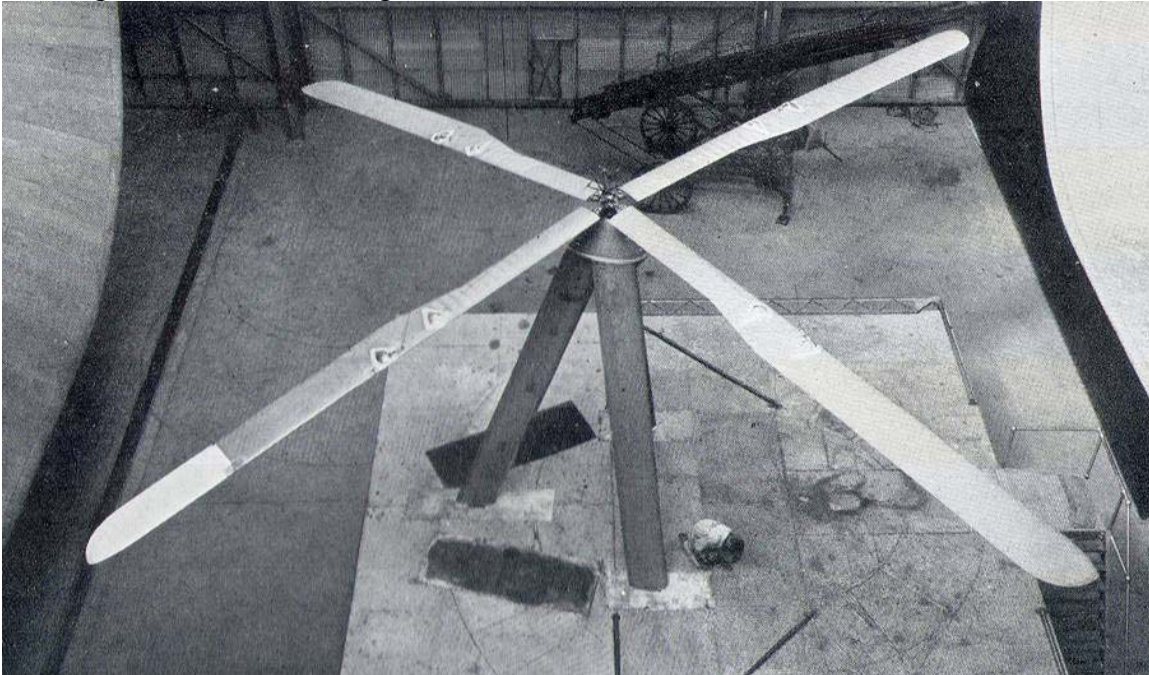


Fig. 3-10. The PCA-2, forty-five foot diameter rotor system installed in the N.A.C.A. Langley 30 by 60 foot wind tunnel during tests in 1934.

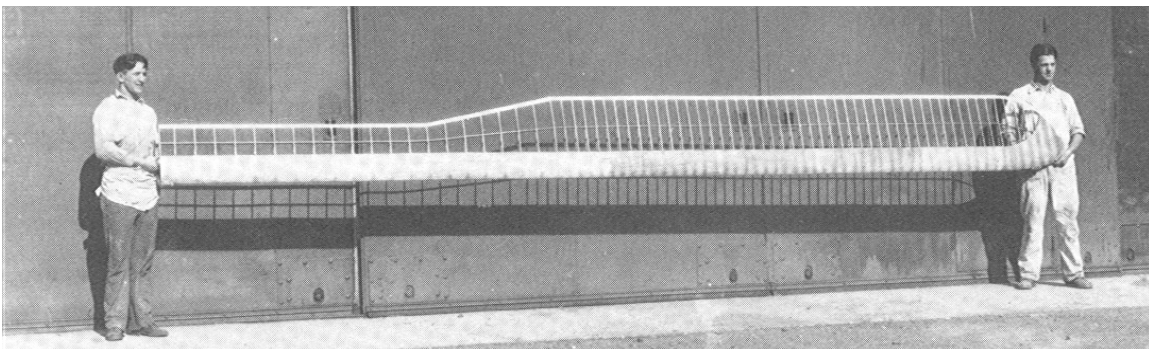


Fig. 3-11. The PCA-2 blade before doped canvas covering. Photo From “Autogyro, The Story of the Windmill Plane” by George Townson

The rotor was supported on the balance by a steel tube tripod having an apex formed by a steel casting containing a mechanism for changing the angle of attack. This mechanism consisted of a double worm and gear reduction operated by a hand crank in the balance house. The angle of attack (the acute angle between the direction of flight and a plane perpendicular to the rotor axis) was indicated by a revolution counter geared to the crank shaft. The entire supporting system beneath the rotor was shielded from the air stream to eliminate tare drag. The rotor speed was obtained from an indicator at the angle-of-attack control station, connected to a tachometer magneto driven by the rotor. An additional indicator was placed at the wind-tunnel control station for the use of the tunnel operator while the rotor was being started.

The rotor was started by the air stream, no mechanical starting gear having been incorporated in the test setup. The rotor was set at about 10° angle of attack, the wind tunnel was started slowly by jogging on and off the lowest-speed switch point, and the air speed was gradually increased as the rotor picked up speed. Force tests were made by the following procedure: The wind tunnel control was set for the lowest air speed, the angle of attack was adjusted so the rotor operated steadily at a desired rotor speed, and the necessary readings were taken. The angle of attack was then adjusted to give other desired rotor speeds, readings were again taken, and the process was repeated at other air speeds. For each condition of operation the readings of all the scales were mechanically recorded and visual readings were taken of rotor speed, rotor angle of attack, and air stream dynamic pressure. In order to compute true air speed, the air temperature, barometric pressure, and wet- and dry-bulb temperatures were obtained by visual observations at internals during the test.

The highest angle of attack at which it was possible to test the rotor in the wind tunnel was limited in some cases by the fact that the tunnel could not be operated below 23 miles per hour and in other cases by the jet size. At the highest angle of attack (26° uncorrected), the blade tips were 3.6 feet and 5.9 feet from the top and bottom boundaries of the jet, respectively. The lowest angle of attack at which the rotor could be tested was limited by the highest air speed available, 119 miles per hour, with the rotor in the jet.

When the pitch setting of the rotor blades was changed it was adjusted within 0.1° with a level protractor. In order to check the track of the blades, the rotor was run and a paint brush was lowered onto the rotor from above until the high blades were marked. Indicated adjustments were then made and the process repeated until the rotor operated smoothly as indicated by the steadiness of the balance scales. When the rotor operation was considered satisfactory, the blade tips tracked to within about $1\frac{1}{2}$ inches.

Wheatley, the author of N.A.C.A. Report 515, provided a small drawing of the blade in planform. His drawing is reproduced here as Fig. 3-12. The description, while adequate to his needs for theoretical calculations in the 1930s, falls far short of the "input" required by advanced theories currently in use. Fortunately, a door to the past opened up and this report would be incomplete if the story were not included. Thanks to some help from Gordon Leishman of the University of Maryland, on January 6, 2008 I got in touch with Stephen Pitcairn, son of Harold Pitcairn, and asked (by E-mail) for

some help (like blade drawings, spar dimensions, etc.). Mr. Pitcairn was in the hospital with pneumonia at the time. BUT, he passed my request to his long time mechanic, Mr. Mike Posey who kept a PCA-2 in flight ready condition at the Pitcairn hanger in Robbinsville, PA for many years. Mr. Posey copied drawings and I received a package in short order. The drawings plus some elbow grease and following Cierva's design manuals led to the material in Appendix 11.5. Mr. Stephen Pitcairn passed away Saturday, March 29, 2008. He was 83. My thank you letter reached him in time.

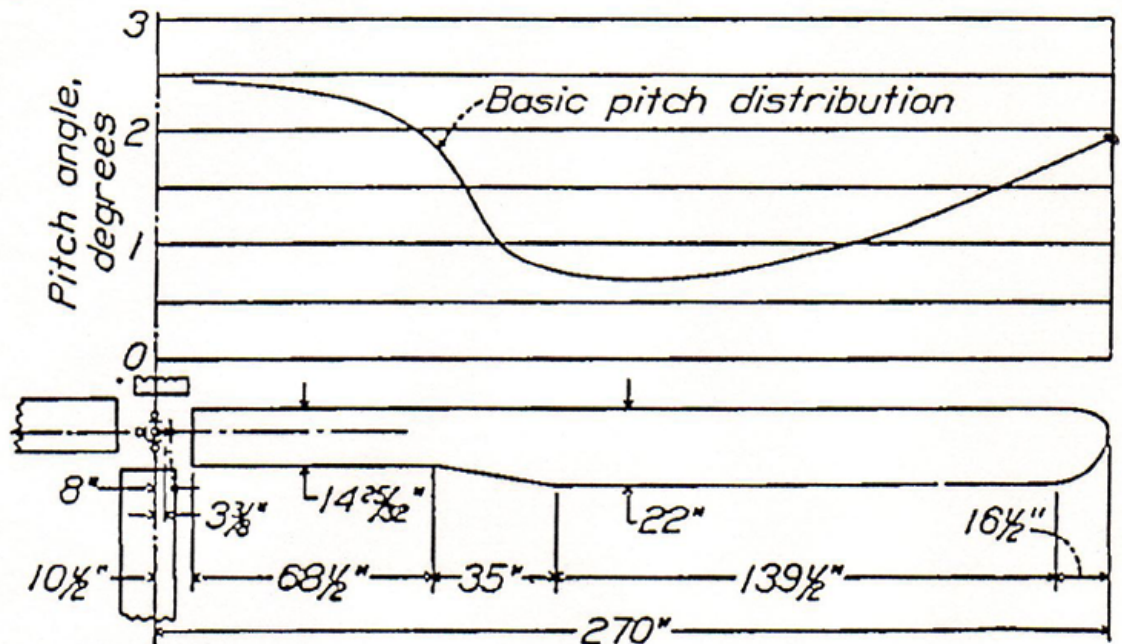


Fig. 3-12. The PCA-2 blade as described in N.A.C.A. Report 515.

The PCA-2 blade airfoils are not ones familiar to today's rotorcraft engineer. As Fig. 3-13 shows, the 22 inch chord airfoil (really 22 3/4 inch per drawing) was symmetrical while the inboard, 14 25/32 inch airfoil was cambered. The twist that Wheatley gave (Fig. 3-12) reflects an approximation to the twist of the airfoil chord line given by drawing. Complete structural and geometry property data used in this study of the PCA-2 rotor system is in Appendix 11.5.

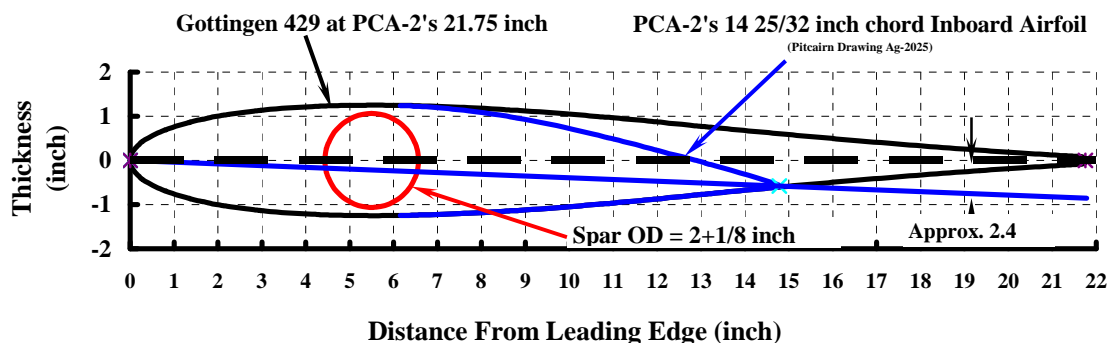


Fig. 3-13. The PCA-2 blade had both cambered and symmetrical airfoils.

4 THEORIES EVALUATED

It is quite safe to say that invention of the autogyro, the helicopter and other V/STOL aircraft came about virtually independent of theory. In fact, the development of these aircraft has largely been accomplished more by experimentation than by theory. This is not to say that considerable refinements of the each aircraft configuration have not been made given theory. And, of course, theory has been the key to solving several destructive phenomena that each class of aircraft has encountered. For example, theory played the primary role in explaining and solving the ground resonance instability that autogyros encountered. A second example where theory played the primary role would be whirl flutter encountered during development of the tilt rotor. Still, theory has developed more slowly than the products the rotorcraft industry has created – at least up until the digital computer came to the aid of theoreticians.

Given the computer, a continuous stream of software programs has been written that progressively removed restrictive theoretical assumptions. In this year of 2008, these software programs have come to be called comprehensive codes. These codes not only capture the aeroelastic behavior of a rotor blade as Cierva sought in the late 1920s, these codes now capture – with varying levels of fidelity – the complete aircraft and its behavior on the ground and in flight. Some of the more developed comprehensive codes can now model (i.e., have input definitions for) a complete aircraft nearly at the level of a detailed drawing.

4.1 Background

Before discussing the five theories that are under evaluation, a brief review of analysis development over the past eight decades is useful. This gives some appreciation of the enormous effort a small band of theoreticians has made to fully understand rotating wings and the aircraft they are attached to. The progress in the first 4⁺ decades is summarized with Table 2, which has been taken from Harris [43] and slightly updated. The breakthrough in Table 2's list occurred in 1955 when Alfred Gessow and Almer Crim, both of the N.A.C.A., used a Bell Telephone Laboratories X-66744 digital computer to solve the rotor blade motion and performance problem. Their report, N.A.C.A. Technical Note 3366, surely qualifies as a quantum jump. In their introduction, they wrote:

The flapping motion of autogyro and helicopter rotor blades has shown itself, both in theory and actual practice, to be very stable for conventional tip-speed ratios (that is, below about 0.5). Some doubt exists, however, as to the stability of blade motion at tip-speed ratios equal to or greater than 1.0, a question that is of interest in connection with the “unloaded rotor” type of helicopter operation. At these extreme tip-speed ratios, the aerodynamic and blade – inflexibility assumptions employed in existing analyses of the problem (in refs. 1 to 5, for example) become questionable. The aerodynamic factors introducing the most uncertainties in these analyses are the assumptions of unstalled blade sections and incompressible flow, the neglect of the reversed velocity region, and the use of small-angle assumptions in connection with the section inflow and blade flapping angles.

Gessow's and Crim's foundation was quickly adopted by the theoreticians in the rotorcraft industry. Such companies as Boeing, Sikorsky, Bell and others supported computer purchases (mostly from IBM) and the Runge-Kutta solution of the rigid blade flapping equation, including simple non-linear blade element aerodynamics, took off in a big way. The era of “comprehensive codes” had begun.

Table 2. Forward Flight, Rotary Wing Theory Assumptions Removed with Time.

No.	Assumption	Removed In	Typical Reference
23	Blade pitch constant with azimuth	1926	Glauert – R&M 1111
22	Only first harmonic blade flapping	1927	Lock – R&M 1127
21	Ignore reverse flow	1934	Wheatley – N.A.C.A. TR 487
20	Blade untwisted	1934	Wheatley – N.A.C.A. TR 487
19	Average drag coefficient	1941	Bailey – N.A.C.A. TR 716
18	Blade untapered in planform	1945	Lichten – Journal AS July 1946
17	Zero pitch-flap coupling	1945	Lichten – Journal AS July 1946
16	Zero flapping hinge offset	1951	Meyer – N.A.C.A. TN 2953
15	All angles are small	1952	Castles & New – N.A.C.A. TN 2656
14	$C_l = (dC_l/d\alpha)\alpha$	1955 Computer	Gessow & Crim – N.A.C.A. TN 3366
13	Ignore blade root cutout	1955	Gessow & Crim – N.A.C.A. TN 3366
12	Incompressible airfoil characteristics	1960	Tanner – NASA CR-114
11	Same airfoil at all blade radii	1961	Kisielowski – AVLABS 66-83
10	Uniform downwash	1962	Miller – Journal AHS Vol. 7 No. 2
9	No potential flow unsteady aerodynamics	1964	Miller – AIAA Vol. 2 No. 7
8	Blade has no elastic deformation	1964	Gabel – NOw 62-0177f
7	Blade lead-lag motion negligible	1967	Jenkins – NASA TN D-4195
6	No dynamic stall unsteady aerodynamics	1969	Gross – AHS 24 th Forum
5	No spanwise flow effects	1970	Harris – Journal AHS Vol. 15 No. 3
4	Boundary layer details	1972	McCroskey – Journal AHS Vol. 17 No. 1
3	Lifting line, not lifting surface	1977	Kocurek – Journal AHS Vol. 22 No. 1
2	Blade element theory (i.e., CFD successfully coupled to CSD)	1986	Tung, Caradonna, and Johnson Journal of the AHS Vol. 31 No.3
1	All the others	TBD	TBD

By 1962 IBM had sold their Model 650, followed by their Models 704 and 7070, to rotorcraft companies. And the several rotorcraft companies had individually expanded rotor system theories which pushed the best IBM could provide. At Lockheed, the code named REXOR [44-48] took on life to support design and development of the AH-56 Cheyenne, Fig. 2-7, and, at Bell Helicopter, Blankenship and Harvey [49] began development of what was to become the comprehensive code called C81. As Corrigan, Bennet and Hsieh relate in their excellent history of C81's development [50], C81 became the U.S. Army's rotorcraft simulation program of choice to evaluate the mid-1970s proposals for the Utility Tactical Transport Assault System (the UTTAS, which became the Blackhawk).

Depending on just one analysis (or one helicopter type) is not the rotorcraft industry's business style. Comprehensive codes different, equal and even superior to C81 began to slowly arrive on the scene as the 1970s ended. Individuals, universities and companies each contributed to improved fidelity of the codes throughout the last four

decades. Fundamental to virtually every code is that the rotor blade can, as a minimum, be represented with a lifting line and a spanwise string of blade elements. An angle of attack (α) and Mach number (M) is computed at each blade element. This blade element environment (α , M) is fed to a table of two dimensional airfoil lift, drag and pitching moment coefficients from which are calculated the blade element forces and moment – commonly called the airloads. Given the airloads along the blade, the problem becomes a relatively simple, though not trivial, case of $F = ma$. Unfortunately for the rotor blade calculation, each blade element's angle of attack depends on the aeroelastic deformation of not just the blade, but the whole aircraft. Of course, the local relative velocity is not constant for any blade element. And the local velocity must include the influence of the wake trailed and shed from each blade because this wake induces velocity at each blade element. Furthermore, the airload computation must also consider the time varying environment of each blade element, which means that both steady and unsteady airfoil aerodynamics are of great importance to the rotorcraft industry.

Such aeroelastic considerations in the rotor system problem as just discussed have meant that getting each improved comprehensive code into everyday, production use has been a major effort in itself. Today's codes require several learning packed months for the uninitiated to become just a beginner. In fact, even the developers of the codes are surprised at times with solutions that do not converge, require excessive run times, and provide results that are just unbelievable. Quite fortunately for the rotorcraft industry, the small band of dedicated theoreticians over successive generations has never given up.

4.2 Selected Theories

Five theories have been selected to assess their accuracy in comparison to the rotors discussed in Chapter 3 and data obtained with these rotors as presented in Chapter 5. One theory represents the state-of-the-art in the 1930s. Three other theories capture comprehensive codes currently in use by the rotorcraft industry. The fifth theory represents the next major step rotor theory will take.

4.3 Wheatley & Bailey (1934)

This report would be incomplete without bench marking this 1930s state of the art theory as was done in Chapter 2. The theory, numerically refined by the author and provided in Appendix 11.2, is compared to the 1960s H-34 experimental data in Chapter 6. This comparison serves as a backdrop for the comprehensive code named CAMRAD.

4.4 CAMRAD II (2008)

The initials for this theory stand for Comprehensive Analytical Model of Rotorcraft Aerodynamics and Dynamics. The comprehensive code CAMRAD was first published in 1980 [51, 52]. This code was created single handedly by Wayne Johnson and further developed to CAMRAD/JA by Johnson Aeronautics located in Palo Alto, California. CAMRAD II was entirely new software, built on the lessons learned from CAMRAD and CAMRAD/JA, but based on multibody dynamics, nonlinear finite

elements, and advanced rotor wake and lifting-line aerodynamics. The first release of CAMRAD II was in 1993, with yearly upgrades since. A somewhat more detailed engineering discussion of CAMRAD II is contained in a paper which Johnson presented in 1998 [53]. In this paper, Johnson's introduction states in part that

CAMRAD II is an aeromechanical analysis of helicopters and rotorcraft that incorporates a combination of advanced technology, including multibody dynamics, nonlinear finite elements, structural dynamics, and rotorcraft aerodynamics. For the design, testing, and evaluation of rotors and rotorcraft - at all stages, including research, conceptual design, detailed design, and development - CAMRAD II calculates performance, loads, vibration, response, and stability - with a consistent, balanced, yet high level of technology in a single computer program -applicable to a wide range of problems, and a wide class of rotorcraft. Such capability is essential for helicopter problems, which are inherently complex and multidisciplinary.

It is only the portions of CAMRAD II that deal with a single rotor tested in a wind tunnel which concern this evaluation. Paraphrasing Johnson, these portions deal with:

1. The basic approach of the analysis is to make no approximations (beyond time and space discretization) at the highest levels, handling exact (nonlinear and time-varying) equations. The analysis solves differential, integral, static, and implicit equations for the motion of the system, and evaluates required output quantities from the response. The trim task finds the equilibrium solution (constant or periodic) for a steady state operating condition.
2. The true geometry of a rotor system, including multiple load paths such as a swashplate and control system, lag dampers; arbitrary elastic axis and arbitrary hinge order; drooped and swept tips; and dissimilar blades. CAMRAD II includes advanced rotor aerodynamics; rigorous kinematics and dynamics (with consistent structural loads and dynamic response, and general interfaces between aerodynamic and structural dynamic components).
3. The input for one rotor in a wind tunnel; with N-bladed rotors having articulated, or teetering root configurations, including a swashplate model. The aerodynamic model includes a sophisticated wake analysis to calculate the rotor non-uniform induced velocities, using rigid, prescribed or free wake geometry. In addition, the aerodynamic model accounts for drag and stall of the rotor blades with a table of airfoil aerodynamic properties.

More specifically the CAMRAD II code, as used for evaluation purposes here, assumed:

1. Full blade elastic properties, hub geometry and control system stiffness properties to the extent known
2. Non-uniform downwash calculated with a rigid wake (self-induced distortion of wake not required at high advance ratio; so wake elements are convected only by wind tunnel velocity and mean rotor induced velocity)
3. No dynamic stall
4. Spanwise flow effects in blade element aerodynamics (yaw and swept flow corrections, and radial drag)
5. Adjustments to the N.A.C.A. 0012, C81 airfoil table to account for excessive drag of the blade root end
6. Adjustments to the N.A.C.A. 0012, C81 airfoil table to account for non-zero blade element pitching moment caused by a trim tab.
7. Lifting line blade representation

There are, of course, many other detailed inputs peculiar to CAMRAD II that Johnson used in the many cases he ran to support this evaluation.

4.5 RCAS (2008)

The initials for this theory stand for Rotorcraft Comprehensive Analysis System. This comprehensive code began as a U.S. Army created – as opposed to C81 and CAMRAD – analysis and was initially called 2GCHAS, which stood for Second Generation Comprehensive Helicopter Analysis System. The combined and very dogged leadership of Robert Ormiston and Michael Rutkowski⁷ led to the initial 2GCHAS program's release to the public in December 1990. Extensions to the initial code followed in rapid succession so that a renamed code, RCAS, was formally released in June 2003. A quite detailed overview of RCAS became available in January 2004 [54] and included these paragraphs

The development of a comprehensive analysis was undertaken by the Government for several reasons. Initially it provided a needed focus and brought to bear substantial resources to address a large interdisciplinary problem beyond the capability of a single organization. The key objectives were to develop a comprehensive rotorcraft analysis system to support rotorcraft R&D, design and development of new and upgraded rotorcraft, and test and evaluation activities. A Government code provides a uniform and independent basis for analytical prediction technology available to the entire rotorcraft technical community and it provides a focus for Government aeromechanics research and a technology transfer medium for Government research products.

The Rotorcraft Comprehensive Analysis System is an advanced computational analysis system for rotorcraft. It is a comprehensive, multi-disciplinary system capable of modeling a complete range of complex rotorcraft configurations operating in hover, forward flight, and maneuvering flight conditions. RCAS is designed to perform a wide variety of rotorcraft engineering analyses including vehicle performance, aerodynamics and rotor loads, vehicle vibration, flight control analyses, aeroelastic stability, flight dynamics, and flight simulation. The system comprises an input data processor for setting up analyses, structural and aerodynamic models, utilities for model assembly and numerical solutions, and an output processor to provide technical data for full range of rotorcraft technical disciplines.

Clearly RCAS' full capability has not been required for this evaluation. The specific rotor alone calculations were made by Ormiston and he assumed:

1. Full blade elastic properties, hub geometry and control system stiffness properties to the extent known
2. Non-uniform downwash calculated with Peters – He dynamic inflow model set to 8 by 8 mode (Comparisons with prescribed vortex wake showed very little difference for selected H-34 cases, so dynamic inflow was used to minimize CPU time. Similar UH-1 comparisons not completed.)
3. Dynamic stall effects blade element aerodynamics
4. Spanwise flow effects blade element aerodynamics
5. Adjustments to the N.A.C.A. 0012, C81 airfoil table to account for excessive drag of the blade root end
6. Adjustments to the N.A.C.A. 0012, C81 airfoil table to account for non-zero blade element pitching moment caused by a trim tab.
7. Lifting line blade representation

There are, of course, many other detailed inputs peculiar to RCAS that Ormiston used in the many cases he ran to support this evaluation.

⁷ Both Ormiston and Rutkowski work at the Aeroflightdynamics Directorate (AMRDEC), a part of the U.S. Army Research, development, & Engineering Command, Ames Research Center, Moffett Field, California.

4.6 CHARM (2008)

The initials for this theory stand for Comprehensive Hierarchical Aeromechanics Rotorcraft Model. This comprehensive code began life as an attack on the lifting line assumption while including a non-uniform inflow calculation, which allowed a completely free-vortex wake. The initial emphasis was on improving the computation of rotor hover performance. The code began with the name Evaluation of Hover Performance using Influence Coefficients (EHPIC) in 1985 [55]. As more and more comprehensive code features were added, EHPIC grew to the second generation called CHARM today. The principle developers of EHPIC and CHARM have been Todd Quackenbush and Dan Wachspress who work at Continuum Dynamics, Inc (CDI) located in Ewing New Jersey. The code is commercially available and the most up to date guide to CHARM, written by Wachspress, is CDI Report 05-11 (Rev. 1), May 2008, entitled “CHARM (Comprehensive Hierarchical Aeromechanics Rotorcraft Model) Version 3.4 User’s Manual.”

In a 2003 paper devoted to the wake calculation analysis portion of CHARM [56], Wachspress, Quackenbush and Boschitsch wrote that

The free wake model described in this paper is part of a comprehensive model of rotorcraft aeromechanics, CHARM, that permits fully coupled development of the rotor wake geometry, the wake-induced loading, blade dynamic response, and vehicle controls, in addition to full airframe flow effects (Refs. 28 and 29). Because the wake and blade dynamics solutions are so closely coupled, the effectiveness of the free wake model depends strongly on the accurate evaluation of the blade loads, motion and deformation. CHARM uses a vortex lattice lifting surface model to determine blade airloads and a modal analysis to determine blade dynamics with either a harmonic analysis solution for periodic solutions or a predictor-corrector time-marching solution for aperiodic solutions. A linear finite element structural analysis is available for determining blade mode shapes from structural properties and standard hub attachments are supported.

It is the lifting surface and free wake capabilities of CHARM that are particularly of interest in this evaluation. The specific rotor alone calculations were made under Wachspress’ guidance and with the assumptions:

1. Full blade elastic properties, hub geometry and control system stiffness properties to the extent known
2. Non-uniform downwash calculated with free wake
3. Dynamic stall effects blade element aerodynamics
4. Spanwise flow effects blade element aerodynamics
5. Blade element lift force and pitching moment calculated with lifting surface theory.
6. Blade element drag force obtained from the N.A.C.A. 0012, C81 airfoil table.

There are, of course, many other detailed inputs peculiar to CHARM that Wachspress used in the many cases he ran to support this evaluation.

4.7 OVERFLOW-2 Coupled with CAMRAD II

Unlike CAMRAD, CHARM and RCAS, OVERFLOW-2 *is not* an acronym. OVERFLOW-2 *is* one of several computer programs that solve fluid dynamic problems using a computer. The development of the several programs has evolved into a special field of aerodynamics called computational fluid dynamics which does have an acronym, namely CFD. Before discussing OVERFLOW-2, some background about CFD is useful.

John Anderson, in his marvelous book *A History of Aerodynamics* [57], suggests on page 13 that CFD had its beginnings in 1962. Anderson provides an introductory discussion of CFD on pages 441 to 445, beginning with the statements:

By the 1970s, a revolution was taking place in aerodynamics, a revolution of such fundamental impact that it would forever change the nature of aerodynamic predictions: the development of computational fluid dynamics (CFD).

It has been a consistent theme in the history of aerodynamics during the past two centuries that although the basic equations of motion – the Euler equations for an inviscid flow (Appendix A) and the Navier-Stokes equations for a viscous, flow (Appendix B) – were known and well established by the middle of the nineteenth century, they could not be solved. They are systems of nonlinear partial differential equations for which there are no known general analytical solutions. Therefore, aerodynamicists over the past 150 years have simplified those equations by making certain approximate assumptions about the flow fields of interest, thus allowing some simplified analytical solutions, albeit at the cost of ignoring some of the physics. Indeed, that has been the world in which aerodynamics theory has functioned. However, because of the development of high-speed digital computers during the past half-century, it is now possible to obtain numerical solutions for the full nonlinear equations shown in Appendixes A and B. We can now obtain "exact" solutions for those equations for virtually any aerodynamic configuration ("exact" meaning that the equations themselves are not simplified, but are solved in their full form). However, the numerical answers are not "exact" in the purest meaning of the term; they are tainted by numerical round-off and truncation errors, and sometimes the numerical algorithms suffer from numerical stability problems that cause the attempted solutions to "blow up" on the computer. In spite of those problems, CFD has matured to the extent that quite accurate predictive solutions for complex flow problems have been obtained, which would be impossible with any other approach.

A more technical and also very well written discussion of CFD used in the rotorcraft industry is available [58]. This survey by Roger Strawn, Frank Caradonna, and Earl Duque, covers the past 30 years and includes many references illustrating progress in solving a number of helicopter and tilt rotor aerodynamic problems.

NASA developed the OVERFLOW analysis which computes fluid flow around bodies (like airfoils, complete aircraft and their components) that are in a steady state condition⁸. The OVERFLOW-2 code extended the analysis to bodies that are in a non-

⁸ If there is one person at NASA who has been a driving force in developing CFD it is Pieter G. Buning. A trip to Pieter's web site (<http://aaac.larc.nasa.gov/~buning/publicat.html>) gives a list of 62 papers and reports beginning in January 1977. Buning was the author or a coauthor of all the work. The first mention of OVERFLOW is reference 35, which is entitled OVERFLOW User's Manual, Version 1.6ab, 26 January 1993 published by NASA Ames Research Center, Moffett Field, California.

steady state condition. This provided a CFD tool that could compute the fluid flow around a rotating wing, more commonly called a rotor blade.

To this author, an applied aerodynamicist, computational fluid dynamics began when Ludwig Prandtl offered the concept of a boundary layer in 1904. The next step came when Heinrich Blasius, a student of Prandtl's, offered equations that calculated the skin friction drag of a flat plate and also calculated the separation points on the back side of a circular cylinder. Blasius' application of the Navier-Stokes equations for a viscous fluid was published in German in 1906 and the N.A.C.A. published an English translation [59] in February 1950. Blasius reduced the skin friction drag problem to a third order, nonlinear, ordinary differential equation which he solved with a Taylor series.

In modern computational fluid dynamics, the Navier-Stokes equations are solved with elegant applications of a Taylor series. The four dimensions of the CFD problem are x , y , z and time. Issues of how to make a Δx or Δy or Δz or Δt adequately approximate a dx or dy or dz or dt have been overcome with enormous effort by applied mathematicians. The objective has been tantamount to trying to keep track of every air particle in a volume that surrounds the body under study. The body under study – perhaps just a simple airfoil – is geometrically introduced as a finely grided surface which the air particles are not allowed to penetrate. The air particles immediately touching the body's surface become the start of the boundary layer just as Prandtl describe in 1904. The overall CFD solution is quite sensitive to the fidelity of the body's grid geometry; so sensitive in fact that the time to set up a problem frequently takes days or weeks before a computer's go button is pushed. The actual computer solution time is measured in hours given today's hardware and operating software.

Members of the CFD community have an insatiable appetite for computer memory and computational speed, which they use to increase their solution's fidelity. The underlying shortcoming of today's CFD is an inability to calculate when and how flow in the boundary layer transitions from laminar to turbulent behavior. This is a century old problem. A number of methods are incorporated in today's CFD code to approximate the boundary layer transition behavior, but none are completely satisfactory and no transition solution has – as yet – been developed from first principals. Another hurdle yet to be overcome is drag prediction of bodies having considerable separated flow; such as a circular cylinder or an airfoil near, at and above stalling angle of attack.

Because structural deformation is so important to rotary wing aerodynamics, CFD is only one-half of the problem. While this deformation is relatively unimportant to rotor blades in hover (a reasonably simple problem), deformation is of paramount importance in studying the rotating wing in forward flight. The structural dynamics of rotorcraft in general and rotor blades in particular is quite well understood. Computer based models such as NASTRAN, CAMRAD II and RCAS are available that can calculate structural response even for a complete aircraft. But these powerful tools are rather helpless without accurate airloads to force a dynamic response. The obvious way taken to solve this shortcoming for a rotorcraft was to couple a CFD code to a high fidelity computational structural dynamics (CSD) code. This step – successfully coupling CFD and CSD – was

first achieved by Chee Tung, Frank Caradonna and Wayne Johnson.⁹ They reported their success at the 40th Annual Forum of the American Helicopter Society held in May 1984 and later published their work in the Society's July 1986 Journal [60].

Now jump ahead some 10 years. From 1987 to mid-1994 the U.S. Army, NASA and Sikorsky collaborated to obtain structural deformation and rotor blade airload data from a Sikorsky UH-60A troop carrying helicopter, better known as the Blackhawk. This flight test program was successfully completed in April 1994. The rotorcraft industry owes Bill Bousman, U.S. Army, and Bob Kufeld, NASA Ames, a debt of gratitude for the program's completion, since these two leaders were faced with NASA upper management wanting to turn off all flight test support at Ames Research Center quite prematurely. Fortunately, more rational thinking prevailed. The UH-60A was heavily instrumented and provided the most comprehensive set of data the rotorcraft industry might possibly imagine. Over 460 data channels were recorded on each flight. Of the 460 data channels, the instrumented pressure blade itself contained 242 absolute pressure transducers. Thirty-one flights were made yielding 960 test points and about 30 gigabytes of data. Bousman organized the massive quantity of flight test data and made it available by computer access. Then industry, government and academia theoreticians, in an extraordinary cooperative effort, began to compare theory and test.

The leading theoreticians formed a loosely organized group that met (and still meets as of this date) informally twice a year for an Airloads Workshop. The organizing force behind the Airloads Workshop was Yung Yu and Bob Ormiston of the U.S. Army, and the first workshop was held February 28, 2002.¹⁰ Following Yu's retirement in early 2005, Mike Rutkowski, Chief Scientist of the NRTC, became the leader, facilitator, secretary and mentor for the group. The theoretical thrust has, from the start, been to see how well several CFD/CSD coupled methods compare to four, carefully selected, UH-60A flight test points. The lessons learned by the Airload Workshop participants has debugged and refined each approach and the progress made would – without question – make the rotorcraft industry pioneers very proud.

That significant progress had made by the Airloads Workshop participants became clearly apparent to the rotorcraft industry worldwide at the 60th Annual Forum of the American Helicopter Society in June 2004. Two papers [61, 62] were presented that showed coupling computational fluid dynamics with computational structural dynamics was going to supplement (in the near term and ultimately replace) current comprehensive analysis codes. In the foreseeable future, reliance on a table of two dimensional airfoil characteristics to compute rotary wing airloads will no longer be necessary. The blade element analysis created by Gessow & Crim in 1955 and set down in N.A.C.A. TN 3366 will have been improved.

⁹ Tung and Caradonna are members of the U.S. Army Aeroflightdynamics Directorate and Johnson is a member of NASA. They are located at the NASA Ames Research Center on Moffett Field in California.

¹⁰ The Airload Workshop activity is carried out by formal agreement between industry, academia and government members of the Rotorcraft Industry Technology Association (RITA) and helped by the National Rotorcraft Technology Center (NRTC). RITA's view is that all Airload Workshop material is non-proprietary which allows the exceptionally free interchange.

The purpose of the above background has been to show that a most advanced theory, capable of predicting performance and loads in the helicopter regime, is available. However, the theory has yet to be evaluated for rotors that may reach much higher advance ratios. To begin an exploratory study, OVERFLOW-2 and OVERFLOW-2 coupled with CAMRAD II have been selected as representative analyses. To use these analyses, a graphical model of a body under study must be created. The H-34 blade has been selected for study in this high advance ratio performance analysis.

An H-34 blade has been geometrically translated into the grid form required by OVERFLOW-2's Navier-Stokes solver. Fig. 4-1 and Fig. 4-2 introduce the current grid patterns used to model the H-34 blades for the OVERFLOW-2 theoretical computations. Additional details of the complete model are included in paragraph 7.4.

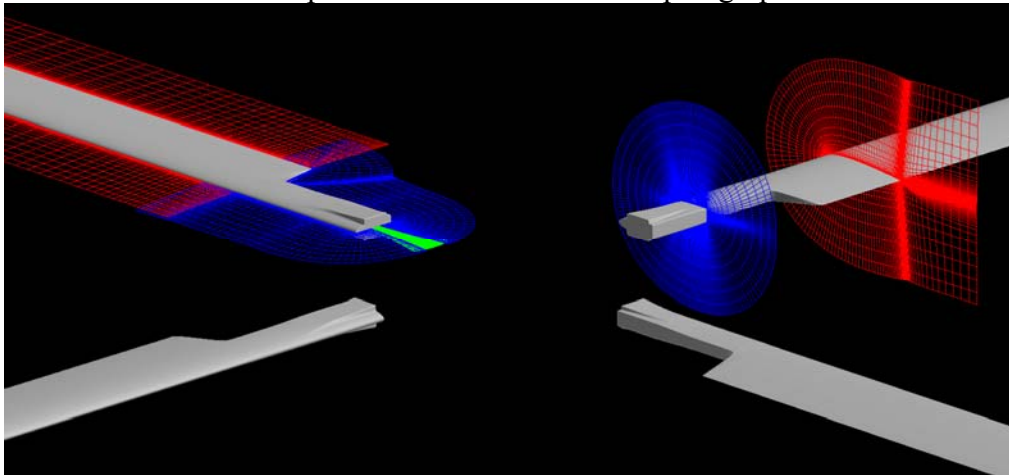


Fig. 4-1. The H-34 blade in early CFD grided form. Details of blade root end complete based on Fig. 3-4 and Fig. 3-5. Contributed by Ethan Romander.

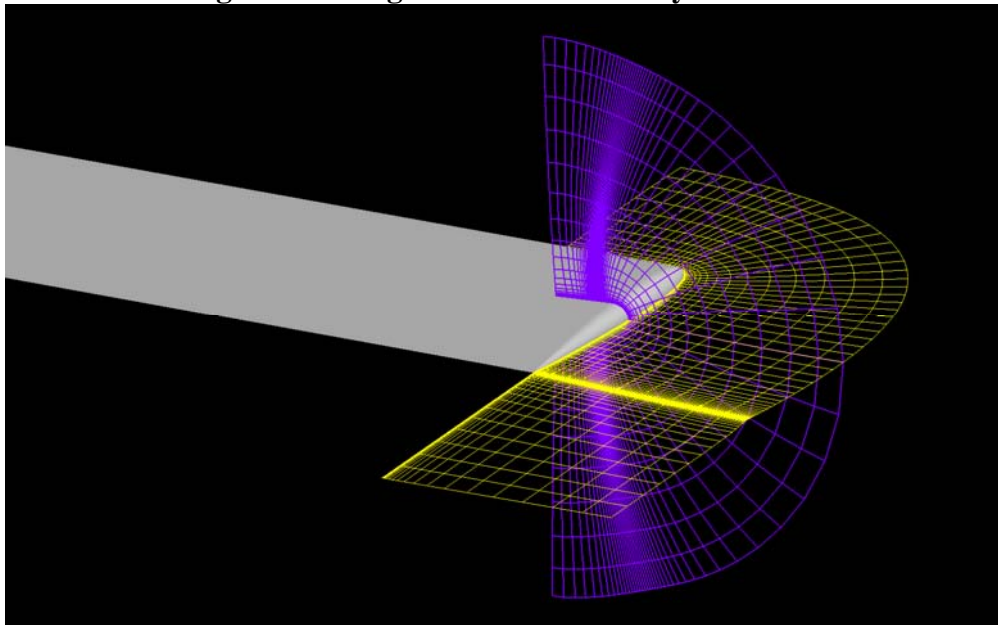


Fig. 4-2. Early CFD grid of H-34 blade with parabolic tip (Fig. 3-6) yet to be included. Contributed by Ethan Romander.

5 EXPERIMENTAL DATA

The three rotors under study (as discussed in Chapter 2 of this report) each had well documented measurements of their aerodynamic performance. This tabulated experimental data base has been put into Microsoft EXCEL spreadsheets and examined in considerable detail. Also, graphs similar to those given in the respective reports were constructed to insure that the original impressions were reasonable. Finally, a simple regression analysis of the H-34 and UH-1 data was used to judge the overall usability of the experimental data for theory versus test correlation. The PCA-2 data was accepted at face value after confirming the graphs that Wheatley gave in N.A.C.A. Report 515 had been reproduced.

The tabulated experimental data for each rotor is reproduced in this report in three Appendices. The H-34 data is in Appendix 11.6, the UH-1 data in Appendix 11.7 and the PCA-2 data is in Appendix 11.8. This tabulated experimental data – in spreadsheet form – is the basis of analysis in this report. Both H-34 and UH-1 rotor systems were tested to high lifts and advance ratios as Fig. 5-1 and Fig. 5-2 show. This matrix was obtained by varying collective pitch at the 3/4 radius station and shaft angle of attack while holding advance ratio constant. At each test point the once per rev flapping was zeroed out using longitudinal and lateral cyclic. Thus the rotor's tip path plane was trimmed normal to the shaft. The UH-1 data is particularly noteworthy because at an advance ratio of 1.1 the rotor was tested to a lift coefficient of C_L/σ equal to 0.1.

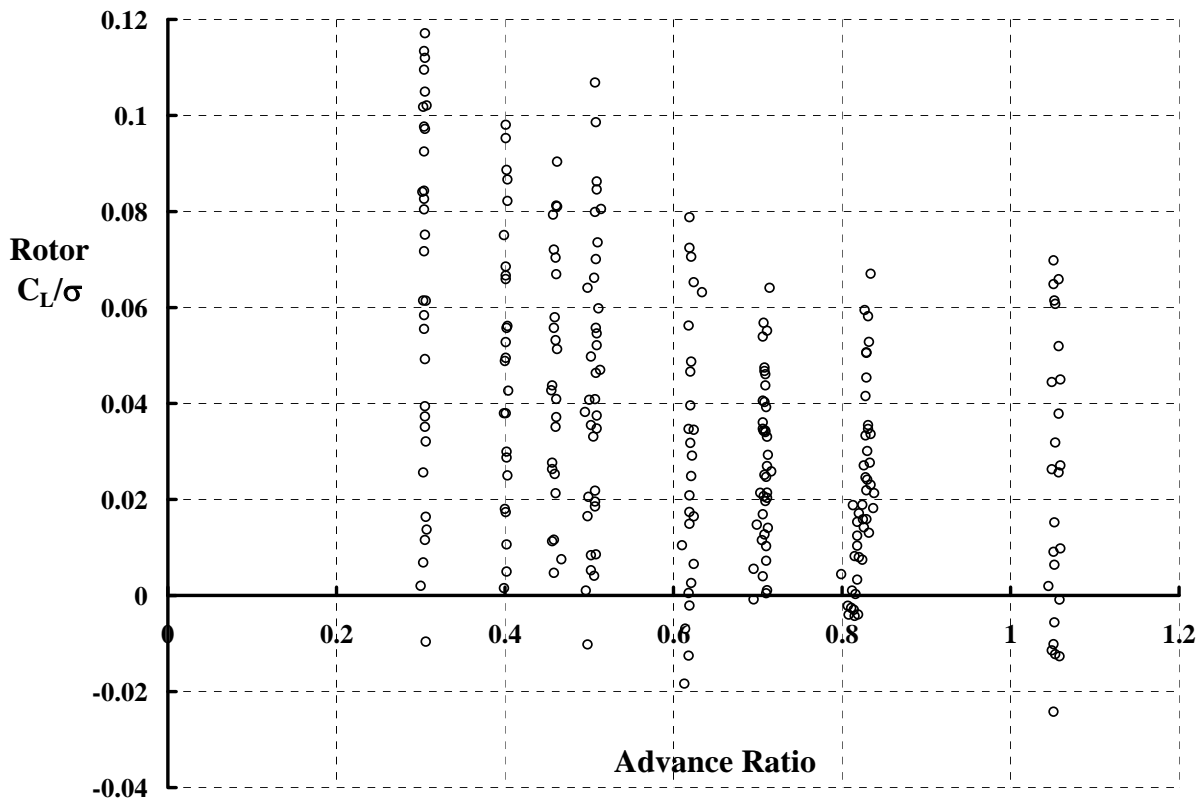


Fig. 5-1. H-34 Test range in rotor lift and advance ratio.

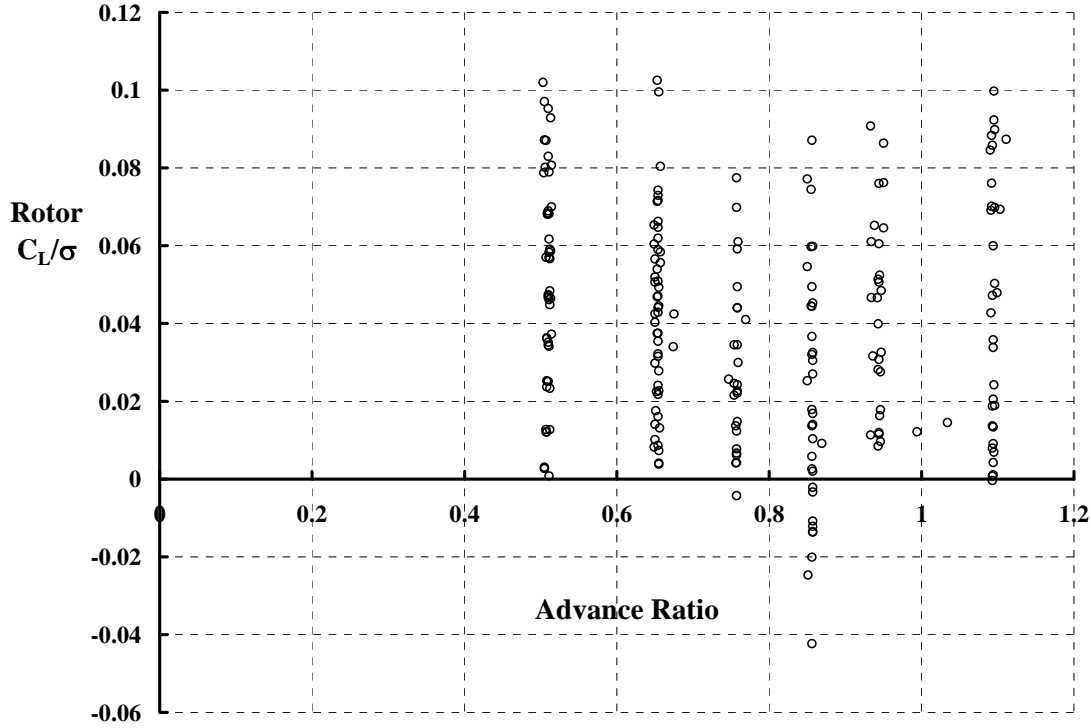


Fig. 5-2. UH-1D Test range in rotor lift and advance ratio.

The regression analysis performed on the H-34 and UH-1 data provided the most concise form to describe the experimental data usability. The analysis was predicated on the assumption that all data (below a $C_L/\sigma < 0.07$ and with the tip path plane trimmed normal to the shaft with less than 0.2 degrees flapping) would behave in a classical, no stall way. That is, *at each advance ratio*:

$$\begin{aligned} \frac{C_L}{\sigma} &= \text{function}(\alpha_s, \theta_{0.75}) & B_{IS} &= \text{function}(\alpha_s, \theta_{0.75}) & A_{IS} &= \text{function}(\alpha_s^2, \alpha_s, \alpha_s \theta_{0.75}, \theta_{0.75}, \theta_{0.75}^2) \\ \frac{C_D}{\sigma} &= \text{function}(\alpha_s^2, \alpha_s, \alpha_s \theta_{0.75}, \theta_{0.75}, \theta_{0.75}^2) & \frac{C_H}{\sigma} &= \text{function}(\alpha_s^2, \alpha_s, \alpha_s \theta_{0.75}, \theta_{0.75}, \theta_{0.75}^2) \\ \frac{C_Y}{\sigma} &= \text{function}(\alpha_s^2, \alpha_s, \alpha_s \theta_{0.75}, \theta_{0.75}, \theta_{0.75}^2) & \frac{C_Q}{\sigma} &= \text{function}(\alpha_s^2, \alpha_s, \alpha_s \theta_{0.75}, \theta_{0.75}, \theta_{0.75}^2) \end{aligned}$$

An example of the presentation form, using H-34 data at an advance ratio of 0.0305, is shown with Fig. 5-3. The regression analysis result for this example is that

$$\frac{C_L}{\sigma} = 0.66591\theta_{0.75R} + 0.30526\alpha_s + 0.01038$$

and the correlation constant, R^2 , is 0.99690. Note that the points *not included* in the regression analysis – the red crosses in Fig. 5-3 – show a distinct deviating trend at the higher lift which is indicative of blade stall at this advance ratio. The “within tolerance” band is illustrated by the \pm range about perfect. Thus, Fig. 5-3 shows that the experimental data below stall (and trimmed) is “good” to within a C_L/σ of ± 0.003 .

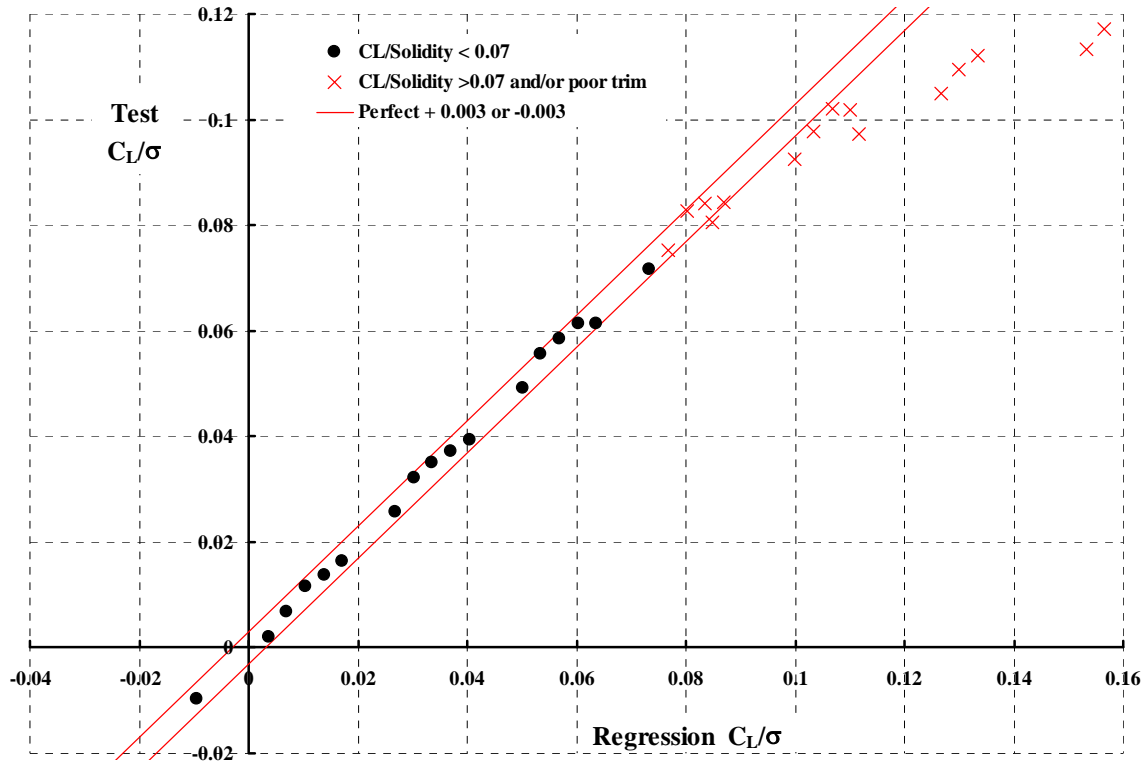


Fig. 5-3. The H-34 Lift Coefficient, C_L/σ , regression analysis for $\mu = 0.0305$.

To consolidate the presentation, the data at all advance ratios for one aerodynamic performance parameter are shown on one graph and the associated regression analysis coefficients are provided with a following table. Keep in mind that the regression coefficients can be helpful in interpolating the experimental data between tested collective pitches and shaft angle of attacks – at least up to $C_L/\sigma = 0.07$.

5.1 H-34

The H-34 Experimental Data Regression Analysis summary is given in Fig. 5-4 through Fig. 5-10 accompanied by Table 3 through Table 9 respectively. Keep in mind that the analysis was based on the assumption that all data below a $C_L/\sigma = 0.07$ and with the tip path plane trimmed normal to the shaft with less than 0.2 degrees flapping would behave in a classical, no stall way.

The summary result of the rotor lift coefficient (C_L/σ) analysis is shown with Fig. 5-4 and the associated regression analysis coefficients are given on Table 3. From Table 3, you will note that R^2 is on the order of 0.99 at low advance ratio, but deteriorates with increasing advance ratio. At $\mu = 0.82$ and 1.05 ($R^2 = 0.982$), the analysis says the experimental data is rather scattered. *In fact, the very high advance ratio data is of questionable use for correlation purposes.* For reference, more detailed analysis (including 57 individual parameter graphs) for each advance ratio is provided by the Harris EXCEL file labeled H-34 Data Regression Analysis (Corrected June 19, 2008).xls.

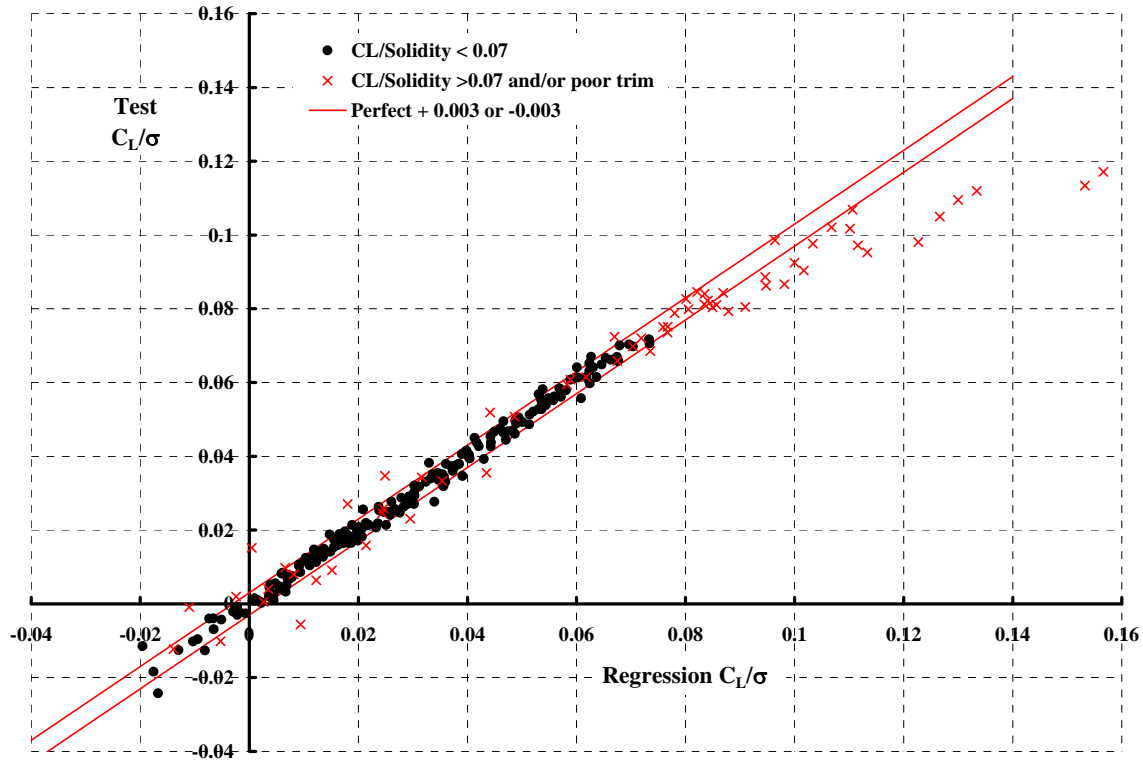


Fig. 5-4. The H-34 Lift Coefficient, C_L/σ , for all advance ratios.

Table 3. H-34 C_L/σ Regression Coefficients

Advance Ratio	Tip Speed (fps)	Tunnel Speed (fps)	Collective at 0.75R (deg)	Alpha Shaft (deg)	Constant	R Squared
0.305	629.34	191.60	0.66591	0.30526	0.010380	0.99690
0.401	664.57	266.73	0.53658	0.33541	0.009145	0.99541
0.460	630.32	289.50	0.45865	0.34148	0.007837	0.99773
0.510	617.86	312.34	0.40787	0.34485	0.007715	0.99190
0.620	505.62	313.47	0.31599	0.38169	0.002631	0.99669
0.710	443.00	313.61	0.20156	0.36472	0.002129	0.98821
0.824	379.77	312.87	0.12678	0.40124	0.002220	0.98239
1.050	295.10	310.86	-0.08209	0.66750	-0.016940	0.98327

The summary analysis for each of the other parameters follows in a similar presentation manner.

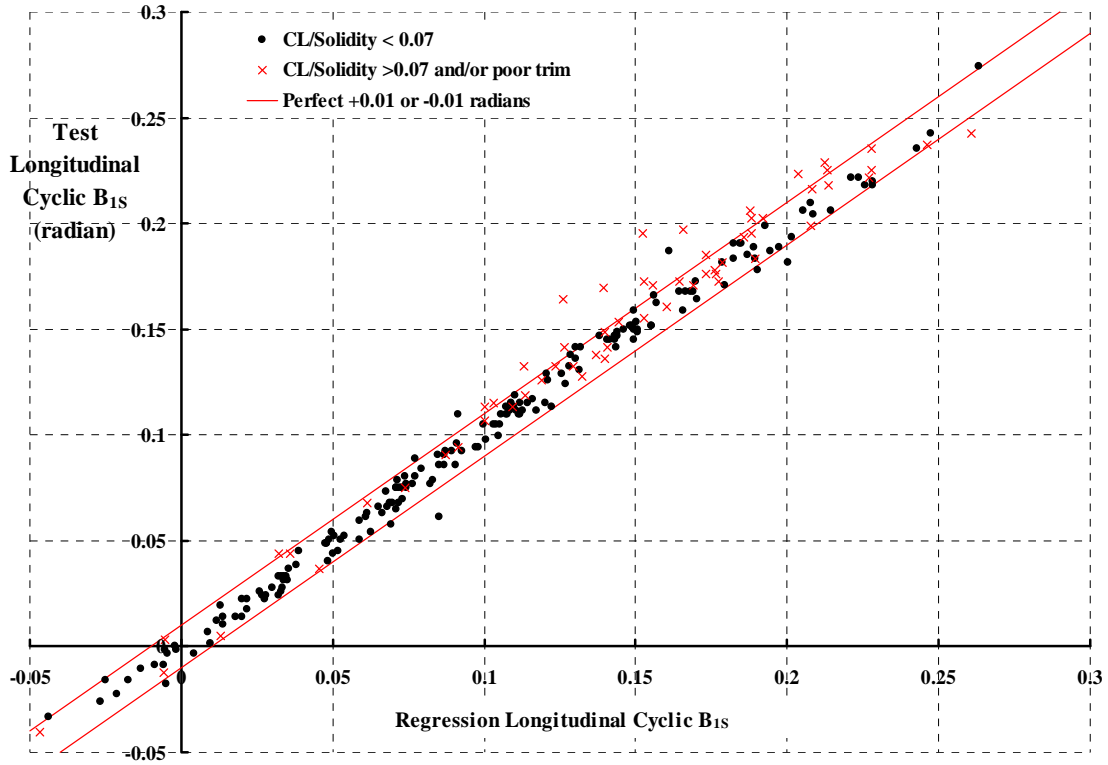


Fig. 5-5. H-34 Longitudinal Cyclic, B_{1s}, for all advance ratios.

Table 4. H-34 Longitudinal Cyclic Regression Coefficients

Advance Ratio	Alpha Shaft (radian)	Collective at 0.75R (radian)	Constant (radians)	R Squared
0.305	0.1483810	0.7489881	0.0218457	0.9957750
0.401	0.2678902	0.9205365	0.0356919	0.9896416
0.460	0.3359510	1.0025594	0.0388165	0.9886141
0.510	0.4021737	1.0264327	0.0347486	0.9846732
0.620	0.4730475	1.1192737	0.0319734	0.9837381
0.710	0.5217808	1.1085577	0.0323536	0.9967368
0.824	0.5932528	1.1148723	0.0336454	0.9859763
1.050	0.7312720	1.1861540	0.0232130	0.9933670

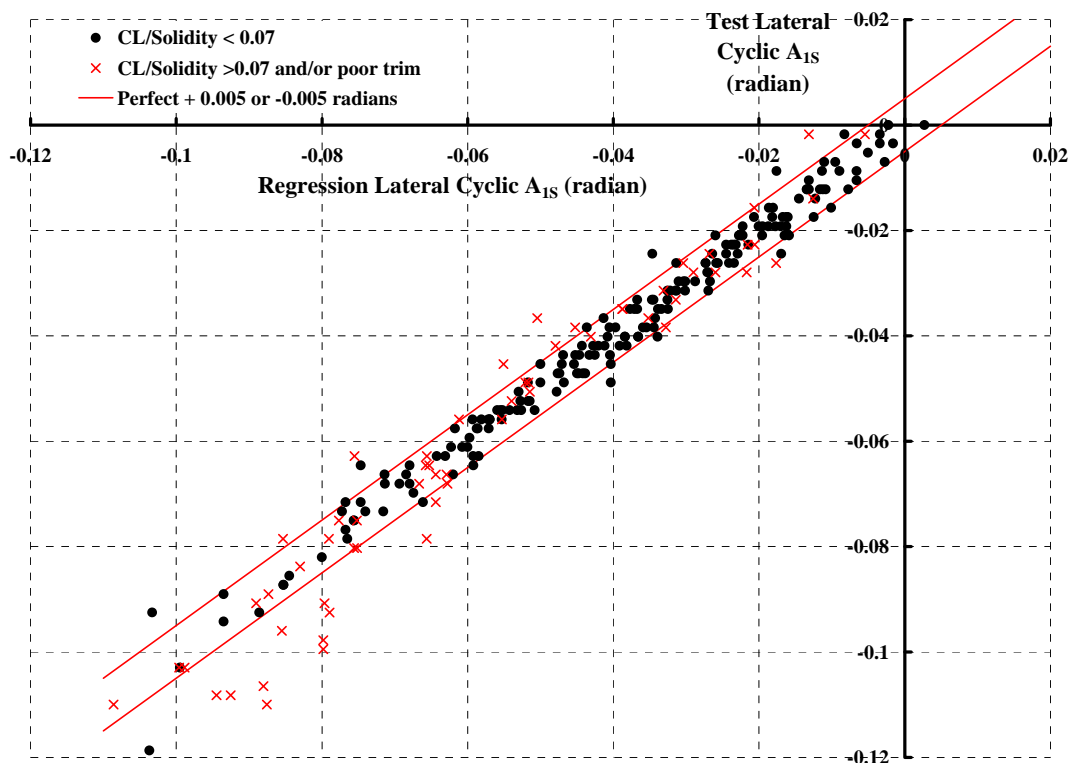


Fig. 5-6. H-34 Lateral Cyclic, A_{1S} , for all advance ratios.

Table 5. H-34 Lateral Cyclic Regression Coefficients

Advance Ratio	Coll ² (rad. ²)	Collective at 0.75R (radian)	Alpha times Collective (Rad. ²)	Alpha Shaft (radian)	Alpha ² (rad. ²)	Constant (radians)	R Squared
0.305	-1.539420	-0.194260	-0.63202	-0.01144	0.11747	-0.018076	0.98892
0.401	-0.557528	-0.320449	-0.07926	-0.04919	0.19456	-0.019573	0.99608
0.460	-0.446941	-0.344868	0.12755	-0.08580	0.22131	-0.018721	0.99504
0.510	-1.277361	-0.249828	-0.96090	-0.04029	-0.06594	-0.020584	0.98085
0.620	-1.273350	-0.228460	-1.60990	-0.06375	-0.42073	-0.020594	0.98667
0.710	-0.386963	-0.238469	-0.92776	-0.10133	-0.16921	-0.022245	0.98637
0.824	-0.066998	-0.273201	-0.13854	-0.22698	-0.13983	-0.016345	0.97877
1.050	0.835650	-0.096580	-1.13005	-0.22911	-0.13691	-0.013608	0.87171

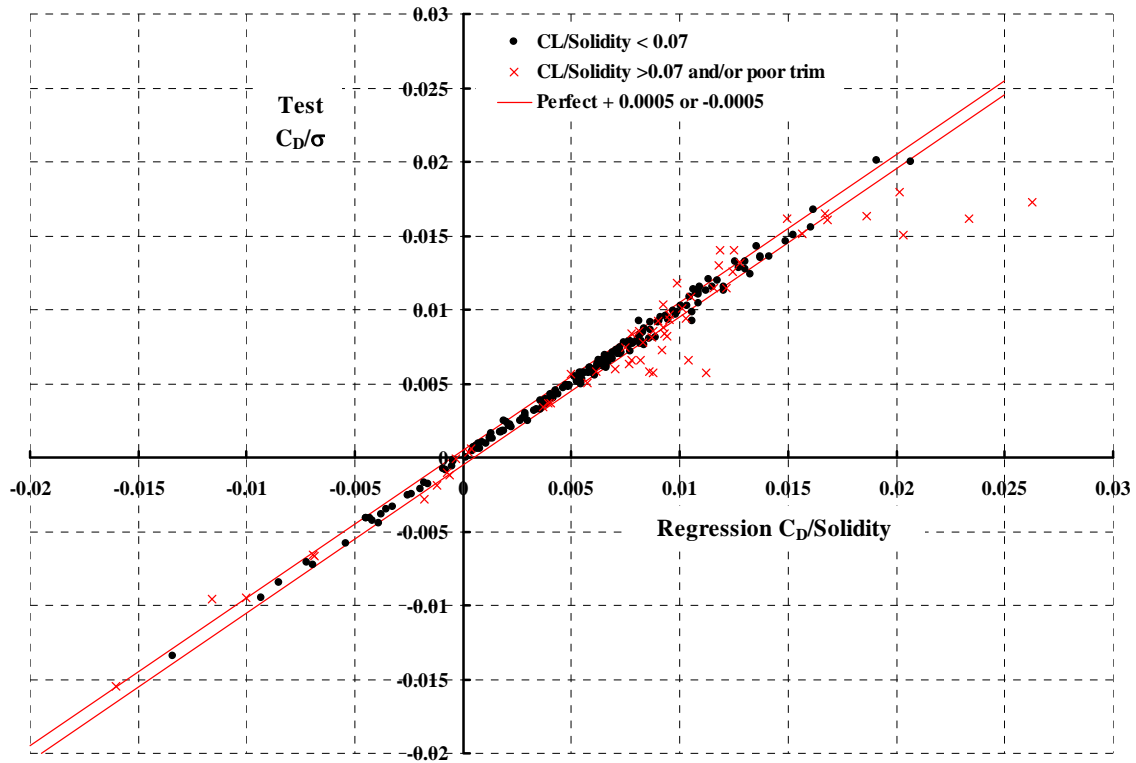


Fig. 5-7. H-34 Drag Coefficient, C_D/σ , for all advance ratios.

Table 6. H-34 C_D/σ Regression Coefficients

Advance Ratio	Coll ² (rad. ²)	Collective at 0.75R (radian)	Alpha times Collective (Rad. ²)	Alpha Shaft (radian)	Alpha ² (rad. ²)	Constant	R Squared
0.305	-0.105648	0.0005262	0.625307	0.012231	0.313008	0.001338	0.999608
0.401	-0.106217	-0.001189	0.455708	0.010291	0.328597	0.001896	0.999153
0.460	-0.113002	0.003047	0.323507	0.012945	0.305438	0.002167	0.999130
0.510	-0.063159	-0.000896	0.340732	0.009566	0.335603	0.002968	0.997380
0.620	-0.049389	0.001705	0.144456	0.006615	0.307882	0.003939	0.982269
0.710	0.035229	0.000202	0.047268	0.005378	0.277993	0.004745	0.964918
0.824	0.101648	0.002142	-0.044168	0.006911	0.243344	0.006070	0.950283
1.050	0.452456	-0.009384	-0.248505	-0.047929	0.675217	0.009897	0.970211

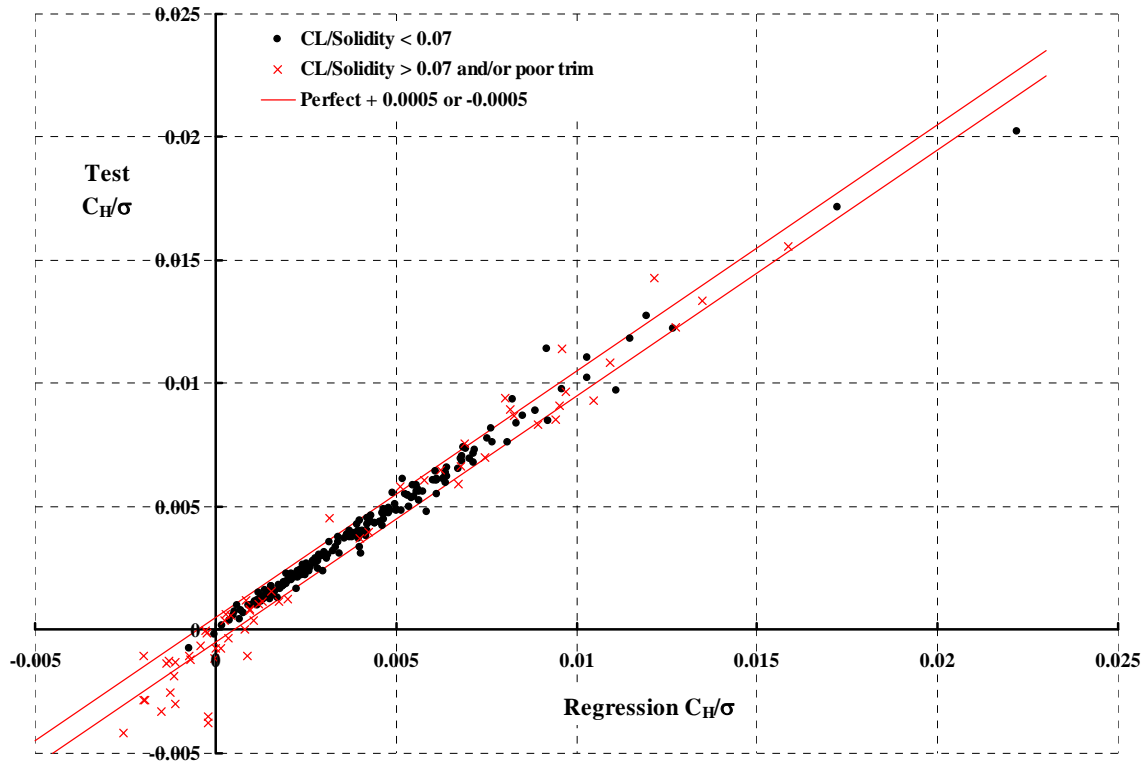


Fig. 5-8. H-34 H-force Coefficient, C_H/σ , for all advance ratios.

Table 7. H-34 C_H/σ Regression Coefficients

Advance Ratio	Coll ² (rad. ²)	Collective at 0.75R (radian)	Alpha times Collective (Rad. ²)	Alpha Shaft (radian)	Alpha ² (rad. ²)	Constant	R Squared
0.305	-0.122478	0.0025028	-0.0585609	0.0033609	0.0013599	0.001334	0.988550
0.401	-0.115967	0.0009282	-0.0938616	0.0028137	-0.0156517	0.001884	0.972158
0.460	-0.112887	0.0027974	-0.1379927	0.0052453	-0.0429657	0.002230	0.950572
0.510	-0.071084	-0.0000188	-0.1042049	0.0034751	-0.0373393	0.003012	0.910805
0.620	-0.038587	0.0006280	-0.1667550	0.0035290	-0.0852280	0.003998	0.917867
0.710	0.035643	0.0009400	-0.1702090	0.0050760	-0.1198190	0.004776	0.939194
0.824	0.100716	0.0030340	-0.1773460	0.0075440	-0.2055060	0.006119	0.956269
1.050	0.492817	-0.0127080	-0.0143830	-0.0385690	0.0246020	0.010098	0.990295

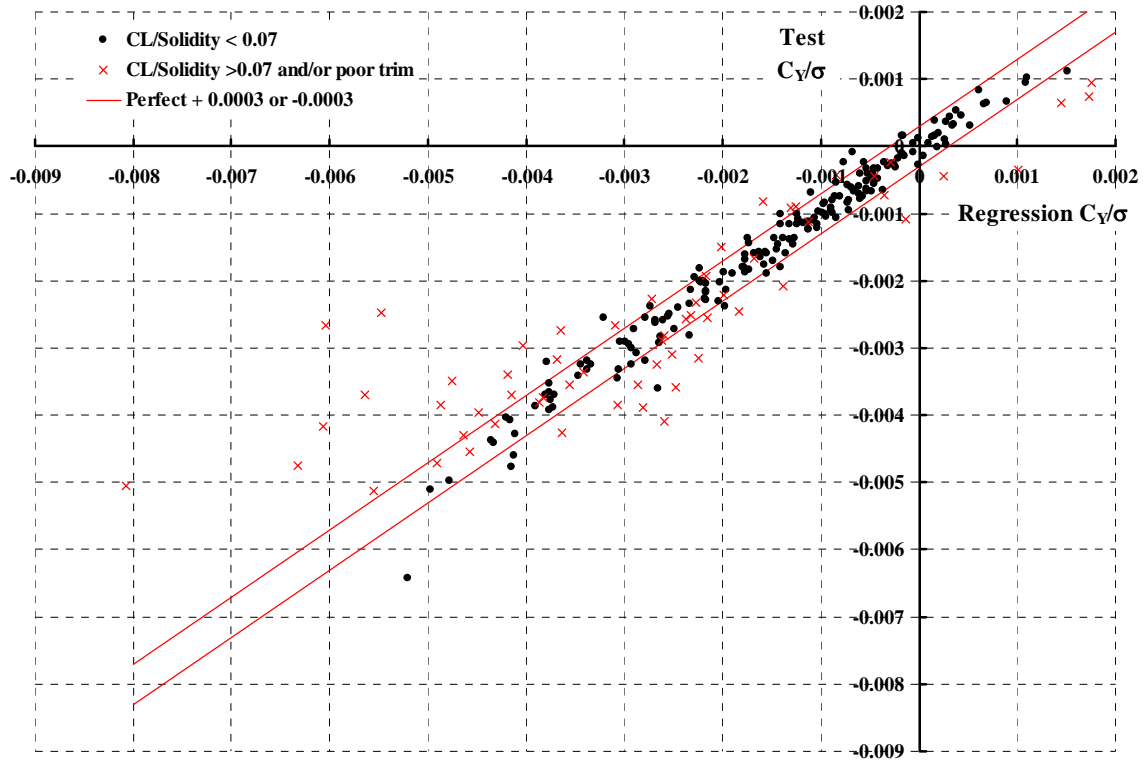


Fig. 5-9. H-34 Y-force Coefficient, C_Y/σ , for all advance ratios.

Table 8. H-34 C_Y/σ Regression Coefficients

Advance Ratio	Coll ² (rad. ²)	Collective at 0.75R (radian)	Alpha times Collective (Rad. ²)	Alpha Shaft (radian)	Alpha ² (rad. ²)	Constant	R Squared
0.305	-0.075468	-0.007551	-0.063003	-0.008032	-0.017008	-0.0000649	0.984248
0.401	-0.042071	-0.009113	-0.040390	-0.012365	-0.007727	-0.0001495	0.995923
0.460	-0.064817	-0.008623	-0.071100	-0.014209	-0.022901	-0.0001560	0.990340
0.510	-0.124332	-0.001561	-0.154431	-0.010578	-0.054730	-0.0002090	0.935476
0.620	-0.062606	-0.006143	-0.109424	-0.013795	-0.078682	-0.0002860	0.989677
0.710	-0.044940	-0.005160	-0.083402	-0.012428	-0.113823	-0.0003740	0.974312
0.824	-0.036946	-0.008524	-0.047420	-0.012166	-0.137476	-0.0002560	0.969449
1.050	-0.106934	-0.003330	0.013153	-0.056087	0.027560	0.0027240	0.968786

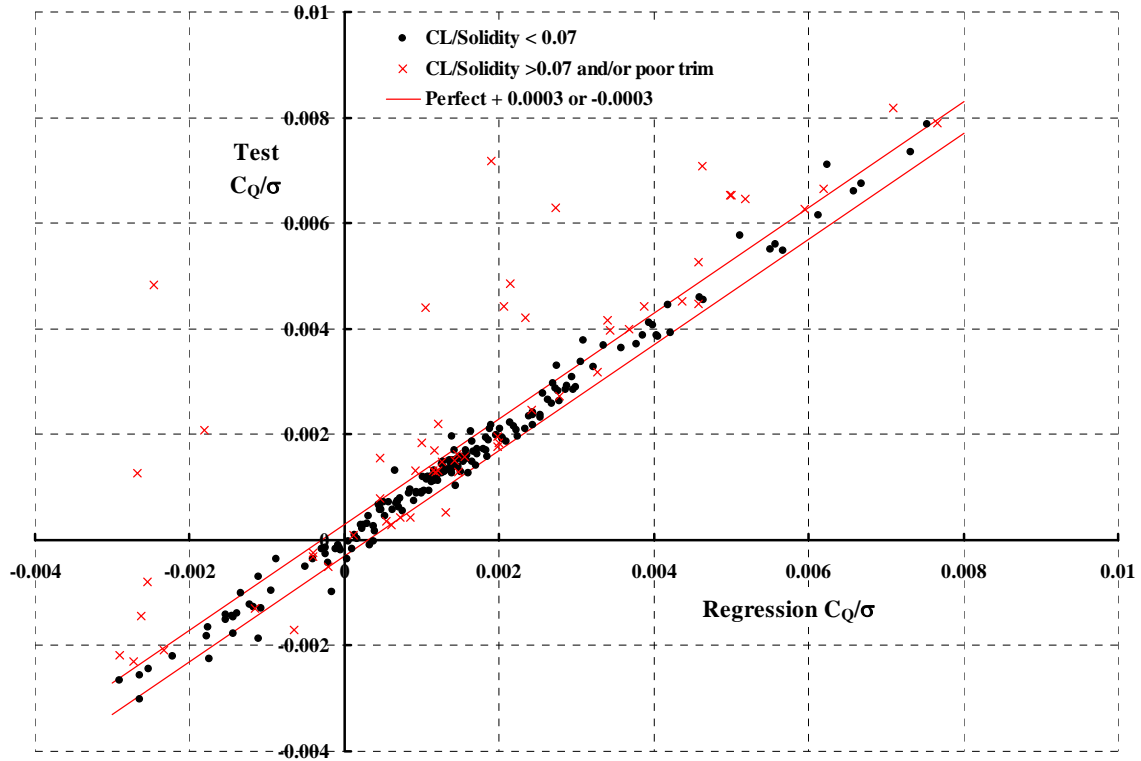


Fig. 5-10. H-34 Torque Coefficient, C_Q/σ , for all advance ratios.

Table 9. H-34 C_Q/σ Regression Coefficients

Advance Ratio	Coll ² (rad. ²)	Collective at 0.75R (radian)	Alpha times Collective (Rad. ²)	Alpha Shaft (radian)	Alpha ² (rad. ²)	Constant	R Squared
0.305	0.105956	0.001922	-0.124545	-0.002836	-0.076705	0.001063	0.99925
0.401	0.133413	0.001365	-0.083807	0.000000	-0.092731	0.001083	0.99784
0.460	0.142503	-0.001840	-0.030781	-0.006694	-0.086595	0.001159	0.99893
0.510	0.152120	-0.002059	-0.019599	-0.005950	-0.099579	0.001172	0.99695
0.620	0.150734	-0.004007	0.068254	-0.006025	-0.097124	0.001209	0.98777
0.710	0.108070	-0.005471	0.130578	-0.010308	-0.055023	0.001436	0.99094
0.824	0.051122	-0.000995	0.113151	-0.005386	-0.066177	0.001389	0.96761
1.050	-0.090083	-0.001928	0.246291	-0.001419	-0.105998	0.001513	0.91928

5.2 UH-1

The UH-1 Data Regression Analysis summary is given in Fig. 5-11 through Fig. 5-16 and Table 10 through Table 15. The analysis was predicated on the assumption that all data below a $C_L/\sigma < 0.07$ and with the tip path plane trimmed normal to the shaft with less than 0.2 degrees flapping would behave in a classical, no stall way. The lateral cyclic values used to trim lateral flapping to zero were not reported. More detailed analysis (including 36 parameter graphs) for each advance ratio is provided by the Harris EXCEL file labeled UH-1 Data Regression Analysis.xls.

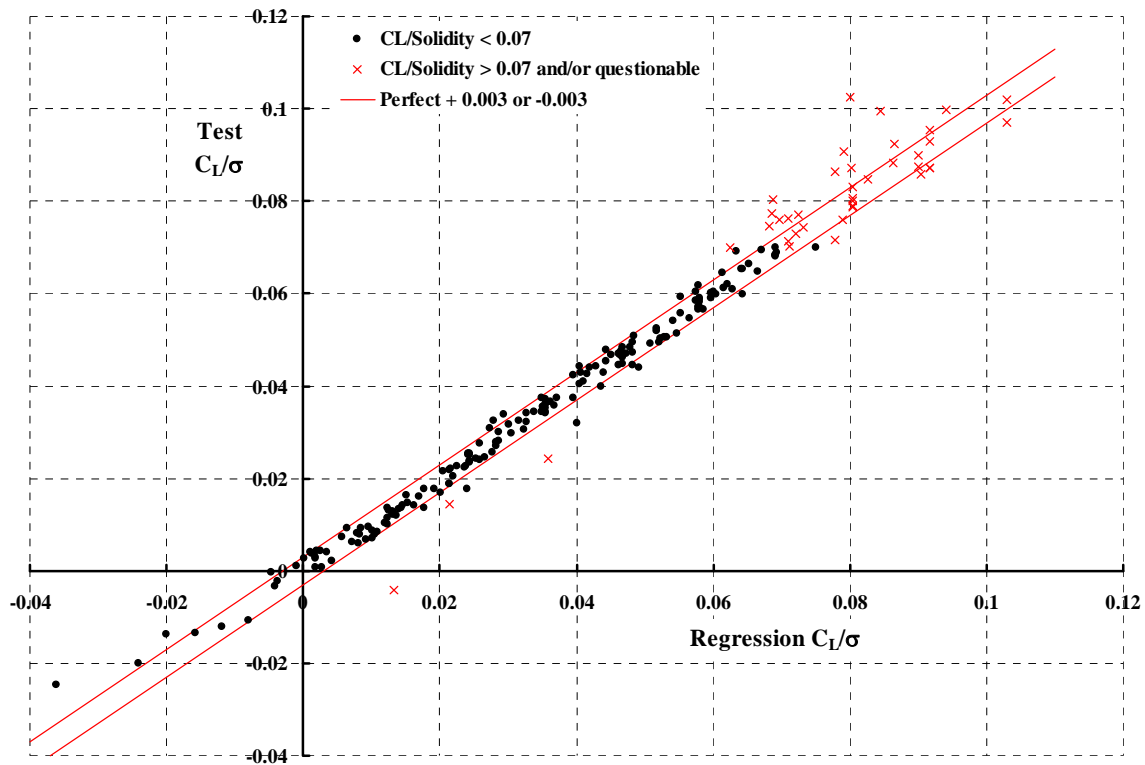


Fig. 5-11. UH-1 Lift Coefficient, C_L/σ , for all advance ratios.

Table 10. UH-1 C_L/σ Regression Coefficients

Advance Ratio	Tunnel Speed (fps)	Tip Speed (fps)	Collective at 0.75R (radian)	Alpha Shaft (radian)	Constant	R Squared
0.510	239.95	470.88	0.3211	0.3219	0.0131	0.9970
0.654	237.93	363.77	0.1944	0.3227	0.0123	0.9940
0.757	240.67	317.86	0.1756	0.3815	0.0093	0.9871
0.856	239.66	279.96	0.1117	0.4588	0.0084	0.9770
0.943	266.89	282.94	-0.0405	0.4689	0.0151	0.9895
1.095	300.13	274.18	-0.2139	0.6558	0.0214	0.9843

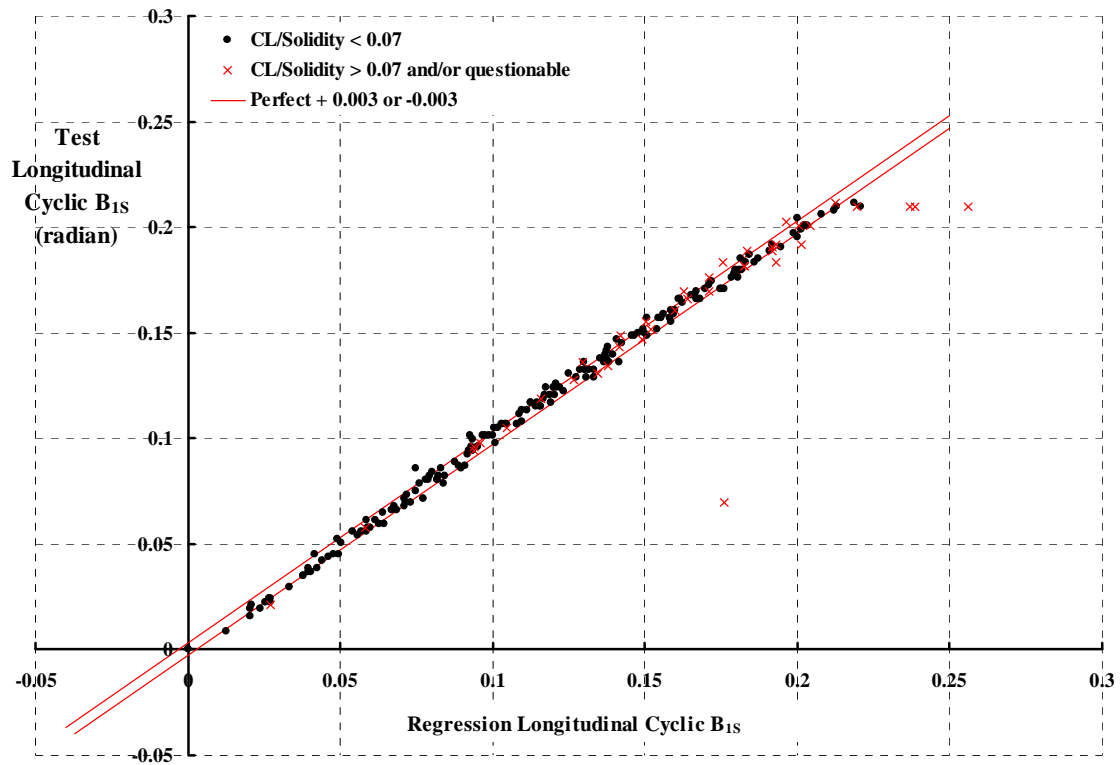


Fig. 5-12. UH-1 Longitudinal Cyclic, B_{1s} , for all advance ratios.

Table 11. UH-1 Longitudinal Cyclic Regression Coefficients

Advance Ratio	Alpha Shaft (radian)	Collective at 0.75R (radian)	Constant (radians)	R Squared
0.510	0.3601	0.9535	0.0128	0.9962
0.654	0.5032	1.0478	0.0205	0.9954
0.757	0.5396	1.1062	0.0206	0.9952
0.856	0.5780	1.1172	0.0239	0.9953
0.943	0.6032	1.1766	0.0266	0.9967
1.095	0.6391	1.2553	0.0271	0.9964

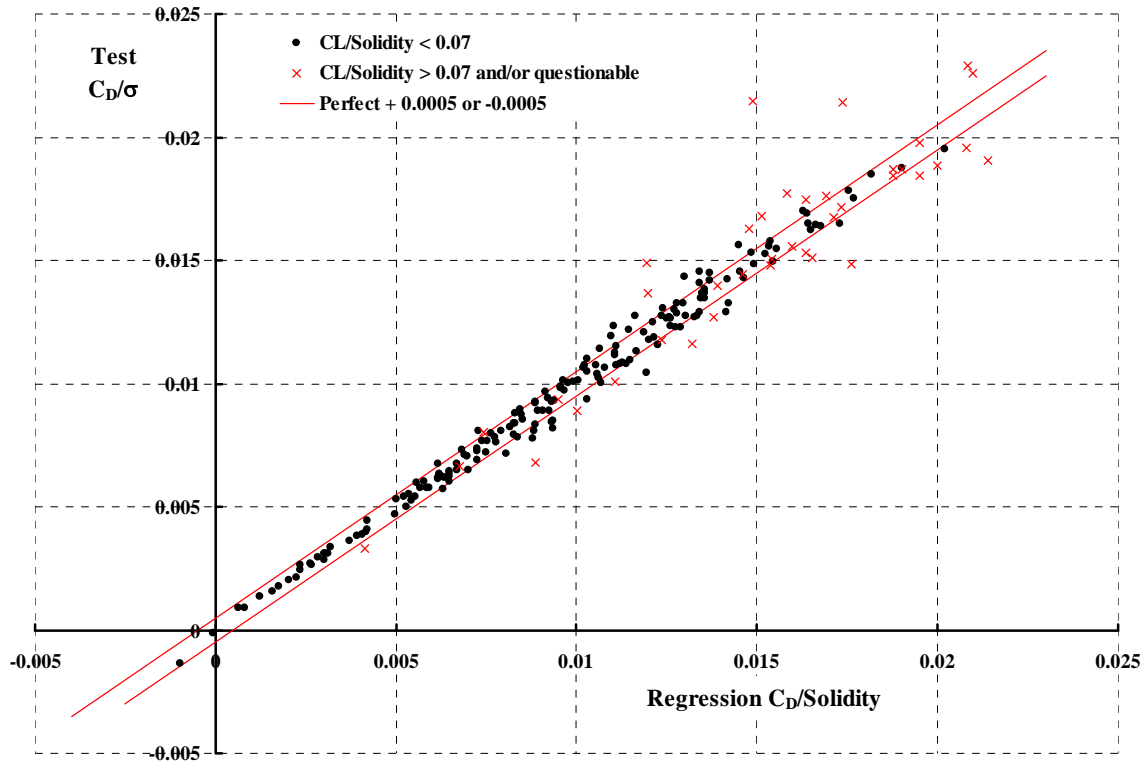


Fig. 5-13. UH-1 Drag Coefficient, C_D/σ , for all advance ratios.

Table 12. UH-1 C_D/σ Regression Coefficients

Advance Ratio	Coll ² (rad. ²)	Collective at 0.75R (radian)	Alpha times Collective (Rad. ²)	Alpha Shaft (radian)	Alpha ² (rad. ²)	Constant	R Squared
0.510	-0.0215	0.0065	0.2155	0.0254	0.2910	0.0037	0.9958
0.654	0.0260	0.0106	0.0864	0.0250	0.2526	0.0053	0.9860
0.757	0.0163	0.0248	0.1964	0.0070	0.2775	0.0056	0.8909
0.856	0.0489	0.0292	-0.1115	0.0284	0.2569	0.0070	0.9238
0.943	0.4438	-0.0099	-0.0566	0.0074	0.3208	0.0091	0.9500
1.095	0.3904	0.0271	-0.5862	0.0238	0.5412	0.0111	0.9722

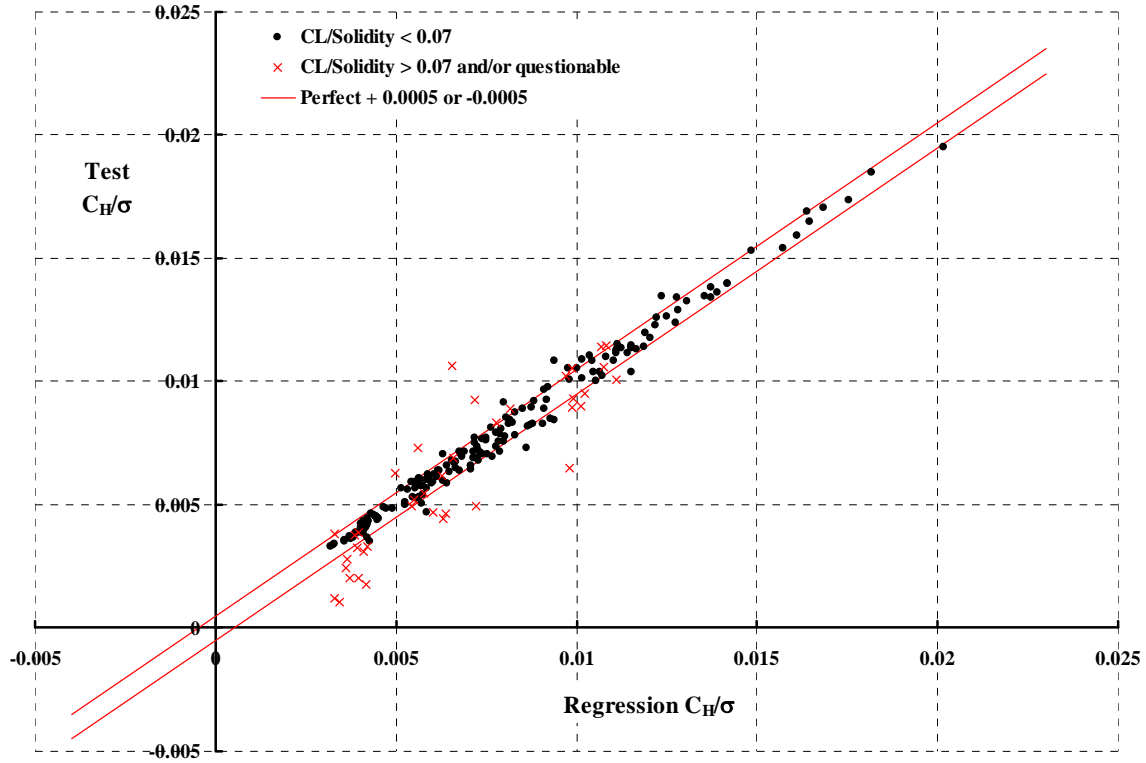


Fig. 5-14. UH-1 H-force Coefficient, C_H/σ , for all advance ratios.

Table 13. UH-1 C_H/σ Regression Coefficients

Advance Ratio	Coll ² (rad. ²)	Collective at 0.75R (radian)	Alpha times Collective (Rad. ²)	Alpha Shaft (radian)	Alpha ² (rad. ²)	Constant	R Squared
0.510	-0.0129	0.0049	-0.1010	0.0116	-0.0272	0.0037	0.8710
0.654	0.0256	0.0107	-0.0984	0.0110	-0.0656	0.0053	0.8952
0.757	0.0152	0.0239	0.0057	-0.0020	-0.1055	0.0056	0.9090
0.856	0.0636	0.0286	-0.2453	0.0231	-0.1871	0.0068	0.9419
0.943	0.4263	-0.0071	-0.0257	-0.0156	-0.0543	0.0091	0.9705
1.095	0.3923	0.0265	-0.2883	-0.0049	-0.0644	0.0111	0.9771

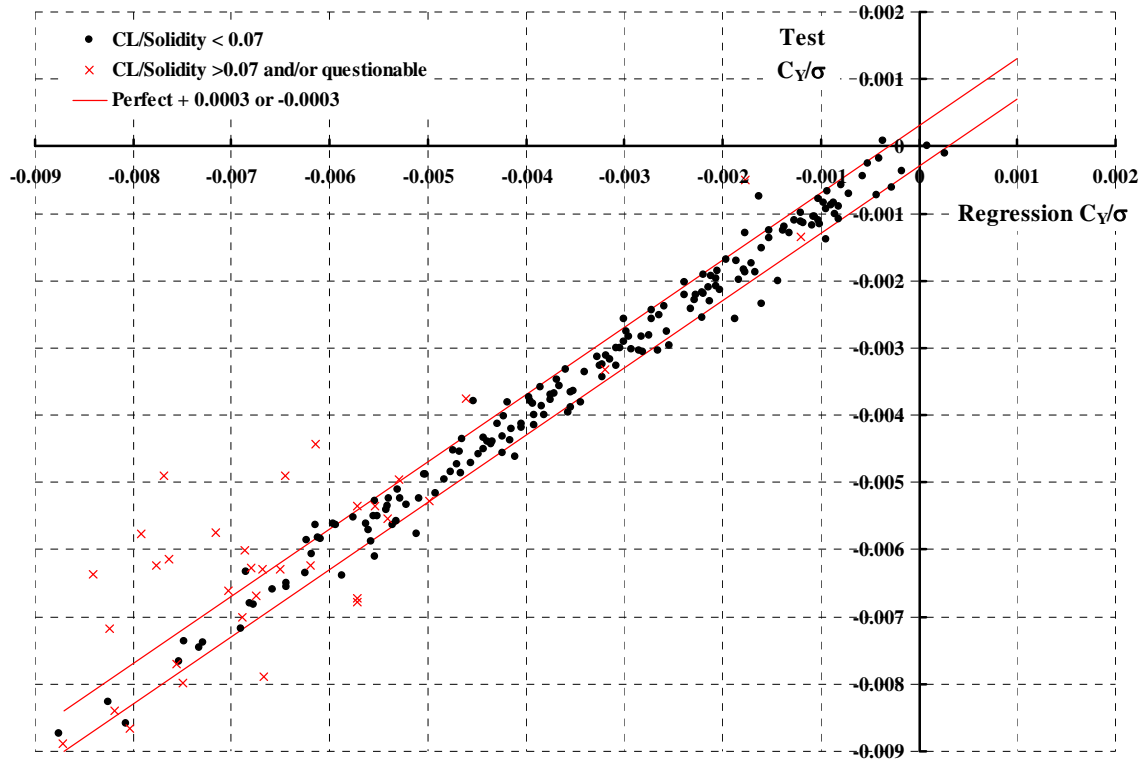


Fig. 5-15. UH-1 Y-force Coefficient, C_Y/σ , for all advance ratios.

Table 14. UH-1 C_Y/σ , Regression Coefficients

Advance Ratio	Coll ² (rad. ²)	Collective at 0.75R (radian)	Alpha times Collective (Rad. ²)	Alpha Shaft (radian)	Alpha ² (rad. ²)	Constant	R Squared
0.510	-0.0155	-0.0139	-0.0790	-0.0155	-0.0371	-0.0010	0.9655
0.654	0.0443	-0.0258	-0.0518	-0.0228	-0.0237	-0.0010	0.9866
0.757	0.0188	-0.0261	-0.1023	-0.0298	-0.0093	-0.0011	0.9865
0.856	-0.0176	-0.0232	-0.1273	-0.0285	-0.0652	-0.0009	0.9716
0.943	0.1105	-0.0417	-0.0466	-0.0430	0.0193	-0.0011	0.9798
1.095	0.2112	-0.0610	0.0267	-0.0526	0.0906	-0.0012	0.9915

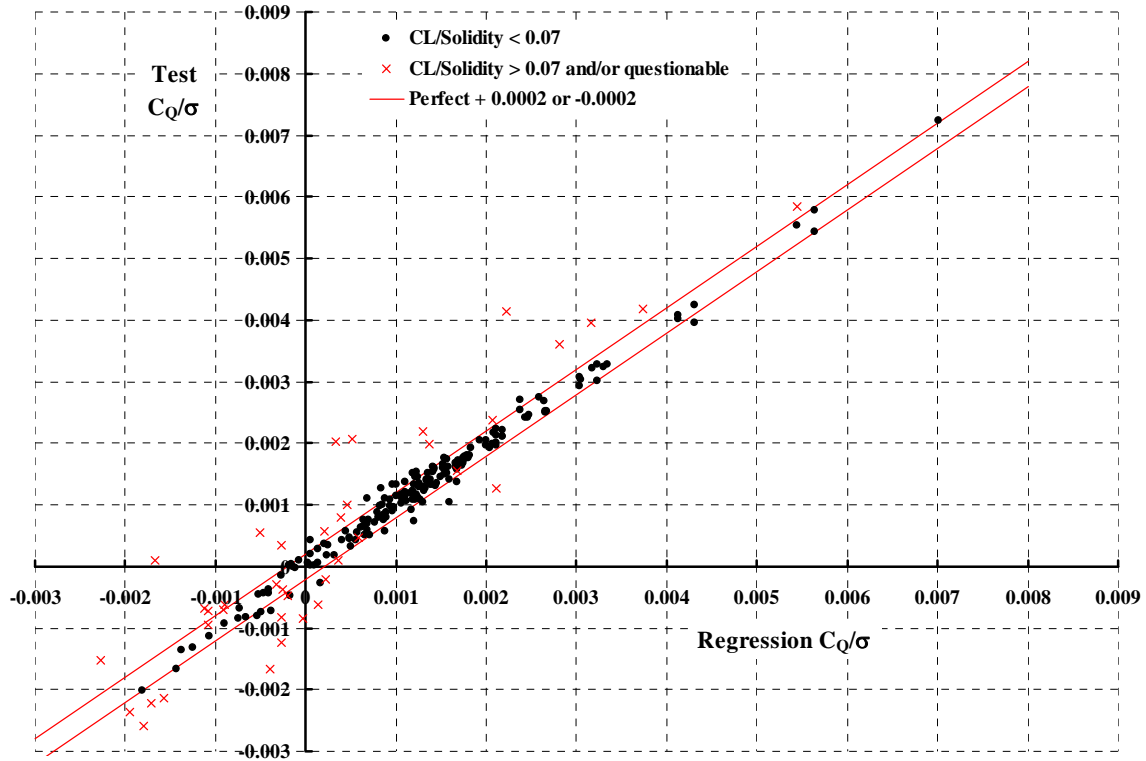


Fig. 5-16. UH-1 Torque Coefficient, C_Q/σ , for all advance ratios.

Table 15. UH-1 C_Q/σ Regression Coefficients

Advance Ratio	Coll ² (rad. ²)	Collective at 0.75R (radian)	Alpha times Collective (Rad. ²)	Alpha Shaft (radian)	Alpha ² (rad. ²)	Constant	R Squared
0.510	0.0972	0.0006	-0.0005	-0.0082	-0.0792	0.0011	0.9925
0.654	0.0548	0.0024	0.0476	-0.0101	-0.0853	0.0013	0.9933
0.757	0.0270	0.0026	0.0032	-0.0036	-0.1239	0.0012	0.9797
0.856	0.0548	-0.0056	0.1018	-0.0085	-0.1065	0.0013	0.9347
0.943	0.0114	-0.0058	0.2167	-0.0079	-0.1537	0.0014	0.9637
1.095	-0.1164	0.0010	0.1392	-0.0044	-0.1356	0.0017	0.8314

5.3 PCA-2

The PCA-2 rotor was tested at four (4) rotor speeds. Nominally these rotor speeds were 98.6, 118.7, 137.6 and 147.9 RPM, which corresponds to tip speeds of 232.3, 279.7, 324.2 and 348.5 feet per second. The wind tunnel speed varied between 32 and 173 feet per second. Wheatley, in N.A.C.A. Report No. 515 graphed rotor lift and drag in airplane coefficients. For rotor analysis, classically defined rotor coefficients are more useful. The PCA-2 rotor data of C_T , C_H , C_Y and shaft angle of attack are shown in Fig. 5-17 through Fig. 5-20. Keep in mind that this autogyro rotor had no feathering or a swashplate to tilt. The rotor simply flapped. Unfortunately, no data about blade motion was reported. More detailed analysis (including 15 parameter graphs) is in Harris EXCEL File PCA-2 Rotor Alone Test Data + Geometry & Properties.xls

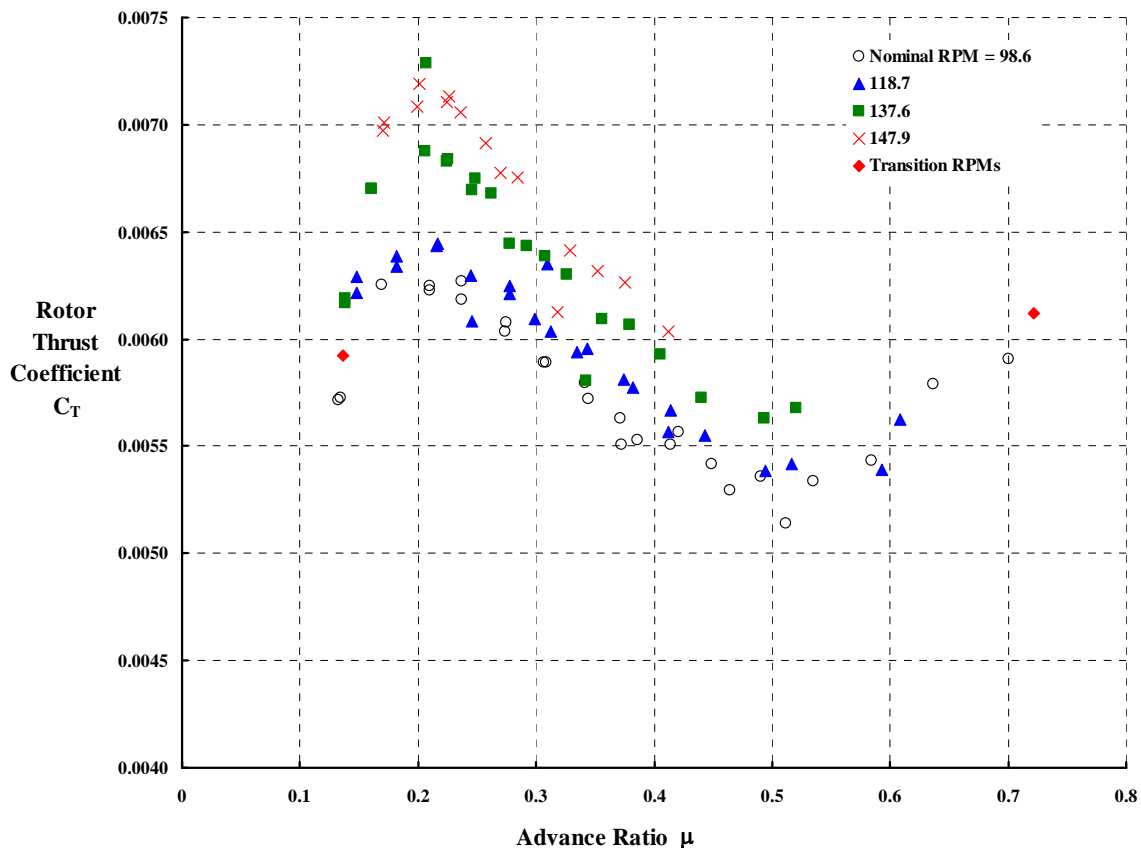


Fig. 5-17. PCA-2 Thrust coefficient at four RPMs versus advance ratio.

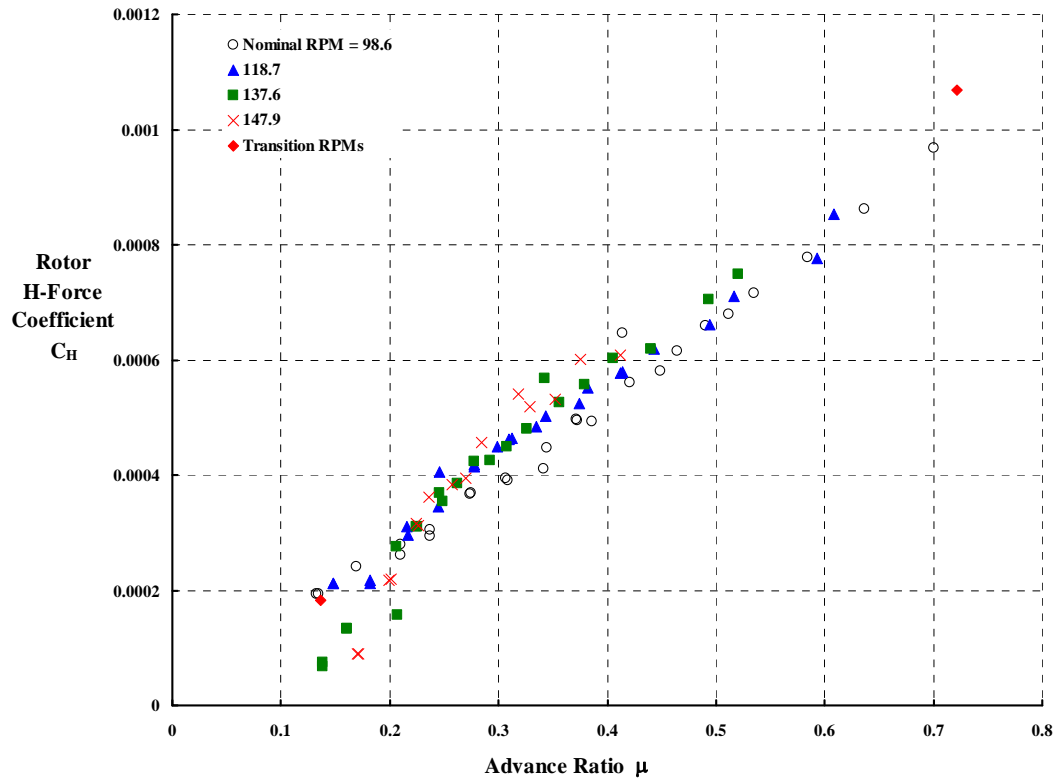


Fig. 5-18. PCA-2 H-Force coefficient at four RPMs versus advance ratio.

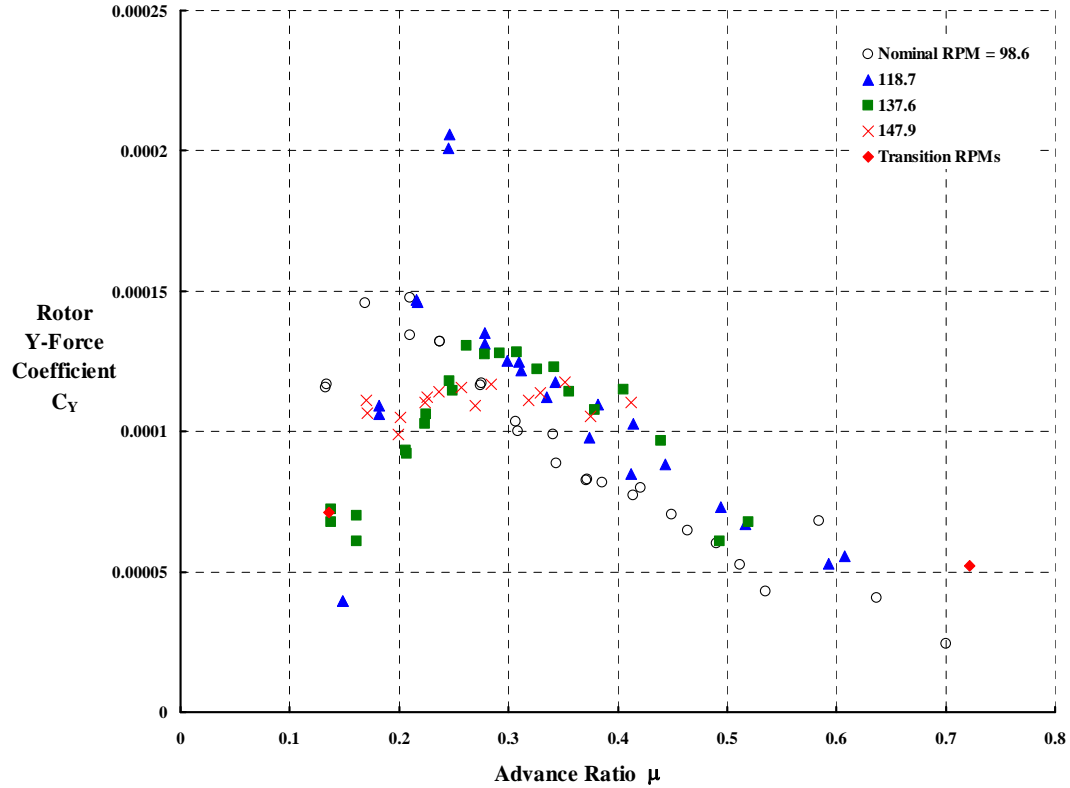


Fig. 5-19. PCA-2 Side force coefficient at four RPMs versus advance ratio.

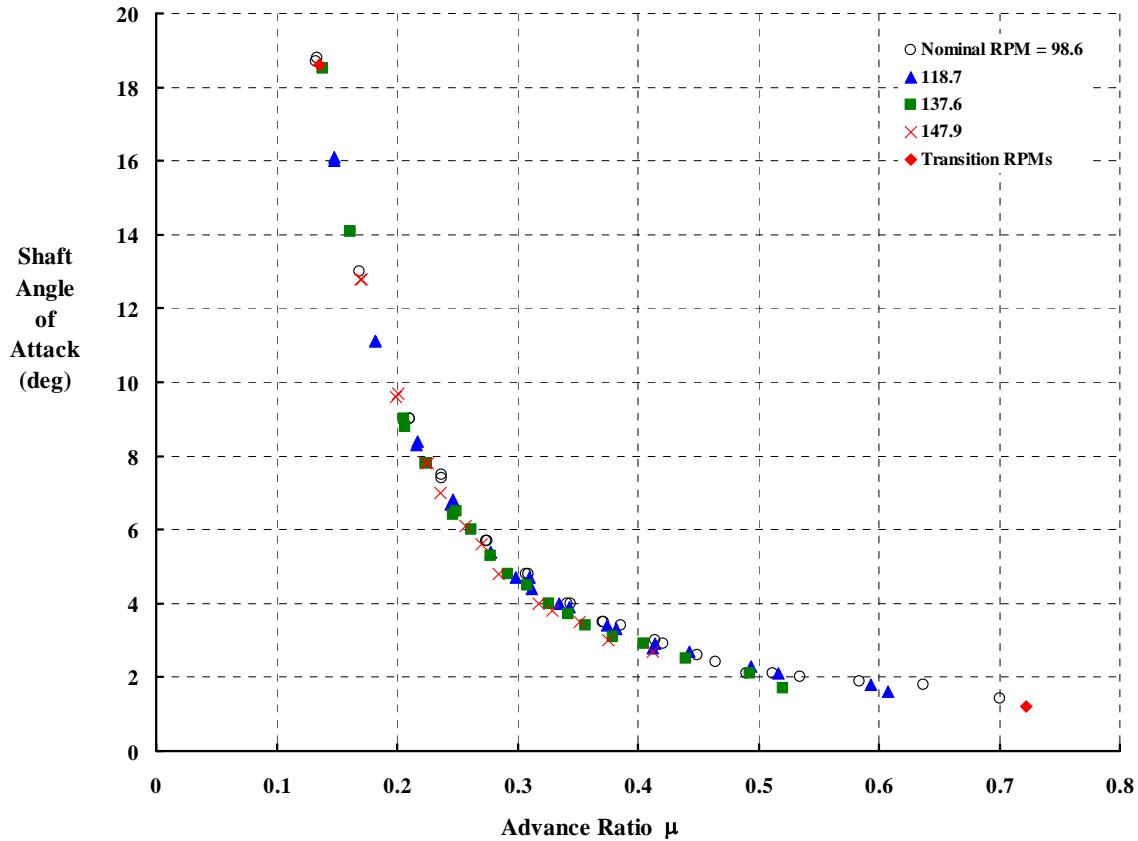


Fig. 5-20. PCA-2 Shaft angle of attack at four RPMs versus advance ratio.

5.4 Discussion

The experimental data as presented above raises several interesting points. Before proceeding to the correlation of theory and test, a discussion of 3 key points is in order.

5.4.1 Performance at zero angles

It is commonly imagined that if an untwisted rotor is tested at zero collective pitch at the $\frac{3}{4}$ radius station and zero shaft angle of attack, then the rotor lift (or thrust) will be zero. Of course, neither the H- and Y-forces nor shaft torque are expected to be zero. Both the H-34 and UH-1 test data say this “lift will be zero” assumption is not a good one.

As Fig. 5-21 and Table 3 show, the H-34 rotor exhibits linear lift curve slopes at all advance ratios tested. The UH-1 also exhibits this behavior as Table 10 shows. However, the lift is not zero at zero collective at $\frac{3}{4}$ R and zero shaft angle of attack. This non-zero lift varies with advance ratio as Fig. 5-22 shows. The UH-1 data does reflect the fact that the twist is -1.42 degrees, not zero. But, the condition is for collective pitch at the $\frac{3}{4}$ R equaling zero, which at low advance ratio is the first approximation for removing twist effects.

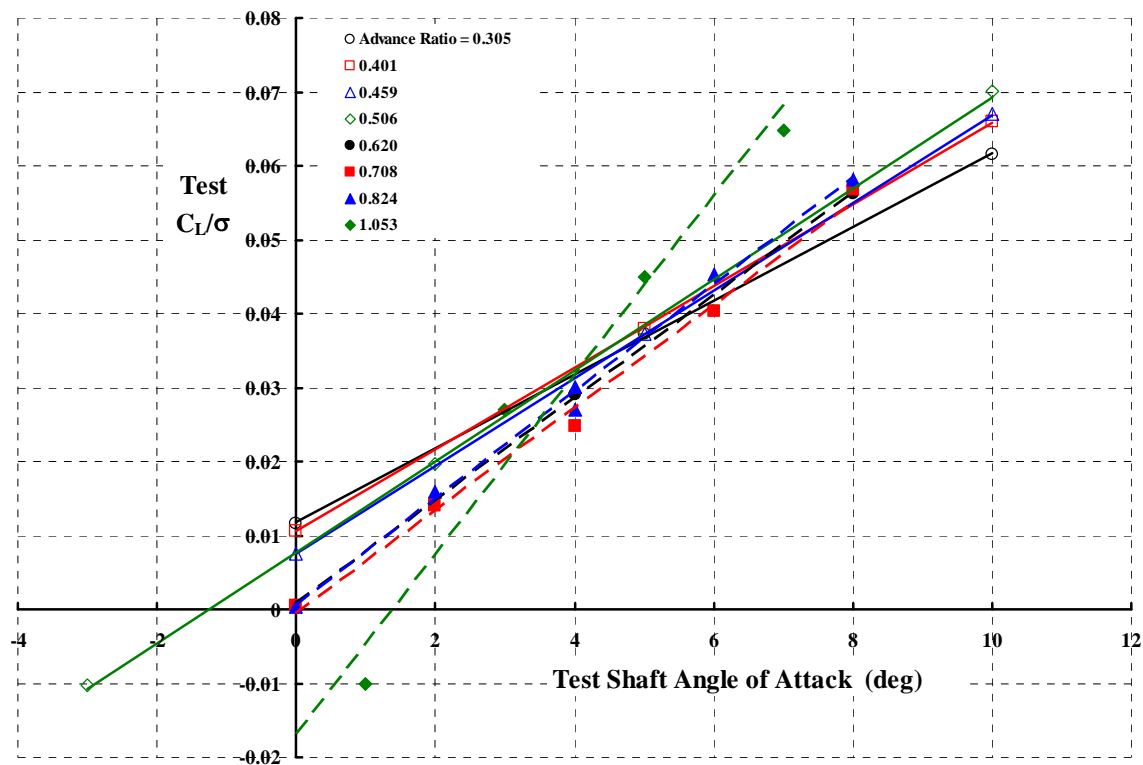


Fig. 5-21. H-34 Lift versus shaft angle of attack at zero collective pitch at $3/4$ R.

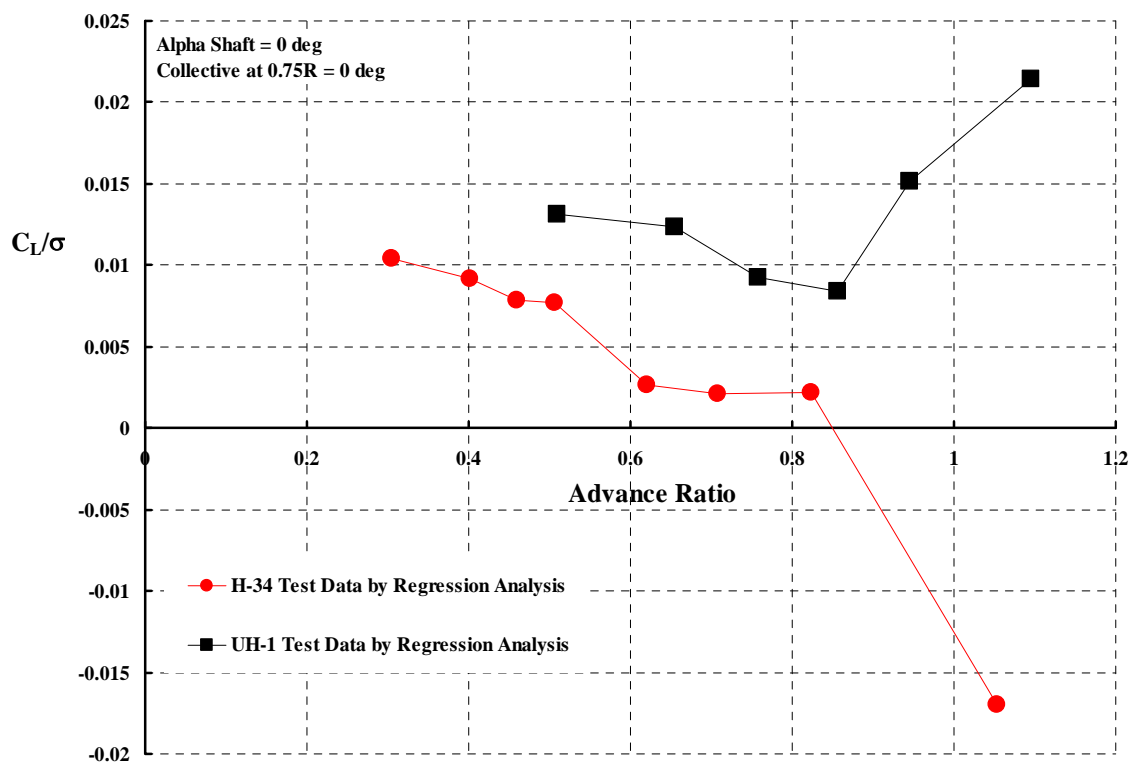


Fig. 5-22. Lift at zero shaft angle of attack and zero collective pitch at $3/4$ R.

The corollary presumption to “ C_L/σ should be zero when θ at $\frac{3}{4} R = 0$ and $\alpha_s = 0$ ” is that there will be no flapping and therefore no cyclic control is required. That is, in the blade feathering equation of

$$\theta_{x,\psi} = \theta_o + x\theta_t - B_{1C} \sin \psi - A_{1C} \cos \psi$$

both longitudinal cyclic (B_{1C}) and lateral cyclic (A_{1C}) should be zero. Neither the H-34 nor the UH-1 rotor systems confirm this presumption as Fig. 5-23 and Fig. 5-24 show.

Investigators in past decades have, in this author’s experience, simply charged the cause of the non-zero lift and cyclic behavior to experimental error. However, in the course of this investigation a more plausible explanation was obtained following Wheatley’s 1937 opinion that elastic twisting was not to be ignored [29]. Wheatley encouraged the view that the blade feathering equation should include at least three additional terms so that

$$\theta_{x,\psi} = \theta_o + x\theta_t - B_{1C} \sin \psi - A_{1C} \cos \psi + x(\theta_{e_x} + \theta_{e_{1s}} \sin \psi + \theta_{e_{1c}} \cos \psi)$$

Admitting any aeroelastic response to blade element pitching moment will lead to flapping. Thus, cyclic control will be required to retrim the rotor tip path plane normal to the shaft (this experiment’s test requirement). As will be seen in the correlation chapter to follow shortly, CAMRAD II could reproduce the “nonzero behavior” by adding a lumped, delta aerodynamic pitching moment to the symmetrical N.A.C.A. 0012. The conclusion of this author is that the trends shown with Fig. 5-22, Fig. 5-23 and Fig. 5-24 are due to aeroelastic deflections, specifically in torsion.

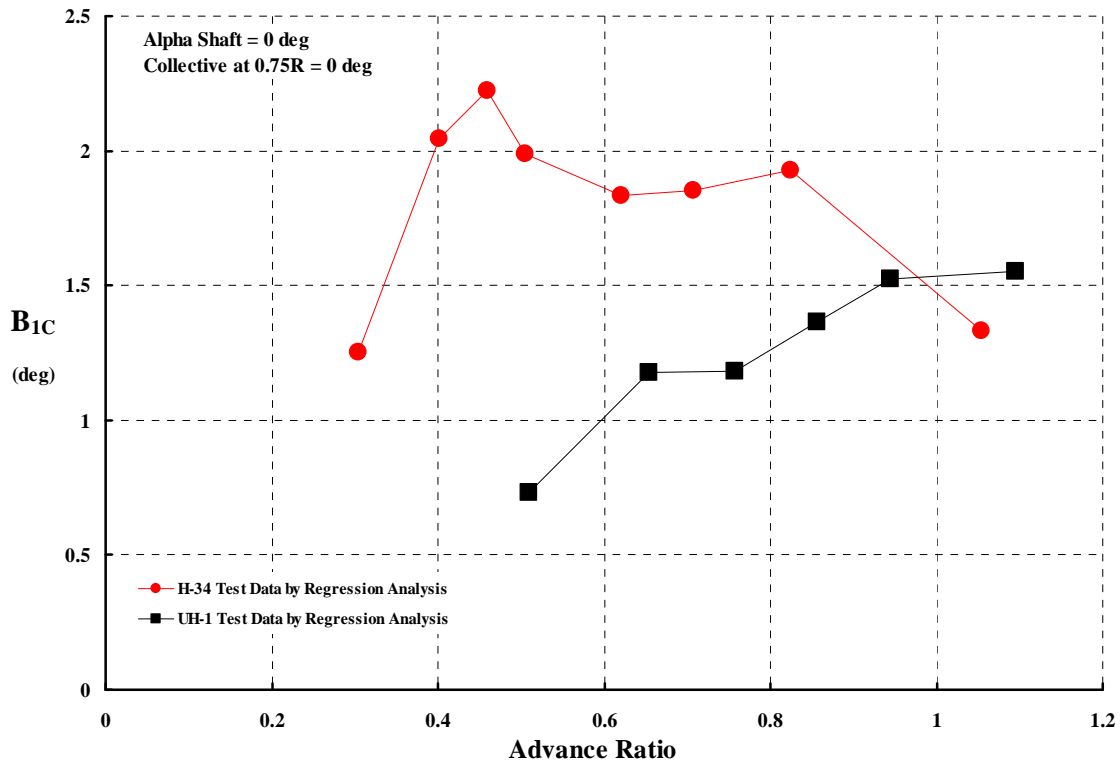


Fig. 5-23. Longitudinal cyclic at zero shaft angle of attack and zero collective pitch at $\frac{3}{4} R$.

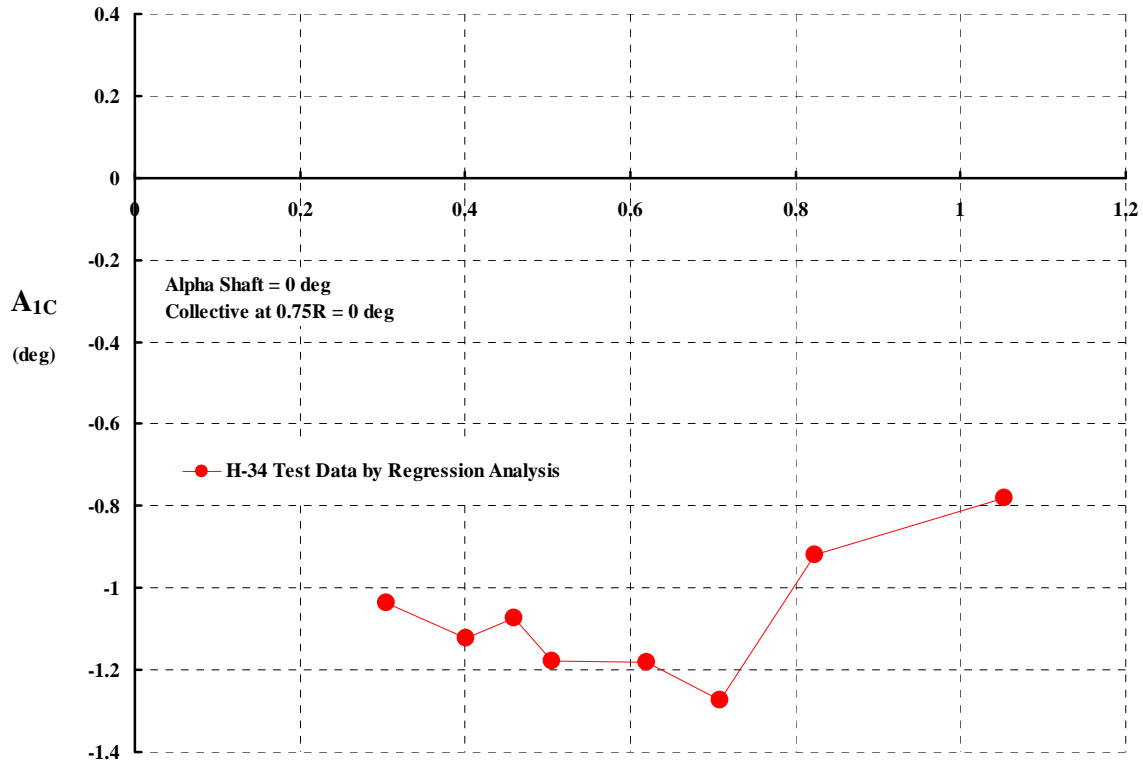


Fig. 5-24. Lateral cyclic at zero shaft angle of attack and zero collective pitch at $\frac{3}{4}$ R
No UH-1 data for lateral cyclic was reported.

The trends of H-force, Y-force and torque with advance ratio when θ at $\frac{3}{4}$ R = 0 and $\alpha_s = 0$ is of particular interest. This is because a compound helicopter is frequently considered where the rotor is operated at zero or near-zero lift and a wing is used to support the aircraft weight. The experimental H-34 and UH-1 data provide a reasonable view of the aerodynamic loads the rotor might impose on the imagined compound helicopter. The H-force, as Fig. 5-25 shows, continually rises with increasing advance ratio. Theoretically, this longitudinal force is zero at zero advance ratio. There is a considerable Y-force at high advance ratio as Fig. 5-26 shows. This side force is also theoretically zero at zero advance ratio. Finally, the rotor requires an input torque (i.e., horsepower from some source) to maintain rotor speed. This evidence is provided by Fig. 5-27. The simplest of theories says that – at zero advance ratio – the torque can be calculated as

$$\frac{C_Q}{\sigma} = \frac{C_{do}}{8}$$

and this suggests that average blade element drag coefficient (C_{do}) is on the order of 0.008, assuming that C_Q/σ is 0.001 at zero advance ratio.

As of October 2008 no experimental, full scale rotor data is available beyond an advance ratio of 1.0 to support a projection of this data to advance ratios on the order of 2 or 3.

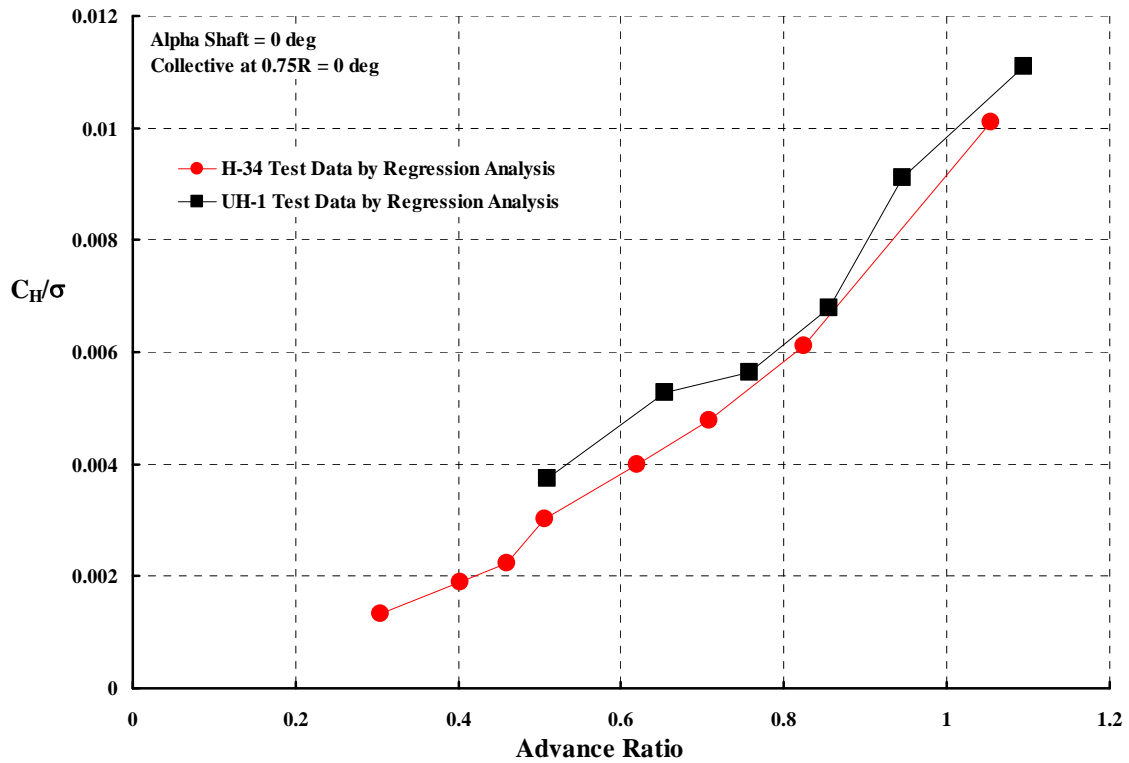


Fig. 5-25. H-Force at zero shaft angle of attack and zero collective pitch at $\frac{3}{4}$ R.

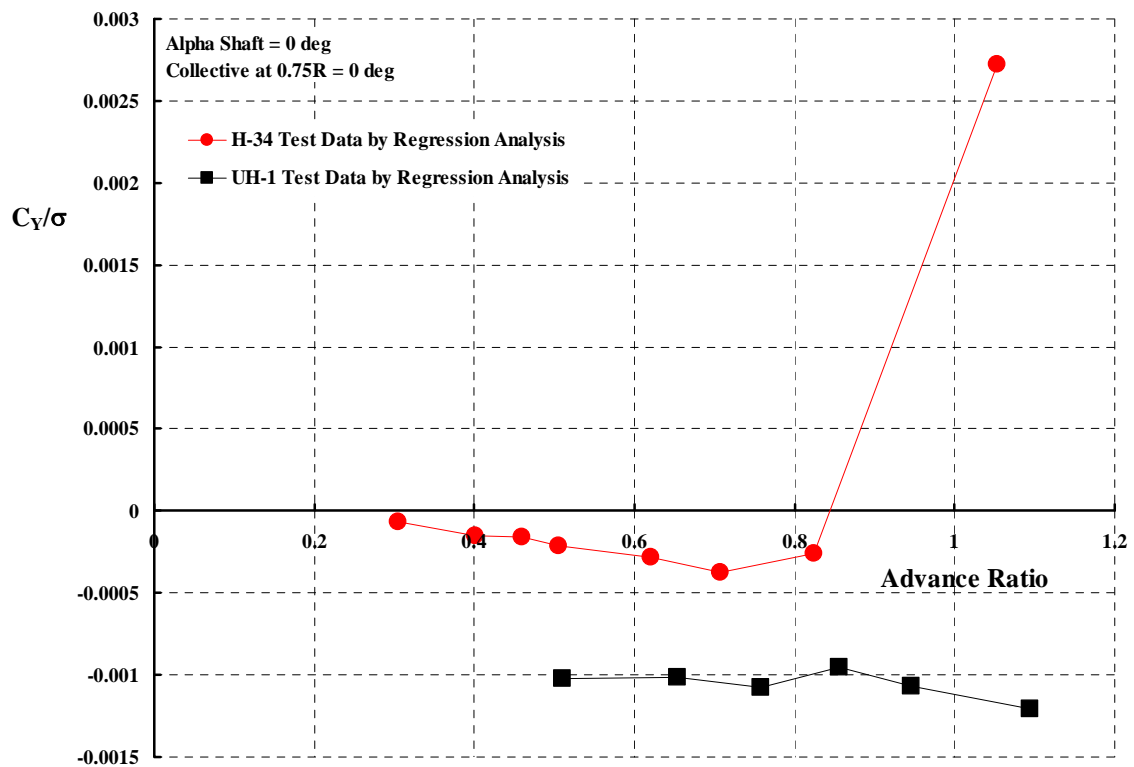


Fig. 5-26. Y-Force at zero shaft angle of attack and zero collective pitch at $\frac{3}{4}$ R.

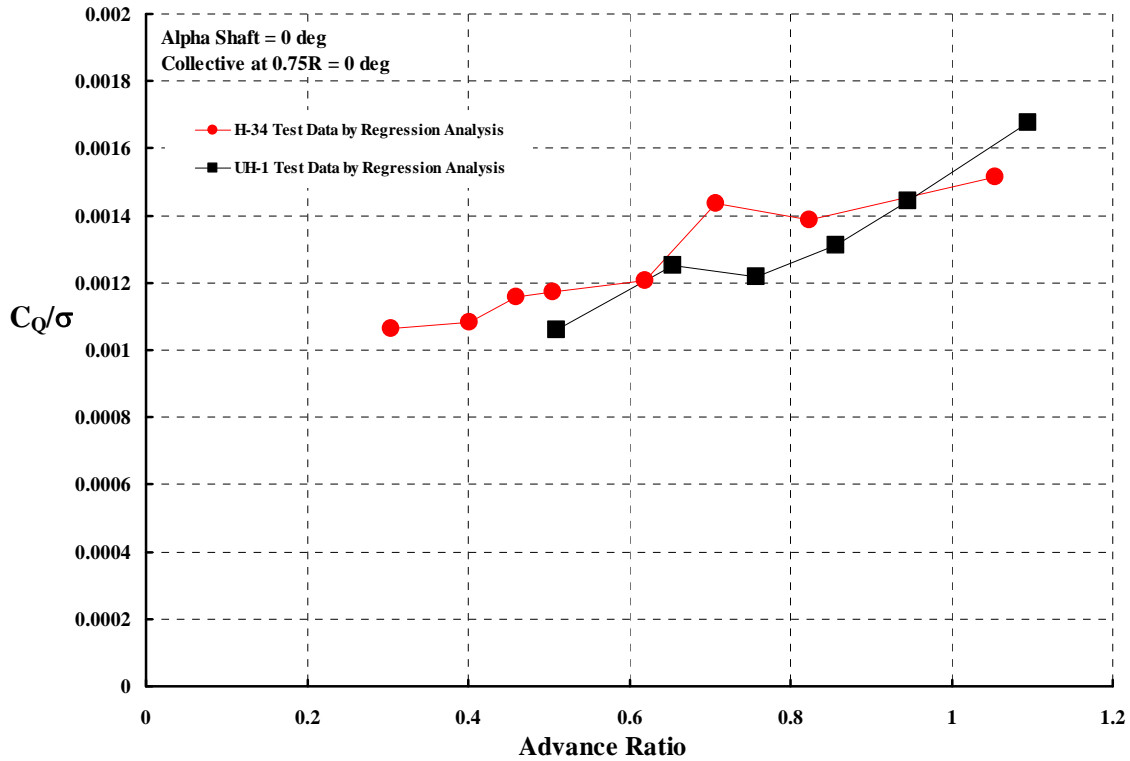


Fig. 5-27. Torque at zero shaft angle of attack and zero collective pitch at $\frac{3}{4}$ R.

5.4.2 Obtaining Lift and Controlling Flapping

Obtaining rotor lift and controlling flapping present serious problems for high speed compound helicopters. Excessive longitudinal flapping, to pick just one example, can create unacceptable vibration and excessive blade loads. Both H-34 and UH-1 experimental data quantify two undesirable behaviors of the typical helicopter rotor when operated at high advance ratio.

The most undesirable behavior is that the rotor lift becomes non-responsive to a collective pitch input at advance ratios near 1.0 – *if the rotor blade flapping is zeroed out by cyclic control*. The magnitude of the problem is quickly seen from the regression collective constant in Table 3 (on page 66 for the H-34) and Table 10 (on page 73 for the UH-1) and is more startling when Fig. 5-28 is viewed. The data indicate that in the advance ratio range of 0.9 to 1.0 there is a control reversal. At advance ratios below 0.9 an increase in collective pitch will increase rotor lift, but at advance ratios above 1.0 an increase in collective pitch reduces lift. Keep in mind that any change in collective pitch causes a change in flapping so that a change in longitudinal cyclic to zero out flapping must accompany the collective pitch change.

At fixed collective pitch, the rotor behaves (in a sense) like a normal wing in that the rotor's lift curve slope is always positive. This point is brought home by Fig. 5-29. The undesirable trend here is that the rotor becomes increasing gust sensitive as advance ratio increases.

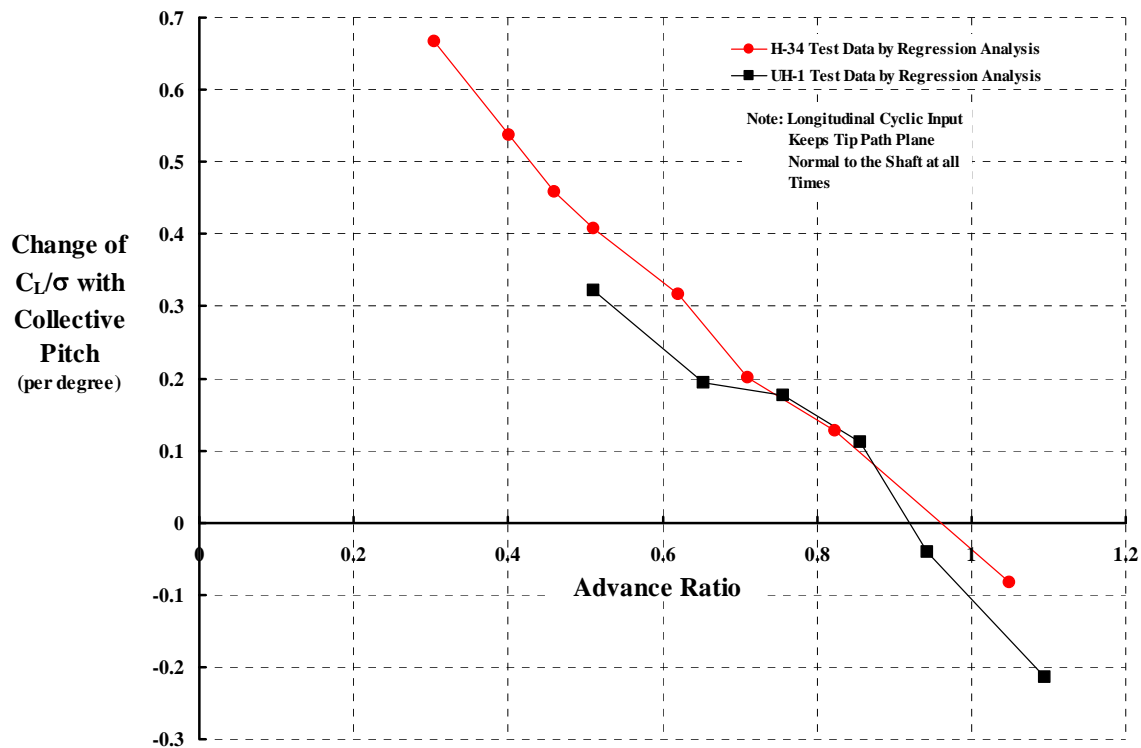


Fig. 5-28. The derivative of lift with collective pitch at fixed shaft angle of attack while holding zero flapping.

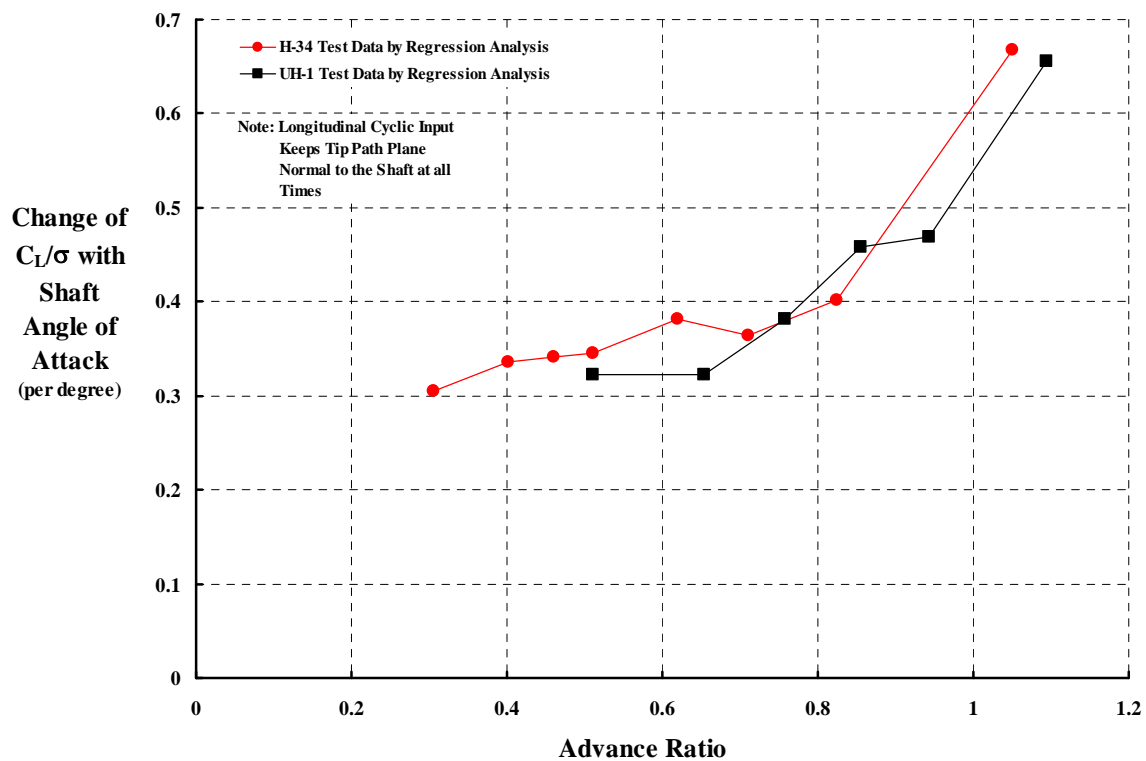


Fig. 5-29. The derivative of lift with shaft angle of attack at fixed collective pitch while holding zero flapping.

The unfavorable trend in $\Delta C_L/\sigma$ due to a $\Delta\theta$ at constant tip path plane angle of attack was first reported by Larry Jenkins in 1965 [63]. His facts were based upon experimental data obtained with a two-bladed, 15.5 foot diameter, and teetering hub rotor system. The test was conducted in the NASA Langley 30 foot by 60 foot wind tunnel. Jenkins used rather simple theory to show that the measured rotor behavior was quite predictable. Harris [9, 10] explored the high advance trends in greater detail.

The simple physics of how the reverse flow region creates this unique conventional rotor thrust characteristic is rather easy to see. Sketch A on Fig. 5-30 shows the velocity diagrams at blade azimuths of 0 and 270 degrees for an advance ratio equal to 1.0. Both regions have exactly the same velocity distributions. Unfortunately, the reverse flow region has the velocity approaching the airfoil's trailing edge.

First, consider the 0 degree azimuth position and the blade element velocity and angle of attack diagram shown on Fig. 5-30, Sketch B. The flow approaches the airfoil leading edge. The blade element is at a positive angle of attack and an increase in collective pitch increases the thrust at the 0 degree azimuth position. Now, consider the root of the blade in the azimuth position of 270 degree as shown by Sketch C on Fig. 5-30. A positive increase in collective pitch will provide a thrust download. At an advance ratio of 1.0, these thrust increments at these two azimuth positions approximately cancel for a positive increase in collective pitch. For a rotor in both rolling and pitching equilibrium, (such as teetering or flapping or articulated rotor system or even a propeller with correct cyclic inputs) the azimuth positions of 90° and 180° have about the same symmetry. *Thus the net effect of a positive change in collective pitch is no change in thrust.* From this discussion, it is clear that the primary culprit in this unusual, conventional rotor characteristic at advance ratios approaching 1.0 is simply (1) the reverse flow region, (2) the velocity orientation in this region, and (3) the ability of airfoils to produce lift proportional to angle of attack in this environment. The accomplice is the statement that the rotor is in at least roll equilibrium.

This rotor thrust characteristic of the conventional rotor is not obvious if the problem is studied in the shaft axis reference system. However, it becomes eminently clear if the tip path plane coordinate system is used. The simplest of algebra that combines the rotor thrust and rolling moment equations can be used to quantify the situation. Consider a set of untwisted blades that have zero root cut out, ignore the concept of a tip loss factor, and assume uniform induced velocity. The rotor thrust and rolling moment equations in steady flight reduce to:

$$\frac{2C_T}{\sigma a} = \lambda_{\text{tip}} \left[\frac{1}{2} + \frac{1}{4} \mu^2 \right] + \theta_o \left[\frac{1}{3} + \frac{1}{2} \mu^2 - \frac{4}{9\pi} \mu^3 \right] - (B_{\text{IC}} + a_{\text{IS}}) \left[\frac{1}{2} \mu + \frac{1}{8} \mu^3 \right]$$

$$\frac{2C_{\text{Roll}}}{\sigma a} = \lambda_{\text{tip}} \left[\frac{1}{4} \mu - \frac{1}{16} \mu^3 \right] + \theta_o \left[\frac{1}{3} \mu + \frac{4}{45\pi} \mu^4 \right] - (B_{\text{IC}} + a_{\text{IS}}) \left[\frac{1}{8} + \frac{3}{16} \mu^2 - \frac{5}{192} \mu^4 \right]$$

It is important at this intermittent point not to jump to the conclusion that the change in thrust with collective pitch is simply proportional to $(1/3 + \mu^2/2 - 4\mu^3/9\pi)$ which does not go to zero until the advance ratio approaches 3.7. That thought process ignores the

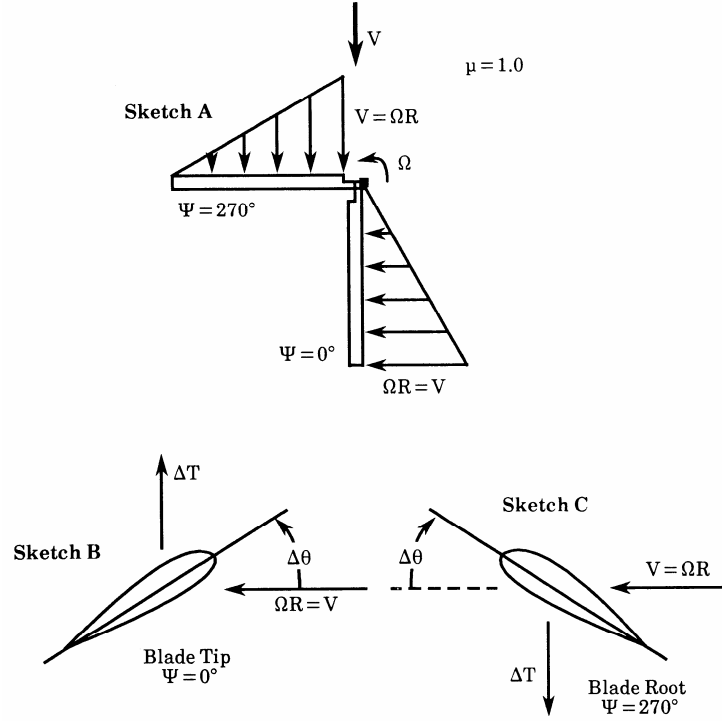


Fig. 5-30. The aerodynamics of rotor thrust near $\mu = 1$.

requirement that the rotor disc not roll over and the fact that $(B_{1C} + a_{1S})$ must change as θ_o is changed to ensure the roll equilibrium.

When the requirement for rolling moment equilibrium of the rotor disc is imposed (i.e., $2C_{ROLL}/\sigma a = 0$), then the required cyclic feathering in the tip path plane $(B_{1C} + a_{1S})$ to obtain this zero rolling moment is uniquely defined in terms of μ , λ_{tp} , and θ_o , as

$$(B_{1C} + a_{1S}) = \frac{\lambda_{tp} \left[\frac{1}{4}\mu - \frac{1}{16}\mu^3 \right] + \theta_o \left[\frac{1}{3}\mu + \frac{4}{45\pi}\mu^4 \right]}{\left[\frac{1}{8} + \frac{3}{16}\mu^2 - \frac{5}{192}\mu^4 \right]} = \frac{\lambda_{tp} \left[2\mu - \frac{1}{2}\mu^3 \right] + \theta_o \left[\frac{8}{3}\mu + \frac{32}{45\pi}\mu^4 \right]}{\left[1 + \frac{3}{2}\mu^2 - \frac{5}{24}\mu^4 \right]}$$

Note that this simple expression says that problems in controlling rotor flapping can be expected when the term $(1 + 3\mu^2/2 - 5\mu^4/24)$ goes to zero. This situation arises near $\mu = 2.8$. This resulting expression for $(B_{1C} + a_{1S})$ can then be imposed on the rotor thrust equation by direct substitution. The result of this algebraic substitution is a thrust equation that is linear in collective pitch and tip path plane inflow as follows:

$$\frac{2C_T}{\sigma a} = \frac{1}{3}\theta_o \left[\frac{1 - \mu^2 - \frac{4}{3\pi}\mu^3 + \frac{25}{24}\mu^4 - \frac{46}{15\pi}\mu^5 - \frac{5}{16}\mu^6 + \frac{1}{90\pi}\mu^7}{1 + \frac{3}{2}\mu^2 - \frac{5}{24}\mu^4} \right] + \frac{1}{2}\lambda_{tp} \left[\frac{1 + \frac{13}{24}\mu^4 + \frac{1}{48}\mu^6}{1 + \frac{3}{2}\mu^2 - \frac{5}{24}\mu^4} \right]$$

It is the partial derivative of $2C_T/\sigma a$ with respect to θ_o that goes to zero when the advance ratio is about 0.85.

This fundamental rotor thrust characteristic (due to reverse flow) presents an apparently insurmountable barrier to very, very high speed helicopters equipped with conventional rotor blades. Considering that the pure helicopter needs a forward component of thrust to propel itself (i.e., a positive C_X/σ), a logical situation exists:

$$\begin{aligned} \text{if} \quad & C_T/\sigma = [\text{ZERO}]\theta_o + \left[\frac{\partial C_T/\sigma}{\partial \alpha_{\text{tp}}} \right] \alpha_{\text{tp}} \\ \text{as} \quad & \mu \quad \text{approaches} \quad 1 \\ \text{and} \quad & C_X/\sigma \quad \text{is dominated by} \quad -(C_T/\sigma)(\alpha_{\text{tp}}) \\ \text{then} \quad & C_X/\sigma \quad \text{acts like} \quad - \left[\frac{\partial C_T/\sigma}{\partial \alpha_{\text{tp}}} \right] (\alpha_{\text{tp}})^2 \end{aligned}$$

In short, if helicopter propulsion requires a forward tilt of the tip path plane (i.e., a negative α_{tp}) then the rotor thrust goes negative and no propulsive force is obtained.

The amount of cyclic control required to maintain the rotor at zero flapping shows that there is no reversal in the derivatives of cyclic with collective or with shaft angle of attack. This fact is established by Fig. 5-31 and Fig. 5-32. Furthermore, the control is quite positive at all advance ratios up to 1.0. Of course, at zero advance ratio both derivatives are theoretically zero. At high advance ratio, the cyclic control becomes very sensitive. At “extreme” advance ratios rotor flapping instabilities are to be expected.

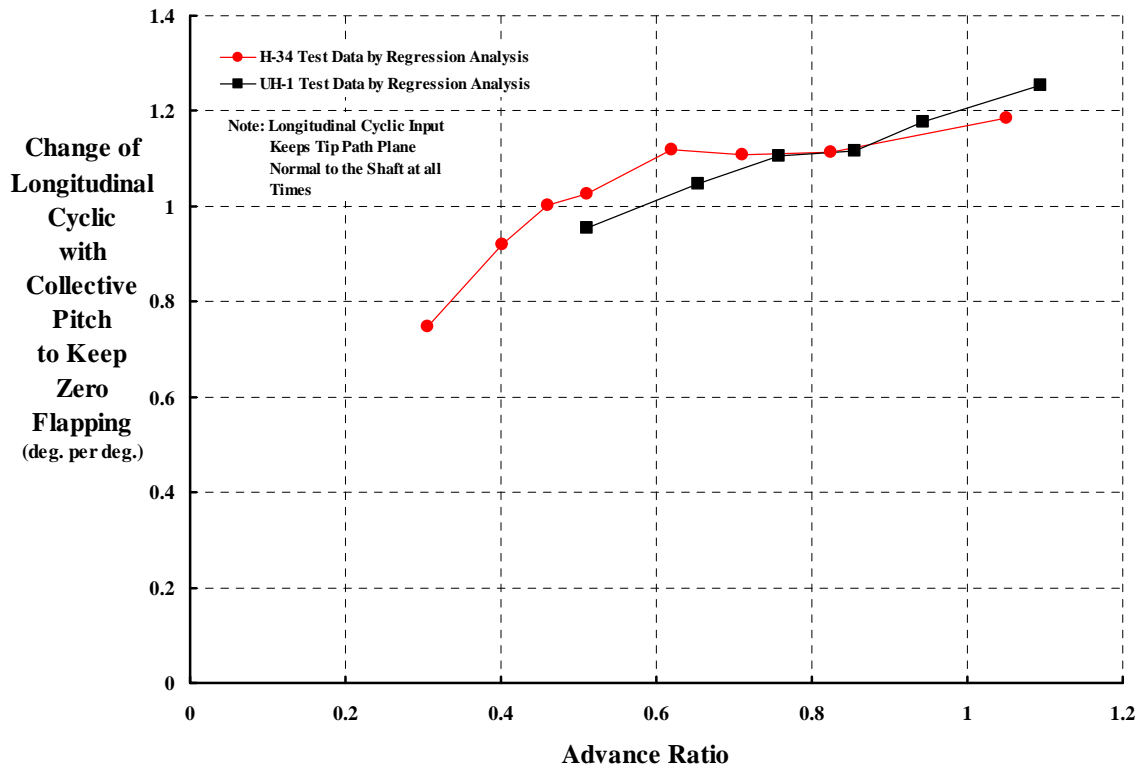


Fig. 5-31. The derivative of longitudinal cyclic with collective pitch to maintain zero flapping.

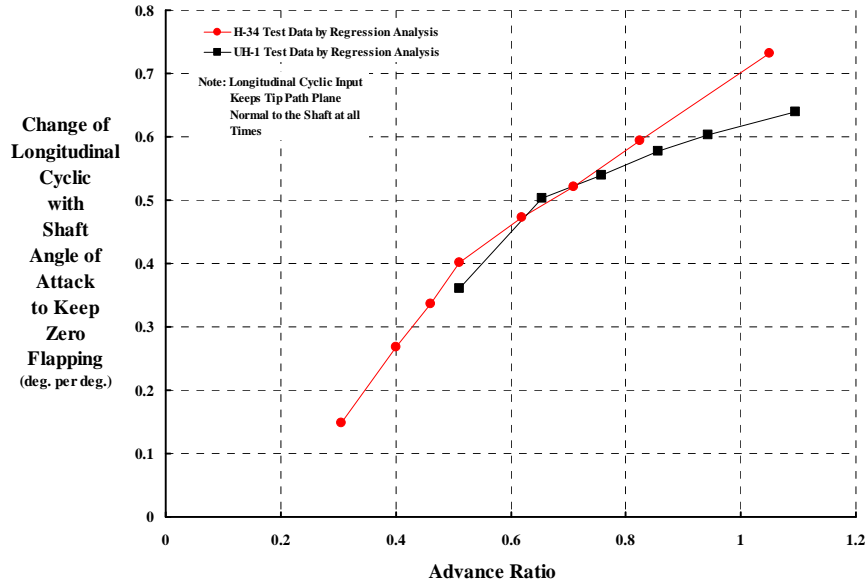


Fig. 5-32. The derivative of longitudinal cyclic with shaft angle of attack to maintain zero flapping.

5.4.3 Blade Stall

The characteristic stall seen at helicopter advance ratios (as shown with Fig. 5-4) is not as clearly evident at high advance ratios. In particular, the UH-1 data at an advance ratio of 1.1 shows that this rotor has a linear lift curve all the way up to $C_L/\sigma = 0.1$ as observed with Fig. 5-33. Furthermore, there is no evidence that the effective drag coefficient, C_{De}/σ , has other than a simple parabolic drag polar. An explanation of this “no stall” behavior is not currently available.

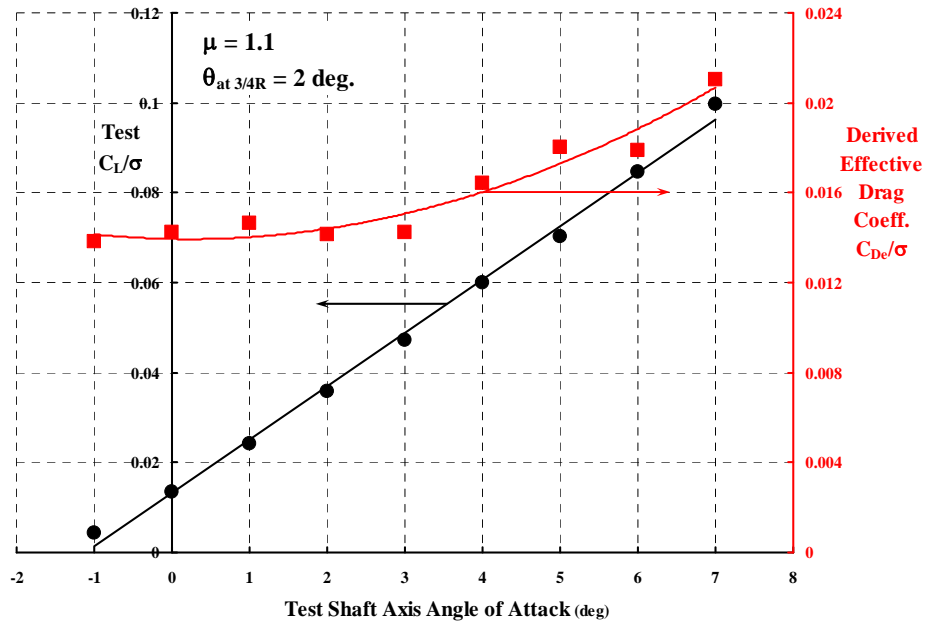


Fig. 5-33. There is little evidence of classical blade stall in this $\mu = 1.1$, UH-1 data.

6 THEORY VERSUS TEST OVERVIEW

The object of this investigation has been to compare theory with available test data at high advance ratio. Five analyses, representative of the state of the art in 2008, have been chosen to compare to experimental data obtained with 3 full scale rotors. This represents a matrix of 15 possible combinations to ultimately be examined in detail. The investigation to date has been able to complete 8 of the possible combinations and initiate a partial completion of a 9th and a 10th.

As a prelude to the detailed results provided in the next chapter, this overview compares Wheatley/Bailey theory of the late 1930s and the comprehensive code CAMRAD II of 2008 to the H-34 experimental obtained in 1965. This overview of theoretical progress after 7 decades, helped by the invention of the digital computer, is very impressive as the reader will see in the following paragraphs. Eight rotor aerodynamic properties of the H-34 are evaluated, the eight parameters being:

Longitudinal and lateral controls, B_{1C} and A_{1C}
Lift, drag, side force and power, C_L/σ , C_D/σ , C_Y/σ and C_Q/σ
Effective drag, C_{DE}/σ
Lift to effective drag ratio, L/D_E

6.1 Evaluation Method

To this author's knowledge virtually all past theory/test correlation reports and papers have presented their results with the vertical axis in a typical graph as an output parameter and the horizontal axis as the input parameter. An example of these past efforts is rotor lift plotted versus collective pitch holding advance ratio and shaft angle of attack constant. Such graphs as shown with Fig. 6-1 through Fig. 6-4 would be representative of "correlation" in past decades. Qualitative terms to describe the correlation have varied, but "good", "fair", "satisfactory", etc. were commonly used. Sometimes "unbelievably good" has been put forth.

A facet of these past correlations is apparent in the four figures under study here. The computations were made using test collective pitch as the input and holding other input (the test advance ratio and test shaft angle of attack) constant. This ground rule puts the Wheatley & Bailey theory in a "very bad light" because this vintage 1930s does not accurately predict the rotor lift at zero collective pitch as Fig. 6-1 shows. Because the Wheatley & Bailey theory seems to have accurately captured the test's data slope, there is a natural urge to slide the calculated curve over to the left, about 1/2 degree along the collective pitch axis. Most past investigators have resisted this urge. Instead, the computations are presented using the rotor lift coefficient as the abscissa instead of collective pitch (in this example). The fact that the rotor lift versus collective pitch is in "poor agreement" is charged off as experimental error.

To illustrate how the comparison looks when the abscissa is changed to rotor lift,

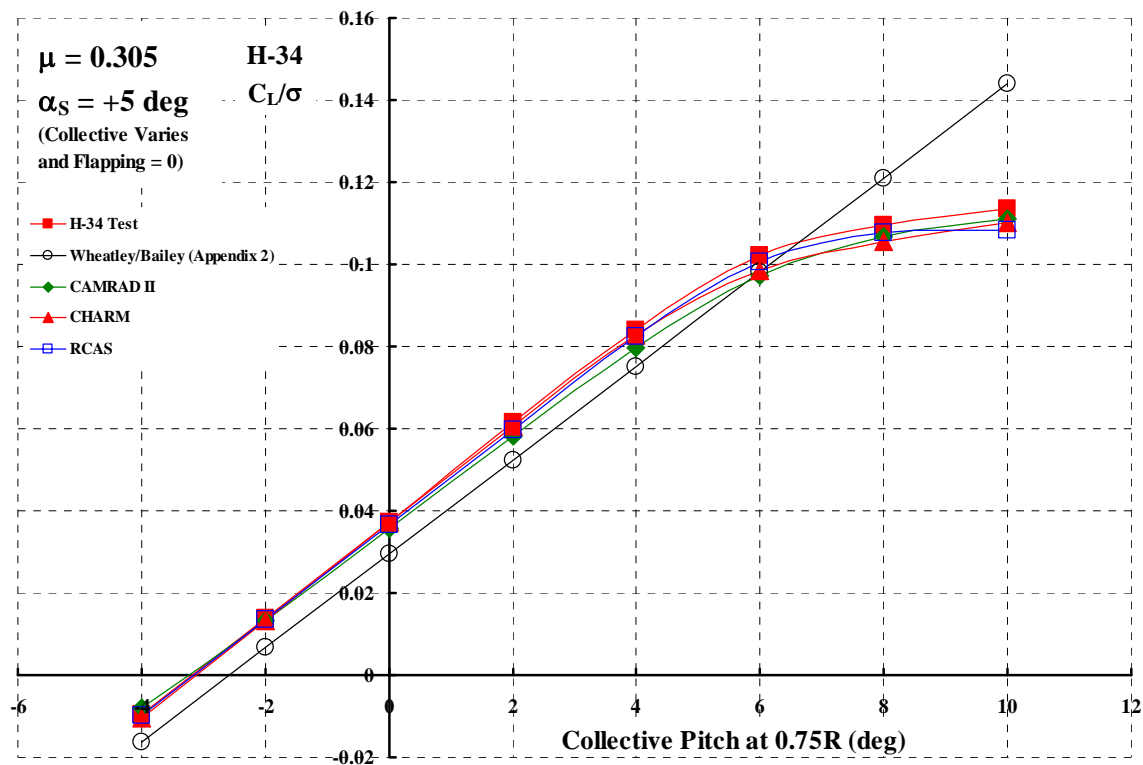


Fig. 6-1. Correlation of rotor lift coefficient with collective pitch.

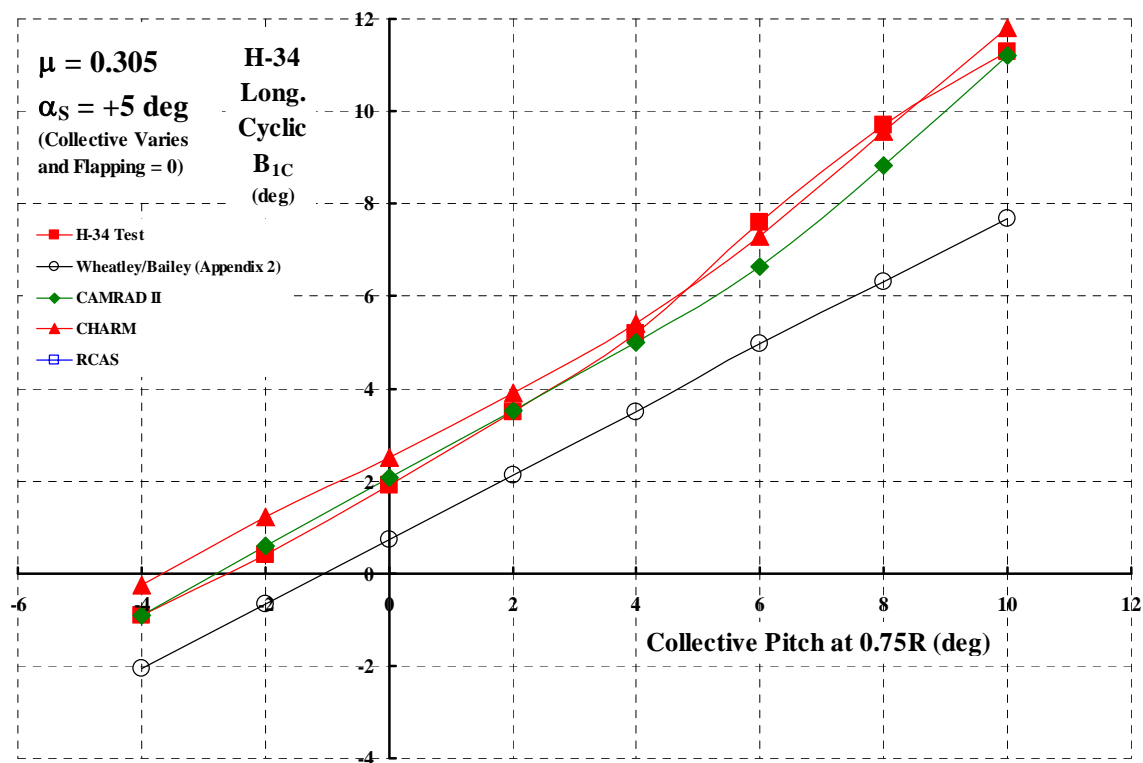


Fig. 6-2. Correlation of longitudinal cyclic with collective pitch.

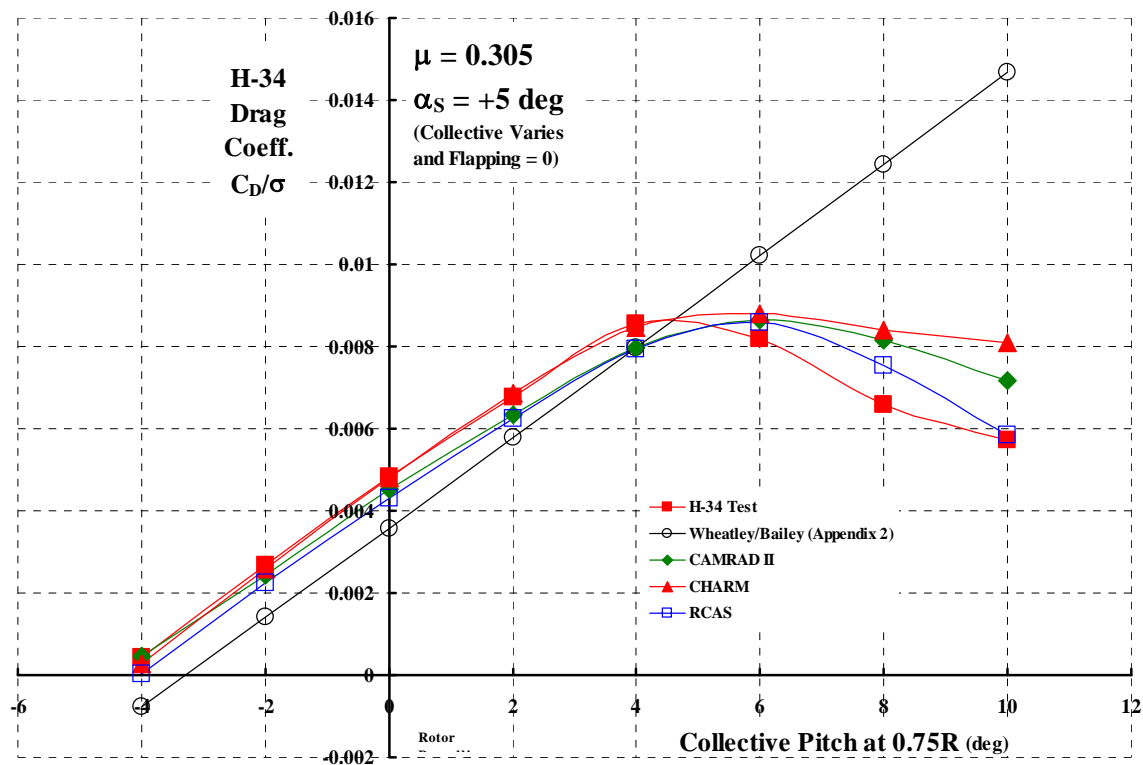


Fig. 6-3. Correlation of rotor drag coefficient with collective pitch.

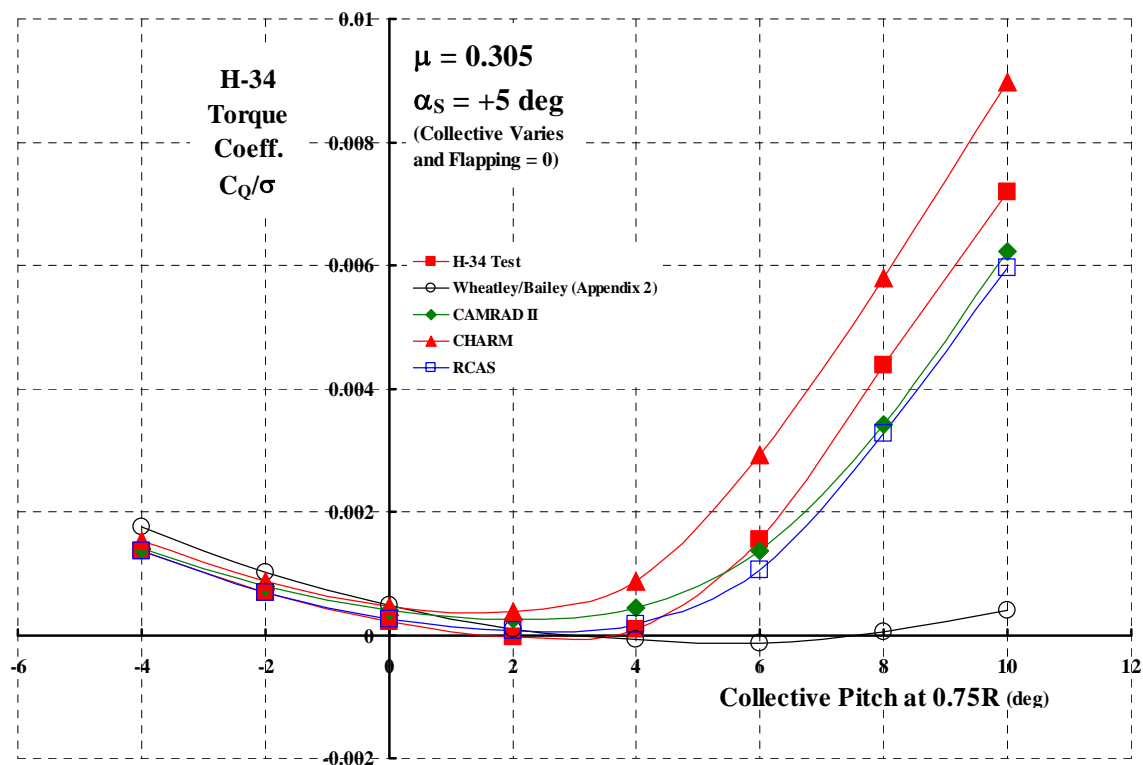


Fig. 6-4. Correlation of rotor torque coefficient with collective pitch.

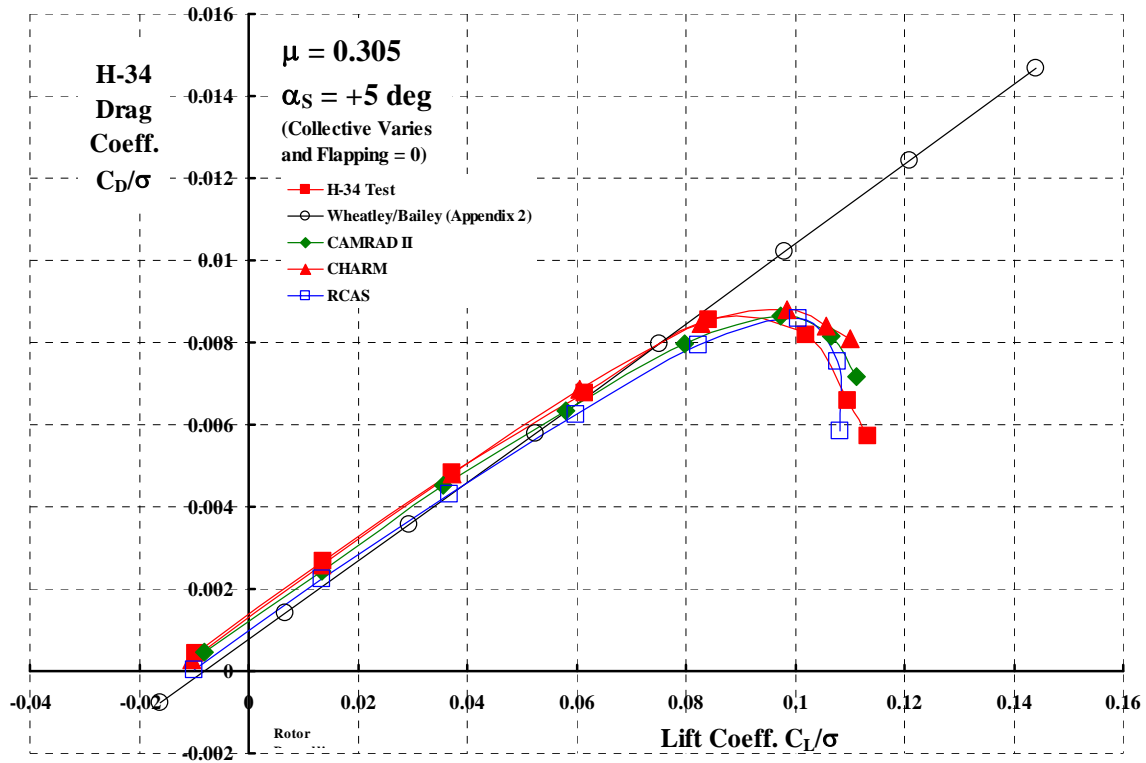


Fig. 6-5. Correlation of rotor drag coefficient with rotor lift coefficient.

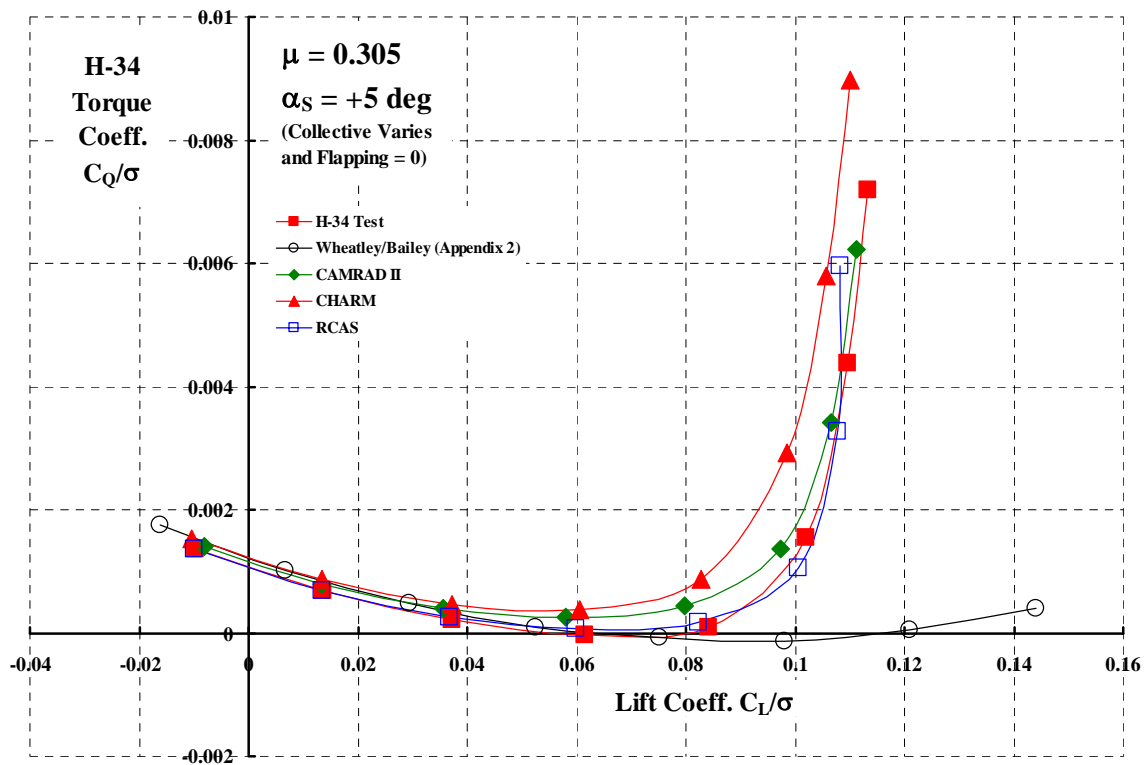


Fig. 6-6. Correlation of rotor torque coefficient with rotor lift coefficient.

consider the drag coefficient as shown with Fig. 6-3 versus Fig. 6-5. Now the theories that account for blade stall (which the Wheatley & Bailey theory clearly does not) are bunched more closely around the test data. This is also true for the torque coefficient when Fig. 6-4 and Fig. 6-6 are compared. However, no quantitative measure of any theory's error is immediately conveyed by the above five figures.

Considering the preceding discussion, a different tack is taken in this investigation. The approach is to graph the test parameter on the ordinate and the theory's calculated value on the abscissa. Furthermore, the calculations are made at the test values of shaft angle of attack, collective pitch, tip speed and tunnel speed. Standard day at sea level atmospheric conditions are assumed because actual test conditions were not reported. However, both wind tunnels in which the rotors were tested are basically at sea level. This approach can be summarized rather simply; if $F = ma$ is the problem then F can be plotted versus ma and the graph should give a straight line of the class $y = x$, which would have a 45 degree slope and pass through zero/zero. Just as simply, if a test value of F and a theory value of F are under study, then the test value can be plotted versus the calculated F . A linear regression analysis will then provide a result of the form $y = Ax + B$ and the coefficients A and B become a quantitative measure of the theory's capability. This capability is, in effect, a measure of how well the theory is performing.

To illustrate this evaluation method, consider Fig. 6-7, where the test value of rotor lift coefficient (C_L/σ) is plotted versus any given theory's prediction of rotor lift coefficient. The Wheatley/Bailey theory's inability to capture blade stall leads to a considerable over prediction of lift as the top three grayed in circles suggest. However, the linear regression of the Wheatley/Bailey theory lift coefficient points at and below $C_L/\sigma = 0.085$ yields the result that

$$y = \text{Test } \frac{C_L}{\sigma} = 1.03514 \left(\text{Theory } \frac{C_L}{\sigma} = x \right) + 0.006993, R^2 = 0.999944$$

which says the lift curve slope is under predicted by about 3.5 percent (very encouraging), but the intercept of +0.006993 is very discouraging. The correlation constant of $R^2 = 0.999944$ (four 9's) says that the regression analysis has extremely high confidence that it is right. *However, the gray symbols connected by the dashed line have not been included in the regression analysis, a fact to keep in mind when reviewing the next several charts.*

The interpretation of CAMRAD II, CHARM and RCAS theories is even more straight forward. The three analyses under predict lift curve slope, but, very encouragingly, the analyses have virtually zero intercept. And, of immense importance, the three analyses make accurate calculations – *with respect to rotor lift* – when there is substantial blade stall as Fig. 6-7 shows.

In a similar manner, the assessment of longitudinal cyclic with Fig. 6-8 immediately points out that all three analyses under predict the amount of longitudinal cyclic required to trim the tip path plane normal to the shaft (i.e., zero out once per rev

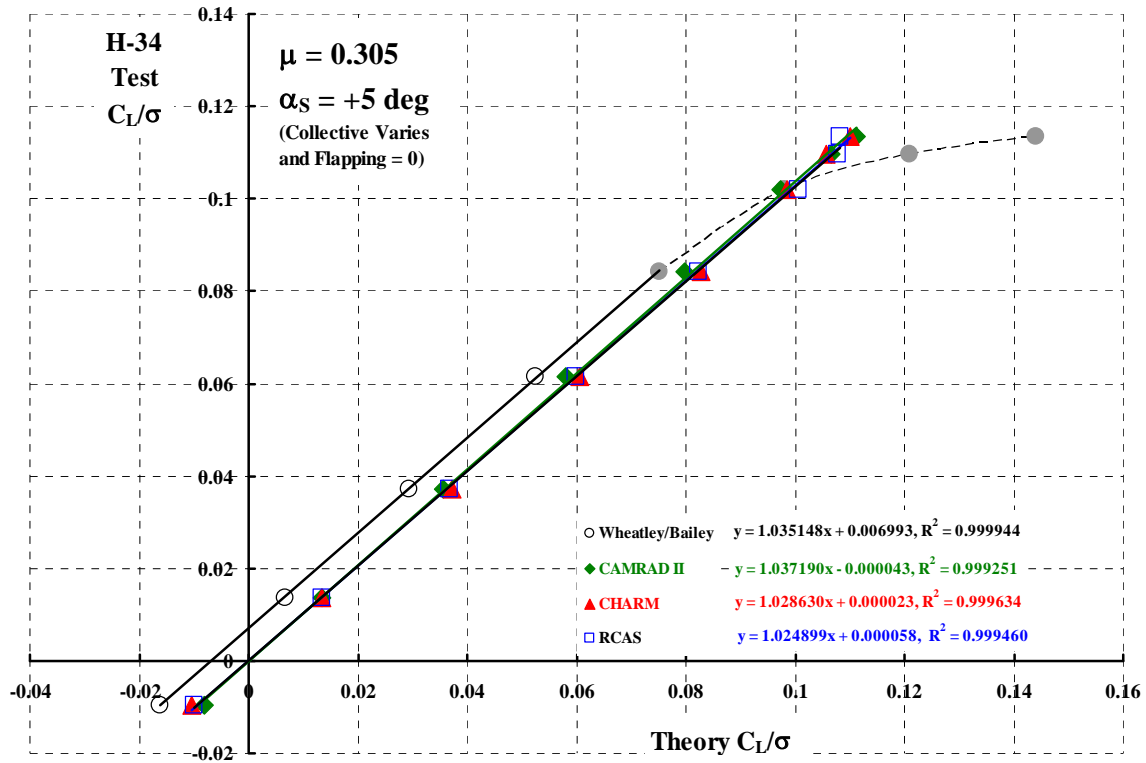


Fig. 6-7. Test versus theory for lift

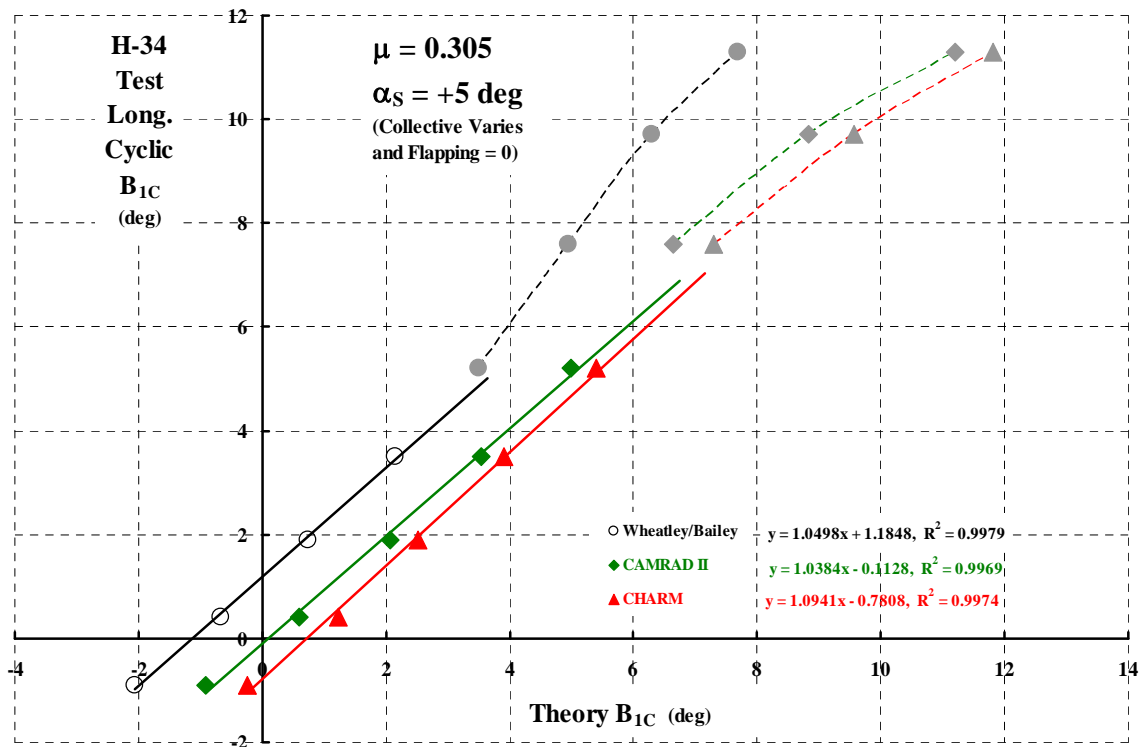


Fig. 6-8. Test versus theory for longitudinal cyclic

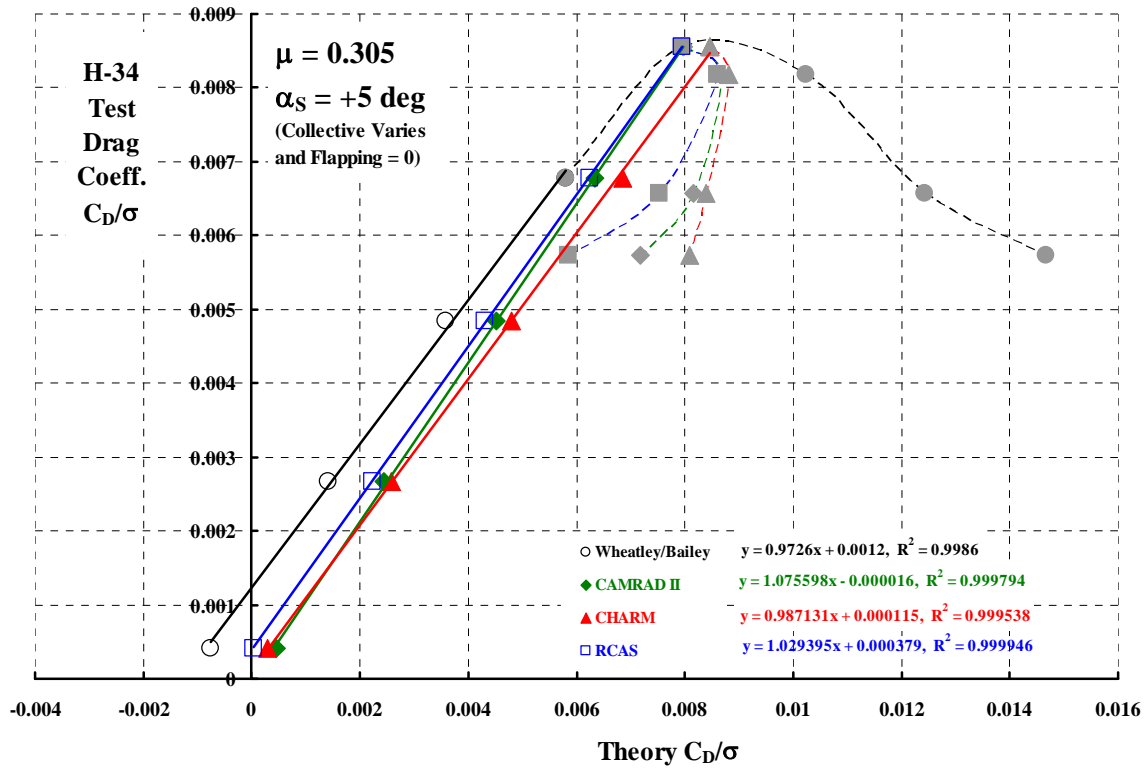


Fig. 6-9. Test versus theory for drag coefficient.

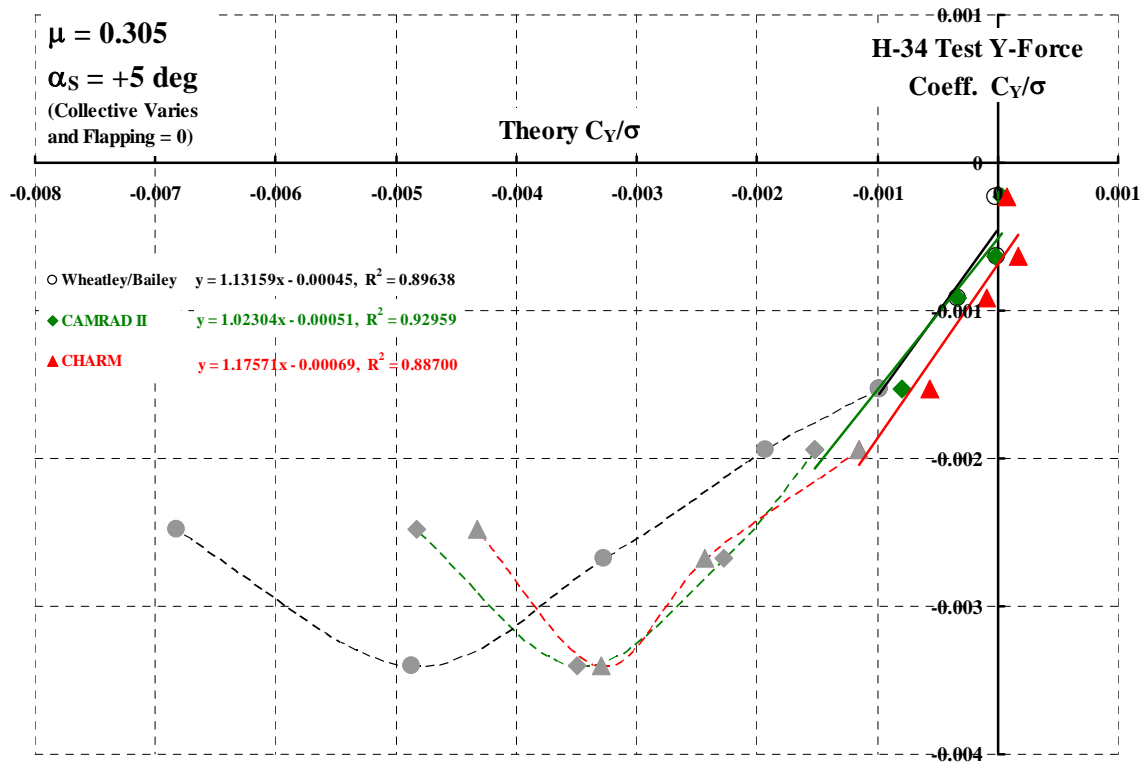


Fig. 6-10. Test versus theory for side force coefficient.

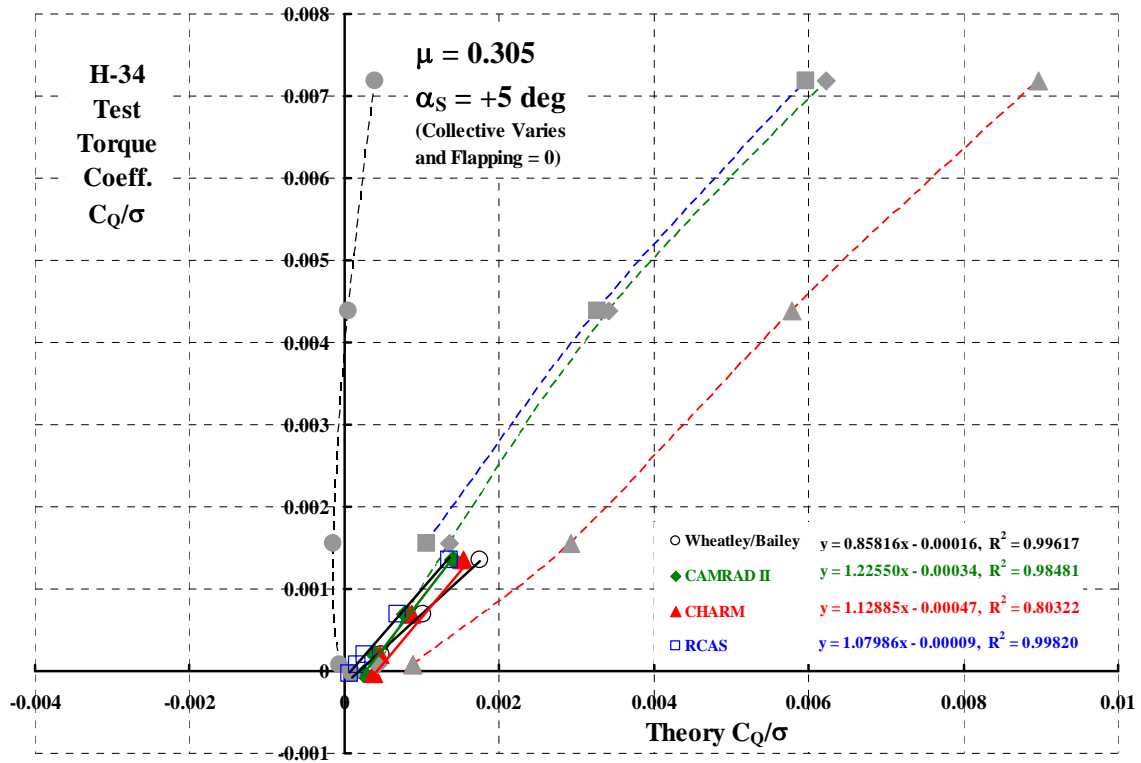


Fig. 6-11. Test versus theory for torque coefficient.

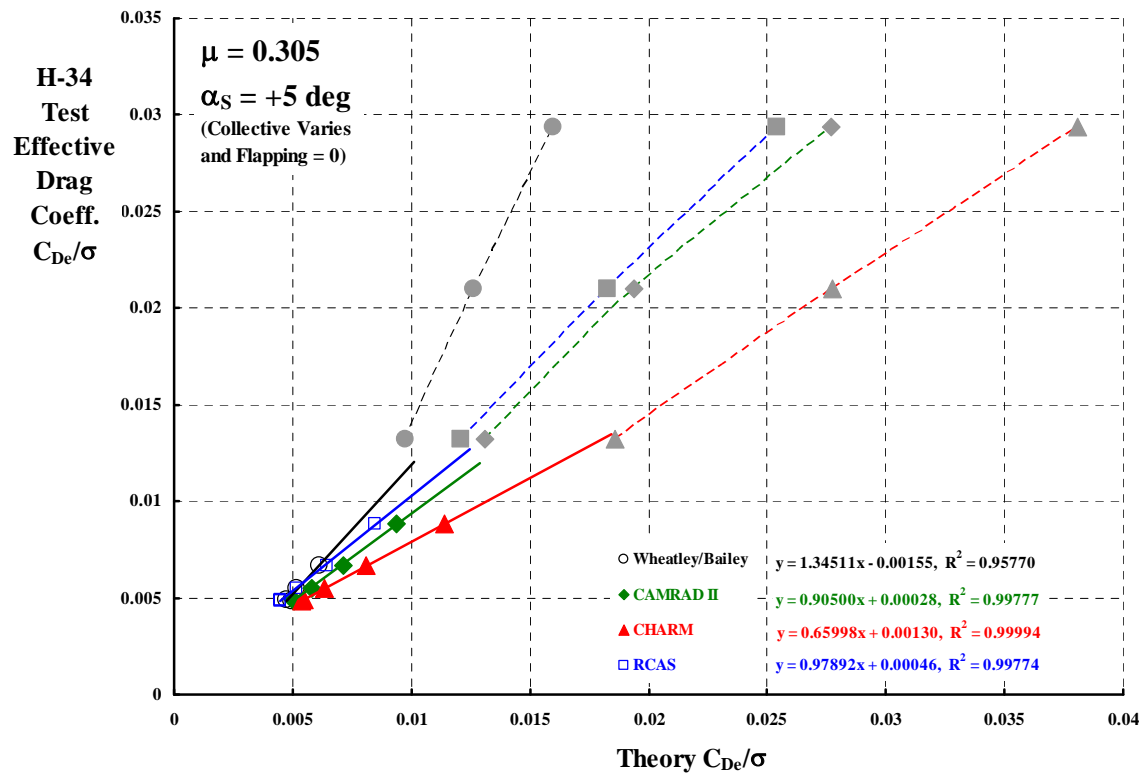


Fig. 6-12. Test versus theory for effective drag coefficient.

flapping) by roughly 5 to 6 percent. Only CAMRAD II predicts the zero-zero intercept. The Wheatley/Bailey theory under predicts the intercept by slightly more than 1 degree and CHARM over predicts by slightly over 0.6 degree. Note that the correlation constant has dropped from R^2 being four 9s for lift to two 9s for the longitudinal cyclic, which is a less confident solution. Most importantly, the data points above a rotor lift coefficient (C_L/σ) of 0.07 to 0.08 (i.e., the solid gray symbols connected by dashed line) clearly would distort the linear regression analysis result if they were included – given the few number of data points under examination.

6.2 Major Progress

The decades spent by many rotorcraft theoreticians to improve prediction of basic rotor aerodynamic performance has paid off. *That is a major fact this study has uncovered.* At present, the CAMRAD II theory is, perhaps arguably, the most advanced comprehensive code to illustrate this pay off. The progress from the late 1930s through 2008 can be illustrated by ten graphs that compare Wheatley/Bailey and CAMRAD II theories to H-34 (untwisted blades) test data.

The ten graphs, Fig. 6-13 to Fig. 6-22, compare the two theories to all 250 experimental data points. This covers an advance ratio range of 0.305 to 1.05, shaft angles of attack from – 10 degrees to + 10 degrees and collective pitch ranging from – 4 degrees to 13.7 degrees. Of course, the H-34 test data did not capture every combination of the three parameters. However, the 250 experimental data points have provided an economical sample with which to display major progress achieved by the industry.

6.2.1 Cyclic Controls, B_{1C} and A_{1C}

Predicting angle of attack and control positions that create the lift required to sustain an aircraft at a given flight condition is an absolutely fundamental task in aeronautics. In the case of a rotor, the reference angle of attack is measured between the flight velocity and a plane perpendicular to the rotor shaft. The control is collective and cyclic blade pitch angles, which geometrically are described by the equation

$$\theta_{x,\psi} = \theta_o + x\theta_t - B_{1C} \sin \psi - A_{1C} \cos \psi$$

To a pilot, the longitudinal cyclic control, B_{1C} , controls aircraft pitching moment and the lateral control, A_{1C} , controls rolling moment.

The contrast between 1930s Wheatley/Bailey theory and 2008 CAMRAD II theory in predicting cyclic controls required to trim the H-34 rotor tip path plane normal to the shaft – given an advance ratio, a shaft angle of attack and a collective pitch – is shown in Fig. 6-13 and Fig. 6-14. Of the two angles, predicting the longitudinal cyclic is the more pressing engineering problem and Fig. 6-13 shows that enormous progress has been made. What use to be at least a 2 degree error has been reduced to less than a 1/2 degree error. Confidence has increased from an $R^2 = 0.9675$ with Wheatley/Bailey theory

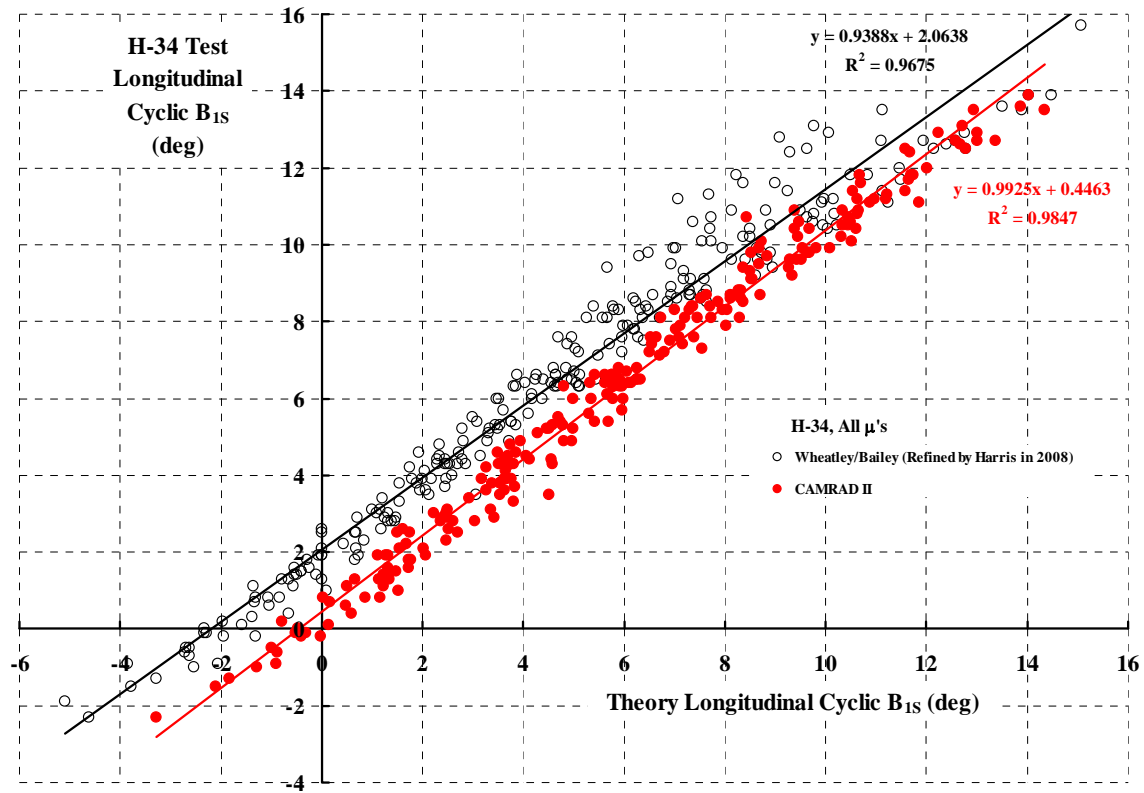


Fig. 6-13. Prediction of H-34 longitudinal cyclic.

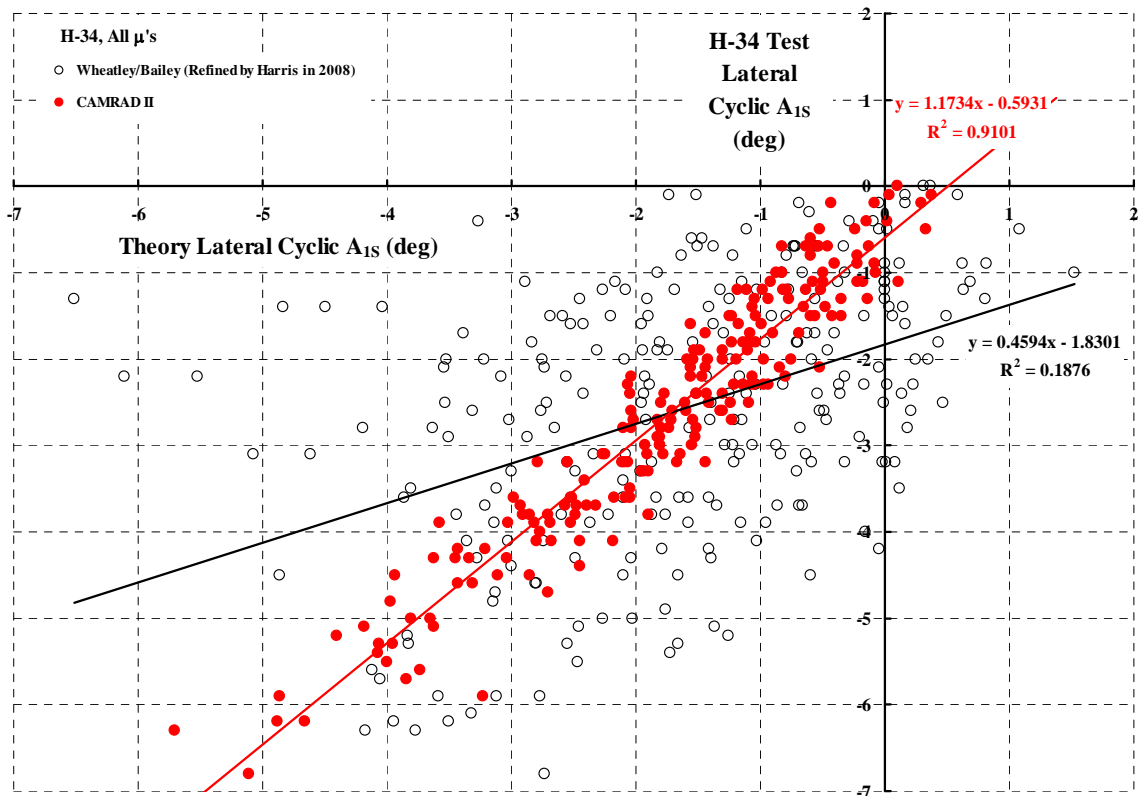


Fig. 6-14. Prediction of H-34 lateral cyclic.

to $R^2 = 0.9847$ with CAMRAD II. And of even greater importance, CAMRAD II is nearly perfect in predicting the slope (0.9925) in comparison to Wheatley/Bailey theory, which shows a 6 percent over prediction (slope = 0.9388).

Predicting lateral cyclic to trim has been a thorn in theoreticians' side since autogyro days. But even with considerable scatter, Fig. 6-14 shows that quite visible progress has been made. Single rotor helicopter engineering has some margin for error in values of lateral cyclic. In contrast, tandem rotor helicopters use differential lateral cyclic for directional control, which means the pedal position to a pilot. The improved prediction of lateral cyclic by CAMRAD II versus Wheatley/Bailey theory is very encouraging, but clearly even this comprehensive code has room for improvement.

6.2.2 Lift Coefficient, C_L/σ

With control positions well predicted for a given advance ratio and shaft angle of attack, the ability to accurately predict the amount of lift a rotor will produce becomes paramount. Fig. 6-15 shows that very gratifying progress in predicting rotor lift has been made since the 1930s. The Wheatley/Bailey theory shows why experimental work was absolutely essential when developing a new helicopter. In contrast, the improvement offered by modern comprehensive codes (in this example CAMRAD II) shows that lift, even with blade stall present, is nearly perfectly predicted, albeit with more scatter than might be hoped for. Of course, an $R^2 = 0.9720$ is too low for such an important parameter and nothing less than an R^2 of 0.99xx should be the goal.

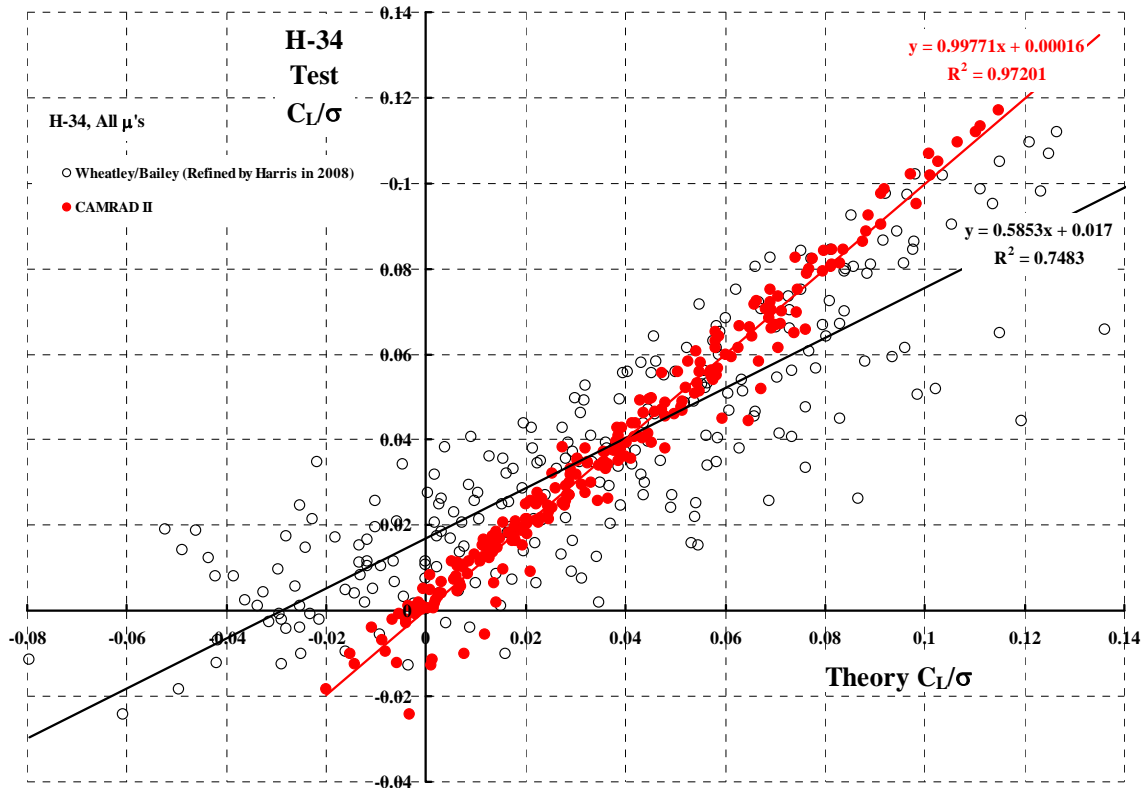


Fig. 6-15. Prediction of lift coefficient.

6.2.3 Drag Coefficient, C_D/σ

The evaluation of how well test and theory agree with respect to rotor drag prediction after nearly 7 decades of investment and effort is shown with Fig. 6-16. The prediction of the rotor drag coefficient by CAMRAD II is rather unsatisfactory as Fig. 6-16 shows. The linear regression analysis slope (0.8174) indicates a serious over estimate of drag (or conversely an under prediction of propulsive force). The error is caused by inaccuracy in the calculation of the rotor H-force. A rotor's drag in the wind axis system is dependent on three shaft oriented parameters as follows:

$$\frac{C_D}{\sigma} = \frac{C_T}{\sigma} \sin \alpha_s + \frac{C_H}{\sigma} \cos \alpha_s$$

The two shaft oriented forces, C_T/σ and C_H/σ , are resolved through the shaft angle of attack, α_s , which for most helicopter, autogyro and compound helicopter configurations is a small angle. In practice, the rotor thrust coefficient C_T/σ is roughly ten times the rotor H-force coefficient, C_H/σ . But because the shaft angle of attack is on the order of 0.1 radians (or less), the contribution of the H-force to overall accuracy can not be ignored. This is obviously true when either thrust or shaft angle of attack is zero, in which case, the H-force is the sole contributor to error.

The theory versus “test” comparisons for the two shaft forces resolved into the wind axis system are provided with Fig. 6-17 and Fig. 6-18. Keep in mind that these two

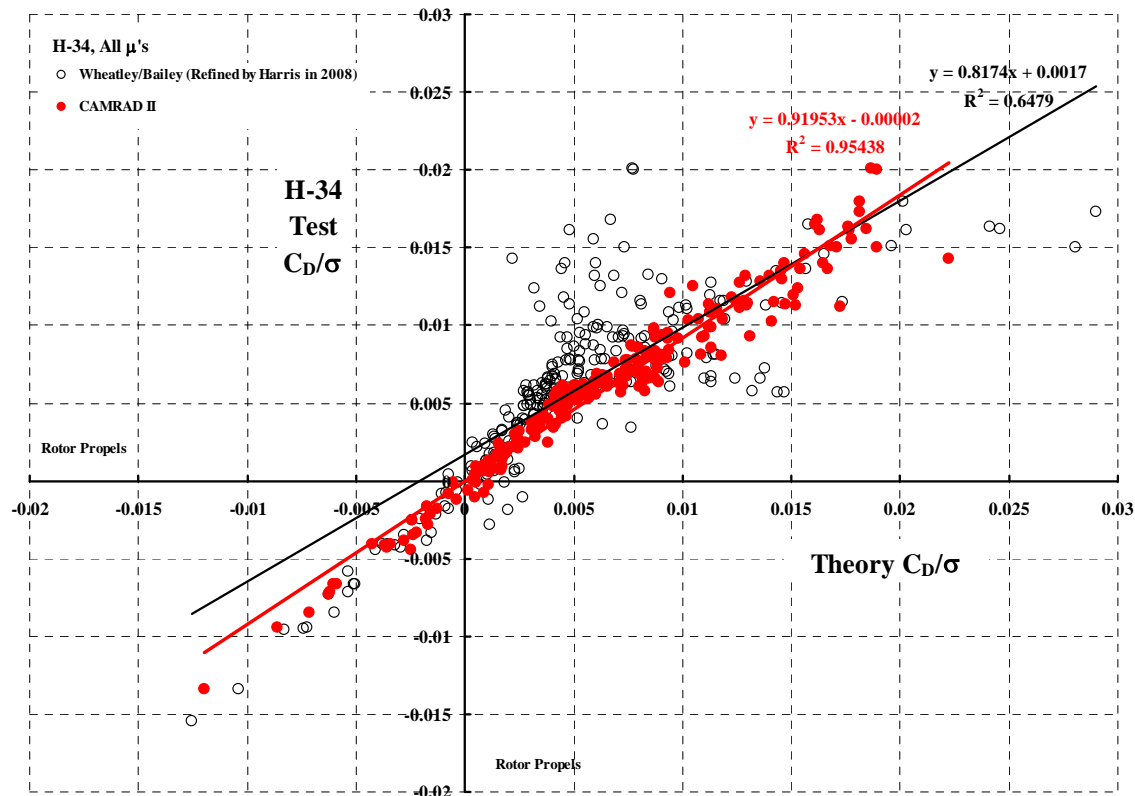


Fig. 6-16. Prediction of drag coefficient.

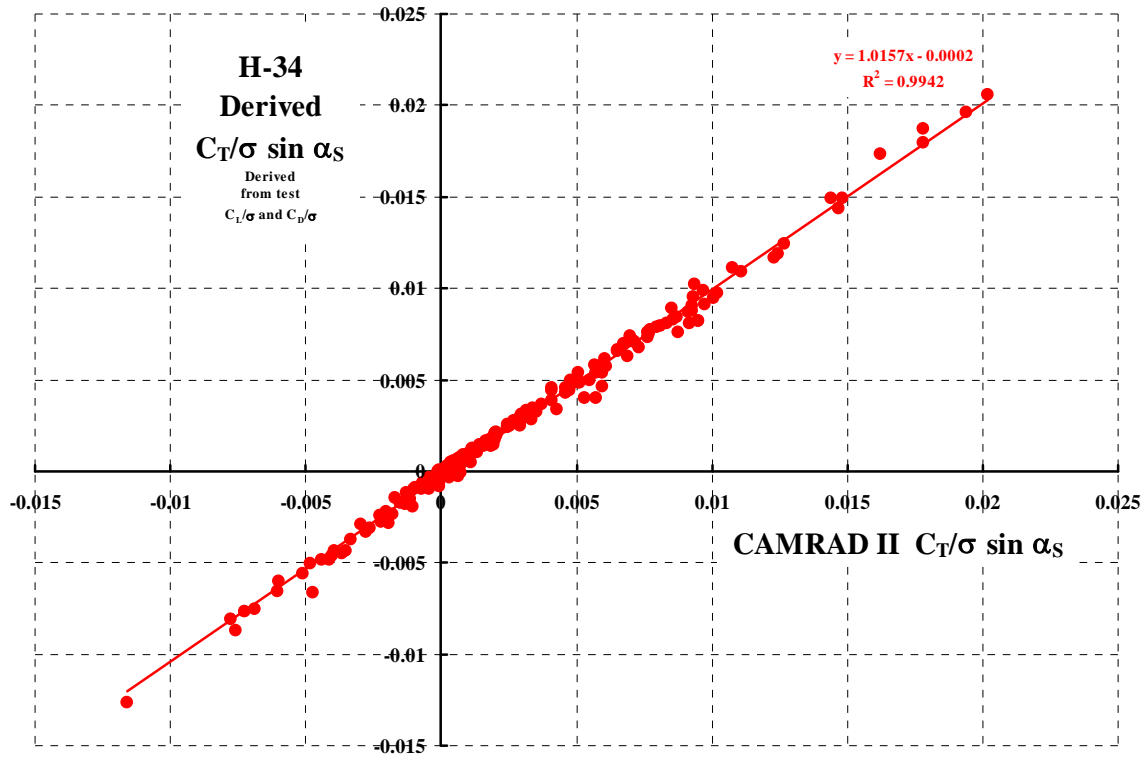


Fig. 6-17. Prediction of thrust contribution to rotor drag.

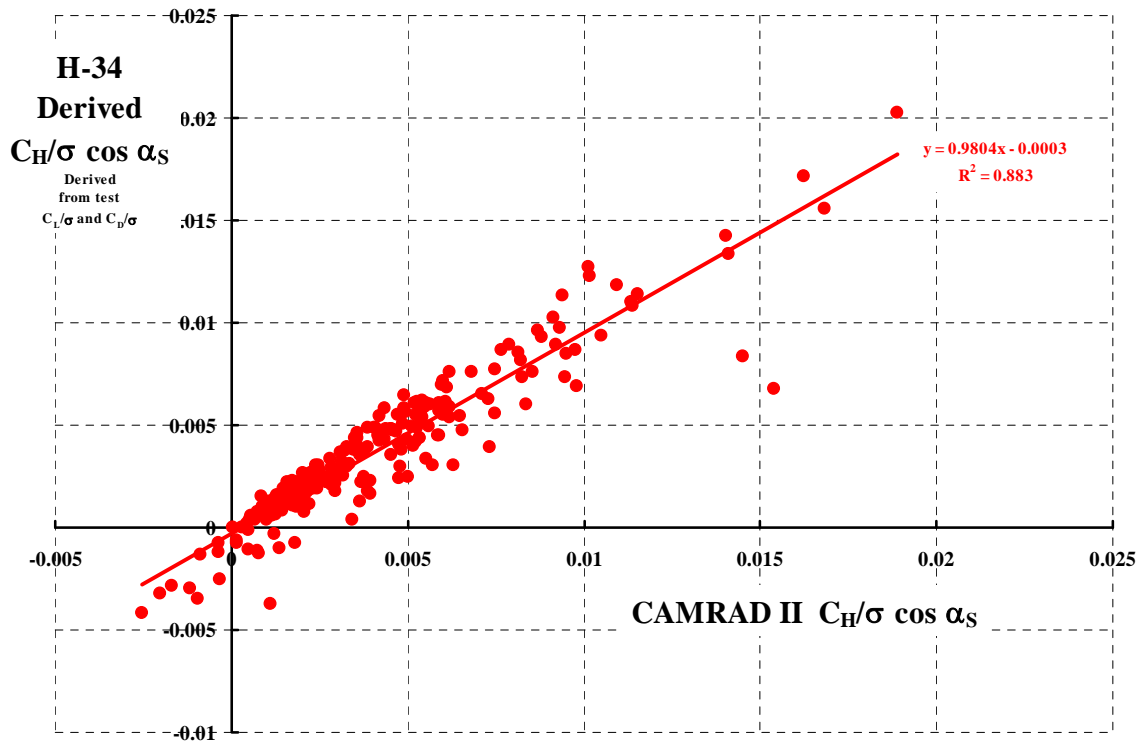


Fig. 6-18. Prediction of H-force contribution to rotor drag.

forces have been derived from the measured wind tunnel wind axis lift and drag, which can mean the difference between two large numbers. In the theories under study, the reverse is true. That is, the theory's calculated C_T/σ and C_H/σ are resolved into the wind axis. According to Fig. 6-17, the thrust contribution to drag – the $C_T/\sigma \sin\alpha_s$ part – is very accurately predicted by CAMRAD II. But unfortunately the H-force contribution to drag – the $C_H/\sigma \cos\alpha_s$ part – has a great deal of scatter, which leads to less than satisfactory prediction of the rotor drag coefficient. Of course, deriving the H-force coefficient from the wind axis experimental data requires the difference of two experimental values having roughly equal – but opposite in sign – quantities.¹¹

6.2.4 Side Force Coefficient, C_Y/σ

No significant progress has been made in predicting the side force coefficient as Fig. 6-19 clearly shows. The primary reason for the lack of progress since Wheatley and Bailey developed the basic theory in the 1930s is that no investigator or theoretician has paid a bit of serious attention to this force. With the tip path plane trimmed normal to the shaft, the side force coefficient is a relatively small force compared to drag and lift. Furthermore, the variation of side force with lateral cyclic has hardly been examined experimentally at any advance ratio.

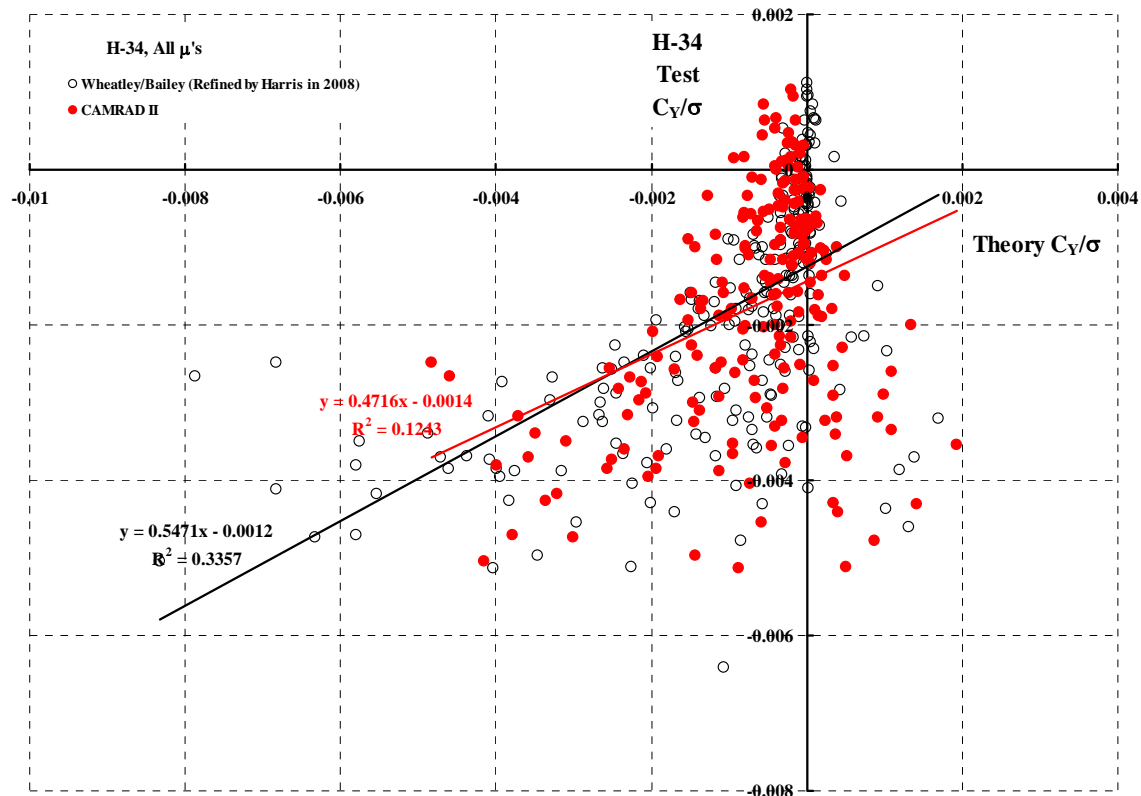


Fig. 6-19. Prediction of Y-force coefficient.

¹¹ Modern rotor testing is accomplished with an internal balance in the shaft axis system and thorough comparisons to the wind axis measurements from the wind tunnel balance are possible.

6.2.5 Torque (or Power) Coefficient, C_Q/σ

The improvement in predicting the torque coefficient, primarily at conditions where blade stall is not encountered, is shown with Fig. 6-20. In contrast to prediction of the lift coefficient, Fig. 6-1 and Fig. 6-15, where advanced theory now accurately predicts lift when blade stall is involved, CAMRAD II (as one example) has room for considerable improvement. The blade element torque equation, as Glauert, Lock and Wheatley proposed, depends upon three variables as follows:

$$\frac{dC_Q/dx}{x} = C_d \cos \phi - C_l \sin \phi$$

Both the blade element drag (C_d) and lift (C_l) forces must be resolved into the shaft axis system through the inflow angle (ϕ). In addition, both forces depend on, as a minimum, the blade element angle of attack, which is the sum of blade pitch angle (θ) and the inflow angle (ϕ). The accumulation of possible errors, particularly when a blade element is computed to be stalled, is really quite mind boggling. The situation is somewhat helped because an integration from blade root to tip is required at each blade azimuth (ψ). This integration over 10 to 20 radially stationed blade elements tends to average out some of the local errors. Even more help comes because the final torque coefficient is the average over a complete blade revolution and this can easily be an average from computations at every tenth to one degree in blade azimuth.

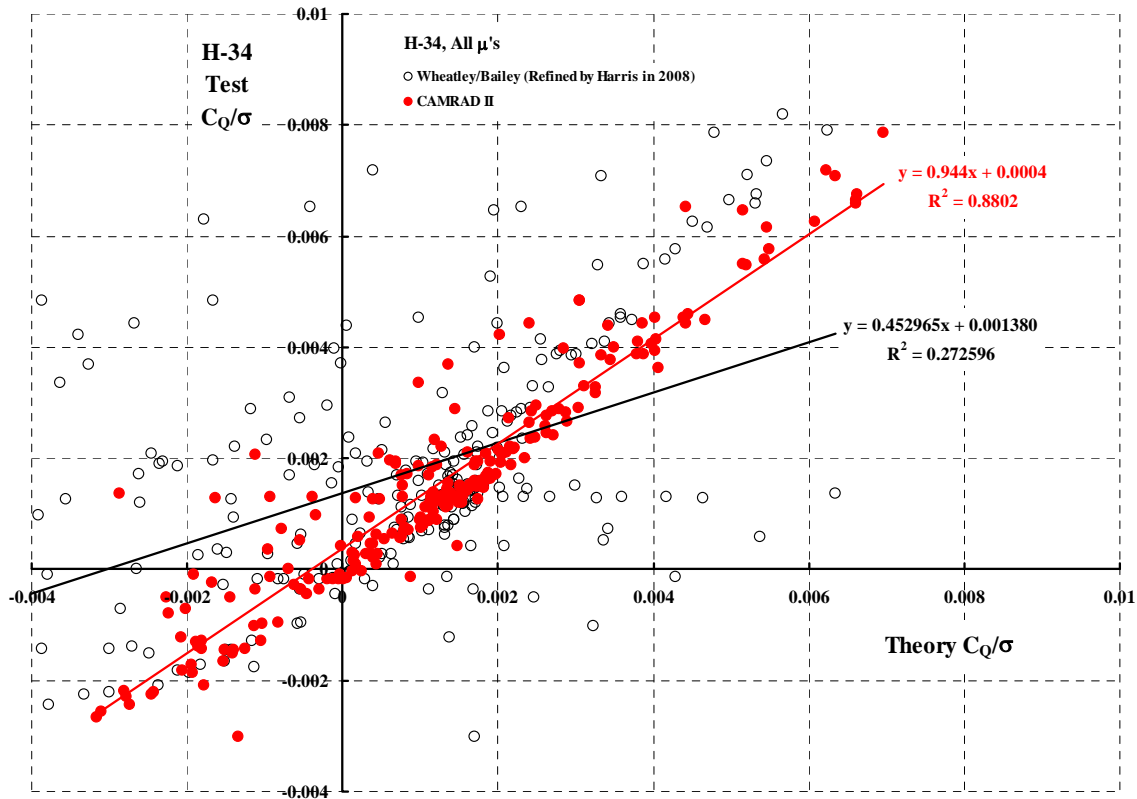


Fig. 6-20. Prediction of torque (or power) coefficient.

6.2.6 Effective Drag Coefficient, C_{De}/σ

The concept and definition of an effective drag coefficient was given with Eq. (19). In coefficient form, this effective drag coefficient is simply

$$\frac{C_{De}}{\sigma} = \frac{C_Q/\sigma}{\mu} - \frac{C_X}{\sigma} = \frac{(C_{Qi}/\sigma)_{\text{induced}} + (C_{Qo}/\sigma)_{\text{profile}}}{\mu}$$

and is the measure of induced plus profile drag of a rotating wing. As Fig. 6-21 shows, the progress from the 1930s Wheatley/Bailey to today's CAMRAD II comprehensive code is impressive and gratifying, to say the least. It is now up to the theoreticians to reduce the scatter of the red, solid circle, points on Fig. 6-21. When that is done, the individual contributions of induced drag and profile drag to rotor performance at high advance ratio will be known with rather high confidence.

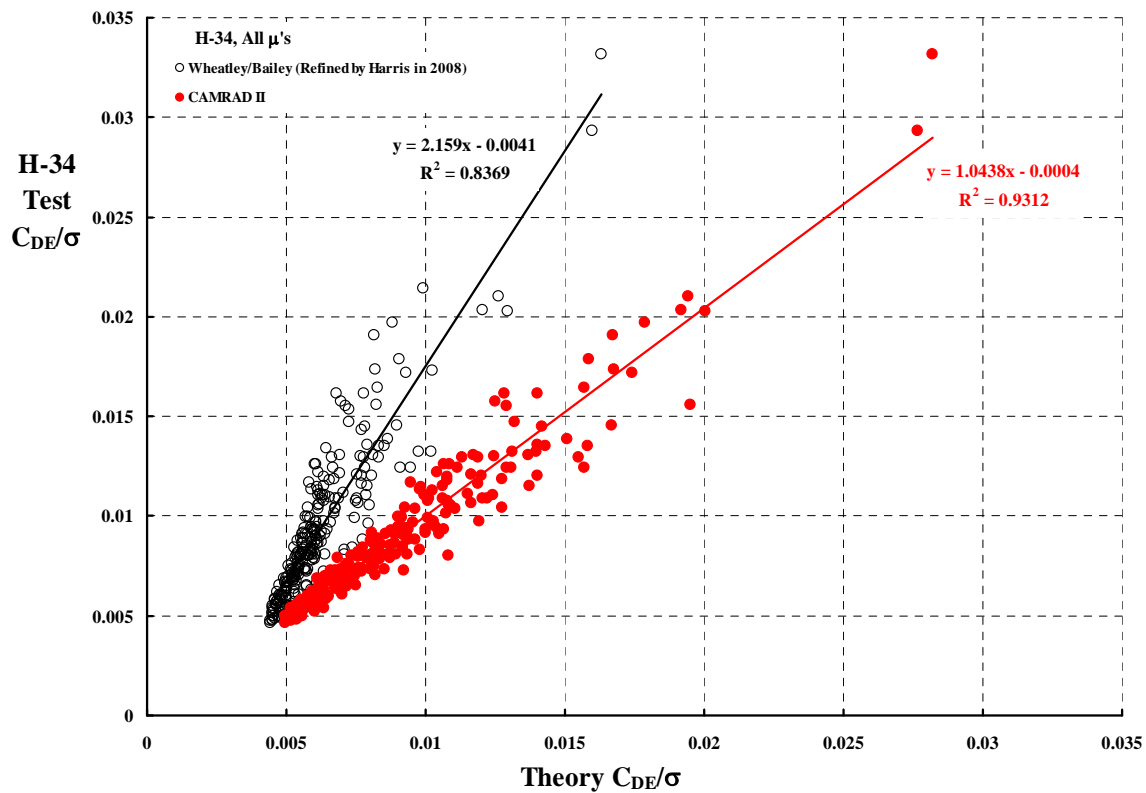


Fig. 6-21. Prediction of effective drag coefficient.

6.2.7 Rotor L/D_E

Frequently, in concept design, it is expeditious to assume a rough order of rotor performance by choosing a maximum rotor L/D_E . All during the 1940s, 1950s and even into the 1960s the assumed value was based on Wheatley/Bailey theory. From Fig. 6-22 there was a tendency to use maximum rotor L/D_E values upwards of 15 based on

Wheatley/Bailey theory. This was done in the face of experimental data (from model scale and a few full scale rotors) that said such a high value was irrational. Fortunately, comprehensive codes such as CAMRAD II provide a great deal of realism even during conceptual design. Unfortunately, a prediction that only bounds the L/D_E value to about ± 1 about $L/D_E = 9$ is still too coarse. Since lift prediction (C_L/σ) is “rather accurate” as Fig. 6-15 shows, the task is to improve prediction of the denominator (i.e., C_{D_e}/σ), which in turn requires accurate prediction of H-force.

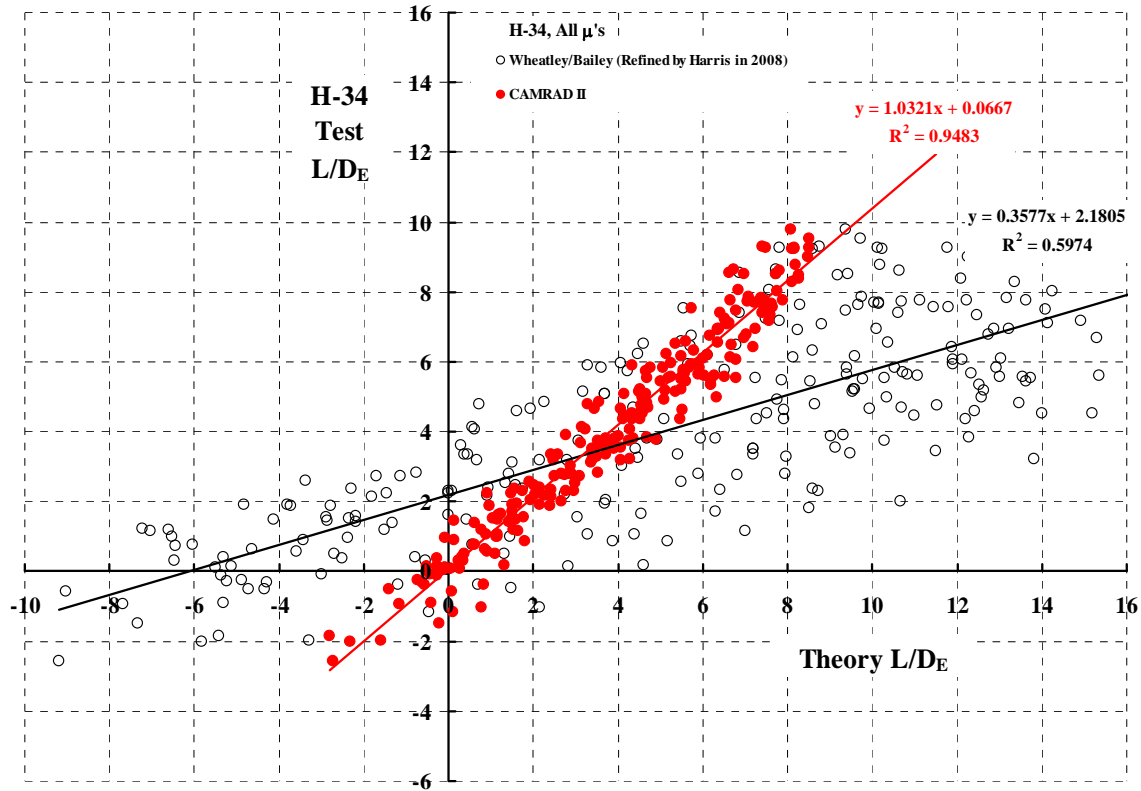


Fig. 6-22. Prediction of rotor L/D_E .

7 THEORY VERSUS TEST DETAILS

The objective of this investigation has been to compare theory with available test data at high advance ratio. Five analyses, four being representative of the state of the art in 2008, have been chosen. Within the time, money, priority and volunteer help available, these five theories are to be compared to three sets of high advance ratio rotor tests. This represents a matrix of 15 possible combinations as displayed with Table 16. The investigation to date must be considered a first step because only 8 of the possible combinations have been completed. However, a partial completion of a 9th and a 10th possible evaluation indicates what can come next. While the Wheatley/Bailey theory is included in the matrix of 15, it is only of historical interest. At the other end of time, the application of computational fluid dynamics (CFD) to the rotating wing in forward flight is just at the very, very beginning of the development cycle.

The three comprehensive codes chosen for this evaluation are only representative of the many codes under development by the worldwide rotorcraft industry. Therefore, it can be hoped that, in time, the theory versus test matrix provided by Table 16 will be expanded. One thing is definitely clear already; there is insufficient experimental data at advance ratios from 0.8 to 2.0.

Table 16. Theory versus Test Matrix.

Rotors	Wheatley & Bailey	CAMRAD II	CHARM	RCAS	Overflow CFD Coupled With CAMRAD II
H-34	✓	✓	✓	✓	Partial
UH-1	✓	Partial		✓	
PCA-2	✓	✓			

The following paragraphs and associated appendices examine each theory's capability and/or evaluation status. Each theory's capability is summarized primarily with a table of regression analysis coefficients for a given parameter at several advance ratios. The appendix associated with each theory provides (1) tabulate data of computed results, (2) graphs of a test parameter versus computed parameter, (3) tabulations of the regression analysis coefficients and (4) graphs of the regression analysis coefficients versus advance ratio. Where only partial evaluation has been completed, the associated appendix is comparably empty and the appendix serves only as a place holder for work to come at some later date.

The evaluation criteria advocated by this author is this: when test is plotted versus theory (calculated at test conditions), a linear regression analysis will yield a $y = Ax + B$ result with some confidence. The confidence is based on the R^2 value the analysis offers. Quantitatively I mean that:

1. There is enough data points so that a meaningful linear regression analysis can be performed. The presentation and analysis of the H-34, UH-1 and PCA-2 experimental data in Chapter 5 illustrate that this quantity of data is adequate. The variables of shaft angle of attack and collective pitch covered operating range sufficiently so that interpolation by regression equation could – with some confidence – be made. The rotorcraft industry is very, very fortunate to have the data bank provided by John Wheatley, John McCloud, Jim Biggers, Bruce Charles and Hank Tanner, to name just a few individuals.

2. A regression analysis R^2 value of at least 0.97 provides the confidence this author considers adequate for rotor trim and performance prediction. An R^2 of 0.97 means that 97 percent of any experimental data trend is captured by theory. The basis for this minimum R^2 level is the several tables included with Chapter 5's analysis of the experimental data. This analysis of the experimental data showed that in the linear range (i.e., blade stall points *were not* included), R^2 values at and well above 0.98 were obtained. Since the theories under consideration account for blade stall and other nonlinearities and their evaluation *does include* points with these nonlinearities, some additional room for error must be given – for now. In short, rotor lift, drag, side force and torque must be accurately predicted if meaningful configuration decisions are to be made.

3. Predicting the slope of test versus theory to within ± 5 percent is, to this author, absolutely mandatory. This means that in the regression analysis, values of the slope coefficient must lay between 0.95 and 1.05. The logic behind this range is rather simple to illustrate. A rotor's lift to drag ratio at zero lift is zero. At the lift for maximum L/D, an ability to predict this maximum L/D to within 5 percent will encourage the rotorcraft industry to pursue the most aerodynamic deserving configurations.

4. A theory must predict the intercept value in the $y = Ax + B$ equation to within the experimental data accuracy. The band widths shown on Chapter 5's graphs with the red lines are an adequate measure of the required accuracy. Therefore, this author advocates that the error in intercept be no greater than:

Longitudinal cyclic, B_{1C} , ± 0.3 degrees

Lateral cyclic, A_{1C} , ± 0.3 degrees

Lift coefficient, C_L/σ , ± 0.003

Drag coefficient, C_D/σ , ± 0.0005

Thrust coefficient, C_T/σ , ± 0.003

H-Force coefficient, C_H/σ , ± 0.0004

Side Force coefficient, C_Y/σ , ± 0.0004

Torque (power) coefficient, C_Q/σ , ± 0.0003

This advocated theory/test correlation method and criteria evaluates both test and theory. However, the resulting regression analysis coefficients can not tell whether test or theory or both are in error. This is an age old question. In fact, it takes a point by point examination of both test and theory to reach a carefully considered opinion. Consider these statements in light of just H-34 test data and CAMRAD II theory at 0.305 and 1.05 advance ratios. The statements become clear just by studying the rotor lift coefficient, C_L/σ , at the two advance ratios. At an advance ratio of 0.305, Fig. 7-1 shows that the experimental data meets the four point criteria advocated by the author – *at least for the data below a lift coefficient below 0.07*. The simple equation used to evaluate the test data has the confidence level of $R^2 = 0.9969$. Now look at Fig. 7-2 where test lift coefficient is plotted versus CAMRAD II's prediction. Theory also meets the advocated criteria and, furthermore, the blade stall points are now well predicted by the theory.

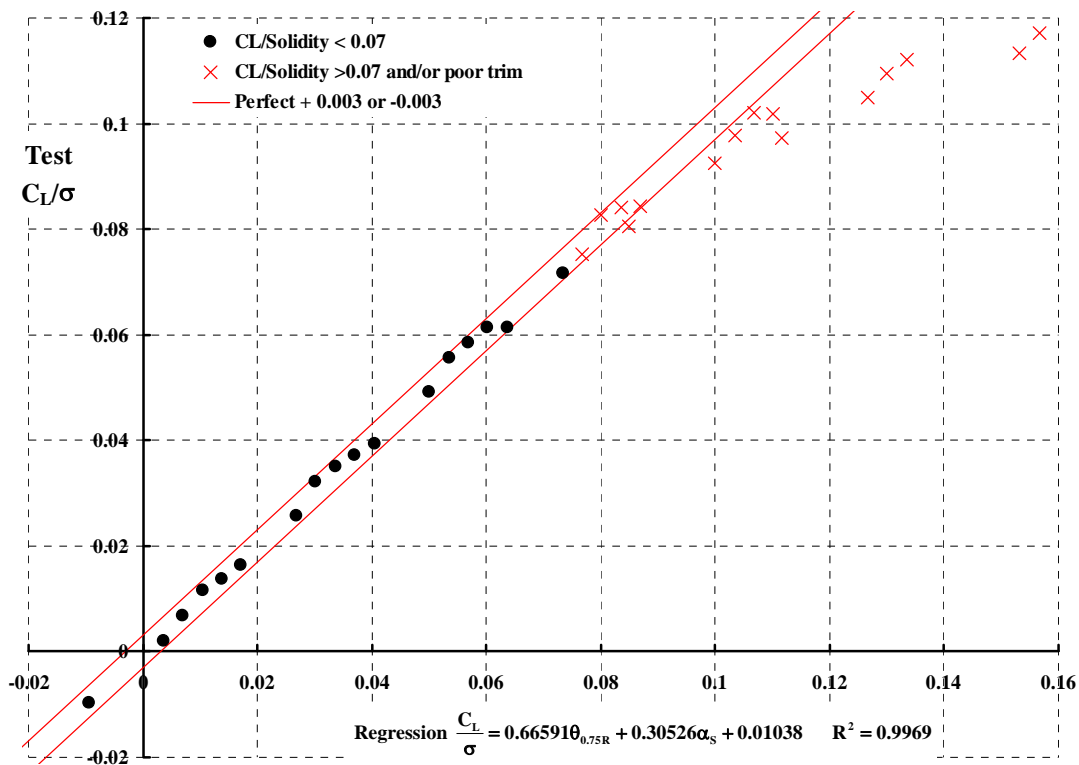


Fig. 7-1. H-34 test lift coefficient regression analyzed at $\mu = 0.305$.

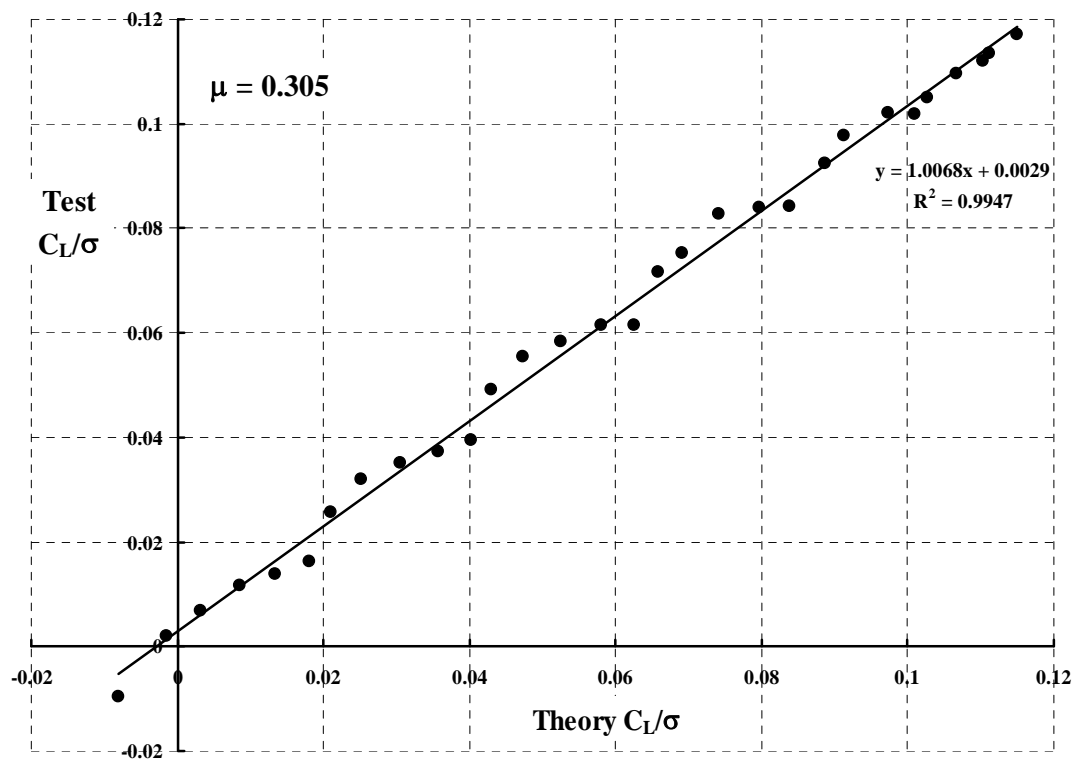


Fig. 7-2. H-34 test lift coefficient versus CAMRAD II theory at $\mu = 0.305$.

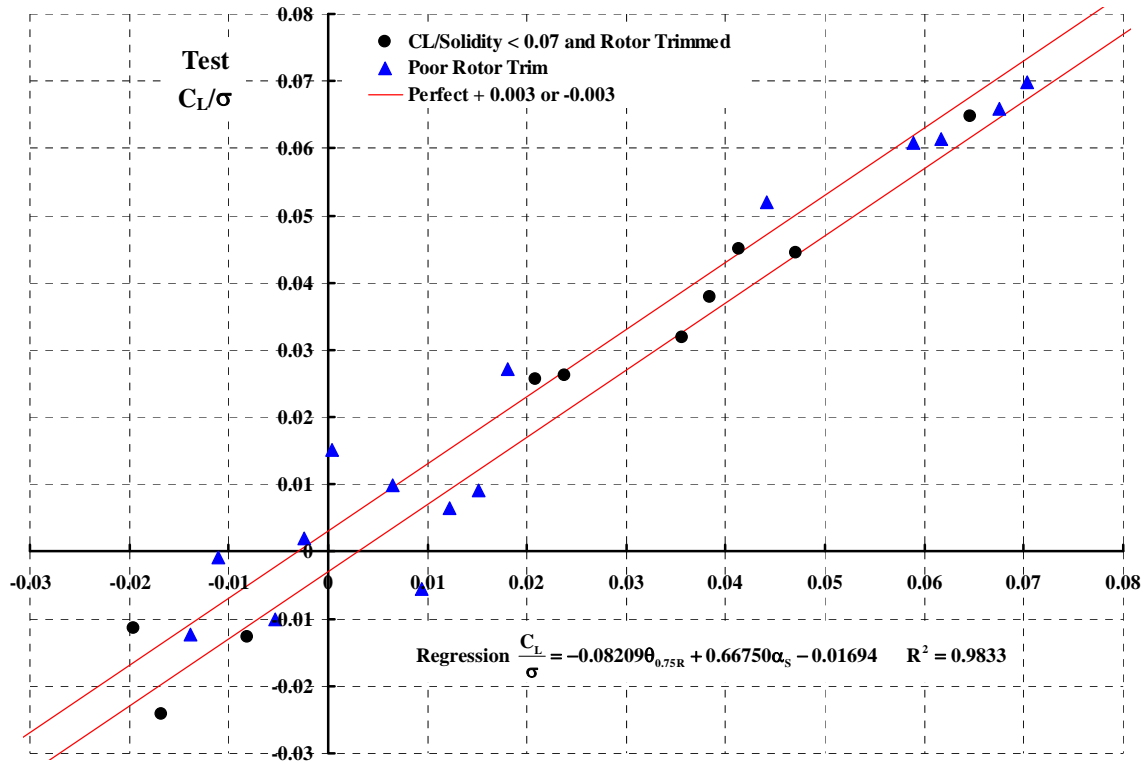


Fig. 7-3. H-34 test lift coefficient regression analyzed at $\mu = 1.05$.

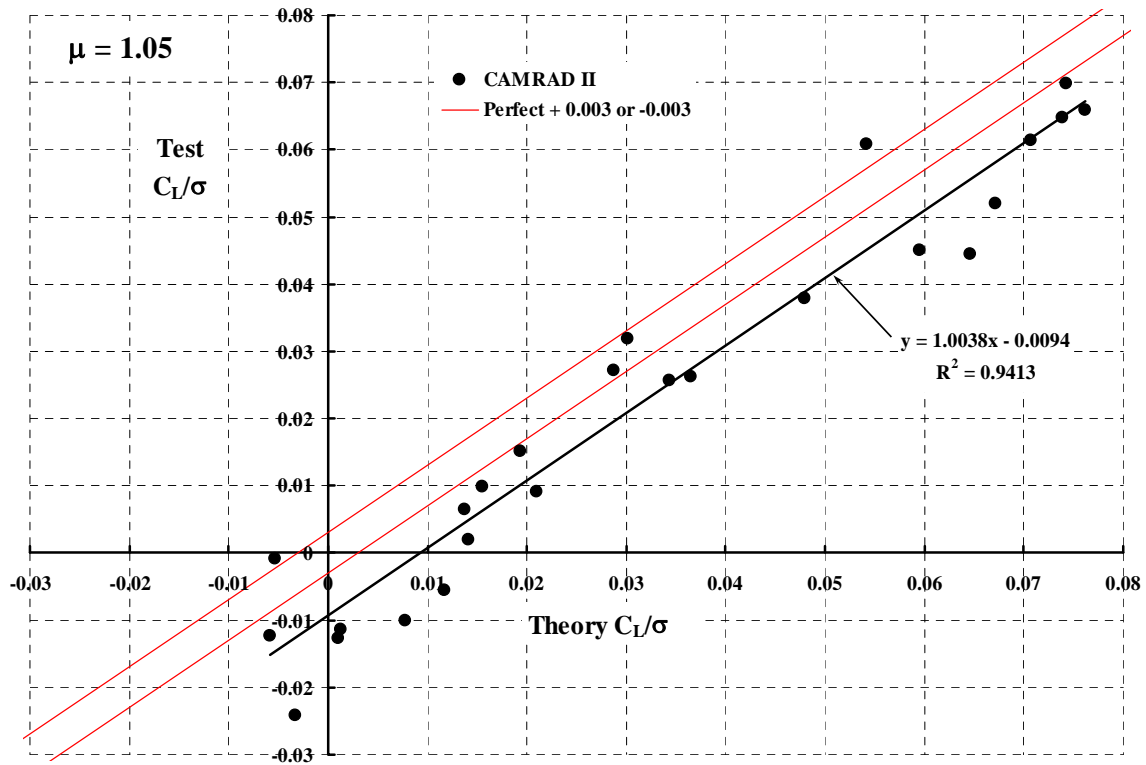


Fig. 7-4. H-34 test lift coefficient versus CAMRAD II theory at $\mu = 1.05$.

Now consider the same lift coefficient examination at an advance ratio of 1.05 as presented by Fig. 7-3 and Fig. 7-4. The regression analysis with the ten, solid black, circle points (reported as being within rotor trim) are an insufficient data quantity in this author's opinion. The regression analysis equation having dependence on two variables does not arrive at a very confident solution. A regression analysis of the form

$$\frac{C_L}{\sigma} = \text{function}(\alpha_s^2, \alpha_s, \alpha_s \theta_{0.75}, \theta_{0.75}, \theta_{0.75}^2)$$

did little to improve the poor impression that Fig. 7-3 gives. One disturbing fact, over and above the question of rotor trim, seen with Fig. 7-3, is that the data "scatters" more at low lift. In pursuing this data dispersion, the author wonders if the wind tunnel balance was so lightly loaded that its accuracy could be questioned.

The prediction of test data by CAMRAD II is, if anything, less encouraging as Fig. 7-4 shows. The slope constant (1.0038) being well within the ± 5 percent criteria advocated by this author is, of course, most encouraging. This positive result is offset by the theory not collecting the data so as to pass close to near zero/zero ($B = -0.0094$). Additionally, a confidence of R^2 of 0.9413 is unacceptably low.

In short, the H-34 experimental data as a basis for evaluating theory at an advance ratio of 1.05 is very questionable. Because theory does not offer an improvement as it did with the blade stall points at $\mu = 0.305$, this author concludes the theory (CAMRAD II) is also questionable at this advance ratio. The situation can be resolved with more carefully testing near and above $\mu = 1$ and providing the new data to the theoreticians who will surely get to the bottom of this problem.

There is a final point to consider. The selected comprehensive codes being evaluated have demonstrated successful prediction of many helicopter parameters and design factors. The codes have been developed for the advance ratio range between hover and 0.4. However, *it is the extension, evaluation and usability of these codes beyond their known capabilities which is under study in this report.*

7.1 H-34 Test versus CAMRAD II (Appendix 11.10)

Chapter 6 showed that CAMRAD II (or any comparable comprehensive code) has made a truly impressive improvement over the Wheatley and Bailey theory as far as predicting rotor trim and performance. The detailed evaluation that now follows summarizes the extensive material provided in Appendix 11.10. The analysis' capability as a function of advance ratio is of particular interest. Each of the following eight rotor parameters that were first examined in Chapter 6 is re-examined in more detail:

- Longitudinal and lateral controls, B_{1C} and A_{1C}
- Lift, drag, side force and power, C_L/σ , C_D/σ , C_Y/σ and C_Q/σ
- Effective drag, C_{DE}/σ
- Lift to effective drag ratio, L/D_E

Appendix 11.10 contains graphs of each test parameter versus theory at each advance ratio. There are 8 parameters and the evaluation is made at 8 advance ratios, which makes a total of 64 graphs. Each graphed parameter is treated with a linear regression analysis and the results in $y = Ax + B$ form along with R^2 are shown on each graph. A tabulation of these many regression constants (i.e., A, B and R^2) constitute the summary evaluation of CAMRAD II's prediction capability. This summary evaluation table is brought forward to this portion of the report for discussion purposes.

The summary of CAMRAD II's prediction capability is given with Table 17. Table 17 evaluates the theory versus the wind tunnel measured parameters. Rotor thrust, H-force, effective drag coefficients and rotor L/D_E are derived from the measured wind tunnel measured parameters. These derived parameters are examined with a table in Appendix 11.10.

Do not be startled by the several cells shaded in yellow or red on Table 17. The meaning of the red color coding is that the regression analysis result does not meet the accuracy criteria advocated by this author. That is, a slope, intercept or R^2 cell is shaded red if:

1. Slope outside of 0.95 to 1.05
2. Intercept outside of
 - Longitudinal cyclic, $B_{1C}, \pm 0.3$ degrees
 - Lateral cyclic, $A_{1C}, \pm 0.3$ degrees
 - Lift coefficient, $C_L/\sigma, \pm 0.003$
 - Drag coefficient, $C_D/\sigma, \pm 0.0005$
 - Side Force coefficient, $C_Y/\sigma, \pm 0.0004$
 - Torque (power) coefficient, $C_Q/\sigma, \pm 0.0003$
3. R^2 less than 0.97

The cells colored yellow indicate a value that is very close to the advocated criteria. Of course, the suggestion might be made that *if the criteria for being colored red were relaxed a bit*, things might look a little more encouraging. In fact, the more important information to be gained from Table 17 is the trends with advance ratio.

A careful scan of Table 17 shows that the theory/test correlation generally deteriorates with advances ratios higher than 0.51 to 0.62. The first parameter in the table, longitudinal cyclic, offers a sufficient example to illustrate this adverse trend as Fig. 7-5 shows. Both the table and the table in graphical form show that the regression analysis is quite confident because R^2 is well above the minimum 0.97 level advocated by this author. The slope trend with advance ratio says that CAMRAD II over predicts the cyclic required to trim the rotor normal to shaft at low advance. Note that at $\mu = 0.62$ the slope is perfectly predicted. But then at the higher advance ratios, the deterioration continues such that theory is under predicting the required longitudinal cyclic. The intercept prediction by CAMRAD II says that as advance ratio increases, the theory needs to calculate increasing increments in cyclic to correctly capture the experimental data.

Table 17. Table of Linear Regression Coefficients For Wind Tunnel Measured Parameters. H-34 Test Versus CAMRAD II.

Mu	Longitudinal Cyclic			Mu	Lateral Cyclic		
	SLOPE	Intercept	R ²		SLOPE	Intercept	R ²
0.305	1.0746	-0.0922	0.9924	0.305	1.0852	-0.4012	0.9718
0.401	1.1252	0.1632	0.9899	0.401	1.3323	-0.1506	0.9439
0.460	1.0627	0.3480	0.9837	0.460	1.3370	-0.2134	0.9647
0.510	1.0215	0.1977	0.9861	0.510	1.2453	-0.4279	0.9497
0.620	1.0001	0.3479	0.9774	0.620	1.3533	-0.5637	0.8995
0.710	0.9639	0.4842	0.9959	0.710	1.0925	-0.7903	0.8766
0.820	0.9543	0.6627	0.9926	0.820	1.2061	-0.8221	0.8649
1.050	0.9287	0.7130	0.9929	1.050	0.4144	-1.1722	0.2450

Mu	Lift Coefficient			Mu	Drag Coefficient		
	SLOPE	Intercept	R ²		SLOPE	Intercept	R ²
0.305	1.0068	0.0029	0.9947	0.305	1.0142	-0.0005	0.9920
0.401	0.9652	0.0030	0.9873	0.401	0.9675	-0.0006	0.9886
0.460	0.9500	0.0032	0.9902	0.460	0.9533	-0.0007	0.9870
0.510	0.9727	0.0037	0.9895	0.510	0.9238	-0.0001	0.9802
0.620	1.0242	0.0014	0.9948	0.620	0.7647	0.0012	0.9487
0.710	0.9144	0.0013	0.9918	0.710	0.6160	0.0025	0.8650
0.820	0.8736	0.0028	0.9912	0.820	0.5852	0.0032	0.7395
1.050	1.0038	-0.0094	0.9413	1.050	0.6771	0.0032	0.6030

Mu	Y-Force Coefficient			Mu	Power Coefficient		
	SLOPE	Intercept	R ²		SLOPE	Intercept	R ²
0.305	0.7234	-0.0004	0.6922	0.305	1.0801	-0.0001	0.9730
0.401	1.1026	-0.0002	0.6415	0.401	1.0510	0.0001	0.9652
0.460	1.2810	-0.0003	0.6729	0.460	1.0235	0.0002	0.9620
0.510	1.2264	-0.0004	0.6549	0.510	0.9958	0.0005	0.9100
0.620	2.0208	-0.0009	0.2213	0.620	0.9028	0.0003	0.8442
0.710	-0.4168	-0.0022	0.0247	0.710	0.8604	0.0004	0.8176
0.820	-1.3183	-0.0017	0.3387	0.820	0.7222	0.0005	0.7723
1.050	-0.5452	-0.0012	0.0821	1.050	0.4049	0.0006	0.2303

The CAMRAD II prediction of lateral cyclic required to trim the rotor normal to the shaft is not satisfactory at any advance ratio. As mentioned earlier, this parameter is rarely studied either with experiment or by theory. The table indicates rather poor confidence based on tabulated R^2 values. Notice that rotor side force is just as poorly predicted.

The most accurate force prediction is rotor lift, although the inaccurate slope prediction at advance ratios of 0.71 and 0.82 should be noted. The drag prediction and torque prediction at a given lift coefficient are the parameters of primary interest to performance engineers. Considerable effort must be devoted to these two parameters before CAMRAD II can be confidently applied at advance ratios much above $\mu = 0.51$.

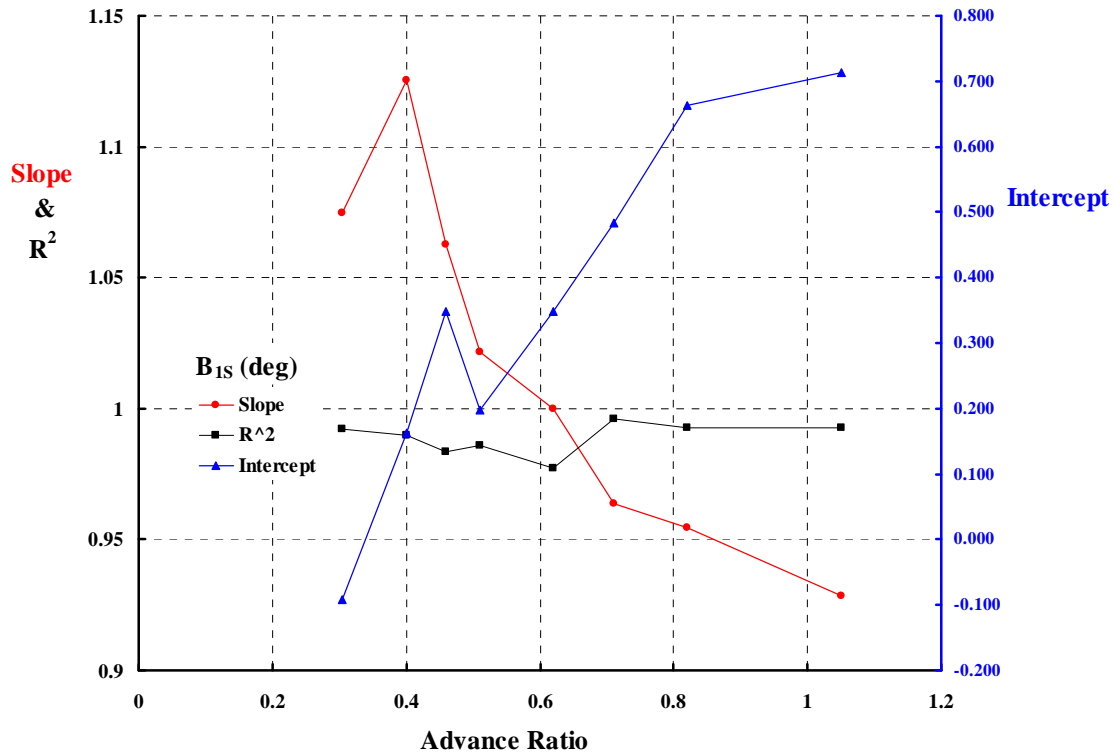


Fig. 7-5. Longitudinal cyclic correlation with CAMRAD II

The key to improving theory (and also test) begins with the intercept values. The problem must be solved at the conditions of shaft angle of attack equal zero and collective pitch at the $3/4$ radius station equal zero. This point was brought home to the author and Wayne Johnson rather early on and the story is worth recounting:

The H-34 test data at this primary condition, as discussed in paragraph 5.4.1, does not give zero lift when θ at $3/4 R = 0$ and $\alpha_s = 0$. Both investigators were taken aback when CAMRAD II also did not calculate zero lift at $\mu = 0.305$ and $\theta_{3/4 R} = 0$ and $\alpha_s = 0$. Johnson, after a weekend's work, traced the culprit to blade torsion deflections. The follow on question as to why there was a torsion deflection given that the standard C81 airfoil deck for the NACA 0012 lists a zero pitching moment coefficient led to Johnson finding that CAMRAD II was using the "standard C81 airfoil deck" but, in addition, the input included a delta pitching moment coefficient for outboard blade elements. The airfoil deck "was an old C81 deck" created by Johnson to analyze Scheiman H-34 flight

test results [64]. It was presumed that the H-34 blade set used in that test included a trim tab over the 0.8 to 0.9 radius station. The trim tab was bent up and Johnson's "old C81 deck" included a positive airfoil pitching moment coefficient of 0.03 over this outboard region of the blade. In essence, CAMRAD II could reproduce the "nonzero lift behavior" by adding a lumped, delta aerodynamic pitching moment to the symmetrical NACA 0012. The reasonably accurate blade structural properties and realistic control system stiffness used by Johnson allowed the torsional deflection.

The only unfortunate part of this story is that no one now knows what the overall trailing edge configuration was for the untwisted H-34 blades under discussion in this report. *The H-34 blade trailing edge is segmented metal and any given segment can be warped or bent up or down.* In fact, there is no assurance that the N.A.C.A. 0012 blade elements remain uncambered in flight since the airloads which create a pitching moment bend the element (i.e., introduce camber). However, there is no disputing the fact that torsional deflection is, just as Wheatley said about his late 1930s theory [29, 30], absolutely essential to accurately predicting rotor lift and blade feathering to trim the rotor. The basic lesson is that a rotating wing is a rotating *flying* wing, which has many unusual aerodynamic characteristics.

Fig. 7-6 gives CAMRAD II lift coefficient results, as a function of advance ratio, with and without blade torsion deflection when $\theta_{3/4 R} = 0$ and $\alpha_S = 0$. Disregarding the test data at $\mu = 1.05$, CAMRAD II captures the basic trend with advance ratio. Increasing the localized airfoil pitching moment coefficient from $C_m = +0.03$ to 0.04 would likely yield even more encouraging results. The non-dimensional parameter to consider is the ratio of airload moment to torsional rigidity, which, from simple blade torsion theory [10], means $\frac{\rho V_t^2 c^2}{GJ}$ for quasi static moments and $\frac{\rho V_t^2 c^2}{GJ} \left(\frac{c}{R} \right)$ for unsteady moments.

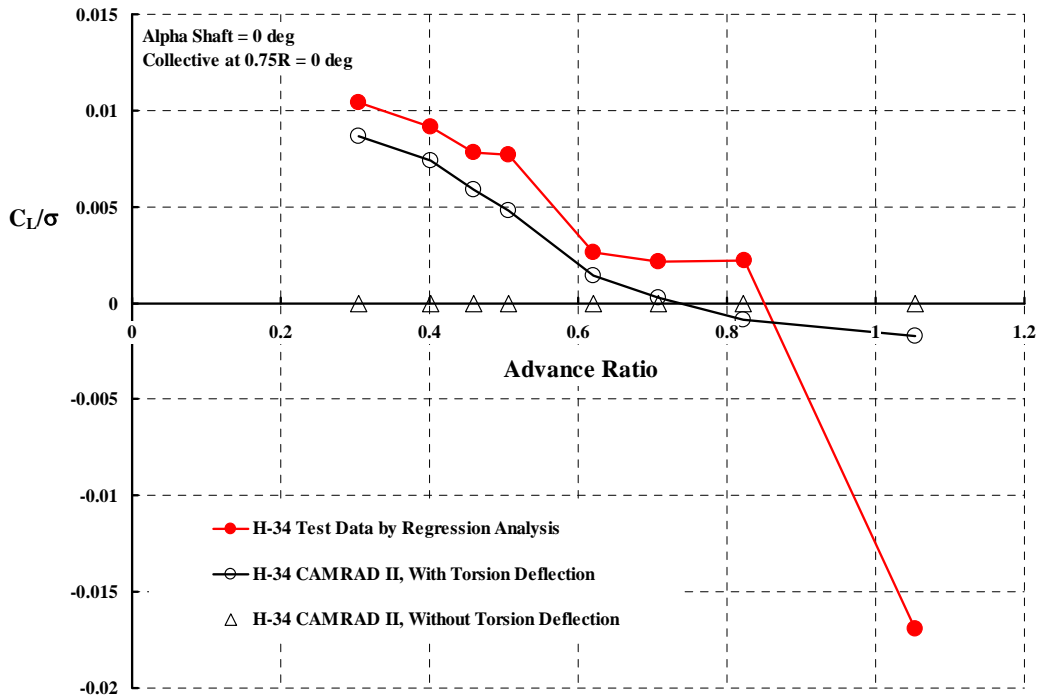


Fig. 7-6. CAMRAD II lift coefficient correlation at $\theta_{3/4 R} = 0$ and $\alpha_S = 0$.

The importance of the blade torsion deflections to both longitudinal (B_{1C}) and lateral cyclic (A_{1C}) required to trim the rotor tip path plane normal to the shaft is confirmed with Fig. 7-7. CAMRAD II confirms that if the torsion degree of freedom is not included in the computation, both cyclic control angles are zero regardless of advance ratio. With torsional deflection included in the computation, both measured cyclic angle trends with advance ratio are captured by CAMRAD II. Wheatley encouraged the view that the blade feathering equation should include at least three additional terms so that

$$\theta_{x,\psi} = \theta_o + x\theta_t - B_{1C} \sin \psi - A_{1C} \cos \psi + x(\theta_{e_o} + \theta_{e_{1s}} \sin \psi + \theta_{e_{1c}} \cos \psi)$$

Admitting any aeroelastic response to blade element pitching moment will lead to flapping. Thus, cyclic control will be required to retrim the rotor tip path plane normal to the shaft (the experiment's test requirement).

The approximate magnitude of the elastic twisting that requires the longitudinal and lateral cyclic trends of Fig. 7-7 are not large. In fact, as Fig. 7-8 shows, CAMRAD II computes that the blade tip is elastically twisting (relative to the blade root) less than 2 degrees. For example, at an advance ratio of 0.506, Wheatley's blade feathering equation (in degrees) becomes

$$\theta_{x,\psi} = 0.122 + 0.122x - 1.609 \sin \psi - 0.491 \cos \psi + x(0.9 + 0.844 \sin \psi + 0.005 \cos \psi)$$

There is, of course, the additional feathering caused by control system elastic deflections, which is relatively small – according to CAMRAD II calculations.

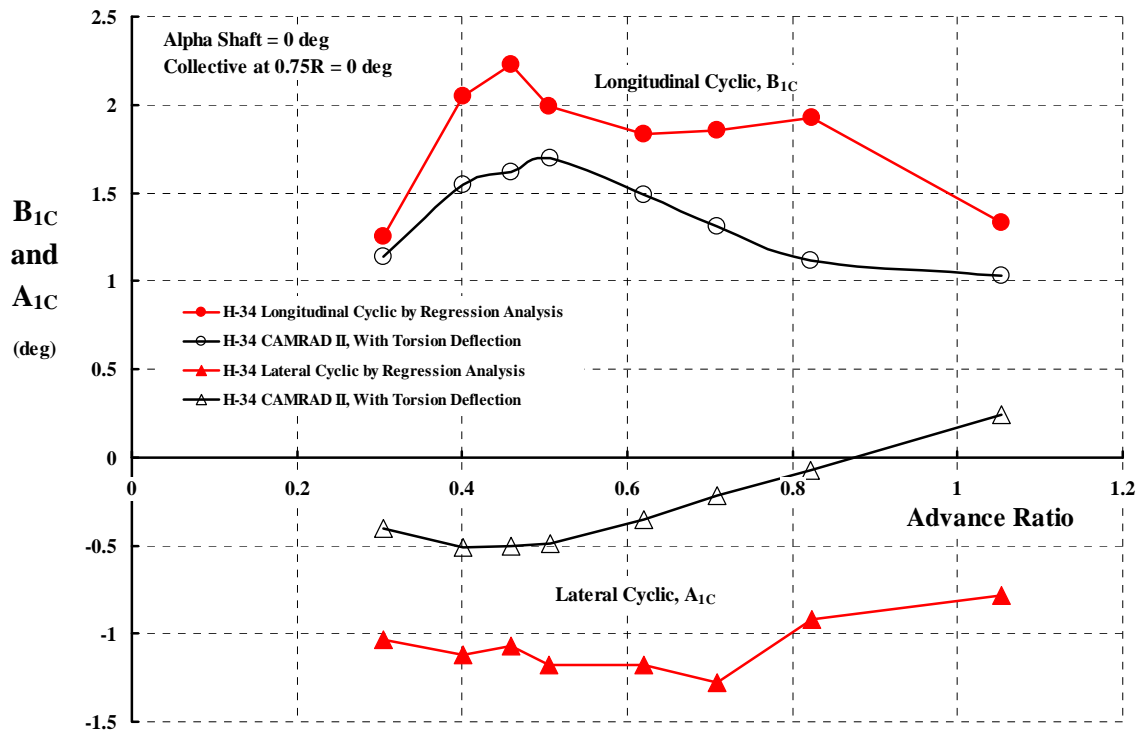


Fig. 7-7. Longitudinal and lateral cyclic correlation with CAMRAD II for the test condition of $\theta_{\frac{3}{4}R} = 0$ and $\alpha_s = 0$.

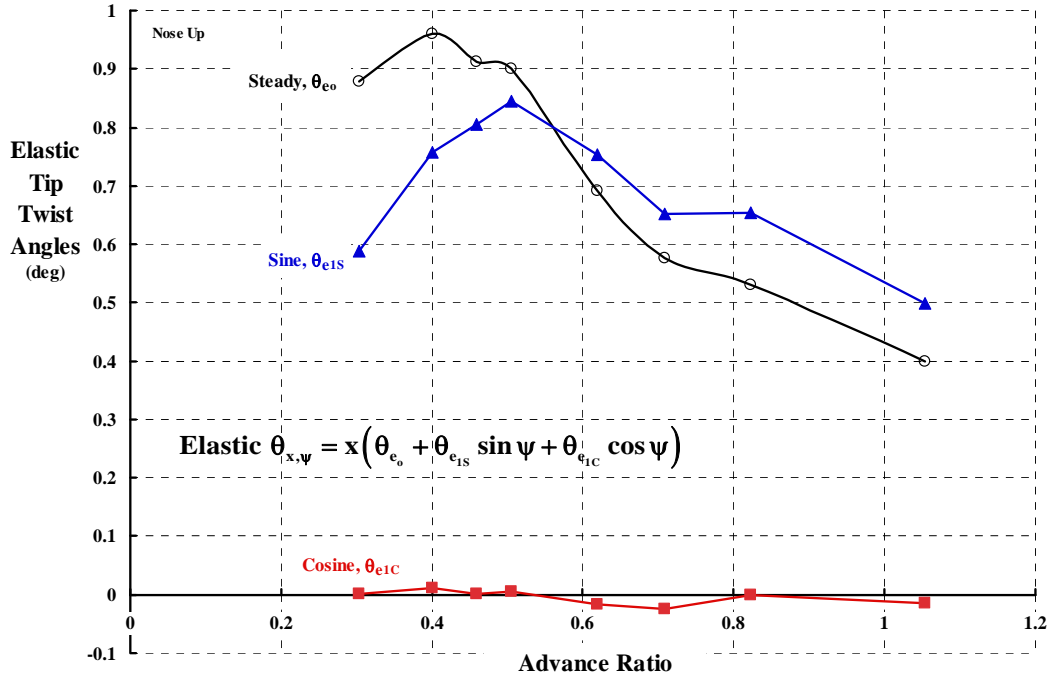


Fig. 7-8. CAMRAD II calculated blade tip elastic deflection; first harmonic coefficients for the test condition of $\theta_{3/4 R} = 0$ and $\alpha_S = 0$.

The rotor H-force, Y-force and shaft torque coefficients at the $\theta_{3/4 R} = 0$ and $\alpha_S = 0$ test condition are shown in Fig. 7-9, Fig. 7-10 and Fig. 7-11 respectively. The H-force, which is identical with rotor drag because the shaft angle of attack is zero, is a very large force. There is, however, always a question about the experimental data when comparisons such as Fig. 7-9 are made. The H-force is a measure of the blades alone drag. Experimentally, this force is obtained by measuring the drag of the blades plus hub (and other components) and then subtracting the hub drag with blades off (a tare). Since the rotor hub drag is 10, 15 or even 20 times the blade alone drag, the experimenter is dealing with the difference of two large and nearly equal forces. Therefore, any difference between test and theory for H-force may or may not be accurately assessed. The side or Y-force and torque do not entail such large tare loads and any differences between test and theory must be seriously studied.

The rotor effective drag coefficient, C_{De}/σ , correlation is shown with Fig. 7-12. It is important to appreciate that this coefficient, at the $\theta_{3/4 R} = 0$ and $\alpha_S = 0$ test condition, is dominated by the H-force at the higher advance ratios. Because the shaft angle of attack is zero, the C_{De}/σ coefficient, following from Eq. (19) and applying Appendix 11.1 thoughts, can be written as

$$(27) \quad \frac{C_{De}}{\sigma} = \frac{C_{p_{rotor induced}} + C_{p_{rotor profile}}}{\sigma \mu} = \frac{1}{\mu} \frac{C_Q}{\sigma} + \frac{C_H}{\sigma}$$

and the two components of C_{De}/σ as calculated by CAMRAD II are also shown on Fig. 7-12.

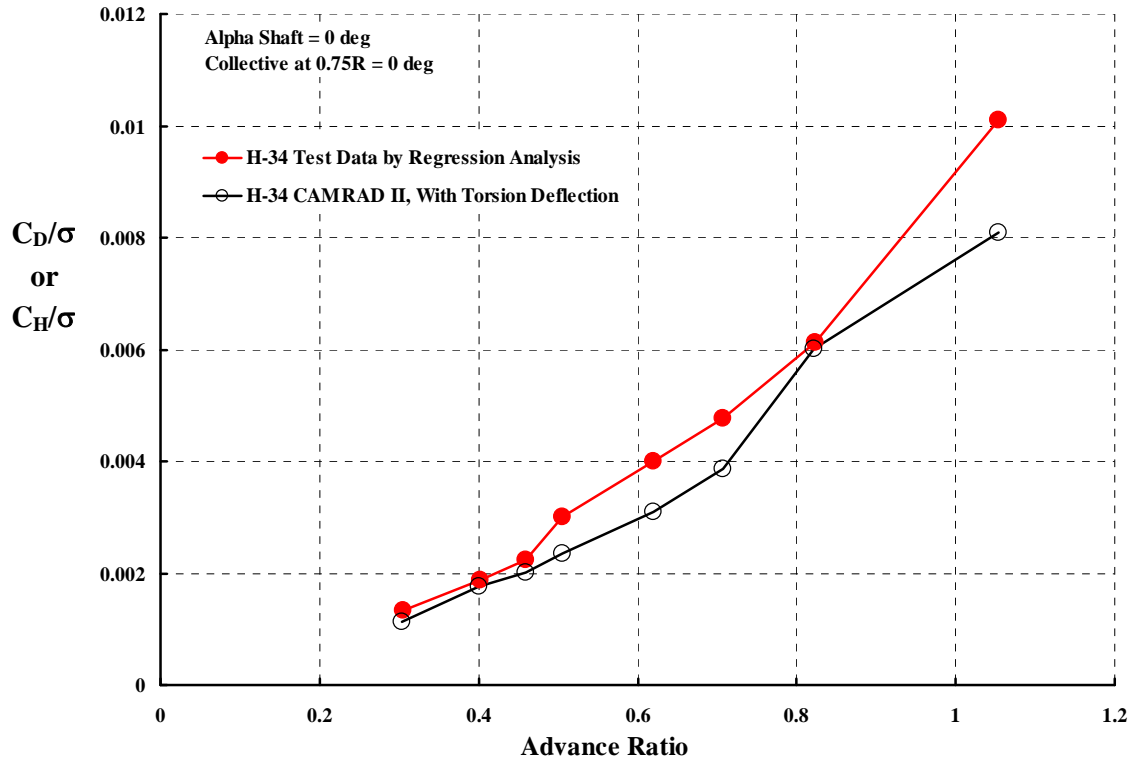


Fig. 7-9. Longitudinal force correlation with CAMRAD II

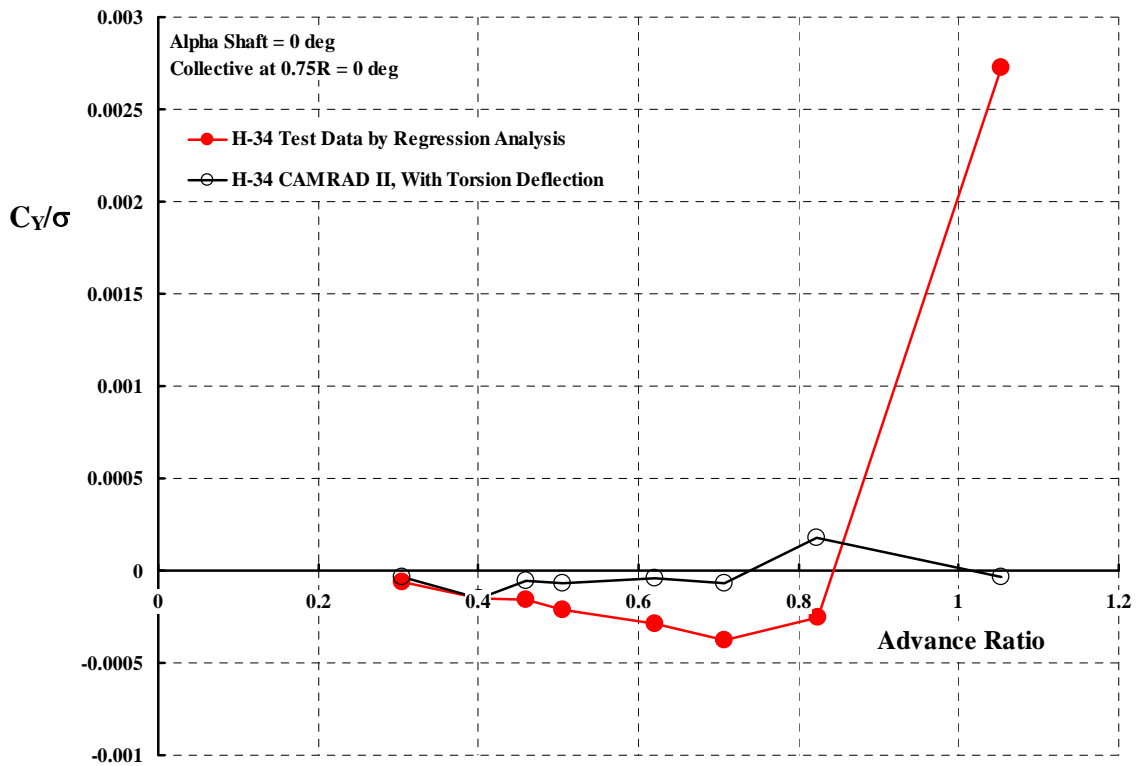


Fig. 7-10. Lateral force correlation with CAMRAD II

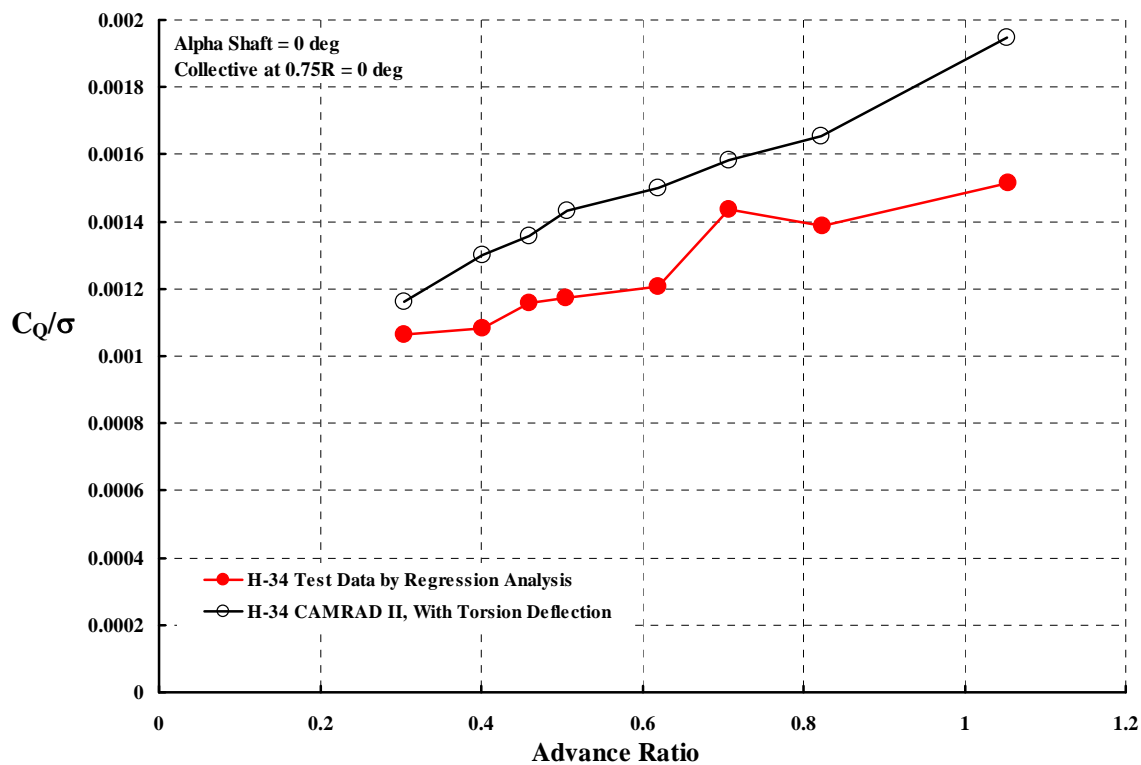


Fig. 7-11. Shaft torque correlation with CAMRAD II

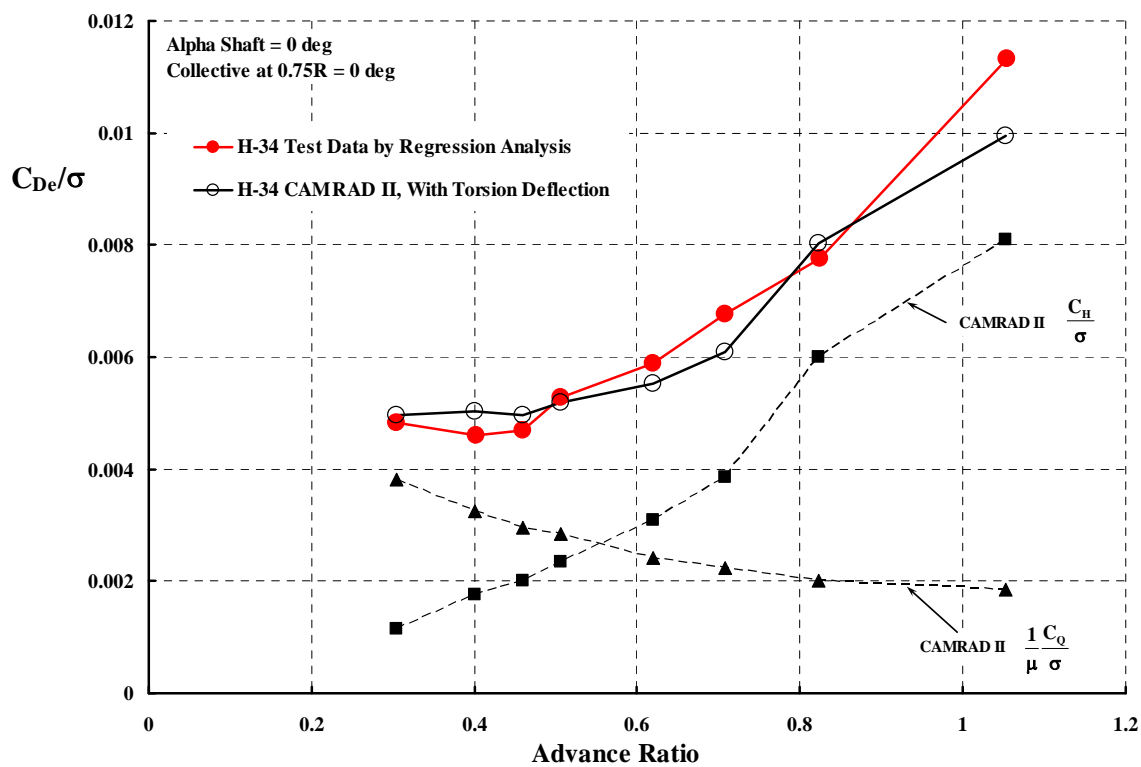


Fig. 7-12. Rotor effective drag correlation with CAMRAD II

A very specific correlation example will close out this comparison of CAMRAD II to the H-34 test data. Based on Table 17, the example is taken from the data at an advance ratio of 0.51, which is the highest advance ratio with a minimum of red cells. At this advance ratio, test collective pitch was varied from -4 degrees up to $+8$ degrees in 2 degree increments while holding a constant $+5$ degree shaft angle of attack. This shaft angle of attack could well be used in a high speed, wingless, propeller driven autogyro, so a condition of zero shaft torque within the collective pitch range was considered in selecting the test conditions for this example. Each of the following parameters will be studied in turn:

Longitudinal and lateral controls, B_{1C} and A_{1C}
 Lift, drag, side force and power, C_L/σ , C_D/σ , C_Y/σ and C_Q/σ
 Effective drag, C_{DE}/σ
 Lift to effective drag ratio, L/D_E

It is difficult to find a more encouraging comparison between theory and test than that shown with Fig. 7-13 and Fig. 7-14. The primary control angle, longitudinal cyclic, is predicted to well within experimental measurements. However, the secondary control angle, lateral cyclic is under predicted. The most heart warming result is that the rotor lift coefficient, C_L/σ , is in virtually perfect agreement with the H-34 test data all the way up to a lift coefficient of 0.065. Above $C_L/\sigma = 0.065$ there appears to be a difference that most likely is due to the blade stall model used by Johnson in CAMRAD II. Note that because predicted and test lift versus collective pitch are in such close agreement, there is no need to graph other parameters versus lift. This crutch, discussed in paragraph 6.1, can be thrown away and the abscissa can be either collective pitch or rotor lift.

Unfortunately, Fig. 7-15 through Fig. 7-17 show that the predictions of drag coefficient, C_D/σ , side force coefficient, C_Y/σ , in particular, and the H-34 torque coefficient, C_Q/σ , are poor relative to the rotor lift coefficient correlation shown with Fig. 7-14. Note from Fig. 7-17 that the rotor will autorotate at both a low collective pitch ($\theta_{\frac{1}{2}R} = -1$ degree) and a high collective pitch ($\theta_{\frac{1}{2}R} = +3$ degree). The low collective pitch autorotation point corresponds to a C_L/σ around 0.03 and the high point occurs at a C_L/σ slightly over 0.06. The test drag coefficient is clearly over predicted at virtually all lift coefficients. The predicted side force coefficient appears to have a serious upward shift. The torque coefficient is over predicted at low rotor lift. This prediction becomes an under – to severely under – prediction as lifts associated with blade stall are reached.

The rotor effective drag coefficient, C_{DE}/σ , and the rotor lift–effective drag ratio, L/D_E , comparisons are, in this author’s opinion, the best way to conclude this detailed comparison of CAMRAD II to H-34 test data given the many choices just discussed. Both parameters, as shown on Fig. 7-18, are plotted versus the rotor lift coefficient. The accurate calculation of these performance parameters very much depends on the blade element drag calculations, which in turn are very dependent on the airfoil drag coefficient characteristics used in the analysis.

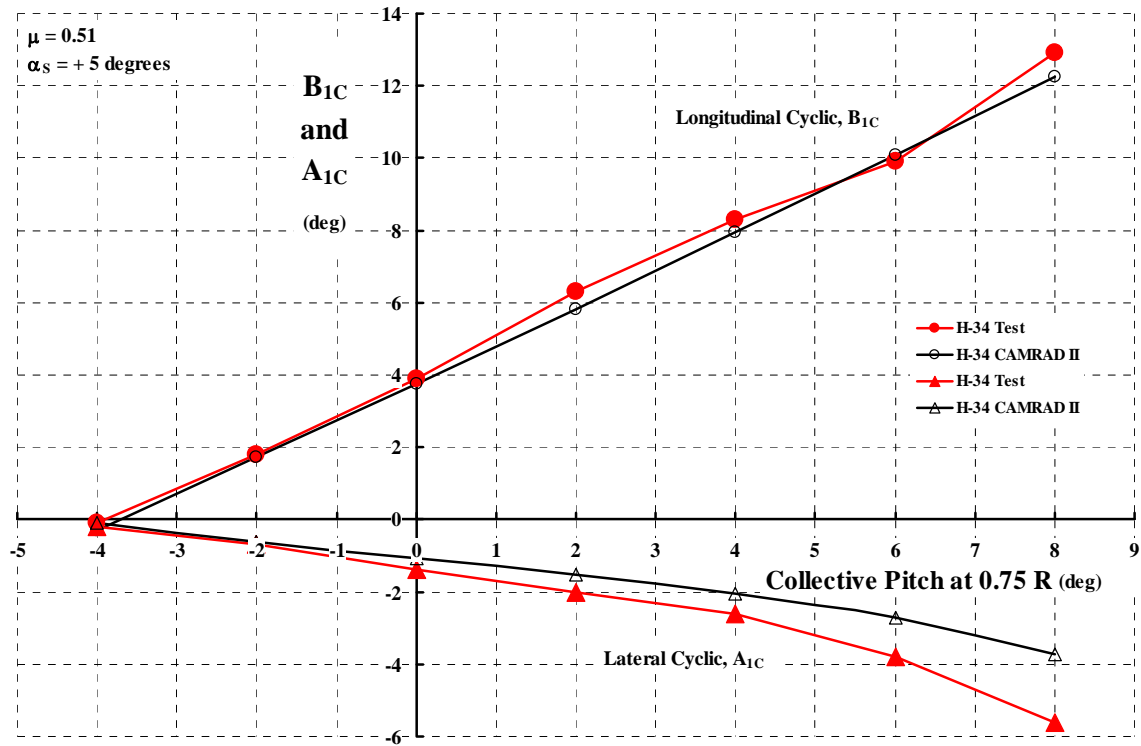


Fig. 7-13. H-34 rotor control angles, test versus CAMRAD II.

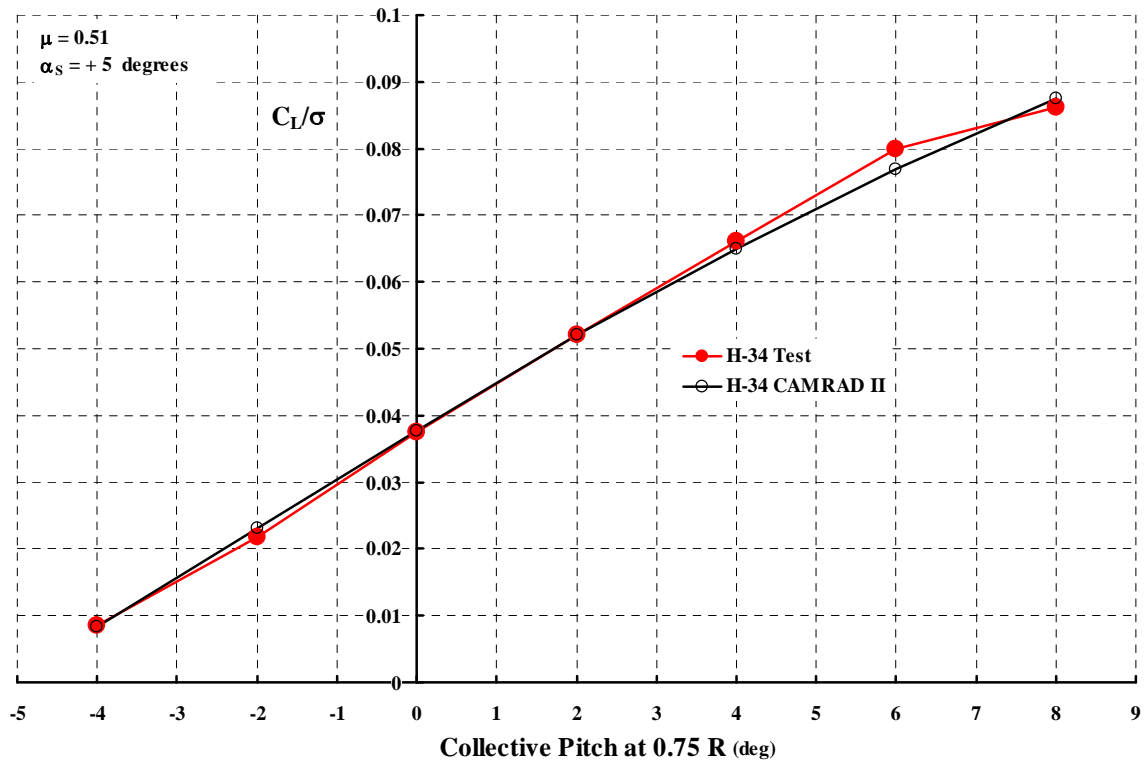


Fig. 7-14. H-34 rotor lift coefficient, test versus CAMRAD II.

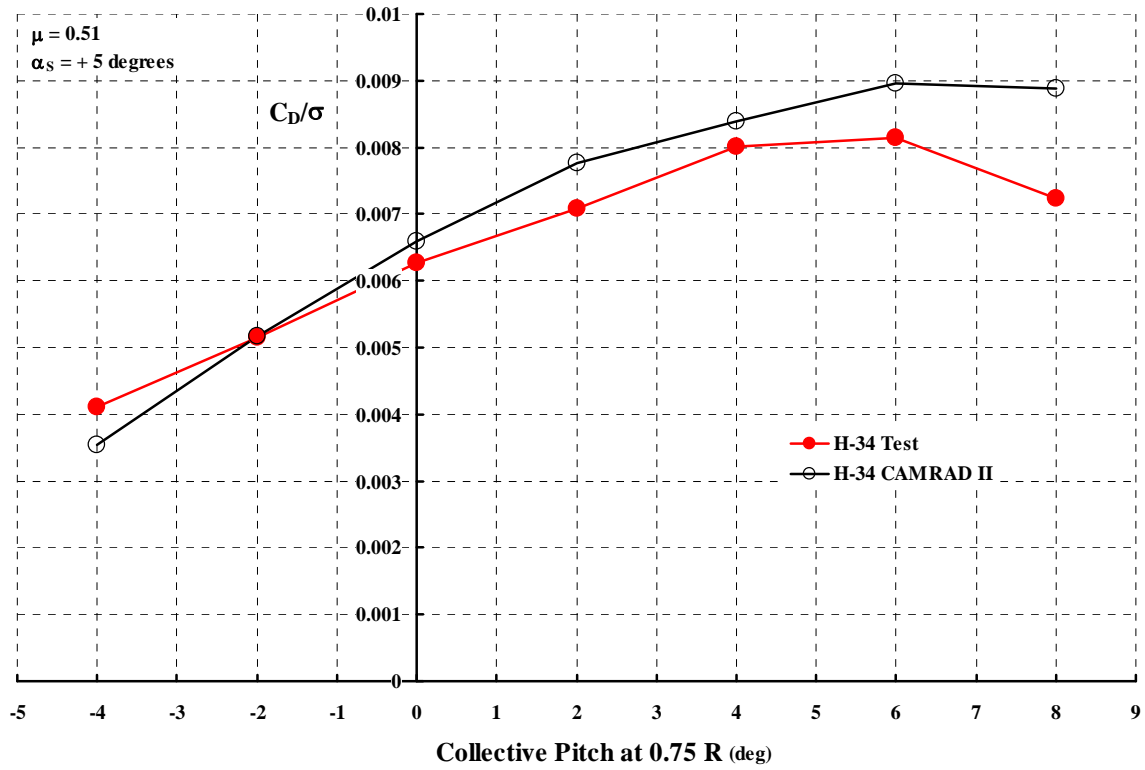


Fig. 7-15. H-34 rotor drag coefficient, test versus CAMRAD II.

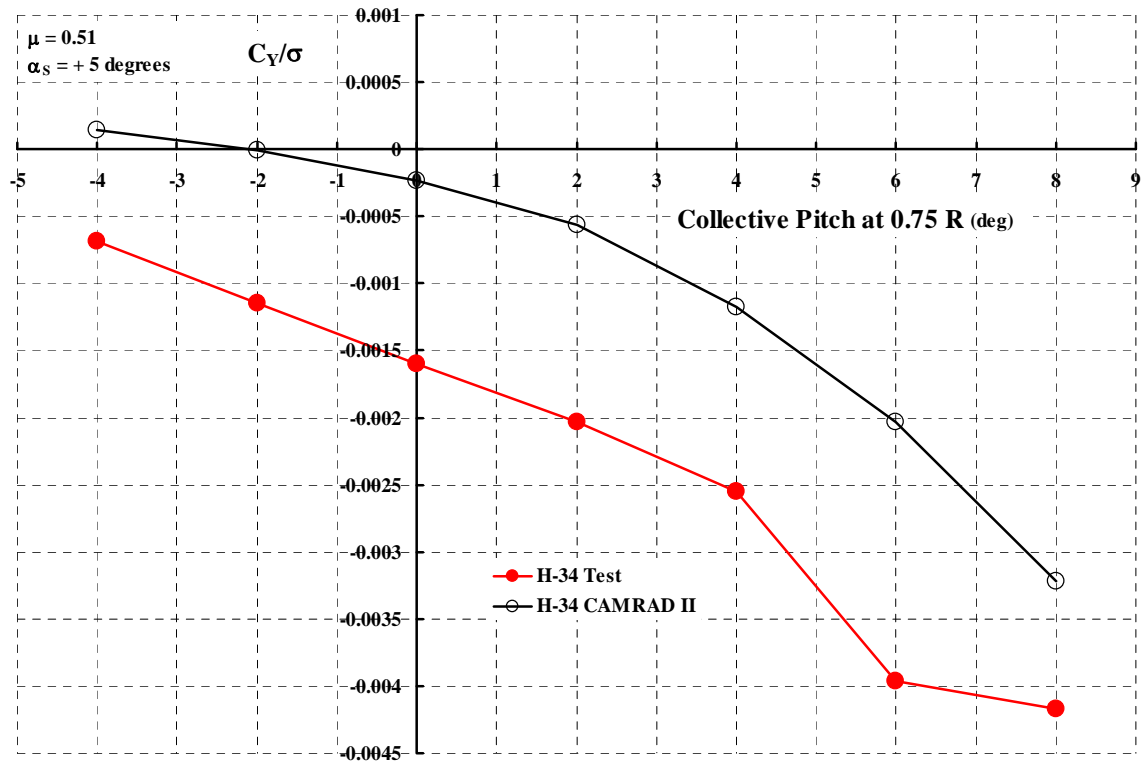


Fig. 7-16. H-34 rotor side force coefficient, test versus CAMRAD II.

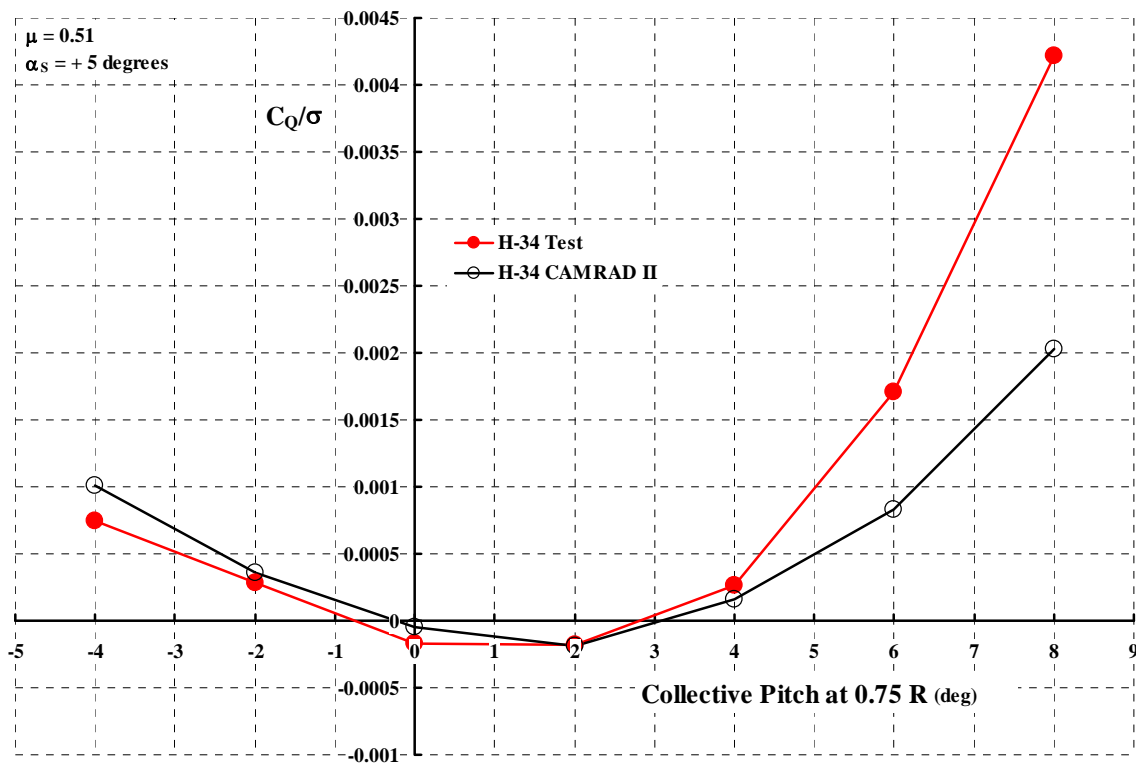


Fig. 7-17. H-34 rotor torque coefficient, test versus CAMRAD II.

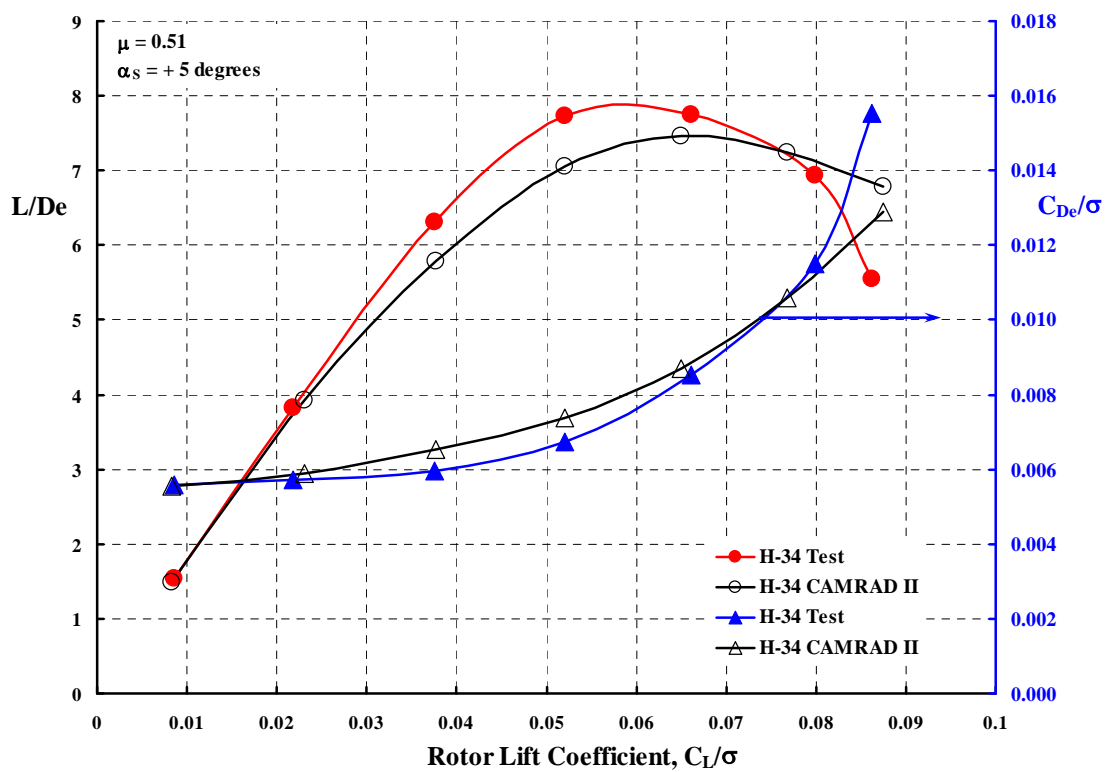


Fig. 7-18. H-34 rotor effective drag coefficient and L/D_E , test versus CAMRAD II.

7.2 H-34 Test versus CHARM (Appendix 11.11)

The summary of CHARM's prediction capability is given in the same tabulated form as used for CAMRAD II's evaluation. CHARM's evaluation, Table 18, compares the theory versus the wind tunnel measured parameters using linear regression analysis. Rotor thrust, H-force, effective drag coefficients and rotor L/D_E are derived from the measured wind tunnel measured parameters. These derived parameters are included in Appendix 11.11. The meaning of the red color coding is that the regression analysis result does not meet the accuracy criteria advocated by this author. That is, a slope, intercept or R^2 cell is shaded red if:

1. Slope outside of 0.95 to 1.05
2. Intercept outside of
 - Longitudinal cyclic, B_{1C} , ± 0.3 degrees
 - Lateral cyclic, A_{1C} , ± 0.3 degrees
 - Lift coefficient, C_L/σ , ± 0.003
 - Drag coefficient, C_D/σ , ± 0.0005
 - Side Force coefficient, C_Y/σ , ± 0.0004
 - Torque (power) coefficient, C_Q/σ , ± 0.0003
3. R^2 less than 0.97

The cells colored yellow indicate a value that is very close to the advocated criteria. Keep in mind that the more important information to be gained from Table 18 is the trends with advance ratio.

The prediction of the cyclic control angles is only half acceptable. The longitudinal cyclic intercept first decreases with advance ratio and then the error reverses so that it is increasing with advance ratio. The lateral cyclic error is characteristic of all theories to date, but the R^2 is so low that little understanding of the reason for the error can be determined. While the lift coefficient is successfully predicted – at least to an advance ratio of 0.51, the drag coefficient is not and neither is the side force coefficient. Prediction of the torque coefficient at any advance ratio is not satisfactory when measured against the criteria advocated by this author.

It is the author's opinion that the key to improving theory (and also test) begins with the intercept values. The problem must be solved at the conditions of shaft angle of attack equal zero and collective pitch at the 3/4 radius station equal zero. The effect of torsional deflections on the rotor parameters is significant as the discussion about CAMRAD II pointed out. No one now knows what the overall trailing edge configuration was for the untwisted H-34 blades under discussion in this report. The H-34 blade trailing edge is segmented metal and any given segment can be warped or bent up or down. In fact, there is no assurance that the N.A.C.A. 0012 blade elements remain uncambered in flight since the airloads that create a pitching moment bend the element.

Table 18. Table of Linear Regression Coefficients for Wind Tunnel Measured Parameters. H-34 Test versus CHARM.

Longitudinal Cyclic				Lateral Cyclic			
Mu	SLOPE	Intercept	R²	SLOPE	Intercept	R²	
0.305	1.0451	-0.5614	0.9922	1.2959	-0.3538	0.8496	
0.401	1.0552	-0.8542	0.9945	1.3952	-0.2108	0.8144	
0.460	1.0430	-0.7550	0.9906	1.3174	-0.3623	0.7361	
0.510	1.0146	-0.9278	0.9906	1.1079	-0.8099	0.6655	
0.620	1.0139	-0.2156	0.9844	0.9999	-1.2132	0.6955	
0.710	0.9554	0.3494	0.9960	1.0147	-1.0047	0.7661	
0.820	0.9519	0.8016	0.9941	0.8192	-1.1448	0.7243	
1.050	0.9387	1.3728	0.9914	0.4445	-0.7214	0.6560	

Lift Coefficient				Drag Coefficient			
Mu	SLOPE	Intercept	R²	SLOPE	Intercept	R²	
0.305	1.0150	0.0019	0.9966	0.9897	-0.0006	0.9926	
0.401	1.0078	-0.0002	0.9828	0.8675	-0.0009	0.9680	
0.460	0.9702	0.0025	0.9739	0.8318	-0.0009	0.9684	
0.510	0.9964	0.0030	0.9743	0.7539	-0.0002	0.9576	
0.620	0.9238	0.0040	0.9774	0.4443	0.0021	0.8293	
0.710	0.7514	0.0047	0.9383	0.2819	0.0037	0.6022	
0.820	0.6515	0.0055	0.9536	0.1965	0.0058	0.3651	
1.050	0.7330	-0.0098	0.9520	0.2115	0.0073	0.2734	

Y-Force Coefficient				Power Coefficient			
Mu	SLOPE	Intercept	R²	SLOPE	Intercept	R²	
0.305	0.7136	-0.0005	0.6664	0.9252	-0.0004	0.9652	
0.401	0.8083	-0.0008	0.4421	0.9329	-0.0003	0.9708	
0.460	0.6389	-0.0014	0.1943	1.0208	-0.0006	0.9612	
0.510	0.5954	-0.0014	0.2245	1.0459	-0.0007	0.9318	
0.620	-0.4216	-0.0014	0.0716	1.1281	-0.0007	0.8909	
0.710	-0.2459	-0.0017	0.0626	1.0488	-0.0007	0.8888	
0.820	-0.3994	-0.0012	0.1937	0.9317	-0.0005	0.4274	
1.050	-0.5421	0.0008	0.2997	-0.5511	0.0015	0.1417	

CHARM lift coefficient results, as a function of advance ratio, including a torsional degree of freedom are presented with Fig. 7-19. The test condition of $\theta_{\frac{3}{4}R} = 0$ and $\alpha_S = 0$ is constant throughout the advance ratio sweep. Disregarding the test data at $\mu = 1.05$, CHARM captures the basic trend with advance ratio. The aerodynamic airfoil pitching moment was obtained by including a trim tab over the outboard radius station in the lifting surface approach. The trim tab was bent up so that the computed lift coefficient at $\mu = 0.305$ was reasonably close to the test data. This configuration remained the same for all higher advance ratios.

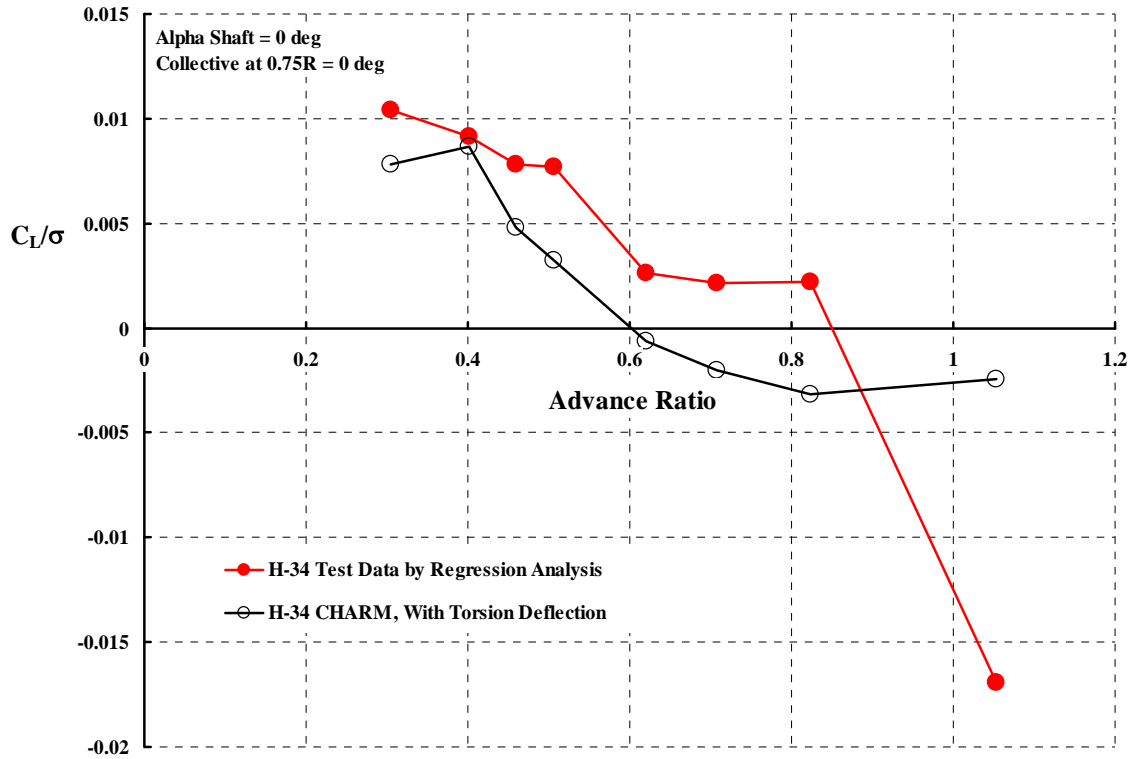


Fig. 7-19. CHARM lift coefficient correlation at $\theta_{\frac{3}{4}R} = 0$ and $\alpha_S = 0$.

CHARM's ability to predict the cyclic control angles, longitudinal cyclic (B_{1C}) and lateral cyclic (A_{1C}), required to trim the rotor tip path plane normal to the shaft is examined with Fig. 7-20. The rotor H-force, Y-force and shaft torque coefficients at the $\theta_{\frac{3}{4}R} = 0$ and $\alpha_S = 0$ test condition are shown in Fig. 7-21, Fig. 7-22 and Fig. 7-23 respectively. The H-force coefficient, which is identical with the rotor drag coefficient because the shaft angle of attack is zero, is a very large force. Fig. 7-21 shows that CHARM's prediction is well within experimental accuracy. In contrast, the Y-force coefficient is a relatively small force and CHARM's prediction is not satisfactory. The torque (or power) coefficient correlation, Fig. 7-23, is clearly well above the experimental trend. The torque and H-force both depend primarily on the blade element drag. That the H-force could be closely predicted and the torque be over predicted requires some careful explaining. Of course, the blade element drag is weighted by radius to compute torque, so the radial and azimuthal distribution of airfoil drag must be examined in detail first.

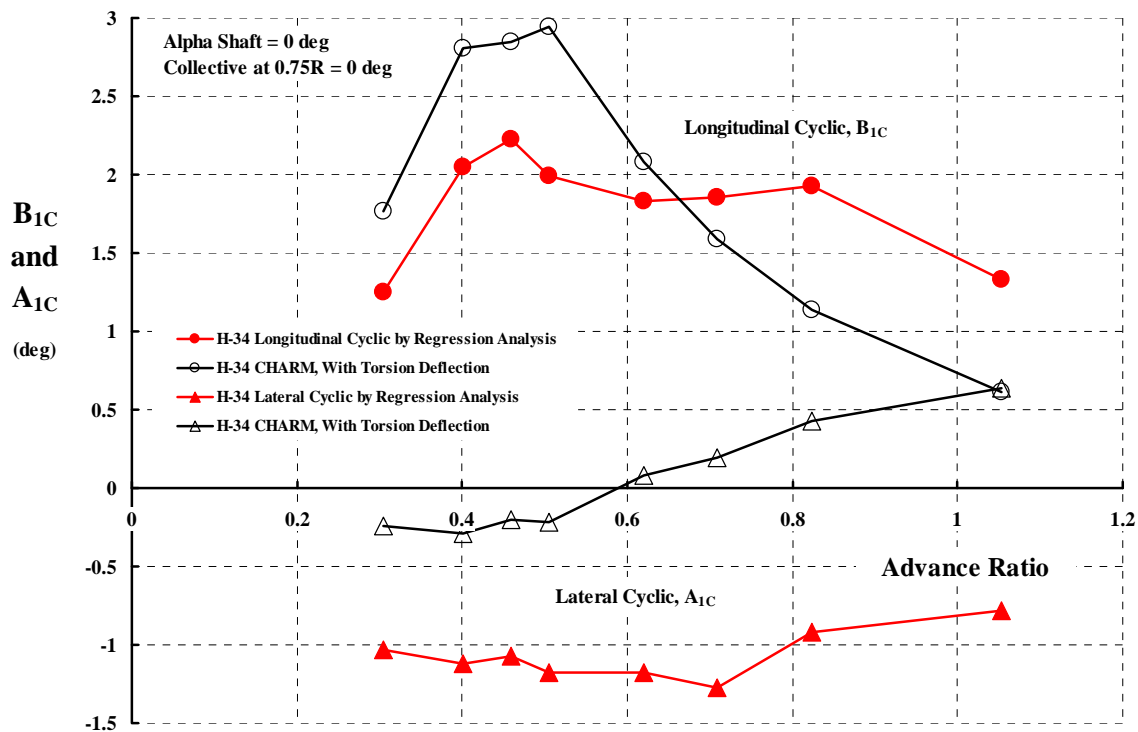


Fig. 7-20. Longitudinal and lateral cyclic correlation with CHARM for the test condition of $\theta_{3/4 R} = 0$ and $\alpha_S = 0$.

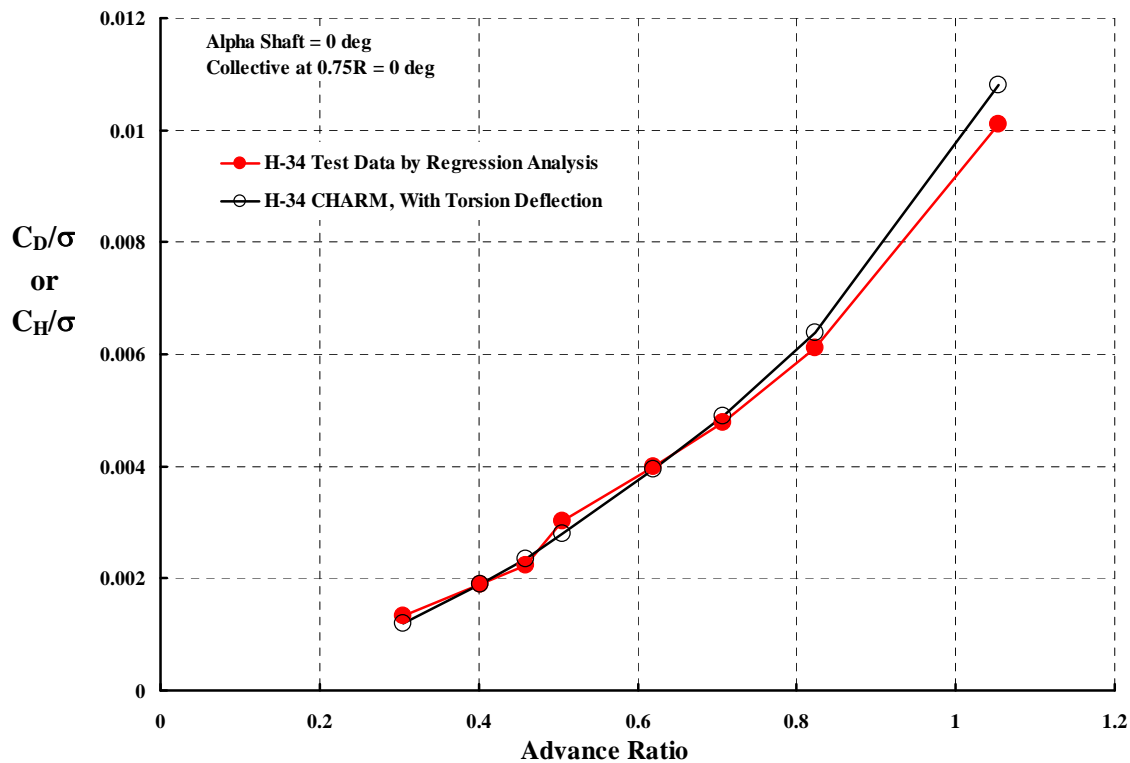


Fig. 7-21. Longitudinal force correlation with CHARM

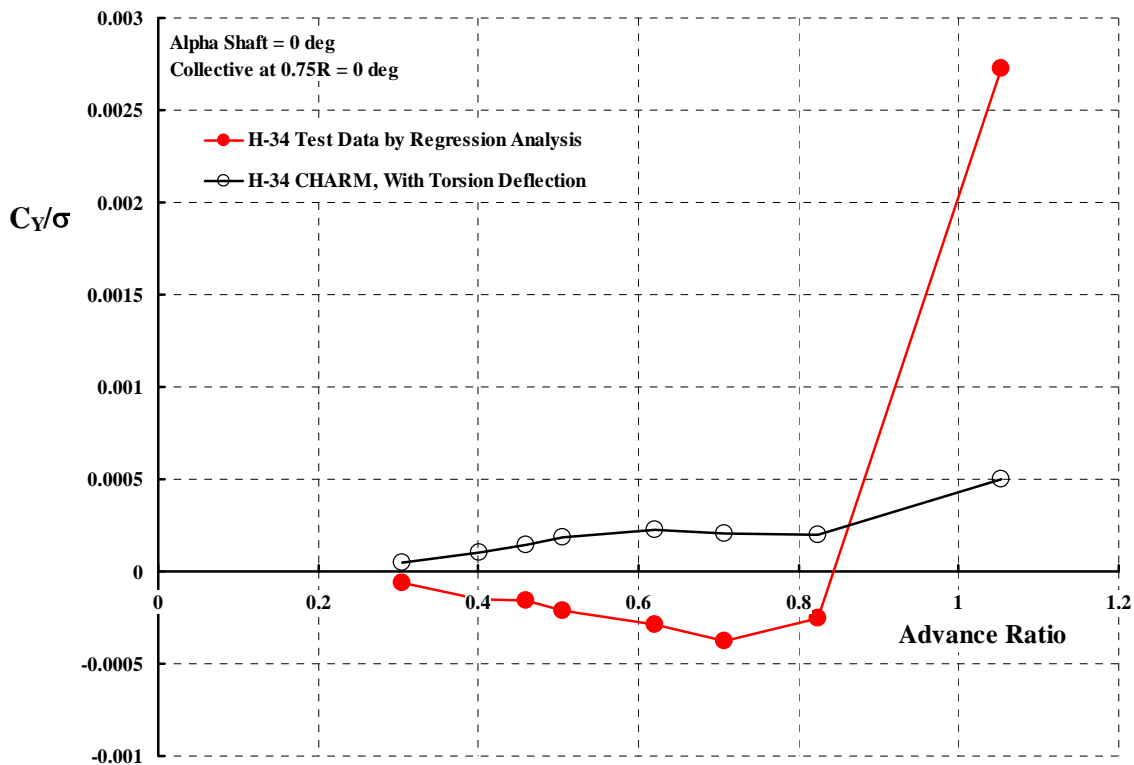


Fig. 7-22. Lateral force correlation with CHARM

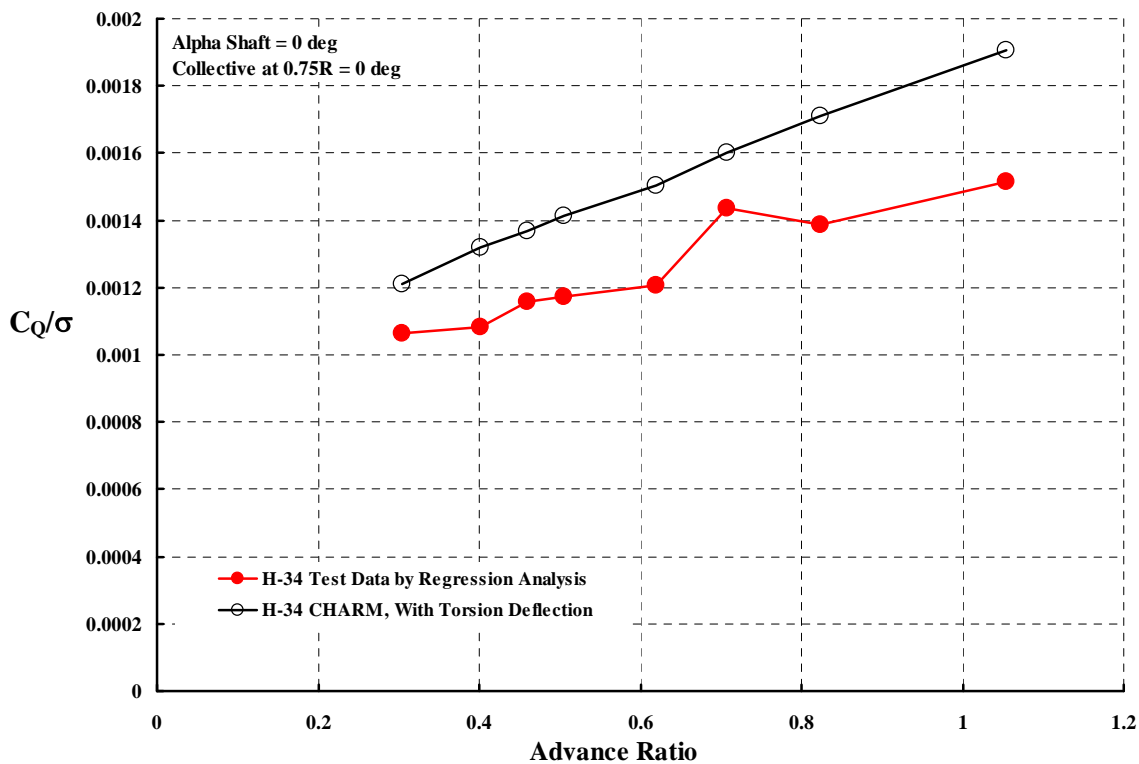


Fig. 7-23. Shaft torque correlation with CHARM

The rotor effective drag coefficient, C_{De}/σ , correlation is shown with Fig. 7-24. It is important to appreciate that this coefficient, at the $\theta_{\frac{3}{4}R} = 0$ and $\alpha_S = 0$ test condition, is dominated by the H-force at the higher advance ratios. Because the shaft angle of attack is zero, the C_{De}/σ coefficient, following from Eq. (19) and applying Appendix 11.1 thoughts, can be written as

$$(28) \quad \frac{C_{De}}{\sigma} = \frac{C_{P_{\text{rotor induced}}} + C_{P_{\text{rotor profile}}}}{\sigma\mu} = \frac{1}{\mu} \frac{C_Q}{\sigma} + \frac{C_H}{\sigma}$$

and the two components of C_{De}/σ as calculated by CHARM are also shown on Fig. 7-12.

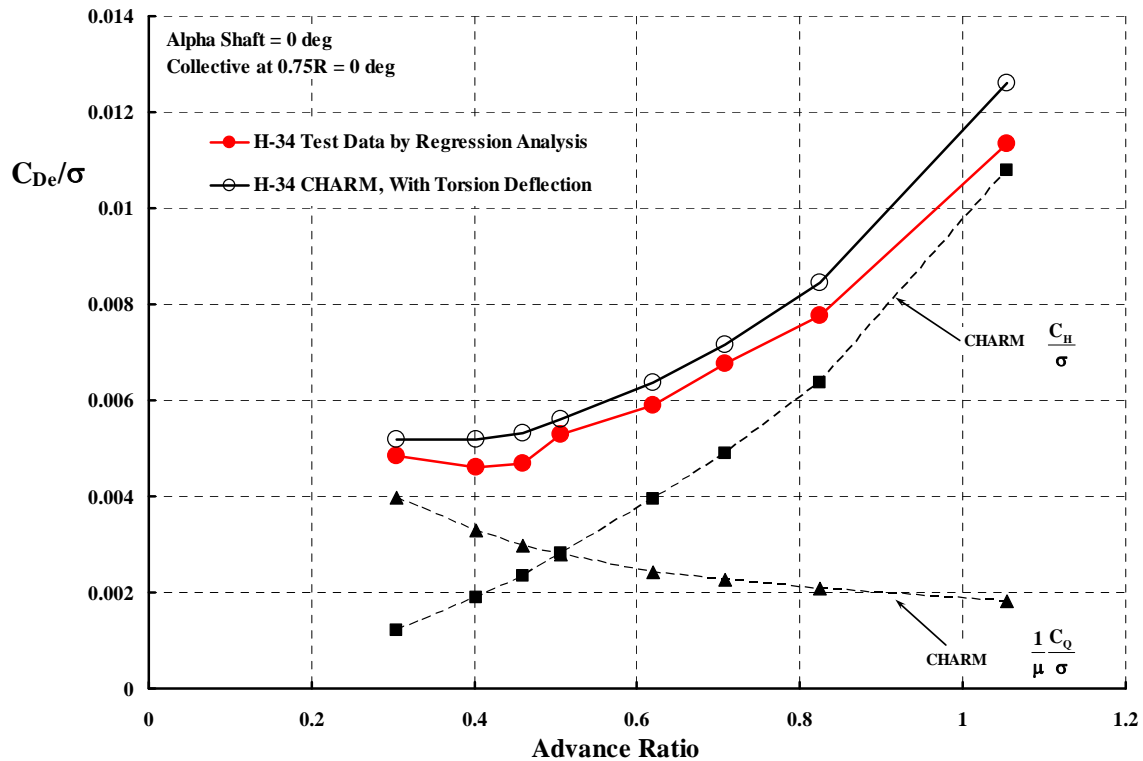


Fig. 7-24. Rotor effective drag correlation with CHARM

A very specific correlation example will close out this comparison of CHARM to the H-34 test data. The example is taken from the test data at an advance ratio of 0.51 and provides a baseline data set to which any theory may be compared. The example was influenced by CAMRAD II's encouraging comparison between theory and test shown with Fig. 7-13 and Fig. 7-14. At this advance ratio, test collective pitch was varied from -4 degrees up to $+8$ degrees in 2 degree increments while holding a constant $+5$ degree shaft angle of attack. This shaft angle of attack could well be used in a high speed, wingless, propeller driven autogyro, so a condition of zero shaft torque within the collective pitch range was considered in selecting the test conditions for this example. Each of the following parameters will be studied in turn:

Longitudinal and lateral controls, B_{1C} and A_{1C}
Lift, drag, side force and power, C_L/σ , C_D/σ , C_Y/σ and C_Q/σ
Effective drag, C_{DE}/σ
Lift to effective drag ratio, L/D_E

CHARM's prediction of the primary control angle, longitudinal cyclic in Fig. 7-25, is an example of where the slope is nearly perfectly predicted. And, most interestingly, correlation with the secondary control angle, lateral cyclic, is – quite frankly – remarkable. The lift coefficient, Fig. 7-26, also is correlated well with respect to slope at low lift, but because of zero shift and an early prediction of blade stall, the overall correlation is not good enough in this author's opinion.

Unfortunately, Fig. 7-27 through Fig. 7-29 show that the predictions of drag coefficient, C_D/σ , side force coefficient, C_Y/σ , in particular, and the H-34 torque coefficient, C_Q/σ , are poor even relative to the rotor lift coefficient correlation shown with Fig. 7-26. Note from Fig. 7-29 that experimentally the H-34 rotor will autorotate at both a low collective pitch ($\theta_{4R} = -1$ degree) and a high collective pitch ($\theta_{4R} = +3$ degree). The low collective pitch autorotation point corresponds to a C_L/σ around 0.03 and the high point occurs at a C_L/σ slightly over 0.06. CHARM does not predict that autorotation can be reached at any collective pitch. The torque coefficient is over predicted through out the collective pitch sweep. The test drag coefficient is clearly over predicted at virtually all lift coefficients. The predicted side force coefficient appears to have a serious upward shift.

The rotor effective drag coefficient, C_{DE}/σ , and the rotor lift–effective drag ratio, L/D_E , comparisons are, in this author's opinion, the best way to conclude this detailed comparison of CAMRAD II to H-34 test data given the many choices just discussed. Both parameters, as shown on Fig. 7-30, are plotted versus the rotor lift coefficient. The accurate calculation of these performance parameters very much depends on the blade element drag calculations. CHARM's prediction is significantly in error, which suggests that the airfoil drag coefficient characteristics used in the analysis are not correct.

Under prediction of the maximum rotor L/D_E is most discouraging. Appendix 11.11 provides graphs of H-34 L/D_E (derived from measured test parameters) versus CHARM's prediction. The correlation is provided for each advance ratio. The under prediction is no less than 12 percent and becomes an under prediction of 60 percent at high advance ratio as Table 19 summarizes.

Table 19. L/D_E Linear Regression Coefficients for H-34 Test versus CHARM.

Mu	SLOPE	Intercept	R²	Mu	SLOPE	Intercept	R²
0.305	1.2375	0.4054	0.9689	0.620	1.2748	1.0794	0.8962
0.401	1.2618	0.1607	0.9181	0.710	1.4272	0.2680	0.8968
0.460	1.3276	0.4071	0.8869	0.820	1.2263	0.7122	0.8868
0.510	1.1293	1.0049	0.8749	1.050	1.6449	-0.7483	0.8220

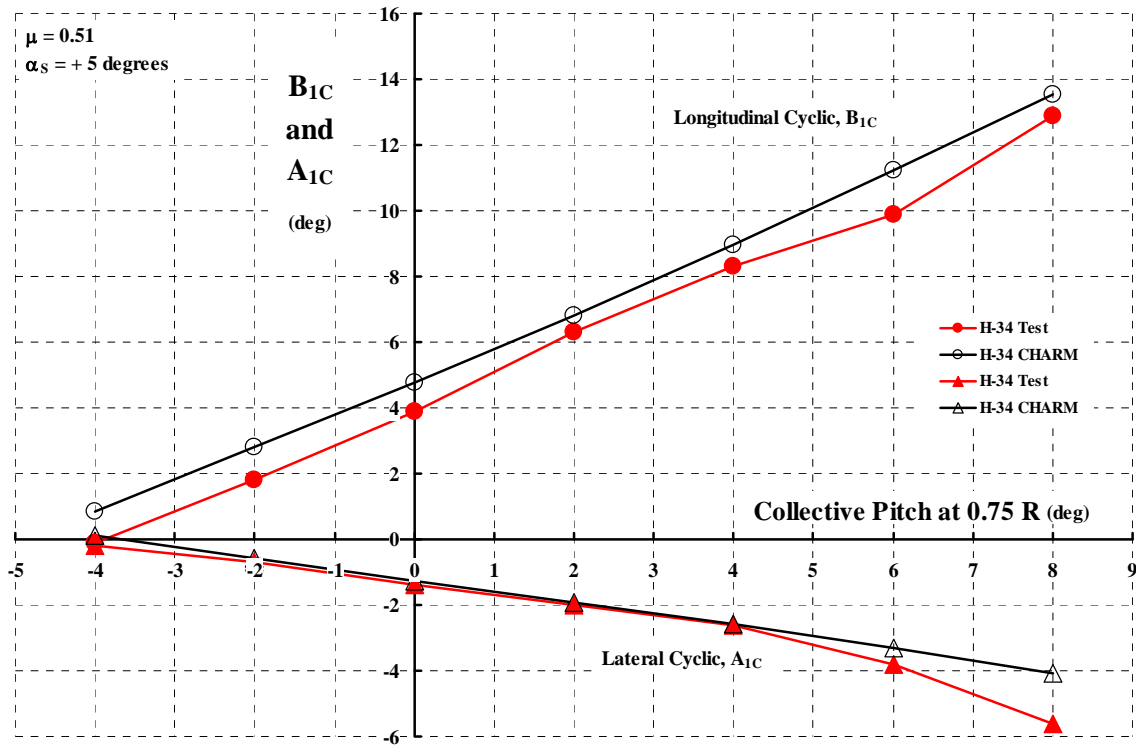


Fig. 7-25. H-34 rotor control angles, test versus CHARM.

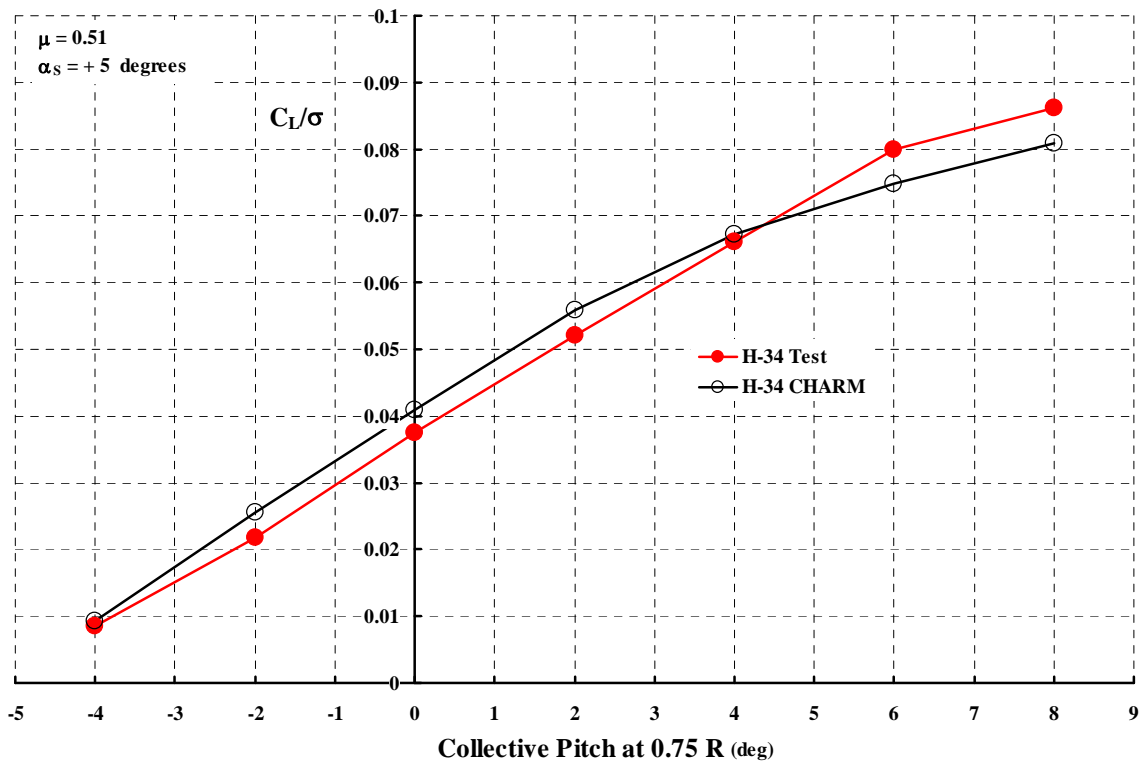


Fig. 7-26. H-34 rotor lift coefficient, test versus CHARM.

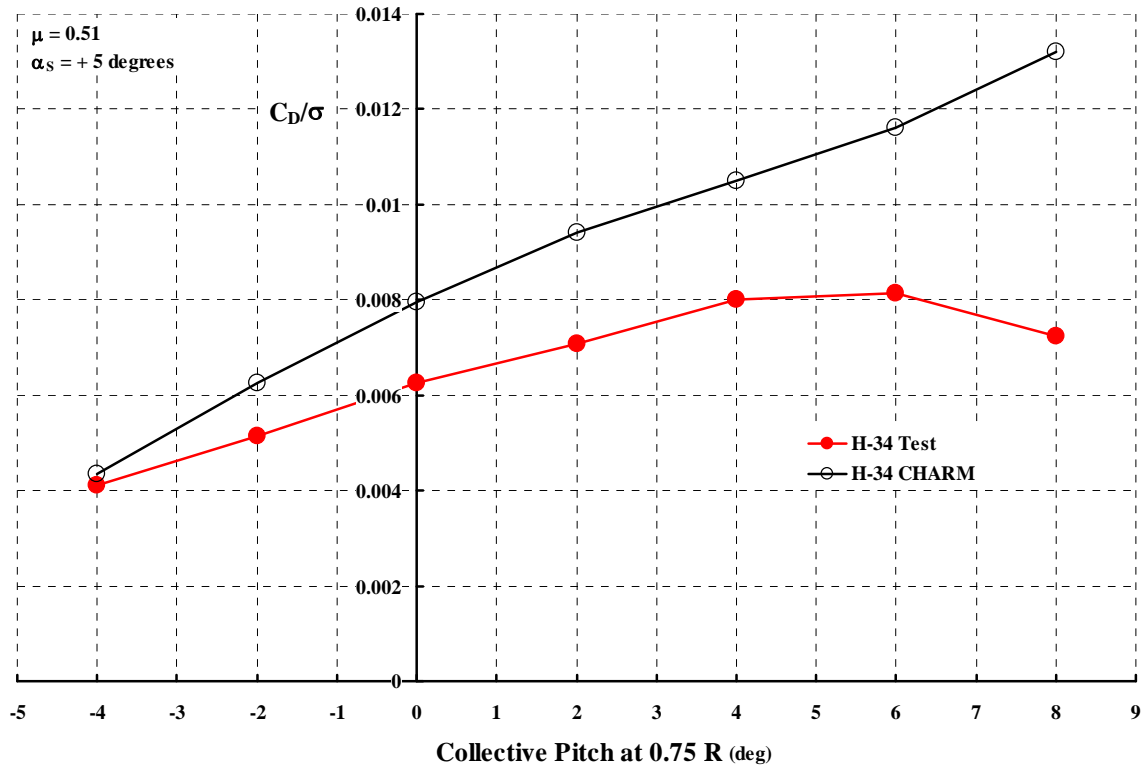


Fig. 7-27. H-34 rotor drag coefficient, test versus CHARM.

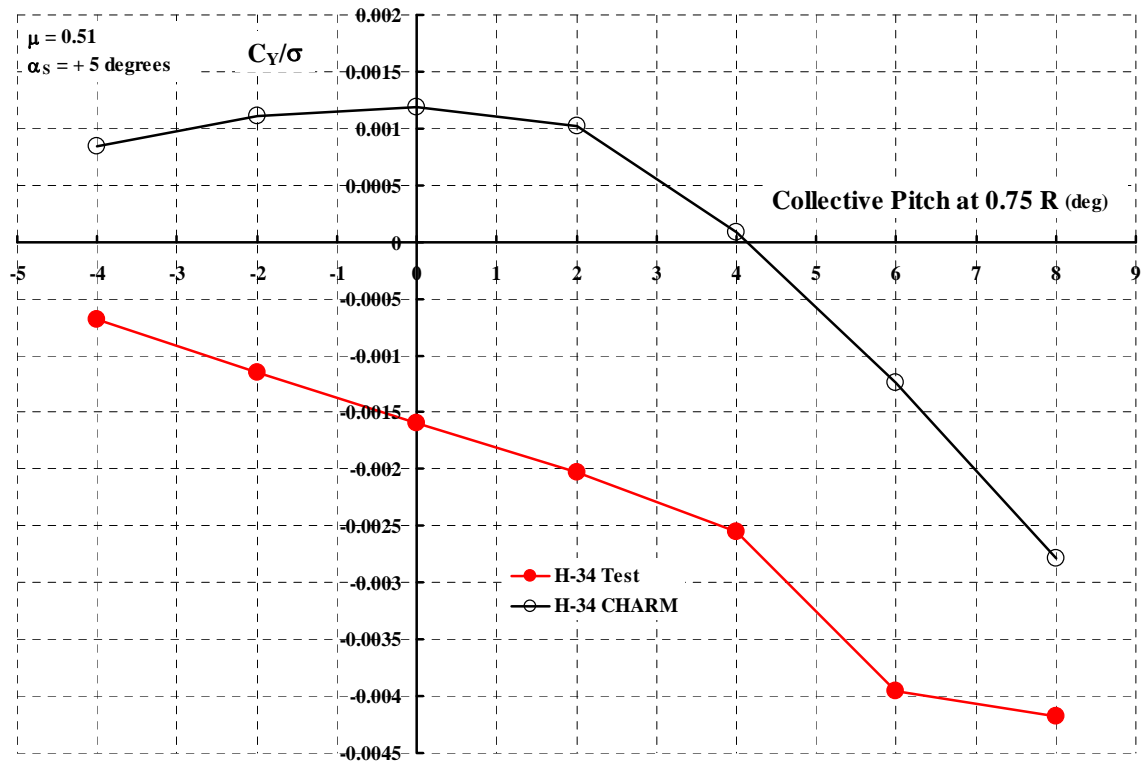


Fig. 7-28. H-34 rotor side force coefficient, test versus CHARM.

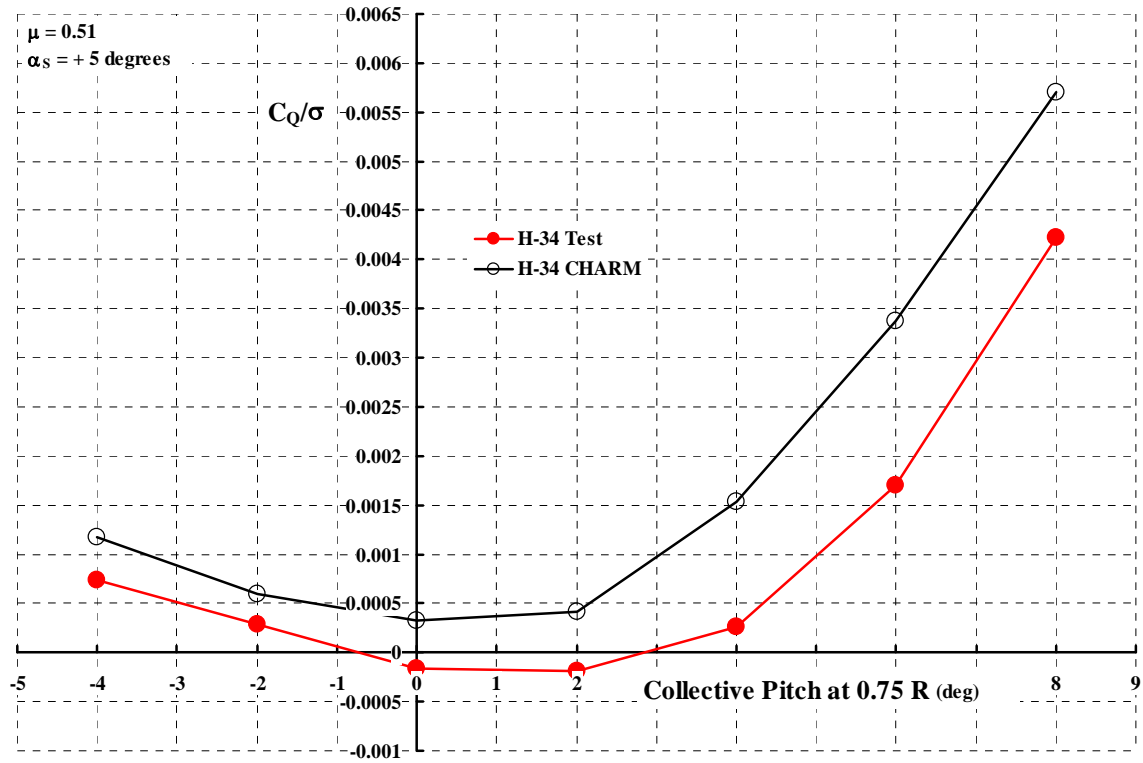


Fig. 7-29. H-34 rotor torque coefficient, test versus CHARM.

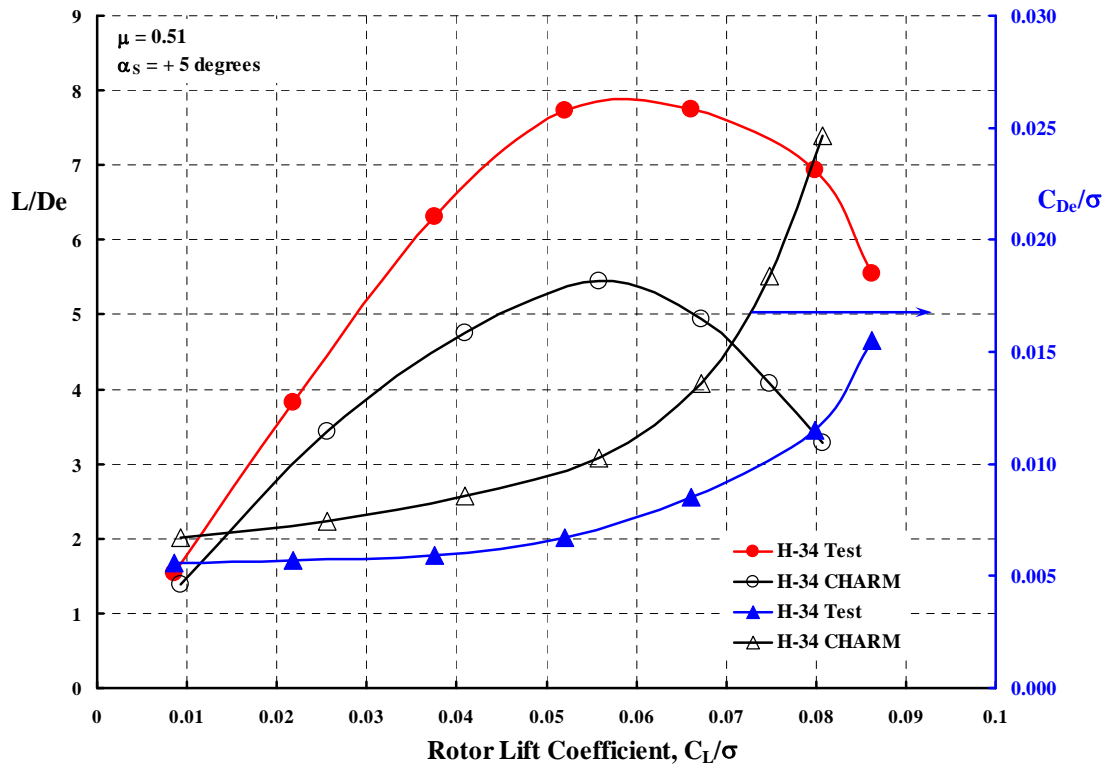


Fig. 7-30. H-34 rotor effective drag coefficient and L/D_E , test versus CHARM.

7.3 H-34 Test versus RCAS (Appendix 11.12)

The summary of RCAS's prediction capability is given in the same tabulated form as used for CAMRAD II's and CHARM's evaluation. RCAS's evaluation, Table 20, compares the theory versus the wind tunnel measured parameters using linear regression analysis. Rotor thrust, H-force, effective drag coefficients and rotor L/De are derived from the measured wind tunnel measured parameters. These derived parameters are included in Appendix 11.12. The meaning of the red color coding is that the regression analysis result does not meet the accuracy criteria advocated by this author. That is, a slope, intercept or R^2 cell is shaded red if:

1. Slope outside of 0.95 to 1.05
2. Intercept outside of
 - Longitudinal cyclic, B_{1C} , ± 0.3 degrees
 - Lateral cyclic, A_{1C} , ± 0.3 degrees
 - Lift coefficient, C_L/σ , ± 0.003
 - Drag coefficient, C_D/σ , ± 0.0005
 - Side Force coefficient, C_Y/σ , ± 0.0004
 - Torque (power) coefficient, C_Q/σ , 0.0003
3. R^2 less than 0.97

The cells colored yellow indicate a value that is very close to the advocated criteria. Keep in mind that the more important information to be gained from Table 20 is the trends with advance ratio.

The prediction of the cyclic control angles is less than half acceptable. The longitudinal intercept steadily increases with advance ratio and the slope is – strangely – not well predicted at the lower advance ratios. The lateral cyclic error is characteristic of all theories to date, but the R^2 is at a value which is encouraging. While the lift coefficient and drag coefficient prediction is encouraging – at least up to an advance ratio of 0.51, the drag coefficient is not and neither is the side force coefficient. Prediction of the torque coefficient is not satisfactory above an advance ratio of 0.51 using the criteria advocated by this author.

As stated earlier, the key to improving theory (and also test) begins with the intercept values. The problem must be solved at the conditions of shaft angle of attack equal zero and collective pitch at the 3/4 radius station equal zero. The effect of torsional deflections on the rotor parameters is significant as the early discussions pointed out. No one now knows what the overall trailing edge configuration was for the untwisted H-34 blades under discussion in this report. The H-34 blade trailing edge is segmented metal and any given segment can be warped or bent up or down. In fact, there is no assurance that the N.A.C.A. 0012 blade elements remain uncambered in flight since the airloads that create a pitching moment bend the element.

Table 20. Table of Linear Regression Coefficients for Wind Tunnel Measured Parameters. H-34 Test versus RCAS.

Mu	Longitudinal Cyclic			Lateral Cyclic		
	SLOPE	Intercept	R²	SLOPE	Intercept	R²
0.305	1.1574	-0.0610	0.9866	1.0661	-0.4305	0.9369
0.401	1.2162	0.1646	0.9860	1.2639	-0.0916	0.9193
0.460	1.1443	0.3687	0.9811	1.2359	-0.1682	0.9438
0.510	1.0800	0.2731	0.9820	1.1075	-0.4114	0.9188
0.620	1.0371	0.4165	0.9772	1.1248	-0.6059	0.9103
0.710	0.9983	0.5338	0.9955	0.9132	-0.8036	0.8927
0.820	0.9676	0.7547	0.9915	1.0258	-0.7181	0.8792
1.050	0.9125	0.9403	0.9819	0.6397	-0.8133	0.3949

Mu	Lift Coefficient			Drag Coefficient		
	SLOPE	Intercept	R²	SLOPE	Intercept	R²
0.305	0.9949	0.0023	0.9956	1.0341	-0.0006	0.9926
0.401	0.9411	0.0020	0.9903	0.9688	-0.0007	0.9899
0.460	0.9247	0.0019	0.9929	0.9415	-0.0005	0.9930
0.510	0.9539	0.0021	0.9856	0.9520	0.0000	0.9938
0.620	0.9726	-0.0003	0.9920	0.7754	0.0013	0.9655
0.710	0.8491	-0.0002	0.9840	0.6338	0.0026	0.8316
0.820	0.8361	0.0010	0.9754	0.6846	0.0028	0.6989
1.050	1.0613	-0.0170	0.9117	1.0117	0.0002	0.7282

Mu	Y-Force Coefficient			Power Coefficient		
	SLOPE	Intercept	R²	SLOPE	Intercept	R²
0.305	0.6896	-0.0003	0.7059	1.0929	0.0000	0.9803
0.401	0.9202	-0.0002	0.6469	1.0296	0.0002	0.9635
0.460	1.0349	-0.0002	0.6313	0.9758	0.0004	0.9610
0.510	0.9566	-0.0002	0.6592	0.9576	0.0006	0.9205
0.620	1.4554	-0.0002	0.5089	0.7440	0.0006	0.8114
0.710	1.4471	-0.0009	0.5819	0.6617	0.0008	0.7168
0.820	2.8038	-0.0009	0.7805	0.4625	0.0009	0.5277
1.050	0.5410	-0.0016	0.1527	0.2347	0.0006	0.0971

RCAS lift coefficient results, as a function of advance ratio, including a torsional degree of freedom are presented with Fig. 7-31. The test condition of $\theta_{3/4R} = 0$ and $\alpha_S = 0$ is constant throughout the advance ratio sweep. Disregarding the test data at $\mu = 1.05$, RCAS captures the basic trend with advance ratio. The aerodynamic airfoil pitching moment was obtained by including an airfoil pitching moment coefficient of $+ 0.03$ over the radius station from $0.8R$ to $0.9R$. This pitching moment coefficient was the configuration used in the CAMRAD II calculations, which yielded a computed lift coefficient at $\mu = 0.305$ reasonably close to the test data. This configuration remained the same for all higher advance ratios.

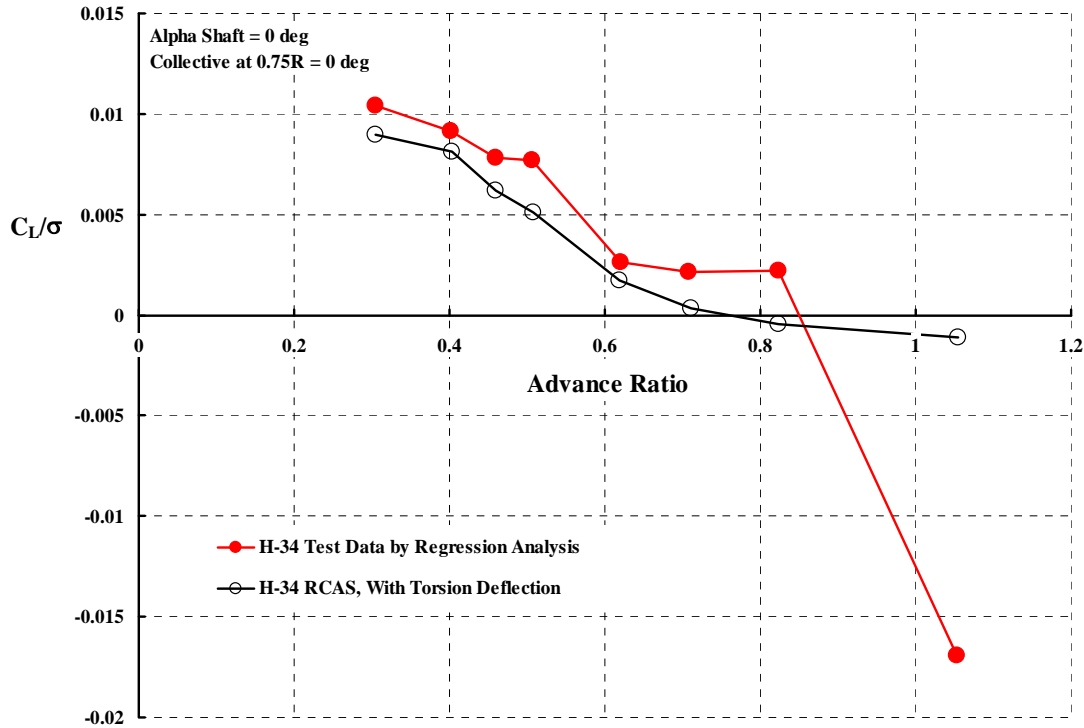


Fig. 7-31. RCAS lift coefficient correlation at $\theta_{3/4R} = 0$ and $\alpha_S = 0$.

RCAS's ability to predict the cyclic control angles, longitudinal cyclic (B_{1C}) and lateral cyclic (A_{1C}), required to trim the rotor tip path plane normal to the shaft is examined with Fig. 7-32. The rotor H-force, Y-force and shaft torque coefficients at the $\theta_{3/4R} = 0$ and $\alpha_S = 0$ test condition are shown in Fig. 7-33, Fig. 7-34 and Fig. 7-35 respectively. The H-force coefficient, which is identical with the rotor drag coefficient because the shaft angle of attack is zero, is a very large force. Fig. 7-33 shows that RCAS's prediction is close to experimental accuracy. In contrast, the Y-force coefficient is a relatively small force and RCAS's prediction is not satisfactory. The torque (or power) coefficient correlation, Fig. 7-35, is clearly well above the experimental trend. The torque and H-force both depend primarily on the blade element drag. That the H-force could be somewhat under predicted and the torque be over predicted requires more careful explaining. Of course, the blade element drag is weighted by radius to compute torque, so the radial and azimuthal distribution of airfoil drag must be examined in detail first.

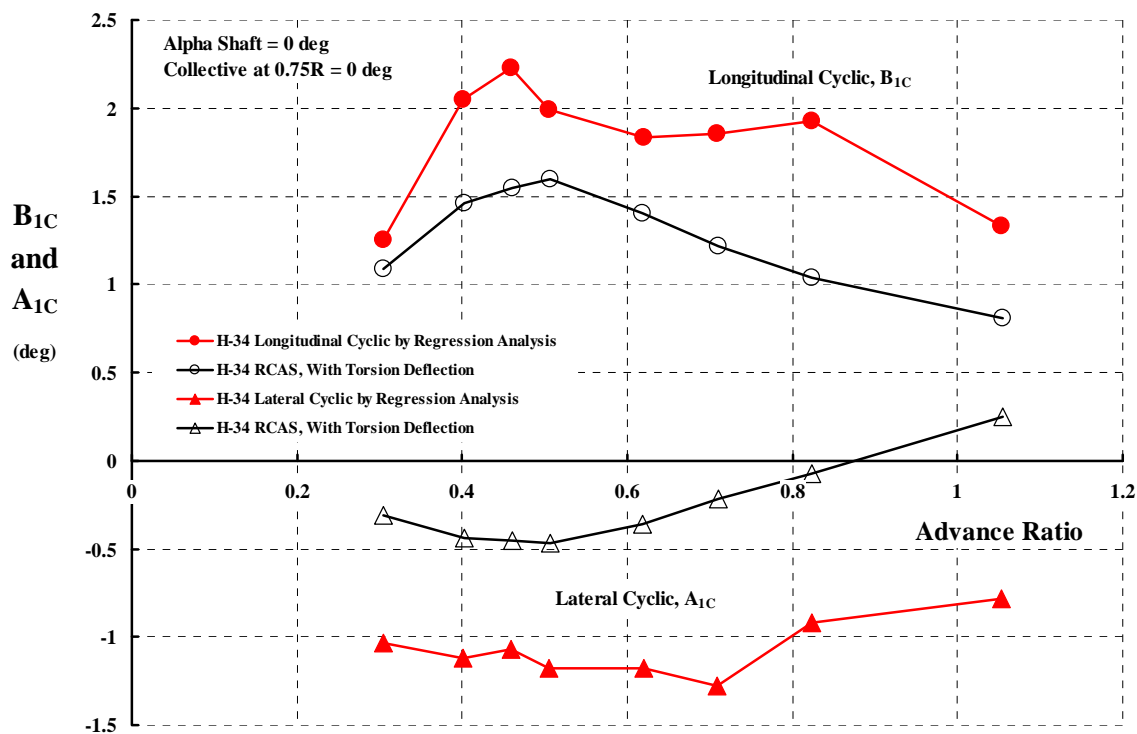


Fig. 7-32. Longitudinal and lateral cyclic correlation with RCAS for the test condition of $\theta_{3/4 R} = 0$ and $\alpha_S = 0$.

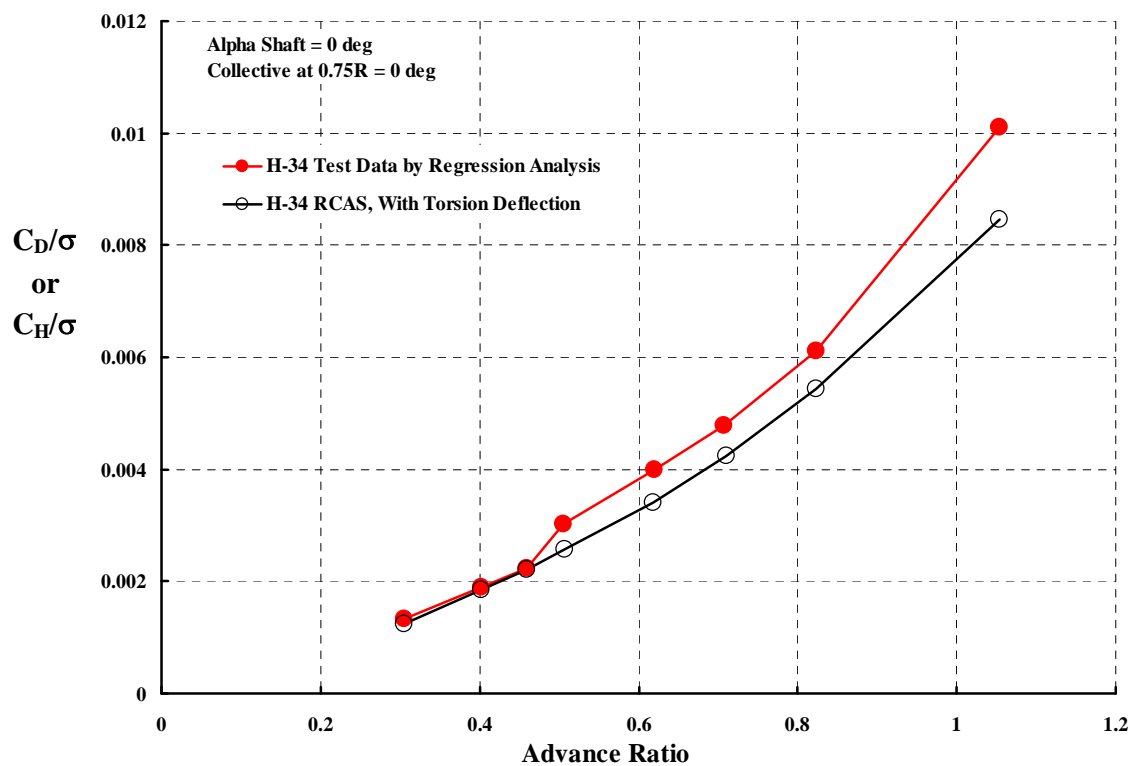


Fig. 7-33. Longitudinal force correlation with RCAS

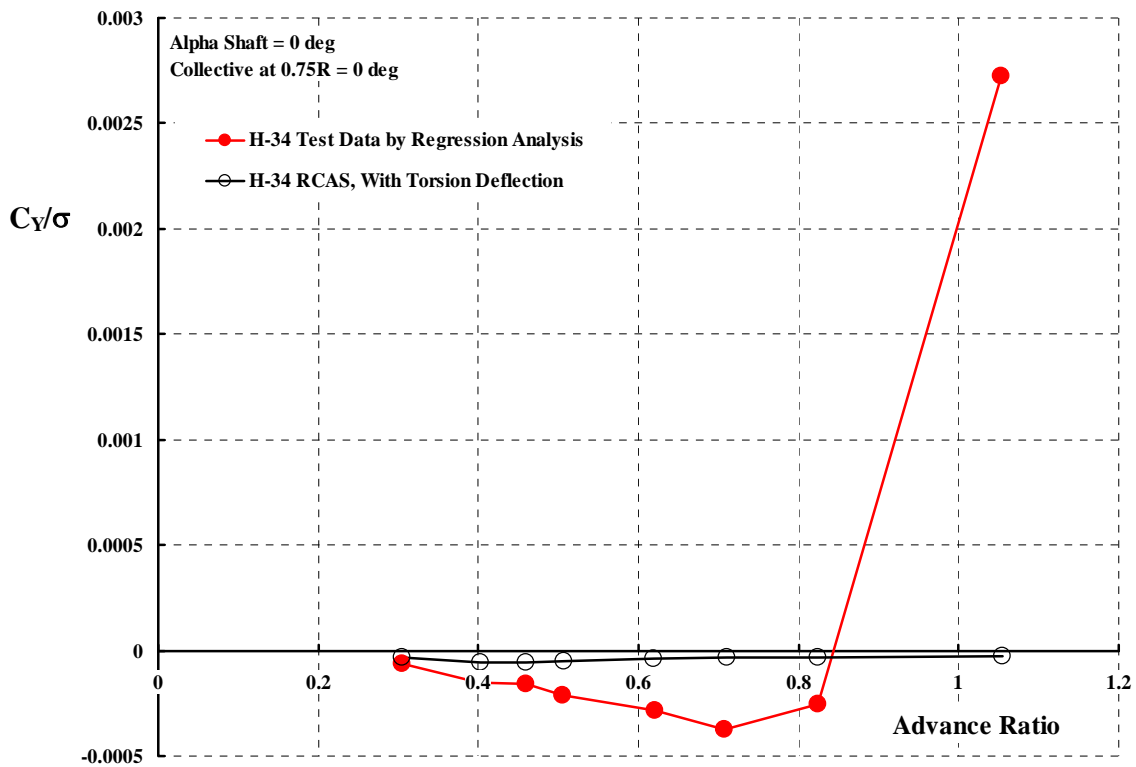


Fig. 7-34. Lateral force correlation with RCAS

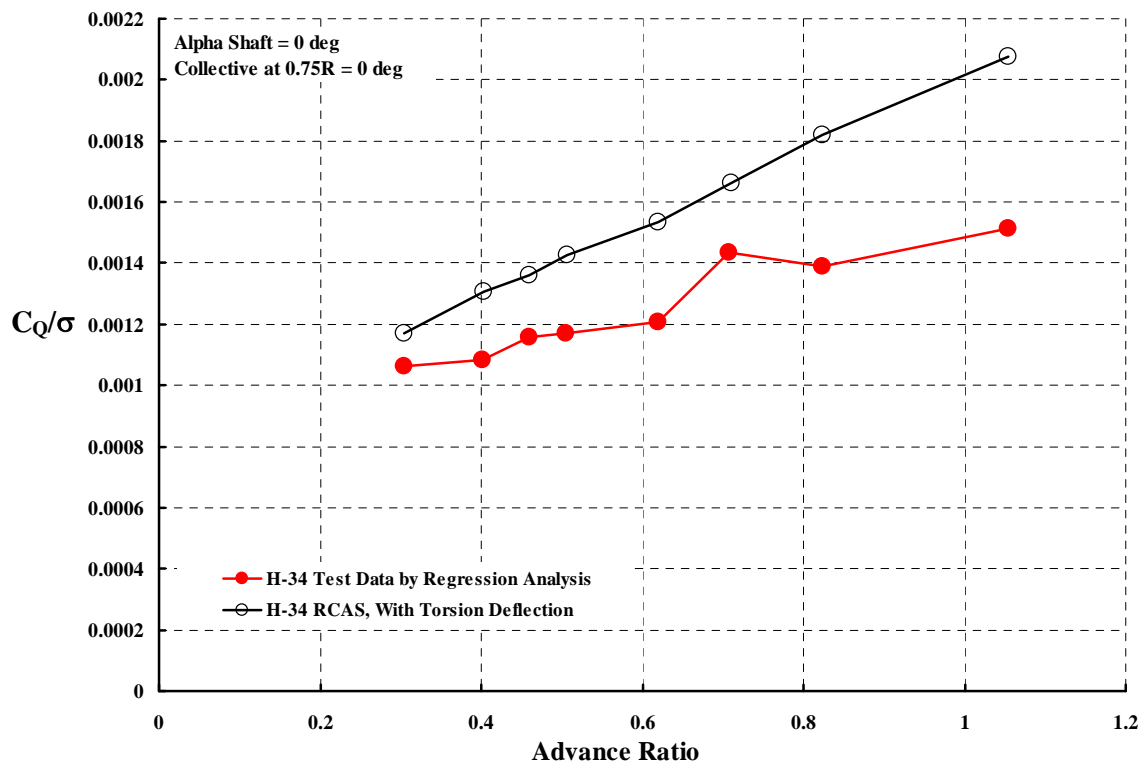


Fig. 7-35. Shaft torque correlation with RCAS

The rotor effective drag coefficient, C_{De}/σ , correlation is shown with Fig. 7-36. It is important to appreciate that this coefficient, at the $\theta_{\frac{3}{4}R} = 0$ and $\alpha_S = 0$ test condition, is dominated by the H-force at the higher advance ratios. Because the shaft angle of attack is zero, the C_{De}/σ coefficient, following from Eq. (19) and applying Appendix 11.1 thoughts, can be written as

$$(29) \quad \frac{C_{De}}{\sigma} = \frac{C_{P_{\text{rotor induced}}} + C_{P_{\text{rotor profile}}}}{\sigma\mu} = \frac{1}{\mu} \frac{C_Q}{\sigma} + \frac{C_H}{\sigma}$$

and the two components of C_{De}/σ as calculated by RCAS are also shown on Fig. 7-36.

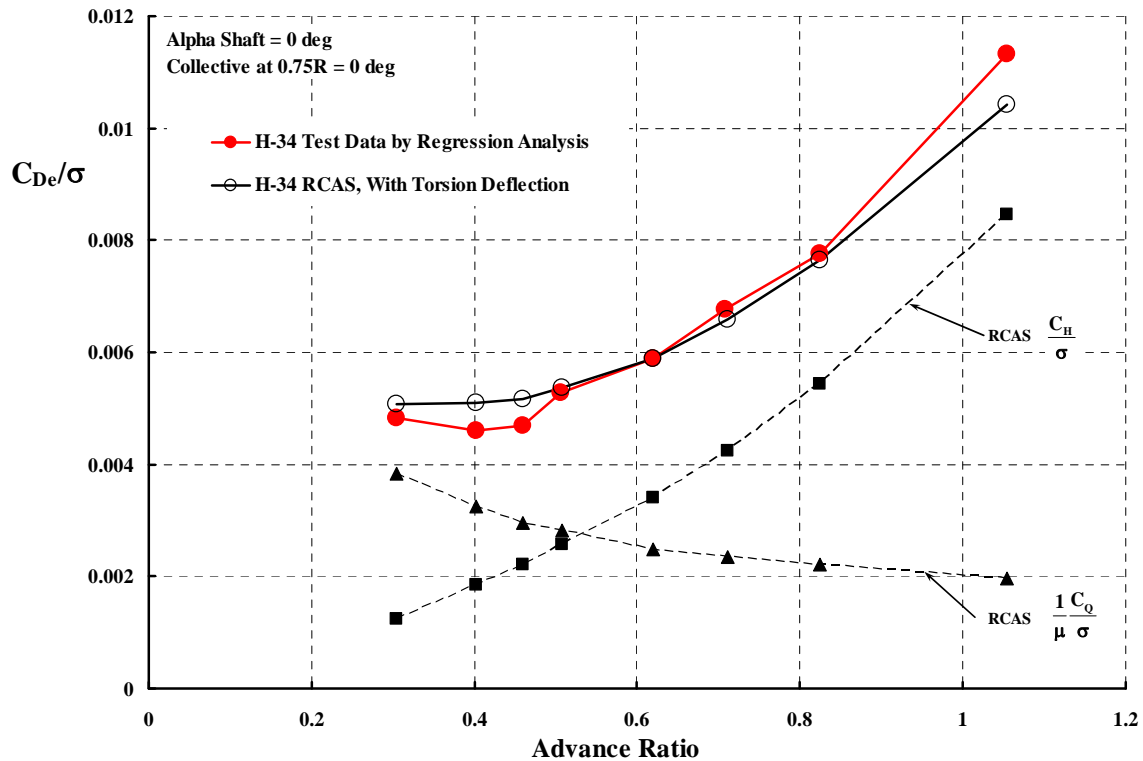


Fig. 7-36. Rotor effective drag correlation with RCAS

A very specific correlation example will close out this comparison of RCAS to the H-34 test data. The example is taken from the test data at an advance ratio of 0.51 and provides a baseline data set to which any theory may be compared. The example was influenced by CAMRAD II's encouraging comparison between theory and test shown with Fig. 7-13 and Fig. 7-14. At this advance ratio, test collective pitch was varied from -4 degrees up to $+8$ degrees in 2 degree increments while holding a constant $+5$ degree shaft angle of attack. This shaft angle of attack could well be used in a high speed, wingless, propeller driven autogyro, so a condition of zero shaft torque within the collective pitch range was considered in selecting the test conditions for this example. Each of the following parameters will be studied in turn:

Longitudinal and lateral controls, B_{1C} and A_{1C}
Lift, drag, side force and power, C_L/σ , C_D/σ , C_Y/σ and C_Q/σ
Effective drag, C_{DE}/σ
Lift to effective drag ratio, L/D_E

RCAS's prediction of the primary control angle, longitudinal cyclic in Fig. 7-37, is an example of where the slope is nearly perfectly predicted. And, most interestingly, correlation with the secondary control angle, lateral cyclic, is – quite frankly – remarkable. The lift coefficient, Fig. 7-38, also is correlated well with respect to slope at low lift, but because of zero shift and an early prediction of blade stall, the overall correlation is not good enough in this author's opinion

Unfortunately, Fig. 7-39 through Fig. 7-41 show that the predictions of drag coefficient, C_D/σ , side force coefficient, C_Y/σ , in particular, and the H-34 torque coefficient, C_Q/σ , are poor even relative to the rotor lift coefficient correlation shown with Fig. 7-38. Note from Fig. 7-41 that experimentally the H-34 rotor will autorotate at both a low collective pitch ($\theta_{\frac{3}{4}R} = -1$ degree) and a high collective pitch ($\theta_{\frac{3}{4}R} = +3$ degree). The low collective pitch autorotation point corresponds to a C_L/σ around 0.03, which RCAS predicts. The high point occurs experimentally at a C_L/σ slightly over 0.06, which RCAS does not agree with. The test drag coefficient is clearly over predicted at virtually all lift coefficients. The predicted side force coefficient appears to have a serious upward shift. The torque coefficient is severely under predicted at lift coefficients useable by an autogyro.

The rotor effective drag coefficient, C_{DE}/σ , and the rotor lift–effective drag ratio, L/D_E , comparisons are, in this author's opinion, the best way to conclude this detailed comparison of RCAS to H-34 test data given the many choices just discussed. Both parameters, as shown on Fig. 7-42, are plotted versus the rotor lift coefficient. The accurate calculation of these performance parameters very much depends on the blade element drag calculations. RCAS's prediction is significantly in error, which suggests that the airfoil drag coefficient characteristics used in the analysis are not correct.

Over prediction of the maximum rotor L/D_E is most discouraging. Appendix 11.12 provides graphs of H-34 L/D_E (derived from measured test parameters) versus RCAS's prediction. The correlation is provided for each advance ratio. There is nearly exact agreement at $\mu = 0.305$, but then a progressive over prediction appears as advance ratio increases.

Table 21. L/D_E Linear Regression Coefficients for H-34 Test versus RCAS.

Mu	SLOPE	Intercept	R²	Mu	SLOPE	Intercept	R²
0.305	1.0591	0.1678	0.9451	0.620	0.8469	0.0341	0.9893
0.401	0.9006	0.6581	0.9406	0.710	0.7362	0.0850	0.9565
0.460	0.8293	0.8214	0.9613	0.820	0.7371	0.1369	0.9643
0.510	0.7511	0.7761	0.9687	1.050	0.9742	-1.2635	0.9292

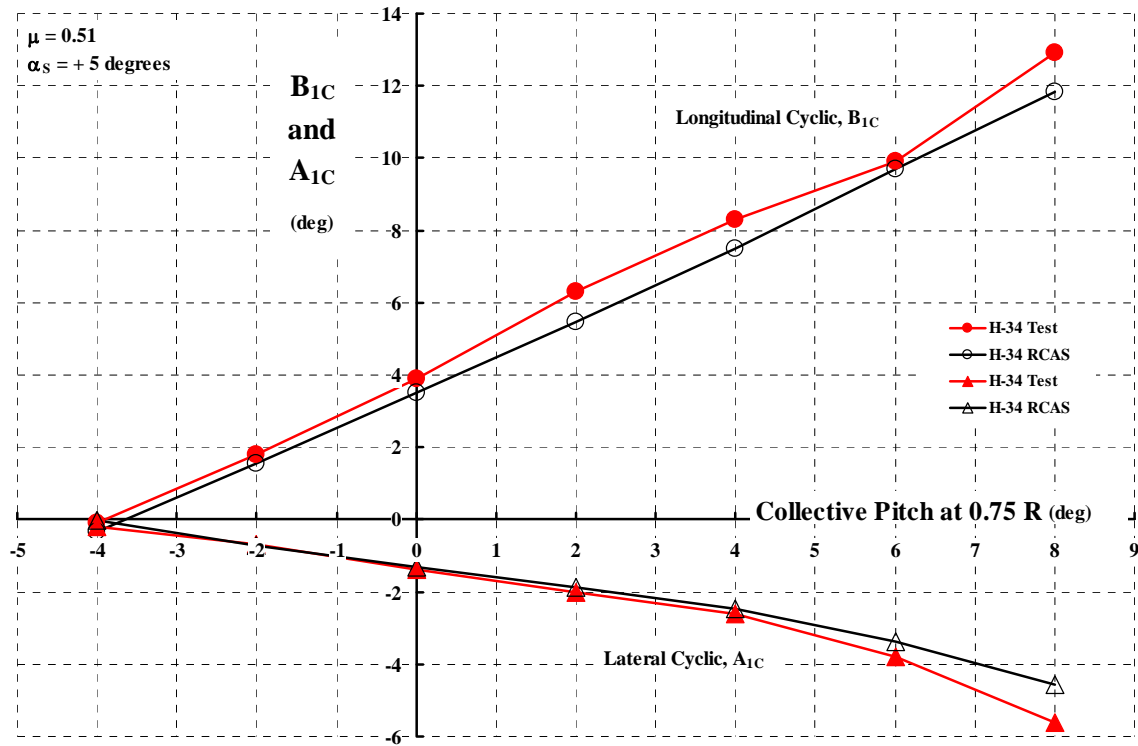


Fig. 7-37. H-34 rotor control angles, test versus RCAS.

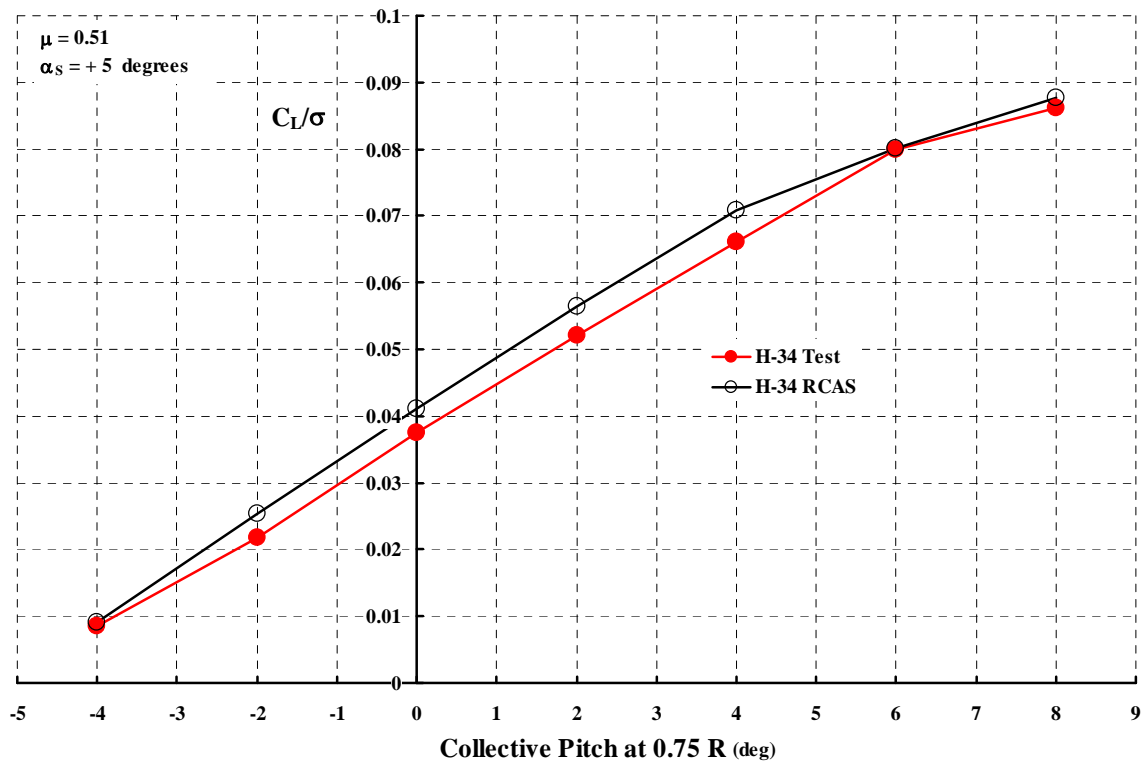


Fig. 7-38. H-34 rotor lift coefficient, test versus RCAS.

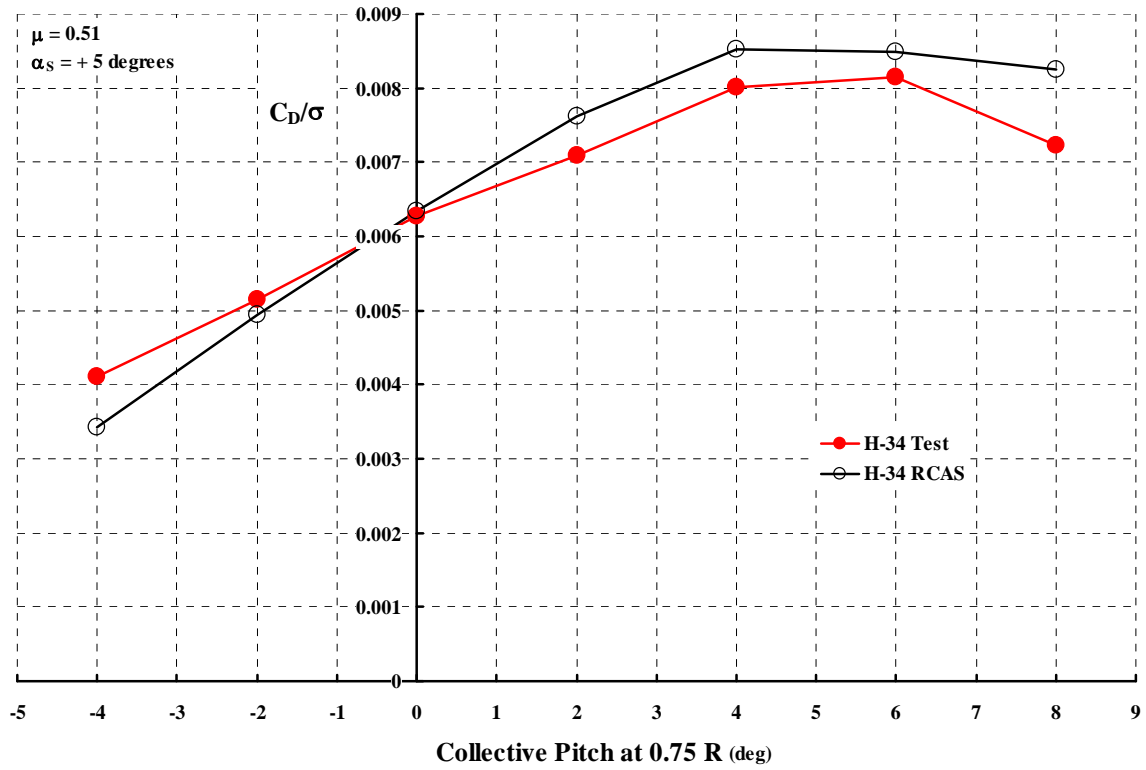


Fig. 7-39. H-34 rotor drag coefficient, test versus RCAS.

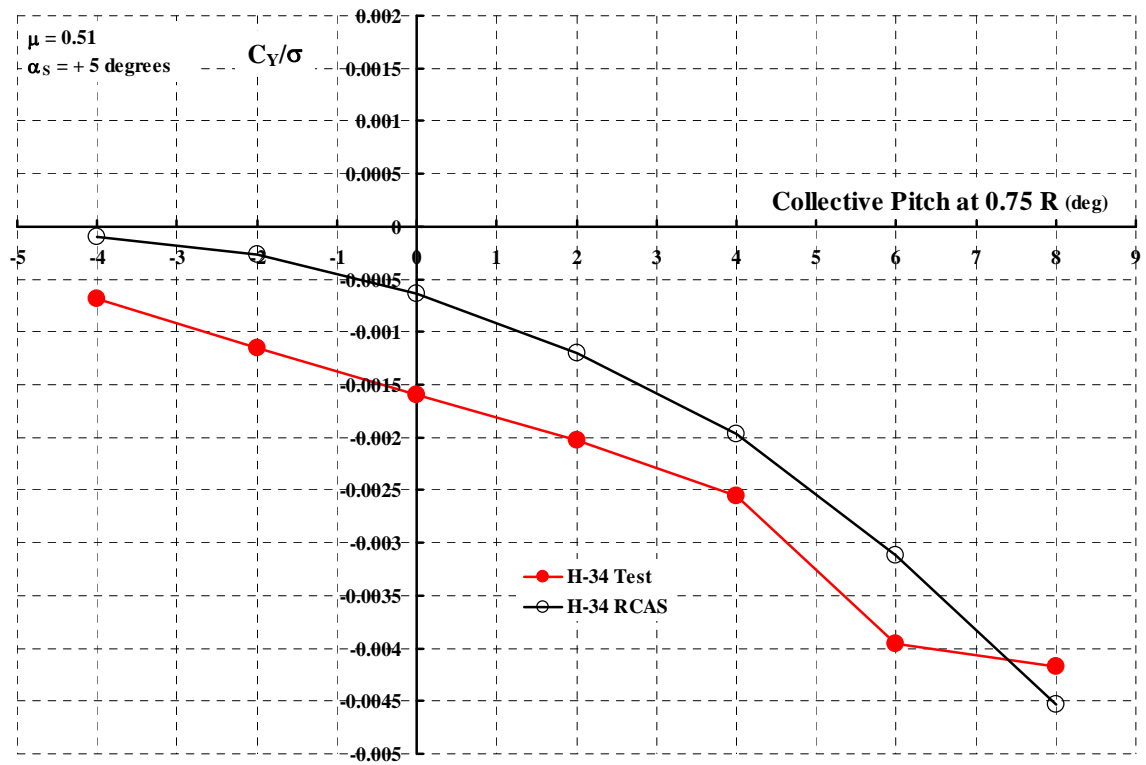


Fig. 7-40. H-34 rotor side force coefficient, test versus RCAS.

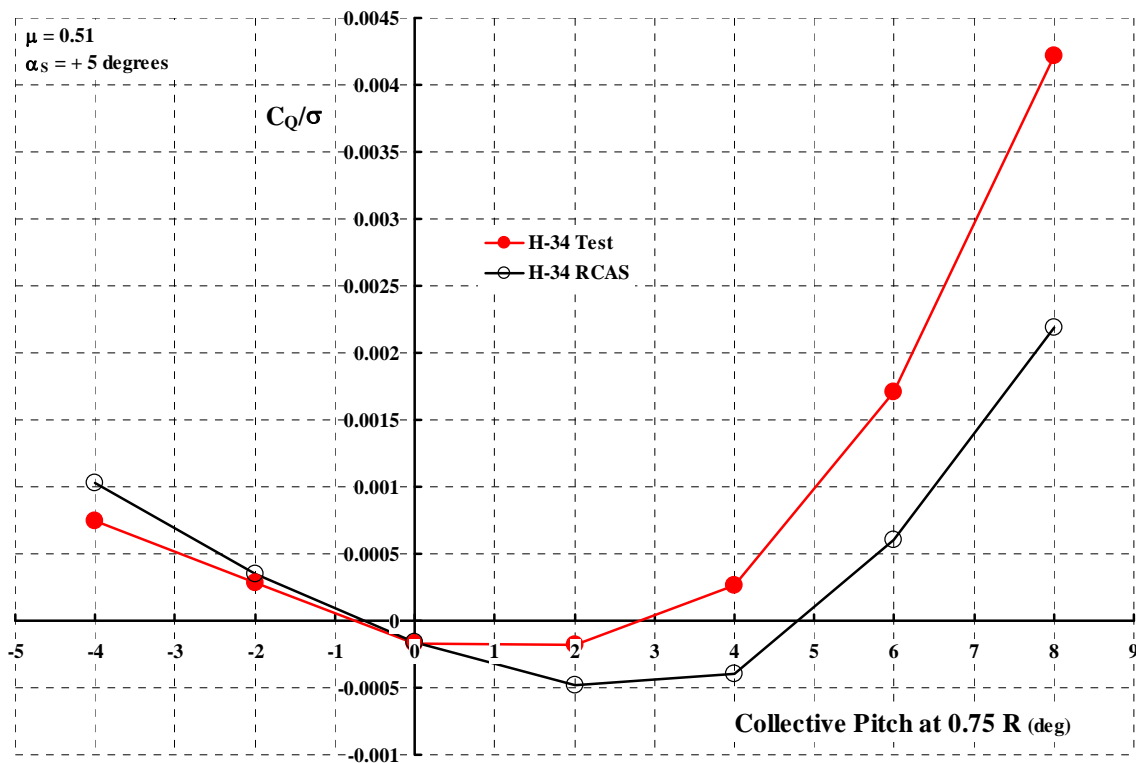


Fig. 7-41. H-34 rotor torque coefficient, test versus RCAS.

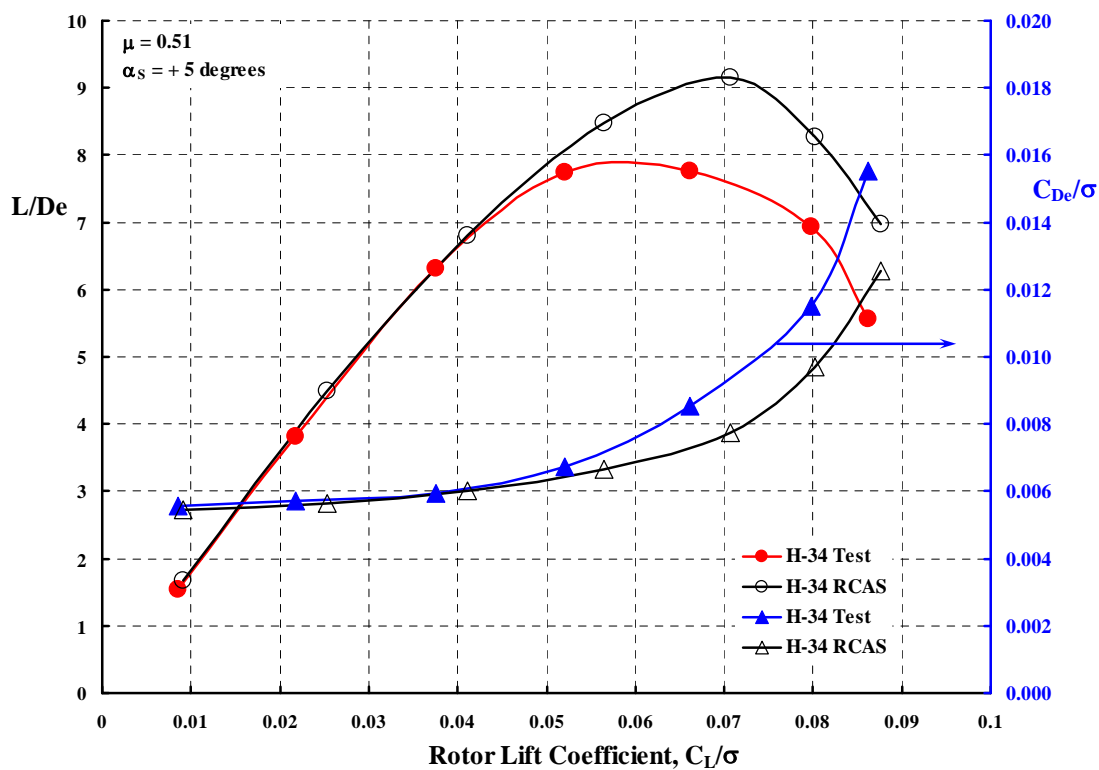


Fig. 7-42. H-34 rotor effective drag coefficient and L/D_E , test versus RCAS.

7.4 H-34 Test versus OVERFLOW-2 with CAMRAD II (Appendix 11.13)

The CFD study of rotor performance at high advance ratio began with a few simple calculations by Roger Strawn in mid-2003. Roger is a member of the U.S. Army Aeroflightdynamics group located at NASA Ames. He approached the author following a seminar the author had given about autogyros.¹² Roger said that CFD could do the high μ problem because OVERFLOW-2 was available. (At the time it was known as OVERFLOW-D, but I have taken some poetic license about OVERFLOW dash numbers for this report). He “sold the author” noting that:

OVERFLOW-2 is a general purpose Navier-Stokes solver for problems that may involve relative motion between configuration components. The code uses overset structured grids to accommodate arbitrarily complex geometries while, on a component-wise basis, retain the computational advantages inherent to structured data. OVERFLOW-2 has recently been released for BETA-testing and comes with complete documentation, a set of examples, and an easy-to-use overset grid generation package called OVERGRID.

OVERFLOW-2 is based on the well known NASA OVERFLOW code, but has been significantly enhanced to accommodate moving body applications, facilitate accuracy control via solution adaption, and run efficiently on scalable computers. Makefiles to compile the software on IBM-SP, Origin 2000, Sun 10000, and Cray T3E platforms are provided with the code. OVERFLOW-2 uses MPI to enable inter-processor communication. OVERFLOW-2 employs a powerful discretization paradigm that partitions the problem domain into near-body and off-body regions. The near-body region includes the surface geometry of all configuration parts being considered and the volume of space that extends a short distance above the respective surfaces. The near-body portion of the domain is discretized in a classical "Chimera" fashion. Near-body grids are generated in a pre-process using standard grid generation packages (OVERGRID is especially well suited to this task).

The off-body portion of the domain encompasses the near-body domain and extends to the far-field boundaries of the problem. OVERFLOW-2 automatically discretizes the off-body domain with uniform Cartesian grid components (structured) of varying levels of resolution capacity. By default, off-body resolution capacity is set based on proximity to near-body components. Users can run simulations on the near-body and default off-body grid systems, or can enable solution adaption. With adaption enabled, OVERFLOW-2 allocates off-body grid resolution based on proximity to near-body components and results of estimates of solution error. Of course, error estimation is carried out automatically by OVERFLOW-2. In all cases, OVERFLOW-2 organizes grid components into groups of equal size. Then, on parallel computers, groups are assigned to processors. Scalability is realized in a group-wise fashion.

OVERFLOW-2 can be used to simulate moving body applications that involve arbitrary rigid-body motion, prescribed motion, or maneuvers. OVERFLOW-2 has a general 6-degrees-of-freedom model (6-DOF) that allows body motion to respond to aerodynamic loads as well as applied forces and moments associated with separation mechanisms. All OVERFLOW-2 functionality is tightly coupled, including 6-DOF, domain connectivity, solution adaption, etc., in order to maximize computational efficiency for such applications.

OVERFLOW-2 has been tested on a range of applications that have practical importance, several of which are described in an AIAA paper [65].

¹² Dr. Michael Scully (US Army AFDD) and Dr. William Warmbrodt (NASA Ames) asked if I would give a seminar about autogyros, which I did on June 18 and 19, 2003. The seminar was titled “Let’s Revisit Autogyros” and, because of their insistence, was later published [9].

Roger proposed to calculate the drag and torque of untwisted rotor blades operating in flat pitch and at zero shaft angle of attack over the advance ratio range of 0.0 to 1.20. Advancing tip Mach number ($M_{1,90}$) for the primary computations was held constant at 0.5, but other combinations of μ and $M_{1,90}$ were examined as tabulated in Appendix 11.13. The rotor dimensions of a standard UH-1 operating at nearly standard day conditions were selected. That is:

Table 22. Rotor Dimensions and Operating Conditions Used by Strawn in 2003 for Constant Advancing Tip Mach Number of 0.50.

Dimensions	Values	Advance Ratio	Tip Speed (fps)	Fwd Speed (fps)
Diameter (ft)	48	0.0	562.664	0
Chord (ft)	1.75	0.2	468.887	93.777
Blade aspect ratio	13.71	0.4	401.903	160.761
Blades (nd)	2	0.6	351.665	210.999
Nominal solidity (nd)	0.04642	0.8	312.591	250.073
Twist (deg)	0.00	1.0	281.332	281.332
Root cutout (ft)	3.60	1.2	255.756	306.908
Tip shape in planform	Square			
Airfoil	N.A.C.A. 0012			
Speed of sound (ft/sec)	1,125.328			
Density (slugs/ft ³)	0.0024254			

Clearly, this idealized computational problem dealt with a simple rectangular rotor having constant chord, untwisted blades and with a N.A.C.A. 0012 airfoil section from the blade's root cutout to the squared-off tip. The calculations used a simplified computational domain based on several factors. First, only the upper half of each rotor blade was modeled in the analysis because the selected configuration had a symmetric airfoil section and no twist. Second, only a single rotor blade was used in the computation, since the non-lifting rotor blades produce a minor rotor wake system. Thus, it was assumed that each rotor blade would effectively operate in isolation. The lack of blade twist or collective pitch angle meant that the idealized rotor produced no lift, which meant no induced power. Thus, any predicted power requirement could be considered a "minimum" when compared to that of a real, twisted rotor blade.

A three-block near-body viscous grid system was used to model the upper half of the rotor blade, consisting of a (106×27×68) tip cap, a (106×27×68) root cap, and a (112×65×68) C-H mesh on the rotor surface. The viscous spacing (y^+) of the first grid point from the rotor surface was everywhere less than one. Another 753,000 grid points were used in a Cartesian background grids with uniform spacing of 0.1 blade chord. These grid sizes typically produced grid-independent rotor performance solutions for earlier rotor problems.

Time accuracy for the problem was ensured by comparing steady and unsteady calculations for the same hovering rotor cases. Using OVERFLOW-2, one can compute hovering rotor cases in a steady-state framework or as time-accurate solutions. If the time-accurate power and torque results for hover match the steady-state ones to within one percent or less, then the time-accurate solution are considered to be independent of

the choice of time-step. The use of this comparison technique guaranteed time-accuracy for the various rotor speeds analyzed in this study. The unsteady calculations typically used time steps of about 0.02 degrees of azimuthal angle.

For all computations, the rotor blade boundary layer was assumed to be fully turbulent and the Spalart-Almaras turbulence model was used for all cases. Using similar grids and these same turbulence models, the OVERFLOW-2 code had recently been used to successfully predict power requirements for both hovering rotors [66] and rotors in forward flight, which was under study at the time [61]. However, none of the “computational simulations” up to Strawn’s 2003 work attacked the high advance ratio conditions under study in this report.

Strawn’s computations were made with no blade root end modeled inboard of the root cutout. The blades were untwisted and the operating condition was shaft angle of attack and control angles set to zero. The primary calculations were made by varying advance ratio holding advancing tip Mach number constant at 0.50. The immediate output was profile power coefficient (C_{P0}/σ), which appeared rather encouraging as Fig. 7-43 shows. However, the components of profile power, C_{Q0}/σ and C_{H0}/σ were not predicted satisfactorily as Fig. 7-44 and Fig. 7-45 clearly point out. Note that Appendix 11.1 theory with $C_{d0} = 0.01$ and $\lambda = 0$ is included on each figure. These points and a number of other operating conditions that Strawn calculated are provided in Appendix 11.13 with tables.

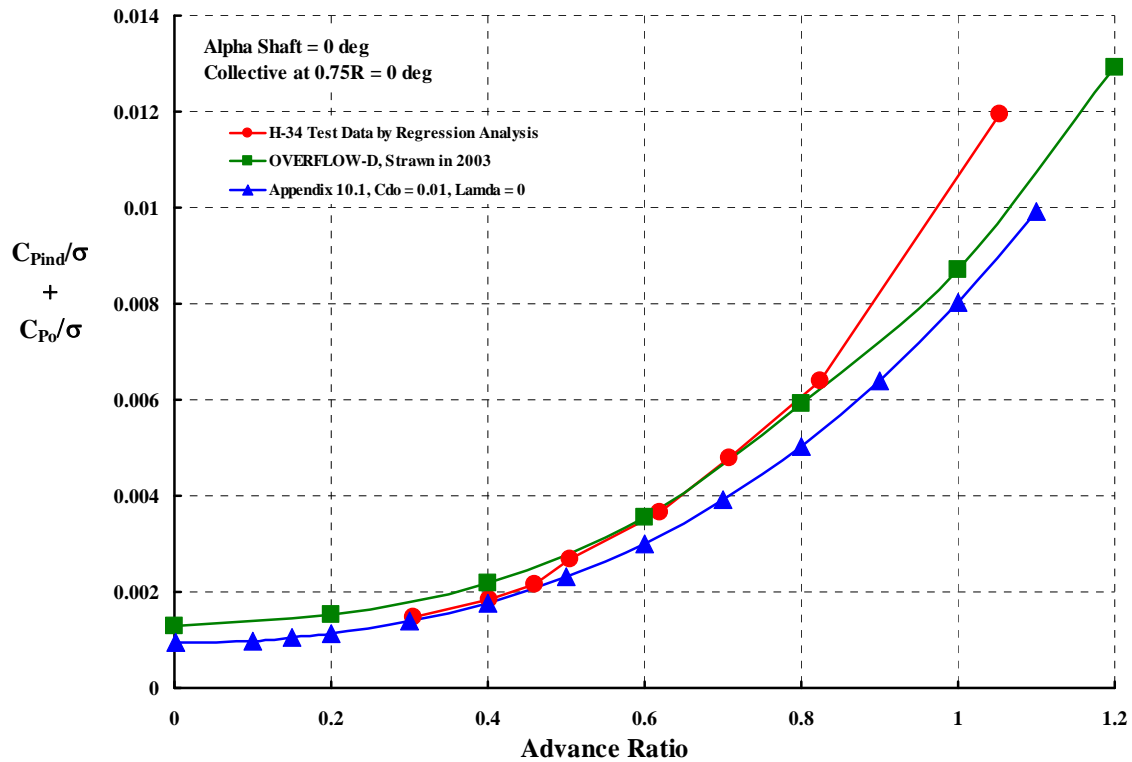


Fig. 7-43. Minimum profile power with Strawn’s idealized configuration.

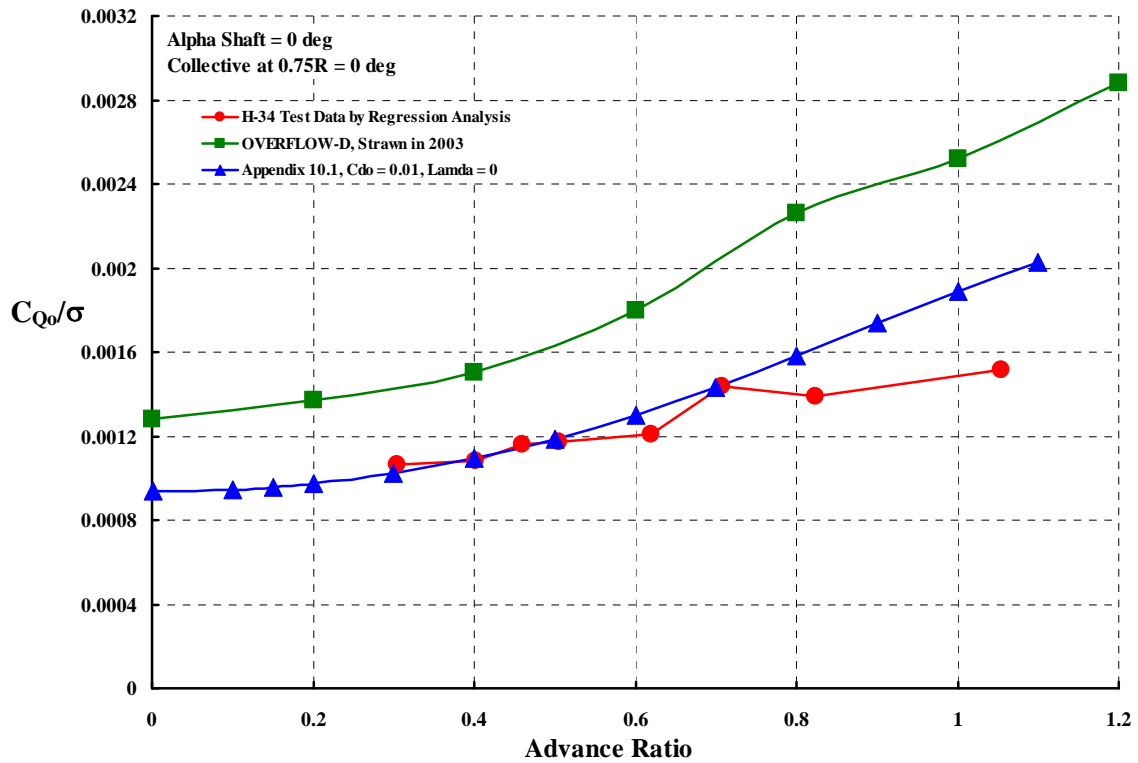


Fig. 7-44. Minimum torque with Strawn's idealized configuration.

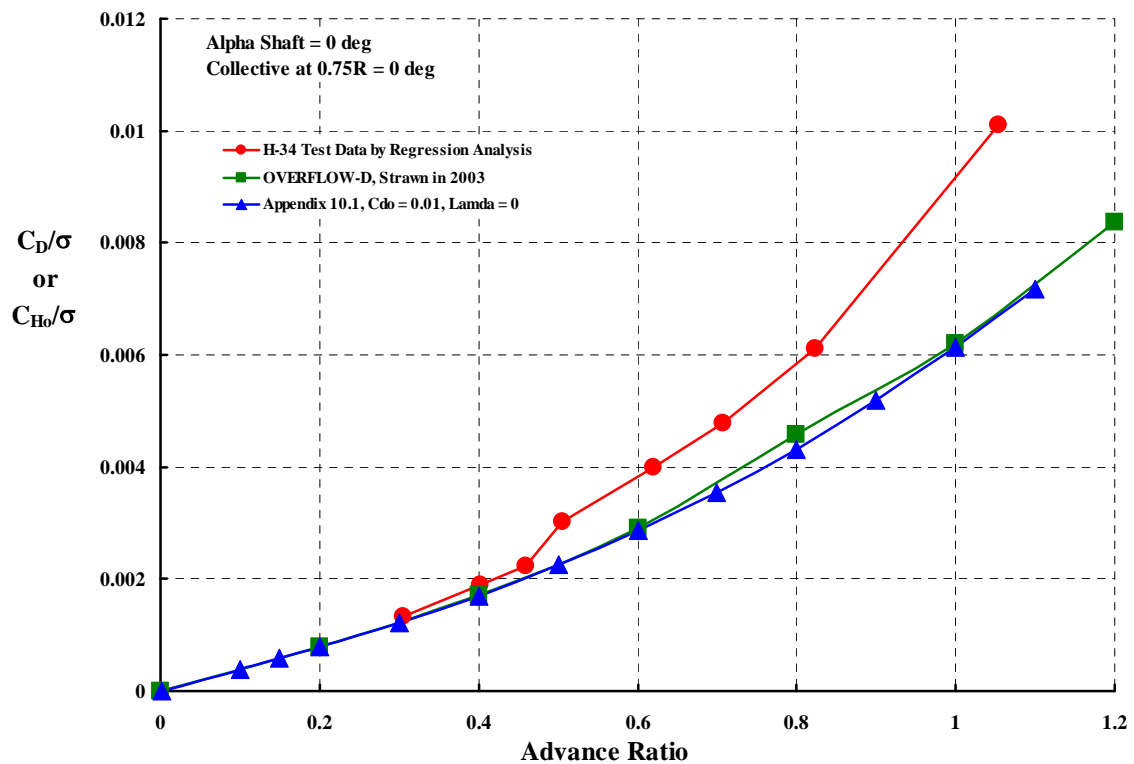


Fig. 7-45. Minimum H-force with Strawn's idealized configuration.

During July and August of 2006, Jan Theron tackled the CFD problem at high advance ratio. At that time Jan was working as a consultant to the Groen Brothers in support of their Heliplane, Fig. 2-9. Jan and the author corresponded during this period to validate his CFD model for the Heliplane with H-34 rotor data. Jan set the H-34 problem up with Table 23's geometry and selected 4 operating conditions to calculate. Following Strawn's lead, the blades were untwisted and the operating condition was shaft angle of attack and control angles set to zero. No blade root end (see Fig. 3-4 and Fig. 3-5) was modeled inboard of the root cutout.

You can see from Fig. 7-46 , Fig. 7-47 and Fig. 7-48 that OVERFLOW-2 results obtained by Jan Theron left something to be desired. Additional results in Appendix 11.13 show azimuthal and radial distributions of chordwise and spanwise drag.

Table 23. H-34 Dimensions and Operating Conditions Used by Jan Theron in 2006.

Dimensions	Values	Advance Ratio	Tip Speed (fps)	Fwd Speed (fps)
Diameter (ft)	56	0.30	627.740	188.322
Chord (ft)	1.337	0.40	662.751	265.100
Blade aspect ratio	20.94	0.71	444.542	315.625
Blades (nd)	4	1.05	294.469	309.193
Nominal solidity (nd)	0.062			
Twist (deg)	0.00			
Root cutout (ft)	4.20			
Tip shape in planform	Square			
Airfoil	N.A.C.A. 0012			
Speed of sound (ft/sec)	1,116.44948			
Density (slugs/ft ³)	0.00237689			

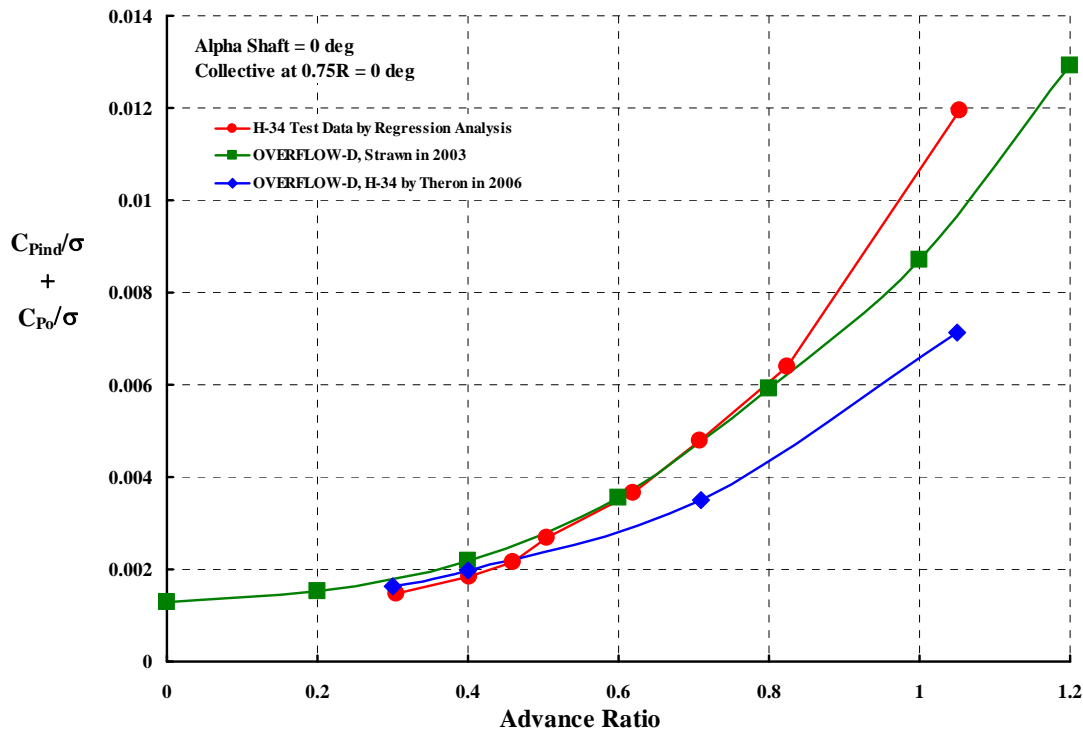


Fig. 7-46. Minimum profile power with Theron's H-34 configuration.

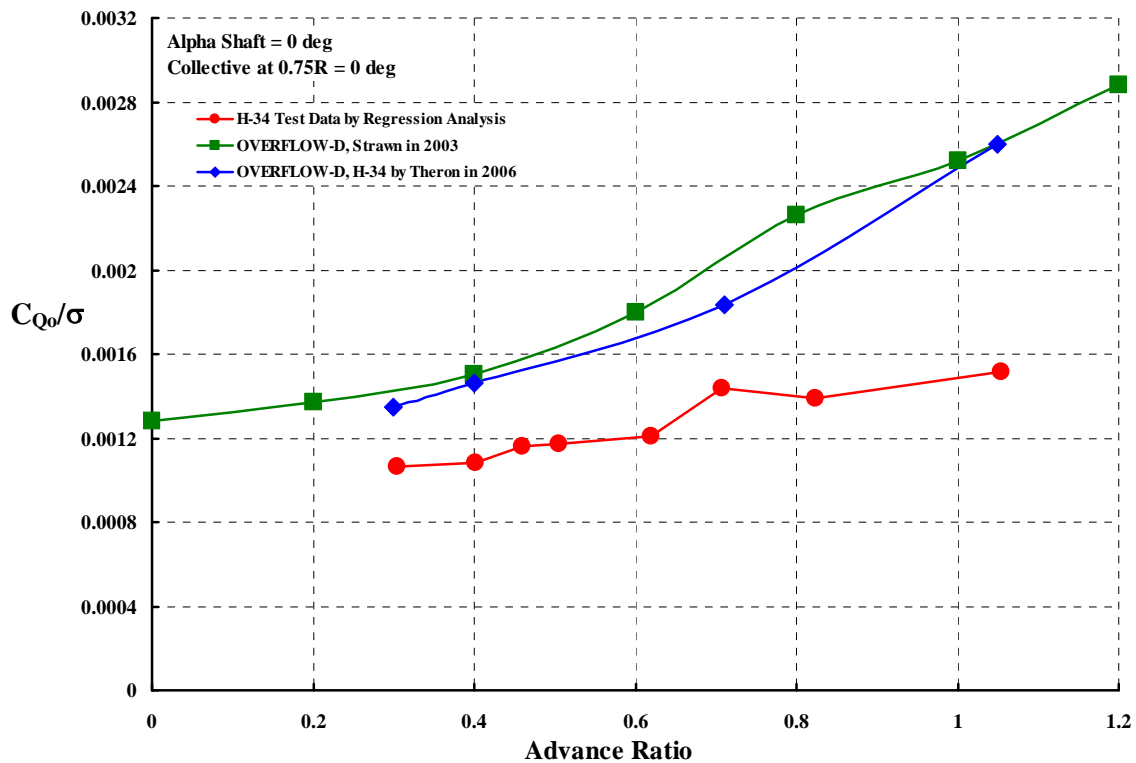


Fig. 7-47. Minimum torque with Theron's H-34 configuration.

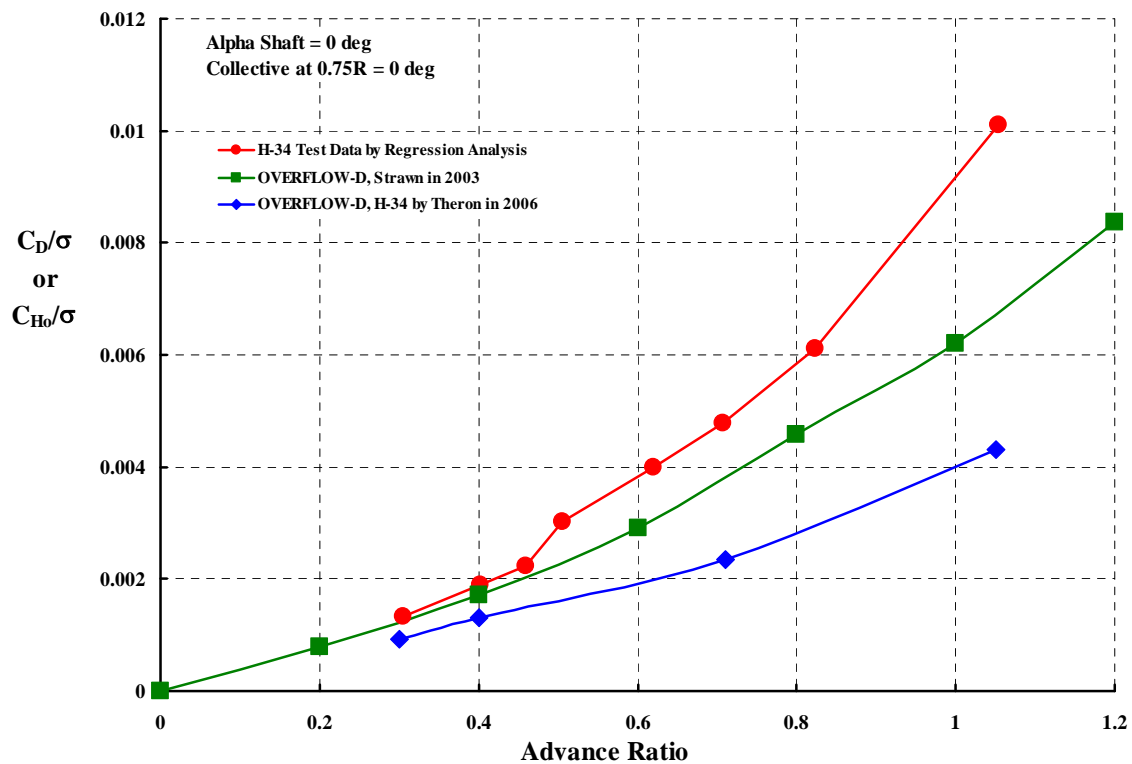


Fig. 7-48. Minimum H-force with Theron's H-34 configuration.

A major contribution of Theron's work was *OVERFLOW-2's* disclosure of a minimum Y-force coefficient that increases nearly linearly with advance ratio. This Y-force coefficient trend at zero shaft angle of attack and with zero control angles is shown on Fig. 7-49. A quick review of comprehensive analysis results (CAMRAD II – Fig. 7-10, CHARM – Fig. 7-22 and RCAS – Fig. 7-34) shows that these theories are missing the contribution of radial flow in the minimum side force calculation. Furthermore, Wheatley's and Bailey's 1930s theory and even the more refined analysis in Appendix 11.1 shows that this minimum side force should be zero for any advance ratio.

Fig. 7-50 illustrates the variation of one blade's Y-force as the blade completes a revolution. Note that there is significant Y-force at azimuth angles of 90 and 270 degrees. To the author's knowledge, no comprehensive code available today accounts for the spanwise drag at these two azimuth angles. The magnitude of a blade element's spanwise drag is shown for several radial stations with Fig. 7-51. The most likely source of the spanwise drag at $\psi = 90$ and 270 degrees is skin friction created by the boundary layer being pumped towards the tip. Comprehensive codes such as CAMRAD II, CHARM and RCAS lack – at the moment – any way to account for this spanwise skin friction drag for a blade at $\psi = 90$ and 270 degrees. Drag in the spanwise direction will, of course, be influenced by blade deflections.

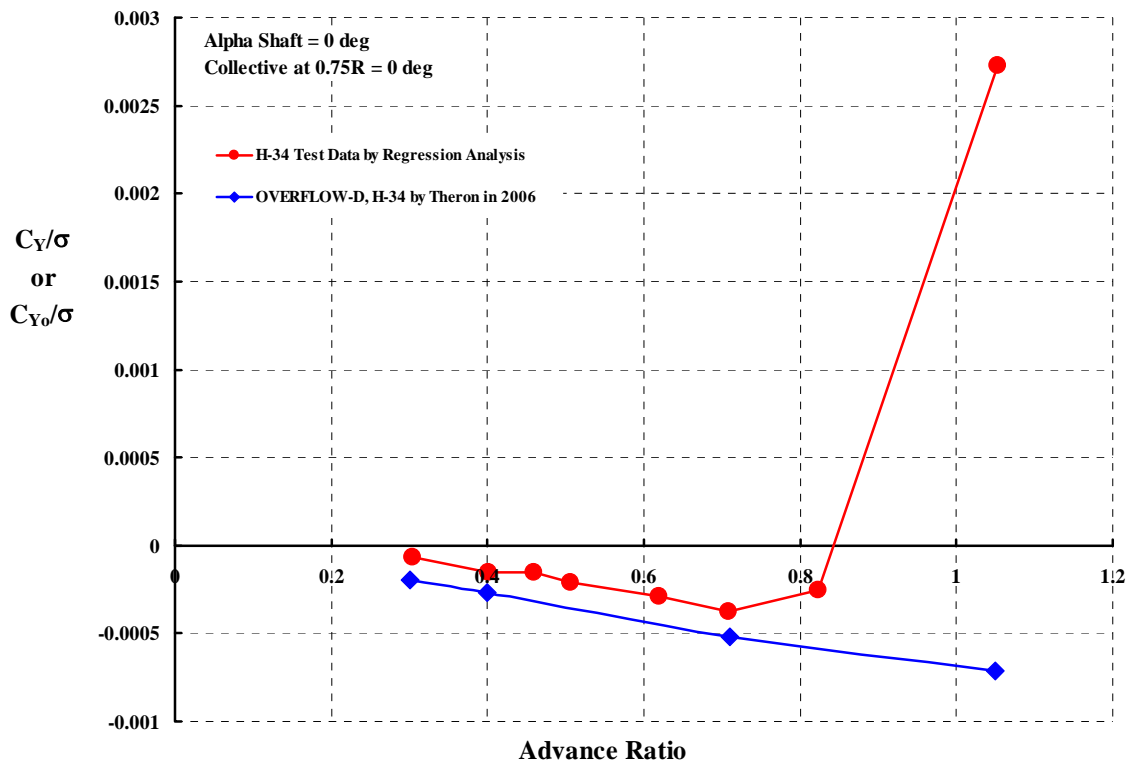


Fig. 7-49. Minimum Y-force with Theron's H-34 configuration.

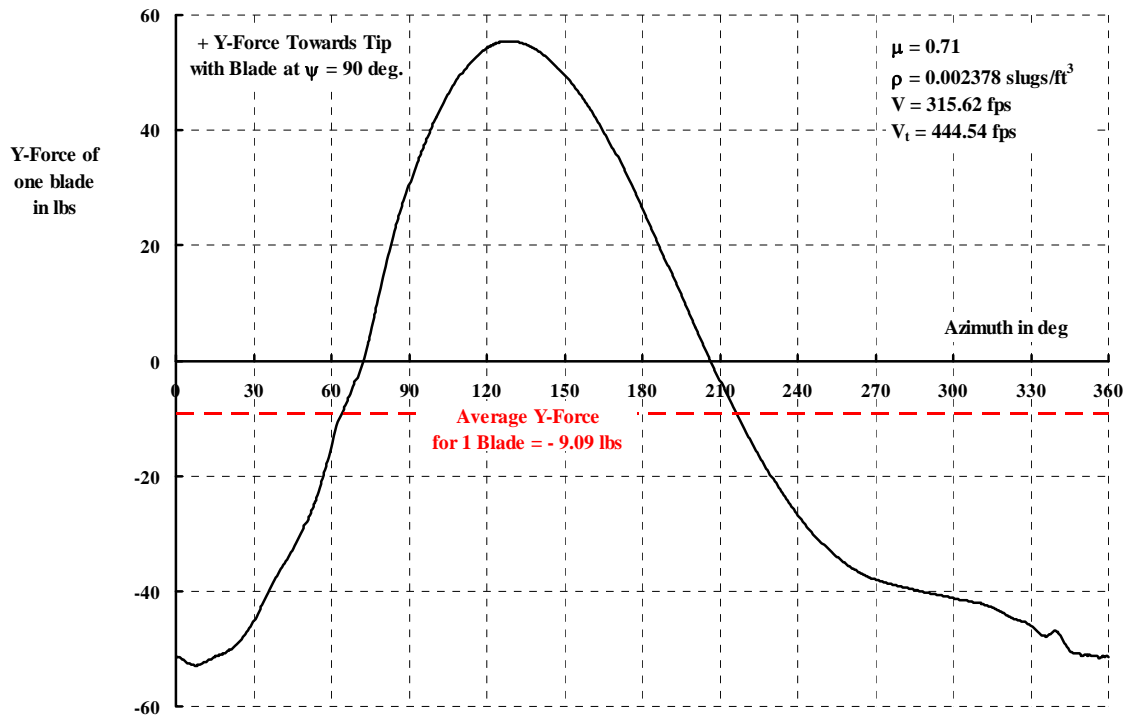


Fig. 7-50. One blade's Y-force versus azimuth with Theron's H-34 configuration at and advance ratio of 0.71.

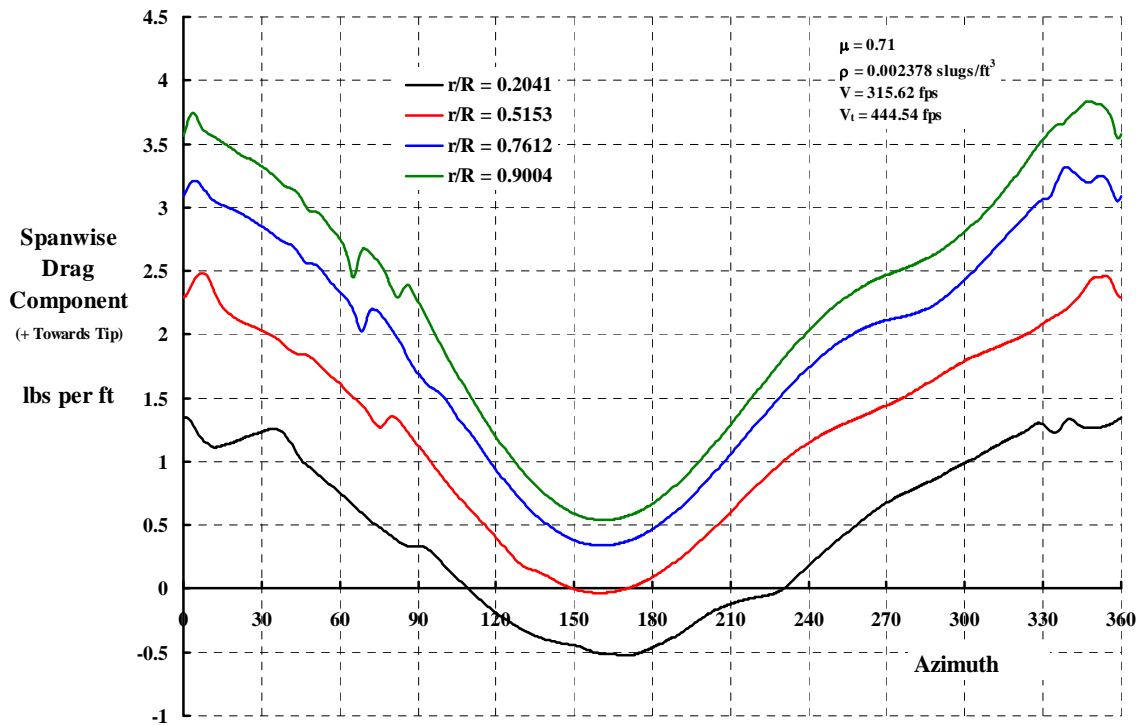


Fig. 7-51. Blade element spanwise drag with Theron's H-34 configuration at an advance ratio of 0.71.

There is, of course, a chordwise component of the blade element drag and this component is shown for several radii with Fig. 7-52. While there is evidence of turbulent wake interaction between blades, the basic one and two per rev wave form is as one would expect. The much more interesting data is shown in Fig. 7-53 and Fig. 7-54. Both of these figures deal with the drag versus radius at the two azimuth locations of $\psi = 90$ degrees and $\psi = 270$ degrees.

Fig. 7-53 shows the blade element drag in pounds per foot as Theron obtained from OVERFLOW-2. At an azimuth of 90 degrees, there is substantial drag and this drag increases from the blade surface's root end (i.e., 0.16R) to the blade tip. The tip region evidently has a significant three dimensional effect on the blade element drag. Of most interest – at least to this author – is the blade element chordwise drag versus radius for the retreating blade azimuth of 270 degrees. Both simple theory and comprehensive codes describe the velocity distribution at this azimuth as

$$V_{x,270} = xV_t - V = V_t(x - \mu)$$

Since the advance ratio is 0.71 for this example, one would expect that the velocity would be zero at the radius station where $x = \mu = 0.71$. But OVERFLOW-2 dismisses that view because the chordwise drag is not zero where the velocity is zero. OVERFLOW-2 calculates the chordwise drag to be zero very close to the 0.6 radial station. This implies that the streamlines are not normal to the leading edge and that there is lag, along with cross flow, in the boundary layer. Obviously more detailed analysis of this behavior is required.

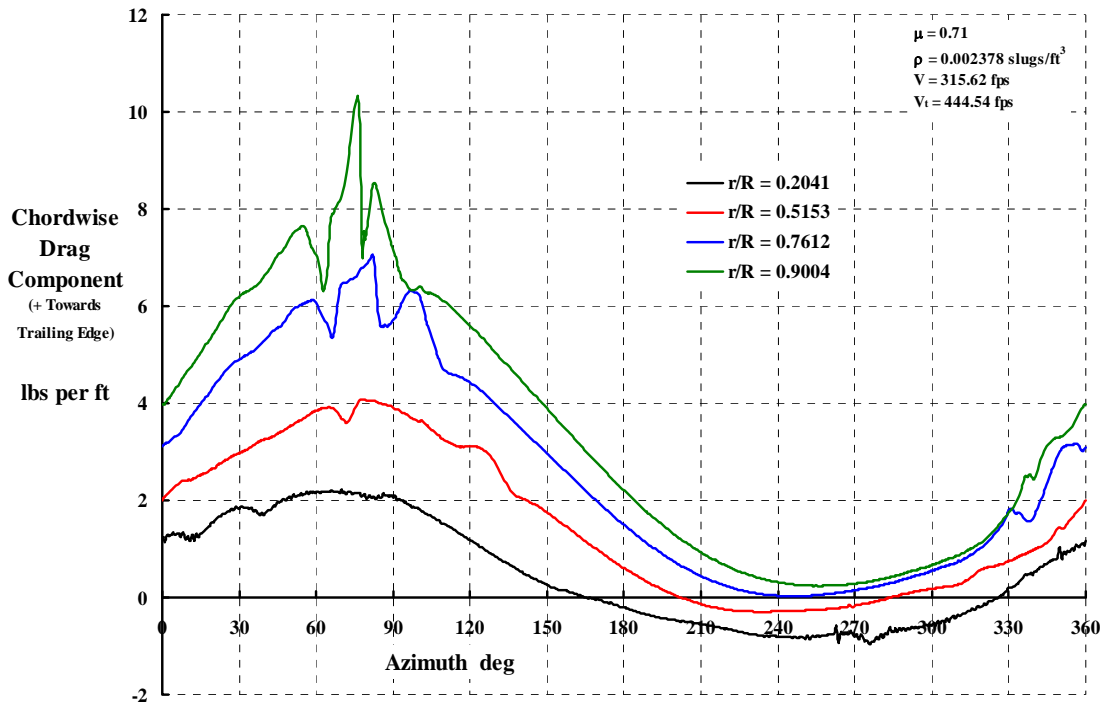


Fig. 7-52. Blade element chordwise drag with Theron's H-34 configuration at an advance ratio of 0.71.

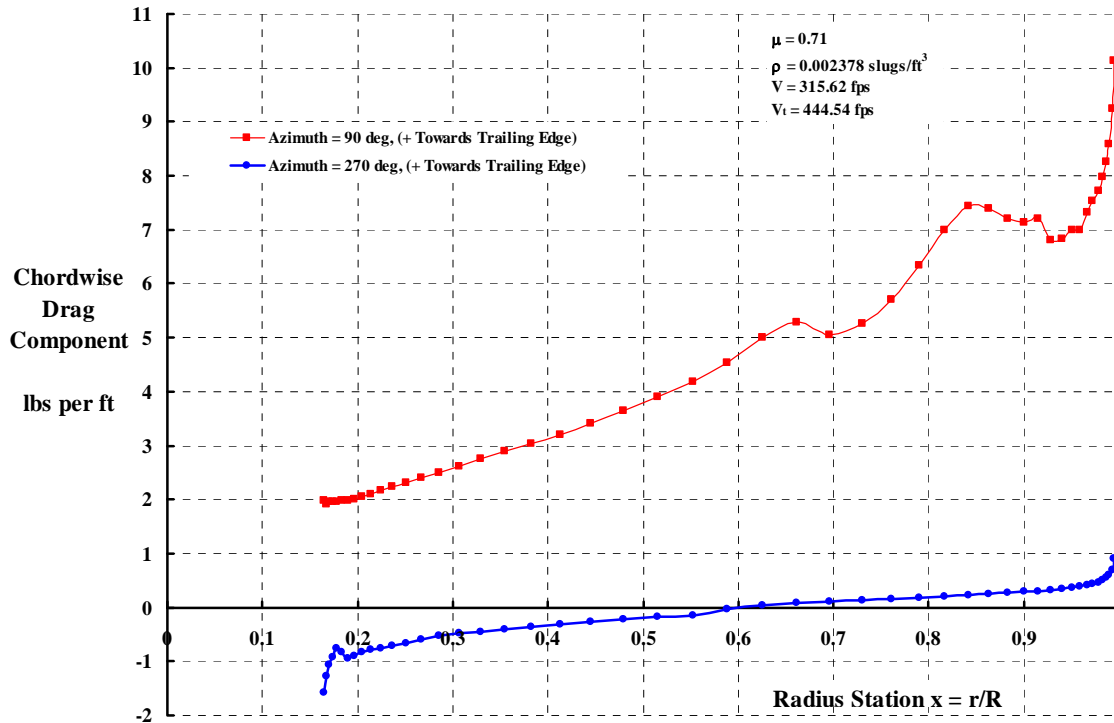


Fig. 7-53. Blade element chordwise drag with Theron's H-34 configuration at an advance ratio of 0.71 for advancing and retreating azimuths.

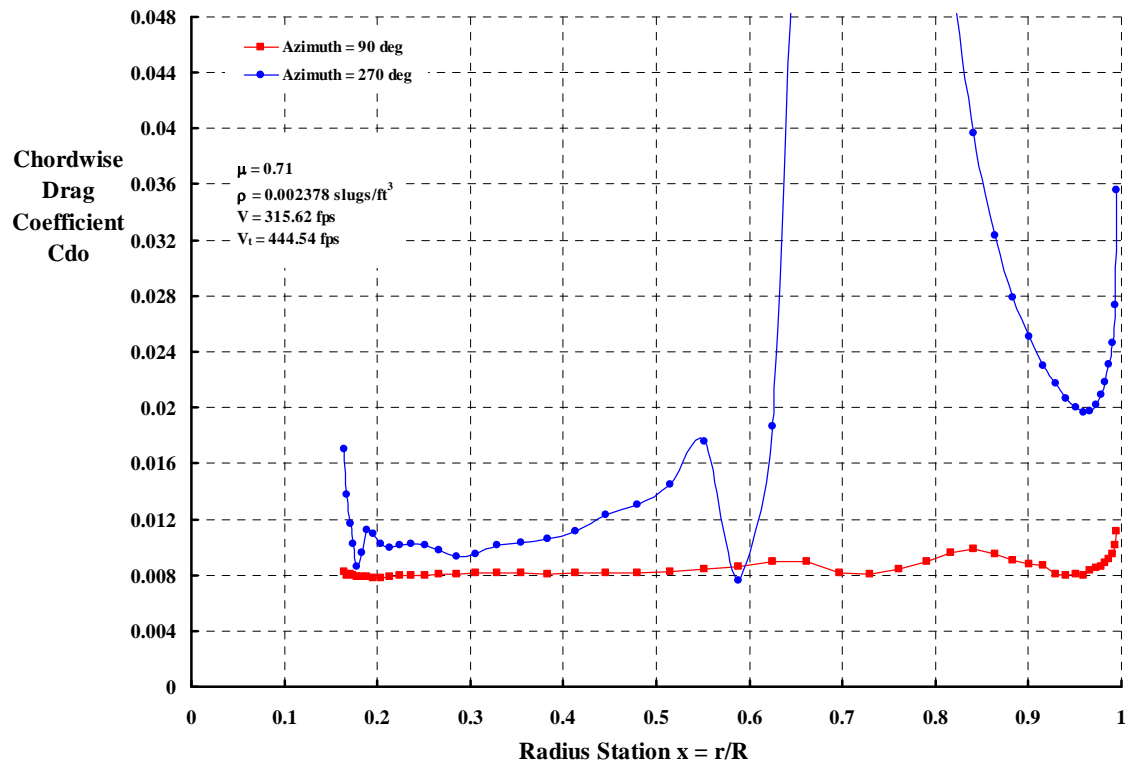


Fig. 7-54. Blade element chordwise drag coefficient with Theron's H-34 configuration at an advance ratio of 0.71 for advancing and retreating azimuths.

The results of translating the chordwise drag from dimensional pounds per foot to a conventional airfoil drag coefficient are shown with Fig. 7-54. The calculation is simply:

$$\text{For } \psi = 90^\circ \quad C_{d_o} = \frac{dD/dr}{\frac{1}{2}\rho[V_t(x+\mu)]^2 c} \quad \text{and for } \psi = 270^\circ \quad C_{d_o} = \frac{|dD/dr|}{\frac{1}{2}\rho[V_t(x-\mu)]^2 c}$$

At the advancing blade azimuth, the airfoil drag coefficient is in the range of 0.008 to 0.01 with a not insignificant drag rise at the blade tip. On the retreating blade side of the disc, calculation of the drag coefficient is distorted because the velocity is zero at $x = 0.71$, but there is a finite dimensional drag. There is also, at $\psi = 270$ degrees and $x = 0.6$, the situation where the dimensional drag is zero but the local velocity is not.

Jan Theron took the time to compare N.A.C.A. 0012 airfoil lift and drag coefficients listed with the C81 airfoil deck and those calculated with OVERFLOW-2. A comparison of minimum drag coefficient (C_{d_o}) versus Mach number is provided with Fig. 7-55. Several other results are tabulated in Appendix 11.13. He used OVERFLOW-2 operating in a steady flow mode. The “standard” C81 N.A.C.A. 0012 airfoil properties do not include a Reynolds number (RN) effect. In contrast, OVERFLOW-2 accounts for Reynolds number as well as Mach number. Theron chose a chord and operating condition such that $RN = 10^7$ times Mach number. Note that the C81 data points are connected with straight line segments because it is common practice with comprehensive codes to interpolate linearly between points – given a well populated table of airfoil properties.

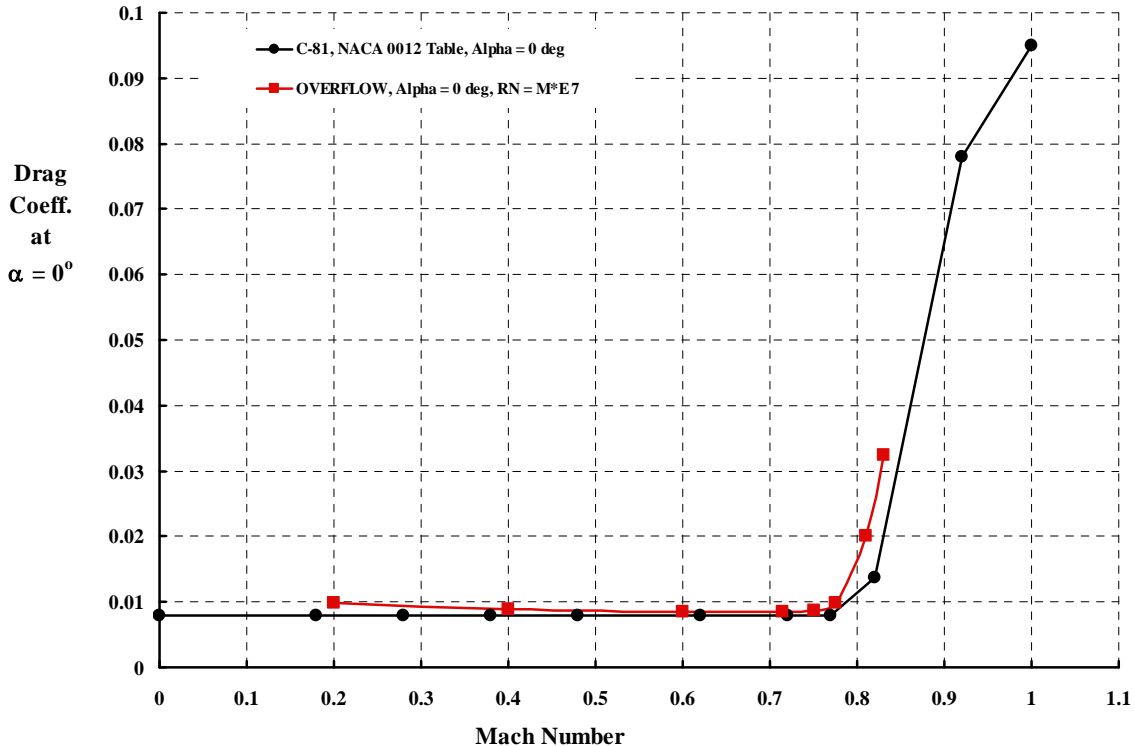


Fig. 7-55. OVERFLOW-2's N.A.C.A. 0012 drag coefficient, *leading edge forward*, versus Mach number by Theron compared to C81 table.

At first glance, Fig. 7-55 suggests that the OVERFLOW-2 results are, for practical engineering purposes, in agreement. This is misleading however as the closer inspection provided by Fig. 7-56 shows. Of course, neither result provided by these two figures need be taken as anything more than representative as McCroskey's critical study of available N.A.C.A. 0012 experimental data reported [67].¹³

The situation is clearly not on such firm ground when the comparison of C_{do} versus Mach number is made with the airfoil at 180 degrees angle of attack. This unfavorable comparison when the airfoil is placed trailing edge forward is shown with Fig. 7-57. There is, even within the CFD community, considerable uncertainty about OVERFLOW-2's and other CFD codes ability to predict drag of bluff bodies. This concern carries over to the rotorcraft world because rotor blades are frequently connected to the rotor hub with a less than satisfactory "airfoil." The H-34 root end, Fig. 3-5, is just one helicopter example.

From Strawn's and Theron's work, it appears that OVERFLOW-2 computations in the reverse flow region (i.e., within the boundary where $x = -\mu \sin\psi$) are quite suspect. Both torque (Fig. 7-47) and H-force (Fig. 7-48) coefficient correlations with H-34 test data would improve significantly if the blade element drag computed in the reverse flow region were increased by a factor of two.

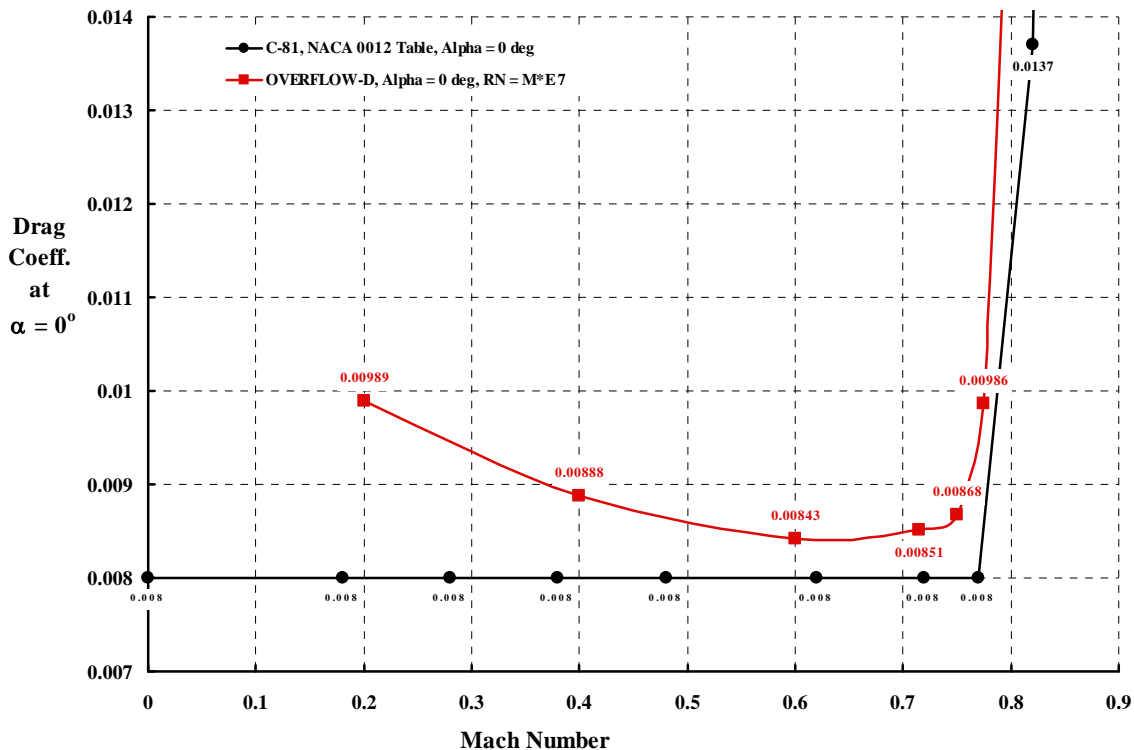


Fig. 7-56. OVERFLOW-2's N.A.C.A. 0012 drag coefficient, leading edge forward, versus Mach number by Theron compared to C81 table. Enlarged scale.

¹³ Bousman, in December 2003, reached a similar conclusion about the SC1095 and SC1094R8 airfoils used on the main rotor blade of the UH-60A Blackhawk helicopter [68].

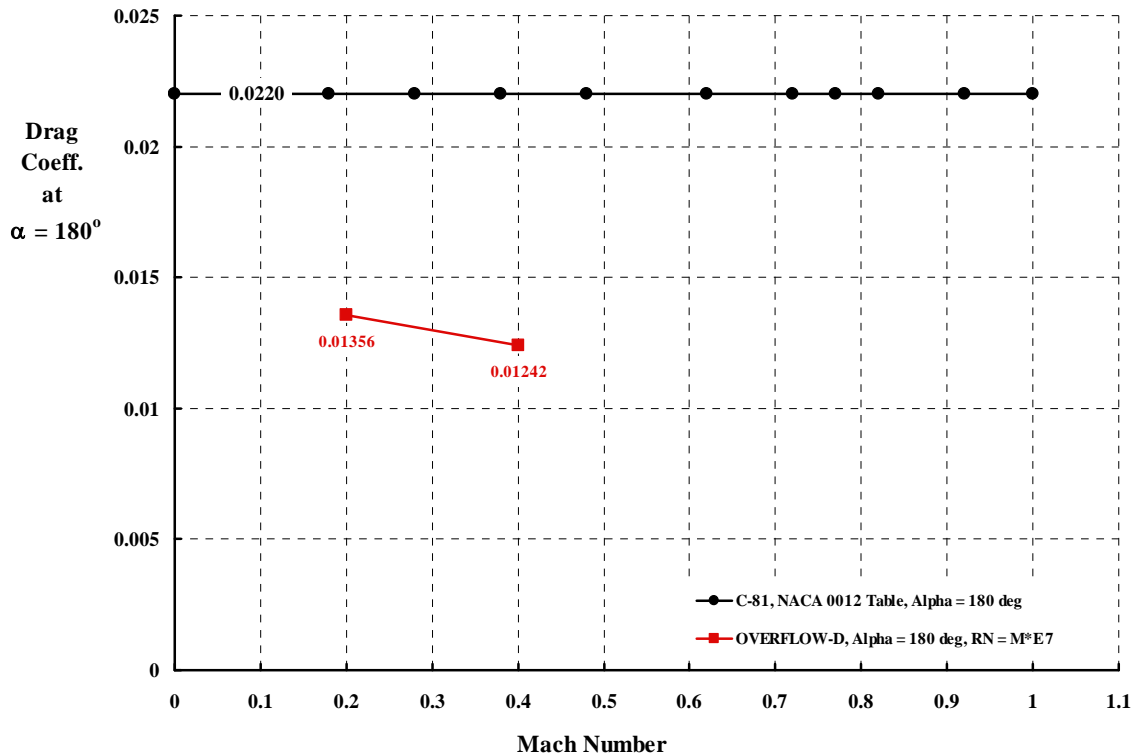


Fig. 7-57. OVERFLOW-2's N.A.C.A. 0012 drag coefficient, *trailing edge forward*, versus Mach number by Theron compared to C81 table.

Jan Theron's contributions to this general high advance ratio problem have been – as you have read – quite significant. When he went on to the Heliplane project as a higher priority, no one stepped in to fill the void until early 2008.

In early 2008 it became apparent that neglecting the H-34 blade root end (see Fig. 3-4 and Fig. 3-5) was a big mistake. Correlations of H-34 experimental data with CAMRAD II, CHARM, RCAS and OVERFLOW-2 all suffered and their early results were discarded. Corrections were made in CAMRAD II, CHARM and RCAS models and these improved correlations are what are included in this report. The primary corrections were to add an increment of C_d to the C81 drag coefficients when a blade element was in the reverse flow region and treat the H-34 blade shank with an additional C_d increment.

The encouraging view at this time was that Strawn's and Theron's calculation of torque coefficient, seen with Fig. 7-47, were in rather close agreement. The substantial difference in the calculated H-force coefficient favored the view that adding the H-34 "blade shank" (i.e., the 28 inch length of D-spar shown with Fig. 3-4 and Fig. 3-5) to Theron's OVERFLOW-2 H-34 configuration would add enough H-force to at least bring agreement with the H-34 experimental data shown on Fig. 7-48. The task of exploring this avenue was thrust upon Ethan Romander, a member of the Aeromechanics Branch at the NASA Ames Research Center.

As of this report, Romander has succeeded in creating a preliminary blade grid which is shown with Fig. 7-58, Fig. 7-59 and Fig. 7-60. He intends to use this configuration for exploration on how OVERFLOW-2 works. Once over the learning process, the more correct “parabolic” tip shape (see Fig. 3-6) will be modeled. To complete the problem set up, the trailing edge over the 0.8 to 0.9 radius station must be bent up to create a localized airfoil pitching moment. After this step, OVERFLOW-2 can be coupled to CAMRAD II and the lengthy computation of some 250 H-34 test points can be made. Then the in depth correlation analysis initiated in this report will tell whether this promising approach to calculating rotor performance is on the right track.

Based on priority and progress to date, the author imagines some conclusion (about how well OVERFLOW-2 coupled to CAMRAD II correlates with H-34 experimental data) in about a year or two.

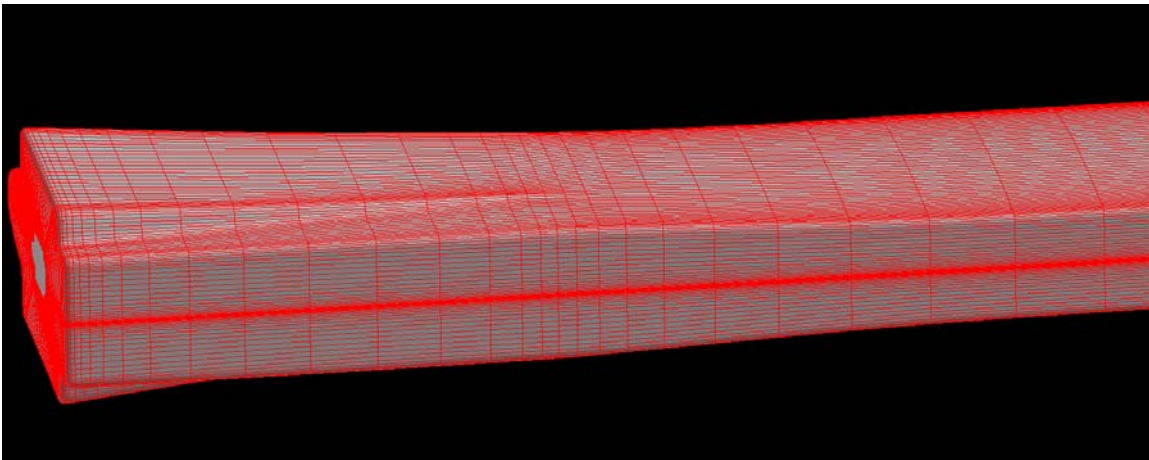


Fig. 7-58. Blade root end or more commonly, the shank.

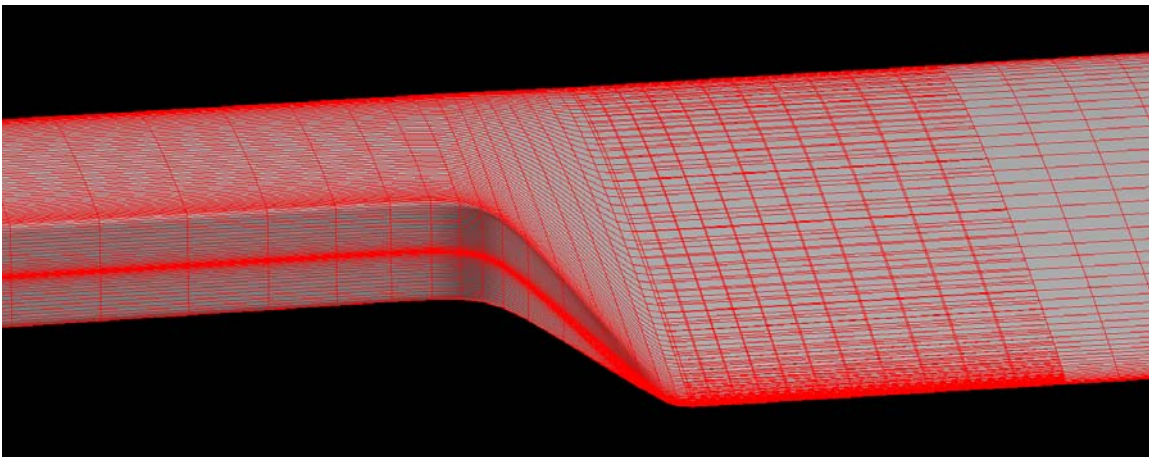


Fig. 7-59. Blade shank transition to blade proper.

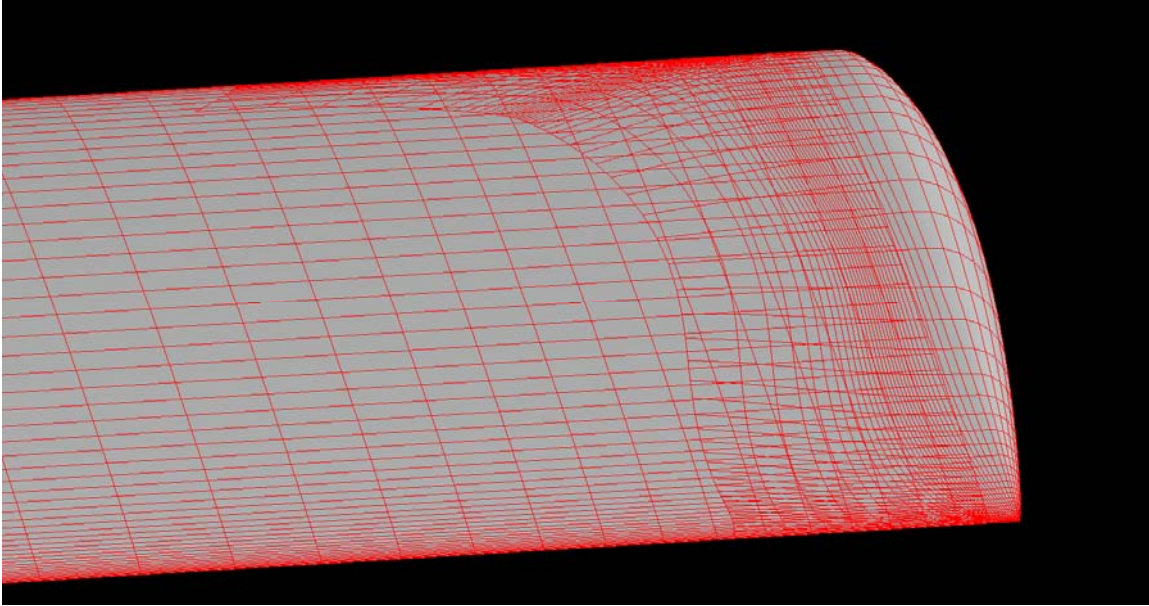


Fig. 7-60. Blade square tip with body of revolution tip cap.

7.5 H-34 Concluding Remarks

There is a final point to remember. The selected comprehensive codes being evaluated have demonstrated successful prediction of many helicopter parameters and design factors. The codes have been developed for the advance ratio range between hover and 0.4. However, *it is the extension, evaluation and usability of these codes beyond their known capabilities which is under study in this report.*

This examination of the selected codes compared to H-34 test data indicates that not one of the codes can predict – to engineering accuracy – the control positions and shaft angle of attack required for a given lift above an advance ratio of 0.62. Two major aspects of the problem are:

1. The questionable accuracy in modeling the blade element lift, drag and pitching moment airloads in the reverse flow region.
2. The impact of torsional deflections on collective and cyclic control positions.

7.6 UH-1 Test versus CAMRAD II (Appendix 11.14)

The detailed evaluation of UH-1 test versus CAMRAD II in the quantitative depth sought by this report is not possible at this time. There are three reasons for this situation:

a. First – and most importantly – the preliminary CAMRAD II computations have not reproduced the measured rotor lift and longitudinal cyclic trim required for zero flapping when the collective pitch at the 0.75 radius station is zero and the shaft angle of attack is zero. The disagreement, illustrated by Fig. 7-61 and Fig. 7-62 for the UH-1, was resolved for the H-34 by allowing an elastic torsion structural response due to a localized bent up trailing edge. This subject was discussed in some detail in paragraph 7.1 and graphically seen with Fig. 7-6 and Fig. 7-7.

b. Second, only about one-half of the 165 calculated points correspond to the 218 UH-1 test points shaft and collective pitch angles. This is far too few correlation points to apply the evaluation method advocated by this author as discussed in paragraph 6.1.

c. Third, CAMRAD II is – at present – very slow to find a converged bound circulation distribution with low aspect ratio blades and high advance. The modified UH-1 blades tested at high advance had a radius of 17 feet and the blade chord was 1.75 feet, which is an aspect ratio of 9.7. In contrast the H-34 blades had an aspect ratio of $28/1.337 = 20.9$.

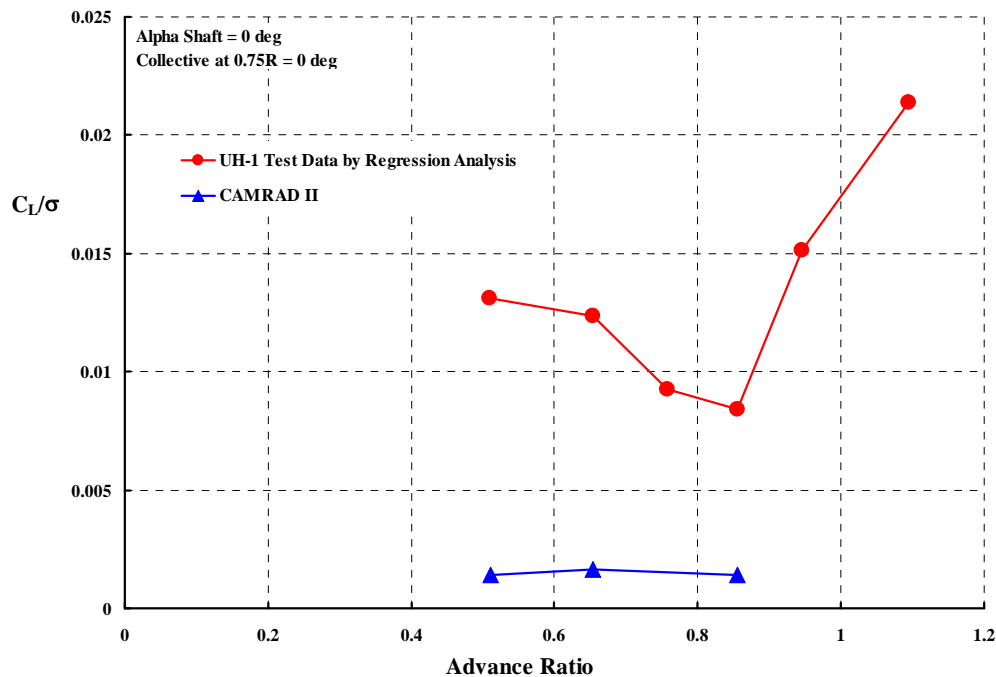


Fig. 7-61. Preliminary CAMRAD II calculations of rotor lift coefficient do not agree with UH-1 test data at $\theta_{3/4 R} = 0$ and $\alpha_S = 0$.

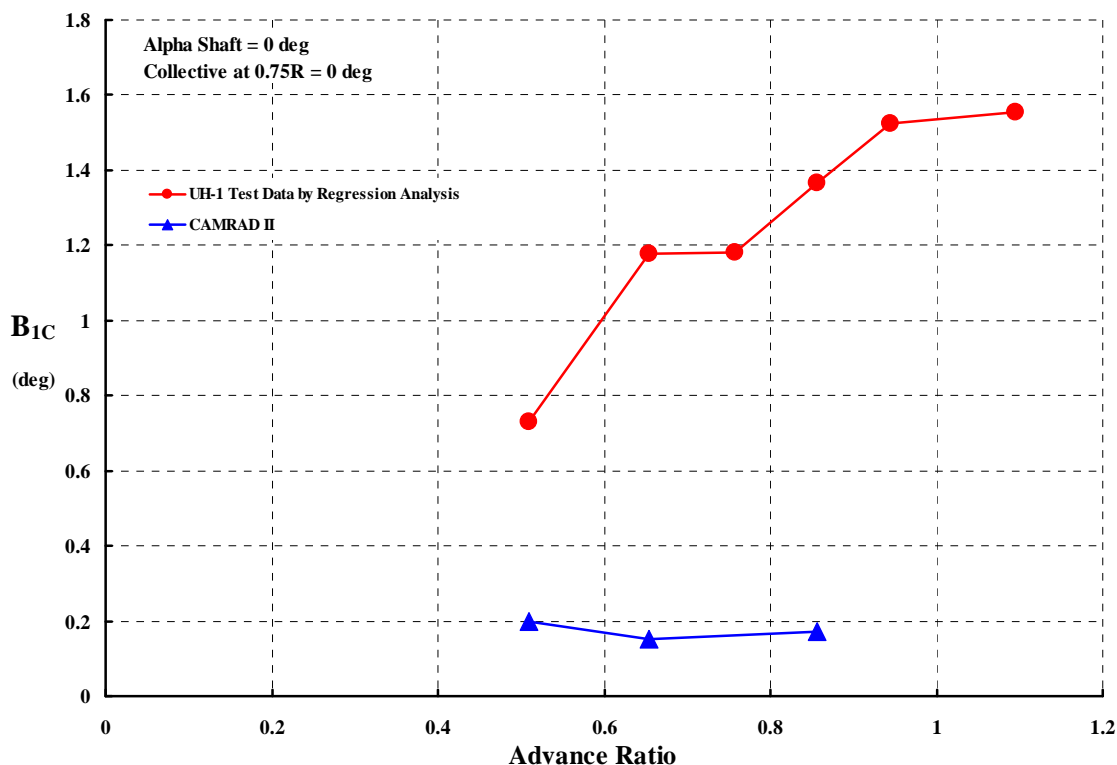


Fig. 7-62. Preliminary CAMRAD II calculations of longitudinal cyclic do not agree with UH-1 test data at $\theta_{3/4 R} = 0$ and $\alpha_S = 0$.

Given CAMRAD II's results shown with Fig. 7-61 and Fig. 7-62, the question arises as to how much elastic twisting might it take to achieve a theory/test match at $\mu = 0.51$ and $\theta_{3/4 R} = 0$ and $\alpha_S = 0$. Ignoring the lateral cyclic control aspects, the CAMRAD II calculation was made with a blade pitch radial and azimuthal distribution of

$$\theta_{x,\psi} = 1.065 - 1.42x - 0.2 \sin \psi$$

CAMRAD II said that the elastic twisting was negligible. The Wheatley/Bailey theory provided in Appendix 11.2 offers the estimated that if

$$\theta_{x,\psi} = 1.065 - 1.42x - 0.73 \sin \psi + x(2.59 - 0.35 \sin \psi)$$

then calculated C_L/σ would equal 0.0131, flapping would be zero and B_{1C} would equal 0.73 degrees, which matches theory and test at a very fundamental point.¹⁴

Notwithstanding the above reservations, a comparison of sorts can be obtained from the preliminary calculations made by Johnson with his CAMARAD II. To begin with, consider the rotor lift coefficient versus shaft angle of attack data shown on Fig. 7-63. At an advance ratio of 0.51, there is a trade of 2 degrees in collective pitch which provides nearly perfect agreement between test and theory. That is, test data at $\theta_{3/4 R} = 0$

¹⁴ It is very difficult for this author to express how strongly he feels about this aspect of theory versus test correlation.

degrees and CAMRAD II at $\theta_{\frac{1}{4}R} = +2$ degrees are well matched. This means that some sort of comparison between measured and predicted performance parameters can be made.

At an advance ratio of 0.51, lift coefficient is matched at each shaft angle of attack shown on Fig. 7-63 (albeit with a disagreement in collective pitch). By the test requirement, the rotor tip path plane was trimmed normal to the shaft at each test and theory point shown on Fig. 7-63. On the basis of matching lift coefficient at any given shaft angle of attack, it is clear that CAMRAD II calculations at $\theta_{\frac{1}{4}R} = +2$ degrees are in “quite reasonable” agreement with UH-1 test data for $\theta_{\frac{1}{4}R} = 0$ degrees. Thus, the performance comparisons can be made using shaft angle of attack or lift coefficient as the independent parameter. For the following graphs and discussion, chose lift coefficient as the abscissa.

The amount of longitudinal cyclic control applied to trim the tip path plane normal to the shaft (i.e., the condition of near zero first harmonic flapping) is shown with Fig. 7-64. CAMRAD II’s matching of lift – but at 2 degree higher collective pitch – forces the longitudinal cyclic to differ by approximately 1.5 degrees. This is in accordance with even the simplest of theory.

The measured drag coefficient versus CAMRAD II’s prediction is provided with Fig. 7-65. Since the component of drag due to rotor thrust (i.e., $C_T/\sigma \sin \alpha_S$) is virtually

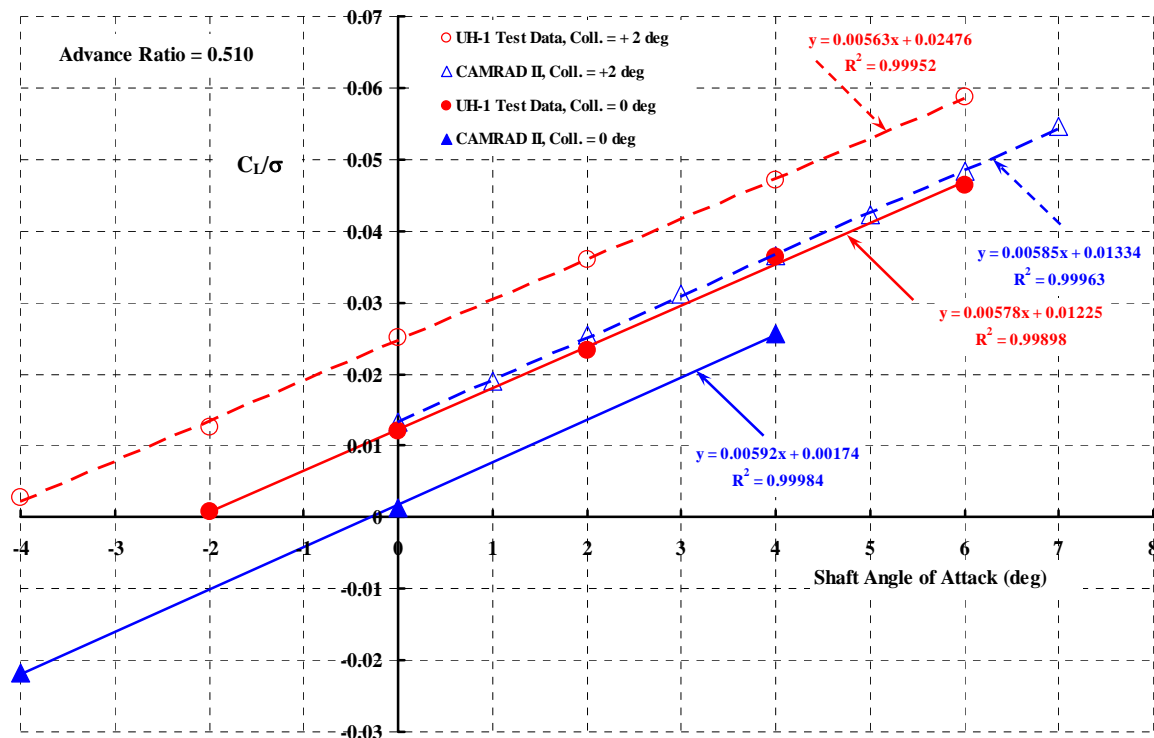


Fig. 7-63. At an advance ratio of 0.51, test and theory lift coefficient can be matched but not at the same collective pitch.

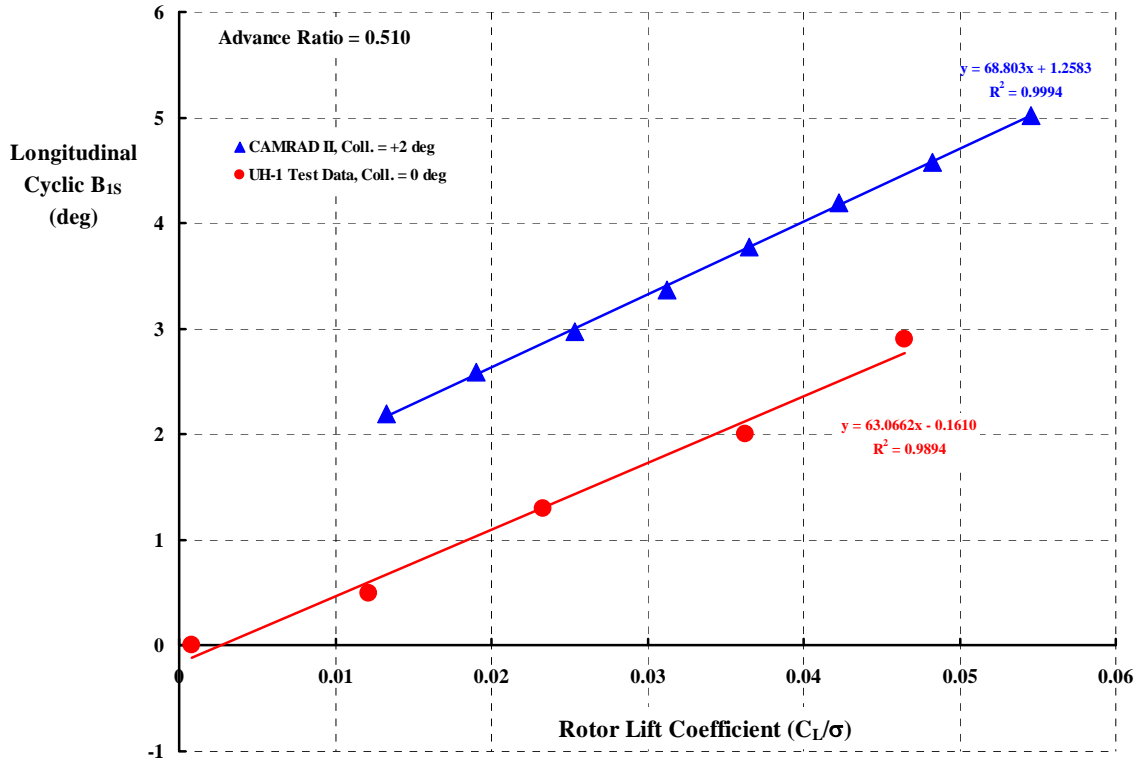


Fig. 7-64. Longitudinal cyclic comparison at nearly equal shaft angle of attack and equal lift coefficient but unequal collective pitch leads to a mismatch in B_{1C} .

exact because thrust and angle of attack are nearly matched, it is the error in the H-force component (i.e., $C_H/\sigma \cos \alpha_s$) that is the major source of the difference seen on Fig. 7-65. The predicted versus measured H-force coefficient, shown with Fig. 7-66, confirms this fact.

The agreement between measured torque (or power) coefficient and CAMRAD II's prediction is seen on Fig. 7-67. The general impression from this small sample is that CAMRAD II over predicts measured power but, from Fig. 7-65, under predicts rotor drag.

While all 165 CAMRAD II predicted points are included in Appendix 11.14, further comparisons are not warranted at this time. The immediate effort must be to understand what additional inputs to this comprehensive code are necessary so that lift and longitudinal cyclic at $\theta_{3/4R} = 0$ and $\alpha_s = 0$ are much more in agreement with the UH-1 experimental data.

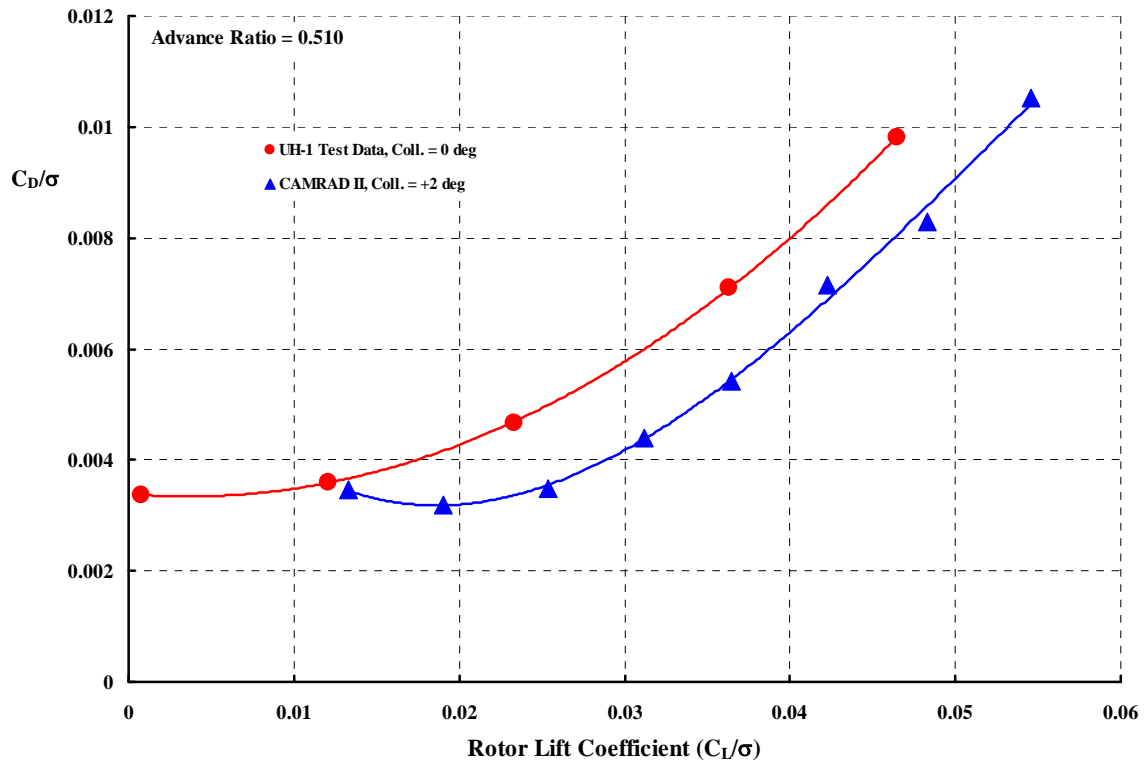


Fig. 7-65. Rotor drag coefficient comparison at nearly equal shaft angle of attack and equal lift coefficient.

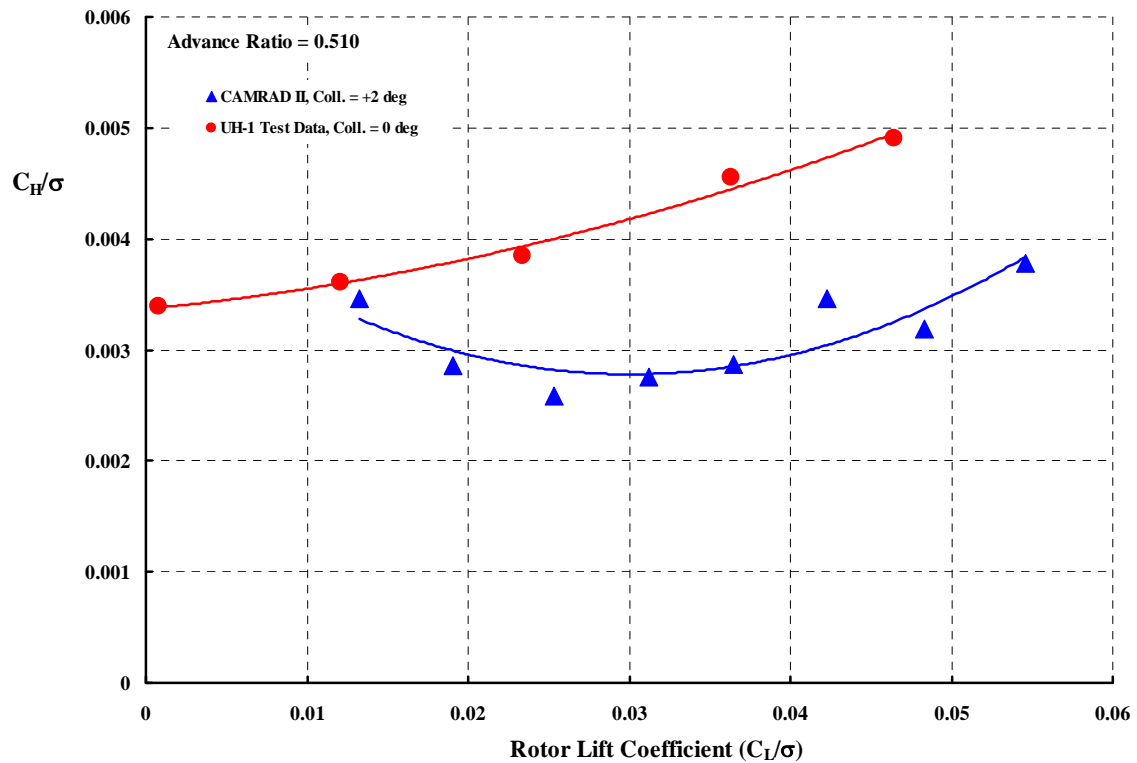


Fig. 7-66. Rotor H-force coefficient comparison at nearly equal shaft angle of attack and equal lift coefficient.

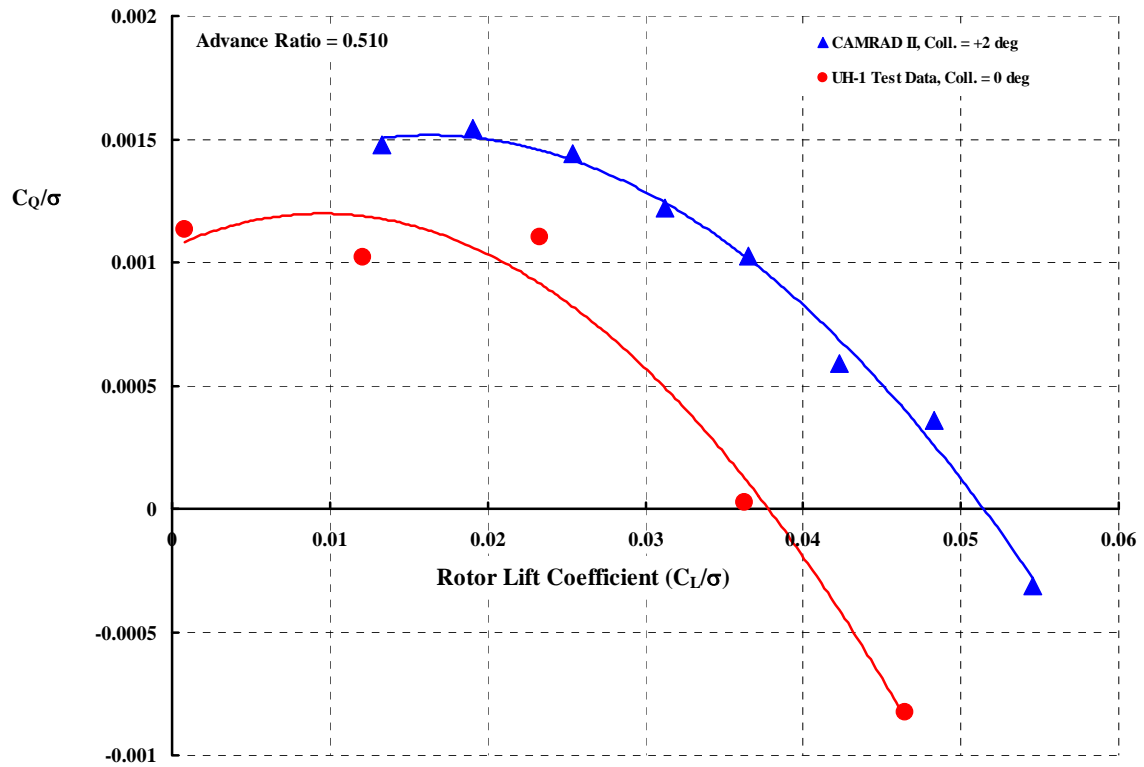


Fig. 7-67. Rotor H-force coefficient comparison at nearly equal shaft angle of attack and equal lift coefficient.

7.7 UH-1 Test versus CHARM (Appendix 11.15)

No UH-1 points were computed by CHARM

7.8 UH-1 Test versus RCAS (Appendix 11.16)

The summary of RCAS's capability to predict UH-1 test data is given here and is supported by tables and graphs in Appendix 11.16. Table 24 compares the theory versus the wind tunnel measured parameters using linear regression analysis. Rotor thrust, H-force, effective drag coefficients and rotor L/D_E are derived from the measured wind tunnel measured parameters. These derived parameters are included in Appendix 11.16. The meaning of the red color coding is that the regression analysis result does not meet the accuracy criteria advocated by this author. That is, a slope, intercept or R^2 cell is shaded red if:

1. Slope outside of 0.95 to 1.05
2. Intercept outside of
 - Longitudinal cyclic, B_{1C} , ± 0.3 degrees
 - Lateral cyclic, A_{1C} , ± 0.3 degrees
 - Lift coefficient, C_L/σ , ± 0.003
 - Drag coefficient, C_D/σ , ± 0.0005
 - Side Force coefficient, C_Y/σ , ± 0.0004
 - Torque (power) coefficient, C_Q/σ , 0.0003
3. R^2 less than 0.97

The cells colored yellow indicate a value that is very close to the advocated criteria. Keep in mind that the more important information to be gained from Table 24 is the trends with advance ratio.

Table 24, with nearly all red cells, immediately says that this very first RCAS computation is not predicting UH-1 test data with any fidelity. The most positive thing that can be said is that the longitudinal cyclic prediction is "very good" – if the intercept is ignored. RCAS's prediction of H-34 test data accomplished this primary correlation requirement, but failed when the UH-1 was tackled. Clearly, there must be several configuration ingredients missing in the RCAS setup at this time.

It is this author's position that correlation begins by predicting the lift and longitudinal cyclic when the shaft angle of attack equals zero and collective pitch at the 3/4 radius station equals zero. Until this fundamental is captured, there is little reason to expect that other aerodynamic performance parameters will be accurately predicted. That there is a serious error in this RCAS computational set is confirmed by Fig. 7-68 and Fig. 7-69. Based on the H-34 examination, it could well be that the torsional deflection is not reflected in these first RCAS predictions of UH-1 test data.

Fig. 7-70, Fig. 7-71 and Table 24 show that there is very little scatter in the lift and longitudinal cyclic correlation, which suggests that RCAS is capturing a fundamental trend. No doubt, additional study will uncover what missing factor about the UH-1 test data and/or RCAS is at the bottom of this correlation problem. For example, the UH-1 blade is stiff inplane and a pre-lag or pre-lead angle is adjustable with a drag strut. A pre-lag or lead angle coupled with a soft control system may be a significant factor.

Table 24. Table of Linear Regression Coefficients for Wind Tunnel Measured Parameters. UH-1 Test versus RCAS.

Longitudinal Cyclic				Lateral Cyclic		
Mu	SLOPE	Intercept	R²	SLOPE	Intercept	R²
0.510	0.9608	0.5881	0.9947	No test data		
0.654	0.9926	0.9332	0.9968	No test data		
0.757	1.0189	0.8470	0.9950	No test data		
0.856	0.9948	1.0992	0.9949	No test data		
0.943	1.0069	1.1839	0.9965	No test data		
1.093	1.0173	1.2481	0.9932	No test data		

Lift Coefficient				Drag Coefficient		
Mu	SLOPE	Intercept	R²	SLOPE	Intercept	R²
0.510	0.8635	0.0098	0.9924	0.9567	0.0025	0.9661
0.654	0.7807	0.0089	0.9883	0.8444	0.0039	0.9498
0.757	0.8439	0.0081	0.9574	0.6476	0.0048	0.7137
0.856	0.9276	0.0060	0.9752	0.8486	0.0050	0.6437
0.943	0.8642	0.0097	0.9717	0.8074	0.0051	0.7104
1.093	0.8617	0.0201	0.9874	1.3736	0.0005	0.9280

Y-Force Coefficient				Power Coefficient		
Mu	SLOPE	Intercept	R²	SLOPE	Intercept	R²
0.510	1.9830	-0.0014	0.8571	0.8479	0.0003	0.9474
0.654	2.9958	-0.0016	0.8938	0.7225	0.0005	0.8759
0.757	3.8110	-0.0016	0.6778	0.7094	0.0003	0.9288
0.856	5.3540	-0.0012	0.4770	0.4453	0.0004	0.5281
0.943	2.0835	-0.0048	0.0781	0.4302	0.0008	0.5165
1.093	0.0611	-0.0053	0.0001	0.5982	0.0007	0.7694

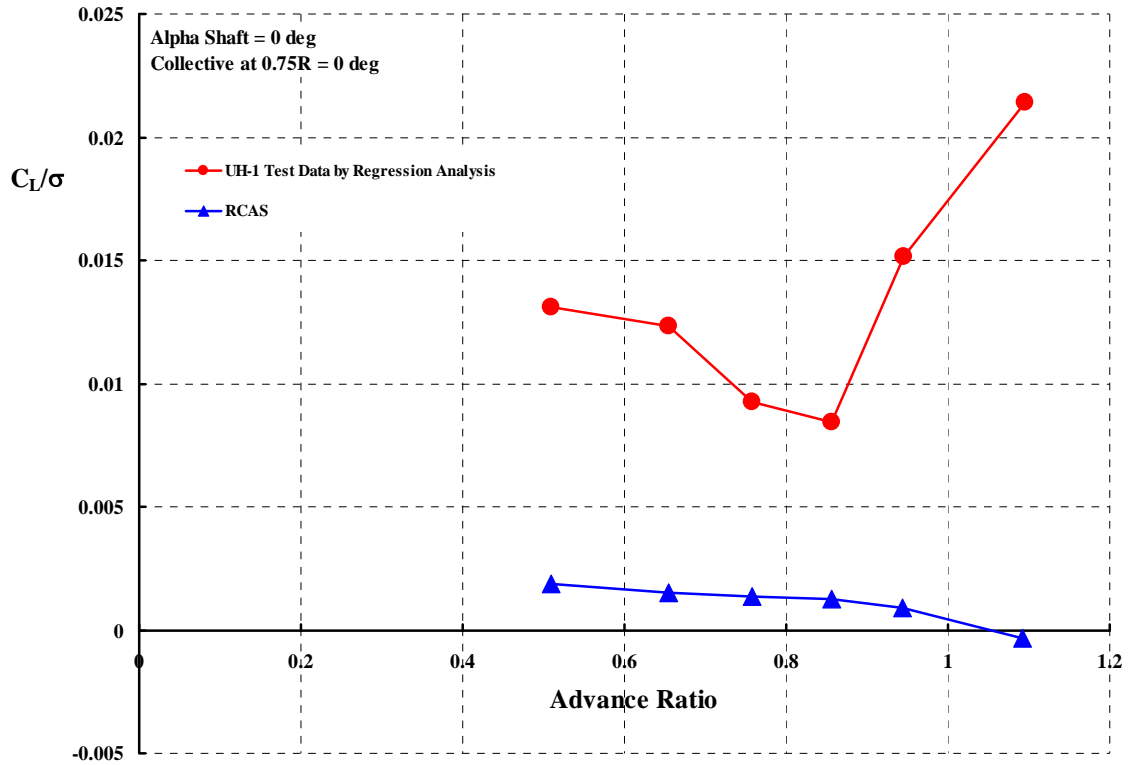


Fig. 7-68. RCAS lift coefficient correlation at $\theta_{3/4 R} = 0$ and $\alpha_S = 0$.

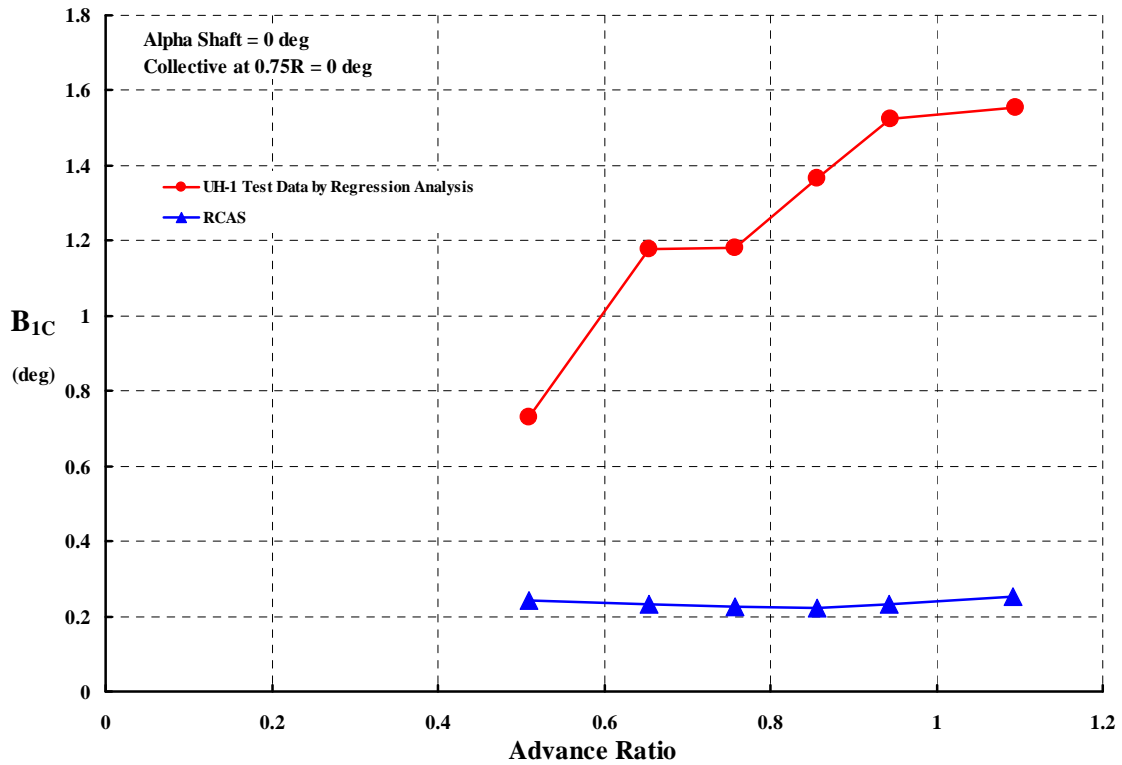


Fig. 7-69. RCAS longitudinal cyclic correlation at $\theta_{3/4 R} = 0$ and $\alpha_S = 0$.

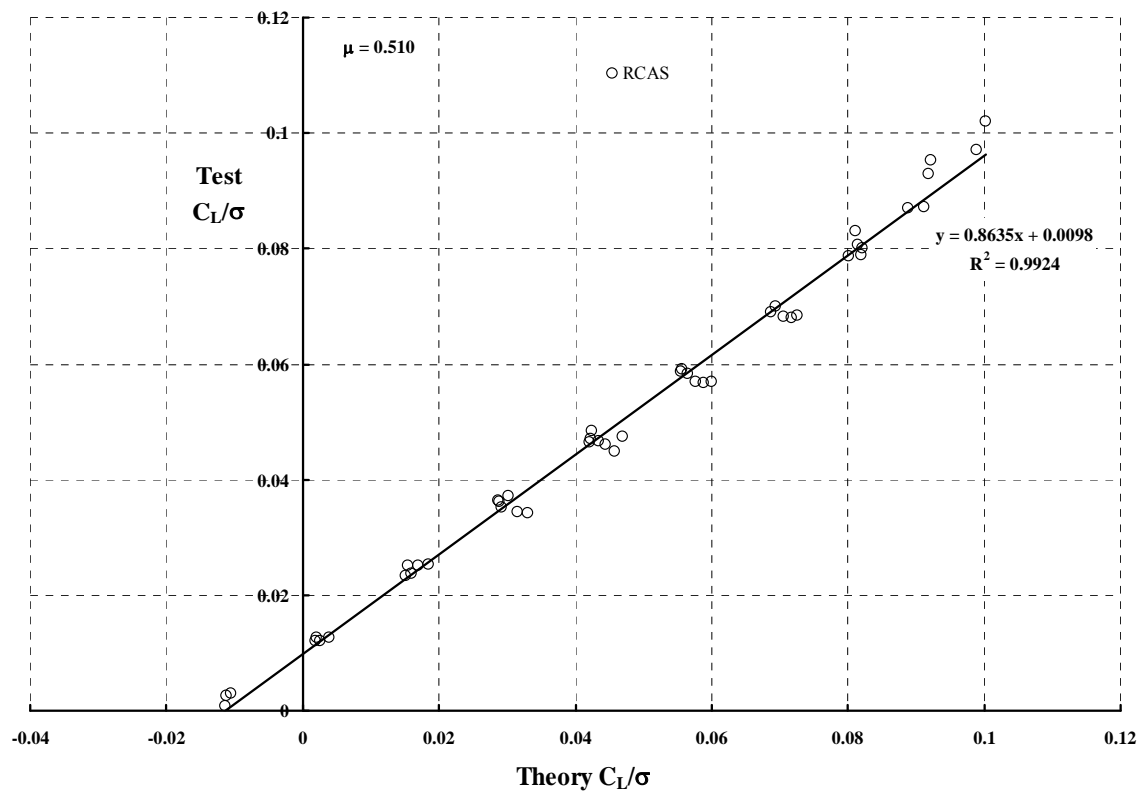


Fig. 7-70. RCAS over predicts lift coefficient slope.

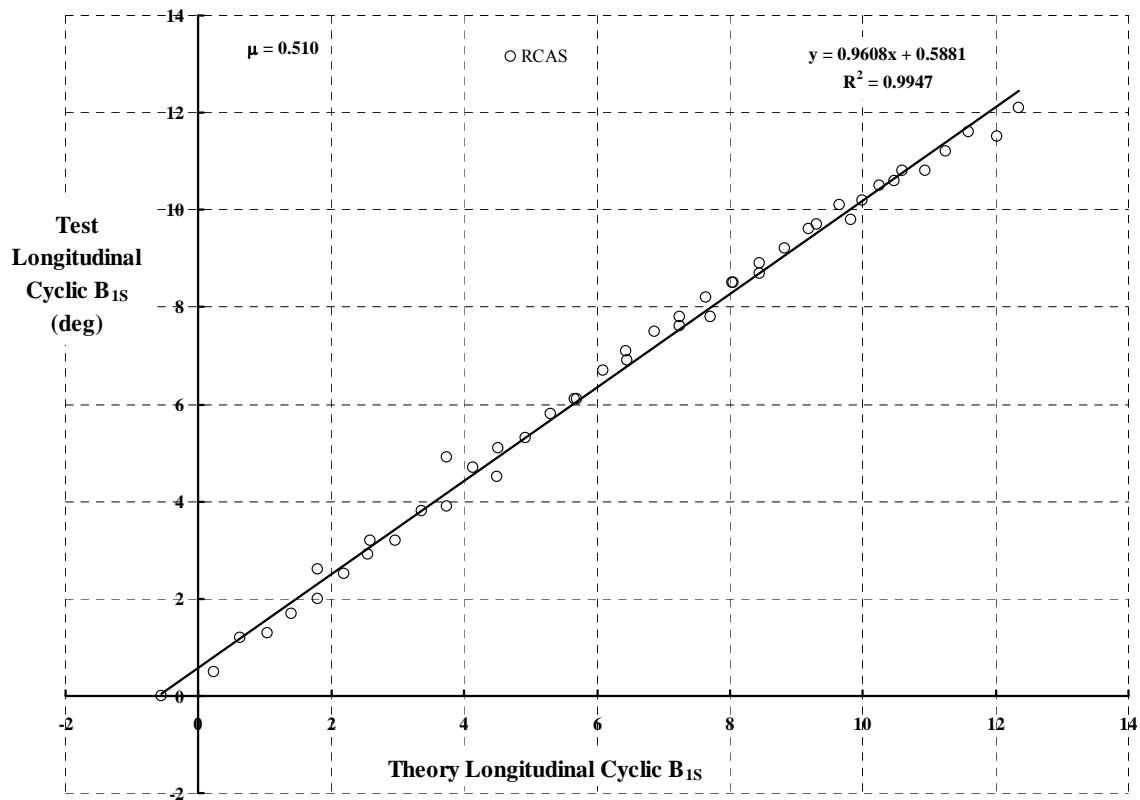


Fig. 7-71. RCAS accurately predicts longitudinal cyclic slope.

7.9 UH-1 Test versus OVERFLOW-2 with CAMRAD II (Appendix 11.17)

No UH-1 points were computed by OVERFLOW-2 or by OVERFLOW-2 coupled with CAMRAD II.

7.10 UH-1 Concluding Remarks

First – and most importantly – the preliminary CAMRAD II and RCAS computations have not reproduced the measured rotor lift and longitudinal cyclic trim required for zero flapping when the collective pitch at the 0.75 radius station is zero and the shaft angle of attack is zero. The disagreement, illustrated for the two codes with Fig. 7-61, Fig. 7-62, Fig. 7-68, and Fig. 7-69 for the UH-1, was resolved for the H-34 by allowing an elastic torsion structural response due to a localized bent up trailing edge. This subject was discussed in some detail in paragraph 7.1 and graphically seen with Fig. 7-6 and Fig. 7-7. An explanation as to why the rotor lift and longitudinal cyclic at this fundamental, UH-1 test condition was not reproduced with theory is not available at this time.

Second, a speculative situation arose about the H-34/UH-1 versus CAMRAD II and RCAS codes. At an advance ratio of 0.51, CAMRAD II accurately predicted rotor lift curve slope for both rotors using a rigid wake model. RCAS accurately predicted rotor lift curve slope *only* for the H-34 using non-uniform downwash calculated with the Peters – He dynamic inflow model set to a 8 by 8 mode. RCAS' predicted lift curve slope was some 15 percent too high for the UH-1 at $\mu = 0.51$. The applicability of dynamic inflow models with low aspect ratio blades operating at high advance ratio is in question.

Third, CAMRAD II is – at present – very slow to find a converged bound circulation distribution with low aspect ratio blades and high advance. The modified UH-1 blades tested at high advance had a radius of 17 feet and the blade chord was 1.75 feet, which is an aspect ratio of 9.7. In contrast the H-34 blades had an aspect ratio of $28/1.337 = 20.9$.

7.11 PCA-2 Test versus CAMRAD II (Appendix 11.18)

The PCA-2 experimental data base has lain dormant for at least 65 years. The author is unaware of any published correlation of modern comprehensive rotor theory with this experiment prior to Wayne Johnson's efforts in mid-2008. His preliminary results are provided in this report. Johnson, in tackling the correlation of CAMRAD II with the PCA-2 data, accepted the PCA-2's structural data reconstructed by the author and contained in Appendix 10.5. For his preliminary calculations, Johnson chose to use the blade twist distribution shown as the Wheatley twist on figure 3 in Appendix 11.5. No root collective pitch was added to this twist distribution. The blade chord distribution Johnson used is shown with figures 1 and 2 in Appendix 11.5. A table of airfoil aerodynamic coefficients in C81 format, created by the author, for the Göttingen 429 was used at all radius stations. This table is provided with Appendix 11.9. A table for the inboard camber airfoil (see Fig. 3-13) had not – at the time – been created to support Johnson's ground breaking efforts.

CAMRAD II was asked to compute the shaft angle of attack at which autorotation would occur given the input blade structural and blade configuration geometry. At selected advance ratios (prescribe rotor RPM and wind tunnel velocity), CAMRAD II searched for the shaft angle of attack that achieved autorotation. Once this shaft angle of was found, the analysis calculated the three forces and two moments associated with the operating condition. (Remember the shaft torque was required to be zero.) This approach reasonably duplicates how Wheatley conducted the PCA-2, rotor alone wind tunnel test.¹⁵

CAMRAD II's output data for the four rotor speeds Wheatley tested is tabulated in Appendix 11.18. The coefficients in common airplane nomenclature are defined as

$$C_L = \frac{\text{Lift}}{(\frac{1}{2}\rho V^2)(\pi R^2)} \quad C_D = \frac{\text{Drag}}{(\frac{1}{2}\rho V^2)(\pi R^2)} \quad C_Y = \frac{\text{Side Force}}{(\frac{1}{2}\rho V^2)(\pi R^2)}$$

$$C_{\text{Roll}} = \frac{\text{Rolling Moment}}{(\frac{1}{2}\rho V^2)(\pi R^2)(2R)} \quad C_{\text{Pitch}} = \frac{\text{Pitching Moment}}{(\frac{1}{2}\rho V^2)(\pi R^2)(2R)}$$

A positive rolling moment is right wing down and a positive pitching moment is nose up. Positive side force is to starboard because the rotor blades are rotating counter clockwise when the disc is viewed from above. The coefficients in rotorcraft nomenclature are defined as

$$C_T = \frac{\text{Thrust}}{(\rho V_t^2)(\pi R^2)} \quad C_H = \frac{\text{H – force}}{(\rho V_t^2)(\pi R^2)} \quad C_Y = \frac{\text{Y – force}}{(\rho V_t^2)(\pi R^2)}$$

$$C_{\text{Roll}} = \frac{\text{Rolling Moment}}{(\rho V_t^2)(\pi R^2)R} \quad C_{\text{Pitch}} = \frac{\text{Pitching Moment}}{(\rho V_t^2)(\pi R^2)R}$$

¹⁵ A different approach, perhaps more suitable for correlation purposes, would be to input the rotor speed, wind tunnel speed *and the test shaft angle of attack*. Then have the analysis search for autorotation by adjusting collective pitch or steady elastic twist. This approach would at least guarantee that whatever thrust was obtained would be resolved to the wind axis through the “correct test angle.”

Neither the airplane or rotor coefficients have been further non-dimensionalized by rotor solidity. The disc area (πR^2) equals 1,590 square feet (a diameter of 45 feet) just as Wheatley used. The nominal rotor speeds of 98.63, 118.7, 137.6 and 147.9 RPM were used by Wheatley. They correspond to average tip speeds of 232.39, 279.68, 324.21 and 348.48 feet per second. Johnson chose 12 ratios of forward speed (V) to tip speed (V_t) at which computations would be made. These ratios were 0.15, 0.20, 0.25, 0.30, 0.35, 0.40, 0.45, 0.50, 0.55, 0.60, 0.65 and 0.70. The actual advance ratio, $\mu = V \cos \alpha_s / V_t$, then depends upon the shaft angle of attack at which autorotation was achieved.

The ability of CAMRAD II to predict the shaft angle of attack at which autorotation occurs for the PCA-2 rotor operating at 98.63 RPM is shown with Fig. 7-72. Roughly speaking CAMRAD II over predicts about 0.5 degrees in the mid-advance ratio range and under predicts by the same amount at the top advance ratios. Fig. 7-73 shows that rotor lift in autorotation is significantly under predicted at all but the lowest advance ratio.

CAMRAD II's prediction of the PCA-2's rotor H-force coefficient, Fig. 7-74, is within experimental error over the helicopter advance ratio region where the analysis is known to be generally accurate. Unfortunately, at and beyond an advance ratio of 0.5, a clear and growing error is apparent. The rotor Y-force coefficient prediction, Fig. 7-75, is, perhaps surprisingly in view of correlations with H-34 and UH-1 examples, encouraging up to an advance ratio of 0.4.

Prediction of the PCA-2 rotor lift to drag ratio by CAMRAD II is shown with Fig. 7-76. Keep in mind that because the rotor is in autorotation, the drag here is the drag auxiliary propulsion (e.g. a propeller) must overcome. The under prediction by about 10 percent of the maximum lift to drag ratio is quite likely due to the under prediction of rotor lift illustrated with Fig. 7-73.

Appendix 11.18 provides similar comparisons of the five rotor parameters under study at rotor speeds of 118.7, 137.6 and 147.9 RPM. CAMRAD II appears not to capture the influence of rotor speed on the PCA-2 performance parameters.

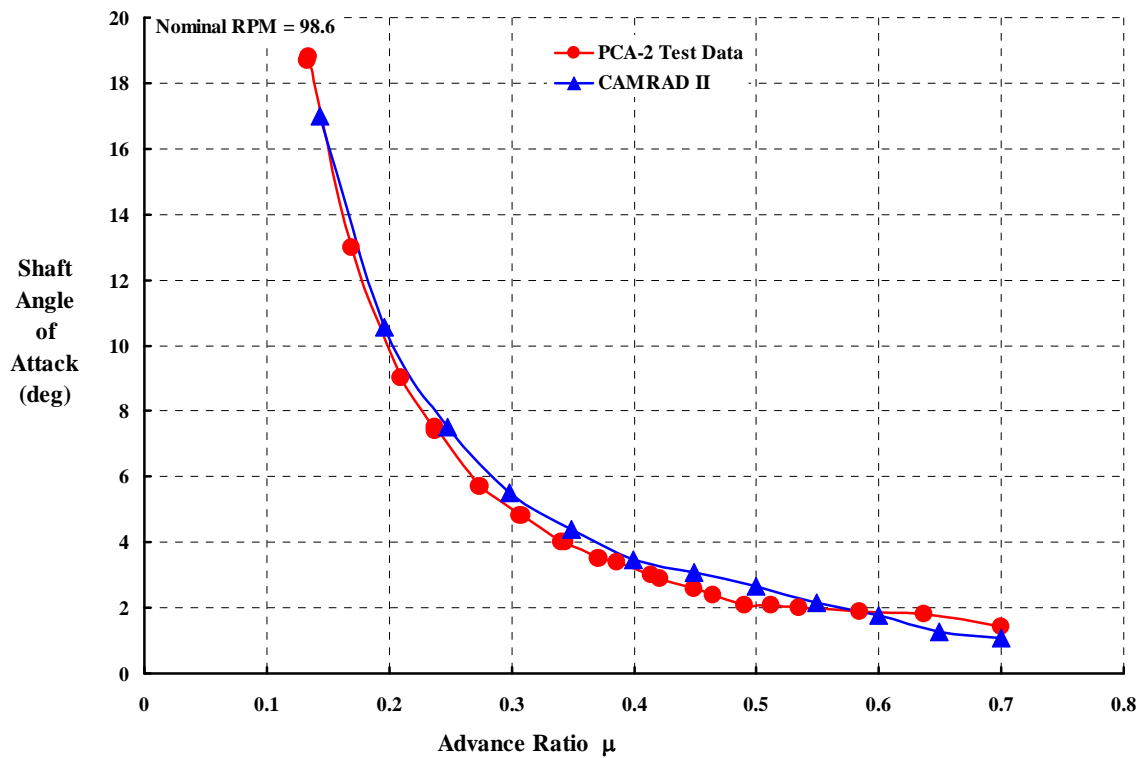


Fig. 7-72. Shaft angle of attack for autorotation, RPM = 98.63.

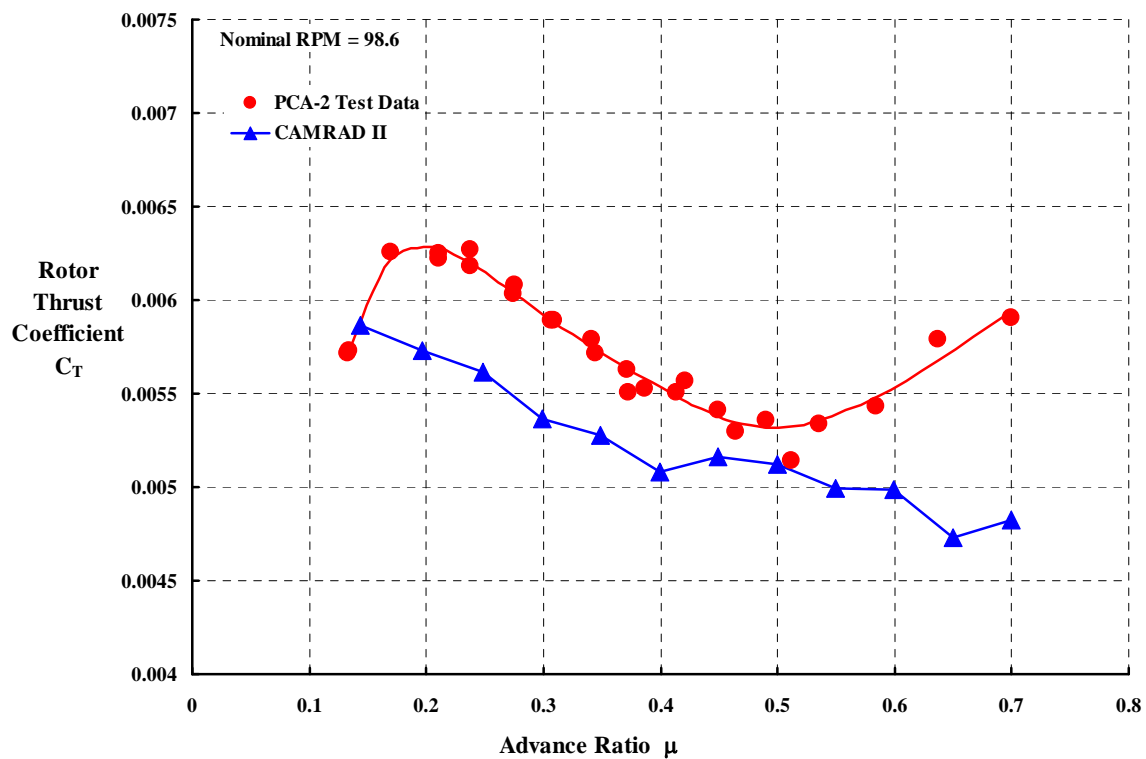


Fig. 7-73. Predicted rotor thrust coefficient, RPM = 98.63

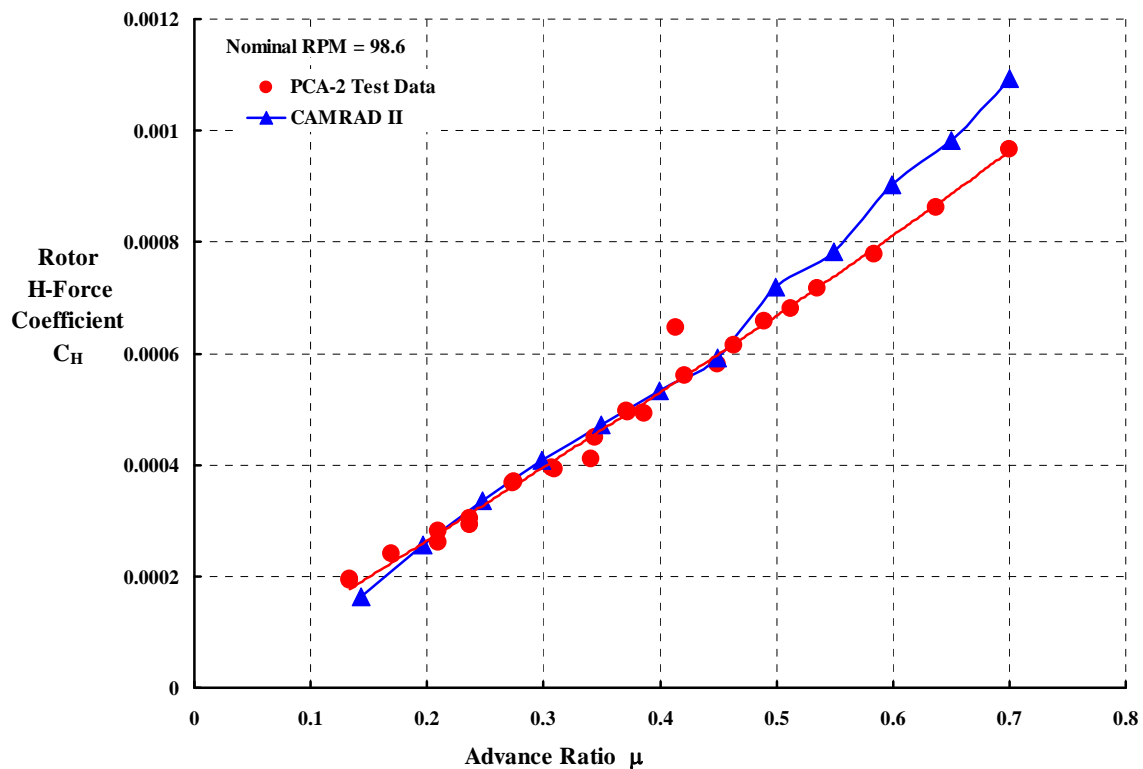


Fig. 7-74. Predicted rotor H–force coefficient, RPM = 98.63

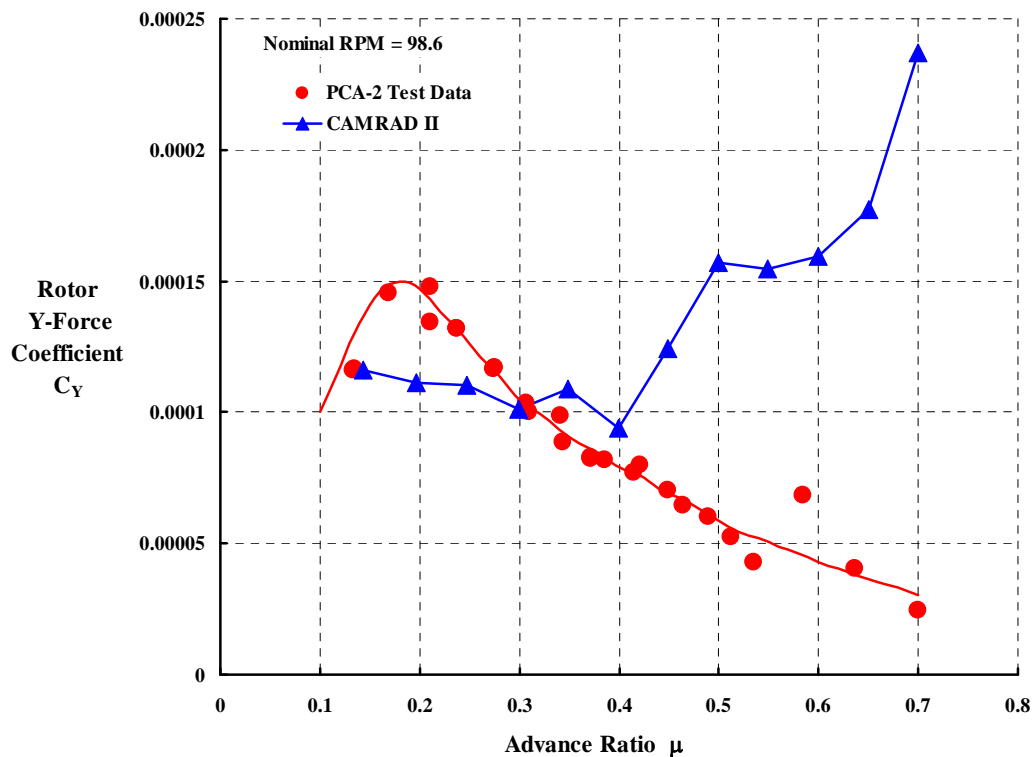


Fig. 7-75. Predicted rotor Y–force coefficient, RPM = 98.63

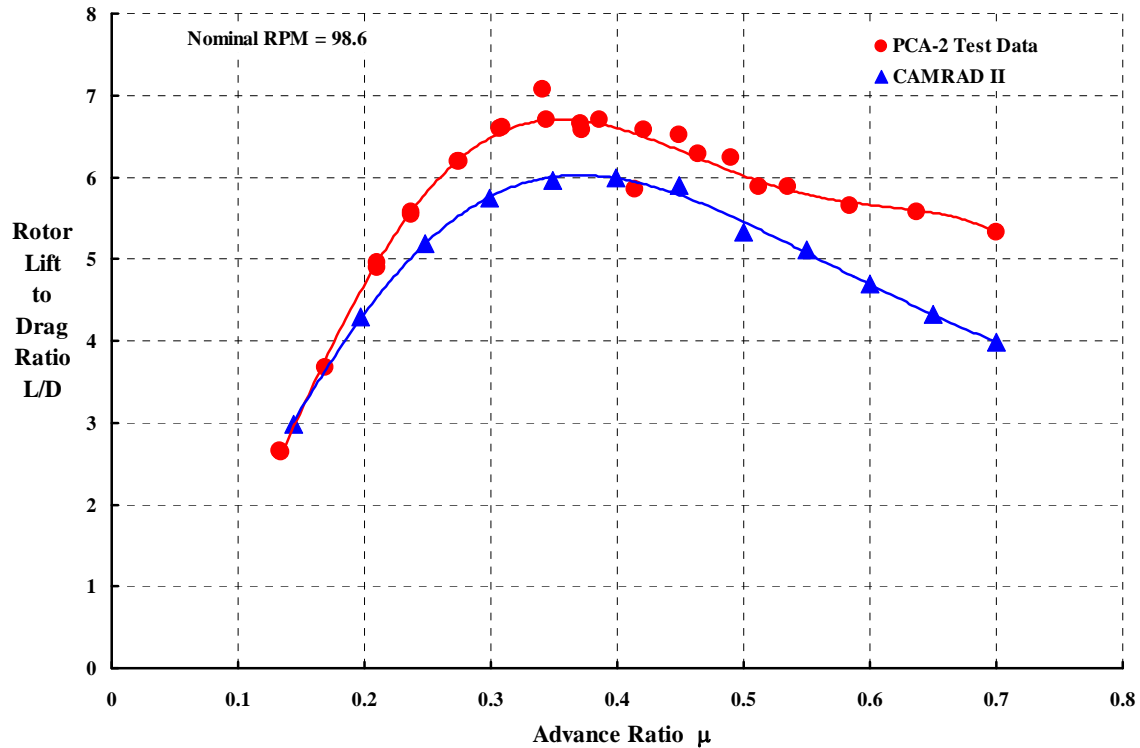


Fig. 7-76. Predicted rotor lift to drag ratio, RPM = 98.63

7.12 PCA-2 Test versus CHARM (Appendix 11.19)

No PCA-2 points were computed by CHARM

7.13 PCA-2 Test versus RCAS (Appendix 11.20)

No PCA-2 points were computed by RCAS

7.14 PCA-2 Test versus OVERFLOW-2 with CAMRAD II (Appendix 11.21)

No PCA-2 points were computed with OVERFLOW-2 or with OVERFLOW-2 coupled to CAMRAD II

Page intentionally blank

8 CONCLUSIONS

Five analytical tools have been chosen to study rotor performance at high advance ratio. One is representative of autogyro rotor theory in 1934 and four are representative of helicopter rotor theory in 2008. Three sets of well documented, full-scale, isolated rotor performance experiments have been selected against which the five theories are measured. This 3 by 5 matrix is summarized by the following table and the progress made as of this report is noted.

Rotors	Wheatley & Bailey	CAMRAD II	CHARM	RCAS	Overflow CFD Coupled With CAMRAD II
H-34	✓	✓	✓	✓	Partial
UH-1	✓	Partial		✓	
PCA-2	✓	✓			

The major finding of this study is that the decades spent by many rotorcraft theoreticians to improve prediction of basic rotor aerodynamic performance has paid off. This payoff, illustrated by comparing the CAMRAD II and Wheatley & Bailey theories to H-34 test data, shows that rational rotor lift to drag ratios are now predictable. The 1934 theory predicted L/D ratios as high as 15. CAMRAD II predictions compared well with H-34 test data having L/D ratios more on the order of 7 to 9. Other findings of note are:

1. The detailed examination of the selected codes compared to H-34 test data indicates that not one of the codes can predict – to engineering accuracy above an advance ratio of 0.62 – the control positions and shaft angle of attack required for a given lift. Two major aspects of the problem are:

- a. the questionable accuracy in modeling the blade element lift, drag and pitching moment airloads in the reverse flow region.
- b. the impact of blade torsional deflections on collective and cyclic control positions.

2. With respect to H-34 experimental data reported in NASA TN D-4632, the data set at an advance ratio of 1.05 is of very doubtful value in any theory/test comparison.

3. With respect to UH-1 experimental data reported in USAAVLABS TR 69-2, there are five (5) points at an advance ratio of 0.65 where there was insufficient longitudinal cyclic to trim the tip path plane normal to the shaft. These points were discarded in this study because all theories used zero first harmonic flapping as a trim requirement.

4. There was an expectation that a rotor with untwisted blades would produce no lift and require no cyclic control input to trim to zero flapping (at any advance ratio) if

operated at zero shaft angle of attack and zero collective pitch at the 3/4 radius station. This was a very incorrect preconceived notion.

5. A speculative situation arose about the H-34/UH-1 versus CAMRAD II and RCAS codes. At an advance ratio of 0.51, CAMRAD II accurately predicted rotor lift curve slope for both rotors using a rigid wake model. RCAS accurately predicted rotor lift curve slope *only* for the H-34 using non-uniform downwash calculated with the Peters – He dynamic inflow model set to 8 by 8 modes. RCAS’ predicted lift curve slope was some 15 percent too high for the UH-1 at $\mu = 0.51$. The applicability of dynamic inflow models with low aspect ratio blades operating at high advance ratio is in question.

6. OVERFLOW–2 coupled to CAMRAD II has shown very promising results in calculating airloads in the helicopter regime where the reverse flow region is quite small and blade root end drag is much less important. However, high advance ratio operation creates a very large portion of the rotor disc where airfoils are “flying backwards.” The collective results from three investigators showed that OVERFLOW–2 failed to calculate measured blade element drag when the airfoil was at an angle of attack of 180 degrees. Computational fluid dynamics cannot – apparently – accurately calculate lift, drag and pitching moment for airfoils flying backwards. Furthermore, OVERFLOW–2 has – apparently – not been tested against the fundamental problem of infinite circular cylinder drag variation with Reynolds number. The ability to calculate pressure drag of a bluff body is absolutely necessary because rotor blade root ends are currently far from airfoil shapes. OVERFLOW–2 (coupled or not) can not – at the present time – be recommended for use beyond an advance ratio of 0.35 to perhaps 0.40.

7. Comprehensive codes appear able to calculate the longitudinal cyclic required to trim a conventional rotor to a desired amount of flapping. On the other hand, the lateral cyclic control required to trim lateral flapping to zero was unpredictable by the comprehensive codes examined with this study. Furthermore, not one of the comprehensive codes came close to predicting measured rotor side force. However, OVERFLOW–2 identified a side force at zero thrust, zero collective pitch and zero shaft angle of attack. Simple and advanced theories do not suggest that there would be a side force at this condition.

8. The several codes were relatively unsuccessful (compared to predicting lift) in calculating rotor H-force and rotor power given test values of μ , α_S , and $\theta_{0.75R}$. High advance ratio flight leads to many blade elements in the reverse flow region operating at large sweep angles in an unsteady flow condition. Airloads for airfoils “flying backwards” are not as well understood as for airfoils in normal flow.

9. The H-34 and UH-1 measurements of H-force and power – at the fundamental condition where $\alpha_S = 0$ and $\theta_{0.75R} = 0$ – varied with advance ratio in approximately the same manner. Unfortunately, the advanced codes did not predict either rotor’s experimental values to within engineering accuracy. The codes over predict power and under predict H-force.

10. Both the H-34 and UH-1 rotors exhibited undesirable lift coefficient sensitivity to changes in collective pitch. The rotor lift becomes non-responsive to a collective pitch input at advance ratios near 1.0 – *if the rotor blade flapping is zeroed out by cyclic control as the collective pitch is changed and the shaft angle of attack remains constant*. The data indicate that in the advance ratio range of 0.9 to 1.0 there is a control reversal. At advance ratios below 0.9 an increase in collective pitch will increase rotor lift, but at advance ratios above 1.0 an increase in collective pitch reduces lift. In contrast, there is no reversal in the rotor lift curve slope (i.e., $\Delta C_L/\sigma$ per $\Delta \alpha_s$ at fixed collective and with cyclic trim for zero flapping), although the sensitivity increases with advance ratio. This rotor behavior may be unfamiliar to some; however, the unfavorable trend in $\Delta C_L/\sigma$ due to a $\Delta \theta$ at constant tip path plane angle of attack was first reported by Larry Jenkins in NASA TN D-2628, which was published in 1965. The comprehensive codes are quite able to capture this undesirable behavior.

11. The blade element airload modeling successfully achieved for helicopter speeds is inadequate when extrapolated to advance ratios above 0.5 to 0.6. In fact, it is even doubtful that increments in performance due to configuration changes can be accurately predicted. Until this technology shortcoming is repaired, the only available experimental data will have to do. The regression analysis equations of the H-34 and UH-1 test data as given in Chapter 5 should suffice for the near term calculation of conventional rotor performance at high advance ratios up to 1.

Page intentionally blank

9 RECOMMENDATIONS

The findings uncovered by this study suggest several recommendations for future efforts. The immediate concern is that the matrix of five theories compared to three experiments was not completed during this study. Therefore, it is recommended that theory comparisons to UH-1 and PCA-2 test data be finished. In addition:

1. Computational fluid dynamic theoreticians must provide the tools to accurately compute airfoil lift, drag and pitching moment when the airfoil is operating in a rotor's reverse flow region. These CFD tools must also be able to accurately predict at least the drag of typical non-airfoil shapes used for rotor blade root ends.

2. Comprehensive code developers must incorporate airfoil tables much more representative of airfoils operating in a rotor's reverse flow region. Inclusion of Reynolds number effects is of utmost priority if these codes are to be useful at advance ratios beyond 0.5 to 0.6. Special attention to modeling blade root end geometry and associated aerodynamic characteristics can no longer be ignored. Furthermore, rotor blade trailing edge geometry and its influence on blade element aerodynamics must be examined in great detail.

3. There is no full-scale rotor performance data available for advance ratios above 1.0 and extrapolation of currently available data to advance ratios on the order of 2.0 is unreasonable despite the needs of future rotorcraft. Therefore, it is recommended that an overly strong full-scale rotor blade set be obtained and tested in a suitable wind tunnel to at least an advance ratio of 2.5. A tail rotor from a Sikorsky CH-53 or other large single rotor helicopter may be adequate for this exploratory experiment.

4. Because so little is known about the reverse flow region, at least two small scale tests of a fundamental research nature should be conducted. Both tests should reach an advance ratio of at least 3.0 and only drag and power need be measured. These two tests, of considerable benefit to the rotorcraft community in general (and CFD theoreticians in particular), are:

- a. Circular cylinders of selected diameters tested as a two bladed rotor, but without a hub (and typical blade retention hardware) and without a control system. In essence, the "rotor" is nothing more than a 6 or 7 foot pipe, center mounted to a shaft so that no aerodynamic tares need be accounted for.
- b. Similarly, a very strong two bladed rotor with no hub or control system and with NACA 0012 airfoil blades should be built. The blades should be of rectangular planform and untwisted. This rotor is nothing more than a 6 or 7 foot carved ruler (i.e., a club), center mounted to a shaft so that no aerodynamic tares need be accounted for.

5. Because of the control reversal characteristic associated with rotor lift, future high advance ratio performance testing should acquire data by fixing collective pitch and varying shaft angle of attack while maintaining the tip path plane normal to the shaft. Additionally, the behavior of side force with lateral cyclic control should be measured.

Page intentionally blank

10 REFERENCES

1. Landis, T. and Jenkins, D.R., *Lockheed AH-56A Cheyenne*. Warbird Tech Series Volume 27: Specialty Press. 2000.(615)
2. Prouty, R.W. and Yackle, A.R. *The Lockheed AH-56 Cheyenne-Lessons Learned*. in AIAA Aircraft Design Systems Meeting, Paper 92-4278.1992. Hilton Head, South Carolina.(618)
3. Anderson, W.D. and Watts, G.A., *Rotor Blade Wake Flutter*, Lockheed Report LR 26213 (Prepared under Contract No. DAAJ01-73-C-0286, Modification P00005). 1973.(632)
4. Johnson, J.F. and Conner, F., *The Reactionless Inplane Mode of Stiff-Inplane Hingeless Rotors*, Lockheed Report LR 26214 (Prepared under Contract No. DAAJ01-73-C-0286, Modification P00005). 1973.(633)
5. Donham, R.E. and Cardinale, S.V., *Flight Test and Analytical Data for Dynamics and Loads in a Hingeless Rotor*, Lockheed Report LR 26215 (Prepared under Contract No. DAAJ01-73-C-0286, Modification P00005). 1973.(634)
6. Potthast, A.J. and Kerr, A.W., *Flying Qualities of a Gyro-Controlled Hingeless-Rotor Compound Helicopter*, Lockheed Report LR 26216 (Prepared under Contract No. DAAJ01-73-C-0286, Modification P00005). 1973.(635)
7. Anderson, W.D. and Gaidelis, J.A., *Vibration Inputs and Response of a Hingeless Rotor Compound Helicopter*, Lockheed Report LR 26523 (Prepared under Contract No. DAAJ01-73-C-0286, Modification P00005). 1974.(636)
8. Harris, F. D., *Performance Analysis of Two Early NACA High Speed Propellers With Application to Civil Tiltrotor Configurations*, NASA Contractor Report 196702. 1996.(416)
9. Harris, F. D, *An Overview of Autogyros and The McDonnell XV-1 Convertiplane*, NASA/CR-2003-212799. 2003.(604)
10. Harris, F. D. *Rotary Wing Aerodynamics-Historical Perspective and Important Issues*. in National Specialist's Meeting on Aerodynamic and Aeroacoustics Sponsored by the American Helicopter Society Southwest Region.1987.(101)
11. McCloud III, John L. and Biggers, James C., *An Investigation of Full-Scale Helicopter Rotors at High Advance Ratios and Advancing Tip Mach Numbers*, NASA Technical Note D-4632. 1968.(605)
12. de la Cierva, J., *Engineering Theory of the Autogiro, (Original Notes)*, ed. D.J.A.J. Bennett. 1929.(11)
13. de la Cierva, J., ed. *Theory of Stresses on Autogiro Rotor Blades (Original Notes)*. ed. D.J.A.J. Bennett. 1934.(12)
14. Glauert, H., *The Theory of the Autogyro*. Journal of the Royal Aeronautical Society. 1927.(125)
15. Glauert, H., *The Analysis of Experimental Results in the Windmill Brake and Vortex Ring States of an Airscrew*, Aeronautical Research Committee R & M No. 1026. February 1926.(116)
16. Glauert, H., *A General Theory of the Autogiro*, Aeronautical Research Committee R & M No. 1111. November 1926.(13)

17. Lock, C.N.H., *Photographs of Streamers Illustrating the Flow Around an Airscrew in the "Vortex Ring State"*, Aeronautical Research Committee R & M No. 1167. 1928.(123)
18. Lock, C.N.H. and Townend, H. C. H., *Wind Tunnel Experiments on a Model Autogyro at Small Angles of Incidence*, Aeronautical Research Committee R & M No. 1154. 1928.(126)
19. Lock, C.N.H., *Note on the Characteristic Curve for an Airscrew or Helicopter*, Aeronautical Research Council R & M No. 2673. 1947.(120)
20. Lock, C.N.H., Bateman, H., and Townend, H. C. H., *An Extension of the Vortex Theory of Airscrews with Applications to Airscrews of Small Pitch, Including Experimental Results*, Aeronautical Research Committee R & M No. 1014. June 1926.(114)
21. Lock, C.N.H., *Further Developments of Autogiro Theory*, Aeronautical Research Committee R & M No. 1127. March 1927.(14)
22. Lock, C.N.H. and Townend, H. C. H., *Photographs of the Flow Round a Model Screw Working in Water, Especially in the "Vortex Ring State"*, Aeronautical Research Committee R & M No. 1043. May 1926.(117)
23. Lock, C.N.H. and Townend, H. C. H., *Wind Tunnel Experiments on a Symmetrical Aerofoil (Gottingen 429 Section)*, Aeronautical Research Committee R & M No. 1066. November 1926.(115)
24. Lock, C.N.H. and Bateman, H., *Some Experiments on Airscrews at Zero Torque, with Applications to a Helicopter Descending with Engine "Off," and to the Design of Windmills*, Aeronautical Research Committee R & M No. 885. September 1923.(113)
25. Beavan, J. A. and Lock, C.N.H., *The Effect of Blade Twist on the Characteristics of the C.30 Autogiro*, Aeronautical Research Committee, Reports and Memoranda No. 1727. April 1936.(51)
26. Wheatley, J. B., *Lift and Drag Characteristics and Gliding Performance of an Autogiro as Determined in Flight*, N.A.C.A. Technical Report No. 434. 1932.(121)
27. Wheatley, J. B., *Wind-Tunnel Tests of a 10-foot Diameter Gyroplane Rotor*, NACA Technical Report No. 536. 1934.(67)
28. Wheatley, J. B., *An Aerodynamic Analysis of the Autogiro Rotor with a Comparison Between Calculated and Experimental Results*, NACA Technical Report 487. 1934.(69)
29. Wheatley, J. B., *An Analytical and Experimental Study of the Effect of Periodic Blade Twist on the Thrust, Torque, and Flapping Motion of an Autogiro Rotor*, NACA Technical Report No. 591. 1937.(52)
30. Wheatley, J. B., *An Analysis of the Factors That Determine the Periodic Twist of an Autogiro Rotor Blade, With a Comparison of Predicted and Measured Results*, NACA Technical Report No. 600. 1937.(53)
31. Wheatley, J. B., *The Influence of Wing Setting on the Wing Load and Rotor Speed of a PCA-2 Autogiro as Determined in Flight*, NACA Technical Report No.523. December 1934.(133)

32. Wheatley, J. B., *Control-Force Measurements in Flight of the Pitcairn YG-2 Autogiro*, NACA Confidential Memorandum Report for Army Air Corps (Langley Library under 1605.4, Pitcairn YG-2/1). February 1936.(56)
33. Wheatley, J. B., *Wing Pressure Distribution and Rotor-Blade Motion of an Autogiro as Determined in Flight*, NACA Technical Report No. 475. July 1933.(132)
34. Wheatley, J. B., *The Aerodynamic Analysis of the Gyroplane Rotating-Wing System*, NACA Technical Note No. 492. March 1934.(66)
35. Wheatley, J. B. and Hood, M. J., *Full Scale Wind Tunnel Tests of a PCA-2 Autogiro Rotor*, NACA Technical Report No. 515. October 1934.(134)
36. Wheatley, J. B. and Carlton, B., *Analysis and Model Tests of Autogiro Jump Take-off*, NACA Technical Note No. 582. October 1936.(76)
37. Bailey, F. J. Jr., *A Study of the Torque Equilibrium of an Autogiro Rotor*, N.A.C.A Report No. 623. 1938.(600)
38. Bailey, F. J. Jr. and Gustafson, F. B., *Observations in Flight of the Region of Stalled Flow over the Blades of an Autogiro Rotor*, N.A.C.A. Technical Note 741. 1939.(602)
39. Bailey, F. J. Jr., *A Simplified Theoretical Method of Determining the Characteristics of a Lifting Rotor in Forward Flight*, N.A.C.A. Report No. 716. 1941.(601)
40. Bailey, F. J. Jr. and Gustafson, F. B., *Charts for Estimation of the Characteristics of a Helicopter Rotor in Forward Flight*, N.A.C.A. ACR L4H07. 1944.(603)
41. Bailey, F. J. Jr., *Flight Investigation of Control-Stick Vibration of the YG-1B Autogiro*, N.A.C.A. Technical Note No. 764. June 1940.(57)
42. Charles, Bruce D. and Tanner, Watson H., *Wind Tunnel Investigation of Semi-rigid Full-Scale Rotors Operating at High Advance Ratios*, USAAVLABS Technical Report 69-2. 1969.(606)
43. Harris, F. D, Tarzanin, F.J. and Fisher, R.K., *Rotor High Speed Performance*. Journal of the American Helicopter Society. Vol. 15 (No. 3). 1970.(609)
44. Kerr, A.W., Potthast, A.J. and Anderson, W.D. *An Interdisciplinary Approach to Integrated Rotor/Body Mathematical Modeling*. in AHS Symposium on the Status of Testing and Modeling for V/STOL Aircraft.1972.(627)
45. Carlson, R. M. and Kerr, A.W., *Integrated Rotor/Body Loads Prediction*, AGARD CP-122. 1973.(628)
46. Lockheed, California Co., *REXOR Rotorcraft Simulation Model, Volume I - Engineering Documentation*, USAAMRDL-TR-76-28A. 1976.(629)
47. Lockheed, California Co., *REXOR Rotorcraft Simulation Model, Volume II - Computer Implementation*, USAAMRDL-TR-76-28B. 1976.(630)
48. Lockheed, California Co., *REXOR Rotorcraft Simulation Model, Volume III- User's Manual*, USAAMRDL-TR-76-28C. 1976.(631)
49. Blankenship, B.L. and Harvey, K.W., *A Digital Analysis for Helicopter Performance and Rotor Blade Bending Moments*. Journal of the American Helicopter Society. Volume 7 (No. 4). 1962.(610)
50. Corrigan, J.J., Bennett, R.L. and Hsieh, P.Y. *COPTER 2000: The QTR and Beyond*. in American Helicopter Society 57th Annual Forum.2001.(611)

51. Johnson, W., *Development of a Comprehensive Analysis for Rotorcraft*. Vertica. Volume 5 (Number 2 for Part I and Number 3 for Part II). 1981.(617)
52. Johnson, W., *A Comprehensive Analytical Model of Rotorcraft Aerodynamics and Dynamics*, NASA TM 81182, TM 81184, TM 81184. 1980.(616)
53. Johnson, Wayne. *Rotorcraft Aeromechanics Applications of a Comprehensive Analysis*. in Heli Japan 98: AHS International Rotorcraft Technology and Disaster Relief.1998. Nagarafukumitsu, Gifu, Japan.(608)
54. Saberi, H., Khoshlahjeh, M., Rutkowski, M.J. and Ormiston, R.A. *Overview of RCAS and Application to Advance Rotorcraft Problems*. in American Helicopter 4th Decennial Specialist's Conference on Aeromechanics.2004. San Francisco, California.(612)
55. Quackenbush, T.R., Bliss, D.B., Wachspress, D.A. and Ong, C.C., *Free Wake Analysis of Hover Performance Using a New Influence Coefficient Method*, NASA Contractor Report 4309. 1990.(624)
56. Wachspress, D. A., Quackenbush, T. R. and Boschitsch, A.H. *First-Principles Free-Vortex Wake Analysis for Helicopters and Tiltrotors*. in American Helicopter Society 59th Annual Forum, May 6-8.2003. Phoenix, Arizona.(613)
57. Anderson, J.D., *A History of Aerodynamics*, Cambridge, United Kingdom: Cambridge University Press. 1997.(137)
58. Strawn, R.C., Caradonna, F.X. and Duque, E.P.N., *30 Years of Rotorcraft Computational Fluid Dynamics Research and Development*. Journal of the American Helicopter Society. Volume 52 (Number 3). 2006.(621)
59. Blasius, H., *The Boundary Layers in Fluids with Little Friction*, NACA Technical Memorandum 1256. 1950.(619)
60. Tung, C., Caradonna, F. X. and Johnson, W., *The prediction of Transonic Flows on an Advancing Rotor*. Journal of the American Helicopter Society. Volume 31 (Number 3). 1986.(620)
61. Potsdam, M.P., Yeo, H. and Johnson, W. *Rotor Airloads Prediction Using Loose Aerodynamic/Structural Coupling*. in American Helicopter Society 60th Annual Forum, Paper Number XXXX.2004.(622)
62. Datta, A., Sitaraman, J., Baeder, J.D. and Chopra, I. *Analysis Refinements for Prediction of Rotor Vibratory Loads in High-Speed Forward Flight*. in American Helicopter Society 60th Annual Forum, Paper Number XXXX.2004.(623)
63. Jenkins Jr., J.L., *Wind-Tunnel Investigation of a Lifting Rotor Operating at Tip-Speed Ratios from 0.65 to 1.45*, NASA TN D-2628. 1965.(607)
64. Scheiman, J., *A Tabulation of Helicopter Rotor-Blade Differential Pressures, Stresses, and Motions as Measured in Flight*, NASA TM X-952. 1964.(614)
65. Meakin, R.L. and Wissink, A.M. *Unsteady Aerodynamics Simulation of Static and Moving Bodies Using Scalable Computers*. in 14th AIAA CFD Conference, AIAA Paper 99-3302-CP.1999.(625)
66. Strawn, R.C. and Djomehri, M.J., *Computational Modeling of Hovering Rotor and Wake Aerodynamics*. AIAA Journal of Aircraft. Volume 39 (No. 5). 2002.(626)
67. McCroskey, W.J., *A Critical Assessment of Wind Tunnel Results for the NACA 0012 Airfoil*, NASA Technical Memorandum 100019. 1987.(638)

68. Bousman, W.G., *Aerodynamic Characteristics of SC1095 and SC1094R8 Airfoils*, NASA/TP-2003-212265. 2003.(639)
69. Lee, B.L. *Experimental Measurements of the Rotating Frequencies and Mode Shapes of a Full Scale Helicopter Rotor in a Vacuum and Correlations with Calculated Results*. in AHS 35th Annual National Forum, Preprint No. 79-18.1979.(637)

Page intentionally blank

11 APPENDICES

11.1 Minimum Profile Power, H and Y Forces, Torque and Thrust Coefficients

The airfoil at any given blade element of a rotor blade has a minimum drag coefficient (C_{do}). At the very least, this airfoil drag coefficient must equate to a skin friction drag. However, there is also some form (i.e., pressure) drag. This blade element drag is classically resolved in a specified direction, summed over the rotor blade's span and then averaged over a blade revolution to give a force at the hub. Based on this integration using a value of C_{do} that is constant over the whole rotor disc, minimum values of profile power coefficient (CP_o), H-force coefficient (CH_o), Y-force coefficient (CY_o), torque coefficient (CQ_o) and thrust coefficient (CT_o) can be defined and calculated. The fundamental relationship that connects four of these coefficients is

$$P_o = \Omega Q_o + (V \cos \alpha) H_o + (V \sin \alpha) T_o$$

In rotor coefficient notation (i.e., divide through by $\rho A V_t^3$) you have

$$CP_o = CQ_o + \mu CH_o + \lambda CT_o$$

where advance ratio (μ) is defined as $\frac{V}{V_t} \cos \alpha$ and inflow ratio (λ) is taken as $\frac{V}{V_t} \sin \alpha$.

Airspeed (V) is the reference forward flight speed and the rotor tip speed is ($V_t = \Omega R$). The angle of attack (α_s) is frequently referenced to the rotor shaft, which is perhaps more correctly the angle between the plane perpendicular to the shaft and the airspeed.

The following paragraphs summarize the classical theory for the five coefficients.

Part 1. Profile Power. As you know, Cierva and then Glauert (R&M 1111) were the first to state that (in my notation)

$$CP_o = \frac{\sigma C_{do}}{8} P_{(\mu, \lambda)}$$

$$(1) \quad \text{where } P_{(\mu, \lambda)} = \frac{1}{2\pi} \int_0^{2\pi} \int_0^1 4 \left[(x + \mu \sin \psi)^2 + (\mu \cos \psi)^2 + \lambda^2 \right]^{3/2} dx d\psi$$

$$= \frac{1}{2\pi} \int_0^{2\pi} \int_0^1 4 \left[x^2 + 2x\mu \sin \psi + \mu^2 + \lambda^2 \right]^{3/2} dx d\psi$$

The assumptions associated with this fundamental problem are (1) the blades are constant chord, untwisted and have no root cutout, and (2) the blade element drag coefficient is constant over the disc.

I found it convenient to let $JJ = \mu^2 + \lambda^2$ in several of the equations that follow.

The integration falls in the elliptic integral world, but less exact and simpler approximations are available. Using MathCad, I found that integrating with respect to radius first (which is exact) and then approximating the azimuthal averaging gives

$$(2) \quad P_{(\mu,\lambda)} = \sqrt{1+JJ} \left[1 + \frac{5}{2}JJ + \frac{3}{8}\mu^2 \frac{4+7JJ+4JJ^2}{(1+JJ)^2} - \frac{9}{16} \frac{\mu^4}{(1+JJ)} \right] \\ + \left(\frac{3}{2}\lambda^4 + \frac{3}{2}\lambda^2\mu^2 + \frac{9}{16}\mu^4 \right) \ln \left(\frac{1+\sqrt{1+JJ}}{\sqrt{JJ}} \right)$$

In the special case where $\lambda = 0$ and $\mu < 0.4$, this lengthy expression reduces to

$$(3) \quad P_{(\mu<0.4,\lambda=0)} = 1 + \frac{9}{2}\mu^2 + \frac{3}{16}\mu^4 \left[5 + 3 \ln \left(\frac{2}{\mu} \right) \right] + \frac{35}{64}\mu^6$$

In the special case where $\mu = 0$, which is the propeller case, the exact solution is

$$(4) \quad P_{(\mu=0,\lambda)} = \left(1 + \frac{5}{2}\lambda^2 \right) \sqrt{1+\lambda^2} + \frac{3}{2}\lambda^4 \ln \left[\frac{1+\sqrt{1+\lambda^2}}{\lambda} \right]$$

In the propeller case, the exact solution has, for $\lambda < 1.0$, the approximation of

$$(5) \quad P_{(\mu=0,\lambda<1)} = 1 + 3\lambda^2 + \frac{3}{8}\lambda^4 \left[3 + 4 \ln \left(\frac{2}{\lambda} \right) \right] + \frac{1}{8}\lambda^6 - \frac{3}{128}\lambda^8$$

Part 2. H-Force. In the general rotor case, there is an H-force acting perpendicular to the shaft and in the downwind direction. This force in rotor notation is

$$CHo = \frac{\sigma C_{do}}{8} H_{(\mu,\lambda)}$$

$$(6) \quad \text{where } H_{(\mu,\lambda)} = \frac{1}{2\pi} \int_0^{2\pi} \int_0^1 4 \left[x^2 + 2x\mu \sin \psi + \mu^2 + \lambda^2 \right] \sin(\psi + \Lambda) dx d\psi \\ = \frac{1}{2\pi} \int_0^{2\pi} \int_0^1 4 \left[x^2 + 2x\mu \sin \psi + \mu^2 + \lambda^2 \right] (\sin \psi \cos \Lambda + \cos \psi \sin \Lambda) dx d\psi$$

Now the sine and cosine of the sweep angle (Λ) are simply

$$(7) \quad \sin \Lambda = \frac{\mu \cos \psi}{\sqrt{x^2 + 2x\mu \sin \psi + \mu^2 + \lambda^2}} \quad \cos \Lambda = \frac{x + \mu \sin \psi}{\sqrt{x^2 + 2x\mu \sin \psi + \mu^2 + \lambda^2}}$$

so that

$$(8) \quad H_{(\mu,\lambda)} = \frac{1}{2\pi} \int_0^{2\pi} \int_0^1 4 \left[x^2 + 2x\mu \sin \psi + \mu^2 + \lambda^2 \right]^{1/2} [x \sin \psi + \mu] dx d\psi$$

and the approximation to the H-force integral is

$$(9) \quad H_{(\mu,\lambda)} = \sqrt{1+JJ} \left[3\mu + \frac{1}{4}\mu^3 \frac{JJ-1}{(1+JJ)^2} \right] + \left(\mu\lambda^2 + \frac{3}{4}\mu^3 \right) \ln \left(\frac{1+\sqrt{1+JJ}}{\sqrt{JJ}} \right)$$

In the special case where $\lambda = 0$ and $\mu < 0.4$, this lengthy expression reduces to

$$(10) \quad H_{(\mu<0.4,\lambda=0)} = 3\mu + \frac{1}{4}\mu^3 \left[5 + 3 \ln \left(\frac{2}{\mu} \right) \right] + \frac{7}{16}\mu^5$$

In the special case where $\mu = 0$, which is the propeller case, the exact solution is

$$(11) \quad H_{(\mu=0,\lambda)} = 0$$

Another interesting case occurs when $\lambda = 0$ and μ approaches infinity. In this case, the rotor approaches a stopped rotor. The H-force in this case is the drag of non-rotating blades. The way to express this drag is to write

$$(12) \quad D = H = \rho(\pi R^2) V_t^2 \frac{\sigma C_{do}}{8} H_{(\mu \rightarrow \infty, \lambda=0)}$$

or in equivalent parasite drag (f_e) form

$$(13) \quad \begin{aligned} \frac{D}{q} = \frac{H}{q} &= \frac{\rho(\pi R^2) V_t^2}{\frac{1}{2}\rho V^2} \left(\frac{bcR}{\pi R^2} \right) \frac{C_{do}}{8} H_{(\mu \rightarrow \infty, \lambda=0)} \\ &= (bcR) C_{do} \frac{H_{(\mu \rightarrow \infty, \lambda=0)}}{4\mu^2} = (bcR) C_{do} \left(1 + \frac{1}{4\mu^2} \right) \end{aligned}$$

Keep in mind that some sort of propulsive device must be used to drag the edgewise rotor through the air. This 100 % efficient device requires power equal to VD.

Part 3. Y-Force. In the general rotor case, there is a Y-force acting perpendicular to the shaft and perpendicular to the free stream velocity. The Y-force is positive towards the right wing tip when the rotor rotation is counter clockwise as viewed from above. This force in rotor notation is

$$(14) \quad \begin{aligned} CY_o &= \frac{\sigma C_{do}}{8} Y_{(\mu,\lambda)} \\ \text{where } Y_{(\mu,\lambda)} &= \frac{1}{2\pi} \int_0^{2\pi} \int_0^1 4 \left[x^2 + 2x\mu \sin \psi + \mu^2 + \lambda^2 \right] \cos(\psi + \Lambda) dx d\psi \\ &= \frac{1}{2\pi} \int_0^{2\pi} \int_0^1 4 \left[x^2 + 2x\mu \sin \psi + \mu^2 + \lambda^2 \right] [\cos \psi \cos \Lambda - \sin \psi \sin \Lambda] dx d\psi \end{aligned}$$

Substituting the sine and cosine of the sweep angle (Λ) relationships from Equation (7) yields

$$(15) \quad Y_{(\mu,\lambda)} = \frac{1}{2\pi} \int_0^{2\pi} \int_0^1 4 \left[x^2 + 2x\mu \sin \psi + \mu^2 + \lambda^2 \right]^{1/2} [x \cos \psi] dx d\psi$$

from which it follows that for all advance ratios and all inflow ratios,

$$(16) \quad Y_{(\mu,\lambda)} \equiv 0$$

Part 4. Torque. In the general rotor case, a torque must be applied to the shaft to maintain rotor speed. This torque might be obtained from an engine if the rotor is not in autorotation. The required torque in rotor notation is

$$(17) \quad CQ_0 = \frac{\sigma C_{do}}{8} Q_{(\mu,\lambda)}$$

where $Q_{(\mu,\lambda)} = \frac{1}{2\pi} \int_0^{2\pi} \int_0^1 4 \left[x^2 + 2x\mu \sin \psi + \mu^2 + \lambda^2 \right]^{1/2} (x + \mu \sin \psi) x dx d\psi$

and the approximation to the torque integral is

$$(18) \quad Q_{(\mu,\lambda)} = \sqrt{1+JJ} \left[1 + \frac{1}{2} JJ + \frac{1}{8} \mu^2 \frac{4+JJ-4JJ^2}{(1+JJ)^2} + \frac{3}{16} \frac{\mu^4}{(1+JJ)} \right] - \left(\frac{1}{2} \lambda^4 + \frac{1}{2} \lambda^2 \mu^2 + \frac{3}{16} \mu^4 \right) \ln \left(\frac{1+\sqrt{1+JJ}}{\sqrt{JJ}} \right)$$

In the special case where $\lambda = 0$ and $\mu < 0.4$, this lengthy expression reduces to

$$(19) \quad Q_{(\mu<0.4,\lambda=0)} = 1 + \frac{3}{2} \mu^2 - \frac{1}{16} \mu^4 \left[5 + 3 \ln \left(\frac{2}{\mu} \right) \right] + \frac{7}{64} \mu^6$$

In the special case where $\mu = 0$, which is the propeller, the exact solution is

$$(20) \quad Q_{(\mu=0,\lambda)} = \frac{1}{2} (2 + \lambda^2) \sqrt{1 + \lambda^2} - \frac{1}{2} \lambda^4 \ln \left(\frac{1 + \sqrt{1 + \lambda^2}}{\lambda} \right)$$

In the special helicopter rotor case where $\lambda = 0$ and advance ratio approaches infinity

$$(21) \quad Q_{(\mu \rightarrow \infty, \lambda=0)} \rightarrow 2\mu$$

Note that CQ_0 goes to infinity, but, in fact, the actual torque goes to zero for the stopped rotor or propeller. You can see this by writing

$$(22) \quad Q = \rho (\pi R^2) V_t^2 R \left(\frac{\sigma C_{do}}{8} \right) (2\mu) = \rho (bcR) RC_{do} \left(\frac{VV_t}{4} \right)$$

This last result applies equally well to a feathered propeller because as the tip speed goes to zero, the torque goes to zero.

Part 5. Thrust. In the general rotor case, when there is an inflow (i.e., λ is not zero), there is a component of minimum blade element drag in the shaft axial direction. This force is a thrust and is given by

$$(23) \quad C_{To} = \frac{\sigma C_{do}}{8} T_{(\mu, \lambda)} \quad \text{where} \quad T_{(\mu, \lambda)} = \frac{\lambda}{2\pi} \int_0^{2\pi} \int_0^1 4 \left[x^2 + 2x\mu \sin \psi + \mu^2 + \lambda^2 \right]^{1/2} dx d\psi$$

and the approximation to the thrust integral is

$$(24) \quad T_{(\mu, \lambda)} = \lambda \sqrt{1 + JJ} \left[2 + \frac{1}{2} \mu^2 \frac{1 + 2JJ}{(1 + JJ)^2} \right] + \lambda (2\lambda^2 + \mu^2) \ln \left(\frac{1 + \sqrt{1 + JJ}}{\sqrt{JJ}} \right)$$

Obviously, if inflow is zero then C_{To} is zero. But, in the special case when $\mu = 0$, which corresponds to a propeller, then

$$(25) \quad T_{(\mu=0, \lambda)} = 2\lambda \sqrt{1 + \lambda^2} + 2\lambda^3 \ln \left(\frac{1 + \sqrt{1 + \lambda^2}}{\lambda} \right)$$

and the series expansion, for $\lambda < 1.0$ is

$$(26) \quad T_{(\mu=0, \lambda < 1)} = 2\lambda + \lambda^3 \left[1 + 2 \ln \left(\frac{2}{\lambda} \right) \right] + \frac{1}{4} \lambda^5 - \frac{1}{16} \lambda^7 + \frac{5}{192} \lambda^9$$

The additionally interesting case when inflow approaches infinity shows that the drag of the feathered propeller is, in equivalent parasite drag form

$$(27) \quad \frac{D}{q} = \frac{T}{q} = \frac{\rho (\pi R^2) V_t^2}{\frac{1}{2} \rho V^2} \left(\frac{bcR}{\pi R^2} \right) \frac{C_{do}}{8} T_{(\mu=0, \lambda \rightarrow \infty)} = (bcR) C_{do} \left(1 + \frac{1}{6\lambda^2} \right)$$

Part 5. A Proof. The preceding results are connected by the fundamental, total energy per unit time equation, which is

$$(28) \quad P_o = \Omega Q_o + (V \cos \alpha) H_o + (V \sin \alpha) T_o$$

which in rotor coefficient notation (i.e., after dividing through by $\rho A V_t^3$) is

$$(29) \quad C_{P_o} = C_{Q_o} + \mu C_{H_o} + \lambda C_{T_o}$$

A simple “proof” of the above relationship can be seen by using the series expansion from the preceding paragraphs. Thus, when $\lambda = 0$ and $\mu < 0.4$,

$$(30) \quad \begin{aligned} C_{P_o} &= C_{Q_o} + \mu C_{H_o} = \frac{\sigma C_{do}}{8} Q_{(\mu, \lambda=0)} + \frac{\sigma C_{do}}{8} \mu H_{(\mu, \lambda=0)} \\ &= \frac{\sigma C_{do}}{8} \left\{ 1 + \frac{3}{2} \mu^2 - \frac{1}{16} \mu^4 \left[5 + 3 \ln \left(\frac{2}{\mu} \right) \right] + \frac{7}{64} \mu^6 \right\} + \frac{\sigma C_{do}}{8} \left\{ \mu \left[3\mu + \frac{1}{4} \mu^3 \left[5 + 3 \ln \left(\frac{2}{\mu} \right) \right] + \frac{7}{16} \mu^5 \right] \right\} \\ &= \frac{\sigma C_{do}}{8} \left\{ 1 + \left(\frac{3}{2} + 3 \right) \mu^2 + \left(-\frac{1}{16} + \frac{1}{4} \right) \mu^4 \left[5 + 3 \ln \left(\frac{2}{\mu} \right) \right] + \left(\frac{7}{64} + \frac{7}{16} \right) \mu^6 \right\} \\ &= \frac{\sigma C_{do}}{8} \left\{ 1 + \frac{9}{2} \mu^2 + \frac{3}{16} \mu^4 \left[5 + 3 \ln \left(\frac{2}{\mu} \right) \right] + \frac{35}{64} \mu^6 \right\} \end{aligned}$$

and you can see by inspection that Eq. (3) has been reproduced. This result supports the frequently used variation on Glauert's work, which is

$$(31) \quad CP_o \approx \frac{\sigma C_{do}}{8} \left\{ 1 + \frac{9}{2} \mu^2 \right\}$$

The same exercise for the propeller case (i.e., $\mu = 0$) will show that Eq. (5) is obtained.

Part 6. Azimuth Integrals. For the sake of completeness, the azimuthal averaging approximations I used were

$$(32) \quad I0 = \frac{1}{2\pi} \int_0^{2\pi} \sqrt{1 + 2\mu \sin \psi + JJ} \, d\psi \approx \sqrt{1 + JJ} - \frac{1}{2} \mu^2 \left[\frac{1}{2(1 + JJ)^{3/2}} \right]$$

$$(33) \quad I1 = \frac{1}{2\pi} \int_0^{2\pi} \sin \psi \sqrt{1 + 2\mu \sin \psi + JJ} \, d\psi \approx \frac{1}{2} \mu \left[\frac{1}{\sqrt{1 + JJ}} \right]$$

$$(34) \quad I2 = \frac{1}{2\pi} \int_0^{2\pi} (\sin \psi)^2 \sqrt{1 + 2\mu \sin \psi + JJ} \, d\psi \approx \frac{1}{2} \sqrt{1 + JJ}$$

$$(35) \quad I3 = \frac{1}{2\pi} \int_0^{2\pi} (\sin \psi)^3 \sqrt{1 + 2\mu \sin \psi + JJ} \, d\psi \approx \frac{3}{8} \mu \left[\frac{1}{\sqrt{1 + JJ}} \right]$$

$$(36) \quad I4 = \frac{1}{2\pi} \int_0^{2\pi} (\sin \psi)^4 \sqrt{1 + 2\mu \sin \psi + JJ} \, d\psi \approx \frac{3}{8} \sqrt{1 + JJ}$$

$$(37) \quad L0 = \frac{1}{2\pi} \int_0^{2\pi} \ln \left(\frac{\sqrt{1 + 2\mu \sin \psi + JJ} + 1 + \mu \sin \psi}{\sqrt{JJ} + \mu \sin \psi} \right) d\psi \approx \ln \left(\frac{\sqrt{1 + JJ} + 1}{\sqrt{JJ}} \right)$$

$$(38) \quad L2 = \frac{1}{2\pi} \int_0^{2\pi} (\sin \psi)^2 \ln \left(\frac{\sqrt{1 + 2\mu \sin \psi + JJ} + 1 + \mu \sin \psi}{\sqrt{JJ} + \mu \sin \psi} \right) d\psi \approx \frac{1}{2} \ln \left(\frac{\sqrt{1 + JJ} + 1}{\sqrt{JJ}} \right)$$

$$(39) \quad L4 = \frac{1}{2\pi} \int_0^{2\pi} (\sin \psi)^4 \ln \left(\frac{\sqrt{1 + 2\mu \sin \psi + JJ} + 1 + \mu \sin \psi}{\sqrt{JJ} + \mu \sin \psi} \right) d\psi \approx \frac{3}{8} \ln \left(\frac{\sqrt{1 + JJ} + 1}{\sqrt{JJ}} \right)$$

The use of these approximations leads to numerical results that are, at most, 1.1 % in error with the MathCad numerical integrations. The greatest error is when $\mu = \lambda = 1.0$.

References

1. Glauert, H., *A General Theory of the Autogiro*, Aeronautical Research Committee R & M No. 1111. November 1926.
2. Harris, F. D., *Preliminary Study of Radial Flow Effects on Rotor Blades*. Journal of the American Helicopter Society. Vol. 11 (No. 3). July 1966.

3. Harris, F. D., *Spanwise Flow Effects on Rotor Blade*. CAL/USAAVLABS Symposium Proceedings, Vol. III, pages 10 and 11. Buffalo, New York, June 22-24, 1966
4. Harris MathCad file: Minimum H_o , Q_o , and P_o and Y_o .MCD

11.2 Wheatley/ Bailey Equations with Sample Case

Advance Ratio Equal To or Less Than 1.0 with zero root cutout

Rotor Equations Including Cyclic, Lamda 1 and Elastic Twist

Ref. (1) MathCad Software: Final Derive Wheatley & Bailey With Cyclic, Lamda 1 & Elastic Twist. mcd

(2) MathCad Software: Final Blade Element Program 2008. mcd

(3) Final Program In EXCEL.xls

Definitions

$$\theta := \theta_0 + x \cdot \theta_t - B1c \cdot \sin(\psi) - A1c \cdot \cos(\psi) + x \cdot \theta e1s \cdot \sin(\psi) + x \cdot \theta e1c \cdot \cos(\psi)$$

$$\beta := \beta_0 - a1s \cdot \cos(\psi) - b1s \cdot \sin(\psi) - a2s \cdot \cos(2 \cdot \psi) - b2s \cdot \sin(2 \cdot \psi)$$

$$UT := x + \mu \cdot \sin(\psi)$$

$$UP := \lambda s + \lambda 1 \cdot x \cdot \cos(\psi) - x \cdot d\beta d\psi - \mu \cdot \beta \cdot \cos(\psi)$$

$$CT := \frac{\sigma \cdot a}{2} \cdot \frac{1}{2 \cdot \pi} \cdot \int_0^{2 \cdot \pi} \int_0^B UT^2 \cdot \left(\theta + \frac{UP}{UT} \right) dx d\psi - \frac{\sigma \cdot a}{2} \cdot \frac{2}{2 \cdot \pi} \cdot \int_{\pi}^{2 \cdot \pi} \int_0^{-\mu \cdot \sin(\psi)} UT^2 \cdot \left(\theta + \frac{UP}{UT} \right) dx d\psi$$

$$CQa := \frac{\sigma \cdot a}{2} \cdot \left[-1 \cdot \frac{1}{2 \cdot \pi} \cdot \int_0^{\pi} \int_0^B \left[UT^2 \cdot \left(\theta + \frac{UP}{UT} \right) \cdot \frac{UP}{UT} \right] \cdot x dx d\psi - \frac{1}{2 \cdot \pi} \cdot \int_{\pi}^{2 \cdot \pi} \int_{-\mu \cdot \sin(\psi)}^B \left[UT^2 \cdot \left(\theta + \frac{UP}{UT} \right) \cdot \frac{UP}{UT} \right] \cdot x dx d\psi \dots \right. \\ \left. + \frac{1}{2 \cdot \pi} \cdot \int_{\pi}^{2 \cdot \pi} \int_0^{-\mu \cdot \sin(\psi)} \left[UT^2 \cdot \left(\theta + \frac{UP}{UT} \right) \cdot \frac{UP}{UT} \right] dx d\psi \right]$$

$$CQd := \frac{\sigma \cdot Cdo}{2} \cdot \left(\frac{1}{2 \cdot \pi} \cdot \int_0^{2 \cdot \pi} \int_0^1 UT^2 \cdot x dx d\psi - \frac{2}{2 \cdot \pi} \cdot \int_{\pi}^{2 \cdot \pi} \int_0^{-\mu \cdot \sin(\psi)} UT^2 \cdot x dx d\psi \right) \dots \\ + \frac{\sigma \cdot \delta 1}{2} \cdot \frac{1}{2 \cdot \pi} \cdot \left[\int_0^{2 \cdot \pi} \int_0^1 UT^2 \cdot \left(\theta + \frac{UP}{UT} \right) \cdot x dx d\psi \right] \dots \\ + \frac{\sigma \cdot \delta 2}{2} \cdot \left[\frac{1}{2 \cdot \pi} \cdot \int_0^{2 \cdot \pi} \int_0^1 UT^2 \cdot \left(\theta + \frac{UP}{UT} \right)^2 \cdot x dx d\psi - \frac{2}{2 \cdot \pi} \cdot \int_{\pi}^{2 \cdot \pi} \int_0^{-\mu \cdot \sin(\psi)} UT^2 \cdot \left(\theta + \frac{UP}{UT} \right)^2 \cdot x dx d\psi \right]$$

$$CHa := \frac{\sigma \cdot a}{2} \cdot \left[-1 \cdot \frac{1}{2 \cdot \pi} \cdot \int_0^\pi \int_0^B \left[UT^2 \cdot \left(\theta + \frac{UP}{UT} \right) \right] \cdot \left(\beta \cdot \cos(\psi) + \frac{UP}{UT} \cdot \sin(\psi) \right) dx d\psi \dots \right. \\
+ 0 - \frac{1}{2 \cdot \pi} \cdot \int_\pi^{2 \cdot \pi} \int_{-\mu \cdot \sin(\psi)}^B \left[UT^2 \cdot \left(\theta + \frac{UP}{UT} \right) \right] \cdot \left(\beta \cdot \cos(\psi) + \frac{UP}{UT} \cdot \sin(\psi) \right) dx d\psi \dots \\
\left. + \frac{1}{2 \cdot \pi} \cdot \left[\int_\pi^{2 \cdot \pi} \int_0^{-\mu \cdot \sin(\psi)} \left[UT^2 \cdot \left(\theta + \frac{UP}{UT} \right) \right] \cdot \left(\beta \cdot \cos(\psi) + \frac{UP}{UT} \cdot \sin(\psi) \right) dx d\psi \right] \right]$$

$$CHd := \frac{\sigma \cdot Cdo}{2} \cdot \left(\frac{1}{2 \cdot \pi} \cdot \int_0^{2 \cdot \pi} \int_0^1 UT^2 \cdot \sin(\psi) dx d\psi - \frac{2}{2 \cdot \pi} \cdot \int_\pi^{2 \cdot \pi} \int_0^{-\mu \cdot \sin(\psi)} UT^2 \cdot \sin(\psi) dx d\psi \right) \dots \\
+ \frac{\sigma \cdot \delta 1}{2} \cdot \frac{1}{2 \cdot \pi} \cdot \left[\int_0^{2 \cdot \pi} \int_0^1 UT^2 \cdot \left(\theta + \frac{UP}{UT} \right) \cdot \sin(\psi) dx d\psi \right] \dots \\
+ \frac{\sigma \cdot \delta 2}{2} \cdot \left[\frac{1}{2 \cdot \pi} \cdot \int_0^{2 \cdot \pi} \int_0^1 UT^2 \cdot \left(\theta + \frac{UP}{UT} \right)^2 \cdot \sin(\psi) dx d\psi \dots \right. \\
\left. + 0 - \frac{2}{2 \cdot \pi} \cdot \left[\int_\pi^{2 \cdot \pi} \int_0^{-\mu \cdot \sin(\psi)} UT^2 \cdot \left(\theta + \frac{UP}{UT} \right)^2 \cdot \sin(\psi) dx d\psi \right] \right]$$

$$CYa := \frac{\sigma \cdot a}{2} \cdot \left[-1 \cdot \frac{1}{2 \cdot \pi} \cdot \int_0^\pi \int_0^B \left[UT^2 \cdot \left(\theta + \frac{UP}{UT} \right) \right] \cdot \left(\beta \cdot \sin(\psi) - \frac{UP}{UT} \cdot \cos(\psi) \right) dx d\psi \dots \right. \\
+ 0 - \frac{1}{2 \cdot \pi} \cdot \int_\pi^{2 \cdot \pi} \int_{-\mu \cdot \sin(\psi)}^B \left[UT^2 \cdot \left(\theta + \frac{UP}{UT} \right) \right] \cdot \left(\beta \cdot \sin(\psi) - \frac{UP}{UT} \cdot \cos(\psi) \right) dx d\psi \dots \\
\left. + \frac{1}{2 \cdot \pi} \cdot \left[\int_\pi^{2 \cdot \pi} \int_0^{-\mu \cdot \sin(\psi)} \left[UT^2 \cdot \left(\theta + \frac{UP}{UT} \right) \right] \cdot \left(\beta \cdot \sin(\psi) - \frac{UP}{UT} \cdot \cos(\psi) \right) dx d\psi \right] \right]$$

$$\begin{aligned}
\text{CYd} := & \frac{\sigma \cdot \text{Cdo}}{2} \cdot \left[\frac{1}{2 \cdot \pi} \cdot \int_0^{2 \cdot \pi} \int_0^1 -1 \cdot \left(\text{UT}^2 \cdot \cos(\psi) \right) \text{d}x \text{d}\psi - \frac{2}{2 \cdot \pi} \cdot \int_{\pi}^{2 \cdot \pi} \int_0^{-\mu \cdot \sin(\psi)} -1 \cdot \left(\text{UT}^2 \cdot \cos(\psi) \right) \text{d}x \text{d}\psi \right] \dots \\
& + \frac{\sigma \cdot \delta 1}{2} \cdot \frac{1}{2 \cdot \pi} \cdot \left[\int_0^{2 \cdot \pi} \int_0^1 -1 \cdot \left[\text{UT}^2 \cdot \left(\frac{\text{UP}}{\text{UT}} + \theta \right) \right] \cdot \cos(\psi) \text{d}x \text{d}\psi \right] \dots \\
& + \frac{\sigma \cdot \delta 2}{2} \cdot \left[\frac{1}{2 \cdot \pi} \cdot \int_0^{2 \cdot \pi} \int_0^1 -1 \cdot \left[\text{UT}^2 \cdot \left(\frac{\text{UP}}{\text{UT}} + \theta \right)^2 \right] \cdot \cos(\psi) \text{d}x \text{d}\psi \dots \right. \\
& \quad \left. + 0 - \frac{2}{2 \cdot \pi} \cdot \int_{\pi}^{2 \cdot \pi} \int_0^{-\mu \cdot \sin(\psi)} -1 \cdot \left[\text{UT}^2 \cdot \left(\frac{\text{UP}}{\text{UT}} + \theta \right)^2 \right] \cdot \cos(\psi) \text{d}x \text{d}\psi \right]
\end{aligned}$$

Input

$$\mu := 0.70 \quad \lambda_s := 0.013 \quad \lambda_1 = -0.007287534590767 \quad \gamma := 19.2 \quad B := .97 \quad \sigma := .0976 \quad a := 5.73$$

$$Cdo := 0.012 \quad \delta_1 := -0.0216 \quad \delta_2 := 0.4$$

$$\theta_o := 1.9 \cdot \frac{\pi}{180} \quad \theta_t := -1 \cdot \frac{\pi}{180} \quad B1c := -2 \cdot \frac{\pi}{180} \quad A1c := 1 \cdot \frac{\pi}{180} \quad \theta e1s := -1 \cdot \frac{\pi}{180} \quad \theta e1c := 1 \cdot \frac{\pi}{180}$$

Calculate β_o , $a1s$, $b1s$, $a2s$ and $b2s$ to use in all calculations

$$M0 := \left(B^4 + \frac{1}{6} \cdot \mu^4 \right) \cdot \left(B^4 - \frac{1}{2} \cdot B^2 \cdot \mu^2 + \frac{7}{24} \cdot \mu^4 \right) - \left(\frac{2}{3} \cdot B^3 \cdot \mu - \frac{88}{315 \pi} \cdot \mu^4 \right) \cdot \left(\frac{2}{3} \cdot B^3 \cdot \mu - \frac{64}{45 \pi} \cdot \mu^4 \right)$$

$$M0 = 0.542330515448621$$

$$M1 := \left(\frac{8}{15 \pi} \cdot \mu^3 \right) \cdot \left(B^4 - \frac{1}{2} \cdot B^2 \cdot \mu^2 + \frac{7}{24} \cdot \mu^4 \right) - \left(\frac{2}{3} \cdot B^3 \cdot \mu - \frac{88}{315 \pi} \cdot \mu^4 \right) \cdot \left(2 \cdot B^2 \cdot \mu - \frac{1}{2} \cdot \mu^3 \right)$$

$$M1 = -0.421327574886569$$

$$M2 := \left(\frac{1}{2} \cdot B^2 \cdot \mu^2 - \frac{1}{12} \cdot \mu^4 \right) \cdot \left(B^4 - \frac{1}{2} \cdot B^2 \cdot \mu^2 + \frac{7}{24} \cdot \mu^4 \right) - \left(\frac{2}{3} \cdot B^3 \cdot \mu - \frac{88}{315 \pi} \cdot \mu^4 \right) \cdot \left(\frac{8}{3} \cdot B^3 \cdot \mu + \frac{32}{45 \pi} \cdot \mu^4 \right)$$

$$M2 = -0.558644204651302$$

$$M3 := \left(\frac{1}{3} \cdot B^3 \cdot \mu^2 - \frac{32}{315 \pi} \cdot \mu^5 \right) \cdot \left(B^4 - \frac{1}{2} \cdot B^2 \cdot \mu^2 + \frac{7}{24} \cdot \mu^4 \right) - \left(\frac{2}{3} \cdot B^3 \cdot \mu - \frac{88}{315 \pi} \cdot \mu^4 \right) \cdot \left(2 \cdot B^4 \cdot \mu + \frac{1}{12} \cdot \mu^5 \right)$$

$$M3 = -0.402978977618712$$

$$M4 := \left(\frac{2}{3} \cdot B^3 \cdot \mu - \frac{88}{315 \pi} \cdot \mu^4 \right) \cdot \left(B^4 + \frac{3}{2} \cdot B^2 \cdot \mu^2 - \frac{5}{24} \cdot \mu^4 \right) - \left(\frac{2}{3} \cdot B^3 \cdot \mu + \frac{16}{63 \pi} \cdot \mu^4 \right) \cdot \left(B^4 - \frac{1}{2} \cdot B^2 \cdot \mu^2 + \frac{7}{24} \cdot \mu^4 \right)$$

$$M4 = 0.294929302420598$$

$$M5 := \left(B^4 - \frac{1}{2} \cdot B^2 \cdot \mu^2 + \frac{7}{24} \cdot \mu^4 \right) \cdot \left(\frac{1}{2} \cdot B^4 \cdot \mu + \frac{1}{32} \cdot \mu^5 \right) - \left(\frac{2}{3} \cdot B^3 \cdot \mu - \frac{88}{315 \pi} \cdot \mu^4 \right) \cdot \left(\frac{4}{5} \cdot B^5 + B^3 \cdot \mu^2 - \frac{128}{525 \pi} \cdot \mu^5 \right)$$

$$M5 = -0.22518921202764$$

$$c1 := \frac{M1}{M0} \quad c1 = -0.776883400223281$$

$$k1 := \frac{M2 \cdot \theta_o + M3 \cdot \theta_t + M4 \cdot B1c + M5 \cdot \theta e1s}{M0} \quad k1 = -0.032925890146846$$

$$b2s := c1 \cdot \lambda_s + k1$$

$$b2s = -0.043025374349748$$

$$c2 := \frac{\left(2 \cdot B^2 \cdot \mu - \frac{1}{2} \cdot \mu^3\right) - \left(\frac{2}{3} \cdot B^3 \cdot \mu - \frac{64}{45 \cdot \pi} \cdot \mu^4\right) \cdot c1}{B^4 - \frac{1}{2} \cdot B^2 \cdot \mu^2 + \frac{7}{24} \cdot \mu^4}$$

$$c2 = 1.920804850449535$$

$$k2 := \frac{\left(\frac{8}{3} \cdot B^3 \cdot \mu + \frac{32}{45 \cdot \pi} \cdot \mu^4\right) \cdot \theta_0 + \left(2 \cdot B^4 \cdot \mu + \frac{1}{12} \cdot \mu^5\right) \cdot \theta_t - \left(B^4 + \frac{3}{2} \cdot B^2 \cdot \mu^2 - \frac{5}{24} \cdot \mu^4\right) \cdot B1c - \left(\frac{2}{3} \cdot B^3 \cdot \mu - \frac{64}{45 \cdot \pi} \cdot \mu^4\right) \cdot k1 \dots}{B^4 - \frac{1}{2} \cdot B^2 \cdot \mu^2 + \frac{7}{24} \cdot \mu^4} + \left(\frac{4}{5} \cdot B^5 + B^3 \cdot \mu^2 - \frac{128}{525 \cdot \pi} \cdot \mu^5\right) \cdot \theta_{e1s}$$

$$k2 = 0.111195718630495$$

$$a1s := c2 \cdot \lambda s + k2$$

$$a1s = 0.136166181686339$$

$$c3 := \frac{\gamma}{2} \cdot \left[\left(B^3 + \frac{2}{3 \cdot \pi} \cdot \mu^3 \right) \cdot \frac{1}{3} + \left(B^2 \cdot \mu^2 - \frac{1}{2} \cdot \mu^4 \right) \cdot \frac{1}{8} \cdot c1 + \left(\frac{2}{15 \cdot \pi} \cdot \mu^4 \right) \cdot c2 \right]$$

$$c3 = 3.02348303009608$$

$$k3 := \frac{\gamma}{2} \cdot \left[\left(B^4 + B^2 \cdot \mu^2 - \frac{1}{8} \cdot \mu^4 \right) \cdot \frac{\theta_0}{4} + \left(B^5 + \frac{5}{6} \cdot B^3 \cdot \mu^2 - \frac{8}{45 \cdot \pi} \cdot \mu^5 \right) \cdot \frac{\theta_t}{5} \dots \right. \\ \left. + \left(B^2 \cdot \mu^2 - \frac{1}{2} \cdot \mu^4 \right) \cdot \frac{1}{8} \cdot k1 - \left(B^3 \cdot \mu + \frac{4}{15 \cdot \pi} \cdot \mu^4 \right) \cdot \frac{B1c}{3} + \left(\frac{2}{15 \cdot \pi} \cdot \mu^4 \right) \cdot k2 + \left(\frac{1}{4} \cdot B^4 \cdot \mu + \frac{1}{96} \cdot \mu^5 \right) \cdot \theta_{e1s} \right]$$

$$k3 = 0.108608361537353$$

$$\beta_0 := c3 \cdot \lambda s + k3$$

$$\beta_0 = 0.147913640928602$$

$$N0 := \left(B^4 + \frac{1}{12} \cdot \mu^4 \right) \cdot \left(B^4 + \frac{1}{2} \cdot B^2 \cdot \mu^2 - \frac{1}{24} \cdot \mu^4 \right) - \left(\frac{2}{3} \cdot B^3 \cdot \mu + \frac{32}{315 \cdot \pi} \cdot \mu^4 \right) \cdot \left(\frac{2}{3} \cdot B^3 \cdot \mu - \frac{16}{45 \cdot \pi} \cdot \mu^4 \right)$$

$$N0 = 0.82816538423059$$

$$N1 := \left(\frac{2}{3} \cdot B^3 \cdot \mu + \frac{32}{315 \cdot \pi} \cdot \mu^4 \right) \cdot \left(\frac{4}{3} \cdot B^3 \cdot \mu + \frac{16}{45 \cdot \pi} \cdot \mu^4 \right) - \left(B^4 + \frac{1}{2} \cdot B^2 \cdot \mu^2 - \frac{1}{24} \cdot \mu^4 \right) \cdot \left(\frac{1}{2} \cdot B^2 \cdot \mu^2 - \frac{1}{12} \cdot \mu^4 \right)$$

$$N1 = 0.148417503634094$$

$$N2 := \left(B^4 + \frac{1}{2} \cdot B^2 \cdot \mu^2 - \frac{1}{24} \cdot \mu^4 \right) \cdot \left(\frac{1}{3} \cdot B^3 \cdot \mu - \frac{32}{315 \cdot \pi} \cdot \mu^4 \right) - \left(\frac{2}{3} \cdot B^3 \cdot \mu + \frac{32}{315 \cdot \pi} \cdot \mu^4 \right) \cdot \left(B^4 + \frac{1}{24} \cdot \mu^4 \right)$$

$$N2 = -0.161366193052923$$

$$N3 := \left(B^4 + \frac{1}{2} \cdot B^2 \cdot \mu^2 - \frac{1}{24} \cdot \mu^4 \right) \cdot \left(\frac{1}{2} \cdot B^4 \cdot \mu + \frac{1}{96} \cdot \mu^5 \right) - \left(\frac{2}{3} \cdot B^3 \cdot \mu + \frac{32}{315 \cdot \pi} \cdot \mu^4 \right) \cdot \left(\frac{4}{5} \cdot B^5 + \frac{1}{3} \cdot B^3 \cdot \mu^2 - \frac{64}{1575 \cdot \pi} \cdot \mu^5 \right)$$

$$N3 = -0.017063134116859$$

$$c4 := \frac{N1 \cdot c3}{N0}$$

$$c4 = 0.541845641162371$$

$$k4 := \frac{N1 \cdot (k3) + (N2) \cdot \lambda 1 + (N3) \cdot \theta e1 c}{N0}$$

$$k4 = 0.020524325285051$$

$$a2s := c4 \cdot \lambda s + k4$$

$$a2s = 0.027568318620162$$

$$c5 := \frac{\left(\frac{4}{3} \cdot B^3 \cdot \mu + \frac{16}{45 \cdot \pi} \cdot \mu^4\right) \cdot c3 + \left(\frac{2}{3} \cdot B^3 \cdot \mu - \frac{16}{45 \cdot \pi} \cdot \mu^4\right) \cdot c4}{B^4 + \frac{1}{2} \cdot B^2 \cdot \mu^2 - \frac{1}{24} \cdot \mu^4}$$

$$c5 = 2.59873326749403$$

$$k5 := \frac{\left[\left(\frac{4}{3} \cdot B^3 \cdot \mu + \frac{16}{45 \cdot \pi} \cdot \mu^4\right) \cdot k3 - \left(B^4 + \frac{1}{24} \cdot \mu^4\right) \cdot \lambda 1 + \left(B^4 + \frac{1}{2} \cdot B^2 \cdot \mu^2 - \frac{1}{24} \cdot \mu^4\right) \cdot A1c \dots\right] + \left(\frac{2}{3} \cdot B^3 \cdot \mu - \frac{16}{45 \cdot \pi} \cdot \mu^4\right) \cdot k4 - \left(\frac{4}{5} \cdot B^5 + \frac{1}{3} \cdot B^3 \cdot \mu^2 - \frac{64}{1575 \pi} \cdot \mu^5\right) \cdot \theta e1 c}{B^4 + \frac{1}{2} \cdot B^2 \cdot \mu^2 - \frac{1}{24} \cdot \mu^4}$$

$$k5 = 0.103925113983945$$

$$b1s := c5 \cdot \lambda s + k5$$

$$b1s = 0.137708646461368$$

Calculate Thrust Coefficient, CT

$$T1 := \left(\frac{1}{2} \cdot B^2 + \frac{1}{4} \cdot \mu^2\right) + \left(\frac{1}{4} \cdot B \cdot \mu^2 - \frac{8}{15 \cdot \pi} \cdot \mu^3\right) \cdot c1 + \left(\frac{1}{8} \cdot \mu^3\right) \cdot c2$$

$$T1 = 0.628228860960388$$

$$T2 := \left(\frac{1}{3} \cdot B^3 + \frac{1}{2} \cdot B \cdot \mu^2 - \frac{4}{9 \cdot \pi} \cdot \mu^3\right) \cdot \theta o + \left(\frac{1}{4} \cdot B^4 + \frac{1}{4} \cdot B^2 \cdot \mu^2 - \frac{1}{32} \cdot \mu^4\right) \cdot \theta t - \left(\frac{1}{2} \cdot B^2 \cdot \mu + \frac{1}{8} \cdot \mu^3\right) \cdot B1c \dots + \left(\frac{1}{4} \cdot B \cdot \mu^2 - \frac{8}{15 \cdot \pi} \cdot \mu^3\right) \cdot k1 + \left(\frac{1}{8} \cdot \mu^3\right) \cdot k2 + \left(\frac{1}{3} \cdot B^3 \cdot \mu + \frac{4}{45 \cdot \pi} \cdot \mu^4\right) \cdot \theta e1 s$$

$$T2 = 0.022545430221145$$

$$CT := \frac{\sigma \cdot a}{2} \cdot (T1 \cdot \lambda s + T2)$$

$$CT = 0.008587925651381$$

Calculate Accelerating Torque, CQa

$$A1 := \left(\frac{1}{2} \cdot B^2 - \frac{1}{4} \cdot \mu^2 \right) + \left(\frac{1}{2} \cdot B^2 \cdot \mu - \frac{3}{8} \cdot \mu^3 \right) \cdot c2 + \left(\frac{8}{5 \cdot \pi} \cdot \mu^3 \right) \cdot c1$$

$$A1 = 0.597723756350029$$

$$A2 := \left(\frac{1}{3} \cdot B^3 + \frac{2}{9 \cdot \pi} \cdot \mu^3 \right) \cdot \theta_0 + \left(\frac{1}{4} \cdot B^4 + \frac{1}{32} \cdot \mu^4 \right) \cdot \theta_t + \left(\frac{1}{2} \cdot B^2 \cdot \mu - \frac{3}{8} \cdot \mu^3 \right) \cdot k2 + \left(\frac{8}{5 \cdot \pi} \cdot \mu^3 \right) \cdot k1 - \left(\frac{1}{4} \cdot B^2 \cdot \mu - \frac{1}{16} \cdot \mu^3 \right) \cdot B1c \dots$$

$$+ \left(\frac{1}{6} \cdot B^3 \cdot \mu - \frac{4}{45 \cdot \pi} \cdot \mu^4 \right) \cdot \theta_{e1s}$$

$$A2 = 0.026722839863594$$

$$\text{Lamda} := A1 \cdot \lambda s^2 + A2 \cdot \lambda s \quad \text{Lamda} = 0.00044841223305$$

$$A3 := \left(\frac{1}{8} \cdot B^2 \cdot \mu^2 - \frac{1}{16} \cdot \mu^4 \right) \cdot c1 \cdot \theta_0 + \left(\frac{2}{15 \cdot \pi} \cdot \mu^4 \right) \cdot c2 \cdot \theta_0$$

$$A3 = -0.000449019030451$$

$$A4 := \left(\frac{1}{8} \cdot B^2 \cdot \mu^2 - \frac{1}{16} \cdot \mu^4 \right) \cdot k1 \cdot \theta_0 + \left(\frac{2}{15 \cdot \pi} \cdot \mu^4 \right) \cdot k2 \cdot \theta_0$$

$$A4 = -0.000008964376402$$

$$\text{Coll} := A3 \cdot \lambda s + A4 \quad \text{Coll} = -0.000014801623798$$

$$A5 := \left(\frac{1}{12} \cdot B^3 \cdot \mu^2 - \frac{32}{315 \cdot \pi} \cdot \mu^5 \right) \cdot c1 \cdot \theta_t + \left(\frac{1}{48} \cdot \mu^5 \right) \cdot c2 \cdot \theta_t$$

$$A5 = 0.000314241300393$$

$$A6 := \left(\frac{1}{12} \cdot B^3 \cdot \mu^2 - \frac{32}{315 \cdot \pi} \cdot \mu^5 \right) \cdot k1 \cdot \theta_t + \left(\frac{1}{48} \cdot \mu^5 \right) \cdot k2 \cdot \theta_t$$

$$A6 = 0.000011497770935$$

$$\text{Twist} := A5 \cdot \lambda s + A6 \quad \text{Twist} = 0.000015582907841$$

$$A7 := \left(\frac{1}{8} \cdot B^4 + \frac{3}{16} \cdot B^2 \cdot \mu^2 - \frac{29}{192} \cdot \mu^4 \right) \cdot c2^2 + \left(\frac{1}{6} \cdot B^3 \cdot \mu + \frac{56}{45 \cdot \pi} \cdot \mu^4 \right) \cdot c1 \cdot c2$$

$$A7 = 0.29260799957433$$

$$A8 := \left(\frac{1}{4} \cdot B^4 + \frac{3}{8} \cdot B^2 \cdot \mu^2 - \frac{29}{96} \cdot \mu^4 \right) \cdot c2 \cdot k2 + \left(\frac{1}{8} \cdot B^4 - \frac{1}{16} \cdot B^2 \cdot \mu^2 + \frac{7}{192} \cdot \mu^4 \right) \cdot B1c \cdot c2 \dots$$

$$+ \left(\frac{1}{6} \cdot B^3 \cdot \mu + \frac{56}{45 \cdot \pi} \cdot \mu^4 \right) \cdot (c1 \cdot k2 + k1 \cdot c2) - \left(\frac{1}{10} \cdot B^5 - \frac{1}{24} \cdot B^3 \cdot \mu^2 + \frac{92}{1575 \cdot \pi} \cdot \mu^5 \right) \cdot \theta_{e1s} \cdot c2$$

$$A8 = 0.034827654259352$$

$$A9 := \left(\frac{1}{8} \cdot B^4 + \frac{3}{16} \cdot B^2 \cdot \mu^2 - \frac{29}{192} \cdot \mu^4 \right) \cdot k2^2 + \left(\frac{1}{8} \cdot B^4 - \frac{1}{16} \cdot B^2 \cdot \mu^2 + \frac{7}{192} \cdot \mu^4 \right) \cdot B1c \cdot k2 \dots$$

$$+ \left(\frac{1}{6} \cdot B^3 \cdot \mu + \frac{56}{45 \cdot \pi} \cdot \mu^4 \right) \cdot k1 \cdot k2 - \left(\frac{1}{10} \cdot B^5 - \frac{1}{24} \cdot B^3 \cdot \mu^2 + \frac{92}{1575 \pi} \cdot \mu^5 \right) \cdot \theta e1s \cdot k2$$

$$A9 = 0.001035569893085$$

$$A1S := A7 \cdot \lambda s^2 + A8 \cdot \lambda s + A9 \quad A1S = 0.001537780150384$$

$$A10 := \left(\frac{1}{8} \cdot B^4 + \frac{1}{16} \cdot B^2 \cdot \mu^2 - \frac{1}{192} \cdot \mu^4 \right) \cdot c5^2 - \left(\frac{1}{3} \cdot B^3 \cdot \mu + \frac{4}{45 \cdot \pi} \cdot \mu^4 \right) \cdot c3 \cdot c5 - \left(\frac{1}{6} \cdot B^3 \cdot \mu - \frac{4}{45 \cdot \pi} \cdot \mu^4 \right) \cdot c4 \cdot c5$$

$$A10 = -0.933498451064171$$

$$A11 := \left(\frac{1}{4} \cdot B^4 + \frac{1}{8} \cdot B^2 \cdot \mu^2 - \frac{1}{96} \cdot \mu^4 \right) \cdot c5 \cdot k5 - \left(\frac{1}{3} \cdot B^3 \cdot \mu + \frac{4}{45 \cdot \pi} \cdot \mu^4 \right) \cdot (c3 \cdot k5 + k3 \cdot c5) - \left(\frac{1}{6} \cdot B^3 \cdot \mu - \frac{4}{45 \cdot \pi} \cdot \mu^4 \right) \cdot (c4 \cdot k5 + k4 \cdot c5) \dots$$

$$+ \left(\frac{1}{4} \cdot B^4 + \frac{1}{96} \cdot \mu^4 \right) \cdot \lambda 1 \cdot c5 - \left(\frac{1}{8} \cdot B^4 + \frac{1}{16} \cdot B^2 \cdot \mu^2 - \frac{1}{192} \cdot \mu^4 \right) \cdot A1c \cdot c5 + \left(\frac{1}{10} \cdot B^5 + \frac{1}{24} \cdot B^3 \cdot \mu^2 - \frac{8}{1575 \pi} \cdot \mu^5 \right) \cdot \theta e1c \cdot c5$$

$$A11 = -0.073120778920482$$

$$A12 := \left(\frac{1}{8} \cdot B^4 + \frac{1}{16} \cdot B^2 \cdot \mu^2 - \frac{1}{192} \cdot \mu^4 \right) \cdot k5^2 - \left(\frac{1}{3} \cdot B^3 \cdot \mu + \frac{4}{45 \cdot \pi} \cdot \mu^4 \right) \cdot k3 \cdot k5 - \left(\frac{1}{6} \cdot B^3 \cdot \mu - \frac{4}{45 \cdot \pi} \cdot \mu^4 \right) \cdot k4 \cdot k5 \dots$$

$$+ \left(\frac{1}{4} \cdot B^4 + \frac{1}{96} \cdot \mu^4 \right) \cdot \lambda 1 \cdot k5 - \left(\frac{1}{8} \cdot B^4 + \frac{1}{16} \cdot B^2 \cdot \mu^2 - \frac{1}{192} \cdot \mu^4 \right) \cdot A1c \cdot k5 + \left(\frac{1}{10} \cdot B^5 + \frac{1}{24} \cdot B^3 \cdot \mu^2 - \frac{8}{1575 \pi} \cdot \mu^5 \right) \cdot \theta e1c \cdot k5$$

$$A12 = -0.001431248082753$$

$$B1S := A10 \cdot \lambda s^2 + A11 \cdot \lambda s + A12 \quad B1S = -0.002539579446949$$

$$A13 := \left(\frac{1}{4} \cdot B^2 \cdot \mu^2 - \frac{1}{16} \cdot \mu^4 \right) \cdot c3^2 - \left(\frac{1}{4} \cdot B^2 \cdot \mu^2 - \frac{1}{6} \cdot \mu^4 \right) \cdot c4 \cdot c3$$

$$A13 = 0.793198255860955$$

$$A14 := \left(\frac{1}{2} \cdot B^2 \cdot \mu^2 - \frac{1}{8} \cdot \mu^4 \right) \cdot c3 \cdot k3 - \left(\frac{1}{4} \cdot B^2 \cdot \mu^2 - \frac{1}{6} \cdot \mu^4 \right) \cdot (c4 \cdot k3 + k4 \cdot c3) \dots$$

$$+ \left(\frac{1}{6} \cdot B^3 \cdot \mu + \frac{2}{45 \cdot \pi} \cdot \mu^4 \right) \cdot A1c \cdot c3 - \left(\frac{1}{3} \cdot B^3 \cdot \mu - \frac{8}{45 \cdot \pi} \cdot \mu^4 \right) \cdot \lambda 1 \cdot c3 - \left(\frac{1}{8} \cdot B^4 \cdot \mu + \frac{1}{192} \cdot \mu^5 \right) \cdot \theta e1c \cdot c3$$

$$A14 = 0.062801733980362$$

$$A15 := \left(\frac{1}{4} \cdot B^2 \cdot \mu^2 - \frac{1}{16} \cdot \mu^4 \right) \cdot k3^2 - \left(\frac{1}{4} \cdot B^2 \cdot \mu^2 - \frac{1}{6} \cdot \mu^4 \right) \cdot k4 \cdot k3 \dots$$

$$+ \left(\frac{1}{6} \cdot B^3 \cdot \mu + \frac{2}{45 \cdot \pi} \cdot \mu^4 \right) \cdot A1c \cdot k3 - \left(\frac{1}{3} \cdot B^3 \cdot \mu - \frac{8}{45 \cdot \pi} \cdot \mu^4 \right) \cdot \lambda 1 \cdot k3 - \left(\frac{1}{8} \cdot B^4 \cdot \mu + \frac{1}{192} \cdot \mu^5 \right) \cdot \theta e1c \cdot k3$$

$$A15 = 0.00123242642384$$

$$\text{Coning} := A13 \cdot \lambda s^2 + A14 \cdot \lambda s + A15 \quad \text{Coning} = 0.002182899470825$$

$$A16 := \left(\frac{1}{6} \cdot B^3 \cdot \mu - \frac{88}{315 \pi} \cdot \mu^4 \right) \cdot \lambda 1 \cdot c4$$

$$A16 = -0.00033614537052$$

$$A17 := \left(\frac{1}{8} \cdot B^4 - \frac{1}{64} \cdot \mu^4 \right) \cdot \lambda 1^2 - \left(\frac{1}{8} \cdot B^4 + \frac{1}{192} \cdot \mu^4 \right) \cdot A1c \cdot \lambda 1 + \left(\frac{1}{6} \cdot B^3 \cdot \mu - \frac{88}{315 \pi} \cdot \mu^4 \right) \cdot \lambda 1 \cdot k4 + \left(\frac{1}{10} \cdot B^5 + \frac{4}{525 \pi} \cdot \mu^5 \right) \cdot \theta e1c \cdot \lambda 1$$

$$A17 = -0.000003794843514$$

$$\text{LamdaONE} := A16 \cdot \lambda s + A17 \quad \text{LamdaONE} = -0.000008164733331$$

$$A18 := \left(\frac{1}{2} \cdot B^4 + \frac{1}{8} \cdot B^2 \cdot \mu^2 - \frac{25}{192} \cdot \mu^4 \right) \cdot c4^2$$

$$A18 = 0.137700818005821$$

$$A19 := \left(B^4 + \frac{1}{4} \cdot B^2 \cdot \mu^2 - \frac{25}{96} \cdot \mu^4 \right) \cdot c4 \cdot k4 + \left(\frac{1}{12} \cdot B^3 \cdot \mu - \frac{2}{45 \pi} \cdot \mu^4 \right) \cdot A1c \cdot c4 - \left(\frac{1}{16} \cdot B^4 \cdot \mu - \frac{5}{768} \cdot \mu^5 \right) \cdot \theta e1c \cdot c4$$

$$A19 = 0.010547237964583$$

$$A20 := \left(\frac{1}{2} \cdot B^4 + \frac{1}{8} \cdot B^2 \cdot \mu^2 - \frac{25}{192} \cdot \mu^4 \right) \cdot k4^2 + \left(\frac{1}{12} \cdot B^3 \cdot \mu - \frac{2}{45 \pi} \cdot \mu^4 \right) \cdot A1c \cdot k4 - \left(\frac{1}{16} \cdot B^4 \cdot \mu - \frac{5}{768} \cdot \mu^5 \right) \cdot \theta e1c \cdot k4$$

$$A20 = 0.000201943073982$$

$$A2S := A18 \cdot \lambda s^2 + A19 \cdot \lambda s + A20 \quad A2S = 0.000362328605764$$

$$A21 := \left(\frac{1}{2} \cdot B^4 + \frac{1}{8} \cdot B^2 \cdot \mu^2 - \frac{59}{192} \cdot \mu^4 \right) \cdot c1^2$$

$$A21 = 0.257410609783993$$

$$A22 := \left(B^4 + \frac{1}{4} \cdot B^2 \cdot \mu^2 - \frac{59}{96} \cdot \mu^4 \right) \cdot c1 \cdot k1 + \left(\frac{1}{12} \cdot B^3 \cdot \mu - \frac{8}{45 \pi} \cdot \mu^4 \right) \cdot B1c \cdot c1 - \left(\frac{1}{16} \cdot B^4 \cdot \mu - \frac{23}{768} \cdot \mu^5 \right) \cdot \theta e1s \cdot c1$$

$$A22 = 0.022437551769387$$

$$A23 := \left(\frac{1}{2} \cdot B^4 + \frac{1}{8} \cdot B^2 \cdot \mu^2 - \frac{59}{192} \cdot \mu^4 \right) \cdot k1^2 + \left(\frac{1}{12} \cdot B^3 \cdot \mu - \frac{8}{45 \pi} \cdot \mu^4 \right) \cdot B1c \cdot k1 - \left(\frac{1}{16} \cdot B^4 \cdot \mu - \frac{23}{768} \cdot \mu^5 \right) \cdot \theta e1s \cdot k1$$

$$A23 = 0.00048857866363$$

$$B2S := A21 \cdot \lambda s^2 + A22 \cdot \lambda s + A23 \quad B2S = 0.000823769229685$$

$$A24 := A13 + A1 + A7 + A21 + A18 + A10 \quad A24 = 1.145142988510958$$

$$A25 := A3 + A14 + A11 + A8 + A5 + A22 + A2 + A16 + A19 \quad A25 = 0.083745315816218$$

$$A26 := A9 + A15 + A20 + A4 + A17 + A6 + A12 + A23 \quad A26 = 0.001526008522803$$

$$CQa := -1 \cdot \frac{\sigma \cdot a}{2} \cdot (A24 \cdot \lambda s^2 + A25 \cdot \lambda s + A26)$$

$$CQa = -0.000785247608898$$

Calculate Decelerating Torque (per Bailey N.A.C.A. TR 716)

$$D0 := 1 + \mu^2 - \frac{1}{8} \cdot \mu^4 \quad D0 = 1.4599875$$

$$CQCd0 := \frac{\sigma \cdot Cdo}{8} \cdot (D0)$$

$$CQCd0 = 0.00021374217$$

$$D1 := \frac{1}{3} + \left(\frac{1}{8} \cdot \mu^2 \right) \cdot c1 \quad D1 = 0.285749225069657$$

$$D2 := \left(\frac{1}{4} + \frac{1}{4} \cdot \mu^2 \right) \cdot \theta_0 + \left(\frac{1}{5} + \frac{1}{6} \cdot \mu^2 \right) \cdot \theta_t + \left(\frac{1}{8} \cdot \mu^2 \right) \cdot k1 - \left(\frac{1}{3} \cdot \mu \right) \cdot B1c + \left(\frac{1}{4} \cdot \mu \right) \cdot \theta_{e1s} \quad D2 = 0.010510389934695$$

$$CQ\delta 1 := \frac{\sigma \cdot \delta 1}{2} \cdot (D1 \cdot \lambda_s + D2)$$

$$CQ\delta 1 = -0.000014994424883$$

$$D3 := \left(\frac{1}{2} - \frac{1}{4} \cdot \mu^2 \right) + \left(\frac{1}{2} \cdot \mu - \frac{3}{8} \cdot \mu^3 \right) \cdot c2 + \left(\frac{8}{5 \cdot \pi} \cdot \mu^3 \right) \cdot c1$$

$$D3 = 0.667005604681578$$

$$D4 := \left(\frac{2}{3} + \frac{4}{9 \cdot \pi} \cdot \mu^3 \right) \cdot \theta_0 + \left(\frac{1}{2} \cdot \mu - \frac{3}{8} \cdot \mu^3 \right) \cdot k2 + \left(\frac{1}{2} + \frac{1}{16} \cdot \mu^4 \right) \cdot \theta_t + \left(\frac{8}{5 \cdot \pi} \cdot \mu^3 \right) \cdot k1 - \left(\frac{1}{2} \cdot \mu - \frac{1}{8} \cdot \mu^3 \right) \cdot B1c + \left(\frac{1}{3} \cdot \mu - \frac{8}{45 \cdot \pi} \cdot \mu^4 \right) \cdot \theta_{e1s}$$

$$D4 = 0.040477649727351$$

$$\text{LamdaD} := D3 \cdot \lambda_s^2 + D4 \cdot \lambda_s \quad \text{LamdaD} = 0.000638933393647$$

$$D5 := \left(\frac{4}{15 \cdot \pi} \cdot \mu^4 \right) \cdot c2 \cdot \theta_0 + \left(\frac{1}{4} \cdot \mu^2 - \frac{1}{8} \cdot \mu^4 \right) \cdot c1 \cdot \theta_0$$

$$D5 = -0.001084551607357$$

$$D6 := \left(\frac{1}{4} + \frac{1}{4} \cdot \mu^2 - \frac{1}{32} \cdot \mu^4 \right) \cdot \theta_0^2 + \left(\frac{1}{4} \cdot \mu^2 - \frac{1}{8} \cdot \mu^4 \right) \cdot k1 \cdot \theta_0 - \left(\frac{2}{3} \cdot \mu + \frac{8}{45 \cdot \pi} \cdot \mu^4 \right) \cdot B1c \cdot \theta_0 + \left(\frac{2}{5} + \frac{1}{3} \cdot \mu^2 - \frac{16}{225 \cdot \pi} \cdot \mu^5 \right) \cdot \theta_t \cdot \theta_0 \dots$$

$$+ \left(\frac{4}{15 \cdot \pi} \cdot \mu^4 \right) \cdot k2 \cdot \theta_0 + \left(\frac{1}{2} \cdot \mu + \frac{1}{48} \cdot \mu^5 \right) \cdot \theta_{e1s} \cdot \theta_0$$

$$D6 = 0.000403020328445$$

$$\text{CollD} := D5 \cdot \lambda_s + D6 \quad \text{CollD} = 0.00038892115755$$

$$D7 := \left(\frac{1}{6} \cdot \mu^2 - \frac{64}{315 \cdot \pi} \cdot \mu^5 \right) \cdot c1 \cdot \theta_t + \left(\frac{1}{24} \cdot \mu^5 \right) \cdot c2 \cdot \theta_t$$

$$D7 = 0.000725182624363$$

$$D8 := \left(\frac{1}{6} + \frac{1}{8} \cdot \mu^2 - \frac{1}{192} \cdot \mu^6 \right) \cdot \theta_t^2 + \left(\frac{1}{6} \cdot \mu^2 - \frac{64}{315 \cdot \pi} \cdot \mu^5 \right) \cdot k1 \cdot \theta_t + \left(\frac{1}{24} \cdot \mu^5 \right) \cdot k2 \cdot \theta_t - \left(\frac{1}{2} \cdot \mu + \frac{1}{48} \cdot \mu^5 \right) \cdot B1c \cdot \theta_t + \left(\frac{2}{5} \cdot \mu + \frac{16}{525 \cdot \pi} \cdot \mu^6 \right) \cdot \theta_{e1s} \cdot \theta_t$$

$$D8 = -0.000033390251961$$

$$\text{TwistD} := D7 \cdot \lambda s + D8 \quad \text{TwistD} = -0.000023962877844$$

$$D9 := \left(\frac{1}{6} \cdot \mu + \frac{56}{45 \cdot \pi} \cdot \mu^4 \right) \cdot c1 \cdot c2 + \left(\frac{1}{8} + \frac{3}{16} \cdot \mu^2 - \frac{29}{192} \cdot \mu^4 \right) \cdot c2^2$$

$$D9 = 0.350339463220244$$

$$D10 := \left(\frac{1}{4} + \frac{3}{8} \cdot \mu^2 - \frac{29}{96} \cdot \mu^4 \right) \cdot k2 \cdot c2 + \left(\frac{1}{6} \cdot \mu + \frac{56}{45 \cdot \pi} \cdot \mu^4 \right) \cdot k1 \cdot c2 + \left(\frac{1}{6} \cdot \mu + \frac{56}{45 \cdot \pi} \cdot \mu^4 \right) \cdot c1 \cdot k2 \dots$$

$$+ \left(\frac{1}{4} - \frac{1}{8} \cdot \mu^2 + \frac{7}{96} \cdot \mu^4 \right) \cdot B1c \cdot c2 - \left(\frac{1}{5} - \frac{1}{12} \cdot \mu^2 + \frac{184}{1575 \pi} \cdot \mu^5 \right) \cdot \theta e1s \cdot c2$$

$$D10 = 0.037179490667527$$

$$D11 := \left(\frac{1}{8} + \frac{3}{16} \cdot \mu^2 - \frac{29}{192} \cdot \mu^4 \right) \cdot k2^2 + \left(\frac{1}{4} - \frac{1}{8} \cdot \mu^2 + \frac{7}{96} \cdot \mu^4 \right) \cdot B1c \cdot k2 + \left(\frac{1}{6} \cdot \mu + \frac{56}{45 \cdot \pi} \cdot \mu^4 \right) \cdot k1 \cdot k2 - \left(\frac{1}{5} - \frac{1}{12} \cdot \mu^2 + \frac{184}{1575 \pi} \cdot \mu^5 \right) \cdot \theta e1s \cdot k2$$

$$D11 = 0.000978244279056$$

$$A1SD := D9 \cdot \lambda s^2 + D10 \cdot \lambda s + D11 \quad A1SD = 0.001520785027018$$

$$D12 := \left(\frac{1}{8} + \frac{1}{16} \cdot \mu^2 - \frac{1}{192} \cdot \mu^4 \right) \cdot c5^2 - \left(\frac{1}{6} \cdot \mu - \frac{4}{45 \cdot \pi} \cdot \mu^4 \right) \cdot c4 \cdot c5 - \left(\frac{1}{3} \cdot \mu + \frac{4}{45 \cdot \pi} \cdot \mu^4 \right) \cdot c3 \cdot c5$$

$$D12 = -0.998889293401722$$

$$D13 := \left(\frac{1}{4} + \frac{1}{8} \cdot \mu^2 - \frac{1}{96} \cdot \mu^4 \right) \cdot k5 \cdot c5 - \left(\frac{1}{6} \cdot \mu - \frac{4}{45 \cdot \pi} \cdot \mu^4 \right) \cdot k4 \cdot c5 - \left(\frac{1}{6} \cdot \mu - \frac{4}{45 \cdot \pi} \cdot \mu^4 \right) \cdot c4 \cdot k5 + \left(\frac{1}{4} + \frac{1}{96} \cdot \mu^4 \right) \cdot \lambda 1 \cdot c5 \dots$$

$$+ 0 - \left(\frac{1}{4} + \frac{1}{8} \cdot \mu^2 - \frac{1}{96} \cdot \mu^4 \right) \cdot A1c \cdot c5 - \left(\frac{\mu}{3} + \frac{4}{45 \cdot \pi} \cdot \mu^4 \right) \cdot k3 \cdot c5 - \left(\frac{\mu}{3} + \frac{4}{45 \cdot \pi} \cdot \mu^4 \right) \cdot c3 \cdot k5 + \left(\frac{1}{5} + \frac{1}{12} \cdot \mu^2 - \frac{16}{1575 \pi} \cdot \mu^5 \right) \cdot \theta e1c \cdot c5$$

$$D13 = -0.079775516833123$$

$$D14 := \left(\frac{1}{8} + \frac{1}{16} \cdot \mu^2 - \frac{1}{192} \cdot \mu^4 \right) \cdot k5^2 + \left(\frac{1}{4} + \frac{1}{96} \cdot \mu^4 \right) \cdot \lambda 1 \cdot k5 - \left(\frac{1}{3} \cdot \mu + \frac{4}{45 \cdot \pi} \cdot \mu^4 \right) \cdot k3 \cdot k5 - \left(\frac{1}{6} \cdot \mu - \frac{4}{45 \cdot \pi} \cdot \mu^4 \right) \cdot k4 \cdot k5 \dots$$

$$+ 0 - \left(\frac{1}{4} + \frac{1}{8} \cdot \mu^2 - \frac{1}{96} \cdot \mu^4 \right) \cdot A1c \cdot k5 + \left(\frac{1}{5} + \frac{1}{12} \cdot \mu^2 - \frac{16}{1575 \pi} \cdot \mu^5 \right) \cdot \theta e1c \cdot k5$$

$$D14 = -0.001592798981$$

$$B1SD := D12 \cdot \lambda s^2 + D13 \cdot \lambda s + D14 \quad B1SD = -0.002798692990415$$

$$D15 := \left(\frac{1}{4} \cdot \mu^2 - \frac{1}{16} \cdot \mu^4 \right) \cdot c3^2 - \left(\frac{1}{4} \cdot \mu^2 - \frac{1}{6} \cdot \mu^4 \right) \cdot c4 \cdot c3$$

$$D15 = 0.847519465037623$$

$$D16 := \left(\frac{1}{2} \cdot \mu^2 - \frac{1}{8} \cdot \mu^4 \right) \cdot k3 \cdot c3 - \left(\frac{1}{3} \cdot \mu - \frac{8}{45 \cdot \pi} \cdot \mu^4 \right) \cdot \lambda 1 \cdot c3 + \left(\frac{1}{3} \cdot \mu + \frac{4}{45 \cdot \pi} \cdot \mu^4 \right) \cdot A1c \cdot c3 \dots$$

$$+ 0 - \left(\frac{1}{4} \cdot \mu^2 - \frac{1}{6} \cdot \mu^4 \right) \cdot k4 \cdot c3 - \left(\frac{1}{4} \cdot \mu^2 - \frac{1}{6} \cdot \mu^4 \right) \cdot c4 \cdot k3 - \left(\frac{1}{4} \cdot \mu + \frac{1}{96} \cdot \mu^5 \right) \cdot \theta e1c \cdot c3$$

$$D16 = 0.068810250513425$$

$$D17 := \left(\frac{1}{4} \cdot \mu^2 - \frac{1}{16} \cdot \mu^4\right) \cdot k3^2 + \left(\frac{\mu}{3} + \frac{4}{45 \cdot \pi} \cdot \mu^4\right) \cdot A1c \cdot k3 - \left(\frac{1}{4} \cdot \mu^2 - \frac{1}{6} \cdot \mu^4\right) \cdot k4 \cdot k3 - \left(\frac{\mu}{3} - \frac{8}{45 \cdot \pi} \cdot \mu^4\right) \cdot \lambda1 \cdot k3 - \left(\frac{1}{4} \cdot \mu + \frac{1}{96} \cdot \mu^5\right) \cdot \theta e1c \cdot k3$$

D17 = 0.001378167972134

$$\text{ConingD} := D15 \cdot \lambda s^2 + D16 \cdot \lambda s + D17 \quad \text{ConingD} = 0.0024159320184$$

$$D18 := \left(\frac{1}{2} + \frac{1}{8} \cdot \mu^2 - \frac{25}{192} \cdot \mu^4\right) \cdot c4^2$$

D18 = 0.155602427515047

$$D19 := \left(\frac{1}{6} \cdot \mu - \frac{88}{315 \cdot \pi} \cdot \mu^4\right) \cdot \lambda1 \cdot c4 + \left(\frac{1}{6} \cdot \mu - \frac{4}{45 \cdot \pi} \cdot \mu^4\right) \cdot A1c \cdot c4 + \left(1 + \frac{1}{4} \cdot \mu^2 - \frac{25}{96} \cdot \mu^4\right) \cdot k4 \cdot c4 - \left(\frac{1}{8} \cdot \mu - \frac{5}{384} \cdot \mu^5\right) \cdot \theta e1c \cdot c4$$

D19 = 0.011643891219549

$$D20 := \left(\frac{1}{2} + \frac{1}{8} \cdot \mu^2 - \frac{25}{192} \cdot \mu^4\right) \cdot k4^2 + \left(\frac{1}{6} \cdot \mu - \frac{88}{315 \cdot \pi} \cdot \mu^4\right) \cdot \lambda1 \cdot k4 + \left(\frac{1}{6} \cdot \mu - \frac{4}{45 \cdot \pi} \cdot \mu^4\right) \cdot A1c \cdot k4 - \left(\frac{1}{8} \cdot \mu - \frac{5}{384} \cdot \mu^5\right) \cdot \theta e1c \cdot k4$$

D20 = 0.000217797757309

$$A2D := D18 \cdot \lambda s^2 + D19 \cdot \lambda s + D20 \quad A2D = 0.000395465153414$$

$$D21 := \left(\frac{1}{2} + \frac{1}{8} \cdot \mu^2 - \frac{59}{192} \cdot \mu^4\right) \cdot c1^2$$

D21 = 0.294211014530486

$$D22 := \left(\frac{1}{6} \cdot \mu - \frac{16}{45 \cdot \pi} \cdot \mu^4\right) \cdot B1c \cdot c1 + \left(1 + \frac{1}{4} \cdot \mu^2 - \frac{59}{96} \cdot \mu^4\right) \cdot k1 \cdot c1 - \left(\frac{1}{8} \cdot \mu - \frac{23}{384} \cdot \mu^5\right) \cdot \theta e1s \cdot c1$$

D22 = 0.026315483963901

$$D23 := \left(\frac{1}{2} + \frac{1}{8} \cdot \mu^2 - \frac{59}{192} \cdot \mu^4\right) \cdot k1^2 + \left(\frac{1}{6} \cdot \mu - \frac{16}{45 \cdot \pi} \cdot \mu^4\right) \cdot B1c \cdot k1 - \left(\frac{1}{8} \cdot \mu - \frac{23}{384} \cdot \mu^5\right) \cdot \theta e1s \cdot k1$$

D23 = 0.000586831067933

$$B2D := D21 \cdot \lambda s^2 + D22 \cdot \lambda s + D23 \quad B2D = 0.000978654020919$$

$$D24 := \left(\frac{1}{8} + \frac{1}{16} \cdot \mu^2 - \frac{1}{192} \cdot \mu^4\right) \cdot A1c^2 - \left(\frac{1}{4} + \frac{1}{96} \cdot \mu^4\right) \cdot \lambda1 \cdot A1c - \left(\frac{1}{5} + \frac{1}{12} \cdot \mu^2 - \frac{16}{1575 \cdot \pi} \cdot \mu^5\right) \cdot \theta e1c \cdot A1c$$

D24 = 0.000005944658361

$$D25 := \left(\frac{1}{8} + \frac{3}{16} \cdot \mu^2 - \frac{5}{192} \cdot \mu^4\right) \cdot B1c^2 - \left(\frac{1}{5} + \frac{1}{4} \cdot \mu^2 - \frac{32}{525 \cdot \pi} \cdot \mu^5\right) \cdot \theta e1s \cdot B1c$$

D25 = 0.000062145391563

$$D26 := \left(\frac{1}{8} - \frac{1}{64} \cdot \mu^4\right) \cdot \lambda1^2 + \left(\frac{1}{5} + \frac{8}{525 \cdot \pi} \cdot \mu^5\right) \cdot \theta e1c \cdot \lambda1 + \left(\frac{1}{12} + \frac{1}{32} \cdot \mu^2 - \frac{1}{1536} \cdot \mu^6\right) \cdot \theta e1c^2 + \left(\frac{1}{12} + \frac{3}{32} \cdot \mu^2 - \frac{7}{1536} \cdot \mu^6\right) \cdot \theta e1s^2$$

D26 = 0.00005013802977

$$D27 := D21 + D18 + D15 + D3 + D12 + D9$$

$$D27 = 1.315788681583257$$

$$D28 := D5 + D16 + D22 + D19 + D4 + D13 + D10 + D7$$

$$D28 = 0.104291880275636$$

$$D29 := D20 + D17 + D26 + D6 + D11 + D8 + D23 + D25 + D14 + D24$$

$$D29 = 0.00205610025161$$

$$CQ\delta 2 := \frac{\sigma \cdot \delta 2}{2} \cdot (D27 \cdot \lambda s^2 + D28 \cdot \lambda s + D29)$$

$$CQ\delta 2 = 0.000070940813416$$

$$D30 := \left(\frac{\sigma \cdot \delta 2}{2} \right) \cdot D27 \quad D30 = 0.025684195064505$$

$$D31 := \left(\frac{\sigma \cdot \delta 1}{2} \right) \cdot D1 + \frac{1}{2} \cdot \sigma \cdot \delta 2 \cdot D28 \quad D31 = 0.001734574959819$$

$$D32 := \left(\frac{\sigma \cdot Cdo}{8} \right) \cdot D0 + \left(\frac{\sigma \cdot \delta 1}{2} \right) \cdot D2 + \left(\frac{\sigma \cdot \delta 2}{2} \right) \cdot D29 \quad D32 = 0.000242798455089$$

$$CQd := D30 \cdot \lambda s^2 + D31 \cdot \lambda s + D32$$

$$CQd = 0.000269688558533$$

Calculate Total Torque

$$CQ := \left[D30 - \left(\frac{\sigma \cdot a}{2} \right) \cdot A24 \right] \cdot \lambda s^2 + \left[D31 - \left(\frac{\sigma \cdot a}{2} \right) \cdot A25 \right] \cdot \lambda s + \left[D32 - \left(\frac{\sigma \cdot a}{2} \right) \cdot A26 \right]$$

$$CQ = -0.000515559050365$$

Calculate Inflow For Autorotation

$$F := \left(D30 - \frac{1}{2} \cdot \sigma \cdot a \cdot A24 \right) \quad F = -0.294525267954883$$

$$D := \left(D31 - \frac{1}{2} \cdot \sigma \cdot a \cdot A25 \right) \quad D = -0.021682625229975$$

$$H := \left(D32 - \frac{1}{2} \cdot \sigma \cdot a \cdot A26 \right) \quad H = -0.000183910152091$$

$$\text{CheckCQ} := F \cdot \lambda s^2 + D \cdot \lambda s + H \quad \text{CheckCQ} = -0.000515559050365$$

$$\lambda s\text{RootONE} := \frac{1}{2 \cdot F} \cdot \left(-D + \sqrt{D^2 - 4 \cdot F \cdot H} \right) \quad \lambda s\text{RootONE} = -0.063837329578679$$

$$\lambda s\text{RootTWO} := \frac{1}{2 \cdot F} \cdot \left(-D - \sqrt{D^2 - 4 \cdot F \cdot H} \right) \quad \lambda s\text{RootTWO} = -0.009781566961283$$

Calculate Accelerating H-Force, CHa

$$\begin{aligned} \text{HLamda} := & \left(\frac{1}{2} \cdot \mu \right) \cdot \lambda s^2 - \left(\frac{1}{2} \cdot B \cdot \mu - \frac{2}{3 \cdot \pi} \cdot \mu^2 \right) \cdot \theta_0 \cdot \lambda s - \left(\frac{1}{4} \cdot B^2 \cdot \mu - \frac{1}{16} \cdot \mu^3 \right) \cdot \theta t \cdot \lambda s + \left(\frac{1}{4} \cdot B^2 + \frac{3}{16} \cdot \mu^2 \right) \cdot B1c \cdot \lambda s \dots \\ & + \left(\frac{3}{4} \cdot B^2 - \frac{9}{16} \cdot \mu^2 \right) \cdot a1s \cdot \lambda s - \left(\frac{1}{4} \cdot B \cdot \mu - \frac{12}{5 \cdot \pi} \cdot \mu^2 \right) \cdot b2s \cdot \lambda s - \left(\frac{1}{6} \cdot B^3 + \frac{8}{45 \cdot \pi} \cdot \mu^3 \right) \cdot \theta e1s \cdot \lambda s \end{aligned}$$

$$\text{HLamda} = 0.000409126548125$$

$$\text{HColl} := \left(\frac{1}{3} \cdot B^3 + \frac{2}{9 \cdot \pi} \cdot \mu^3 \right) \cdot a1s \cdot \theta_0 + \left(\frac{3}{8} \cdot B^2 \cdot \mu - \frac{5}{48} \cdot \mu^3 \right) \cdot b2s \cdot \theta_0$$

$$\text{HColl} = 0.001181845724661$$

$$\text{HTwist} := \left(\frac{1}{4} \cdot B^4 + \frac{1}{32} \cdot \mu^4 \right) \cdot a1s \cdot \theta t + \left(\frac{1}{4} \cdot B^3 \cdot \mu - \frac{16}{105 \cdot \pi} \cdot \mu^4 \right) \cdot b2s \cdot \theta t$$

$$\text{HTwist} = -0.000432624523905$$

$$\text{HA1S} := \left(\frac{1}{4} \cdot B^2 \cdot \mu - \frac{3}{16} \cdot \mu^3 \right) \cdot a1s^2 - \left(\frac{1}{4} \cdot B^2 \cdot \mu - \frac{1}{16} \cdot \mu^3 \right) \cdot B1c \cdot a1s - \left(\frac{1}{4} \cdot B^3 - \frac{164}{105 \cdot \pi} \cdot \mu^3 \right) \cdot b2s \cdot a1s + \left(\frac{1}{6} \cdot B^3 \cdot \mu - \frac{4}{45 \cdot \pi} \cdot \mu^4 \right) \cdot \theta e1s \cdot a1s$$

$$\text{HA1S} = 0.002642035801963$$

$$\text{HB1S} := \left(\frac{1}{4} \cdot B^3 + \frac{2}{21 \cdot \pi} \cdot \mu^3 \right) \cdot a2s \cdot b1s - \left(\frac{1}{6} \cdot B^3 + \frac{2}{45 \cdot \pi} \cdot \mu^3 \right) \cdot \beta_0 \cdot b1s - \left(\frac{1}{16} \cdot B^2 \cdot \mu - \frac{1}{96} \cdot \mu^3 \right) \cdot \lambda 1 \cdot b1s$$

$$\text{HB1S} = -0.002253792891716$$

$$\begin{aligned} \text{HConing} := & \left(\frac{1}{4} \cdot B^2 \cdot \mu - \frac{1}{16} \cdot \mu^3 \right) \cdot \beta_0^2 + \left(\frac{1}{6} \cdot B^3 + \frac{2}{45 \cdot \pi} \cdot \mu^3 \right) \cdot A1c \cdot \beta_0 - \left(\frac{1}{6} \cdot B^3 - \frac{2}{9 \cdot \pi} \cdot \mu^3 \right) \cdot \lambda 1 \cdot \beta_0 \dots \\ & + 0 - \left(\frac{1}{2} \cdot B^2 \cdot \mu - \frac{5}{24} \cdot \mu^3 \right) \cdot a2s \cdot \beta_0 - \left(\frac{1}{8} \cdot B^4 + \frac{1}{192} \cdot \mu^4 \right) \cdot \theta e1c \cdot \beta_0 \end{aligned}$$

$$\text{HConing} = 0.002336080274585$$

$$\text{HA2S} := \left(\frac{1}{8} \cdot B^2 \cdot \mu - \frac{11}{64} \cdot \mu^3 \right) \cdot a2s^2 - \left(\frac{1}{4} \cdot B^3 + \frac{2}{21 \cdot \pi} \cdot \mu^3 \right) \cdot A1c \cdot a2s + \left(\frac{3}{16} \cdot B^4 + \frac{3}{256} \cdot \mu^4 \right) \cdot \theta e1c \cdot a2s$$

$$\text{HA2S} = -0.000015799961115$$

$$\text{HB2S} := \left(\frac{1}{8} \cdot B^2 \cdot \mu - \frac{25}{64} \cdot \mu^3 \right) \cdot b2s^2 - \left(\frac{1}{4} \cdot B^3 + \frac{32}{105 \cdot \pi} \cdot \mu^3 \right) \cdot b2s \cdot B1c + \left(\frac{3}{16} \cdot B^4 + \frac{35}{768} \cdot \mu^4 \right) \cdot b2s \cdot \theta e1s$$

$$\text{HB2S} = -0.000355409798295$$

$$\text{HLamdaONE} := \left(\frac{1}{16} \cdot B^2 \cdot \mu - \frac{1}{96} \cdot \mu^3 \right) \cdot A1c \cdot \lambda 1 + \left(\frac{5}{12} \cdot B^3 - \frac{118}{315 \cdot \pi} \cdot \mu^3 \right) \cdot a2s \cdot \lambda 1 - \left(\frac{1}{24} \cdot B^3 \cdot \mu - \frac{4}{315 \cdot \pi} \cdot \mu^4 \right) \cdot \theta e1c \cdot \lambda 1 - \left(\frac{1}{48} \cdot \mu^3 \right) \cdot \lambda 1^2$$

$$\text{HLamdaONE} = -0.000070081855597$$

$$\text{CHa} := \frac{\sigma \cdot a}{2} \cdot (\text{HLamda} + \text{HConing} + \text{HColl} + \text{HTwist} + \text{HA1S} + \text{HB1S} + \text{HA2S} + \text{HB2S} + \text{HLamdaONE})$$

$$\text{CHa} = 0.000962292250614$$

Derive CHa due to inflow from $CHa := \frac{-1 \cdot (CT \cdot \lambda s + CQa)}{\mu}$

$$CHaCheck := \frac{-1 \cdot (CT \cdot \lambda s + CQa)}{\mu} \quad CHaCheck = 0.000962292250614$$

$$\mu \cdot CHa + (CT \cdot \lambda s + CQa) = 0$$

Calculate CH due to Cd

$$CHCdo := \frac{\sigma \cdot Cdo}{8} \cdot \left(2 \cdot \mu + \frac{1}{2} \cdot \mu^3 \right) \quad CHCdo = 0.0002300676$$

$$CH\delta 1 := \sigma \cdot \delta 1 \cdot \left[\left(\frac{1}{4} \cdot \mu \right) \cdot \lambda s + \left(\frac{1}{4} \cdot \mu \right) \cdot \theta o + \left(\frac{1}{6} \cdot \mu \right) \cdot \theta t - \left(\frac{3}{16} \cdot \mu^2 \right) \cdot B1c + \left(\frac{1}{16} \cdot \mu^2 \right) \cdot a1s - \left(\frac{1}{16} \cdot \mu \right) \cdot b2s - \frac{1}{12} \cdot B1c - \frac{1}{12} \cdot a1s + \left(\frac{1}{16} + \frac{3}{32} \cdot \mu^2 \right) \cdot \theta e1s \right]$$

$$CH\delta 1 = -0.000010478826666$$

$$Lamda := \left(\frac{1}{2} \cdot \mu \right) \cdot \lambda s^2 - \left(\frac{1}{2} - \frac{5}{8} \cdot \mu^2 \right) \cdot a1s \cdot \lambda s + \left(\frac{1}{2} \cdot \mu - \frac{1}{8} \cdot \mu^3 \right) \cdot \theta t \cdot \lambda s + \left(\mu - \frac{4}{3 \cdot \pi} \cdot \mu^2 \right) \cdot \theta o \cdot \lambda s \dots$$

$$+ \left(\frac{1}{2} \cdot \mu - \frac{8}{3 \cdot \pi} \cdot \mu^2 \right) \cdot b2s \cdot \lambda s - \left(\frac{1}{2} + \frac{3}{8} \cdot \mu^2 \right) \cdot B1c \cdot \lambda s + \left(\frac{1}{3} + \frac{16}{45 \cdot \pi} \cdot \mu^3 \right) \cdot \theta e1s \cdot \lambda s$$

$$Lamda = 0.000121323401491$$

$$Coll := \left(\frac{1}{2} \cdot \mu + \frac{1}{8} \cdot \mu^3 \right) \cdot \theta o^2 + \left(\frac{2}{3} \cdot \mu + \frac{8}{45 \cdot \pi} \cdot \mu^4 \right) \cdot \theta t \cdot \theta o - \left(\frac{1}{3} - \frac{1}{4} \cdot \mu^2 + \frac{28}{45 \cdot \pi} \cdot \mu^3 \right) \cdot a1s \cdot \theta o \dots$$

$$+ 0 - \left(\frac{1}{4} \cdot \mu - \frac{7}{24} \cdot \mu^3 \right) \cdot b2s \cdot \theta o - \left(\frac{1}{3} + \frac{3}{4} \cdot \mu^2 - \frac{32}{45 \cdot \pi} \cdot \mu^3 \right) \cdot B1c \cdot \theta o + \left(\frac{1}{4} - \frac{5}{96} \cdot \mu^4 + \frac{3}{8} \cdot \mu^2 \right) \cdot \theta e1s \cdot \theta o$$

$$Coll = -0.00052016543129$$

$$Twist := \left(\frac{1}{4} \cdot \mu + \frac{1}{96} \cdot \mu^5 \right) \cdot \theta t^2 - \left(\frac{1}{4} - \frac{1}{8} \cdot \mu^2 + \frac{7}{96} \cdot \mu^4 \right) \cdot a1s \cdot \theta t - \left(\frac{1}{6} \cdot \mu - \frac{16}{45 \cdot \pi} \cdot \mu^4 \right) \cdot b2s \cdot \theta t \dots$$

$$+ 0 - \left(\frac{1}{4} + \frac{3}{8} \cdot \mu^2 - \frac{5}{96} \cdot \mu^4 \right) \cdot B1c \cdot \theta t + \left(\frac{1}{5} + \frac{1}{4} \cdot \mu^2 - \frac{32}{525 \cdot \pi} \cdot \mu^5 \right) \cdot \theta e1s \cdot \theta t$$

$$Twist = 0.000317427243898$$

$$Coning := \left(\frac{1}{8} \cdot \mu^3 \right) \cdot \beta o^2 + \left(\frac{1}{2} \cdot \mu - \frac{1}{4} \cdot \mu^3 \right) \cdot a2s \cdot \beta o - \left(\frac{1}{4} \cdot \mu^2 - \frac{4}{15 \cdot \pi} \cdot \mu^3 \right) \cdot b1s \cdot \beta o \dots$$

$$+ \left(\frac{1}{4} \cdot \mu^2 - \frac{4}{15 \cdot \pi} \cdot \mu^3 \right) \cdot A1c \cdot \beta o - \left(\frac{4}{15 \cdot \pi} \cdot \mu^3 \right) \cdot \lambda 1 \cdot \beta o + \left(\frac{1}{48} \cdot \mu^4 - \frac{1}{8} \cdot \mu^2 \right) \cdot \theta e1c \cdot \beta o$$

$$Coning = 0.000240672049834$$

$$A1S := \left(\frac{1}{3} + \frac{1}{4} \cdot \mu^2 - \frac{584}{315 \cdot \pi} \cdot \mu^3 \right) \cdot b2s \cdot a1s - \left(\frac{1}{8} \cdot \mu - \frac{11}{48} \cdot \mu^3 \right) \cdot a1s^2 + \left(\frac{1}{4} \cdot \mu - \frac{1}{6} \cdot \mu^3 \right) \cdot B1c \cdot a1s - \left(\frac{1}{6} \cdot \mu - \frac{64}{315 \cdot \pi} \cdot \mu^4 \right) \cdot \theta e1s \cdot a1s$$

$$A1S = -0.001969318014698$$

$$B1S := \left(\frac{1}{8} \cdot \mu + \frac{1}{48} \cdot \mu^3 \right) \cdot b1s^2 - \left(\frac{1}{3} + \frac{52}{315\pi} \cdot \mu^3 \right) \cdot a2s \cdot b1s + \left(\frac{1}{8} \cdot \mu - \frac{1}{48} \cdot \mu^3 \right) \cdot \lambda1 \cdot b1s - \left(\frac{1}{4} \cdot \mu + \frac{1}{24} \cdot \mu^3 \right) \cdot A1c \cdot b1s \dots$$

$$+ \left(\frac{1}{6} \cdot \mu + \frac{8}{315\pi} \cdot \mu^4 \right) \cdot \theta e1c \cdot b1s$$

$$B1S = 0.000210416370366$$

$$A2B2 := \left(\frac{43}{96} \cdot \mu^3 \right) \cdot b2s^2 + \left(\frac{17}{96} \cdot \mu^3 \right) \cdot a2s^2$$

$$A2B2 = 0.000330570070475$$

$$EXTRAone := \left(\frac{3}{8} \cdot \mu + \frac{5}{48} \cdot \mu^3 \right) \cdot B1c^2 + \left(\frac{1}{3} - \frac{1}{4} \cdot \mu^2 + \frac{256}{315\pi} \cdot \mu^3 \right) \cdot b2s \cdot B1c + \left(\frac{1}{8} \cdot \mu + \frac{1}{48} \cdot \mu^3 \right) \cdot A1c^2 + \left(\frac{1}{3} + \frac{52}{315\pi} \cdot \mu^3 \right) \cdot a2s \cdot A1c$$

$$EXTRAone = 0.001011177876538$$

$$EXTRAtwo := \left(\frac{1}{48} \cdot \mu^3 \right) \cdot \lambda1^2 - \left(\frac{1}{3} - \frac{116}{315\pi} \cdot \mu^3 \right) \cdot a2s \cdot \lambda1 - \left(\frac{1}{8} \cdot \mu - \frac{1}{48} \cdot \mu^3 \right) \cdot A1c \cdot \lambda1$$

$$EXTRAtwo = 0.000069490620782$$

$$Elastic := \left(\frac{1}{12} \cdot \mu - \frac{8}{315\pi} \cdot \mu^4 \right) \cdot \theta e1c \cdot \lambda1 - \left(\frac{1}{6} \cdot \mu + \frac{8}{315\pi} \cdot \mu^4 \right) \cdot \theta e1c \cdot A1c - \left(\frac{16}{105\pi} \cdot \mu^4 + \frac{1}{2} \cdot \mu \right) \cdot \theta e1s \cdot B1c \dots$$

$$+ \left(\frac{3}{16} \cdot \mu + \frac{7}{768} \cdot \mu^5 \right) \cdot \theta e1s^2 + \left(\frac{1}{16} \cdot \mu + \frac{1}{768} \cdot \mu^5 \right) \cdot \theta e1c^2 - \left(\frac{1}{4} - \frac{1}{8} \cdot \mu^2 + \frac{5}{48} \cdot \mu^4 \right) \cdot \theta e1s \cdot b2s - \left(\frac{1}{4} + \frac{1}{48} \cdot \mu^4 \right) \cdot \theta e1c \cdot a2s$$

$$Elastic = -0.00049300484576$$

$$CH\delta2 := \frac{\sigma \cdot \delta2}{2} \cdot (Lamda + Coll + Twist + Coning + A1S + B1S + A2B2 + EXTRAone + EXTRAtwo + Elastic)$$

$$CH\delta2 = -0.000013301136051$$

$$CHd := CHCdo + CH\delta1 + CH\delta2$$

$$CHd = 0.000206287637283$$

Calculate Total CH

$$CH := CHa + CHd$$

$$CH = 0.001168579887897$$

Calculate CY due to CL (Y-force positive to $\psi = 90$ deg)

$$Lamda := \left(\frac{3}{4} \cdot B^2 + \frac{5}{16} \cdot \mu^2 \right) \cdot b1s \cdot \lambda s - \left(\frac{3}{2} \cdot B \cdot \mu - \frac{2}{\pi} \cdot \mu^2 \right) \cdot \beta o \cdot \lambda s + \left(\frac{1}{4} \cdot B \cdot \mu - \frac{14}{15\pi} \cdot \mu^2 \right) \cdot a2s \cdot \lambda s \dots$$

$$+ \left(\frac{1}{2} \cdot B^2 - \frac{1}{8} \cdot \mu^2 \right) \cdot \lambda1 \cdot \lambda s - \left(\frac{1}{4} \cdot B^2 + \frac{1}{16} \cdot \mu^2 \right) \cdot A1c \cdot \lambda s + \left(\frac{1}{6} \cdot B^3 + \frac{2}{45\pi} \cdot \mu^3 \right) \cdot \theta e1c \cdot \lambda s$$

$$Lamda = 0.000124005711733$$

$$\text{Coll} := \left(\frac{1}{3} \cdot B^3 + \frac{1}{2} \cdot B \cdot \mu^2 - \frac{4}{9 \cdot \pi} \cdot \mu^3 \right) \cdot b1s \cdot \theta o - \left(\frac{3}{4} \cdot B^2 \cdot \mu + \frac{3}{16} \cdot \mu^3 \right) \cdot \beta o \cdot \theta o - \left(\frac{3}{8} \cdot B^2 \cdot \mu + \frac{1}{24} \cdot \mu^3 \right) \cdot a2s \cdot \theta o + \left(\frac{1}{6} \cdot B^3 + \frac{2}{45 \cdot \pi} \cdot \mu^3 \right) \cdot \lambda 1 \cdot \theta o$$

Coll = -0.000762255150436

$$\text{Twist} := \left(\frac{1}{4} \cdot B^4 + \frac{1}{4} \cdot B^2 \cdot \mu^2 - \frac{1}{32} \cdot \mu^4 \right) \cdot b1s \cdot \theta t - \left(\frac{1}{2} \cdot B^3 \cdot \mu + \frac{2}{15 \cdot \pi} \cdot \mu^4 \right) \cdot \beta o \cdot \theta t - \left(\frac{1}{4} \cdot B^3 \cdot \mu + \frac{2}{105 \cdot \pi} \cdot \mu^4 \right) \cdot a2s \cdot \theta t + \left(\frac{1}{8} \cdot B^4 + \frac{1}{192} \cdot \mu^4 \right) \cdot \lambda 1 \cdot \theta t$$

Twist = 0.00015180487599

$$\begin{aligned} \text{Coning} := & \left(\frac{1}{6} \cdot B^3 - B \cdot \mu^2 + \frac{68}{45 \cdot \pi} \cdot \mu^3 \right) \cdot a1s \cdot \beta o - \left(\frac{1}{2} \cdot B^2 \cdot \mu + \frac{11}{24} \cdot \mu^3 \right) \cdot b2s \cdot \beta o \dots \\ & + \left(\frac{1}{6} \cdot B^3 + \frac{1}{2} \cdot B \cdot \mu^2 - \frac{22}{45 \cdot \pi} \cdot \mu^3 \right) \cdot B1c \cdot \beta o - \left(\frac{1}{8} \cdot B^4 + \frac{1}{4} \cdot B^2 \cdot \mu^2 - \frac{7}{192} \cdot \mu^4 \right) \cdot \theta e1s \cdot \beta o \end{aligned}$$

Coning = -0.001266285819158

$$\begin{aligned} A1S := & \left(\frac{1}{4} \cdot B^2 \cdot \mu + \frac{3}{16} \cdot \mu^3 \right) \cdot a1s \cdot b1s + \left(\frac{1}{4} \cdot B^3 + \frac{1}{2} \cdot B \cdot \mu^2 - \frac{116}{105 \cdot \pi} \cdot \mu^3 \right) \cdot a2s \cdot a1s \dots \\ & + \left(\frac{7}{16} \cdot B^2 \cdot \mu - \frac{11}{96} \cdot \mu^3 \right) \cdot \lambda 1 \cdot a1s - \left(\frac{1}{4} \cdot B^2 \cdot \mu + \frac{1}{16} \cdot \mu^3 \right) \cdot A1c \cdot a1s + \left(\frac{1}{6} \cdot B^3 \cdot \mu + \frac{2}{45 \cdot \pi} \cdot \mu^4 \right) \cdot \theta e1c \cdot a1s \end{aligned}$$

A1S = 0.005161236802228

$$B1S := \left(\frac{1}{4} \cdot B^3 + \frac{1}{2} \cdot B \cdot \mu^2 - \frac{16}{21 \cdot \pi} \cdot \mu^3 \right) \cdot b2s \cdot b1s - \left(\frac{1}{2} \cdot B^2 \cdot \mu + \frac{1}{8} \cdot \mu^3 \right) \cdot B1c \cdot b1s + \left(\frac{1}{3} \cdot B^3 \cdot \mu + \frac{4}{45 \cdot \pi} \cdot \mu^4 \right) \cdot \theta e1s \cdot b1s$$

B1S = -0.001006158164124

$$A2 := \left(\frac{7}{32} \cdot \mu^3 \right) \cdot b2s \cdot a2s + \left(\frac{1}{4} \cdot B^3 + \frac{1}{4} \cdot B \cdot \mu^2 - \frac{6}{35 \cdot \pi} \cdot \mu^3 \right) \cdot B1c \cdot a2s - \left(\frac{3}{16} \cdot B^4 + \frac{1}{8} \cdot B^2 \cdot \mu^2 - \frac{7}{768} \cdot \mu^4 \right) \cdot \theta e1s \cdot a2s$$

A2 = -0.000298358384238

$$B2 := \left(\frac{5}{12} \cdot B^3 + \frac{104}{315 \cdot \pi} \cdot \mu^3 \right) \cdot \lambda 1 \cdot b2s - \left(\frac{1}{4} \cdot B^3 + \frac{1}{4} \cdot B \cdot \mu^2 - \frac{8}{35 \cdot \pi} \cdot \mu^3 \right) \cdot A1c \cdot b2s + \left(\frac{3}{16} \cdot B^4 + \frac{1}{8} \cdot B^2 \cdot \mu^2 - \frac{13}{768} \cdot \mu^4 \right) \cdot \theta e1c \cdot b2s$$

B2 = 0.000207494277531

$$\text{EXTRA} := \left(\frac{1}{24} \cdot B^3 \cdot \mu - \frac{4}{315 \cdot \pi} \cdot \mu^4 \right) \cdot \theta e1s \cdot \lambda 1 - \left(\frac{1}{16} \cdot \mu \cdot B^2 - \frac{1}{96} \cdot \mu^3 \right) \cdot B1c \cdot \lambda 1 \quad \text{EXTRA} = -0.000006300274309$$

$$\text{CYa} := \frac{\sigma \cdot a}{2} \cdot (\text{Lamda} + \text{Coning} + \text{Coll} + \text{Twist} + A1S + B1S + A2 + B2 + \text{EXTRA})$$

CYa = 0.000644584735924

Calculate CY due to Cd

$$\text{CYCdo} := 0$$

$$\text{CY}\delta 1 := \frac{\sigma \cdot \delta 1}{2} \cdot \left[\left(\frac{1}{6} + \frac{1}{8} \cdot \mu^2 \right) \cdot A1c - \left(\frac{1}{6} + \frac{1}{8} \cdot \mu^2 \right) \cdot b1s - \left(\frac{1}{8} + \frac{1}{16} \cdot \mu^2 \right) \cdot \theta e1c + \left(\frac{1}{4} \cdot \mu \right) \cdot \beta o + \left(\frac{1}{8} \cdot \mu \right) \cdot a2s - \frac{1}{6} \cdot \lambda 1 \right]$$

$$\text{CY}\delta 1 = 6.45796792525479310^{-7}$$

$$\begin{aligned} \text{Lamda} := & \left(\frac{1}{2} + \frac{1}{8} \cdot \mu^2 \right) \cdot b1s \cdot \lambda s - \left(\mu - \frac{4}{3 \cdot \pi} \cdot \mu^2 \right) \cdot \beta o \cdot \lambda s + \left(\frac{1}{2} \cdot \mu - \frac{4}{3 \cdot \pi} \cdot \mu^2 \right) \cdot a2s \cdot \lambda s - \left(\frac{1}{2} + \frac{1}{16} \cdot \mu^2 \right) \cdot A1c \cdot \lambda s \dots \\ & + \left(\frac{1}{2} - \frac{1}{8} \cdot \mu^2 \right) \cdot \lambda 1 \cdot \lambda s + \left(\frac{1}{3} + \frac{2}{45 \cdot \pi} \cdot \mu^3 \right) \cdot \theta e1c \cdot \lambda s \end{aligned}$$

$$\text{Lamda} = 0.000024304101028$$

$$\begin{aligned} \text{Coll} := & \left(\frac{1}{3} + \frac{1}{4} \cdot \mu^2 - \frac{4}{45 \cdot \pi} \cdot \mu^3 \right) \cdot \theta o \cdot b1s - \left(\frac{1}{2} \cdot \mu + \frac{1}{16} \cdot \mu^3 \right) \cdot \theta o \cdot \beta o - \left(\frac{1}{4} \cdot \mu - \frac{1}{24} \cdot \mu^3 \right) \cdot \theta o \cdot a2s - \left(\frac{1}{3} + \frac{1}{4} \cdot \mu^2 - \frac{8}{45 \cdot \pi} \cdot \mu^3 \right) \cdot \theta o \cdot A1c \dots \\ & + \left(\frac{1}{3} + \frac{2}{45 \cdot \pi} \cdot \mu^3 \right) \cdot \theta o \cdot \lambda 1 + \left(\frac{1}{4} + \frac{1}{8} \cdot \mu^2 - \frac{1}{96} \cdot \mu^4 \right) \cdot \theta o \cdot \theta e1c \end{aligned}$$

$$\text{Coll} = -0.00008715682354$$

$$\begin{aligned} \text{Twist} := & \left(\frac{1}{4} + \frac{1}{8} \cdot \mu^2 - \frac{1}{192} \cdot \mu^4 \right) \cdot \theta t \cdot b1s - \left(\frac{1}{3} \cdot \mu + \frac{2}{45 \cdot \pi} \cdot \mu^4 \right) \cdot \theta t \cdot \beta o - \left(\frac{1}{6} \cdot \mu - \frac{2}{45 \cdot \pi} \cdot \mu^4 \right) \cdot \theta t \cdot a2s - \left(\frac{1}{4} + \frac{1}{8} \cdot \mu^2 - \frac{1}{96} \cdot \mu^4 \right) \cdot \theta t \cdot A1c \dots \\ & + \left(\frac{1}{4} + \frac{1}{192} \cdot \mu^4 \right) \cdot \theta t \cdot \lambda 1 + \left(\frac{1}{5} + \frac{1}{12} \cdot \mu^2 - \frac{16}{1575 \cdot \pi} \cdot \mu^5 \right) \cdot \theta t \cdot \theta e1c \end{aligned}$$

$$\text{Twist} = -0.000026625155014$$

$$\text{Coning} := \left(\frac{1}{4} \cdot \mu^2 - \frac{2}{15 \cdot \pi} \cdot \mu^3 \right) \cdot \beta o \cdot B1c - \left(\frac{3}{4} \cdot \mu^2 - \frac{16}{15 \cdot \pi} \cdot \mu^3 \right) \cdot \beta o \cdot a1s - \left(\frac{1}{2} \cdot \mu + \frac{1}{4} \cdot \mu^3 \right) \cdot \beta o \cdot b2s - \left(\frac{1}{8} \cdot \mu^2 - \frac{1}{96} \cdot \mu^4 \right) \cdot \theta e1s \cdot \beta o$$

$$\text{Coning} = -0.002688705597424$$

$$\begin{aligned} A1S := & \left(\frac{1}{4} \cdot \mu + \frac{1}{12} \cdot \mu^3 \right) \cdot a1s \cdot b1s + \left(\frac{1}{3} + \frac{1}{2} \cdot \mu^2 - \frac{368}{315 \cdot \pi} \cdot \mu^3 \right) \cdot a1s \cdot a2s - \left(\frac{1}{4} \cdot \mu + \frac{1}{24} \cdot \mu^3 \right) \cdot a1s \cdot A1c \dots \\ & + \left(\frac{3}{8} \cdot \mu - \frac{5}{48} \cdot \mu^3 \right) \cdot a1s \cdot \lambda 1 + \left(\frac{1}{6} \cdot \mu + \frac{2}{63 \cdot \pi} \cdot \mu^4 \right) \cdot a1s \cdot \theta e1c \end{aligned}$$

$$A1S = 0.005117767180249$$

$$B1S := \left(\frac{1}{3} + \frac{1}{4} \cdot \mu^2 - \frac{16}{63 \cdot \pi} \cdot \mu^3 \right) \cdot b1s \cdot b2s - \left(\frac{1}{4} \cdot \mu + \frac{1}{48} \cdot \mu^3 \right) \cdot b1s \cdot B1c + \left(\frac{1}{6} \cdot \mu + \frac{4}{315 \cdot \pi} \cdot \mu^4 \right) \cdot b1s \cdot \theta e1s$$

$$B1S = -0.001943681093466$$

$$A2 := \left(\frac{1}{3} + \frac{26}{315 \cdot \pi} \cdot \mu^3 \right) \cdot a2s \cdot B1c - \left(\frac{1}{4} + \frac{1}{96} \cdot \mu^4 \right) \cdot a2s \cdot \theta e1s + \left(\frac{13}{48} \cdot \mu^3 \right) \cdot b2s \cdot a2s$$

$$A2 = -0.000318138388903$$

$$B2 := \left(\frac{1}{3} + \frac{88}{315 \cdot \pi} \cdot \mu^3 \right) \cdot b2s \cdot \lambda 1 - \left(\frac{1}{3} + \frac{1}{4} \cdot \mu^2 - \frac{8}{63 \cdot \pi} \cdot \mu^3 \right) \cdot b2s \cdot A1c + \left(\frac{1}{4} + \frac{1}{8} \cdot \mu^2 - \frac{1}{96} \cdot \mu^4 \right) \cdot b2s \cdot \theta e1c$$

$$B2 = 0.000214119551942$$

$$\lambda_{11} := \left(\frac{1}{12} \cdot \mu - \frac{4}{315\pi} \cdot \mu^4 \right) \cdot \lambda_1 \cdot \theta_{e1s} - \left(\frac{1}{8} \cdot \mu - \frac{1}{96} \cdot \mu^3 \right) \cdot \lambda_1 \cdot B1c$$

$$\lambda_{11} = -0.000014053554352$$

$$\text{Extra} := \left(\frac{1}{4} \cdot \mu + \frac{1}{24} \cdot \mu^3 \right) \cdot A1c \cdot B1c - \left(\frac{1}{6} \cdot \mu + \frac{8}{315\pi} \cdot \mu^4 \right) \cdot A1c \cdot \theta_{e1s} - \left(\frac{1}{6} \cdot \mu + \frac{8}{315\pi} \cdot \mu^4 \right) \cdot B1c \cdot \theta_{e1c} + \left(\frac{1}{8} \cdot \mu + \frac{1}{384} \cdot \mu^5 \right) \cdot \theta_{e1s} \cdot \theta_{e1c}$$

$$\text{Extra} = -0.000033720559476$$

$$CY_{\delta 2} := \left(-1 \cdot \frac{\sigma \cdot \delta 2}{2} \right) \cdot (\text{Lamda} + \text{Coll} + \text{Twist} + \text{Coning} + A1S + B1S + A2 + B2 + \lambda_{11} + \text{Extra})$$

$$CY_{\delta 2} = -0.000004765020584$$

$$CY_d := CY_{Cdo} + CY_{\delta 1} + CY_{\delta 2}$$

$$CY_d = -0.000004119223791$$

Calculate Total CY

$$CY := CY_a + CY_d$$

$$CY = 0.000640465512133$$

Calculate Shaft Angle of Attack

$$\alpha_s := \text{atan} \left(\frac{\lambda_s}{\mu} + \frac{1}{2} \cdot \frac{CT}{\mu \cdot \sqrt{\mu^2 + \lambda_s^2}} \right) \quad \alpha_s = 0.027326303405535$$

Repeat Input (Angles now in degrees)

$$\mu = 0.7 \quad \lambda_s = 0.013 \quad \lambda_1 = -0.007287534590767 \quad \gamma = 19.2 \quad B = 0.97 \quad \sigma = 0.0976$$
$$a = 5.73$$

$$\theta_o \cdot \frac{180}{\pi} = 1.9 \quad \theta_t \cdot \frac{180}{\pi} = -1 \quad B1c \cdot \frac{180}{\pi} = -2 \quad A1c \cdot \frac{180}{\pi} = 1 \quad \theta_{e1s} \cdot \frac{180}{\pi} = -1 \quad \theta_{e1c} \cdot \frac{180}{\pi} = 1$$

$$Cdo = 0.012 \quad \delta_1 = -0.0216 \quad \delta_2 = 0.4$$

Summarize Output

$$\beta_o \cdot \frac{180}{\pi} = 8.474827357622401 \quad a1s \cdot \frac{180}{\pi} = 7.801747523038808 \quad b1s \cdot \frac{180}{\pi} = 7.890124244695535$$
$$a2s \cdot \frac{180}{\pi} = 1.579548305207202 \quad b2s \cdot \frac{180}{\pi} = -2.465172362211013$$

$$CT = 0.008587925651381 \quad CH = 0.001168579887897 \quad CY = 0.000640465512133$$

$$CQ = -0.000515559050365$$

$$\alpha_s \cdot \frac{180}{\pi} = 1.565681854831141$$

$$\text{RotorCL} := CT \cdot \cos(\alpha_s) - CH \cdot \sin(\alpha_s)$$

$$\text{RotorCL} = 0.008552790439016$$

$$\text{RotorCD} := CT \cdot \sin(\alpha_s) + CH \cdot \cos(\alpha_s)$$

$$\text{RotorCD} = 0.001402790666605$$

$$\text{RotorCY} := CY$$

$$\text{RotorCY} = 0.000640465512133$$

$$\text{AirplaneCL} := \frac{2}{\mu^2} \cdot (\text{RotorCL})$$

$$\text{AirplaneCL} = 0.034909348730678$$

$$\text{AirplaneCD} := \frac{2}{\mu^2} \cdot (\text{RotorCD})$$

$$\text{AirplaneCD} = 0.005725676190225$$

$$\text{AirplaneCY} := 2 \cdot \frac{CY}{\mu^2}$$

$$\text{AirplaneCY} = 0.002614144947481$$

11.3 H-34 Blade Section Properties

Notations

MASS: section mass

EIFLAP: flap bending stiffness

EILAG: lag bending stiffness

EA: axial stiffness

GJ: torsion stiffness

ITHETA: section moment of inertia

IPOLAR: section polar inertia

XEA: chordwise beam axis

XI: chordwise center of gravity

KP: polar radius of gyration

KT: extension/torsion coupling

r/R	MASS	EIFLAP	EILAG	EA	GJ	ITHETA	IPOLAR	XEA	XI	KP	KT
	slug/ft	lb-ft ²	lb-ft ²	lb	lb-ft ²	slug-ft ² /ft	slug-ft ² /ft	x/R	x/R	x/R	x/R
0	2.05	5.40E+05	6.50E+06	1.40E+07	8.30E+05	0.129	0.129	0	0	0.0104	0.0104
0.033	2.05	5.40E+05	6.50E+06	1.40E+07	8.30E+05	0.129	0.129	0	0	0.0104	0.0104
0.038	2.05	1.04E+06	1.74E+06	1.40E+07	8.30E+05	0.129	0.129	0	0	0.0104	0.0104
0.049	2.05	3.47E+06	3.21E+06	1.40E+07	8.30E+05	0.129	0.129	0	0	0.0104	0.0104
0.068	1.77	3.47E+06	3.21E+06	1.40E+07	8.30E+05	6.80E-02	6.80E-02	0	0	0.0104	0.0104
0.082	0.612	2.23E+06	6.40E+05	1.40E+07	3.10E+05	4.80E-02	4.80E-02	0	0	0.0104	0.0104
0.093	0.399	1.10E+06	2.36E+06	1.40E+07	3.10E+05	2.30E-02	2.30E-02	0	0	0.0104	0.0104
0.109	0.131	2.10E+05	1.39E+06	1.40E+07	1.53E+05	6.00E-03	6.00E-03	0	0	0.0104	0.0104
0.15	0.131	1.19E+05	1.19E+06	1.40E+07	1.46E+05	1.20E-02	1.20E-02	0	0	0.0104	0.0104
0.199	0.157	1.19E+05	1.19E+06	1.40E+07	1.39E+05	1.60E-02	1.60E-02	0	0	0.0104	0.0104
0.219	0.205	1.02E+05	1.11E+06	1.40E+07	1.25E+05	1.75E-02	1.75E-02	0	0	0.0104	0.0104
0.861	0.205	1.02E+05	1.11E+06	1.40E+07	1.25E+05	1.75E-02	1.75E-02	0	0	0.0104	0.0104
0.885	0.354	1.02E+05	1.11E+06	1.40E+07	1.25E+05	1.75E-02	1.75E-02	0	0	0.0104	0.0104
1	0.093	1.02E+05	1.11E+06	1.40E+07	1.25E+05	1.75E-02	1.75E-02	0	0	0.0104	0.0104

11.4 UH-1 Blade Section Properties

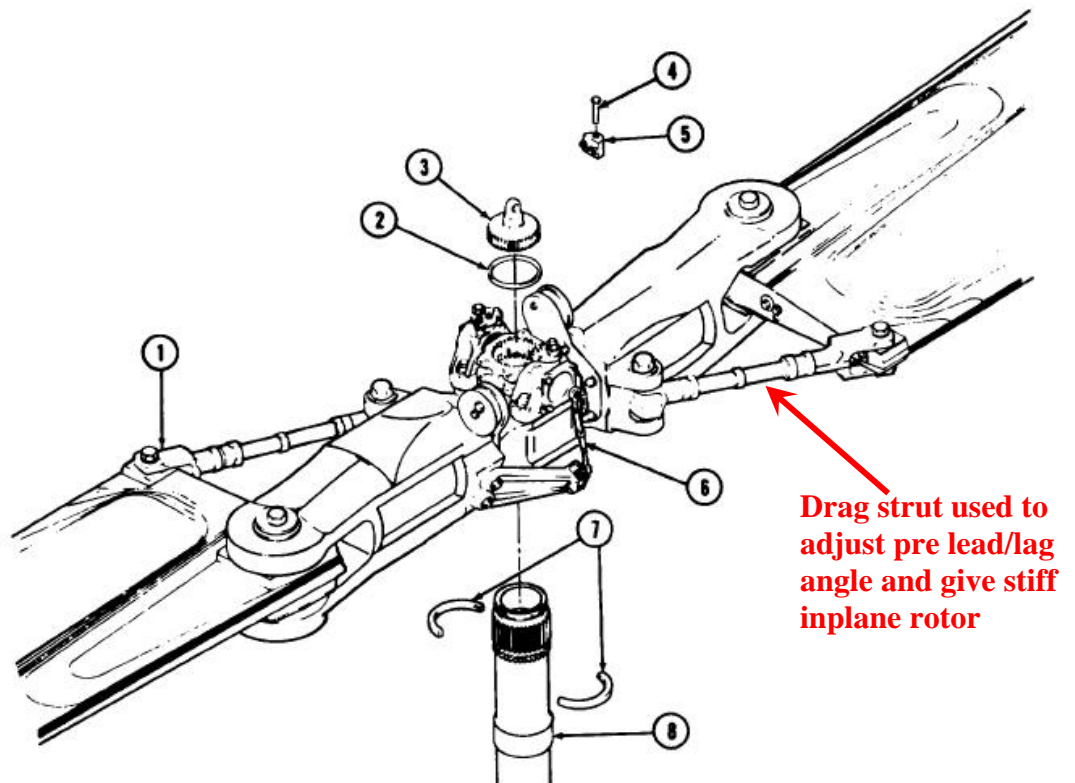
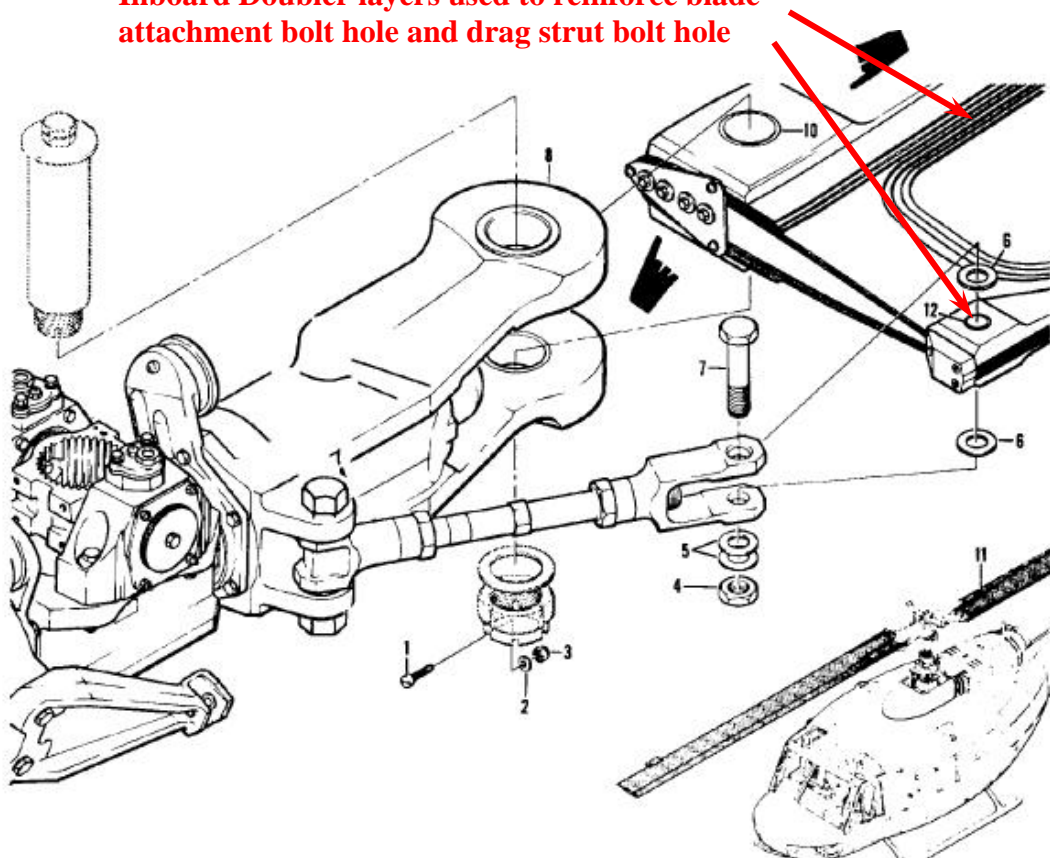
Notations: See Appendix 11.3

Reference: Lee, B.L. Experimental Measurements of the Rotating Frequencies and Mode Shapes of a Full Scale Helicopter Rotor in a Vacuum and Correlations with Calculated Results [69]

r/R	MASS	EI FLAP	EI LAG	EA	GJ	ITHETA	IPOLAR	XEA	XI	KP	KT
	slug/ft	lb-ft ²	lb-ft ²	lb	lb-ft ²	slug-ft ² /ft	slug-ft ² /ft	x/R	x/R	x/R	x/R
0	4.9689	5.24E+07	2.32E+08	1.40E+08	1.17E+08	0.94267	0.56107	-0.0056	0	0.06375	0.06375
0.0168	4.9689	5.24E+07	2.32E+08	1.40E+08	1.17E+08	0.94267	0.56107	-0.0056	0	0.06375	0.06375
0.0298	2.4559	2.95E+07	7.27E+07	1.36E+08	1.83E+07	0.38255	0.16735	-0.0056	0.00666	0.03885	0.03885
0.0429	0.7751	2.43E+06	5.63E+07	1.31E+08	4.81E+05	0.20882	0.19078	-0.00588	0.01198	0.02993	0.02993
0.0504	0.5139	1.06E+06	3.43E+07	1.29E+08	3.83E+05	0.13245	0.12417	-0.00603	0.01087	0.02343	0.02343
0.0578	0.4954	1.01E+06	3.13E+07	1.27E+08	3.76E+05	0.15821	7.90E-02	-0.00614	0.01035	0.02261	0.02261
0.0839	0.4660	9.12E+05	2.87E+07	1.18E+08	3.64E+05	0.11271	0.10549	-0.00638	0.01022	0.02244	0.02244
0.1082	0.4252	7.69E+05	2.61E+07	1.10E+08	3.53E+05	0.13016	6.86E-02	-0.00674	0.01028	0.02212	0.02212
0.1269	0.3863	6.33E+05	2.46E+07	1.04E+08	3.31E+05	9.63E-02	9.11E-02	-0.00703	0.01058	0.02207	0.02207
0.1436	0.3567	5.44E+05	2.35E+07	9.85E+07	3.12E+05	9.15E-02	8.71E-02	-0.00729	0.01071	0.0221	0.0221
0.1567	0.3345	4.77E+05	2.30E+07	9.42E+07	2.97E+05	8.92E-02	8.54E-02	-0.00752	0.01106	0.02233	0.02233
0.1772	0.3119	4.22E+05	2.12E+07	8.75E+07	2.89E+05	8.27E-02	7.92E-02	-0.00774	0.01091	0.02225	0.02225
0.19.04	0.2896	3.65E+05	2.04E+07	8.20E+07	2.82E+05	7.96E-02	7.66E-02	-0.008	0.01139	0.02254	0.02254
0.2108	0.2721	3.24E+05	1.98E+07	7.65E+07	2.52E+05	7.70E-02	7.43E-02	-0.00825	0.01189	0.02294	0.02294
0.2257	0.2567	2.92E+05	1.91E+07	7.16E+07	2.46E+05	7.43E-02	7.19E-02	-0.00847	0.01243	0.0233	0.0233
0.2612	0.2417	2.66E+05	1.81E+07	6.00E+07	2.36E+05	7.07E-02	6.85E-02	-0.00853	0.0127	0.02479	0.02479
0.2985	0.2387	2.66E+05	1.70E+07	6.00E+07	2.15E+05	6.74E-02	6.53E-02	-0.00843	0.01202	0.02404	0.02404
0.3358	0.2357	2.65E+05	1.59E+07	6.00E+07	2.08E+05	6.41E-02	6.19E-02	-0.00834	0.01133	0.02325	0.02325
0.3731	0.2328	2.65E+05	1.48E+07	6.00E+07	2.02E+05	6.08E-02	5.86E-02	-0.00823	0.01063	0.02246	0.02246
0.4104	0.1970	2.09E+05	1.34E+07	6.00E+07	1.87E+05	5.49E-02	5.32E-02	-0.00812	0.01166	0.02135	0.02135
0.4477	0.1946	2.08E+05	1.25E+07	6.00E+07	1.80E+05	5.20E-02	5.03E-02	-0.008	0.01094	0.02058	0.02058
0.4850	0.1922	2.08E+05	1.15E+07	6.00E+07	1.74E+05	4.90E-02	4.73E-02	-0.00791	0.01023	0.01978	0.01978
0.5223	0.1901	2.08E+05	1.06E+07	6.00E+07	1.71E+05	4.62E-02	4.45E-02	-0.00782	0.00957	0.01903	0.01903
0.6007	0.1872	2.08E+05	9.42E+06	6.00E+07	1.71E+05	4.21E-02	4.04E-02	-0.00765	0.0086	0.01794	0.01794
0.6716	0.2239	2.09E+05	8.40E+06	6.00E+07	1.71E+05	4.29E-02	4.12E-02	-0.00744	0.00423	0.01696	0.01696
0.7089	0.2219	2.09E+05	7.58E+06	6.00E+07	1.71E+05	3.94E-02	3.76E-02	-0.00729	0.00357	0.01613	0.01613
0.7462	0.2213	2.09E+05	7.30E+06	6.00E+07	1.71E+05	3.82E-02	3.65E-02	-0.00718	0.00329	0.01584	0.01584
0.8208	0.2214	2.09E+05	7.30E+06	6.00E+07	1.71E+05	3.86E-02	3.69E-02	-0.00703	0.00317	0.01584	0.01584
0.8955	0.2217	2.09E+05	7.30E+06	6.00E+07	1.71E+05	3.90E-02	3.73E-02	-0.00683	0.00303	0.01584	0.01584
0.9380	0.2327	2.23E+05	7.70E+06	6.00E+07	1.76E+05	4.01E-02	3.83E-02	-0.00666	0.00234	0.01627	0.01627
0.9503	0.3983	2.23E+05	7.70E+06	6.00E+07	1.76E+05	4.01E-02	3.83E-02	-0.00658	0.00226	0.01627	0.01627
0.9802	0.6300	4.32E+05	8.36E+06	6.00E+07	5.23E+05	4.15E-02	3.83E-02	-0.00652	0.00293	0.01714	0.01714
1	0.2327	2.23E+05	7.70E+06	6.00E+07	1.76E+05	4.01E-02	3.83E-02	-0.00645	0.00213	0.01627	0.01627



Inboard Doubler layers used to reinforce blade attachment bolt hole and drag strut bolt hole

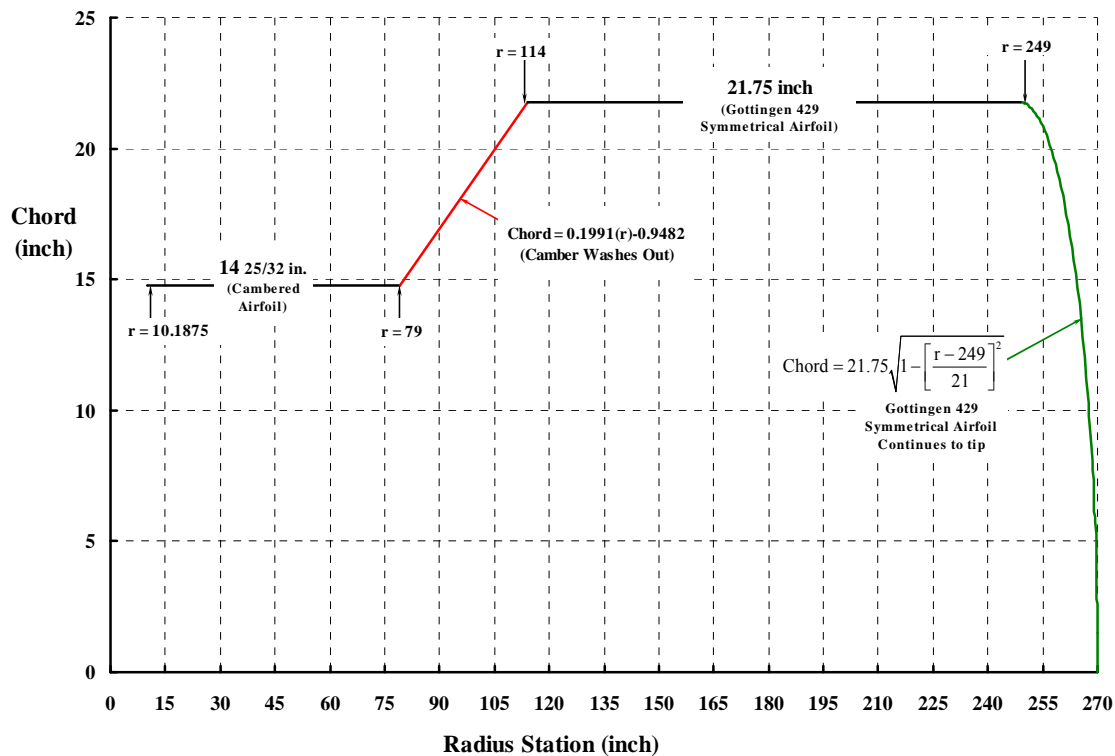


Appendix 11.4. Figure 2. Courtesy of Tom Wood, Bell Helicopter

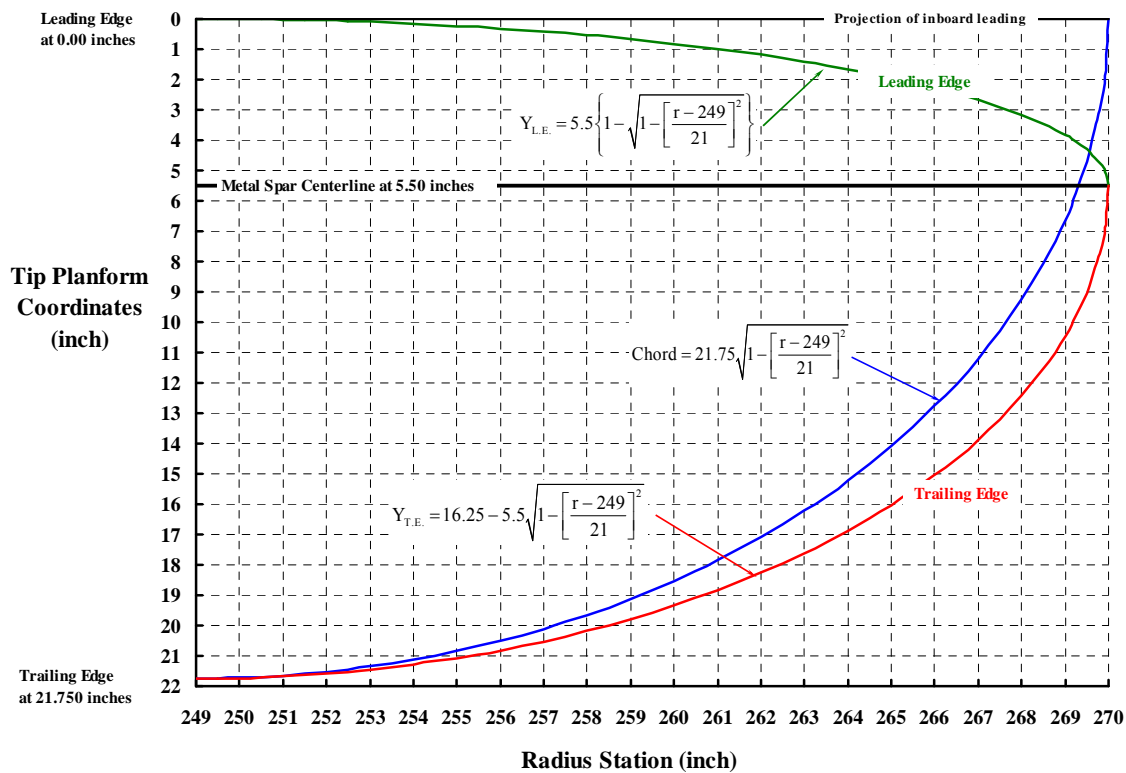
11.5 PCA-2 Blade Section Properties

Notations: See Appendix 11.3

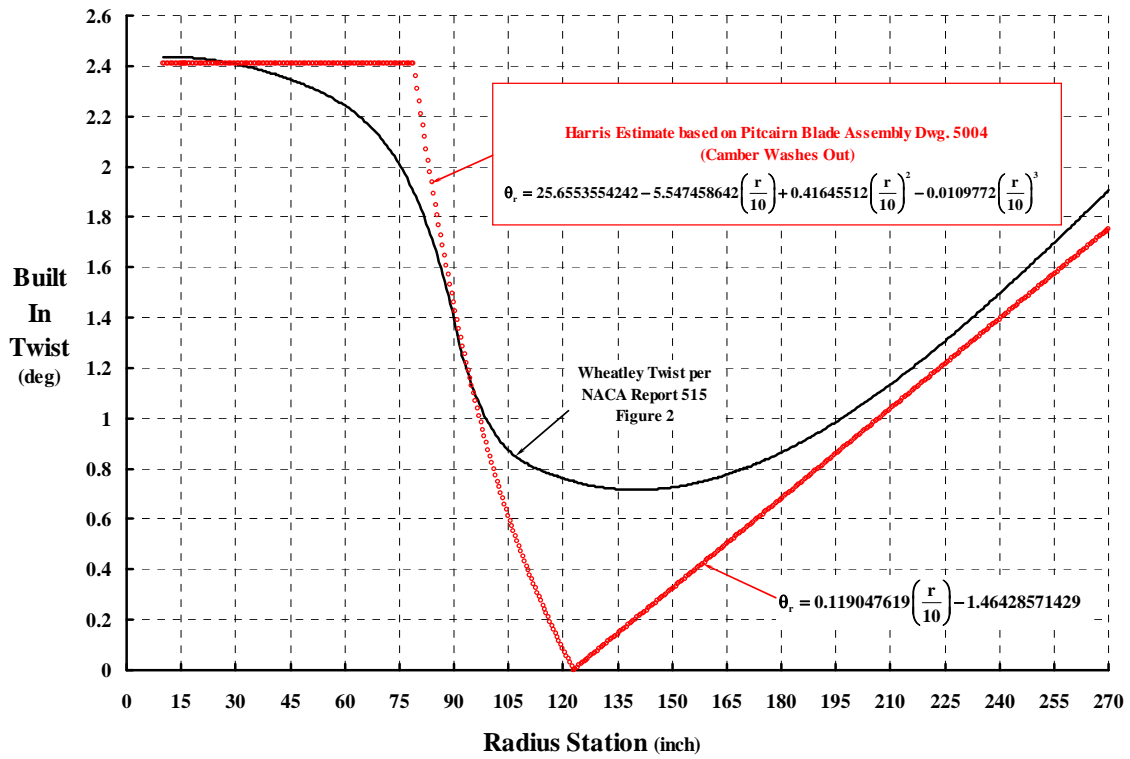
r/R	MASS slug/ft	EI/FLAP lb-ft ²	EI/LAG lb-ft ²	EA lb	GJ lb-ft ²	ITHETA slug-ft ² /ft	IPOLAR slug-ft ² /ft	XEA x/R	XI x/R	KP x/R	KT x/R	CHORD XEA	CHORD XQC
0	0.2941	1.21E+05	1.21E+06	3.80E+07	1.26E+05	3.46E-02	3.46E-02	-0.0006	0	0.0152	0.0152	-0.0006	-0.00668
0.05	0.2941	1.21E+05	1.21E+06	3.80E+07	1.26E+05	3.46E-02	3.46E-02	-0.0006	0	0.0152	0.0152	-0.0006	-0.00668
0.063	0.1195	78376	7.84E+05	1.54E+07	57914	1.41E-02	1.41E-02	-0.0006	0	0.0152	0.0152	-0.0006	-0.00668
0.1	0.1195	78376	7.84E+05	1.54E+07	57914	1.41E-02	1.41E-02	-0.0006	0	0.0152	0.0152	-0.0006	-0.00668
0.15	0.1195	78376	7.84E+05	1.54E+07	57914	1.41E-02	1.41E-02	-0.0006	0	0.0152	0.0152	-0.0006	-0.00668
0.2	0.1195	78376	7.84E+05	1.54E+07	57914	1.41E-02	1.41E-02	-0.0006	0	0.0152	0.0152	-0.0006	-0.00668
0.25	0.1195	78376	7.84E+05	1.54E+07	57914	1.41E-02	1.41E-02	-0.0006	0	0.0152	0.0152	-0.0006	-0.00668
0.2926	0.1195	78376	7.84E+05	1.54E+07	57914	1.41E-02	1.41E-02	-0.0006	0	0.0152	0.0152	-0.0006	-0.00668
0.3	0.1178	78376	7.84E+05	1.54E+07	57914	1.44E-02	1.44E-02	-0.0042	0.00008	0.0155	0.0155	-0.0042	-0.00632
0.3259	0.1119	78376	7.84E+05	1.54E+07	57914	1.54E-02	1.54E-02	0.00022	0.0003	0.0165	0.0165	0.0022	-0.00502
0.35	0.1063	78376	7.84E+05	1.54E+07	57914	1.59E-02	1.59E-02	0.00082	0.0004	0.0172	0.0172	0.00082	-0.00383
0.3759	0.1003	78376	7.84E+05	1.54E+07	57914	1.61E-02	1.61E-02	0.00146	0.0004	0.0178	0.0178	0.00146	-0.00254
0.4	9.48E-02	78376	7.84E+05	1.54E+07	57914	1.59E-02	1.59E-02	0.00206	0.00026	0.0182	0.0182	0.00206	-0.00134
0.422	8.97E-02	78376	7.84E+05	1.54E+07	57914	1.52E-02	1.52E-02	0.00261	0	0.0183	0.0183	0.00261	-0.00023
0.45	8.97E-02	78376	7.84E+05	1.54E+07	57914	1.52E-02	1.52E-02	0.00261	0	0.0183	0.0183	0.00261	-0.00023
0.4556	8.97E-02	78376	7.84E+05	1.54E+07	57914	1.52E-02	1.52E-02	0.00261	0	0.0183	0.0183	0.00261	-0.00023
0.4557	0.7824	78376	7.84E+05	1.54E+07	57914	1.52E-02	1.52E-02	0.00261	0	0.0062	0.0062	0.00261	-0.00023
0.4683	0.7824	78376	7.84E+05	1.54E+07	57914	1.52E-02	1.52E-02	0.00261	0	0.0062	0.0062	0.00261	-0.00023
0.4685	8.97E-02	78376	7.84E+05	1.54E+07	57914	1.52E-02	1.52E-02	0.00261	0	0.0183	0.0183	0.00261	-0.00023
0.5	8.97E-02	78376	7.84E+05	1.54E+07	57914	1.52E-02	1.52E-02	0.00261	0	0.0183	0.0183	0.00261	-0.00023
0.55	8.97E-02	78376	7.84E+05	1.54E+07	57914	1.52E-02	1.52E-02	0.00261	0	0.0183	0.0183	0.00261	-0.00023
0.6	8.97E-02	78376	7.84E+05	1.54E+07	57914	1.52E-02	1.52E-02	0.00261	0	0.0183	0.0183	0.00261	-0.00023
0.65	8.97E-02	78376	7.84E+05	1.54E+07	57914	1.52E-02	1.52E-02	0.00261	0	0.0183	0.0183	0.00261	-0.00023
0.7	8.97E-02	78376	7.84E+05	1.54E+07	57914	1.52E-02	1.52E-02	0.00261	0	0.0183	0.0183	0.00261	-0.00023
0.75	8.97E-02	78376	7.84E+05	1.54E+07	57914	1.52E-02	1.52E-02	0.00261	0	0.0183	0.0183	0.00261	-0.00023
0.8	8.97E-02	78376	7.84E+05	1.54E+07	57914	1.52E-02	1.52E-02	0.00261	0	0.0183	0.0183	0.00261	-0.00023
0.85	8.97E-02	78376	7.84E+05	1.54E+07	57914	1.52E-02	1.52E-02	0.00261	0	0.0183	0.0183	0.00261	-0.00023
0.9	8.97E-02	78376	7.84E+05	1.54E+07	57914	1.52E-02	1.52E-02	0.00261	0	0.0183	0.0183	0.00261	-0.00023
0.922	8.97E-02	78376	7.84E+05	1.54E+07	57914	1.52E-02	1.52E-02	0.00261	0	0.0183	0.0183	0.00261	-0.00023
0.9407	4.96E-02	5276	52758	5.34E+06	4232	1.35E-02	1.35E-02	0.00261	0.00183	0.0232	0.0232	0.00261	-0.00022
0.9593	4.44E-02	3545	35449	5.34E+06	4232	9.08E-03	9.08E-03	0.00261	0.00107	0.0201	0.0201	0.00261	-0.0002
0.9704	3.96E-02	2255	22555	5.34E+06	4232	5.79E-03	5.79E-03	0.00261	0.00033	0.017	0.017	0.00261	-0.00018
0.9796	3.46E-02	1229	12286	5.34E+06	4232	3.17E-03	3.17E-03	0.00261	-0.00048	0.0134	0.0134	0.00261	-0.00016
0.9907	2.44E-02	297	2973	4.53E+06	1042	7.60E-04	7.60E-04	0.00261	-0.00157	0.0078	0.0078	0.00261	-0.00011



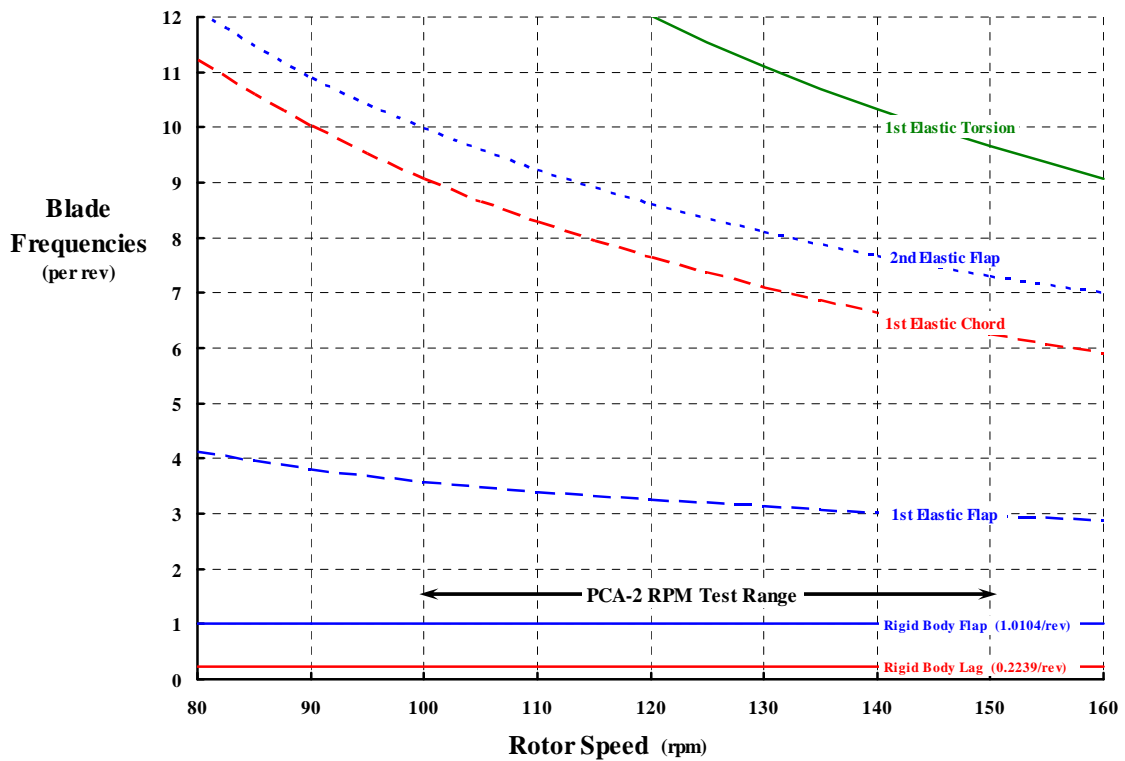
Appendix 11.5. Figure 1.



Appendix 11.5. Figure 2.



Appendix 11.5. Figure 3.



Appendix 11.5. Figure 4.

11.6 H-34 Experimental Data Set

- References:
1. NASA TN D-4632, An Investigation of Full-Scale Helicopter Rotors at High Advance Ratios and Advancing Tip Mach Numbers by John McCloud III and Jim Biggers, July 1968
 2. Harris EXCEL File: H-34 Data Regression Analysis (Corrected June 19, 2008)
 3. Harris EXCEL File: H-34 Data Regression Analysis (Corrected June 19, 2008) Page 2
 4. Theory vs Test Alpha = Coll = Zero.xls
 5. SUMMARY H-34 versus Theory (Matched Alpha and Collective).xls

Airfoil	N.A.C.A. 0012
Chord	1.337 ft
Diameter	56.00 ft
Twist	0.00 deg
Disc Area	2,463 sq. ft
Reference Area (4 blades)	153.1 sq. ft
Nominal Solidity	0.062
Lock Number	8.86
Flap Moment of inertia	1264 slug ft ²
Weight Moment	2,265 lb-ft
Flap/Lag Hinge Offset	1.00 ft

- Notes:
1. Wind axis data measured. Shaft axis data derived.
 2. Shaft torque derived from strain cage on shaft.
 3. Coefficients based on rotor tip speed and total blade area ($\sigma A = 153.1$ sq. ft.)
 4. Articulated hub with coincident flap and lag hinges at $r/R = 0.0357$
 5. Pitch bearing at $r/R = 0.079$

Advance	Collective at	Shaft Angle of	Long	Lat			Derived	Derived				Derived	Derived Rotor Alone
Ratio	0.75R (deg)	(deg)	Cyclic (deg)	Cyclic (deg)	C _L /Solidity	C _D /Solidity	C _T /Solidity	C _H /Solidity	C _Y /Solidity	C _Q /Solidity	C _{De} /Solidity	L/De	
0.306	-4.0	5.0	-0.90	-0.10	-0.009605	0.000417	-0.009532	0.001253	-0.000235	0.001361	0.004863	-1.98	
0.306	-4.0	10.0	-0.20	-0.40	0.016385	0.004846	0.016978	0.001927	-0.001071	0.000098	0.005167	3.17	
0.307	-2.0	5.0	0.40	-0.50	0.013741	0.002668	0.013921	0.001460	-0.000633	0.000689	0.004913	2.80	
0.305	-2.0	10.0	1.00	-0.70	0.039440	0.009224	0.040443	0.002235	-0.001455	-0.000962	0.006071	6.50	
0.305	0.0	0.0	1.30	-0.90	0.011576	0.001281	0.011576	0.001281	-0.000090	0.001135	0.005003	2.31	
0.305	0.0	5.0	1.90	-1.00	0.037296	0.004846	0.037576	0.001577	-0.000915	0.000206	0.005523	6.75	
0.303	0.0	10.0	2.80	-1.20	0.061465	0.012725	0.062741	0.001858	-0.001875	-0.001664	0.007233	8.50	
0.303	2.0	-5.0	1.80	-1.40	0.006869	0.000598	0.006791	0.001194	0.000302	0.001320	0.004955	1.39	
0.305	2.0	0.0	2.80	-1.70	0.035131	0.001256	0.035131	0.001256	-0.000482	0.001259	0.005385	6.52	
0.306	2.0	5.0	3.50	-1.70	0.061393	0.006773	0.061750	0.001396	-0.001534	-0.000038	0.006648	9.23	
0.304	2.0	10.0	4.30	-1.60	0.084323	0.016471	0.085902	0.001578	-0.002268	-0.002085	0.009614	8.77	
0.300	4.0	-10.0	2.80	-1.50	0.002033	0.000806	0.001862	0.001147	0.000637	0.001335	0.005255	0.39	
0.306	4.0	-5.0	3.60	-2.00	0.032069	-0.001797	0.032104	0.001005	0.000122	0.002213	0.005436	5.90	
0.304	4.0	0.0	4.40	-2.40	0.058405	0.000996	0.058405	0.000996	-0.001013	0.001616	0.006311	9.25	
0.302	4.0	5.0	5.20	-2.30	0.084087	0.008555	0.084513	0.001194	-0.001937	0.000084	0.008832	9.52	
0.303	4.0	10.0	6.50	-2.20	0.101766	0.017961	0.103339	0.000017	-0.002733	-0.001436	0.013221	7.70	
0.303	6.0	-10.0	4.30	-2.40	0.025630	-0.003840	0.025907	0.000669	0.000335	0.002837	0.005521	4.64	
0.304	6.0	-5.0	5.30	-2.70	0.055523	-0.004266	0.055684	0.000589	-0.000340	0.003273	0.006499	8.54	
0.304	6.0	0.0	6.10	-3.20	0.082647	0.000384	0.082647	0.000384	-0.001676	0.002450	0.008443	9.79	
0.307	6.0	5.0	7.60	-3.20	0.102068	0.008180	0.102393	-0.000747	-0.002672	0.001553	0.013237	7.71	
0.305	6.0	10.0	9.40	-3.70	0.111988	0.016171	0.113095	-0.003521	-0.003495	0.001254	0.020282	5.52	
0.305	8.0	-10.0	5.60	-3.10	0.049258	-0.008496	0.049985	0.000187	-0.000101	0.004587	0.006543	7.53	
0.305	8.0	-5.0	6.80	-3.60	0.075162	-0.006604	0.075452	-0.000028	-0.000892	0.004482	0.008092	9.29	
0.304	8.0	0.0	8.10	-4.30	0.097650	-0.001206	0.097650	-0.001206	-0.002817	0.004149	0.012443	7.85	
0.304	8.0	5.0	9.70	-4.80	0.109527	0.006575	0.109683	-0.002996	-0.003403	0.004389	0.021011	5.21	
0.305	8.0	10.0	11.20	-5.20	0.117120	0.017300	0.118345	-0.003301	-0.002669	0.004835	0.033152	3.53	
0.304	10.0	-10.0	7.10	-4.20	0.071694	-0.013409	0.072933	-0.000756	-0.000995	0.006595	0.008285	8.65	
0.304	10.0	-5.0	8.50	-5.10	0.092491	-0.009460	0.092964	-0.001363	-0.002553	0.006649	0.012411	7.45	
0.305	10.0	0.0	9.90	-5.90	0.104978	-0.002847	0.104978	-0.002847	-0.003175	0.007078	0.020360	5.16	

0.304	10.0	5.0	11.30	-6.30	0.113408	0.005727	0.113476	-0.004179	-0.002479	0.007184	0.029357	3.86
0.304	11.0	-10.0	7.80	-4.50	0.080413	-0.015462	0.081876	-0.001264	-0.000908	0.007901	0.010528	7.64
0.305	11.0	-5.0	8.90	-5.90	0.097181	-0.009578	0.097646	-0.001072	-0.003243	0.008191	0.017278	5.62
0.399	-4.0	5.0	-0.10	0.00	0.001537	0.002139	0.001718	0.001997	-0.000598	0.001033	0.004727	0.33
0.402	-4.0	10.0	0.80	-0.20	0.029977	0.007836	0.030882	0.002512	-0.001619	-0.000975	0.005411	5.54
0.400	-2.0	5.0	1.40	-0.70	0.018014	0.003610	0.018260	0.002026	-0.000951	0.000542	0.004965	3.63
0.400	-2.0	10.0	2.50	-0.70	0.048863	0.011039	0.050038	0.002386	-0.002018	-0.001865	0.006378	7.66
0.402	0.0	0.0	2.10	-1.20	0.010644	0.001797	0.010644	0.001797	-0.000137	0.001190	0.004756	2.24
0.399	0.0	5.0	3.40	-1.20	0.037958	0.005309	0.038276	0.001981	-0.001405	-0.000028	0.005240	7.24
0.401	0.0	10.0	4.40	-1.20	0.065931	0.013491	0.067272	0.001837	-0.002487	-0.002257	0.007862	8.39
0.402	2.0	0.0	4.20	-1.80	0.028737	0.001692	0.028737	0.001692	-0.000399	0.001333	0.005007	5.74
0.403	2.0	5.0	5.50	-1.90	0.056138	0.006320	0.056475	0.001403	-0.001798	-0.000098	0.006077	9.24
0.401	4.0	-5.0	4.40	-2.30	0.017354	0.000037	0.017285	0.001549	0.000358	0.002058	0.005169	3.36
0.401	4.0	0.0	6.00	-2.50	0.049499	0.001610	0.049499	0.001610	-0.000987	0.001687	0.005816	8.51
0.399	4.0	5.0	7.60	-2.40	0.075066	0.007404	0.075426	0.000833	-0.002573	0.000277	0.008098	9.27
0.402	6.0	-10.0	4.90	-2.50	0.004963	0.000716	0.004763	0.001567	0.001025	0.001948	0.005561	0.89
0.401	6.0	-5.0	6.40	-3.00	0.037980	-0.002143	0.038022	0.001175	-0.000133	0.003302	0.006090	6.24
0.401	6.0	0.0	8.10	-3.60	0.066657	0.000770	0.066657	0.000770	-0.001581	0.002576	0.007194	9.27
0.402	6.0	5.0	9.80	-3.90	0.088635	0.006607	0.088874	-0.001143	-0.003846	0.002199	0.012076	7.34
0.403	8.0	-10.0	6.40	-3.30	0.024990	-0.003336	0.025190	0.001054	0.000632	0.003773	0.006025	4.15
0.402	8.0	-5.0	8.30	-3.80	0.055746	-0.004134	0.055894	0.000740	-0.000838	0.004439	0.006908	8.07
0.403	8.0	0.0	9.90	-4.60	0.082204	-0.000106	0.082204	-0.000106	-0.003161	0.004425	0.010874	7.56
0.401	8.0	5.0	11.80	-5.30	0.095261	0.005774	0.095402	-0.002551	-0.003808	0.004845	0.017856	5.33
0.404	10.0	-10.0	8.30	-4.30	0.042669	-0.007136	0.043260	0.000382	0.000146	0.005773	0.007154	5.96
0.401	10.0	-5.0	10.10	-5.50	0.068526	-0.006636	0.068844	-0.000638	-0.002087	0.006264	0.008984	7.63
0.401	9.0	5.0	12.80	-6.30	0.098072	0.005709	0.098196	-0.002860	-0.004124	0.006301	0.021421	4.58
0.403	9.5	0.0	11.60	-6.10	0.086655	-0.001876	0.086655	-0.001876	-0.003889	0.006530	0.014328	6.05
0.401	11.0	-10.0	9.10	-4.90	0.052771	-0.009500	0.053619	-0.000192	-0.000113	0.007093	0.008188	6.44
0.458	-4.0	5.0	0.00	-0.10	0.004717	0.002856	0.004948	0.002434	-0.000746	0.000893	0.004805	0.98
0.460	-4.0	10.0	1.30	-0.50	0.035152	0.009159	0.036208	0.002916	-0.002263	-0.001446	0.006015	5.84
0.460	-2.0	5.0	1.50	-0.70	0.021283	0.004296	0.021576	0.002425	-0.001235	0.000274	0.004892	4.35
0.462	-2.0	10.0	3.10	-1.00	0.051303	0.011564	0.052532	0.002480	-0.002619	-0.002207	0.006786	7.56
0.467	0.0	0.0	2.60	-1.10	0.007521	0.002190	0.007521	0.002190	-0.000116	0.001137	0.004625	1.63
0.461	0.0	5.0	3.80	-1.30	0.037189	0.005700	0.037544	0.002437	-0.001758	-0.000148	0.005379	6.91
0.461	0.0	10.0	5.40	-1.60	0.066925	0.013622	0.068274	0.001794	-0.003255	-0.002556	0.008078	8.28

0.459	2.0	0.0	4.60	-1.80	0.025336	0.002134	0.025336	0.002134	-0.000515	0.001315	0.004999	5.07
0.460	2.0	5.0	6.00	-1.90	0.053182	0.006561	0.053551	0.001901	-0.002052	-0.000179	0.006171	8.62
0.461	2.0	10.0	7.30	-2.00	0.081219	0.015108	0.082609	0.000775	-0.003694	-0.002302	0.010115	8.03
0.458	4.0	-5.0	4.80	-2.30	0.011628	0.000938	0.011502	0.001948	0.000465	0.001937	0.005166	2.25
0.461	4.0	0.0	6.60	-2.70	0.040930	0.001775	0.040930	0.001775	-0.001109	0.001726	0.005518	7.42
0.460	4.0	5.0	8.40	-2.80	0.070360	0.007153	0.070716	0.000994	-0.002998	0.000304	0.007815	9.00
0.456	6.0	-5.0	6.60	-3.00	0.027663	-0.000607	0.027611	0.001806	0.000049	0.002878	0.005704	4.85
0.458	6.0	0.0	8.40	-3.40	0.055761	0.001363	0.055761	0.001363	-0.001684	0.002376	0.006551	8.51
0.462	6.0	5.0	10.60	-4.10	0.081036	0.006352	0.081281	-0.000735	-0.003738	0.001850	0.010357	7.82
0.456	8.0	-10.0	6.60	-3.20	0.011314	-0.000217	0.011180	0.001751	0.000657	0.002850	0.006033	1.88
0.455	8.0	-5.0	8.60	-3.90	0.042727	-0.002464	0.042779	0.001269	-0.000620	0.004067	0.006474	6.60
0.458	8.0	0.0	10.40	-4.60	0.072057	0.000571	0.072057	0.000571	-0.002886	0.003990	0.009283	7.76
0.462	8.0	5.0	12.40	-5.70	0.090369	0.006607	0.090601	-0.001294	-0.004710	0.004421	0.016176	5.59
0.456	10.0	-10.0	8.70	-4.10	0.026313	-0.003462	0.026514	0.001160	0.000439	0.004537	0.006488	4.06
0.459	10.0	-5.0	10.90	-5.00	0.057941	-0.004091	0.058077	0.000974	-0.001702	0.005589	0.008085	7.17
0.457	10.0	0.0	12.50	-6.20	0.079317	-0.001045	0.079317	-0.001045	-0.004263	0.006457	0.013083	6.06
0.456	12.0	-10.0	10.20	-5.40	0.043778	-0.007300	0.044381	0.000413	-0.000334	0.006751	0.007506	5.83
0.508	-4.0	5.0	-0.10	-0.20	0.008569	0.004114	0.008895	0.003352	-0.000686	0.000741	0.005573	1.54
0.507	-4.0	10.0	1.60	-0.60	0.040903	0.010852	0.042166	0.003584	-0.002820	-0.001823	0.007256	5.64
0.506	-2.0	2.0	1.10	-0.90	0.004095	0.003178	0.004203	0.003033	-0.000233	0.001109	0.005369	0.76
0.507	-2.0	5.0	1.80	-0.70	0.021813	0.005151	0.022179	0.003230	-0.001148	0.000281	0.005706	3.82
0.509	-2.0	10.0	3.30	-1.10	0.054615	0.012818	0.056011	0.003139	-0.003078	-0.002433	0.008039	6.79
0.498	0.0	-3.0	0.60	-0.90	-0.010197	0.003289	-0.010355	0.002751	0.000200	0.001118	0.005534	-1.84
0.507	0.0	2.0	2.90	-1.30	0.019575	0.003604	0.019689	0.002919	-0.000647	0.000878	0.005336	3.67
0.509	0.0	5.0	3.90	-1.40	0.037500	0.006269	0.037904	0.002977	-0.001595	-0.000167	0.005942	6.31
0.508	0.0	10.0	5.70	-1.80	0.070077	0.014602	0.071548	0.002211	-0.003878	-0.002670	0.009347	7.50
0.502	2.0	-3.0	3.10	-1.40	0.005233	0.002520	0.005094	0.002790	0.000028	0.001505	0.005518	0.95
0.509	2.0	2.0	5.20	-2.00	0.034767	0.004256	0.034894	0.003040	-0.001165	0.000900	0.006025	5.77
0.509	2.0	5.0	6.30	-2.00	0.052098	0.007092	0.052518	0.002524	-0.002033	-0.000184	0.006731	7.74
0.509	2.0	10.0	8.10	-2.00	0.084568	0.016092	0.086078	0.001162	-0.003847	-0.002186	0.011797	7.17
0.502	4.0	-5.0	4.50	-2.30	0.008397	0.002079	0.008184	0.002803	0.000315	0.001870	0.005804	1.45
0.507	4.0	-3.0	3.50	-2.60	0.018562	0.001720	0.018447	0.002689	-0.000150	0.002097	0.005856	3.17
0.513	4.0	2.0	7.40	-2.70	0.047002	0.004168	0.047119	0.002525	-0.001450	0.001273	0.006649	7.07
0.506	4.0	5.0	8.30	-2.60	0.066162	0.008009	0.066608	0.002212	-0.002553	0.000264	0.008530	7.76
0.508	4.0	10.0	10.10	-2.80	0.098575	0.016311	0.099910	-0.001054	-0.004742	-0.000801	0.014734	6.69

0.499	6.0	-5.0	6.50	-2.80	0.020553	0.000618	0.020421	0.002407	-0.000007	0.002767	0.006163	3.33
0.505	6.0	-3.0	7.20	-3.20	0.033092	0.000944	0.032997	0.002675	-0.000662	0.002822	0.006531	5.07
0.511	6.0	2.0	9.50	-3.80	0.059795	0.004006	0.059898	0.001917	-0.002390	0.002086	0.008089	7.39
0.507	6.0	5.0	9.90	-3.80	0.079870	0.008147	0.080276	0.001155	-0.003960	0.001707	0.011514	6.94
0.507	6.0	10.0	13.10	-4.50	0.106878	0.015000	0.107859	-0.003787	-0.005047	0.002073	0.019089	5.60
0.496	8.0	-10.0	6.30	-3.20	0.001020	0.002477	0.000574	0.002616	0.000942	0.002109	0.006730	0.15
0.502	8.0	-5.0	8.40	-3.70	0.035485	-0.000841	0.035423	0.002255	-0.000557	0.003880	0.006888	5.15
0.508	8.0	-3.0	9.30	-3.80	0.046355	-0.000132	0.046298	0.002294	-0.001168	0.003869	0.007484	6.19
0.510	8.0	2.0	11.60	-4.30	0.073569	0.003638	0.073651	0.001068	-0.002973	0.003981	0.011443	6.43
0.509	8.0	5.0	12.90	-5.60	0.086239	0.007232	0.086541	-0.000312	-0.004174	0.004220	0.015523	5.56
0.498	10.0	-10.0	8.10	-3.70	0.016522	-0.000756	0.016402	0.002125	0.000834	0.003862	0.006998	2.36
0.502	10.0	-5.0	10.40	-5.00	0.049762	-0.002555	0.049795	0.001792	-0.001791	0.005502	0.008406	5.92
0.508	10.0	-3.0	11.40	-5.30	0.055738	-0.001678	0.055749	0.001241	-0.002406	0.005472	0.009093	6.13
0.514	10.0	2.0	13.50	-6.20	0.080522	0.003429	0.080593	0.000617	-0.003706	0.006530	0.016134	4.99
0.495	12.0	-10.0	9.80	-5.10	0.038248	-0.004430	0.038436	0.002279	0.000156	0.006157	0.008008	4.78
0.498	12.0	-5.0	11.80	-6.80	0.064089	-0.004097	0.064202	0.001504	-0.003602	0.007865	0.011695	5.48
0.500	13.0	-10.0	10.80	-5.30	0.040732	-0.005841	0.041127	0.001321	-0.000082	0.007350	0.008859	4.60
0.624	-4.0	4.0	-0.60	-0.40	0.006577	0.004822	0.006897	0.004351	-0.000853	0.000897	0.006259	1.05
0.618	-4.0	8.0	0.80	-0.80	0.034702	0.009465	0.035682	0.004543	-0.002532	-0.001278	0.007396	4.69
0.624	-2.0	4.0	1.50	-1.00	0.016457	0.004968	0.016763	0.003808	-0.001090	0.000578	0.005895	2.79
0.620	-2.0	8.0	2.90	-1.50	0.046648	0.010299	0.047627	0.003707	-0.003451	-0.001509	0.007865	5.93
0.618	0.0	0.0	2.50	-1.30	0.000526	0.003693	0.000526	0.003693	-0.000245	0.001301	0.005799	0.09
0.622	0.0	4.0	3.80	-1.60	0.029119	0.005959	0.029464	0.003913	-0.001567	0.000453	0.006686	4.35
0.618	0.0	8.0	5.40	-2.00	0.056221	0.010390	0.057120	0.002464	-0.003779	-0.001424	0.008085	6.95
0.618	2.0	-4.0	2.20	-1.30	-0.012523	0.004677	-0.012819	0.003792	0.000100	0.000933	0.006187	-2.02
0.619	2.0	0.0	4.30	-1.70	0.014925	0.003718	0.014925	0.003718	-0.000740	0.001423	0.006017	2.48
0.620	2.0	4.0	6.00	-2.20	0.039601	0.006557	0.039962	0.003779	-0.002003	0.000452	0.007287	5.43
0.619	2.0	8.0	7.90	-2.60	0.072395	0.011444	0.073283	0.001257	-0.004541	-0.001305	0.009335	7.75
0.619	4.0	-4.0	4.60	-2.00	-0.002084	0.003976	-0.002356	0.003821	0.000040	0.001469	0.006350	-0.33
0.621	4.0	0.0	6.80	-2.40	0.024862	0.003920	0.024862	0.003920	-0.000973	0.001679	0.006623	3.75
0.621	4.0	4.0	8.30	-3.30	0.048701	0.006372	0.049027	0.002959	-0.002727	0.000942	0.007888	6.17
0.619	4.0	8.0	10.20	-3.60	0.078796	0.011470	0.079625	0.000392	-0.005131	-0.000232	0.011096	7.10
0.613	6.0	-8.0	4.50	-2.10	-0.018372	0.006889	-0.019152	0.004265	0.000525	0.000155	0.007142	-2.57
0.610	6.0	-4.0	6.70	-2.40	0.010472	0.003283	0.010217	0.004005	-0.000310	0.002185	0.006865	1.53
0.624	6.0	0.0	8.70	-3.60	0.034521	0.003877	0.034521	0.003877	-0.001655	0.002174	0.007361	4.69

0.634	6.0	4.0	10.50	-4.40	0.063186	0.006085	0.063457	0.001663	-0.003668	0.001900	0.009081	6.96
0.624	6.0	4.0	10.90	-4.10	0.065267	0.006868	0.065587	0.002298	-0.003534	0.001935	0.009968	6.55
0.614	8.0	-8.0	6.50	-2.50	-0.006915	0.005340	-0.007591	0.004326	0.000165	0.001243	0.007365	-0.94
0.619	8.0	-4.0	8.70	-3.70	0.020839	0.002949	0.020583	0.004395	-0.000799	0.002907	0.007645	2.73
0.621	8.0	4.0	12.70	-5.90	0.070578	0.006689	0.070873	0.001749	-0.004969	0.003681	0.012616	5.59
0.621	10.0	-8.0	10.70	-3.20	0.002570	0.004524	0.001915	0.004838	-0.000175	0.002353	0.008314	0.31
0.620	10.0	-4.0	10.70	-4.20	0.031783	0.002426	0.031536	0.004637	-0.001591	0.003930	0.008764	3.63
0.619	12.0	-8.0	10.40	-4.50	0.017413	0.002453	0.016902	0.004853	-0.000579	0.004109	0.009091	1.92
0.711	-4.0	2.0	-1.50	-0.50	0.001084	0.005490	0.001275	0.005449	-0.000407	0.001262	0.007265	0.15
0.708	-4.0	4.0	-0.50	-0.70	0.012720	0.006299	0.013128	0.005396	-0.001008	0.000783	0.007404	1.72
0.708	-4.0	6.0	0.10	-0.70	0.025133	0.007657	0.025796	0.004988	-0.002290	-0.000176	0.007409	3.39
0.706	-4.0	8.0	1.40	-1.20	0.040553	0.011341	0.041737	0.005587	-0.003186	-0.001453	0.009283	4.37
0.710	-2.0	2.0	0.70	-1.10	0.007222	0.005156	0.007398	0.004901	-0.000960	0.001198	0.006844	1.06
0.711	-2.0	4.0	1.60	-1.10	0.020303	0.006527	0.020709	0.005095	-0.001375	0.000564	0.007320	2.77
0.709	-2.0	6.0	2.30	-1.30	0.034042	0.007822	0.034673	0.004221	-0.002722	-0.000367	0.007304	4.66
0.708	-2.0	8.0	3.60	-1.50	0.047483	0.011150	0.048573	0.004433	-0.003695	-0.001389	0.009188	5.17
0.710	0.0	0.0	1.90	-1.10	0.000461	0.004866	0.000461	0.004866	-0.000653	0.001415	0.006859	0.07
0.712	0.0	2.0	3.00	-1.20	0.014077	0.005221	0.014251	0.004727	-0.001038	0.001199	0.006904	2.04
0.710	0.0	4.0	3.90	-1.80	0.024718	0.006129	0.025085	0.004390	-0.001798	0.000655	0.007052	3.51
0.708	0.0	6.0	4.90	-1.90	0.040292	0.007636	0.040869	0.003383	-0.003237	-0.000272	0.007253	5.56
0.707	0.0	8.0	6.00	-2.20	0.056809	0.011567	0.057866	0.003548	-0.004419	-0.001294	0.009737	5.83
0.710	2.0	0.0	4.30	-1.70	0.010286	0.004858	0.010286	0.004858	-0.000716	0.001493	0.006961	1.48
0.711	2.0	2.0	5.30	-2.20	0.021427	0.005461	0.021605	0.004710	-0.001460	0.001166	0.007101	3.02
0.709	2.0	4.0	6.30	-2.40	0.034345	0.006695	0.034728	0.004283	-0.001814	0.000623	0.007574	4.53
0.708	2.0	6.0	7.40	-2.50	0.046774	0.008012	0.047355	0.003079	-0.003408	0.000016	0.008035	5.82
0.714	2.0	8.0	8.50	-2.90	0.064117	0.011243	0.065058	0.002210	-0.005115	-0.000502	0.010540	6.08
0.706	4.0	-2.0	5.40	-2.10	0.003982	0.005663	0.003782	0.005799	-0.000442	0.001585	0.007909	0.50
0.706	4.0	0.0	6.50	-2.30	0.016931	0.004837	0.016931	0.004837	-0.000830	0.001594	0.007095	2.39
0.711	4.0	2.0	7.60	-2.80	0.026947	0.005687	0.027129	0.004743	-0.001843	0.001390	0.007642	3.53
0.709	4.0	4.0	8.60	-3.10	0.043748	0.007103	0.044137	0.004034	-0.002555	0.001262	0.008883	4.93
0.706	4.0	6.0	9.60	-3.50	0.053930	0.008085	0.054480	0.002403	-0.004288	0.000966	0.009453	5.71
0.695	6.0	-4.0	6.60	-2.30	-0.000823	0.005691	-0.001218	0.005620	-0.000465	0.001568	0.007947	-0.10
0.705	6.0	-2.0	7.80	-2.70	0.011521	0.005458	0.011324	0.005857	-0.000745	0.001877	0.008121	1.42
0.707	6.0	0.0	8.70	-3.00	0.020691	0.005492	0.020691	0.005492	-0.001158	0.001913	0.008198	2.52
0.711	6.0	2.0	9.60	-3.30	0.033070	0.006043	0.033261	0.004885	-0.001956	0.001869	0.008672	3.81

0.709	6.0	4.0	10.90	-4.10	0.046086	0.007007	0.046463	0.003775	-0.003241	0.002092	0.009958	4.63
0.695	8.0	-4.0	8.60	-2.90	0.005570	0.005761	0.005155	0.006136	-0.000545	0.001994	0.008630	0.65
0.709	8.0	-2.0	9.60	-3.10	0.019636	0.005752	0.019423	0.006434	-0.001374	0.002415	0.009158	2.14
0.712	8.0	0.0	10.60	-3.60	0.029314	0.005713	0.029314	0.005713	-0.002389	0.002633	0.009411	3.11
0.710	8.0	2.0	11.80	-3.90	0.039266	0.006341	0.039463	0.004967	-0.002942	0.002891	0.010413	3.77
0.711	8.0	4.0	12.70	-4.70	0.055190	0.007876	0.055605	0.004007	-0.004045	0.003367	0.012611	4.38
0.699	10.0	-4.0	10.50	-3.20	0.014729	0.006132	0.014265	0.007145	-0.001393	0.002657	0.009933	1.48
0.716	10.0	-2.0	11.40	-3.90	0.025829	0.005019	0.025638	0.005917	-0.002449	0.003176	0.009454	2.73
0.706	10.0	0.0	12.50	-4.30	0.036062	0.006055	0.036062	0.006055	-0.002925	0.003715	0.011317	3.19
0.703	12.0	-4.0	12.60	-3.90	0.021382	0.006137	0.020902	0.007614	-0.001888	0.003632	0.011303	1.89
0.707	12.0	-2.0	13.60	-4.50	0.034292	0.005784	0.034069	0.006977	-0.003101	0.004529	0.012189	2.81
0.706	13.7	-4.0	13.90	-5.20	0.034737	0.005943	0.034238	0.008352	-0.003588	0.005272	0.013410	2.59
0.819	-4.0	0.0	-1.90	0.00	-0.003950	0.006583	-0.003950	0.006583	0.000380	0.001403	0.008296	-0.48
0.824	-4.0	2.0	-0.90	-0.30	0.007447	0.007301	0.007697	0.007037	-0.000285	0.001131	0.008674	0.86
0.829	-4.0	4.0	-0.50	-0.60	0.021902	0.008480	0.022440	0.006932	-0.001225	0.000620	0.009228	2.37
0.814	-2.0	0.0	-1.00	-0.20	-0.002999	0.006089	-0.002999	0.006089	-0.000272	0.001574	0.008023	-0.37
0.832	-2.0	2.0	0.80	-0.80	0.013079	0.006460	0.013296	0.006000	-0.000675	0.001191	0.007891	1.66
0.830	-2.0	4.0	1.90	-1.20	0.024126	0.007794	0.024611	0.006092	-0.001002	0.000710	0.008650	2.79
0.816	0.0	0.0	1.90	-1.00	0.000272	0.005514	0.000272	0.005514	-0.000270	0.001495	0.007345	0.04
0.829	0.0	2.0	2.90	-1.50	0.015917	0.006706	0.016141	0.006146	-0.001068	0.001190	0.008142	1.95
0.830	0.0	4.0	4.30	-1.90	0.030098	0.007718	0.030563	0.005600	-0.001616	0.000710	0.008574	3.51
0.808	2.0	-2.0	3.00	-1.10	-0.003983	0.006244	-0.004198	0.006101	-0.000265	0.001423	0.008005	-0.50
0.818	2.0	0.0	4.30	-1.50	0.003292	0.006177	0.003292	0.006177	-0.000782	0.001497	0.008008	0.41
0.837	2.0	2.0	6.30	-2.30	0.018192	0.006698	0.018415	0.006059	-0.001159	0.001294	0.008244	2.21
0.834	2.0	4.0	6.40	-2.50	0.033628	0.007731	0.034085	0.005366	-0.001999	0.000891	0.008799	3.82
0.815	3.0	-2.0	4.00	-1.20	-0.004284	0.006557	-0.004510	0.006403	-0.000332	0.001454	0.008341	-0.51
0.807	4.0	-2.0	5.30	-1.50	-0.002134	0.006628	-0.002364	0.006549	-0.000675	0.001482	0.008465	-0.25
0.818	4.0	0.0	6.30	-2.20	0.010384	0.006847	0.010384	0.006847	-0.001206	0.001540	0.008730	1.19
0.838	4.0	2.0	8.10	-2.70	0.021359	0.006991	0.021590	0.006241	-0.001372	0.001696	0.009015	2.37
0.831	4.0	4.0	9.10	-3.10	0.034693	0.008318	0.035189	0.005878	-0.003185	0.001692	0.010354	3.35
0.811	5.0	-2.0	6.30	-1.80	-0.002584	0.007428	-0.002842	0.007333	-0.000810	0.001527	0.009310	-0.28
0.812	6.0	-2.0	7.50	-2.00	0.001027	0.007593	0.000761	0.007624	-0.001115	0.001491	0.009429	0.11
0.818	6.0	0.0	8.80	-2.60	0.015332	0.007747	0.015332	0.007747	-0.001899	0.001586	0.009685	1.58
0.834	6.0	2.0	9.80	-3.00	0.023050	0.008390	0.023329	0.007580	-0.002513	0.001829	0.010583	2.18
0.831	6.0	4.0	11.20	-3.80	0.035487	0.008550	0.035997	0.006054	-0.003352	0.001963	0.010912	3.25

0.799	7.0	-2.0	8.50	-2.40	0.004423	0.009199	0.004099	0.009348	-0.001370	0.001491	0.011065	0.40
0.815	8.0	-2.0	9.40	-2.60	0.008199	0.008639	0.007893	0.008920	-0.001600	0.001723	0.010753	0.76
0.820	8.0	0.0	10.80	-3.10	0.017134	0.008680	0.017134	0.008680	-0.002162	0.001950	0.011058	1.55
0.833	8.0	2.0	12.00	-3.60	0.027647	0.009153	0.027950	0.008183	-0.002907	0.002327	0.011947	2.31
0.820	9.0	-2.0	10.50	-2.80	0.007990	0.008804	0.007678	0.009077	-0.002218	0.001772	0.010965	0.73
0.818	10.0	-2.0	11.70	-3.20	0.012444	0.009800	0.012094	0.010228	-0.002146	0.002155	0.012435	1.00
0.828	10.0	0.0	12.90	-3.70	0.024631	0.009645	0.024631	0.009645	-0.003555	0.002720	0.012930	1.90
0.826	11.0	-2.0	12.50	-3.50	0.014224	0.009245	0.013893	0.009736	-0.002581	0.002373	0.012118	1.17
0.813	12.0	-2.0	13.90	-4.00	0.018826	0.012090	0.018393	0.012740	-0.003315	0.002957	0.015727	1.20
0.824	12.8	-2.0	15.70	-4.20	0.018902	0.011578	0.018486	0.012231	-0.003326	0.003095	0.015334	1.23
0.825	-4.0	4.0	-0.70	-0.10	0.015851	0.007752	0.016353	0.006627	-0.001121	0.000784	0.008702	1.82
0.826	0.0	4.0	3.90	-1.80	0.027084	0.007159	0.027517	0.005252	-0.001881	0.000743	0.008058	3.36
0.828	-4.0	6.0	0.30	-1.30	0.033317	0.010048	0.034185	0.006510	-0.002327	-0.000307	0.009678	3.44
0.828	-2.0	6.0	2.60	-1.50	0.041549	0.009874	0.042354	0.005477	-0.002596	-0.000438	0.009345	4.45
0.829	0.0	6.0	4.90	-2.10	0.045377	0.009306	0.046101	0.004512	-0.002903	-0.000176	0.009094	4.99
0.829	2.0	6.0	7.60	-2.90	0.050676	0.009300	0.051371	0.003952	-0.003551	0.000353	0.009725	5.21
0.832	4.0	6.0	9.60	-3.30	0.052808	0.009619	0.053524	0.004046	-0.004074	0.001202	0.011064	4.77
0.829	-4.0	8.0	1.40	-1.70	0.050514	0.013277	0.051870	0.006118	-0.003927	-0.001769	0.011143	4.53
0.827	-2.0	8.0	3.70	-2.10	0.059451	0.012960	0.060676	0.004560	-0.004307	-0.001708	0.010895	5.46
0.831	0.0	8.0	6.50	-2.80	0.058174	0.011305	0.059181	0.003099	-0.004778	-0.000709	0.010452	5.57
0.834	2.0	8.0	8.70	-3.50	0.067017	0.011957	0.068029	0.002514	-0.006416	-0.000090	0.011850	5.66
1.052	-4.0	1.0	-2.30	-0.10	0.015213	0.012551	0.015430	0.012284	0.000641	0.000427	0.012957	1.17
1.049	-4.0	3.0	-1.30	-0.40	0.026288	0.013214	0.026944	0.011820	-0.000414	-0.000142	0.013078	2.01
1.049	-4.0	5.0	-0.20	-1.40	0.044451	0.015001	0.045589	0.011070	-0.002338	-0.001217	0.013841	3.21
1.051	-4.0	7.0	1.10	-1.30	0.069819	0.020074	0.071745	0.011416	-0.004603	-0.003016	0.017205	4.06
1.045	-2.0	1.0	0.20	-0.80	0.001981	0.009363	0.002144	0.009327	0.000748	0.001476	0.010775	0.18
1.057	-2.0	3.0	1.30	-1.10	0.025610	0.009850	0.026090	0.008496	0.000156	0.001303	0.011082	2.31
1.057	-2.0	5.0	2.10	-1.40	0.051927	0.013996	0.052949	0.009417	-0.001504	-0.000508	0.013515	3.84
1.057	-2.0	7.0	4.10	-2.20	0.065862	0.015532	0.067264	0.007390	-0.003213	-0.001018	0.014569	4.52
1.051	0.0	1.0	2.50	-1.50	-0.010139	0.008368	-0.009991	0.008544	0.000956	0.001633	0.009922	-1.02
1.059	0.0	3.0	3.90	-1.60	0.027072	0.010378	0.027578	0.008947	-0.001086	0.001303	0.011608	2.33
1.059	0.0	5.0	5.20	-1.40	0.044998	0.011339	0.045815	0.007374	-0.002145	0.000726	0.012025	3.74
1.051	0.0	7.0	6.40	-2.20	0.064844	0.013628	0.066021	0.005624	-0.003703	-0.000144	0.013491	4.81
1.058	2.0	1.0	5.10	-1.00	-0.012657	0.009543	-0.012489	0.009762	0.001111	0.001438	0.010902	-1.16
1.051	2.0	3.0	6.60	-1.50	0.009098	0.009202	0.009567	0.008713	-0.000719	0.001501	0.010630	0.86

1.057	2.0	5.0	7.90	-2.50	0.037892	0.010270	0.038643	0.006928	-0.002165	0.001307	0.011506	3.29
1.052	2.0	7.0	9.10	-3.10	0.061455	0.012395	0.062507	0.004813	-0.003868	0.000575	0.012941	4.75
1.058	4.0	1.0	7.20	-1.60	-0.000865	0.010814	-0.000676	0.010827	-0.000351	0.001297	0.012039	-0.07
1.052	4.0	3.0	8.80	-2.20	0.006390	0.011763	0.006997	0.011412	-0.000424	0.001289	0.012988	0.49
1.053	4.0	5.0	9.90	-2.70	0.031877	0.011206	0.032732	0.008385	-0.002837	0.001293	0.012434	2.56
1.053	4.0	7.0	11.20	-3.10	0.060753	0.014310	0.062044	0.006799	-0.004372	0.001365	0.015606	3.89
1.053	6.0	1.0	9.20	-0.90	-0.012238	0.013151	-0.012007	0.013363	-0.000445	0.000428	0.013557	-0.90
1.052	6.0	3.0	11.10	-1.80	-0.005611	0.014013	-0.004870	0.014287	-0.000823	0.000531	0.014518	-0.39
1.051	8.0	1.0	11.10	-0.50	-0.024233	0.016758	-0.023937	0.017178	-0.000234	-0.000356	0.016419	-1.48
1.059	8.0	3.0	12.70	-1.90	0.009791	0.016115	0.010621	0.015580	-0.004101	0.001305	0.017348	0.56
1.049	10.0	1.0	13.50	-1.00	-0.011436	0.020033	-0.011085	0.020230	-0.002303	-0.000356	0.019694	-0.58

11.7 UH-1 Experimental Data Set

References: 1. USAAVLABS Technical Report 69-2, Wind Tunnel Investigation of Semirigid Full-Scale Rotors Operating at High Advance Ratios by Bruce Charles and Watson (Hank) Tanner January 1969
2. Harris EXCEL File: UH-1D Data Regression Analysis.xls

Airfoil	N.A.C.A. 0012
Chord	1.75 ft
Diameter	34.00 ft
Twist	-1.42 deg Washout
Disc Area	908 sq. ft
Reference Area (2 blades)	59.5 sq. ft
Nominal Solidity	0.0656
Lock Number	3.62
Flap Moment of inertia	1,584 slug ft ²

Notes: 1. Wind axis data measured. Shaft axis data derived.
2. Shaft torque derived from wind tunnel balance forces and moments.
3. Coefficients based on rotor tip speed and total blade area ($\sigma A = 59.5$ sq. ft.)
4. Teetering, under slung hub with $z/R = 0.0256$
5. Pitch bearing at $r/R = 0.0578$
6. Hub precone angle of 2.75 degrees
7. Lateral cyclic to remove lateral flapping not provided.

Advance	Collective at 0.75R	Alpha Shaft	Longitudinal Cyclic B1s			Derived	Derived			Derived	Derived Rotor Alone
Ratio	(deg)	(deg)	(deg)	C _L /Solidity	C _D /Solidity	C _T /Solidity	C _H /Solidity	C _V /Solidity	C _Q /Solidity	C _{De} /Solidity	L/De
0.511	0.0	-2.0	0.00	0.000790	0.003366	0.000672	0.003392	-0.000252	0.001133	0.005583	0.14
0.505	2.0	-4.0	1.20	0.002667	0.003105	0.002444	0.003283	-0.000724	0.001406	0.005889	0.45
0.505	4.0	-6.0	2.60	0.003011	0.003077	0.002673	0.003375	-0.000607	0.001504	0.006055	0.50
0.508	0.0	0.0	0.50	0.012107	0.003608	0.012107	0.003608	-0.000774	0.001023	0.005622	2.15
0.507	4.0	-4.0	3.20	0.012107	0.002654	0.011892	0.003492	-0.000585	0.001744	0.006094	1.99
0.512	2.0	-2.0	1.70	0.012665	0.003122	0.012548	0.003562	-0.000668	0.001333	0.005726	2.21
0.507	6.0	-6.0	4.90	0.012714	0.002425	0.012391	0.003741	-0.000451	0.002109	0.006585	1.93
0.512	0.0	2.0	1.30	0.023335	0.004668	0.023484	0.003851	-0.002350	0.001103	0.006822	3.42
0.508	4.0	-2.0	3.80	0.023677	0.002850	0.023563	0.003675	-0.001259	0.001788	0.006370	3.72
0.509	6.0	-4.0	5.10	0.025109	0.002136	0.024899	0.003882	-0.001145	0.002545	0.007136	3.52
0.51	2.0	0.0	2.50	0.025141	0.003805	0.025141	0.003805	-0.001369	0.001162	0.006083	4.13
0.508	8.0	-6.0	6.10	0.025259	0.001573	0.024956	0.004205	-0.000874	0.003075	0.007626	3.31
0.511	10.0	-6.0	7.80	0.034121	0.000881	0.033842	0.004443	-0.001108	0.004067	0.008840	3.86
0.51	8.0	-4.0	7.10	0.034428	0.001771	0.034221	0.004168	-0.001515	0.003276	0.008195	4.20
0.51	4.0	0.0	4.70	0.035182	0.003859	0.035182	0.003859	-0.001962	0.001623	0.007041	5.00
0.508	2.0	2.0	3.20	0.036099	0.005268	0.036261	0.004005	-0.002182	0.000790	0.006823	5.29
0.508	0.0	4.0	2.00	0.036310	0.007106	0.036717	0.004556	-0.002292	0.000024	0.007153	5.08
0.514	6.0	-2.0	5.80	0.037260	0.002936	0.037135	0.004235	-0.002568	0.002707	0.008203	4.54
0.512	10.0	-4.0	8.70	0.044839	0.001340	0.044636	0.004465	-0.002082	0.004233	0.009608	4.67
0.511	8.0	-2.0	7.60	0.046128	0.002715	0.046005	0.004323	-0.002206	0.003015	0.008615	5.35
0.513	0.0	6.0	2.90	0.046460	0.009814	0.047231	0.004904	-0.003002	-0.000824	0.008208	5.66
0.51	6.0	0.0	6.70	0.046701	0.003978	0.046701	0.003978	-0.002521	0.002210	0.008311	5.62
0.511	2.0	4.0	3.90	0.047105	0.007965	0.047546	0.004660	-0.002766	0.000187	0.008331	5.65
0.51	12.0	-6.0	9.80	0.047435	-0.000117	0.047187	0.004842	-0.001865	0.005531	0.010728	4.42
0.512	4.0	2.0	5.30	0.048393	0.005751	0.048564	0.004059	-0.003036	0.001220	0.008134	5.95
0.512	10.0	-2.0	9.60	0.056642	0.002633	0.056516	0.004608	-0.002827	0.003963	0.010373	5.46
0.511	8.0	0.0	8.50	0.056982	0.004081	0.056982	0.004081	-0.003142	0.002922	0.009799	5.81
0.507	12.0	-4.0	10.60	0.056992	0.000886	0.056791	0.004859	-0.002757	0.005433	0.011602	4.91
0.511	6.0	2.0	7.50	0.058285	0.006354	0.058471	0.004316	-0.003638	0.001762	0.009802	5.95

0.513	2.0	6.0	4.50	0.058647	0.010736	0.059448	0.004547	-0.003858	-0.000800	0.009177	6.39
0.512	4.0	4.0	6.10	0.059128	0.008394	0.059570	0.004249	-0.003687	0.000628	0.009621	6.15
0.511	14.0	-6.0	11.80	0.061678	-0.001358	0.061482	0.005097	-0.001935	0.007227	0.012785	4.82
0.509	10.0	0.0	10.20	0.068045	0.004457	0.068045	0.004457	-0.003828	0.004008	0.012331	5.52
0.511	8.0	2.0	9.20	0.068211	0.006441	0.068394	0.004057	-0.004321	0.002674	0.011674	5.84
0.509	12.0	-2.0	11.20	0.068407	0.002004	0.068295	0.004390	-0.003666	0.005772	0.013344	5.13
0.51	4.0	6.0	6.90	0.068953	0.010935	0.069718	0.003668	-0.004547	0.000035	0.011004	6.27
0.514	6.0	4.0	8.20	0.070018	0.008894	0.070468	0.003988	-0.004576	0.001524	0.011859	5.90
0.504	12.0	0.0	12.10	0.078739	0.003302	0.078739	0.003302	-0.003746	0.005844	0.014897	5.29
0.511	10.0	2.0	10.80	0.078962	0.006637	0.079146	0.003877	-0.005276	0.004177	0.014811	5.33
0.506	8.0	4.0	10.10	0.080157	0.009377	0.080616	0.003763	-0.004952	0.002365	0.014051	5.70
0.514	6.0	6.0	8.90	0.080700	0.011746	0.081486	0.003246	-0.005350	0.000999	0.013690	5.89
0.51	4.0	8.0	7.80	0.083009	0.014777	0.084258	0.003081	-0.005358	-0.000692	0.013420	6.19
0.507	10.0	4.0	11.50	0.087047	0.008878	0.087454	0.002784	-0.004439	0.003950	0.016669	5.22
0.505	8.0	6.0	10.80	0.087236	0.011638	0.087975	0.002456	-0.004895	0.002198	0.015990	5.46
0.513	6.0	8.0	9.70	0.092874	0.015077	0.094068	0.002005	-0.006294	0.000548	0.016145	5.75
0.51	4.0	10.0	8.50	0.095287	0.018864	0.097115	0.002031	-0.006016	-0.001515	0.015893	6.00
0.505	8.0	8.0	11.60	0.097067	0.014866	0.098191	0.001212	-0.004902	0.002034	0.018894	5.14
0.503	6.0	10.0	10.50	0.101994	0.019034	0.103750	0.001034	-0.005766	0.000092	0.019217	5.31
0.655	10.0	-8.0	7.40	0.003851	0.007262	0.002803	0.007727	-0.000367	0.002048	0.010389	0.37
0.655	4.0	-4.0	3.50	0.004067	0.005402	0.003680	0.005673	-0.000847	0.001679	0.007965	0.51
0.655	8.0	-6.0	6.60	0.007338	0.006191	0.006651	0.006924	-0.001012	0.002172	0.009507	0.77
0.649	2.0	-2.0	2.20	0.008193	0.005309	0.008003	0.005592	-0.001097	0.001407	0.007477	1.10
0.654	6.0	-4.0	5.50	0.008660	0.005405	0.008262	0.005996	-0.001188	0.001923	0.008345	1.04
0.65	0.0	0.0	0.90	0.010147	0.004982	0.010147	0.004982	-0.001162	0.001320	0.007013	1.45
0.656	10.0	-6.0	8.50	0.013116	0.006206	0.012395	0.007543	-0.001178	0.002735	0.010375	1.26
0.65	4.0	-2.0	4.50	0.014098	0.005532	0.013896	0.006021	-0.001745	0.001794	0.008292	1.70
0.654	8.0	-4.0	7.60	0.016060	0.005794	0.015617	0.006900	-0.001297	0.002450	0.009540	1.68
0.651	2.0	0.0	3.20	0.017574	0.005761	0.017574	0.005761	-0.001695	0.001333	0.007809	2.25
0.654	6.0	-2.0	6.70	0.021724	0.006038	0.021500	0.006792	-0.002208	0.002103	0.009254	2.35
0.652	0.0	2.0	2.00	0.022483	0.006042	0.022680	0.005254	-0.001985	0.000875	0.007384	3.04
0.655	10.0	-4.0	9.50	0.022676	0.006194	0.022189	0.007761	-0.001849	0.003040	0.010835	2.09
0.654	4.0	0.0	5.70	0.024088	0.006110	0.024088	0.006110	-0.002373	0.001728	0.008752	2.75

0.655	8.0	-2.0	8.70	0.027809	0.006252	0.027574	0.007219	-0.002432	0.002527	0.010110	2.75
0.65	2.0	2.0	4.30	0.029816	0.007067	0.030044	0.006022	-0.002813	0.001333	0.009118	3.27
0.654	6.0	0.0	7.60	0.032187	0.006727	0.032187	0.006727	-0.003426	0.001974	0.009745	3.30
0.674	6.0	0.0	7.60	0.034035	0.006486	0.034035	0.006486	-0.003241	0.002138	0.009658	3.52
0.654	10.0	-2.0	10.50	0.035409	0.007286	0.035133	0.008517	-0.003269	0.003237	0.012236	2.89
0.653	0.0	4.0	3.10	0.037459	0.008408	0.037954	0.005775	-0.002577	0.000057	0.008495	4.41
0.654	4.0	2.0	6.50	0.037528	0.007674	0.037773	0.006360	-0.003885	0.001397	0.009810	3.83
0.654	8.0	0.0	9.70	0.037534	0.006920	0.037534	0.006920	-0.003765	0.002524	0.010779	3.48
0.65	0.0	5.0	3.40	0.040322	0.009311	0.040980	0.005761	-0.003115	-0.000149	0.009082	4.44
0.675	8.0	0.0	9.50	0.042433	0.007378	0.042433	0.007378	-0.003689	0.002507	0.011092	3.83
0.65	2.0	4.0	5.40	0.042469	0.009225	0.043009	0.006240	-0.003465	0.000429	0.009885	4.30
0.654	6.0	2.0	8.60	0.042896	0.008218	0.043157	0.006716	-0.004556	0.001929	0.011168	3.84
0.654	4.0	3.0	7.10	0.044141	0.008722	0.044537	0.006400	-0.004132	0.001148	0.010477	4.21
0.655	10.0	0.0	11.50	0.044512	0.008054	0.044512	0.008054	-0.004379	0.003279	0.013060	3.41
0.653	2.0	5.0	5.60	0.046860	0.010144	0.047566	0.006021	-0.003810	0.000049	0.010219	4.59
0.654	0.0	6.0	4.00	0.047077	0.010030	0.047868	0.005054	-0.003570	-0.000684	0.008984	5.24
0.655	8.0	2.0	10.70	0.049291	0.008325	0.049552	0.006600	-0.004949	0.002420	0.012020	4.10
0.65	2.0	6.0	6.20	0.050666	0.010776	0.051515	0.005421	-0.004735	-0.000367	0.010211	4.96
0.654	4.0	4.0	7.60	0.050881	0.009872	0.051446	0.006299	-0.004709	0.000797	0.011091	4.59
0.65	0.0	7.0	4.60	0.051923	0.012493	0.053058	0.006072	-0.004197	-0.001327	0.010451	4.97
0.653	4.0	5.0	8.10	0.053976	0.010619	0.054696	0.005874	-0.005235	0.000575	0.011500	4.69
0.657	6.0	4.0	9.60	0.055625	0.010494	0.056222	0.006588	-0.005583	0.001413	0.012645	4.40
0.65	2.0	7.0	6.90	0.056556	0.012295	0.057633	0.005311	-0.005338	-0.000937	0.010853	5.21
0.657	10.0	2.0	12.00	0.058412	0.010149	0.058731	0.008104	-0.005109	0.003206	0.015029	3.89
0.654	4.0	6.0	8.50	0.058981	0.011881	0.059900	0.005651	-0.005619	0.000207	0.012198	4.84
0.649	0.0	8.0	5.00	0.060443	0.014462	0.061867	0.005909	-0.004864	-0.002008	0.011368	5.32
0.654	8.0	4.0	11.50	0.061954	0.010735	0.062552	0.006387	-0.005614	0.002046	0.013863	4.47
0.654	6.0	6.0	10.50	0.064735	0.012742	0.065712	0.005906	-0.006552	0.000752	0.013892	4.66
0.649	2.0	8.0	7.40	0.065347	0.014536	0.066734	0.005300	-0.005516	-0.001668	0.011966	5.46
0.654	4.0	7.0	9.00	0.066281	0.014205	0.067518	0.006021	-0.006063	-0.000446	0.013523	4.90
0.653	4.0	8.0	9.50	0.071390	0.015049	0.072790	0.004967	-0.006685	-0.000695	0.013985	5.10
0.654	6.0	8.0	11.50	0.071654	0.015319	0.073089	0.005198	-0.006134	0.000344	0.015845	4.52
0.654	6.0	7.0	10.90	0.072951	0.014447	0.074168	0.005449	-0.006615	0.000567	0.015314	4.76

0.654	8.0	6.0	12.00	0.074285	0.013998	0.075341	0.006156	-0.005741	0.001984	0.017032	4.36
0.657	10.0	4.0	12.00	0.080400	0.014919	0.081245	0.009274	-0.006284	0.003596	0.020392	3.94
0.655	8.0	8.0	12.00	0.099529	0.021385	0.101537	0.007325	-0.006365	0.002073	0.024550	4.05
0.653	10.0	6.0	12.00	0.102562	0.021474	0.104245	0.010636	-0.006245	0.004141	0.027816	3.69
0.757	10.0	-4.0	4.00	-0.004284	0.006792	-0.004747	0.006477	-0.000497	0.001260	0.008456	-0.51
0.756	6.0	-4.0	5.80	0.004121	0.007621	0.003579	0.007890	-0.001079	0.001538	0.009655	0.43
0.757	2.0	-2.0	2.10	0.004178	0.005738	0.003975	0.005880	-0.000898	0.001277	0.007425	0.56
0.757	8.0	-4.0	7.90	0.006192	0.008782	0.005564	0.009193	-0.001291	0.001641	0.010950	0.57
0.757	0.0	0.0	1.10	0.006686	0.005992	0.006686	0.005992	-0.001049	0.001091	0.007433	0.90
0.757	4.0	-2.0	4.60	0.007763	0.006507	0.007531	0.006774	-0.001258	0.001446	0.008417	0.92
0.757	10.0	-4.0	9.80	0.012330	0.009237	0.011656	0.010075	-0.001868	0.002232	0.012185	1.01
0.756	6.0	-2.0	7.10	0.013661	0.007842	0.013379	0.008314	-0.001913	0.001749	0.010155	1.35
0.758	2.0	0.0	3.30	0.014783	0.006337	0.014783	0.006337	-0.001688	0.001389	0.008169	1.81
0.754	8.0	-2.0	9.10	0.021555	0.008527	0.021244	0.009274	-0.002841	0.001978	0.011150	1.93
0.758	4.0	0.0	5.80	0.022084	0.007645	0.022084	0.007645	-0.003065	0.001502	0.009627	2.29
0.758	0.0	2.0	2.10	0.022658	0.006735	0.022879	0.005940	-0.002303	0.001090	0.008173	2.77
0.754	10.0	-2.0	10.90	0.024571	0.009255	0.024233	0.010107	-0.003354	0.002424	0.012470	1.97
0.747	6.0	0.0	7.80	0.025665	0.007814	0.025665	0.007814	-0.003312	0.001803	0.010228	2.51
0.759	2.0	2.0	4.60	0.029972	0.008096	0.030236	0.007045	-0.003177	0.001164	0.009630	3.11
0.754	8.0	0.0	9.80	0.034513	0.008471	0.034513	0.008471	-0.004429	0.002015	0.011143	3.10
0.758	4.0	2.0	6.80	0.034527	0.008925	0.034817	0.007715	-0.004611	0.001287	0.010623	3.25
0.769	6.0	2.0	9.00	0.040999	0.009735	0.041314	0.008298	-0.004883	0.001598	0.011813	3.47
0.758	0.0	6.0	4.10	0.043995	0.008164	0.044607	0.003521	-0.004136	-0.000462	0.007555	5.82
0.758	2.0	4.0	5.80	0.044084	0.007786	0.044520	0.004692	-0.004394	0.000470	0.008406	5.24
0.758	4.0	4.0	7.90	0.049453	0.010625	0.050074	0.007149	-0.005402	0.000691	0.011537	4.29
0.758	2.0	6.0	6.60	0.059174	0.011942	0.060098	0.005691	-0.005508	-0.000728	0.010982	5.39
0.759	4.0	6.0	9.00	0.061068	0.012662	0.062057	0.006209	-0.006819	0.000019	0.012687	4.81
0.758	0.0	4.0	3.30	0.024302	0.008015	0.024802	0.006300	-0.003314	0.000105	0.008154	2.98
0.757	0.0	8.0	5.60	0.069857	0.013652	0.071077	0.003797	-0.005547	-0.002218	0.010722	6.52
0.757	2.0	8.0	7.50	0.077460	0.012668	0.078469	0.001764	-0.006270	-0.002131	0.009853	7.86
0.856	6.0	-6.0	4.80	-0.042337	0.012749	-0.043438	0.008254	0.000001	0.000095	0.012860	-3.29
0.851	10.0	-8.0	7.80	-0.024691	0.016487	-0.026745	0.012890	-0.000103	-0.001364	0.014884	-1.66
0.856	8.0	-6.0	6.70	-0.020121	0.013683	-0.021441	0.011505	-0.000182	-0.000478	0.013125	-1.53

0.857	10.0	-6.0	9.00	-0.013660	0.014925	-0.015145	0.013415	-0.001386	-0.000007	0.014917	-0.92
0.857	4.0	-4.0	3.50	-0.013518	0.008901	-0.014106	0.007936	0.000086	0.000723	0.009745	-1.39
0.857	6.0	-4.0	6.00	-0.012185	0.011411	-0.012951	0.010533	-0.000839	0.000505	0.012000	-1.02
0.857	8.0	-4.0	8.00	-0.010774	0.012739	-0.011636	0.011956	-0.000748	0.000588	0.013425	-0.80
0.857	10.0	-4.0	10.10	-0.003352	0.014224	-0.004336	0.013956	-0.002418	0.001268	0.015704	-0.21
0.857	2.0	-2.0	2.20	-0.002154	0.007212	-0.002404	0.007132	-0.000710	0.001157	0.008562	-0.25
0.857	6.0	-2.0	7.20	0.001999	0.010986	0.001614	0.011049	-0.002194	0.001053	0.012215	0.16
0.856	4.0	-2.0	4.60	0.002573	0.008071	0.002290	0.008156	-0.002013	0.001372	0.009674	0.27
0.856	8.0	-2.0	9.20	0.005842	0.012090	0.005417	0.012287	-0.002571	0.001092	0.013366	0.44
0.869	0.0	0.0	1.10	0.009157	0.007066	0.009157	0.007066	-0.000928	0.001227	0.008478	1.08
0.857	10.0	-2.0	11.30	0.010328	0.013647	0.009845	0.013999	-0.003584	0.001573	0.015482	0.67
0.856	2.0	0.0	3.40	0.013687	0.007142	0.013687	0.007142	-0.001837	0.001087	0.008412	1.63
0.857	4.0	0.0	6.00	0.014054	0.008878	0.014054	0.008878	-0.003038	0.001504	0.010633	1.32
0.857	6.0	0.0	8.40	0.016861	0.010392	0.016861	0.010392	-0.003967	0.001262	0.011865	1.42
0.856	8.0	0.0	10.30	0.017837	0.011751	0.017837	0.011751	-0.003784	0.001039	0.012965	1.38
0.85	0.0	2.0	2.40	0.025285	0.007946	0.025547	0.007059	-0.002131	0.000885	0.008987	2.81
0.857	2.0	2.0	4.90	0.027029	0.009406	0.027341	0.008457	-0.002906	0.001093	0.010681	2.53
0.857	4.0	2.0	7.10	0.030507	0.009361	0.030815	0.008291	-0.004190	0.001139	0.010690	2.85
0.856	8.0	2.0	11.70	0.032029	0.012296	0.032439	0.011171	-0.005867	0.001610	0.014177	2.26
0.857	10.0	0.0	12.10	0.032562	0.013828	0.032562	0.013828	-0.006097	0.001969	0.016126	2.02
0.856	6.0	2.0	9.50	0.036642	0.012173	0.037045	0.010887	-0.005773	0.001303	0.013695	2.68
0.856	0.0	4.0	3.70	0.044369	0.010758	0.045011	0.007637	-0.003270	0.000358	0.011176	3.97
0.855	4.0	4.0	8.30	0.044482	0.010418	0.045100	0.007290	-0.005873	0.000550	0.011061	4.02
0.857	2.0	4.0	6.10	0.045267	0.012326	0.046017	0.009138	-0.004386	0.000170	0.012524	3.61
0.856	6.0	4.0	10.60	0.049443	0.014345	0.050323	0.010861	-0.006794	0.001338	0.015908	3.11
0.85	0.0	6.0	4.70	0.054647	0.013275	0.055735	0.007490	-0.004359	-0.000846	0.012280	4.45
0.855	2.0	6.0	7.00	0.059741	0.013436	0.060818	0.007118	-0.005632	-0.000753	0.012555	4.76
0.857	4.0	6.0	9.40	0.059869	0.013269	0.060928	0.006938	-0.007381	-0.000016	0.013250	4.52
0.855	6.0	6.0	11.00	0.074493	0.016773	0.075838	0.008894	-0.009339	0.000787	0.017693	4.21
0.85	0.0	8.0	6.00	0.077153	0.015555	0.078567	0.004666	-0.006229	-0.002354	0.012786	6.03
0.856	4.0	8.0	10.40	0.087129	0.016728	0.088609	0.004439	-0.008449	-0.000731	0.015874	5.49
0.943	6.0	0.0	8.60	0.008460	0.013235	0.008460	0.013235	-0.004009	0.000893	0.014182	0.60
0.946	8.0	0.0	10.80	0.009641	0.016465	0.009641	0.016465	-0.004516	0.000839	0.017352	0.56

0.944	4.0	0.0	6.40	0.011544	0.010247	0.011544	0.010247	-0.003813	0.001215	0.011534	1.00
0.944	2.0	0.0	3.90	0.011960	0.008421	0.011960	0.008421	-0.002032	0.001351	0.009852	1.21
0.945	0.0	0.0	1.40	0.016292	0.009670	0.016292	0.009670	-0.001045	0.001309	0.011055	1.47
0.946	8.0	1.0	11.40	0.017816	0.016220	0.018096	0.015907	-0.005715	0.001334	0.017630	1.01
0.946	8.0	2.0	11.90	0.027558	0.016400	0.028114	0.015428	-0.006503	0.001354	0.017831	1.55
0.943	4.0	2.0	7.80	0.028182	0.011534	0.028567	0.010543	-0.004876	0.001186	0.012792	2.20
0.944	6.0	2.0	9.90	0.030758	0.014543	0.031247	0.013461	-0.006390	0.001047	0.015652	1.97
0.936	2.0	2.0	5.00	0.031664	0.010052	0.031996	0.008941	-0.004002	0.001117	0.011245	2.82
0.947	0.0	2.0	2.60	0.032574	0.010043	0.032905	0.008900	-0.002956	0.000949	0.011045	2.95
0.943	6.0	4.0	11.00	0.039885	0.014295	0.040785	0.011478	-0.007371	0.001454	0.015837	2.52
0.942	4.0	4.0	9.00	0.046599	0.013040	0.047395	0.009758	-0.006599	0.000999	0.014101	3.30
0.934	2.0	4.0	6.50	0.046688	0.010841	0.047331	0.007558	-0.005357	0.000439	0.011311	4.13
0.947	0.0	4.0	3.80	0.048434	0.010786	0.049068	0.007381	-0.003729	0.000276	0.011077	4.37
0.944	4.0	5.0	9.50	0.050625	0.012742	0.051543	0.008281	-0.007456	0.000430	0.013198	3.84
0.943	2.0	5.0	6.90	0.051355	0.011579	0.052169	0.007059	-0.005627	0.000020	0.011600	4.43
0.945	6.0	5.0	11.50	0.052430	0.015486	0.053580	0.010857	-0.008258	0.001081	0.016630	3.15
0.944	6.0	6.0	12.00	0.060495	0.016417	0.061880	0.010004	-0.008561	0.000989	0.017465	3.46
0.934	2.0	6.0	7.40	0.061049	0.012904	0.062063	0.006452	-0.006331	-0.000439	0.012434	4.91
0.95	4.0	6.0	10.00	0.064593	0.015600	0.065870	0.008763	-0.008583	-0.000275	0.015311	4.22
0.938	0.0	6.0	4.90	0.065219	0.014055	0.066331	0.007161	-0.005639	-0.001133	0.012847	5.08
0.944	4.0	7.0	10.40	0.076014	0.017715	0.077606	0.008319	-0.009071	-0.000283	0.017415	4.36
0.95	2.0	7.0	8.20	0.076214	0.016296	0.077632	0.006886	-0.007694	-0.000947	0.015299	4.98
0.95	4.0	8.0	11.00	0.086372	0.017158	0.087919	0.004970	-0.007570	-0.000624	0.016501	5.23
0.933	2.0	8.0	8.70	0.090781	0.017473	0.092329	0.004669	-0.007170	-0.002595	0.014692	6.18
1.093	7.0	0.0	10.10	-0.000393	0.019516	-0.000393	0.019516	-0.005506	0.000422	0.019902	-0.02
1.093	5.0	0.0	7.90	0.000770	0.016904	0.000770	0.016904	-0.005155	0.000565	0.017421	0.04
1.094	6.0	0.0	8.90	0.001113	0.018485	0.001113	0.018485	-0.005240	0.000315	0.018773	0.06
1.094	2.0	-1.0	3.30	0.004248	0.012316	0.004032	0.012388	-0.002103	0.001656	0.013830	0.31
1.095	3.0	0.0	5.80	0.006914	0.013469	0.006914	0.013469	-0.003994	0.001608	0.014937	0.46
1.093	6.0	1.0	9.80	0.007938	0.017515	0.008242	0.017374	-0.005828	0.000648	0.018108	0.44
1.094	4.0	0.0	6.70	0.009104	0.015327	0.009104	0.015327	-0.004345	0.000912	0.016161	0.56
1.094	2.0	0.0	4.10	0.013370	0.012627	0.013370	0.012627	-0.003006	0.001739	0.014217	0.94
1.093	1.0	0.0	3.00	0.013696	0.011292	0.013696	0.011292	-0.002549	0.001671	0.012821	1.07

1.093	0.0	0.0	1.30	0.018777	0.011240	0.018777	0.011240	-0.001123	0.001568	0.012675	1.48
1.096	0.0	0.0	1.40	0.018883	0.011155	0.018883	0.011155	-0.000991	0.001378	0.012412	1.52
1.094	6.0	2.0	10.30	0.020529	0.017801	0.021138	0.017074	-0.007167	0.000746	0.018483	1.11
1.095	2.0	1.0	4.70	0.024251	0.013024	0.024475	0.012599	-0.003789	0.001760	0.014631	1.66
1.094	4.0	2.0	8.00	0.033820	0.014827	0.034317	0.013638	-0.005848	0.000743	0.015506	2.18
1.094	2.0	2.0	5.50	0.035843	0.012671	0.036263	0.011412	-0.004838	0.001605	0.014138	2.54
1.091	1.0	2.0	4.00	0.042760	0.012857	0.043183	0.011357	-0.004154	0.001572	0.014298	2.99
1.093	2.0	3.0	6.10	0.047212	0.012895	0.047822	0.010406	-0.005277	0.001444	0.014216	3.32
1.099	0.0	2.0	2.60	0.047906	0.012696	0.048320	0.011016	-0.003014	0.001512	0.014072	3.40
1.096	4.0	4.0	9.10	0.050287	0.016977	0.051349	0.013428	-0.007666	0.000791	0.017699	2.84
1.094	2.0	4.0	6.60	0.059979	0.015556	0.060918	0.011334	-0.006349	0.000975	0.016447	3.65
1.091	1.0	4.0	5.40	0.069081	0.015253	0.069977	0.010397	-0.005233	0.000756	0.015946	4.33
1.103	0.0	4.0	4.20	0.069374	0.015749	0.070304	0.010871	-0.004502	0.000512	0.016213	4.28
1.096	4.0	6.0	10.30	0.069839	0.018768	0.071418	0.011365	-0.008729	0.000336	0.019075	3.66
1.092	2.0	5.0	7.30	0.070154	0.017612	0.071422	0.011431	-0.007001	0.000462	0.018035	3.89
1.092	3.0	6.0	9.20	0.076078	0.018667	0.077612	0.010612	-0.008400	-0.000217	0.018468	4.12
1.09	2.0	6.0	7.70	0.084591	0.018434	0.086054	0.009491	-0.007993	-0.000611	0.017873	4.73
1.093	3.0	7.0	9.70	0.085803	0.019579	0.087550	0.008976	-0.008884	-0.000373	0.019238	4.46
1.111	0.0	6.0	5.50	0.087370	0.019777	0.088959	0.010536	-0.006727	-0.000835	0.019025	4.59
1.092	1.0	6.0	6.80	0.088362	0.018668	0.089829	0.009329	-0.007899	-0.000851	0.017889	4.94
1.096	0.0	6.0	5.40	0.089867	0.018441	0.091302	0.008946	-0.006787	-0.001243	0.017307	5.19
1.095	4.0	7.0	10.50	0.092317	0.022889	0.094418	0.011468	-0.009389	-0.000467	0.022463	4.11
1.095	2.0	7.0	8.40	0.099758	0.022567	0.101765	0.010241	-0.008670	-0.001661	0.021050	4.74
1.034	0.0	0.0	1.20	0.014520	0.010062	0.014520	0.010062	-0.001343	0.001564	0.011575	1.25

11.8 PCA-2 Experimental Data Set

References: 1. N.A.C.A. Report No. 515, Full-Scale Wind-Tunnel Tests of a PCA-2 Autogiro Rotor by John B. Wheatley and Manley J. Hood, October 1934
2. Harris EXCEL File: PCA-2 Rotor Alone Test Data + Geometry & Properties.xls

Airfoil	See Appendix 11.5
Chord	See Appendix 11.5
Diameter	45.00 ft
Twist	See Appendix 11.5
Disc Area	1,588 sq. ft
Reference Area (4 blades)	154.4 sq. ft
Nominal Solidity	0.0971
Lock Number	19.2
Flap Moment of inertia	334 slug ft ²
Weight Moment	780 lb-ft
Flap Hinge Radius	3.375 inches
Lag Hinge Radius	7.75 inches

Notes: 1. Wind axis data measured. Shaft axis data derived.
2. Shaft torque equal zero for all data points because rotor unpowered.
3. Wind axis coefficients based on wind tunnel dynamic pressure and rotor disc area ($A = 1,590$ sq. ft.).
4. Derived shaft axis coefficients based on rotor tip speed and rotor disc area ($A = 1,590$ sq. ft.).
5. Data includes hub drag and droop and blade to blade lag cable drag.
7. Articulated flap and lag hub but with no in-flight pitch change provisions.

Advance Ratio	Shaft Angle of Attack (deg)	Airplane Lift Coeff. C_L	Airplane Drag Coeff. C_D	L / D	RPM	Airplane Rolling Moment Coeff. C_l	Airplane Pitching Moment Coeff. C_m	Airplane Lateral Force Coeff. C_Y	Derived Rotor C_T	Derived Rotor C_H	Derived Rotor C_Y
0.1330	18.70	0.6050	0.2280	2.65	98.3	0.001574	0.000130	0.013100	0.005715	0.000195	0.000116
0.1340	18.80	0.5970	0.2260	2.64	97.5	0.001242	-0.000103	0.013000	0.005728	0.000193	0.000117
0.1690	13.00	0.4230	0.1150	3.68	98.8	0.001287	0.000192	0.010200	0.006255	0.000241	0.000146
0.2100	9.00	0.2780	0.0569	4.89	99.6	0.000997	0.000117	0.006100	0.006251	0.000280	0.000135
0.2100	9.00	0.2770	0.0559	4.95	98.3	0.000931	0.000140	0.006700	0.006225	0.000262	0.000148
0.2370	7.40	0.2200	0.0395	5.57	100.0	0.000717	0.000076	0.004700	0.006270	0.000304	0.000132
0.2370	7.50	0.2170	0.0391	5.55	100.0	0.000715	0.000085	0.004700	0.006186	0.000293	0.000132
0.2740	5.70	0.1590	0.0257	6.19	98.8	0.000414	0.000070	0.003100	0.006035	0.000367	0.000116
0.2750	5.70	0.1590	0.0257	6.19	98.8	0.000566	0.000075	0.003100	0.006079	0.000370	0.000117
0.3070	4.80	0.1239	0.0188	6.59	99.6	0.000236	0.000045	0.002200	0.005892	0.000394	0.000104
0.3090	4.80	0.1223	0.0185	6.61	98.8	0.000316	0.000051	0.002100	0.005892	0.000392	0.000100
0.3410	4.00	0.0989	0.0140	7.07	98.0	0.000256	0.000055	0.001700	0.005793	0.000411	0.000099
0.3440	4.00	0.0959	0.0143	6.71	97.1	0.000216	0.000048	0.001500	0.005719	0.000448	0.000089
0.3710	3.50	0.0812	0.0122	6.66	98.0	0.000296	0.000045	0.001200	0.005629	0.000497	0.000083
0.3720	3.50	0.0790	0.0120	6.58	98.0	0.000886	0.000017	0.001200	0.005507	0.000495	0.000083
0.3860	3.40	0.0737	0.0110	6.70	98.0	0.000159	0.000011	0.001100	0.005529	0.000492	0.000082
0.4140	3.00	0.0638	0.0109	5.85	97.5	0.000110	0.000016	0.000900	0.005509	0.000647	0.000077
0.4210	2.90	0.0624	0.0095	6.58	99.2	0.000258	0.000038	0.000900	0.005565	0.000561	0.000080
0.4490	2.60	0.0534	0.0082	6.51	98.3	0.000081	0.000054	0.000700	0.005415	0.000582	0.000071
0.4640	2.40	0.0489	0.0078	6.29	98.8	0.000050	0.000048	0.000600	0.005294	0.000615	0.000065
0.4900	2.10	0.0444	0.0071	6.24	98.8	0.000144	0.000019	0.000500	0.005358	0.000659	0.000060
0.5120	2.10	0.0390	0.0066	5.89	98.8	0.000099	0.000032	0.000400	0.005140	0.000680	0.000052
0.5350	2.00	0.0371	0.0063	5.89	99.7	0.000150	0.000015	0.000300	0.005338	0.000716	0.000043
0.5840	1.90	0.0317	0.0056	5.66	99.7	0.000298	0.000033	0.000400	0.005435	0.000779	0.000068
0.6370	1.80	0.0284	0.0051	5.57	98.8	0.000289	0.000018	0.000200	0.005792	0.000861	0.000041
0.7000	1.41	0.0240	0.0045	5.33	97.1	0.000149	0.000033	0.000100	0.005906	0.000967	0.000025
0.7220	1.20	0.0234	0.0046	5.09	102.1	0.000218	0.000026	0.00020	0.006123	0.001068	0.000052
0.1360	18.60	0.6010	0.2230	2.69	109.2	0.001845	0.000028	0.007700	0.005926	0.000182	0.000071

0.1480	16.00	0.5470	0.1770	3.09	119.2	0.001653	0.000272	0.003600	0.006293	0.000212	0.000039
0.1480	16.10	0.5400	0.1760	3.07	119.7	0.002695	0.000756	0.003600	0.006217	0.000212	0.000039
0.1820	11.10	0.3730	0.0866	4.31	118.9	0.000639	0.000018	0.006600	0.006338	0.000218	0.000109
0.1820	11.10	0.3760	0.0868	4.33	118.9	0.001001	0.000174	0.006400	0.006388	0.000212	0.000106
0.2160	8.30	0.2710	0.0530	5.11	117.6	0.000752	0.000116	0.006300	0.006434	0.000311	0.000147
0.2170	8.40	0.2690	0.0524	5.13	117.1	0.000646	0.000081	0.006200	0.006446	0.000295	0.000146
0.2450	6.70	0.2070	0.0359	5.76	118.1	0.000560	0.000109	0.006700	0.006296	0.000345	0.000201
0.2460	6.80	0.1980	0.0371	5.33	118.5	0.000502	0.000090	0.006800	0.006082	0.000405	0.000206
0.2780	5.40	0.1590	0.0259	6.14	117.6	0.000455	0.000073	0.003400	0.006211	0.000418	0.000131
0.2780	5.40	0.1600	0.0259	6.18	117.6	0.000565	0.000000	0.003500	0.006249	0.000415	0.000135
0.2990	4.70	0.1350	0.0212	6.37	118.9	0.000386	0.000059	0.002800	0.006092	0.000450	0.000125
0.3100	4.70	0.1309	0.0204	6.42	118.1	0.000256	0.000047	0.002600	0.006349	0.000462	0.000125
0.3120	4.40	0.1229	0.0190	6.47	118.5	0.000282	-0.000005	0.002500	0.006035	0.000463	0.000122
0.3350	4.00	0.1050	0.0160	6.56	119.7	0.000278	0.000036	0.002000	0.005940	0.000485	0.000112
0.3430	3.90	0.1004	0.0154	6.52	121.4	0.000448	0.000049	0.002000	0.005954	0.000502	0.000118
0.3740	3.40	0.0825	0.0124	6.65	117.1	0.000319	0.000029	0.001400	0.005811	0.000524	0.000098
0.3820	3.30	0.0786	0.0121	6.59	119.7	0.000317	0.000049	0.001500	0.005776	0.000551	0.000109
0.4120	2.80	0.0652	0.0100	6.52	117.1	0.000257	0.000046	0.001000	0.005569	0.000577	0.000085
0.4140	2.90	0.0657	0.0101	6.50	121.4	0.000339	0.000027	0.001200	0.005667	0.000580	0.000103
0.4430	2.70	0.0562	0.0090	6.26	119.7	0.000259	0.000024	0.000900	0.005550	0.000619	0.000088
0.4940	2.30	0.0439	0.0072	6.11	117.6	0.000094	0.000012	0.000600	0.005387	0.000660	0.000073
0.5170	2.10	0.0403	0.0068	5.93	120.5	0.000129	0.000018	0.000500	0.005416	0.000711	0.000067
0.5930	1.80	0.0305	0.0054	5.75	114.7	0.000009	0.000015	0.000300	0.005390	0.000777	0.000053
0.6080	1.60	0.0303	0.0055	5.61	120.5	0.000198	0.000034	0.000300	0.005626	0.000852	0.000055
0.1380	18.50	0.6140	0.2130	2.88	133.5	0.001509	0.000352	0.007100	0.006188	0.000068	0.000068
0.1380	18.50	0.6120	0.2130	2.87	133.9	0.001594	0.000313	0.007600	0.006170	0.000074	0.000072
0.1610	14.10	0.4990	0.1360	3.67	137.6	0.002114	0.000789	0.004700	0.006702	0.000134	0.000061
0.1610	14.10	0.4990	0.1360	3.67	137.6	0.001598	0.000499	0.005400	0.006702	0.000134	0.000070
0.2060	9.00	0.3180	0.0635	5.01	133.5	0.001057	0.000271	0.004400	0.006875	0.000275	0.000093
0.2070	8.80	0.3350	0.0593	5.65	132.8	0.000941	0.000243	0.004300	0.007287	0.000158	0.000092
0.2240	7.80	0.2680	0.0492	5.44	137.3	0.000580	0.000061	0.004100	0.006829	0.000310	0.000103
0.2250	7.80	0.2660	0.0488	5.45	137.3	0.000832	0.000176	0.004200	0.006838	0.000310	0.000106

0.2460	6.40	0.2185	0.0368	5.94	138.5	0.000439	0.000042	0.003900	0.006694	0.000370	0.000118
0.2490	6.50	0.2150	0.0360	5.97	137.6	0.000492	0.000090	0.003700	0.006749	0.000354	0.000115
0.2620	6.00	0.1924	0.0315	6.11	137.6	0.000484	0.000072	0.003800	0.006680	0.000385	0.000130
0.2780	5.30	0.1650	0.0263	6.27	138.5	0.000512	0.000091	0.003300	0.006443	0.000423	0.000128
0.2920	4.80	0.1496	0.0226	6.61	138.5	0.000329	0.000026	0.003000	0.006436	0.000426	0.000128
0.3080	4.50	0.1335	0.0200	6.68	138.5	0.000397	0.000046	0.002700	0.006387	0.000449	0.000128
0.3260	4.00	0.1177	0.0173	6.80	136.8	0.000416	0.000062	0.002300	0.006303	0.000481	0.000122
0.3420	3.70	0.0984	0.0161	6.11	139.2	0.000377	0.000050	0.002100	0.005803	0.000568	0.000123
0.3560	3.40	0.0955	0.0140	6.82	139.2	0.000137	0.000029	0.001800	0.006094	0.000527	0.000114
0.3790	3.10	0.0839	0.0123	6.82	138.5	0.000268	0.000008	0.001500	0.006065	0.000556	0.000108
0.4050	2.90	0.0718	0.0110	6.53	141.7	0.000348	0.000042	0.001400	0.005927	0.000603	0.000115
0.4400	2.50	0.0588	0.0090	6.60	140.9	0.000278	0.000030	0.001000	0.005724	0.000619	0.000097
0.4930	2.10	0.0461	0.0075	6.23	137.7	0.000229	0.000022	0.000500	0.005632	0.000704	0.000061
0.5200	1.70	0.0418	0.0068	6.15	140.9	0.000287	0.000050	0.000500	0.005676	0.000749	0.000068
0.1700	12.80	0.4690	0.1129	4.16	148.2	0.000986	0.000051	0.007700	0.006970	0.000089	0.000111
0.1710	12.80	0.4660	0.1122	4.15	147.7	0.001300	0.000150	0.007300	0.007007	0.000090	0.000107
0.1990	9.60	0.3510	0.0705	4.98	146.9	0.000721	0.000070	0.005000	0.007085	0.000217	0.000099
0.2010	9.70	0.3490	0.0707	4.93	147.7	0.001174	0.000083	0.005200	0.007190	0.000220	0.000105
0.2240	7.80	0.2790	0.0509	5.48	148.6	0.000698	0.000079	0.004400	0.007108	0.000315	0.000110
0.2260	7.80	0.2750	0.0500	5.50	147.7	0.000723	0.000106	0.004400	0.007131	0.000312	0.000112
0.2360	7.00	0.2500	0.0438	5.71	146.5	0.000744	0.000102	0.004100	0.007059	0.000362	0.000114
0.2570	6.10	0.2070	0.0338	6.12	147.4	0.000585	0.000081	0.003500	0.006916	0.000383	0.000116
0.2700	5.60	0.1840	0.0289	6.37	146.1	0.000515	0.000075	0.003000	0.006778	0.000394	0.000109
0.2840	4.80	0.1660	0.0253	6.56	146.9	0.000456	0.000056	0.002900	0.006756	0.000457	0.000117
0.3180	4.00	0.1201	0.0191	6.29	147.4	0.000426	0.000067	0.002200	0.006125	0.000540	0.000111
0.3290	3.80	0.1176	0.0174	6.75	148.2	0.000525	0.000082	0.002100	0.006413	0.000518	0.000114
0.3520	3.50	0.1013	0.0148	6.84	147.4	0.000429	0.000047	0.001900	0.006320	0.000532	0.000118
0.3750	3.00	0.0885	0.0132	6.70	152.3	0.000553	-0.000004	0.001500	0.006263	0.000601	0.000105
0.4120	2.70	0.0707	0.0105	6.73	149.0	0.000471	0.000008	0.001300	0.006036	0.000608	0.000110

11.9 Göttingen 429 and N.A.C.A. 0012 Airfoil Tables

The Göttingen 429 airfoil properties in C81 format were constructed by the author from test data. See Lock, C.N.H. and Townend, H. C. H., *Wind Tunnel Experiments on a Symmetrical Aerofoil (Göttingen 429 Section)*, Aeronautical Research Committee R & M No. 1066. November 1926. Ref: Harris EXCEL File: Gottingen 429, C81 Table.xls

The N.A.C.A. 0012 airfoil properties in C81 format are commonly used by many comprehensive code developers and have been included in this report for the sake of completeness. Ref: Harris EXCEL File: NACA0012-StdC81 Table.xls

Gottingen 429 Airfoil Table

CL	RN															
alpha	10,000	20,000	63,939	85,251	106,564	127,877	149,190	200,000	287,724	383,632	575,448	767,263	1,000,000	2,000,000	3,000,000	5,000,000
-180.0	0.0000	0.0000	0.0000	0.0000	0.0000	0.0000	0.0000	0.0000	0.0000	0.0000	0.0000	0.0000	0.0000	0.0000	0.0000	0.0000
-179.0	0.1200	0.1200	0.1200	0.1200	0.1200	0.1200	0.1200	0.1200	0.1200	0.1200	0.1200	0.1200	0.1200	0.1200	0.1200	0.1200
-178.0	0.2400	0.2400	0.2400	0.2400	0.2400	0.2400	0.2400	0.2400	0.2400	0.2400	0.2400	0.2400	0.2400	0.2400	0.2400	0.2400
-177.0	0.3600	0.3600	0.3600	0.3600	0.3600	0.3600	0.3600	0.3600	0.3600	0.3600	0.3600	0.3600	0.3600	0.3600	0.3600	0.3600
-176.0	0.4800	0.4800	0.4800	0.4800	0.4800	0.4800	0.4800	0.4800	0.4800	0.4800	0.4800	0.4800	0.4800	0.4800	0.4800	0.4800
-175.0	0.6000	0.6000	0.6000	0.6000	0.6000	0.6000	0.6000	0.6000	0.6000	0.6000	0.6000	0.6000	0.6000	0.6000	0.6000	0.6000
-174.0	0.6800	0.6800	0.6800	0.6800	0.6800	0.6800	0.6800	0.6800	0.6800	0.6800	0.6800	0.6800	0.6800	0.6800	0.6800	0.6800
-173.0	0.7320	0.7320	0.7320	0.7320	0.7320	0.7320	0.7320	0.7320	0.7320	0.7320	0.7320	0.7320	0.7320	0.7320	0.7320	0.7320
-172.0	0.7690	0.7690	0.7690	0.7690	0.7690	0.7690	0.7690	0.7690	0.7690	0.7690	0.7690	0.7690	0.7690	0.7690	0.7690	0.7690
-171.0	0.7939	0.7939	0.7939	0.7939	0.7939	0.7939	0.7939	0.7939	0.7939	0.7939	0.7939	0.7939	0.7939	0.7939	0.7939	0.7939
-170.0	0.8090	0.8090	0.8090	0.8090	0.8090	0.8090	0.8090	0.8090	0.8090	0.8090	0.8090	0.8090	0.8090	0.8090	0.8090	0.8090
-169.0	0.8175	0.8175	0.8175	0.8175	0.8175	0.8175	0.8175	0.8175	0.8175	0.8175	0.8175	0.8175	0.8175	0.8175	0.8175	0.8175
-168.0	0.8200	0.8200	0.8200	0.8200	0.8200	0.8200	0.8200	0.8200	0.8200	0.8200	0.8200	0.8200	0.8200	0.8200	0.8200	0.8200
-167.0	0.8158	0.8158	0.8158	0.8158	0.8158	0.8158	0.8158	0.8158	0.8158	0.8158	0.8158	0.8158	0.8158	0.8158	0.8158	0.8158
-166.0	0.8077	0.8077	0.8077	0.8077	0.8077	0.8077	0.8077	0.8077	0.8077	0.8077	0.8077	0.8077	0.8077	0.8077	0.8077	0.8077
-165.0	0.7950	0.7950	0.7950	0.7950	0.7950	0.7950	0.7950	0.7950	0.7950	0.7950	0.7950	0.7950	0.7950	0.7950	0.7950	0.7950
-164.0	0.7800	0.7800	0.7800	0.7800	0.7800	0.7800	0.7800	0.7800	0.7800	0.7800	0.7800	0.7800	0.7800	0.7800	0.7800	0.7800
-163.0	0.7633	0.7633	0.7633	0.7633	0.7633	0.7633	0.7633	0.7633	0.7633	0.7633	0.7633	0.7633	0.7633	0.7633	0.7633	0.7633
-162.0	0.7460	0.7460	0.7460	0.7460	0.7460	0.7460	0.7460	0.7460	0.7460	0.7460	0.7460	0.7460	0.7460	0.7460	0.7460	0.7460
-161.0	0.7281	0.7281	0.7281	0.7281	0.7281	0.7281	0.7281	0.7281	0.7281	0.7281	0.7281	0.7281	0.7281	0.7281	0.7281	0.7281
-160.0	0.7137	0.7137	0.7137	0.7137	0.7137	0.7137	0.7137	0.7137	0.7137	0.7137	0.7137	0.7137	0.7137	0.7137	0.7137	0.7137
-159.0	0.7033	0.7033	0.7033	0.7033	0.7033	0.7033	0.7033	0.7033	0.7033	0.7033	0.7033	0.7033	0.7033	0.7033	0.7033	0.7033
-158.0	0.6964	0.6964	0.6964	0.6964	0.6964	0.6964	0.6964	0.6964	0.6964	0.6964	0.6964	0.6964	0.6964	0.6964	0.6964	0.6964
-157.0	0.6941	0.6941	0.6941	0.6941	0.6941	0.6941	0.6941	0.6941	0.6941	0.6941	0.6941	0.6941	0.6941	0.6941	0.6941	0.6941
-156.0	0.6947	0.6947	0.6947	0.6947	0.6947	0.6947	0.6947	0.6947	0.6947	0.6947	0.6947	0.6947	0.6947	0.6947	0.6947	0.6947
-155.0	0.6993	0.6993	0.6993	0.6993	0.6993	0.6993	0.6993	0.6993	0.6993	0.6993	0.6993	0.6993	0.6993	0.6993	0.6993	0.6993
-152.5	0.7264	0.7264	0.7264	0.7264	0.7264	0.7264	0.7264	0.7264	0.7264	0.7264	0.7264	0.7264	0.7264	0.7264	0.7264	0.7264

-150.0	0.7780	0.7780	0.7780	0.7780	0.7780	0.7780	0.7780	0.7780	0.7780	0.7780	0.7780	0.7780	0.7780	0.7780	0.7780	0.7780
-140.0	1.0000	1.0000	1.0000	1.0000	1.0000	1.0000	1.0000	1.0000	1.0000	1.0000	1.0000	1.0000	1.0000	1.0000	1.0000	1.0000
-130.0	1.0550	1.0550	1.0550	1.0550	1.0550	1.0550	1.0550	1.0550	1.0550	1.0550	1.0550	1.0550	1.0550	1.0550	1.0550	1.0550
-120.0	0.9510	0.9510	0.9510	0.9510	0.9510	0.9510	0.9510	0.9510	0.9510	0.9510	0.9510	0.9510	0.9510	0.9510	0.9510	0.9510
-110.0	0.6920	0.6920	0.6920	0.6920	0.6920	0.6920	0.6920	0.6920	0.6920	0.6920	0.6920	0.6920	0.6920	0.6920	0.6920	0.6920
-100.0	0.3560	0.3560	0.3560	0.3560	0.3560	0.3560	0.3560	0.3560	0.3560	0.3560	0.3560	0.3560	0.3560	0.3560	0.3560	0.3560
-90.0	0.0000	0.0000	0.0000	0.0000	0.0000	0.0000	0.0000	0.0000	0.0000	0.0000	0.0000	0.0000	0.0000	0.0000	0.0000	0.0000
-80.0	-0.3560	-0.3560	-0.3560	-0.3560	-0.3560	-0.3560	-0.3560	-0.3560	-0.3560	-0.3560	-0.3560	-0.3560	-0.3560	-0.3560	-0.3560	-0.3560
-70.0	-0.6920	-0.6920	-0.6920	-0.6920	-0.6920	-0.6920	-0.6920	-0.6920	-0.6920	-0.6920	-0.6920	-0.6920	-0.6920	-0.6920	-0.6920	-0.6920
-60.0	-0.9510	-0.9510	-0.9510	-0.9510	-0.9510	-0.9510	-0.9510	-0.9510	-0.9510	-0.9510	-0.9510	-0.9510	-0.9510	-0.9510	-0.9510	-0.9510
-50.0	-1.1000	-1.1000	-1.1000	-1.1000	-1.1000	-1.1000	-1.1000	-1.1000	-1.1000	-1.1000	-1.1000	-1.1000	-1.1000	-1.1000	-1.1000	-1.1000
-40.0	-1.1000	-1.1000	-1.1000	-1.1000	-1.1000	-1.1000	-1.1000	-1.1000	-1.1000	-1.1000	-1.1000	-1.1000	-1.1000	-1.1000	-1.1000	-1.1000
-30.0	-0.9600	-0.9600	-0.9600	-0.9600	-0.9600	-0.9600	-0.9600	-0.9600	-0.9600	-0.9600	-0.9600	-0.9600	-0.9600	-0.9600	-0.9600	-0.9600
-25.0	-0.8470	-0.8470	-0.8470	-0.8470	-0.8470	-0.8470	-0.8470	-0.8470	-0.8470	-0.8470	-0.8600	-0.8600	-0.8600	-0.8600	-0.8600	-0.8600
-24.0	-0.8240	-0.8240	-0.8240	-0.8240	-0.8240	-0.8240	-0.8240	-0.8240	-0.8240	-0.8240	-0.8420	-0.8420	-0.8420	-0.8420	-0.8420	-0.8420
-23.0	-0.8030	-0.8030	-0.8030	-0.8030	-0.8030	-0.8030	-0.8030	-0.8030	-0.8030	-0.8030	-0.8253	-0.8253	-0.8253	-0.8253	-0.8253	-0.8253
-22.0	-0.7860	-0.7860	-0.7860	-0.7860	-0.7860	-0.7860	-0.7860	-0.7860	-0.7860	-0.7860	-0.8097	-0.8097	-0.8097	-0.8097	-0.8097	-0.8097
-21.0	-0.7700	-0.7700	-0.7700	-0.7700	-0.7700	-0.7700	-0.7700	-0.7700	-0.7700	-0.7700	-0.7981	-0.8006	-0.8006	-0.8006	-0.8006	-0.8006
-20.0	-0.7580	-0.7580	-0.7580	-0.7580	-0.7580	-0.7580	-0.7580	-0.7580	-0.7580	-0.7580	-0.7899	-0.7970	-0.7970	-0.7970	-0.7970	-0.7970
-19.0	-0.7480	-0.7480	-0.7480	-0.7480	-0.7480	-0.7480	-0.7480	-0.7480	-0.7480	-0.7480	-0.7833	-0.8000	-0.8050	-0.8110	-0.8167	-0.8238
-18.0	-0.7420	-0.7420	-0.7420	-0.7420	-0.7420	-0.7420	-0.7420	-0.7420	-0.7420	-0.7420	-0.7808	-0.8141	-0.8260	-0.8374	-0.8484	-0.8620
-17.0	-0.7380	-0.7380	-0.7380	-0.7380	-0.7380	-0.7380	-0.7380	-0.7380	-0.7380	-0.7380	-0.7792	-0.8350	-0.8530	-0.8711	-0.8860	-0.9035
-16.0	-0.7374	-0.7374	-0.7374	-0.7374	-0.7385	-0.7385	-0.7385	-0.7385	-0.7385	-0.7420	-0.7849	-0.8620	-0.8940	-0.9191	-0.9392	-0.9600
-15.0	-0.7390	-0.7390	-0.7390	-0.7390	-0.7411	-0.7423	-0.7432	-0.7432	-0.7432	-0.7510	-0.7960	-0.9000	-0.9420	-0.9781	-1.0040	-1.0293
-14.0	-0.7442	-0.7442	-0.7442	-0.7442	-0.7463	-0.7482	-0.7507	-0.7530	-0.7530	-0.7700	-0.8160	-0.9547	-1.0080	-1.0772	-1.1083	-1.1360
-13.5	-0.7500	-0.7500	-0.7500	-0.7500	-0.7564	-0.7564	-0.7564	-0.7564	-0.7609	-0.7804	-0.8309	-0.9819	-1.0519	-1.1518	-1.1848	-1.2146
-13.0	-0.7555	-0.7555	-0.7555	-0.7555	-0.7571	-0.7600	-0.7634	-0.7664	-0.7677	-0.7940	-0.8500	-1.0130	-1.0980	-1.2231	-1.2420	-1.2671
-12.5	-0.7620	-0.7620	-0.7620	-0.7620	-0.7644	-0.7669	-0.7708	-0.7747	-0.7781	-0.8077	-0.8698	-1.0430	-1.1420	-1.2566	-1.2675	-1.2820
-12.0	-0.7690	-0.7690	-0.7690	-0.7690	-0.7721	-0.7742	-0.7779	-0.7843	-0.7903	-0.8260	-0.8950	-1.0770	-1.1720	-1.2438	-1.2549	-1.2660
-11.5	-0.7764	-0.7764	-0.7764	-0.7764	-0.7794	-0.7816	-0.7850	-0.7929	-0.8031	-0.8450	-0.9320	-1.0970	-1.1740	-1.2133	-1.2194	-1.2255
-11.0	-0.7840	-0.7840	-0.7840	-0.7840	-0.7865	-0.7885	-0.7929	-0.8015	-0.8167	-0.8670	-0.9704	-1.0970	-1.1576	-1.1763	-1.1770	-1.1770

-10.5	-0.7911	-0.7911	-0.7911	-0.7911	-0.7936	-0.7963	-0.7998	-0.8101	-0.8299	-0.8880	-0.9940	-1.0820	-1.1180	-1.1286	-1.1290	-1.1290
-10.0	-0.7975	-0.7975	-0.7975	-0.7975	-0.8000	-0.8022	-0.8066	-0.8169	-0.8420	-0.9070	-0.9940	-1.0480	-1.0714	-1.0809	-1.0809	-1.0809
-9.5	-0.8028	-0.8028	-0.8028	-0.8028	-0.8055	-0.8077	-0.8110	-0.8208	-0.8459	-0.9070	-0.9638	-1.0004	-1.0200	-1.0269	-1.0269	-1.0269
-9.0	-0.8040	-0.8040	-0.8040	-0.8040	-0.8074	-0.8090	-0.8117	-0.8208	-0.8436	-0.8860	-0.9230	-0.9478	-0.9728	-0.9728	-0.9728	-0.9728
-8.5	-0.7945	-0.7945	-0.7945	-0.7945	-0.7985	-0.8012	-0.8052	-0.8126	-0.8281	-0.8470	-0.8777	-0.8951	-0.9188	-0.9188	-0.9188	-0.9188
-8.0	-0.7696	-0.7696	-0.7696	-0.7696	-0.7721	-0.7757	-0.7811	-0.7869	-0.7963	-0.8050	-0.8261	-0.8425	-0.8648	-0.8648	-0.8648	-0.8648
-7.5	-0.7350	-0.7350	-0.7350	-0.7350	-0.7380	-0.7394	-0.7418	-0.7448	-0.7545	-0.7607	-0.7745	-0.7898	-0.8107	-0.8107	-0.8107	-0.8107
-7.0	-0.6932	-0.6932	-0.6932	-0.6932	-0.6943	-0.6965	-0.6965	-0.6992	-0.7042	-0.7100	-0.7228	-0.7372	-0.7567	-0.7567	-0.7567	-0.7567
-6.5	-0.6437	-0.6437	-0.6437	-0.6437	-0.6447	-0.6468	-0.6468	-0.6493	-0.6539	-0.6593	-0.6712	-0.6845	-0.7026	-0.7026	-0.7026	-0.7026
-6.0	-0.5942	-0.5942	-0.5942	-0.5942	-0.5951	-0.5970	-0.5970	-0.5993	-0.6036	-0.6086	-0.6196	-0.6319	-0.6486	-0.6486	-0.6486	-0.6486
-5.0	-0.4952	-0.4952	-0.4952	-0.4952	-0.4959	-0.4975	-0.4975	-0.4995	-0.5030	-0.5072	-0.5163	-0.5266	-0.5405	-0.5405	-0.5405	-0.5405
-4.0	-0.3961	-0.3961	-0.3961	-0.3961	-0.3967	-0.3980	-0.3980	-0.3996	-0.4024	-0.4057	-0.4130	-0.4212	-0.4324	-0.4324	-0.4324	-0.4324
-3.0	-0.2971	-0.2971	-0.2971	-0.2971	-0.2976	-0.2985	-0.2985	-0.2997	-0.3018	-0.3043	-0.3098	-0.3159	-0.3243	-0.3243	-0.3243	-0.3243
-2.0	-0.1981	-0.1981	-0.1981	-0.1981	-0.1984	-0.1990	-0.1990	-0.1998	-0.2012	-0.2029	-0.2065	-0.2106	-0.2162	-0.2162	-0.2162	-0.2162
-1.0	-0.0990	-0.0990	-0.0990	-0.0990	-0.0992	-0.0995	-0.0995	-0.0999	-0.1006	-0.1014	-0.1033	-0.1053	-0.1081	-0.1081	-0.1081	-0.1081
0.0	0.0000	0.0000	0.0000	0.0000	0.0000	0.0000	0.0000	0.0000	0.0000	0.0000	0.0000	0.0000	0.0000	0.0000	0.0000	0.0000
1.0	0.0990	0.0990	0.0990	0.0990	0.0992	0.0995	0.0995	0.0999	0.1006	0.1014	0.1033	0.1053	0.1081	0.1081	0.1081	0.1081
2.0	0.1981	0.1981	0.1981	0.1981	0.1984	0.1990	0.1990	0.1998	0.2012	0.2029	0.2065	0.2106	0.2162	0.2162	0.2162	0.2162
3.0	0.2971	0.2971	0.2971	0.2971	0.2976	0.2985	0.2985	0.2997	0.3018	0.3043	0.3098	0.3159	0.3243	0.3243	0.3243	0.3243
4.0	0.3961	0.3961	0.3961	0.3961	0.3967	0.3980	0.3980	0.3996	0.4024	0.4057	0.4130	0.4212	0.4324	0.4324	0.4324	0.4324
5.0	0.4952	0.4952	0.4952	0.4952	0.4959	0.4975	0.4975	0.4995	0.5030	0.5072	0.5163	0.5266	0.5405	0.5405	0.5405	0.5405
6.0	0.5942	0.5942	0.5942	0.5942	0.5951	0.5970	0.5970	0.5993	0.6036	0.6086	0.6196	0.6319	0.6486	0.6486	0.6486	0.6486
6.5	0.6437	0.6437	0.6437	0.6437	0.6447	0.6468	0.6468	0.6493	0.6539	0.6593	0.6712	0.6845	0.7026	0.7026	0.7026	0.7026
7.0	0.6932	0.6932	0.6932	0.6932	0.6943	0.6965	0.6965	0.6992	0.7042	0.7100	0.7228	0.7372	0.7567	0.7567	0.7567	0.7567
7.5	0.7350	0.7350	0.7350	0.7350	0.7380	0.7394	0.7418	0.7448	0.7545	0.7607	0.7745	0.7898	0.8107	0.8107	0.8107	0.8107
8.0	0.7696	0.7696	0.7696	0.7696	0.7721	0.7757	0.7811	0.7869	0.7963	0.8050	0.8261	0.8425	0.8648	0.8648	0.8648	0.8648
8.5	0.7945	0.7945	0.7945	0.7945	0.7985	0.8012	0.8052	0.8126	0.8281	0.8470	0.8777	0.8951	0.9188	0.9188	0.9188	0.9188
9.0	0.8040	0.8040	0.8040	0.8040	0.8074	0.8090	0.8117	0.8208	0.8436	0.8860	0.9230	0.9478	0.9728	0.9728	0.9728	0.9728
9.5	0.8028	0.8028	0.8028	0.8028	0.8055	0.8077	0.8110	0.8208	0.8459	0.9070	0.9638	1.0004	1.0200	1.0269	1.0269	1.0269
10.0	0.7975	0.7975	0.7975	0.7975	0.8000	0.8022	0.8066	0.8169	0.8420	0.9070	0.9940	1.0480	1.0714	1.0809	1.0809	1.0809
10.5	0.7911	0.7911	0.7911	0.7911	0.7936	0.7963	0.7998	0.8101	0.8299	0.8880	0.9940	1.0820	1.1180	1.1286	1.1290	1.1290

11.0	0.7840	0.7840	0.7840	0.7840	0.7865	0.7885	0.7929	0.8015	0.8167	0.8670	0.9704	1.0970	1.1576	1.1763	1.1770	1.1770
11.5	0.7764	0.7764	0.7764	0.7764	0.7794	0.7816	0.7850	0.7929	0.8031	0.8450	0.9320	1.0970	1.1740	1.2133	1.2194	1.2255
12.0	0.7690	0.7690	0.7690	0.7690	0.7721	0.7742	0.7779	0.7843	0.7903	0.8260	0.8950	1.0770	1.1720	1.2438	1.2549	1.2660
12.5	0.7620	0.7620	0.7620	0.7620	0.7644	0.7669	0.7708	0.7747	0.7781	0.8077	0.8698	1.0430	1.1420	1.2566	1.2675	1.2820
13.0	0.7555	0.7555	0.7555	0.7555	0.7571	0.7600	0.7634	0.7664	0.7677	0.7940	0.8500	1.0130	1.0980	1.2231	1.2420	1.2671
13.5	0.7500	0.7500	0.7500	0.7500	0.7564	0.7564	0.7564	0.7564	0.7609	0.7804	0.8309	0.9819	1.0519	1.1518	1.1848	1.2146
14.0	0.7442	0.7442	0.7442	0.7442	0.7463	0.7482	0.7507	0.7530	0.7530	0.7700	0.8160	0.9547	1.0080	1.0772	1.1083	1.1360
15.0	0.7390	0.7390	0.7390	0.7390	0.7411	0.7423	0.7432	0.7432	0.7432	0.7510	0.7960	0.9000	0.9420	0.9781	1.0040	1.0293
16.0	0.7374	0.7374	0.7374	0.7374	0.7385	0.7385	0.7385	0.7385	0.7385	0.7420	0.7849	0.8620	0.8940	0.9191	0.9392	0.9600
17.0	0.7380	0.7380	0.7380	0.7380	0.7380	0.7380	0.7380	0.7380	0.7380	0.7380	0.7792	0.8350	0.8530	0.8711	0.8860	0.9035
18.0	0.7420	0.7420	0.7420	0.7420	0.7420	0.7420	0.7420	0.7420	0.7420	0.7420	0.7808	0.8141	0.8260	0.8374	0.8484	0.8620
19.0	0.7480	0.7480	0.7480	0.7480	0.7480	0.7480	0.7480	0.7480	0.7480	0.7480	0.7833	0.8000	0.8050	0.8110	0.8167	0.8238
20.0	0.7580	0.7580	0.7580	0.7580	0.7580	0.7580	0.7580	0.7580	0.7580	0.7580	0.7899	0.7970	0.7970	0.7970	0.7970	0.7970
21.0	0.7700	0.7700	0.7700	0.7700	0.7700	0.7700	0.7700	0.7700	0.7700	0.7700	0.7981	0.8006	0.8006	0.8006	0.8006	0.8006
22.0	0.7860	0.7860	0.7860	0.7860	0.7860	0.7860	0.7860	0.7860	0.7860	0.7860	0.8097	0.8097	0.8097	0.8097	0.8097	0.8097
23.0	0.8030	0.8030	0.8030	0.8030	0.8030	0.8030	0.8030	0.8030	0.8030	0.8030	0.8253	0.8253	0.8253	0.8253	0.8253	0.8253
24.0	0.8240	0.8240	0.8240	0.8240	0.8240	0.8240	0.8240	0.8240	0.8240	0.8240	0.8420	0.8420	0.8420	0.8420	0.8420	0.8420
25.0	0.8470	0.8470	0.8470	0.8470	0.8470	0.8470	0.8470	0.8470	0.8470	0.8470	0.8600	0.8600	0.8600	0.8600	0.8600	0.8600
30.0	0.9600	0.9600	0.9600	0.9600	0.9600	0.9600	0.9600	0.9600	0.9600	0.9600	0.9600	0.9600	0.9600	0.9600	0.9600	0.9600
40.0	1.1000	1.1000	1.1000	1.1000	1.1000	1.1000	1.1000	1.1000	1.1000	1.1000	1.1000	1.1000	1.1000	1.1000	1.1000	1.1000
50.0	1.1000	1.1000	1.1000	1.1000	1.1000	1.1000	1.1000	1.1000	1.1000	1.1000	1.1000	1.1000	1.1000	1.1000	1.1000	1.1000
60.0	0.9510	0.9510	0.9510	0.9510	0.9510	0.9510	0.9510	0.9510	0.9510	0.9510	0.9510	0.9510	0.9510	0.9510	0.9510	0.9510
70.0	0.6920	0.6920	0.6920	0.6920	0.6920	0.6920	0.6920	0.6920	0.6920	0.6920	0.6920	0.6920	0.6920	0.6920	0.6920	0.6920
80.0	0.3560	0.3560	0.3560	0.3560	0.3560	0.3560	0.3560	0.3560	0.3560	0.3560	0.3560	0.3560	0.3560	0.3560	0.3560	0.3560
90.0	0.0000	0.0000	0.0000	0.0000	0.0000	0.0000	0.0000	0.0000	0.0000	0.0000	0.0000	0.0000	0.0000	0.0000	0.0000	0.0000
100.0	-0.3560	-0.3560	-0.3560	-0.3560	-0.3560	-0.3560	-0.3560	-0.3560	-0.3560	-0.3560	-0.3560	-0.3560	-0.3560	-0.3560	-0.3560	-0.3560
110.0	-0.6920	-0.6920	-0.6920	-0.6920	-0.6920	-0.6920	-0.6920	-0.6920	-0.6920	-0.6920	-0.6920	-0.6920	-0.6920	-0.6920	-0.6920	-0.6920
120.0	-0.9510	-0.9510	-0.9510	-0.9510	-0.9510	-0.9510	-0.9510	-0.9510	-0.9510	-0.9510	-0.9510	-0.9510	-0.9510	-0.9510	-0.9510	-0.9510
130.0	-1.0550	-1.0550	-1.0550	-1.0550	-1.0550	-1.0550	-1.0550	-1.0550	-1.0550	-1.0550	-1.0550	-1.0550	-1.0550	-1.0550	-1.0550	-1.0550
140.0	-1.0000	-1.0000	-1.0000	-1.0000	-1.0000	-1.0000	-1.0000	-1.0000	-1.0000	-1.0000	-1.0000	-1.0000	-1.0000	-1.0000	-1.0000	-1.0000
150.0	-0.7780	-0.7780	-0.7780	-0.7780	-0.7780	-0.7780	-0.7780	-0.7780	-0.7780	-0.7780	-0.7780	-0.7780	-0.7780	-0.7780	-0.7780	-0.7780

[illegible]

CD	RN															
alpha	10,000	20,000	63,939	85,251	106,564	127,877	149,190	200,000	287,724	383,632	575,448	767,263	1,000,000	2,000,000	3,000,000	5,000,000
-180.0	0.04400	0.03986	0.03435	0.03322	0.03239	0.03175	0.03123	0.03029	0.02943	0.02889	0.02844	0.02820	0.02820	0.02820	0.02820	0.02820
-179.0	0.04383	0.03970	0.03419	0.03305	0.03222	0.03158	0.03106	0.03013	0.02926	0.02871	0.02822	0.02786	0.02786	0.02786	0.02786	0.02786
-178.0	0.04730	0.04316	0.03765	0.03652	0.03569	0.03505	0.03453	0.03359	0.03273	0.03220	0.03161	0.03119	0.03119	0.03119	0.03119	0.03119
-177.0	0.05419	0.05005	0.04454	0.04340	0.04258	0.04193	0.04141	0.04048	0.03961	0.03912	0.03837	0.03794	0.03794	0.03794	0.03794	0.03794
-176.0	0.06434	0.06021	0.05469	0.05356	0.05273	0.05209	0.05157	0.05064	0.04977	0.04926	0.04825	0.04785	0.04785	0.04785	0.04785	0.04785
-175.0	0.07768	0.07354	0.06803	0.06689	0.06607	0.06543	0.06491	0.06397	0.06310	0.06244	0.06106	0.06066	0.06066	0.06066	0.06066	0.06066
-174.0	0.09416	0.09002	0.08451	0.08338	0.08255	0.08191	0.08139	0.08046	0.07959	0.07851	0.07660	0.07610	0.07570	0.07570	0.07570	0.07570
-173.0	0.11148	0.10734	0.10183	0.10069	0.09987	0.09923	0.09871	0.09777	0.09690	0.09547	0.09323	0.09262	0.09204	0.09204	0.09204	0.09204
-172.0	0.13074	0.12660	0.12109	0.11996	0.11913	0.11849	0.11797	0.11704	0.11617	0.11427	0.11164	0.11085	0.10986	0.10986	0.10986	0.10986
-171.0	0.15170	0.14757	0.14206	0.14092	0.14010	0.13945	0.13893	0.13800	0.13713	0.13462	0.13154	0.13049	0.12905	0.12905	0.12905	0.12905
-170.0	0.17491	0.17077	0.16526	0.16412	0.16330	0.16266	0.16214	0.16120	0.16033	0.15703	0.15267	0.15126	0.14953	0.14953	0.14953	0.14953
-169.0	0.20557	0.20143	0.19592	0.19478	0.19396	0.19331	0.19279	0.19186	0.19099	0.18489	0.17689	0.17285	0.17079	0.17079	0.17079	0.17079
-168.0	0.26091	0.25677	0.25126	0.25012	0.24930	0.24865	0.24813	0.24380	0.23340	0.22210	0.20583	0.19498	0.19273	0.19273	0.19273	0.19273
-167.0	0.32523	0.32109	0.31773	0.31578	0.31437	0.31298	0.30590	0.29180	0.27200	0.25320	0.23620	0.21795	0.21495	0.21495	0.21495	0.21495
-166.0	0.37213	0.37010	0.36730	0.36480	0.36052	0.35520	0.34540	0.32690	0.30490	0.28800	0.26730	0.24426	0.24426	0.24426	0.24426	0.24426
-165.0	0.41102	0.41190	0.40790	0.40440	0.39941	0.38920	0.37460	0.35760	0.34000	0.32000	0.29460	0.27400	0.27400	0.27400	0.27400	0.27400
-164.0	0.43600	0.43390	0.43070	0.42650	0.42310	0.41130	0.39620	0.37810	0.35760	0.33880	0.31060	0.29400	0.29400	0.29400	0.29400	0.29400
-163.0	0.45500	0.45090	0.44560	0.44000	0.43530	0.42400	0.41040	0.39250	0.37080	0.35110	0.32280	0.30600	0.30600	0.30600	0.30600	0.30600
-162.0	0.47300	0.46710	0.45700	0.45160	0.44630	0.43530	0.42160	0.40190	0.38210	0.36240	0.33640	0.31900	0.31900	0.31900	0.31900	0.31900
-161.0	0.48700	0.48000	0.46680	0.46000	0.45480	0.44450	0.43040	0.41060	0.39150	0.37550	0.35010	0.33600	0.33600	0.33600	0.33600	0.33600
-160.0	0.49700	0.49190	0.47590	0.46960	0.46270	0.45160	0.43670	0.42000	0.40280	0.38780	0.36610	0.35600	0.35600	0.35600	0.35600	0.35600
-159.0	0.51000	0.49300	0.48530	0.47840	0.47210	0.46040	0.44710	0.43070	0.41320	0.39910	0.38490	0.37600	0.37600	0.37600	0.37600	0.37600
-158.0	0.52500	0.51000	0.49940	0.49000	0.48430	0.47110	0.45930	0.44330	0.42650	0.41410	0.40560	0.39800	0.39800	0.39800	0.39800	0.39800
-157.0	0.54000	0.52700	0.51260	0.50000	0.49750	0.48900	0.48000	0.46400	0.44890	0.44140	0.43390	0.42700	0.42700	0.42700	0.42700	0.42700
-156.0	0.55600	0.54500	0.53140	0.52670	0.52200	0.50980	0.50070	0.48940	0.47720	0.47060	0.46590	0.45700	0.45700	0.45700	0.45700	0.45700
-155.0	0.57900	0.56500	0.55780	0.55410	0.54650	0.53710	0.53180	0.52330	0.51480	0.50540	0.49790	0.49100	0.49100	0.49100	0.49100	0.49100
-152.5	0.63700	0.63100	0.61292	0.62570	0.62380	0.62100	0.61930	0.61460	0.60800	0.60140	0.59580	0.58600	0.58600	0.58600	0.58600	0.58600

-150.0	0.71000	0.70400	0.69952	0.70290	0.70110	0.69692	0.69840	0.69547	0.69460	0.68890	0.68330	0.68000	0.68000	0.68000	0.68000	0.68000
-140.0	1.07957	1.07544	1.06992	1.06879	1.06796	1.06732	1.06680	1.06587	1.06500	1.06500	1.06500	1.06500	1.06500	1.06500	1.06500	1.06500
-130.0	1.40357	1.39944	1.39392	1.39279	1.39196	1.39132	1.39080	1.38987	1.38900	1.38900	1.38900	1.38900	1.38900	1.38900	1.38900	1.38900
-120.0	1.68457	1.68044	1.67492	1.67379	1.67296	1.67232	1.67180	1.67087	1.67000	1.67000	1.67000	1.67000	1.67000	1.67000	1.67000	1.67000
-110.0	1.87457	1.87044	1.86492	1.86379	1.86296	1.86232	1.86180	1.86087	1.86000	1.86000	1.86000	1.86000	1.86000	1.86000	1.86000	1.86000
-100.0	2.02057	2.01644	2.01092	2.00979	2.00896	2.00832	2.00780	2.00687	2.00600	2.00600	2.00600	2.00600	2.00600	2.00600	2.00600	2.00600
-90.0	2.04857	2.04444	2.03892	2.03779	2.03696	2.03632	2.03580	2.03487	2.03400	2.03400	2.03400	2.03400	2.03400	2.03400	2.03400	2.03400
-80.0	1.99057	1.98644	1.98092	1.97979	1.97896	1.97832	1.97780	1.97687	1.97600	1.97600	1.97600	1.97600	1.97600	1.97600	1.97600	1.97600
-70.0	1.87457	1.87044	1.86492	1.86379	1.86296	1.86232	1.86180	1.86087	1.86000	1.86000	1.86000	1.86000	1.86000	1.86000	1.86000	1.86000
-60.0	1.68457	1.68044	1.67492	1.67379	1.67296	1.67232	1.67180	1.67087	1.67000	1.67000	1.67000	1.67000	1.67000	1.67000	1.67000	1.67000
-50.0	1.41857	1.41444	1.40892	1.40779	1.40696	1.40632	1.40580	1.40487	1.40400	1.40400	1.40400	1.40400	1.40400	1.40400	1.40400	1.40400
-40.0	0.99657	0.99244	0.98692	0.98579	0.98496	0.98432	0.98380	0.98287	0.98200	0.98200	0.98200	0.98200	0.98200	0.98200	0.98200	0.98200
-30.0	0.58657	0.58244	0.57692	0.57579	0.57496	0.57432	0.57380	0.57287	0.57200	0.57200	0.57200	0.57200	0.57200	0.57200	0.57200	0.57200
-25.0	0.45757	0.45344	0.44792	0.44679	0.44596	0.44532	0.44480	0.44387	0.44300	0.44300	0.44300	0.44300	0.44300	0.44300	0.44300	0.44300
-24.0	0.43957	0.43544	0.42992	0.42879	0.42796	0.42732	0.42680	0.42587	0.42500	0.42500	0.42500	0.42500	0.42500	0.42500	0.42500	0.42500
-23.0	0.42327	0.41914	0.41362	0.41249	0.41166	0.41102	0.41050	0.40957	0.40870	0.40870	0.40870	0.40870	0.40870	0.40490	0.40440	0.40490
-22.0	0.40657	0.40244	0.39692	0.39579	0.39496	0.39432	0.39380	0.39287	0.39200	0.39200	0.39200	0.39200	0.39200	0.38760	0.38370	0.38060
-21.0	0.38657	0.38244	0.37692	0.37579	0.37496	0.37432	0.37380	0.37287	0.37200	0.37200	0.37200	0.37200	0.37200	0.36740	0.36160	0.35610
-20.0	0.36657	0.36244	0.35692	0.35579	0.35496	0.35432	0.35380	0.35287	0.35200	0.35200	0.35200	0.35200	0.35200	0.34530	0.33810	0.33130
-19.0	0.34557	0.34144	0.33592	0.33479	0.33396	0.33332	0.33280	0.33187	0.33100	0.33100	0.33100	0.33100	0.33100	0.32250	0.31440	0.30000
-18.0	0.32577	0.32164	0.31612	0.31499	0.31416	0.31352	0.31300	0.31207	0.31120	0.31120	0.31120	0.31120	0.31120	0.29820	0.28540	0.26450
-17.0	0.30967	0.30554	0.30002	0.29889	0.29806	0.29742	0.29690	0.29597	0.29510	0.29320	0.29220	0.29050	0.29050	0.26800	0.25190	0.22820
-16.0	0.29037	0.28624	0.28072	0.27959	0.27876	0.27812	0.27760	0.27667	0.27580	0.27390	0.27150	0.26970	0.26400	0.23430	0.21820	0.18950
-15.0	0.27197	0.26784	0.26232	0.26119	0.26036	0.25972	0.25920	0.25827	0.25740	0.25410	0.24920	0.24560	0.23210	0.19450	0.17540	0.14370
-14.0	0.25247	0.24834	0.24282	0.24169	0.24086	0.24022	0.23970	0.23877	0.23790	0.23480	0.23060	0.22150	0.19420	0.14680	0.12020	0.07120
-13.5	0.24357	0.23944	0.23392	0.23279	0.23196	0.23132	0.23080	0.22987	0.22900	0.22500	0.22000	0.21000	0.17000	0.11610	0.09000	0.05000
-13.0	0.23357	0.22944	0.22392	0.22279	0.22196	0.22132	0.22080	0.21987	0.21900	0.21550	0.21040	0.19590	0.14000	0.08050	0.06130	0.04060
-12.5	0.22447	0.22034	0.21482	0.21369	0.21286	0.21222	0.21170	0.21077	0.20990	0.20560	0.19950	0.18090	0.10850	0.05680	0.04640	0.03620
-12.0	0.21497	0.21084	0.20532	0.20419	0.20336	0.20272	0.20220	0.20127	0.20040	0.19530	0.18870	0.16450	0.07660	0.04520	0.03810	0.03340
-11.5	0.20517	0.20104	0.19552	0.19439	0.19356	0.19292	0.19240	0.19147	0.19060	0.18540	0.17740	0.13750	0.04830	0.03780	0.03330	0.03120
-11.0	0.19437	0.19024	0.18472	0.18359	0.18276	0.18212	0.18160	0.18067	0.17980	0.17510	0.16470	0.08670	0.03650	0.03230	0.03000	0.02930

-10.5	0.18117	0.17704	0.17152	0.17039	0.16956	0.16892	0.16840	0.16747	0.16660	0.16240	0.14780	0.05000	0.03070	0.02870	0.02775	0.02775
-10.0	0.16187	0.15774	0.15222	0.15109	0.15026	0.14962	0.14910	0.14817	0.14730	0.14210	0.11910	0.03400	0.02650	0.02650	0.02680	0.02650
-9.5	0.13507	0.13094	0.12542	0.12429	0.12346	0.12282	0.12230	0.12137	0.12050	0.11340	0.06780	0.02780	0.02480	0.02480	0.02480	0.02480
-9.0	0.09107	0.08694	0.08142	0.08029	0.07946	0.07882	0.07830	0.07737	0.07650	0.06400	0.03600	0.02515	0.02290	0.02290	0.02290	0.02290
-8.5	0.05597	0.05184	0.04632	0.04519	0.04436	0.04372	0.04320	0.04227	0.04140	0.03530	0.02730	0.02326	0.02120	0.02120	0.02120	0.02120
-8.0	0.04517	0.04104	0.03552	0.03439	0.03356	0.03292	0.03240	0.03147	0.03060	0.02730	0.02294	0.02153	0.01980	0.01980	0.01980	0.01980
-7.5	0.04115	0.03701	0.03150	0.03037	0.02954	0.02890	0.02838	0.02744	0.02658	0.02406	0.02099	0.01994	0.01850	0.01850	0.01850	0.01850
-7.0	0.03838	0.03425	0.02873	0.02760	0.02677	0.02613	0.02561	0.02468	0.02381	0.02191	0.01928	0.01849	0.01750	0.01750	0.01750	0.01750
-6.5	0.03604	0.03190	0.02639	0.02525	0.02443	0.02379	0.02327	0.02233	0.02146	0.02003	0.01779	0.01718	0.01660	0.01660	0.01660	0.01660
-6.0	0.03406	0.02993	0.02441	0.02328	0.02245	0.02181	0.02129	0.02036	0.01949	0.01841	0.01650	0.01600	0.01560	0.01560	0.01560	0.01560
-5.0	0.03104	0.02690	0.02139	0.02025	0.01943	0.01879	0.01827	0.01733	0.01646	0.01580	0.01442	0.01402	0.01402	0.01402	0.01402	0.01402
-4.0	0.02899	0.02485	0.01934	0.01820	0.01738	0.01673	0.01621	0.01528	0.01441	0.01390	0.01290	0.01249	0.01249	0.01249	0.01249	0.01249
-3.0	0.02763	0.02350	0.01798	0.01685	0.01602	0.01538	0.01486	0.01393	0.01306	0.01257	0.01182	0.01139	0.01139	0.01139	0.01139	0.01139
-2.0	0.02677	0.02264	0.01713	0.01599	0.01517	0.01452	0.01400	0.01307	0.01220	0.01168	0.01109	0.01067	0.01067	0.01067	0.01067	0.01067
-1.0	0.02626	0.02212	0.01661	0.01548	0.01465	0.01401	0.01349	0.01256	0.01169	0.01113	0.01064	0.01029	0.01029	0.01029	0.01029	0.01029
0.0	0.02600	0.02186	0.01635	0.01522	0.01439	0.01375	0.01323	0.01229	0.01143	0.01089	0.01044	0.01020	0.01020	0.01020	0.01020	0.01020
1.0	0.02626	0.02212	0.01661	0.01548	0.01465	0.01401	0.01349	0.01256	0.01169	0.01113	0.01064	0.01029	0.01029	0.01029	0.01029	0.01029
2.0	0.02677	0.02264	0.01713	0.01599	0.01517	0.01452	0.01400	0.01307	0.01220	0.01168	0.01109	0.01067	0.01067	0.01067	0.01067	0.01067
3.0	0.02763	0.02350	0.01798	0.01685	0.01602	0.01538	0.01486	0.01393	0.01306	0.01257	0.01182	0.01139	0.01139	0.01139	0.01139	0.01139
4.0	0.02899	0.02485	0.01934	0.01820	0.01738	0.01673	0.01621	0.01528	0.01441	0.01390	0.01290	0.01249	0.01249	0.01249	0.01249	0.01249
5.0	0.03104	0.02690	0.02139	0.02025	0.01943	0.01879	0.01827	0.01733	0.01646	0.01580	0.01442	0.01402	0.01402	0.01402	0.01402	0.01402
6.0	0.03406	0.02993	0.02441	0.02328	0.02245	0.02181	0.02129	0.02036	0.01949	0.01841	0.01650	0.01600	0.01560	0.01560	0.01560	0.01560
6.5	0.03604	0.03190	0.02639	0.02525	0.02443	0.02379	0.02327	0.02233	0.02146	0.02003	0.01779	0.01718	0.01660	0.01660	0.01660	0.01660
7.0	0.03838	0.03425	0.02873	0.02760	0.02677	0.02613	0.02561	0.02468	0.02381	0.02191	0.01928	0.01849	0.01750	0.01750	0.01750	0.01750
7.5	0.04115	0.03701	0.03150	0.03037	0.02954	0.02890	0.02838	0.02744	0.02658	0.02406	0.02099	0.01994	0.01850	0.01850	0.01850	0.01850
8.0	0.04517	0.04104	0.03552	0.03439	0.03356	0.03292	0.03240	0.03147	0.03060	0.02730	0.02294	0.02153	0.01980	0.01980	0.01980	0.01980
8.5	0.05597	0.05184	0.04632	0.04519	0.04436	0.04372	0.04320	0.04227	0.04140	0.03530	0.02730	0.02326	0.02120	0.02120	0.02120	0.02120
9.0	0.09107	0.08694	0.08142	0.08029	0.07946	0.07882	0.07830	0.07737	0.07650	0.06400	0.03600	0.02515	0.02290	0.02290	0.02290	0.02290
9.5	0.13507	0.13094	0.12542	0.12429	0.12346	0.12282	0.12230	0.12137	0.12050	0.11340	0.06780	0.02780	0.02480	0.02480	0.02480	0.02480
10.0	0.16187	0.15774	0.15222	0.15109	0.15026	0.14962	0.14910	0.14817	0.14730	0.14210	0.11910	0.03400	0.02650	0.02650	0.02680	0.02650
10.5	0.18117	0.17704	0.17152	0.17039	0.16956	0.16892	0.16840	0.16747	0.16660	0.16240	0.14780	0.05000	0.03070	0.02870	0.02775	0.02775

11.0	0.19437	0.19024	0.18472	0.18359	0.18276	0.18212	0.18160	0.18067	0.17980	0.17510	0.16470	0.08670	0.03650	0.03230	0.03000	0.02930
11.5	0.20517	0.20104	0.19552	0.19439	0.19356	0.19292	0.19240	0.19147	0.19060	0.18540	0.17740	0.13750	0.04830	0.03780	0.03330	0.03120
12.0	0.21497	0.21084	0.20532	0.20419	0.20336	0.20272	0.20220	0.20127	0.20040	0.19530	0.18870	0.16450	0.07660	0.04520	0.03810	0.03340
12.5	0.22447	0.22034	0.21482	0.21369	0.21286	0.21222	0.21170	0.21077	0.20990	0.20560	0.19950	0.18090	0.10850	0.05680	0.04640	0.03620
13.0	0.23357	0.22944	0.22392	0.22279	0.22196	0.22132	0.22080	0.21987	0.21900	0.21550	0.21040	0.19590	0.14000	0.08050	0.06130	0.04060
13.5	0.24357	0.23944	0.23392	0.23279	0.23196	0.23132	0.23080	0.22987	0.22900	0.22500	0.22000	0.21000	0.17000	0.11610	0.09000	0.05000
14.0	0.25247	0.24834	0.24282	0.24169	0.24086	0.24022	0.23970	0.23877	0.23790	0.23480	0.23060	0.22150	0.19420	0.14680	0.12020	0.07120
15.0	0.27197	0.26784	0.26232	0.26119	0.26036	0.25972	0.25920	0.25827	0.25740	0.25410	0.24920	0.24560	0.23210	0.19450	0.17540	0.14370
16.0	0.29037	0.28624	0.28072	0.27959	0.27876	0.27812	0.27760	0.27667	0.27580	0.27390	0.27150	0.26970	0.26400	0.23430	0.21820	0.18950
17.0	0.30967	0.30554	0.30002	0.29889	0.29806	0.29742	0.29690	0.29597	0.29510	0.29320	0.29220	0.29050	0.29050	0.26800	0.25190	0.22820
18.0	0.32577	0.32164	0.31612	0.31499	0.31416	0.31352	0.31300	0.31207	0.31120	0.31120	0.31120	0.31120	0.31120	0.29820	0.28540	0.26450
19.0	0.34557	0.34144	0.33592	0.33479	0.33396	0.33332	0.33280	0.33187	0.33100	0.33100	0.33100	0.33100	0.33100	0.32250	0.31440	0.30000
20.0	0.36657	0.36244	0.35692	0.35579	0.35496	0.35432	0.35380	0.35287	0.35200	0.35200	0.35200	0.35200	0.35200	0.34530	0.33810	0.33130
21.0	0.38657	0.38244	0.37692	0.37579	0.37496	0.37432	0.37380	0.37287	0.37200	0.37200	0.37200	0.37200	0.37200	0.36740	0.36160	0.35610
22.0	0.40657	0.40244	0.39692	0.39579	0.39496	0.39432	0.39380	0.39287	0.39200	0.39200	0.39200	0.39200	0.39200	0.38760	0.38370	0.38060
23.0	0.42327	0.41914	0.41362	0.41249	0.41166	0.41102	0.41050	0.40957	0.40870	0.40870	0.40870	0.40870	0.40870	0.40490	0.40440	0.40490
24.0	0.43957	0.43544	0.42992	0.42879	0.42796	0.42732	0.42680	0.42587	0.42500	0.42500	0.42500	0.42500	0.42500	0.42500	0.42500	0.42500
25.0	0.45757	0.45344	0.44792	0.44679	0.44596	0.44532	0.44480	0.44387	0.44300	0.44300	0.44300	0.44300	0.44300	0.44300	0.44300	0.44300
30.0	0.58657	0.58244	0.57692	0.57579	0.57496	0.57432	0.57380	0.57287	0.57200	0.57200	0.57200	0.57200	0.57200	0.57200	0.57200	0.57200
40.0	0.99657	0.99244	0.98692	0.98579	0.98496	0.98432	0.98380	0.98287	0.98200	0.98200	0.98200	0.98200	0.98200	0.98200	0.98200	0.98200
50.0	1.41857	1.41444	1.40892	1.40779	1.40696	1.40632	1.40580	1.40487	1.40400	1.40400	1.40400	1.40400	1.40400	1.40400	1.40400	1.40400
60.0	1.68457	1.68044	1.67492	1.67379	1.67296	1.67232	1.67180	1.67087	1.67000	1.67000	1.67000	1.67000	1.67000	1.67000	1.67000	1.67000
70.0	1.87457	1.87044	1.86492	1.86379	1.86296	1.86232	1.86180	1.86087	1.86000	1.86000	1.86000	1.86000	1.86000	1.86000	1.86000	1.86000
80.0	1.99057	1.98644	1.98092	1.97979	1.97896	1.97832	1.97780	1.97687	1.97600	1.97600	1.97600	1.97600	1.97600	1.97600	1.97600	1.97600
90.0	2.04857	2.04444	2.03892	2.03779	2.03696	2.03632	2.03580	2.03487	2.03400	2.03400	2.03400	2.03400	2.03400	2.03400	2.03400	2.03400
100.0	2.02057	2.01644	2.01092	2.00979	2.00896	2.00832	2.00780	2.00687	2.00600	2.00600	2.00600	2.00600	2.00600	2.00600	2.00600	2.00600
110.0	1.87457	1.87044	1.86492	1.86379	1.86296	1.86232	1.86180	1.86087	1.86000	1.86000	1.86000	1.86000	1.86000	1.86000	1.86000	1.86000
120.0	1.68457	1.68044	1.67492	1.67379	1.67296	1.67232	1.67180	1.67087	1.67000	1.67000	1.67000	1.67000	1.67000	1.67000	1.67000	1.67000
130.0	1.40357	1.39944	1.39392	1.39279	1.39196	1.39132	1.39080	1.38987	1.38900	1.38900	1.38900	1.38900	1.38900	1.38900	1.38900	1.38900
140.0	1.07957	1.07544	1.06992	1.06879	1.06796	1.06732	1.06680	1.06587	1.06500	1.06500	1.06500	1.06500	1.06500	1.06500	1.06500	1.06500
150.0	0.71000	0.70400	0.69952	0.70290	0.70110	0.69692	0.69840	0.69547	0.69460	0.68890	0.68330	0.68000	0.68000	0.68000	0.68000	0.68000

152.5	0.63700	0.63100	0.61292	0.62570	0.62380	0.62100	0.61930	0.61460	0.60800	0.60140	0.59580	0.58600	0.58600	0.58600	0.58600	0.58600
155.0	0.57900	0.56500	0.55780	0.55410	0.54650	0.53710	0.53180	0.52330	0.51480	0.50540	0.49790	0.49100	0.49100	0.49100	0.49100	0.49100
156.0	0.55600	0.54500	0.53140	0.52670	0.52200	0.50980	0.50070	0.48940	0.47720	0.47060	0.46590	0.45700	0.45700	0.45700	0.45700	0.45700
157.0	0.54000	0.52700	0.51260	0.50000	0.49750	0.48900	0.48000	0.46400	0.44890	0.44140	0.43390	0.42700	0.42700	0.42700	0.42700	0.42700
158.0	0.52500	0.51000	0.49940	0.49000	0.48430	0.47110	0.45930	0.44330	0.42650	0.41410	0.40560	0.39800	0.39800	0.39800	0.39800	0.39800
159.0	0.51000	0.49300	0.48530	0.47840	0.47210	0.46040	0.44710	0.43070	0.41320	0.39910	0.38490	0.37600	0.37600	0.37600	0.37600	0.37600
160.0	0.49700	0.49190	0.47590	0.46960	0.46270	0.45160	0.43670	0.42000	0.40280	0.38780	0.36610	0.35600	0.35600	0.35600	0.35600	0.35600
161.0	0.48700	0.48000	0.46680	0.46000	0.45480	0.44450	0.43040	0.41060	0.39150	0.37550	0.35010	0.33600	0.33600	0.33600	0.33600	0.33600
162.0	0.47300	0.46710	0.45700	0.45160	0.44630	0.43530	0.42160	0.40190	0.38210	0.36240	0.33640	0.31900	0.31900	0.31900	0.31900	0.31900
163.0	0.45500	0.45090	0.44560	0.44000	0.43530	0.42400	0.41040	0.39250	0.37080	0.35110	0.32280	0.30600	0.30600	0.30600	0.30600	0.30600
164.0	0.43600	0.43390	0.43070	0.42650	0.42310	0.41130	0.39620	0.37810	0.35760	0.33880	0.31060	0.29400	0.29400	0.29400	0.29400	0.29400
165.0	0.41102	0.41190	0.40790	0.40440	0.39941	0.38920	0.37460	0.35760	0.34000	0.32000	0.29460	0.27400	0.27400	0.27400	0.27400	0.27400
166.0	0.37213	0.37010	0.36730	0.36480	0.36052	0.35520	0.34540	0.32690	0.30490	0.28800	0.26730	0.24426	0.24426	0.24426	0.24426	0.24426
167.0	0.32523	0.32109	0.31773	0.31578	0.31437	0.31298	0.30590	0.29180	0.27200	0.25320	0.23620	0.21795	0.21495	0.21495	0.21495	0.21495
168.0	0.26091	0.25677	0.25126	0.25012	0.24930	0.24865	0.24813	0.24380	0.23340	0.22210	0.20583	0.19498	0.19273	0.19273	0.19273	0.19273
169.0	0.20557	0.20143	0.19592	0.19478	0.19396	0.19331	0.19279	0.19186	0.19099	0.18489	0.17689	0.17285	0.17079	0.17079	0.17079	0.17079
170.0	0.17491	0.17077	0.16526	0.16412	0.16330	0.16266	0.16214	0.16120	0.16033	0.15703	0.15267	0.15126	0.14953	0.14953	0.14953	0.14953
171.0	0.15170	0.14757	0.14206	0.14092	0.14010	0.13945	0.13893	0.13800	0.13713	0.13462	0.13154	0.13049	0.12905	0.12905	0.12905	0.12905
172.0	0.13074	0.12660	0.12109	0.11996	0.11913	0.11849	0.11797	0.11704	0.11617	0.11427	0.11164	0.11085	0.10986	0.10986	0.10986	0.10986
173.0	0.11148	0.10734	0.10183	0.10069	0.09987	0.09923	0.09871	0.09777	0.09690	0.09547	0.09323	0.09262	0.09204	0.09204	0.09204	0.09204
174.0	0.09416	0.09002	0.08451	0.08338	0.08255	0.08191	0.08139	0.08046	0.07959	0.07851	0.07660	0.07610	0.07570	0.07570	0.07570	0.07570
175.0	0.07768	0.07354	0.06803	0.06689	0.06607	0.06543	0.06491	0.06397	0.06310	0.06244	0.06106	0.06066	0.06066	0.06066	0.06066	0.06066
176.0	0.06434	0.06021	0.05469	0.05356	0.05273	0.05209	0.05157	0.05064	0.04977	0.04926	0.04825	0.04785	0.04785	0.04785	0.04785	0.04785
177.0	0.05419	0.05005	0.04454	0.04340	0.04258	0.04193	0.04141	0.04048	0.03961	0.03912	0.03837	0.03794	0.03794	0.03794	0.03794	0.03794
178.0	0.04730	0.04316	0.03765	0.03652	0.03569	0.03505	0.03453	0.03359	0.03273	0.03220	0.03161	0.03119	0.03119	0.03119	0.03119	0.03119
179.0	0.04383	0.03970	0.03419	0.03305	0.03222	0.03158	0.03106	0.03013	0.02926	0.02871	0.02822	0.02786	0.02786	0.02786	0.02786	0.02786
180.0	0.04400	0.03986	0.03435	0.03322	0.03239	0.03175	0.03123	0.03029	0.02943	0.02889	0.02844	0.02820	0.02820	0.02820	0.02820	0.02820

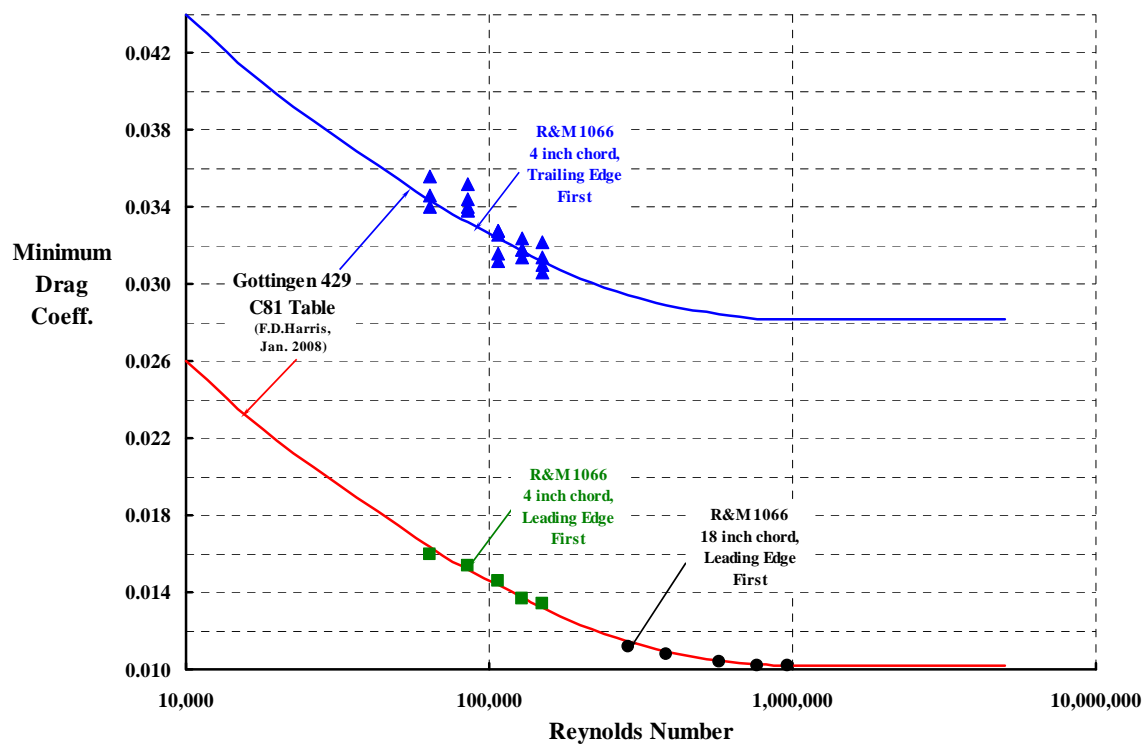
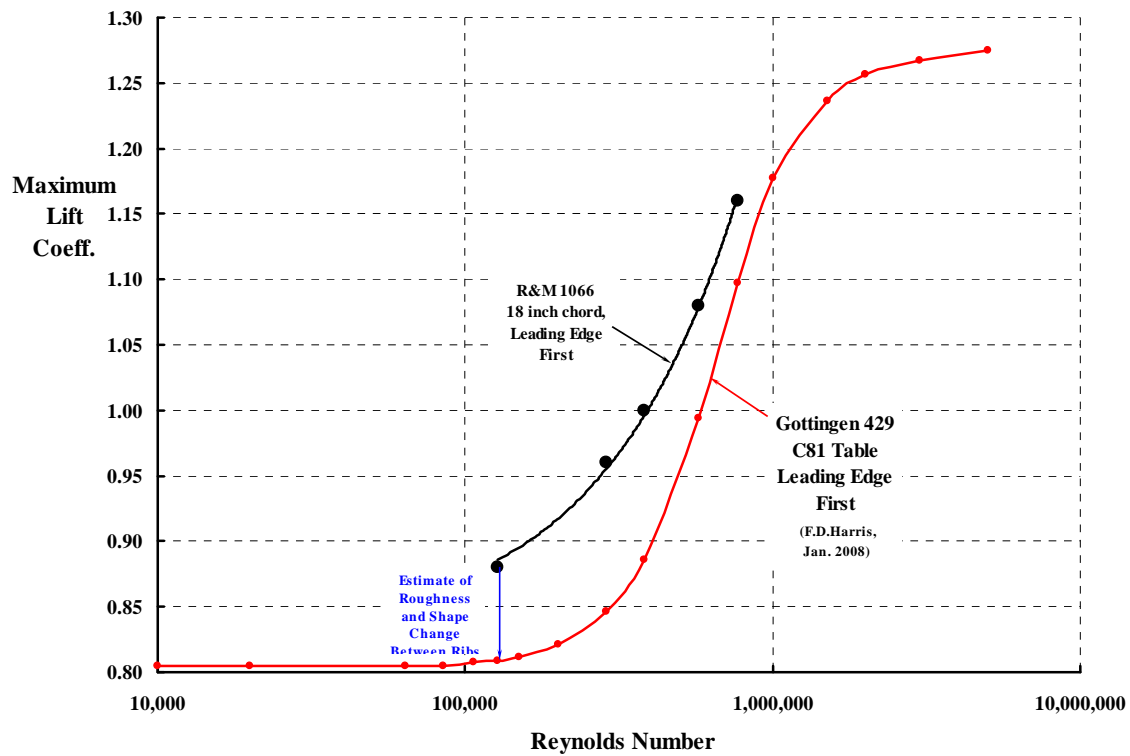
Cm	about	0.25	Chord													
	RN															
alpha	10,000	20,000	63,939	85,251	106,564	127,877	149,190	200,000	287,724	383,632	575,448	767,263	1,000,000	2,000,000	3,000,000	5,000,000
-180.0	0.0000	0.0000	0.0000	0.0000	0.0000	0.0000	0.0000	0.0000	0.0000	0.0000	0.0000	0.0000	0.0000	0.0000	0.0000	0.0000
-179.0	0.0600	0.0600	0.0600	0.0600	0.0600	0.0600	0.0600	0.0600	0.0600	0.0600	0.0600	0.0600	0.0600	0.0600	0.0600	0.0600
-178.0	0.1200	0.1200	0.1200	0.1200	0.1200	0.1200	0.1200	0.1200	0.1200	0.1200	0.1200	0.1200	0.1200	0.1200	0.1200	0.1200
-177.0	0.1800	0.1800	0.1800	0.1800	0.1800	0.1800	0.1800	0.1800	0.1800	0.1800	0.1800	0.1800	0.1800	0.1800	0.1800	0.1800
-176.0	0.2400	0.2400	0.2400	0.2400	0.2400	0.2400	0.2400	0.2400	0.2400	0.2400	0.2400	0.2400	0.2400	0.2400	0.2400	0.2400
-175.0	0.2908	0.2908	0.2908	0.2908	0.2908	0.2908	0.2908	0.2908	0.2908	0.2908	0.2908	0.2908	0.2908	0.2908	0.2908	0.2908
-174.0	0.3367	0.3367	0.3367	0.3367	0.3367	0.3367	0.3367	0.3367	0.3367	0.3367	0.3367	0.3367	0.3367	0.3367	0.3367	0.3367
-173.0	0.3660	0.3660	0.3660	0.3660	0.3660	0.3660	0.3660	0.3660	0.3660	0.3660	0.3660	0.3660	0.3660	0.3660	0.3660	0.3660
-172.0	0.3845	0.3845	0.3845	0.3845	0.3845	0.3845	0.3845	0.3845	0.3845	0.3845	0.3845	0.3845	0.3845	0.3845	0.3845	0.3845
-171.0	0.3912	0.3912	0.3912	0.3912	0.3912	0.3912	0.3912	0.3912	0.3912	0.3912	0.3912	0.3912	0.3912	0.3912	0.3912	0.3912
-170.0	0.3869	0.3869	0.3869	0.3869	0.3869	0.3869	0.3869	0.3869	0.3869	0.3869	0.3869	0.3869	0.3869	0.3869	0.3869	0.3869
-169.0	0.3800	0.3800	0.3800	0.3800	0.3800	0.3800	0.3800	0.3800	0.3800	0.3800	0.3800	0.3800	0.3800	0.3800	0.3800	0.3800
-168.0	0.3730	0.3730	0.3730	0.3730	0.3730	0.3730	0.3730	0.3730	0.3730	0.3730	0.3730	0.3730	0.3730	0.3730	0.3730	0.3730
-167.0	0.3644	0.3644	0.3644	0.3644	0.3644	0.3644	0.3644	0.3644	0.3644	0.3644	0.3644	0.3644	0.3644	0.3644	0.3644	0.3644
-166.0	0.3583	0.3583	0.3583	0.3583	0.3583	0.3583	0.3583	0.3583	0.3583	0.3583	0.3583	0.3583	0.3583	0.3583	0.3583	0.3583
-165.0	0.3514	0.3514	0.3514	0.3514	0.3514	0.3514	0.3514	0.3514	0.3514	0.3514	0.3514	0.3514	0.3514	0.3514	0.3514	0.3514
-164.0	0.3462	0.3462	0.3462	0.3462	0.3462	0.3462	0.3462	0.3462	0.3462	0.3462	0.3462	0.3462	0.3462	0.3462	0.3462	0.3462
-163.0	0.3427	0.3427	0.3427	0.3427	0.3427	0.3427	0.3427	0.3427	0.3427	0.3427	0.3427	0.3427	0.3427	0.3427	0.3427	0.3427
-162.0	0.3419	0.3419	0.3419	0.3419	0.3419	0.3419	0.3419	0.3419	0.3419	0.3419	0.3419	0.3419	0.3419	0.3419	0.3419	0.3419
-161.0	0.3453	0.3453	0.3453	0.3453	0.3453	0.3453	0.3453	0.3453	0.3453	0.3453	0.3453	0.3453	0.3453	0.3453	0.3453	0.3453
-160.0	0.3505	0.3505	0.3505	0.3505	0.3505	0.3505	0.3505	0.3505	0.3505	0.3505	0.3505	0.3505	0.3505	0.3505	0.3505	0.3505
-159.0	0.3600	0.3600	0.3600	0.3600	0.3600	0.3600	0.3600	0.3600	0.3600	0.3600	0.3600	0.3600	0.3600	0.3600	0.3600	0.3600
-158.0	0.3713	0.3713	0.3713	0.3713	0.3713	0.3713	0.3713	0.3713	0.3713	0.3713	0.3713	0.3713	0.3713	0.3713	0.3713	0.3713
-157.0	0.3808	0.3808	0.3808	0.3808	0.3808	0.3808	0.3808	0.3808	0.3808	0.3808	0.3808	0.3808	0.3808	0.3808	0.3808	0.3808
-156.0	0.3912	0.3912	0.3912	0.3912	0.3912	0.3912	0.3912	0.3912	0.3912	0.3912	0.3912	0.3912	0.3912	0.3912	0.3912	0.3912
-155.0	0.4016	0.4016	0.4016	0.4016	0.4016	0.4016	0.4016	0.4016	0.4016	0.4016	0.4016	0.4016	0.4016	0.4016	0.4016	0.4016

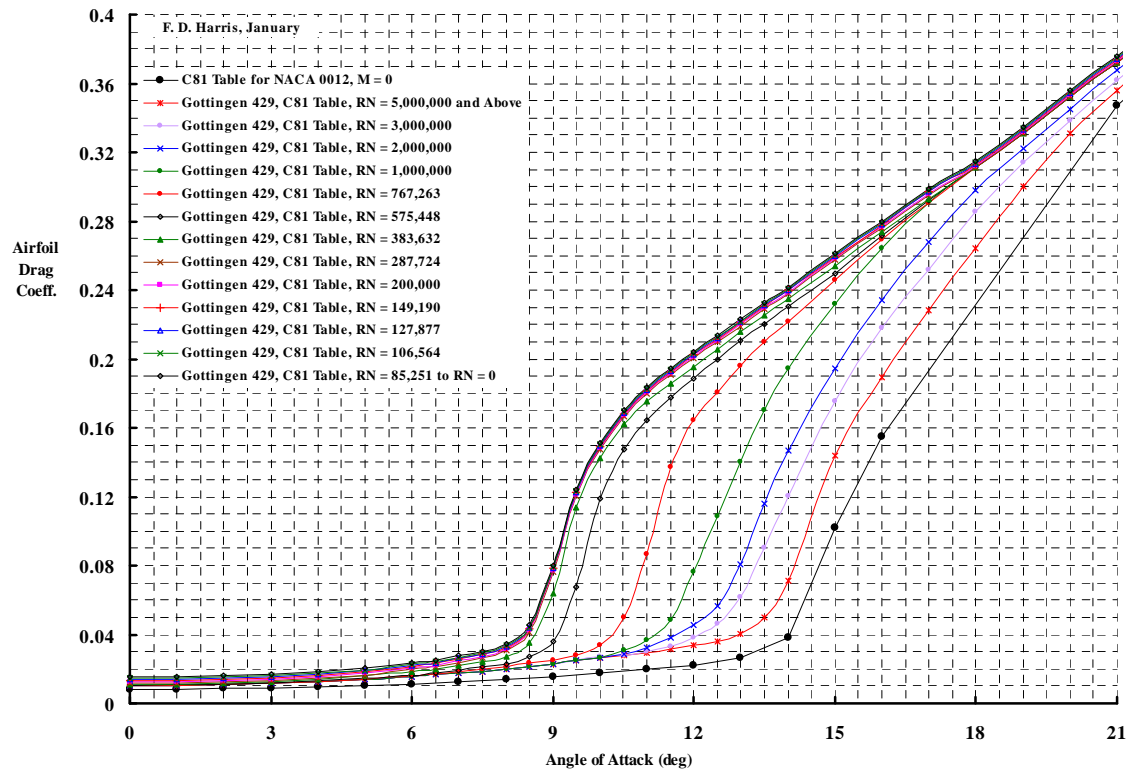
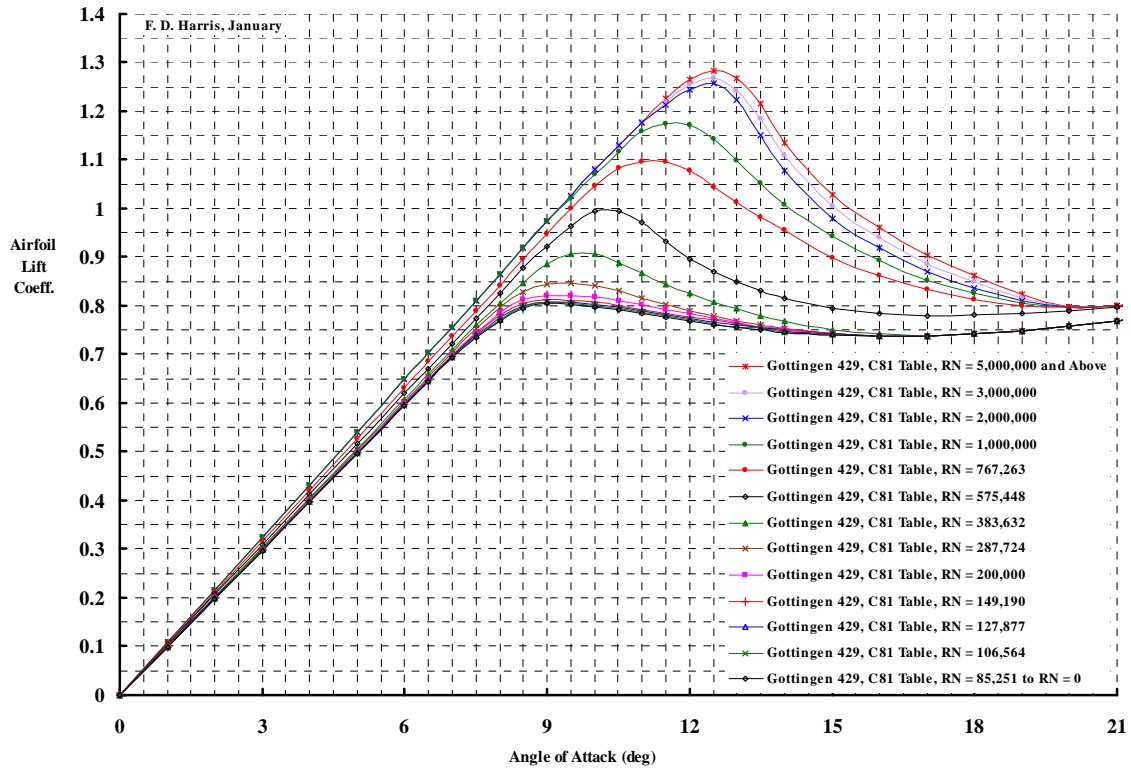
-152.5	0.4284	0.4284	0.4284	0.4284	0.4284	0.4284	0.4284	0.4284	0.4284	0.4284	0.4284	0.4284	0.4284	0.4284	0.4284	0.4284
-150.0	0.4530	0.4530	0.4530	0.4530	0.4530	0.4530	0.4530	0.4530	0.4530	0.4530	0.4530	0.4530	0.4530	0.4530	0.4530	0.4530
-140.0	0.5300	0.5300	0.5300	0.5300	0.5300	0.5300	0.5300	0.5300	0.5300	0.5300	0.5300	0.5300	0.5300	0.5300	0.5300	0.5300
-130.0	0.5800	0.5800	0.5800	0.5800	0.5800	0.5800	0.5800	0.5800	0.5800	0.5800	0.5800	0.5800	0.5800	0.5800	0.5800	0.5800
-120.0	0.6050	0.6050	0.6050	0.6050	0.6050	0.6050	0.6050	0.6050	0.6050	0.6050	0.6050	0.6050	0.6050	0.6050	0.6050	0.6050
-110.0	0.6050	0.6050	0.6050	0.6050	0.6050	0.6050	0.6050	0.6050	0.6050	0.6050	0.6050	0.6050	0.6050	0.6050	0.6050	0.6050
-100.0	0.5900	0.5900	0.5900	0.5900	0.5900	0.5900	0.5900	0.5900	0.5900	0.5900	0.5900	0.5900	0.5900	0.5900	0.5900	0.5900
-90.0	0.5600	0.5600	0.5600	0.5600	0.5600	0.5600	0.5600	0.5600	0.5600	0.5600	0.5600	0.5600	0.5600	0.5600	0.5600	0.5600
-80.0	0.5200	0.5200	0.5200	0.5200	0.5200	0.5200	0.5200	0.5200	0.5200	0.5200	0.5200	0.5200	0.5200	0.5200	0.5200	0.5200
-70.0	0.4708	0.4708	0.4708	0.4708	0.4708	0.4708	0.4708	0.4708	0.4708	0.4708	0.4708	0.4708	0.4708	0.4708	0.4708	0.4708
-60.0	0.4100	0.4100	0.4100	0.4100	0.4100	0.4100	0.4100	0.4100	0.4100	0.4100	0.4100	0.4100	0.4100	0.4100	0.4100	0.4100
-50.0	0.3500	0.3500	0.3500	0.3500	0.3500	0.3500	0.3500	0.3500	0.3500	0.3500	0.3500	0.3500	0.3500	0.3500	0.3500	0.3500
-40.0	0.2804	0.2804	0.2804	0.2804	0.2804	0.2804	0.2804	0.2804	0.2804	0.2804	0.2804	0.2804	0.2804	0.2804	0.2804	0.2804
-30.0	0.2000	0.2000	0.2000	0.2000	0.2000	0.2000	0.2000	0.2000	0.2000	0.2000	0.2000	0.2000	0.1983	0.1968	0.1947	0.1929
-25.0	0.1549	0.1549	0.1549	0.1549	0.1549	0.1549	0.1549	0.1549	0.1549	0.1506	0.1487	0.1487	0.1466	0.1447	0.1429	0.1402
-24.0	0.1450	0.1450	0.1450	0.1450	0.1450	0.1450	0.1450	0.1450	0.1450	0.1398	0.1372	0.1363	0.1336	0.1313	0.1291	0.1267
-23.0	0.1356	0.1356	0.1356	0.1356	0.1356	0.1356	0.1356	0.1356	0.1356	0.1297	0.1253	0.1230	0.1214	0.1181	0.1156	0.1111
-22.0	0.1275	0.1275	0.1275	0.1275	0.1275	0.1275	0.1275	0.1275	0.1275	0.1208	0.1147	0.1075	0.1053	0.1030	0.0996	0.0967
-21.0	0.1215	0.1215	0.1215	0.1215	0.1215	0.1215	0.1215	0.1215	0.1215	0.1133	0.1051	0.0922	0.0904	0.0875	0.0842	0.0807
-20.0	0.1154	0.1154	0.1154	0.1154	0.1154	0.1154	0.1154	0.1154	0.1154	0.1067	0.0951	0.0803	0.0784	0.0757	0.0728	0.0692
-19.0	0.1107	0.1107	0.1107	0.1107	0.1107	0.1107	0.1107	0.1107	0.1107	0.1018	0.0891	0.0738	0.0725	0.0696	0.0665	0.0630
-18.0	0.1067	0.1067	0.1067	0.1067	0.1067	0.1067	0.1067	0.1067	0.1067	0.0982	0.0880	0.0726	0.0699	0.0676	0.0634	0.0595
-17.0	0.1040	0.1040	0.1040	0.1040	0.1040	0.1040	0.1040	0.1040	0.1040	0.0952	0.0893	0.0737	0.0693	0.0656	0.0615	0.0566
-16.0	0.1004	0.1004	0.1004	0.1004	0.1004	0.1004	0.1004	0.1004	0.1004	0.0928	0.0883	0.0766	0.0696	0.0628	0.0575	0.0505
-15.0	0.0957	0.0957	0.0957	0.0957	0.0957	0.0957	0.0957	0.0957	0.0957	0.0893	0.0847	0.0772	0.0675	0.0585	0.0492	0.0347
-14.0	0.0893	0.0893	0.0893	0.0893	0.0893	0.0893	0.0893	0.0893	0.0893	0.0841	0.0788	0.0741	0.0602	0.0503	0.0331	0.0090
-13.5	0.0848	0.0848	0.0848	0.0848	0.0848	0.0848	0.0848	0.0848	0.0848	0.0803	0.0750	0.0692	0.0550	0.0412	0.0165	0.0011
-13.0	0.0787	0.0787	0.0787	0.0787	0.0787	0.0787	0.0787	0.0787	0.0787	0.0738	0.0692	0.0610	0.0471	0.0257	0.0051	0.0000
-12.5	0.0696	0.0696	0.0696	0.0696	0.0696	0.0696	0.0696	0.0696	0.0696	0.0656	0.0603	0.0476	0.0338	0.0083	0.0003	-0.0002
-12.0	0.0587	0.0587	0.0587	0.0587	0.0587	0.0587	0.0587	0.0587	0.0587	0.0545	0.0494	0.0324	0.0162	0.0012	-0.0002	-0.0002
-11.5	0.0443	0.0443	0.0443	0.0443	0.0443	0.0443	0.0443	0.0443	0.0443	0.0409	0.0365	0.0157	0.0030	-0.0004	-0.0003	-0.0002

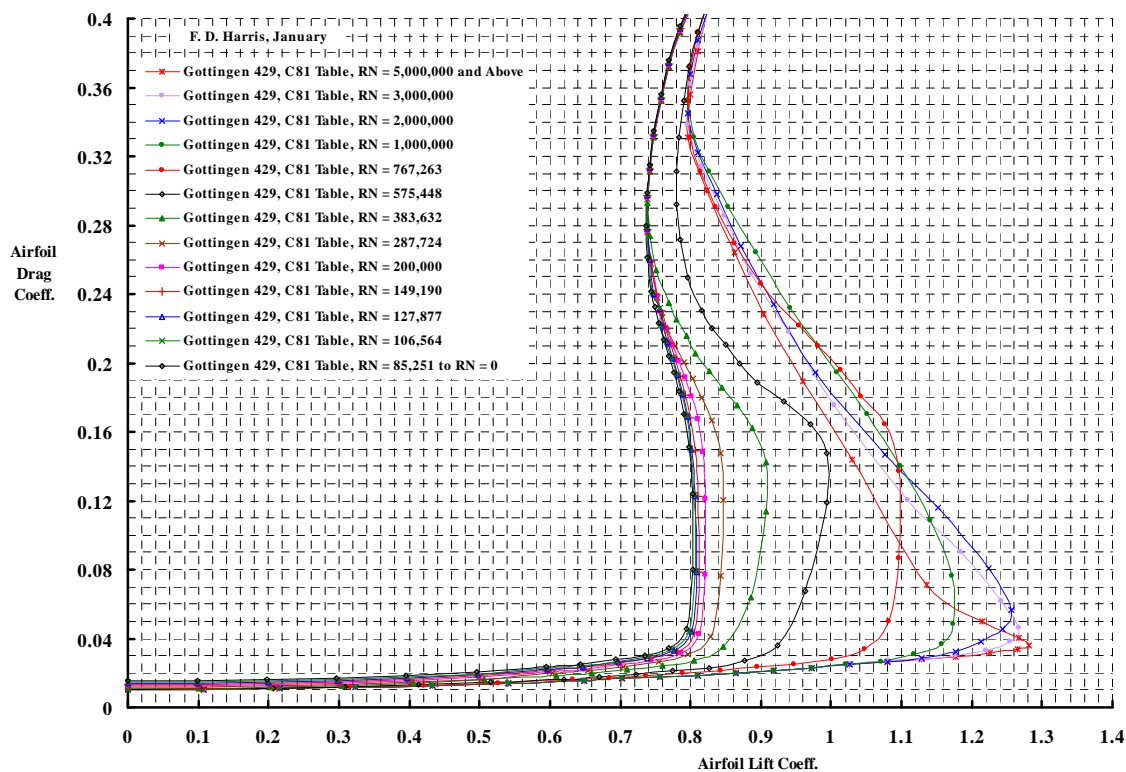
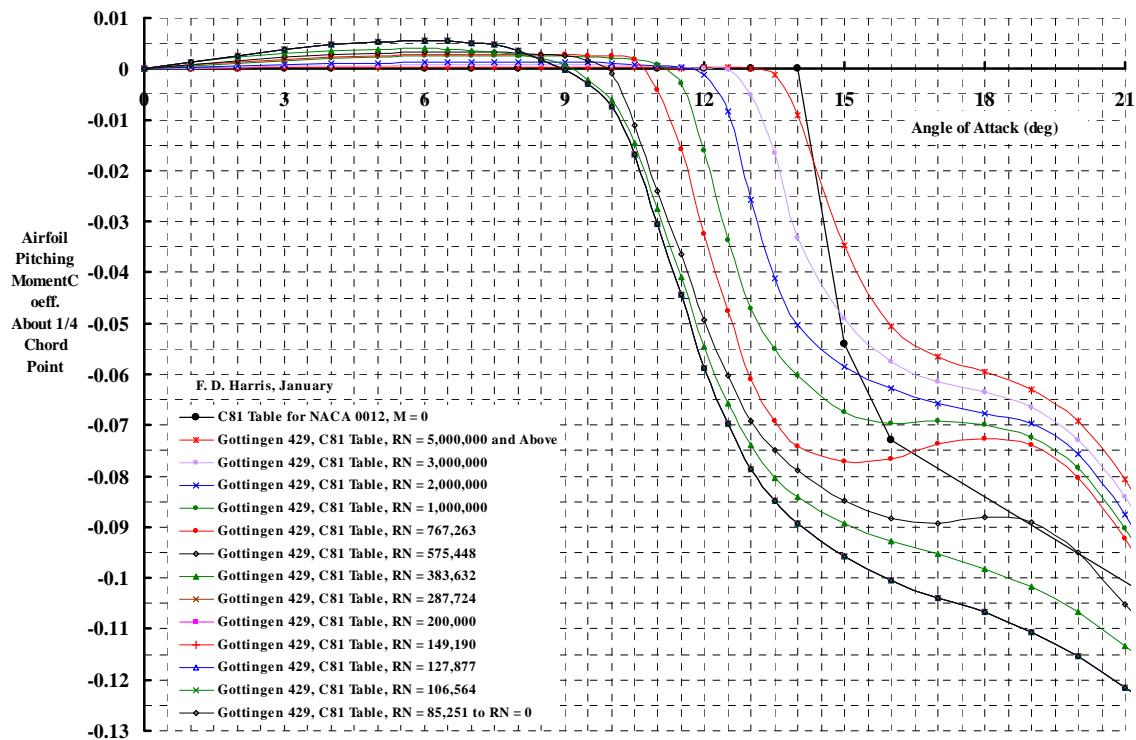
-11.0	0.0304	0.0304	0.0304	0.0304	0.0304	0.0304	0.0304	0.0304	0.0304	0.0304	0.0274	0.0240	0.0042	-0.0009	-0.0007	-0.0005	-0.0002
-10.5	0.0167	0.0167	0.0167	0.0167	0.0167	0.0167	0.0167	0.0167	0.0167	0.0167	0.0146	0.0111	-0.0019	-0.0017	-0.0009	-0.0005	-0.0003
-10.0	0.0074	0.0074	0.0074	0.0074	0.0074	0.0074	0.0074	0.0074	0.0074	0.0074	0.0061	0.0010	-0.0025	-0.0021	-0.0011	-0.0007	-0.0003
-9.5	0.0030	0.0030	0.0030	0.0030	0.0030	0.0030	0.0030	0.0030	0.0030	0.0030	0.0021	-0.0015	-0.0027	-0.0024	-0.0012	-0.0007	-0.0004
-9.0	0.0003	0.0003	0.0003	0.0003	0.0003	0.0003	0.0003	0.0003	0.0003	0.0003	-0.0007	-0.0024	-0.0027	-0.0025	-0.0012	-0.0007	-0.0004
-8.5	-0.0019	-0.0019	-0.0019	-0.0019	-0.0019	-0.0019	-0.0019	-0.0019	-0.0019	-0.0019	-0.0021	-0.0029	-0.0028	-0.0025	-0.0013	-0.0008	-0.0004
-8.0	-0.0036	-0.0036	-0.0036	-0.0036	-0.0036	-0.0036	-0.0036	-0.0036	-0.0036	-0.0036	-0.0028	-0.0031	-0.0028	-0.0026	-0.0013	-0.0008	-0.0004
-7.5	-0.0047	-0.0047	-0.0047	-0.0047	-0.0047	-0.0047	-0.0047	-0.0047	-0.0047	-0.0047	-0.0033	-0.0032	-0.0029	-0.0026	-0.0013	-0.0008	-0.0004
-7.0	-0.0052	-0.0052	-0.0052	-0.0052	-0.0052	-0.0052	-0.0052	-0.0052	-0.0052	-0.0052	-0.0036	-0.0032	-0.0028	-0.0026	-0.0013	-0.0008	-0.0004
-6.5	-0.0054	-0.0054	-0.0054	-0.0054	-0.0054	-0.0054	-0.0054	-0.0054	-0.0054	-0.0054	-0.0039	-0.0032	-0.0028	-0.0025	-0.0013	-0.0008	-0.0004
-6.0	-0.0055	-0.0055	-0.0055	-0.0055	-0.0055	-0.0055	-0.0055	-0.0055	-0.0055	-0.0055	-0.0039	-0.0032	-0.0027	-0.0025	-0.0012	-0.0007	-0.0004
-5.0	-0.0053	-0.0053	-0.0053	-0.0053	-0.0053	-0.0053	-0.0053	-0.0053	-0.0053	-0.0053	-0.0039	-0.0030	-0.0025	-0.0023	-0.0011	-0.0007	-0.0003
-4.0	-0.0047	-0.0047	-0.0047	-0.0047	-0.0047	-0.0047	-0.0047	-0.0047	-0.0047	-0.0047	-0.0036	-0.0027	-0.0022	-0.0020	-0.0010	-0.0006	-0.0003
-3.0	-0.0037	-0.0037	-0.0037	-0.0037	-0.0037	-0.0037	-0.0037	-0.0037	-0.0037	-0.0037	-0.0030	-0.0023	-0.0018	-0.0016	-0.0008	-0.0005	-0.0002
-2.0	-0.0025	-0.0025	-0.0025	-0.0025	-0.0025	-0.0025	-0.0025	-0.0025	-0.0025	-0.0025	-0.0022	-0.0017	-0.0013	-0.0012	-0.0006	-0.0004	-0.0002
-1.0	-0.0012	-0.0012	-0.0012	-0.0012	-0.0012	-0.0012	-0.0012	-0.0012	-0.0012	-0.0012	-0.0012	-0.0009	-0.0007	-0.0006	-0.0003	-0.0002	-0.0001
0.0	0.0000	0.0000	0.0000	0.0000	0.0000	0.0000	0.0000	0.0000	0.0000	0.0000	0.0000	0.0000	0.0000	0.0000	0.0000	0.0000	0.0000
1.0	0.0012	0.0012	0.0012	0.0012	0.0012	0.0012	0.0012	0.0012	0.0012	0.0012	0.0012	0.0009	0.0007	0.0006	0.0003	0.0002	0.0001
2.0	0.0025	0.0025	0.0025	0.0025	0.0025	0.0025	0.0025	0.0025	0.0025	0.0025	0.0022	0.0017	0.0013	0.0012	0.0006	0.0004	0.0002
3.0	0.0037	0.0037	0.0037	0.0037	0.0037	0.0037	0.0037	0.0037	0.0037	0.0037	0.0030	0.0023	0.0018	0.0016	0.0008	0.0005	0.0002
4.0	0.0047	0.0047	0.0047	0.0047	0.0047	0.0047	0.0047	0.0047	0.0047	0.0047	0.0036	0.0027	0.0022	0.0020	0.0010	0.0006	0.0003
5.0	0.0053	0.0053	0.0053	0.0053	0.0053	0.0053	0.0053	0.0053	0.0053	0.0053	0.0039	0.0030	0.0025	0.0023	0.0011	0.0007	0.0003
6.0	0.0055	0.0055	0.0055	0.0055	0.0055	0.0055	0.0055	0.0055	0.0055	0.0055	0.0039	0.0032	0.0027	0.0025	0.0012	0.0007	0.0004
6.5	0.0054	0.0054	0.0054	0.0054	0.0054	0.0054	0.0054	0.0054	0.0054	0.0054	0.0039	0.0032	0.0028	0.0025	0.0013	0.0008	0.0004
7.0	0.0052	0.0052	0.0052	0.0052	0.0052	0.0052	0.0052	0.0052	0.0052	0.0052	0.0036	0.0032	0.0028	0.0026	0.0013	0.0008	0.0004
7.5	0.0047	0.0047	0.0047	0.0047	0.0047	0.0047	0.0047	0.0047	0.0047	0.0047	0.0033	0.0032	0.0029	0.0026	0.0013	0.0008	0.0004
8.0	0.0036	0.0036	0.0036	0.0036	0.0036	0.0036	0.0036	0.0036	0.0036	0.0036	0.0028	0.0031	0.0028	0.0026	0.0013	0.0008	0.0004
8.5	0.0019	0.0019	0.0019	0.0019	0.0019	0.0019	0.0019	0.0019	0.0019	0.0019	0.0021	0.0029	0.0028	0.0025	0.0013	0.0008	0.0004
9.0	-0.0003	-0.0003	-0.0003	-0.0003	-0.0003	-0.0003	-0.0003	-0.0003	-0.0003	-0.0003	0.0007	0.0024	0.0027	0.0025	0.0012	0.0007	0.0004
9.5	-0.0030	-0.0030	-0.0030	-0.0030	-0.0030	-0.0030	-0.0030	-0.0030	-0.0030	-0.0030	-0.0021	0.0015	0.0027	0.0024	0.0012	0.0007	0.0004
10.0	-0.0074	-0.0074	-0.0074	-0.0074	-0.0074	-0.0074	-0.0074	-0.0074	-0.0074	-0.0074	-0.0061	-0.0010	0.0025	0.0021	0.0011	0.0007	0.0003

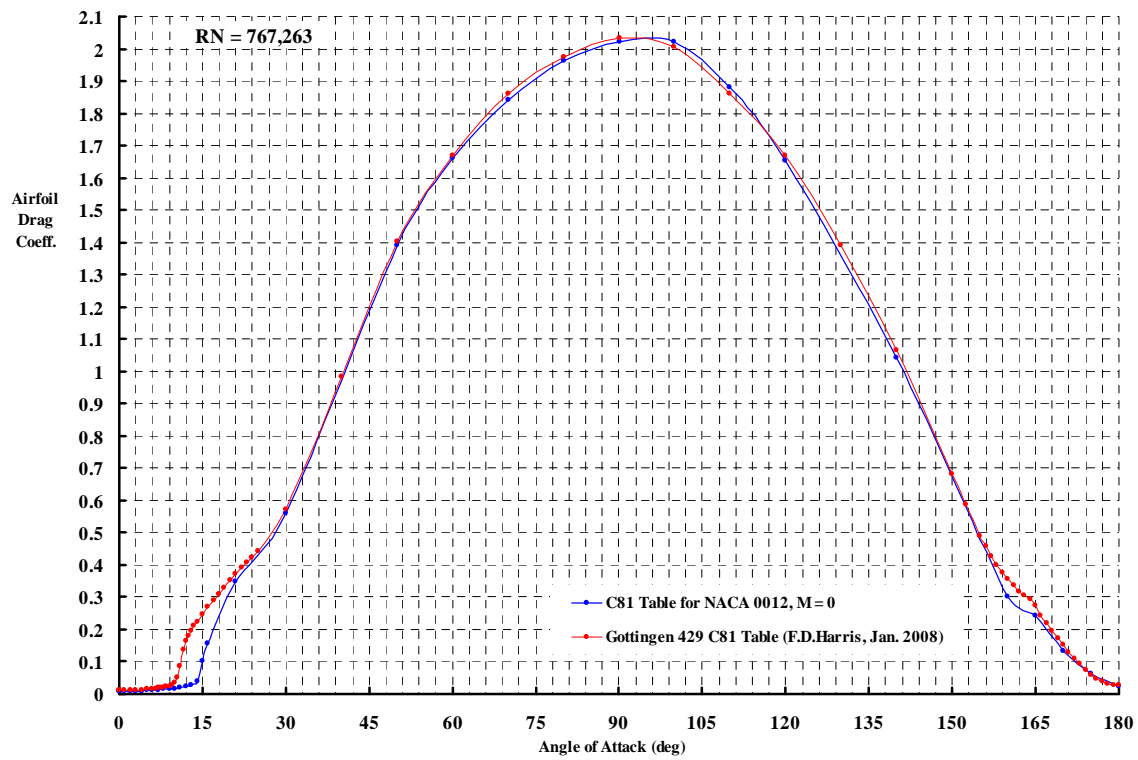
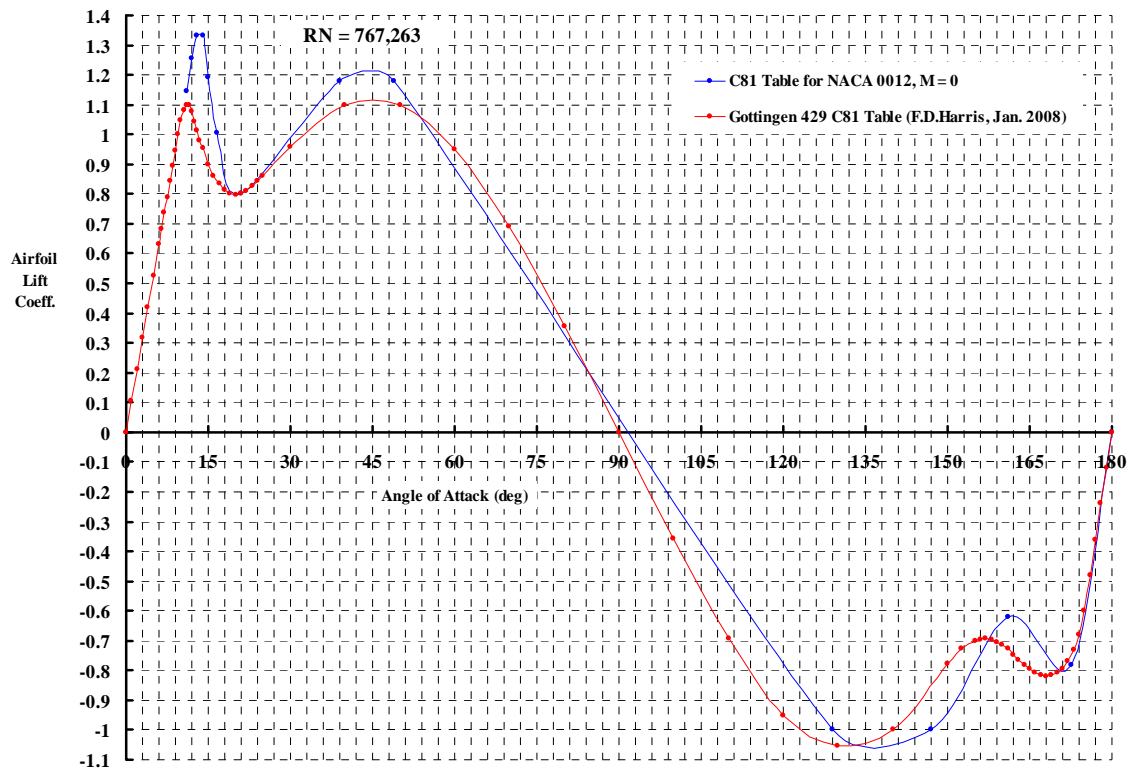
10.5	-0.0167	-0.0167	-0.0167	-0.0167	-0.0167	-0.0167	-0.0167	-0.0167	-0.0167	-0.0167	-0.0146	-0.0111	0.0019	0.0017	0.0009	0.0005	0.0003
11.0	-0.0304	-0.0304	-0.0304	-0.0304	-0.0304	-0.0304	-0.0304	-0.0304	-0.0304	-0.0304	-0.0274	-0.0240	-0.0042	0.0009	0.0007	0.0005	0.0002
11.5	-0.0443	-0.0443	-0.0443	-0.0443	-0.0443	-0.0443	-0.0443	-0.0443	-0.0443	-0.0443	-0.0409	-0.0365	-0.0157	-0.0030	0.0004	0.0003	0.0002
12.0	-0.0587	-0.0587	-0.0587	-0.0587	-0.0587	-0.0587	-0.0587	-0.0587	-0.0587	-0.0587	-0.0545	-0.0494	-0.0324	-0.0162	-0.0012	0.0002	0.0002
12.5	-0.0696	-0.0696	-0.0696	-0.0696	-0.0696	-0.0696	-0.0696	-0.0696	-0.0696	-0.0696	-0.0656	-0.0603	-0.0476	-0.0338	-0.0083	-0.0003	0.0002
13.0	-0.0787	-0.0787	-0.0787	-0.0787	-0.0787	-0.0787	-0.0787	-0.0787	-0.0787	-0.0787	-0.0738	-0.0692	-0.0610	-0.0471	-0.0257	-0.0051	0.0000
13.5	-0.0848	-0.0848	-0.0848	-0.0848	-0.0848	-0.0848	-0.0848	-0.0848	-0.0848	-0.0848	-0.0803	-0.0750	-0.0692	-0.0550	-0.0412	-0.0165	-0.0011
14.0	-0.0893	-0.0893	-0.0893	-0.0893	-0.0893	-0.0893	-0.0893	-0.0893	-0.0893	-0.0893	-0.0841	-0.0788	-0.0741	-0.0602	-0.0503	-0.0331	-0.0090
15.0	-0.0957	-0.0957	-0.0957	-0.0957	-0.0957	-0.0957	-0.0957	-0.0957	-0.0957	-0.0957	-0.0893	-0.0847	-0.0772	-0.0675	-0.0585	-0.0492	-0.0347
16.0	-0.1004	-0.1004	-0.1004	-0.1004	-0.1004	-0.1004	-0.1004	-0.1004	-0.1004	-0.1004	-0.0928	-0.0883	-0.0766	-0.0696	-0.0628	-0.0575	-0.0505
17.0	-0.1040	-0.1040	-0.1040	-0.1040	-0.1040	-0.1040	-0.1040	-0.1040	-0.1040	-0.1040	-0.0952	-0.0893	-0.0737	-0.0693	-0.0656	-0.0615	-0.0566
18.0	-0.1067	-0.1067	-0.1067	-0.1067	-0.1067	-0.1067	-0.1067	-0.1067	-0.1067	-0.1067	-0.0982	-0.0880	-0.0726	-0.0699	-0.0676	-0.0634	-0.0595
19.0	-0.1107	-0.1107	-0.1107	-0.1107	-0.1107	-0.1107	-0.1107	-0.1107	-0.1107	-0.1107	-0.1018	-0.0891	-0.0738	-0.0725	-0.0696	-0.0665	-0.0630
20.0	-0.1154	-0.1154	-0.1154	-0.1154	-0.1154	-0.1154	-0.1154	-0.1154	-0.1154	-0.1154	-0.1067	-0.0951	-0.0803	-0.0784	-0.0757	-0.0728	-0.0692
21.0	-0.1215	-0.1215	-0.1215	-0.1215	-0.1215	-0.1215	-0.1215	-0.1215	-0.1215	-0.1215	-0.1133	-0.1051	-0.0922	-0.0904	-0.0875	-0.0842	-0.0807
22.0	-0.1275	-0.1275	-0.1275	-0.1275	-0.1275	-0.1275	-0.1275	-0.1275	-0.1275	-0.1275	-0.1208	-0.1147	-0.1075	-0.1053	-0.1030	-0.0996	-0.0967
23.0	-0.1356	-0.1356	-0.1356	-0.1356	-0.1356	-0.1356	-0.1356	-0.1356	-0.1356	-0.1356	-0.1297	-0.1253	-0.1230	-0.1214	-0.1181	-0.1156	-0.1111
24.0	-0.1450	-0.1450	-0.1450	-0.1450	-0.1450	-0.1450	-0.1450	-0.1450	-0.1450	-0.1450	-0.1398	-0.1372	-0.1363	-0.1336	-0.1313	-0.1291	-0.1267
25.0	-0.1549	-0.1549	-0.1549	-0.1549	-0.1549	-0.1549	-0.1549	-0.1549	-0.1549	-0.1549	-0.1506	-0.1487	-0.1487	-0.1466	-0.1447	-0.1429	-0.1402
30.0	-0.2000	-0.2000	-0.2000	-0.2000	-0.2000	-0.2000	-0.2000	-0.2000	-0.2000	-0.2000	-0.2000	-0.2000	-0.2000	-0.2000	-0.1983	-0.1968	-0.1929
40.0	-0.2804	-0.2804	-0.2804	-0.2804	-0.2804	-0.2804	-0.2804	-0.2804	-0.2804	-0.2804	-0.2804	-0.2804	-0.2804	-0.2804	-0.2804	-0.2804	-0.2804
50.0	-0.3500	-0.3500	-0.3500	-0.3500	-0.3500	-0.3500	-0.3500	-0.3500	-0.3500	-0.3500	-0.3500	-0.3500	-0.3500	-0.3500	-0.3500	-0.3500	-0.3500
60.0	-0.4100	-0.4100	-0.4100	-0.4100	-0.4100	-0.4100	-0.4100	-0.4100	-0.4100	-0.4100	-0.4100	-0.4100	-0.4100	-0.4100	-0.4100	-0.4100	-0.4100
70.0	-0.4708	-0.4708	-0.4708	-0.4708	-0.4708	-0.4708	-0.4708	-0.4708	-0.4708	-0.4708	-0.4708	-0.4708	-0.4708	-0.4708	-0.4708	-0.4708	-0.4708
80.0	-0.5200	-0.5200	-0.5200	-0.5200	-0.5200	-0.5200	-0.5200	-0.5200	-0.5200	-0.5200	-0.5200	-0.5200	-0.5200	-0.5200	-0.5200	-0.5200	-0.5200
90.0	-0.5600	-0.5600	-0.5600	-0.5600	-0.5600	-0.5600	-0.5600	-0.5600	-0.5600	-0.5600	-0.5600	-0.5600	-0.5600	-0.5600	-0.5600	-0.5600	-0.5600
100.0	-0.5900	-0.5900	-0.5900	-0.5900	-0.5900	-0.5900	-0.5900	-0.5900	-0.5900	-0.5900	-0.5900	-0.5900	-0.5900	-0.5900	-0.5900	-0.5900	-0.5900
110.0	-0.6050	-0.6050	-0.6050	-0.6050	-0.6050	-0.6050	-0.6050	-0.6050	-0.6050	-0.6050	-0.6050	-0.6050	-0.6050	-0.6050	-0.6050	-0.6050	-0.6050
120.0	-0.6050	-0.6050	-0.6050	-0.6050	-0.6050	-0.6050	-0.6050	-0.6050	-0.6050	-0.6050	-0.6050	-0.6050	-0.6050	-0.6050	-0.6050	-0.6050	-0.6050
130.0	-0.5800	-0.5800	-0.5800	-0.5800	-0.5800	-0.5800	-0.5800	-0.5800	-0.5800	-0.5800	-0.5800	-0.5800	-0.5800	-0.5800	-0.5800	-0.5800	-0.5800
140.0	-0.5300	-0.5300	-0.5300	-0.5300	-0.5300	-0.5300	-0.5300	-0.5300	-0.5300	-0.5300	-0.5300	-0.5300	-0.5300	-0.5300	-0.5300	-0.5300	-0.5300

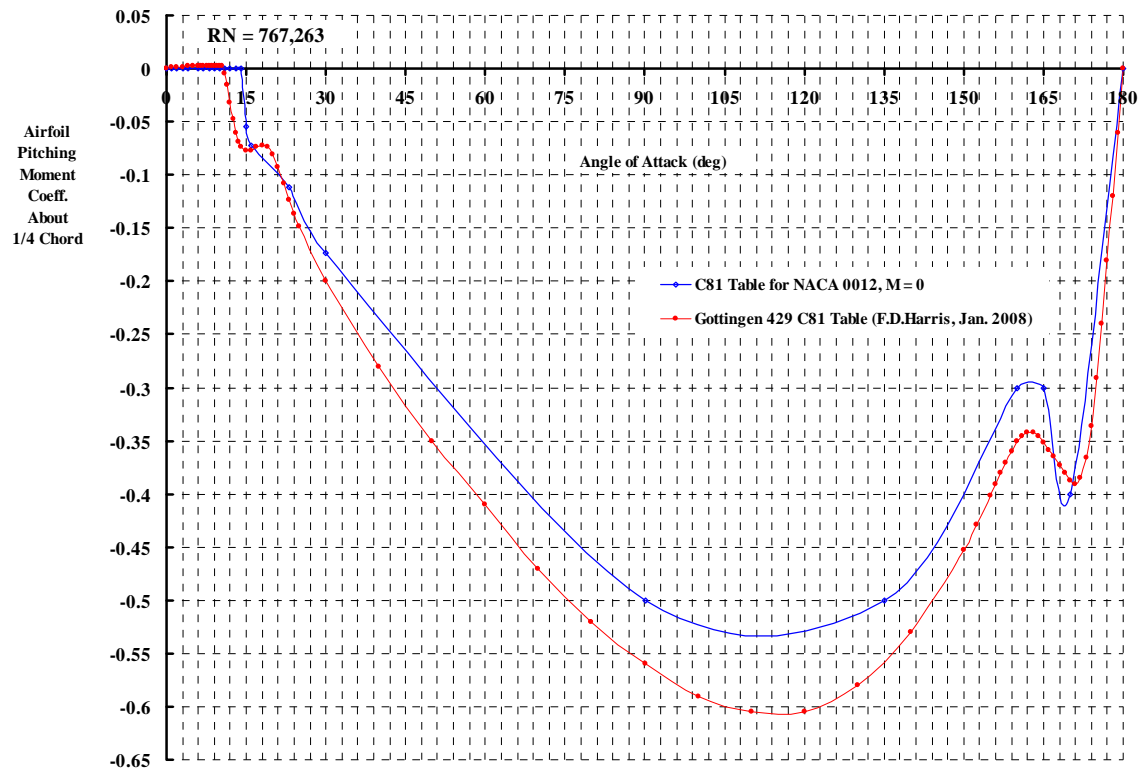
[illegible]











Standard N.A.C.A. 0012 Airfoil Table

CL	Mach No.										
alpha	0.000	0.200	0.300	0.400	0.500	0.600	0.700	0.750	0.800	0.900	1.000
-180.0	0.000	0.000	0.000	0.000	0.000	0.000	0.000	0.000	0.000	0.000	0.000
-172.5	0.780	0.780	0.780	0.780	0.780	0.780	0.780	0.780	0.780	0.780	0.780
-161.0	0.620	0.620	0.620	0.620	0.620	0.620	0.620	0.620	0.620	0.620	0.620
-147.0	1.000	1.000	1.000	1.000	1.000	1.000	1.000	1.000	1.000	1.000	1.000
-129.0	1.000	1.000	1.000	1.000	1.000	1.000	1.000	1.000	1.000	1.000	1.000
-49.0	-1.180	-1.180	-1.180	-1.180	-1.180	-1.180	-1.180	-1.180	-1.180	-1.180	-1.180
-39.0	-1.180	-1.180	-1.180	-1.180	-1.180	-1.180	-1.180	-1.180	-1.180	-1.180	-1.180
-21.0	-0.800	-0.800	-0.810	-0.830	-0.850	-0.850	-0.850	-0.710	-0.680	-0.640	-0.640
-16.5	-1.007	-1.007	-0.944	-0.960	-0.965	-0.965	-0.965	-0.795	-0.760	-0.700	-0.700
-15.0	-1.190	-1.190	-1.090	-1.055	-0.990	-0.980	-0.980	-0.830	-0.790	-0.720	-0.720
-14.0	-1.333	-1.333	-1.220	-1.096	-1.000	-0.970	-0.970	-0.840	-0.805	-0.730	-0.730
-13.0	-1.334	-1.334	-1.280	-1.120	-1.000	-0.960	-0.960	-0.850	-0.815	-0.735	-0.735
-12.0	-1.255	-1.255	-1.260	-1.130	-1.000	-0.947	-0.940	-0.850	-0.820	-0.740	-0.740
-11.0	-1.161	-1.161	-1.190	-1.120	-0.994	-0.930	-0.923	-0.850	-0.810	-0.740	-0.740
-10.0	-1.055	-1.055	-1.010	-1.082	-0.985	-0.910	-0.900	-0.845	-0.805	-0.730	-0.730
-8.0	-0.844	-0.844	-0.880	-0.907	-0.922	-0.870	-0.840	-0.820	-0.770	-0.695	-0.695
-6.0	-0.633	-0.633	-0.660	-0.684	-0.741	-0.770	-0.750	-0.770	-0.720	-0.593	-0.593
-4.0	-0.422	-0.422	-0.440	-0.456	-0.494	-0.544	-0.578	-0.627	-0.603	-0.396	-0.396
-2.0	-0.211	-0.211	-0.220	-0.228	-0.247	-0.272	-0.313	-0.350	-0.395	-0.200	-0.200
0.0	0.000	0.000	0.000	0.000	0.000	0.000	0.000	0.000	0.000	0.000	0.000
2.0	0.211	0.211	0.220	0.228	0.247	0.272	0.313	0.350	0.395	0.200	0.200
4.0	0.422	0.422	0.440	0.456	0.494	0.544	0.578	0.627	0.603	0.396	0.396
6.0	0.633	0.633	0.660	0.684	0.741	0.770	0.750	0.770	0.720	0.593	0.593
8.0	0.844	0.844	0.880	0.907	0.922	0.870	0.840	0.820	0.770	0.695	0.695
10.0	1.055	1.055	1.100	1.082	0.985	0.910	0.900	0.845	0.805	0.730	0.730
11.0	1.161	1.161	1.190	1.120	0.994	0.930	0.923	0.850	0.810	0.740	0.740
12.0	1.255	1.255	1.260	1.130	1.000	0.947	0.940	0.850	0.820	0.740	0.740

13.0	1.334	1.334	1.280	1.120	1.000	0.960	0.960	0.850	0.815	0.735	0.735
14.0	1.333	1.333	1.220	1.096	1.000	0.970	0.970	0.840	0.805	0.730	0.730
15.0	1.190	1.190	1.090	1.055	0.990	0.980	0.980	0.830	0.790	0.730	0.730
16.5	1.007	1.007	0.944	0.960	0.965	0.965	0.965	0.795	0.760	0.700	0.700
21.0	0.800	0.800	0.810	0.830	0.850	0.850	0.850	0.710	0.680	0.640	0.640
39.0	1.180	1.180	1.180	1.180	1.180	1.180	1.180	1.180	1.180	1.180	1.180
49.0	1.180	1.180	1.180	1.180	1.180	1.180	1.180	1.180	1.180	1.180	1.180
129.0	-1.000	-1.000	-1.000	-1.000	-1.000	-1.000	-1.000	-1.000	-1.000	-1.000	-1.000
147.0	-1.000	-1.000	-1.000	-1.000	-1.000	-1.000	-1.000	-1.000	-1.000	-1.000	-1.000
161.0	-0.620	-0.620	-0.620	-0.620	-0.620	-0.620	-0.620	-0.620	-0.620	-0.620	-0.620
172.5	-0.780	-0.780	-0.780	-0.780	-0.780	-0.780	-0.780	-0.780	-0.780	-0.780	-0.780
180.0	0.000	0.000	0.000	0.000	0.000	0.000	0.000	0.000	0.000	0.000	0.000

CD	M										
alpha	0.000	0.180	0.280	0.380	0.480	0.620	0.720	0.770	0.820	0.920	1.000
-180.0	0.0220	0.0220	0.0220	0.0220	0.0220	0.0220	0.0220	0.0220	0.0220	0.0220	0.0220
-175.0	0.0620	0.0620	0.0620	0.0620	0.0620	0.0620	0.0620	0.0620	0.0620	0.0620	0.0620
-170.0	0.1320	0.1320	0.1320	0.1320	0.1320	0.1320	0.1320	0.1320	0.1320	0.1320	0.1320
-165.0	0.2420	0.2420	0.2420	0.2420	0.2420	0.2420	0.2420	0.2420	0.2420	0.2420	0.2420
-160.0	0.3020	0.3020	0.3020	0.3020	0.3020	0.3020	0.3020	0.3020	0.3020	0.3020	0.3020
-140.0	1.0420	1.0420	1.0420	1.0420	1.0420	1.0420	1.0420	1.0420	1.0420	1.0420	1.0420
-120.0	1.6520	1.6520	1.6520	1.6520	1.6520	1.6520	1.6520	1.6520	1.6520	1.6520	1.6520
-110.0	1.8520	1.8520	1.8520	1.8520	1.8520	1.8520	1.8520	1.8520	1.8520	1.8520	1.8520
-100.0	2.0220	2.0220	2.0220	2.0220	2.0220	2.0220	2.0220	2.0220	2.0220	2.0220	2.0220
-90.0	2.0220	2.0220	2.0220	2.0220	2.0220	2.0220	2.0220	2.0220	2.0220	2.0220	2.0220
-80.0	1.9620	1.9620	1.9620	1.9620	1.9620	1.9620	1.9620	1.9620	1.9620	1.9620	1.9620
-70.0	1.8420	1.8420	1.8420	1.8420	1.8420	1.8420	1.8420	1.8420	1.8420	1.8420	1.8420
-60.0	1.6620	1.6620	1.6620	1.6620	1.6620	1.6620	1.6620	1.6620	1.6620	1.6620	1.6620
-50.0	1.3920	1.3920	1.3920	1.3920	1.3920	1.3990	1.3920	1.3920	1.3920	1.3920	1.3920
-30.0	0.5620	0.5620	0.5620	0.5620	0.5620	0.5620	0.5620	0.5620	0.5620	0.5620	0.5620
-21.0	0.3320	0.3320	0.3320	0.3320	0.3320	0.3320	0.3320	0.3320	0.3320	0.3420	0.3420

-16.0	0.1550	0.1550	0.1810	0.2070	0.2350	0.2570	0.2740	0.2920	0.3050	0.3420	0.3420
-15.0	0.1020	0.1020	0.1480	0.1810	0.2090	0.2330	0.2520	0.2710	0.2820	0.2980	0.2980
-14.0	0.0380	0.0380	0.0990	0.1460	0.1800	0.2120	0.2330	0.2490	0.2600	0.2930	0.2930
-13.0	0.0264	0.0264	0.0455	0.0940	0.1480	0.1910	0.2160	0.2310	0.2390	0.2720	0.2920
-12.0	0.0220	0.0220	0.0300	0.0600	0.1110	0.1640	0.1980	0.2110	0.2200	0.2520	0.2910
-11.0	0.0196	0.0196	0.0232	0.0380	0.0780	0.1350	0.1700	0.1920	0.2020	0.2320	0.2750
-10.0	0.0174	0.0174	0.0189	0.0259	0.0530	0.1050	0.1450	0.1760	0.1860	0.2130	0.2540
-9.0	0.0154	0.0154	0.0159	0.0187	0.0351	0.0770	0.1220	0.1590	0.1720	0.1990	0.2320
-8.0	0.0138	0.0138	0.0138	0.0147	0.0220	0.0530	0.1010	0.1400	0.1550	0.1830	0.2140
-7.0	0.0122	0.0122	0.0122	0.0123	0.0141	0.0350	0.0820	0.1110	0.1390	0.1690	0.1920
-6.0	0.0110	0.0110	0.0110	0.0110	0.0110	0.0212	0.0615	0.0820	0.1200	0.1400	0.1700
-5.0	0.0100	0.0100	0.0100	0.0100	0.0100	0.0132	0.0380	0.0540	0.0880	0.1110	0.1400
-4.0	0.0093	0.0093	0.0093	0.0093	0.0093	0.0100	0.0167	0.0300	0.0575	0.0950	0.1120
-3.0	0.0088	0.0088	0.0088	0.0088	0.0088	0.0090	0.0102	0.0175	0.0355	0.0860	0.1020
-2.0	0.0085	0.0085	0.0085	0.0085	0.0085	0.0085	0.0086	0.0117	0.0240	0.0810	0.0980
-1.0	0.0083	0.0083	0.0083	0.0083	0.0083	0.0083	0.0083	0.0091	0.0175	0.0780	0.0960
0.0	0.0080	0.0080	0.0080	0.0080	0.0080	0.0080	0.0080	0.0080	0.0137	0.0780	0.0950
1.0	0.0083	0.0083	0.0083	0.0083	0.0083	0.0083	0.0083	0.0091	0.0175	0.0780	0.0960
2.0	0.0085	0.0085	0.0085	0.0085	0.0085	0.0085	0.0086	0.0117	0.0240	0.0810	0.0980
3.0	0.0088	0.0088	0.0088	0.0088	0.0088	0.0090	0.0102	0.0175	0.0355	0.0860	0.1020
4.0	0.0093	0.0093	0.0093	0.0093	0.0093	0.0100	0.0167	0.0300	0.0575	0.0950	0.1120
5.0	0.0100	0.0100	0.0100	0.0100	0.0100	0.0132	0.0380	0.0540	0.0880	0.1110	0.1400
6.0	0.0110	0.0110	0.0110	0.0110	0.0110	0.0212	0.0615	0.0820	0.1200	0.1400	0.1700
7.0	0.0122	0.0122	0.0122	0.0123	0.0141	0.0350	0.0820	0.1110	0.1390	0.1690	0.1920
8.0	0.0138	0.0138	0.0138	0.0147	0.0220	0.0530	0.1010	0.1400	0.1550	0.1830	0.2140
9.0	0.0154	0.0154	0.0159	0.0187	0.0351	0.0770	0.1220	0.1590	0.1720	0.1990	0.2320
10.0	0.0174	0.0174	0.0189	0.0259	0.0530	0.1050	0.1450	0.1760	0.1860	0.2130	0.2540
11.0	0.0196	0.0196	0.0232	0.0380	0.0780	0.1350	0.1700	0.1920	0.2020	0.2320	0.2750
12.0	0.0220	0.0220	0.0300	0.0600	0.1110	0.1640	0.1980	0.2110	0.2200	0.2520	0.2910
13.0	0.0264	0.0264	0.0455	0.0940	0.1480	0.1910	0.2160	0.2310	0.2390	0.2720	0.2920
14.0	0.0380	0.0380	0.0990	0.1460	0.1800	0.2120	0.2330	0.2490	0.2600	0.2930	0.2930

15.0	0.1020	0.1020	0.1480	0.1810	0.2090	0.2330	0.2520	0.2710	0.2820	0.2980	0.2980
16.0	0.1550	0.1550	0.1810	0.2070	0.2350	0.2570	0.2740	0.2920	0.3050	0.3420	0.3420
21.0	0.3320	0.3320	0.3320	0.3320	0.3320	0.3320	0.3320	0.3320	0.3320	0.3420	0.3420
30.0	0.5620	0.5620	0.5620	0.5620	0.5620	0.5620	0.5620	0.5620	0.5620	0.5620	0.5620
50.0	1.3920	1.3920	1.3920	1.3920	1.3920	1.3920	1.3920	1.3920	1.3920	1.3920	1.3920
60.0	1.6620	1.6620	1.6620	1.6620	1.6620	1.6620	1.6620	1.6620	1.6620	1.6620	1.6620
70.0	1.8420	1.8420	1.8420	1.8420	1.8420	1.8420	1.8420	1.8420	1.8420	1.8420	1.8420
80.0	1.9620	1.9620	1.9620	1.9620	1.9620	1.9620	1.9620	1.9620	1.9620	1.9620	1.9620
90.0	2.0220	2.0220	2.0220	2.0220	2.0220	2.0220	2.0220	2.0220	2.0220	2.0220	2.0220
100.0	2.0220	2.0220	2.0220	2.0220	2.0220	2.0220	2.0220	2.0220	2.0220	2.0220	2.0220
110.0	1.8520	1.8520	1.8520	1.8520	1.8520	1.8520	1.8520	1.8520	1.8520	1.8520	1.8520
120.0	1.6520	1.6520	1.6520	1.6520	1.6520	1.6520	1.6520	1.6520	1.6520	1.6520	1.6520
140.0	1.0420	1.0420	1.0420	1.0420	1.0420	1.0420	1.0420	1.0420	1.0420	1.0420	1.0420
160.0	0.3020	0.3020	0.3020	0.3020	0.3020	0.3020	0.3020	0.3020	0.3020	0.3020	0.3020
165.0	0.2420	0.2420	0.2420	0.2420	0.2420	0.2420	0.2420	0.2420	0.2420	0.2420	0.2420
170.0	0.1320	0.1320	0.1320	0.1320	0.1320	0.1320	0.1320	0.1320	0.1320	0.1320	0.1320
175.0	0.0620	0.0620	0.0620	0.0620	0.0620	0.0620	0.0620	0.0620	0.0620	0.0620	0.0620
180.0	0.0220	0.0220	0.0220	0.0220	0.0220	0.0220	0.0220	0.0220	0.0220	0.0220	0.0220

CM	Mach No.									
alpha	0.20000	0.30000	0.40000	0.50000	0.60000	0.70000	0.75000	0.80000	0.90000	
-180.0	0.0000	0.0000	0.0000	0.0000	0.0000	0.0000	0.0000	0.0000	0.0000	
-170.0	0.4000	0.4000	0.4000	0.4000	0.4000	0.4000	0.4000	0.4000	0.4000	
-165.0	0.3000	0.3000	0.3000	0.3000	0.3000	0.3000	0.3000	0.3000	0.3000	
-160.0	0.3000	0.3000	0.3000	0.3000	0.3000	0.3000	0.3000	0.3000	0.3000	
-135.0	0.5000	0.5000	0.5000	0.5000	0.5000	0.5000	0.5000	0.5000	0.5000	
-90.0	0.5000	0.5000	0.5000	0.5000	0.5000	0.5000	0.5000	0.5000	0.5000	
-30.0	0.1740	0.1840	0.1960	0.2140	0.2350	0.2500	0.2640	0.2770	0.2980	
-23.0	0.1120	0.1180	0.1280	0.1440	0.1570	0.1710	0.1830	0.2060	0.2320	
-16.0	0.0730	0.0780	0.0860	0.0970	0.1080	0.1170	0.1370	0.1760	0.2000	
-15.0	0.0540	0.0650	0.0730	0.0840	0.0970	0.1110	0.1330	0.1730	0.1950	

-14.0	0.0000	0.0270	0.0540	0.0680	0.0860	0.1030	0.1270	0.1670	0.1890
-13.0	0.0000	0.0015	0.0250	0.0500	0.0740	0.0930	0.1220	0.1630	0.1840
-12.0	0.0000	0.0000	0.0020	0.0300	0.0600	0.0830	0.1160	0.1570	0.1760
-11.0	0.0000	0.0000	-0.0030	0.0140	0.0460	0.0740	0.1080	0.1490	0.1700
-10.0	0.0000	0.0000	-0.0015	0.0020	0.0320	0.0650	0.1000	0.1420	0.1630
-9.0	0.0000	0.0000	0.0000	-0.0030	0.0160	0.0540	0.0890	0.1320	0.1540
-8.0	0.0000	0.0000	0.0000	-0.0040	0.0050	0.0410	0.0820	0.1230	0.1450
-7.0	0.0000	0.0000	0.0000	0.0000	-0.0040	0.0275	0.0720	0.1125	0.1360
-6.0	0.0000	0.0000	0.0000	0.0000	-0.0030	0.0160	0.0625	0.1000	0.1250
-4.0	0.0000	0.0000	0.0000	0.0000	0.0000	0.0050	0.0400	0.0760	0.1020
-3.0	0.0000	0.0000	0.0000	0.0000	0.0000	-0.0025	0.0260	0.0665	0.0870
-2.0	0.0000	0.0000	0.0000	0.0000	0.0000	0.0000	0.0130	0.0530	0.0700
-1.0	0.0000	0.0000	0.0000	0.0000	0.0000	0.0000	0.0035	0.0330	0.0450
0.0	0.0000	0.0000	0.0000	0.0000	0.0000	0.0000	0.0000	0.0000	0.0000
1.0	0.0000	0.0000	0.0000	0.0000	0.0000	0.0000	-0.0035	-0.0330	-0.0450
2.0	0.0000	0.0000	0.0000	0.0000	0.0000	0.0000	-0.0130	-0.0530	-0.0700
3.0	0.0000	0.0000	0.0000	0.0000	0.0000	0.0025	-0.0260	-0.0665	-0.0870
4.0	0.0000	0.0000	0.0000	0.0000	0.0000	-0.0050	-0.0400	-0.0760	-0.1020
6.0	0.0000	0.0000	0.0000	0.0000	0.0030	-0.0160	-0.0625	-0.1000	-0.1250
7.0	0.0000	0.0000	0.0000	0.0000	0.0040	-0.0275	-0.0720	-0.1125	-0.1360
8.0	0.0000	0.0000	0.0000	0.0040	-0.0050	-0.0410	-0.0820	-0.1230	-0.1450
9.0	0.0000	0.0000	0.0000	0.0030	-0.0160	-0.0540	-0.0890	-0.1320	-0.1540
10.0	0.0000	0.0000	0.0015	-0.0020	-0.0320	-0.0650	-0.1000	-0.1420	-0.1630
11.0	0.0000	0.0000	0.0030	-0.0140	-0.0460	-0.0740	-0.1080	-0.1490	-0.1700
12.0	0.0000	0.0000	-0.0020	-0.0300	-0.0600	-0.0830	-0.1160	-0.1570	-0.1760
13.0	0.0000	-0.0015	-0.0250	-0.0500	-0.0740	-0.0930	-0.1220	-0.1630	-0.1840
14.0	0.0000	-0.0270	-0.0540	-0.0680	-0.0860	-0.1030	-0.1270	-0.1670	-0.1890
15.0	-0.0540	-0.0650	-0.0730	-0.0840	-0.0970	-0.1110	-0.1330	-0.1730	-0.1950
16.0	-0.0730	-0.0780	-0.0860	-0.0970	-0.1080	-0.1170	-0.1370	-0.1760	-0.2000
23.0	-0.1120	-0.1180	-0.1280	-0.1440	-0.1570	-0.1710	-0.1830	-0.2060	-0.2320
30.0	-0.1740	-0.1840	-0.1960	-0.2140	-0.2350	-0.2500	-0.2640	-0.2770	-0.2980

90.0	-0.5000	-0.5000	-0.5000	-0.5000	-0.5000	-0.5000	-0.5000	-0.5000	-0.5000
135.0	-0.5000	-0.5000	-0.5000	-0.5000	-0.5000	-0.5000	-0.5000	-0.5000	-0.5000
160.0	-0.3000	-0.3000	-0.3000	-0.3000	-0.3000	-0.3000	-0.3000	-0.3000	-0.3000
165.0	-0.3000	-0.3000	-0.3000	-0.3000	-0.3000	-0.3000	-0.3000	-0.3000	-0.3000
170.0	-0.4000	-0.4000	-0.4000	-0.4000	-0.4000	-0.4000	-0.4000	-0.4000	-0.4000
180.0	0.0000	0.0000	0.0000	0.0000	0.0000	0.0000	0.0000	0.0000	0.0000

11.10 H-34 versus CAMRAD II

References: 1. NASA TN D-4632, An Investigation of Full-Scale Helicopter Rotors at High Advance Ratios and Advancing Tip Mach Numbers by John McCloud III and Jim Biggers, July 1968
2. Harris EXCEL File: MASTER H-34 versus CAMRAD II (Final June 20, 2008).xls

Airfoil	N.A.C.A. 0012
Chord	1.337 ft
Diameter	56.00 ft
Twist	0.00 deg
Disc Area	2,463 sq. ft
Reference Area (4 blades)	153.1 sq. ft
Nominal Solidity	0.062
Lock Number	8.86
Flap Moment of inertia	1264 slug ft ²
Weight Moment	2,265 lb-ft
Flap/Lag Hinge Offset	1.00 ft

Notes: 1. Wind axis data measured. Shaft axis data derived.
2. Shaft torque derived from strain cage on shaft.
3. Coefficients based on rotor tip speed and total blade area ($\sigma A = 153.1$ sq. ft.)
4. Articulated hub with coincident flap and lag hinges at $r/R = 0.0357$
5. Pitch bearing at $r/R = 0.079$

Table of CAMRAD II Output

Advance Ratio	Collective at 0.75R (deg)	Shaft Angle of Attack (deg)	Long Cyclic (deg)	Lat Cyclic (deg)	C_L/σ	C_D/σ	C_T/σ	C_H/σ	C_Y/σ	C_Q/σ	C_{De}/σ	Rotor Alone L/De
0.306	-4.0	5.0	-0.91	0.38	-0.008090	0.000450	-0.008020	0.001150	0.000031	0.001406	0.005080	-1.59
0.306	-4.0	10.0	-0.01	-0.15	0.017990	0.004710	0.018530	0.001510	-0.000102	0.000177	0.005290	3.40
0.307	-2.0	5.0	0.60	-0.24	0.013360	0.002430	0.013520	0.001260	-0.000017	0.000787	0.005020	2.66
0.305	-2.0	10.0	1.53	-0.63	0.040280	0.008760	0.041190	0.001630	-0.000461	-0.000825	0.006040	6.67
0.305	0.0	0.0	1.14	-0.40	0.008640	0.001140	0.008640	0.001140	-0.000034	0.001162	0.004970	1.74
0.305	0.0	5.0	2.06	-0.83	0.035690	0.004510	0.035950	0.001380	-0.000335	0.000392	0.005800	6.15
0.303	0.0	10.0	3.05	-1.11	0.062510	0.012620	0.063740	0.001570	-0.001018	-0.001536	0.007560	8.27
0.303	2.0	-5.0	1.78	-0.48	0.003110	0.000880	0.003020	0.001140	-0.000044	0.001293	0.005130	0.61
0.305	2.0	0.0	2.62	-1.08	0.030450	0.001070	0.030450	0.001070	-0.000307	0.001398	0.005670	5.37
0.306	2.0	5.0	3.53	-1.44	0.058050	0.006340	0.058380	0.001250	-0.000801	0.000251	0.007160	8.11
0.304	2.0	10.0	4.59	-1.56	0.083790	0.016090	0.085300	0.001300	-0.001475	-0.001777	0.010250	8.17
0.300	4.0	-10.0	2.35	-0.56	-0.001480	0.001520	-0.001710	0.001240	-0.000136	0.001185	0.005420	-0.27
0.306	4.0	-5.0	3.26	-1.19	0.025210	-0.001290	0.025230	0.000910	-0.000261	0.002155	0.005800	4.35
0.304	4.0	0.0	4.13	-1.77	0.052540	0.000890	0.052530	0.000890	-0.000791	0.001866	0.007020	7.48
0.302	4.0	5.0	4.99	-2.06	0.079730	0.007970	0.080110	0.000990	-0.001519	0.000431	0.009380	8.50
0.303	4.0	10.0	6.32	-2.04	0.100980	0.018120	0.102570	0.000310	-0.002120	-0.001256	0.013980	7.22
0.303	6.0	-10.0	3.80	-1.30	0.021020	-0.002810	0.021190	0.000880	-0.000246	0.002703	0.006080	3.46
0.304	6.0	-5.0	4.78	-2.02	0.047250	-0.003590	0.047380	0.000550	-0.000760	0.003260	0.007140	6.62
0.304	6.0	0.0	5.66	-2.55	0.074070	0.000520	0.074050	0.000520	-0.001633	0.002631	0.009170	8.08
0.307	6.0	5.0	6.64	-2.79	0.097280	0.008650	0.097640	0.000140	-0.002272	0.001357	0.013120	7.41
0.305	6.0	10.0	8.37	-2.93	0.110290	0.018440	0.111770	-0.000980	-0.003095	0.000487	0.020050	5.50
0.305	8.0	-10.0	5.31	-2.25	0.043010	-0.007120	0.043590	0.000460	-0.000702	0.004446	0.007510	5.73
0.305	8.0	-5.0	6.26	-2.98	0.069140	-0.006020	0.069380	0.000030	-0.001519	0.004668	0.009340	7.40
0.304	8.0	0.0	7.46	-3.45	0.091210	-0.000380	0.091180	-0.000380	-0.002425	0.004038	0.012900	7.07
0.304	8.0	5.0	8.83	-3.97	0.106640	0.008160	0.106880	-0.001160	-0.003499	0.003421	0.019410	5.49
0.305	8.0	10.0	10.63	-4.40	0.114920	0.018160	0.116230	-0.002060	-0.004601	0.003057	0.028210	4.07
0.304	10.0	-10.0	6.72	-3.43	0.065820	-0.011960	0.066880	-0.000350	-0.001431	0.006613	0.009790	6.72

0.304	10.0	-5.0	7.87	-4.18	0.088750	-0.008630	0.089130	-0.000870	-0.002540	0.006606	0.013090	6.78
0.305	10.0	0.0	9.54	-4.86	0.102720	-0.001690	0.102650	-0.001690	-0.003711	0.006347	0.019190	5.35
0.304	10.0	5.0	11.21	-5.71	0.111230	0.007170	0.111330	-0.002540	-0.004831	0.006230	0.027670	4.02
0.304	11.0	-10.0	N C	N C	N C	N C	N C	N C	N C	N C	N C	N C
0.305	11.0	-5.0	N C	N C	N C	N C	N C	N C	N C	N C	N C	N C
0.399	-4.0	5.0	-0.51	0.10	0.001790	0.002220	0.001970	0.002060	0.000117	0.001174	0.005150	0.35
0.402	-4.0	10.0	0.87	-0.43	0.033150	0.008940	0.034200	0.003050	-0.000423	-0.001030	0.006370	5.20
0.400	-2.0	5.0	1.22	-0.46	0.020310	0.003990	0.020580	0.002210	-0.000044	0.000539	0.005340	3.80
0.400	-2.0	10.0	2.71	-0.83	0.051460	0.011560	0.052680	0.002450	-0.000786	-0.001923	0.006760	7.61
0.402	0.0	0.0	1.55	-0.51	0.007370	0.001770	0.007370	0.001770	-0.000149	0.001303	0.005020	1.47
0.399	0.0	5.0	2.93	-0.98	0.039110	0.005700	0.039450	0.002270	-0.000370	0.000125	0.006010	6.51
0.401	0.0	10.0	4.55	-1.18	0.069360	0.014500	0.070820	0.002240	-0.001098	-0.002456	0.008380	8.28
0.402	2.0	0.0	3.26	-1.14	0.026070	0.001800	0.026070	0.001800	-0.000269	0.001522	0.005590	4.66
0.403	2.0	5.0	4.69	-1.49	0.057360	0.007090	0.057750	0.002060	-0.000959	-0.000028	0.007020	8.17
0.401	4.0	-5.0	3.62	-1.14	0.013300	0.000380	0.013210	0.001530	-0.000182	0.002053	0.005500	2.42
0.401	4.0	0.0	5.00	-1.80	0.044710	0.001560	0.044700	0.001560	-0.000783	0.001949	0.006420	6.96
0.399	4.0	5.0	6.54	-2.05	0.074580	0.007990	0.074970	0.001460	-0.001700	0.000307	0.008760	8.51
0.402	6.0	-10.0	3.95	-1.09	0.000790	0.001690	0.000460	0.001800	-0.000200	0.001712	0.005960	0.13
0.401	6.0	-5.0	5.32	-1.93	0.031880	-0.001570	0.031890	0.001210	-0.000584	0.003111	0.006190	5.15
0.401	6.0	0.0	6.74	-2.51	0.062790	0.001170	0.062770	0.001170	-0.001485	0.002617	0.007700	8.15
0.402	6.0	5.0	8.53	-2.82	0.088150	0.008460	0.088520	0.000750	-0.002561	0.001268	0.011620	7.59
0.403	8.0	-10.0	5.62	-1.94	0.020100	-0.002210	0.020180	0.001310	-0.000536	0.003444	0.006380	3.15
0.402	8.0	-5.0	7.01	-2.85	0.050410	-0.003670	0.050530	0.000740	-0.001164	0.004423	0.007360	6.85
0.403	8.0	0.0	8.68	-3.43	0.077400	0.000500	0.077370	0.000500	-0.002309	0.003855	0.010120	7.65
0.401	8.0	5.0	10.67	-3.95	0.098340	0.008260	0.098600	-0.000330	-0.003986	0.003049	0.015860	6.20
0.404	10.0	-10.0	7.30	-3.04	0.039180	-0.006200	0.039650	0.000690	-0.000934	0.005487	0.007480	5.24
0.401	10.0	-5.0	8.72	-4.00	0.068780	-0.005870	0.069000	0.000140	-0.001975	0.006074	0.009270	7.42
0.401	9.0	5.0	N C	N C	N C	N C	N C	N C	N C	N C	N C	N C
0.403	9.5	0.0	N C	N C	N C	N C	N C	N C	N C	N C	N C	N C
0.401	11.0	-10.0	N C	N C	N C	N C	N C	N C	N C	N C	N C	N C
0.458	-4.0	5.0	-0.47	0.04	0.006220	0.003230	0.006480	0.002670	0.000034	0.000991	0.005380	1.16
0.460	-4.0	10.0	1.35	-0.52	0.038490	0.009820	0.039600	0.002980	-0.000338	-0.001522	0.006500	5.92
0.460	-2.0	5.0	1.48	-0.53	0.022210	0.004430	0.022510	0.002480	-0.000194	0.000449	0.005410	4.11

0.462	-2.0	10.0	3.36	-0.87	0.054740	0.012500	0.056070	0.002800	-0.000925	-0.002434	0.007190	7.61
0.467	0.0	0.0	1.62	-0.50	0.005880	0.002010	0.005880	0.002010	-0.000055	0.001356	0.004970	1.18
0.461	0.0	5.0	3.39	-1.05	0.038590	0.005970	0.038960	0.002580	-0.000379	0.000050	0.006080	6.35
0.461	0.0	10.0	5.41	-1.17	0.070170	0.015410	0.071770	0.002990	-0.001444	-0.003105	0.008650	8.11
0.459	2.0	0.0	3.50	-1.10	0.022410	0.002040	0.022410	0.002040	-0.000476	0.001547	0.005410	4.14
0.460	2.0	5.0	5.35	-1.53	0.054490	0.007240	0.054910	0.002460	-0.000812	-0.000122	0.006970	7.82
0.461	2.0	10.0	7.55	-1.54	0.083050	0.016780	0.084680	0.002110	-0.001903	-0.002782	0.010720	7.75
0.458	4.0	-5.0	3.74	-1.05	0.005050	0.001730	0.004870	0.002160	-0.000237	0.001739	0.005520	0.91
0.461	4.0	0.0	5.41	-1.72	0.038650	0.001940	0.038640	0.001940	-0.000751	0.001880	0.006030	6.41
0.460	4.0	5.0	7.37	-2.04	0.069150	0.007890	0.069560	0.001840	-0.001460	0.000122	0.008160	8.47
0.456	6.0	-5.0	5.62	-1.81	0.022230	0.000160	0.022130	0.002100	-0.000404	0.002788	0.006240	3.56
0.458	6.0	0.0	7.35	-2.41	0.054760	0.001700	0.054740	0.001700	-0.001332	0.002476	0.007090	7.72
0.462	6.0	5.0	9.47	-2.80	0.081430	0.008930	0.081850	0.001800	-0.002509	0.000974	0.011050	7.37
0.456	8.0	-10.0	5.77	-1.67	0.006240	0.001100	0.005940	0.002170	-0.000387	0.002429	0.006390	0.98
0.455	8.0	-5.0	7.52	-2.69	0.038390	-0.001800	0.038400	0.001550	-0.000813	0.003980	0.006870	5.59
0.458	8.0	0.0	9.39	-3.31	0.069100	0.001140	0.069060	0.001140	-0.002068	0.003493	0.008750	7.90
0.462	8.0	5.0	11.68	-3.84	0.091210	0.008760	0.091550	0.000790	-0.003780	0.002406	0.014010	6.51
0.456	10.0	-10.0	7.64	-2.68	0.023260	-0.002390	0.023320	0.001690	-0.000562	0.004392	0.007180	3.24
0.459	10.0	-5.0	9.38	-3.81	0.055140	-0.003410	0.055210	0.001410	-0.001369	0.005432	0.008430	6.54
0.457	10.0	0.0	11.58	-4.66	0.079470	0.000470	0.079400	0.000470	-0.003367	0.005157	0.011710	6.79
0.456	12.0	-10.0	9.46	-4.07	0.041330	-0.006240	0.041770	0.001030	-0.001267	0.006616	0.008170	5.06
0.508	-4.0	5.0	-0.31	-0.08	0.008270	0.003550	0.008550	0.002810	0.000141	0.001008	0.005540	1.49
0.507	-4.0	10.0	1.72	-0.60	0.042580	0.011290	0.043890	0.003720	-0.000301	-0.002057	0.007220	5.90
0.506	-2.0	2.0	0.50	-0.22	0.003180	0.002530	0.003270	0.002410	0.000012	0.001328	0.005150	0.62
0.507	-2.0	5.0	1.73	-0.60	0.023120	0.005170	0.023490	0.003140	-0.000010	0.000360	0.005880	3.93
0.509	-2.0	10.0	3.82	-0.92	0.057300	0.013560	0.058790	0.003400	-0.000516	-0.002735	0.008150	7.03
0.498	0.0	-3.0	0.49	-0.08	-0.015110	0.003240	-0.015260	0.002440	-0.000084	0.001071	0.005360	-2.82
0.507	0.0	2.0	2.50	-0.77	0.017710	0.003460	0.017820	0.002840	-0.000221	0.001118	0.005670	3.12
0.509	0.0	5.0	3.76	-1.06	0.037710	0.006600	0.038140	0.003290	-0.000232	-0.000044	0.006520	5.78
0.508	0.0	10.0	5.97	-1.23	0.071400	0.015640	0.073030	0.003010	-0.001120	-0.003159	0.009400	7.60
0.502	2.0	-3.0	2.50	-0.65	-0.000490	0.002390	-0.000600	0.002360	-0.000106	0.001504	0.005360	-0.09
0.509	2.0	2.0	4.51	-1.30	0.032460	0.003630	0.032560	0.002490	-0.000459	0.001131	0.005860	5.54
0.509	2.0	5.0	5.81	-1.54	0.052090	0.007760	0.052560	0.003190	-0.000560	-0.000191	0.007380	7.06

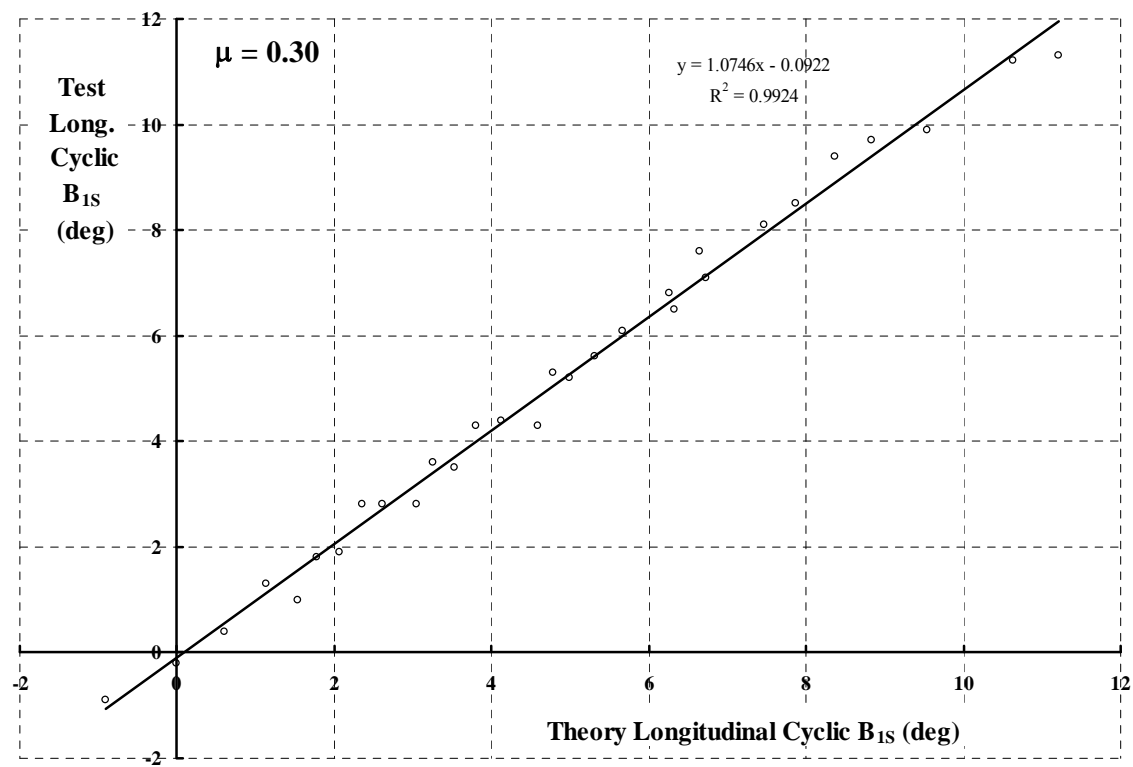
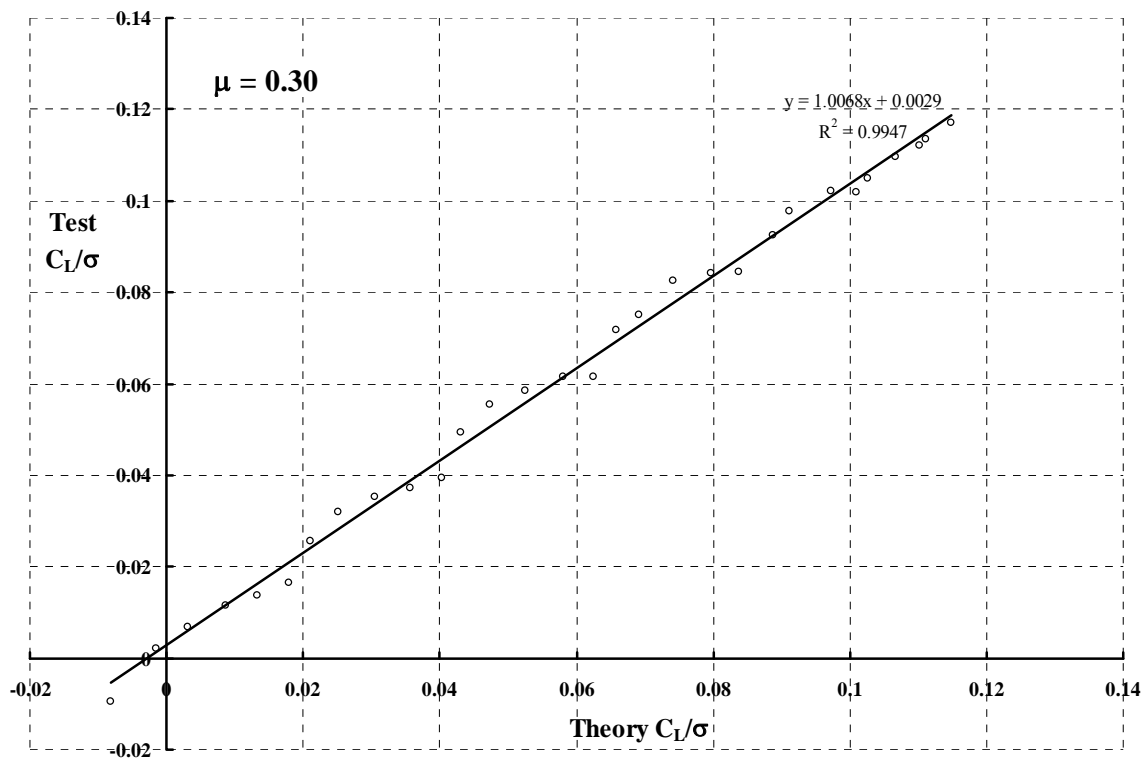
0.509	2.0	10.0	8.29	-1.59	0.081360	0.016320	0.082940	0.001950	-0.001941	-0.002810	0.010760	7.56
0.502	4.0	-5.0	3.70	-0.97	0.000720	0.002450	0.000480	0.002510	-0.000150	0.001702	0.005820	0.12
0.507	4.0	-3.0	4.51	-1.30	0.014030	0.001520	0.013930	0.002250	-0.000282	0.002109	0.005680	2.47
0.513	4.0	2.0	6.56	-1.83	0.047170	0.004650	0.047290	0.003000	-0.001076	0.001284	0.007190	6.56
0.506	4.0	5.0	7.95	-2.04	0.064910	0.008390	0.065380	0.002700	-0.001174	0.000164	0.008710	7.45
0.508	4.0	10.0	10.51	-2.10	0.091830	0.017610	0.093450	0.001400	-0.003012	-0.002239	0.013180	6.97
0.499	6.0	-5.0	5.71	-1.73	0.015570	0.000850	0.015430	0.002200	-0.000395	0.002621	0.006030	2.58
0.505	6.0	-3.0	6.50	-2.06	0.028910	0.000520	0.028840	0.002030	-0.000621	0.002876	0.006200	4.66
0.511	6.0	2.0	8.68	-2.49	0.060010	0.004430	0.060110	0.002330	-0.001409	0.001853	0.008090	7.42
0.507	6.0	5.0	10.09	-2.71	0.076820	0.008960	0.077280	0.002230	-0.002033	0.000827	0.010600	7.25
0.507	6.0	10.0	12.72	-2.85	0.100920	0.018930	0.102590	0.001140	-0.004159	-0.001127	0.016710	6.04
0.496	8.0	-10.0	5.79	-1.44	-0.003620	0.003830	-0.004220	0.003140	-0.000175	0.001610	0.007010	-0.52
0.502	8.0	-5.0	7.71	-2.57	0.030240	-0.000740	0.030180	0.001900	-0.000798	0.003782	0.006730	4.49
0.508	8.0	-3.0	8.49	-2.91	0.043570	-0.000540	0.043520	0.001740	-0.001151	0.003880	0.007130	6.11
0.510	8.0	2.0	10.70	-3.62	0.070600	0.004200	0.070670	0.001730	-0.002160	0.002842	0.009820	7.19
0.509	8.0	5.0	12.25	-3.73	0.087530	0.008880	0.087910	0.001220	-0.003218	0.002027	0.012890	6.79
0.498	10.0	-10.0	7.74	-2.39	0.011560	0.000890	0.011220	0.002880	-0.000552	0.003325	0.007460	1.55
0.502	10.0	-5.0	9.68	-3.65	0.045320	-0.002440	0.045340	0.001520	-0.001356	0.005156	0.007750	5.85
0.508	10.0	-3.0	10.54	-4.06	0.056790	-0.001730	0.056770	0.001240	-0.001924	0.005201	0.008550	6.64
0.514	10.0	2.0	12.93	-4.88	0.081210	0.004100	0.081230	0.001260	-0.003584	0.004421	0.012840	6.32
0.495	12.0	-10.0	9.69	-3.62	0.027360	-0.002480	0.027360	0.002310	-0.000803	0.005457	0.008310	3.29
0.498	12.0	-5.0	11.69	-5.11	0.058630	-0.004270	0.058730	0.000850	-0.002345	0.006958	0.009480	6.18
0.500	13.0	-10.0	N C	N C	N C	N C	N C	N C	N C	N C	N C	N C
0.624	-4.0	4.0	-0.89	0.02	0.006800	0.004010	0.007070	0.003520	-0.000050	0.001210	0.005960	1.14
0.618	-4.0	8.0	1.16	-0.60	0.035620	0.009270	0.036560	0.004220	0.000346	-0.001053	0.007570	4.71
0.624	-2.0	4.0	1.34	-0.50	0.017350	0.004760	0.017640	0.003540	-0.000094	0.000754	0.005980	2.90
0.620	-2.0	8.0	3.43	-1.04	0.045900	0.010280	0.046880	0.003790	-0.000050	-0.001412	0.008000	5.74
0.618	0.0	0.0	1.49	-0.35	0.001420	0.003100	0.001420	0.003100	-0.000038	0.001500	0.005520	0.26
0.622	0.0	4.0	3.54	-0.99	0.028100	0.005840	0.028430	0.003870	-0.000106	0.000395	0.006480	4.34
0.618	0.0	8.0	5.69	-1.42	0.057050	0.011850	0.058150	0.003790	-0.000275	-0.001805	0.008930	6.39
0.618	2.0	-4.0	1.67	-0.14	-0.014200	0.004480	-0.014480	0.003480	-0.000315	0.001010	0.006110	-2.32
0.619	2.0	0.0	3.70	-0.90	0.011730	0.003210	0.011730	0.003210	-0.000147	0.001601	0.005790	2.03
0.620	2.0	4.0	5.79	-1.47	0.038050	0.006180	0.038390	0.003510	-0.000400	0.000368	0.006780	5.61

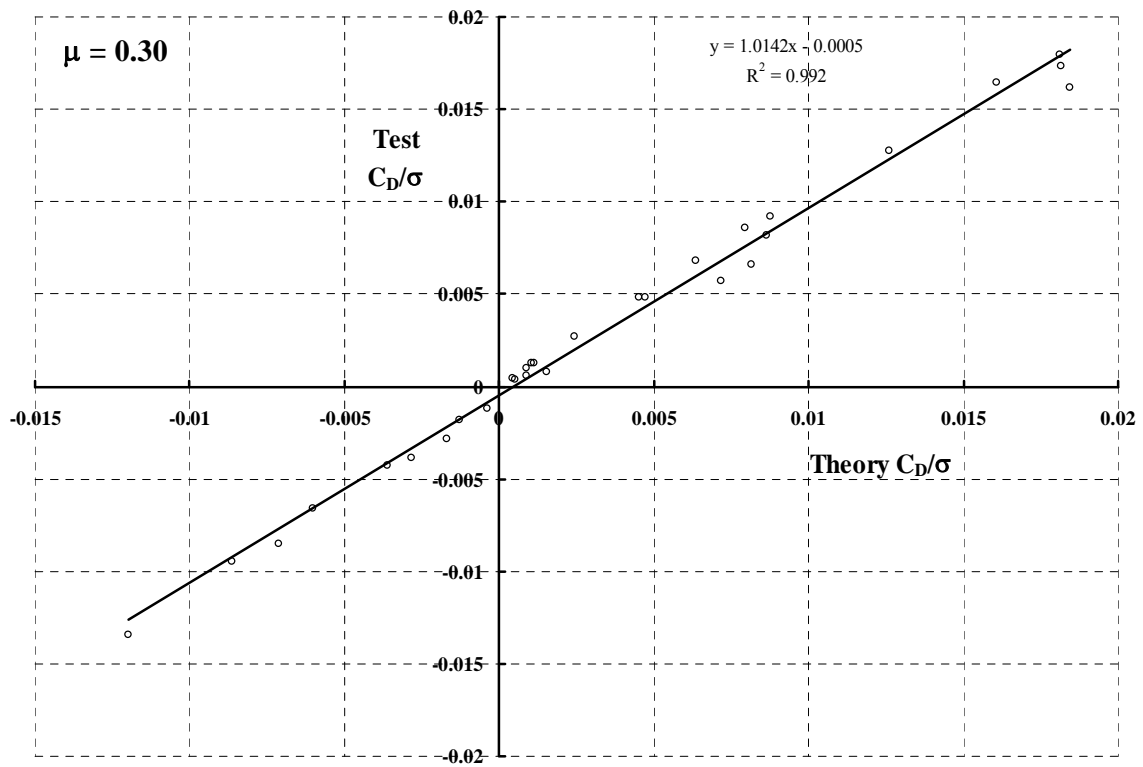
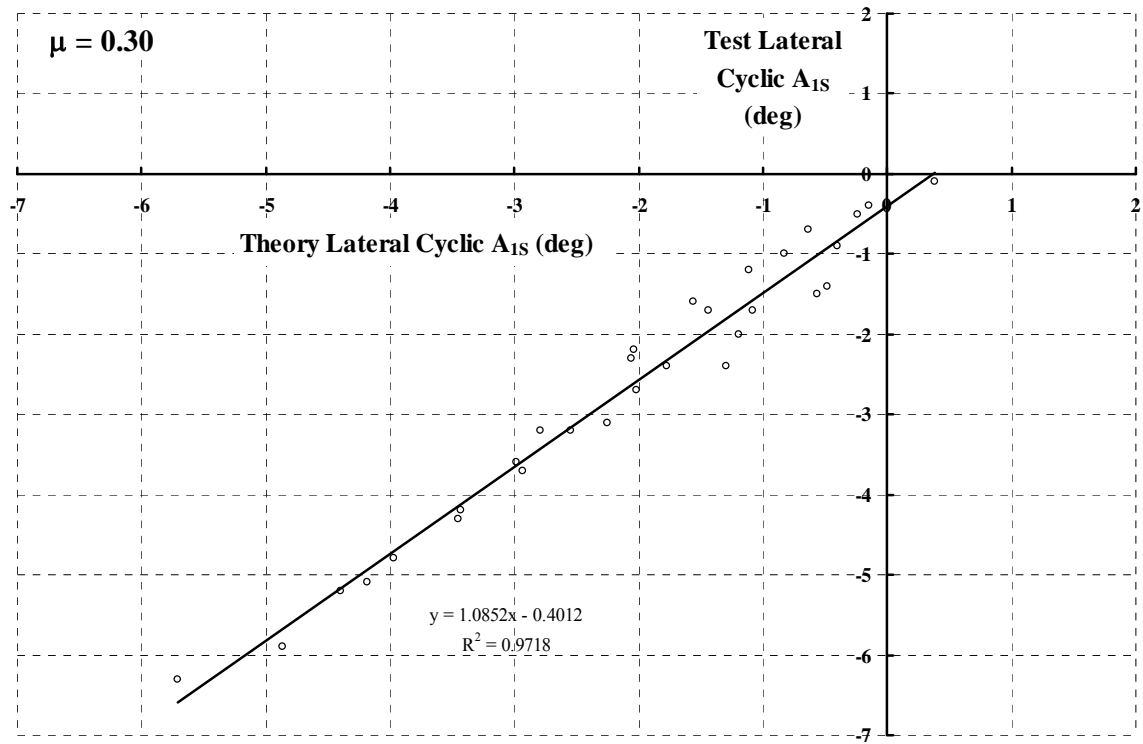
0.619	2.0	8.0	8.02	-1.71	0.066270	0.013020	0.067430	0.003670	-0.000586	-0.001882	0.009980	6.64
0.619	4.0	-4.0	3.86	-0.75	-0.003940	0.003830	-0.004190	0.003550	-0.000234	0.001530	0.006300	-0.63
0.621	4.0	0.0	5.90	-1.51	0.022100	0.003270	0.022100	0.003270	-0.000414	0.001848	0.006250	3.54
0.621	4.0	4.0	8.05	-1.90	0.047970	0.008170	0.048420	0.004800	-0.000672	0.000349	0.008730	5.49
0.619	4.0	8.0	10.31	-2.08	0.076250	0.014210	0.077480	0.003460	-0.000875	-0.001677	0.011500	6.63
0.613	6.0	-8.0	4.07	-0.52	-0.019930	0.007100	-0.020720	0.004250	-0.000410	0.000136	0.007320	-2.72
0.610	6.0	-4.0	6.05	-1.51	0.006940	0.003110	0.006700	0.003590	-0.000364	0.002209	0.006670	1.04
0.624	6.0	0.0	8.12	-2.17	0.032300	0.003430	0.032290	0.003430	-0.000702	0.002195	0.006970	4.63
0.634	6.0	4.0	10.33	-2.45	0.057960	0.008020	0.058370	0.003960	-0.000958	0.000691	0.009140	6.34
0.624	6.0	4.0	10.33	-2.45	0.057960	0.008020	0.058370	0.003960	-0.000958	0.000691	0.009140	6.34
0.614	8.0	-8.0	6.26	-1.24	-0.008860	0.005700	-0.009570	0.004410	-0.000203	0.001223	0.007670	-1.16
0.619	8.0	-4.0	8.26	-2.32	0.018070	0.002320	0.017850	0.003570	-0.000649	0.003038	0.007220	2.50
0.621	8.0	4.0	12.57	-3.23	0.068110	0.008670	0.068540	0.003890	-0.001430	0.001368	0.010870	6.27
0.621	10.0	-8.0	8.44	-2.09	0.002040	0.004330	0.001390	0.004570	-0.000303	0.002426	0.008250	0.25
0.620	10.0	-4.0	10.45	-3.21	0.028970	0.001550	0.028770	0.003570	-0.001071	0.004016	0.008030	3.61
0.619	12.0	-8.0	10.60	-3.11	0.013290	0.002770	0.012750	0.004590	-0.000711	0.003799	0.008900	1.49
0.711	-4.0	2.0	-2.11	0.33	-0.001860	0.004130	-0.001710	0.004190	-0.000105	0.001739	0.006590	-0.28
0.708	-4.0	4.0	-1.00	-0.13	0.011570	0.006250	0.011970	0.005430	0.000184	0.001041	0.007720	1.50
0.708	-4.0	6.0	0.13	-0.53	0.027290	0.008040	0.027980	0.005150	0.000455	0.000012	0.008060	3.39
0.706	-4.0	8.0	1.31	-0.82	0.041790	0.011210	0.042940	0.005280	0.000389	-0.001398	0.009230	4.53
0.710	-2.0	2.0	0.17	-0.17	0.005640	0.004270	0.005790	0.004070	-0.000018	0.001487	0.006370	0.89
0.711	-2.0	4.0	1.32	-0.58	0.020190	0.006290	0.020580	0.004860	0.000191	0.000740	0.007330	2.75
0.709	-2.0	6.0	2.48	-0.94	0.034690	0.008940	0.035440	0.005270	0.000098	-0.000302	0.008520	4.07
0.708	-2.0	8.0	3.64	-1.23	0.051160	0.012620	0.052420	0.005380	0.000524	-0.001857	0.010000	5.12
0.710	0.0	0.0	1.31	-0.22	0.000290	0.003860	0.000280	0.003860	-0.000070	0.001582	0.006100	0.05
0.712	0.0	2.0	2.47	-0.63	0.013010	0.005090	0.013180	0.004630	0.000220	0.001128	0.006680	1.95
0.710	0.0	4.0	3.62	-1.04	0.027910	0.007300	0.028350	0.005340	0.000326	0.000638	0.008200	3.40
0.708	0.0	6.0	4.81	-1.30	0.043310	0.010120	0.044130	0.005540	0.000243	-0.000627	0.009230	4.69
0.707	0.0	8.0	5.99	-1.56	0.058570	0.012840	0.059780	0.004570	0.000400	-0.001810	0.010290	5.69
0.710	2.0	0.0	3.62	-0.69	0.007450	0.004090	0.007450	0.004090	-0.000058	0.001641	0.006410	1.16
0.711	2.0	2.0	4.78	-1.06	0.020230	0.005380	0.020410	0.004670	0.000050	0.001145	0.007000	2.89
0.709	2.0	4.0	5.96	-1.43	0.035080	0.007450	0.035520	0.004990	0.000110	0.000438	0.008070	4.35
0.708	2.0	6.0	7.17	-1.61	0.051370	0.011780	0.052320	0.006350	0.000370	-0.000697	0.010800	4.76

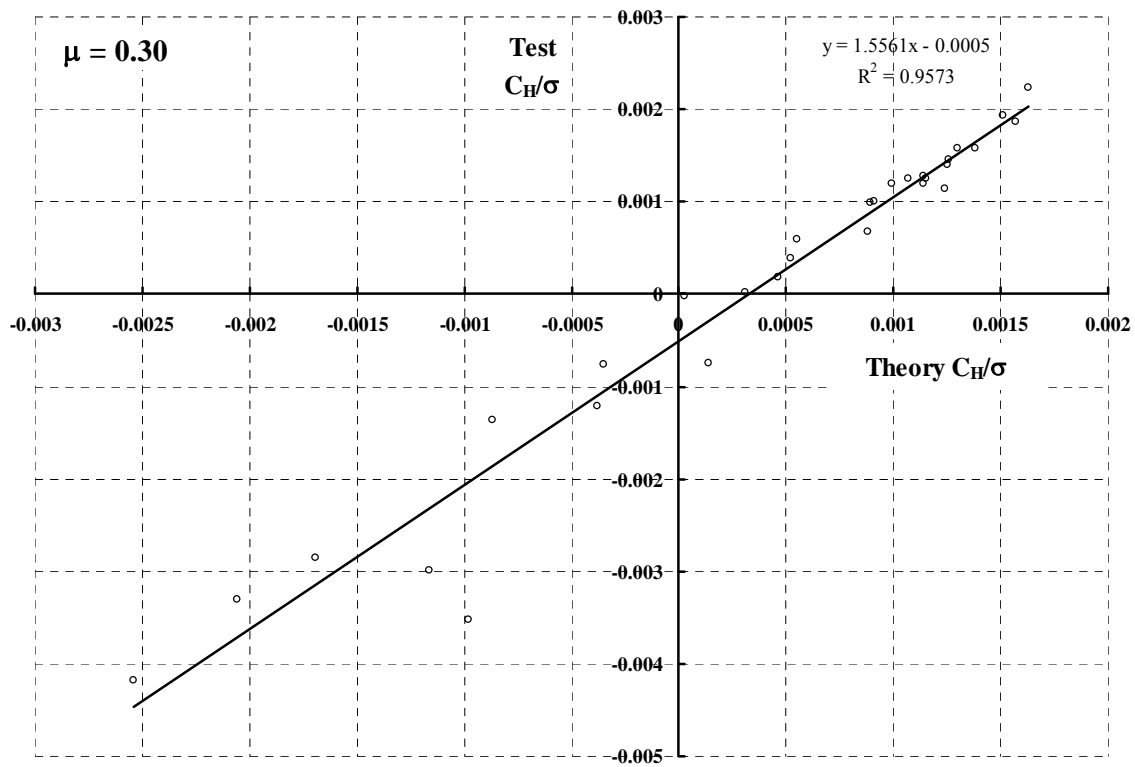
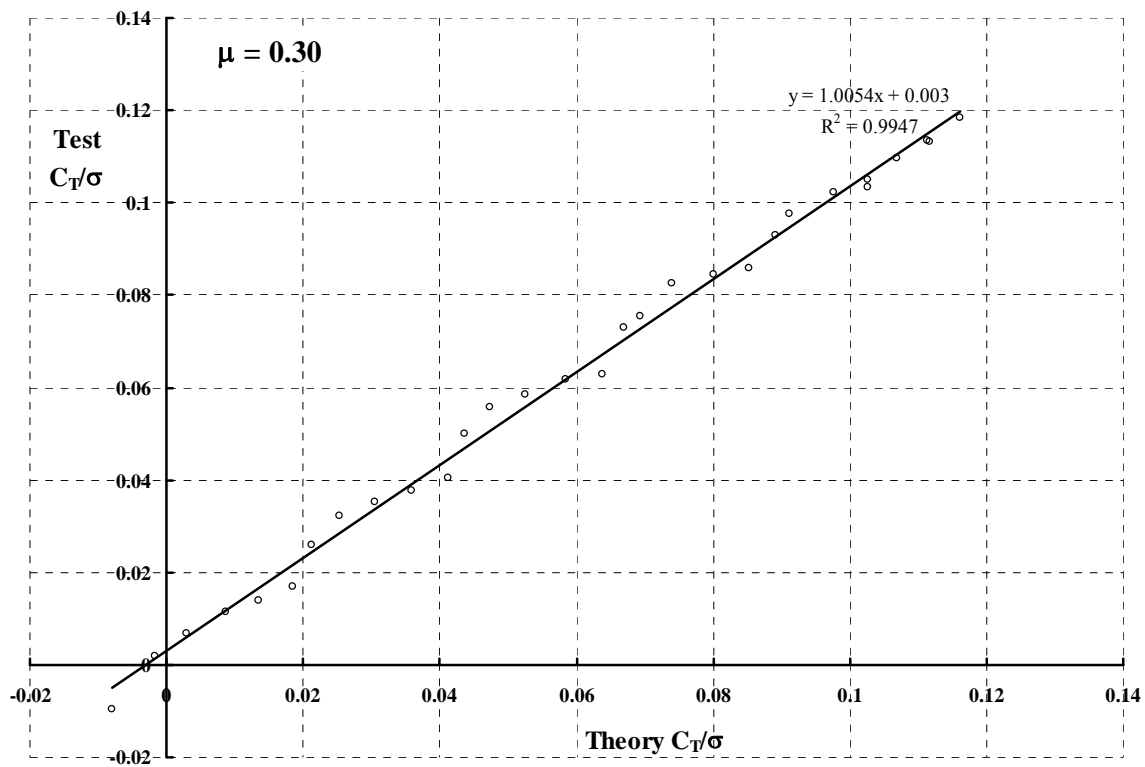
0.714	2.0	8.0	8.37	-1.83	0.065400	0.012930	0.066560	0.003710	0.000510	-0.001450	0.010890	6.01
0.706	4.0	-2.0	4.74	-0.84	0.002570	0.004260	0.002420	0.004340	-0.000151	0.001823	0.006830	0.38
0.706	4.0	0.0	5.92	-1.21	0.014820	0.004390	0.014820	0.004390	-0.000154	0.001772	0.006890	2.15
0.711	4.0	2.0	7.10	-1.51	0.028310	0.005580	0.028490	0.004590	-0.000097	0.001174	0.007240	3.91
0.709	4.0	4.0	8.31	-1.78	0.042090	0.007740	0.042530	0.004780	-0.000288	0.000393	0.008290	5.08
0.706	4.0	6.0	9.53	-2.05	0.057610	0.010850	0.058430	0.004770	0.000346	-0.000341	0.010370	5.56
0.695	6.0	-4.0	5.85	-1.07	-0.002050	0.005090	-0.002360	0.004940	-0.000367	0.001768	0.007590	-0.27
0.705	6.0	-2.0	7.02	-1.54	0.010810	0.004530	0.010640	0.004910	-0.000338	0.002173	0.007600	1.42
0.707	6.0	0.0	8.21	-1.81	0.022660	0.004710	0.022660	0.004710	-0.000304	0.002036	0.007580	2.99
0.711	6.0	2.0	9.44	-1.95	0.036170	0.006560	0.036380	0.005290	-0.000196	0.001216	0.008280	4.37
0.709	6.0	4.0	10.66	-2.18	0.049830	0.008350	0.050290	0.004850	-0.000318	0.000471	0.009010	5.53
0.695	8.0	-4.0	8.12	-1.81	0.006900	0.004810	0.006520	0.005270	-0.000548	0.002342	0.008110	0.85
0.709	8.0	-2.0	9.29	-2.27	0.019530	0.004220	0.019360	0.004900	-0.000543	0.002718	0.008060	2.42
0.712	8.0	0.0	10.50	-2.52	0.031260	0.005900	0.031260	0.005900	-0.000411	0.002412	0.009310	3.36
0.710	8.0	2.0	11.75	-2.52	0.045310	0.007210	0.045530	0.005620	-0.000661	0.001454	0.009260	4.89
0.711	8.0	4.0	13.00	-2.71	0.058220	0.009270	0.058720	0.005180	-0.000737	0.000975	0.010640	5.47
0.699	10.0	-4.0	10.44	-2.55	0.014390	0.005040	0.014000	0.006030	-0.000475	0.002890	0.009120	1.58
0.716	10.0	-2.0	11.59	-3.03	0.028060	0.004500	0.027870	0.005480	-0.000815	0.003259	0.009100	3.08
0.706	10.0	0.0	12.79	-3.34	0.039880	0.005480	0.039860	0.005480	-0.001125	0.003056	0.009790	4.07
0.703	12.0	-4.0	12.68	-3.58	0.024540	0.004510	0.024140	0.006210	-0.001133	0.004069	0.010250	2.39
0.707	12.0	-2.0	13.86	-3.94	0.036500	0.004710	0.036290	0.005980	-0.001379	0.004022	0.010390	3.51
0.706	13.7	-4.0	N C	N C	N C	N C	N C	N C	N C	N C	N C	N C
0.819	-4.0	0.0	N C	N C	N C	N C	N C	N C	N C	N C	N C	N C
0.824	-4.0	2.0	N C	N C	N C	N C	N C	N C	N C	N C	N C	N C
0.829	-4.0	4.0	N C	N C	N C	N C	N C	N C	N C	N C	N C	N C
0.814	-2.0	0.0	-1.28	0.29	-0.004110	0.005180	-0.004110	0.005180	-0.000126	0.001780	0.007340	-0.56
0.832	-2.0	2.0	0.03	-0.22	0.009760	0.005980	0.009970	0.005640	0.000125	0.001538	0.007850	1.24
0.830	-2.0	4.0	1.28	-0.79	0.025280	0.007860	0.025760	0.006080	0.000388	0.000847	0.008890	2.84
0.816	0.0	0.0	1.12	-0.07	-0.000880	0.006010	-0.000870	0.006010	0.000175	0.001654	0.008020	-0.11
0.829	0.0	2.0	2.41	-0.60	0.013190	0.006560	0.013410	0.006090	0.000065	0.001323	0.008170	1.61
0.830	0.0	4.0	3.68	-1.10	0.028790	0.007410	0.029230	0.005390	0.000153	0.000801	0.008390	3.43
0.808	2.0	-2.0	2.22	0.11	-0.010960	0.005900	-0.011150	0.005520	-0.000155	0.001608	0.007860	-1.39
0.818	2.0	0.0	3.52	-0.42	0.002470	0.005430	0.002470	0.005430	0.000005	0.001732	0.007530	0.33

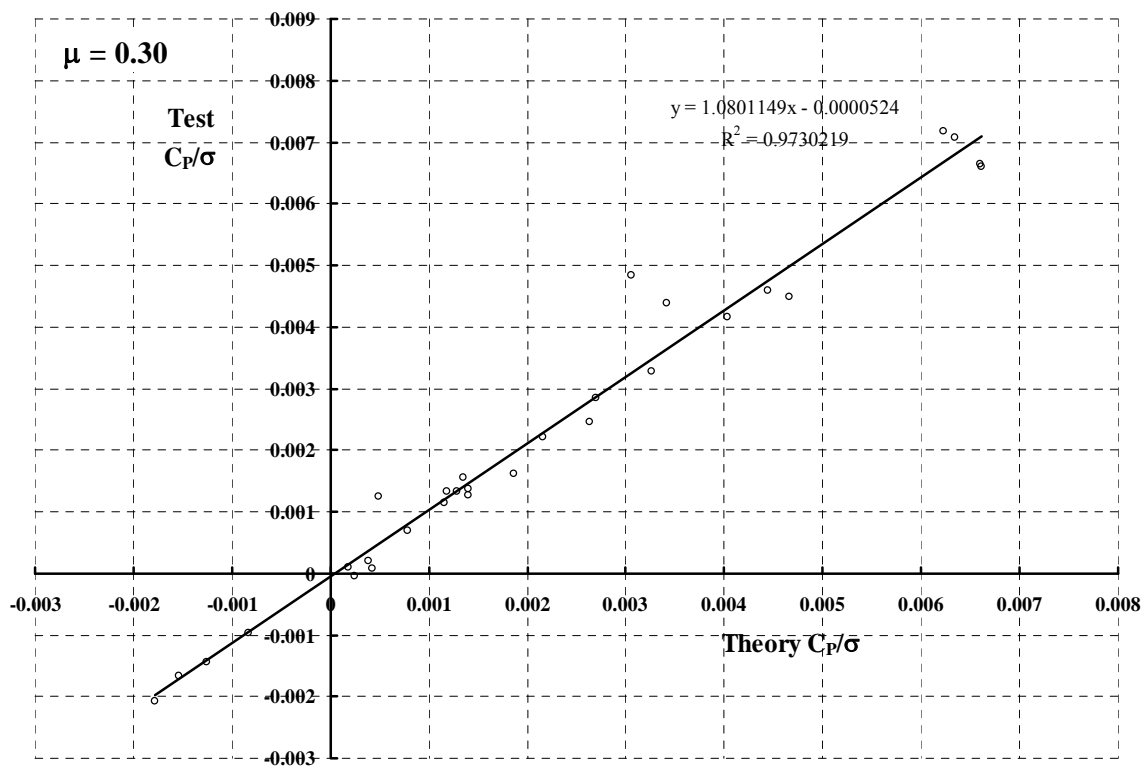
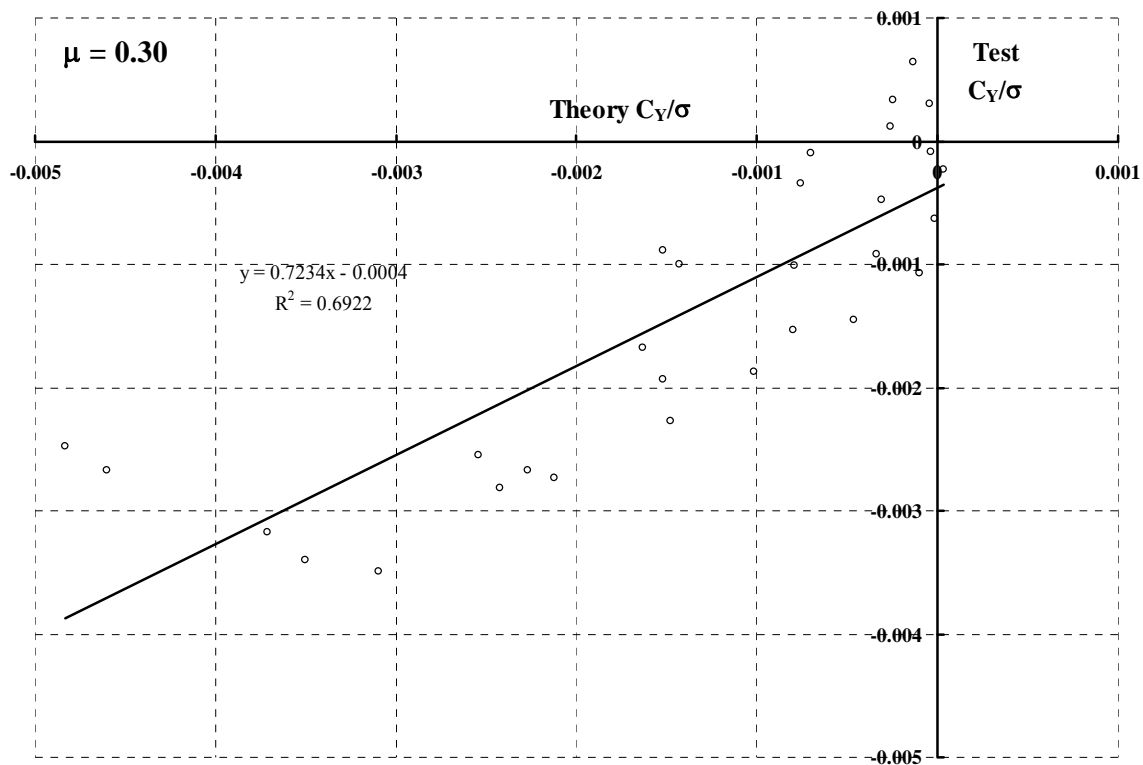
0.837	2.0	2.0	4.80	-0.94	0.016680	0.006490	0.016900	0.005900	0.000249	0.001388	0.008180	2.04
0.834	2.0	4.0	6.09	-1.41	0.035940	0.008730	0.035380	0.006200	0.001341	0.000760	0.009650	3.72
0.815	3.0	-2.0	N C	N C	N C	N C	N C	N C	N C	N C	N C	N C
0.807	4.0	-2.0	4.57	-0.35	-0.006690	0.007340	-0.006940	0.007100	0.000057	0.001520	0.009190	-0.73
0.818	4.0	0.0	5.91	-0.80	0.006340	0.006100	0.006340	0.006100	0.000047	0.001645	0.008100	0.78
0.838	4.0	2.0	7.22	-1.23	0.020000	0.007990	0.020260	0.007290	0.000487	0.001117	0.009360	2.14
0.831	4.0	4.0	8.54	-1.64	0.035940	0.008730	0.036450	0.006200	0.000917	0.000760	0.009650	3.72
0.811	5.0	-2.0	N C	N C	N C	N C	N C	N C	N C	N C	N C	N C
0.812	6.0	-2.0	6.92	-0.97	-0.000750	0.006850	-0.000970	0.006820	-0.000171	0.001791	0.009030	-0.08
0.818	6.0	0.0	8.27	-1.32	0.011390	0.007470	0.011390	0.007470	0.000189	0.001705	0.009540	1.19
0.834	6.0	2.0	9.64	-1.55	0.024520	0.009400	0.024830	0.008540	-0.000079	0.001162	0.010810	2.27
0.831	6.0	4.0	10.96	-1.90	0.041170	0.011300	0.041840	0.008400	0.001094	0.000609	0.012040	3.42
0.799	7.0	-2.0	N C	N C	N C	N C	N C	N C	N C	N C	N C	N C
0.815	8.0	-2.0	9.28	-1.60	0.006030	0.007680	0.005750	0.007880	-0.000388	0.001976	0.010080	0.60
0.820	8.0	0.0	10.63	-1.91	0.017770	0.007650	0.017770	0.007650	-0.000196	0.001904	0.009970	1.78
0.833	8.0	2.0	12.01	-2.05	0.031870	0.009350	0.032170	0.008230	0.000348	0.001184	0.010790	2.95
0.820	9.0	-2.0	N C	N C	N C	N C	N C	N C	N C	N C	N C	N C
0.818	10.0	-2.0	11.65	-2.11	0.012700	0.008700	0.012380	0.009130	-0.000352	0.002009	0.011140	1.14
0.828	10.0	0.0	13.00	-2.48	0.024330	0.008710	0.024330	0.008710	-0.000444	0.002139	0.011310	2.15
0.826	11.0	-2.0	N C	N C	N C	N C	N C	N C	N C	N C	N C	N C
0.813	12.0	-2.0	14.02	-2.77	0.019230	0.009450	0.018880	0.010120	-0.000406	0.002490	0.012480	1.54
0.824	12.8	-2.0	N C	N C	N C	N C	N C	N C	N C	N C	N C	N C
0.825	-4.0	4.0	N C	N C	N C	N C	N C	N C	N C	N C	N C	N C
0.826	0.0	4.0	3.68	-1.10	0.028790	0.007410	0.029230	0.005390	0.000153	0.000801	0.008390	3.43
0.828	-4.0	6.0	N C	N C	N C	N C	N C	N C	N C	N C	N C	N C
0.828	-2.0	6.0	2.51	-1.25	0.044560	0.011230	0.045480	0.006510	0.001090	-0.000461	0.010670	4.18
0.829	0.0	6.0	4.97	-1.44	0.048030	0.011010	0.048910	0.005930	0.000990	-0.000437	0.010480	4.58
0.829	2.0	6.0	7.38	-1.52	0.053900	0.013100	0.054940	0.007390	0.001924	-0.000957	0.011930	4.52
0.832	4.0	6.0	N C	N C	N C	N C	N C	N C	N C	N C	N C	N C
0.829	-4.0	8.0	N C	N C	N C	N C	N C	N C	N C	N C	N C	N C
0.827	-2.0	8.0	3.83	-1.56	0.061280	0.014590	0.062700	0.005920	0.001416	-0.001950	0.012210	5.02
0.831	0.0	8.0	6.25	-1.80	0.066730	0.015190	0.068190	0.005750	0.000871	-0.002016	0.012740	5.24
0.834	2.0	8.0	8.70	-1.90	0.071020	0.015100	0.072410	0.005070	0.001554	-0.001920	0.012760	5.57

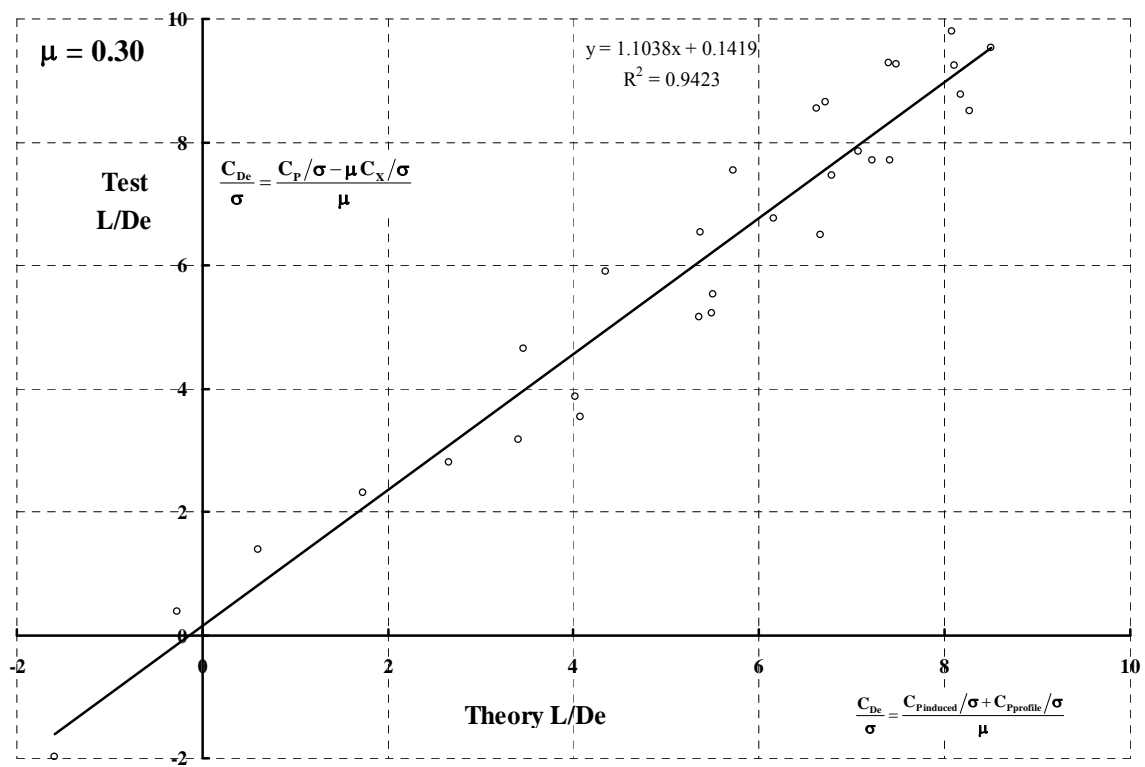
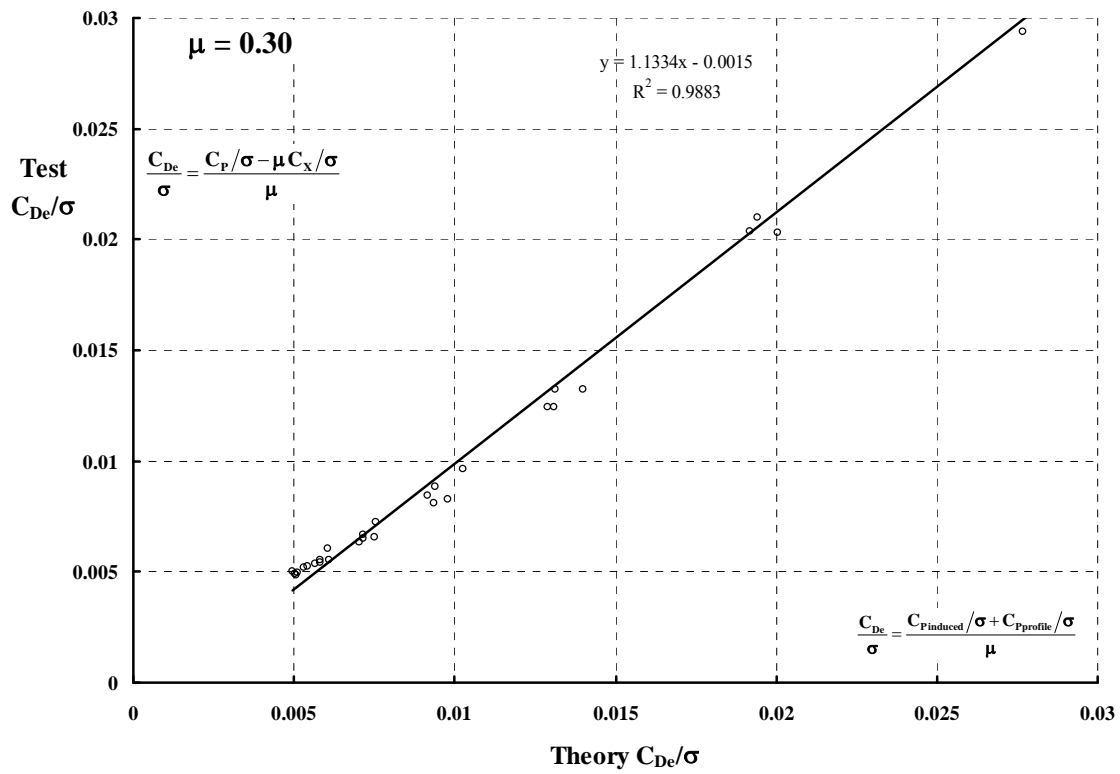
1.052	-4.0	1.0	-3.29	-0.21	0.019370	0.010490	0.019550	0.010150	-0.000305	0.001480	0.011890	1.63
1.049	-4.0	3.0	-1.83	-0.87	0.036560	0.012870	0.037180	0.010940	-0.000406	0.000870	0.013690	2.67
1.049	-4.0	5.0	-0.41	-2.17	0.064570	0.017080	0.065810	0.011380	-0.000043	-0.002080	0.015100	4.28
1.051	-4.0	7.0	1.23	-2.05	0.074290	0.018680	0.076010	0.009480	-0.000702	-0.001345	0.017400	4.27
1.045	-2.0	1.0	-0.78	-0.13	0.014090	0.009050	0.014250	0.008800	-0.000236	0.001815	0.010770	1.31
1.057	-2.0	3.0	0.66	-0.85	0.034360	0.011330	0.034900	0.009510	-0.000248	0.001136	0.012400	2.77
1.057	-2.0	5.0	2.03	-2.32	0.067140	0.016460	0.068320	0.010540	0.000038	-0.002270	0.014300	4.70
1.057	-2.0	7.0	3.66	-2.21	0.076230	0.017760	0.077820	0.008330	-0.000561	-0.001133	0.016680	4.57
1.051	0.0	1.0	1.75	-0.13	0.007740	0.008280	0.007890	0.008150	-0.000003	0.001907	0.010100	0.77
1.059	0.0	3.0	3.18	-0.78	0.028750	0.010740	0.029270	0.009220	-0.000252	0.001216	0.011890	2.42
1.059	0.0	5.0	4.47	-2.13	0.059530	0.014750	0.060590	0.009510	0.000402	-0.000778	0.014010	4.25
1.051	0.0	7.0	6.14	-2.15	0.073920	0.016690	0.075400	0.007550	-0.000366	-0.000923	0.015810	4.68
1.058	2.0	1.0	4.28	-0.04	0.001050	0.009330	0.001160	0.009310	0.000344	0.001350	0.010610	0.10
1.051	2.0	3.0	5.75	-0.67	0.020970	0.010890	0.021490	0.009780	0.000988	0.000780	0.011630	1.80
1.057	2.0	5.0	7.12	-1.62	0.047980	0.014080	0.049010	0.009850	0.001041	-0.000385	0.013710	3.50
1.052	2.0	7.0	8.53	-2.48	0.070710	0.015320	0.072010	0.006600	0.002487	0.000198	0.015510	4.56
1.058	4.0	1.0	6.81	0.24	-0.005330	0.011280	-0.005060	0.011370	0.000875	0.000778	0.012010	-0.44
1.052	4.0	3.0	8.32	-0.30	0.013720	0.012290	0.014300	0.011560	0.001208	0.000172	0.012460	1.10
1.053	4.0	5.0	9.82	-0.97	0.030110	0.017260	0.038170	0.014570	0.001112	-0.001629	0.015710	1.92
1.053	4.0	7.0	11.20	-1.70	0.054230	0.022250	0.062700	0.015500	0.001690	-0.002874	0.019520	2.78
1.053	6.0	1.0	9.35	0.22	-0.005780	0.014020	-0.005470	0.014120	0.000907	-0.000014	0.014010	-0.41
1.052	6.0	3.0	10.88	-0.10	0.011760	0.014680	0.012410	0.014050	0.001504	-0.000549	0.014160	0.83
1.051	8.0	1.0	11.86	0.08	-0.003350	0.016200	-0.002830	0.016250	0.001242	-0.000535	0.015690	-0.21
1.059	8.0	3.0	13.37	-0.46	0.015490	0.017660	0.016170	0.016840	0.002615	-0.000930	0.016780	0.92
1.049	10.0	1.0	14.34	-0.08	0.001230	0.018920	0.000630	0.018910	0.001193	-0.001120	0.017860	0.07

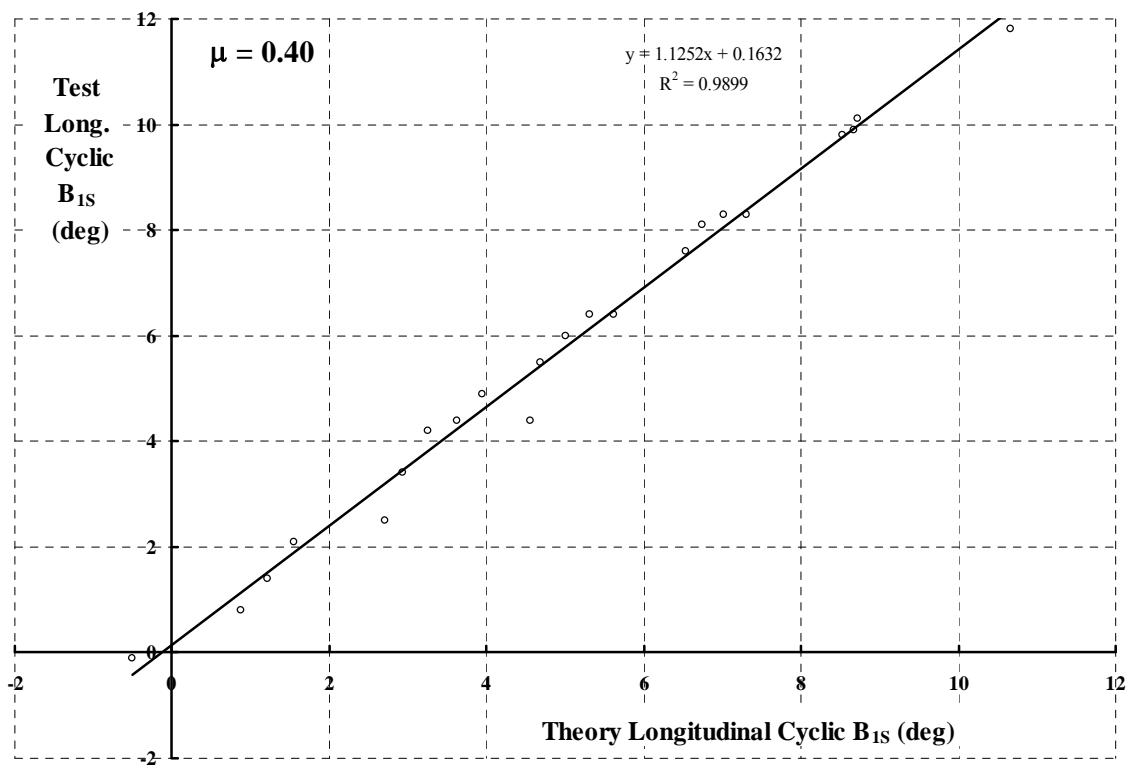
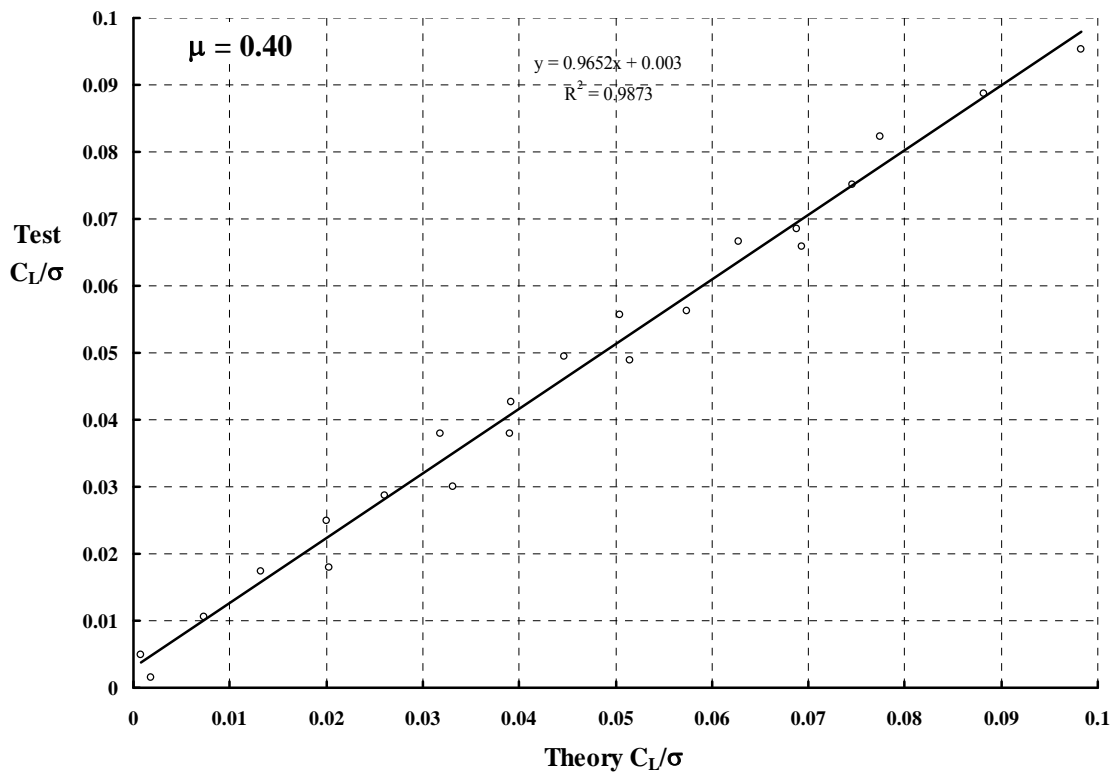


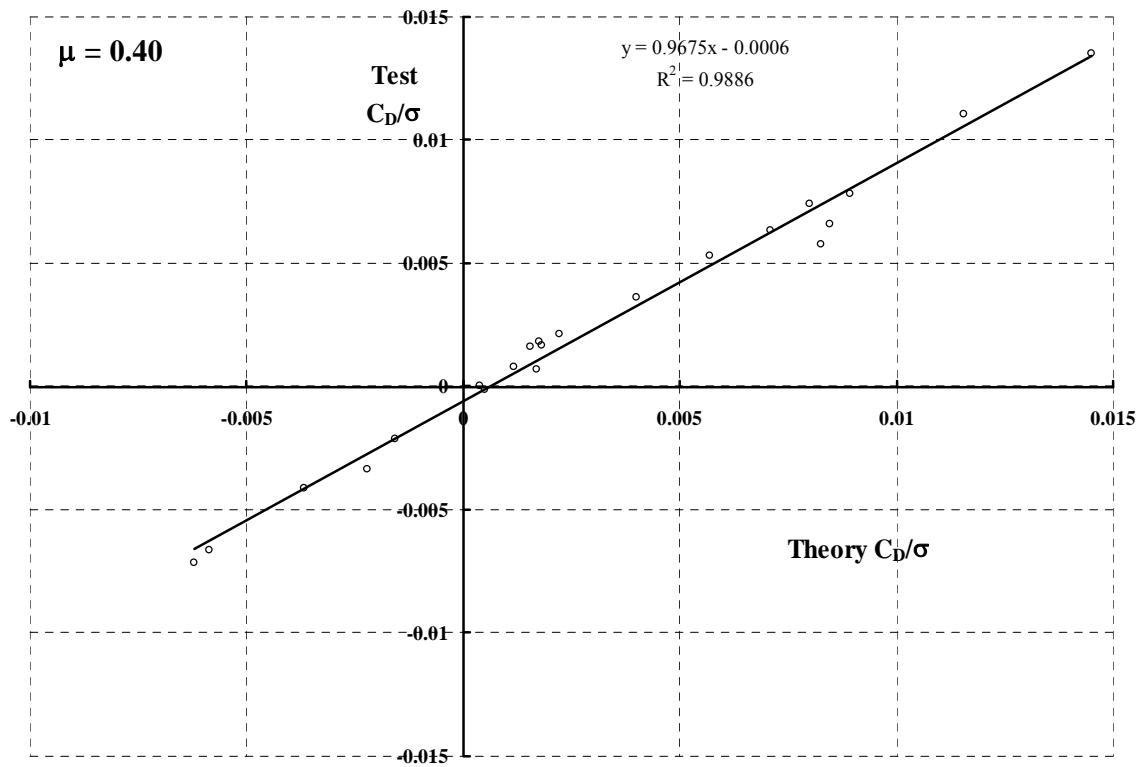
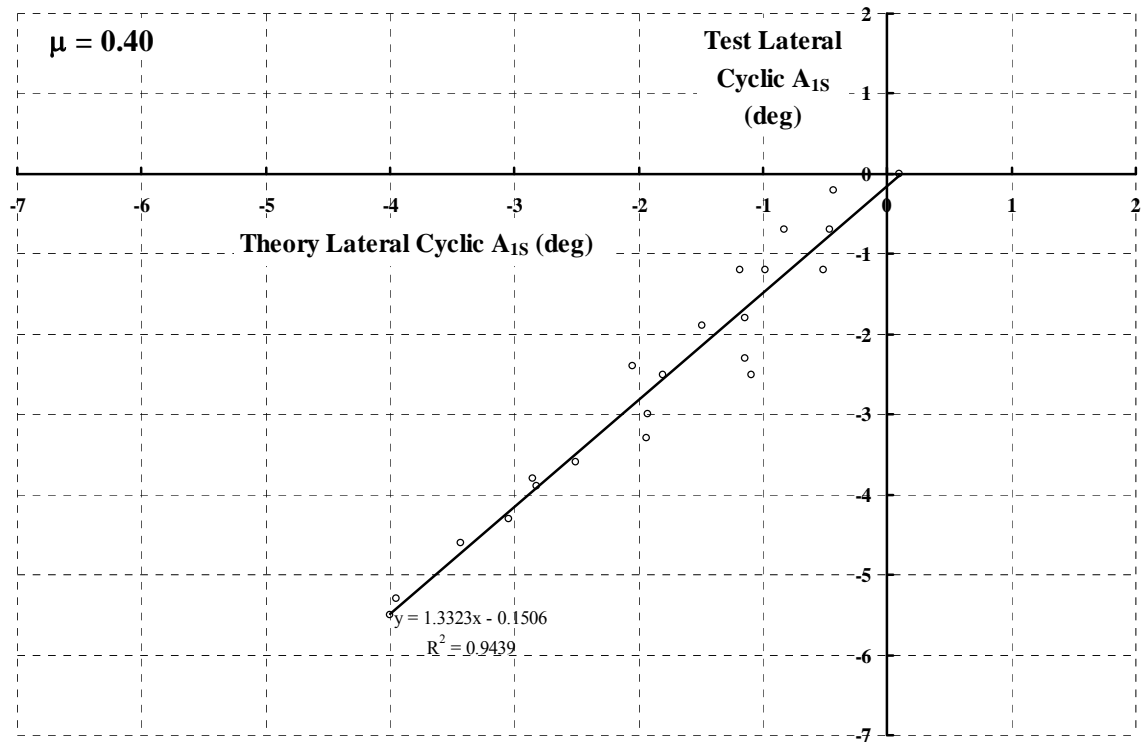


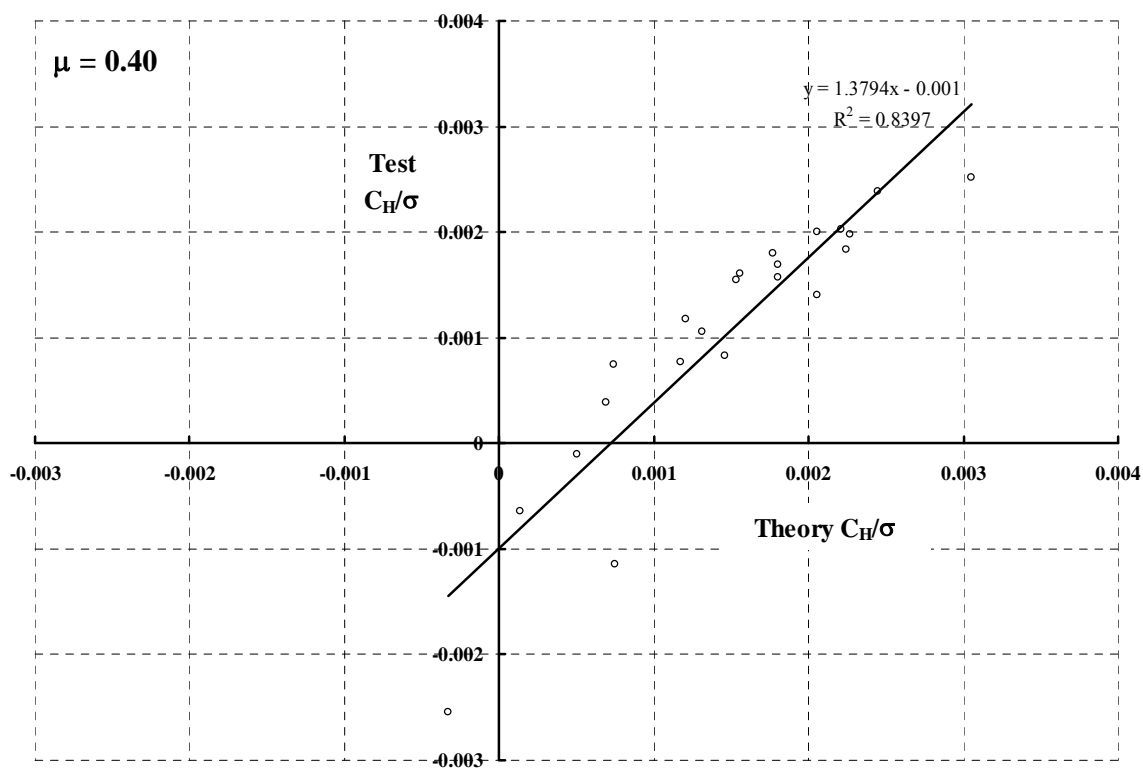
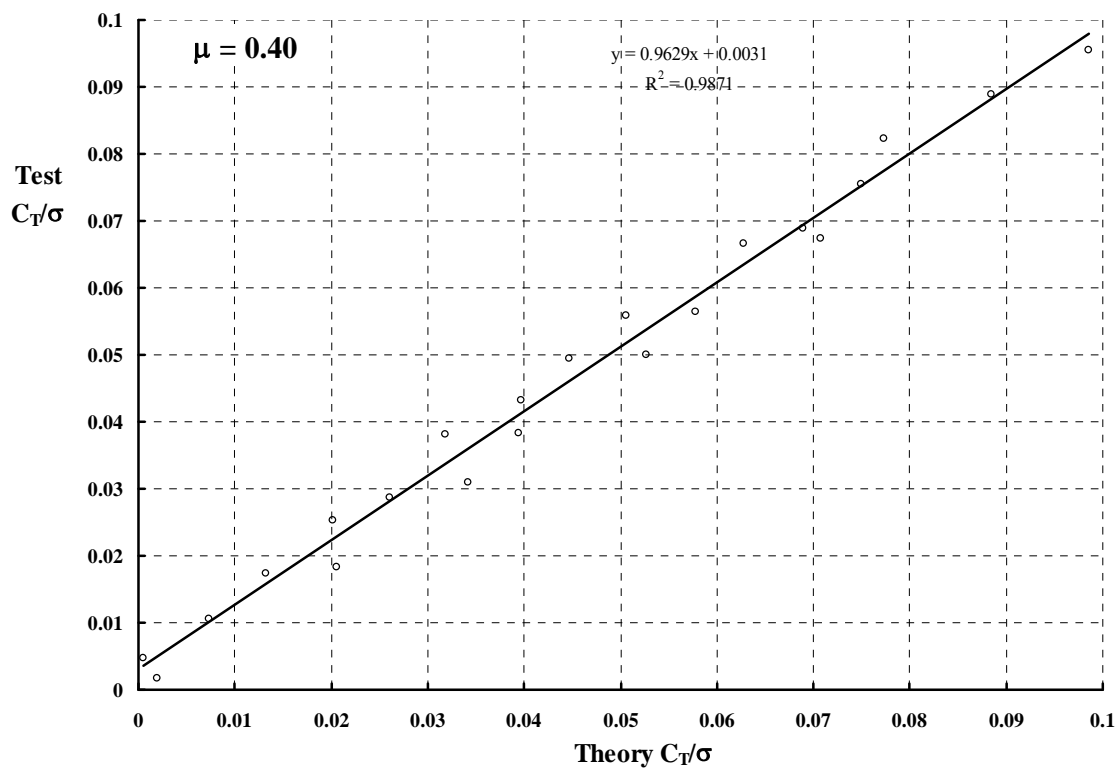


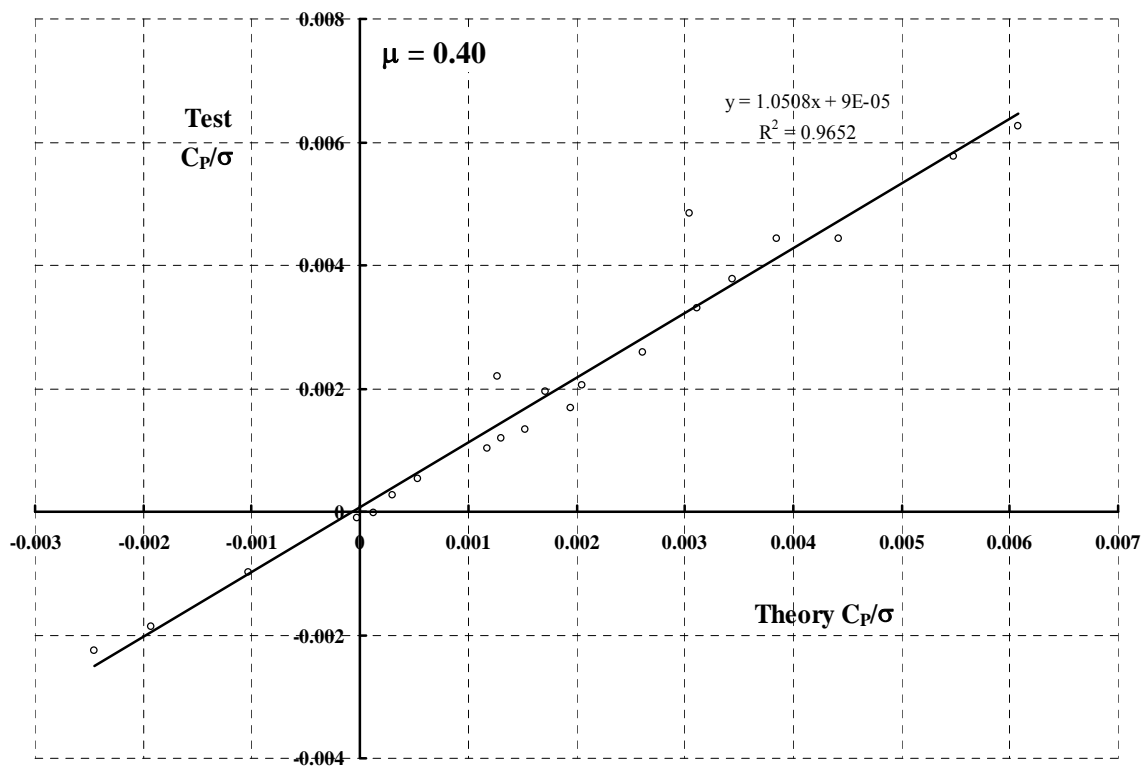
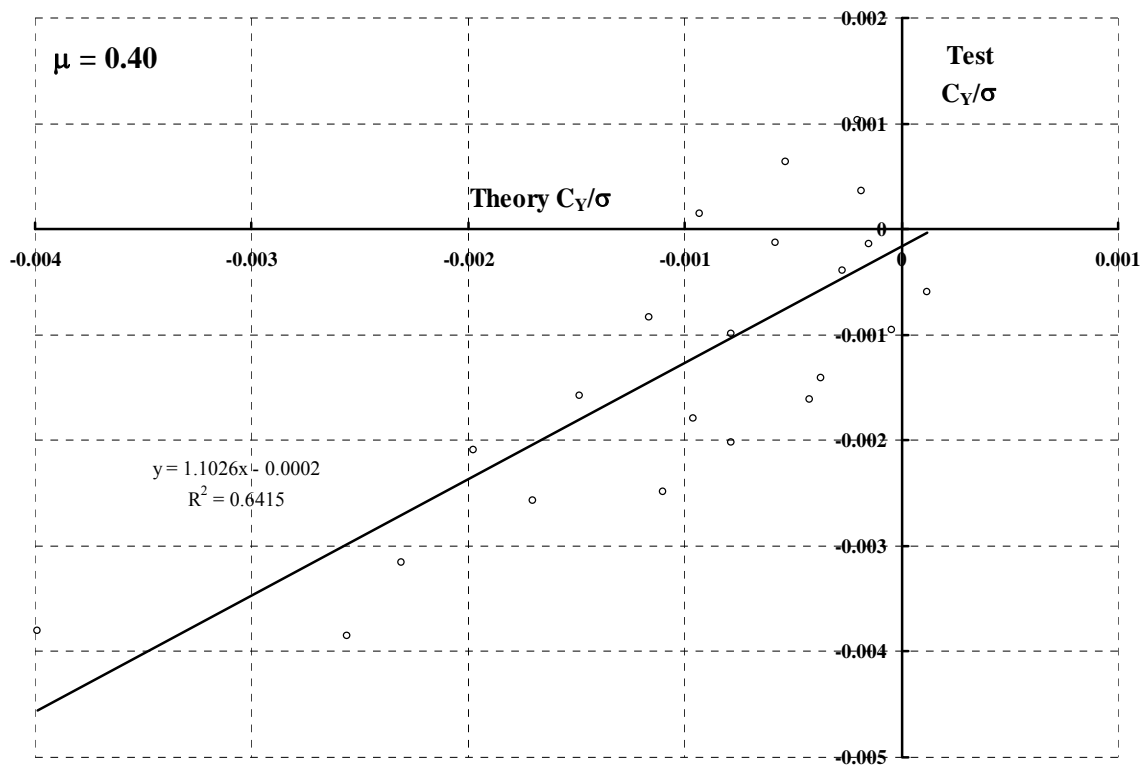


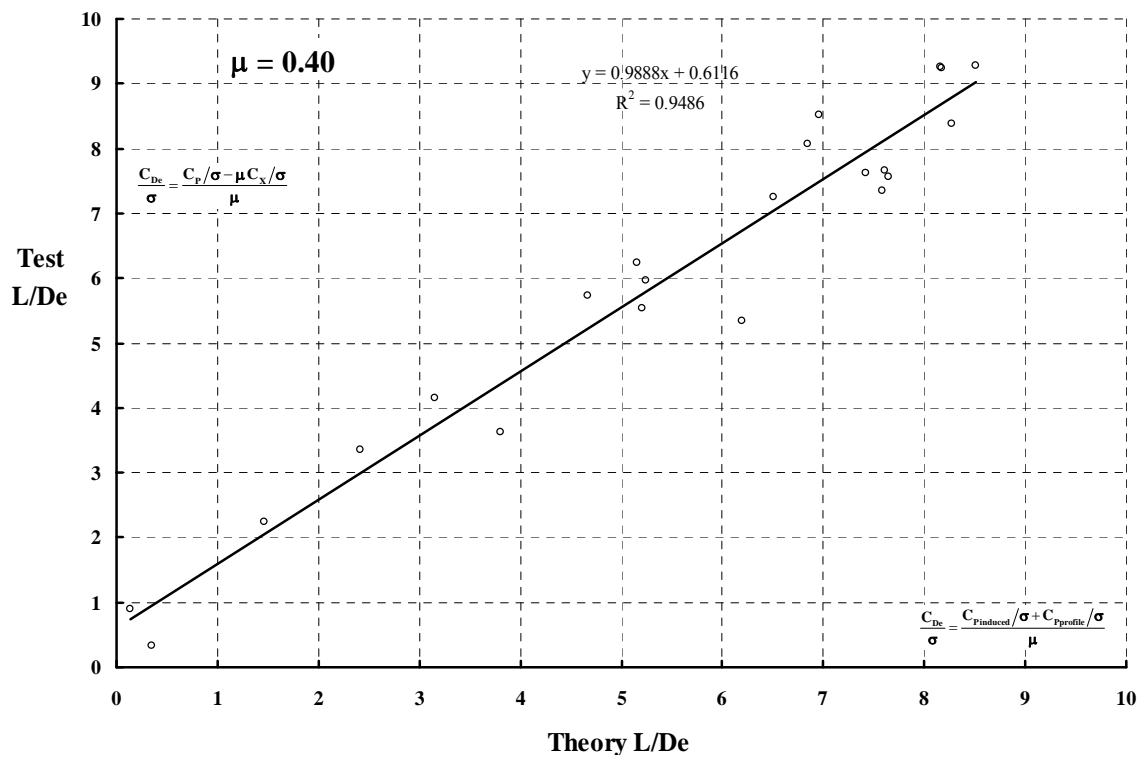
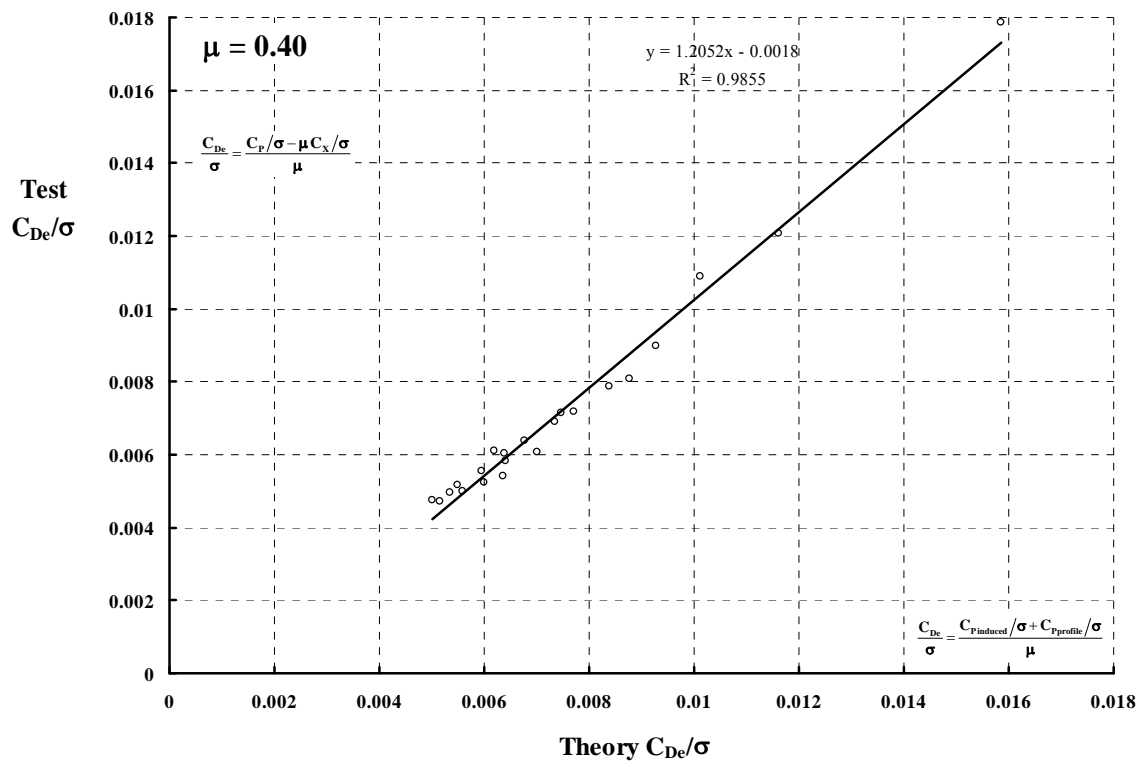


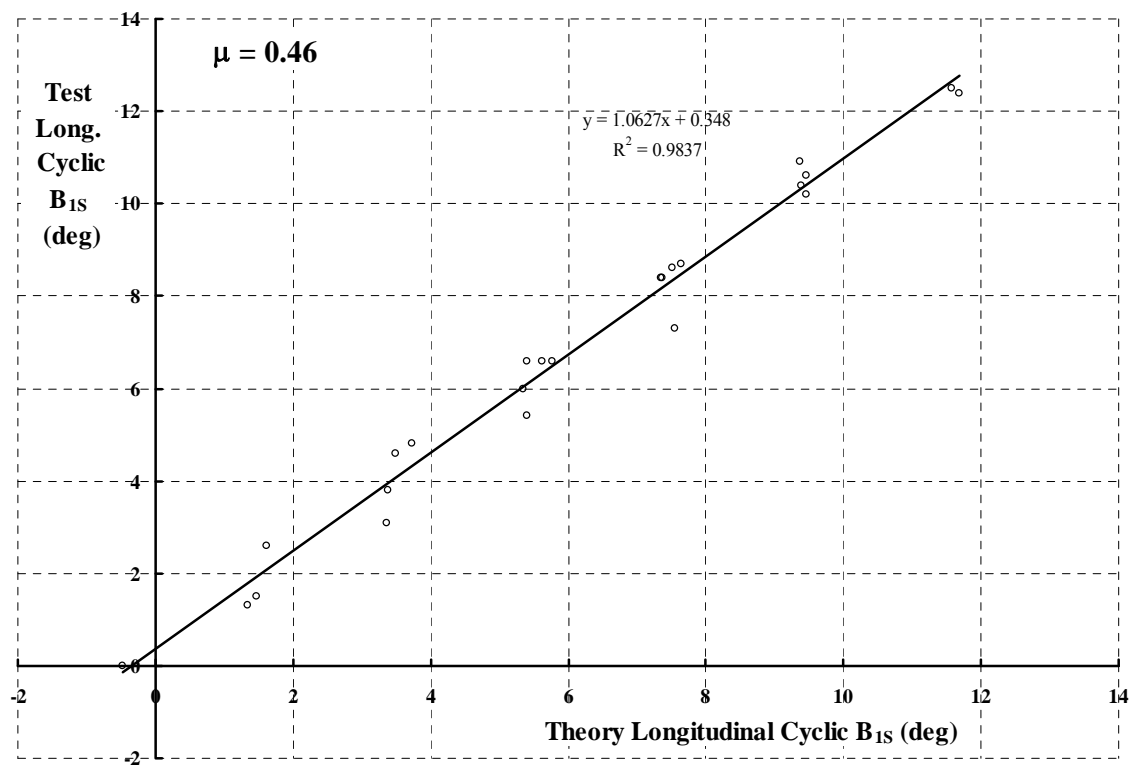
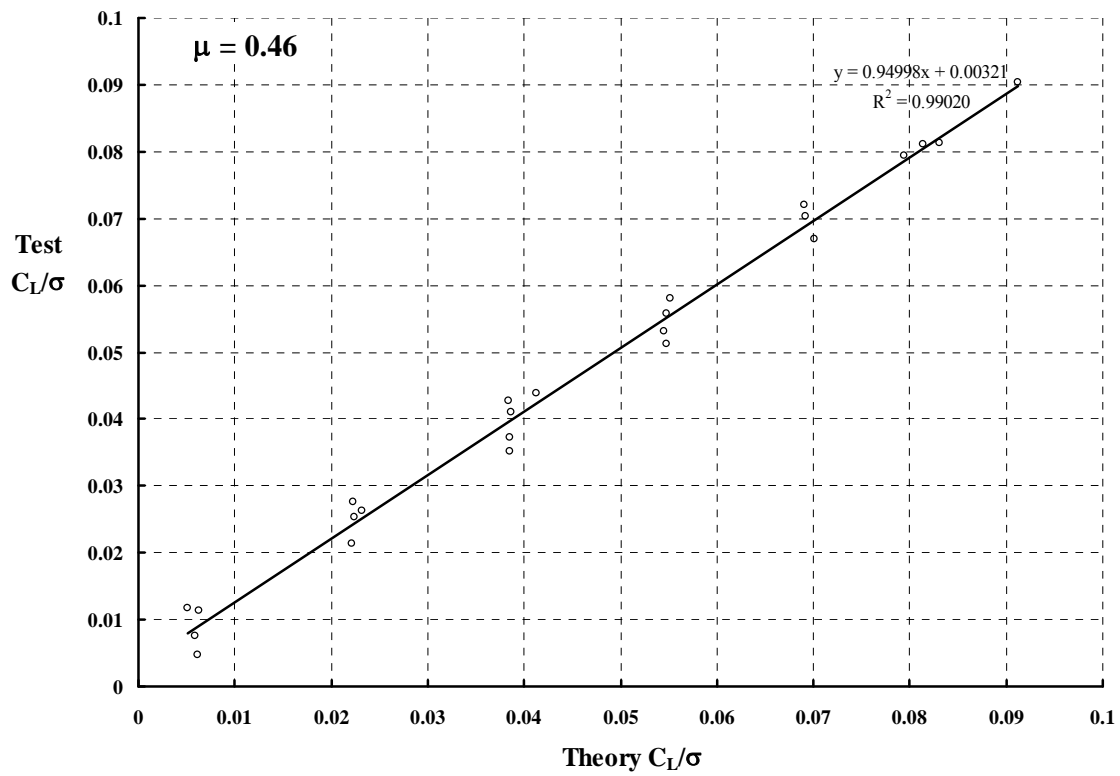


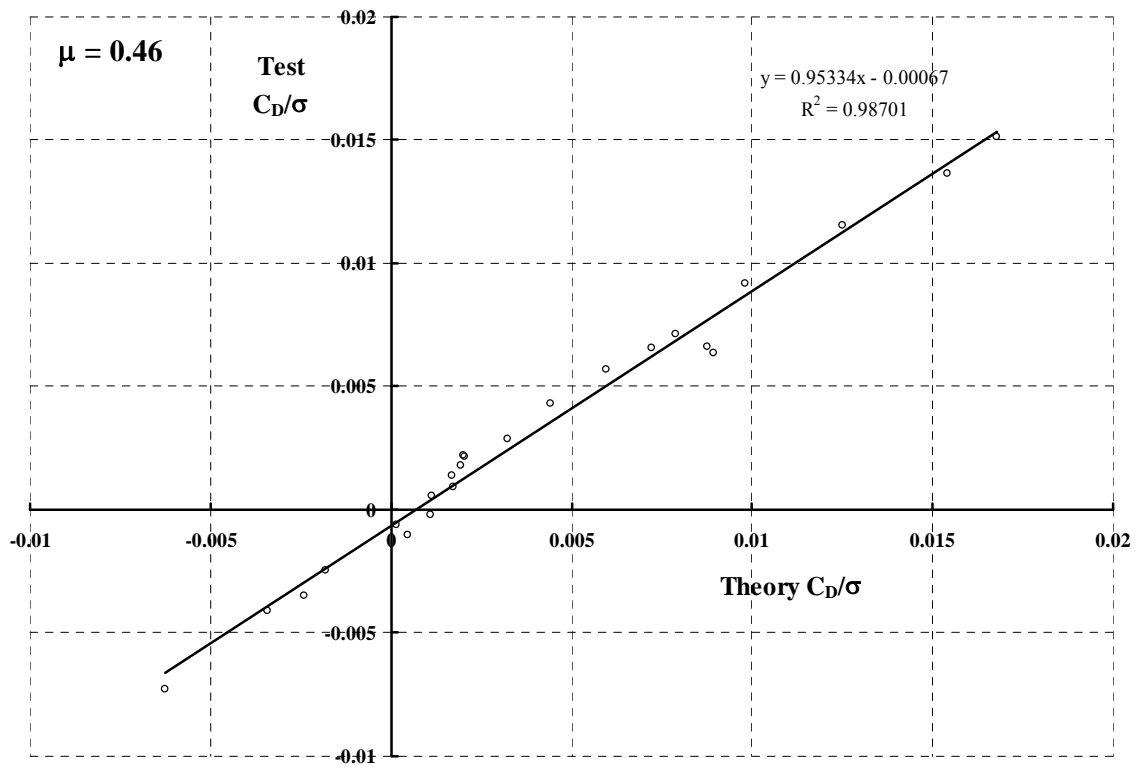
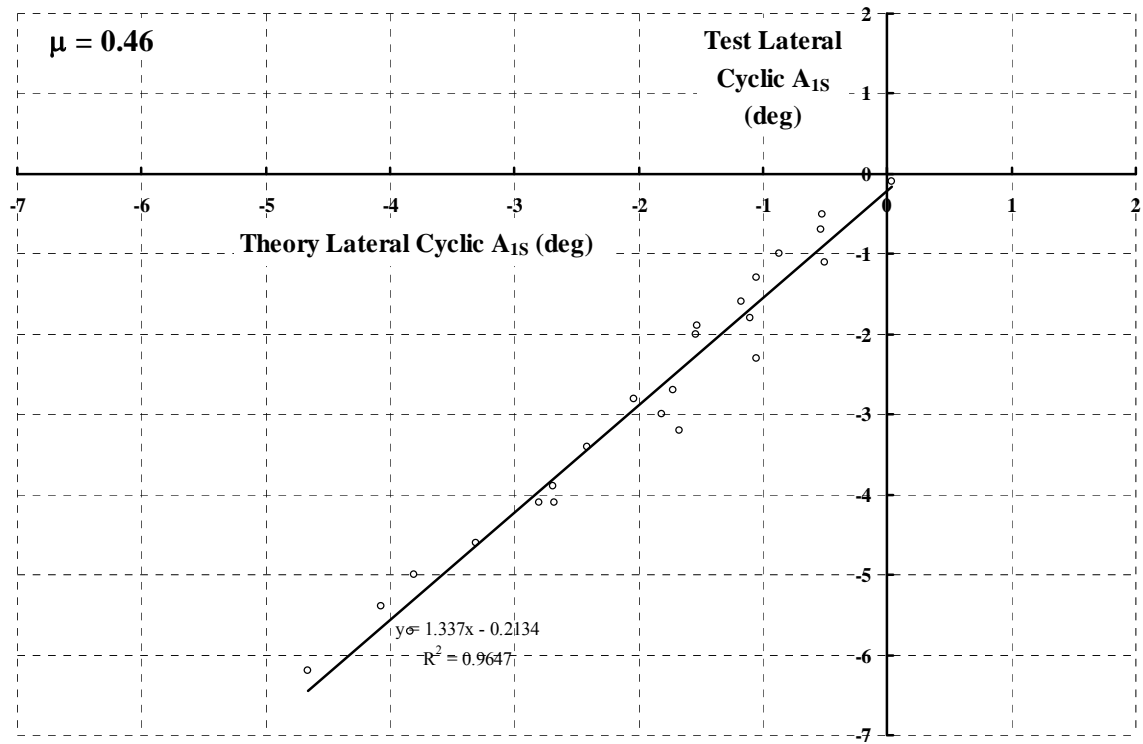


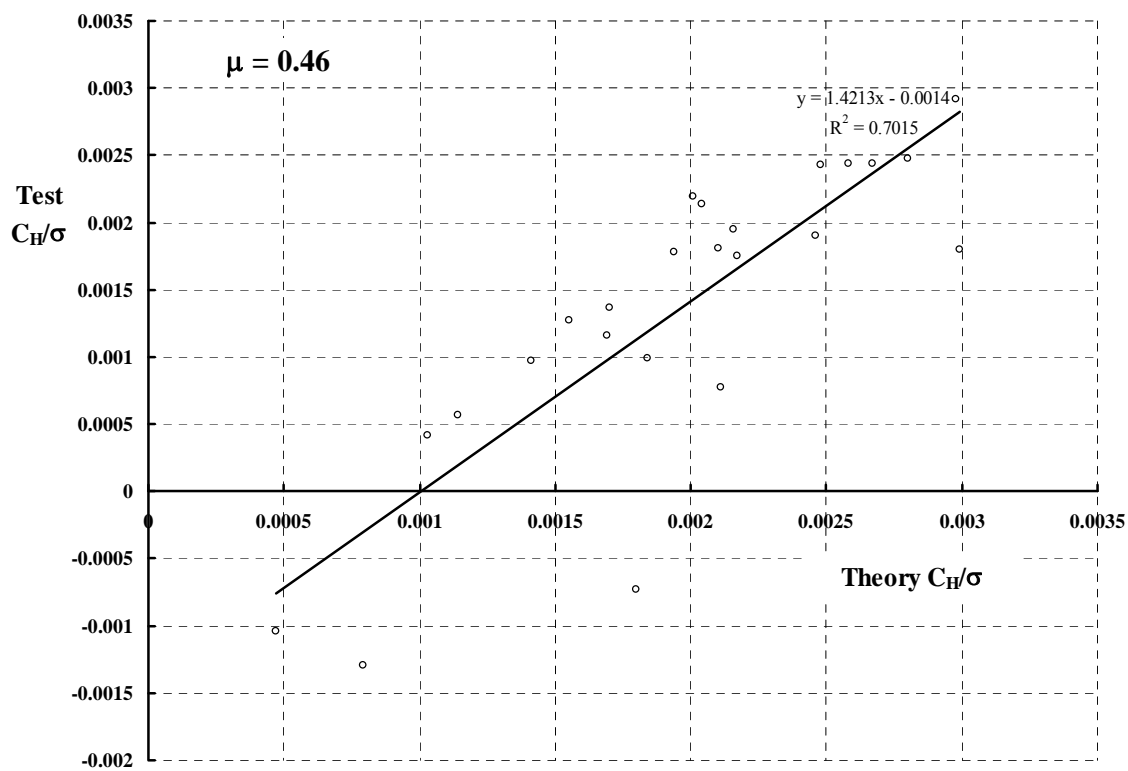
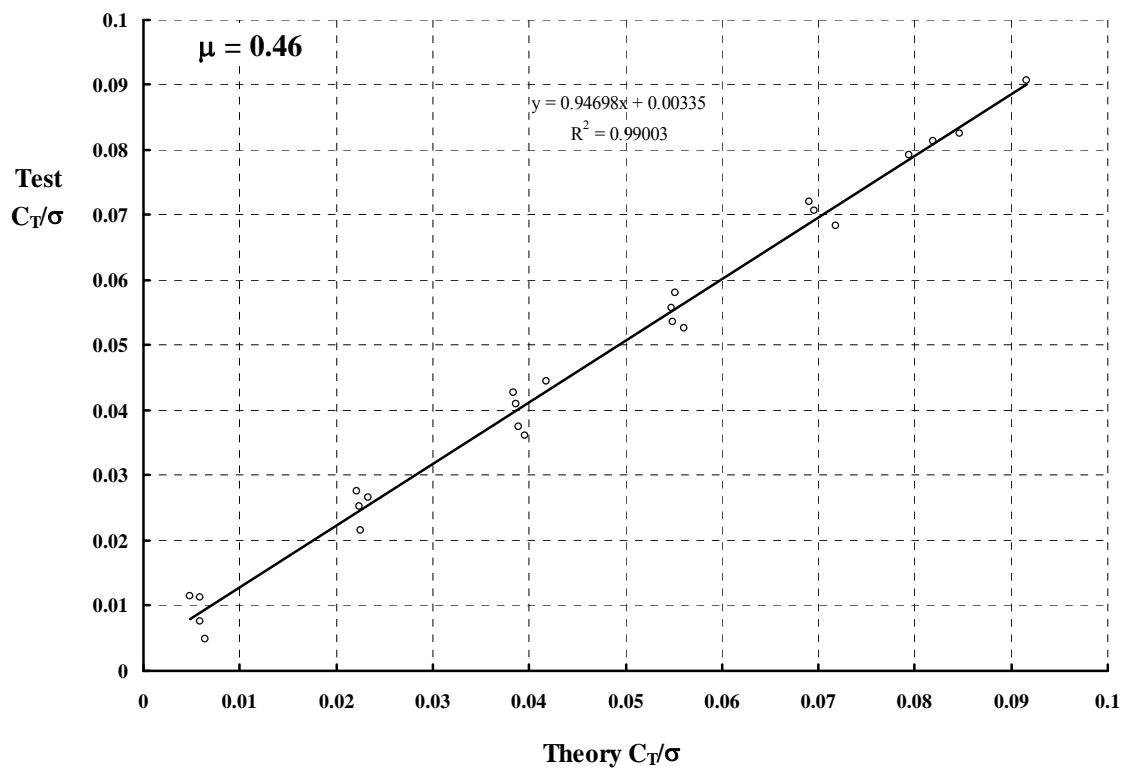


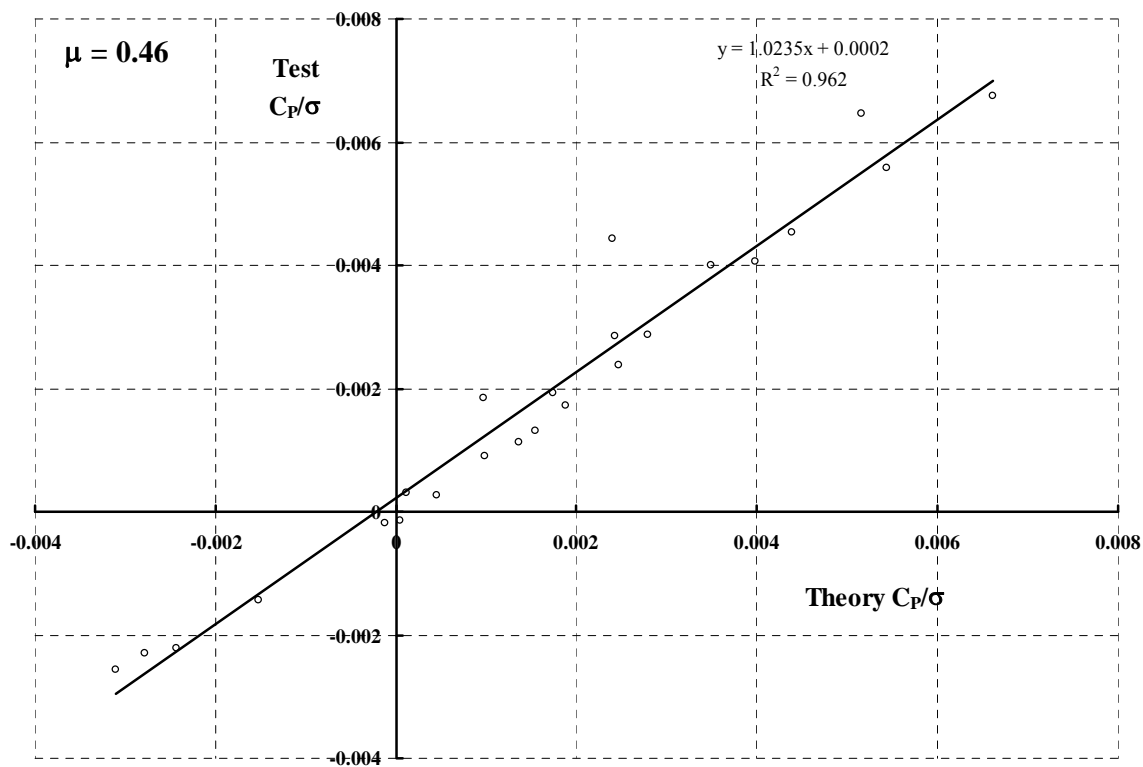
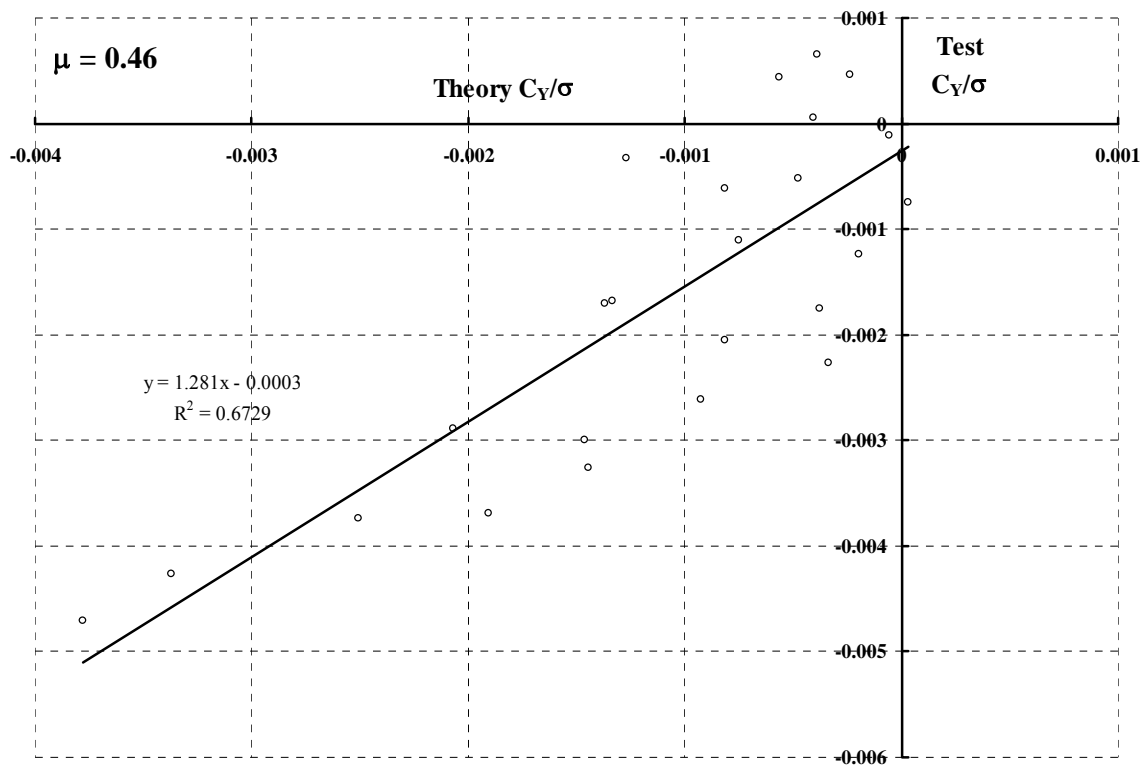


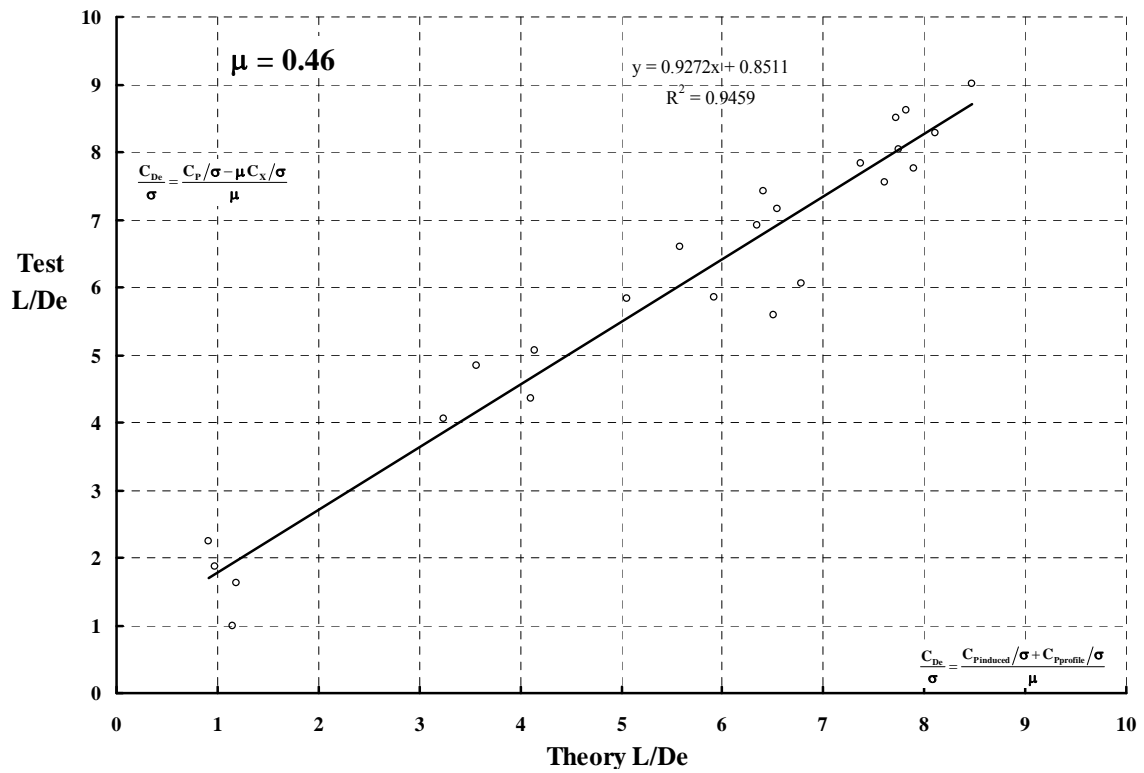
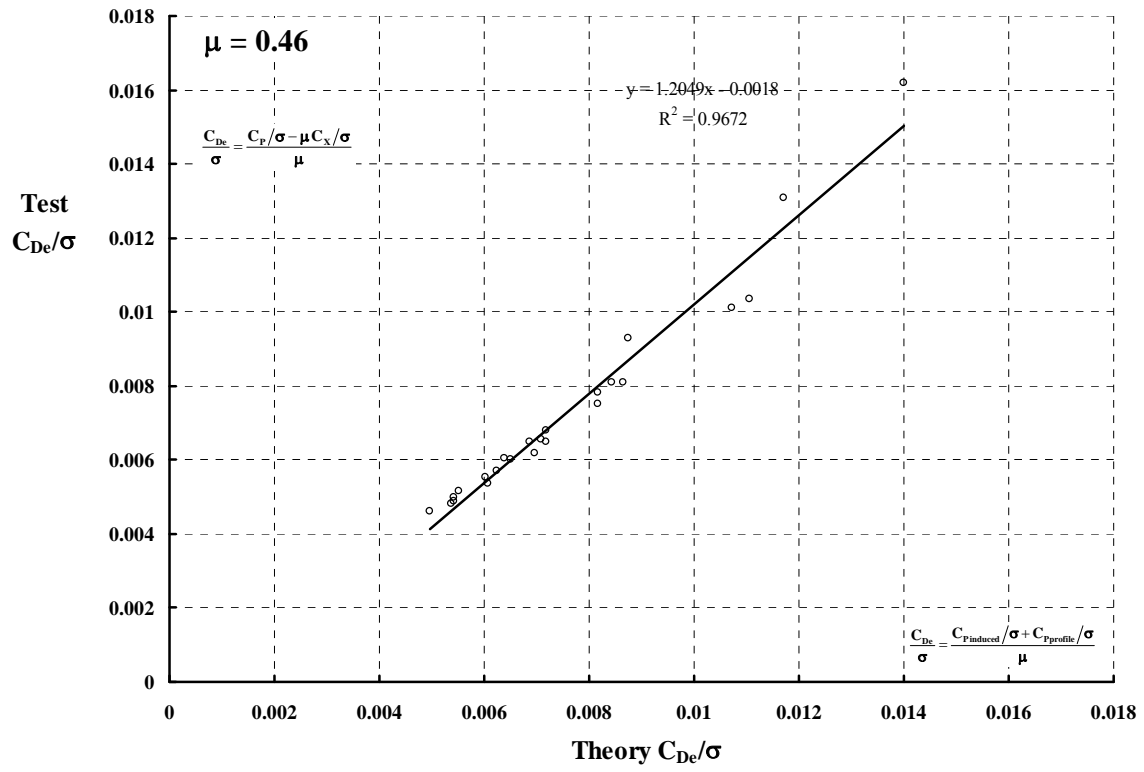


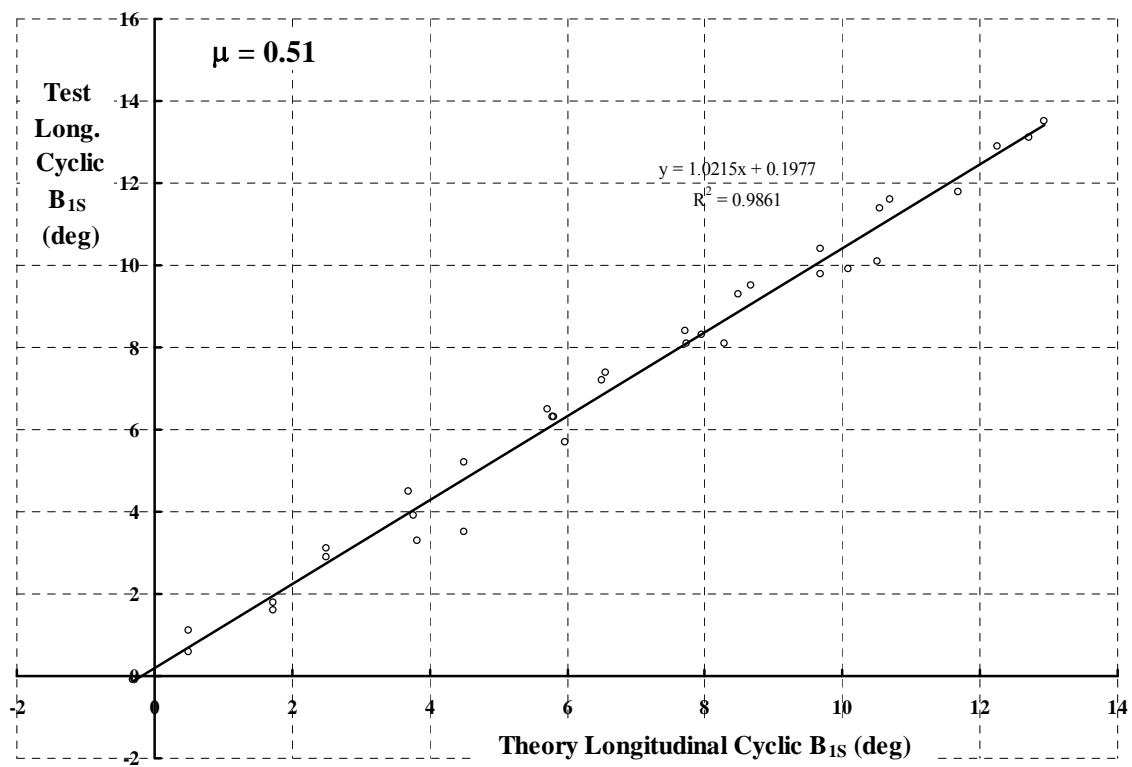
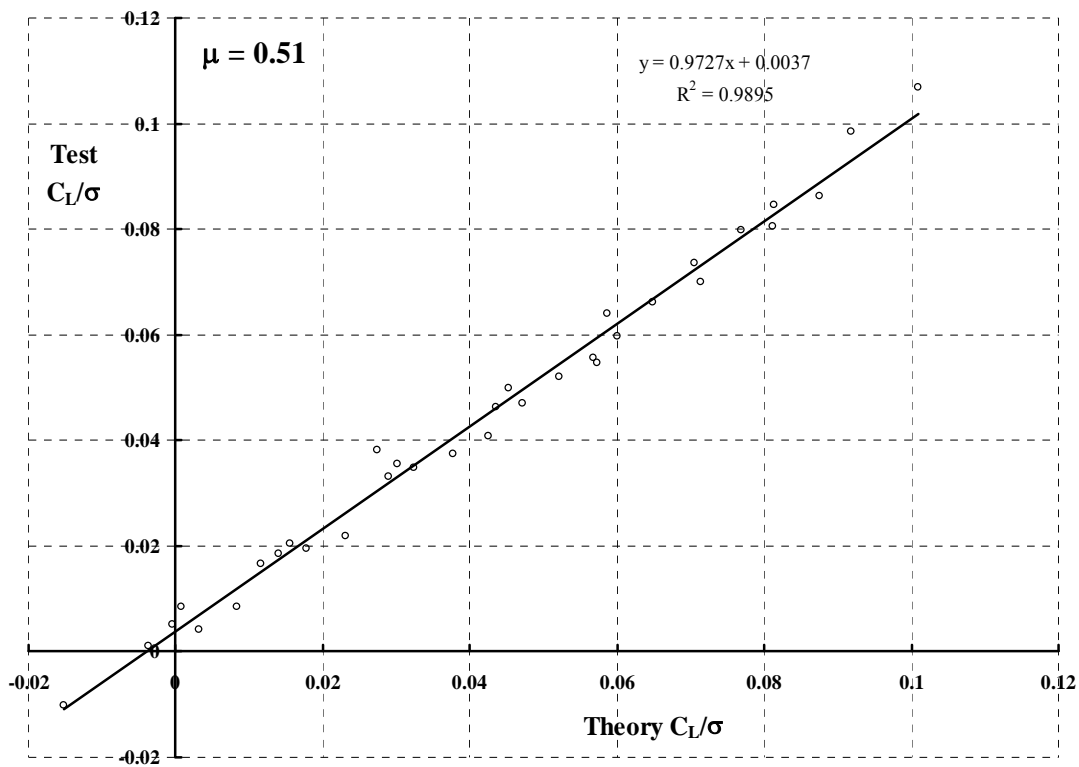


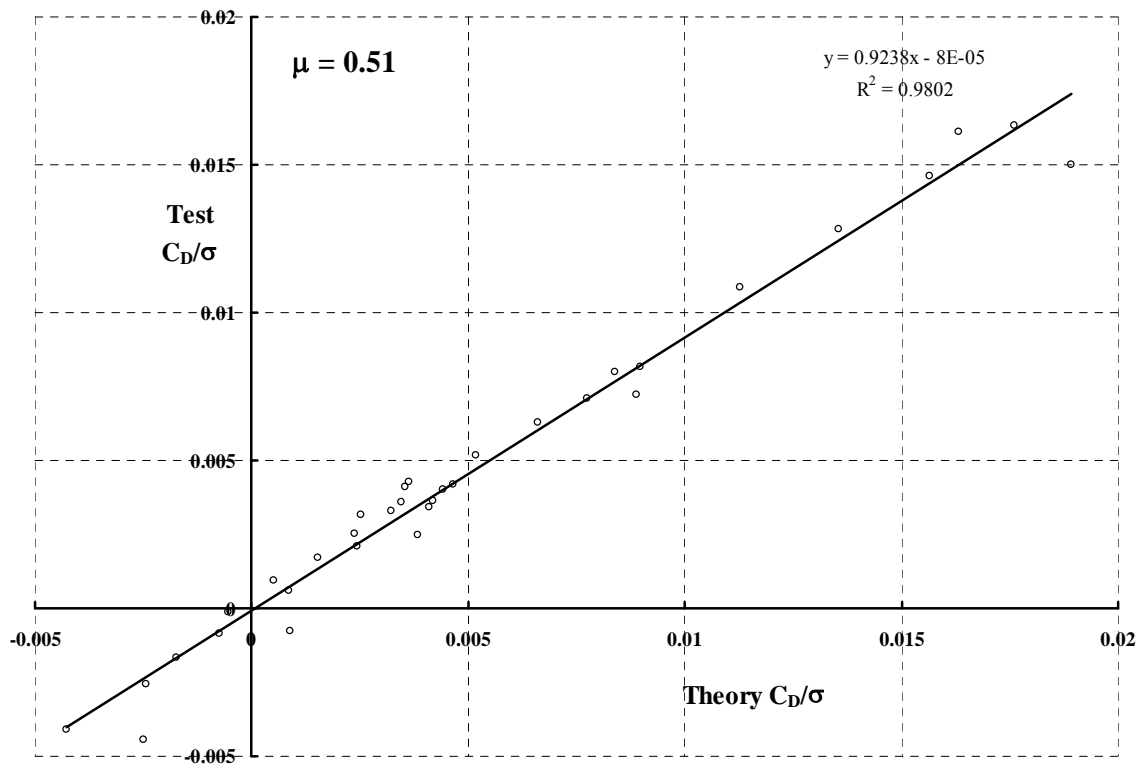
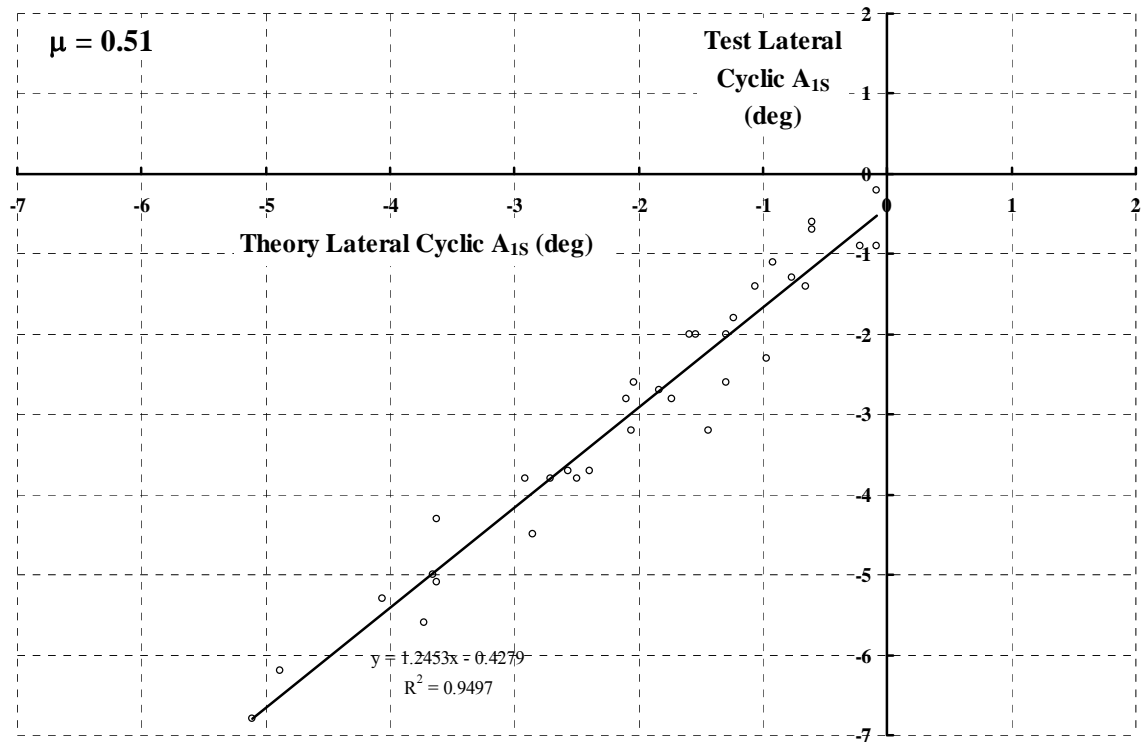


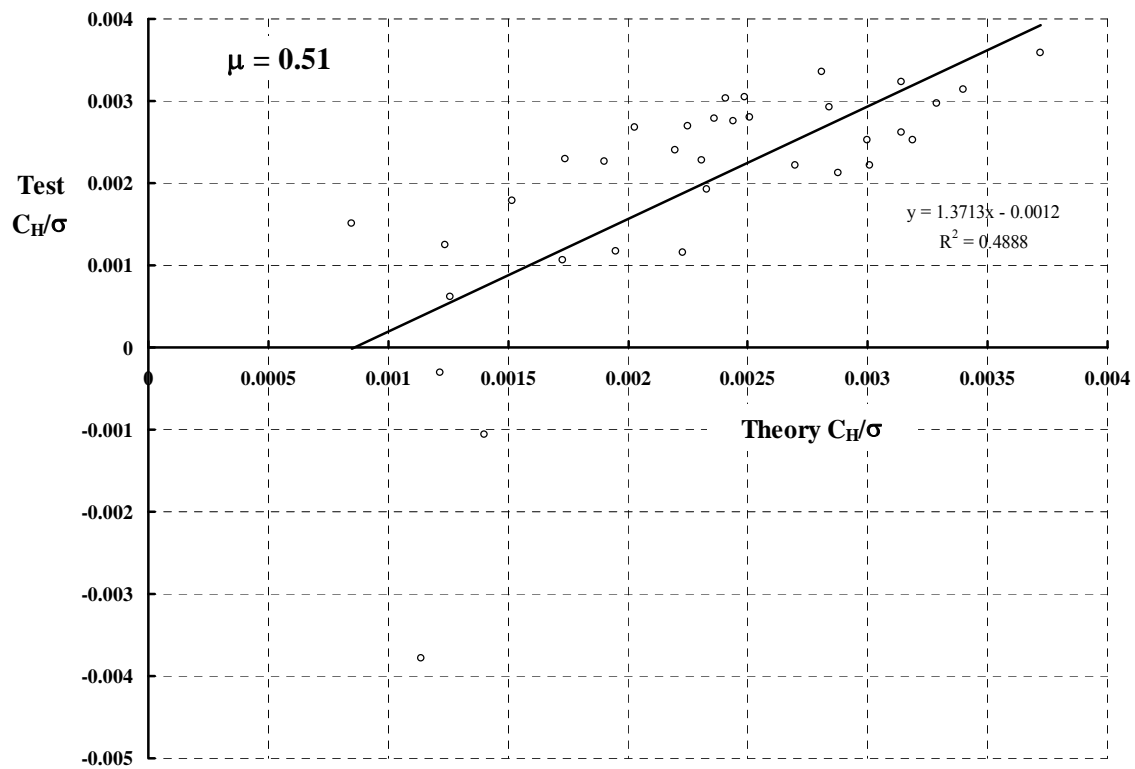
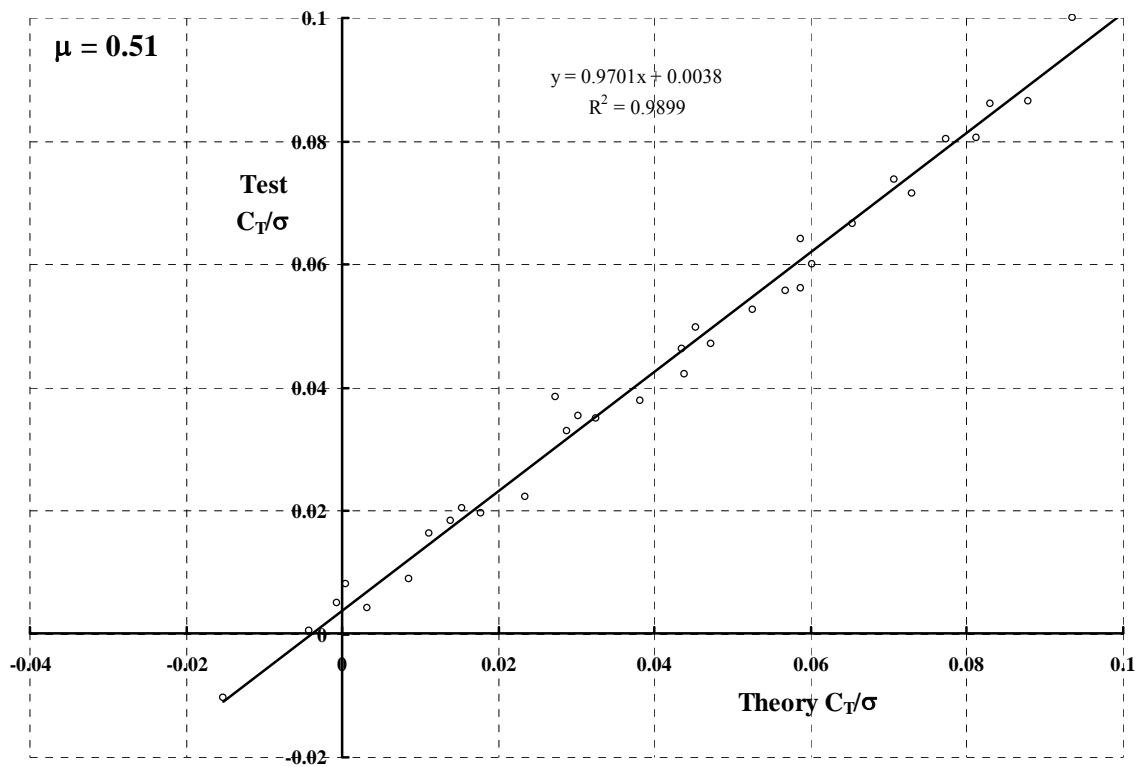


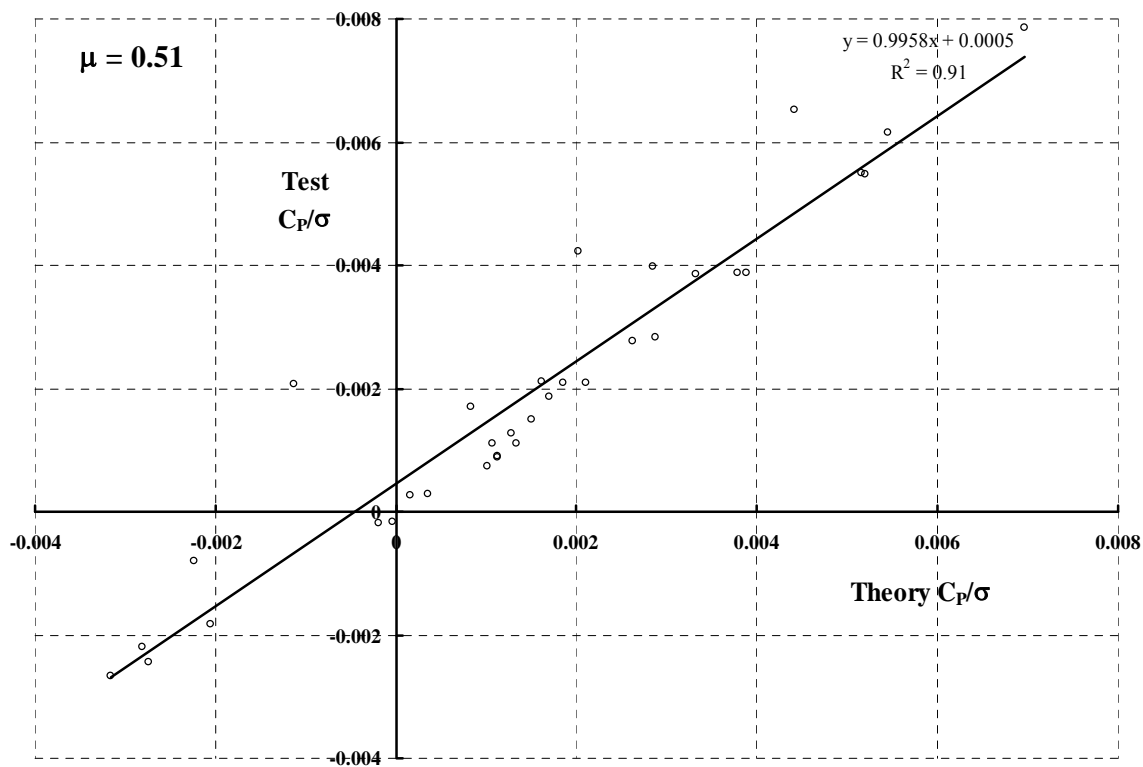
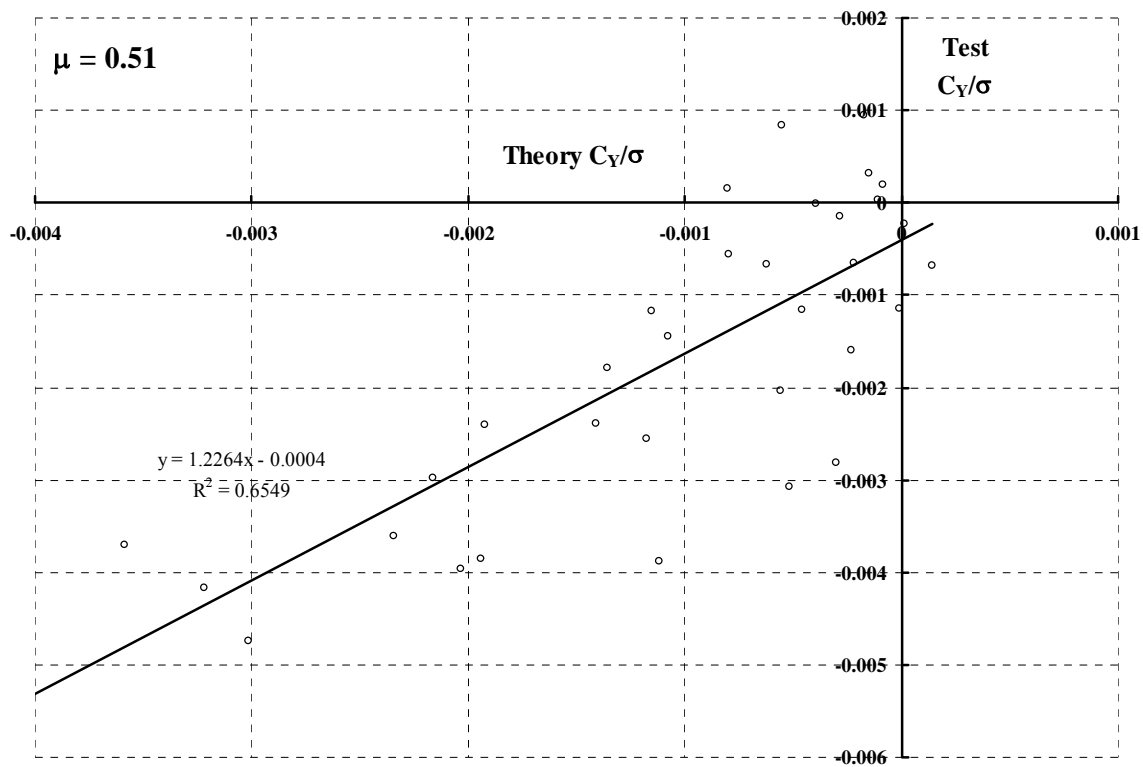


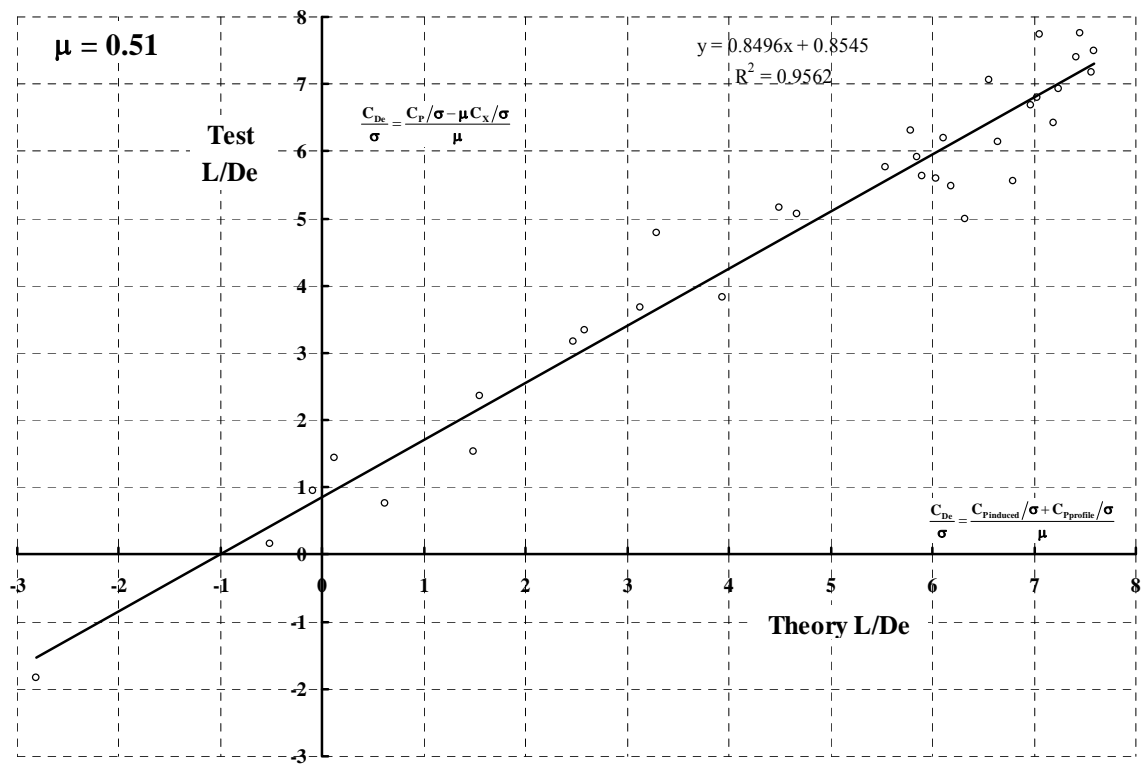
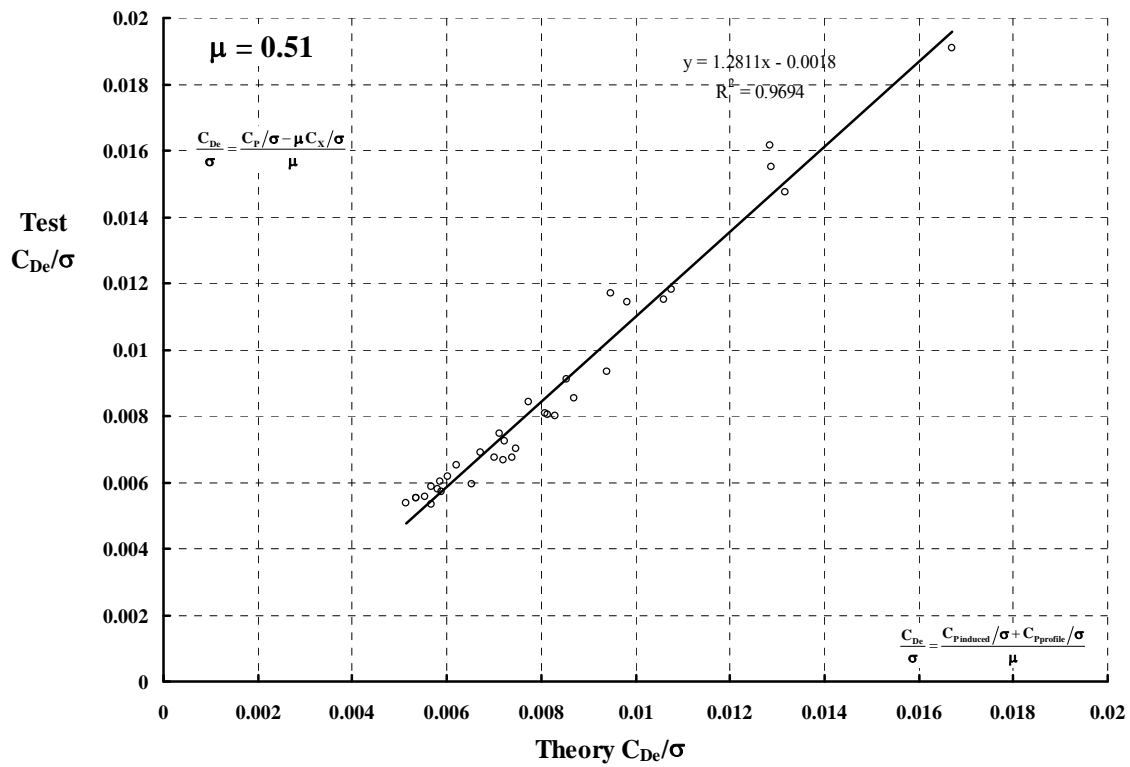


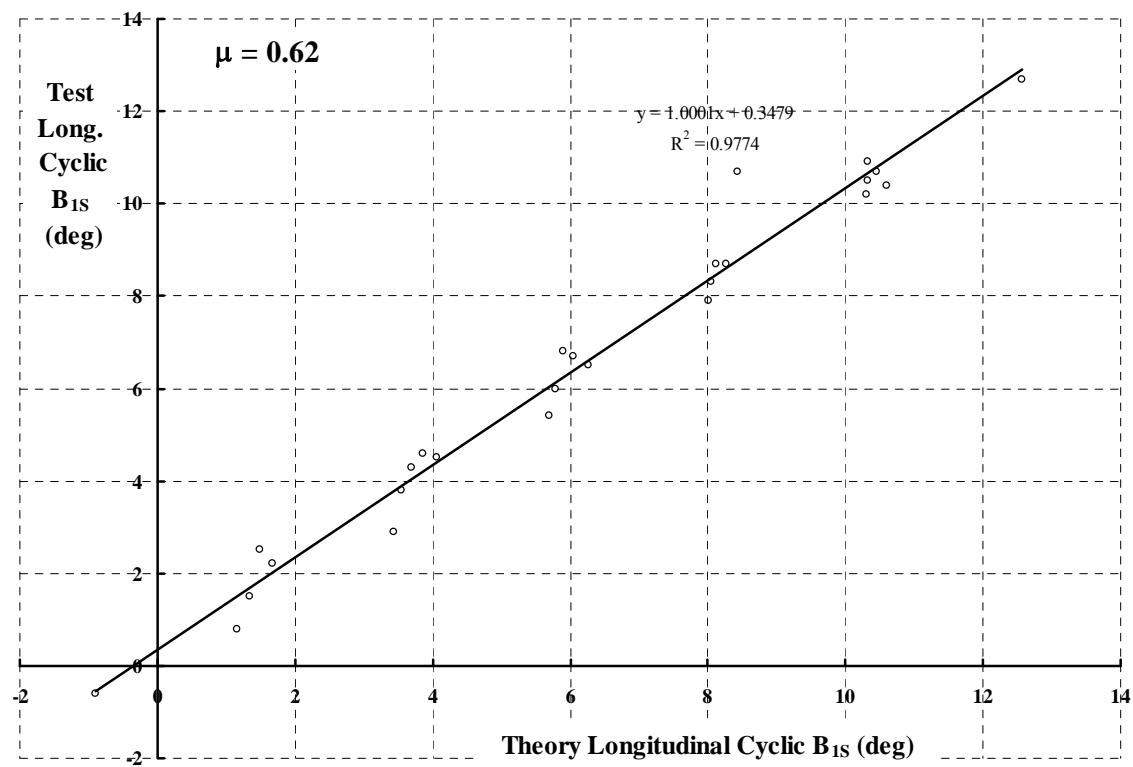
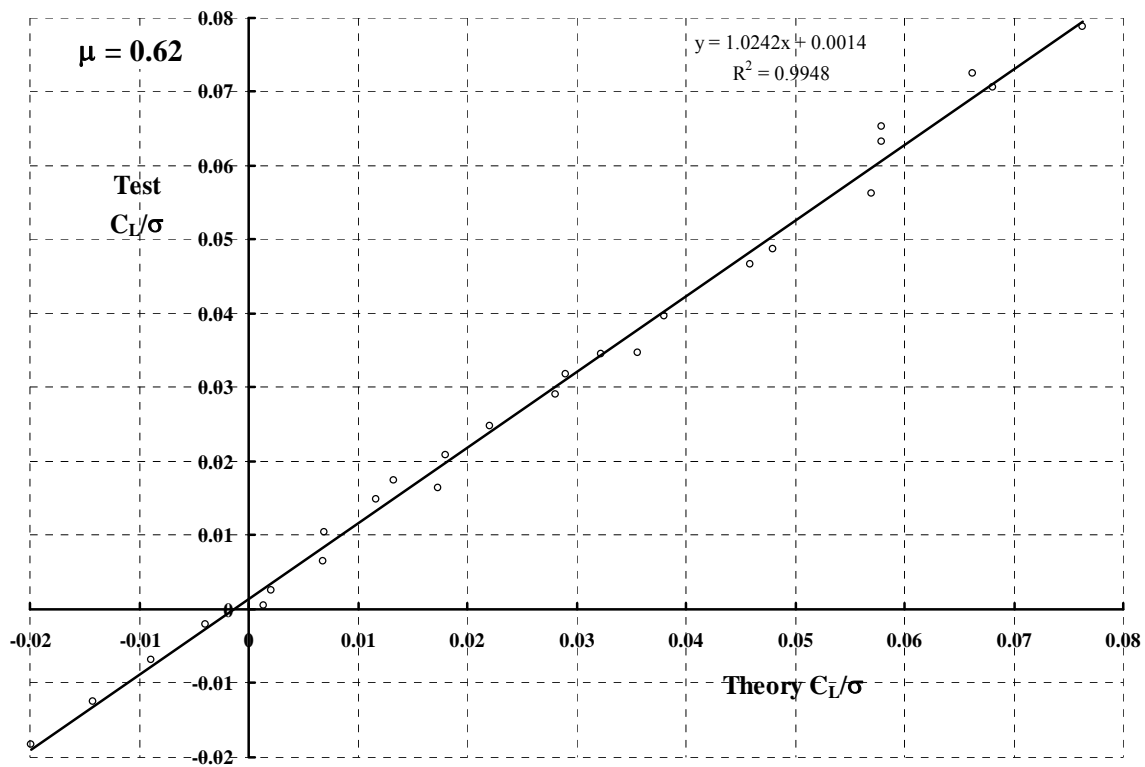


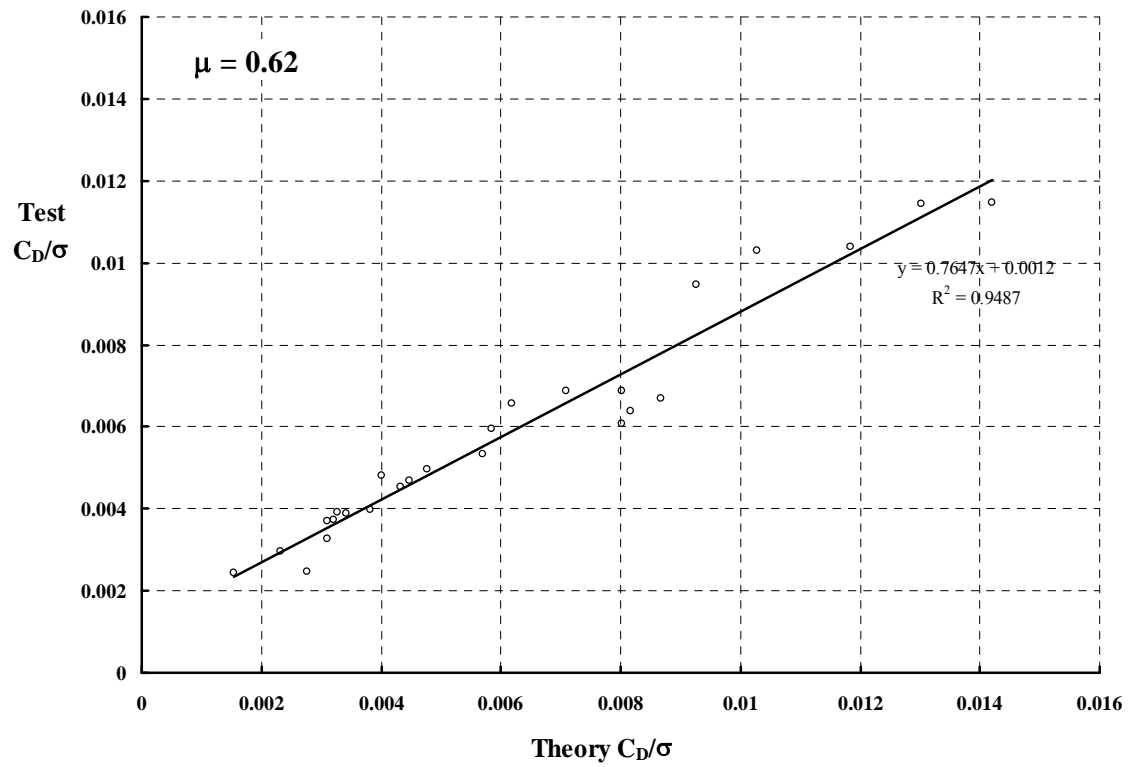
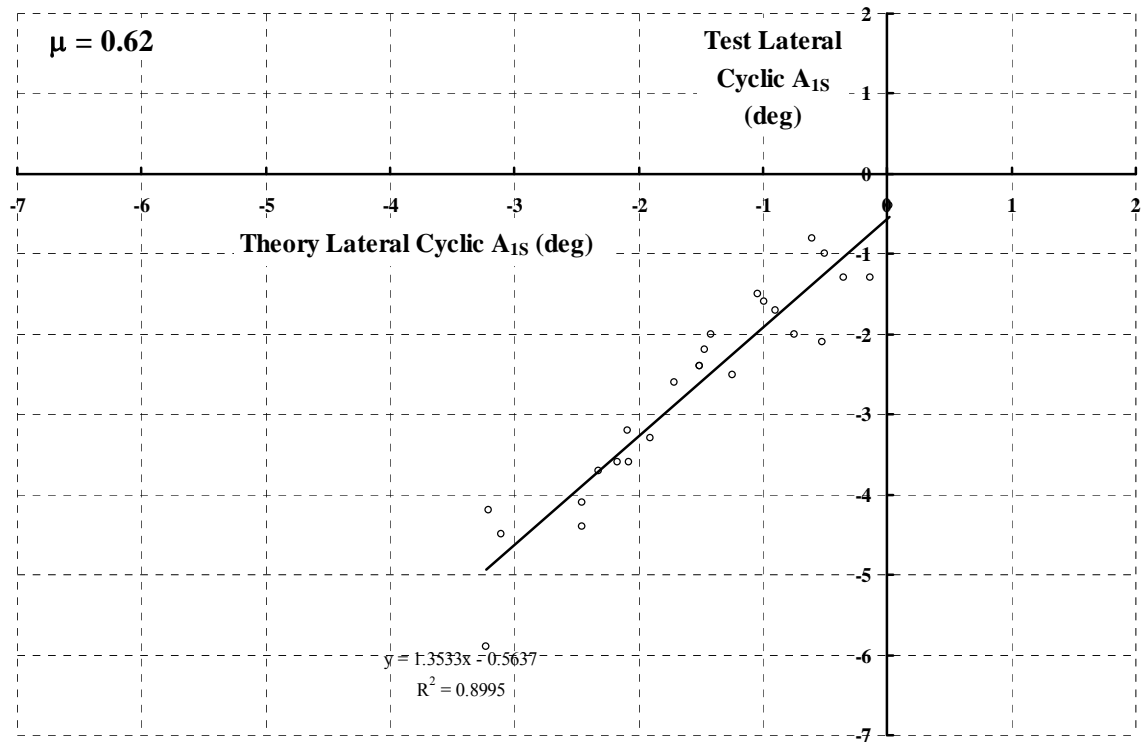


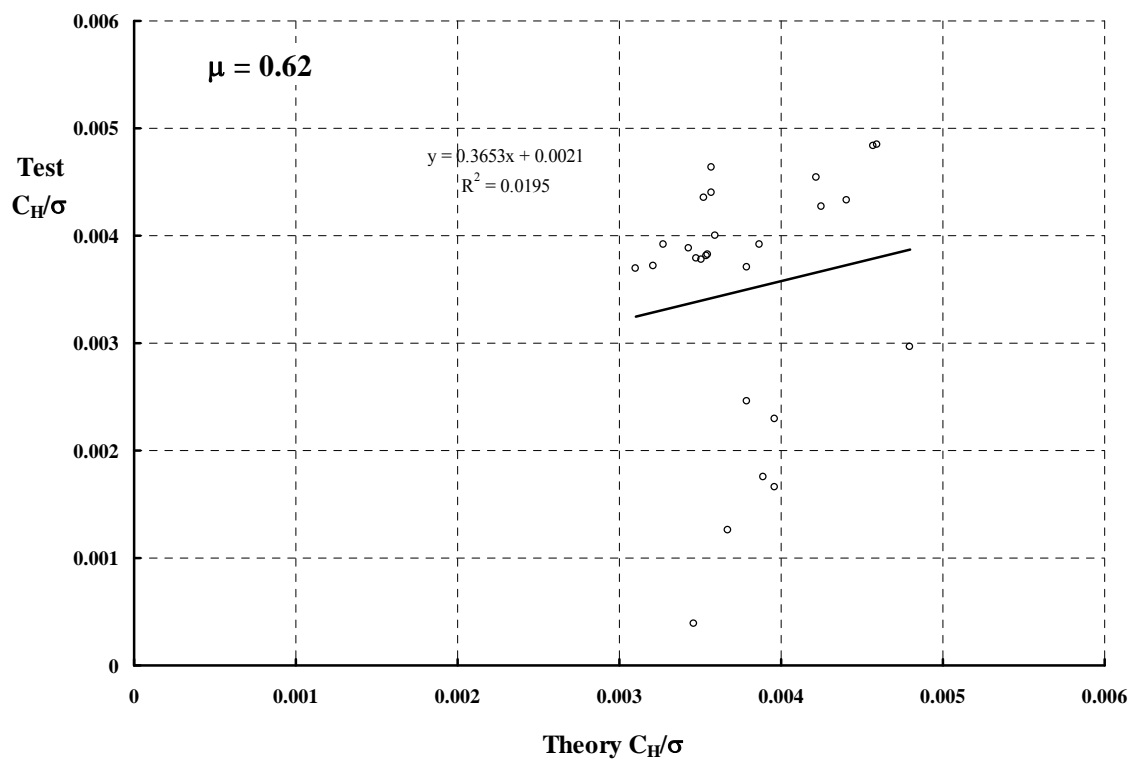
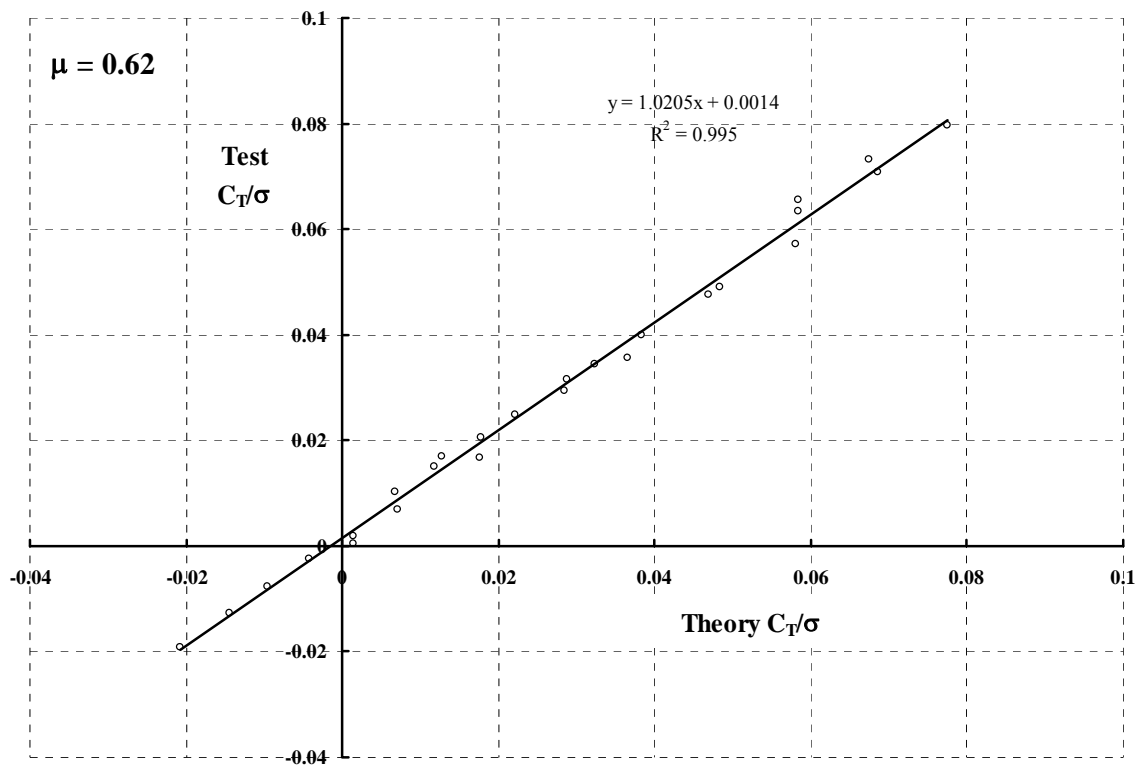


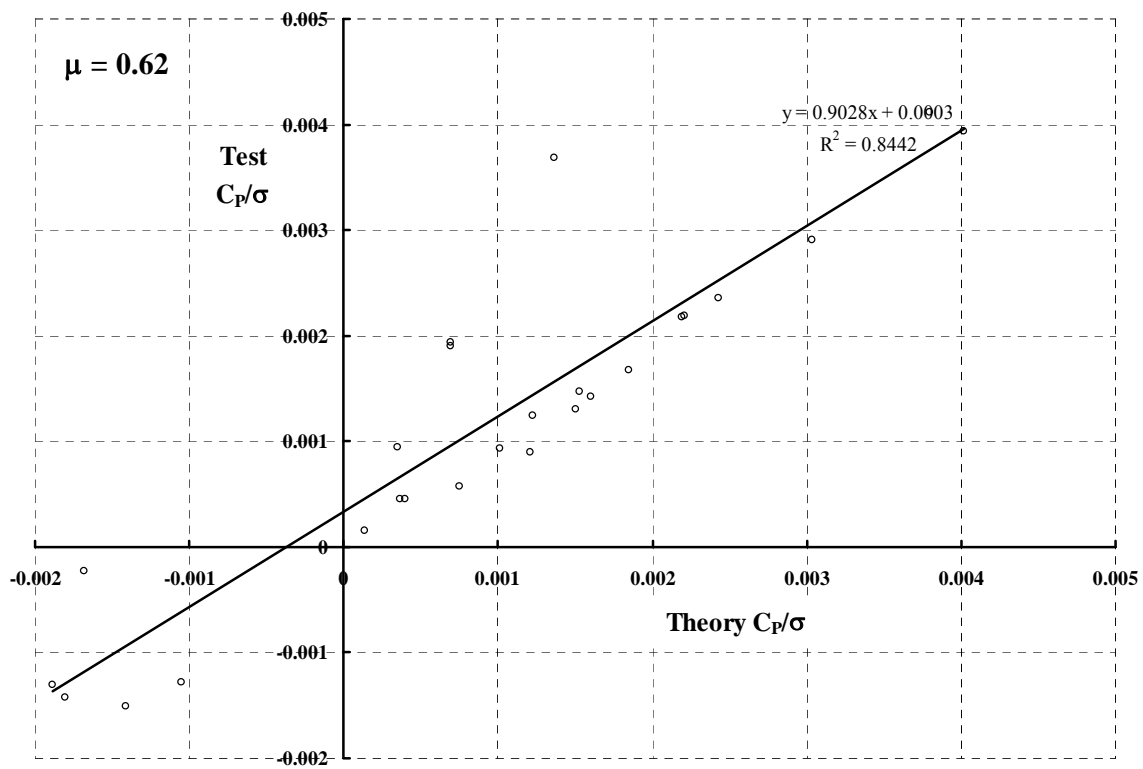
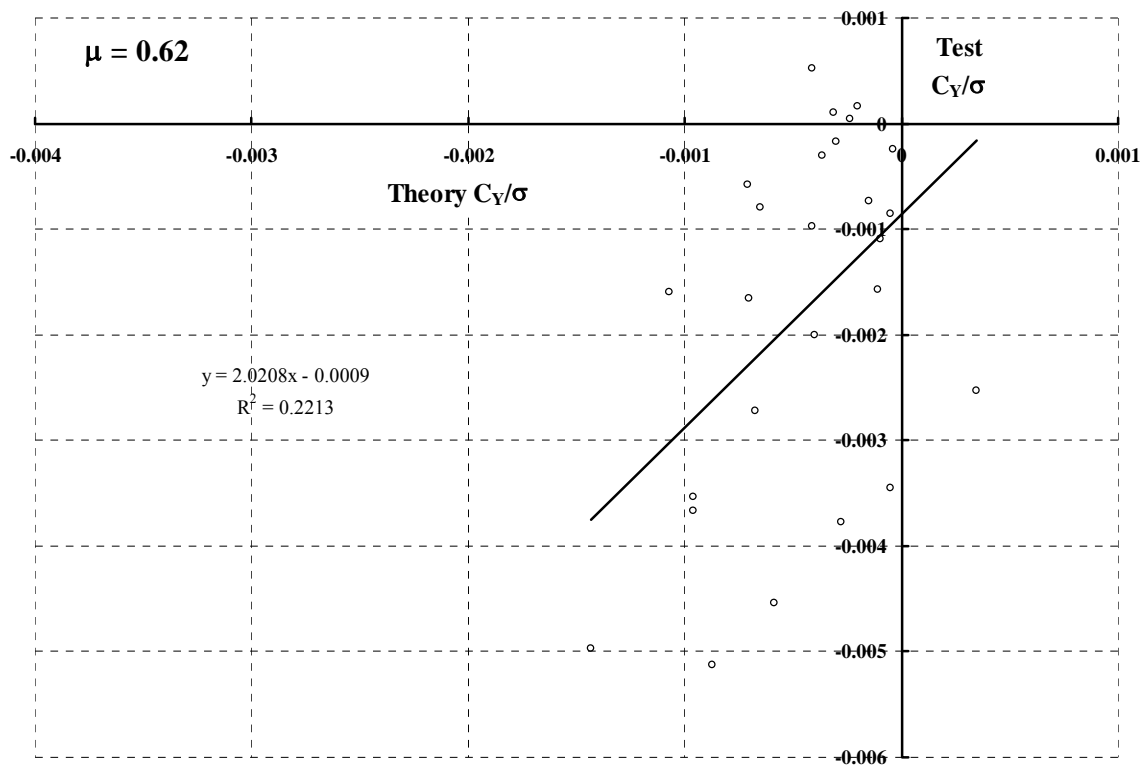


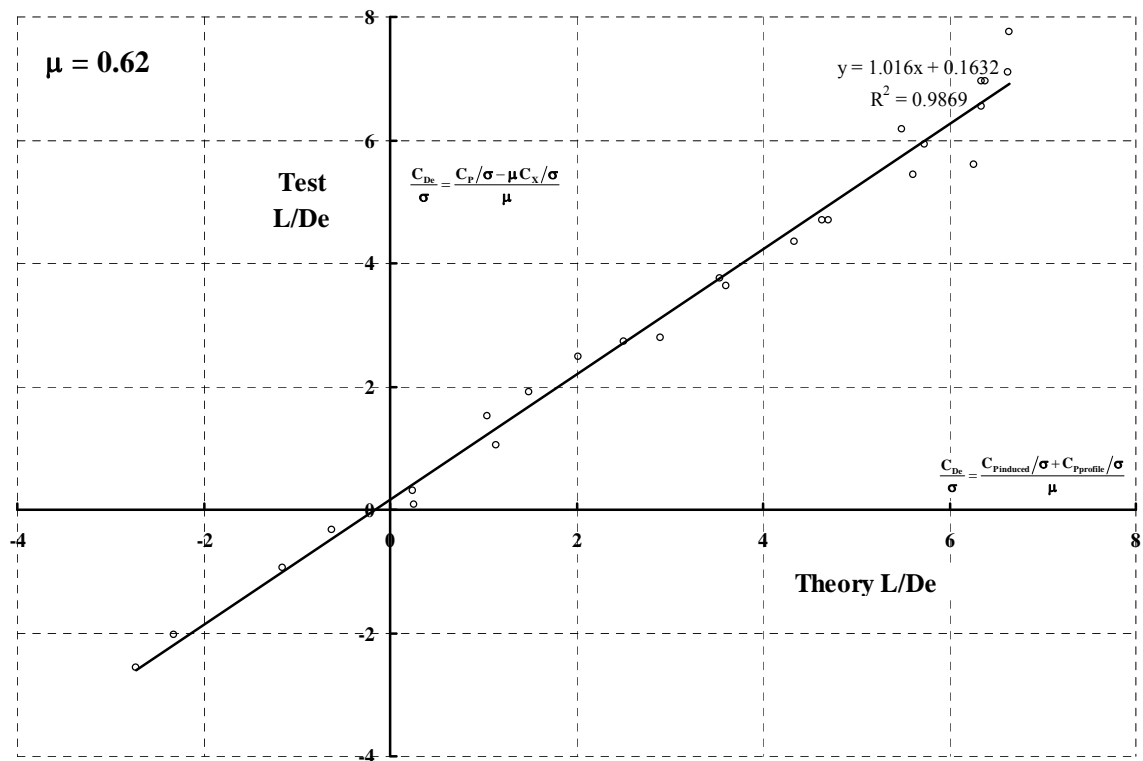
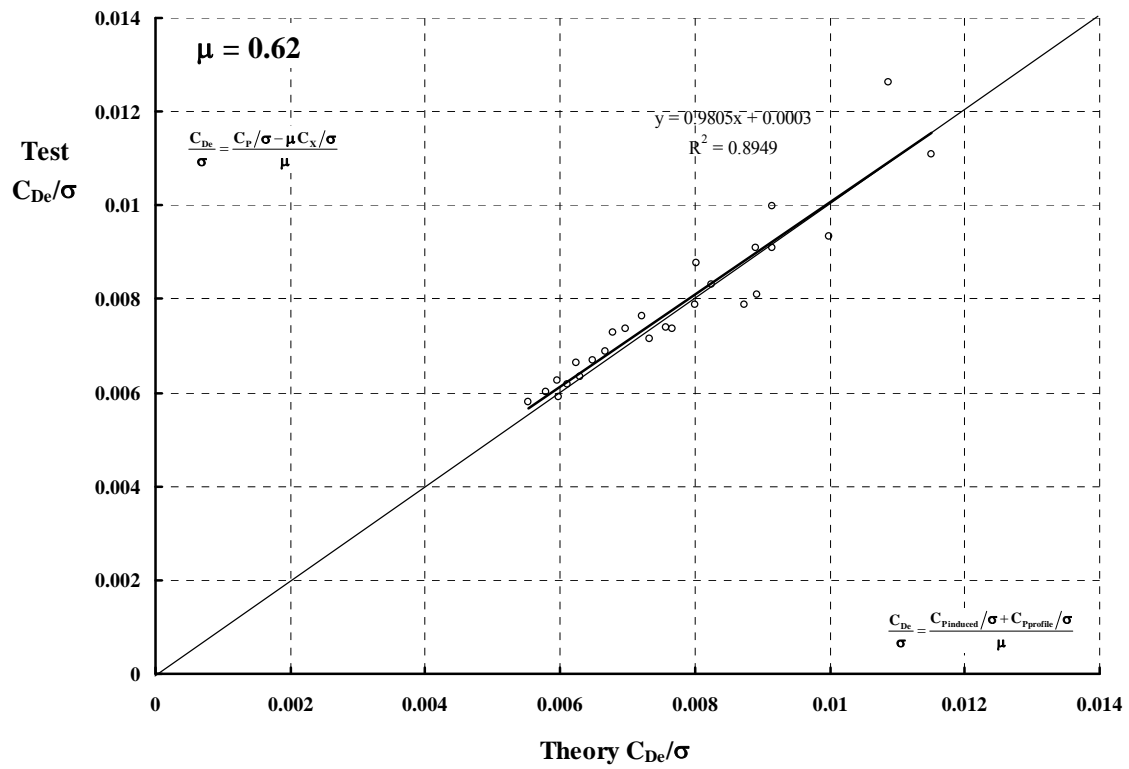


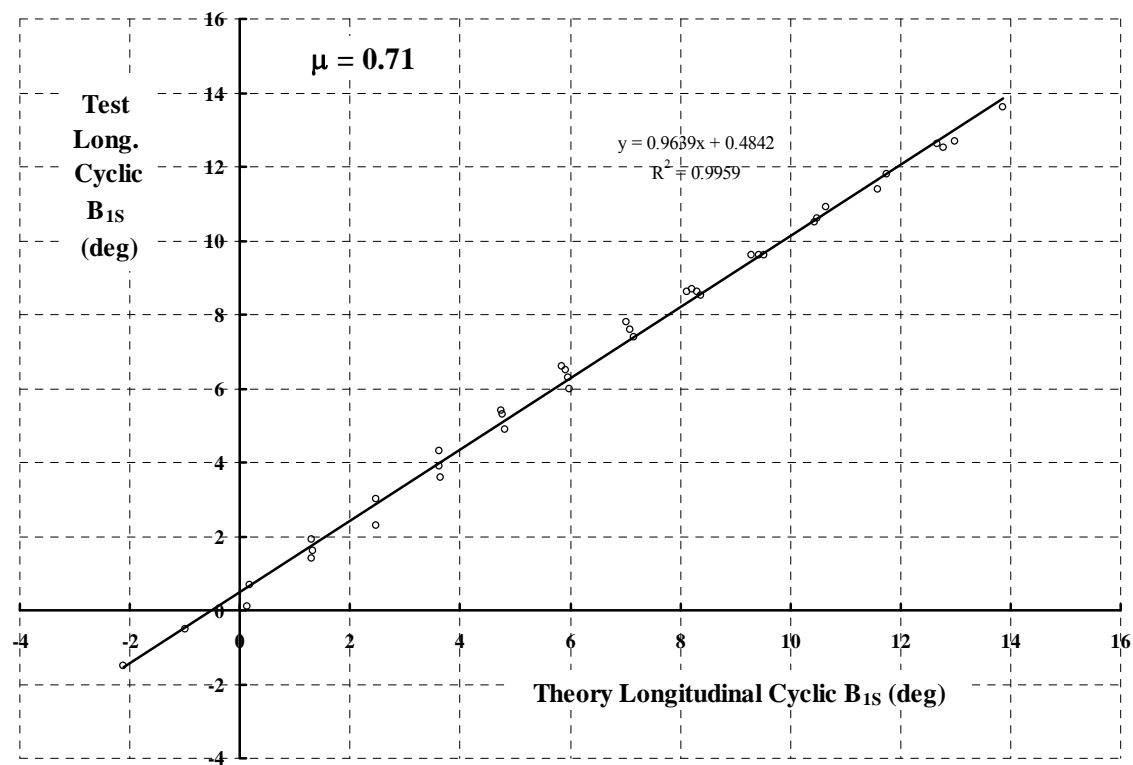
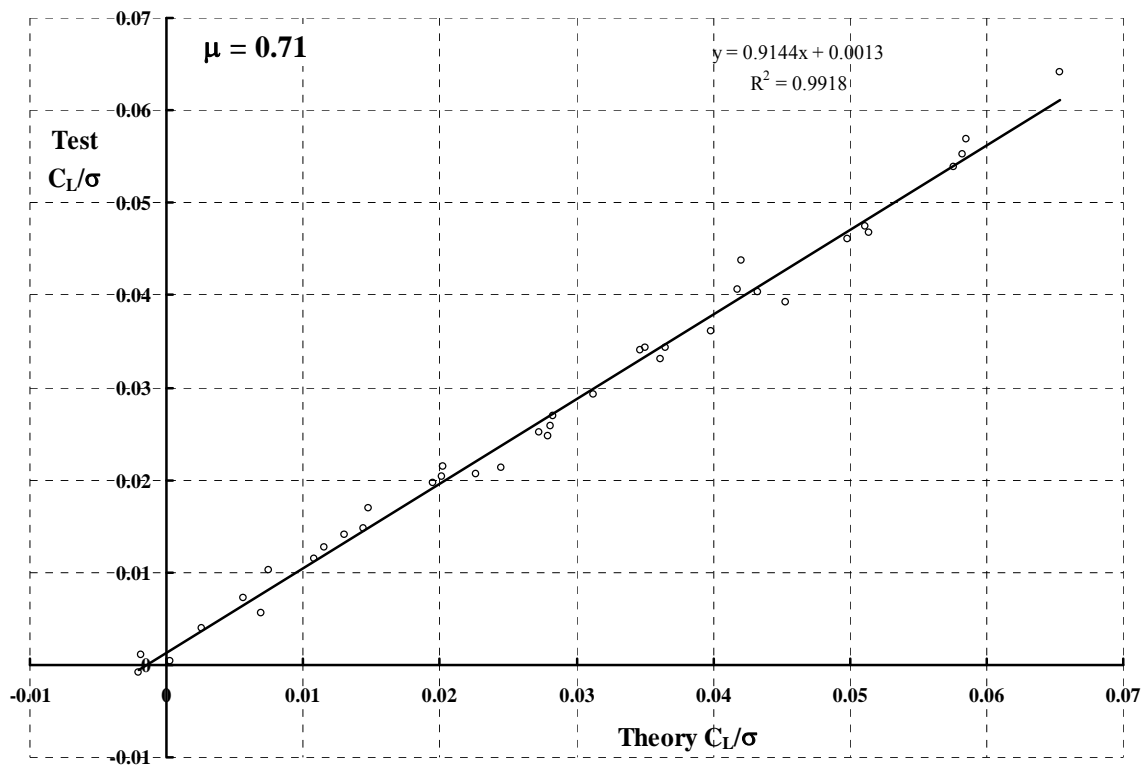


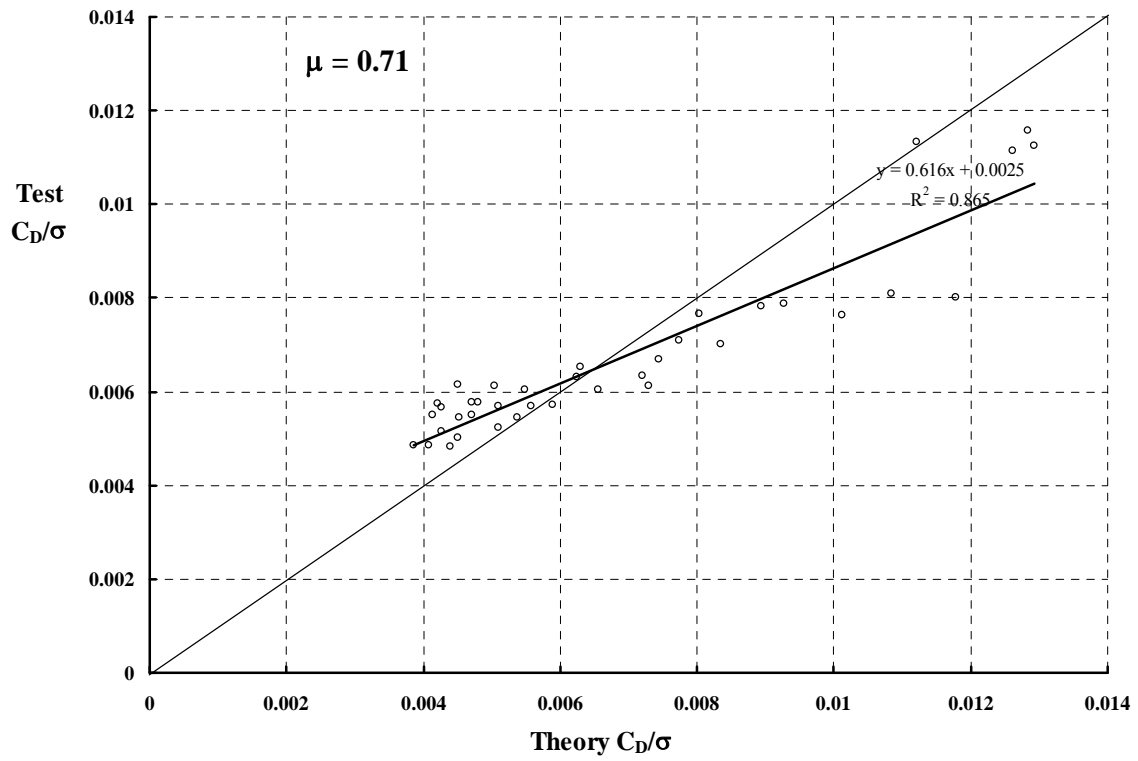
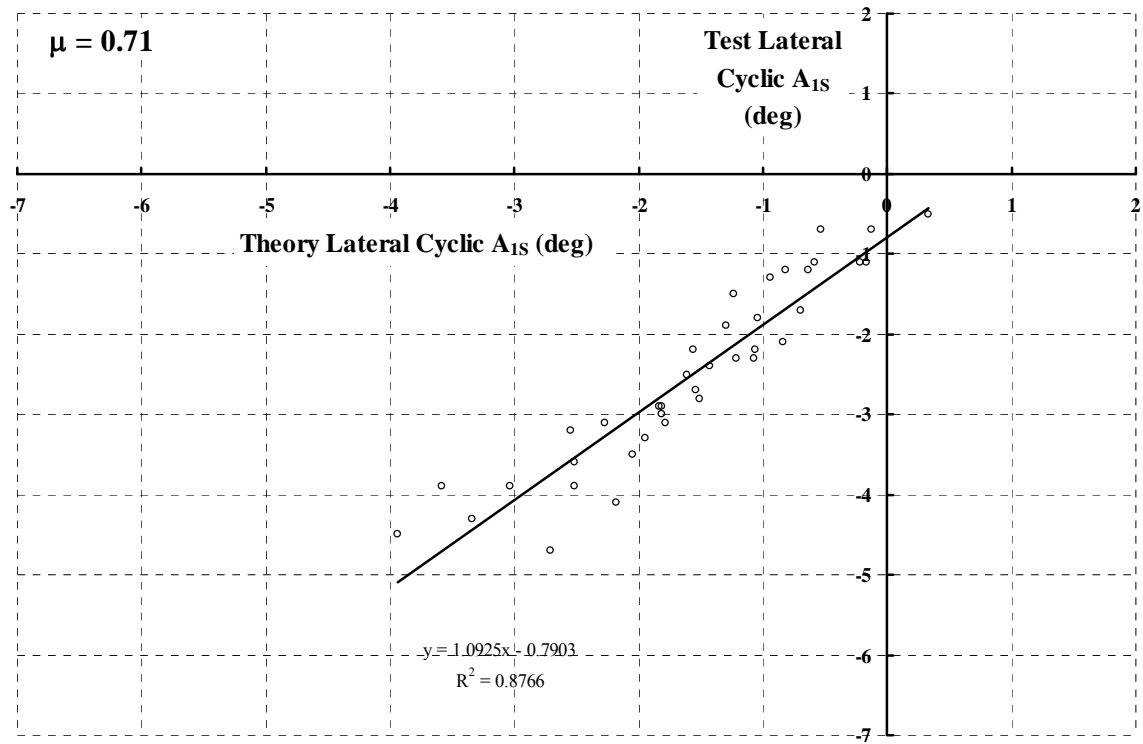


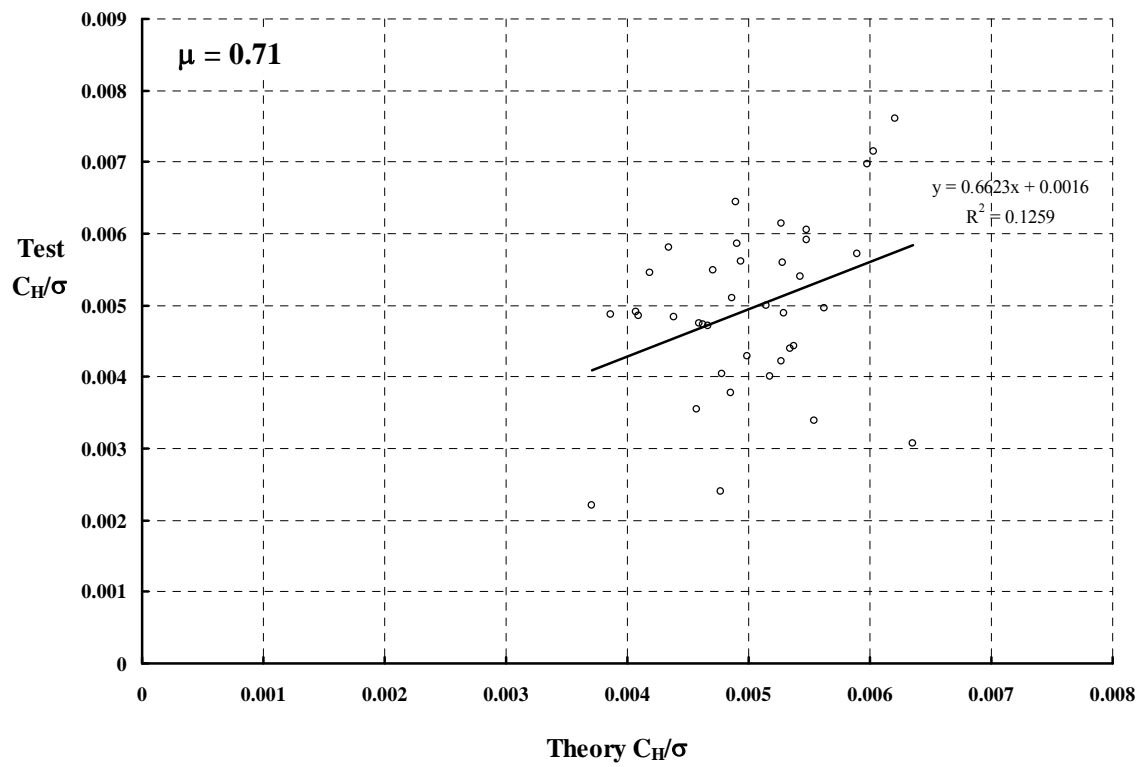
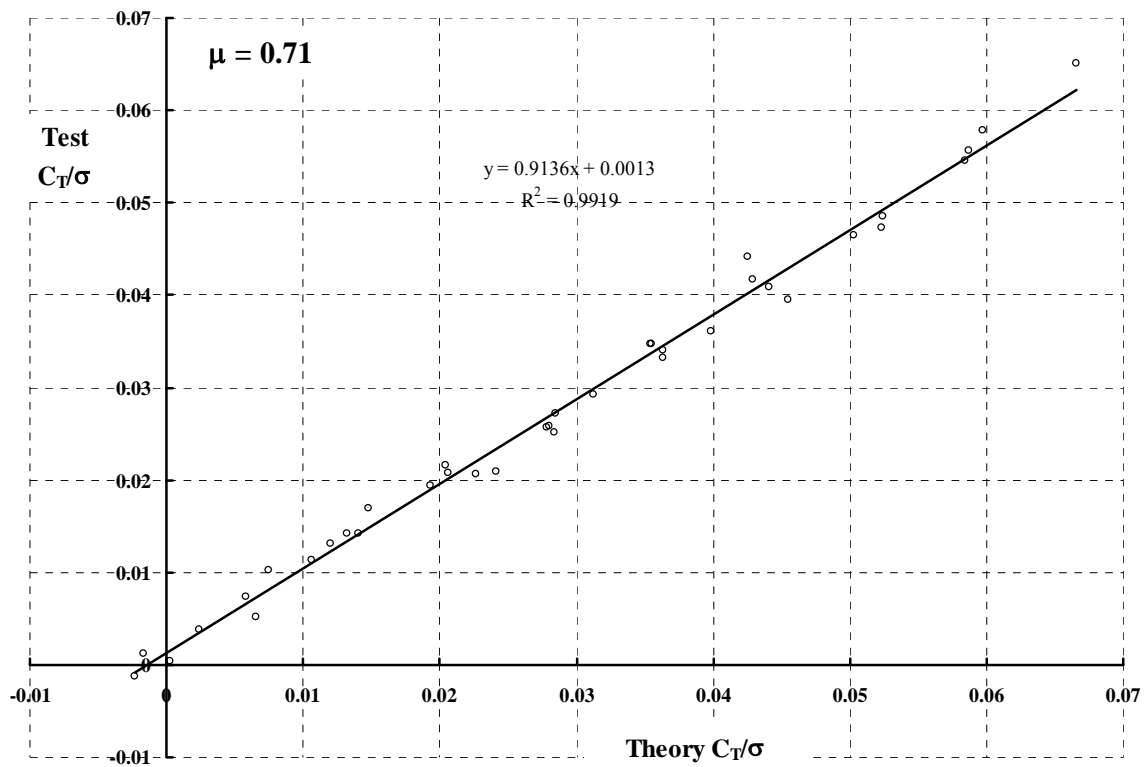


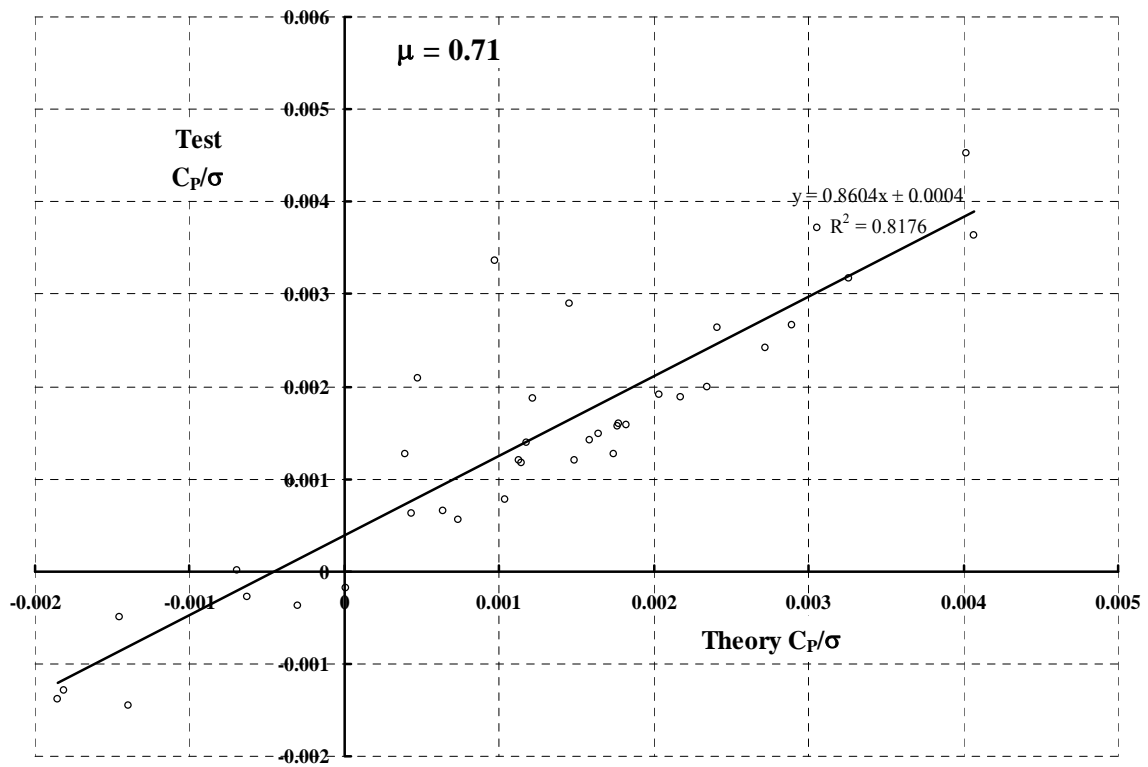
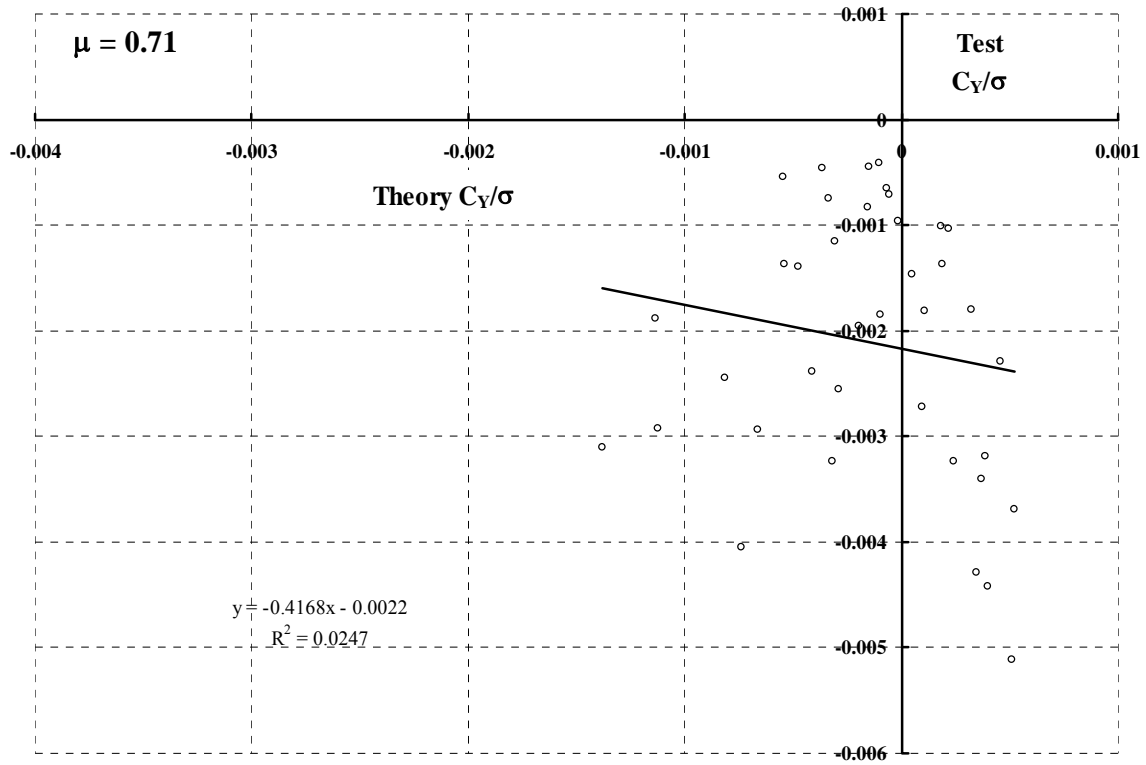


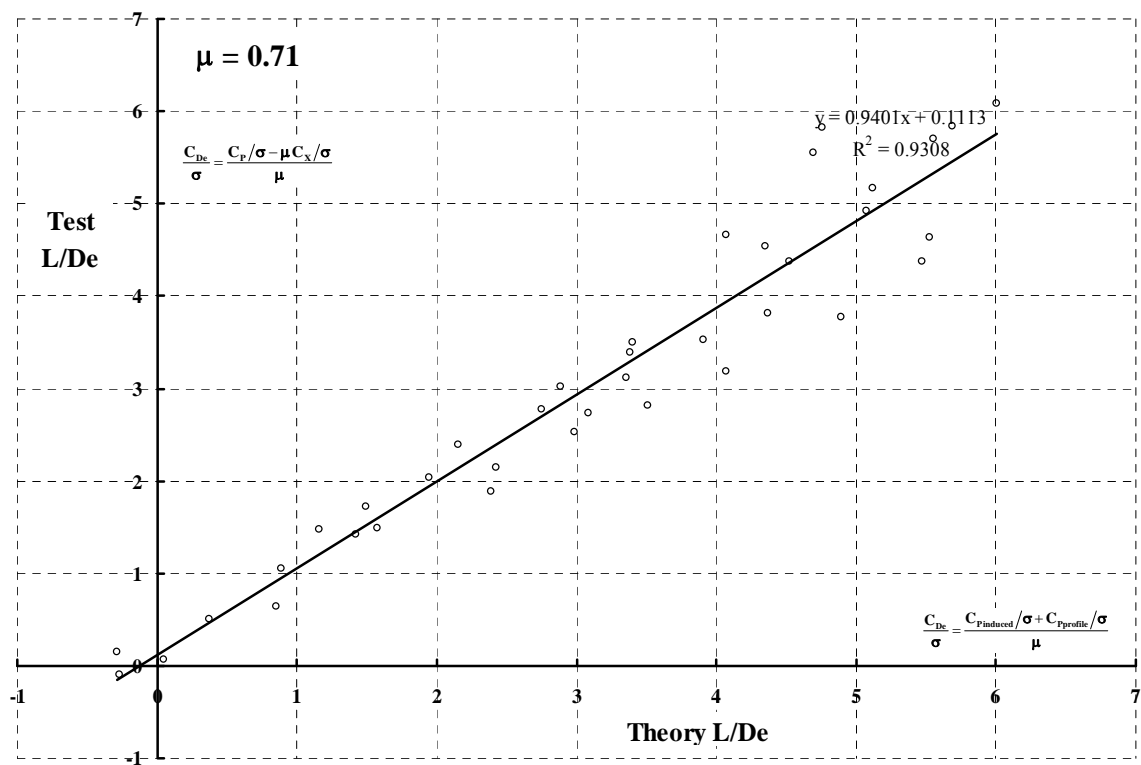
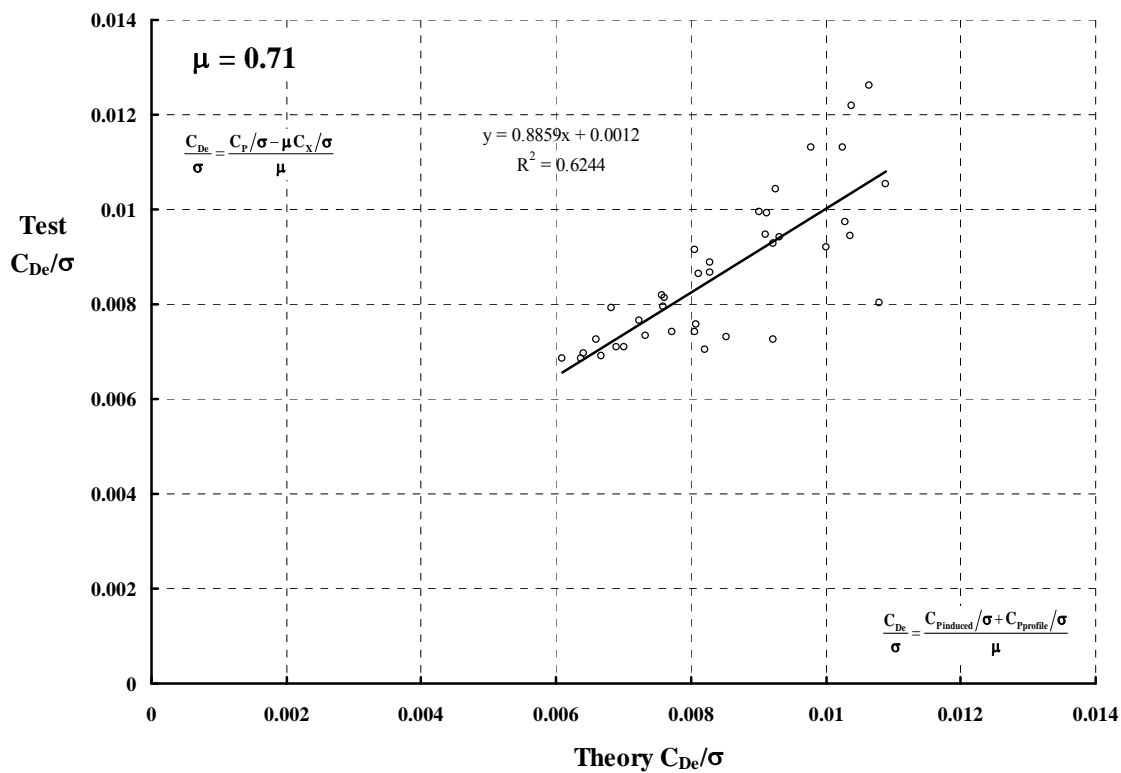


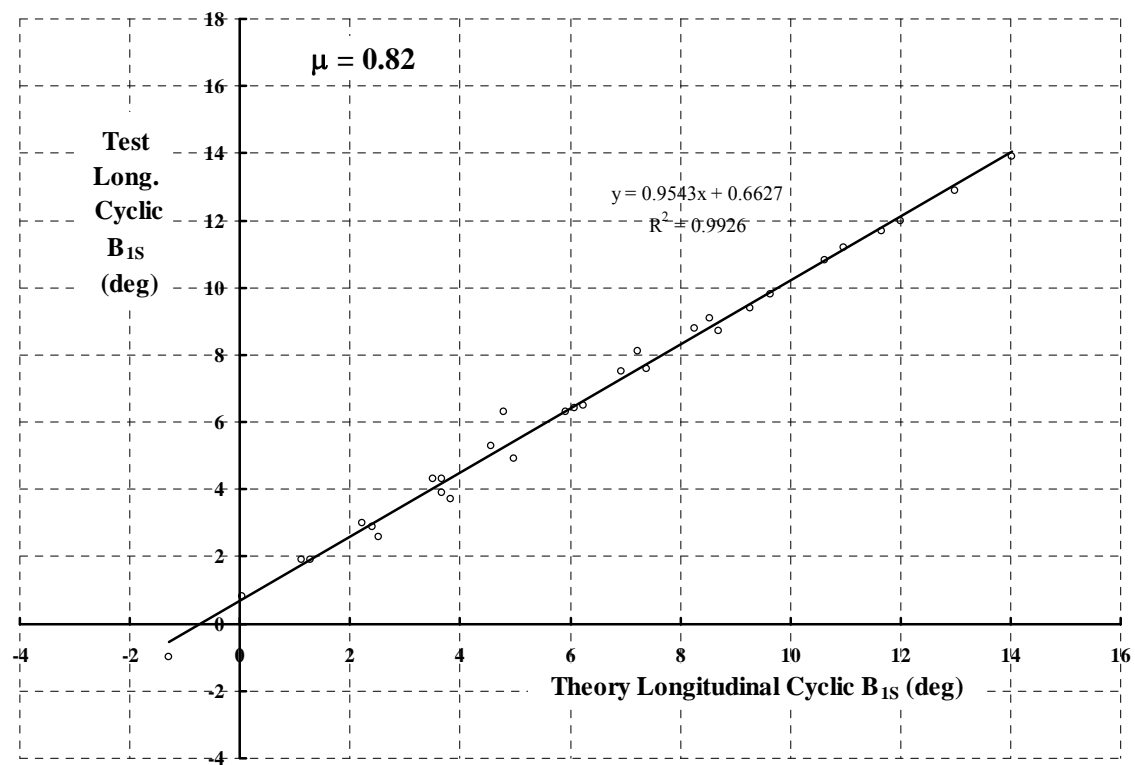
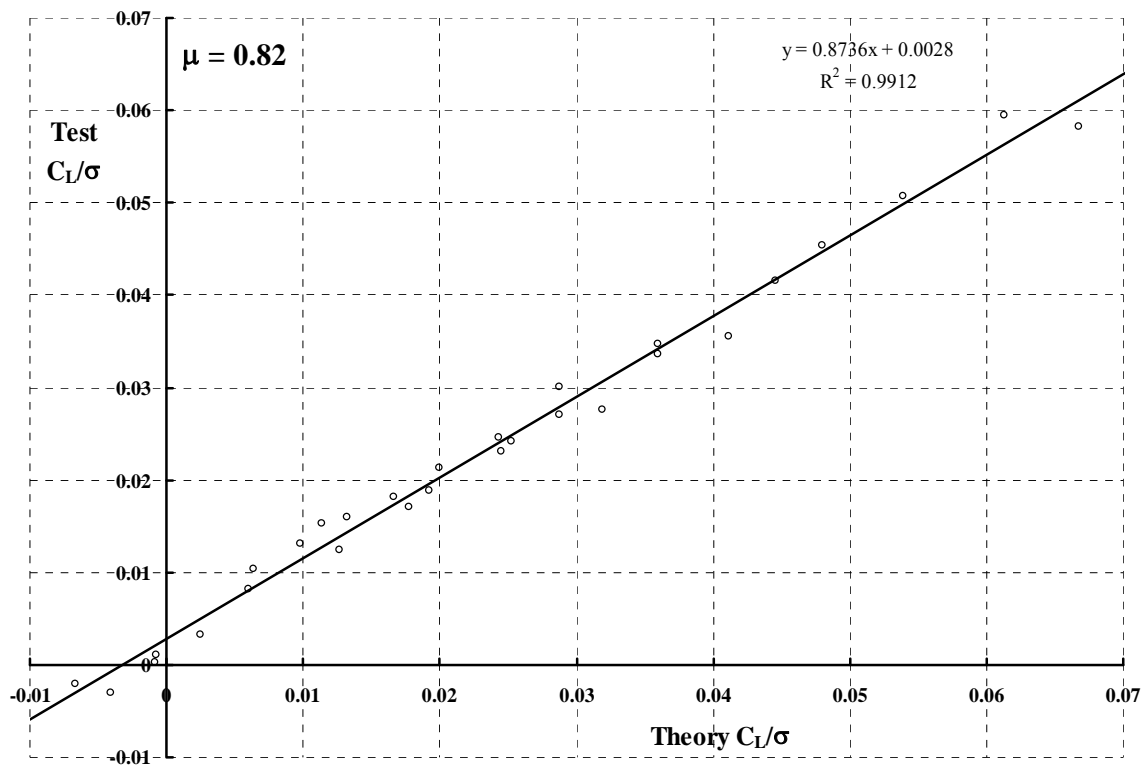


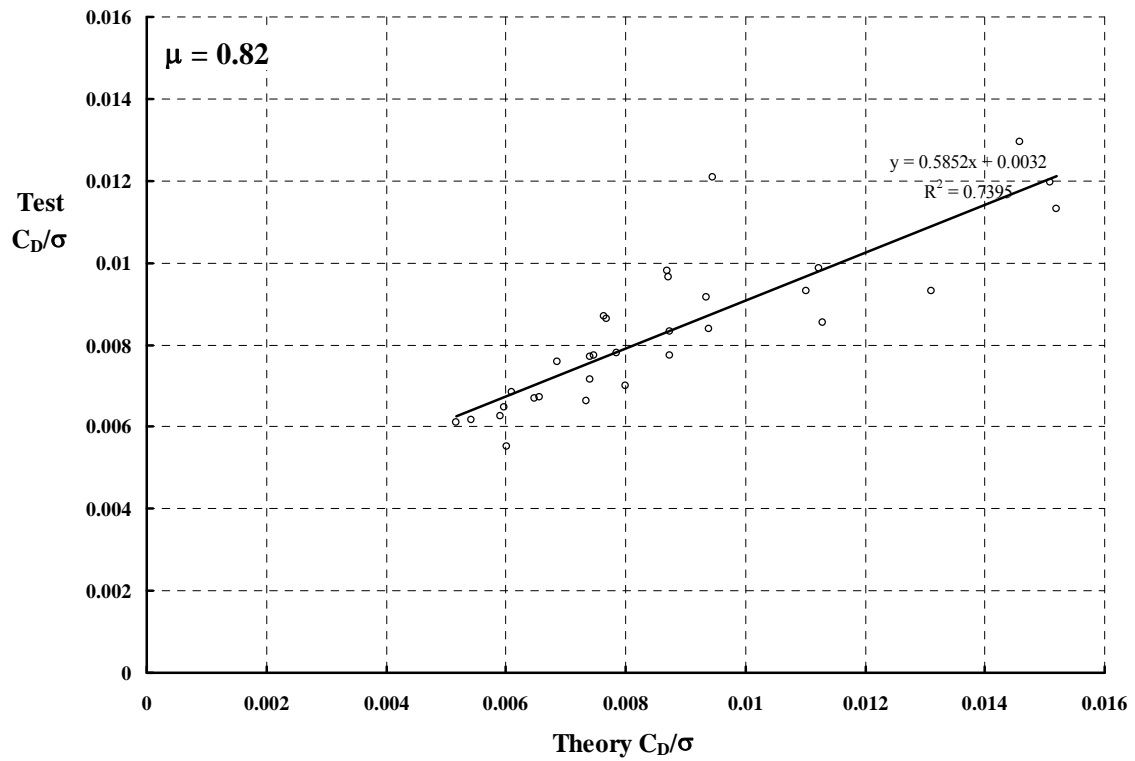
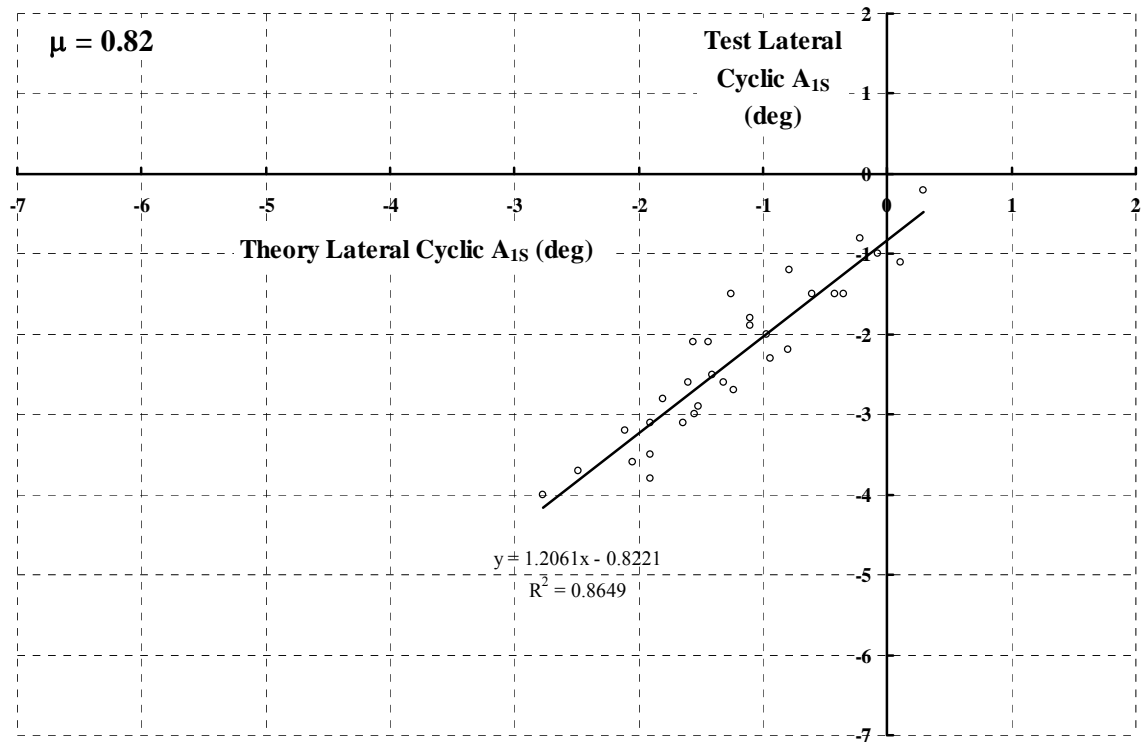


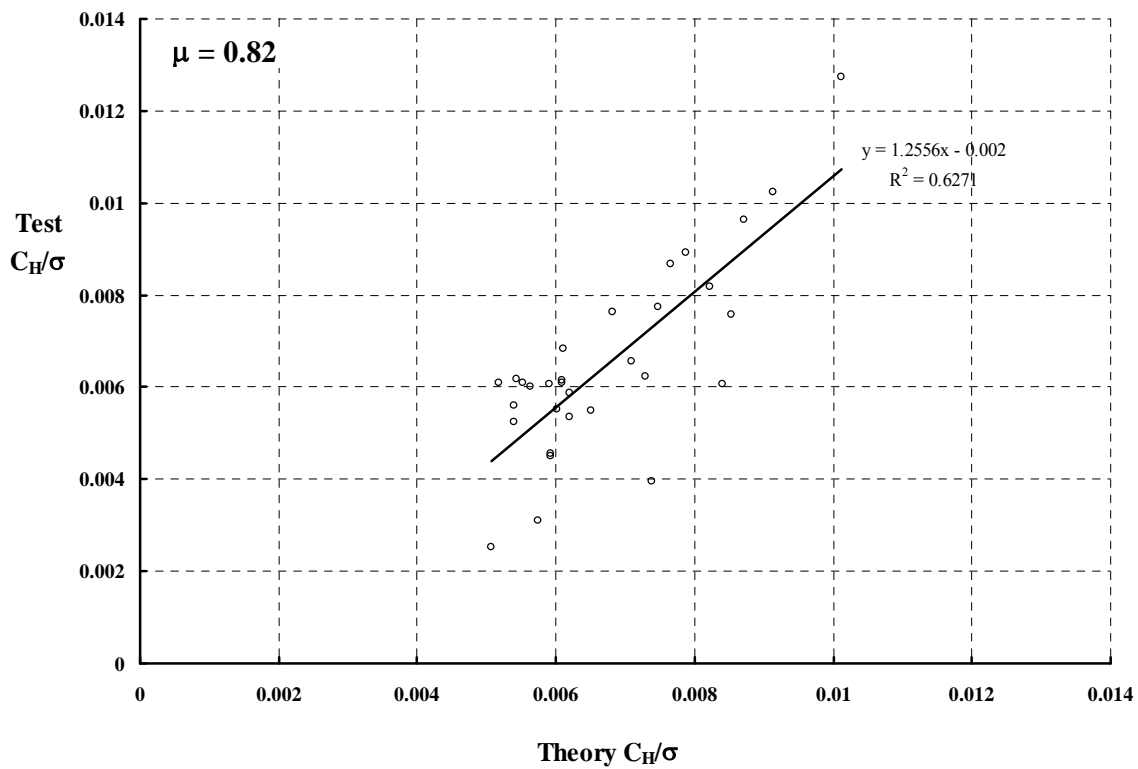
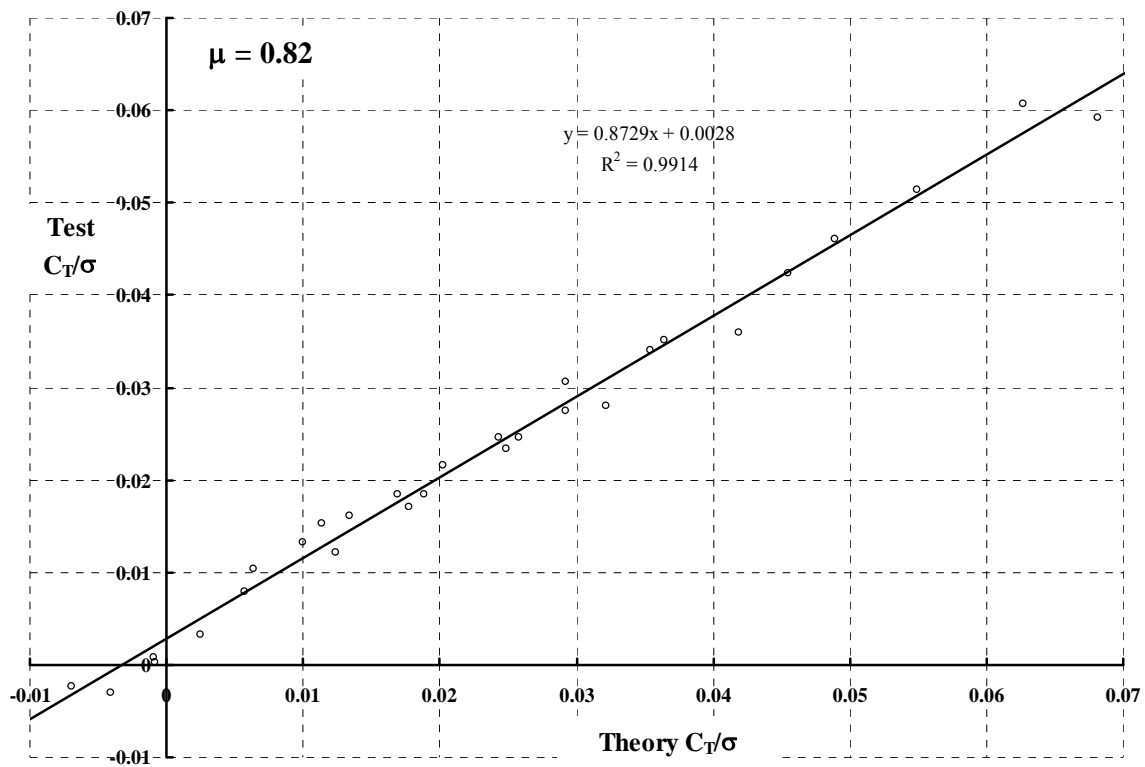


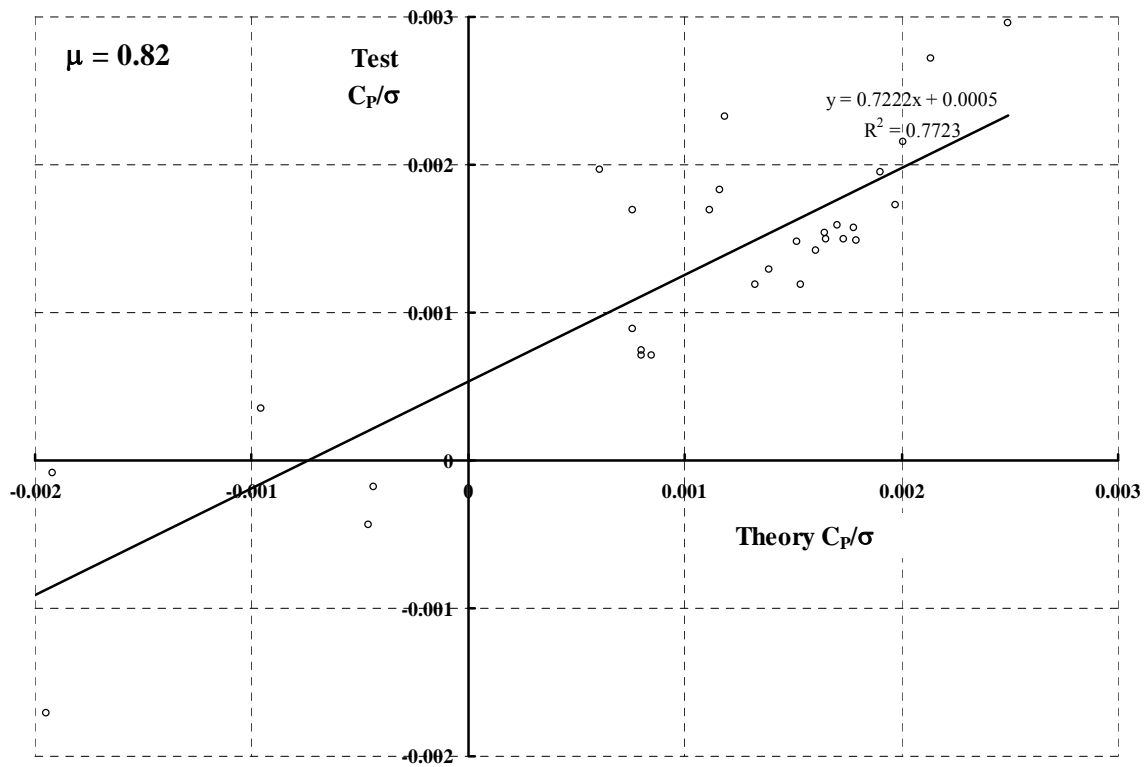
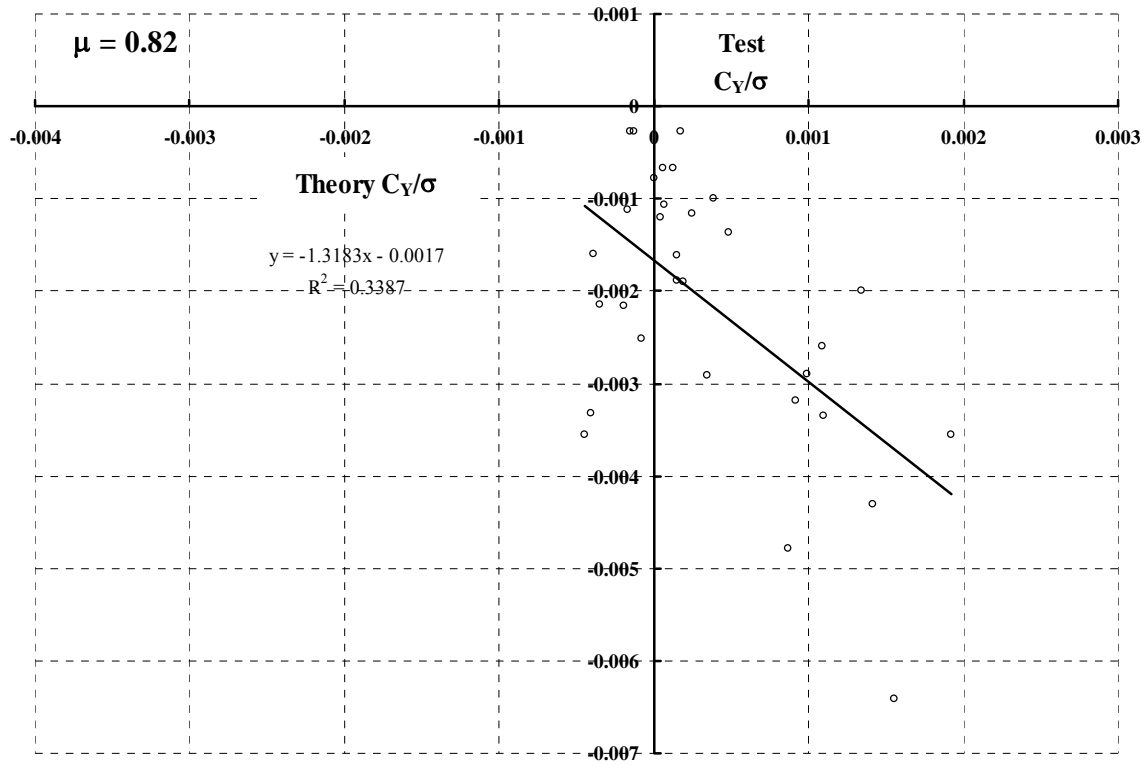


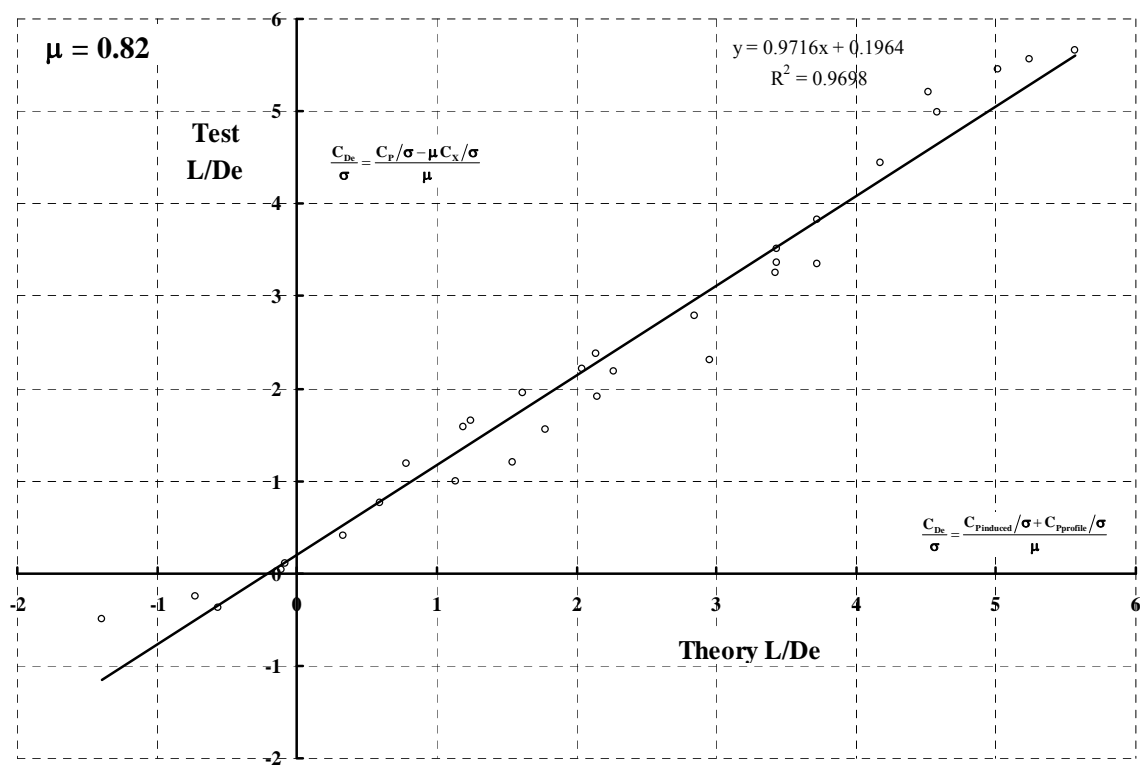
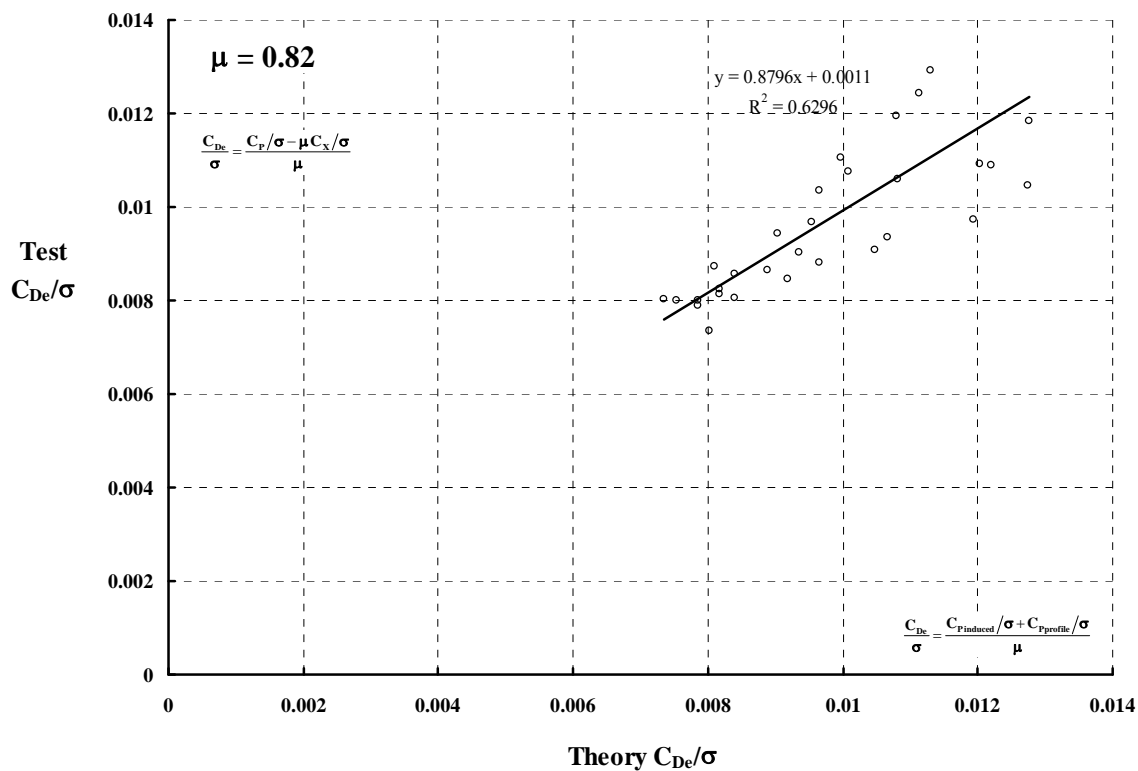


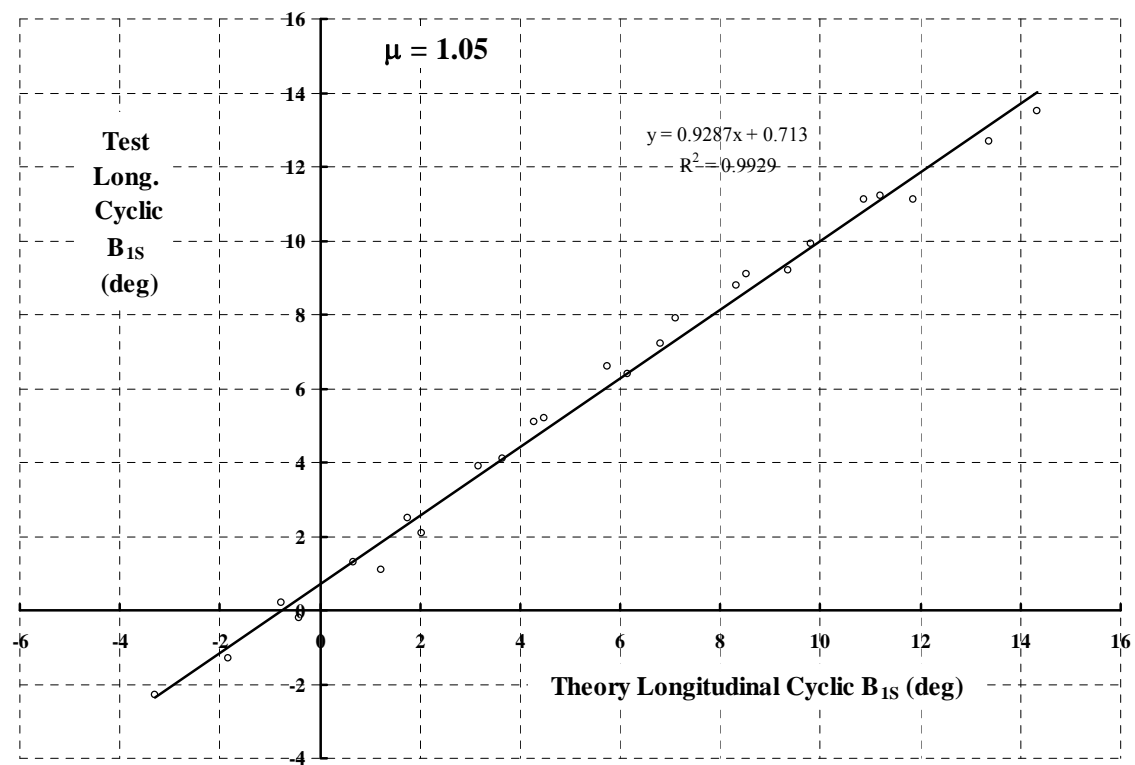
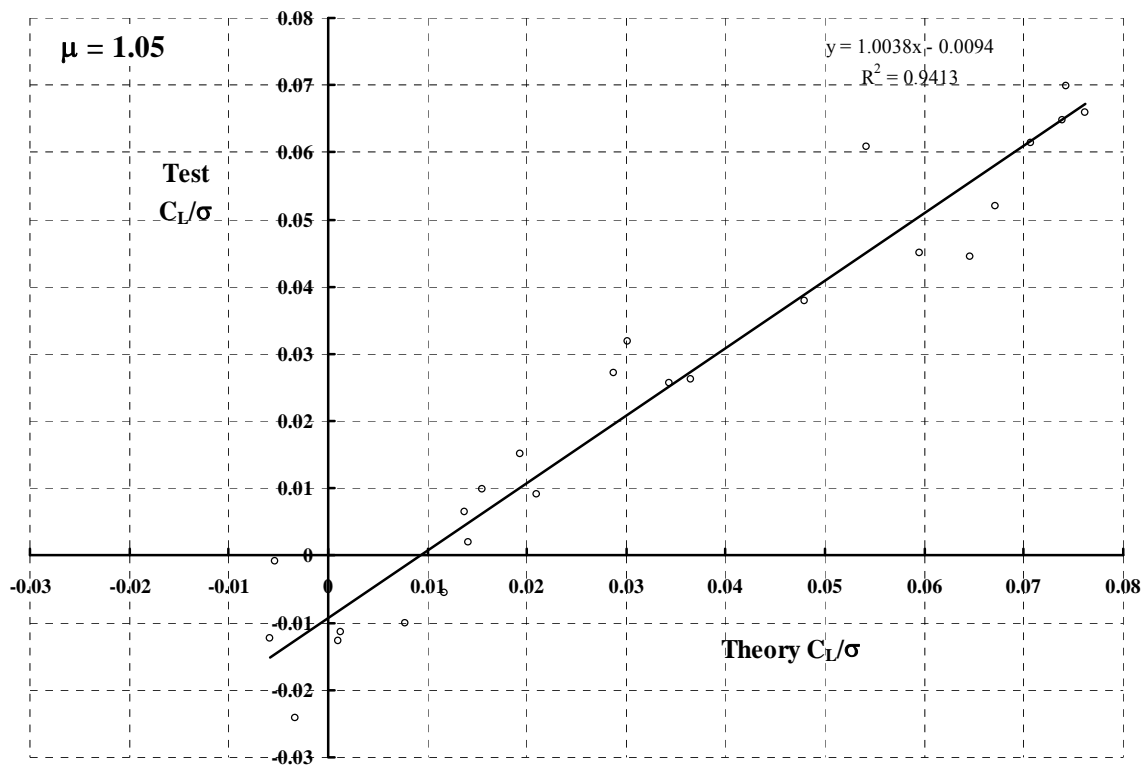


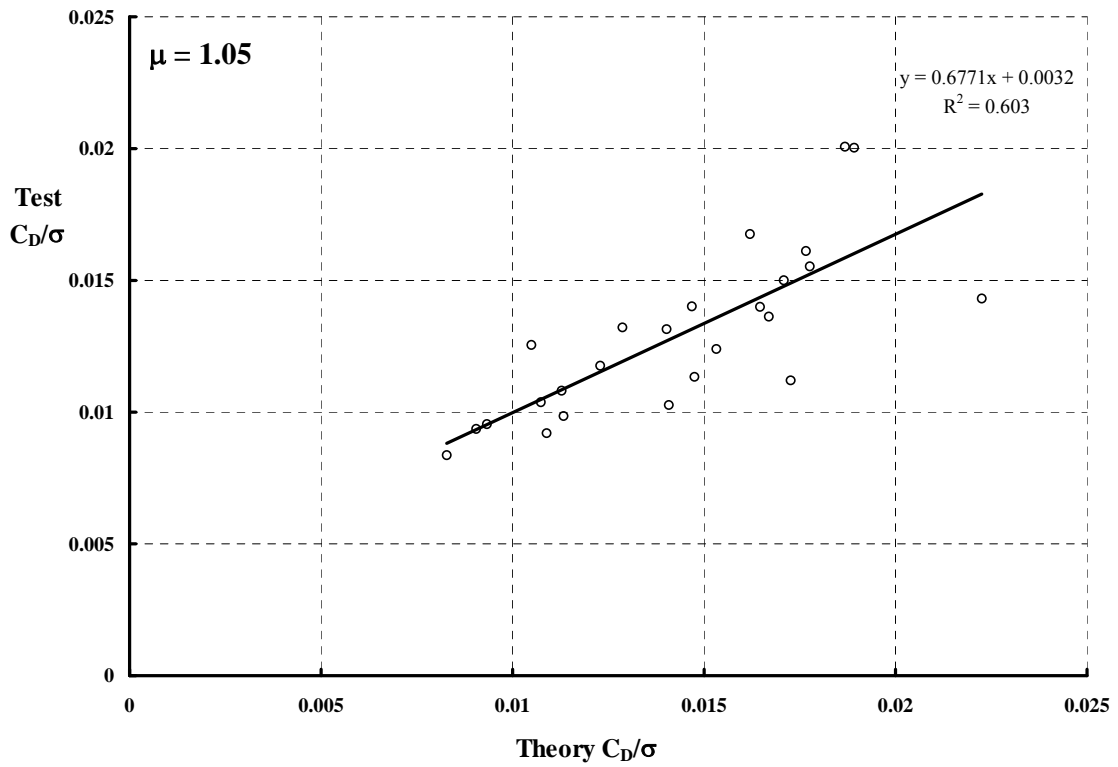
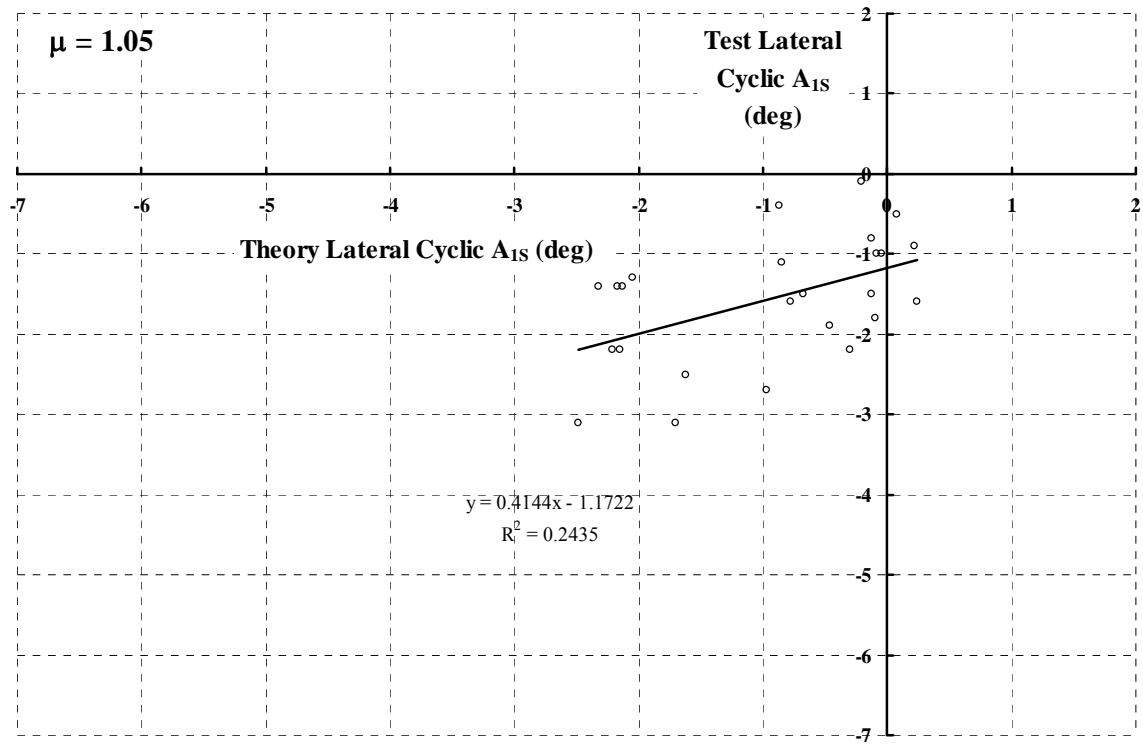


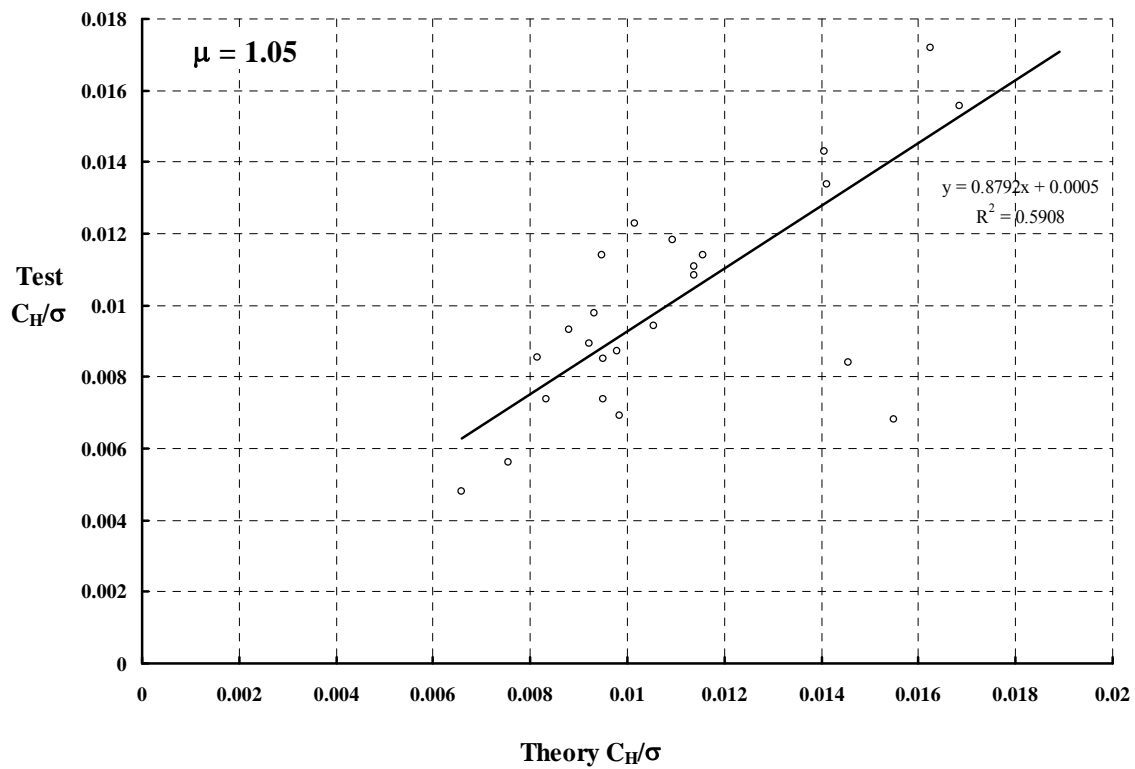
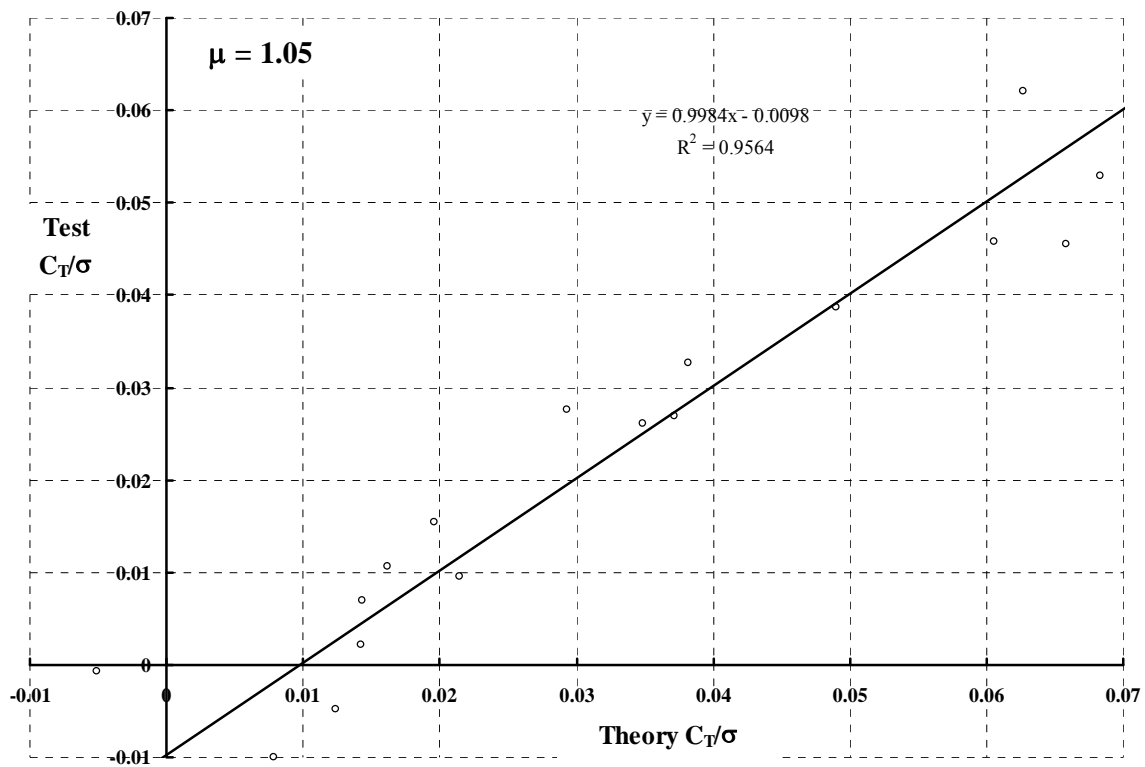


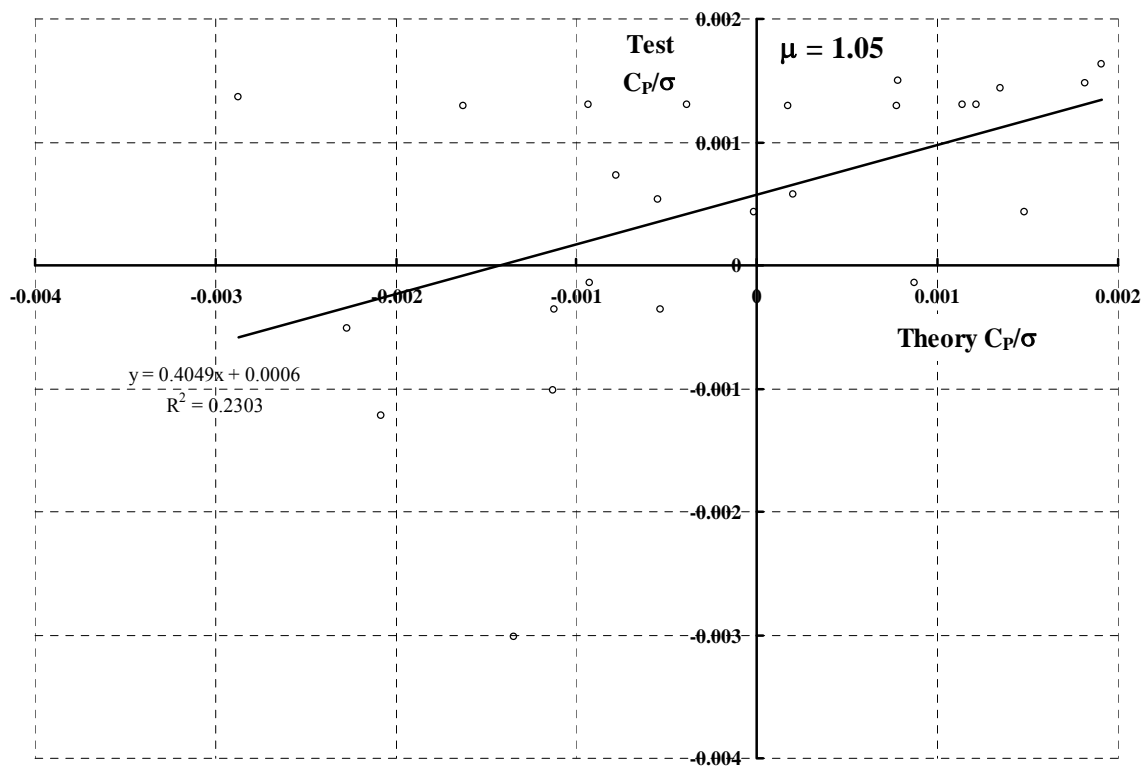
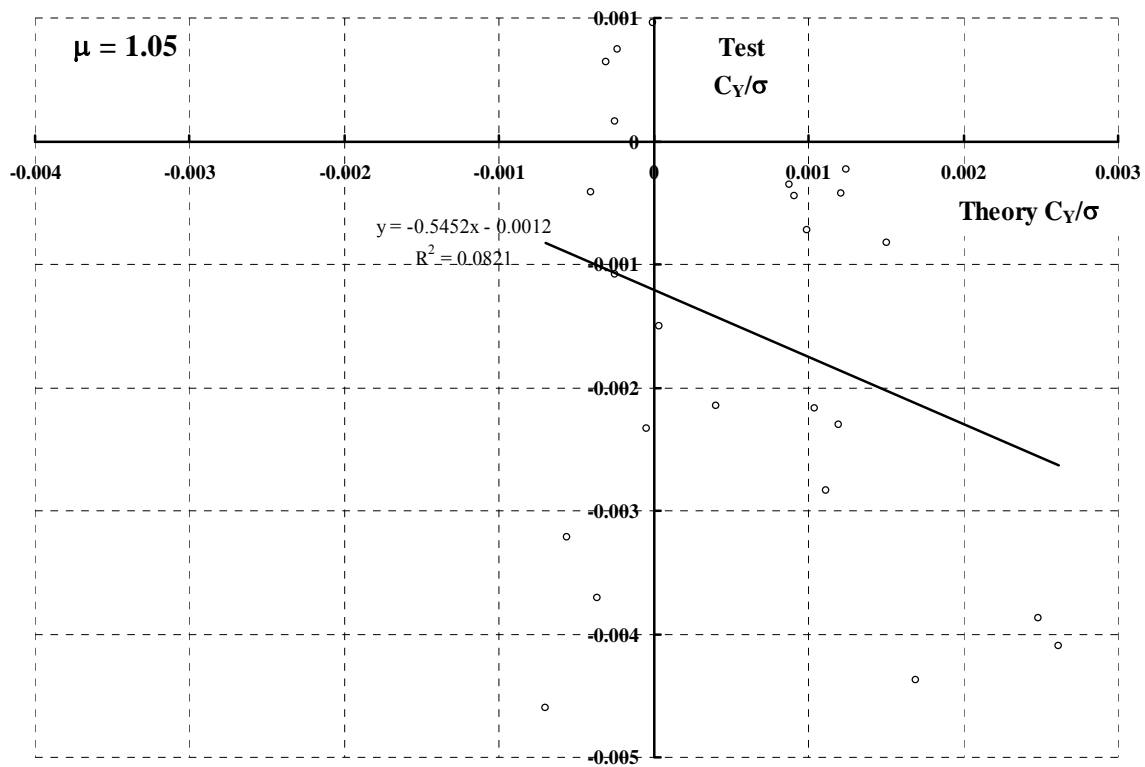












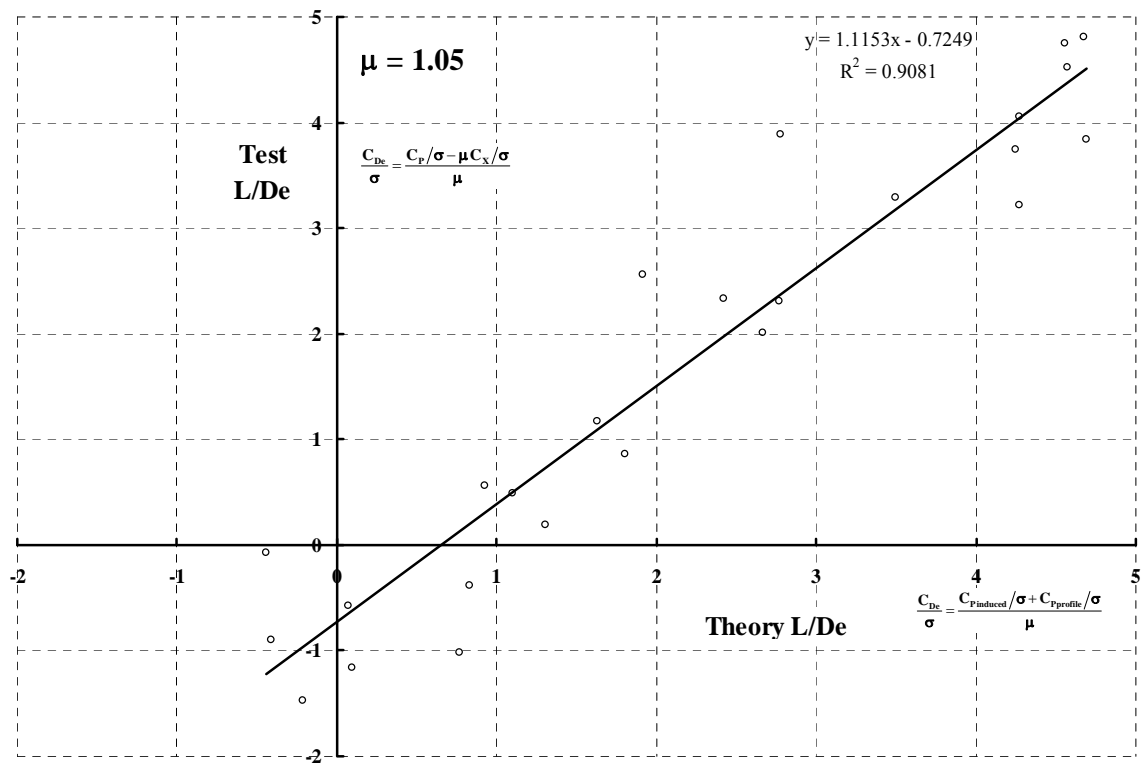
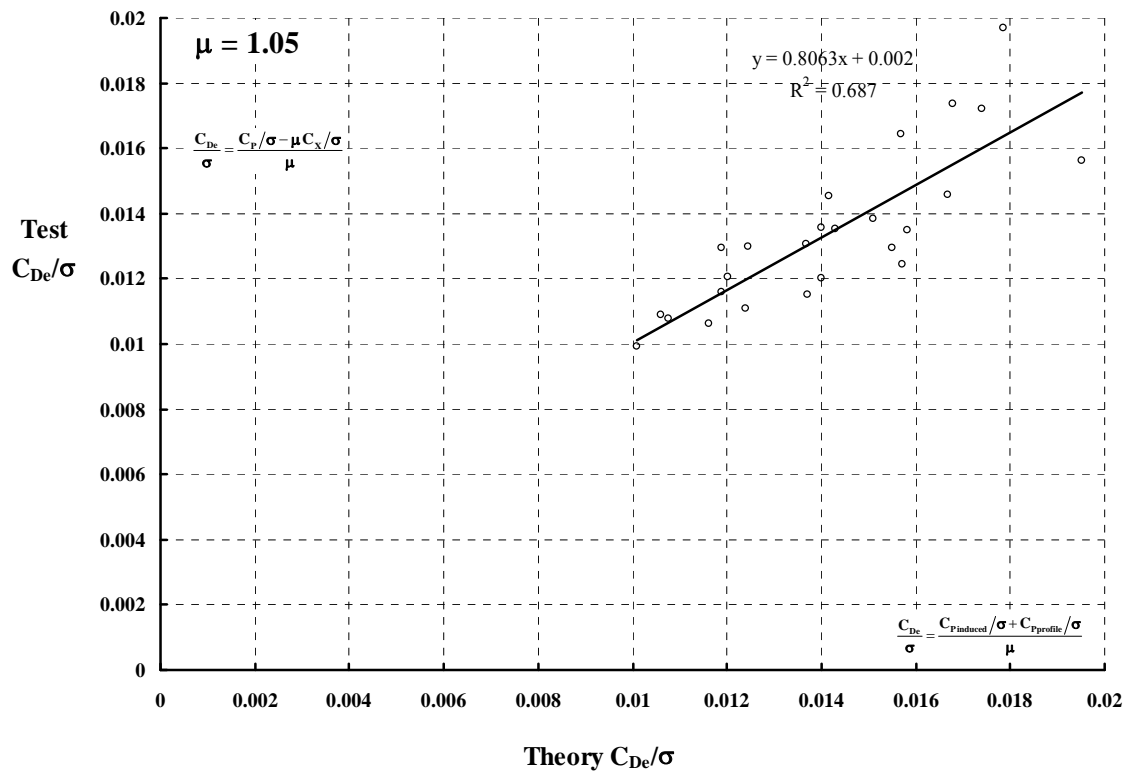


Table of Linear Regression Coefficients

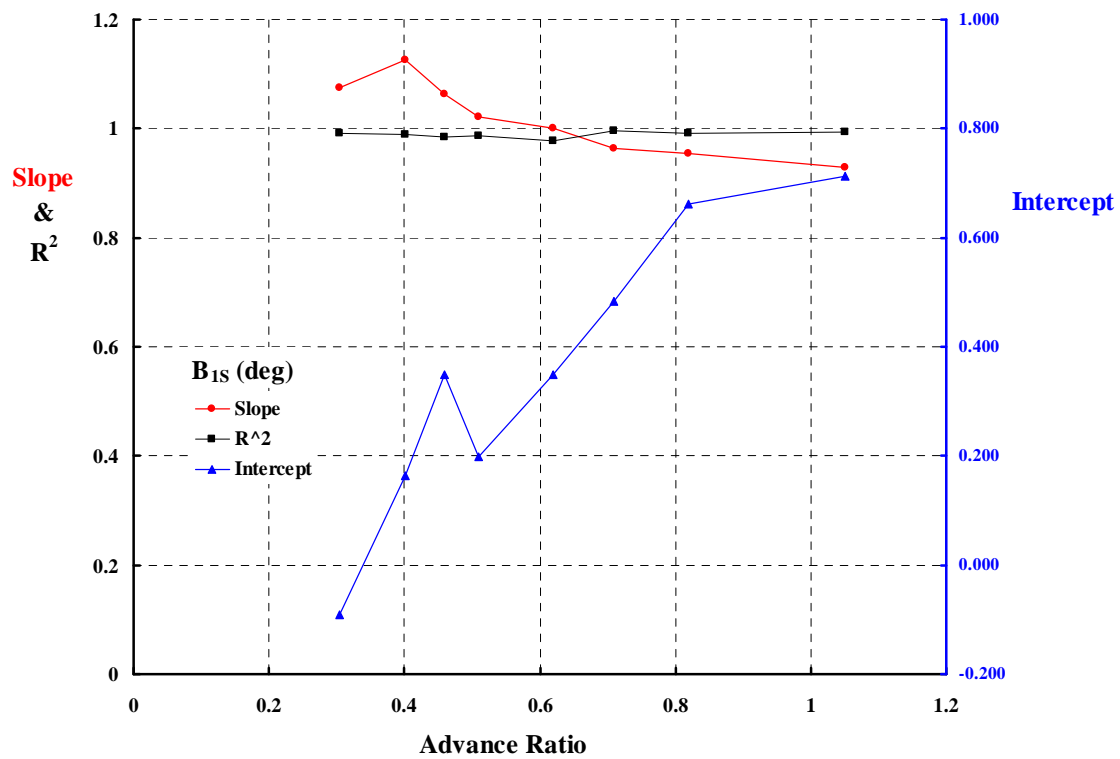
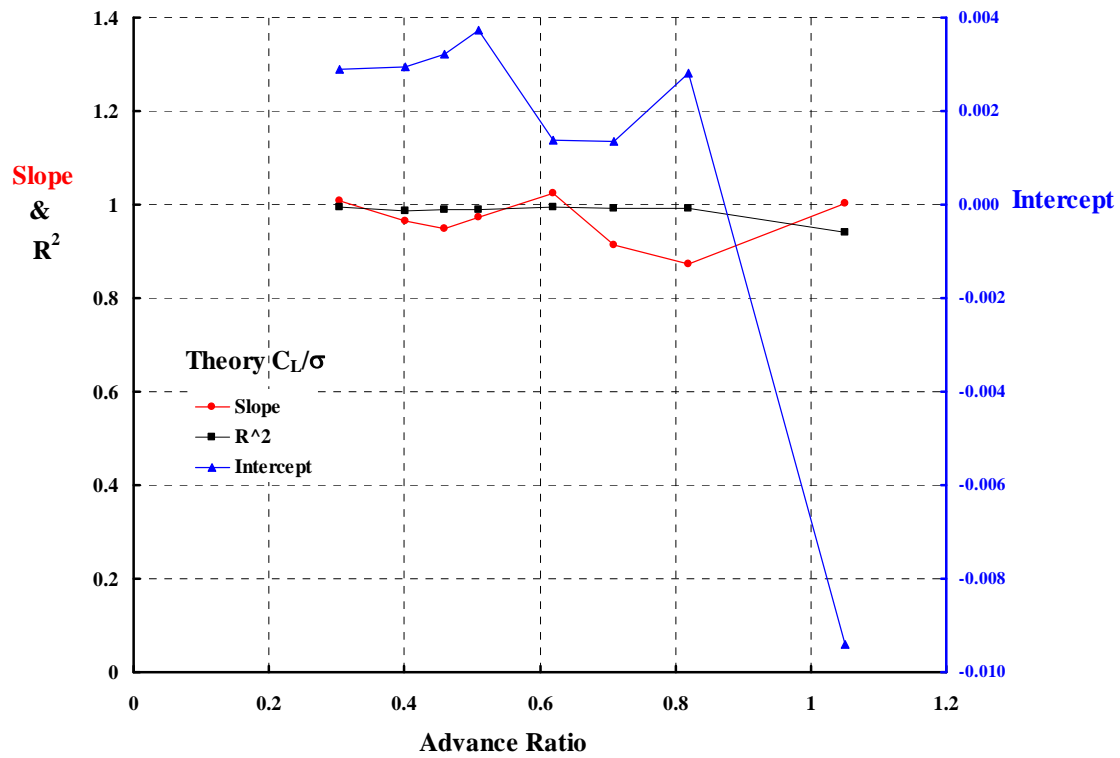
Longitudinal Cyclic				Lateral Cyclic		
Mu	SLOPE	Intercept	R²	SLOPE	Intercept	R²
0.305	1.0746	-0.0922	0.9924	1.0852	-0.4012	0.9718
0.401	1.1252	0.1632	0.9899	1.3323	-0.1506	0.9439
0.460	1.0627	0.3480	0.9837	1.3370	-0.2134	0.9647
0.510	1.0215	0.1977	0.9861	1.2453	-0.4279	0.9497
0.620	1.0001	0.3479	0.9774	1.3533	-0.5637	0.8995
0.710	0.9639	0.4842	0.9959	1.0925	-0.7903	0.8766
0.820	0.9543	0.6627	0.9926	1.2061	-0.8221	0.8649
1.050	0.9287	0.7130	0.9929	0.4144	-1.1722	0.2450

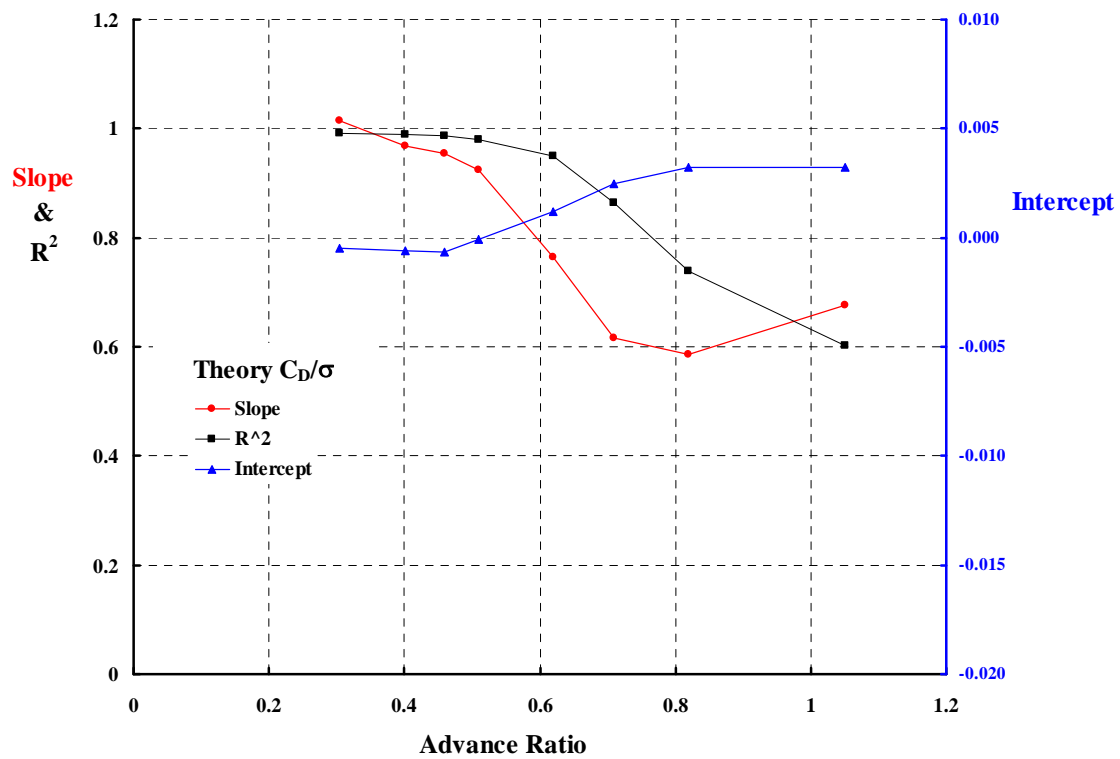
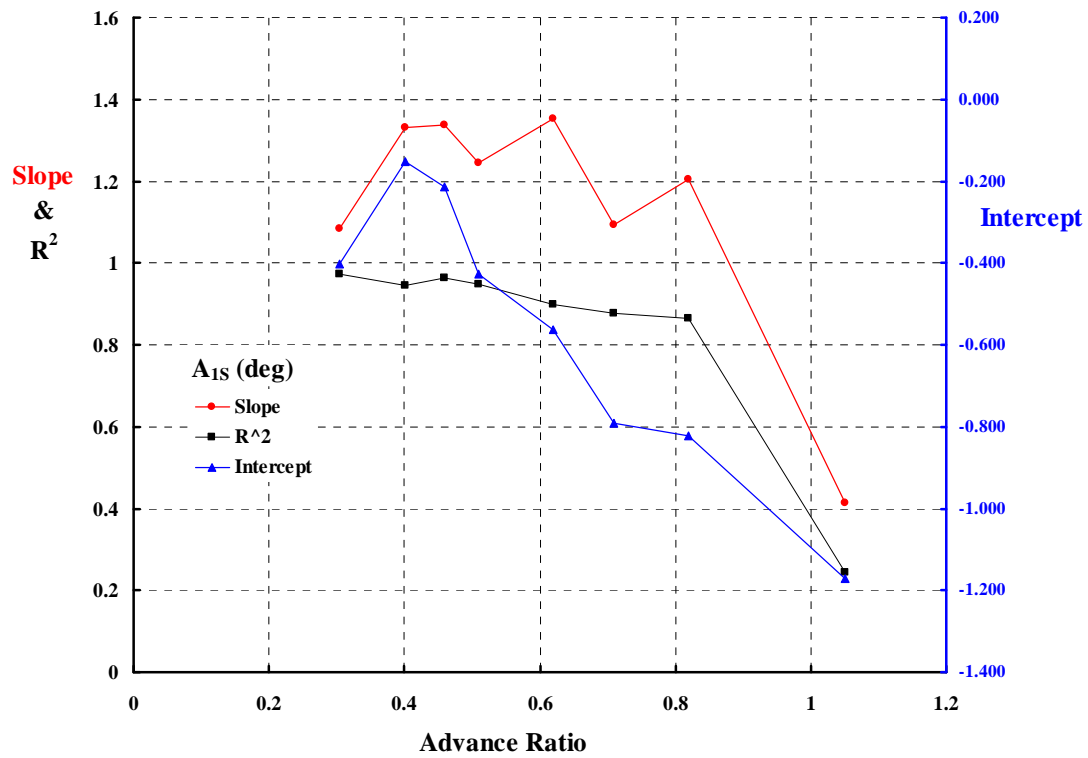
Lift Coefficient				Drag Coefficient		
Mu	SLOPE	Intercept	R²	SLOPE	Intercept	R²
0.305	1.0068	0.0029	0.9947	1.0142	-0.0005	0.9920
0.401	0.9652	0.0030	0.9873	0.9675	-0.0006	0.9886
0.460	0.9500	0.0032	0.9902	0.9533	-0.0007	0.9870
0.510	0.9727	0.0037	0.9895	0.9238	-0.0001	0.9802
0.620	1.0242	0.0014	0.9948	0.7647	0.0012	0.9487
0.710	0.9144	0.0013	0.9918	0.6160	0.0025	0.8650
0.820	0.8736	0.0028	0.9912	0.5852	0.0032	0.7395
1.050	1.0038	-0.0094	0.9413	0.6771	0.0032	0.6030

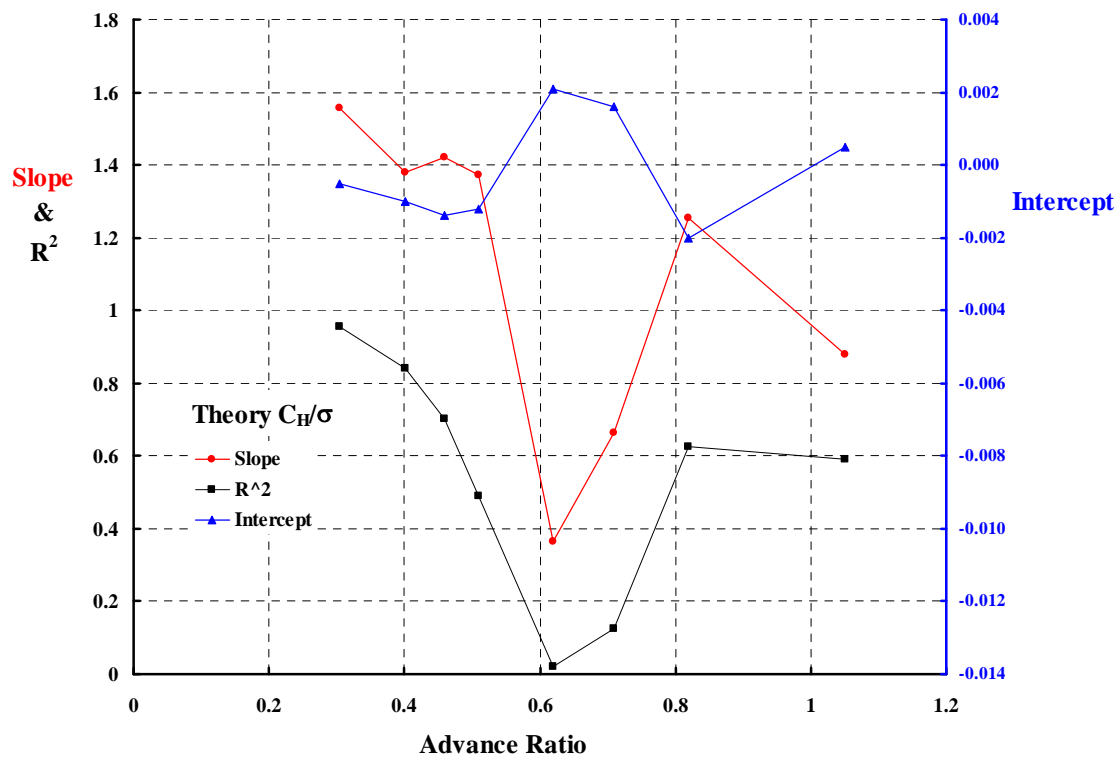
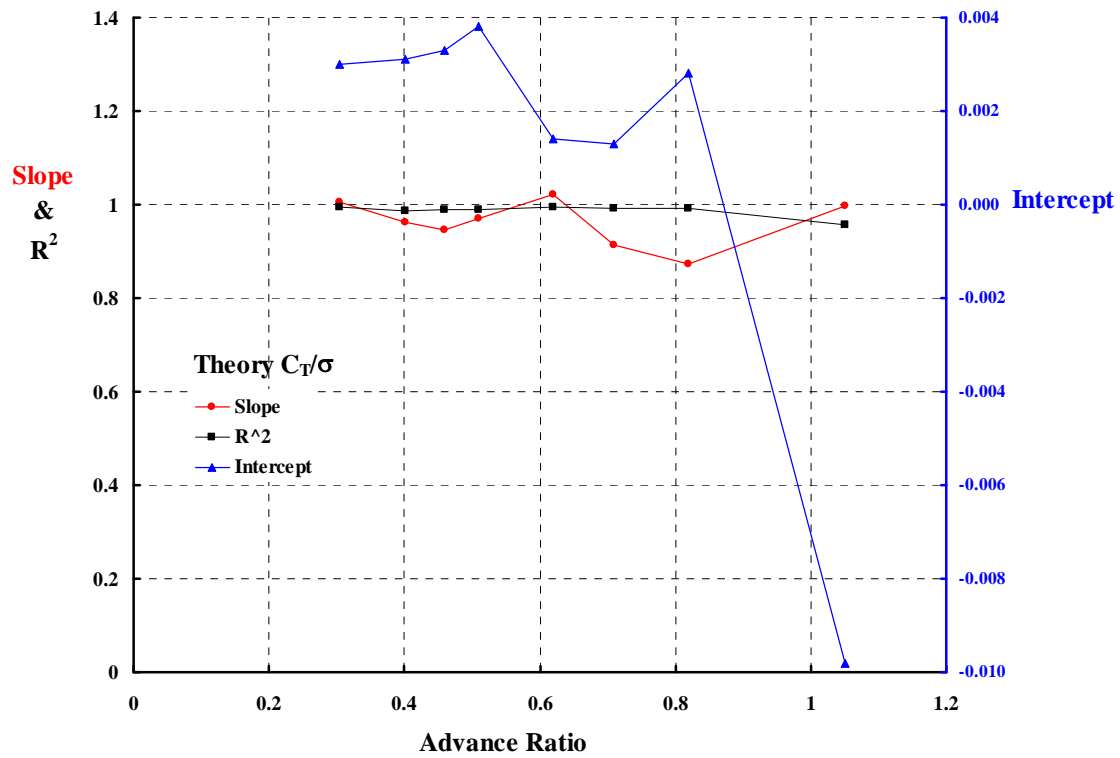
Thrust Coefficient				H-Force Coefficient		
Mu	SLOPE	Intercept	R²	SLOPE	Intercept	R²
0.305	1.0054	0.0030	0.9947	1.5561	-0.0005	0.9573
0.401	0.9629	0.0031	0.9871	1.3794	-0.0010	0.8397
0.460	0.9470	0.0033	0.9900	1.4213	-0.0014	0.7015
0.510	0.9701	0.0038	0.9899	1.3713	-0.0012	0.4888
0.620	1.0205	0.0014	0.9950	0.3653	0.0021	0.0195
0.710	0.9136	0.0013	0.9919	0.6623	0.0016	0.1259
0.820	0.8729	0.0028	0.9914	1.2556	-0.0020	0.6271
1.050	0.9984	-0.0098	0.9564	0.8792	0.0005	0.5908

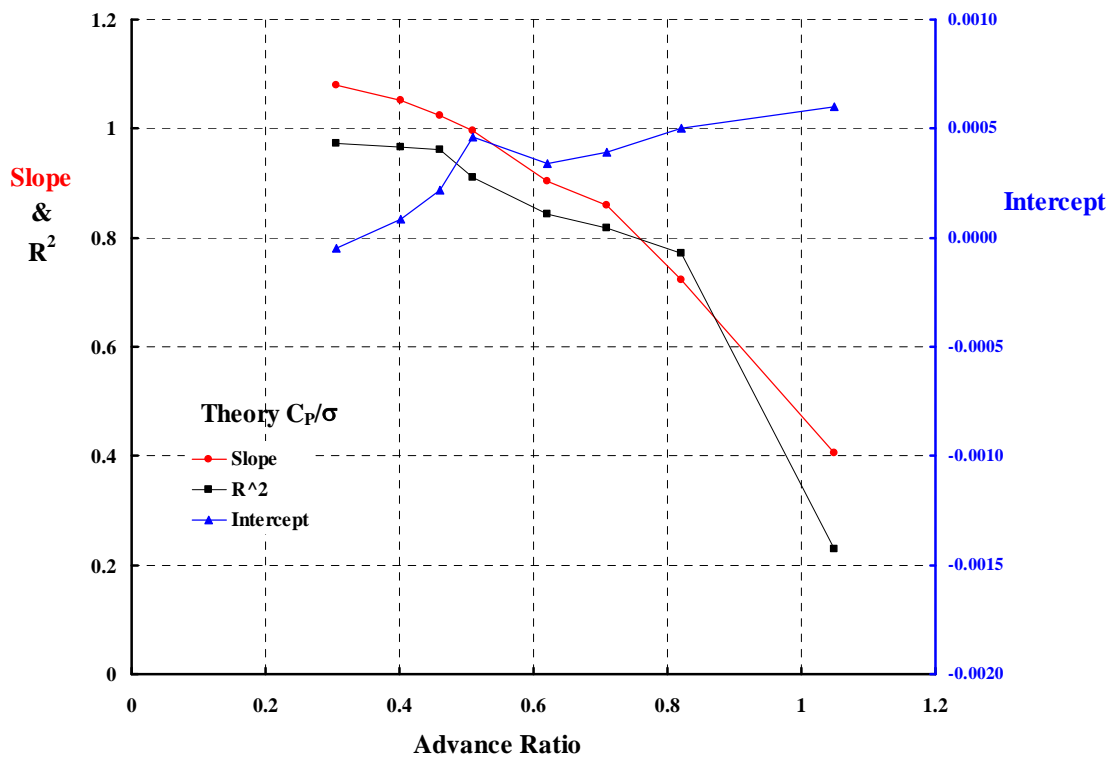
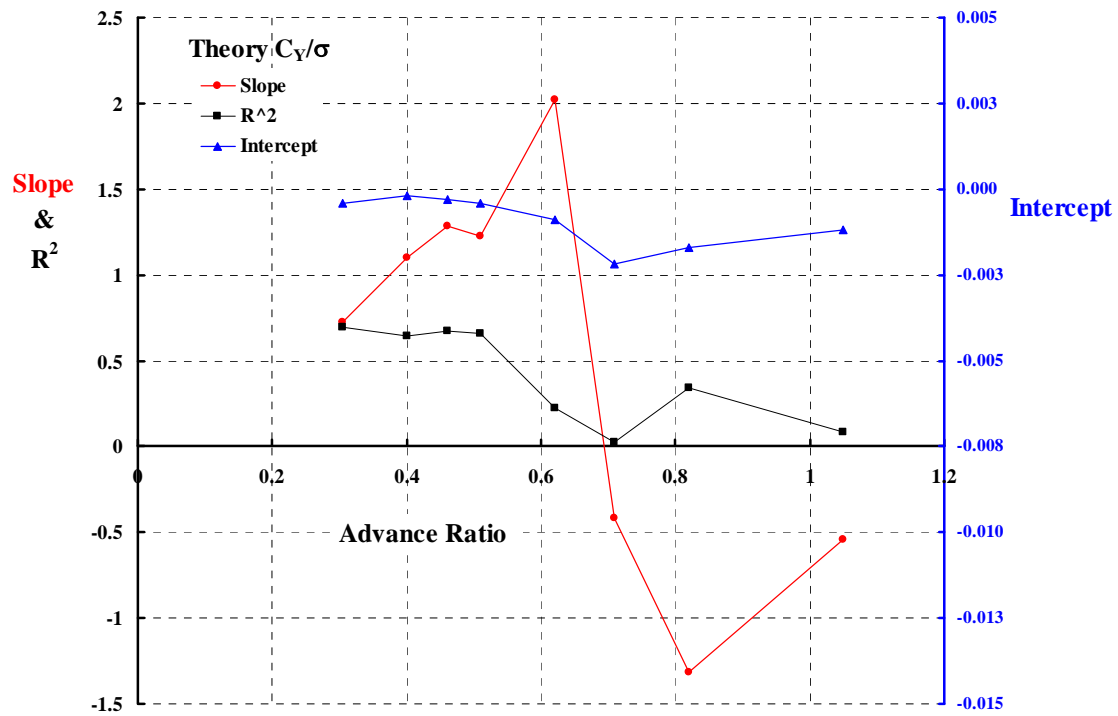
Y-Force Coefficient				Power Coefficient		
Mu	SLOPE	Intercept	R²	SLOPE	Intercept	R²
0.305	0.7234	-0.0004	0.6922	1.0801	-0.0001	0.9730
0.401	1.1026	-0.0002	0.6415	1.0510	0.0001	0.9652
0.460	1.2810	-0.0003	0.6729	1.0235	0.0002	0.9620
0.510	1.2264	-0.0004	0.6549	0.9958	0.0005	0.9100
0.620	2.0208	-0.0009	0.2213	0.9028	0.0003	0.8442
0.710	-0.4168	-0.0022	0.0247	0.8604	0.0004	0.8176
0.820	-1.3183	-0.0017	0.3387	0.7222	0.0005	0.7723
1.050	-0.5452	-0.0012	0.0821	0.4049	0.0006	0.2303

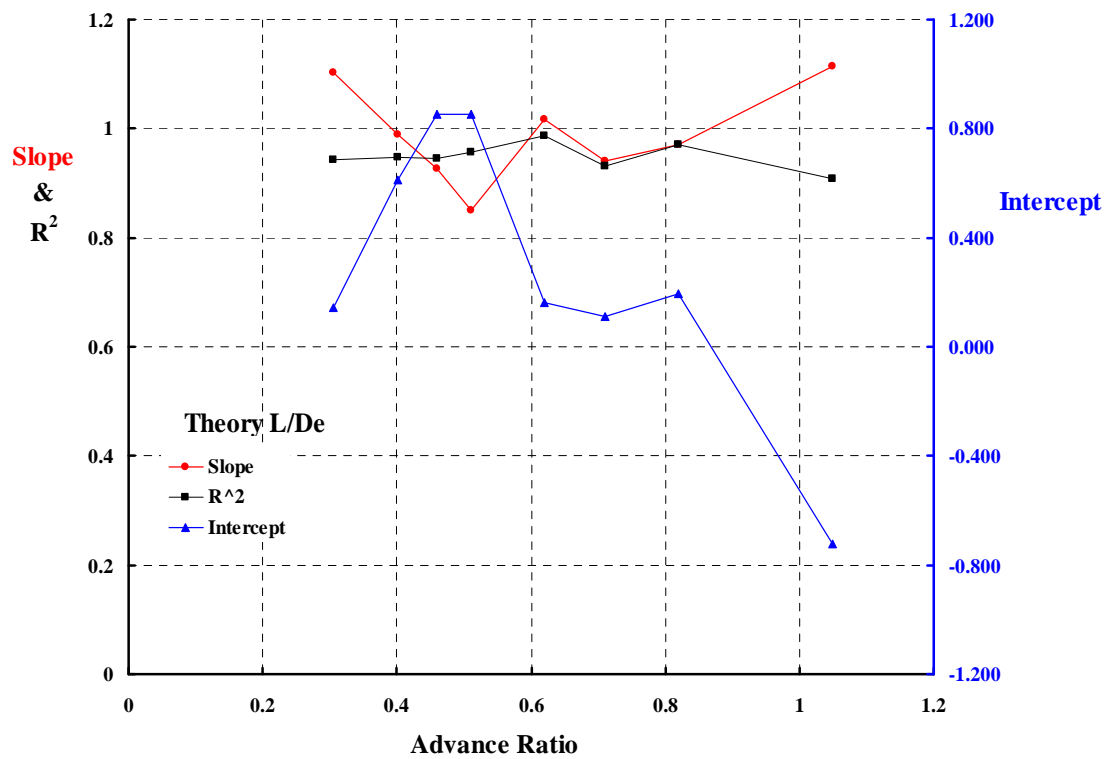
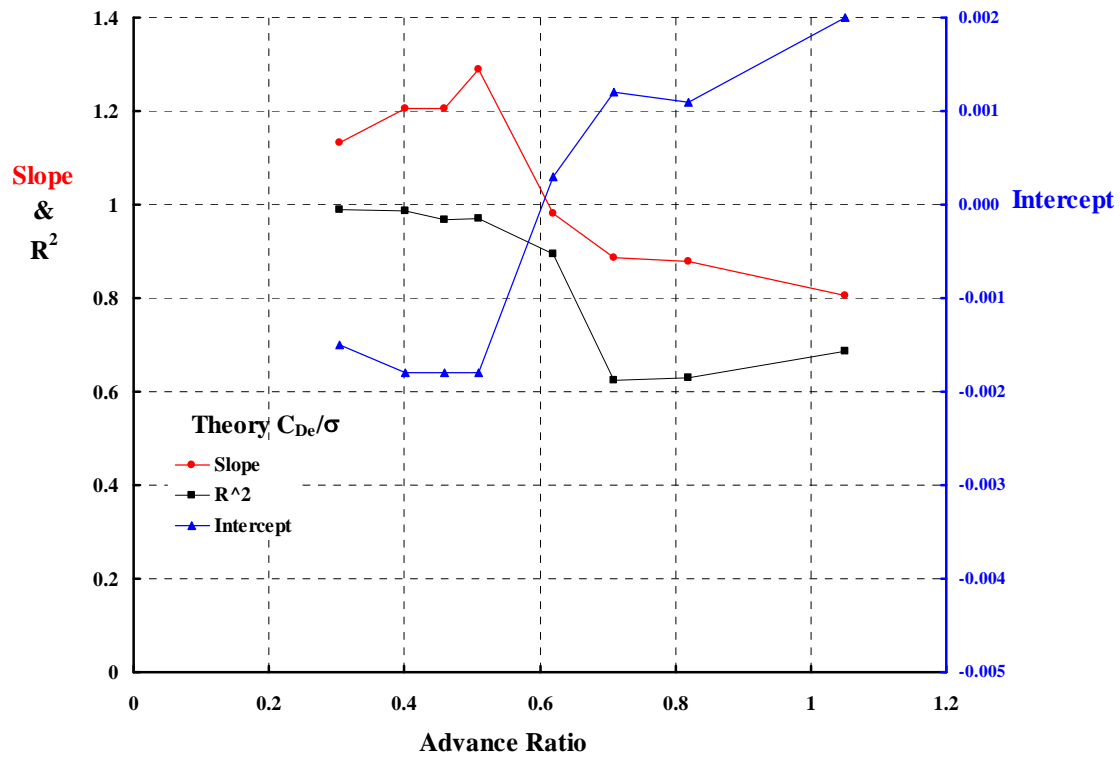
Effective Drag Coefficient				L/De		
Mu	SLOPE	Intercept	R²	SLOPE	Intercept	R²
0.305	1.1334	-0.0015	0.9883	1.1038	0.1419	0.9423
0.401	1.2052	-0.0018	0.9855	0.9888	0.6116	0.9486
0.460	1.2049	-0.0018	0.9672	0.9272	0.8511	0.9459
0.510	1.2881	-0.0018	0.9694	0.8496	0.8545	0.9562
0.620	0.9805	0.0003	0.8939	1.0160	0.1632	0.9869
0.710	0.8859	0.0012	0.6244	0.9401	0.1113	0.9308
0.820	0.8796	0.0011	0.6296	0.9716	0.1964	0.9698
1.050	0.8063	0.0020	0.6870	1.1153	-0.7249	0.9084











11.11 H-34 versus CHARM

References: 1. NASA TN D-4632, An Investigation of Full-Scale Helicopter Rotors at High Advance Ratios and Advancing Tip Mach Numbers by John McCloud III and Jim Biggers, July 1968
2. Harris EXCEL File: MASTER H-34 versus CHARM (Final July 30, 2008).xls

Airfoil	N.A.C.A. 0012
Chord	1.337 ft
Diameter	56.00 ft
Twist	0.00 deg
Disc Area	2,463 sq. ft
Reference Area (4 blades)	153.1 sq. ft
Nominal Solidity	0.062
Lock Number	8.86
Flap Moment of inertia	1264 slug ft ²
Weight Moment	2,265 lb-ft
Flap/Lag Hinge Offset	1.00 ft

Notes: 1. Wind axis data measured. Shaft axis data derived.
2. Shaft torque derived from strain cage on shaft.
3. Coefficients based on rotor tip speed and total blade area ($\sigma A = 153.1$ sq. ft.)
4. Articulated hub with coincident flap and lag hinges at $r/R = 0.0357$
5. Pitch bearing at $r/R = 0.079$

Table of CHARM Output

Advance	Collective at 0.75R	Shaft Angle of Attack	Long Cyclic	Lat Cyclic								Rotor Alone L/De
Ratio	(deg)	(deg)	(deg)	(deg)	C_L/σ	C_D/σ	C_T/σ	C_H/σ	C_Y/σ	C_Q/σ	C_{De}/σ	
0.306	-4.0	5.0	-0.25	0.51	-0.010432	0.000285	-0.010367	0.001193	0.000080	0.001530	0.005405	-1.93
0.306	-4.0	10.0	0.53	-0.15	0.016655	0.004570	0.017196	0.001609	0.000155	0.000409	0.005954	2.80
0.307	-2.0	5.0	1.23	-0.13	0.013353	0.002580	0.013527	0.001406	0.000174	0.000867	0.005481	2.44
0.305	-2.0	10.0	1.86	-0.80	0.040674	0.009086	0.041634	0.001885	-0.000052	-0.000629	0.006958	5.85
0.305	0.0	0.0	1.76	-0.24	0.008011	0.001176	0.008011	0.001176	0.000055	0.001212	0.005215	1.54
0.305	0.0	5.0	2.51	-0.91	0.037209	0.004801	0.037486	0.001540	-0.000087	0.000466	0.006360	5.85
0.303	0.0	10.0	3.36	-1.38	0.064080	0.013263	0.065409	0.001934	-0.000456	-0.001299	0.008865	7.23
0.303	2.0	-5.0	2.35	-0.25	0.003721	0.000785	0.003639	0.001106	-0.000013	0.001348	0.005294	0.70
0.305	2.0	0.0	3.15	-0.94	0.031530	0.001199	0.031530	0.001199	-0.000152	0.001443	0.006008	5.25
0.306	2.0	5.0	3.91	-1.61	0.060507	0.006851	0.060874	0.001552	-0.000561	0.000378	0.008115	7.46
0.304	2.0	10.0	4.83	-1.99	0.085848	0.016777	0.087457	0.001614	-0.001035	-0.001316	0.012322	6.97
0.300	4.0	-10.0	2.94	-0.35	-0.000496	0.001190	-0.000695	0.001086	-0.000104	0.001275	0.005506	-0.09
0.306	4.0	-5.0	3.82	-0.96	0.026859	-0.001415	0.026881	0.000931	-0.000209	0.002215	0.005997	4.48
0.304	4.0	0.0	4.62	-1.66	0.055145	0.001086	0.055145	0.001086	-0.000660	0.001943	0.007562	7.29
0.302	4.0	5.0	5.40	-2.24	0.082745	0.008461	0.083168	0.001217	-0.001150	0.000880	0.011407	7.25
0.303	4.0	10.0	6.72	-2.57	0.100710	0.018339	0.102365	0.000572	-0.002230	0.000407	0.019716	5.11
0.303	6.0	-10.0	4.37	-1.02	0.022146	-0.003125	0.022352	0.000768	-0.000169	0.002789	0.006315	3.51
0.304	6.0	-5.0	5.28	-1.69	0.049561	-0.003667	0.049692	0.000667	-0.000726	0.003349	0.007540	6.57
0.304	6.0	0.0	6.17	-2.26	0.077617	0.000715	0.077617	0.000715	-0.001300	0.002932	0.010487	7.40
0.307	6.0	5.0	7.29	-2.89	0.098385	0.008812	0.098779	0.000204	-0.002437	0.002919	0.018581	5.30
0.305	6.0	10.0	8.93	-3.17	0.108658	0.018819	0.110275	-0.000335	-0.003241	0.003095	0.029296	3.71
0.305	8.0	-10.0	5.88	-1.70	0.044860	-0.007530	0.045486	0.000375	-0.000618	0.004591	0.008009	5.60
0.305	8.0	-5.0	6.83	-2.35	0.071704	-0.006063	0.071959	0.000210	-0.001571	0.004895	0.010317	6.95
0.304	8.0	0.0	8.07	-3.02	0.092003	-0.000198	0.092003	-0.000198	-0.002528	0.005336	0.017589	5.23
0.304	8.0	5.0	9.57	-3.50	0.105649	0.008399	0.105979	-0.000840	-0.003298	0.005787	0.027762	3.81
0.305	8.0	10.0	11.17	-3.78	0.113830	0.019024	0.115404	-0.001032	-0.004309	0.006112	0.039712	2.87
0.304	10.0	-10.0	7.44	-2.33	0.068091	-0.012266	0.069186	-0.000255	-0.001428	0.006858	0.010946	6.22

0.304	10.0	-5.0	8.78	-3.11	0.086923	-0.008396	0.087324	-0.000788	-0.002855	0.007603	0.017045	5.10
0.305	10.0	0.0	10.28	-3.68	0.099842	-0.001125	0.099842	-0.001125	-0.003312	0.008254	0.026389	3.78
0.304	10.0	5.0	11.81	-4.17	0.110072	0.008084	0.110358	-0.001541	-0.004326	0.008972	0.038106	2.89
0.304	11.0	-10.0	8.20	-2.73	0.077064	-0.014329	0.078381	-0.000729	-0.002166	0.008362	0.013975	5.51
0.305	11.0	-5.0	9.89	-3.41	0.091276	-0.009235	0.091733	-0.001244	-0.003221	0.009180	0.021482	4.25
0.399	-4.0	5.0	0.69	0.27	0.002646	0.002375	0.002842	0.002135	0.000345	0.001239	0.005485	0.48
0.402	-4.0	10.0	1.92	-0.58	0.035256	0.009105	0.036301	0.002845	0.000538	-0.000689	0.007356	4.79
0.400	-2.0	5.0	2.36	-0.47	0.022988	0.004544	0.023297	0.002523	0.000475	0.000610	0.006075	3.78
0.400	-2.0	10.0	3.60	-1.23	0.054700	0.012748	0.056083	0.003056	0.000360	-0.001553	0.008805	6.21
0.402	0.0	0.0	2.82	-0.30	0.008428	0.001850	0.008428	0.001850	0.000078	0.001319	0.005148	1.64
0.399	0.0	5.0	4.07	-1.17	0.042825	0.006495	0.043228	0.002738	0.000371	0.000260	0.007148	5.99
0.401	0.0	10.0	5.40	-1.88	0.072308	0.015759	0.073946	0.002963	-0.000133	-0.001728	0.011372	6.36
0.402	2.0	0.0	4.48	-1.04	0.028821	0.001999	0.028821	0.001999	0.000054	0.001528	0.005819	4.95
0.403	2.0	5.0	5.85	-1.83	0.062407	0.008180	0.062883	0.002710	0.000049	0.000286	0.008897	7.01
0.401	4.0	-5.0	4.86	-0.93	0.014343	0.000159	0.014274	0.001409	-0.000160	0.002135	0.005160	2.60
0.401	4.0	0.0	6.19	-1.79	0.048618	0.002044	0.048618	0.002044	-0.000206	0.002015	0.007081	6.87
0.399	4.0	5.0	7.79	-2.51	0.077282	0.009070	0.077779	0.002300	-0.001013	0.001544	0.012943	5.97
0.402	6.0	-10.0	5.24	-0.84	0.001763	0.000979	0.001566	0.001270	-0.000328	0.001859	0.005699	0.31
0.401	6.0	-5.0	6.62	-1.67	0.034186	-0.001885	0.034220	0.001101	-0.000548	0.003267	0.006313	5.42
0.401	6.0	0.0	8.11	-2.45	0.065904	0.001793	0.065904	0.001793	-0.000933	0.003210	0.009819	6.71
0.402	6.0	5.0	10.02	-3.20	0.086068	0.009533	0.086571	0.001996	-0.002157	0.003705	0.018832	4.57
0.403	8.0	-10.0	6.98	-1.56	0.021244	-0.003095	0.021459	0.000641	-0.000422	0.003760	0.006451	3.29
0.402	8.0	-5.0	8.38	-2.36	0.054126	-0.003946	0.054264	0.000786	-0.001197	0.004740	0.007948	6.81
0.403	8.0	0.0	10.18	-3.18	0.077543	0.001452	0.077543	0.001452	-0.002187	0.005439	0.015049	5.15
0.401	8.0	5.0	12.25	-3.97	0.092064	0.010171	0.092600	0.002109	-0.003250	0.006335	0.026069	3.53
0.404	10.0	-10.0	8.74	-2.27	0.040438	-0.007076	0.041052	0.000053	-0.000922	0.005871	0.007826	5.17
0.401	10.0	-5.0	10.32	-3.10	0.068899	-0.005591	0.069124	0.000435	-0.002417	0.007132	0.012308	5.60
0.401	9.0	5.0	13.43	-4.30	0.094135	0.010374	0.094681	0.002130	-0.003670	0.007710	0.029723	3.17
0.403	9.5	0.0	11.68	-3.73	0.081799	0.001226	0.081799	0.001226	-0.002956	0.007179	0.019173	4.27
0.401	11.0	-10.0	9.61	-2.60	0.050420	-0.009126	0.051239	-0.000232	-0.001390	0.007173	0.009083	5.55
0.458	-4.0	5.0	0.74	0.22	0.006237	0.003522	0.006520	0.002965	0.000594	0.001210	0.006162	1.01
0.460	-4.0	10.0	2.30	-0.73	0.040880	0.010956	0.042161	0.003691	0.000922	-0.000975	0.008803	4.64
0.460	-2.0	5.0	2.63	-0.49	0.023839	0.005527	0.024230	0.003429	0.000816	0.000607	0.006852	3.48

0.462	-2.0	10.0	4.20	-1.35	0.057593	0.014229	0.059188	0.004012	0.000811	-0.001709	0.010456	5.51
0.467	0.0	0.0	2.84	-0.23	0.005037	0.002389	0.005037	0.002389	0.000173	0.001372	0.005372	0.94
0.461	0.0	5.0	4.46	-1.25	0.041459	0.007339	0.041941	0.003698	0.000801	0.000269	0.007925	5.23
0.461	0.0	10.0	6.18	-2.02	0.071953	0.016755	0.073769	0.004006	0.000200	-0.001606	0.013210	5.45
0.459	2.0	0.0	4.69	-0.98	0.022620	0.002648	0.022620	0.002648	0.000301	0.001551	0.006020	3.76
0.460	2.0	5.0	6.46	-1.85	0.057687	0.008785	0.058233	0.003723	0.000673	0.000333	0.009511	6.07
0.461	2.0	10.0	8.41	-2.60	0.082563	0.018664	0.084549	0.004044	-0.000969	-0.000371	0.017845	4.63
0.458	4.0	-5.0	4.96	-0.70	0.005406	0.001474	0.005257	0.001940	-0.000105	0.001852	0.005515	0.98
0.461	4.0	0.0	6.59	-1.66	0.040301	0.002852	0.040301	0.002852	0.000258	0.001979	0.007155	5.63
0.460	4.0	5.0	8.54	-2.52	0.070615	0.009810	0.071201	0.003618	-0.000318	0.001465	0.013007	5.43
0.456	6.0	-5.0	6.87	-1.44	0.022128	-0.000402	0.022079	0.001528	-0.000338	0.002926	0.005984	3.70
0.458	6.0	0.0	8.47	-2.44	0.056127	0.002857	0.056127	0.002857	-0.000239	0.002942	0.009254	6.07
0.462	6.0	5.0	10.77	-3.24	0.078787	0.010625	0.079413	0.003718	-0.001555	0.003376	0.017993	4.38
0.456	8.0	-10.0	7.09	-1.22	0.005372	0.000237	0.005249	0.001166	-0.000401	0.002681	0.006156	0.87
0.455	8.0	-5.0	8.78	-2.19	0.038986	-0.002248	0.039033	0.001158	-0.000856	0.004191	0.006898	5.65
0.458	8.0	0.0	10.70	-3.14	0.066311	0.002845	0.066311	0.002845	-0.001334	0.004770	0.013215	5.02
0.462	8.0	5.0	13.06	-3.98	0.085033	0.011635	0.085724	0.004179	-0.002827	0.005768	0.024221	3.51
0.456	10.0	-10.0	8.98	-1.91	0.023457	-0.003583	0.023723	0.000545	-0.000608	0.004750	0.006904	3.40
0.459	10.0	-5.0	10.76	-2.96	0.053813	-0.003768	0.053937	0.000936	-0.001812	0.006024	0.009376	5.74
0.457	10.0	0.0	12.89	-4.02	0.073960	0.003122	0.073960	0.003122	-0.002831	0.007248	0.018880	3.92
0.456	12.0	-10.0	10.66	-2.62	0.037398	-0.006729	0.037999	-0.000132	-0.001095	0.006688	0.008034	4.66
0.508	-4.0	5.0	0.85	0.13	0.009327	0.004346	0.009670	0.003517	0.000840	0.001168	0.006691	1.39
0.507	-4.0	10.0	2.62	-0.87	0.044983	0.012275	0.046432	0.004277	0.001213	-0.001090	0.010062	4.47
0.506	-2.0	2.0	1.70	0.05	0.002870	0.003161	0.002979	0.003059	0.000408	0.001341	0.005844	0.49
0.507	-2.0	5.0	2.81	-0.57	0.025612	0.006268	0.026061	0.004012	0.001105	0.000599	0.007470	3.43
0.509	-2.0	10.0	4.60	-1.52	0.059779	0.015265	0.061522	0.004653	0.001098	-0.001674	0.011866	5.04
0.498	0.0	-3.0	1.74	0.37	-0.017645	0.003549	-0.017806	0.002621	-0.000258	0.000980	0.005512	-3.20
0.507	0.0	2.0	3.73	-0.61	0.019007	0.004289	0.019145	0.003623	0.000812	0.001184	0.006659	2.85
0.509	0.0	5.0	4.78	-1.27	0.040878	0.007943	0.041415	0.004350	0.001191	0.000322	0.008589	4.76
0.508	0.0	10.0	6.72	-2.11	0.072434	0.017734	0.074413	0.004887	0.000365	-0.001382	0.014927	4.85
0.502	2.0	-3.0	3.77	-0.31	-0.000865	0.002606	-0.001001	0.002558	-0.000053	0.001473	0.005556	-0.16
0.509	2.0	2.0	5.65	-1.35	0.035316	0.005239	0.035477	0.004003	0.000895	0.001236	0.007711	4.58
0.509	2.0	5.0	6.80	-1.94	0.055787	0.009421	0.056395	0.004523	0.001017	0.000416	0.010255	5.44

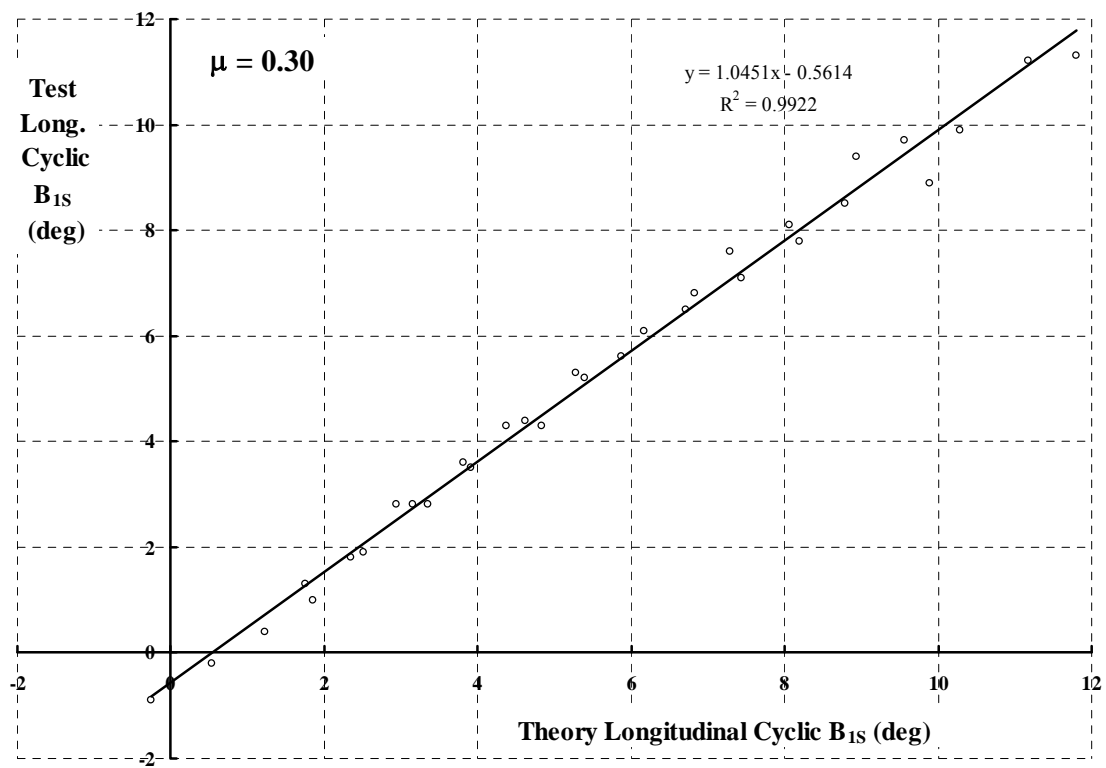
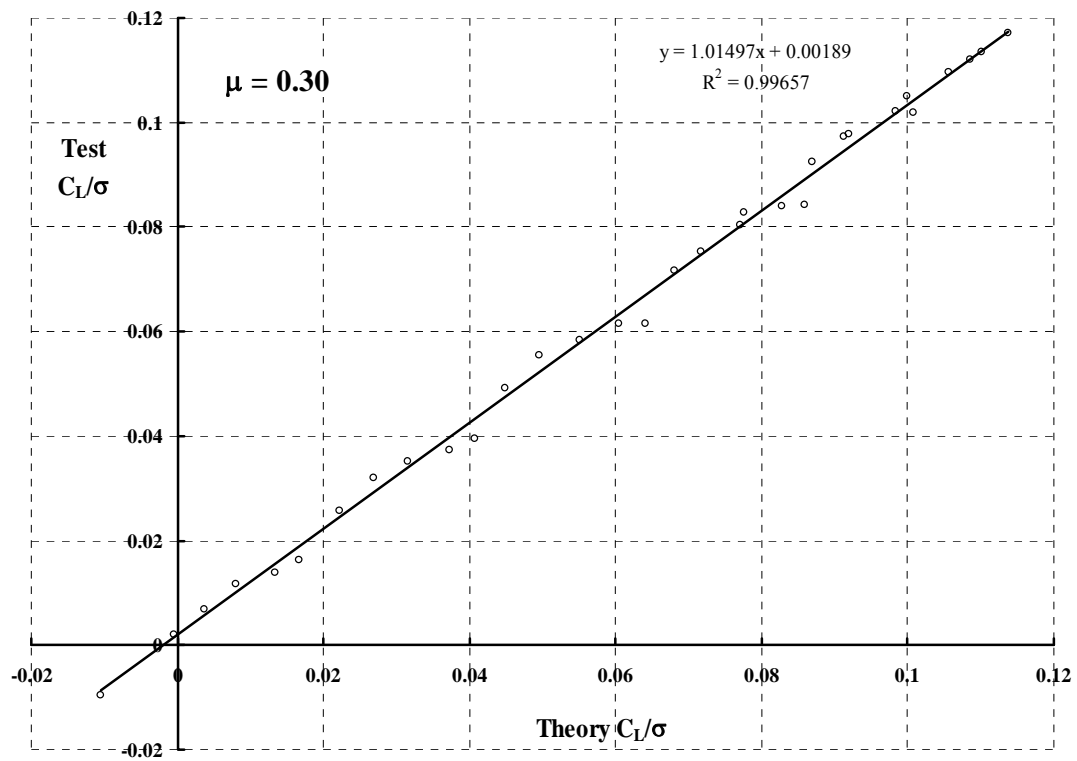
0.509	2.0	10.0	8.95	-2.76	0.081775	0.019786	0.083968	0.005286	-0.001029	-0.000075	0.019635	4.17
0.502	4.0	-5.0	5.01	-0.60	0.000654	0.002280	0.000453	0.002329	-0.000134	0.001707	0.005707	0.12
0.507	4.0	-3.0	5.76	-1.04	0.014047	0.001580	0.013945	0.002313	-0.000165	0.002104	0.005794	2.42
0.513	4.0	2.0	7.70	-2.03	0.050065	0.006012	0.050245	0.004261	0.000814	0.001648	0.009311	5.38
0.506	4.0	5.0	8.97	-2.59	0.067183	0.010507	0.067844	0.004612	0.000084	0.001536	0.013591	4.94
0.508	4.0	10.0	11.23	-3.46	0.088545	0.021605	0.090952	0.005901	-0.002388	0.001774	0.025206	3.51
0.499	6.0	-5.0	6.96	-1.34	0.015557	0.000571	0.015448	0.001925	-0.000292	0.002738	0.006068	2.56
0.505	6.0	-3.0	7.76	-1.72	0.030115	0.000482	0.030049	0.002058	-0.000470	0.002941	0.006373	4.73
0.511	6.0	2.0	9.86	-2.71	0.061807	0.006413	0.061993	0.004252	-0.000084	0.002956	0.012328	5.01
0.507	6.0	5.0	11.25	-3.30	0.074862	0.011602	0.075588	0.005033	-0.001242	0.003375	0.018377	4.07
0.507	6.0	10.0	13.42	-4.31	0.094825	0.023812	0.097520	0.006984	-0.004115	0.004052	0.032042	2.96
0.496	8.0	-10.0	7.08	-1.03	-0.002787	0.002068	-0.003104	0.001553	-0.000546	0.002090	0.006313	-0.44
0.502	8.0	-5.0	9.00	-2.04	0.031097	-0.001165	0.031080	0.001550	-0.000666	0.003964	0.006793	4.58
0.508	8.0	-3.0	9.77	-2.47	0.044713	0.000061	0.044649	0.002401	-0.000567	0.004142	0.008357	5.35
0.510	8.0	2.0	12.14	-3.42	0.069761	0.007224	0.069970	0.004785	-0.001554	0.005038	0.017306	4.03
0.509	8.0	5.0	13.55	-4.07	0.080795	0.013199	0.081638	0.006107	-0.002781	0.005698	0.024638	3.28
0.498	10.0	-10.0	9.07	-1.75	0.012648	-0.001319	0.012685	0.000898	-0.000572	0.004031	0.006868	1.84
0.502	10.0	-5.0	11.01	-2.78	0.045579	-0.002887	0.045657	0.001096	-0.001638	0.005621	0.008398	5.43
0.508	10.0	-3.0	11.98	-3.16	0.055696	-0.000212	0.055631	0.002703	-0.001405	0.006097	0.011998	4.64
0.514	10.0	2.0	14.45	-4.29	0.074553	0.008616	0.074808	0.006009	-0.003206	0.007496	0.023618	3.16
0.495	12.0	-10.0	10.80	-2.43	0.026194	-0.004416	0.026563	0.000200	-0.000927	0.005941	0.007649	3.43
0.498	12.0	-5.0	12.97	-3.49	0.053819	-0.003645	0.053932	0.001060	-0.002734	0.007625	0.011664	4.61
0.500	13.0	-10.0	11.79	-2.76	0.033538	-0.006074	0.034083	-0.000158	-0.001395	0.007219	0.008587	3.91
0.624	-4.0	4.0	-0.35	0.34	0.009025	0.005744	0.009404	0.005100	0.001145	0.001499	0.008168	1.11
0.618	-4.0	8.0	1.46	-0.70	0.040850	0.011715	0.042083	0.005915	0.002084	0.000171	0.011993	3.41
0.624	-2.0	4.0	1.84	-0.33	0.020778	0.007258	0.021234	0.005791	0.001592	0.001058	0.008969	2.32
0.620	-2.0	8.0	3.67	-1.31	0.051756	0.014067	0.053210	0.006728	0.002311	-0.000288	0.013598	3.81
0.618	0.0	0.0	2.10	0.08	-0.000617	0.003940	-0.000617	0.003940	0.000227	0.001503	0.006365	-0.10
0.622	0.0	4.0	4.02	-1.00	0.031484	0.008526	0.032002	0.006309	0.001985	0.000867	0.009929	3.17
0.618	0.0	8.0	5.87	-1.95	0.061825	0.016457	0.063514	0.007693	0.002003	-0.000317	0.015941	3.88
0.618	2.0	-4.0	2.32	0.34	-0.018595	0.005115	-0.018906	0.003805	-0.000255	0.000834	0.006463	-2.88
0.619	2.0	0.0	4.29	-0.58	0.010614	0.004930	0.010614	0.004930	0.000815	0.001566	0.007455	1.42
0.620	2.0	4.0	6.20	-1.66	0.042914	0.009923	0.043502	0.006905	0.002287	0.000885	0.011354	3.78

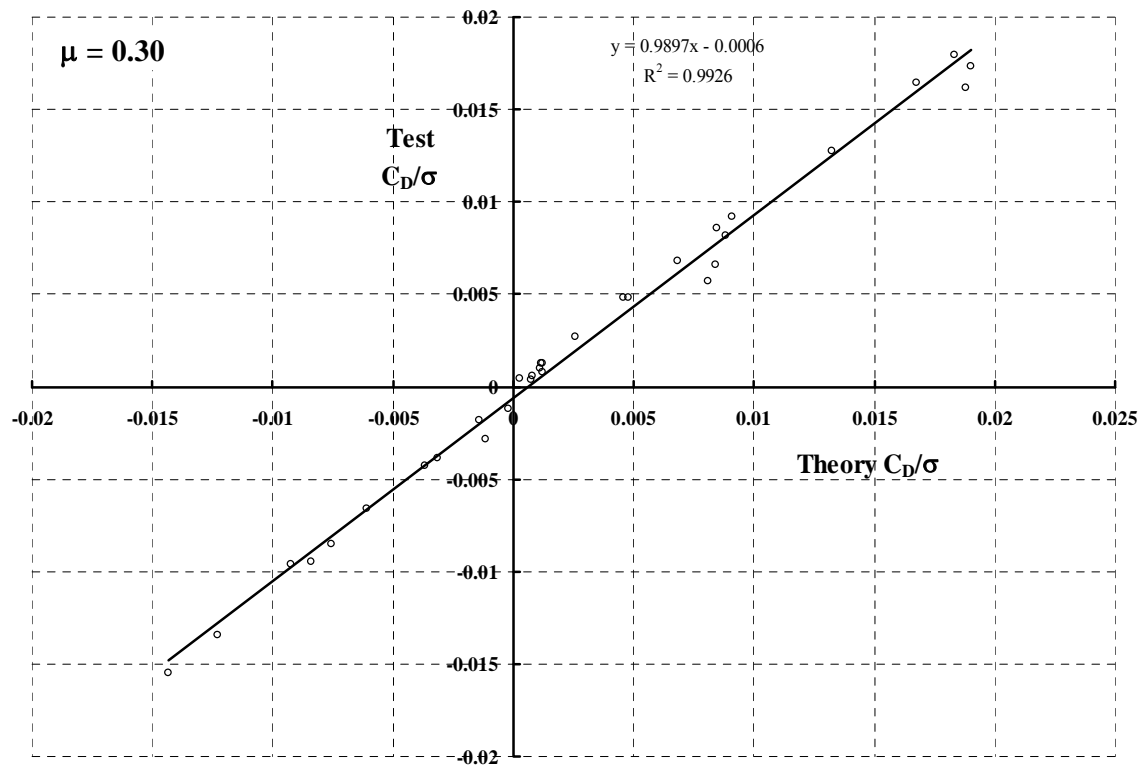
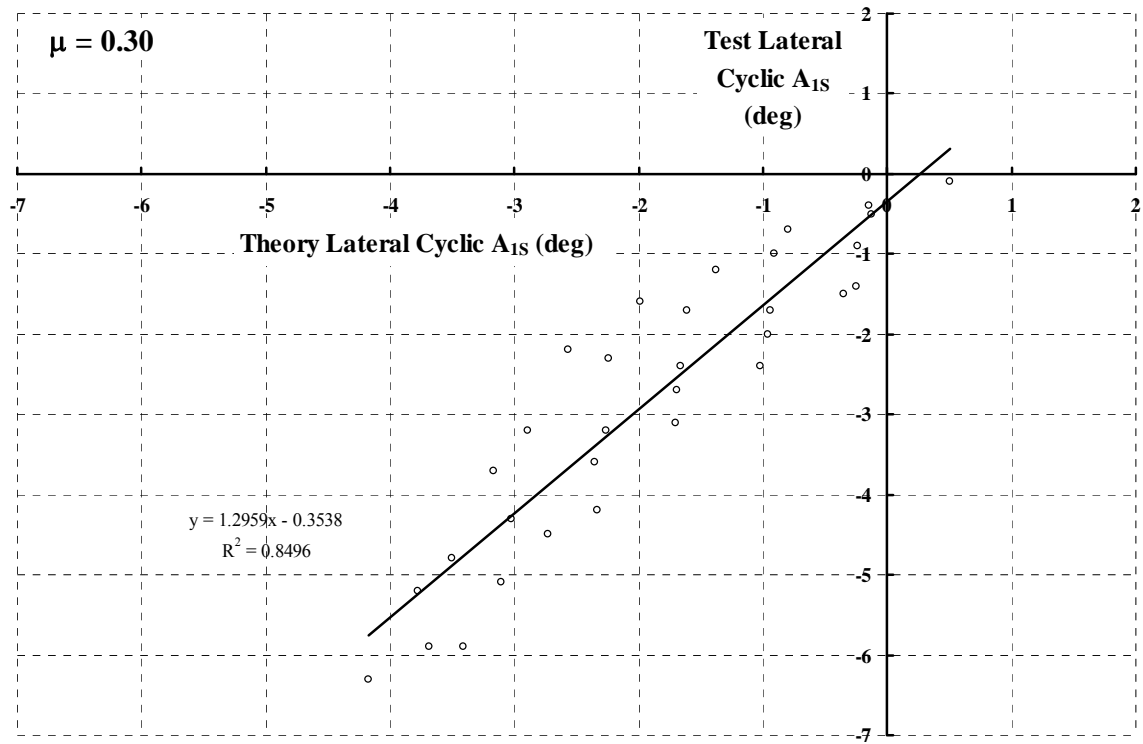
0.619	2.0	8.0	8.12	-2.57	0.069729	0.018422	0.071614	0.008538	0.001105	0.000335	0.018968	3.68
0.619	4.0	-4.0	4.51	-0.30	-0.007268	0.004163	-0.007541	0.003646	-0.000003	0.001433	0.006479	-1.12
0.621	4.0	0.0	6.42	-1.33	0.023213	0.006517	0.023213	0.006517	0.001621	0.001697	0.009254	2.51
0.621	4.0	4.0	8.41	-2.29	0.052795	0.011350	0.053458	0.007640	0.002218	0.001281	0.013422	3.93
0.619	4.0	8.0	10.40	-3.22	0.077108	0.021077	0.079291	0.010141	-0.000606	0.001658	0.023779	3.24
0.613	6.0	-8.0	4.74	-0.05	-0.025685	0.006635	-0.026358	0.002996	-0.000643	0.000175	0.006919	-3.71
0.610	6.0	-4.0	6.72	-0.93	0.003335	0.003178	0.003106	0.003403	0.000040	0.002167	0.006682	0.50
0.624	6.0	0.0	8.64	-1.95	0.034375	0.007518	0.034375	0.007518	0.002092	0.002116	0.010931	3.15
0.634	6.0	4.0	10.67	-2.95	0.060382	0.013109	0.061149	0.008865	0.001010	0.002542	0.017219	3.51
0.624	6.0	4.0	10.67	-2.95	0.060382	0.013109	0.061149	0.008865	0.001010	0.002542	0.017219	3.51
0.614	8.0	-8.0	6.93	-0.70	-0.013996	0.004629	-0.014504	0.002636	-0.000280	0.001479	0.007038	-1.99
0.619	8.0	-4.0	8.88	-1.60	0.014901	0.002172	0.014713	0.003206	-0.000090	0.003049	0.007101	2.10
0.621	8.0	4.0	13.02	-3.56	0.065801	0.015247	0.066704	0.010620	-0.000757	0.004345	0.022273	2.95
0.621	10.0	-8.0	9.10	-1.35	-0.002370	0.002549	-0.002702	0.002194	-0.000126	0.002943	0.007342	-0.32
0.620	10.0	-4.0	11.07	-2.26	0.025156	0.001268	0.025006	0.003020	-0.000555	0.004140	0.007961	3.16
0.619	12.0	-8.0	11.11	-1.98	0.007194	0.000724	0.007024	0.001718	-0.000286	0.004386	0.007868	0.91
0.711	-4.0	2.0	-1.79	0.80	0.001336	0.005705	-0.001136	0.005748	0.000492	0.001810	0.008256	-0.16
0.708	-4.0	4.0	-0.76	0.17	0.016451	0.008018	0.016970	0.006851	0.001674	0.001557	0.010216	1.61
0.708	-4.0	6.0	0.26	-0.46	0.034374	0.011053	0.035341	0.007399	0.002409	0.001118	0.012636	2.72
0.706	-4.0	8.0	1.28	-1.06	0.051576	0.014956	0.053156	0.007633	0.002882	0.000562	0.015756	3.27
0.710	-2.0	2.0	0.49	0.17	0.007905	0.007267	0.008153	0.006987	0.001439	0.001466	0.009333	0.85
0.711	-2.0	4.0	1.52	-0.46	0.025665	0.009529	0.026268	0.007715	0.002162	0.001157	0.011163	2.30
0.709	-2.0	6.0	2.54	-1.07	0.043274	0.013084	0.044404	0.008489	0.002804	0.000723	0.014108	3.07
0.708	-2.0	8.0	3.57	-1.64	0.059869	0.017311	0.061696	0.008810	0.003111	0.000237	0.017648	3.39
0.710	0.0	0.0	1.66	0.18	-0.001968	0.004967	-0.001968	0.004967	0.000233	0.001603	0.007225	-0.27
0.712	0.0	2.0	2.74	-0.48	0.017166	0.008703	0.017459	0.008099	0.002110	0.001271	0.010494	1.64
0.710	0.0	4.0	3.80	-1.07	0.033783	0.010821	0.034456	0.008438	0.002684	0.001028	0.012273	2.75
0.708	0.0	6.0	4.81	-1.68	0.050953	0.014845	0.052226	0.009438	0.003187	0.000601	0.015697	3.25
0.707	0.0	8.0	5.85	-2.24	0.067567	0.019660	0.069645	0.010065	0.002741	0.000286	0.020067	3.37
0.710	2.0	0.0	3.93	-0.44	0.007108	0.006299	0.007108	0.006299	0.001068	0.001583	0.008528	0.83
0.711	2.0	2.0	5.01	-1.10	0.025582	0.009706	0.025905	0.008808	0.002525	0.001288	0.011522	2.22
0.709	2.0	4.0	6.07	-1.67	0.041901	0.012235	0.042653	0.009282	0.003179	0.001053	0.013721	3.05
0.708	2.0	6.0	7.10	-2.28	0.058276	0.016705	0.059703	0.010522	0.003092	0.000839	0.017894	3.26

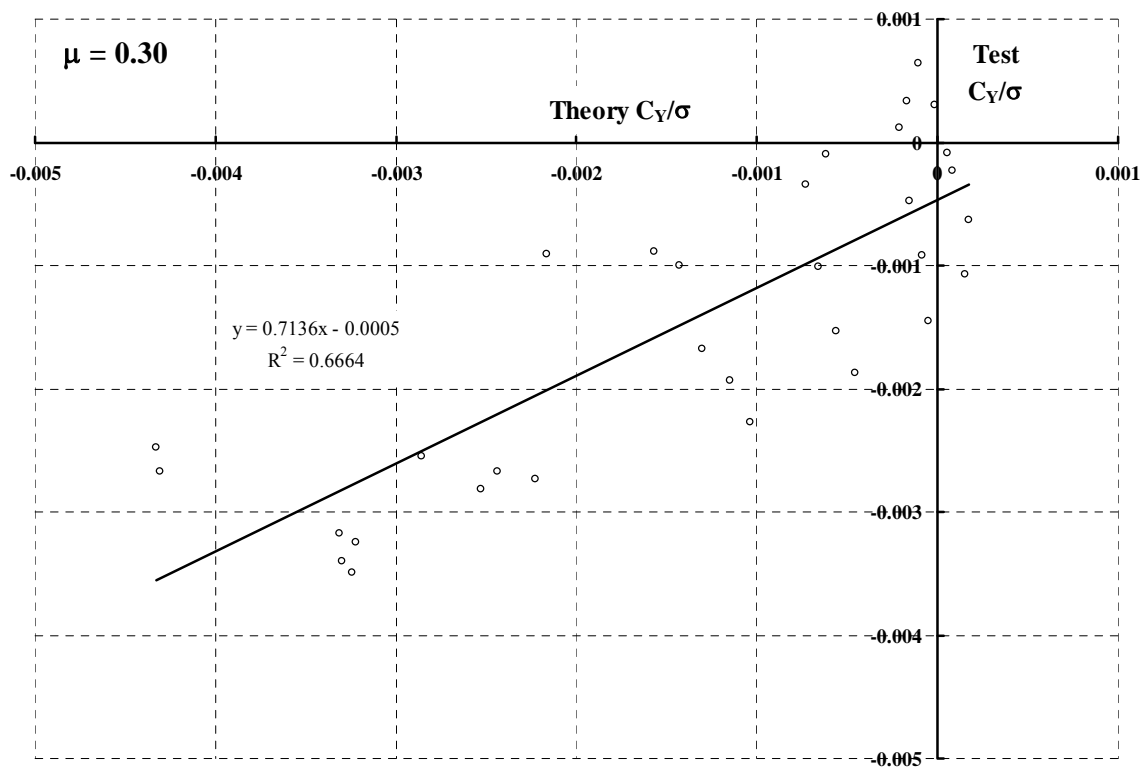
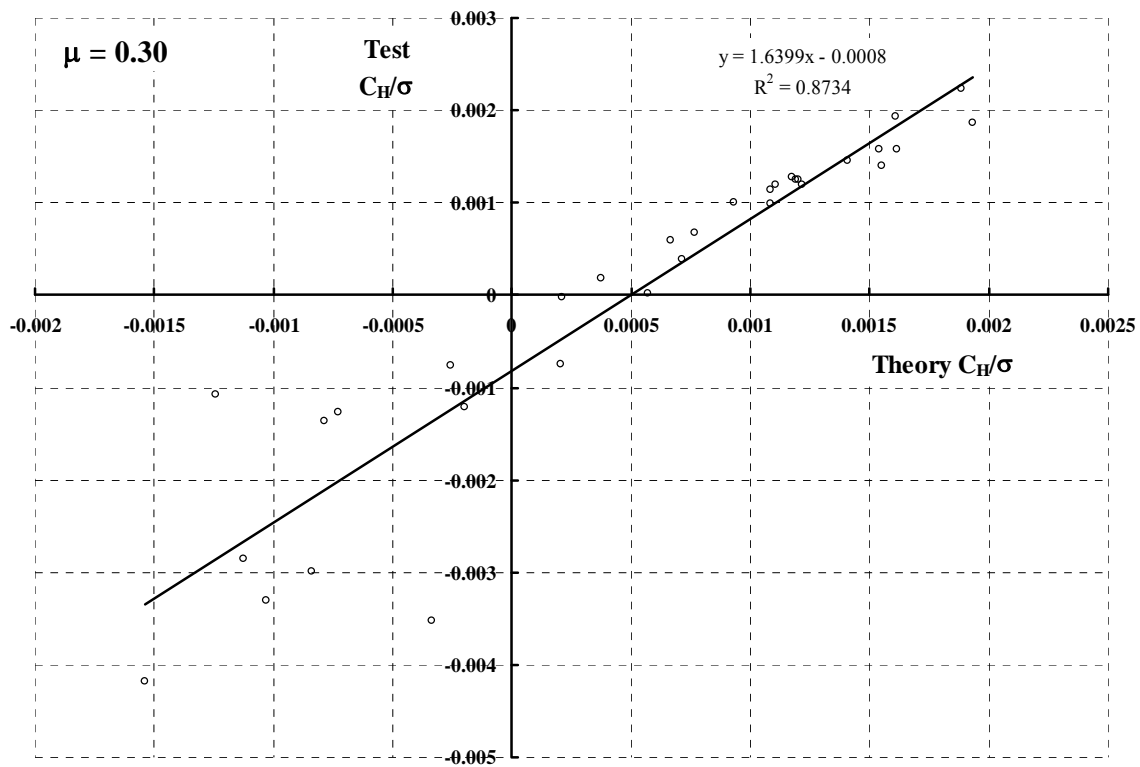
0.714	2.0	8.0	8.13	-2.87	0.073915	0.022098	0.076271	0.011596	0.001737	0.000869	0.023335	3.17
0.706	4.0	-2.0	5.10	-0.49	-0.001041	0.005175	-0.001221	0.005136	0.000201	0.001700	0.007572	-0.14
0.706	4.0	0.0	6.17	-1.09	0.016933	0.008829	0.016933	0.008829	0.002291	0.001560	0.011027	1.54
0.711	4.0	2.0	7.28	-1.70	0.033450	0.010513	0.033797	0.009340	0.002594	0.001523	0.012660	2.64
0.709	4.0	4.0	8.33	-2.29	0.049788	0.014068	0.050648	0.010561	0.003210	0.001371	0.016004	3.11
0.706	4.0	6.0	9.41	-2.87	0.064691	0.019270	0.066351	0.012403	0.001957	0.001650	0.021607	2.99
0.695	6.0	-4.0	6.26	-0.58	-0.007737	0.005305	-0.008088	0.004752	0.000199	0.001758	0.007787	-0.99
0.705	6.0	-2.0	7.35	-1.10	0.006988	0.004809	0.006816	0.005050	0.000226	0.002074	0.007732	0.90
0.707	6.0	0.0	8.43	-1.68	0.025882	0.010324	0.025882	0.010324	0.002886	0.001752	0.012792	2.02
0.711	6.0	2.0	9.58	-2.25	0.040601	0.011937	0.040993	0.010512	0.002980	0.001949	0.014683	2.77
0.709	6.0	4.0	10.66	-2.88	0.055407	0.016545	0.056426	0.012640	0.002040	0.002427	0.019972	2.77
0.695	8.0	-4.0	8.53	-1.19	0.000857	0.004641	0.000531	0.004689	0.000308	0.002461	0.008116	0.11
0.709	8.0	-2.0	9.65	-1.64	0.014609	0.004685	0.014436	0.005192	0.000341	0.002554	0.008284	1.76
0.712	8.0	0.0	10.74	-2.24	0.033372	0.011413	0.033372	0.011413	0.003142	0.002438	0.014847	2.25
0.710	8.0	2.0	11.90	-2.88	0.046409	0.014070	0.046872	0.012442	0.001889	0.003291	0.018709	2.48
0.711	8.0	4.0	13.00	-3.49	0.060236	0.019495	0.061449	0.015246	0.000352	0.004015	0.025165	2.39
0.699	10.0	-4.0	10.81	-1.78	0.008266	0.004115	0.007959	0.004682	0.000163	0.003352	0.008848	0.93
0.716	10.0	-2.0	11.97	-2.21	0.020474	0.006650	0.020230	0.007360	0.000647	0.003781	0.011979	1.71
0.706	10.0	0.0	13.05	-2.88	0.037651	0.011901	0.037651	0.011901	0.001735	0.004209	0.017829	2.11
0.703	12.0	-4.0	12.97	-2.32	0.015249	0.004172	0.014921	0.005226	-0.000654	0.004703	0.010813	1.41
0.707	12.0	-2.0	14.20	-2.71	0.026205	0.008548	0.025891	0.009458	0.000154	0.005314	0.016037	1.63
0.706	13.7	-4.0	14.95	-2.86	0.020374	0.004553	0.020006	0.005963	-0.001849	0.006121	0.013194	1.54
0.819	-4.0	0.0	-3.52	1.40	-0.010122	0.007393	-0.010122	0.007393	-0.000182	0.001685	0.009422	-1.07
0.824	-4.0	2.0	-2.36	0.62	0.008783	0.009263	0.009101	0.008951	0.001016	0.001737	0.011358	0.77
0.829	-4.0	4.0	-1.24	-0.21	0.029547	0.012212	0.030327	0.010121	0.002555	0.001694	0.014258	2.07
0.814	-2.0	0.0	-1.16	0.90	-0.006417	0.006623	-0.006417	0.006623	-0.000095	0.001702	0.008673	-0.74
0.832	-2.0	2.0	-0.01	0.05	0.014372	0.010174	0.014718	0.009667	0.001779	0.001547	0.012039	1.19
0.830	-2.0	4.0	1.11	-0.78	0.035074	0.013562	0.035934	0.011082	0.003071	0.001395	0.015246	2.30
0.816	0.0	0.0	1.21	0.38	-0.003174	0.006501	-0.003174	0.006501	0.000275	0.001708	0.008559	-0.37
0.829	0.0	2.0	2.33	-0.50	0.019261	0.010780	0.019625	0.010101	0.002353	0.001530	0.012624	1.53
0.830	0.0	4.0	3.47	-1.33	0.040308	0.014915	0.041250	0.012067	0.003629	0.001239	0.016412	2.46
0.808	2.0	-2.0	2.26	0.43	-0.014326	0.007566	-0.014581	0.007061	0.000084	0.001339	0.009180	-1.56
0.818	2.0	0.0	3.57	-0.17	0.002122	0.009031	0.002122	0.009031	0.001275	0.001614	0.010975	0.19

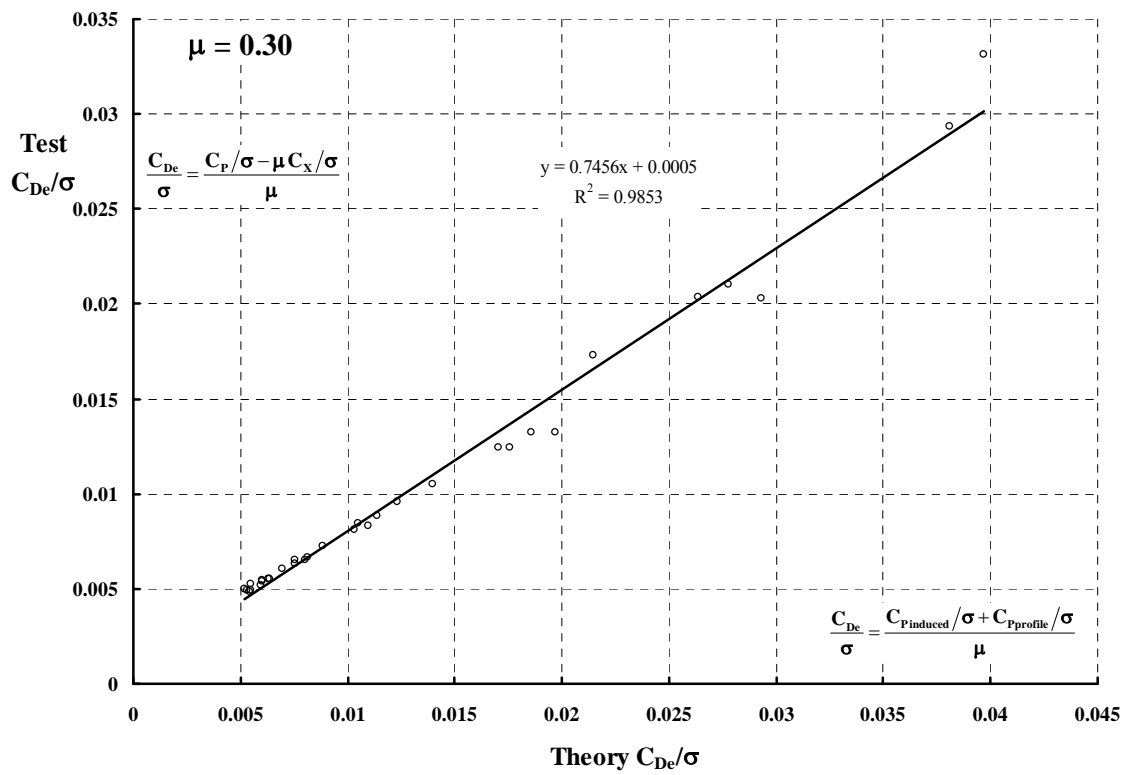
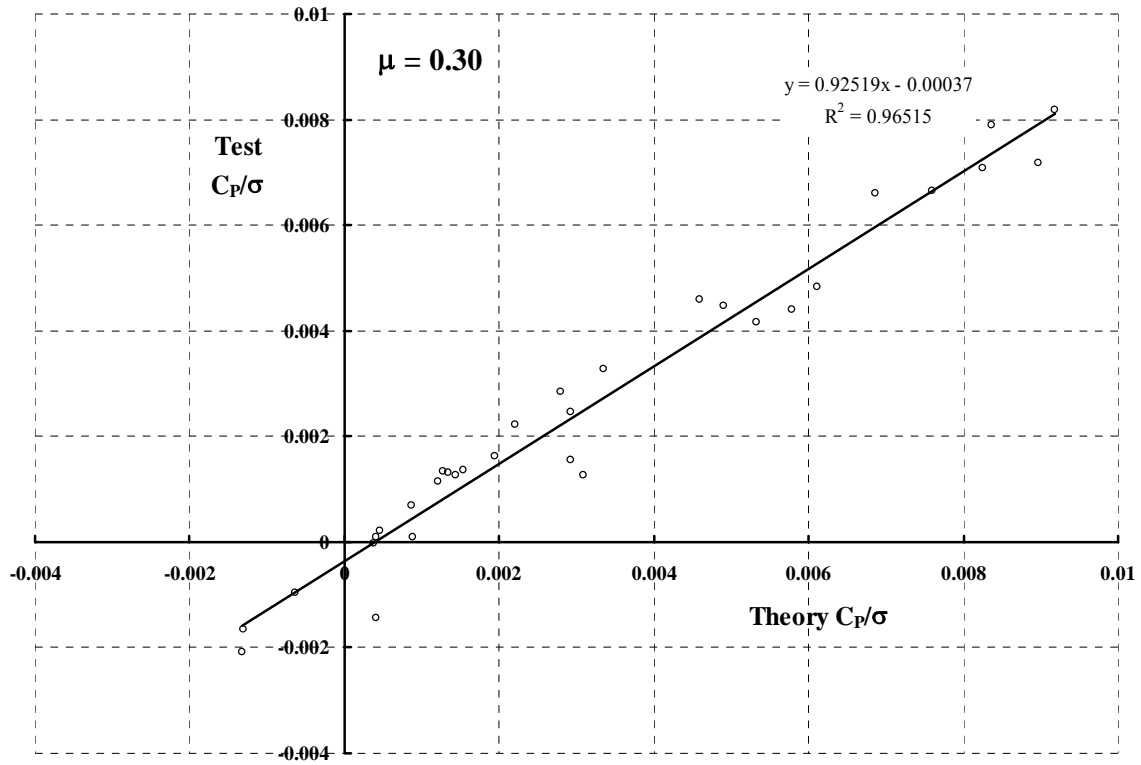
0.837	2.0	2.0	4.69	-1.02	0.023768	0.011819	0.024166	0.010982	0.003056	0.001475	0.013597	1.75
0.834	2.0	4.0	5.83	-1.87	0.044688	0.016381	0.045722	0.013223	0.004219	0.001192	0.017821	2.51
0.815	3.0	-2.0	3.45	0.17	-0.012598	0.007704	-0.012859	0.007260	0.000219	0.001401	0.009393	-1.34
0.807	4.0	-2.0	4.63	-0.10	-0.011051	0.007746	-0.011315	0.007355	0.000334	0.001514	0.009571	-1.16
0.818	4.0	0.0	5.90	-0.73	0.007810	0.012259	0.007810	0.012259	0.002624	0.001438	0.013992	0.56
0.838	4.0	2.0	7.05	-1.57	0.027456	0.013822	0.027922	0.012855	0.003465	0.001404	0.015515	1.77
0.831	4.0	4.0	8.20	-2.36	0.048387	0.018796	0.049580	0.015375	0.004237	0.001447	0.020544	2.36
0.811	5.0	-2.0	5.80	-0.36	-0.008577	0.007763	-0.008842	0.007459	0.000451	0.001629	0.009727	-0.88
0.812	6.0	-2.0	6.99	-0.59	-0.006389	0.007733	-0.006655	0.007506	0.000601	0.001741	0.009832	-0.65
0.818	6.0	0.0	8.24	-1.31	0.012116	0.013110	0.012116	0.013110	0.003383	0.001427	0.014830	0.82
0.834	6.0	2.0	9.40	-2.10	0.031916	0.016130	0.032460	0.015007	0.003970	0.001609	0.018070	1.77
0.831	6.0	4.0	10.59	-2.87	0.050905	0.022441	0.052347	0.018835	0.003016	0.002386	0.025323	2.01
0.799	7.0	-2.0	8.16	-0.90	-0.005044	0.007677	-0.005309	0.007497	0.000765	0.001884	0.009949	-0.51
0.815	8.0	-2.0	9.34	-1.13	-0.002426	0.007823	-0.002698	0.007733	0.000968	0.001990	0.010221	-0.24
0.820	8.0	0.0	10.63	-1.76	0.014503	0.013885	0.014503	0.013885	0.003404	0.002123	0.016444	0.88
0.833	8.0	2.0	11.80	-2.61	0.034815	0.019222	0.035465	0.017995	0.003186	0.002703	0.022480	1.55
0.820	9.0	-2.0	10.52	-1.38	-0.000571	0.008175	-0.000856	0.008150	0.000818	0.002321	0.010974	-0.05
0.818	10.0	-2.0	11.69	-1.65	0.001952	0.008751	0.001645	0.008814	0.000450	0.002830	0.012162	0.16
0.828	10.0	0.0	13.01	-2.29	0.017927	0.016618	0.017927	0.016618	0.002866	0.003353	0.020658	0.87
0.826	11.0	-2.0	12.91	-1.90	0.002968	0.009344	0.002640	0.009442	-0.000092	0.003402	0.013445	0.22
0.813	12.0	-2.0	14.02	-2.05	0.005023	0.010101	0.004667	0.010270	-0.000362	0.003944	0.014855	0.34
0.824	12.8	-2.0	14.97	-2.26	0.006441	0.010859	0.006058	0.001108	-0.000759	0.004462	0.016238	0.40
0.825	-4.0	4.0	-1.24	-0.21	0.029547	0.012212	0.030327	0.010121	0.002555	0.001694	0.014258	2.07
0.826	0.0	4.0	3.47	-1.33	0.040308	0.014915	0.041250	0.012067	0.003629	0.001239	0.016412	2.46
0.828	-4.0	6.0	-0.11	-1.05	0.050412	0.015945	0.051802	0.010588	0.003611	0.001612	0.017899	2.82
0.828	-2.0	6.0	2.25	-1.59	0.055735	0.017930	0.057304	0.012006	0.003881	0.001287	0.019489	2.86
0.829	0.0	6.0	4.60	-2.13	0.060398	0.019872	0.062144	0.013450	0.004144	0.001140	0.021254	2.84
0.829	2.0	6.0	6.97	-2.66	0.064409	0.022067	0.066363	0.015214	0.003871	0.001399	0.023761	2.71
0.832	4.0	6.0	9.34	-3.17	0.067582	0.025303	0.069856	0.018100	0.002828	0.002135	0.027889	2.42
0.829	-4.0	8.0	1.00	-1.86	0.071386	0.020419	0.073533	0.010286	0.003947	0.001464	0.022201	3.22
0.827	-2.0	8.0	3.36	-2.36	0.076134	0.022820	0.078569	0.012002	0.003918	0.001219	0.024303	3.13
0.831	0.0	8.0	5.71	-2.86	0.080503	0.025521	0.083271	0.014068	0.003468	0.001306	0.027110	2.97
0.834	2.0	8.0	8.08	-3.41	0.084157	0.028742	0.087338	0.016749	0.002329	0.001857	0.031000	2.72

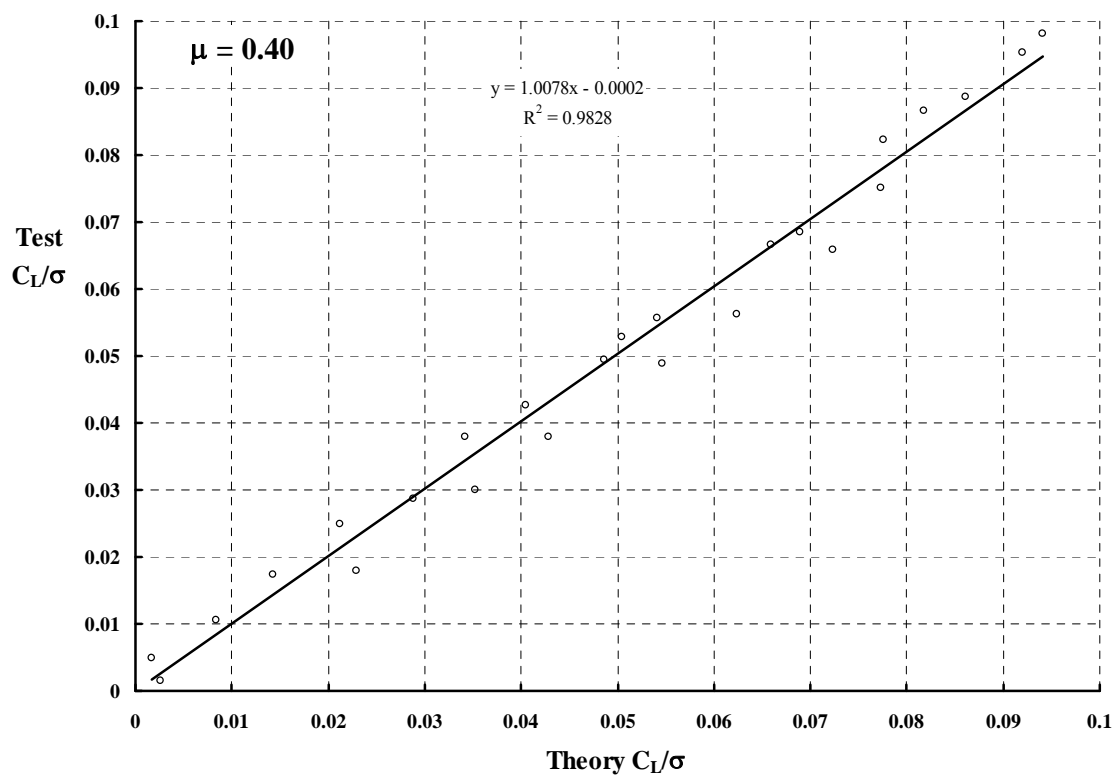
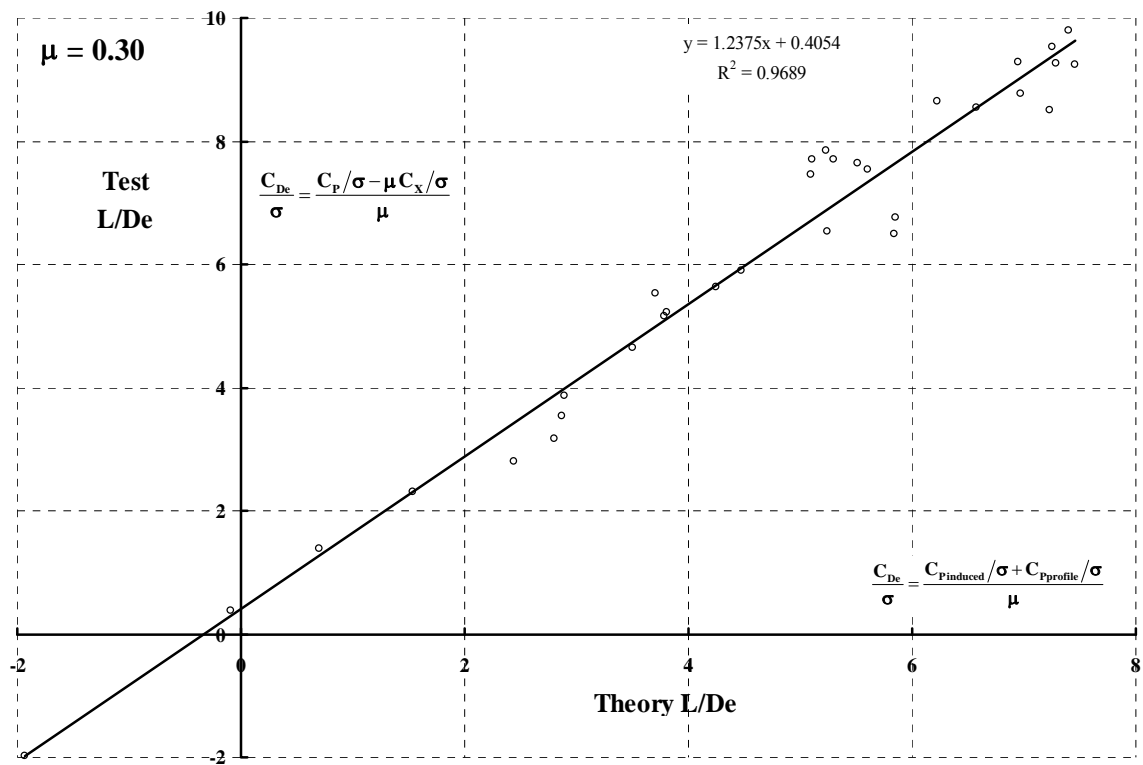
1.052	-4.0	1.0	-3.75	0.43	0.024337	0.016783	0.024626	0.016356	0.001751	0.001050	0.017783	1.37
1.049	-4.0	3.0	-2.48	-0.92	0.051995	0.021441	0.053046	0.018690	0.004296	0.001554	0.022923	2.27
1.049	-4.0	5.0	-1.19	-2.22	0.079971	0.026044	0.081937	0.018975	0.006292	0.002244	0.028190	2.84
1.051	-4.0	7.0	0.12	-3.40	0.107700	0.030141	0.110571	0.016791	0.007793	0.003165	0.033178	3.25
1.045	-2.0	1.0	-1.26	0.11	0.018924	0.015162	0.019186	0.014829	0.001941	0.001502	0.016593	1.14
1.057	-2.0	3.0	-0.01	-1.28	0.048280	0.021420	0.049335	0.018864	0.004170	0.001598	0.022944	2.10
1.057	-2.0	5.0	1.28	-2.55	0.077030	0.026706	0.079064	0.019891	0.006068	0.002034	0.028651	2.69
1.057	-2.0	7.0	2.61	-3.71	0.103489	0.031354	0.106539	0.018508	0.007217	0.002841	0.034080	3.04
1.051	0.0	1.0	1.24	-0.11	0.013229	0.014170	0.013474	0.013937	0.002031	0.001808	0.015893	0.83
1.059	0.0	3.0	2.49	-1.54	0.043322	0.021336	0.044379	0.019040	0.004445	0.001622	0.022883	1.89
1.059	0.0	5.0	3.78	-2.82	0.072222	0.027556	0.074349	0.021157	0.006272	0.001760	0.029239	2.47
1.051	0.0	7.0	5.08	-3.99	0.100024	0.033483	0.103359	0.021043	0.006716	0.002659	0.036034	2.78
1.058	2.0	1.0	3.74	-0.30	0.006677	0.015406	0.006945	0.015287	0.002392	0.001494	0.016829	0.40
1.051	2.0	3.0	4.99	-1.70	0.037205	0.022012	0.038306	0.020035	0.005063	0.001357	0.023307	1.60
1.057	2.0	5.0	6.26	-3.05	0.067444	0.029767	0.069782	0.023775	0.005986	0.001647	0.031341	2.15
1.052	2.0	7.0	7.58	-4.23	0.094097	0.037750	0.097997	0.026001	0.005149	0.002881	0.040515	2.32
1.058	4.0	1.0	6.25	-0.44	0.000239	0.017929	0.000551	0.017922	0.003150	0.000717	0.018612	0.01
1.052	4.0	3.0	7.50	-1.84	0.031143	0.025287	0.032424	0.023623	0.005049	0.000949	0.026193	1.19
1.053	4.0	5.0	8.76	-3.24	0.060825	0.034661	0.063614	0.029228	0.004663	0.001910	0.036487	1.67
1.053	4.0	7.0	10.06	-4.46	0.088381	0.043493	0.093023	0.032398	0.003033	0.003471	0.046823	1.89
1.053	6.0	1.0	8.77	-0.56	-0.007416	0.020774	-0.007052	0.020900	0.003456	0.000448	0.021200	-0.35
1.052	6.0	3.0	10.02	-1.98	0.023516	0.031163	0.025115	0.029890	0.003749	0.001184	0.032292	0.73
1.051	8.0	1.0	11.27	-0.70	-0.013822	0.025961	-0.013367	0.026198	0.003052	0.000832	0.026754	-0.52
1.059	8.0	3.0	12.53	-2.22	0.014775	0.037350	0.016710	0.036525	0.002188	0.001929	0.039189	0.38
1.049	10.0	1.0	13.76	-0.90	-0.019645	0.030918	-0.019103	0.031257	0.002524	0.001469	0.032317	-0.61

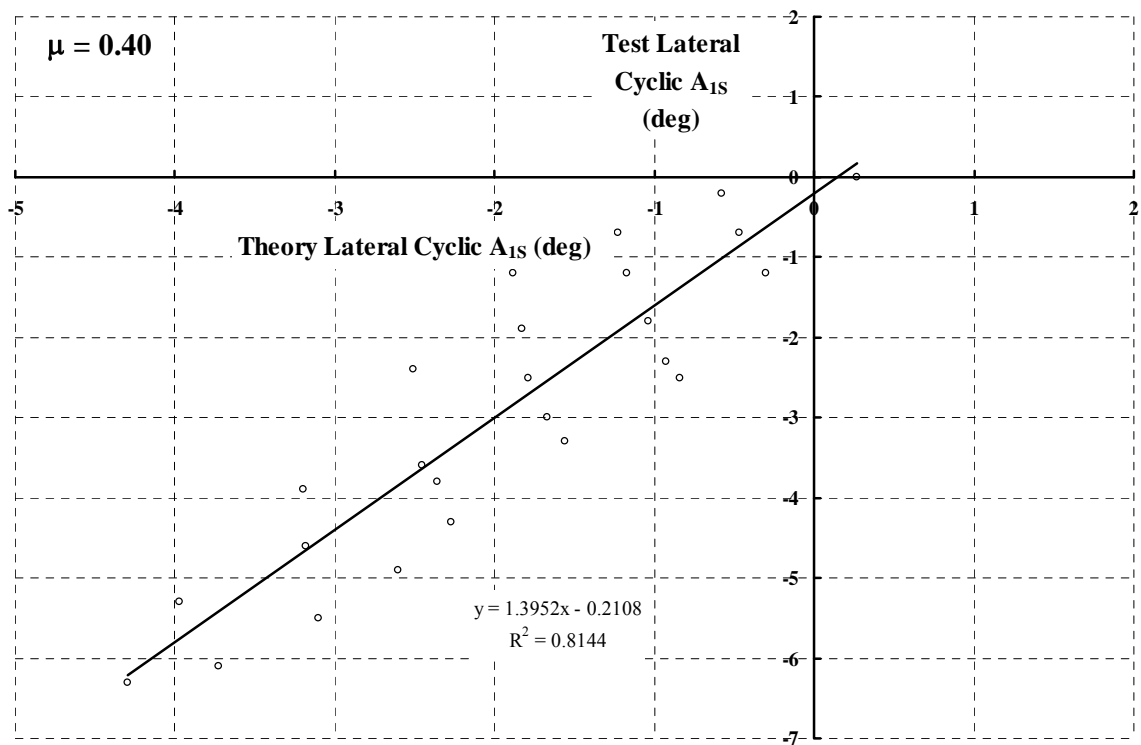
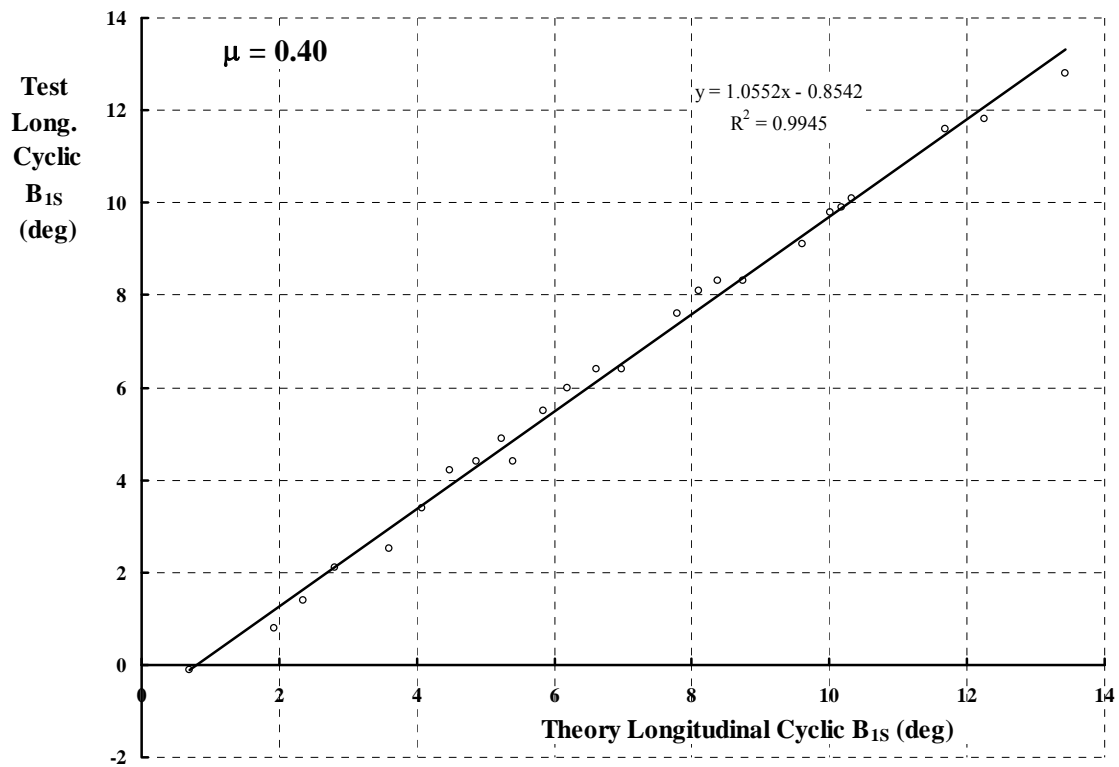


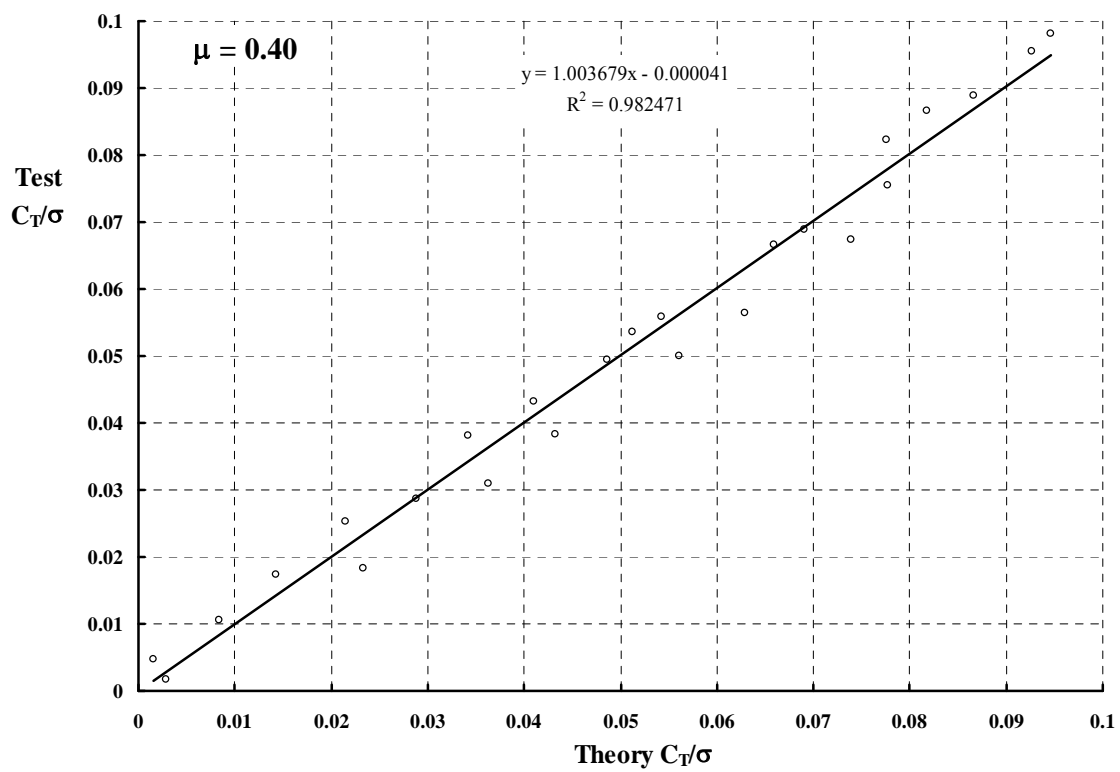
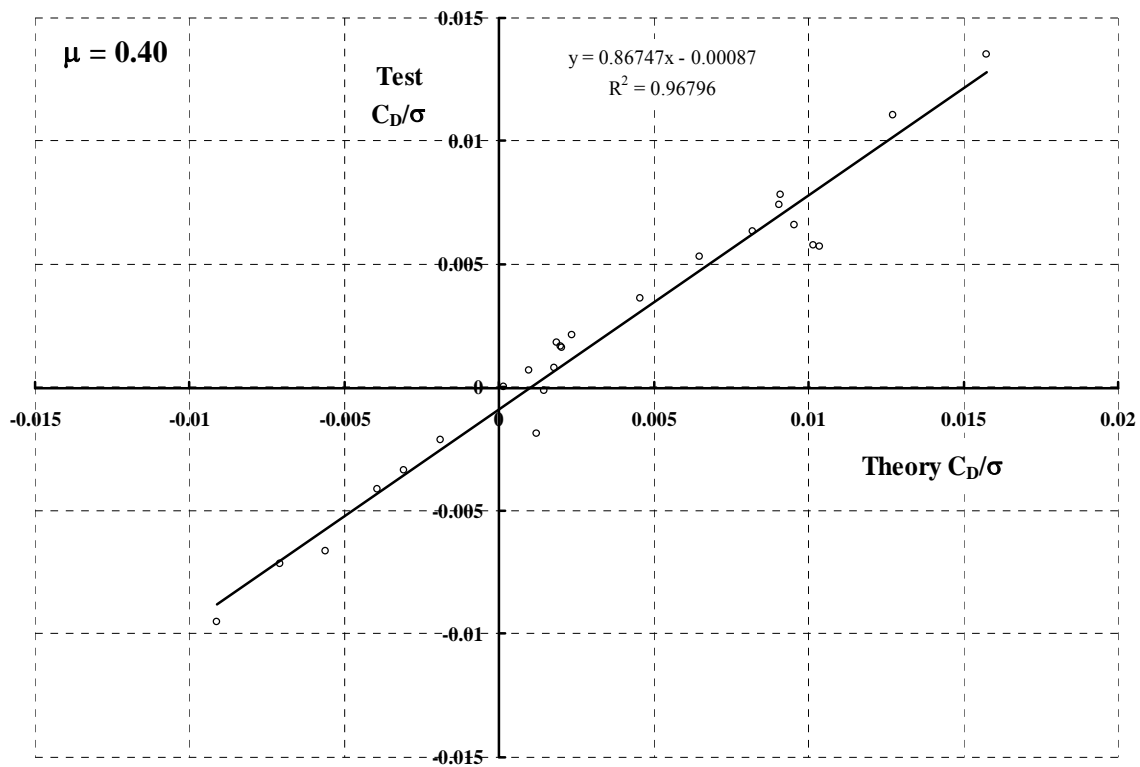


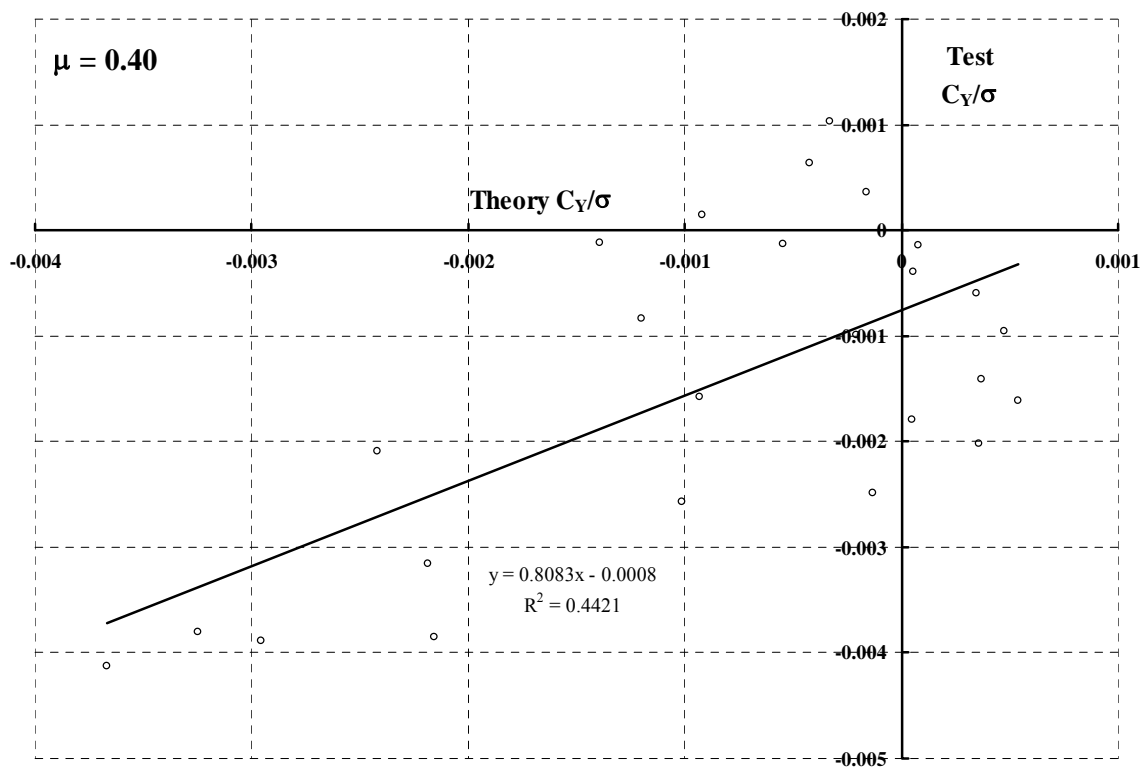
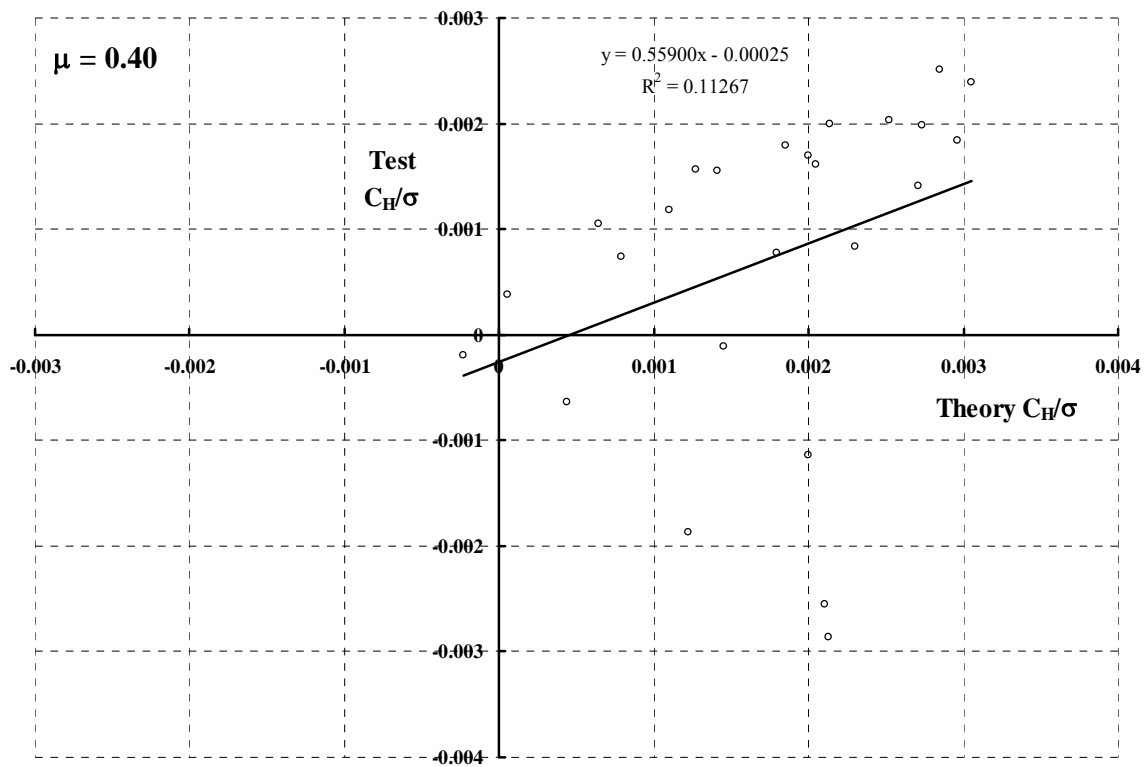


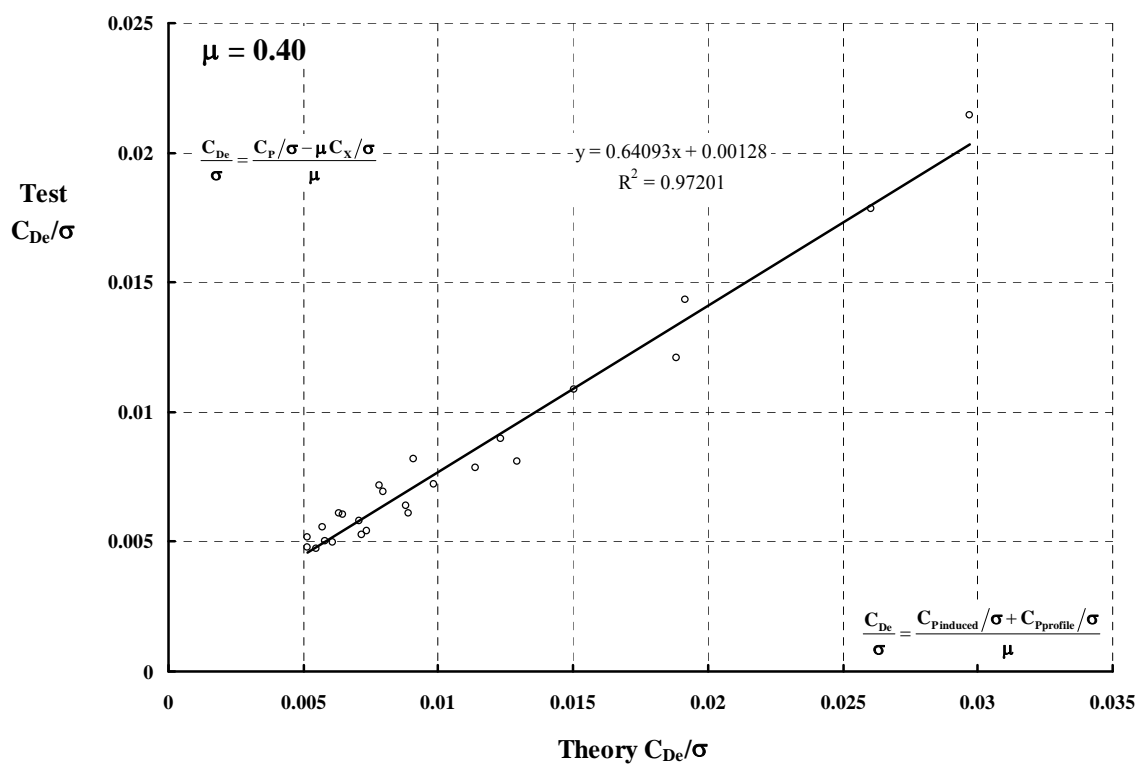
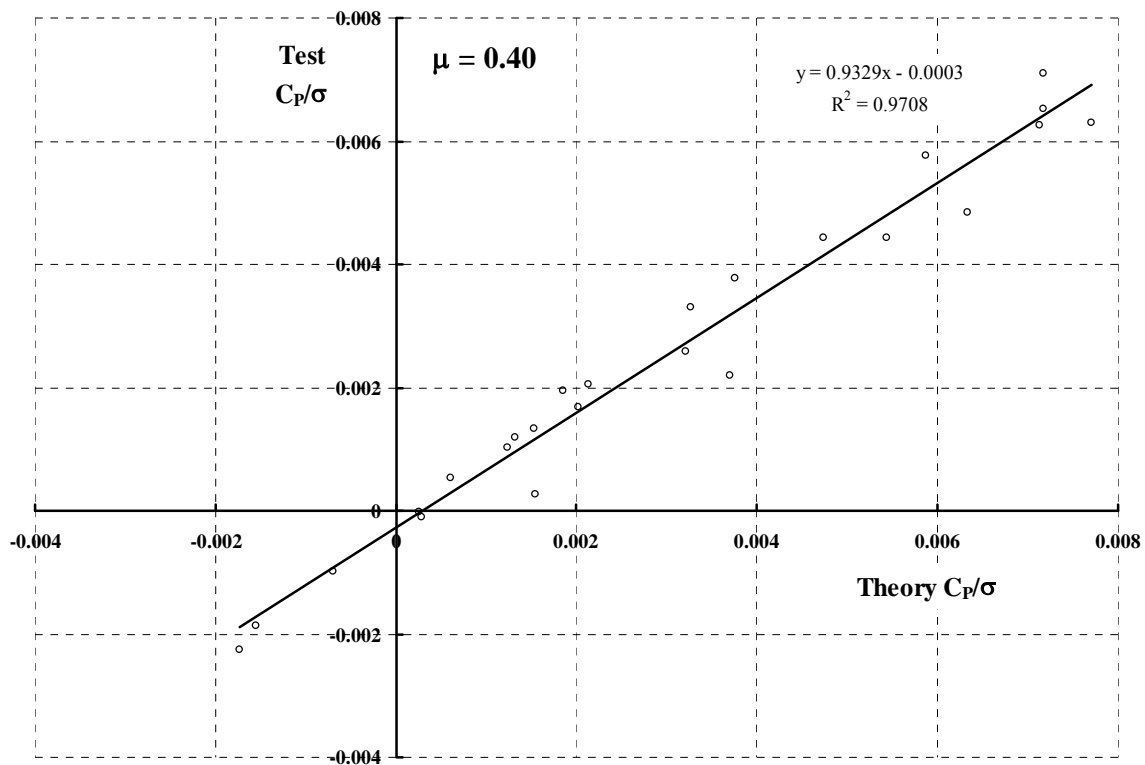


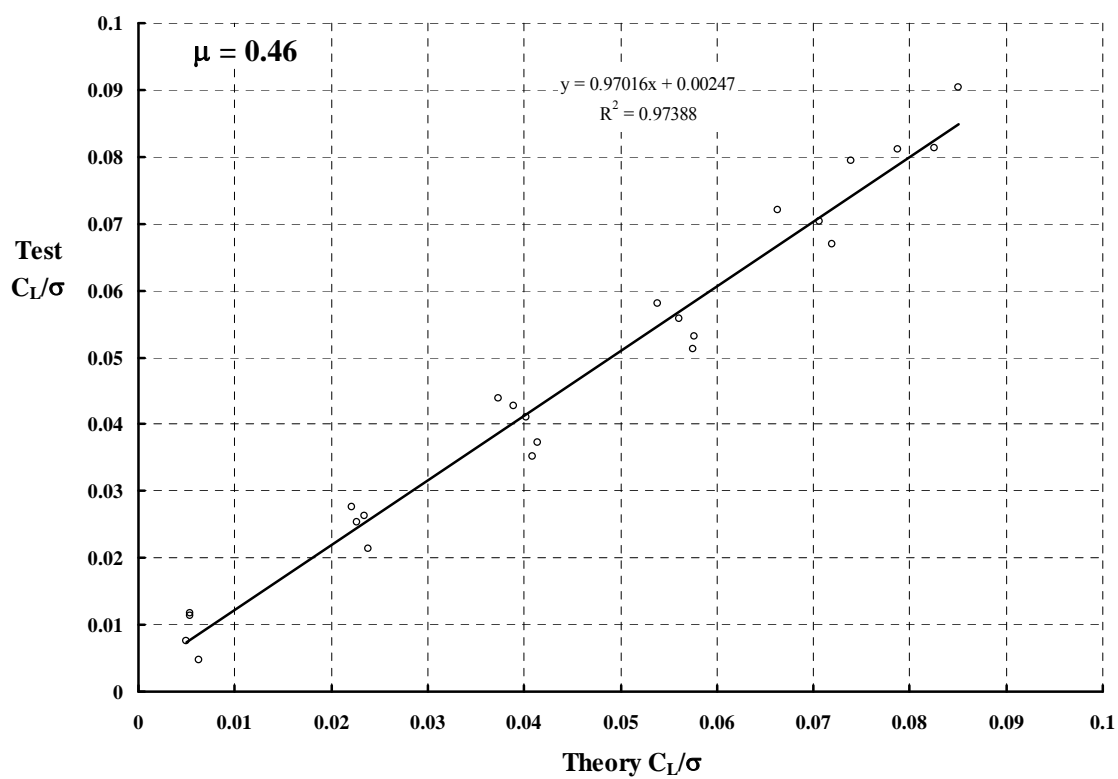
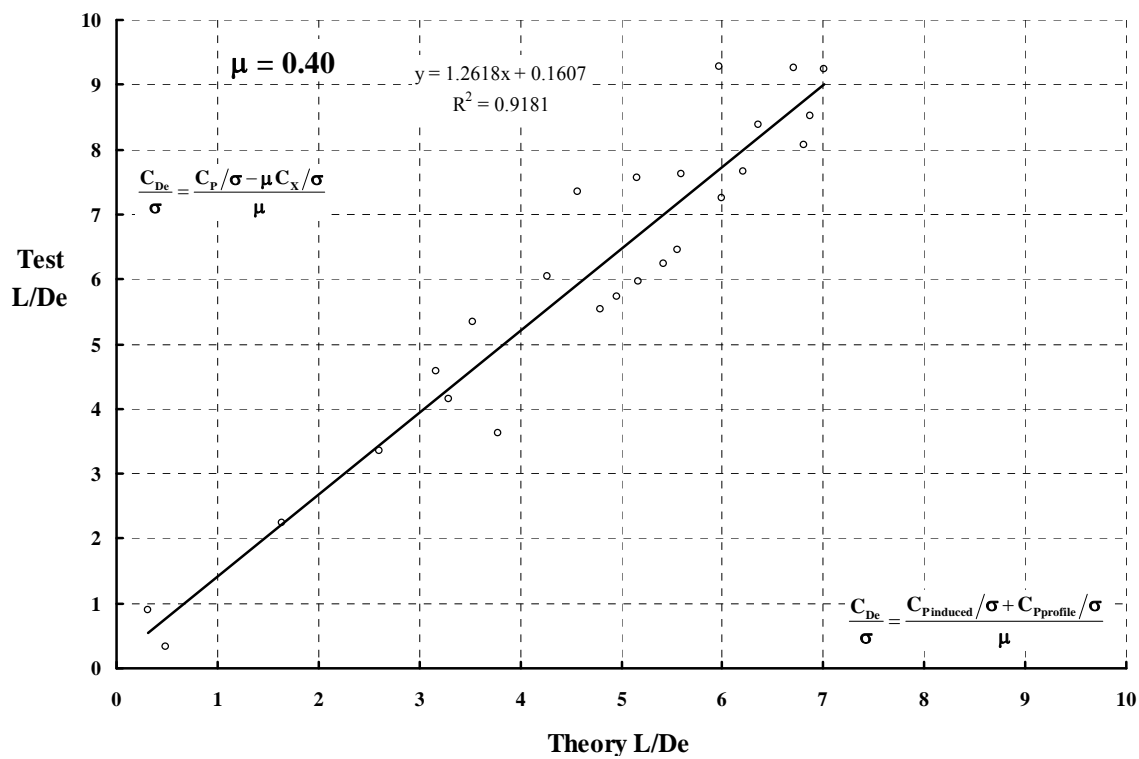


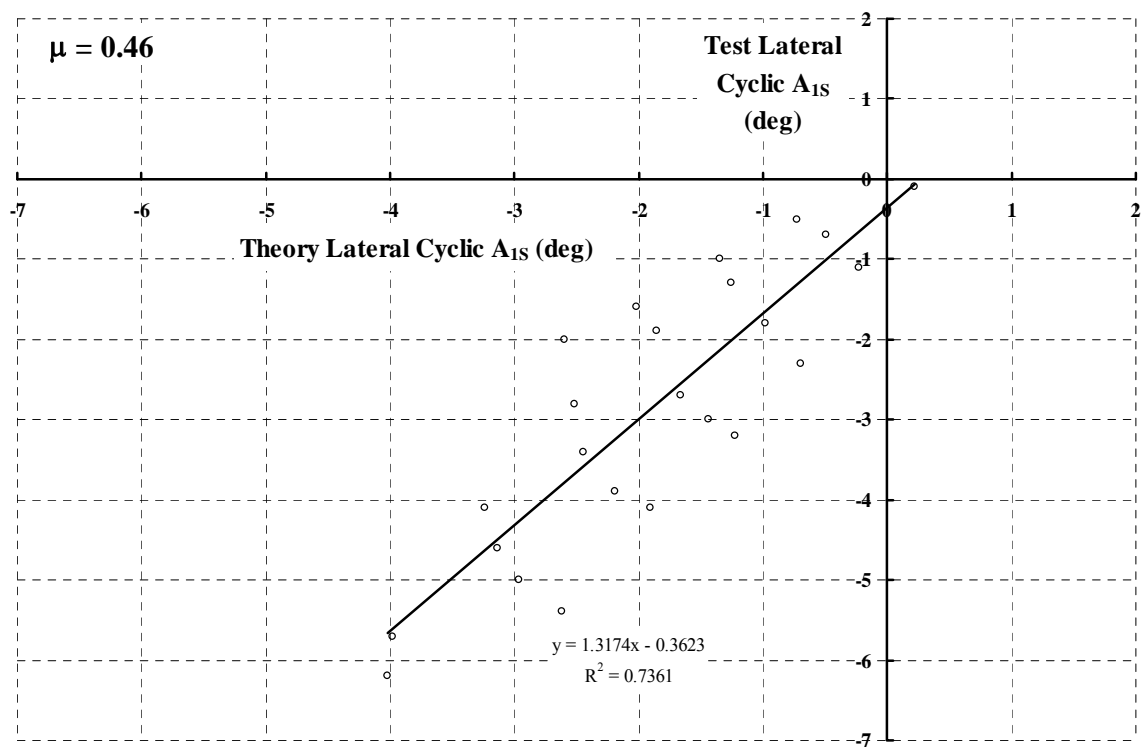
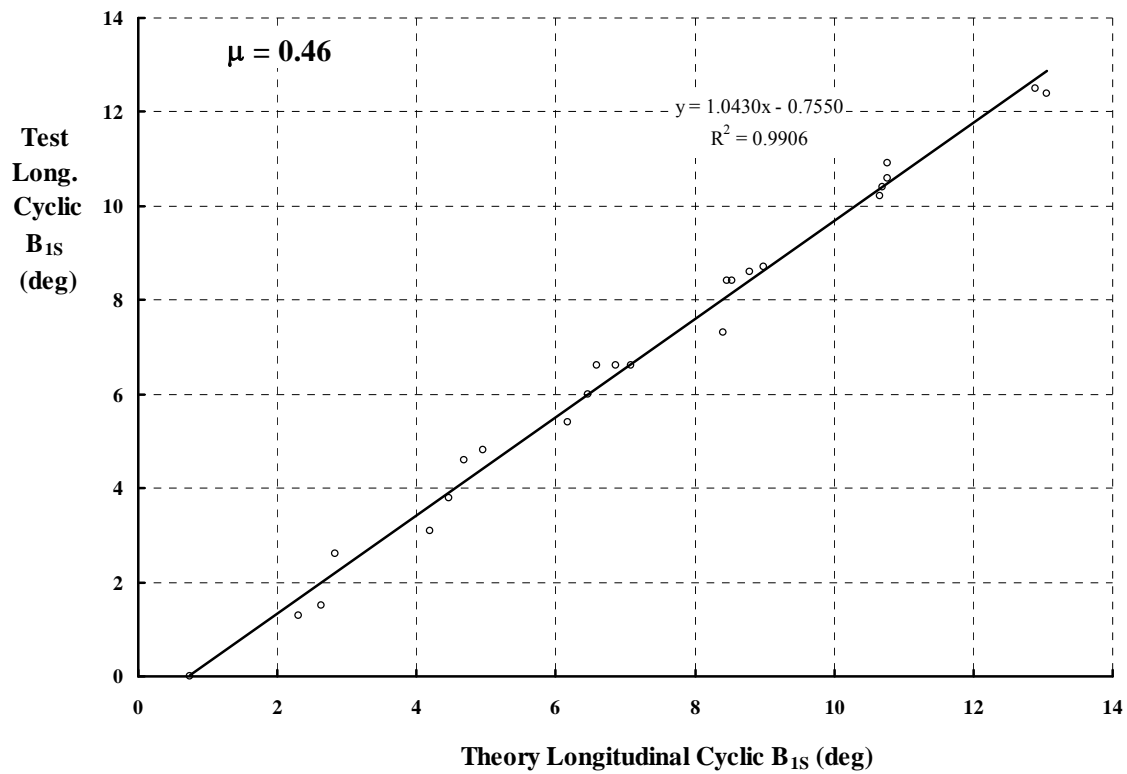


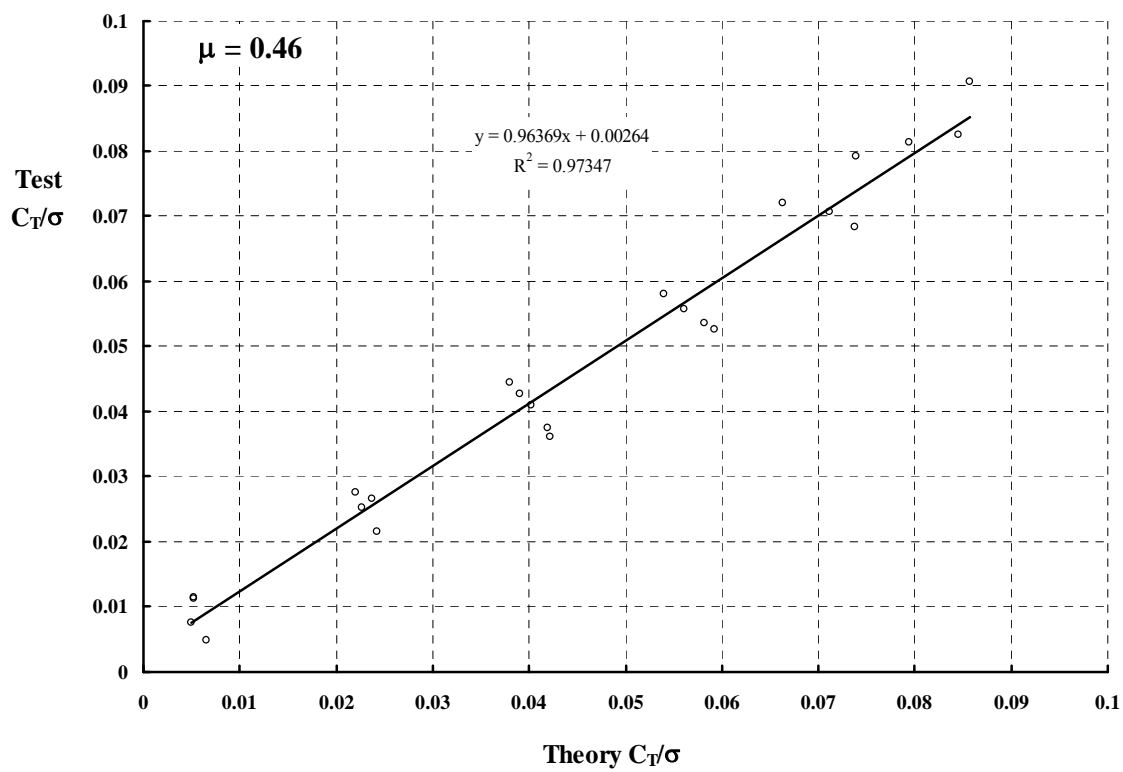
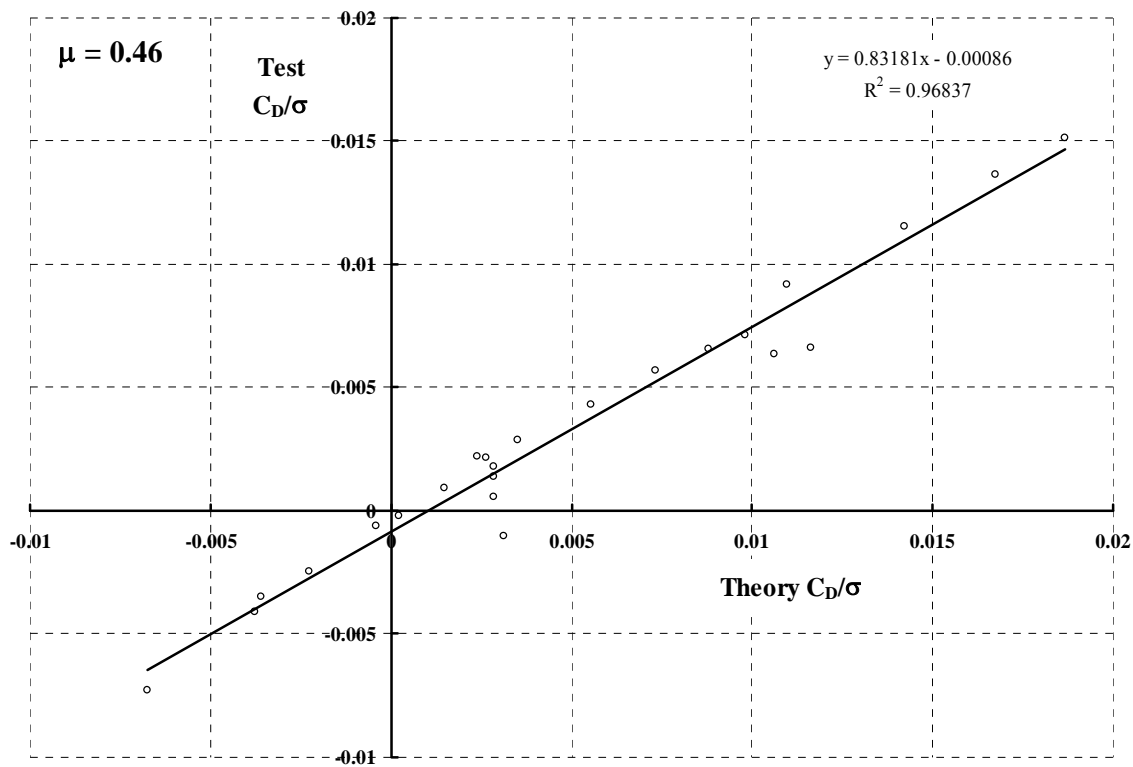


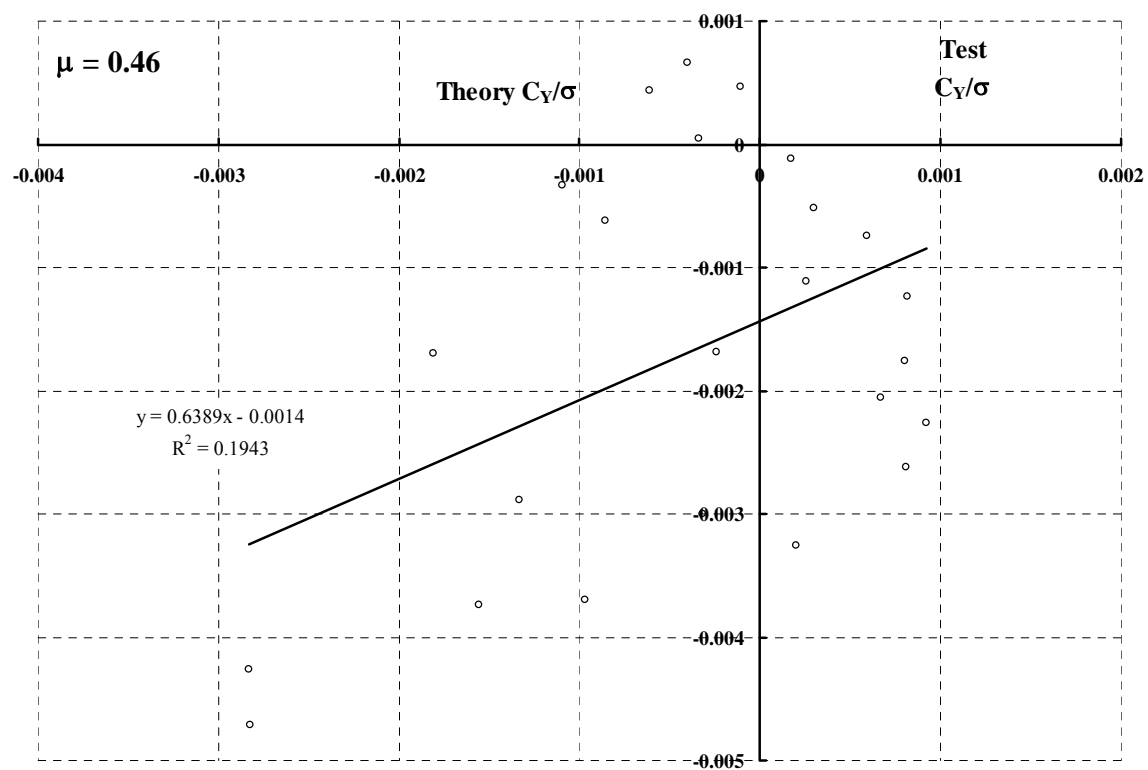
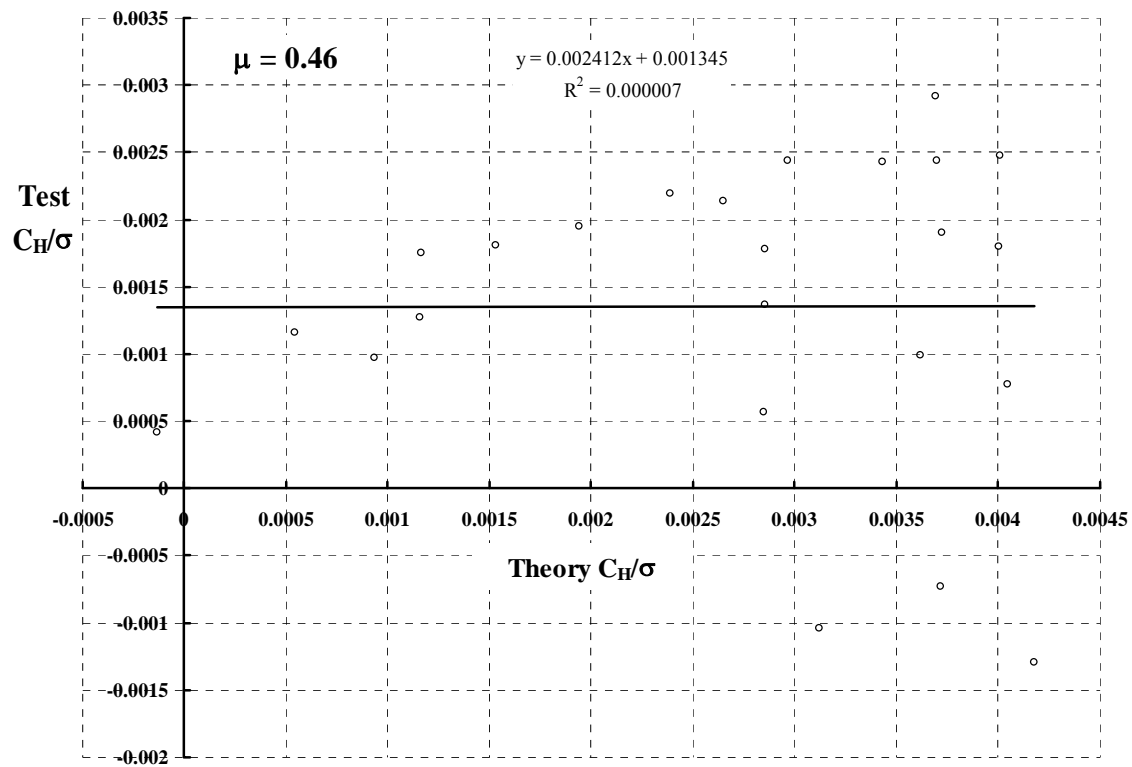


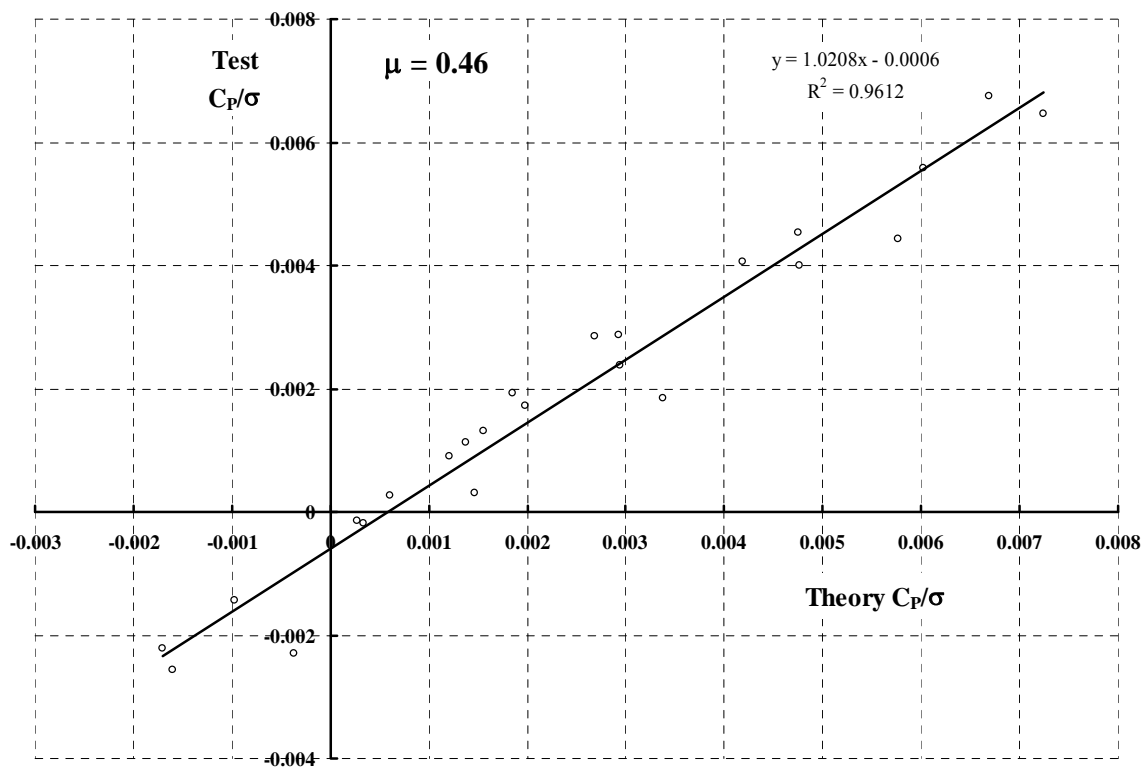
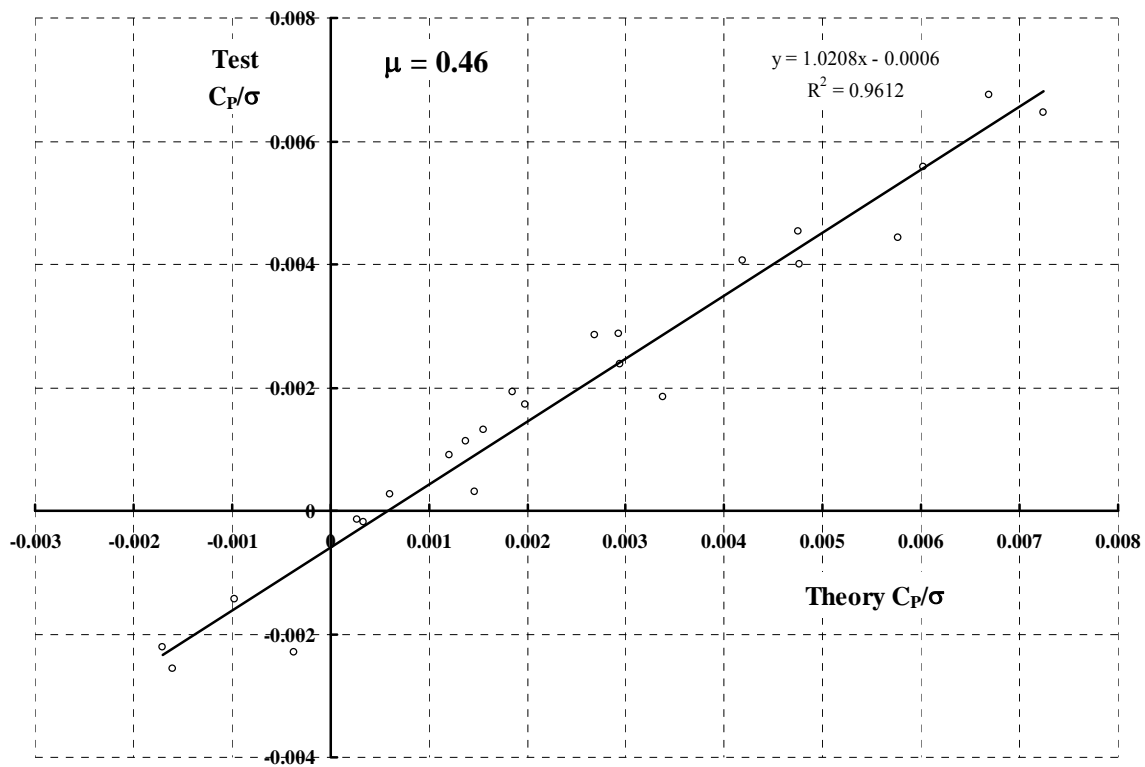


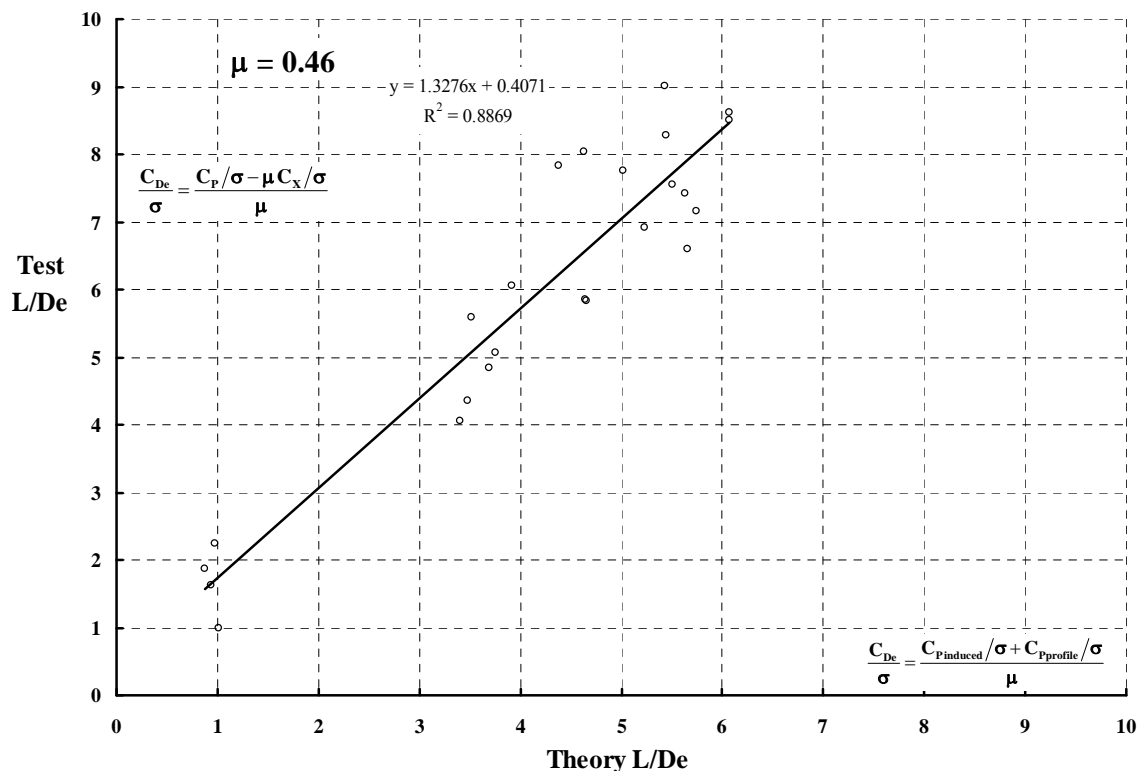
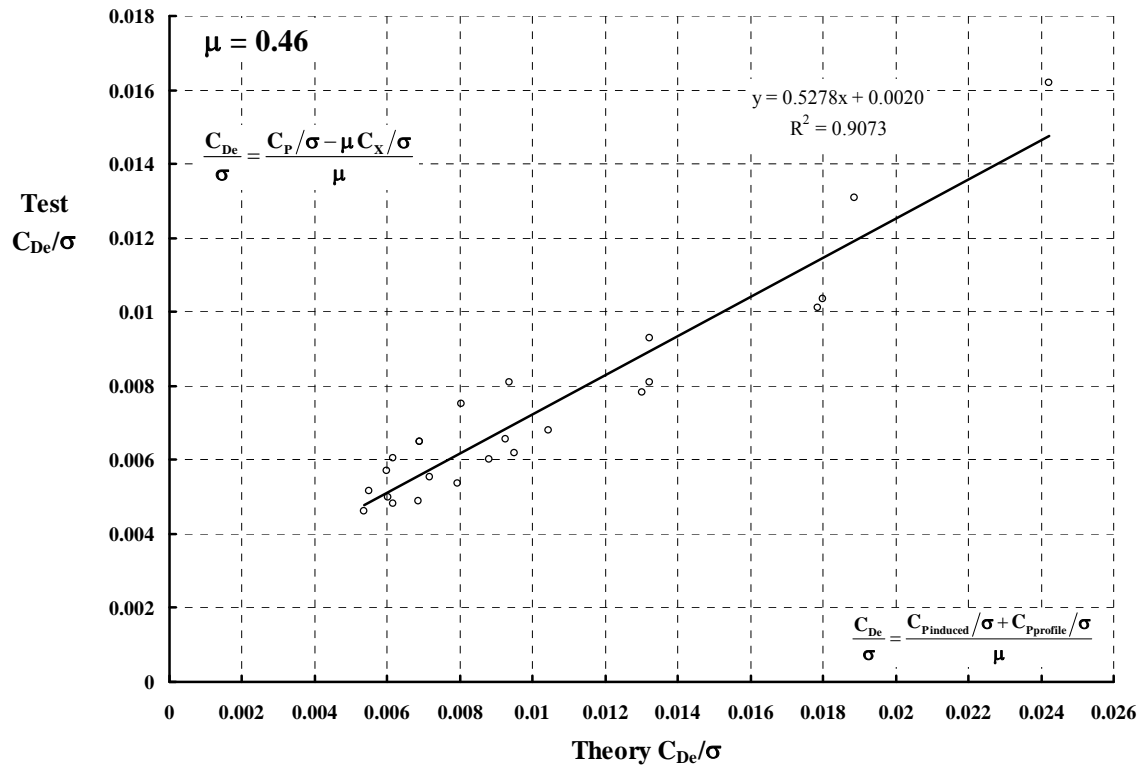


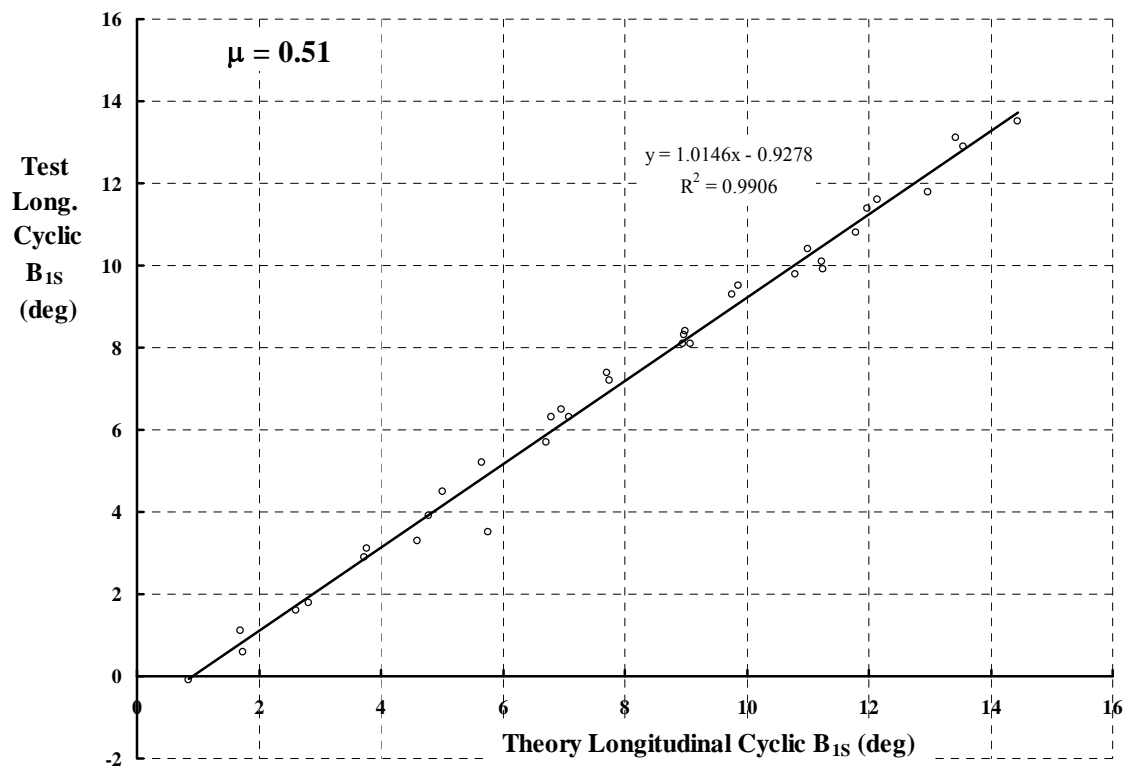
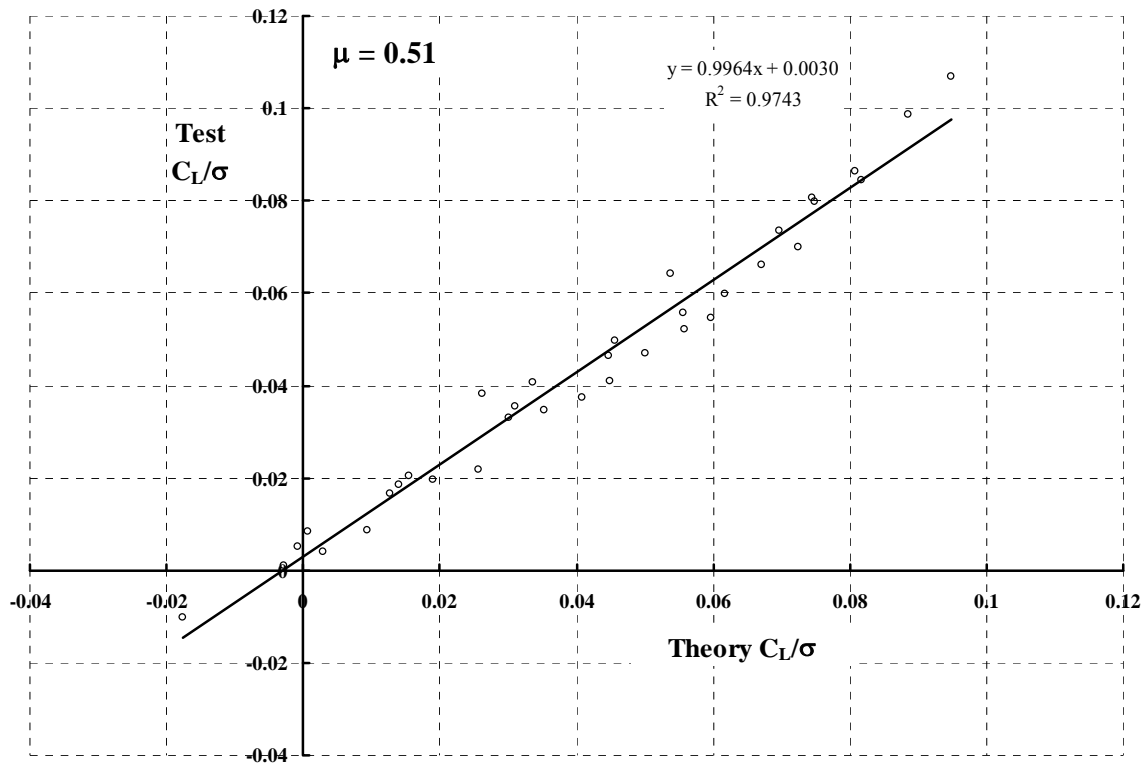


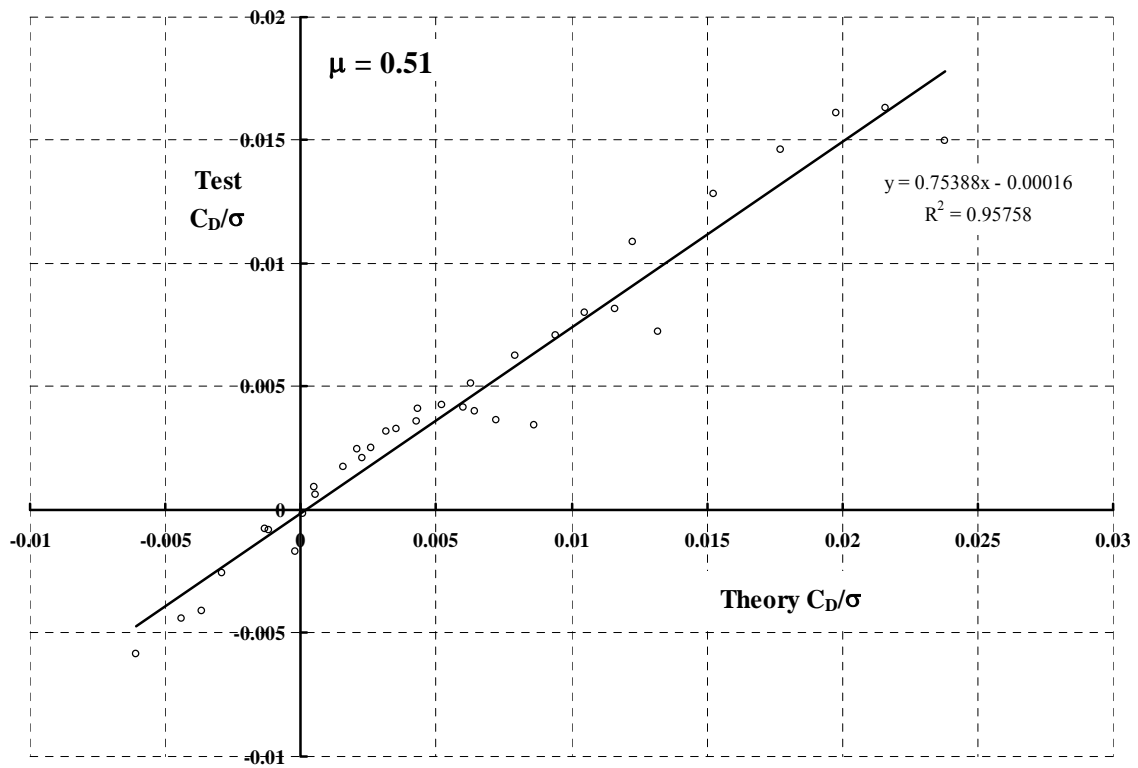
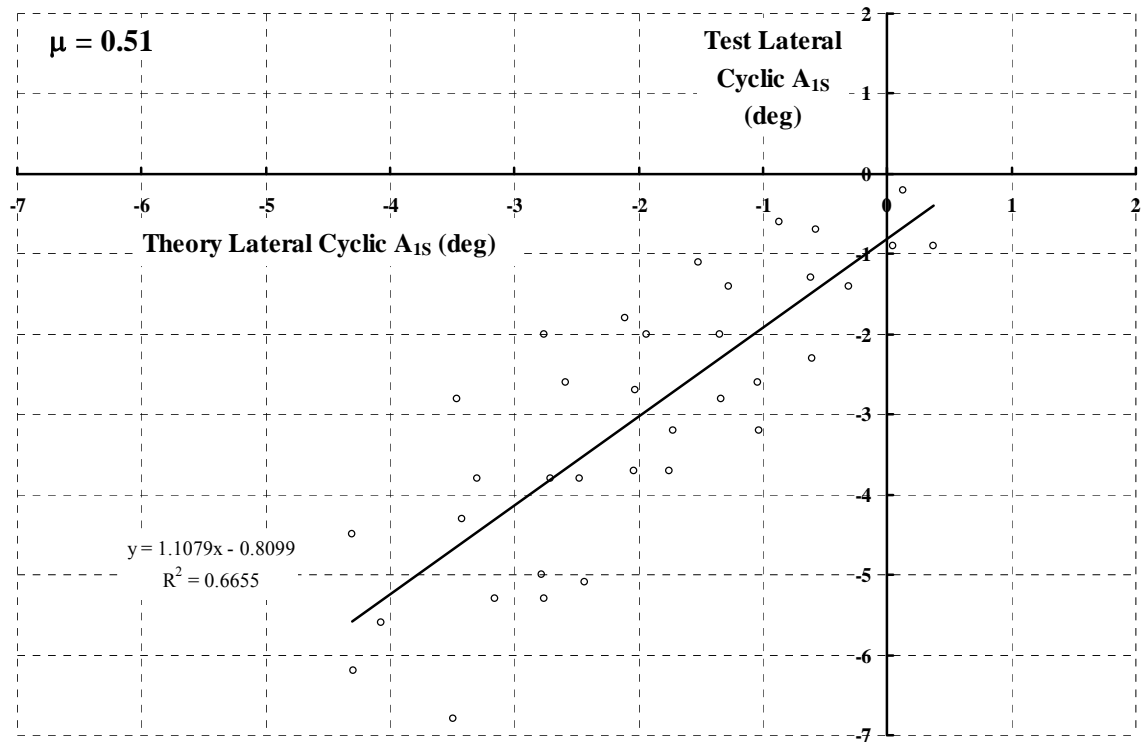


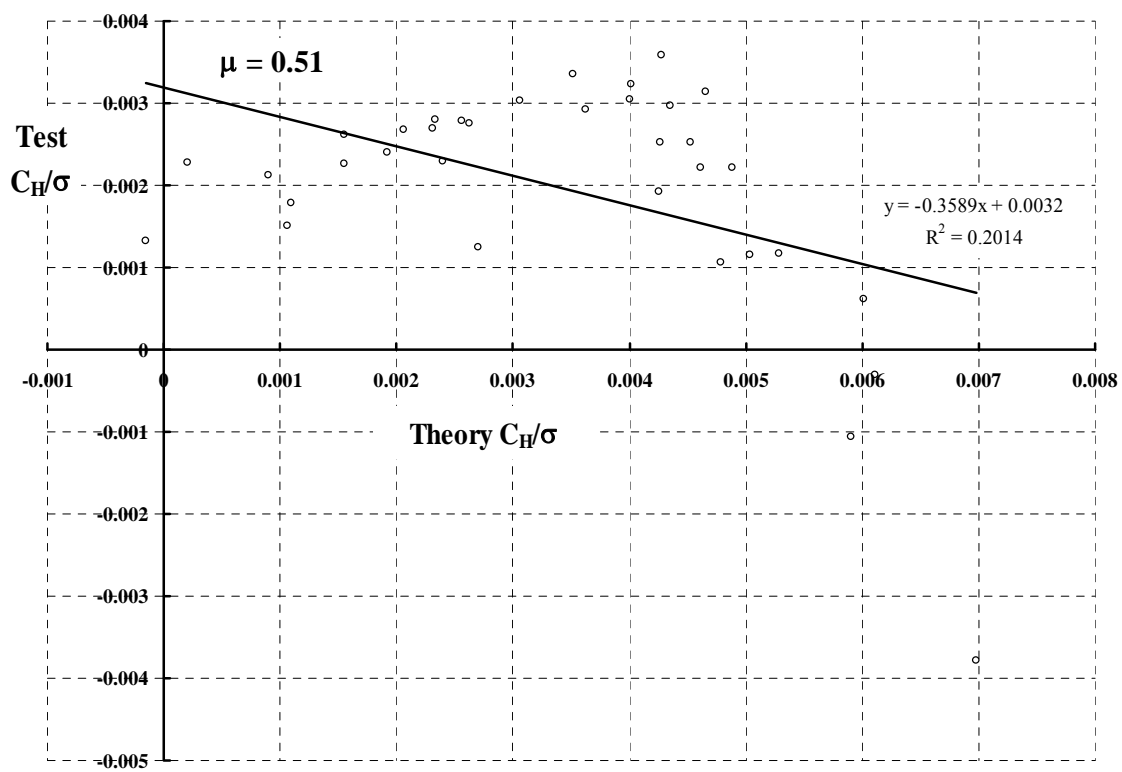
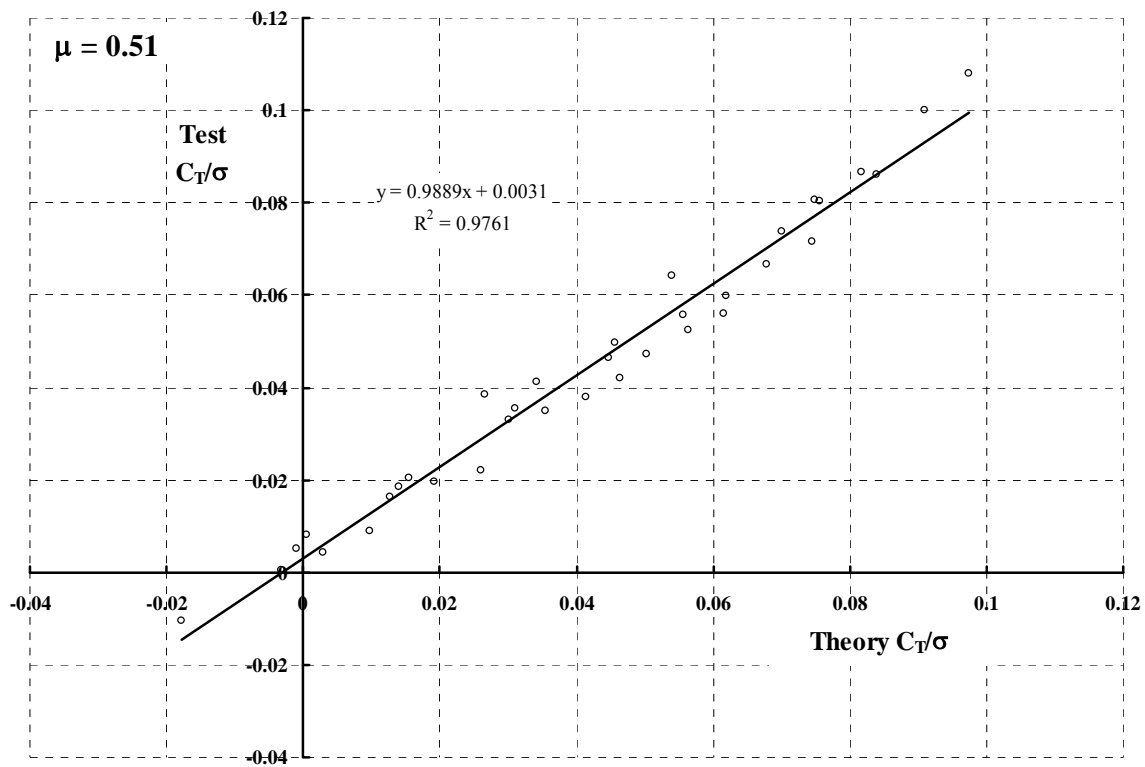


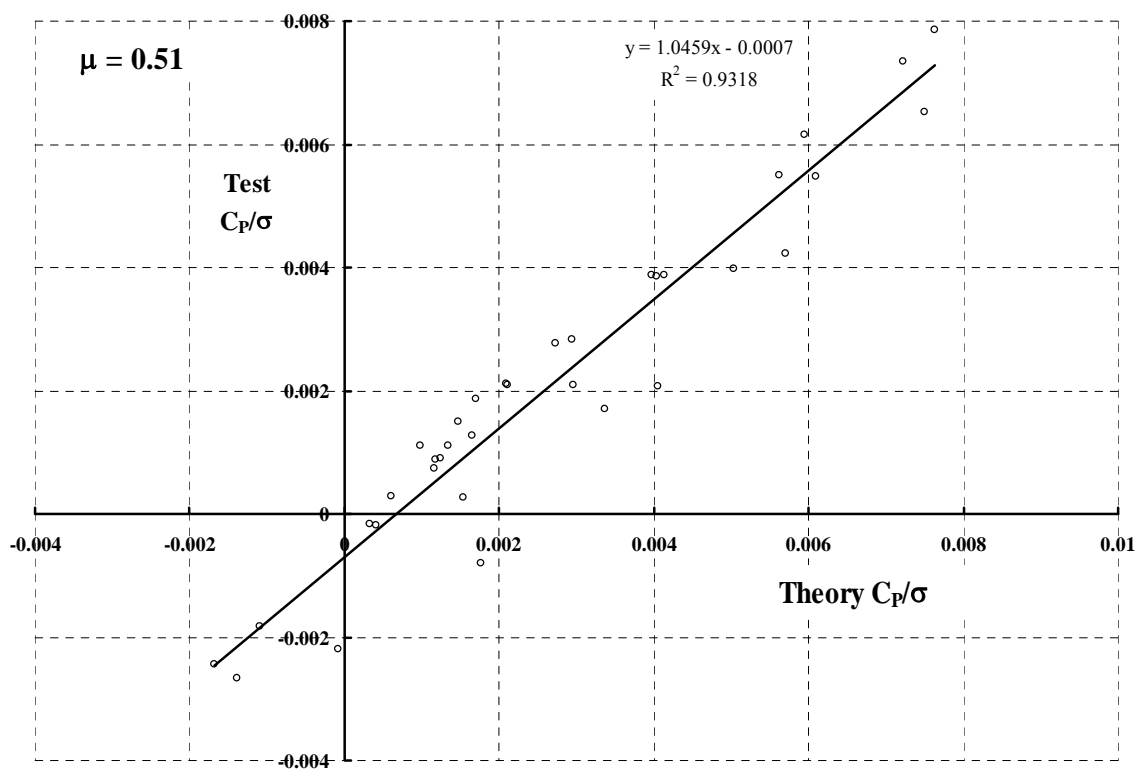
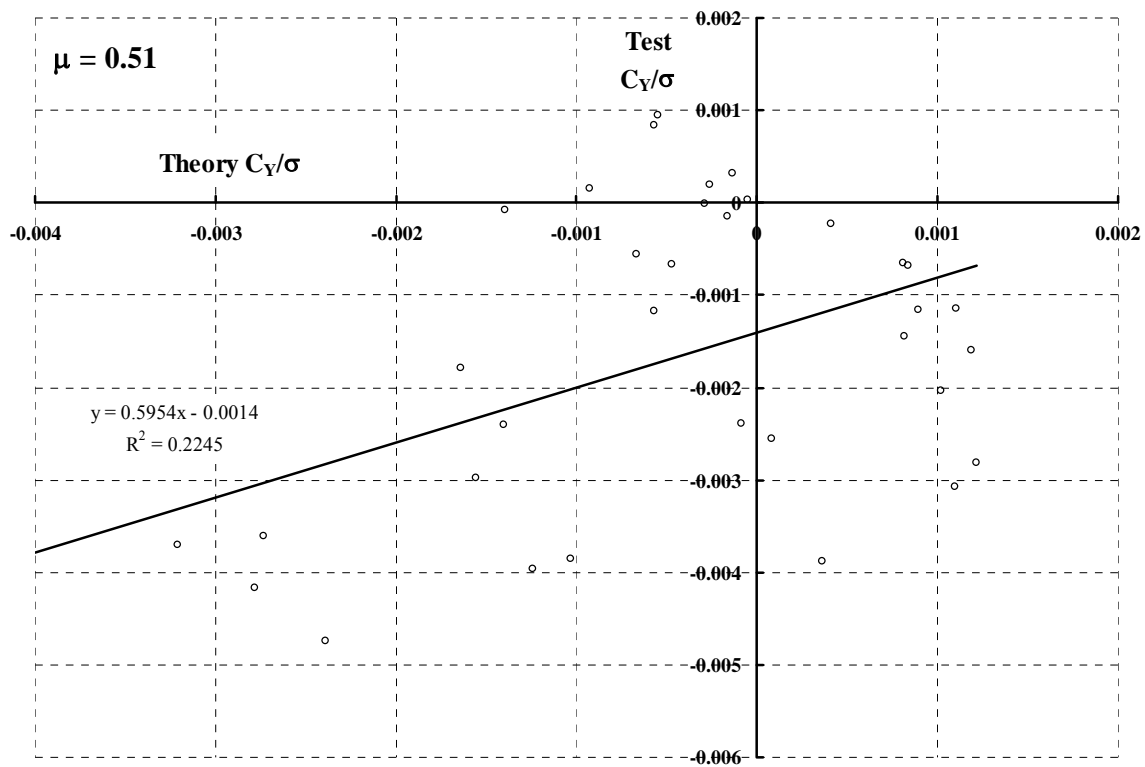


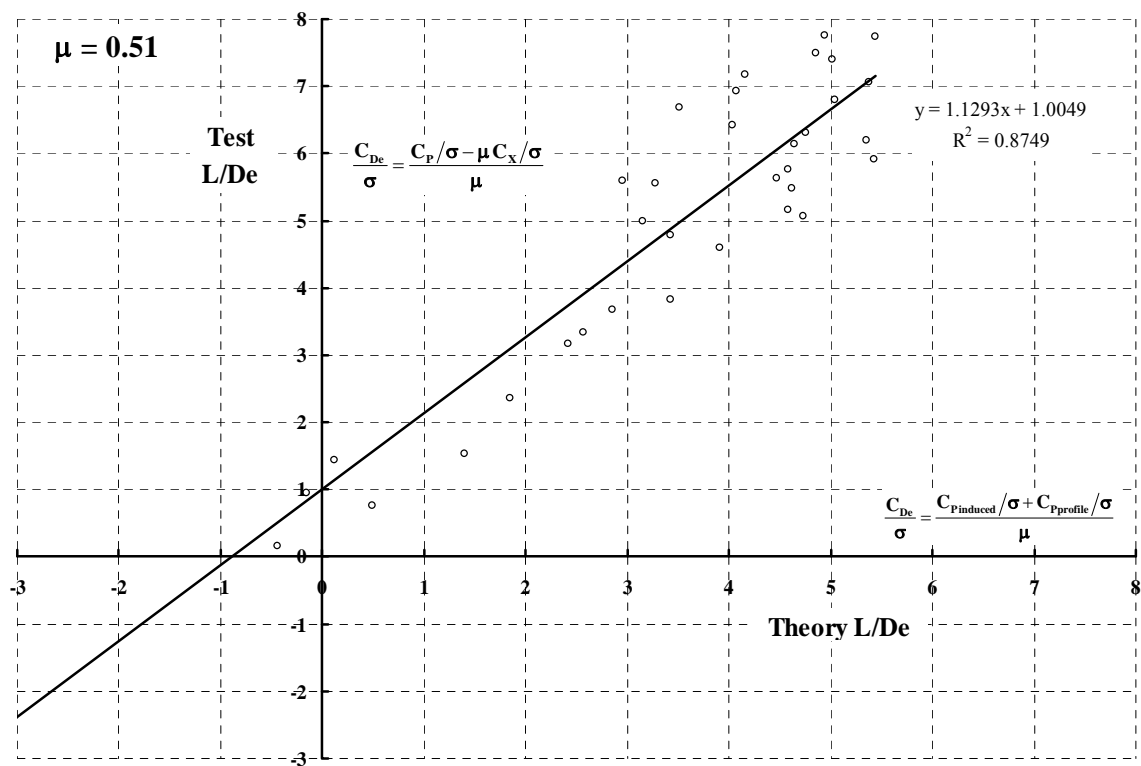
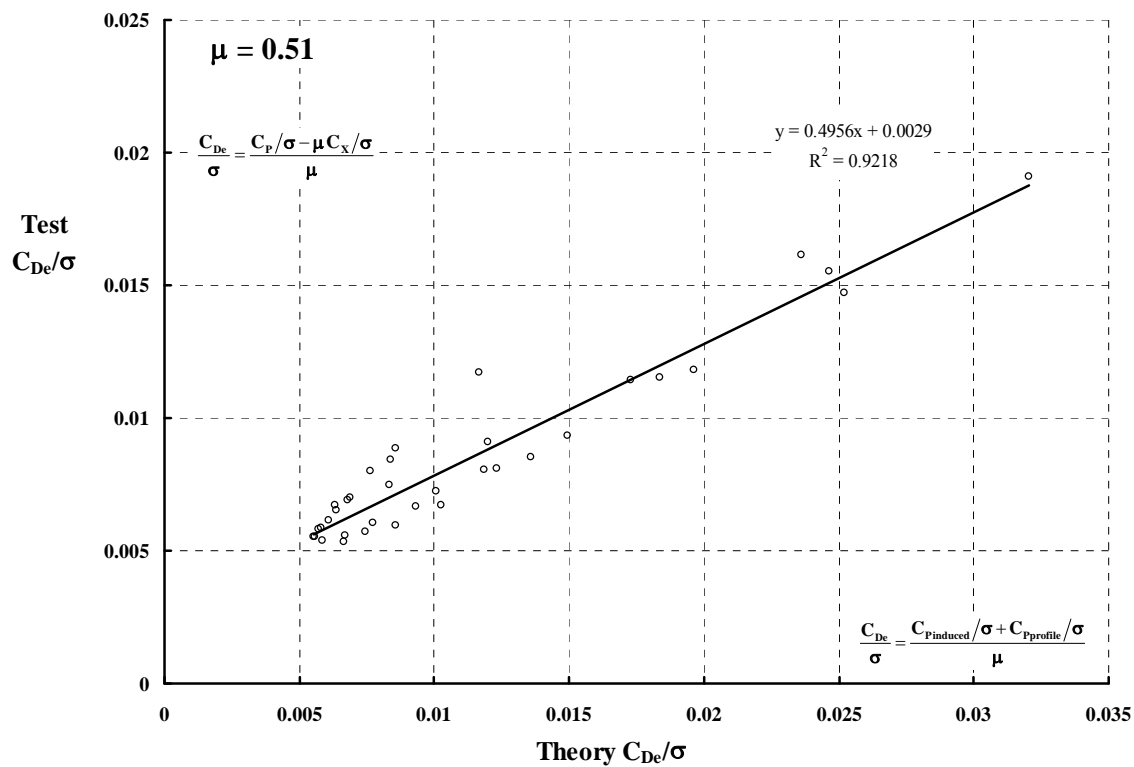


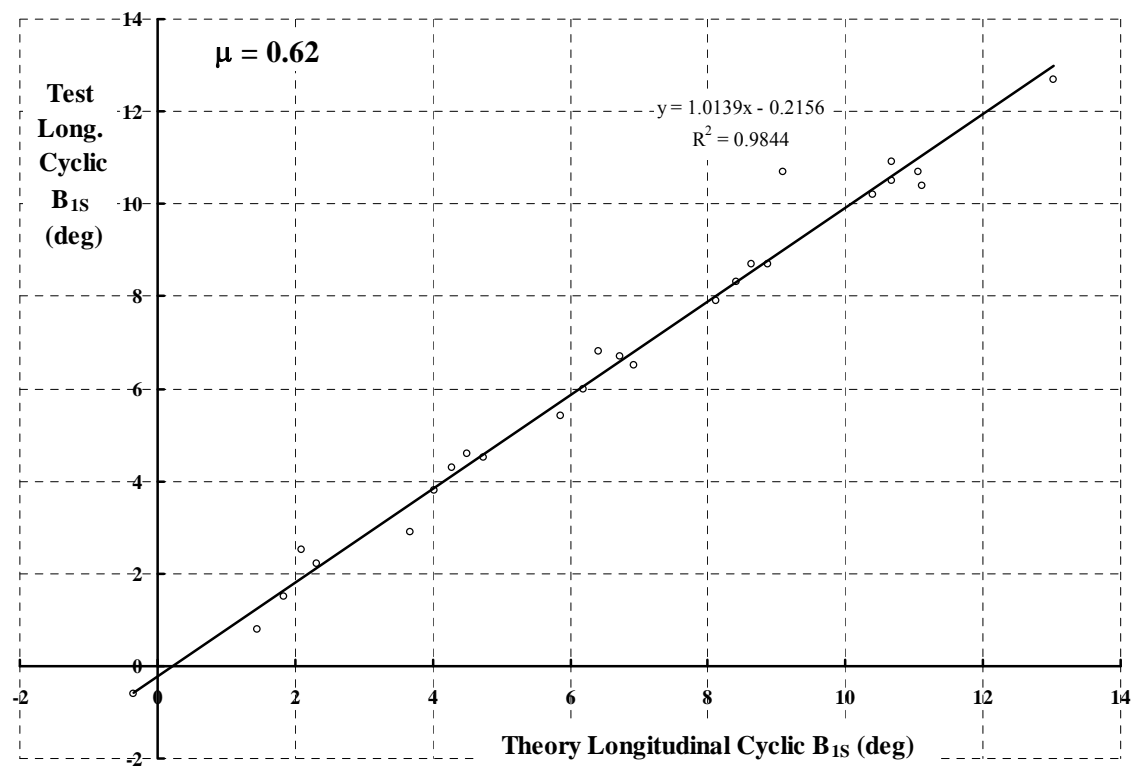
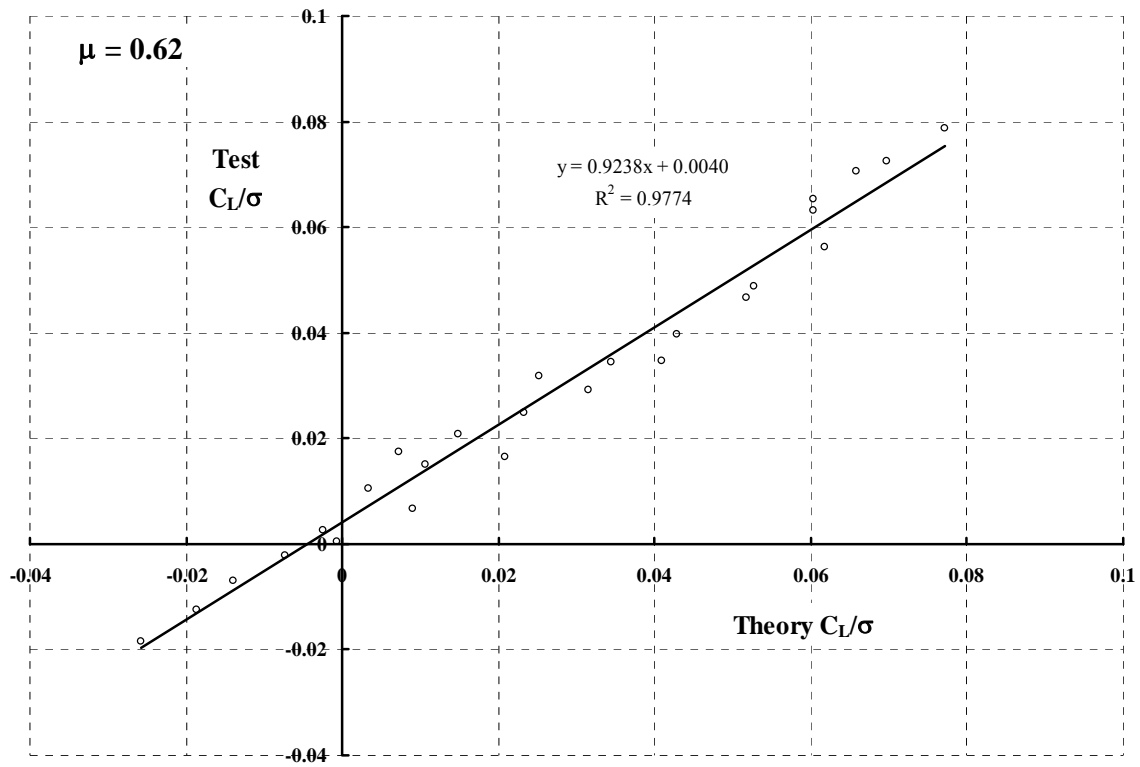


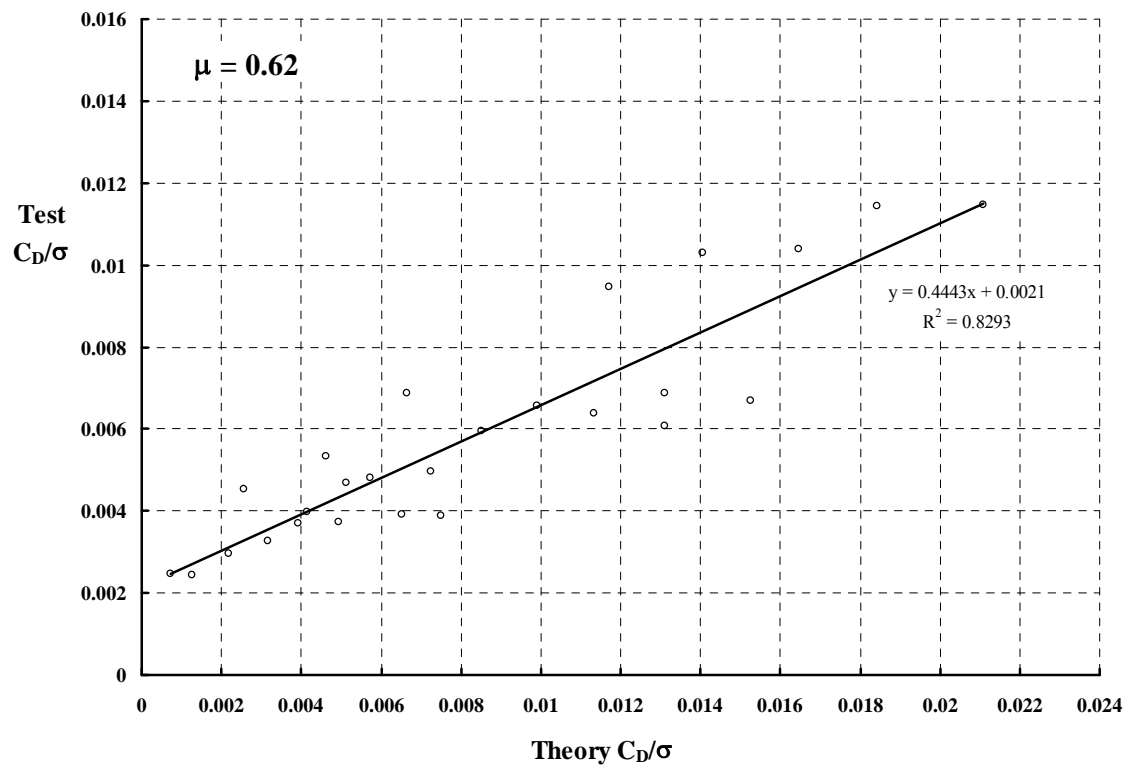
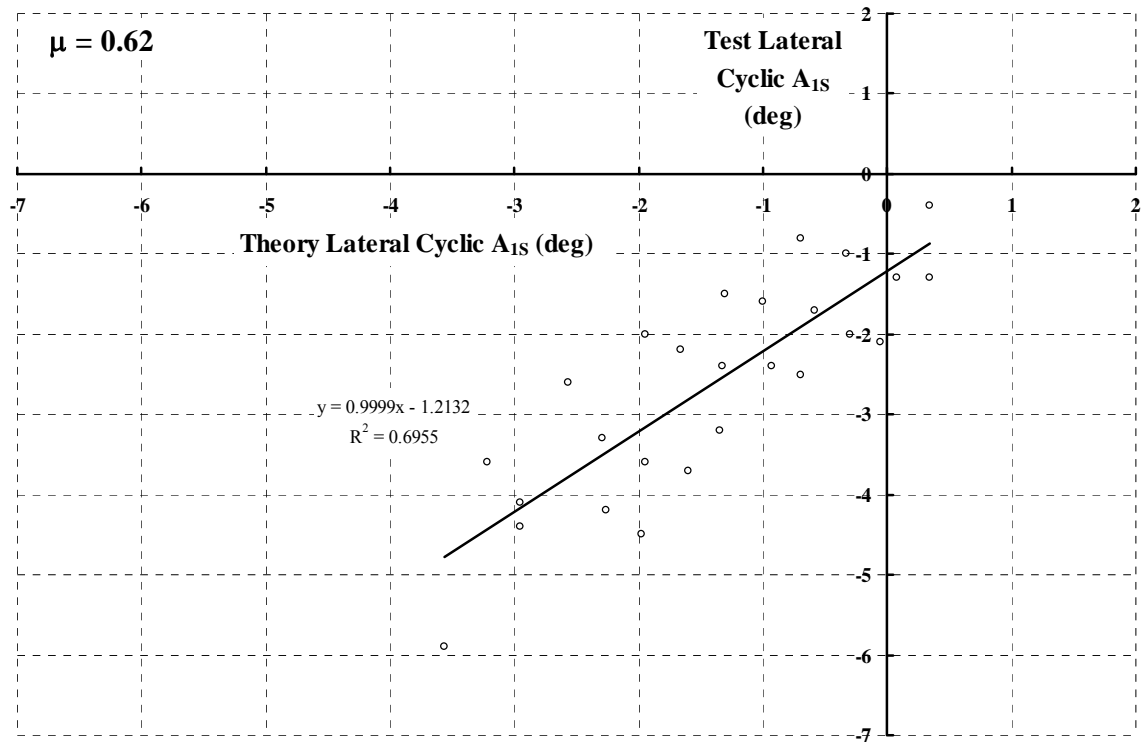


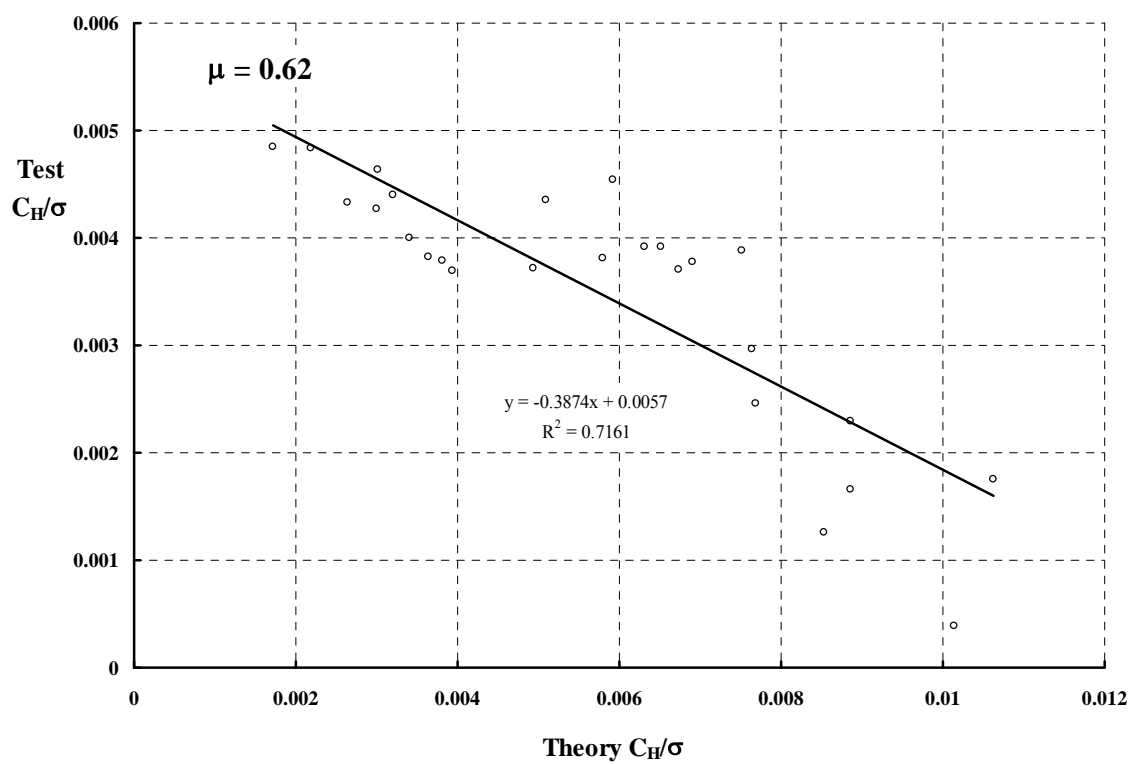
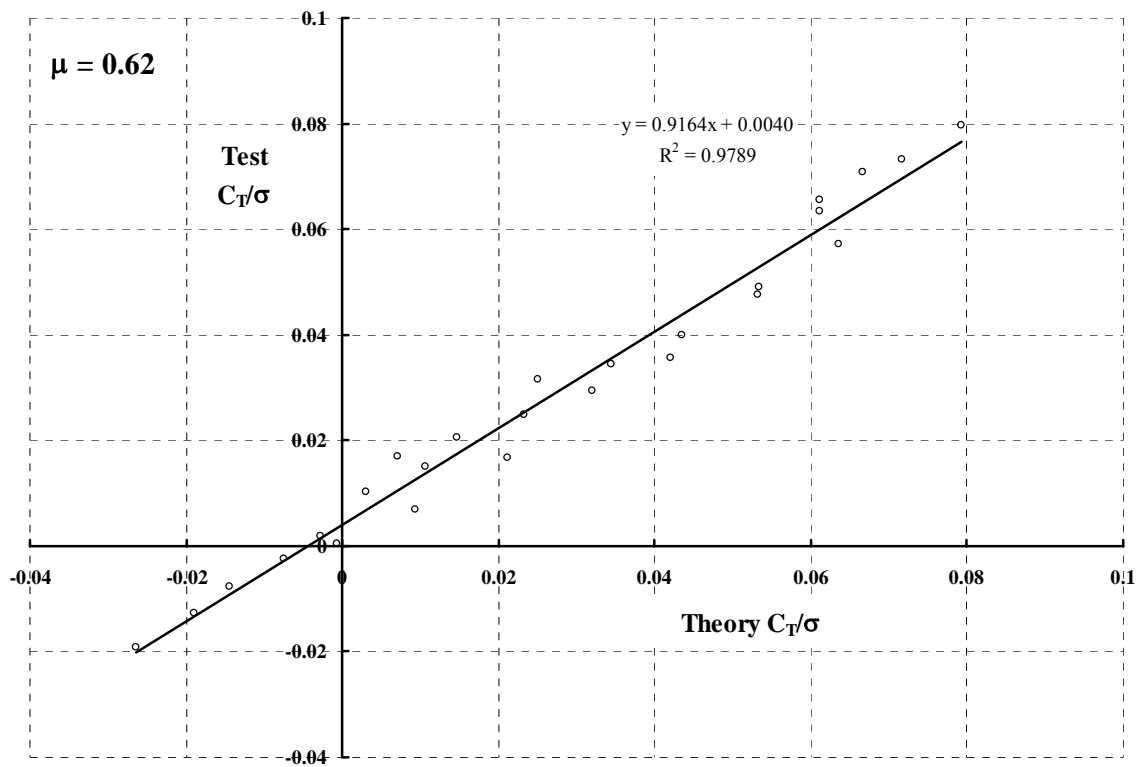


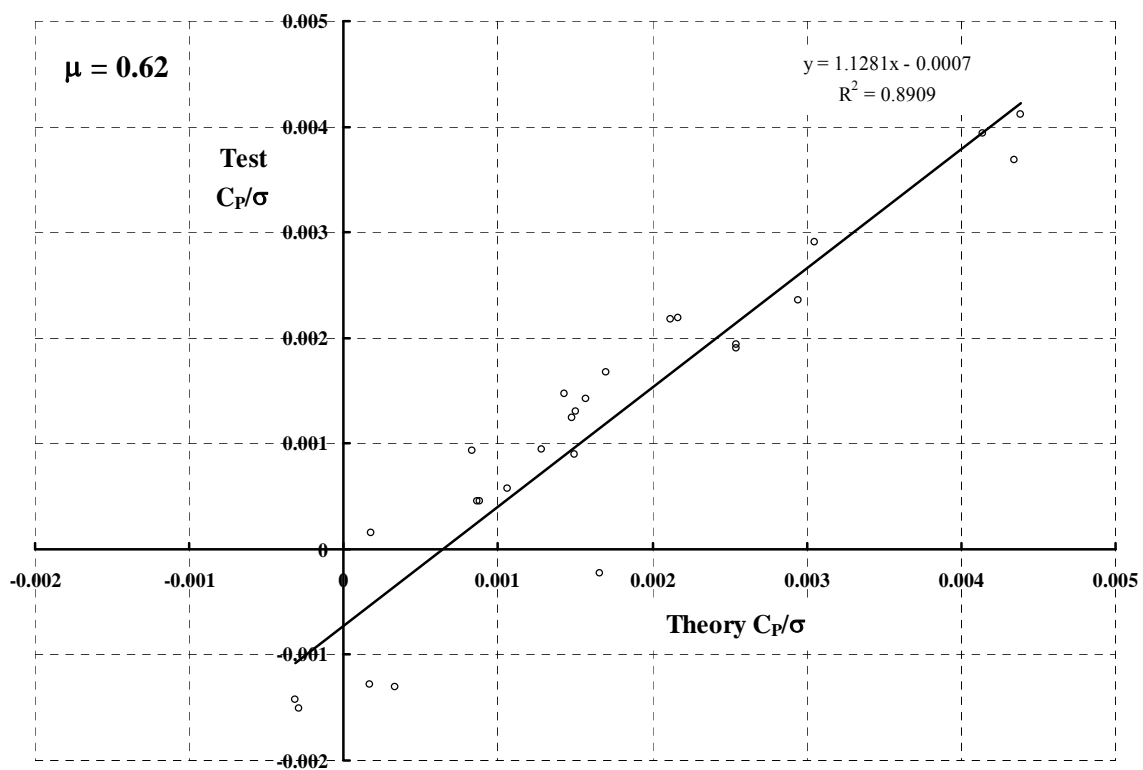
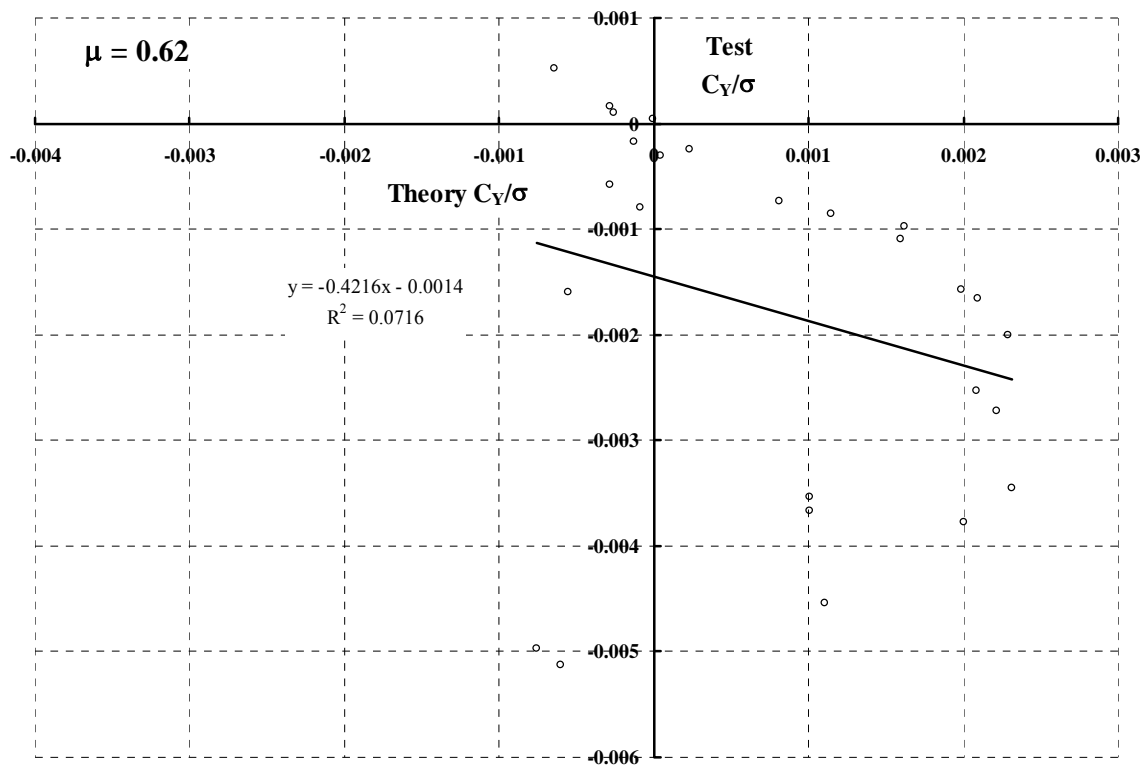


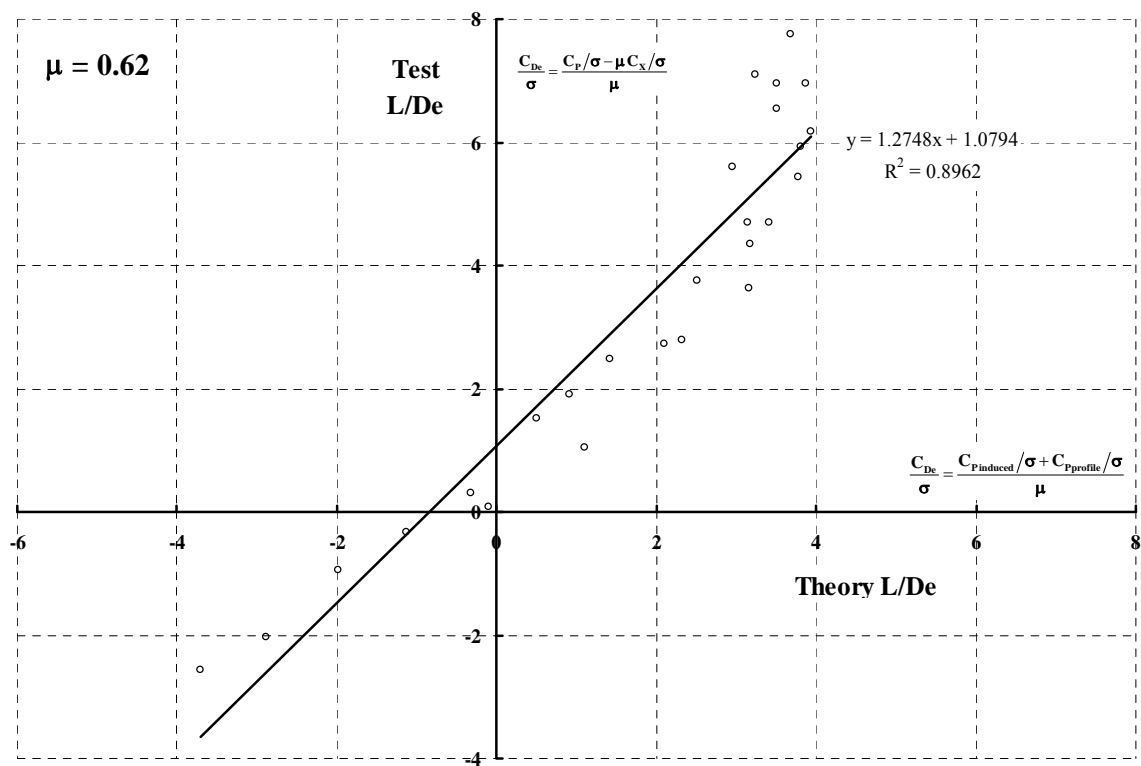
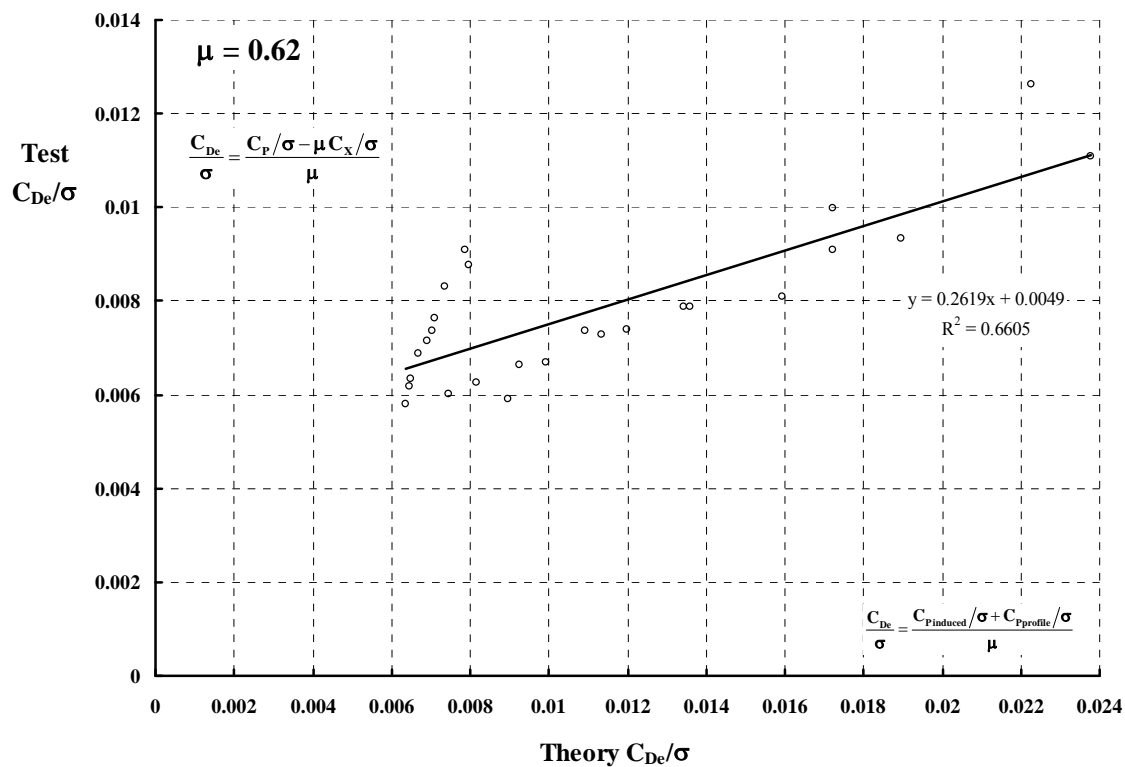


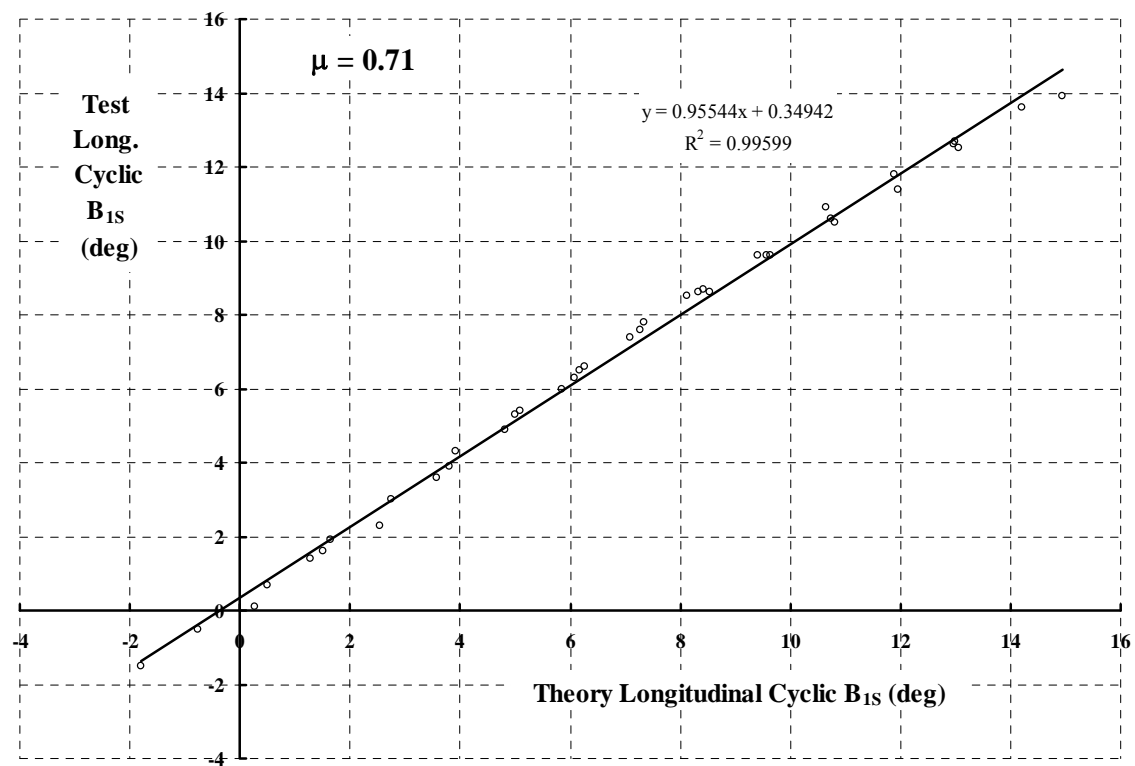
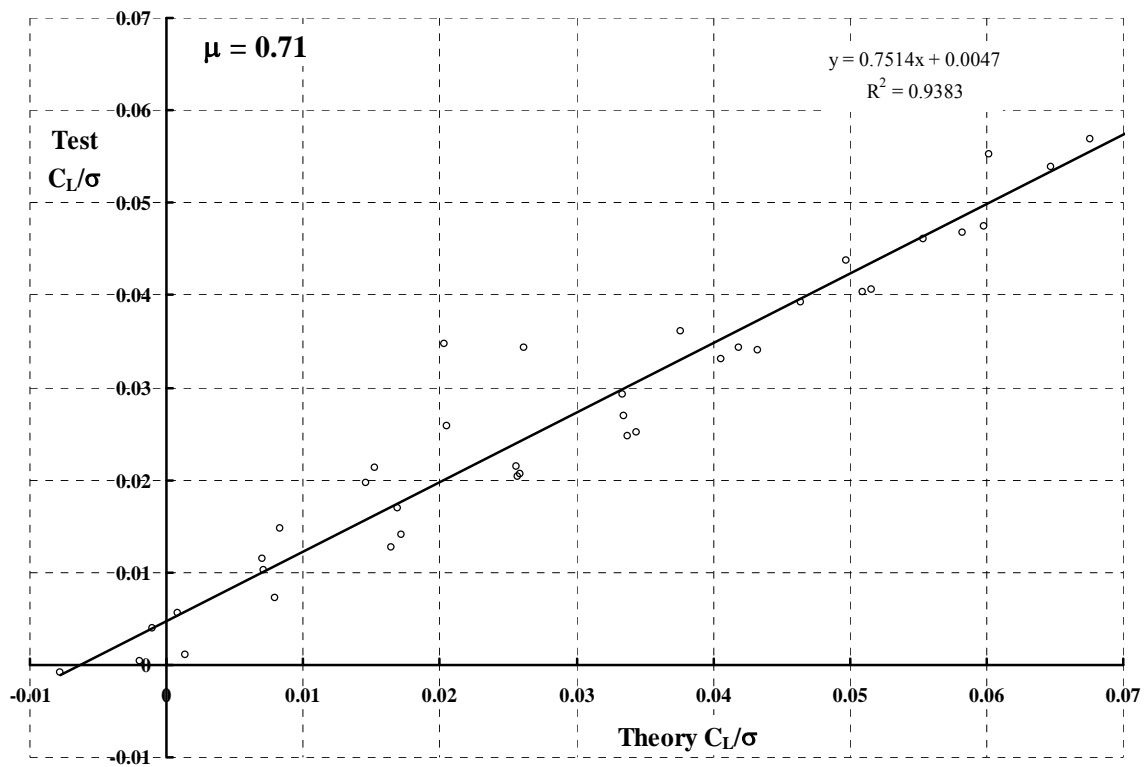


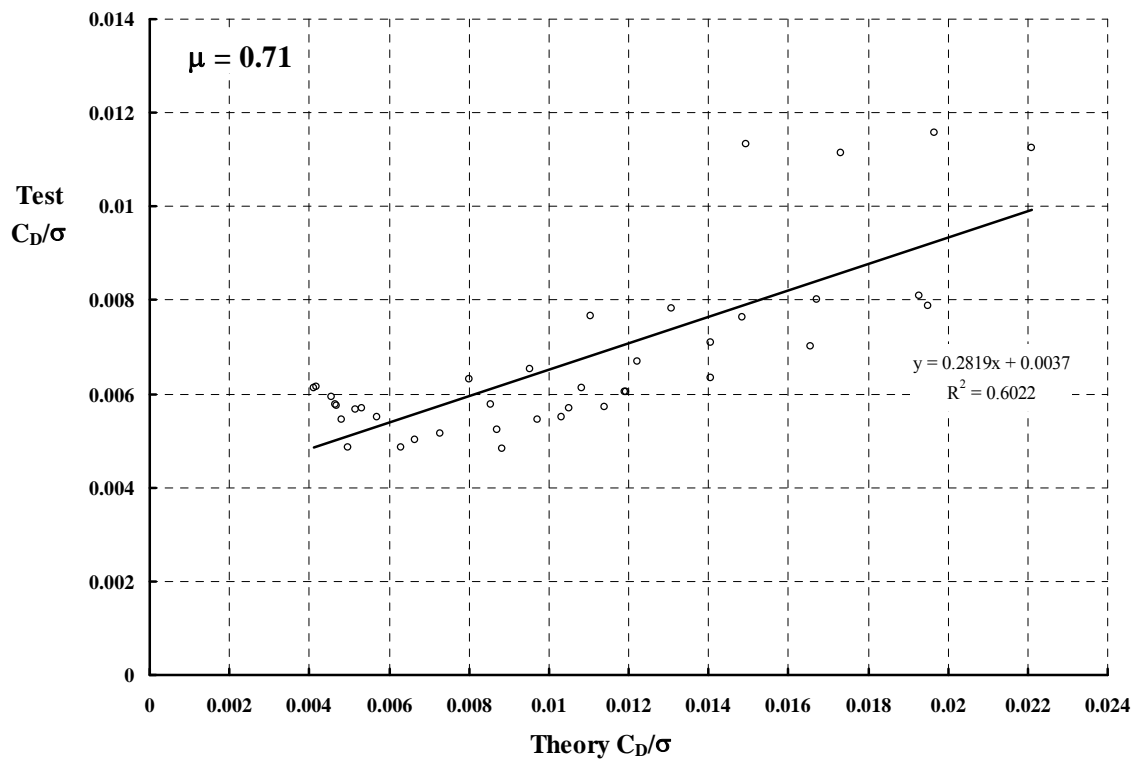
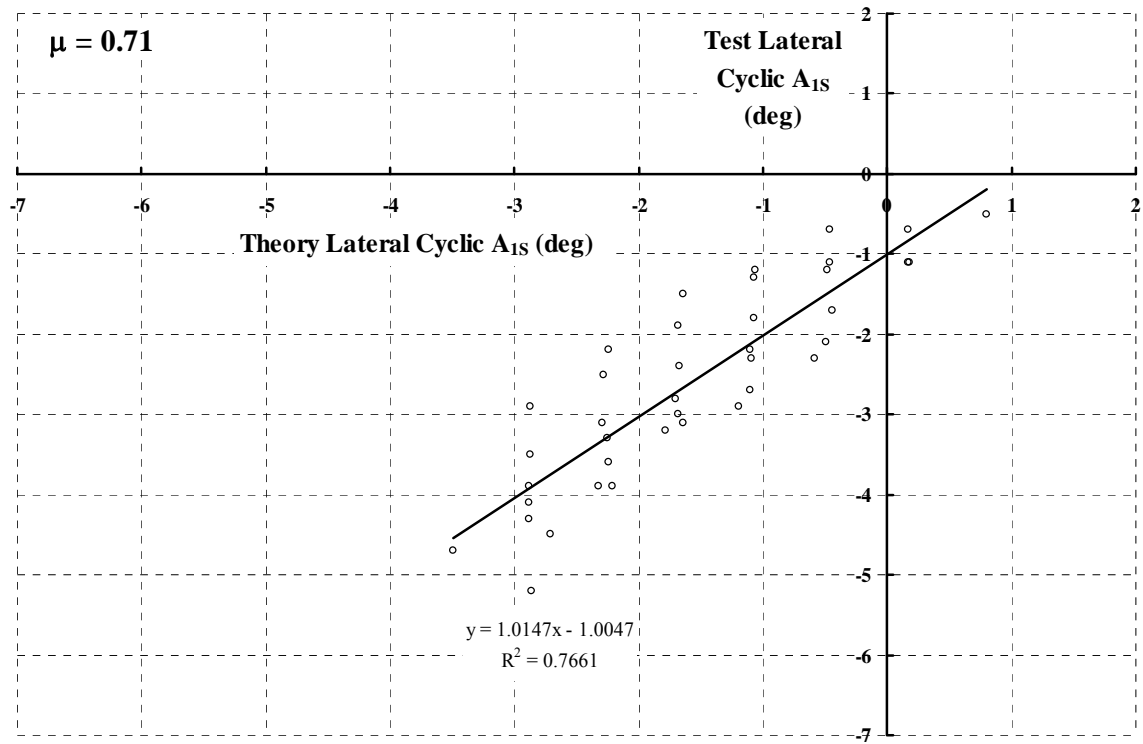


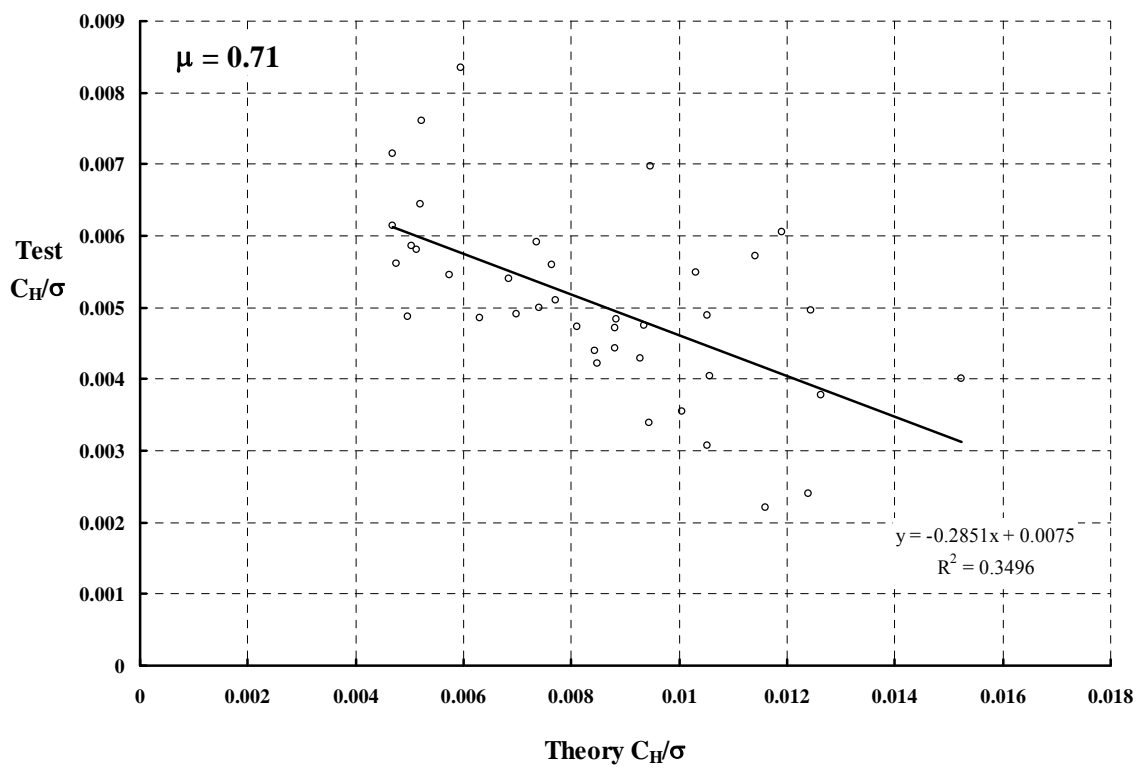
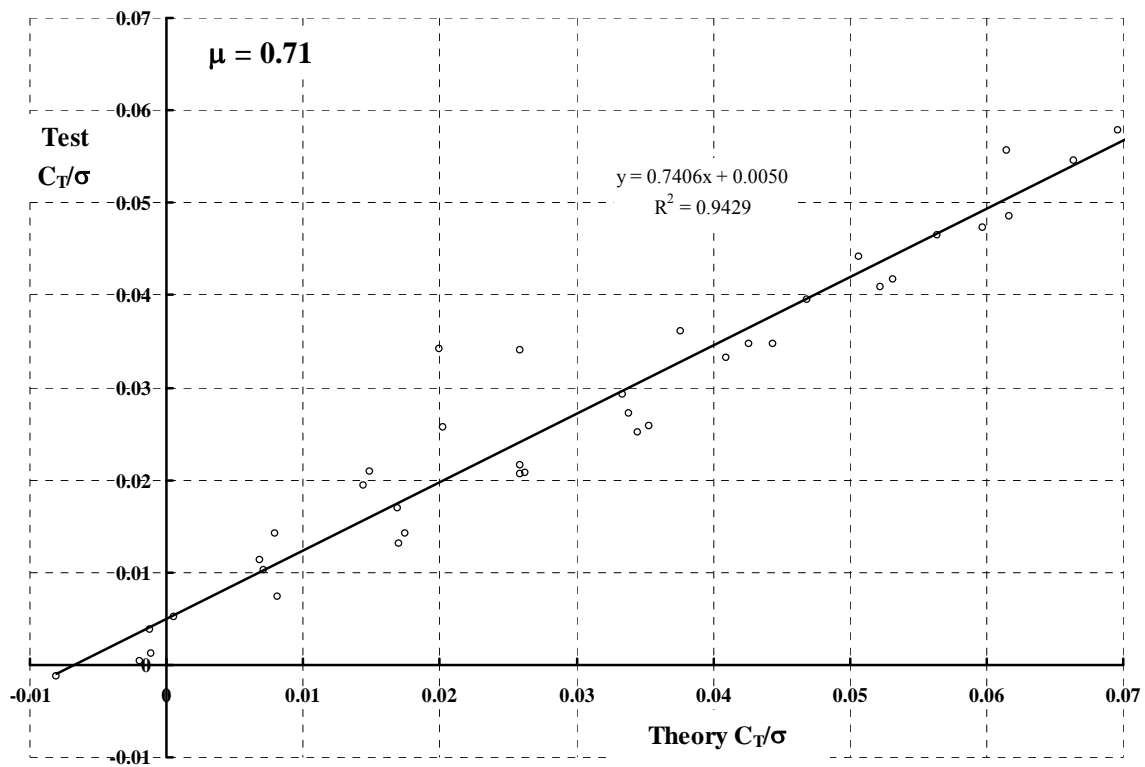


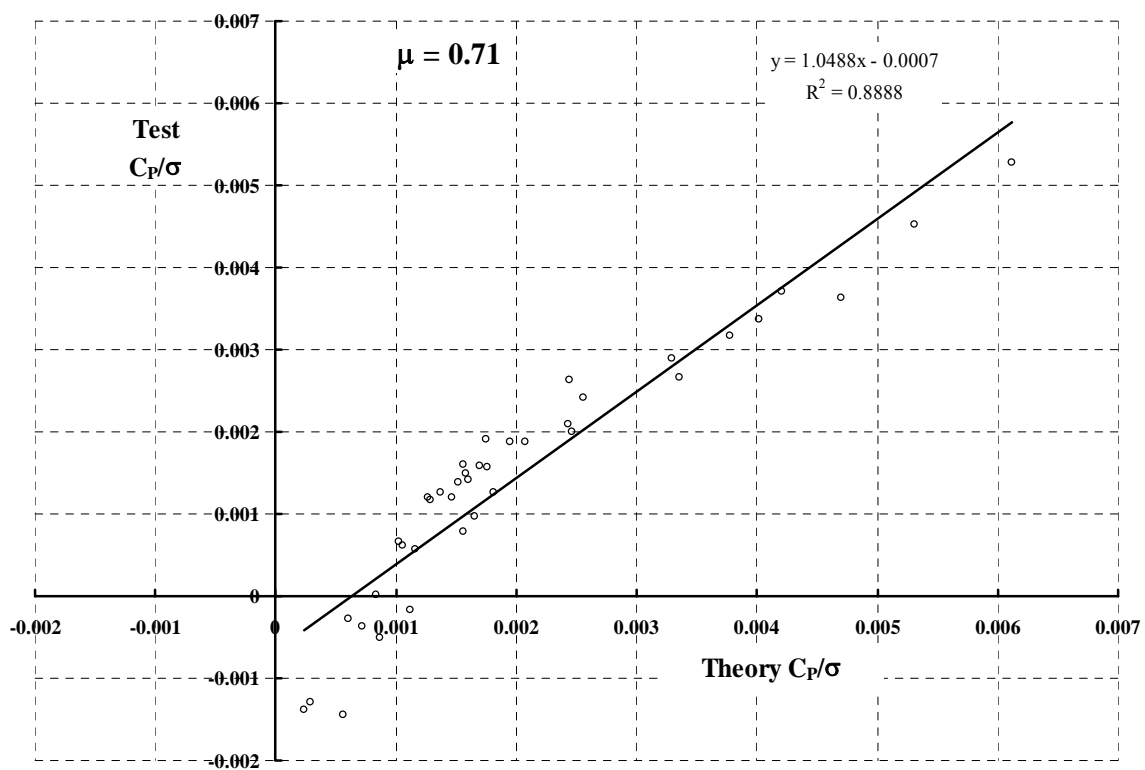
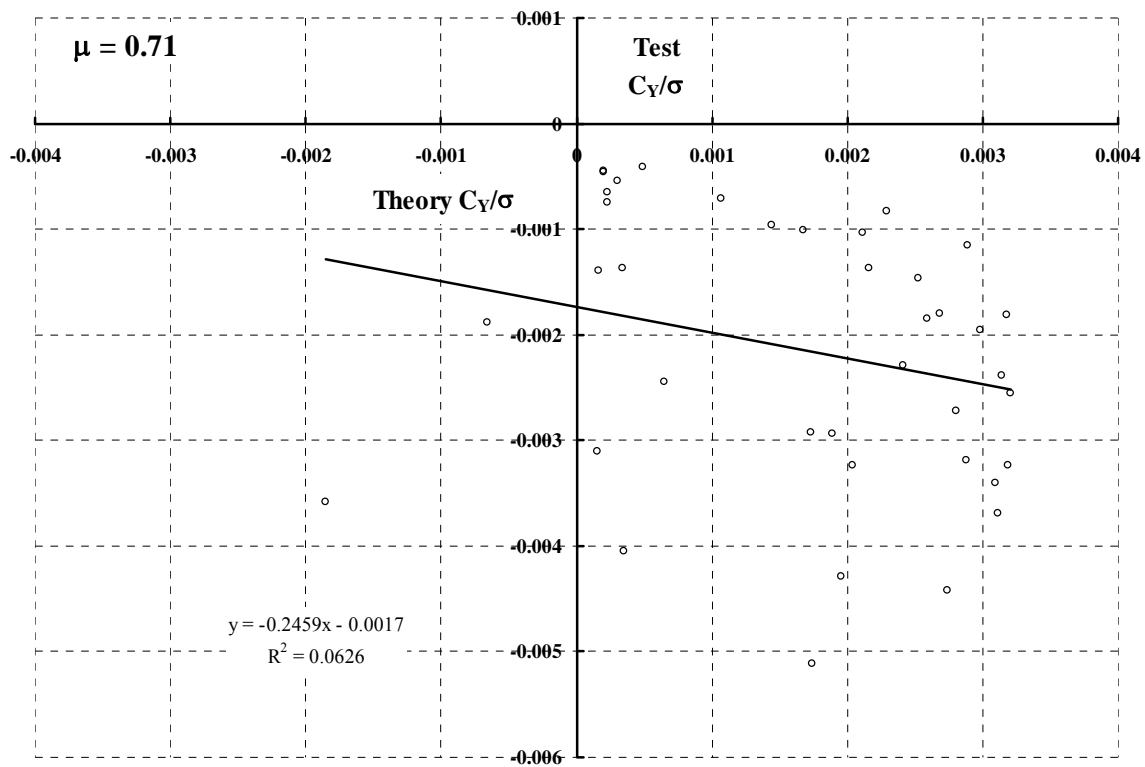


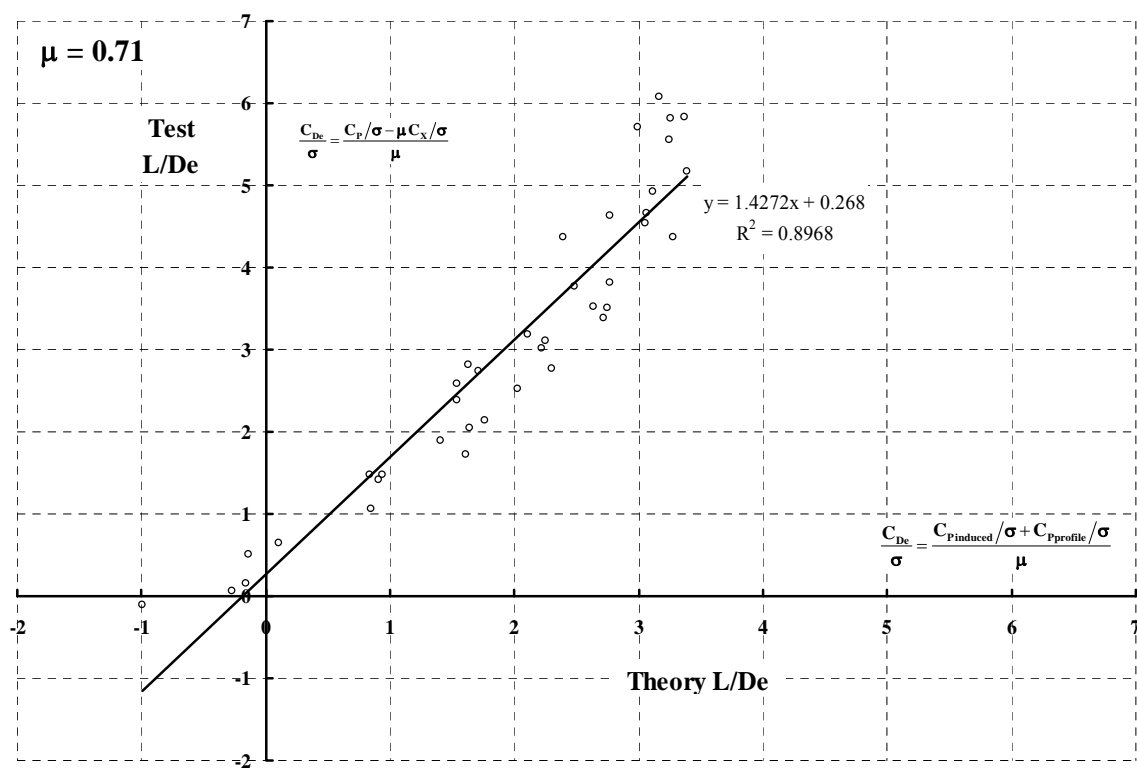
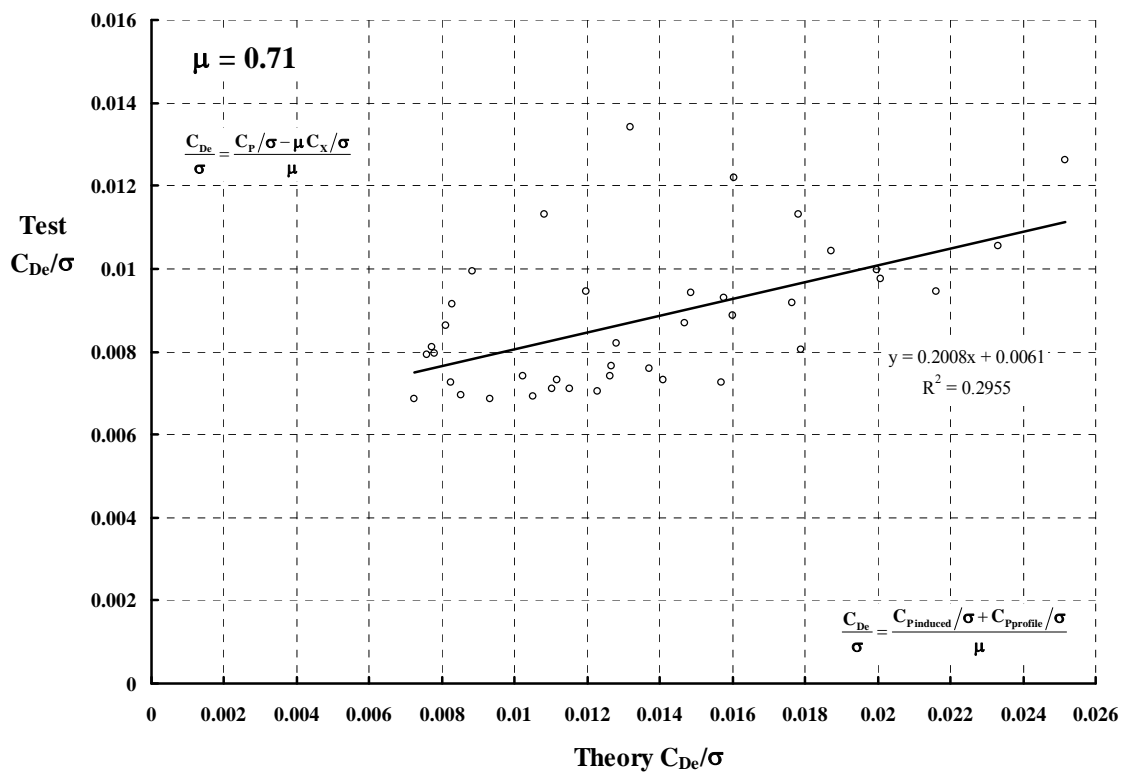


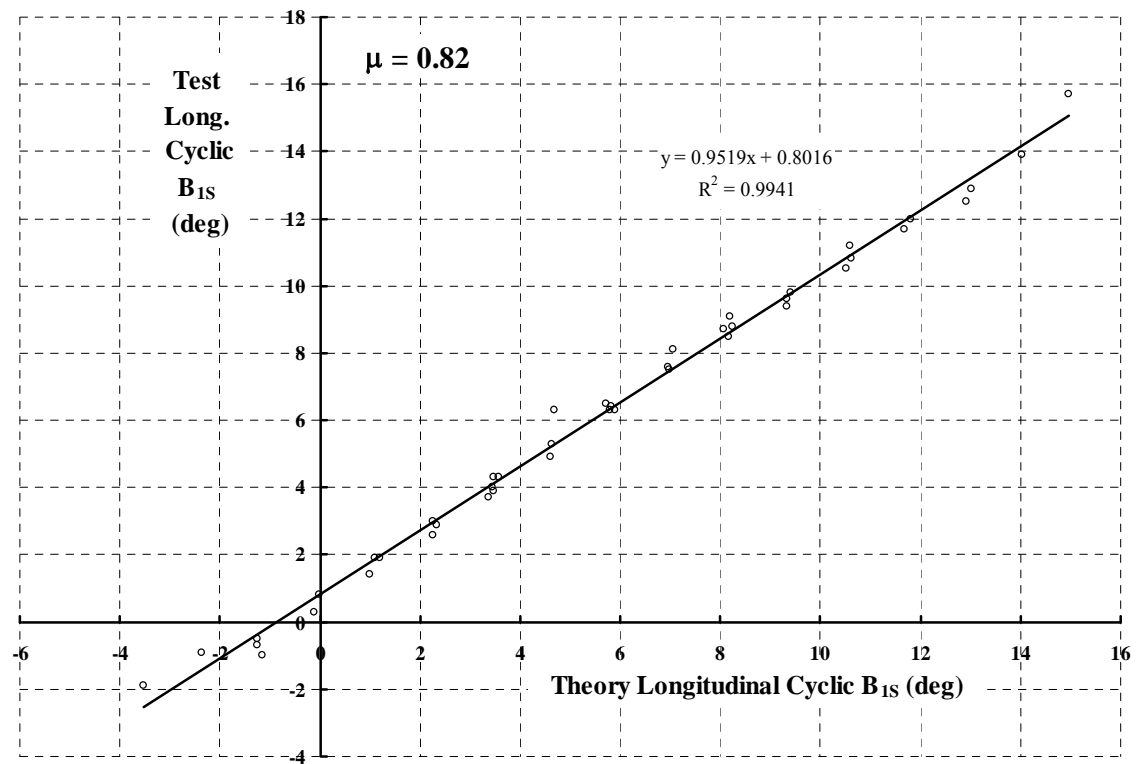
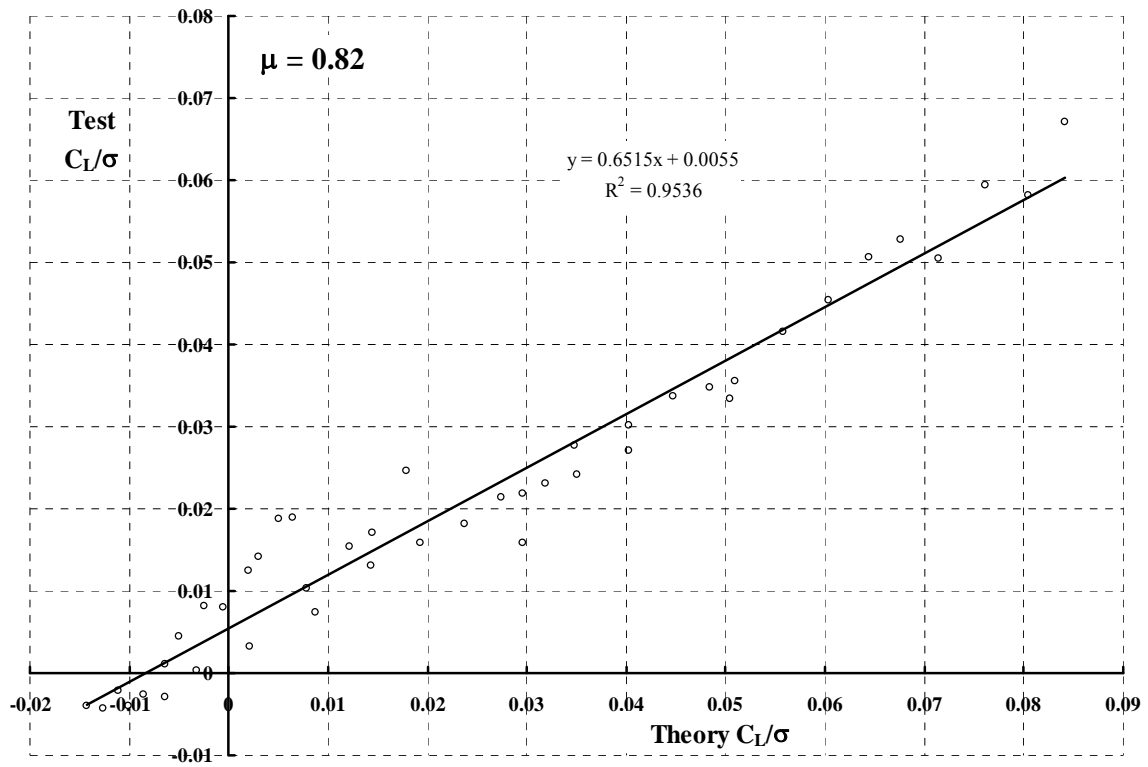


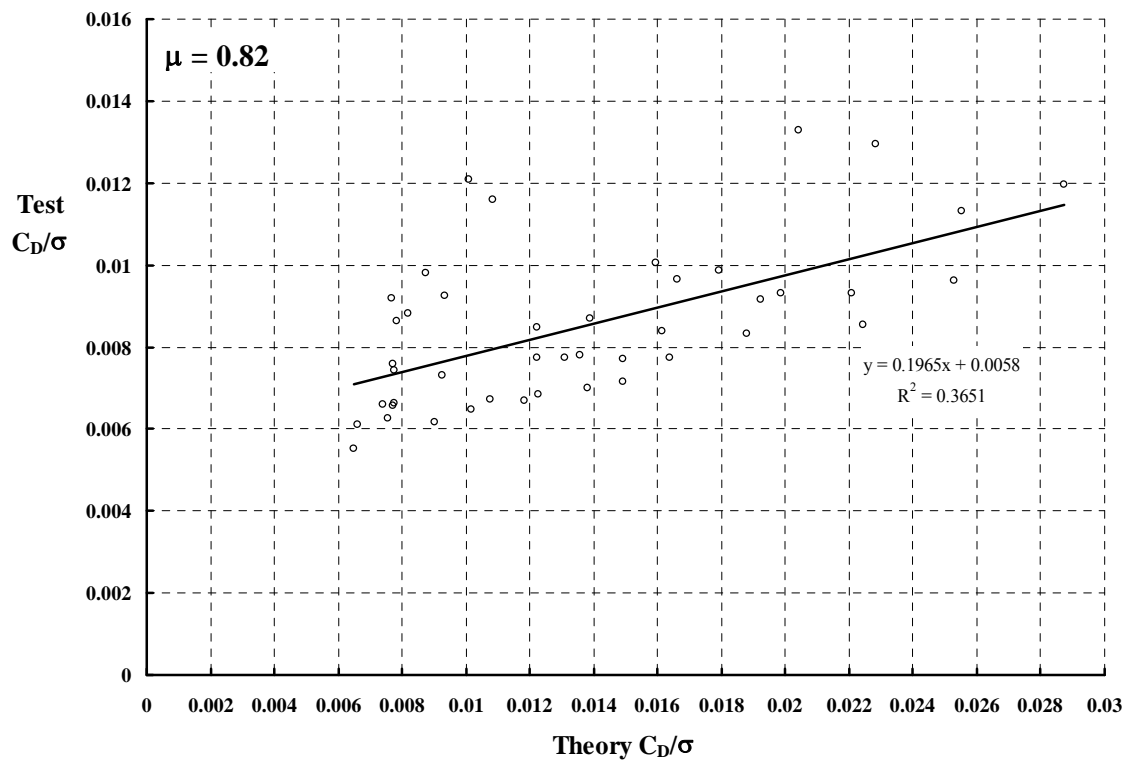
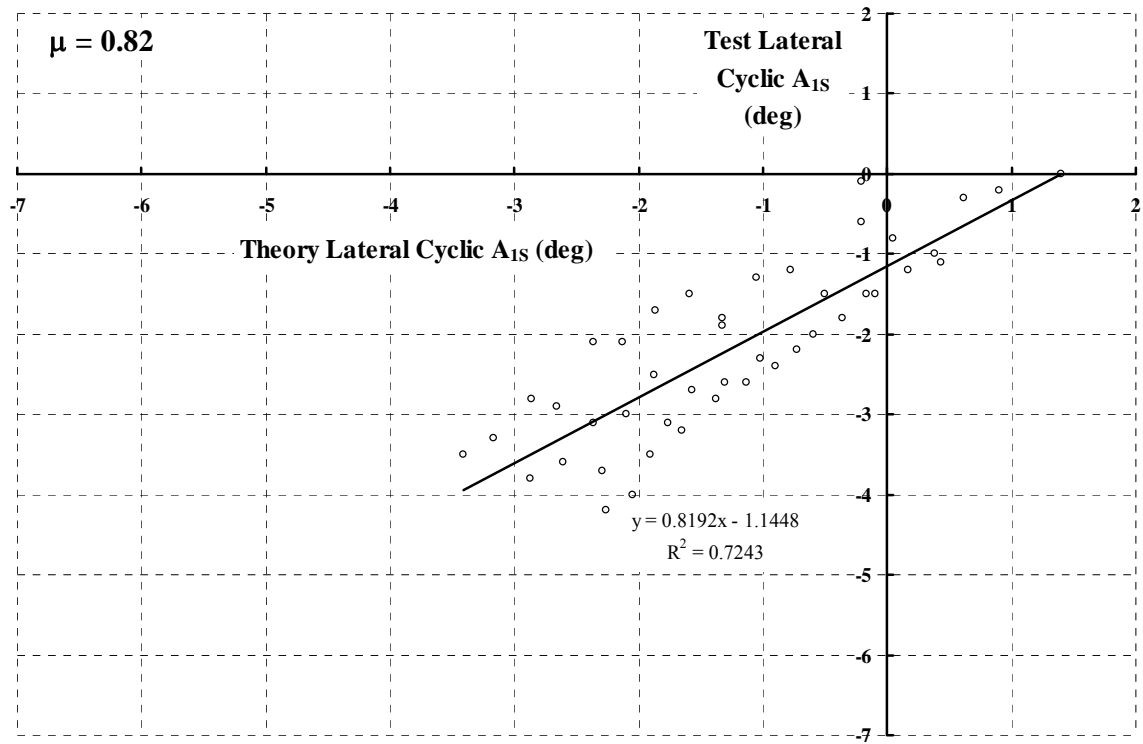


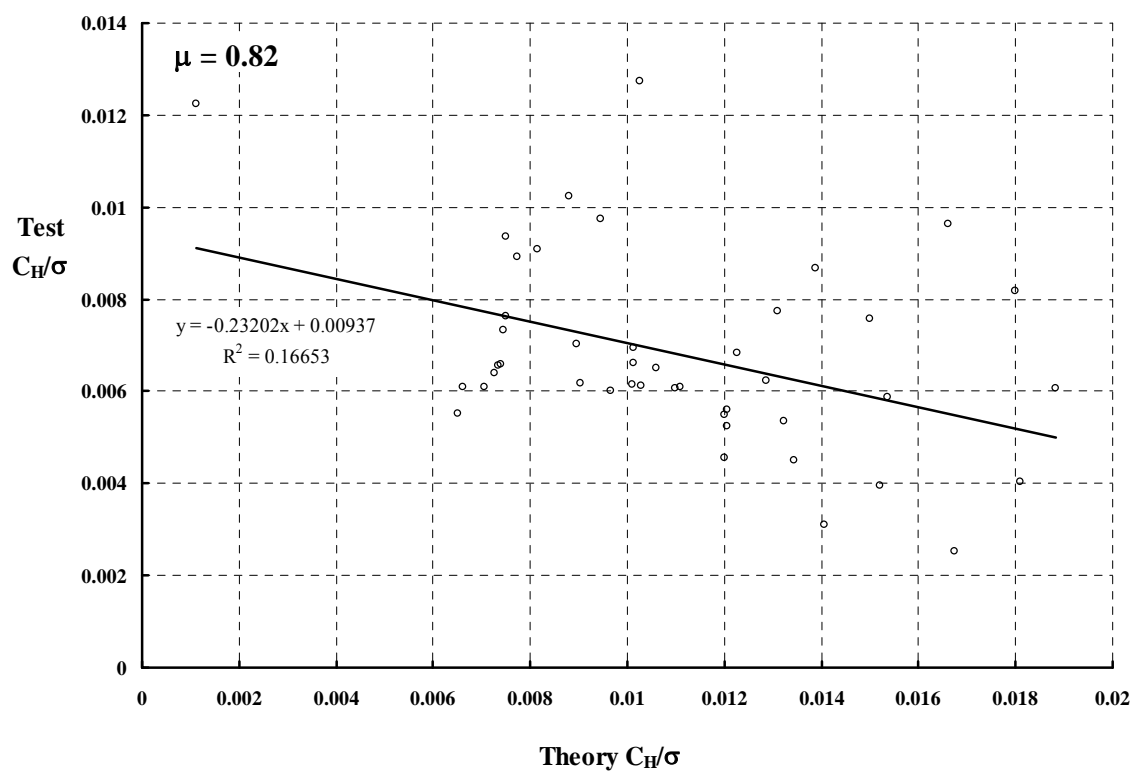
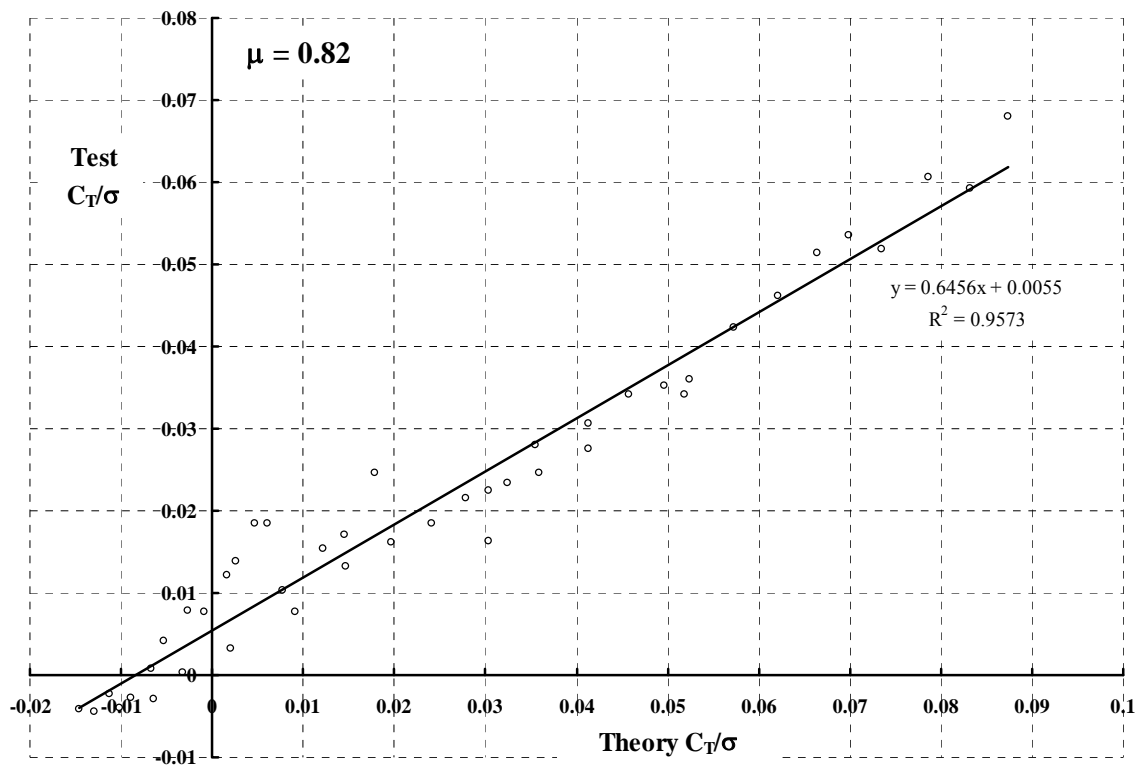


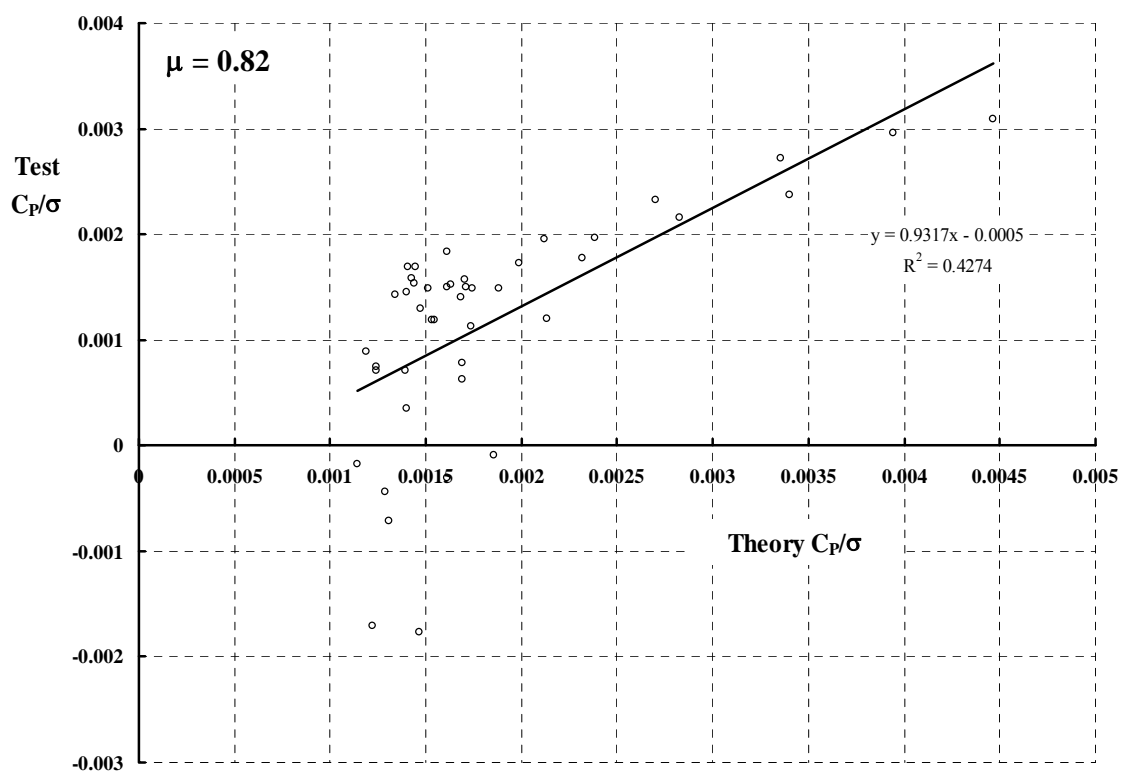
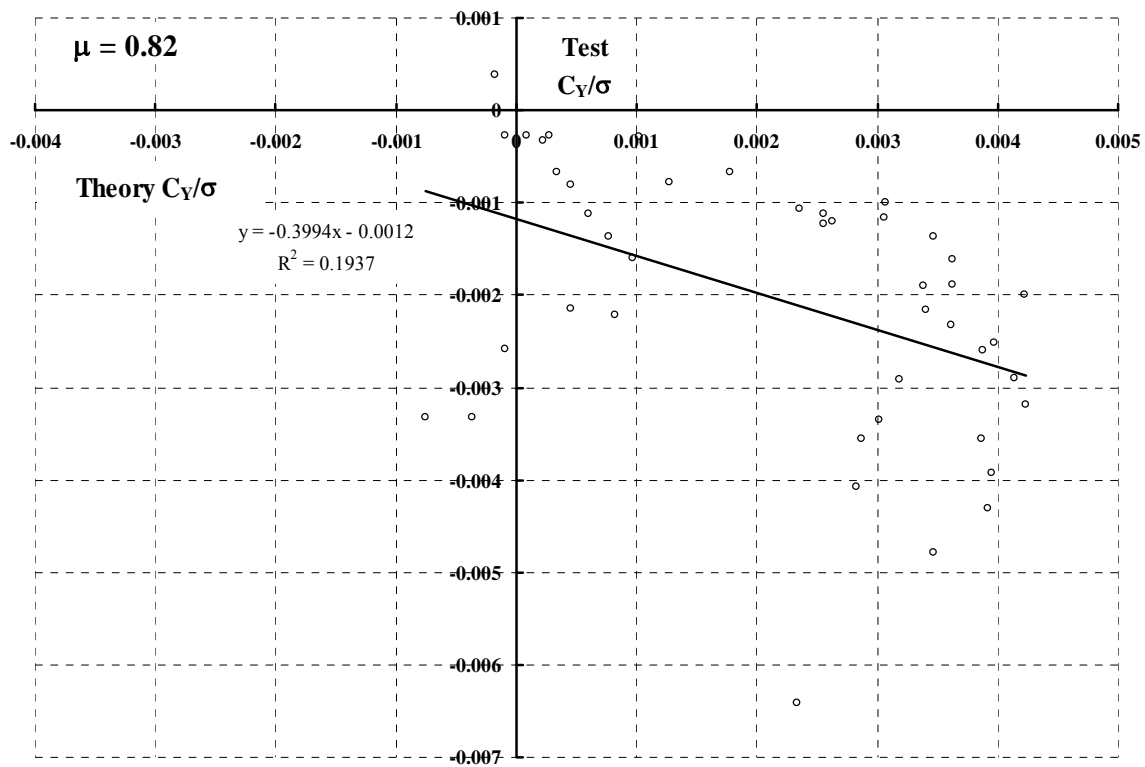


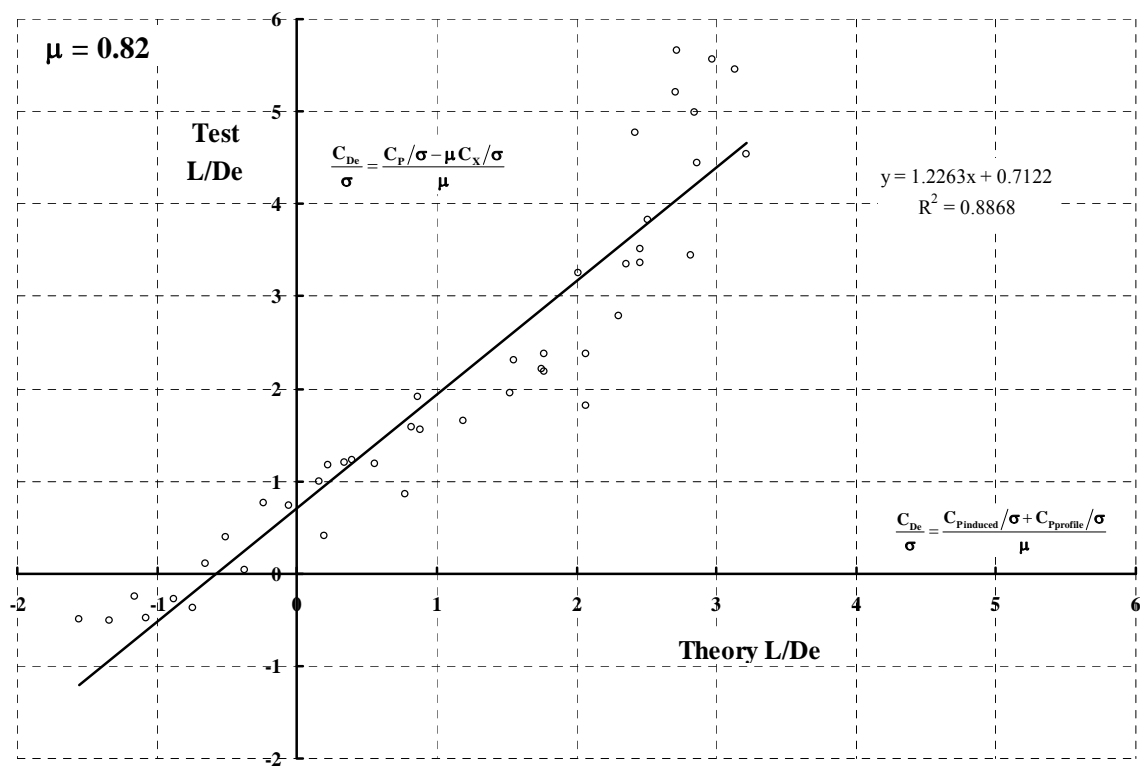
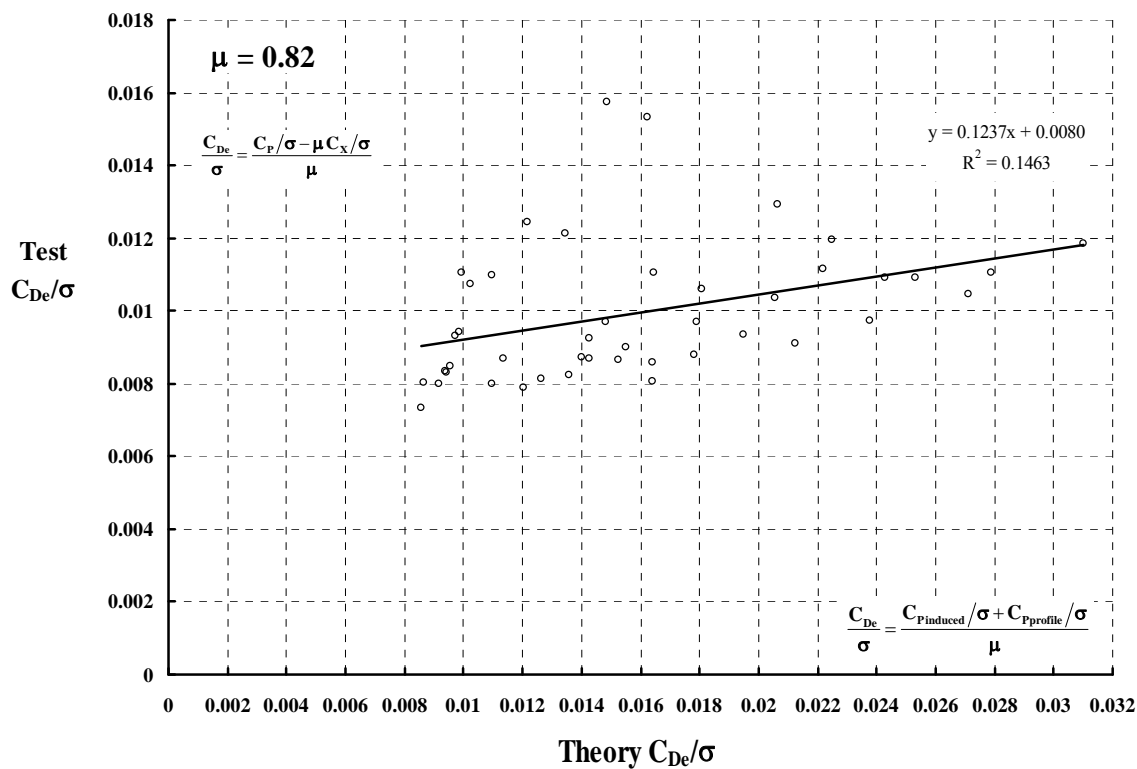


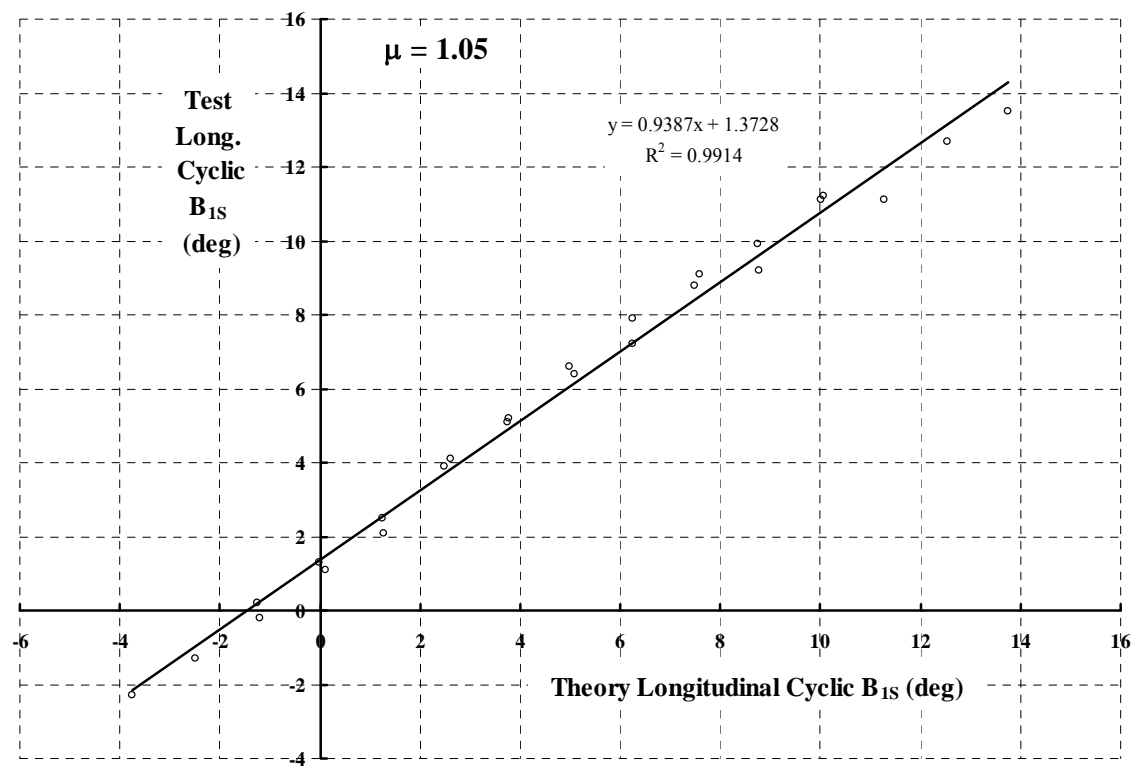
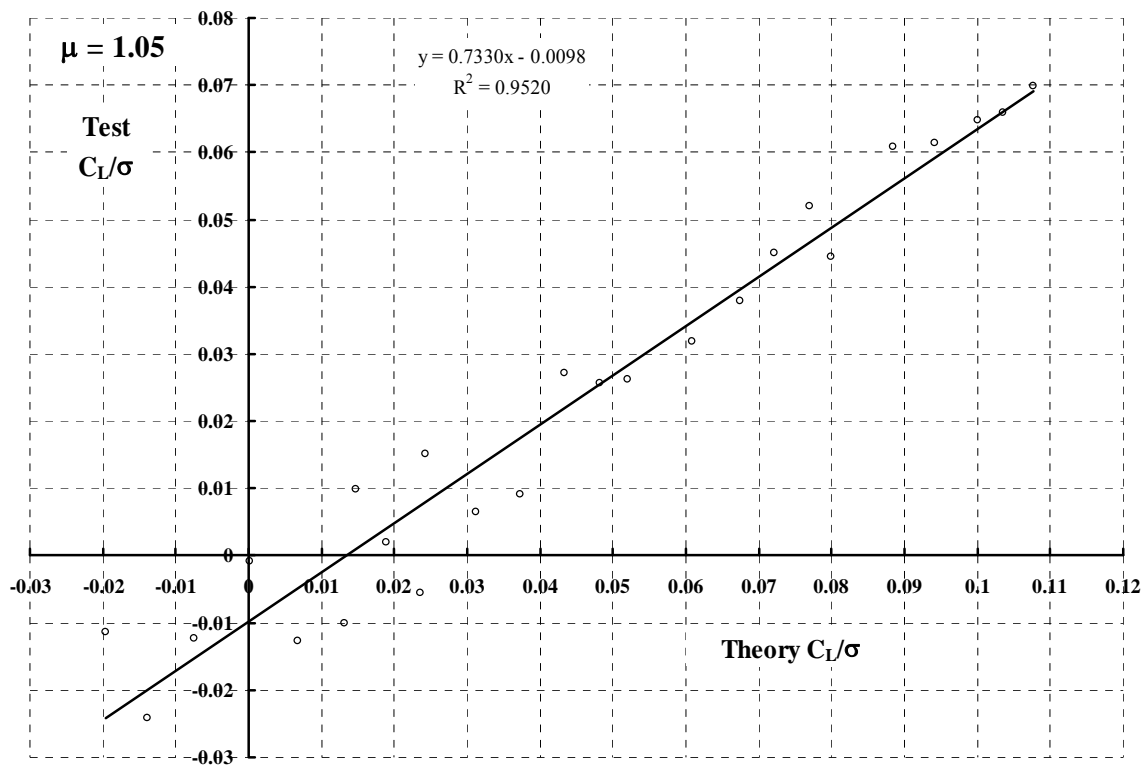


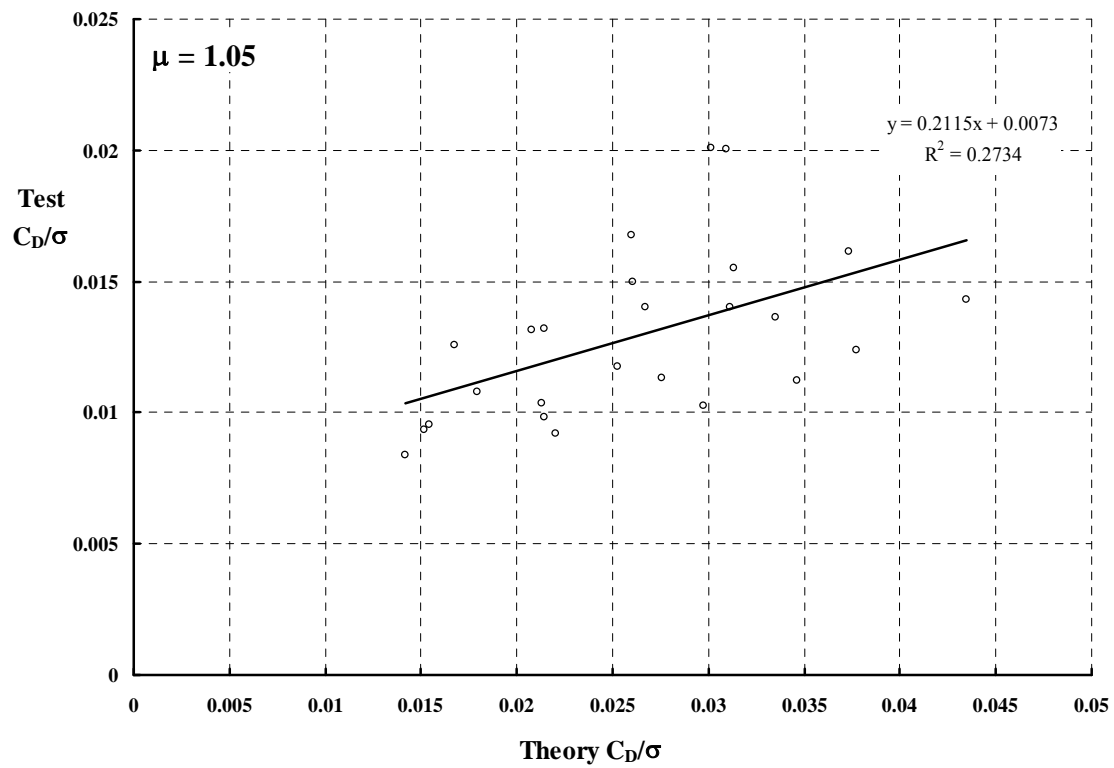
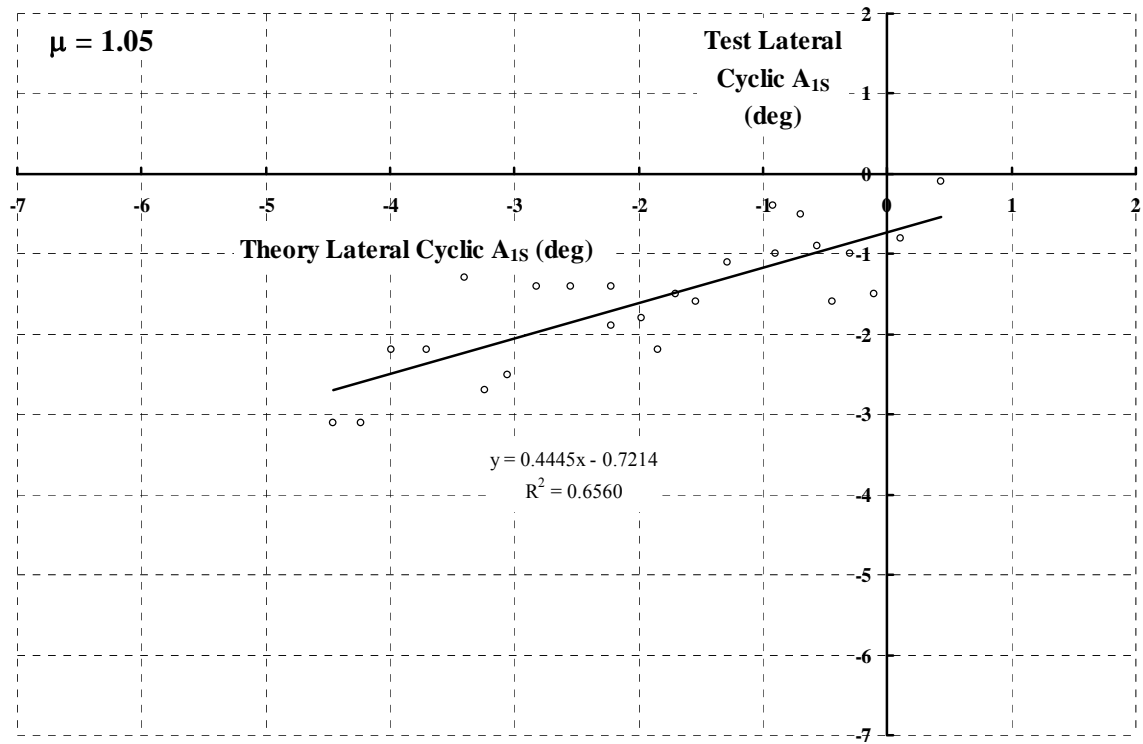


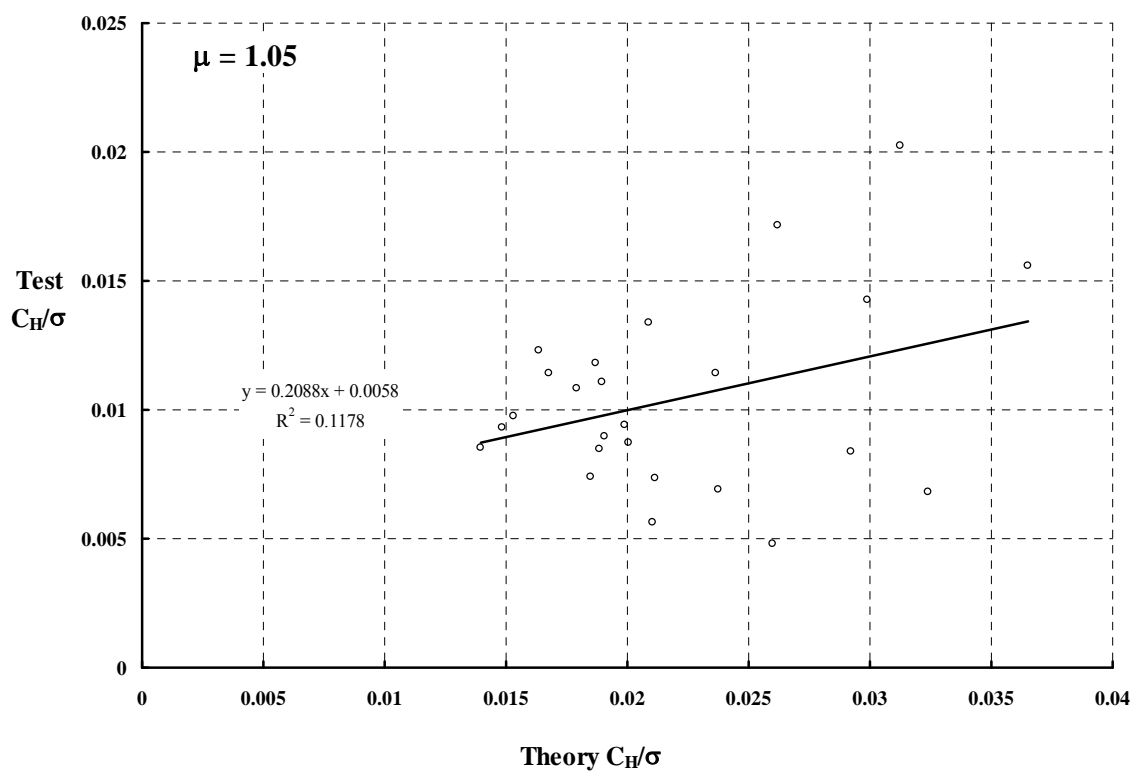
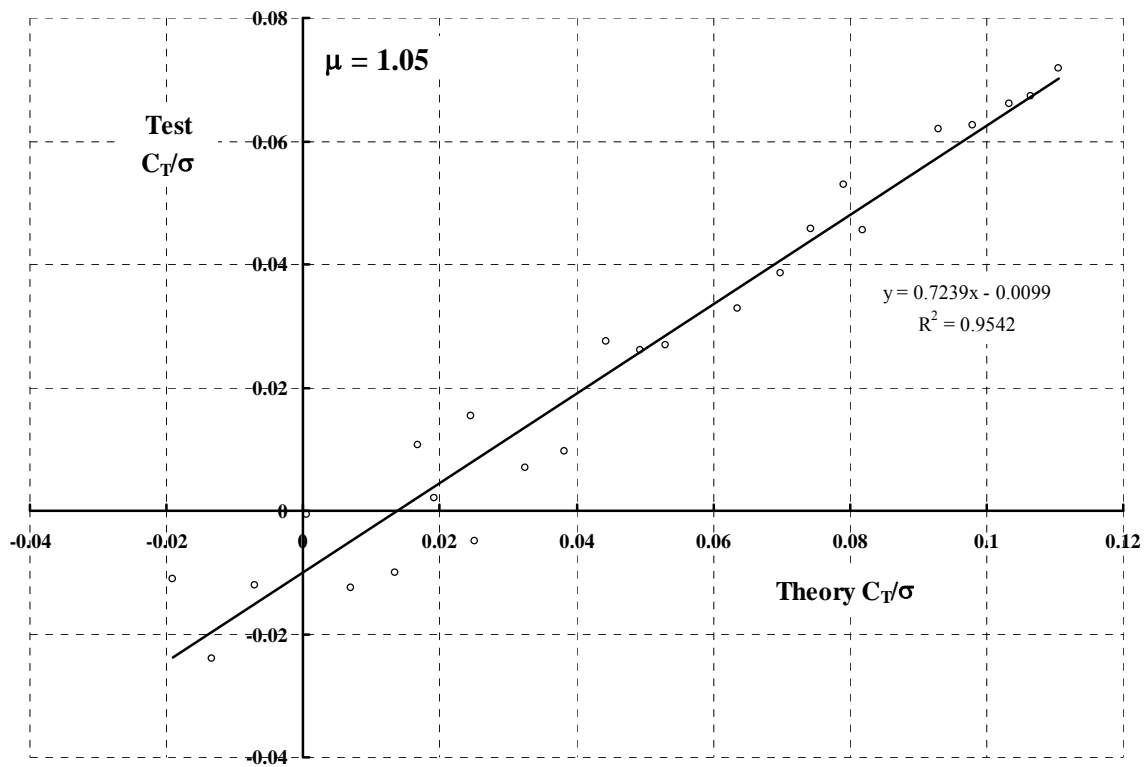


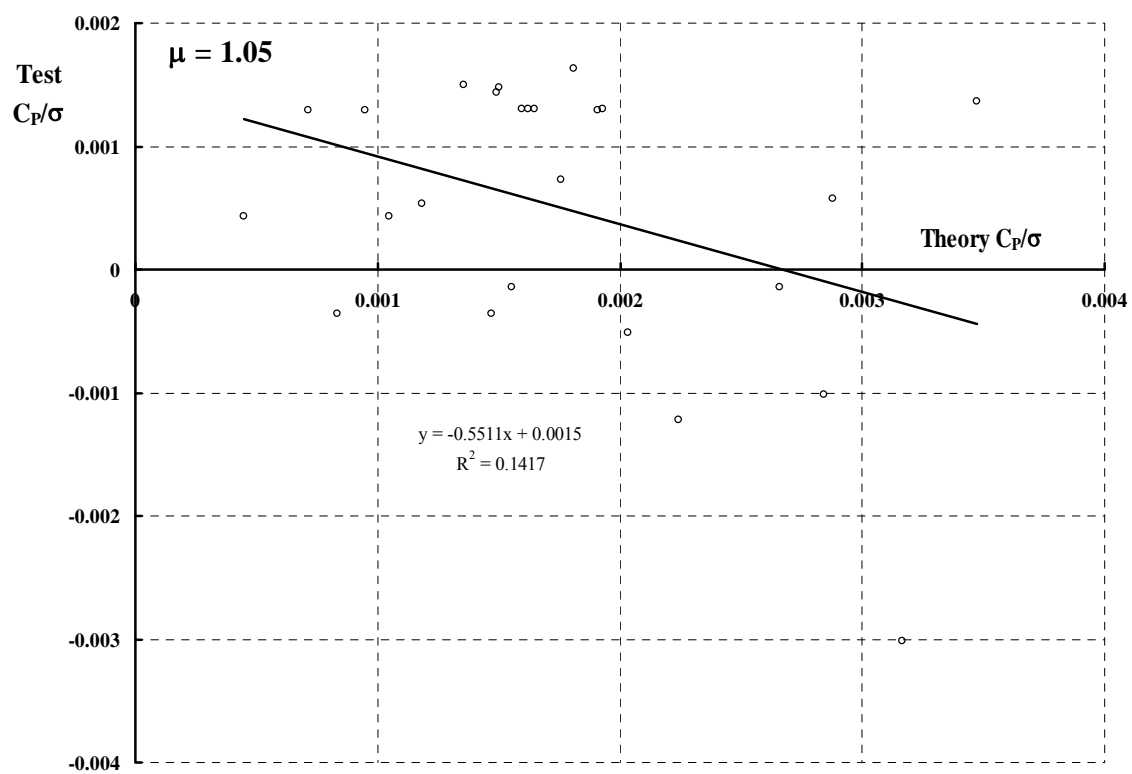
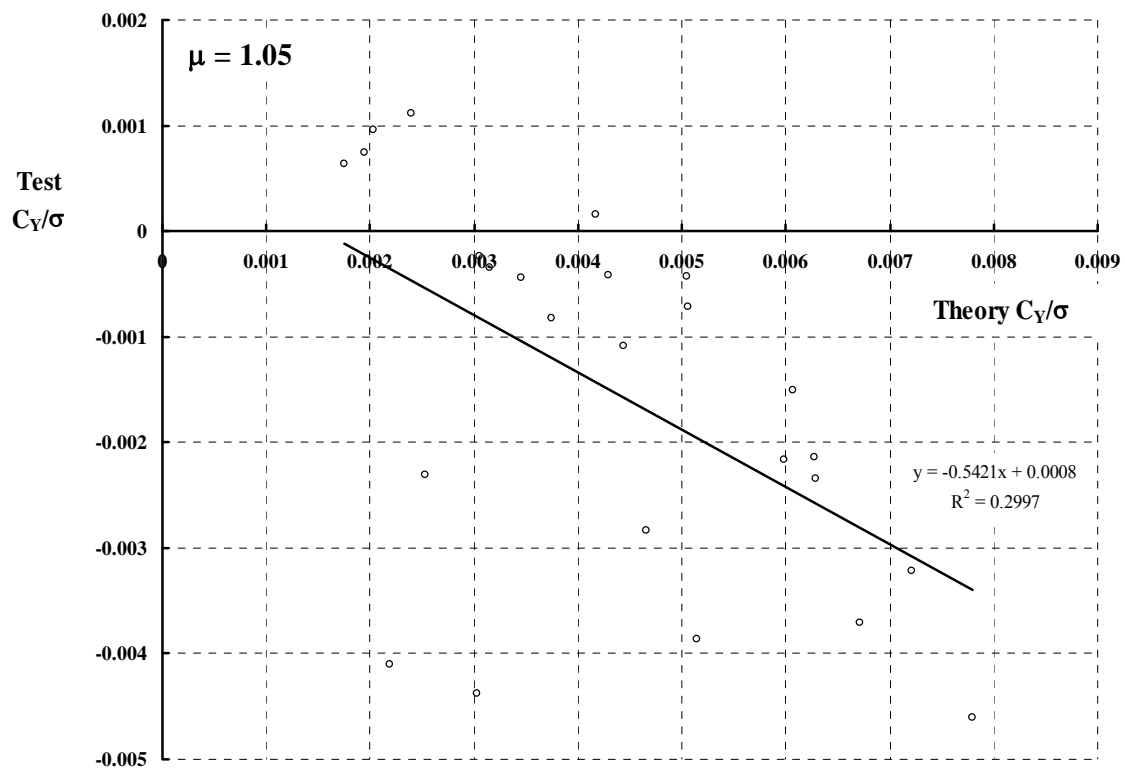


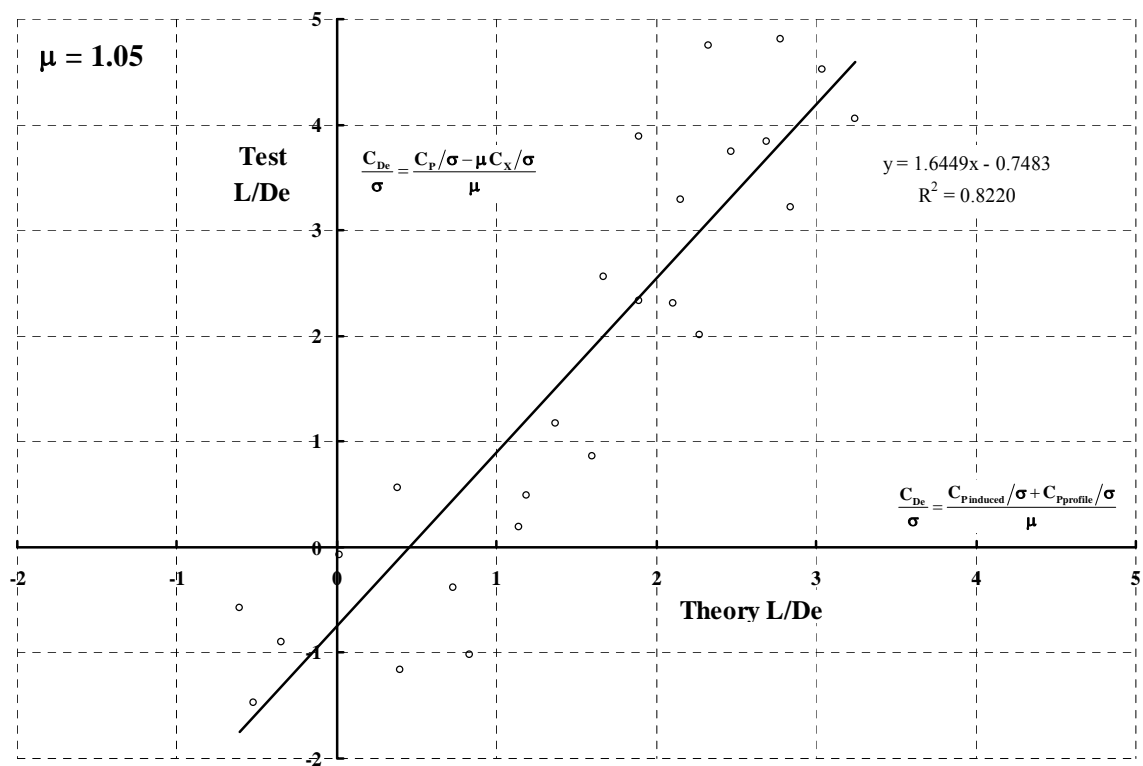
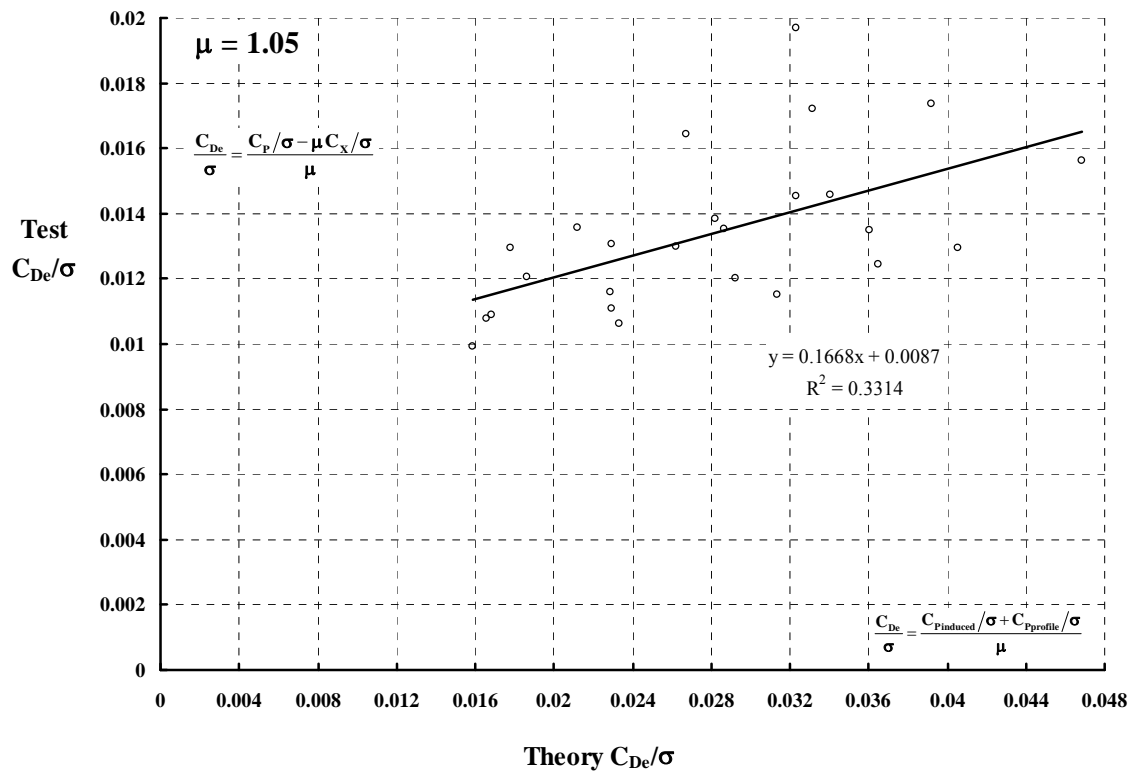












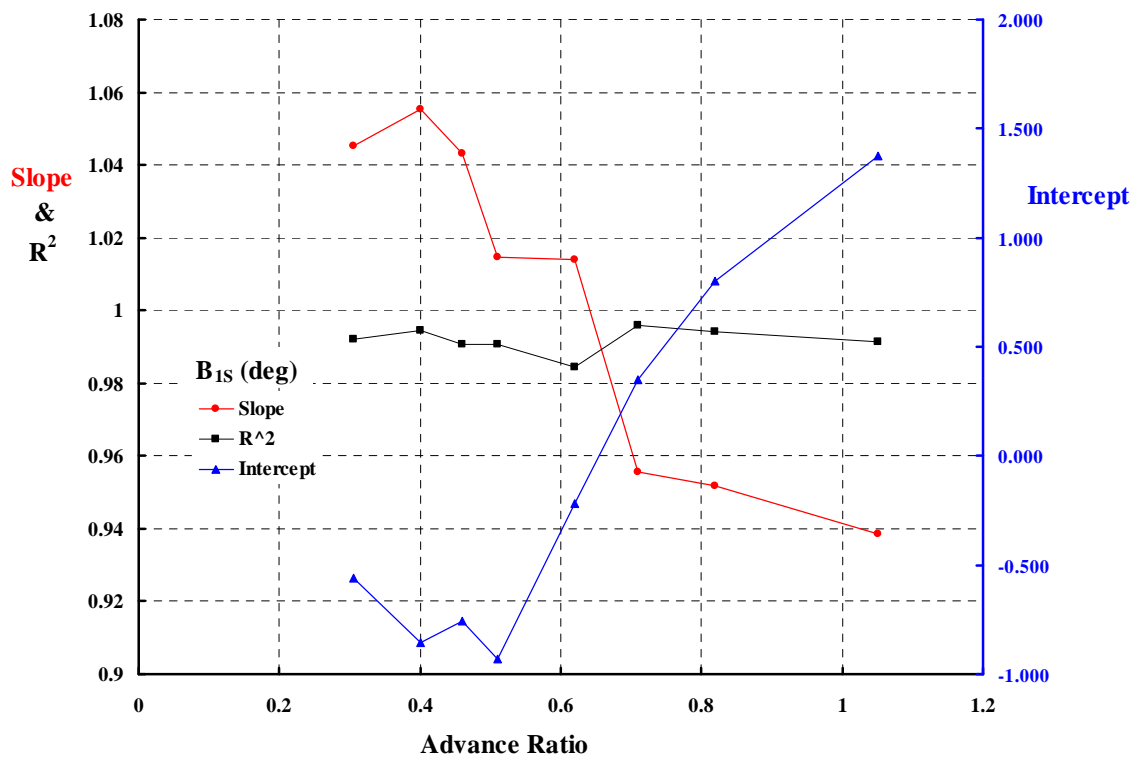
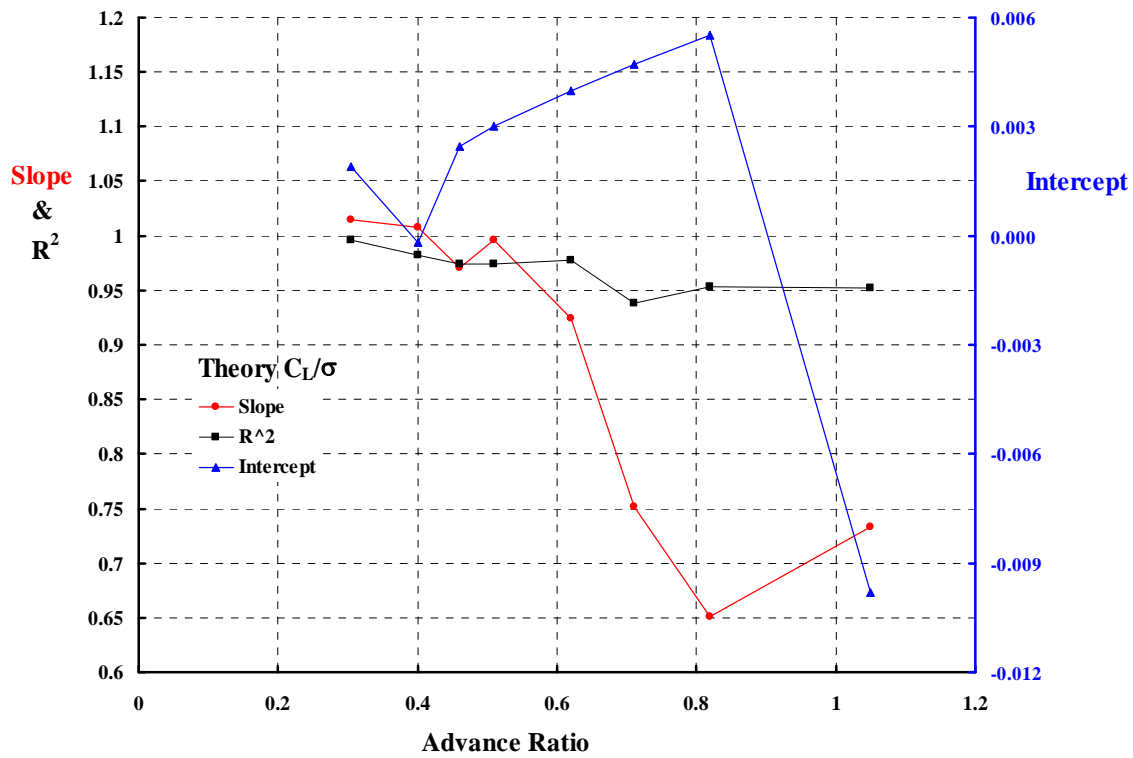
Longitudinal Cyclic				Lateral Cyclic		
Mu	SLOPE	Intercept	R²	SLOPE	Intercept	R²
0.305	1.0451	-0.5614	0.9922	1.2959	-0.3538	0.8496
0.401	1.0552	-0.8542	0.9945	1.3952	-0.2108	0.8144
0.460	1.0430	-0.7550	0.9906	1.3174	-0.3623	0.7361
0.510	1.0146	-0.9278	0.9906	1.1079	-0.8099	0.6655
0.620	1.0139	-0.2156	0.9844	0.9999	-1.2132	0.6955
0.710	0.9554	0.3494	0.9960	1.0147	-1.0047	0.7661
0.820	0.9519	0.8016	0.9941	0.8192	-1.1448	0.7243
1.050	0.9387	1.3728	0.9914	0.4445	-0.7214	0.6560

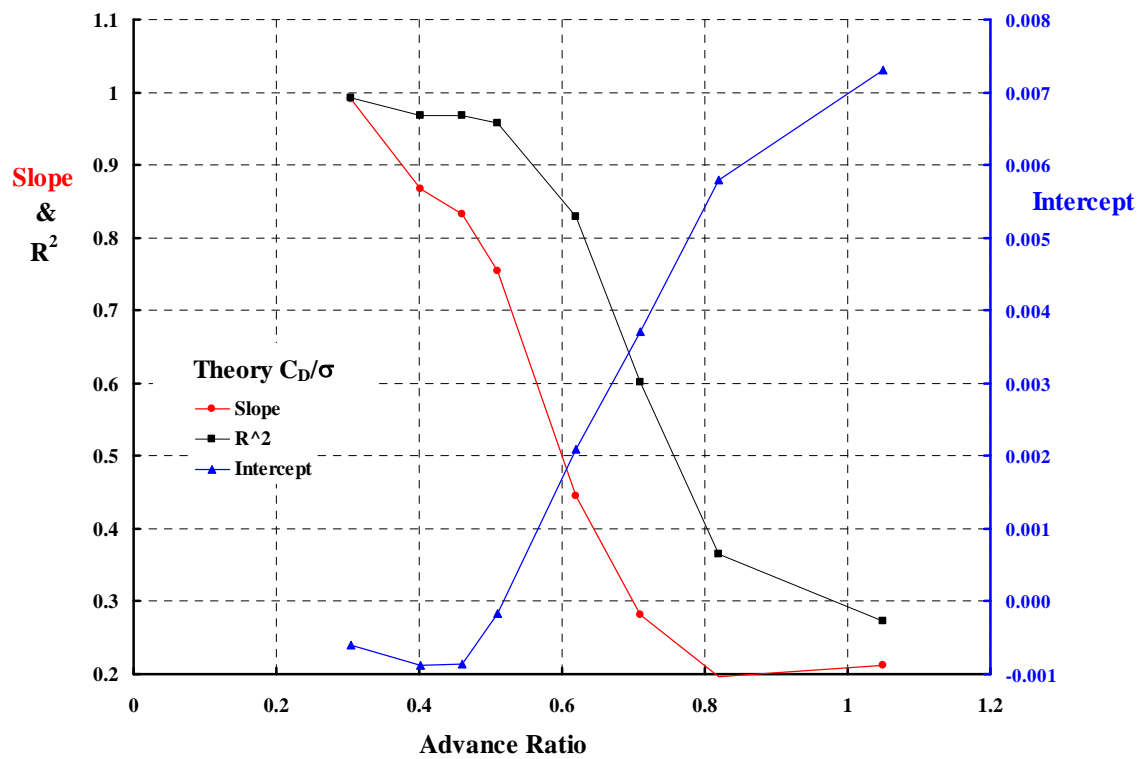
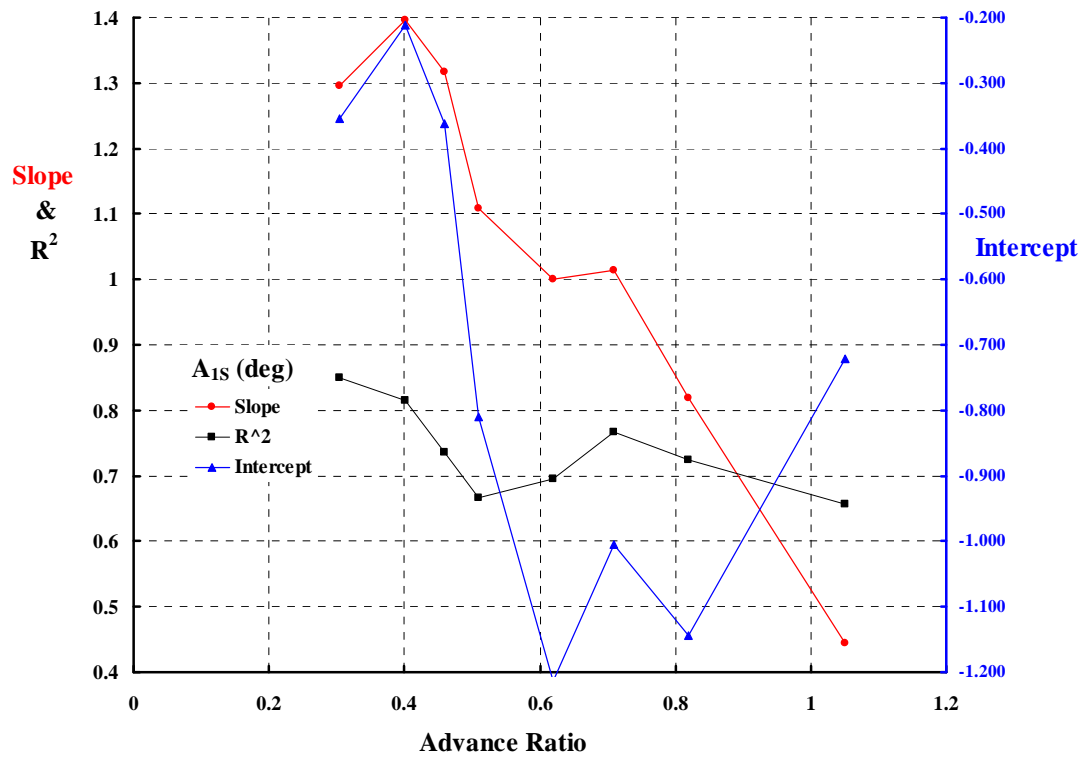
Lift Coefficient				Drag Coefficient		
Mu	SLOPE	Intercept	R²	SLOPE	Intercept	R²
0.305	1.0150	0.0019	0.9966	0.9897	-0.0006	0.9926
0.401	1.0078	-0.0002	0.9828	0.8675	-0.0009	0.9680
0.460	0.9702	0.0025	0.9739	0.8318	-0.0009	0.9684
0.510	0.9964	0.0030	0.9743	0.7539	-0.0002	0.9576
0.620	0.9238	0.0040	0.9774	0.4443	0.0021	0.8293
0.710	0.7514	0.0047	0.9383	0.2819	0.0037	0.6022
0.820	0.6515	0.0055	0.9536	0.1965	0.0058	0.3651
1.050	0.7330	-0.00983	0.9520	0.2115	0.0073	0.2734

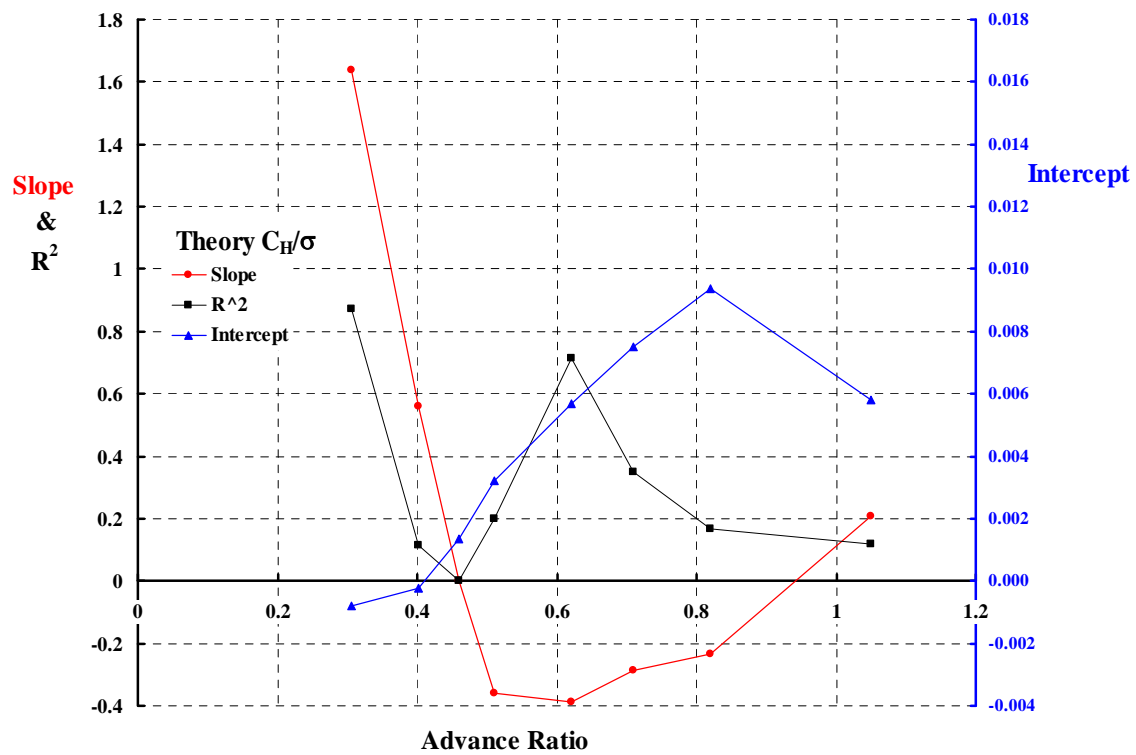
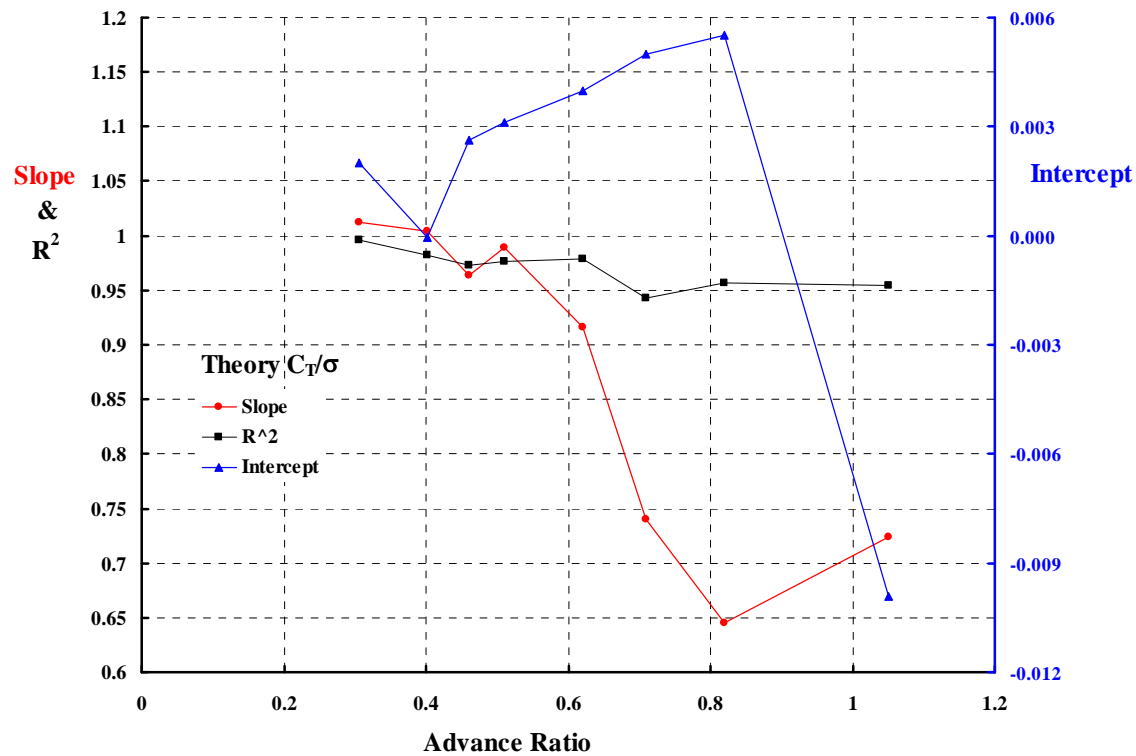
Thrust Coefficient				H-Force Coefficient		
Mu	SLOPE	Intercept	R²	SLOPE	Intercept	R²
0.305	1.0126	0.0020	0.9965	1.6399	-0.0008	0.8734
0.401	1.0037	0.0000	0.9825	0.5590	-0.0003	0.1127
0.460	0.9637	0.0026	0.9735	0.0024	0.0013	0.0000
0.510	0.9889	0.0031	0.9761	-0.3589	0.0032	0.2014
0.620	0.9164	0.0040	0.9789	-0.3874	0.0057	0.7161
0.710	0.7406	0.0050	0.9429	-0.2851	0.0075	0.3496
0.820	0.6456	0.0055	0.9573	-0.2320	0.0094	0.1665
1.050	0.7239	-0.0099	0.9542	0.2088	0.0058	0.1178

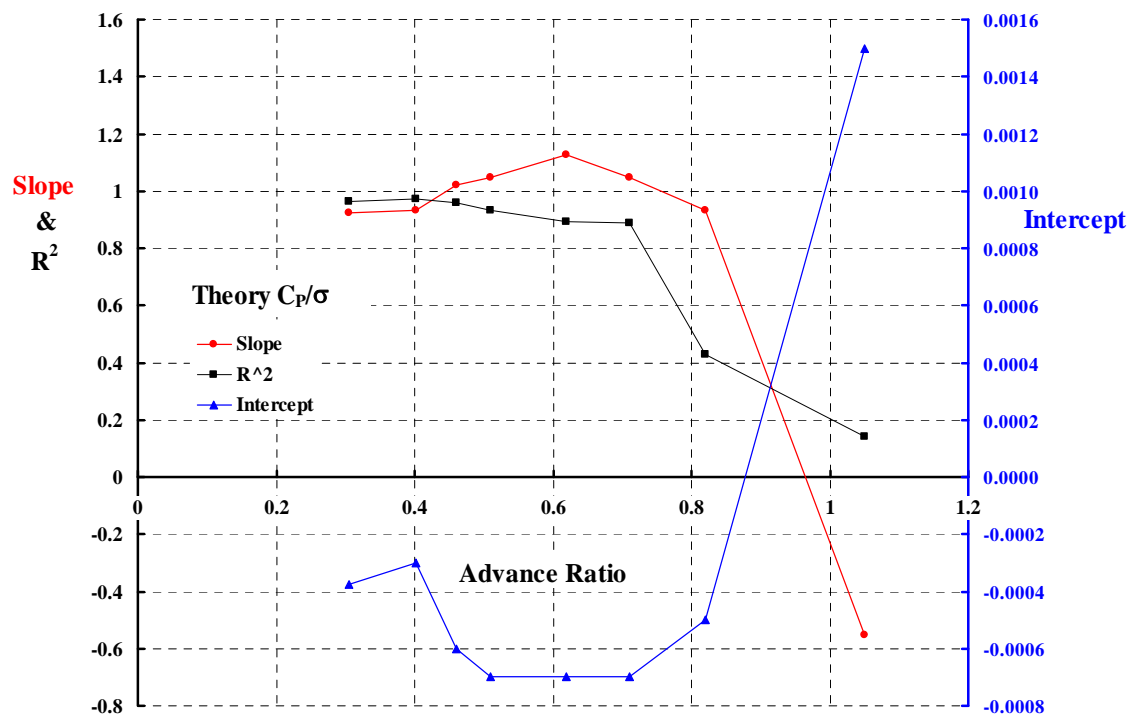
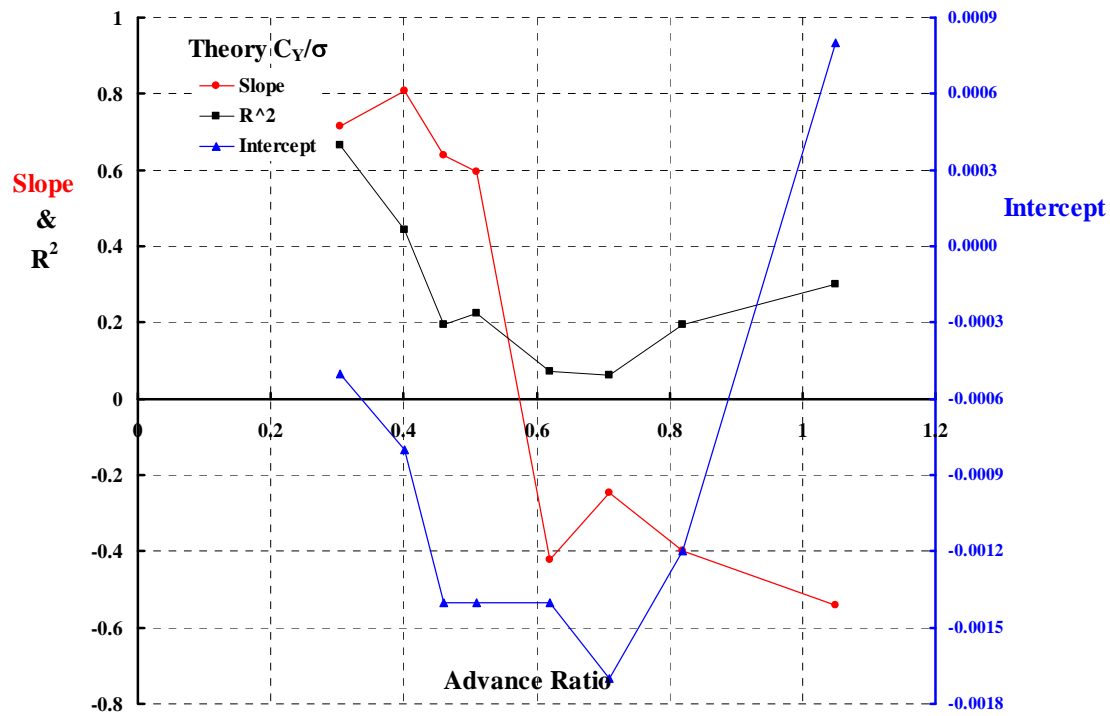
Y-Force Coefficient				Power Coefficient		
Mu	SLOPE	Intercept	R²	SLOPE	Intercept	R²
0.305	0.7136	-0.0005	0.6664	0.9252	-0.0004	0.9652
0.401	0.8083	-0.0008	0.4421	0.9329	-0.0003	0.9708
0.460	0.6389	-0.0014	0.1943	1.0208	-0.0006	0.9612
0.510	0.5954	-0.0014	0.2245	1.0459	-0.0007	0.9318
0.620	-0.4216	-0.0014	0.0716	1.1281	-0.0007	0.8909
0.710	-0.2459	-0.0017	0.0626	1.0488	-0.0007	0.8888
0.820	-0.3994	-0.0012	0.1937	0.9317	-0.0005	0.4274
1.050	-0.5421	0.0008	0.2997	-0.5511	0.0015	0.1417

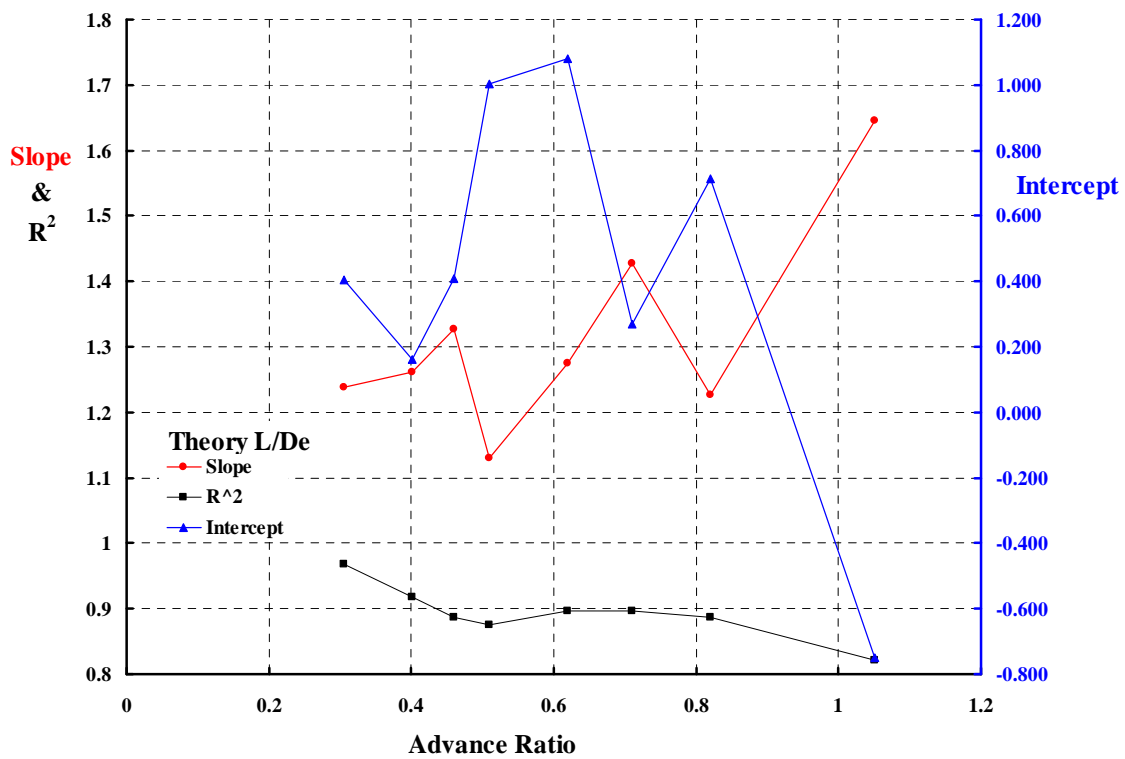
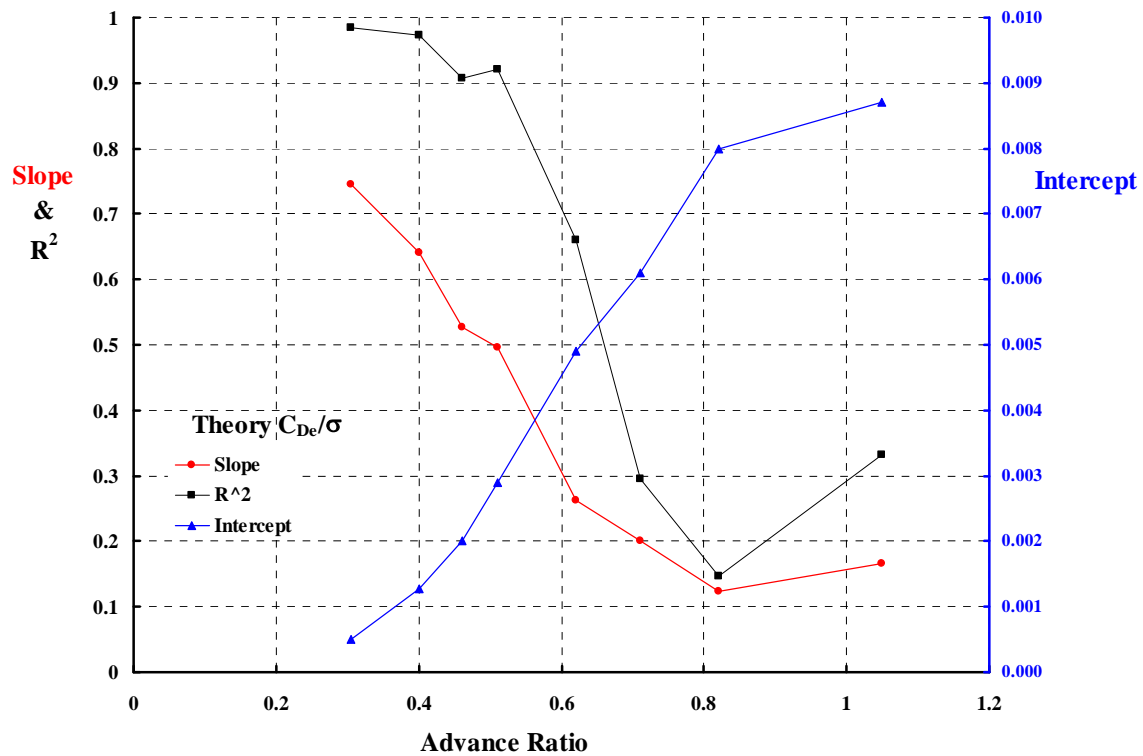
Effective Drag Coefficient				L/De		
Mu	SLOPE	Intercept	R²	SLOPE	Intercept	R²
0.305	0.7456	0.0005	0.9853	1.2375	0.4054	0.9689
0.401	0.6409	0.0013	0.9720	1.2618	0.1607	0.9181
0.460	0.5278	0.0020	0.9073	1.3276	0.4071	0.8869
0.510	0.4956	0.0029	0.9218	1.1293	1.0049	0.8749
0.620	0.2619	0.0049	0.6605	1.2748	1.0794	0.8962
0.710	0.2008	0.0061	0.2955	1.4272	0.2680	0.8968
0.820	0.1237	0.0080	0.1463	1.2263	0.7122	0.8868
1.050	0.1668	0.0087	0.3314	1.6449	-0.7483	0.8220











11.12 H-34 versus RCAS

References: 1. NASA TN D-4632, An Investigation of Full-Scale Helicopter Rotors at High Advance Ratios and Advancing Tip Mach Numbers by John McCloud III and Jim Biggers, July 1968
2. Harris EXCEL File: MASTER H-34 versus RCAS (Final August 23, 2008).xls

Airfoil	N.A.C.A. 0012
Chord	1.337 ft
Diameter	56.00 ft
Twist	0.00 deg
Disc Area	2,463 sq. ft
Reference Area (4 blades)	153.1 sq. ft
Nominal Solidity	0.062
Lock Number	8.86
Flap Moment of inertia	1264 slug ft ²
Weight Moment	2,265 lb-ft
Flap/Lag Hinge Offset	1.00 ft

Notes: 1. Wind axis data measured. Shaft axis data derived.
2. Shaft torque derived from strain cage on shaft.
3. Coefficients based on rotor tip speed and total blade area ($\sigma A = 153.1$ sq. ft.)
4. Articulated hub with coincident flap and lag hinges at $r/R = 0.0357$
5. Pitch bearing at $r/R = 0.079$

Table of RCAS Output

Advance Ratio	Collective at 0.75R (deg)	Shaft Angle of Attack (deg)	Long Cyclic (deg)	Lat Cyclic (deg)	C_L/σ	C_D/σ	C_T/σ	C_H/σ	C_Y/σ	C_P/σ	C_{De}/σ	Rotor Alone L/De
0.306	-4.00	5.00	-0.85	0.43	-0.009648	0.000381	-0.009579	0.001220	-0.000042	0.001454	0.005154	-1.87
0.306	-4.00	10.00	-0.01	-0.18	0.017823	0.004714	0.018370	0.001548	-0.000162	0.000165	0.005254	3.39
0.307	-2.00	5.00	0.54	-0.26	0.013629	0.002563	0.013801	0.001365	-0.000065	0.000779	0.005120	2.66
0.305	-2.00	10.00	1.41	-0.76	0.040640	0.008861	0.041561	0.001669	-0.000447	-0.000860	0.006038	6.73
0.305	0.00	0.00	1.09	-0.33	0.008782	0.001241	0.008782	0.001241	-0.000038	0.001172	0.005088	1.73
0.305	0.00	5.00	1.96	-0.90	0.036762	0.004646	0.037027	0.001424	-0.000344	0.000367	0.005850	6.28
0.303	0.00	10.00	2.84	-1.29	0.063227	0.012837	0.064495	0.001663	-0.000963	-0.001613	0.007541	8.38
0.303	2.00	-5.00	1.65	-0.39	0.003839	0.000891	0.003746	0.001223	-0.000107	0.001303	0.005171	0.74
0.305	2.00	0.00	2.48	-1.04	0.031949	0.001190	0.031949	0.001190	-0.000300	0.001393	0.005764	5.54
0.306	2.00	5.00	3.36	-1.57	0.059891	0.006643	0.060242	0.001398	-0.000910	0.000192	0.007274	8.23
0.304	2.00	10.00	4.34	-1.76	0.084863	0.016346	0.086412	0.001361	-0.001617	-0.001979	0.009848	8.62
0.300	4.00	-10.00	2.20	-0.46	-0.000501	0.001397	-0.000736	0.001289	-0.000248	0.001210	0.005372	-0.09
0.306	4.00	-5.00	3.01	-1.12	0.026767	-0.001306	0.026779	0.001032	-0.000324	0.002171	0.005823	4.60
0.304	4.00	0.00	3.85	-1.78	0.055013	0.001044	0.055013	0.001044	-0.000828	0.001852	0.007125	7.72
0.302	4.00	5.00	4.80	-2.20	0.082311	0.008356	0.082726	0.001151	-0.001668	0.000342	0.009478	8.68
0.303	4.00	10.00	6.03	-2.31	0.103199	0.018661	0.104872	0.000457	-0.002488	-0.001561	0.013534	7.63
0.303	6.00	-10.00	3.52	-1.22	0.022056	-0.002874	0.022220	0.000999	-0.000428	0.002707	0.006017	3.67
0.304	6.00	-5.00	4.30	-1.92	0.049479	-0.003575	0.049603	0.000751	-0.000788	0.003275	0.007178	6.89
0.304	6.00	0.00	5.18	-2.56	0.077765	0.000773	0.077765	0.000773	-0.001617	0.002589	0.009276	8.38
0.307	6.00	5.00	6.37	-2.91	0.101372	0.009261	0.101794	0.000390	-0.002600	0.001141	0.013006	7.79
0.305	6.00	10.00	8.18	-3.31	0.111141	0.018067	0.112590	-0.001507	-0.003720	0.000589	0.020002	5.56
0.305	8.00	-10.00	4.74	-2.08	0.044210	-0.007182	0.044785	0.000604	-0.000835	0.004433	0.007374	6.00
0.305	8.00	-5.00	5.53	-2.80	0.071711	-0.005920	0.071954	0.000352	-0.001489	0.004639	0.009313	7.70
0.304	8.00	0.00	6.57	-3.43	0.097730	0.000177	0.097730	0.000177	-0.002611	0.003785	0.012608	7.75
0.304	8.00	5.00	8.35	-4.07	0.108932	0.008029	0.109218	-0.001496	-0.003878	0.003419	0.019255	5.66
0.305	8.00	10.00	10.39	-4.87	0.111080	0.016060	0.112181	-0.003472	-0.004900	0.003484	0.027501	4.04
0.304	10.00	-10.00	5.83	-3.04	0.065615	-0.011476	0.066611	0.000092	-0.001449	0.006386	0.009493	6.91

0.304	10.00	-5.00	6.71	-3.79	0.091875	-0.008302	0.092249	-0.000263	-0.002424	0.006332	0.012490	7.36
0.305	10.00	0.00	8.26	-4.63	0.106691	-0.001434	0.106691	-0.001434	-0.003808	0.006045	0.018417	5.79
0.304	10.00	5.00	10.39	-5.70	0.108140	0.006091	0.108259	-0.003357	-0.004968	0.006149	0.026283	4.11
0.304	11.00	-10.00										
0.305	11.00	-5.00										
0.399	-4.00	5.00	-0.48	0.18	0.001404	0.002021	0.001575	0.001891	-0.000046	0.001225	0.005064	0.28
0.402	-4.00	10.00	0.79	-0.49	0.033508	0.008321	0.034444	0.002376	-0.000477	-0.001076	0.005648	5.93
0.4	-2.00	5.00	1.13	-0.51	0.021419	0.003915	0.021679	0.002034	-0.000182	0.000537	0.005249	4.08
0.4	-2.00	10.00	2.46	-1.00	0.052752	0.011707	0.053984	0.002369	-0.000902	-0.002130	0.006416	8.22
0.402	0.00	0.00	1.45	-0.48	0.008158	0.001854	0.008158	0.001854	-0.000063	0.001308	0.005104	1.60
0.399	0.00	5.00	2.77	-1.11	0.041077	0.005683	0.041416	0.002081	-0.000538	0.000054	0.005818	7.06
0.401	0.00	10.00	4.18	-1.45	0.071445	0.014789	0.072927	0.002158	-0.001506	-0.002877	0.007643	9.35
0.402	2.00	0.00	3.04	-1.18	0.027983	0.001837	0.027983	0.001837	-0.000342	0.001477	0.005505	5.08
0.403	2.00	5.00	4.42	-1.73	0.060613	0.007323	0.061020	0.002012	-0.001155	-0.000210	0.006800	8.91
0.401	4.00	-5.00	3.39	-1.13	0.014355	0.000414	0.014264	0.001664	-0.000333	0.002038	0.005478	2.62
0.401	4.00	0.00	4.62	-1.91	0.047732	0.001736	0.047732	0.001736	-0.000863	0.001831	0.006284	7.60
0.399	4.00	5.00	6.13	-2.35	0.079088	0.008622	0.079538	0.001697	-0.001968	-0.000110	0.008348	9.47
0.402	6.00	-10.00										
0.401	6.00	-5.00	4.90	-1.95	0.033974	-0.001557	0.033981	0.001410	-0.000715	0.003101	0.006146	5.53
0.401	6.00	0.00	6.20	-2.68	0.067062	0.001477	0.067062	0.001477	-0.001612	0.002436	0.007529	8.91
0.402	6.00	5.00	8.05	-3.18	0.092325	0.008674	0.092729	0.000595	-0.003166	0.001048	0.011277	8.19
0.403	8.00	-10.00	5.22	-1.94	0.021397	-0.002272	0.021467	0.001478	-0.000816	0.003423	0.006230	3.43
0.402	8.00	-5.00	6.34	-2.86	0.053298	-0.003593	0.053409	0.001065	-0.001318	0.004372	0.007266	7.34
0.403	8.00	0.00	7.80	-3.59	0.083834	0.000838	0.083834	0.000838	-0.002693	0.003576	0.009721	8.62
0.401	8.00	5.00	10.24	-4.52	0.096853	0.007697	0.097155	-0.000773	-0.004553	0.003184	0.015607	6.21
0.404	10.00	-10.00	6.55	-2.94	0.040323	-0.006075	0.040765	0.001020	-0.001277	0.005355	0.007228	5.58
0.401	10.00	-5.00	7.70	-3.90	0.071504	-0.005710	0.071730	0.000544	-0.002165	0.005907	0.008963	7.98
0.401	9.00	5.00										
0.403	9.50	0.00										
0.401	11.00	-10.00										
0.458	-4.00	5.00	-0.43	0.09	0.005528	0.002761	0.005747	0.002269	-0.000073	0.001118	0.005193	1.06
0.46	-4.00	10.00	1.16	-0.62	0.039326	0.009783	0.040428	0.002806	-0.000679	-0.001762	0.005953	6.61
0.46	-2.00	5.00	1.35	-0.61	0.023716	0.004482	0.024016	0.002398	-0.000234	0.000411	0.005376	4.41

0.462	-2.00	10.00	3.02	-1.09	0.056559	0.012739	0.057912	0.002725	-0.001122	-0.002806	0.006640	8.52
0.467	0.00	0.00	1.51	-0.47	0.006461	0.002218	0.006461	0.002218	-0.000057	0.001357	0.005167	1.25
0.461	0.00	5.00	3.19	-1.22	0.041258	0.006061	0.041629	0.002442	-0.000610	-0.000104	0.005835	7.07
0.461	0.00	10.00	4.95	-1.48	0.072870	0.015263	0.074413	0.002377	-0.001710	-0.003487	0.007684	9.48
0.459	2.00	0.00	3.30	-1.18	0.024095	0.002205	0.024095	0.002205	-0.000297	0.001488	0.005439	4.43
0.46	2.00	5.00	5.04	-1.80	0.058526	0.007487	0.058956	0.002358	-0.001181	-0.000411	0.006594	8.88
0.461	2.00	10.00	7.05	-1.95	0.086536	0.016728	0.088126	0.001447	-0.002577	-0.003327	0.009495	9.11
0.458	4.00	-5.00	3.51	-1.05	0.006795	0.001474	0.006641	0.002061	-0.000343	0.001834	0.005461	1.24
0.461	4.00	0.00	5.08	-1.91	0.041750	0.002104	0.041750	0.002104	-0.000766	0.001779	0.005971	6.99
0.46	4.00	5.00	6.94	-2.40	0.074695	0.008557	0.075157	0.002015	-0.001971	-0.000345	0.007808	9.57
0.456	6.00	-5.00	5.22	-1.89	0.024508	-0.000290	0.024440	0.001847	-0.000647	0.002840	0.005883	4.17
0.458	6.00	0.00	6.83	-2.71	0.059368	0.001887	0.059368	0.001887	-0.001478	0.002277	0.006837	8.68
0.462	6.00	5.00	9.07	-3.30	0.085272	0.008405	0.085680	0.000941	-0.003183	0.000807	0.010160	8.39
0.456	8.00	-10.00	5.44	-1.75	0.008715	0.000596	0.008479	0.002100	-0.000864	0.002532	0.006099	1.43
0.455	8.00	-5.00	6.85	-2.84	0.042081	-0.002121	0.042106	0.001554	-0.001164	0.004026	0.006631	6.35
0.458	8.00	0.00	8.59	-3.66	0.074928	0.001251	0.074928	0.001251	-0.002575	0.003315	0.008457	8.86
0.462	8.00	5.00	11.21	-4.59	0.091354	0.007871	0.091692	-0.000121	-0.004607	0.002649	0.013629	6.70
0.456	10.00	-10.00	7.00	-2.78	0.026101	-0.002867	0.026202	0.001709	-0.001227	0.004411	0.006722	3.88
0.459	10.00	-5.00	8.39	-3.89	0.059290	-0.004032	0.059416	0.001150	-0.001908	0.005436	0.007784	7.62
0.457	10.00	0.00	10.58	-5.02	0.082033	0.000243	0.082033	0.000243	-0.003982	0.005092	0.011312	7.25
0.456	12.00	-10.00	8.40	-3.95	0.043056	-0.006381	0.043510	0.001193	-0.001781	0.006476	0.007696	5.59
0.508	-4.00	5.00	-0.35	-0.02	0.009122	0.003434	0.009387	0.002626	-0.000094	0.001027	0.005458	1.67
0.507	-4.00	10.00	1.51	-0.72	0.043529	0.010889	0.044758	0.003165	-0.000833	-0.002299	0.006355	6.85
0.506	-2.00	2.00	0.43	-0.18	0.003784	0.002708	0.003877	0.002574	-0.000014	0.001339	0.005348	0.71
0.507	-2.00	5.00	1.57	-0.71	0.025324	0.004938	0.025658	0.002712	-0.000271	0.000350	0.005629	4.50
0.509	-2.00	10.00	3.48	-1.16	0.059098	0.013453	0.060536	0.002987	-0.001278	-0.003283	0.006980	8.47
0.498	0.00	-3.00	0.49	0.11	-0.016490	0.003408	-0.016646	0.002541	-0.000197	0.001053	0.005485	-3.01
0.507	0.00	2.00	2.35	-0.85	0.019464	0.003307	0.019568	0.002626	-0.000172	0.001117	0.005509	3.53
0.509	0.00	5.00	3.51	-1.31	0.041043	0.006341	0.041439	0.002740	-0.000636	-0.000160	0.006025	6.81
0.508	0.00	10.00	5.54	-1.55	0.073516	0.015514	0.075093	0.002513	-0.001883	-0.003840	0.007942	9.26
0.502	2.00	-3.00	2.38	-0.60	-0.000765	0.002534	-0.000897	0.002490	-0.000185	0.001496	0.005484	-0.14
0.509	2.00	2.00	4.25	-1.52	0.035247	0.003869	0.035361	0.002637	-0.000531	0.001024	0.005889	5.99
0.509	2.00	5.00	5.47	-1.87	0.056517	0.007628	0.056967	0.002673	-0.001196	-0.000486	0.006670	8.47

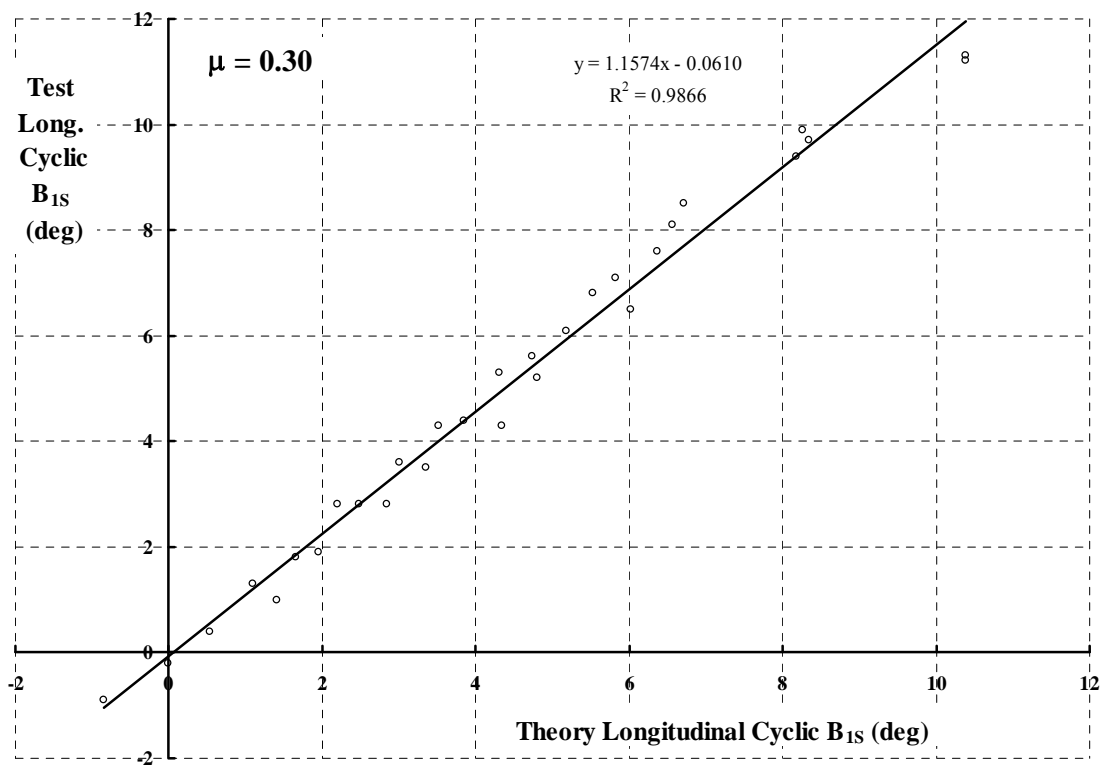
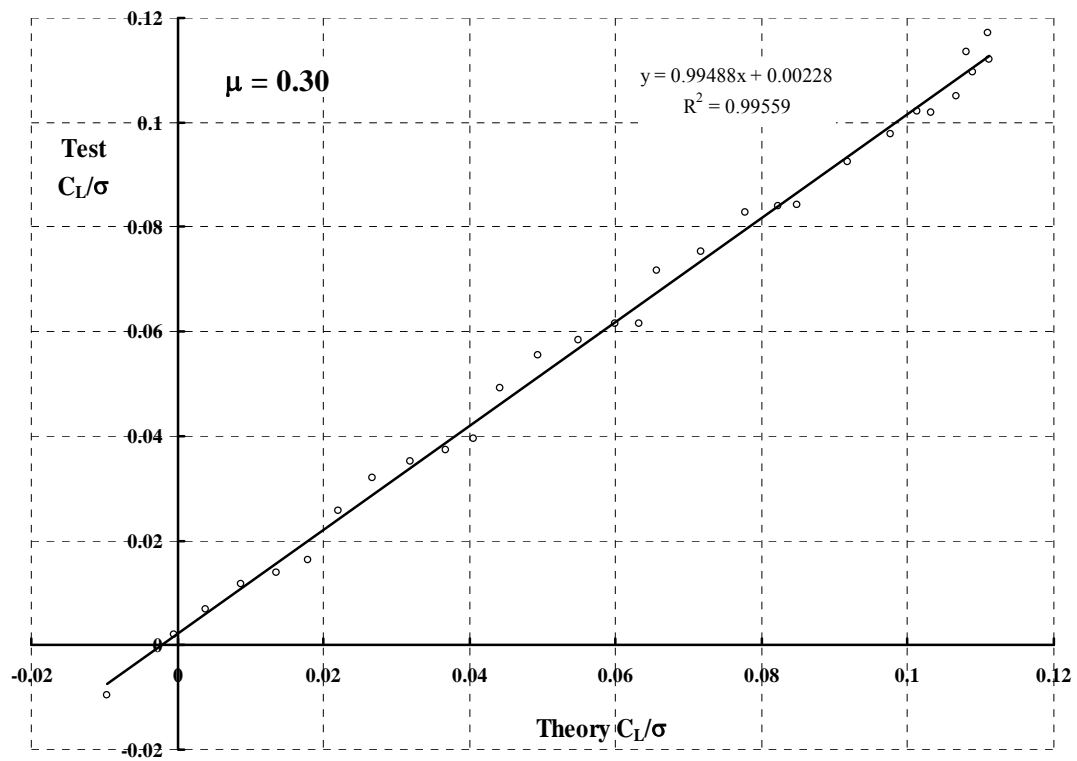
0.509	2.00	10.00	7.80	-2.06	0.084609	0.016430	0.086177	0.001488	-0.002759	-0.003473	0.009581	8.83
0.502	4.00	-5.00	3.53	-0.98	0.001251	0.002345	0.001042	0.002445	-0.000385	0.001687	0.005672	0.22
0.507	4.00	-3.00	4.25	-1.38	0.015209	0.001597	0.015105	0.002391	-0.000392	0.002093	0.005725	2.66
0.513	4.00	2.00	6.17	-2.20	0.050794	0.004308	0.050913	0.002533	-0.001098	0.001112	0.006502	7.81
0.506	4.00	5.00	7.49	-2.48	0.070739	0.008519	0.071212	0.002321	-0.001969	-0.000399	0.007731	9.15
0.508	4.00	10.00	10.18	-2.84	0.093010	0.016710	0.094499	0.000305	-0.004088	-0.002277	0.012219	7.61
0.499	6.00	-5.00	5.35	-1.83	0.017428	0.000766	0.017295	0.002282	-0.000644	0.002646	0.005984	2.91
0.505	6.00	-3.00	6.07	-2.24	0.031316	0.000572	0.031244	0.002210	-0.000819	0.002849	0.006190	5.06
0.511	6.00	2.00	8.10	-2.98	0.065928	0.004536	0.066046	0.002232	-0.001947	0.001497	0.007488	8.80
0.507	6.00	5.00	9.69	-3.37	0.080169	0.008491	0.080603	0.001471	-0.003114	0.000605	0.009684	8.28
0.507	6.00	10.00	12.45	-3.87	0.100230	0.016979	0.101656	-0.000684	-0.005468	-0.000754	0.015492	6.47
0.496	8.00	-10.00	5.47	-1.57	-0.000558	0.002844	-0.001044	0.002704	-0.000989	0.001778	0.006351	-0.09
0.502	8.00	-5.00	7.11	-2.78	0.033502	-0.000855	0.033449	0.002068	-0.001099	0.003764	0.006567	5.10
0.508	8.00	-3.00	7.83	-3.19	0.047391	-0.000525	0.047353	0.001956	-0.001456	0.003781	0.006931	6.84
0.51	8.00	2.00	10.16	-4.08	0.075917	0.004018	0.076011	0.001366	-0.003267	0.002765	0.009472	8.02
0.509	8.00	5.00	11.85	-4.56	0.087627	0.008245	0.088012	0.000577	-0.004532	0.002187	0.012558	6.98
0.498	10.00	-10.00	7.17	-2.58	0.015564	-0.000293	0.015379	0.002414	-0.001285	0.003600	0.006806	2.29
0.502	10.00	-5.00	8.77	-3.84	0.049326	-0.002559	0.049361	0.001750	-0.001755	0.005081	0.007460	6.61
0.508	10.00	-3.00	9.54	-4.26	0.062608	-0.001713	0.062612	0.001566	-0.002354	0.004977	0.008102	7.73
0.514	10.00	2.00	12.18	-5.48	0.082736	0.003442	0.082805	0.000552	-0.004689	0.004492	0.012299	6.73
0.495	12.00	-10.00	8.72	-3.75	0.031421	-0.003505	0.031553	0.002005	-0.001771	0.005600	0.007538	4.17
0.498	12.00	-5.00	10.34	-5.08	0.063618	-0.004379	0.063758	0.001182	-0.002733	0.006722	0.008876	7.17
0.5	13.00	-10.00										
0.624	-4.00	4.00	-0.95	0.07	0.008826	0.004042	0.009086	0.003417	-0.000070	0.001275	0.006101	1.45
0.618	-4.00	8.00	0.99	-0.70	0.037608	0.009129	0.038513	0.003807	-0.000642	-0.001460	0.006771	5.55
0.624	-2.00	4.00	1.18	-0.63	0.021050	0.004953	0.021344	0.003473	-0.000154	0.000719	0.006114	3.44
0.62	-2.00	8.00	3.16	-1.21	0.050219	0.010670	0.051216	0.003577	-0.000936	-0.002240	0.007052	7.12
0.618	0.00	0.00	1.39	-0.34	0.001904	0.003410	0.001904	0.003410	-0.000035	0.001534	0.005887	0.32
0.622	0.00	4.00	3.34	-1.21	0.032480	0.005852	0.032809	0.003572	-0.000377	0.000271	0.006289	5.16
0.618	0.00	8.00	5.41	-1.68	0.061069	0.011800	0.062117	0.003186	-0.001356	-0.002634	0.007544	8.09
0.618	2.00	-4.00	1.63	-0.03	-0.016873	0.004523	-0.017147	0.003335	-0.000370	0.001014	0.006160	-2.74
0.619	2.00	0.00	3.52	-1.01	0.013041	0.003498	0.013041	0.003498	-0.000139	0.001580	0.006050	2.16
0.62	2.00	4.00	5.51	-1.76	0.043648	0.006713	0.044010	0.003652	-0.000730	-0.000045	0.006640	6.57

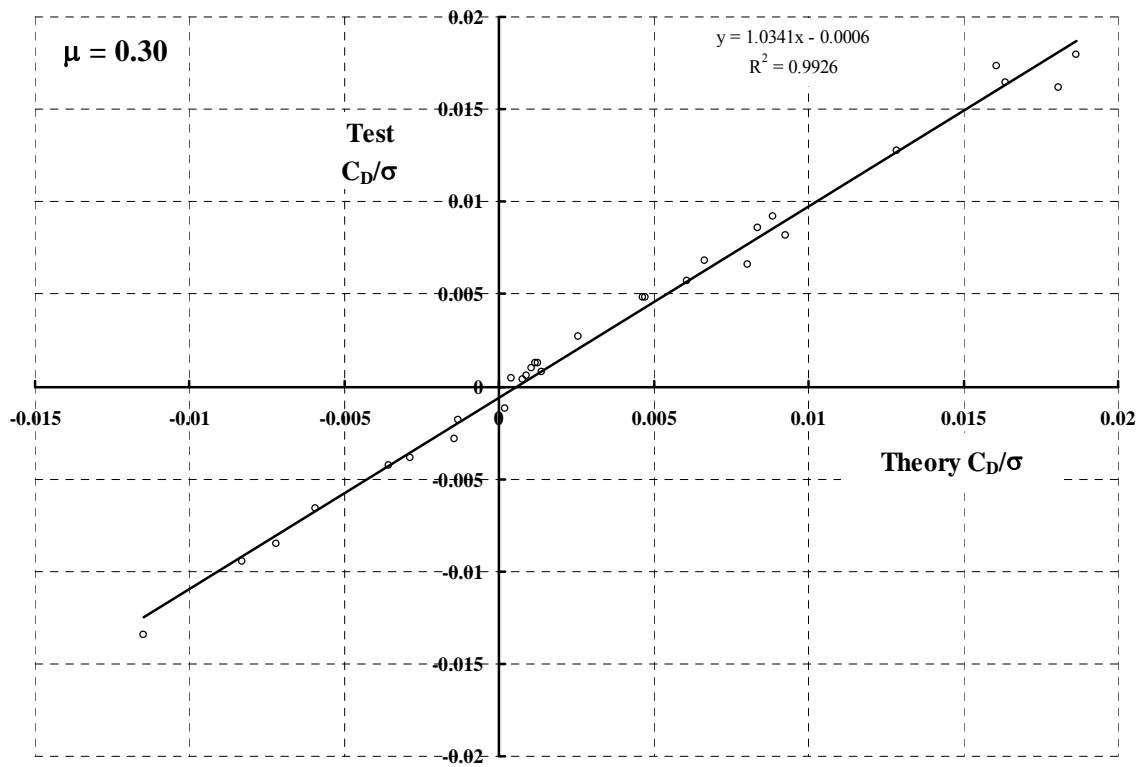
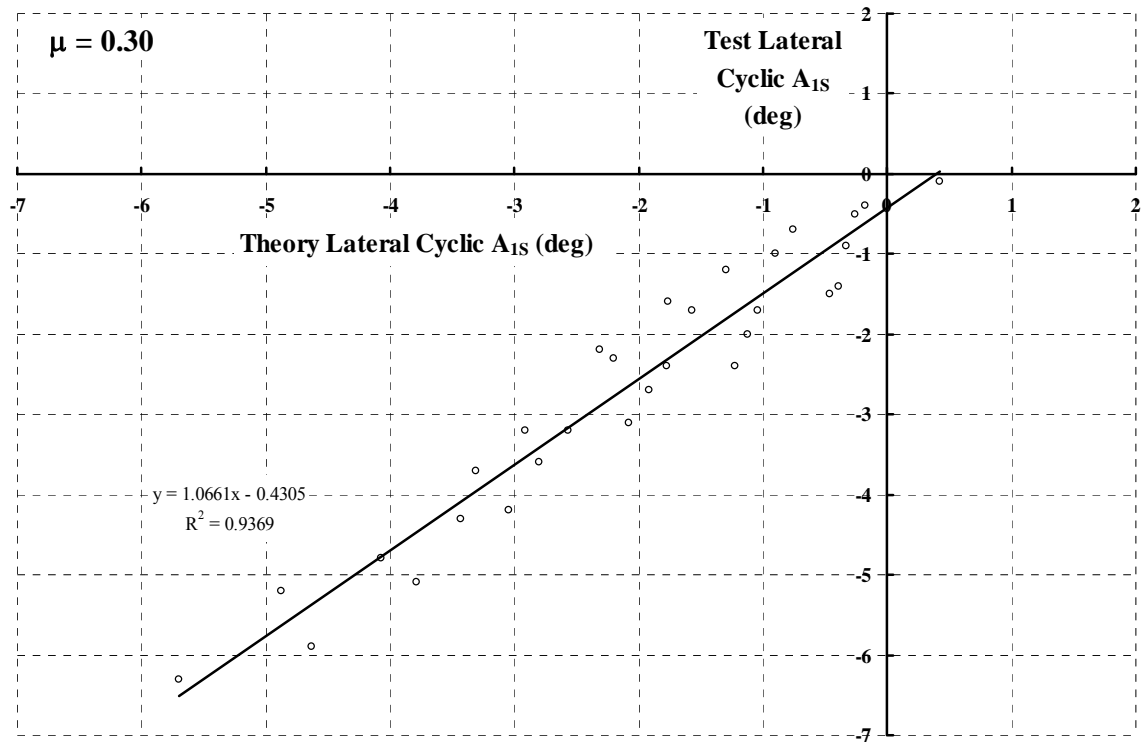
0.619	2.00	8.00	7.73	-2.11	0.070209	0.012606	0.071280	0.002712	-0.001923	-0.002668	0.008297	8.46
0.619	4.00	-4.00	3.73	-0.80	-0.004367	0.003688	-0.004614	0.003374	-0.000385	0.001597	0.006268	-0.70
0.621	4.00	0.00	5.62	-1.73	0.024808	0.003567	0.024808	0.003567	-0.000421	0.001733	0.006367	3.90
0.621	4.00	4.00	7.73	-2.34	0.053788	0.007392	0.054172	0.003621	-0.001234	-0.000085	0.007254	7.41
0.619	4.00	8.00	10.08	-2.61	0.078634	0.013151	0.079699	0.002079	-0.002814	-0.002290	0.009451	8.32
0.613	6.00	-8.00	3.97	-0.62	-0.019682	0.006558	-0.020403	0.003755	-0.001038	0.000160	0.006817	-2.89
0.61	6.00	-4.00	5.78	-1.67	0.008487	0.002784	0.008272	0.003369	-0.000595	0.002308	0.006513	1.30
0.624	6.00	0.00	7.73	-2.54	0.036986	0.003572	0.036986	0.003572	-0.000930	0.002039	0.006866	5.39
0.634	6.00	4.00	9.98	-3.04	0.063327	0.007791	0.063717	0.003354	-0.001997	0.000247	0.008190	7.73
0.624	6.00	4.00	9.98	-3.04	0.063327	0.007791	0.063717	0.003354	-0.001997	0.000247	0.008190	7.73
0.614	8.00	-8.00	6.03	-1.48	-0.006458	0.004823	-0.007067	0.003877	-0.001123	0.001383	0.007057	-0.92
0.619	8.00	-4.00	7.79	-2.61	0.021373	0.001872	0.021190	0.003358	-0.000982	0.003135	0.006937	3.08
0.621	8.00	4.00	12.18	-3.98	0.072610	0.007855	0.072981	0.002771	-0.003264	0.001155	0.009722	7.47
0.621	10.00	-8.00	8.02	-2.44	0.006397	0.003066	0.005908	0.003926	-0.001371	0.002733	0.007481	0.86
0.62	10.00	-4.00	9.74	-3.65	0.034198	0.000989	0.034046	0.003372	-0.001537	0.004085	0.007588	4.51
0.619	12.00	-8.00	9.89	-3.58	0.019331	0.001194	0.018977	0.003873	-0.001785	0.004256	0.008069	2.40
0.711	-4.00	2.00	-2.16	0.47	-0.000178	0.004290	-0.000028	0.004294	-0.000048	0.001825	0.006859	-0.03
0.708	-4.00	4.00	-1.05	-0.05	0.014951	0.005321	0.015286	0.004265	-0.000097	0.001184	0.006987	2.14
0.708	-4.00	6.00	0.06	-0.57	0.030101	0.007525	0.030723	0.004338	-0.000384	-0.000141	0.007327	4.11
0.706	-4.00	8.00	1.21	-0.90	0.044056	0.010629	0.045107	0.004394	-0.000839	-0.001948	0.007886	5.59
0.71	-2.00	2.00	0.06	-0.21	0.008592	0.004564	0.008746	0.004261	-0.000011	0.001502	0.006679	1.29
0.711	-2.00	4.00	1.17	-0.74	0.024612	0.005977	0.024969	0.004246	-0.000170	0.000661	0.006908	3.56
0.709	-2.00	6.00	2.33	-1.16	0.040065	0.008347	0.040718	0.004114	-0.000525	-0.000719	0.007336	5.46
0.708	-2.00	8.00	3.52	-1.39	0.054180	0.011499	0.055253	0.003847	-0.001067	-0.002472	0.008019	6.76
0.71	0.00	0.00	1.20	-0.23	0.000617	0.004243	0.000617	0.004243	-0.000030	0.001660	0.006580	0.09
0.712	0.00	2.00	2.30	-0.78	0.016653	0.004913	0.016815	0.004328	-0.000063	0.001254	0.006677	2.49
0.71	0.00	4.00	3.43	-1.24	0.032836	0.006658	0.033220	0.004351	-0.000320	0.000225	0.006974	4.71
0.708	0.00	6.00	4.64	-1.57	0.048084	0.009116	0.048773	0.004039	-0.000762	-0.001153	0.007493	6.42
0.707	0.00	8.00	5.87	-1.75	0.062888	0.012284	0.063986	0.003412	-0.001432	-0.002819	0.008316	7.56
0.71	2.00	0.00	3.43	-0.82	0.008571	0.004453	0.008571	0.004453	-0.000048	0.001625	0.006741	1.27
0.711	2.00	2.00	4.54	-1.32	0.024867	0.005458	0.025042	0.004587	-0.000179	0.001009	0.006879	3.62
0.709	2.00	4.00	5.73	-1.68	0.040415	0.007342	0.040829	0.004504	-0.000539	-0.000087	0.007219	5.60
0.708	2.00	6.00	6.97	-1.93	0.055574	0.009888	0.056303	0.004024	-0.001110	-0.001456	0.007838	7.09

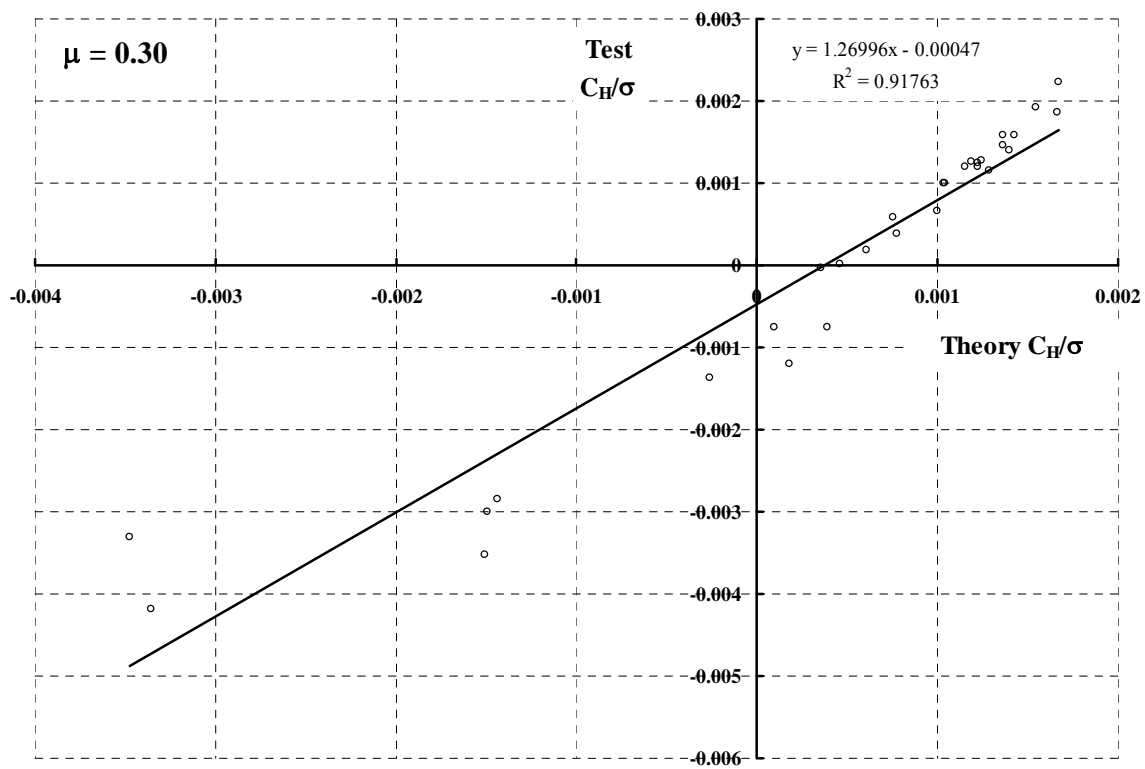
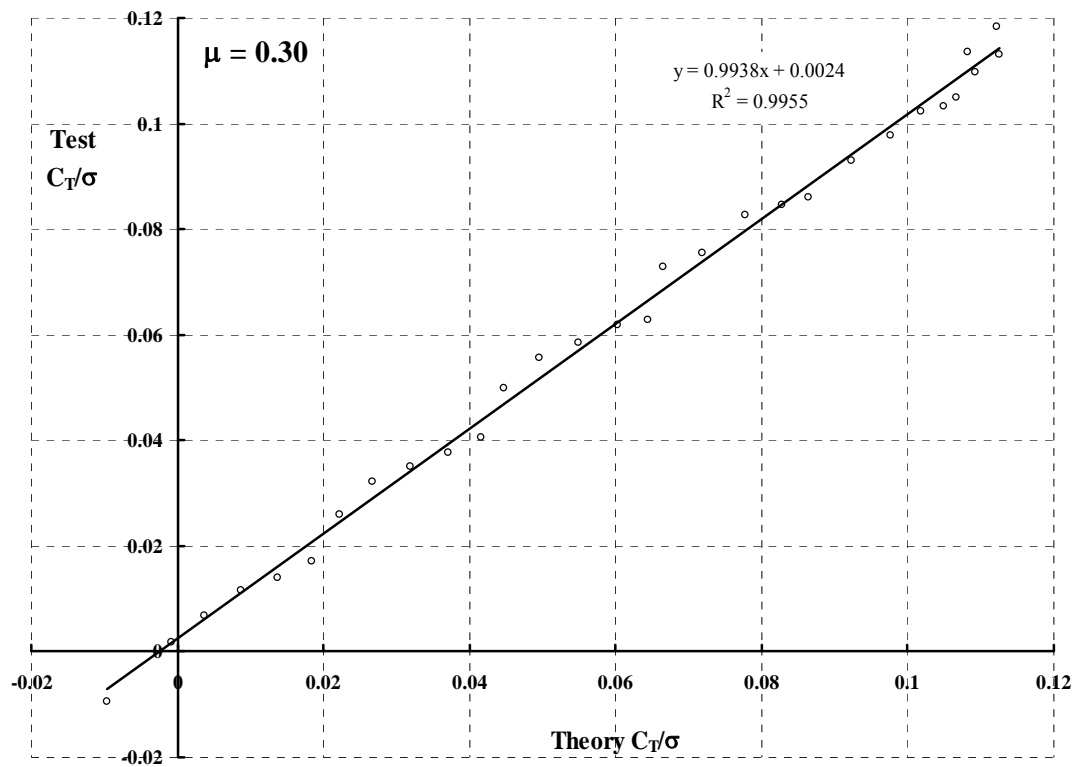
0.714	2.00	8.00	8.24	-2.03	0.070301	0.012983	0.071424	0.003073	-0.001913	-0.002944	0.008839	7.95
0.706	4.00	-2.00	4.55	-0.95	0.001902	0.004410	0.001747	0.004473	-0.000198	0.001851	0.007016	0.27
0.706	4.00	0.00	5.66	-1.45	0.017043	0.004711	0.017043	0.004711	-0.000170	0.001644	0.007026	2.43
0.711	4.00	2.00	6.82	-1.83	0.032651	0.006064	0.032843	0.004921	-0.000384	0.000838	0.007243	4.51
0.709	4.00	4.00	8.05	-2.11	0.047792	0.008107	0.048242	0.004753	-0.000853	-0.000298	0.007688	6.22
0.706	4.00	6.00	9.32	-2.28	0.062727	0.010679	0.063500	0.004064	-0.001588	-0.001569	0.008471	7.40
0.695	6.00	-4.00	5.64	-1.25	-0.002303	0.004685	-0.002624	0.004513	-0.000563	0.001944	0.007421	-0.31
0.705	6.00	-2.00	6.72	-1.77	0.012214	0.004270	0.012058	0.004694	-0.000418	0.002212	0.007385	1.65
0.707	6.00	0.00	7.86	-2.19	0.027195	0.005002	0.027195	0.005002	-0.000496	0.001755	0.007472	3.64
0.711	6.00	2.00	9.09	-2.46	0.041636	0.006605	0.041841	0.005148	-0.000803	0.000846	0.007795	5.34
0.709	6.00	4.00	10.37	-2.67	0.055702	0.008743	0.056176	0.004836	-0.001429	-0.000241	0.008403	6.63
0.695	8.00	-4.00	7.78	-2.15	0.008579	0.004115	0.008271	0.004704	-0.000814	0.002621	0.007805	1.10
0.709	8.00	-2.00	8.87	-2.66	0.023002	0.004024	0.022848	0.004824	-0.000830	0.002697	0.007820	2.94
0.712	8.00	0.00	10.07	-3.03	0.037223	0.005099	0.037223	0.005099	-0.001065	0.002074	0.008019	4.64
0.71	8.00	2.00	11.35	-3.25	0.050980	0.006917	0.051190	0.005133	-0.001546	0.001173	0.008568	5.95
0.711	8.00	4.00	12.66	-3.45	0.064211	0.009120	0.064690	0.004619	-0.002498	0.000348	0.009611	6.68
0.699	10.00	-4.00	9.88	-3.10	0.019386	0.003705	0.019080	0.005048	-0.001193	0.003356	0.008430	2.30
0.716	10.00	-2.00	11.01	-3.58	0.033495	0.003952	0.033337	0.005119	-0.001371	0.003243	0.008517	3.93
0.706	10.00	0.00	12.27	-3.94	0.046878	0.005154	0.046878	0.005154	-0.001855	0.002640	0.008871	5.28
0.703	12.00	-4.00	11.92	-4.15	0.030187	0.003330	0.029881	0.005427	-0.001705	0.004185	0.009220	3.27
0.707	12.00	-2.00	13.10	-4.63	0.043355	0.003806	0.043196	0.005316	-0.002141	0.004041	0.009495	4.57
0.706	13.70	-4.00										
0.819	-4.00	0.00	-3.61	0.89	-0.008291	0.005919	-0.008291	0.005919	-0.000163	0.001787	0.008089	-1.03
0.824	-4.00	2.00	-2.38	0.26	0.008183	0.005963	0.008386	0.005674	-0.000038	0.001804	0.008154	1.00
0.829	-4.00	4.00	-1.11	-0.37	0.023974	0.007090	0.024410	0.005400	-0.000178	0.001073	0.008393	2.86
0.814	-2.00	0.00	-1.29	0.39	-0.004277	0.005546	-0.004277	0.005546	-0.000097	0.001828	0.007766	-0.55
0.832	-2.00	2.00	-0.05	-0.30	0.012851	0.005902	0.013049	0.005450	-0.000016	0.001602	0.007846	1.64
0.83	-2.00	4.00	1.22	-0.93	0.029999	0.007283	0.030434	0.005173	-0.000188	0.000709	0.008144	3.68
0.816	0.00	0.00	1.04	-0.08	-0.000402	0.005432	-0.000402	0.005432	-0.000030	0.001818	0.007639	-0.05
0.829	0.00	2.00	2.28	-0.75	0.016869	0.006064	0.017071	0.005471	0.000005	0.001380	0.007739	2.18
0.83	0.00	4.00	3.57	-1.31	0.034221	0.007654	0.034672	0.005248	-0.000211	0.000339	0.008065	4.24
0.808	2.00	-2.00	2.14	0.14	-0.013641	0.006080	-0.013845	0.005600	-0.000188	0.001572	0.007988	-1.71
0.818	2.00	0.00	3.37	-0.55	0.003507	0.005839	0.003507	0.005839	0.000067	0.001667	0.007863	0.45

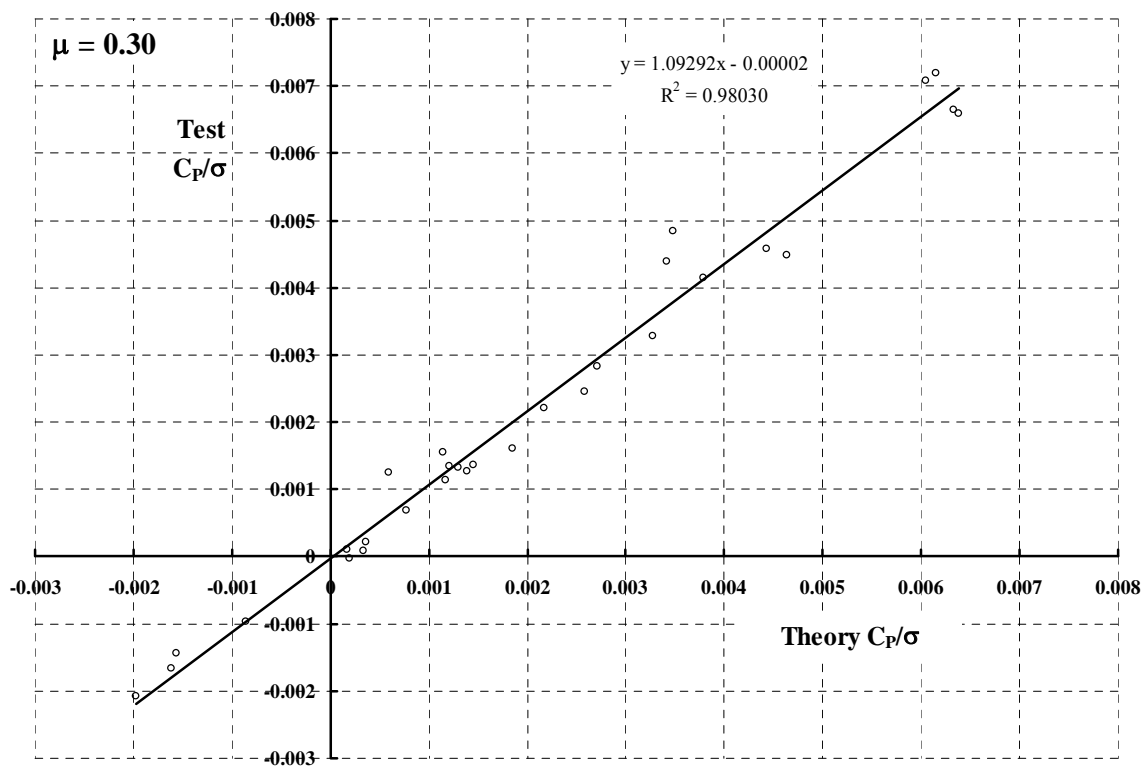
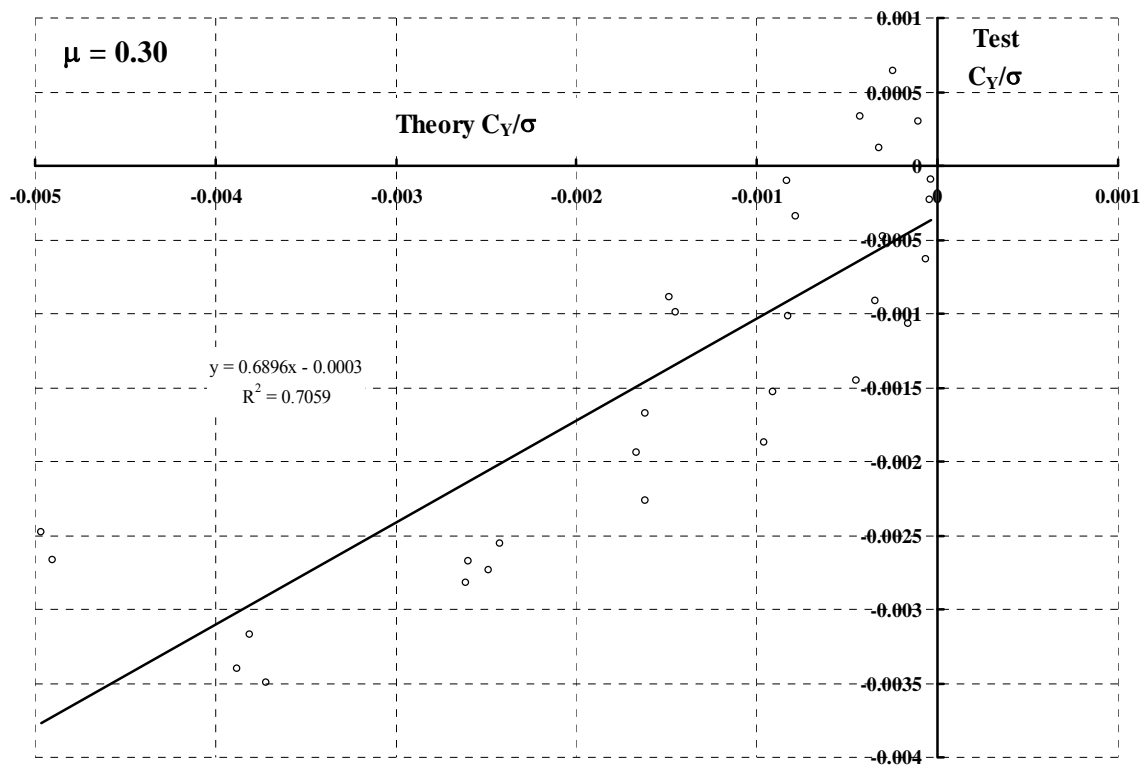
0.837	2.00	2.00	4.63	-1.15	0.020796	0.006633	0.021015	0.005903	0.000058	0.001065	0.007926	2.62
0.834	2.00	4.00	5.93	-1.63	0.038208	0.008311	0.038695	0.005626	-0.000248	-0.000076	0.008218	4.65
0.815	3.00	-2.00										
0.807	4.00	-2.00	4.45	-0.45	-0.008046	0.006318	-0.008262	0.006033	-0.000099	0.001666	0.008339	-0.96
0.818	4.00	0.00	5.70	-1.03	0.008022	0.006438	0.008022	0.006438	0.000153	0.001482	0.008237	0.97
0.838	4.00	2.00	6.99	-1.51	0.024792	0.007517	0.025039	0.006647	0.000104	0.000670	0.008331	2.98
0.831	4.00	4.00	8.31	-1.89	0.041889	0.009263	0.042433	0.006318	-0.000297	-0.000503	0.008653	4.84
0.811	5.00	-2.00										
0.812	6.00	-2.00	6.72	-1.20	-0.000258	0.006636	-0.000489	0.006623	-0.000165	0.001817	0.008842	-0.03
0.818	6.00	0.00	8.00	-1.68	0.015180	0.007125	0.015180	0.007125	0.000053	0.001359	0.008775	1.73
0.834	6.00	2.00	9.32	-2.01	0.031119	0.008474	0.031396	0.007382	-0.000036	0.000372	0.008925	3.49
0.831	6.00	4.00	10.68	-2.25	0.046944	0.010272	0.047547	0.006972	-0.000574	-0.000735	0.009379	5.01
0.799	7.00	-2.00										
0.815	8.00	-2.00	8.97	-2.03	0.008491	0.006781	0.008249	0.007074	-0.000379	0.002092	0.009321	0.91
0.82	8.00	0.00	10.28	-2.41	0.023548	0.007695	0.023548	0.007695	-0.000248	0.001368	0.009356	2.52
0.833	8.00	2.00	11.64	-2.65	0.038722	0.009229	0.039021	0.007872	-0.000576	0.000415	0.009733	3.98
0.82	9.00	-2.00										
0.818	10.00	-2.00	11.21	-2.83	0.017071	0.007302	0.016806	0.007893	-0.000644	0.002323	0.010122	1.69
0.828	10.00	0.00	12.56	-3.17	0.031820	0.008283	0.031820	0.008283	-0.000759	0.001576	0.010196	3.12
0.826	11.00	-2.00										
0.813	12.00	-2.00	13.43	-3.68	0.025877	0.007958	0.025584	0.008856	-0.001053	0.002653	0.011178	2.32
0.824	12.80	-2.00										
0.825	-4.00	4.00	-1.11	-0.37	0.023974	0.007090	0.024410	0.005400	-0.000178	0.001073	0.008393	2.86
0.826	0.00	4.00	3.57	-1.31	0.034221	0.005919	0.034672	0.005248	-0.000211	0.000339	0.008065	4.24
0.828	-4.00	6.00	0.18	-0.87	0.039484	0.009330	0.040243	0.005152	-0.000520	-0.000369	0.008882	4.45
0.828	-2.00	6.00	2.52	-1.40	0.046941	0.009621	0.047690	0.004662	-0.000607	-0.000771	0.008686	5.40
0.829	0.00	6.00	4.88	-1.70	0.051636	0.010044	0.052403	0.004591	-0.000718	-0.001148	0.008650	5.97
0.829	2.00	6.00	7.26	-1.94	0.055594	0.010654	0.056403	0.004784	-0.000838	-0.001504	0.008828	6.30
0.832	4.00	6.00	9.64	-2.13	0.059076	0.011540	0.059959	0.005302	-0.001023	-0.001810	0.009343	6.32
0.829	-4.00	8.00										
0.827	-2.00	8.00	3.84	-1.65	0.062644	0.012869	0.063825	0.004025	-0.001247	-0.002744	0.009538	6.57
0.831	0.00	8.00	6.22	-1.93	0.068464	0.013136	0.069626	0.003480	-0.001507	-0.002923	0.009588	7.14
0.834	2.00	8.00	8.61	-2.10	0.072248	0.013550	0.073431	0.003363	-0.001758	-0.003065	0.009829	7.35

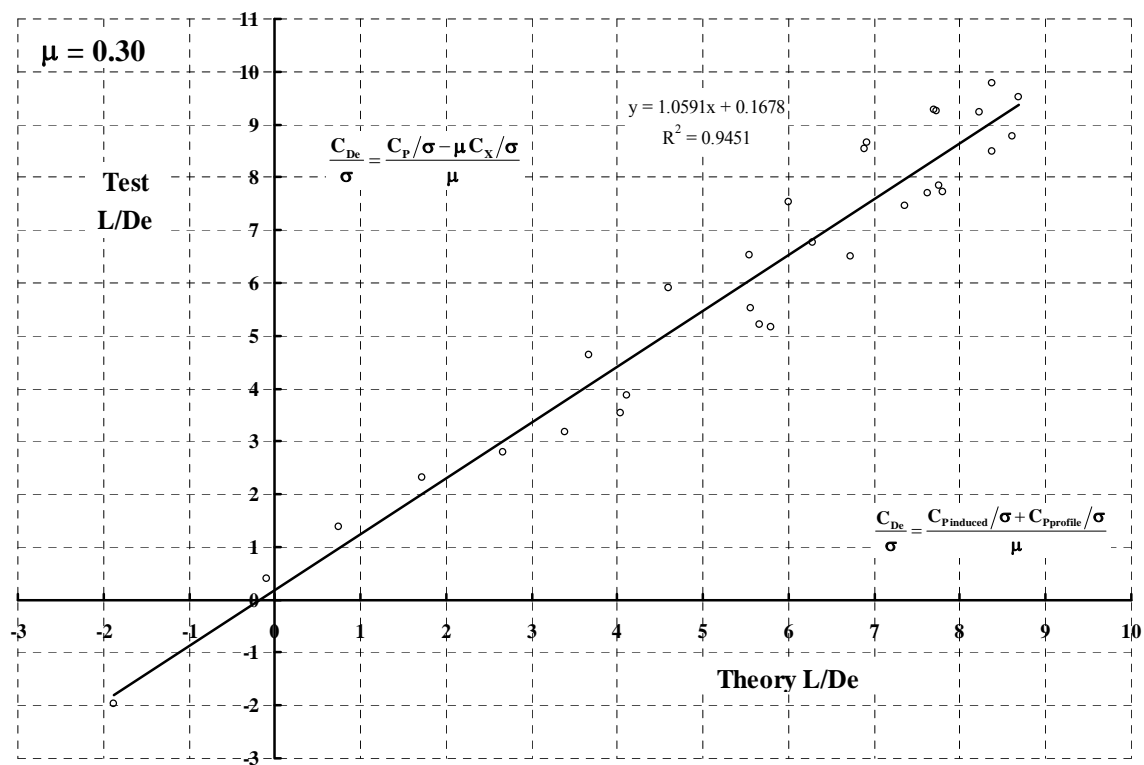
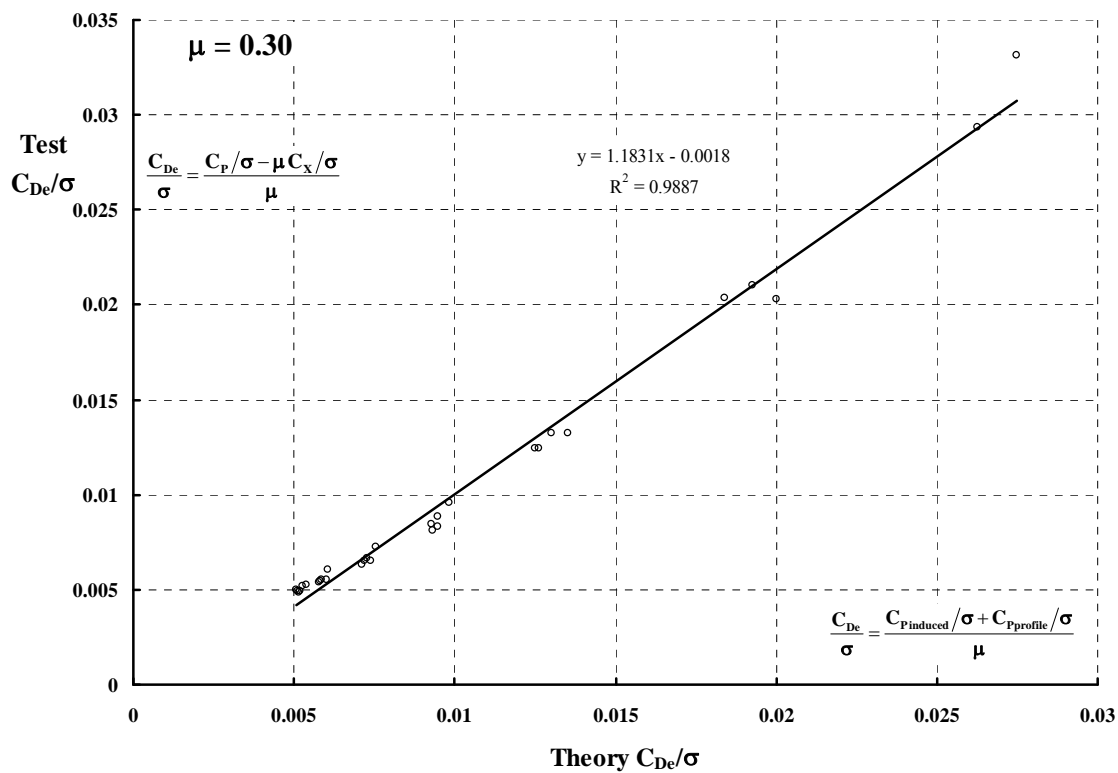
1.052	-4.00	1.00	-3.39	-0.04	0.022004	0.010334	0.022181	0.009948	0.000116	0.001387	0.011649	1.89
1.049	-4.00	3.00	-1.94	-0.82	0.042026	0.010960	0.042542	0.008746	-0.000332	0.001175	0.012074	3.48
1.049	-4.00	5.00	-0.44	-1.51	0.060447	0.012621	0.061317	0.007305	-0.001105	0.000189	0.012800	4.72
1.051	-4.00	7.00	1.09	-2.01	0.077369	0.015566	0.078689	0.006021	-0.002074	-0.001713	0.013941	5.55
1.045	-2.00	1.00	-0.96	-0.13	0.016952	0.009044	0.017107	0.008746	-0.000084	0.001921	0.010865	1.56
1.057	-2.00	3.00	0.48	-1.03	0.039031	0.009785	0.039489	0.007729	-0.000344	0.001539	0.011245	3.47
1.057	-2.00	5.00	1.96	-1.85	0.060608	0.011505	0.061380	0.006179	-0.001062	0.000490	0.011970	5.06
1.057	-2.00	7.00	3.50	-2.44	0.081146	0.014196	0.082271	0.004201	-0.002162	-0.001177	0.013080	6.20
1.051	0.00	1.00	1.50	-0.23	0.010866	0.008554	0.011014	0.008363	0.000107	0.001984	0.010435	1.04
1.059	0.00	3.00	2.93	-1.12	0.033479	0.009405	0.033925	0.007640	-0.000072	0.001477	0.010806	3.10
1.059	0.00	5.00	4.40	-1.90	0.055960	0.011018	0.056707	0.006099	-0.000672	0.000456	0.011450	4.89
1.051	0.00	7.00	5.92	-2.51	0.078025	0.013496	0.079088	0.003887	-0.001718	-0.001055	0.012496	6.24
1.058	2.00	1.00	3.98	-0.26	0.004388	0.009641	0.004555	0.009563	0.000679	0.001294	0.010868	0.40
1.051	2.00	3.00	5.42	-1.08	0.027393	0.010210	0.027890	0.008762	0.000622	0.000795	0.010963	2.50
1.057	2.00	5.00	6.88	-1.79	0.050588	0.011612	0.051408	0.007159	0.000113	-0.000178	0.011443	4.42
1.052	2.00	7.00	8.39	-2.36	0.072939	0.013778	0.074074	0.004786	-0.000870	-0.001503	0.012352	5.91
1.058	4.00	1.00	6.46	-0.10	-0.001770	0.011695	-0.001566	0.011724	0.001573	0.000041	0.011734	-0.15
1.052	4.00	3.00	7.91	-0.81	0.020903	0.012224	0.021514	0.011113	0.001670	-0.000518	0.011733	1.78
1.053	4.00	5.00	9.38	-1.46	0.043979	0.013380	0.044978	0.009496	0.001125	-0.001357	0.012094	3.64
1.053	4.00	7.00	10.87	-1.96	0.066697	0.015254	0.068059	0.007012	0.000172	-0.002487	0.012895	5.17
1.053	6.00	1.00	8.94	-0.24	-0.002236	0.013710	-0.001996	0.013747	0.001892	-0.000842	0.012911	-0.17
1.052	6.00	3.00	10.40	-0.70	0.018158	0.014488	0.018891	0.013518	0.002153	-0.001627	0.012945	1.40
1.051	8.00	3.00	12.86	-0.92	0.020265	0.016483	0.021100	0.015400	0.001924	-0.002201	0.014396	1.41
1.059	8.00	5.00	14.36	-1.25	0.039210	0.017915	0.040622	0.014429	0.001579	-0.003092	0.014982	2.62
1.049	10.00	1.00	13.76	-0.98	0.006792	0.017445	0.007096	0.017324	0.001551	-0.001808	0.015730	0.43

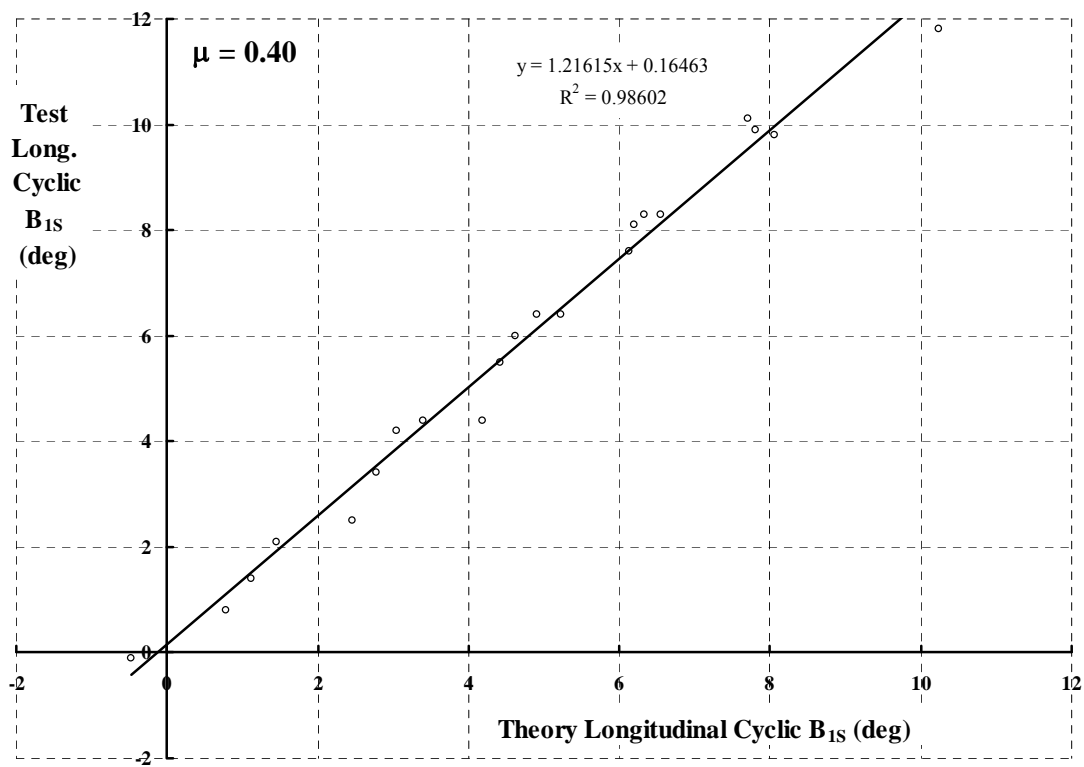
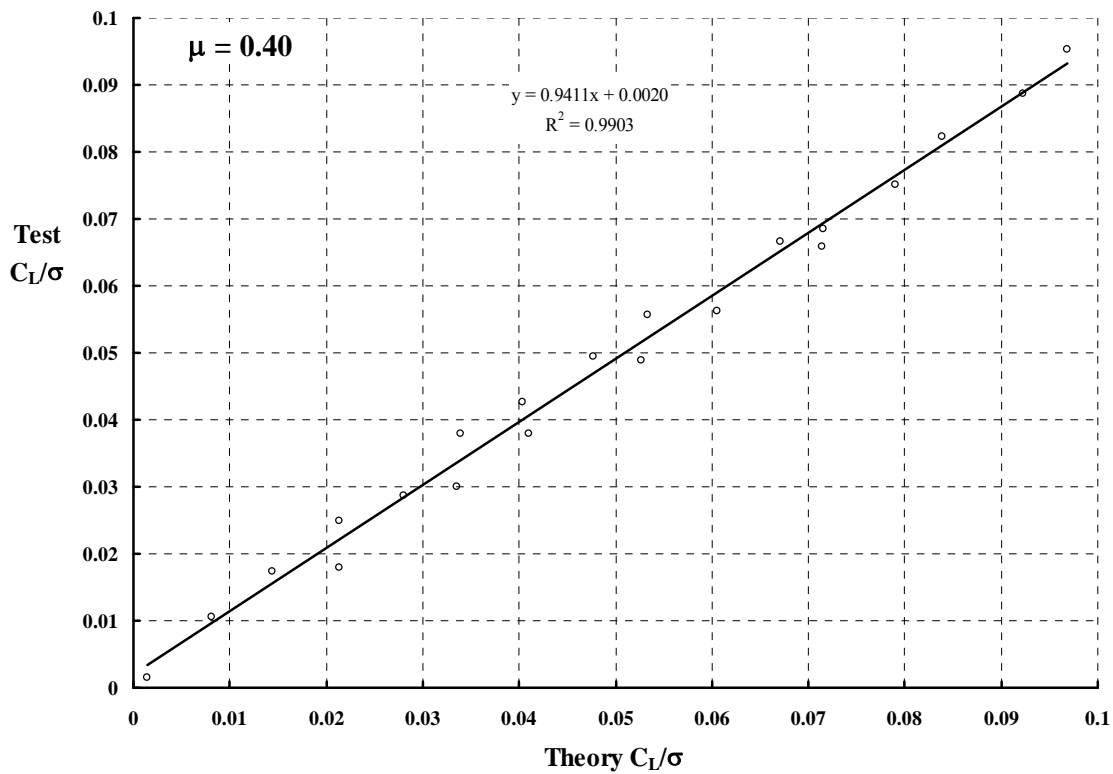


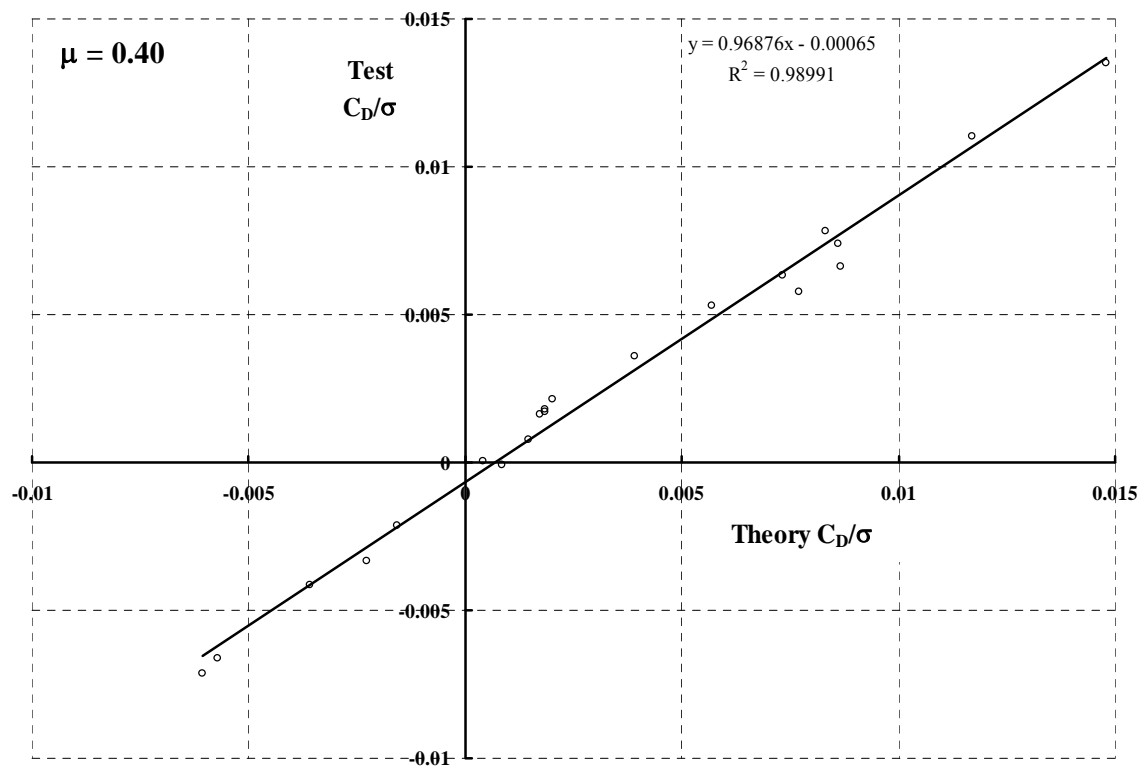
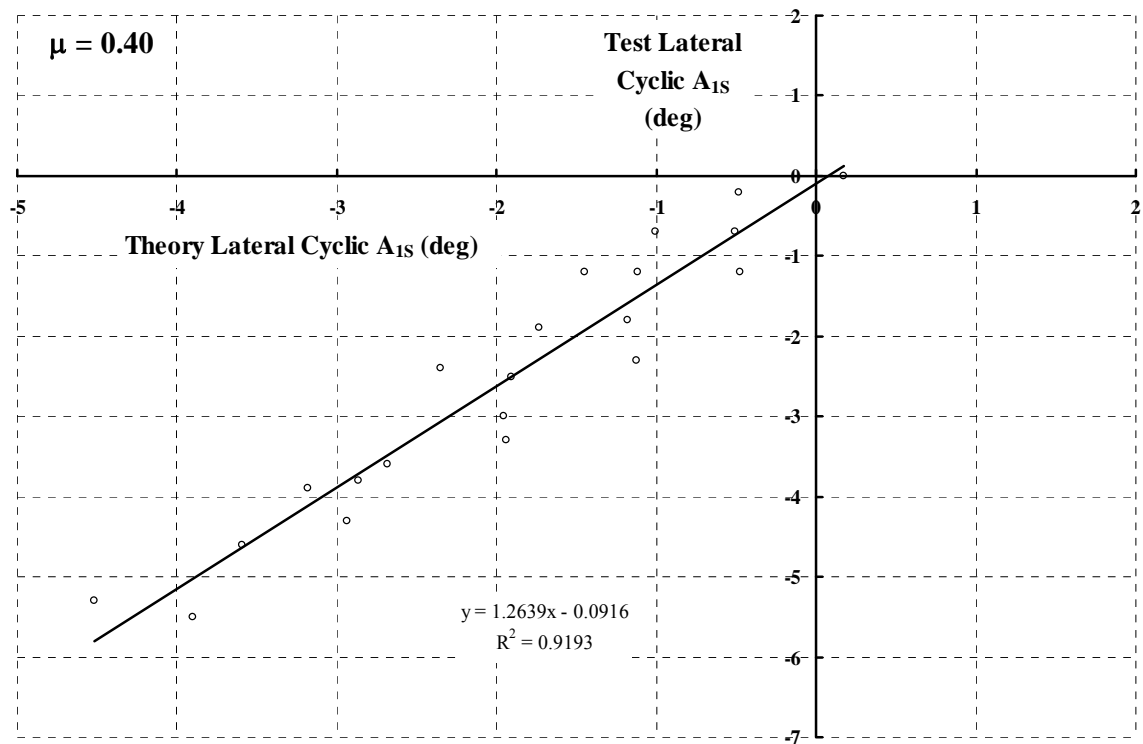


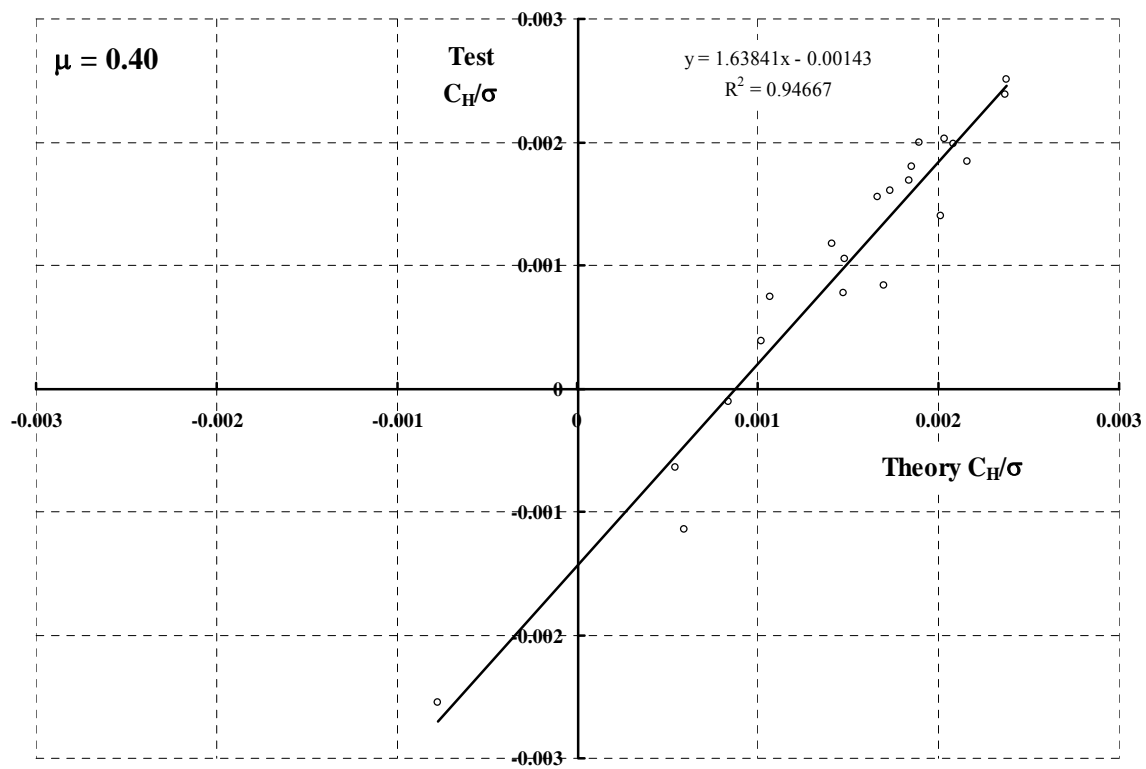
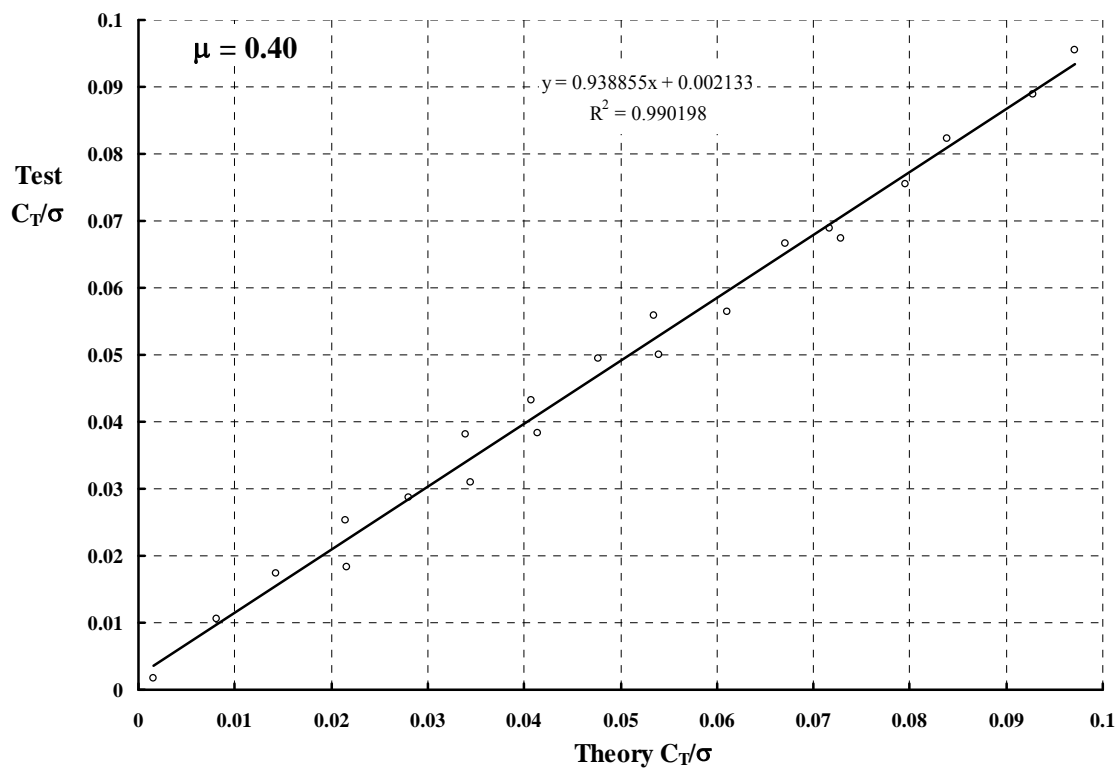


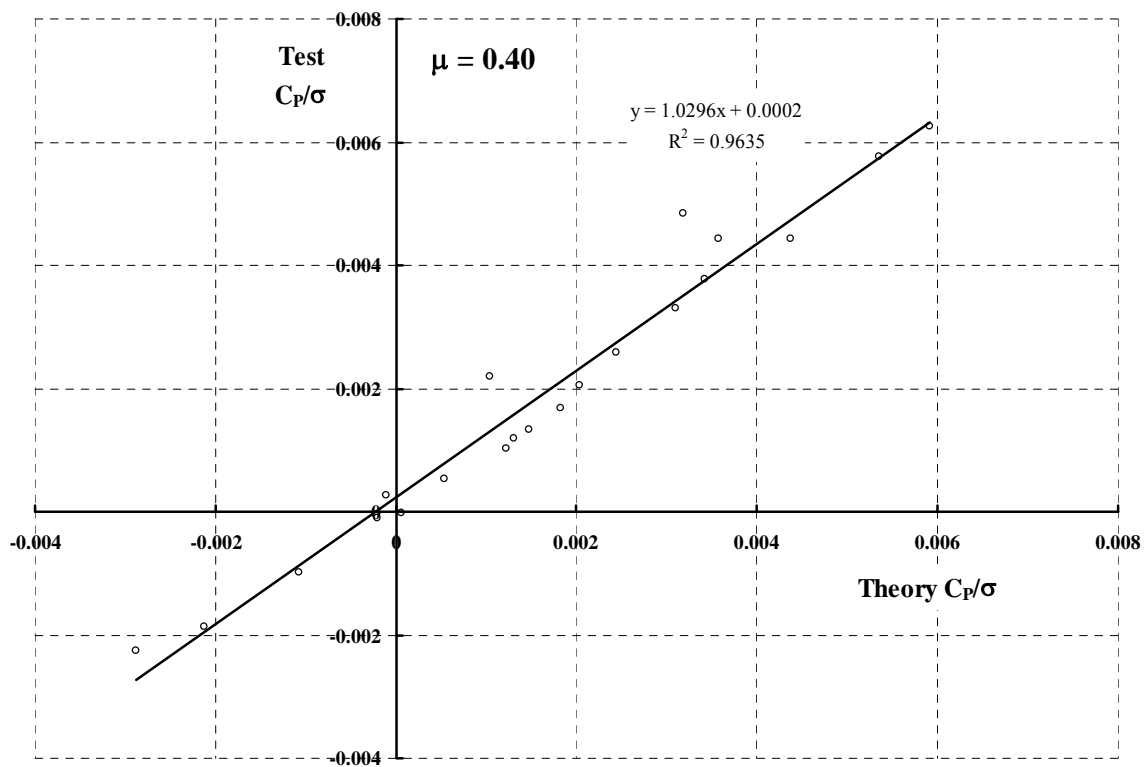
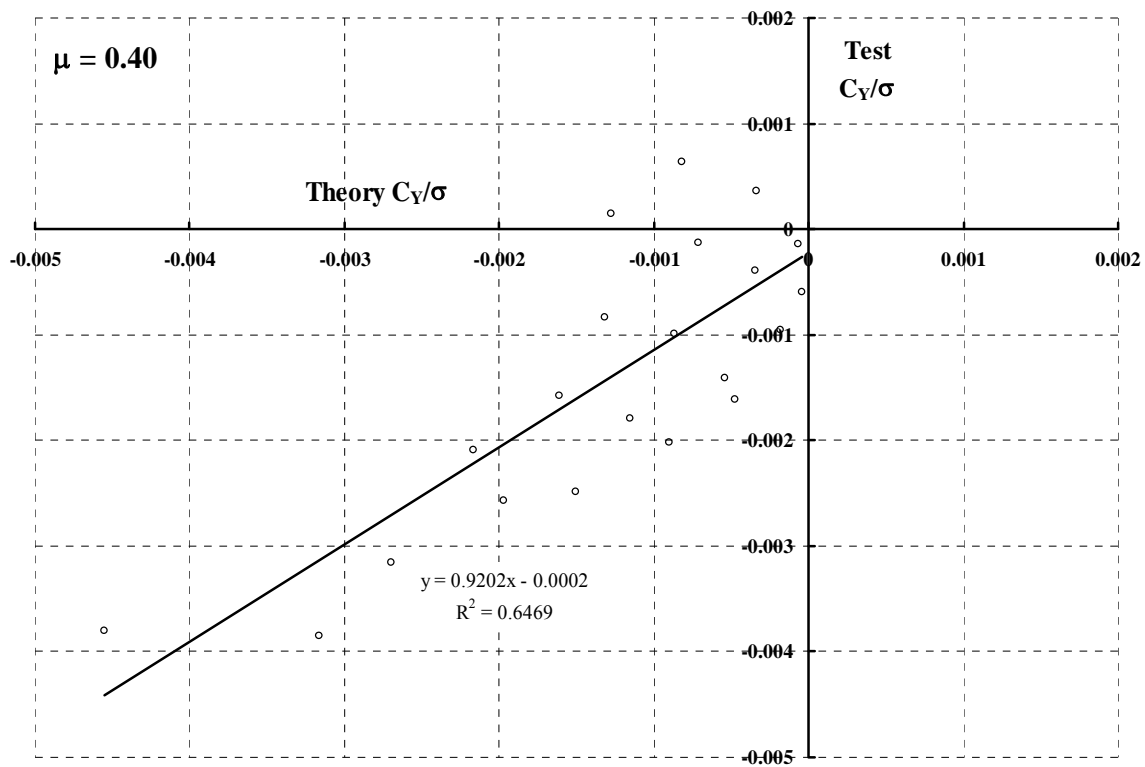


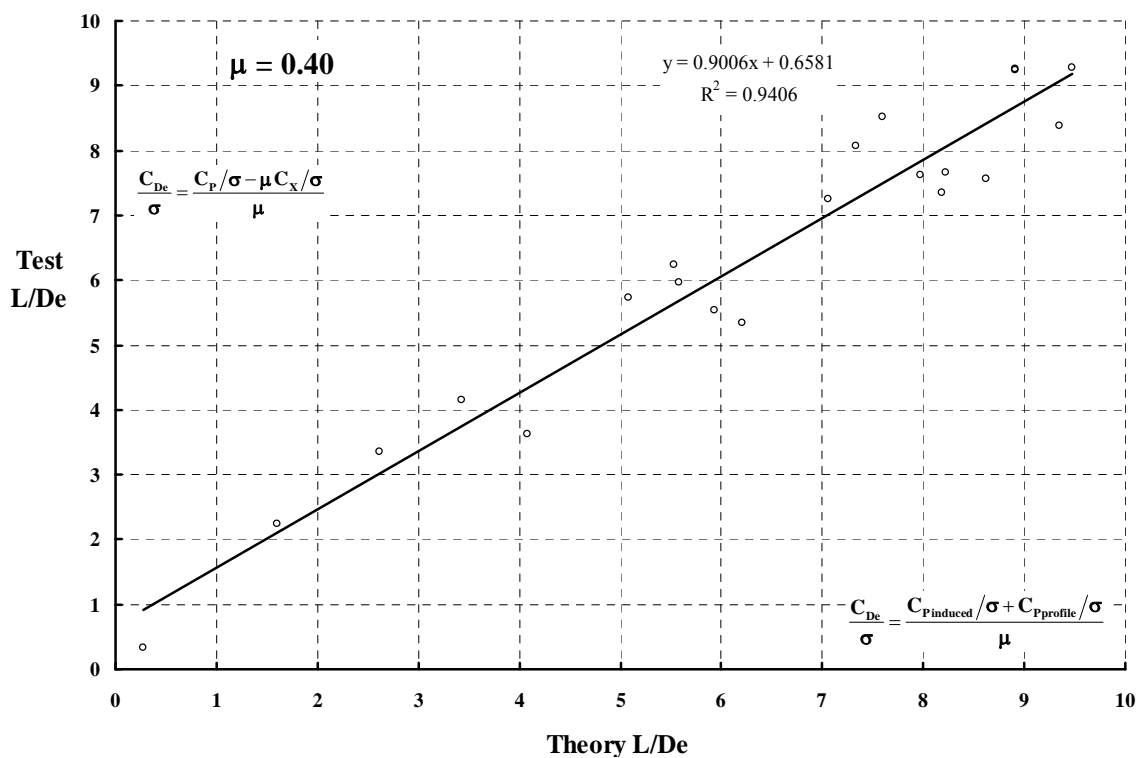
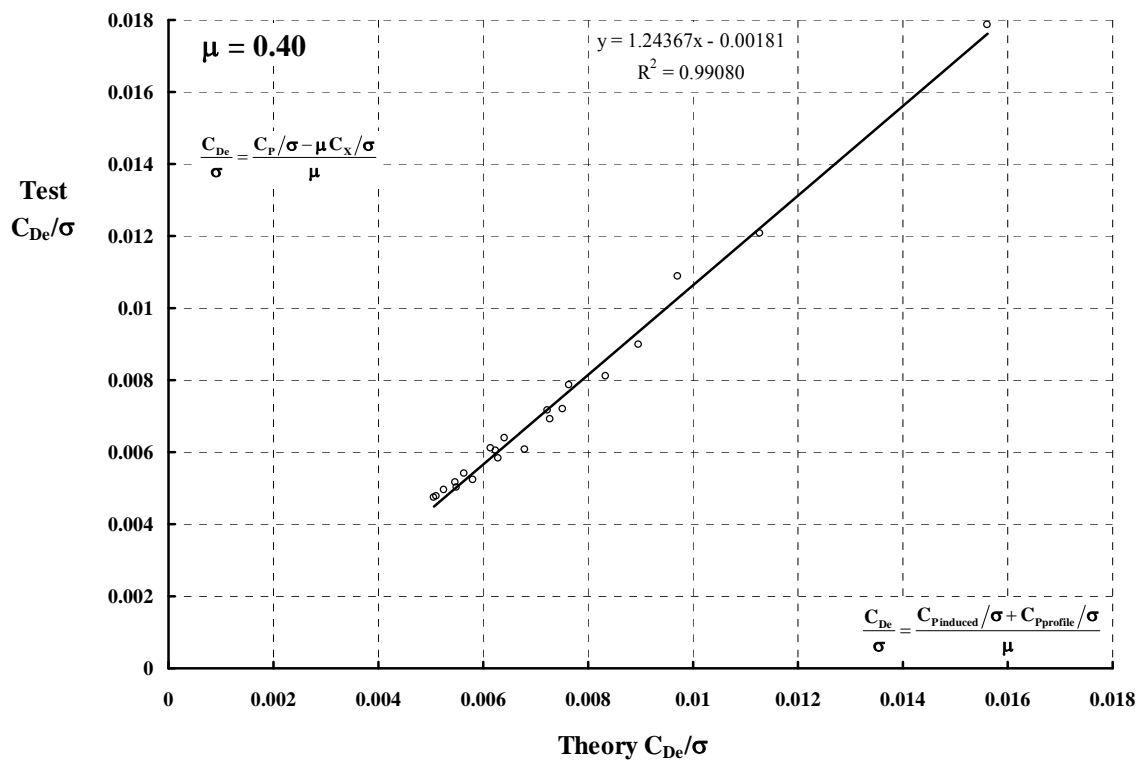


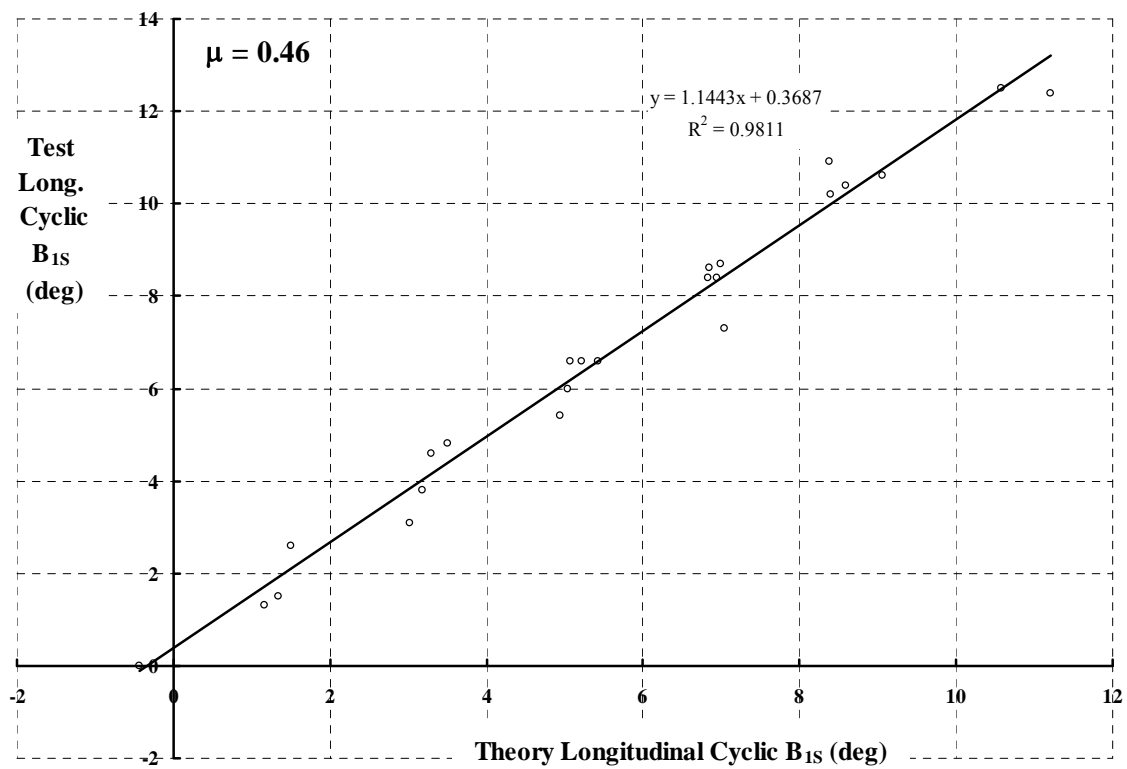
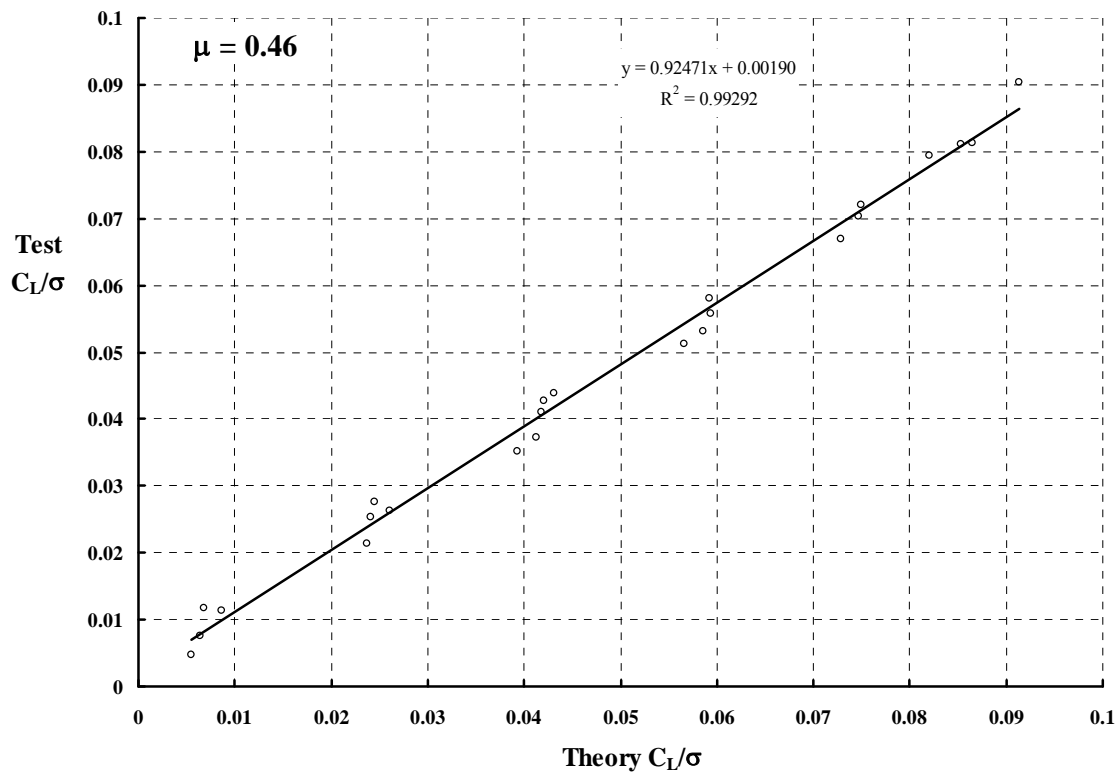


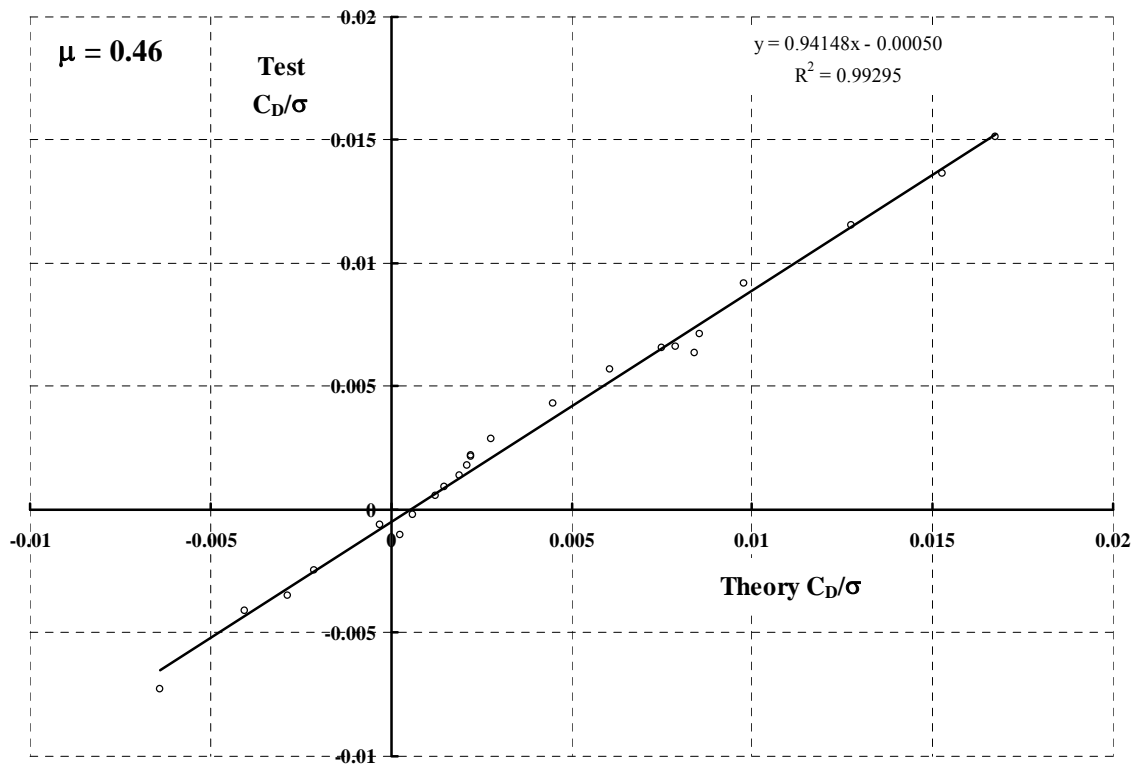
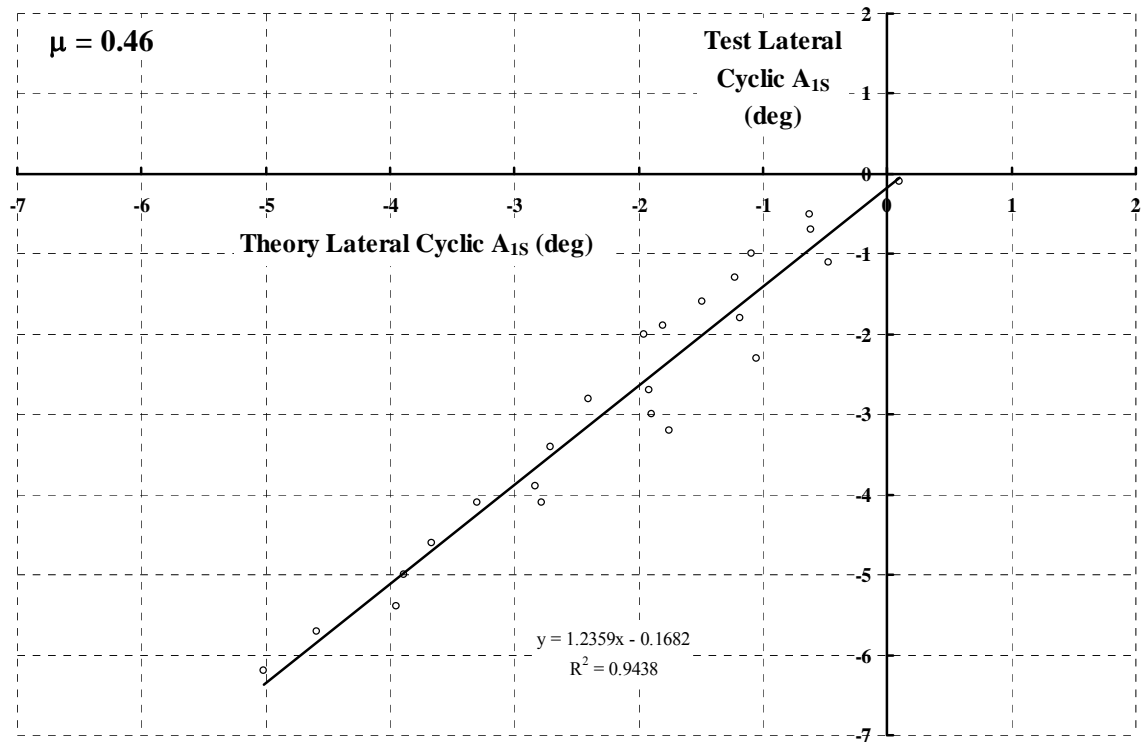


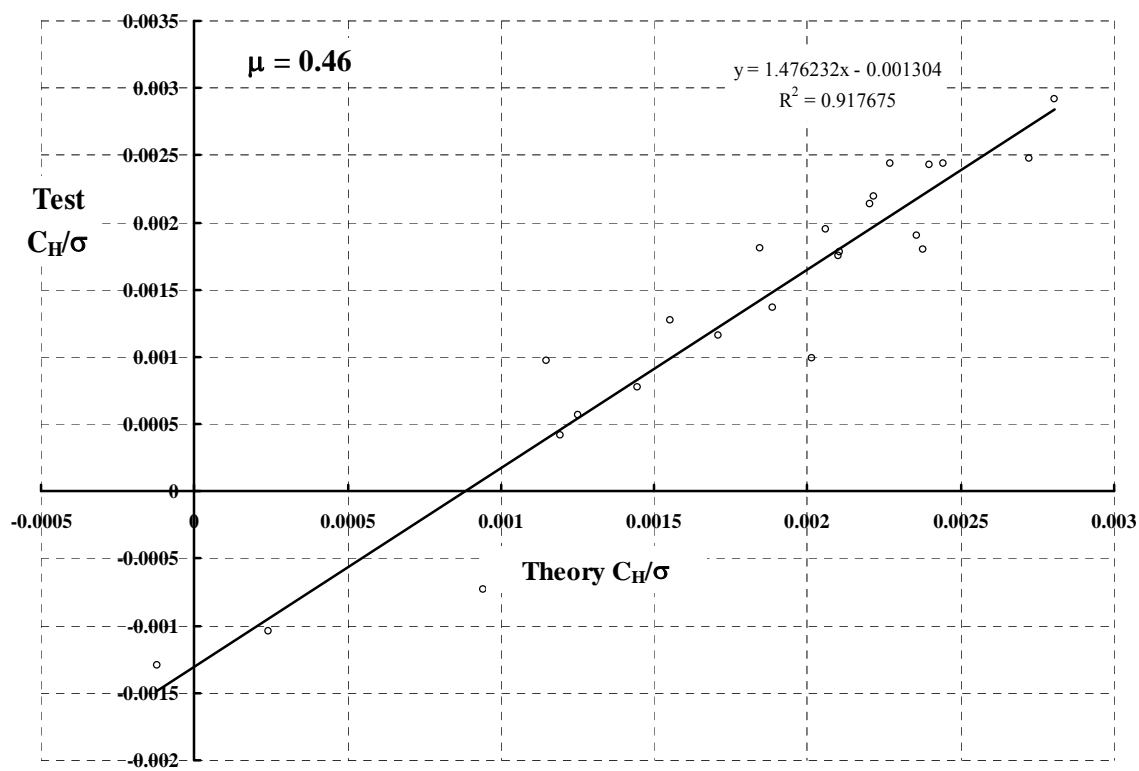
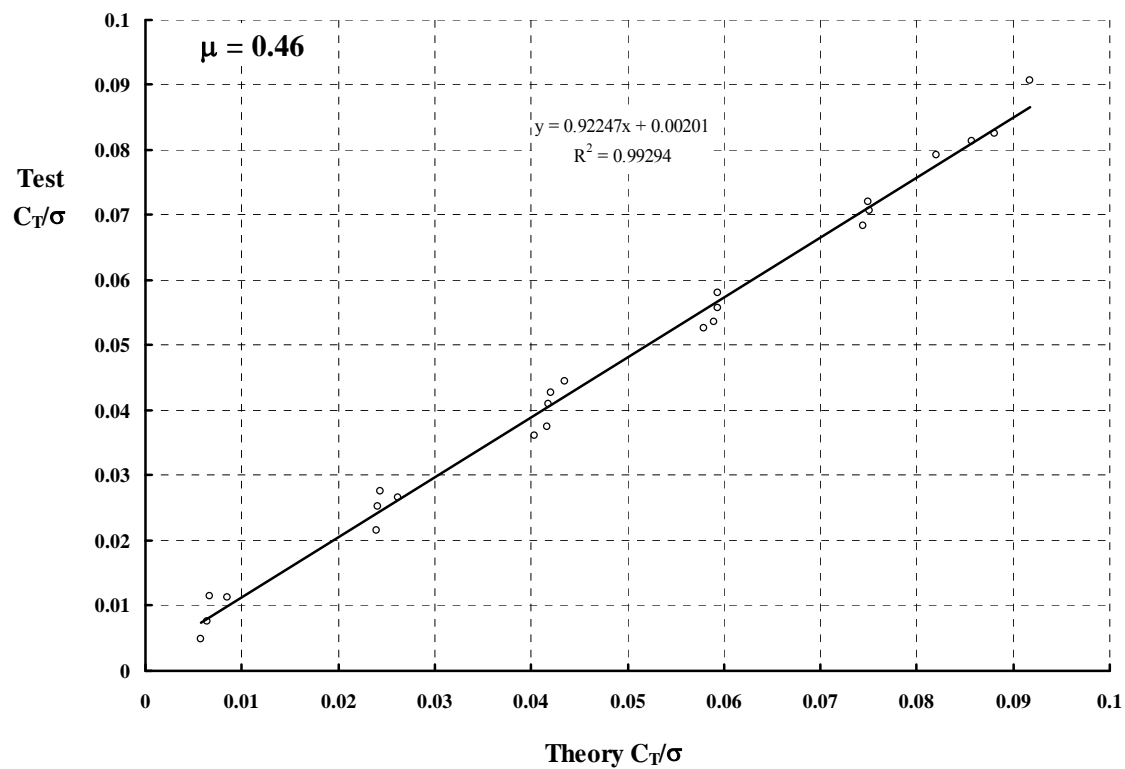


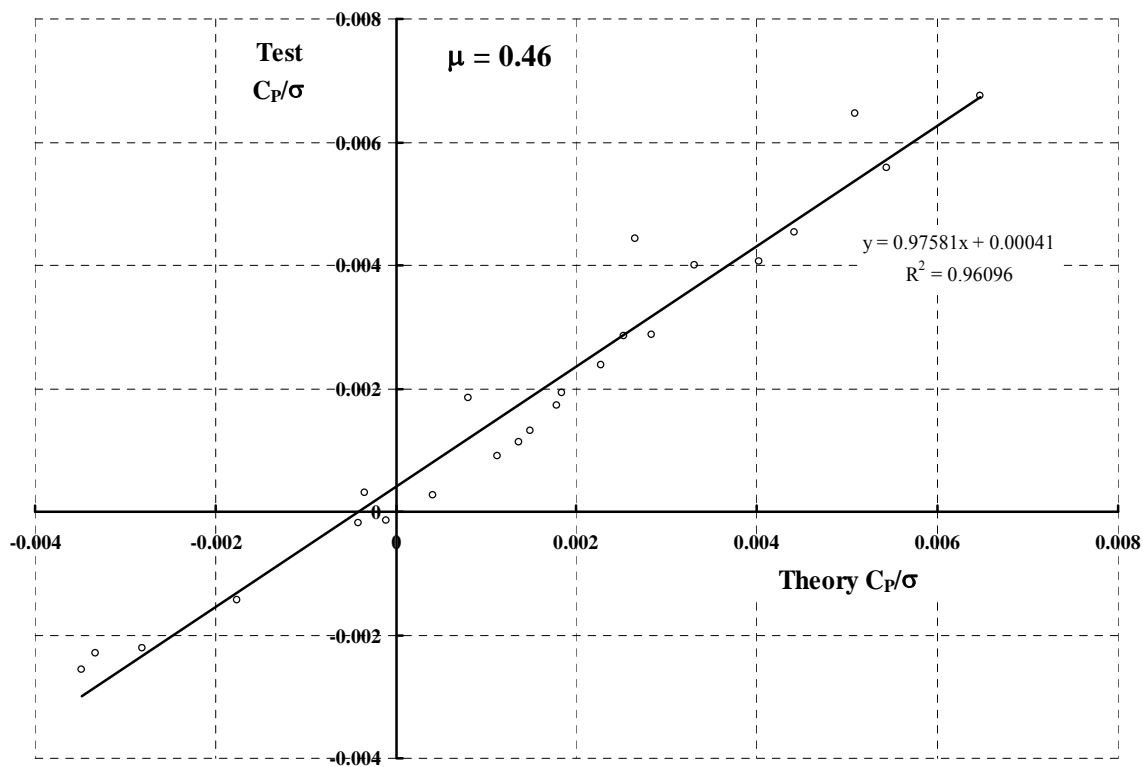
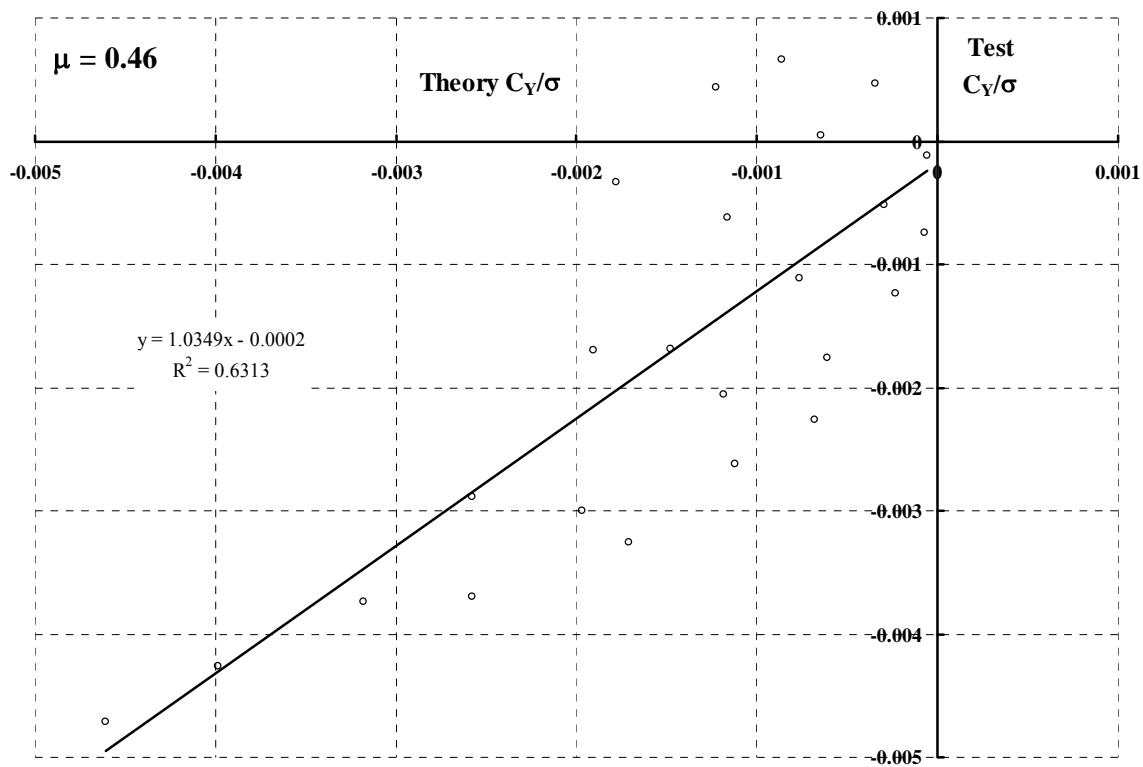


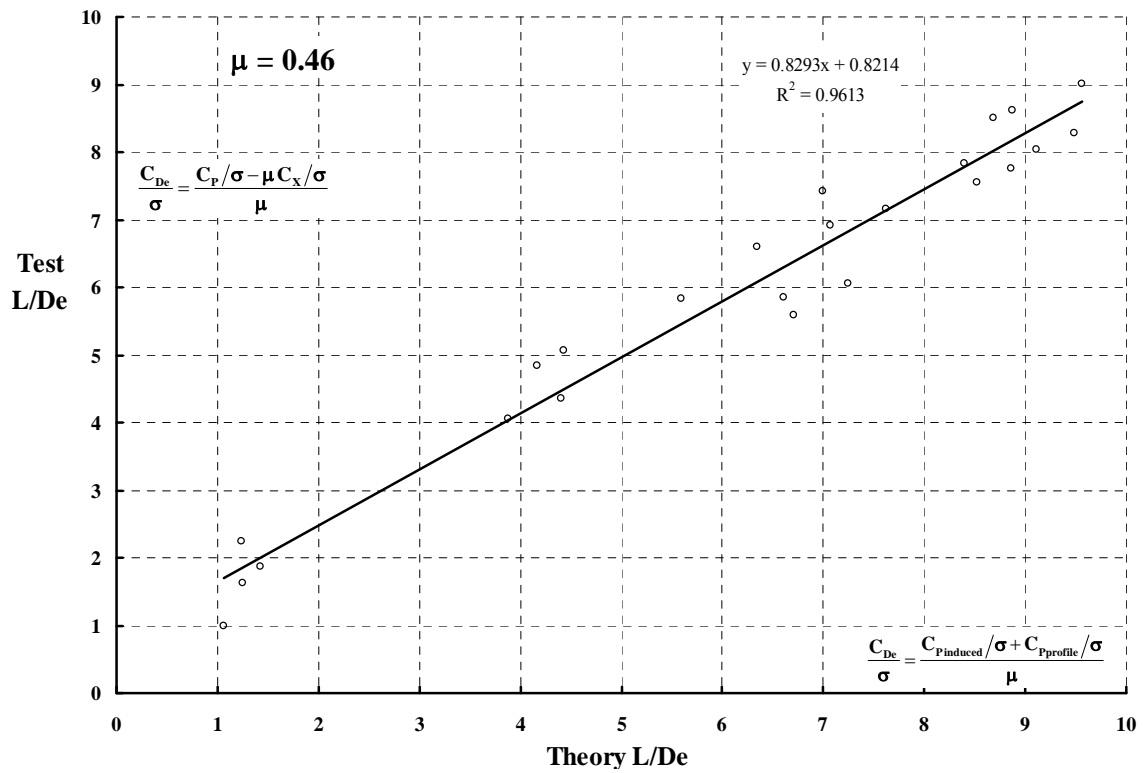
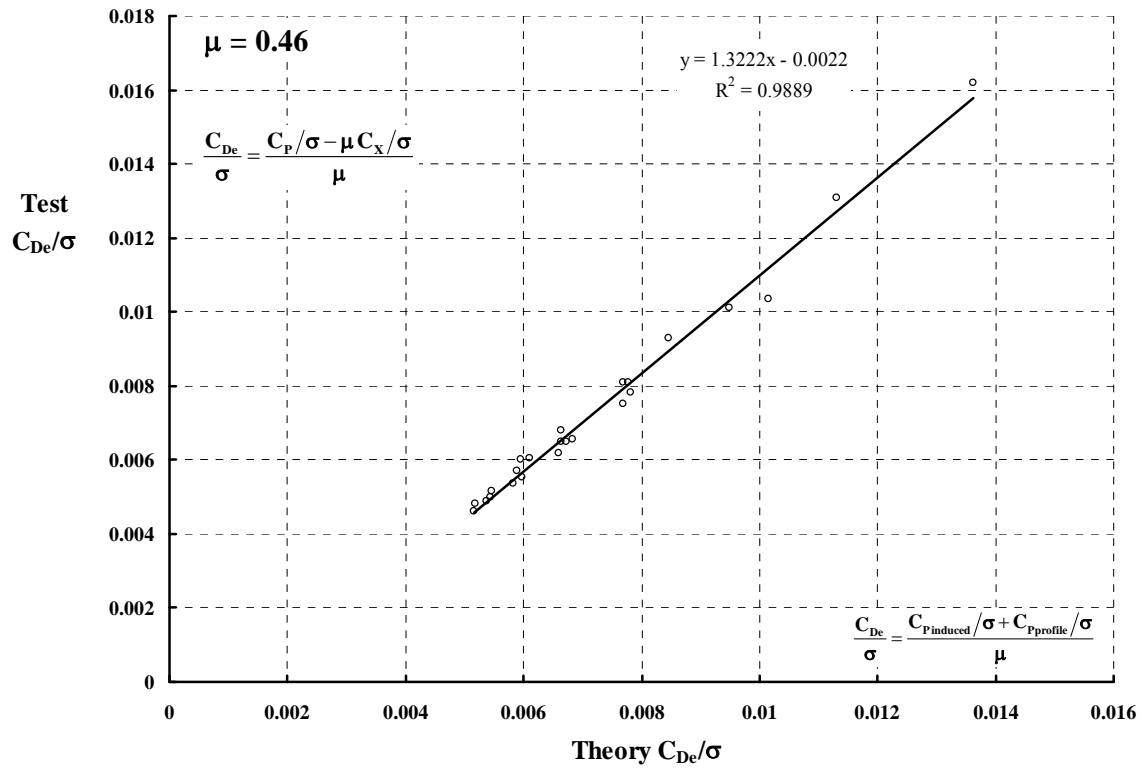


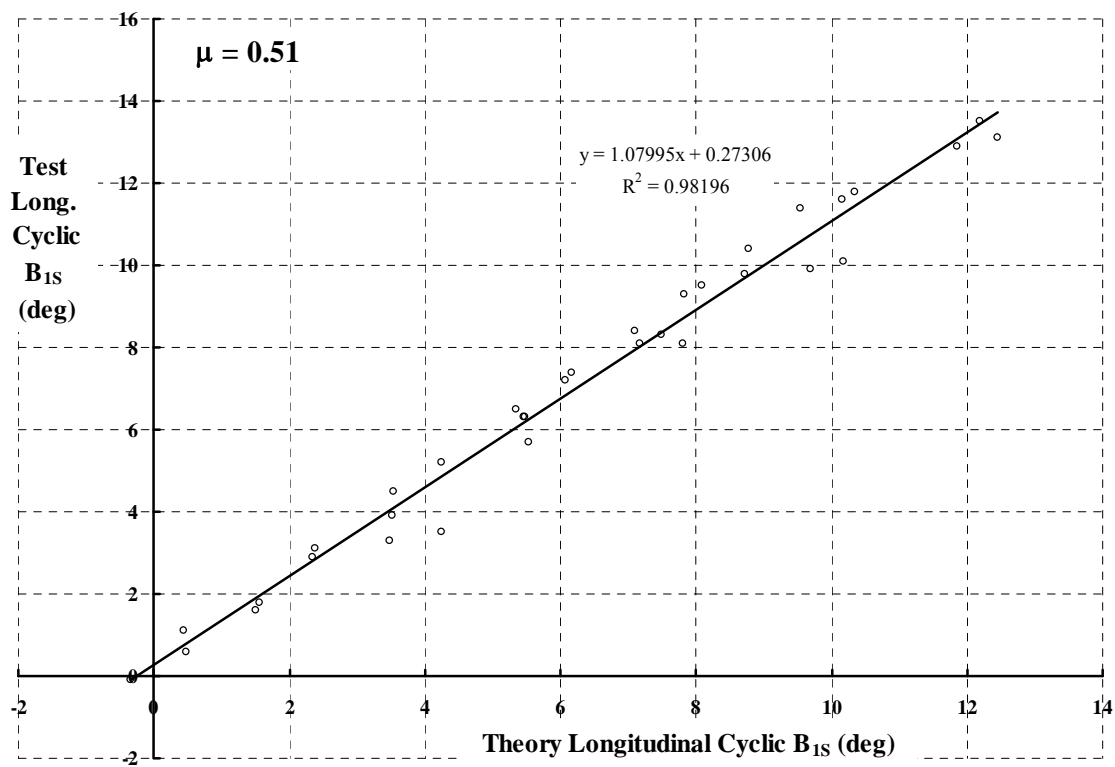
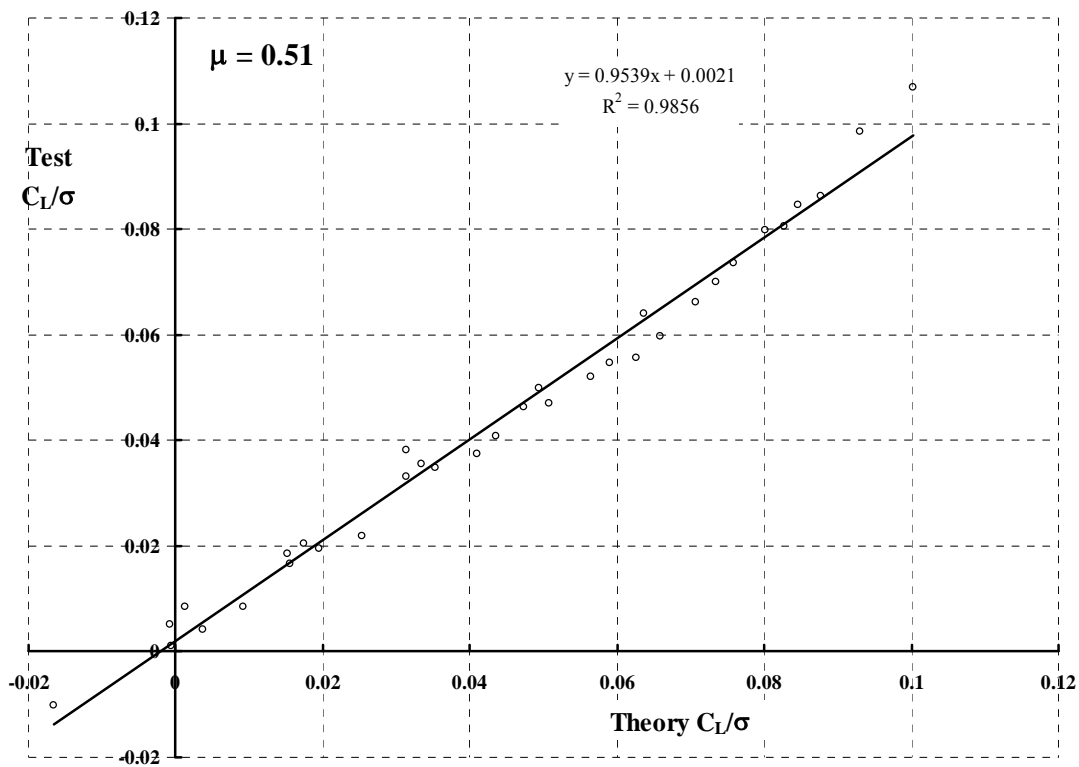


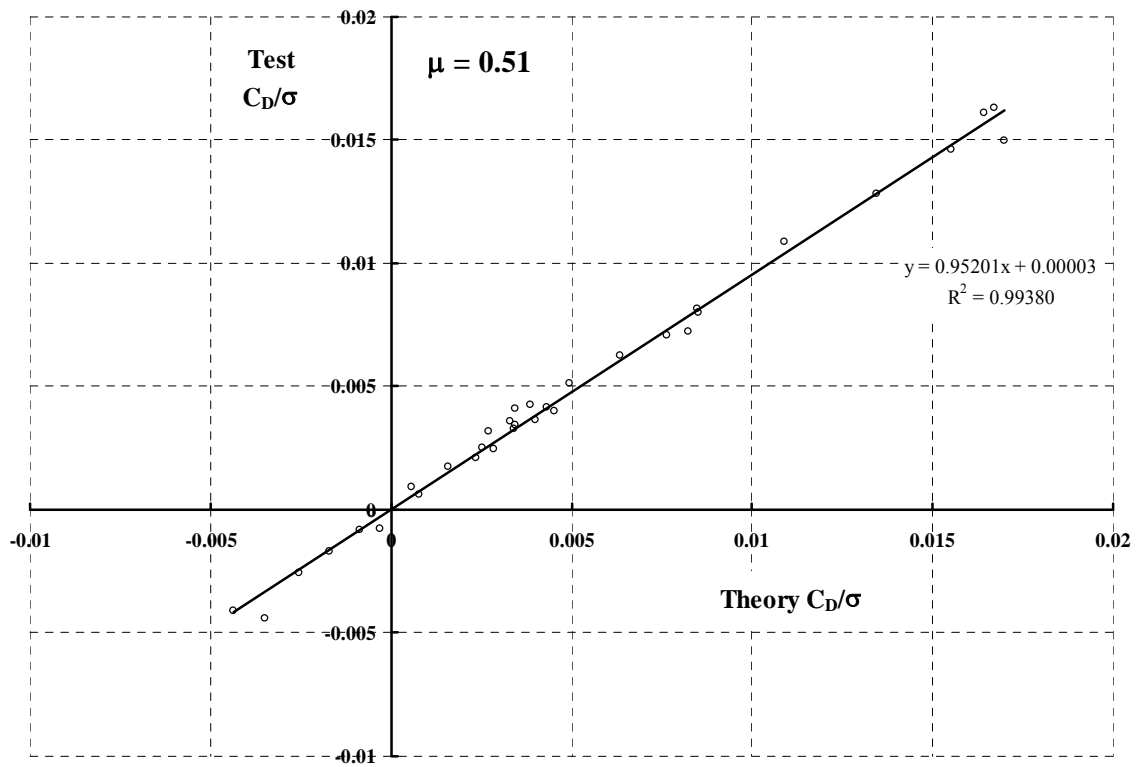
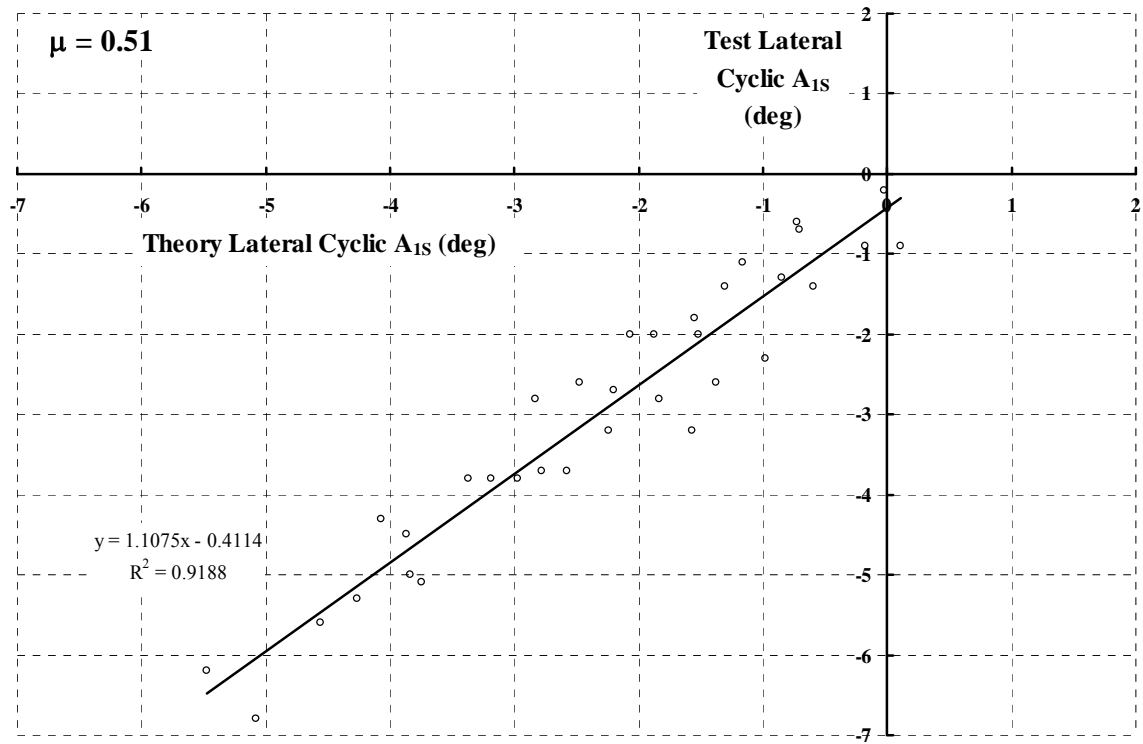


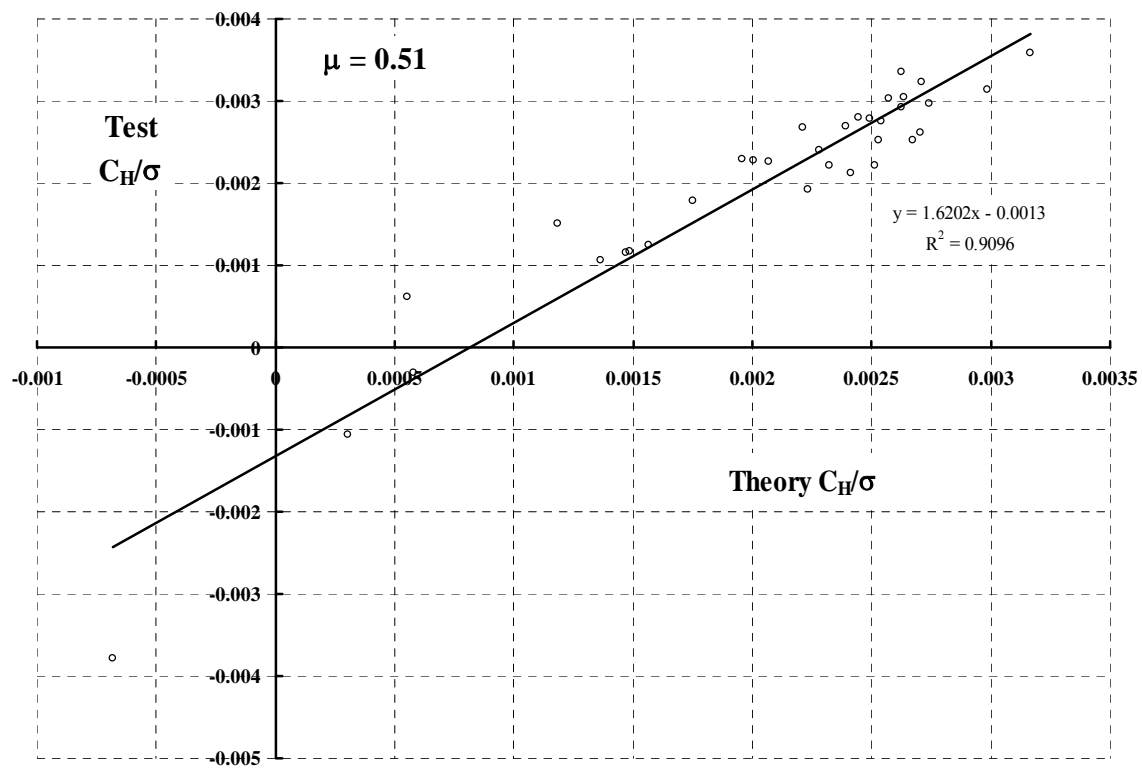
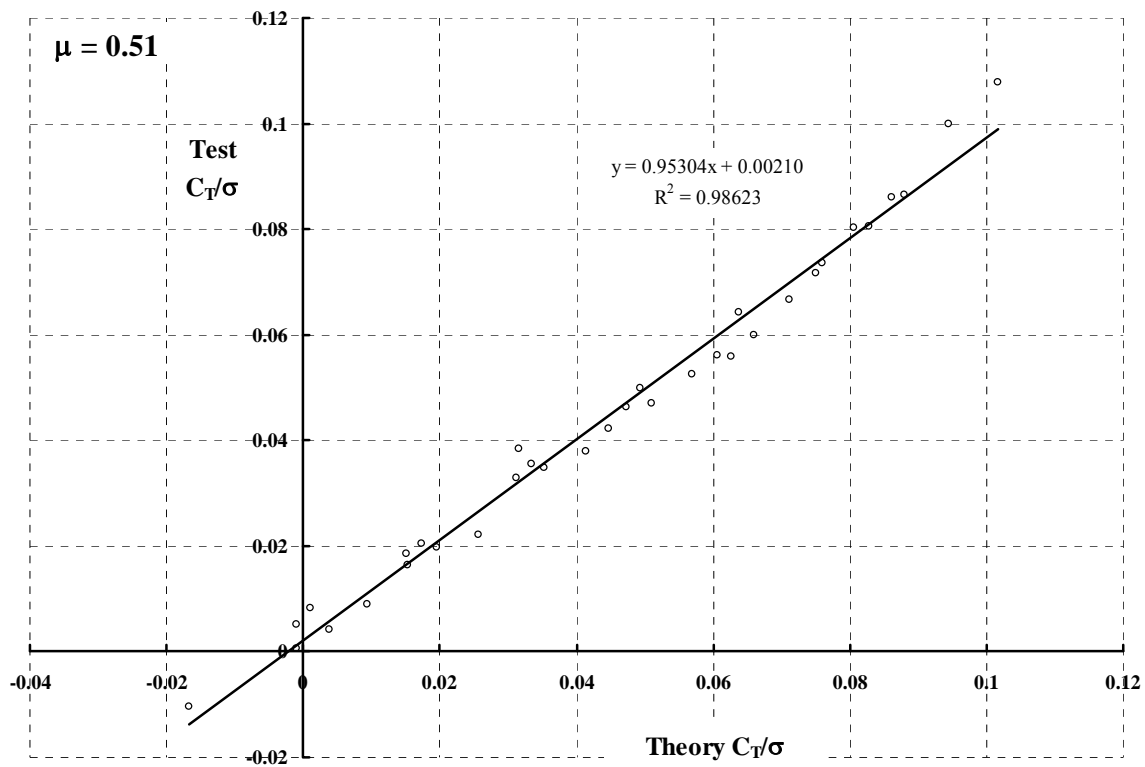


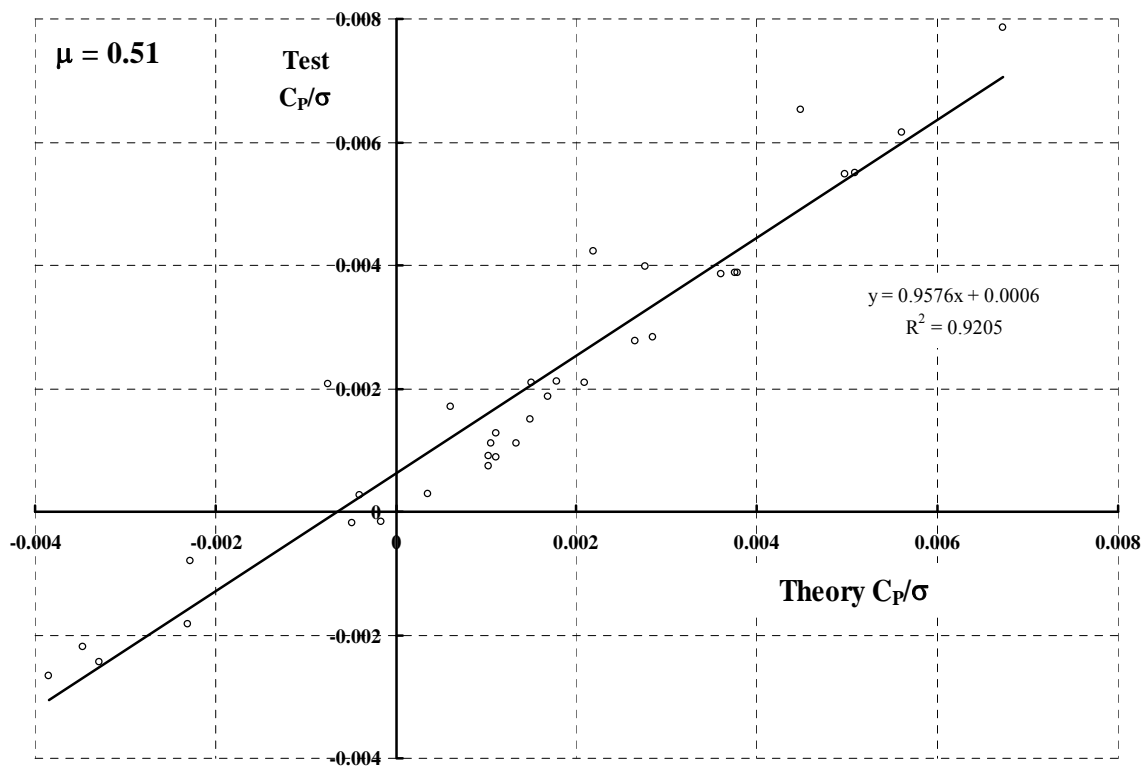
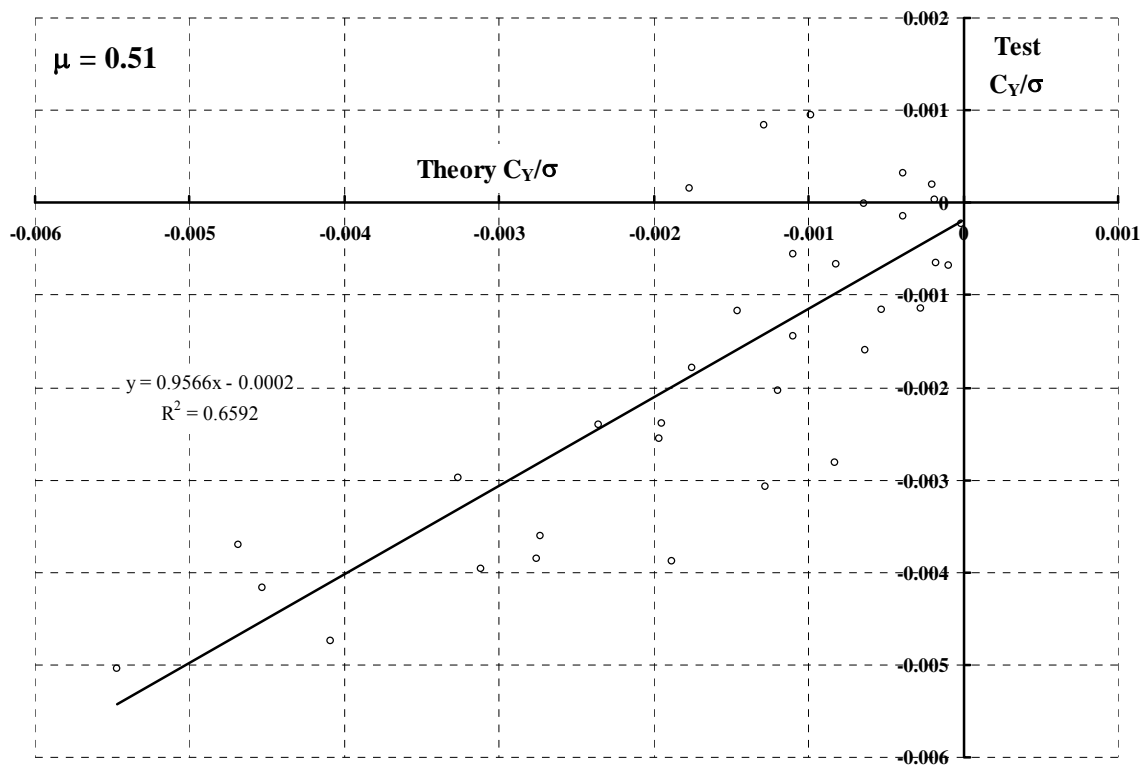


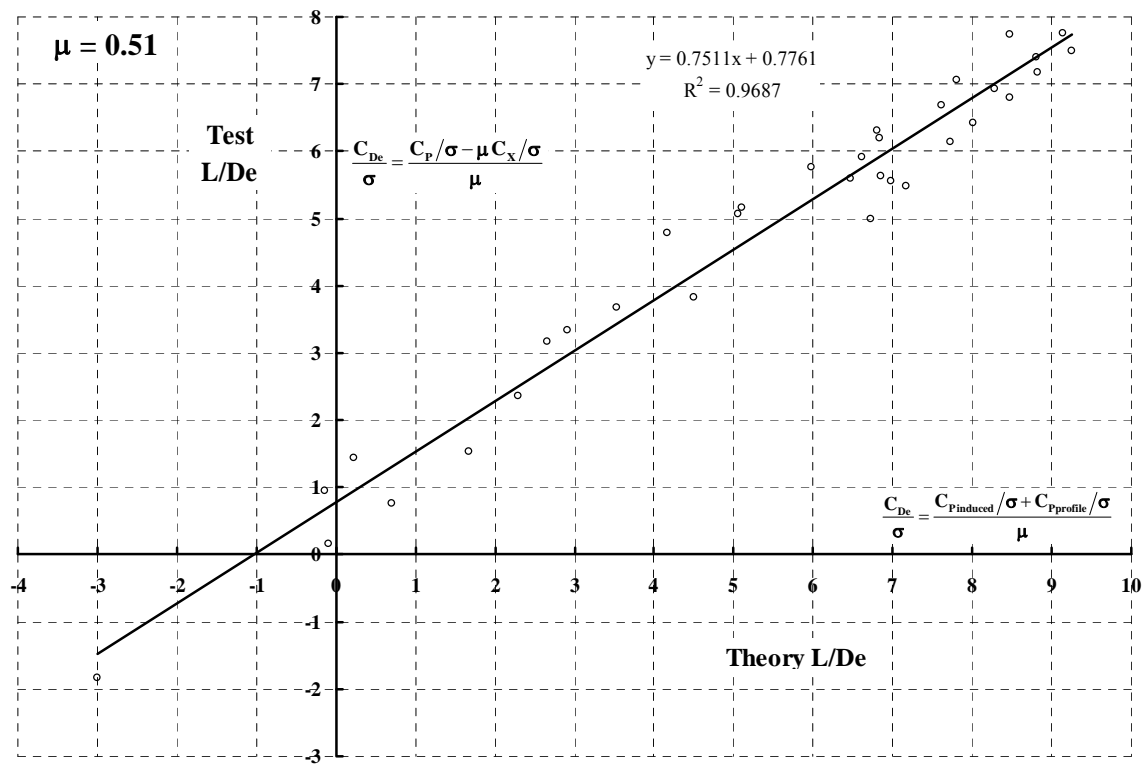
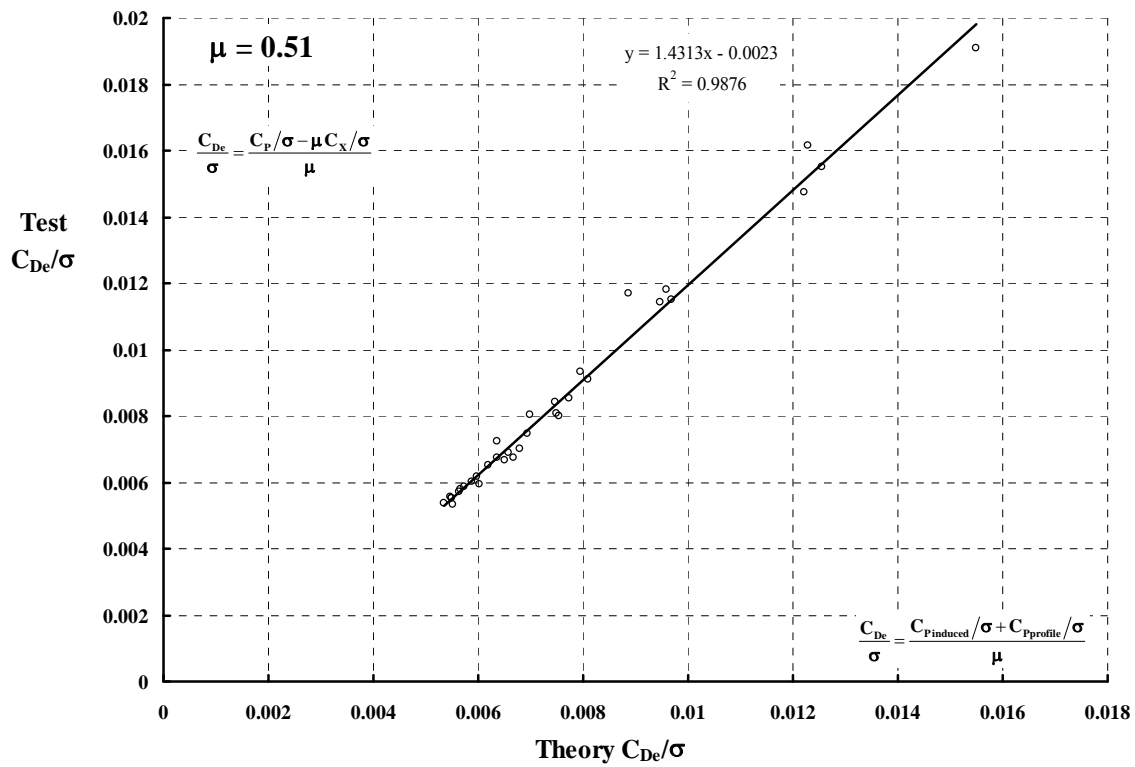


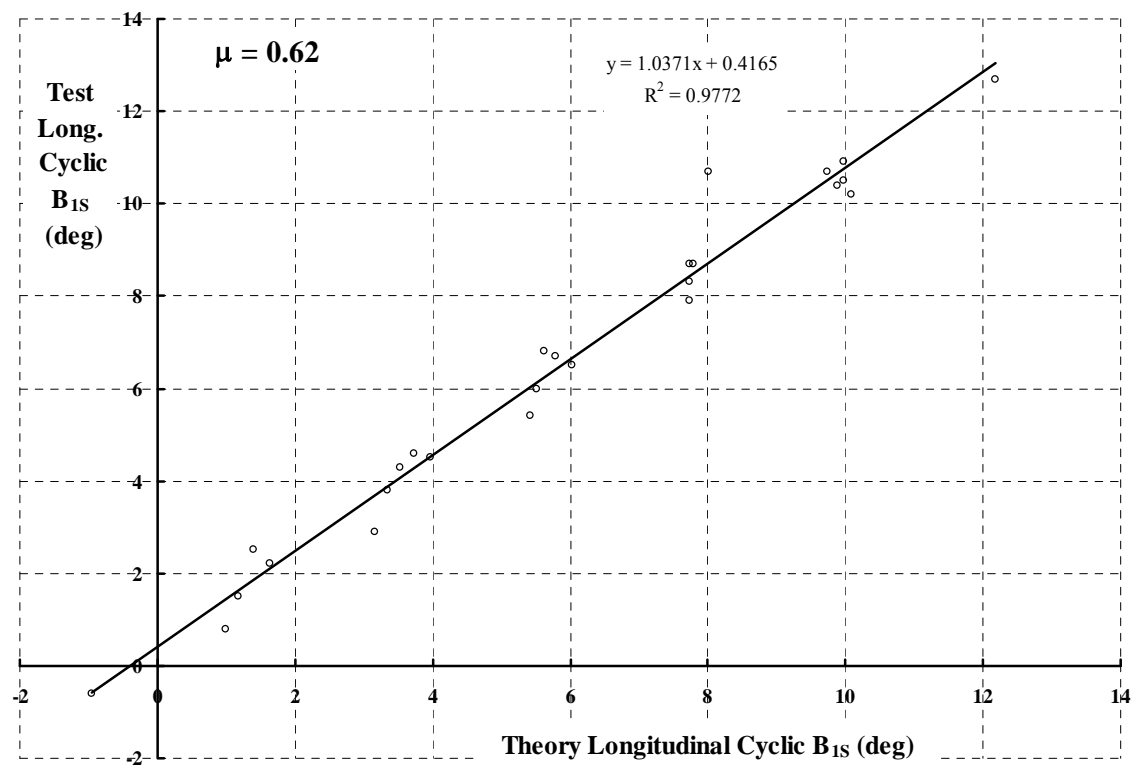
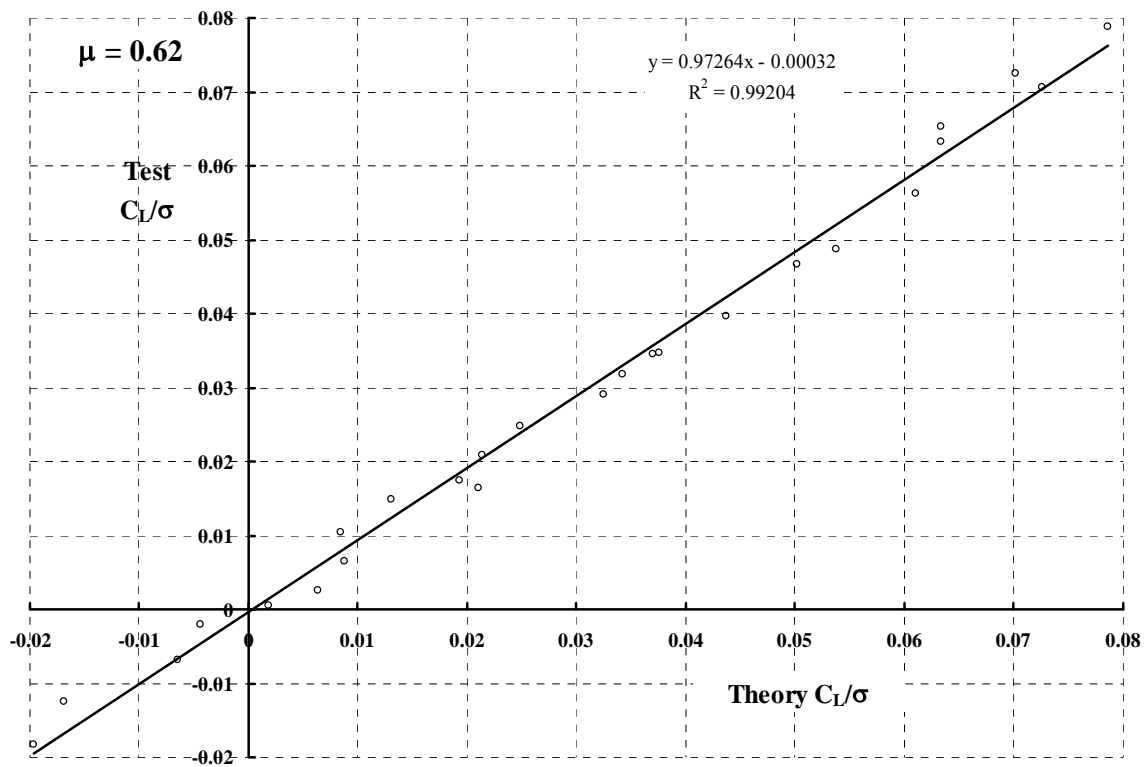


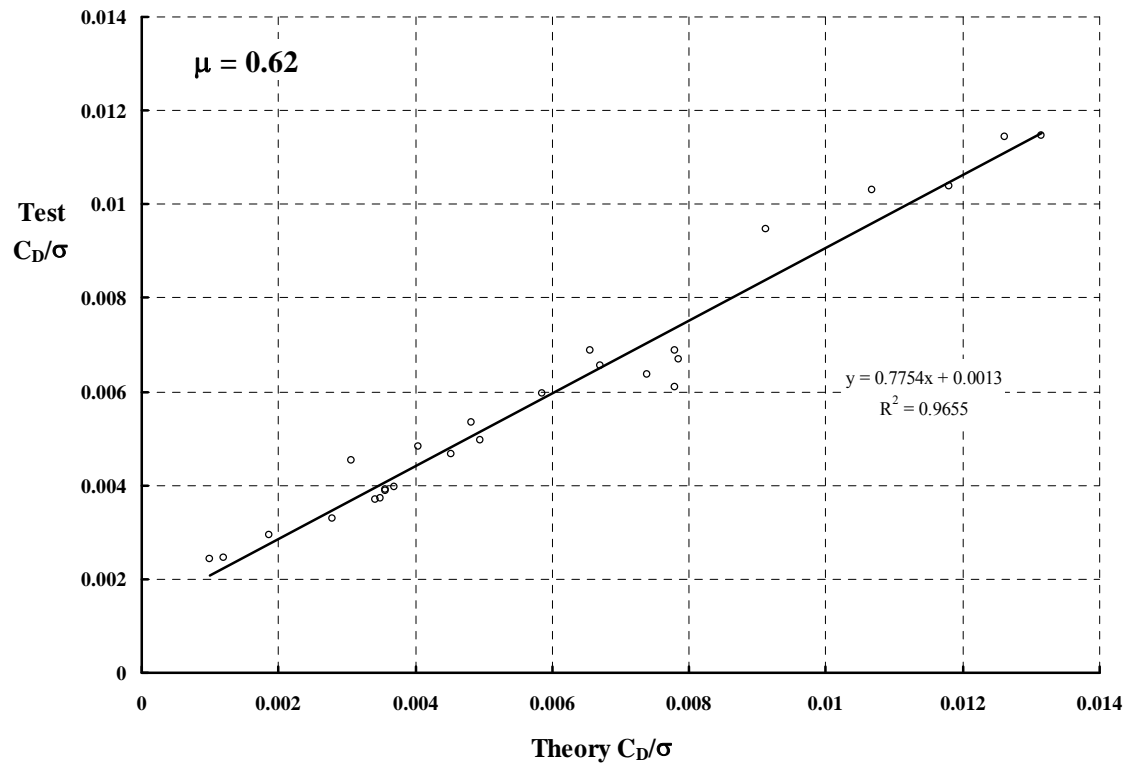
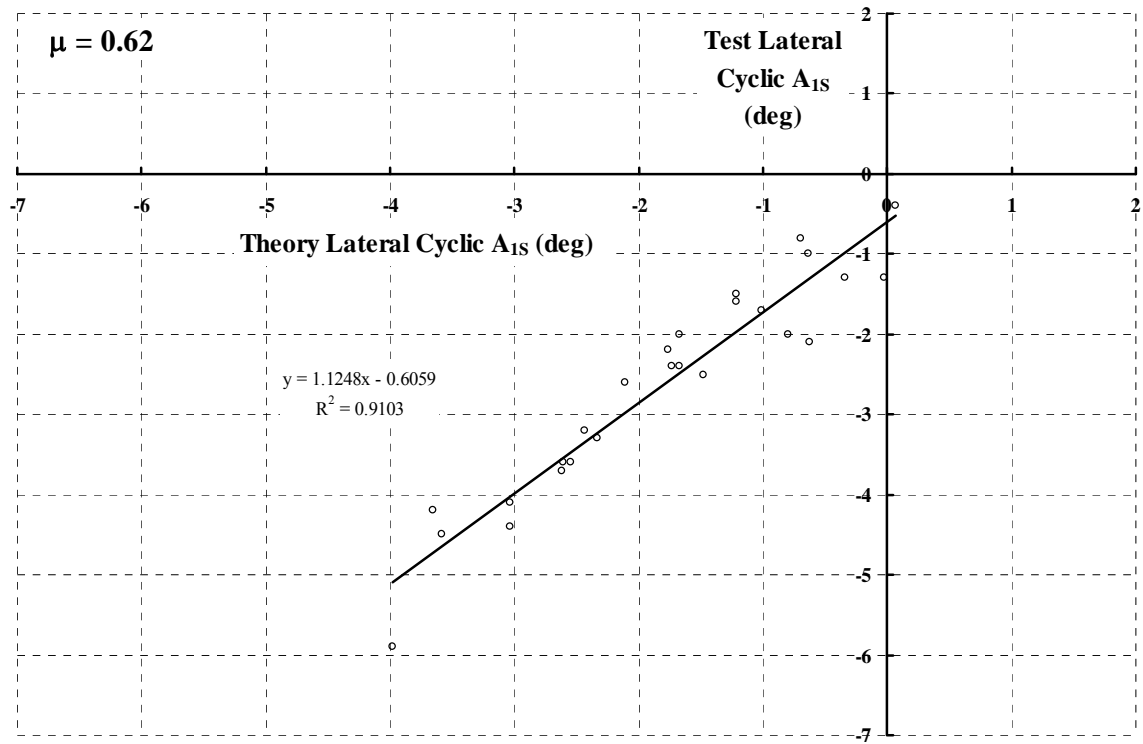


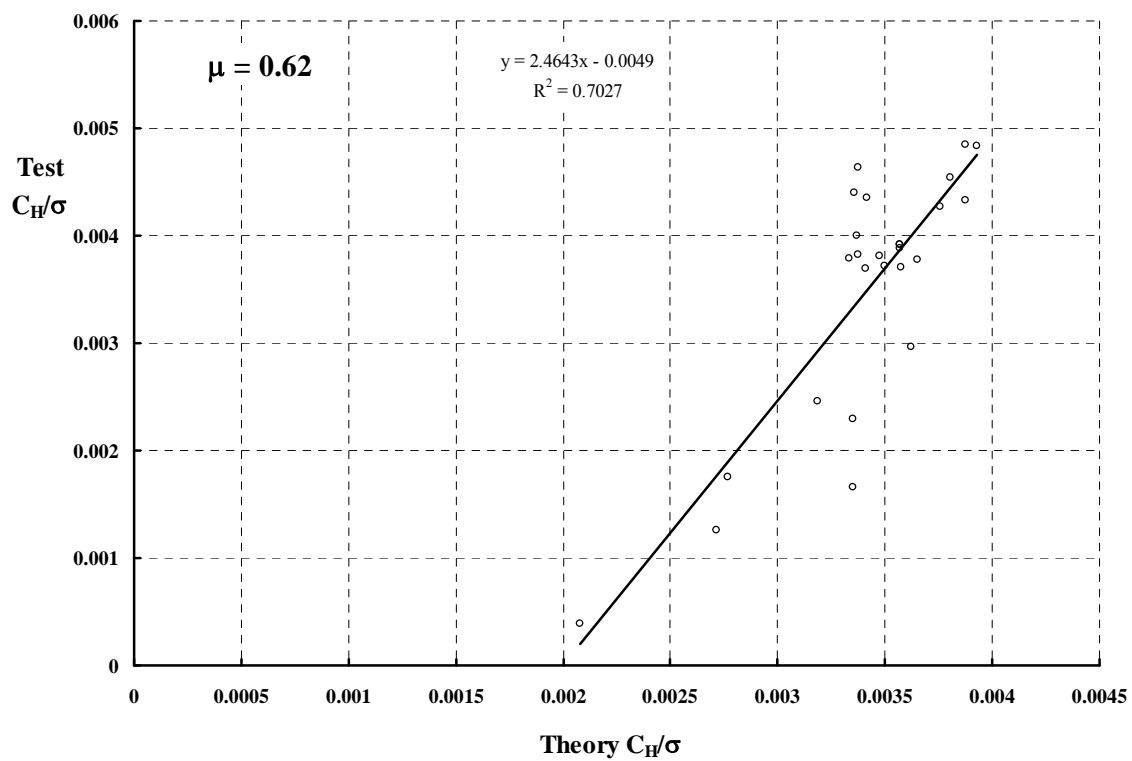
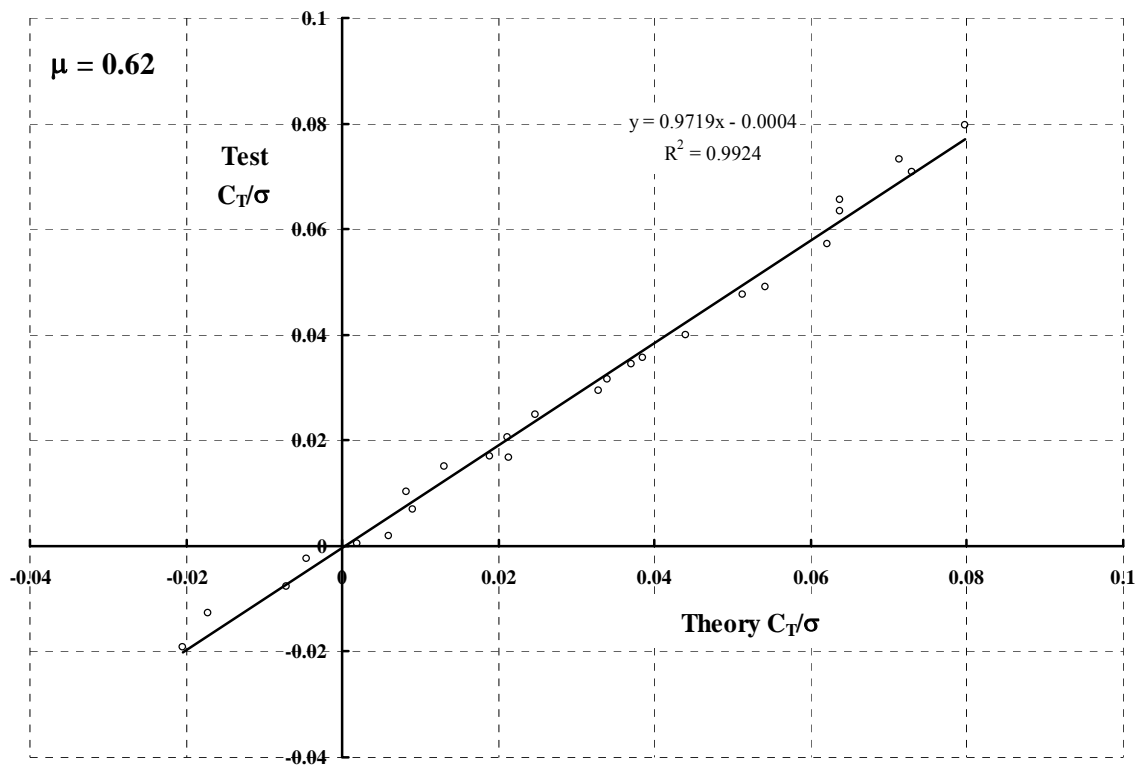


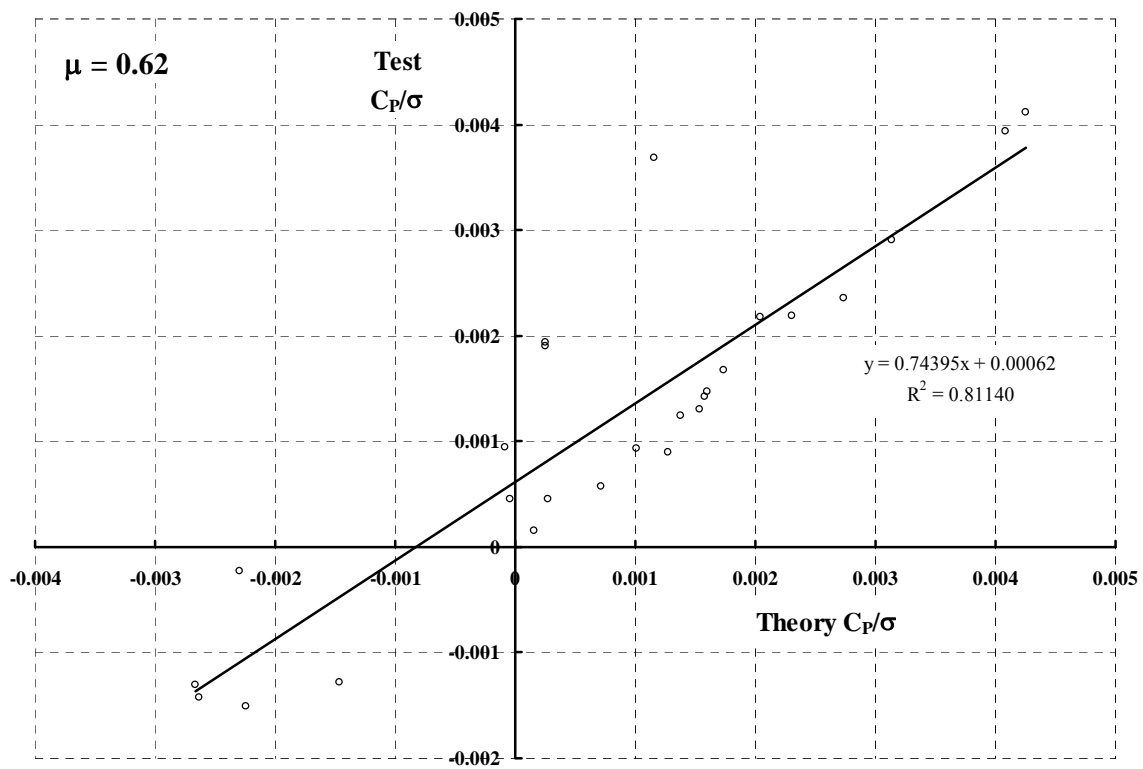
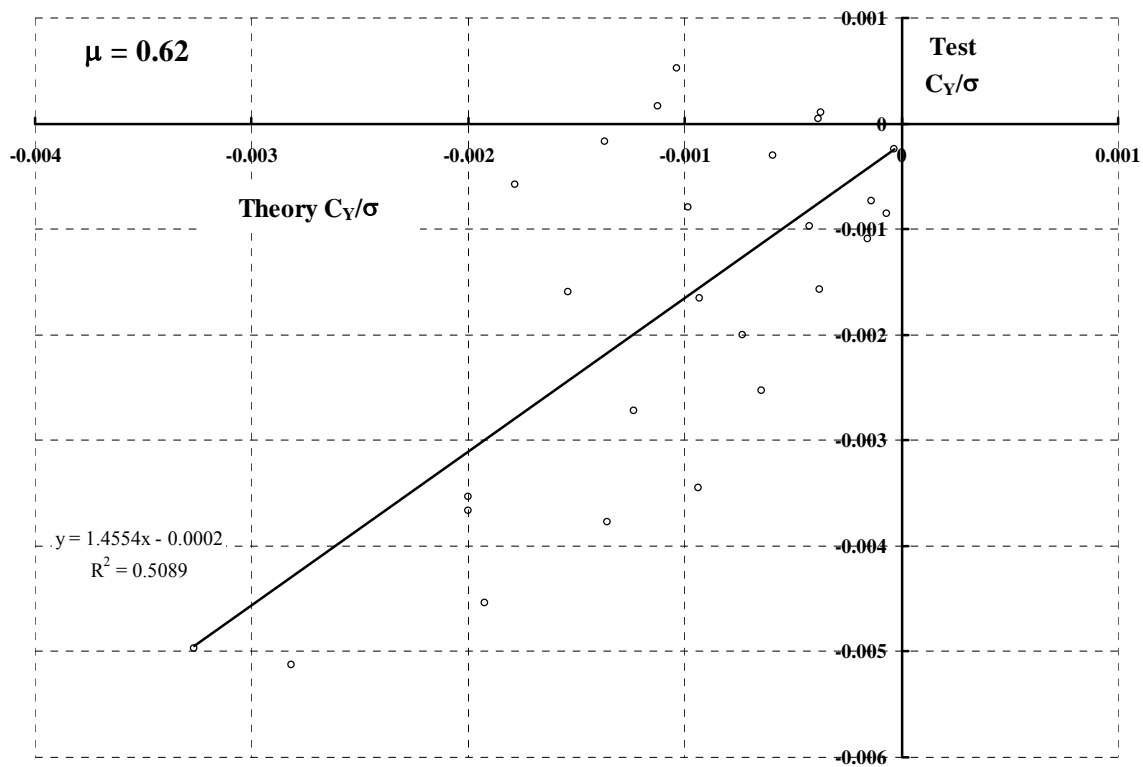


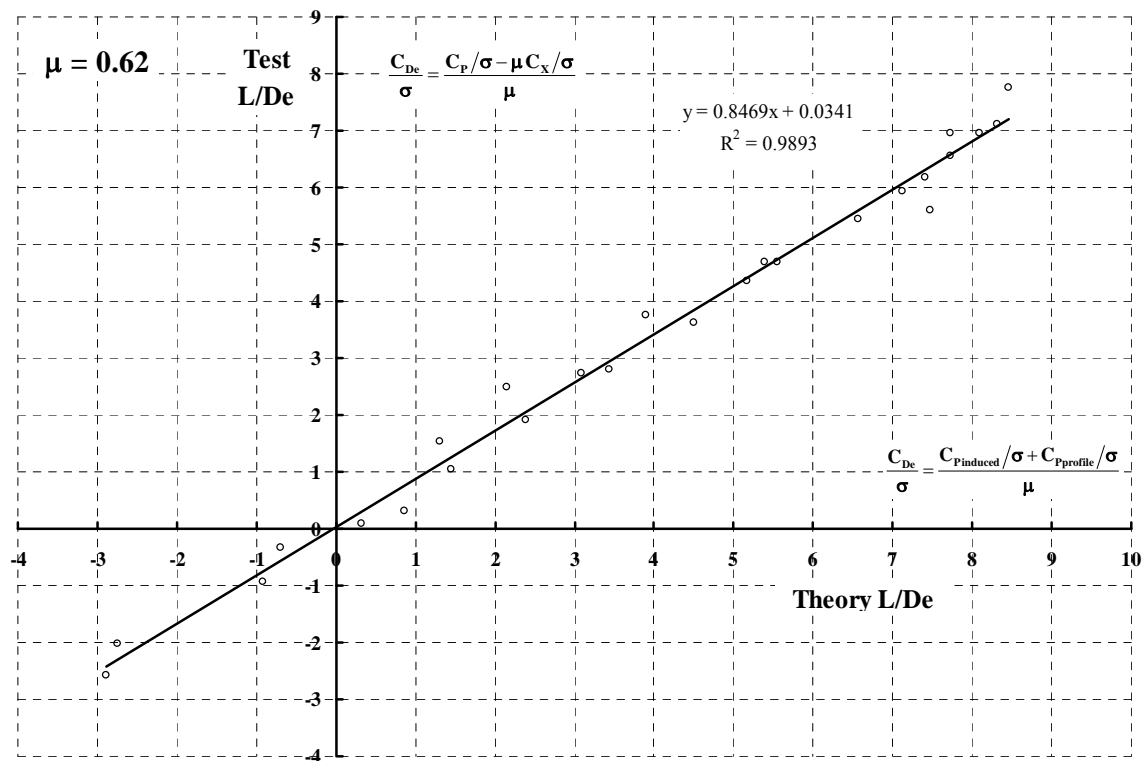
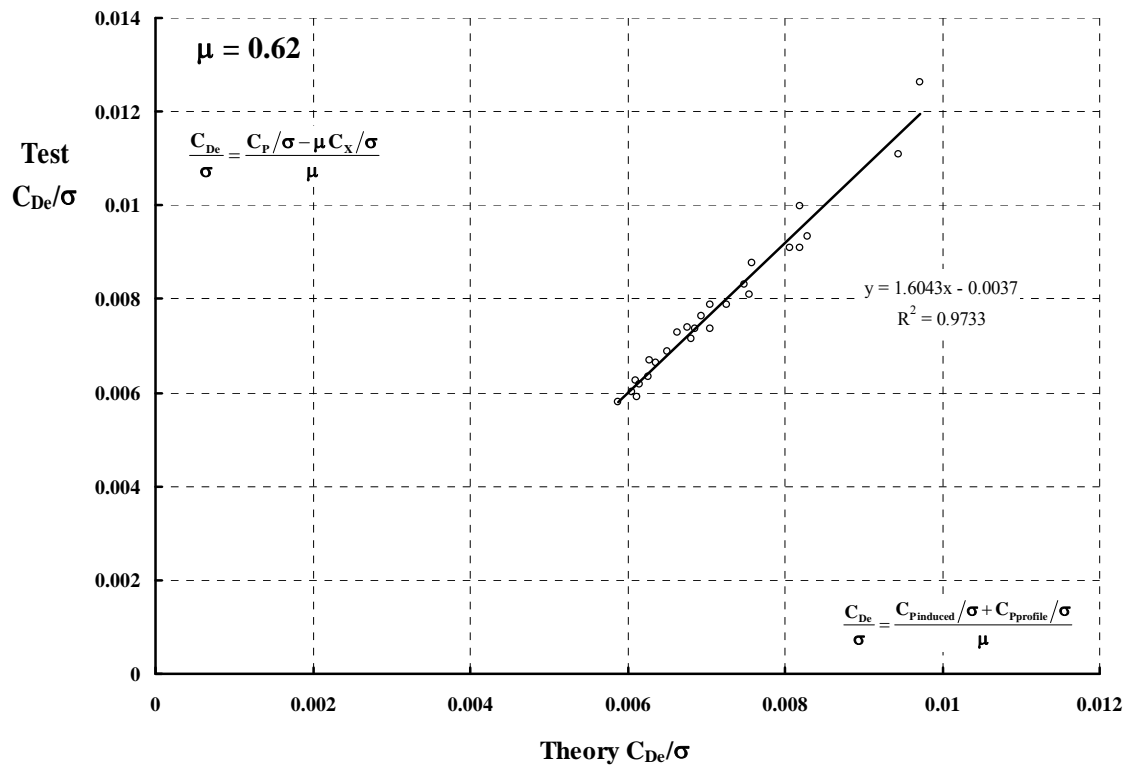


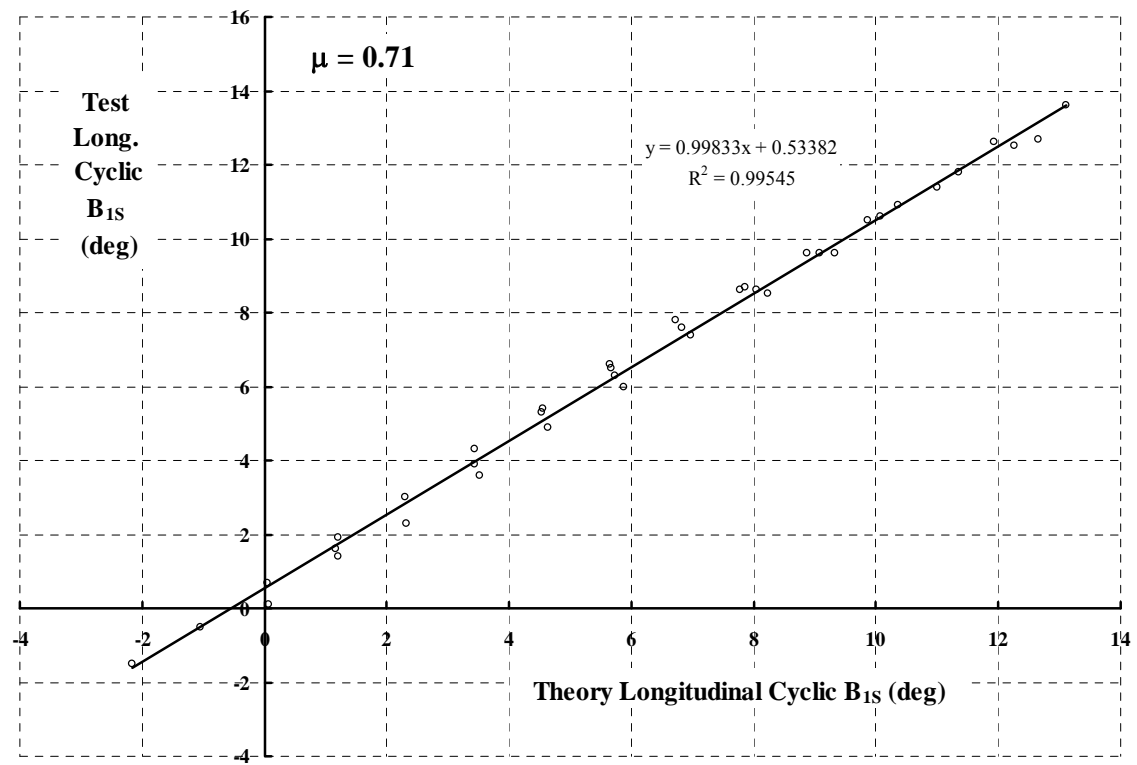
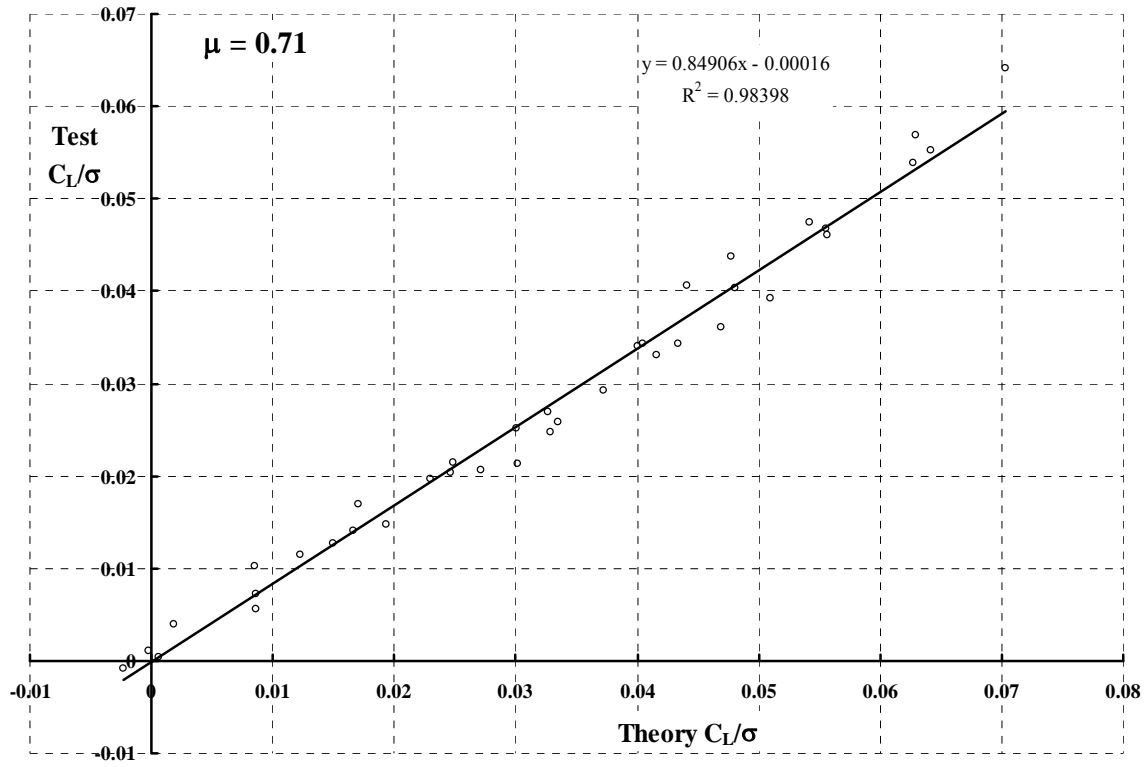


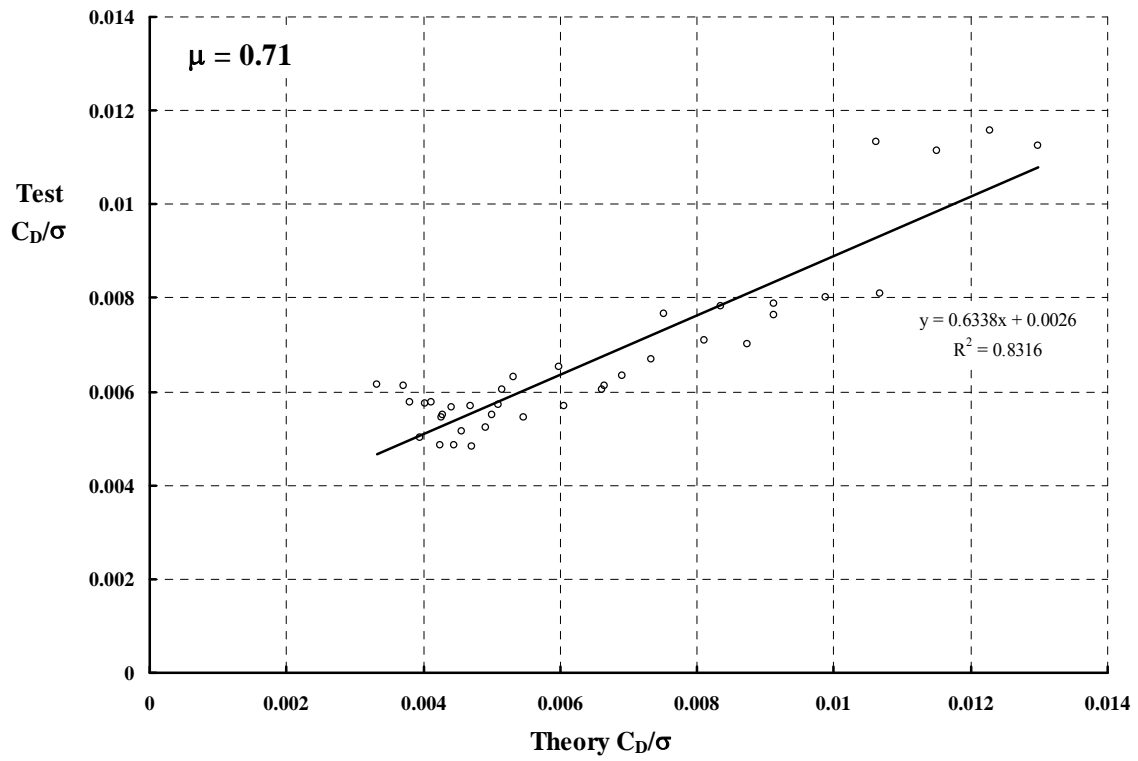
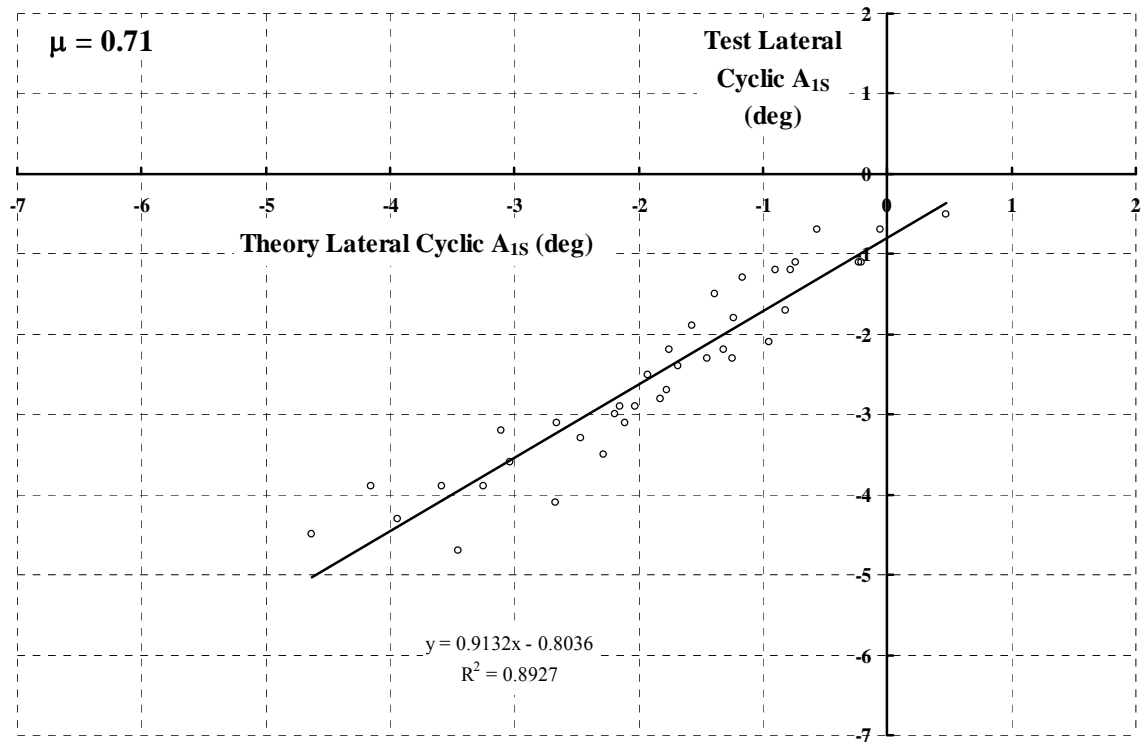


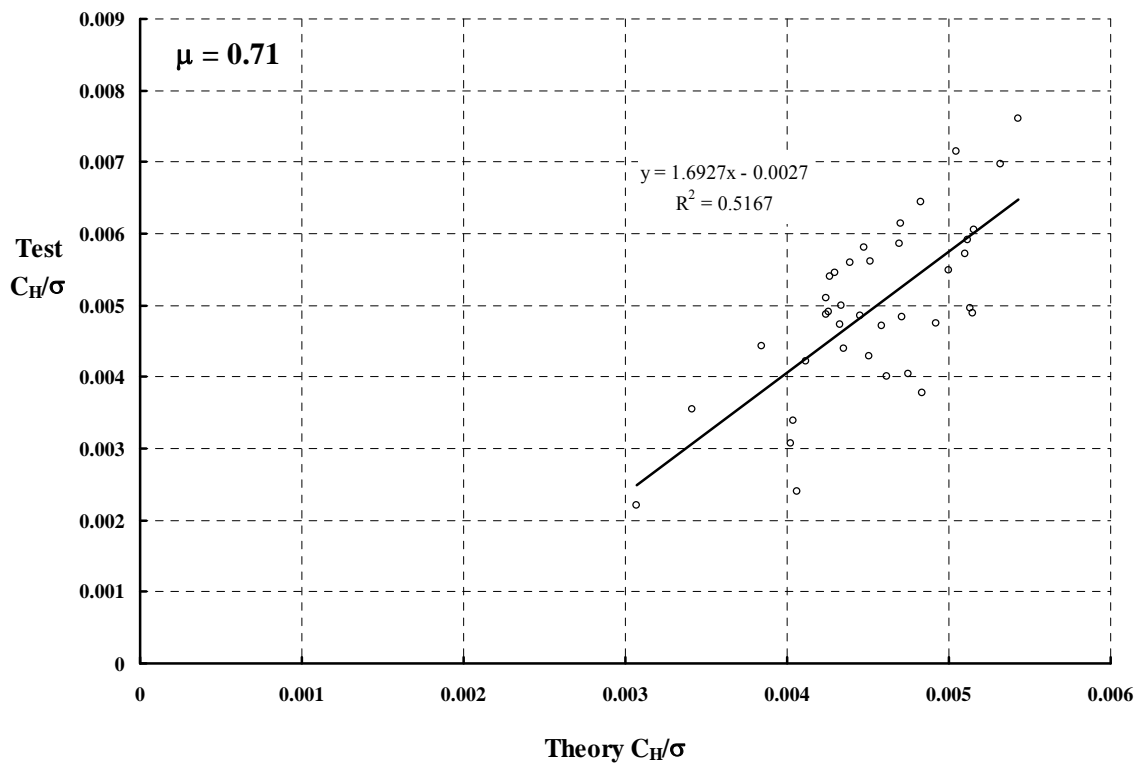
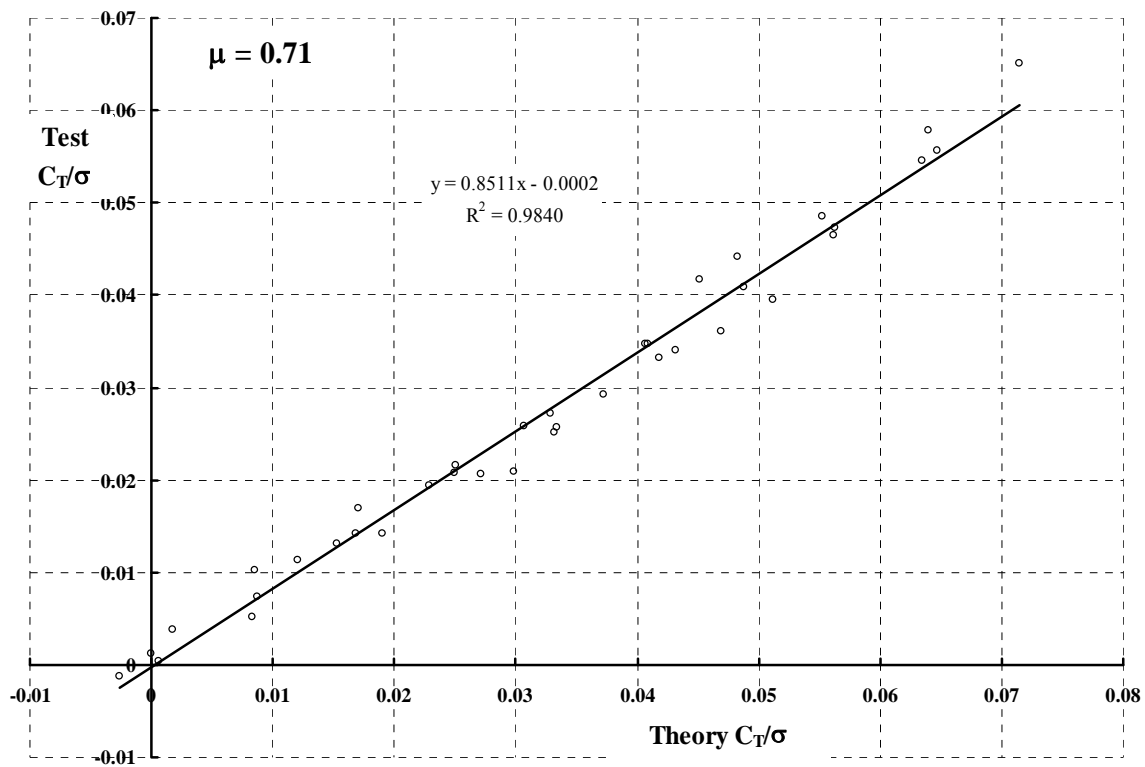


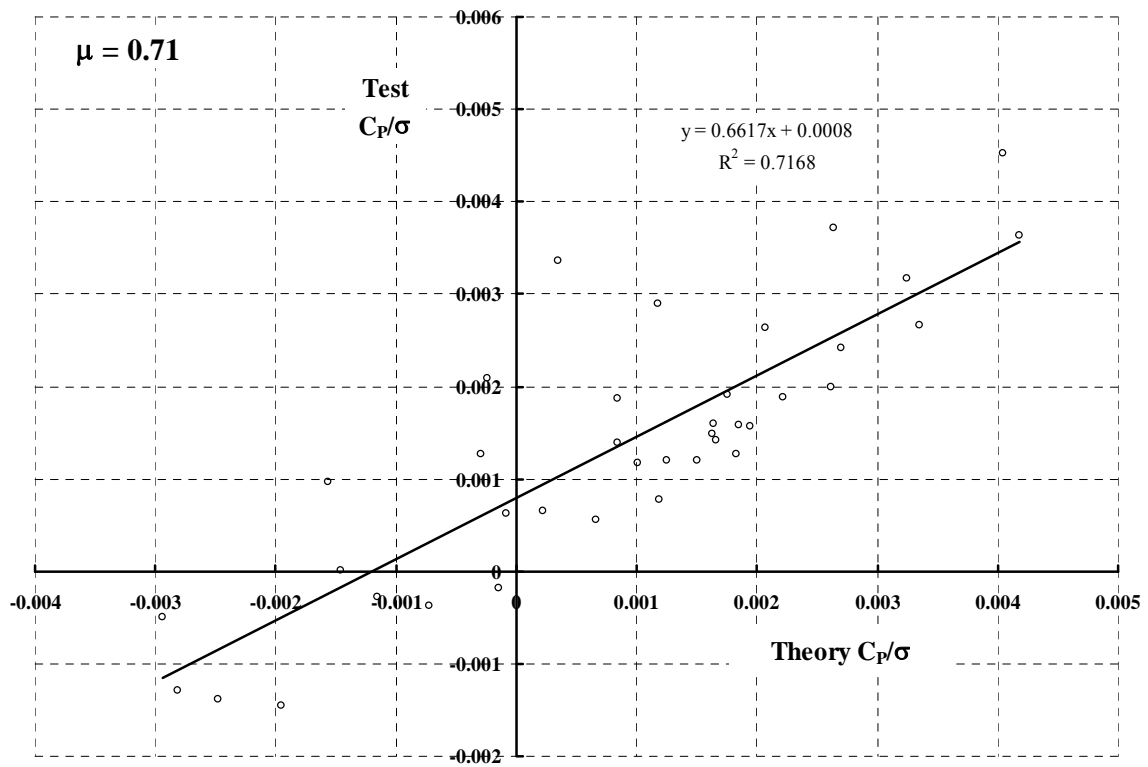
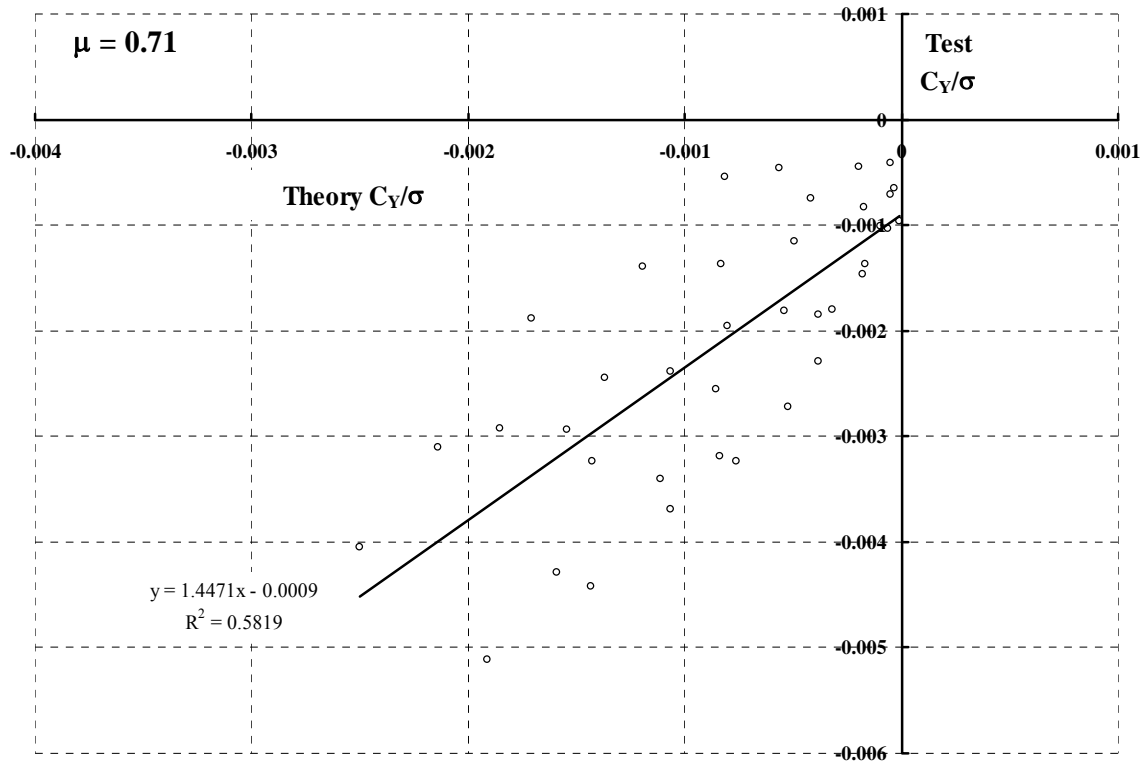


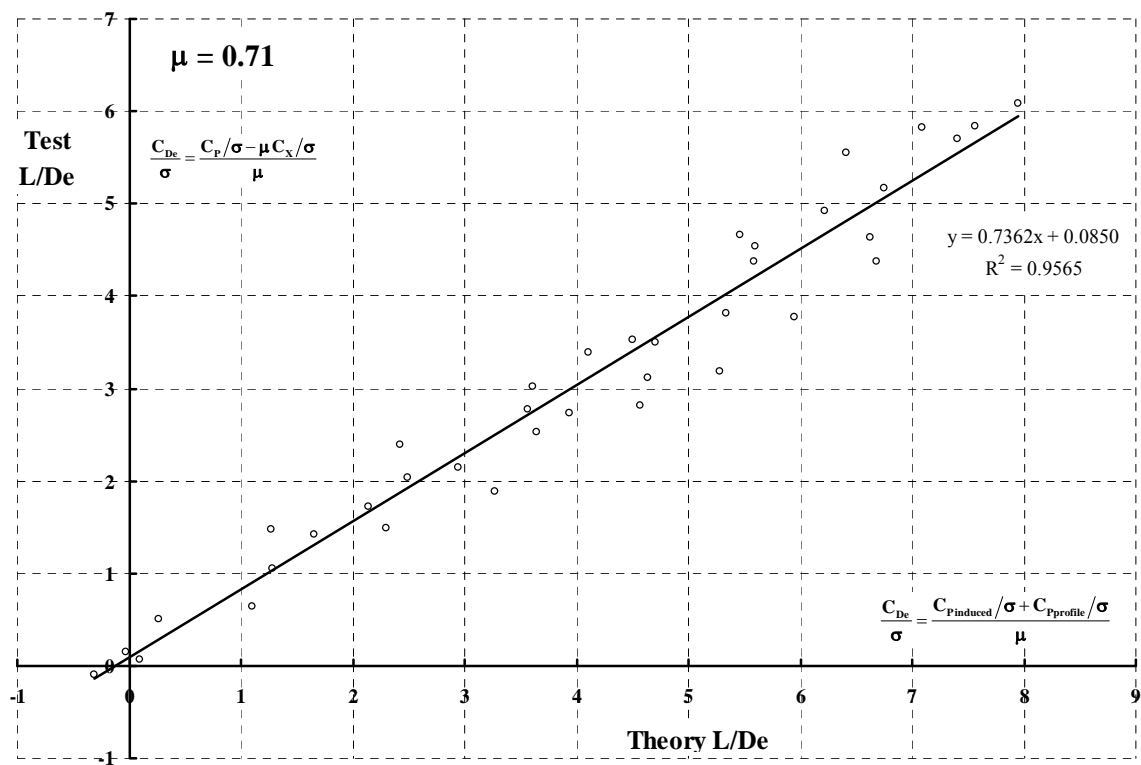
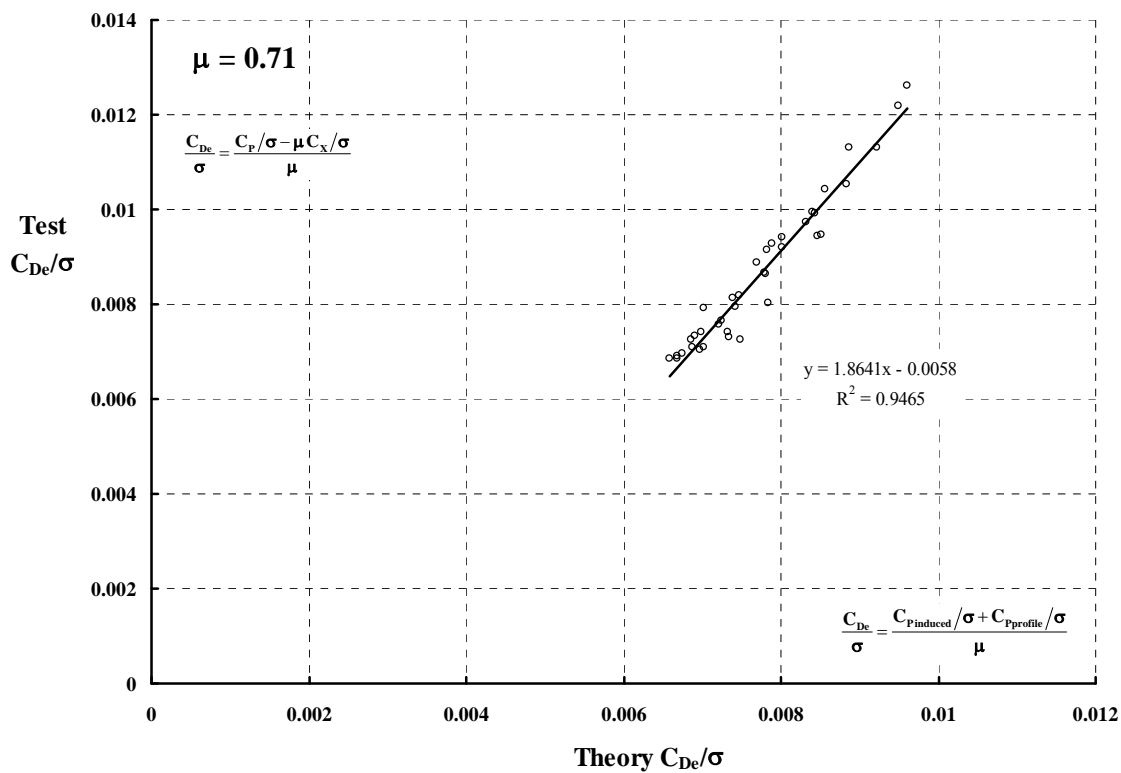


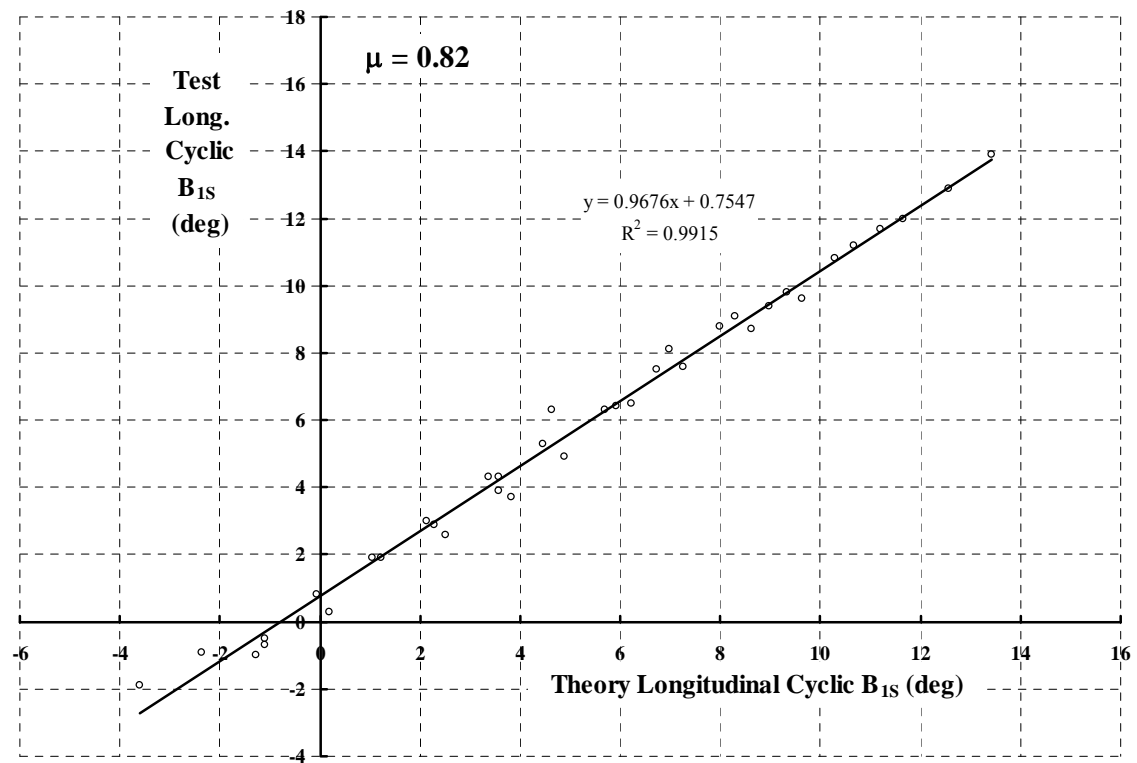
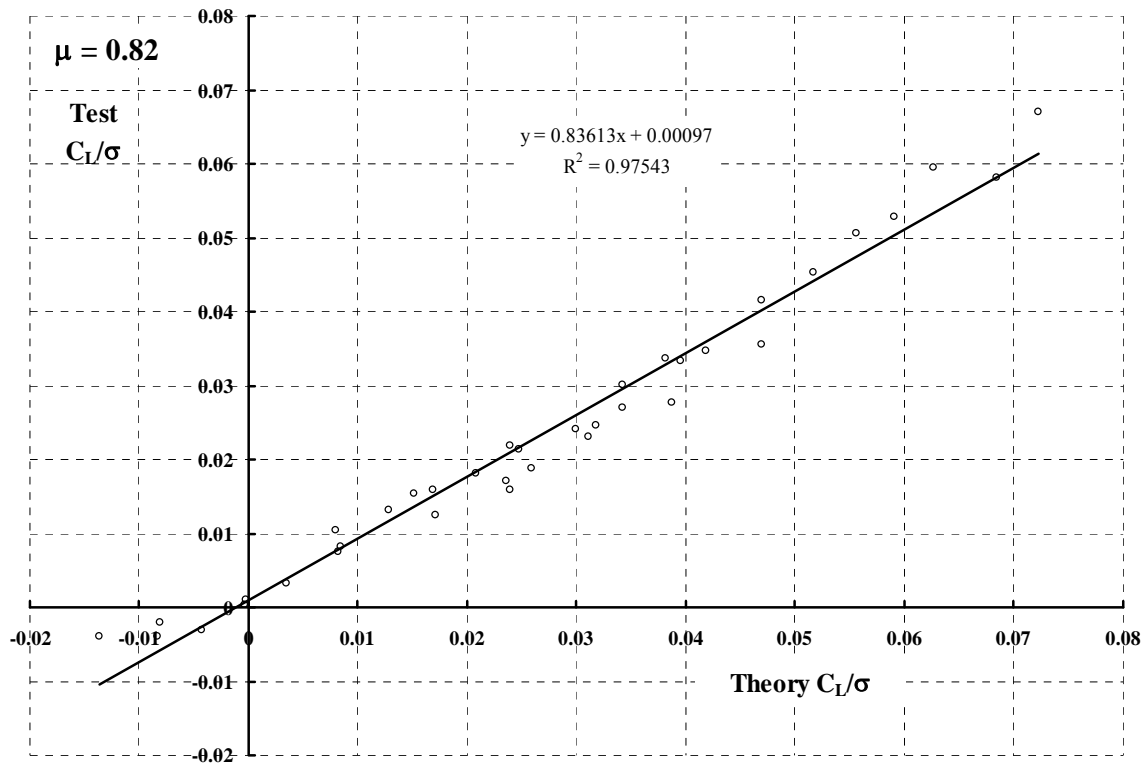


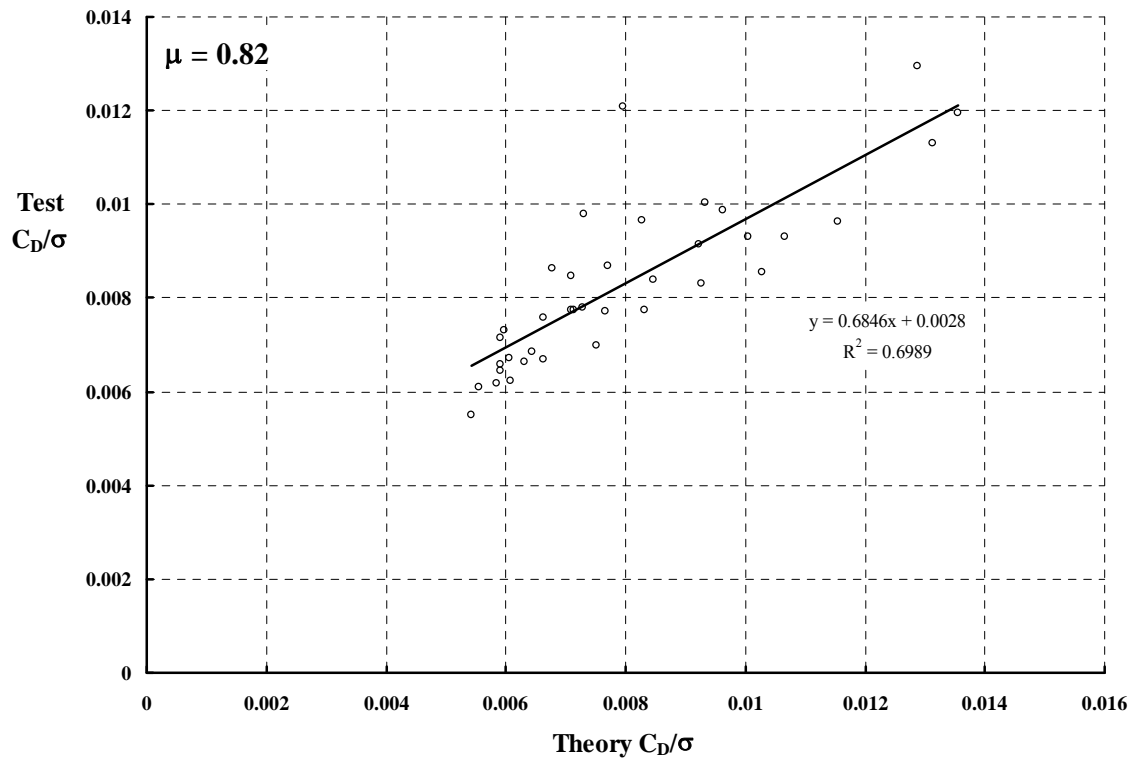
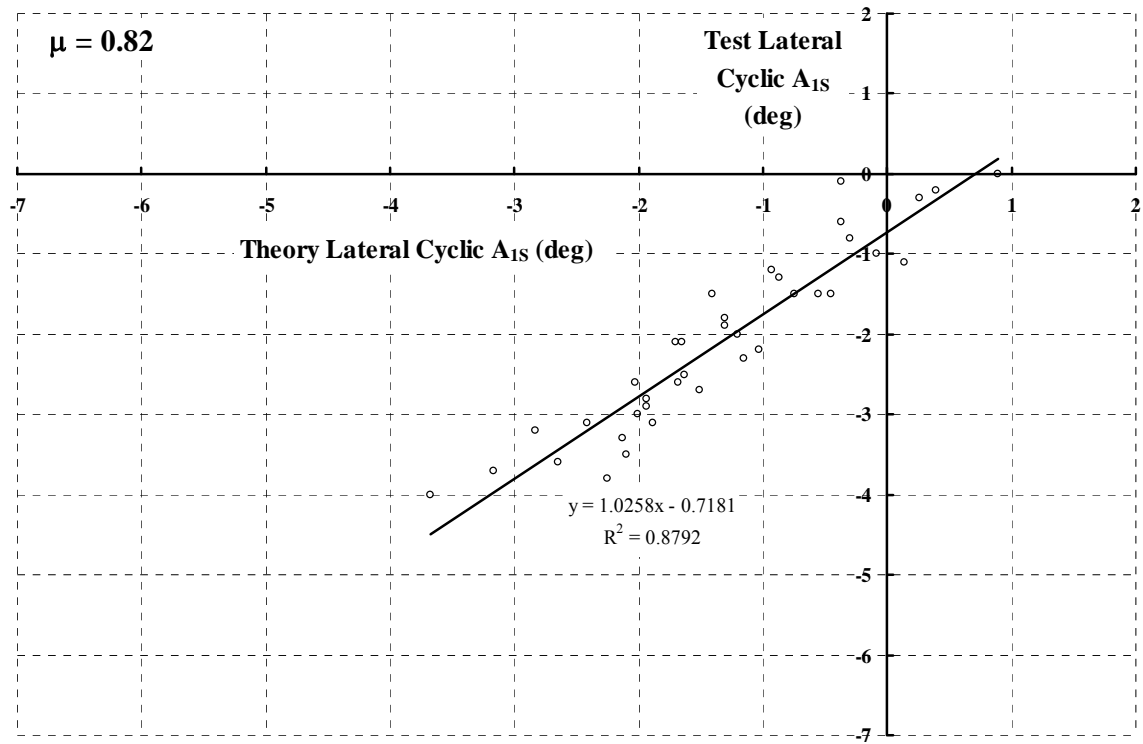


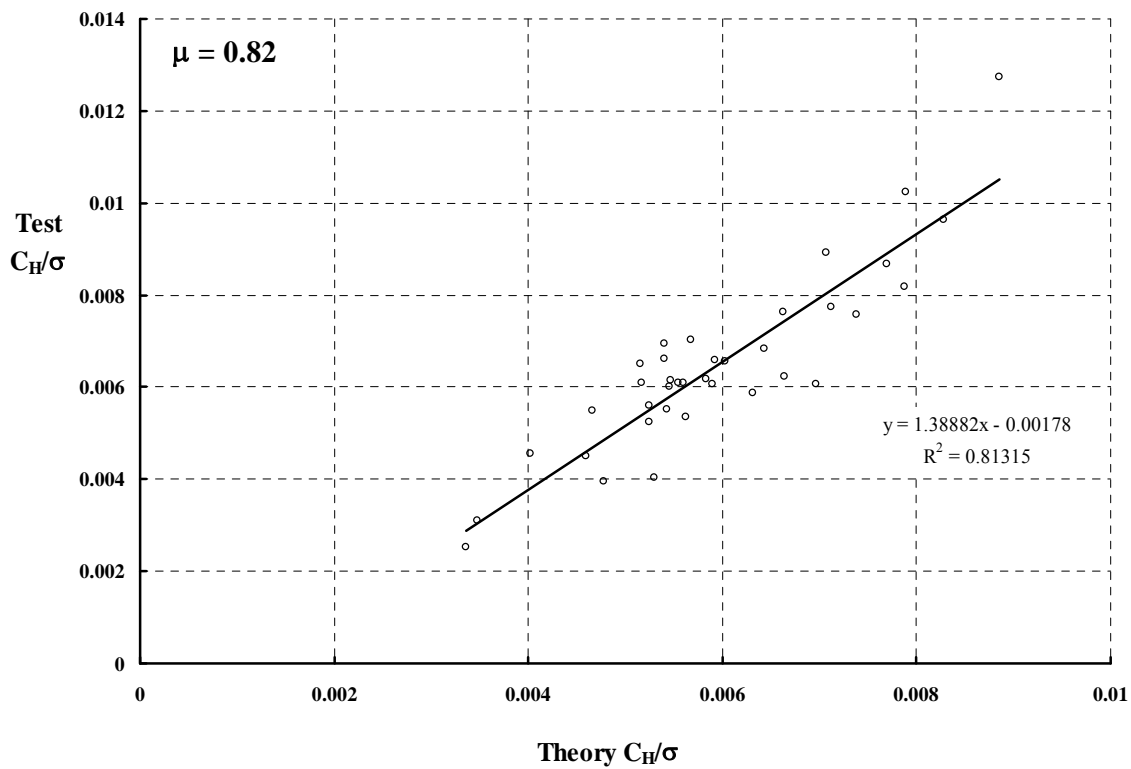
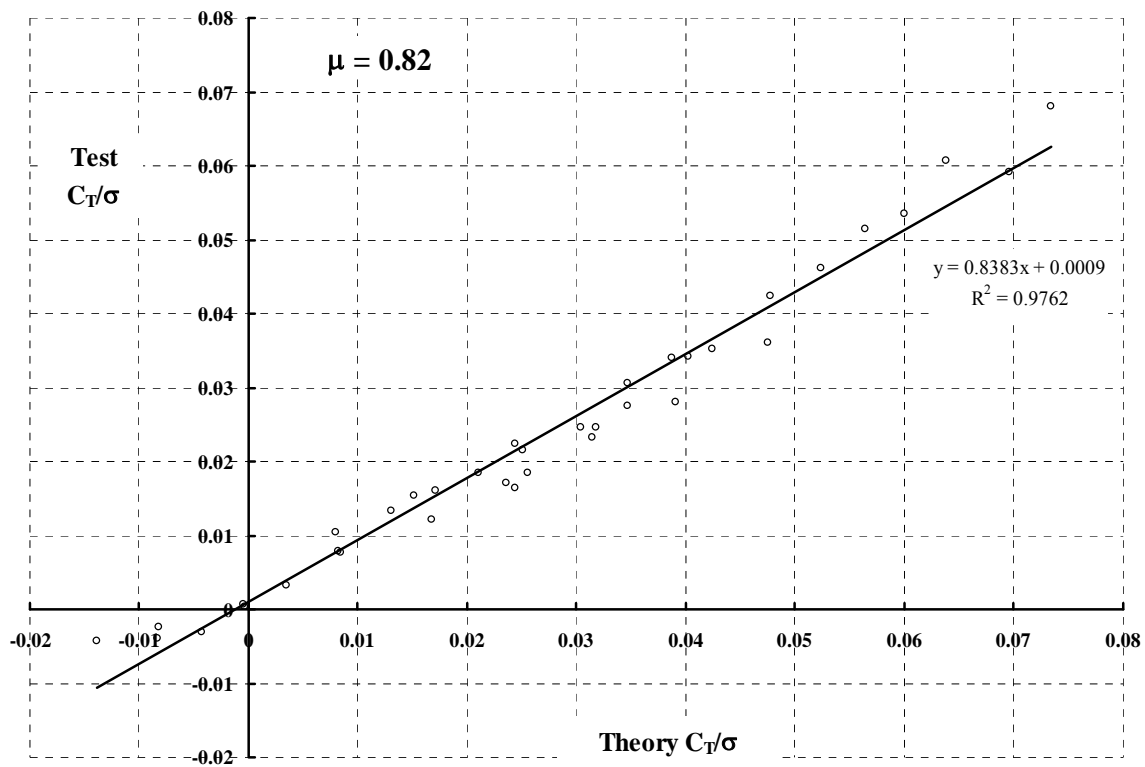


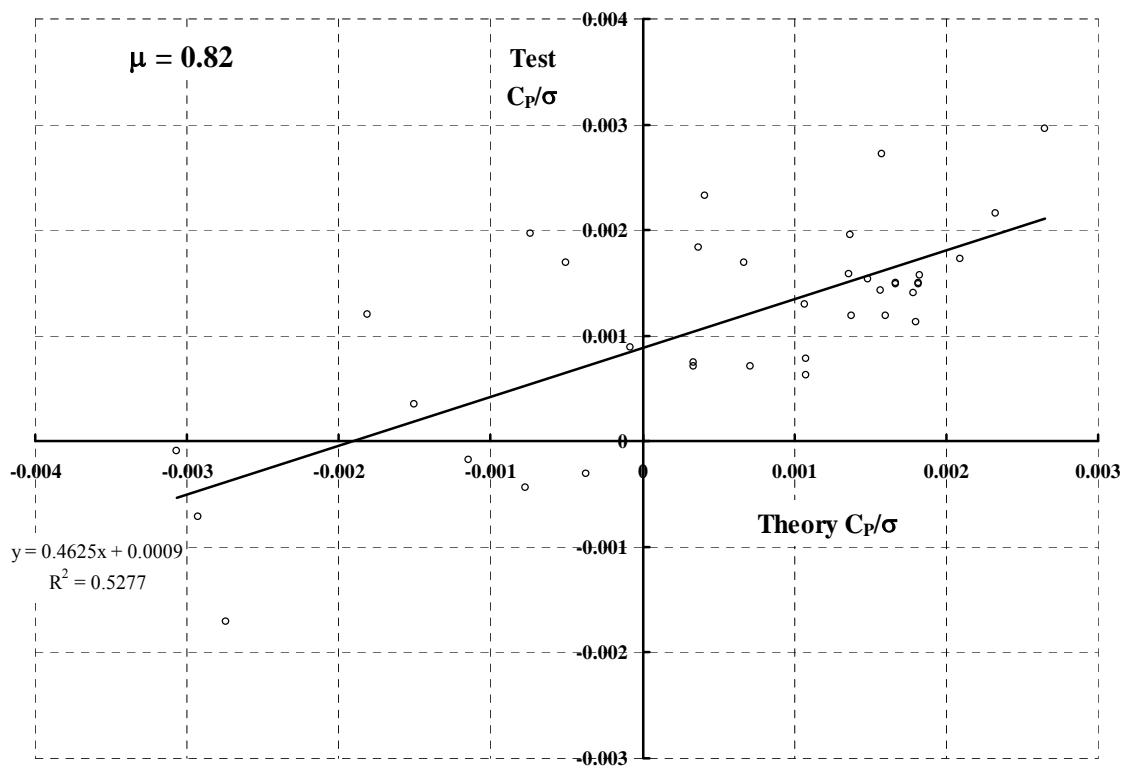
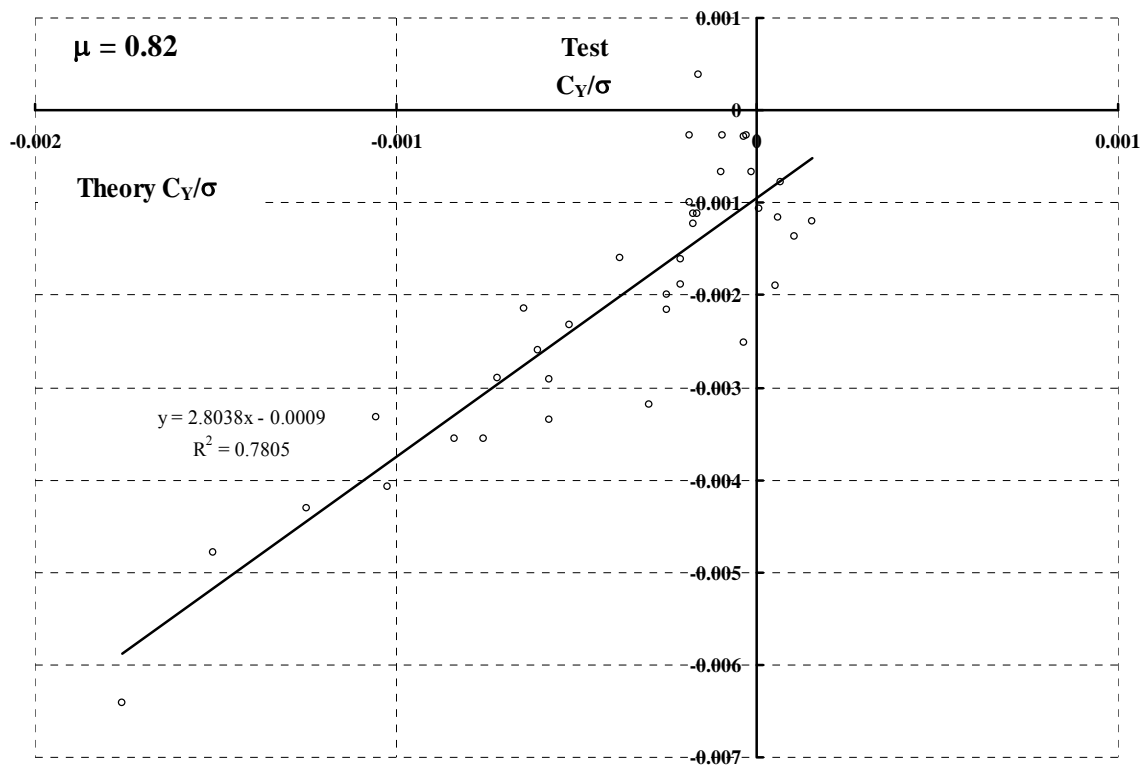


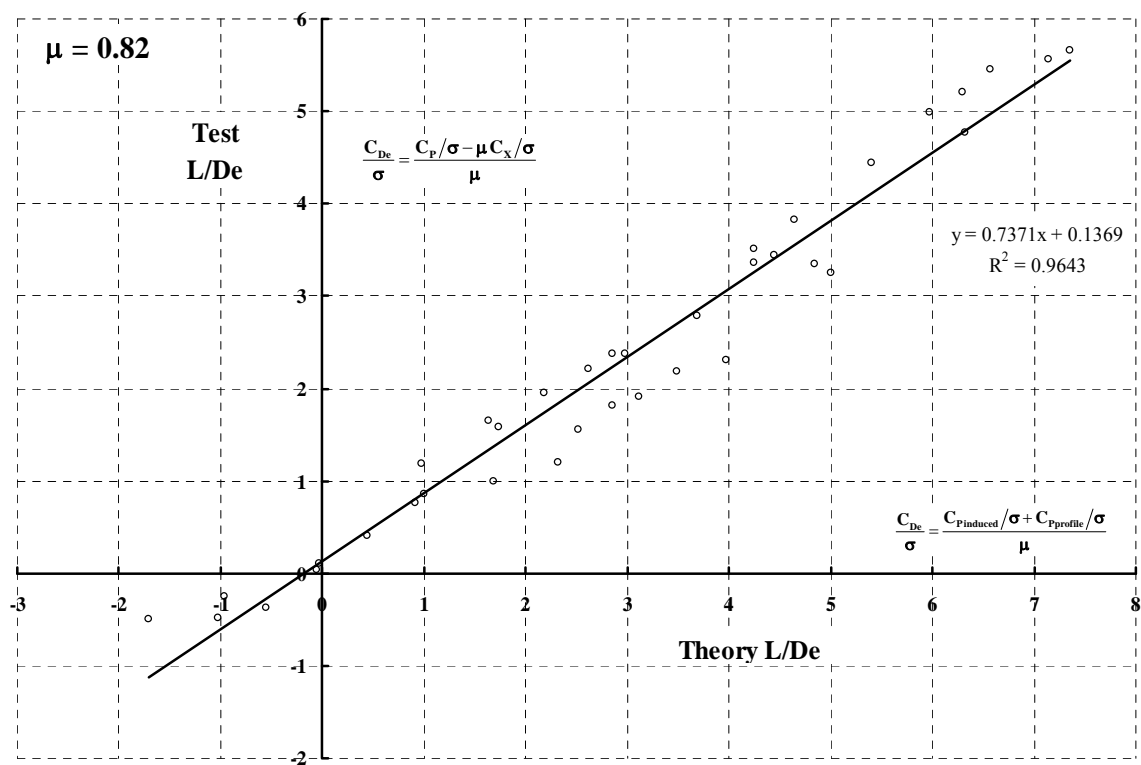
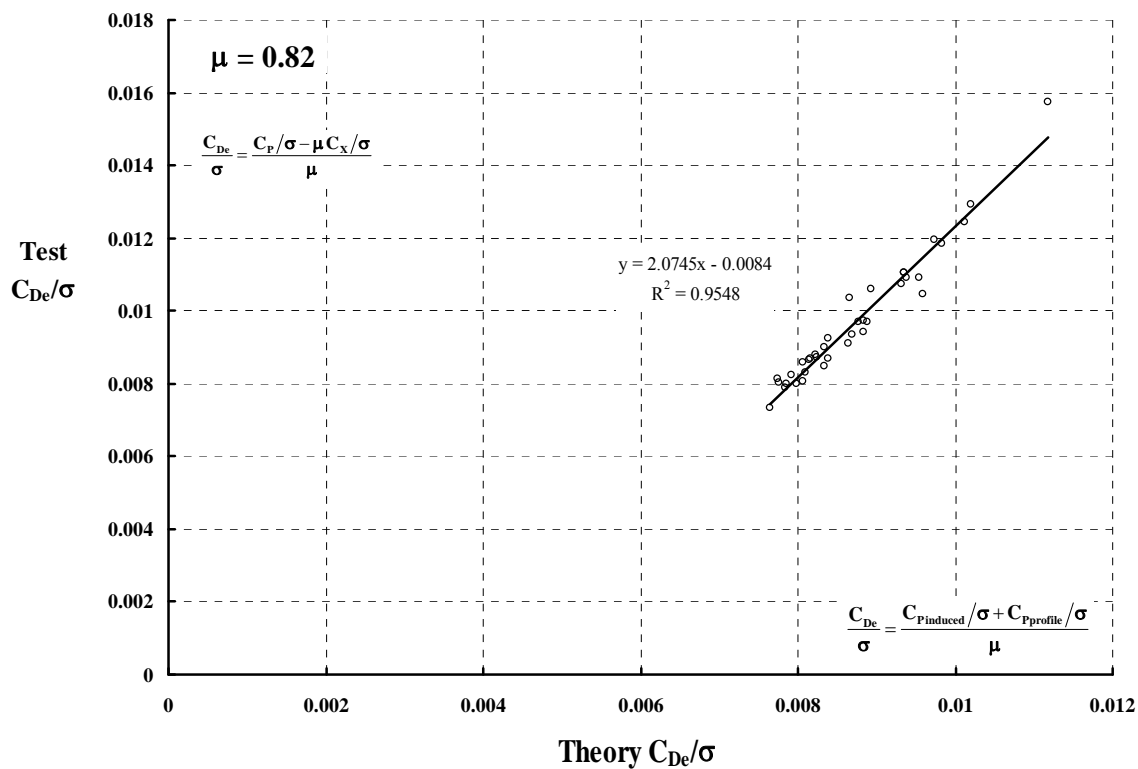


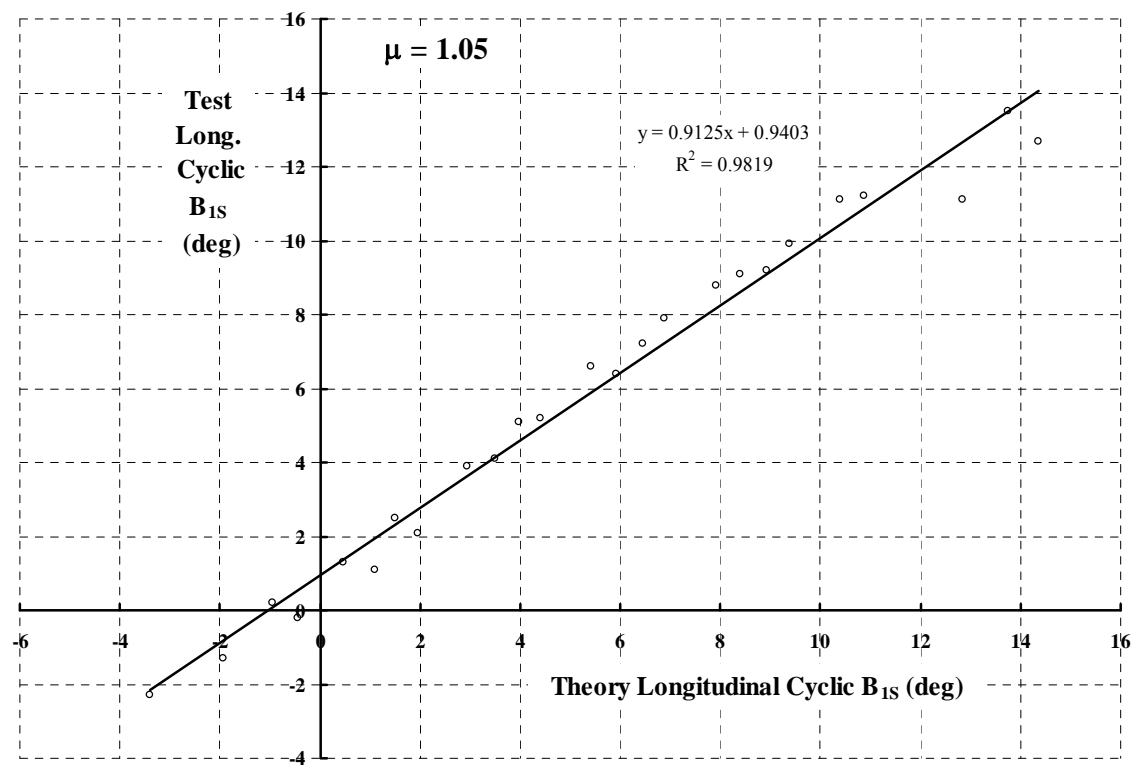
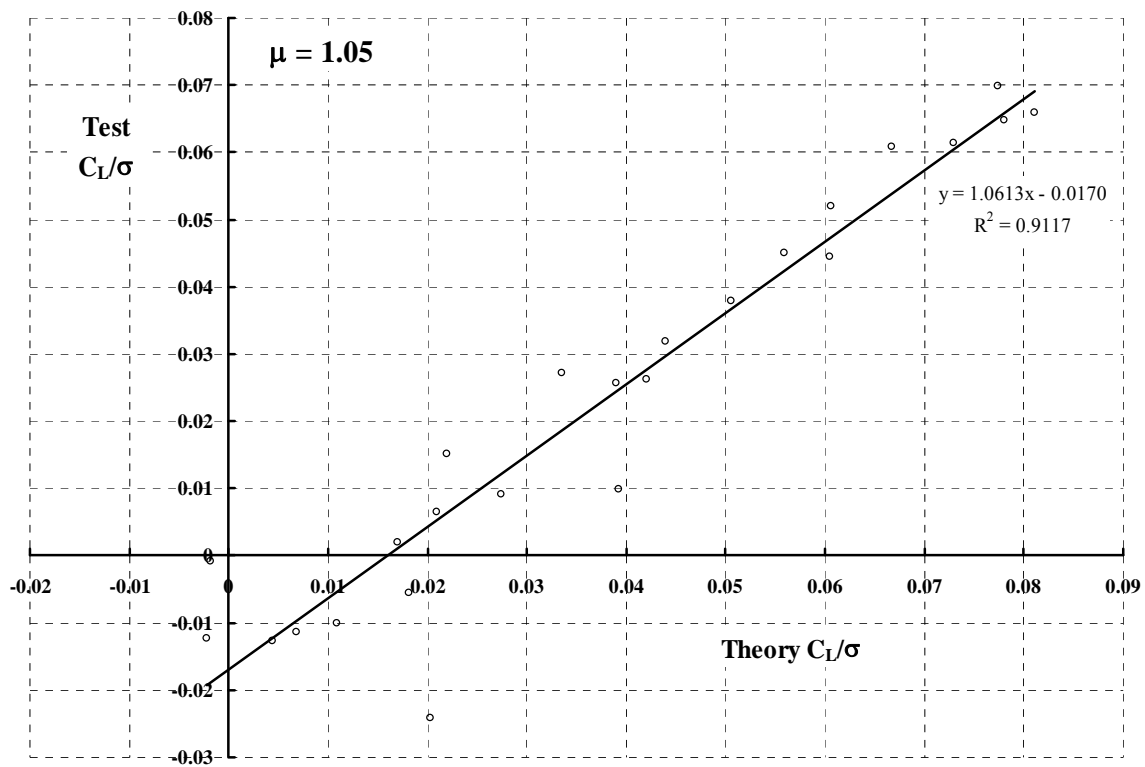


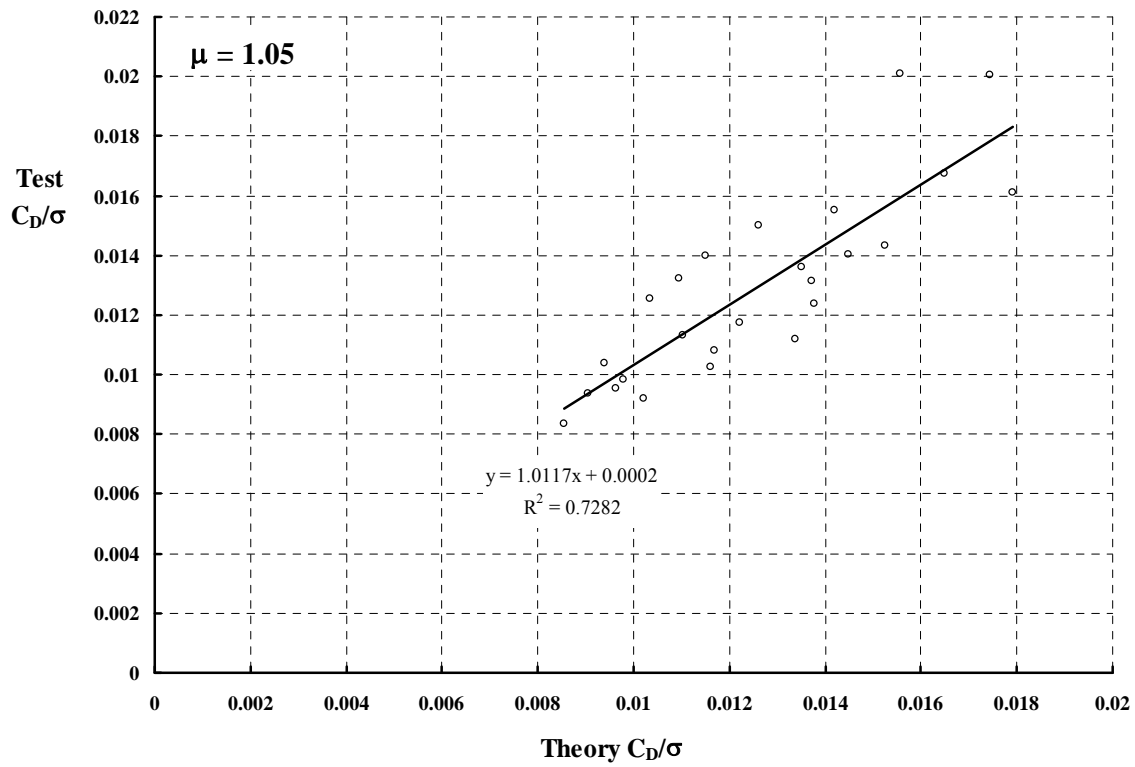
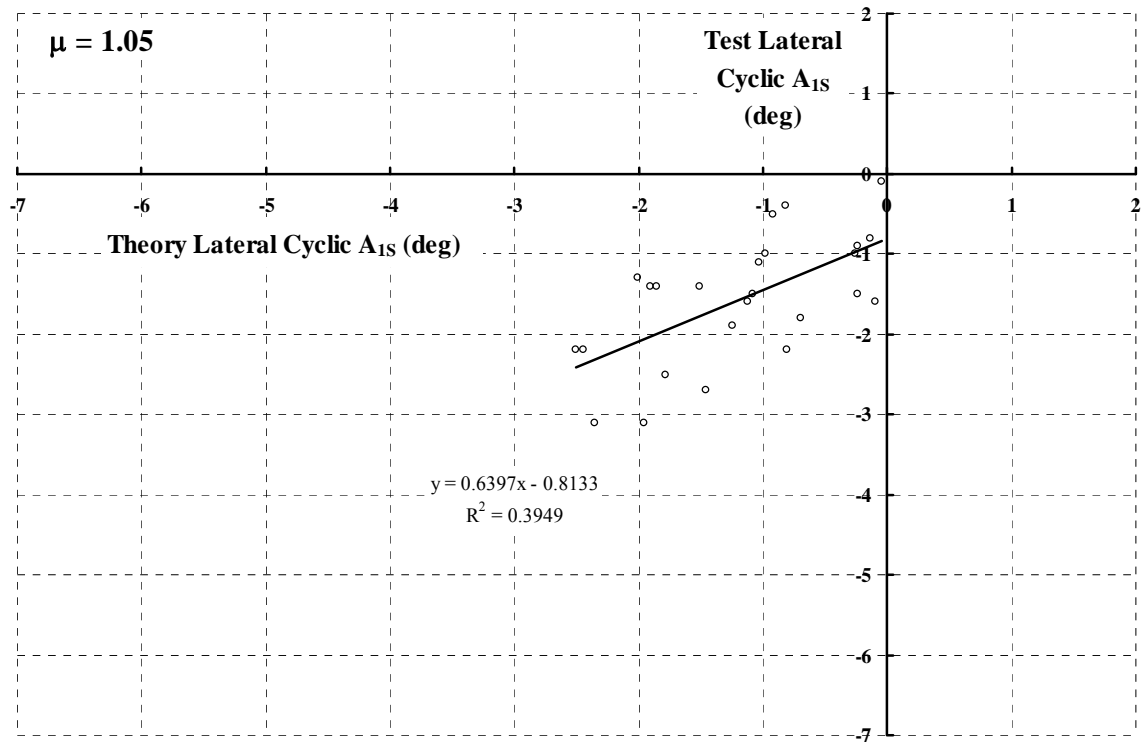


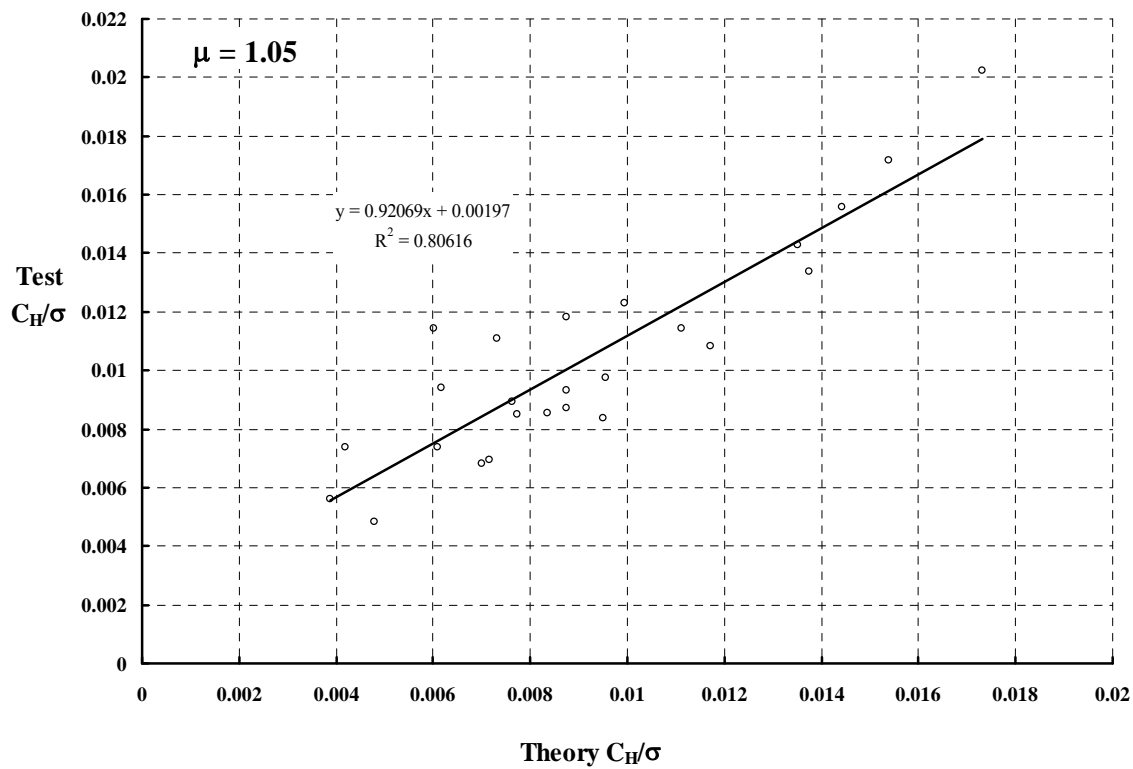
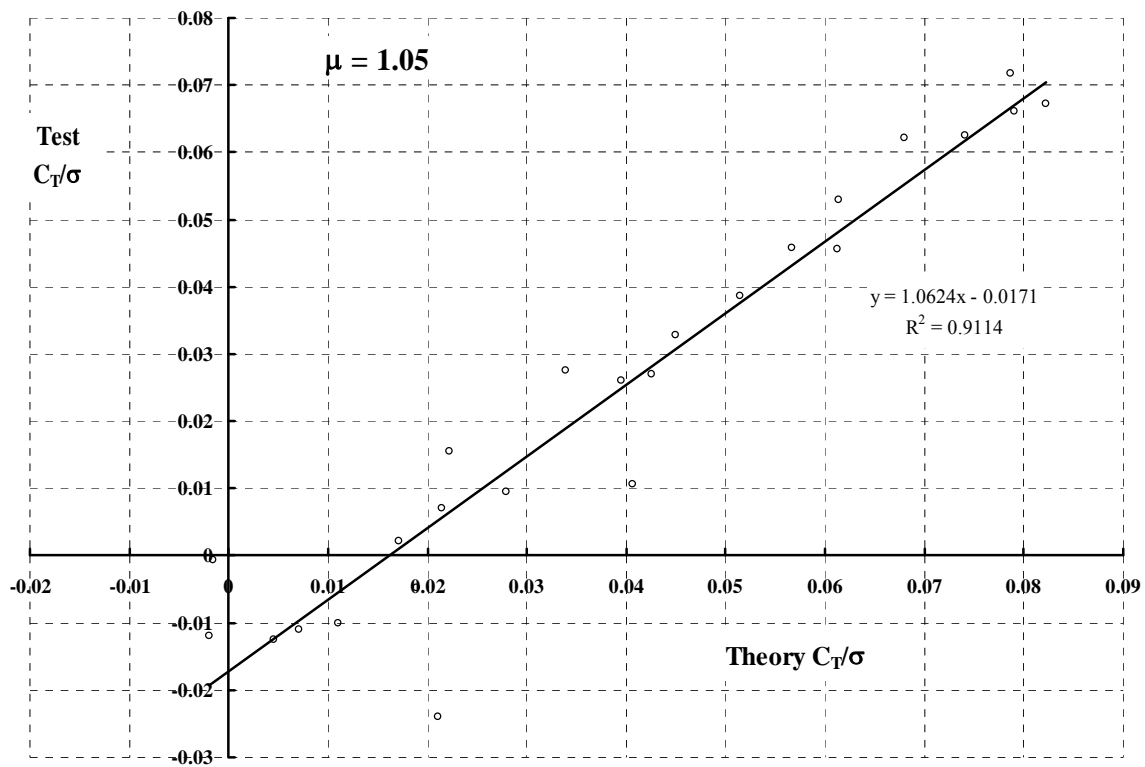


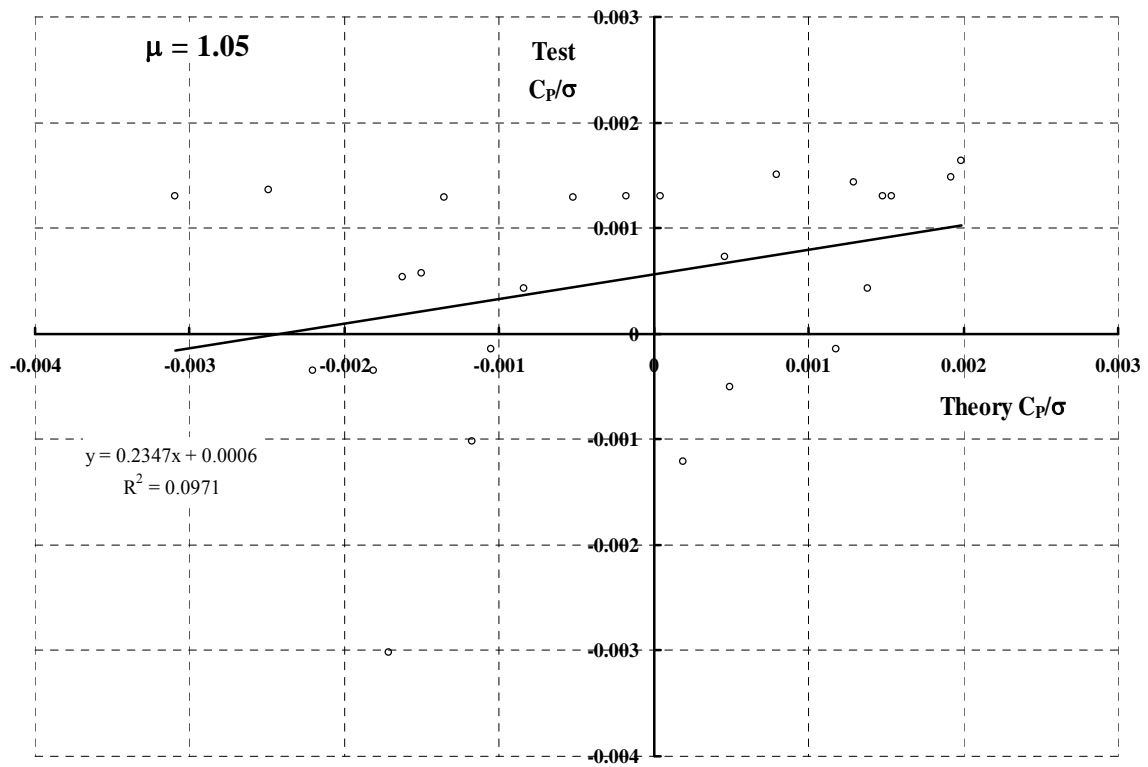
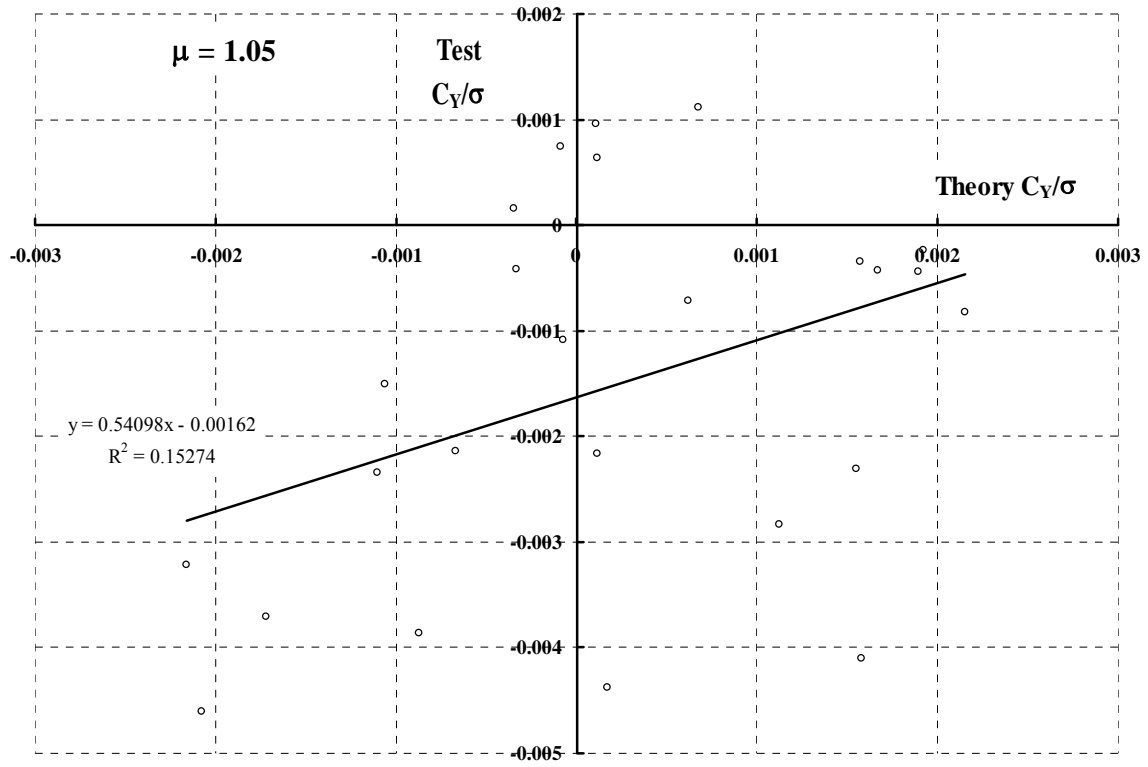


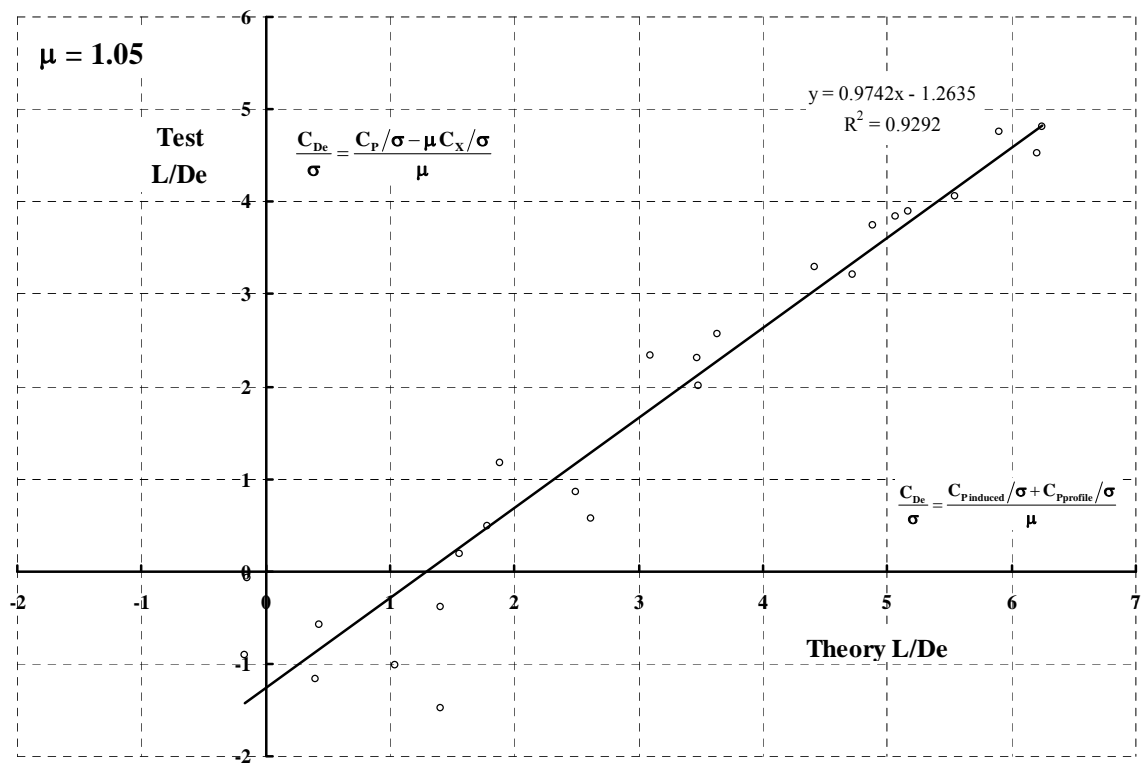
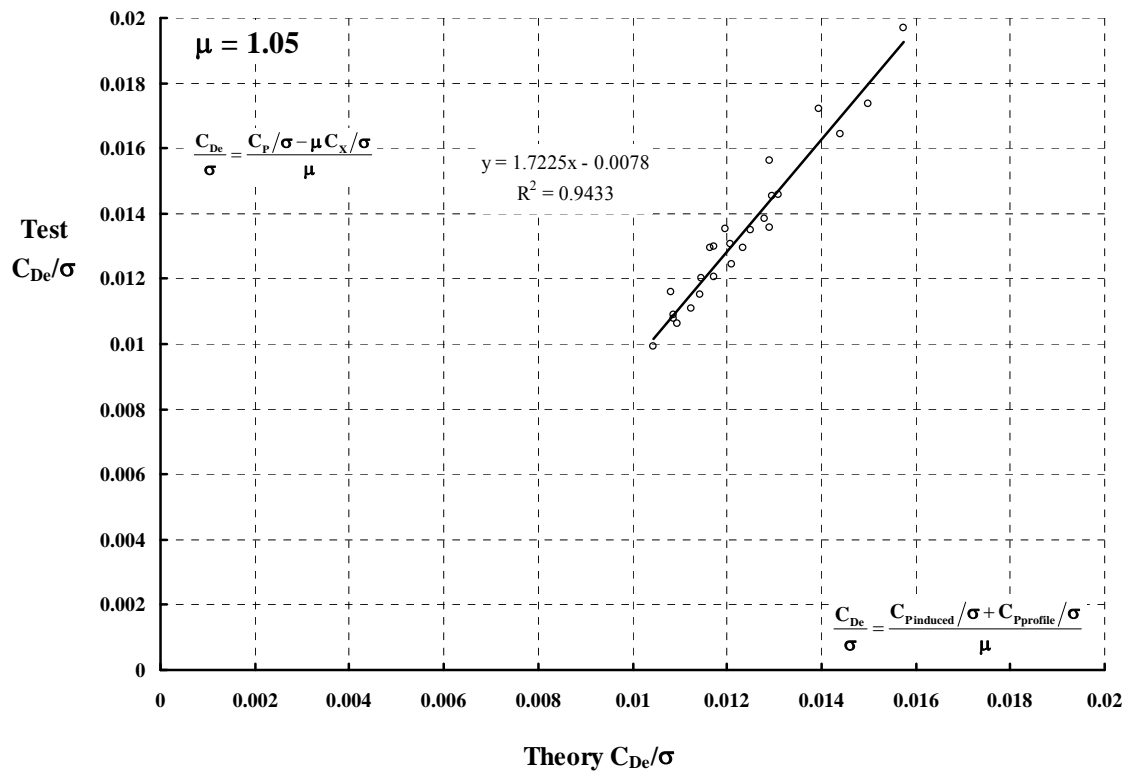












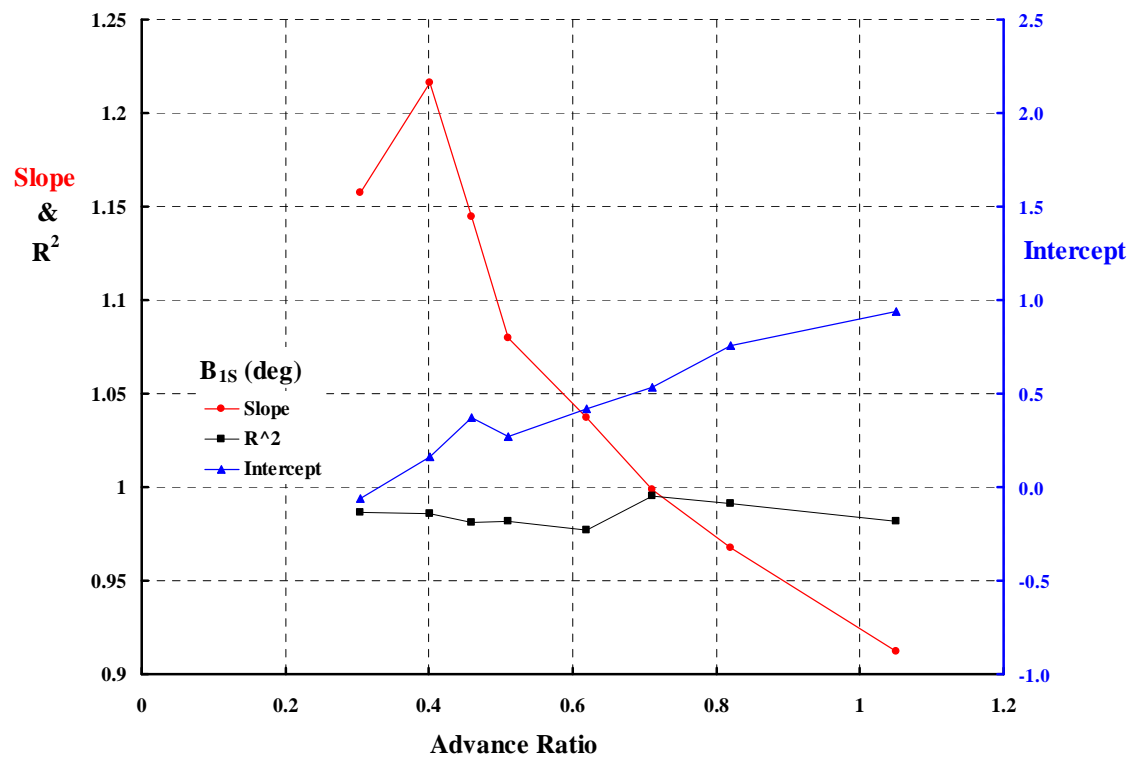
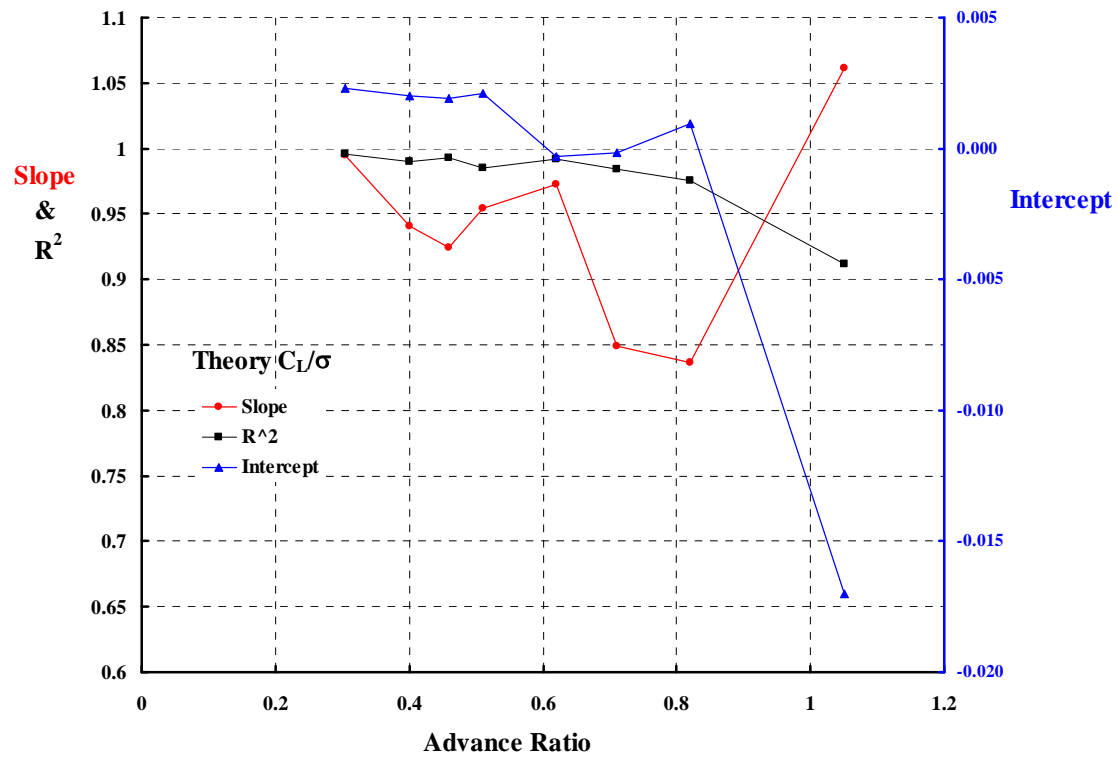
Longitudinal Cyclic				Lateral Cyclic		
Mu	SLOPE	Intercept	R ²	SLOPE	Intercept	R ²
0.305	1.1574	-0.0610	0.9866	1.0661	-0.4305	0.9369
0.401	1.2162	0.1646	0.9860	1.2639	-0.0916	0.9193
0.460	1.1443	0.3687	0.9811	1.2359	-0.1682	0.9438
0.510	1.0800	0.2731	0.9820	1.1075	-0.4114	0.9188
0.620	1.0371	0.4165	0.9772	1.1248	-0.6059	0.9103
0.710	0.9983	0.5338	0.9955	0.9132	-0.8036	0.8927
0.820	0.9676	0.7547	0.9915	1.0258	-0.7181	0.8792
1.050	0.9125	0.9403	0.9819	0.6397	-0.8133	0.3949

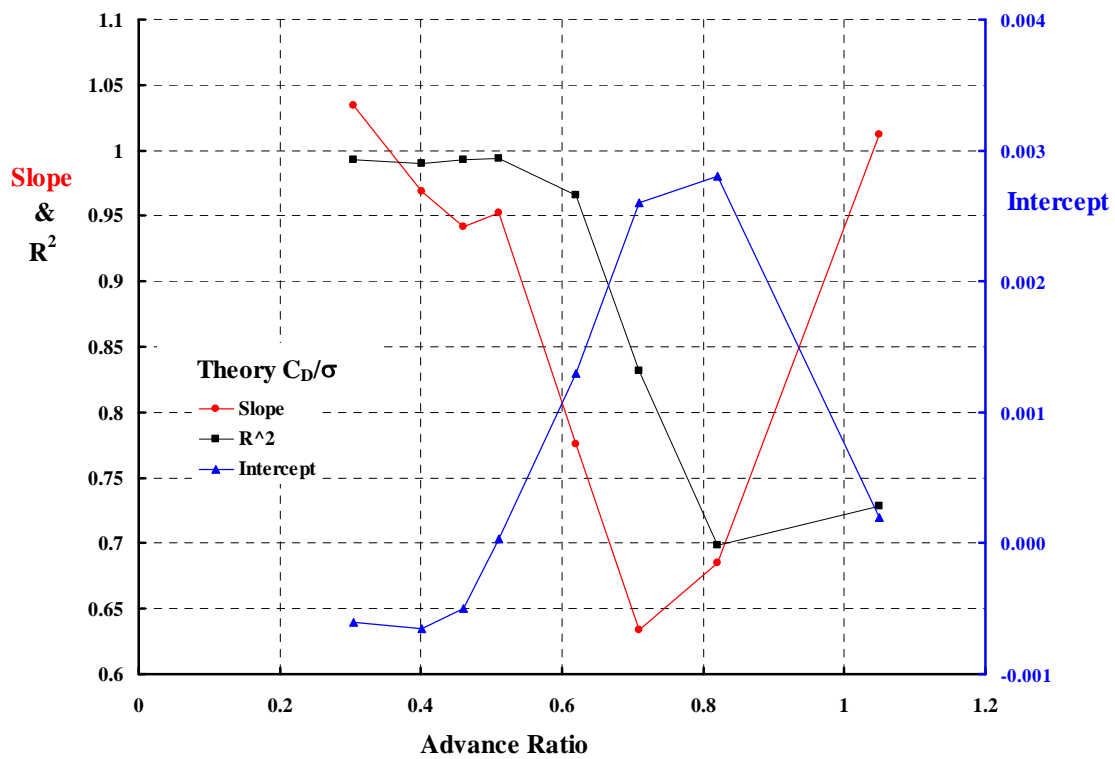
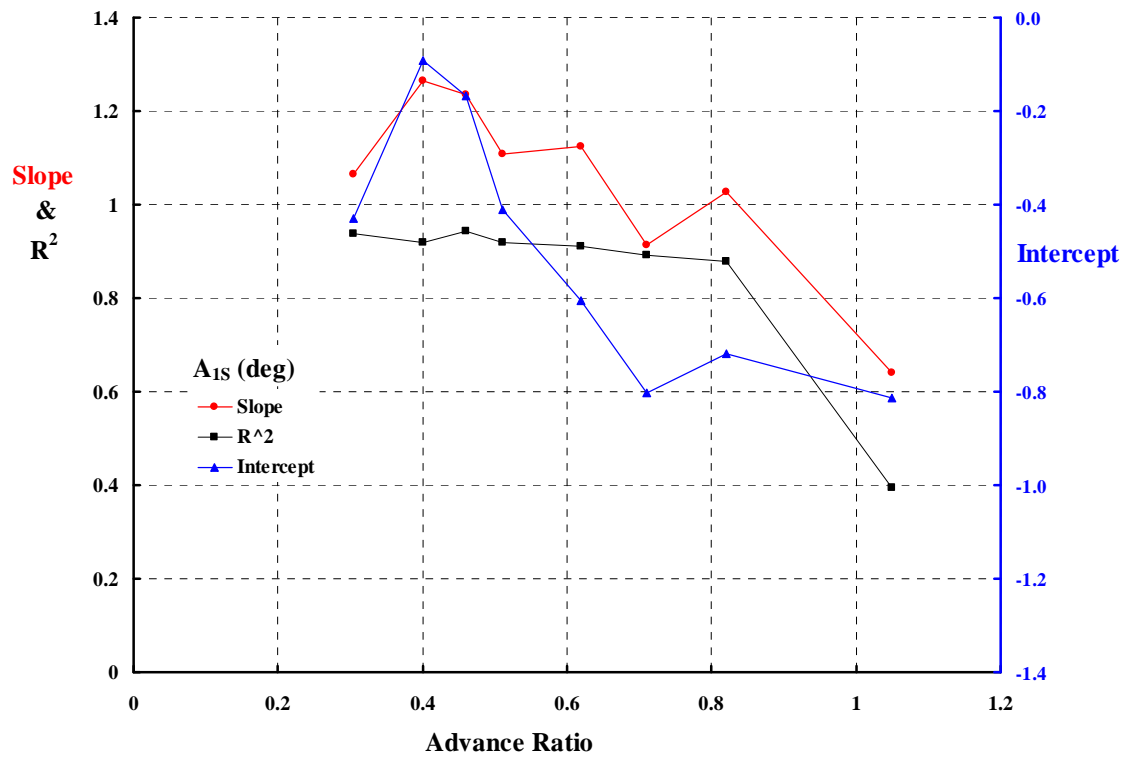
Lift Coefficient				Drag Coefficient		
Mu	SLOPE	Intercept	R ²	SLOPE	Intercept	R ²
0.305	0.9949	0.0023	0.9956	1.0341	-0.0006	0.9926
0.401	0.9411	0.0020	0.9903	0.9688	-0.0007	0.9899
0.460	0.9247	0.0019	0.9929	0.9415	-0.0005	0.9930
0.510	0.9539	0.0021	0.9856	0.9520	0.0000	0.9938
0.620	0.9726	-0.0003	0.9920	0.7754	0.0013	0.9655
0.710	0.8491	-0.0002	0.9840	0.6338	0.0026	0.8316
0.820	0.8361	0.0010	0.9754	0.6846	0.0028	0.6989
1.050	1.0613	-0.0170	0.9117	1.0117	0.0002	0.7282

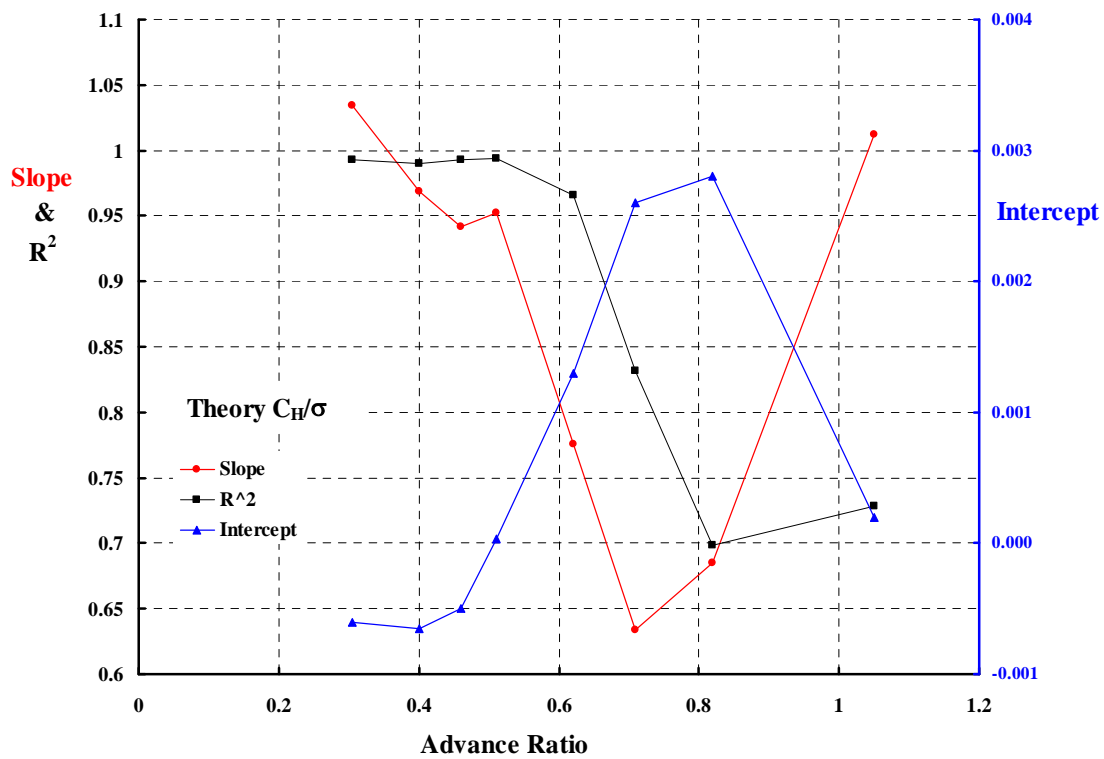
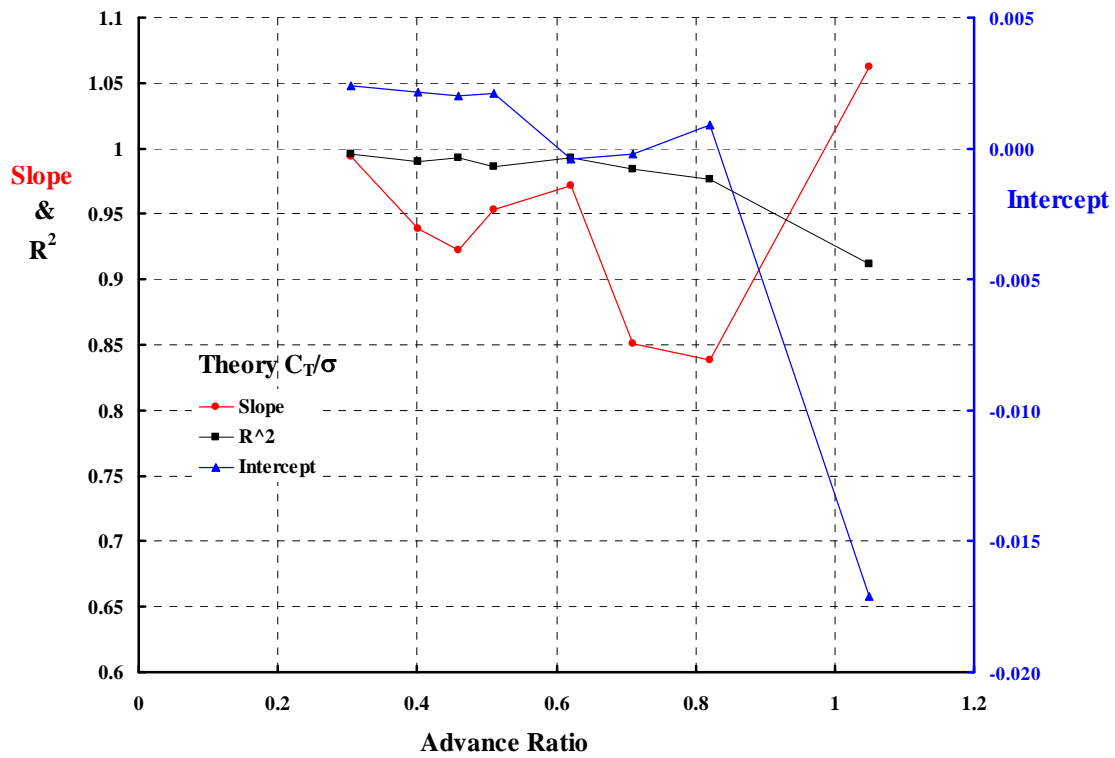
Thrust Coefficient				H-Force Coefficient		
Mu	SLOPE	Intercept	R ²	SLOPE	Intercept	R ²
0.305	0.9938	0.0024	0.9955	1.2700	-0.0005	0.9176
0.401	0.9389	0.0021	0.9902	1.6384	-0.0014	0.9467
0.460	0.9225	0.0020	0.9929	1.4762	-0.0013	0.9177
0.510	0.9530	0.0021	0.9862	1.6202	-0.0013	0.9096
0.620	0.9719	-0.0004	0.9924	2.4643	-0.0049	0.7027
0.710	0.8511	-0.0002	0.9840	1.6927	-0.0027	0.5167
0.820	0.8383	0.0009	0.9762	1.3888	-0.0018	0.8132
1.050	1.0624	-0.0171	0.9114	0.9207	0.0020	0.8062

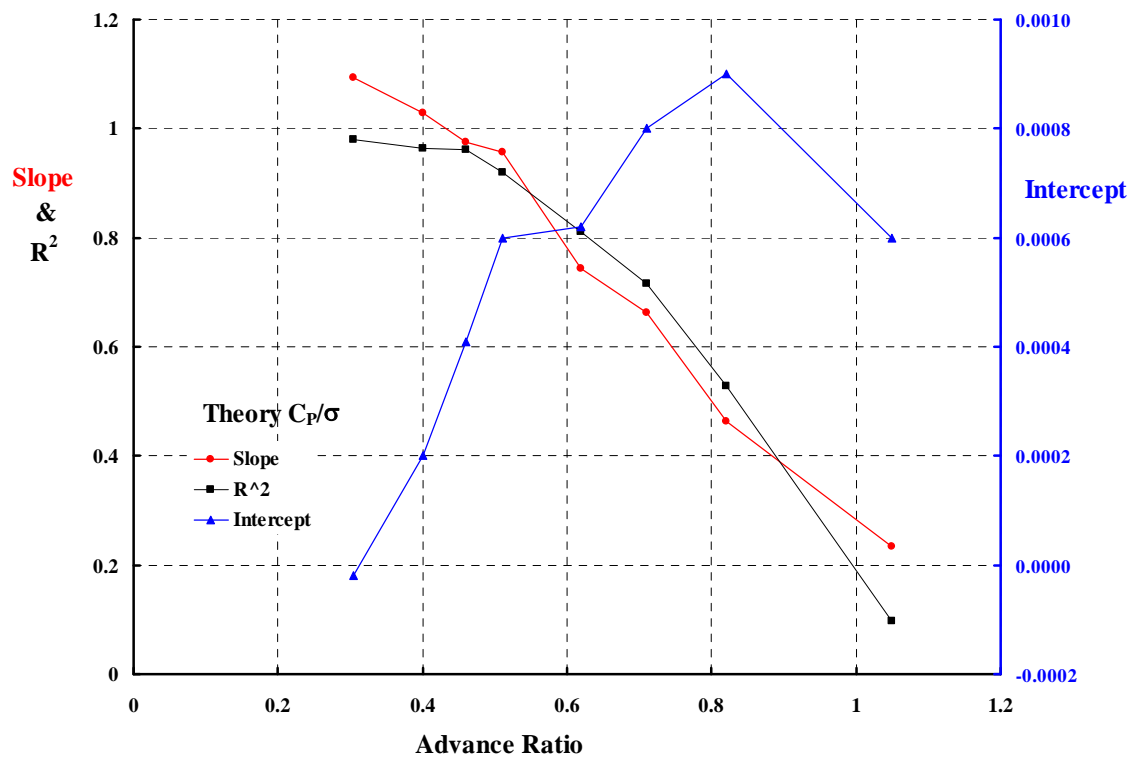
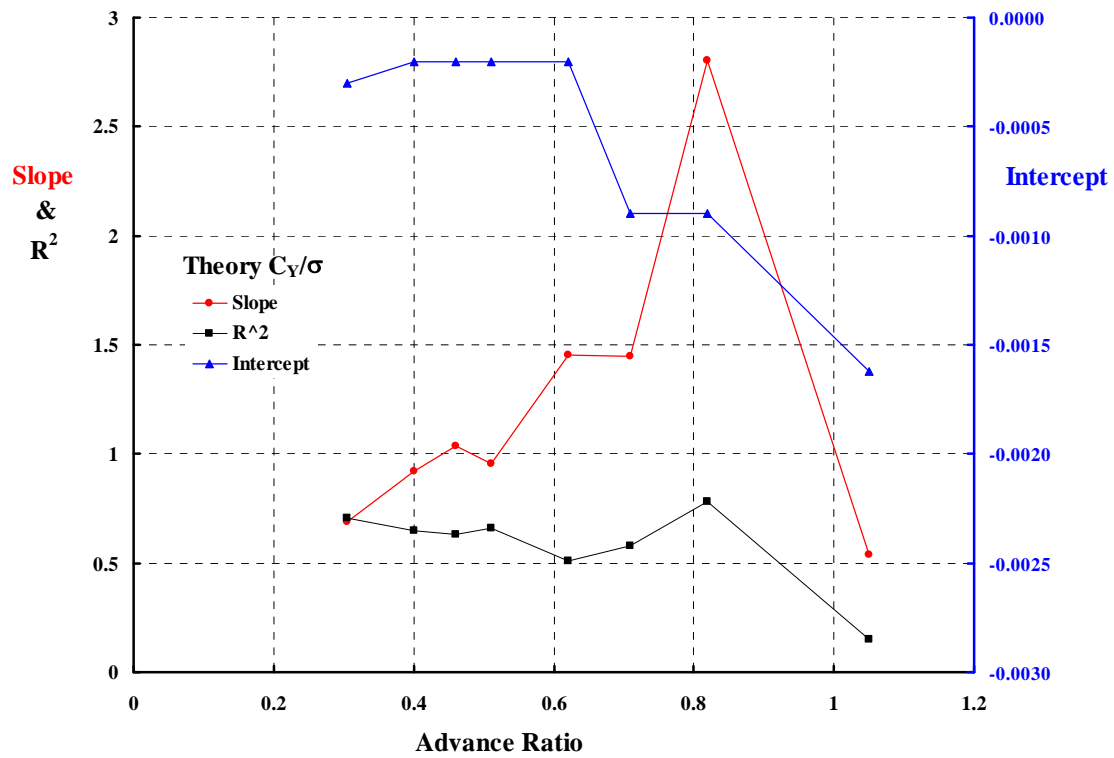
Mu	Y-Force Coefficient			Power Coefficient		
	SLOPE	Intercept	R²	SLOPE	Intercept	R²
0.305	0.6896	-0.0003	0.7059	1.0929	0.0000	0.9803
0.401	0.9202	-0.0002	0.6469	1.0296	0.0002	0.9635
0.460	1.0349	-0.0002	0.6313	0.9758	0.0004	0.9610
0.510	0.9566	-0.0002	0.6592	0.9576	0.0006	0.9205
0.620	1.4554	-0.0002	0.5089	0.7440	0.0006	0.8114
0.710	1.4471	-0.0009	0.5819	0.6617	0.0008	0.7168
0.820	2.8038	-0.0009	0.7805	0.4625	0.0009	0.5277
1.050	0.5410	-0.0016	0.1527	0.2347	0.0006	0.0971

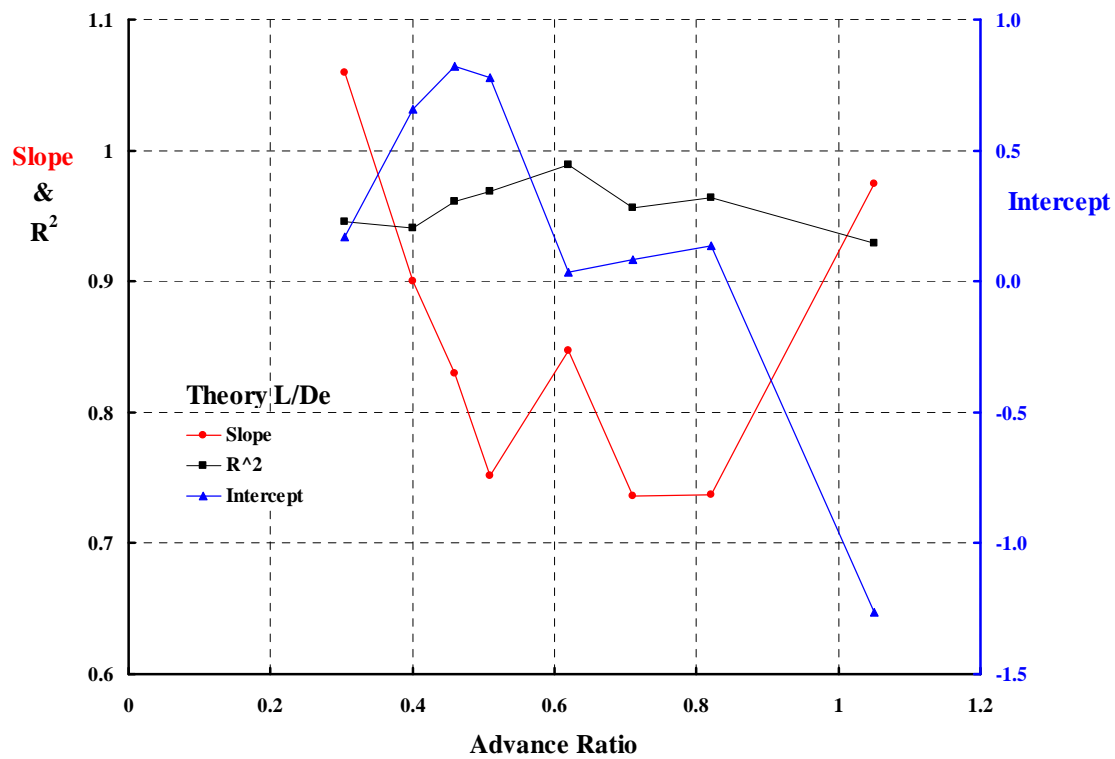
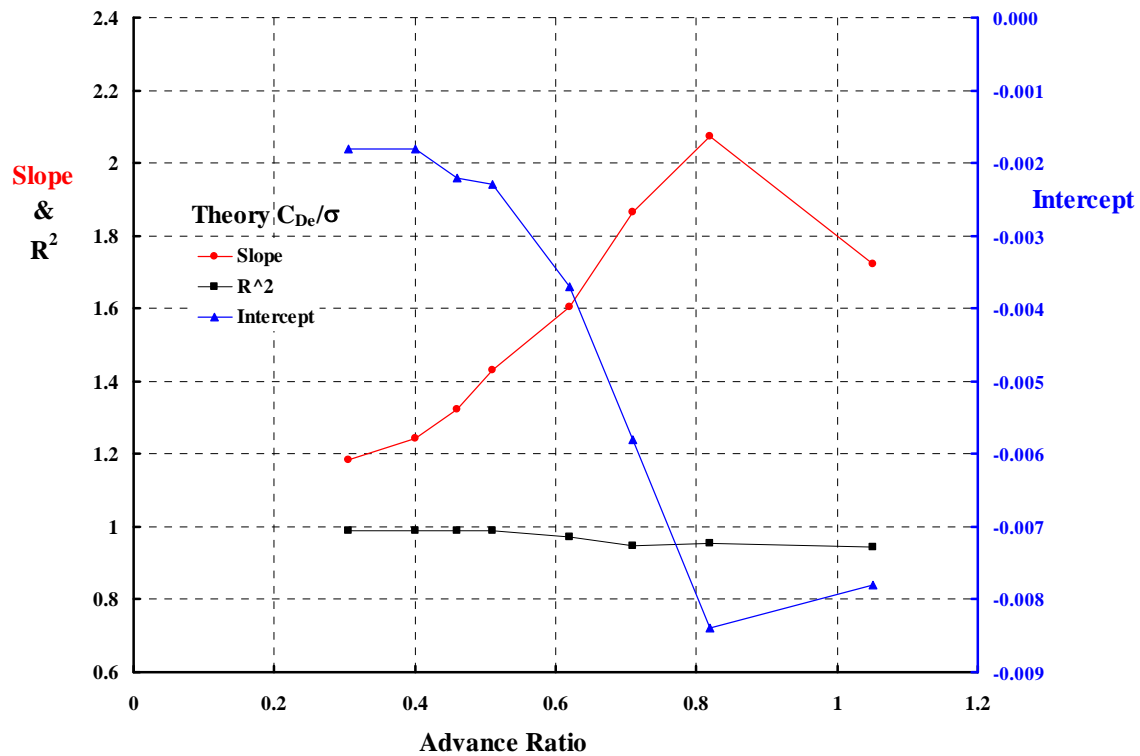
Mu	Effective Drag Coefficient			L/De		
	SLOPE	Intercept	R²	SLOPE	Intercept	R²
0.305	1.1831	-0.0018	0.9887	1.0591	0.1678	0.9451
0.401	1.2437	-0.0018	0.9908	0.9006	0.6581	0.9406
0.460	1.3222	-0.0022	0.9889	0.8293	0.8214	0.9613
0.510	1.4313	-0.0023	0.9876	0.7511	0.7761	0.9687
0.620	1.6043	-0.0037	0.9733	0.8469	0.0341	0.9893
0.710	1.8641	-0.0058	0.9465	0.7362	0.0850	0.9565
0.820	2.0745	-0.0084	0.9548	0.7371	0.1369	0.9643
1.050	1.7225	-0.0078	0.9433	0.9742	-1.2635	0.9292











11.13 H-34 versus OVERFLOW-2 Coupled with CAMRAD II

This appendix contains work Roger Strawn completed in 2003 and the work Jan Theron completed in 2006. Tables of performance data and selected graphs are included for each investigator. Strawn's work shows the influence of advancing tip Mach number on profile power, H-force and torque coefficients. Theron's work shows the torque, H-force and Y-force for one blade as the azimuth angle advances. Finally, Theron used OVERFLOW-2 to calculate N.A.C.A. 0012 airfoil C_l and C_d coefficients at a few Mach numbers and angles of attack for comparison to the C81 airfoil deck.

Roger Strawn Data From 2003

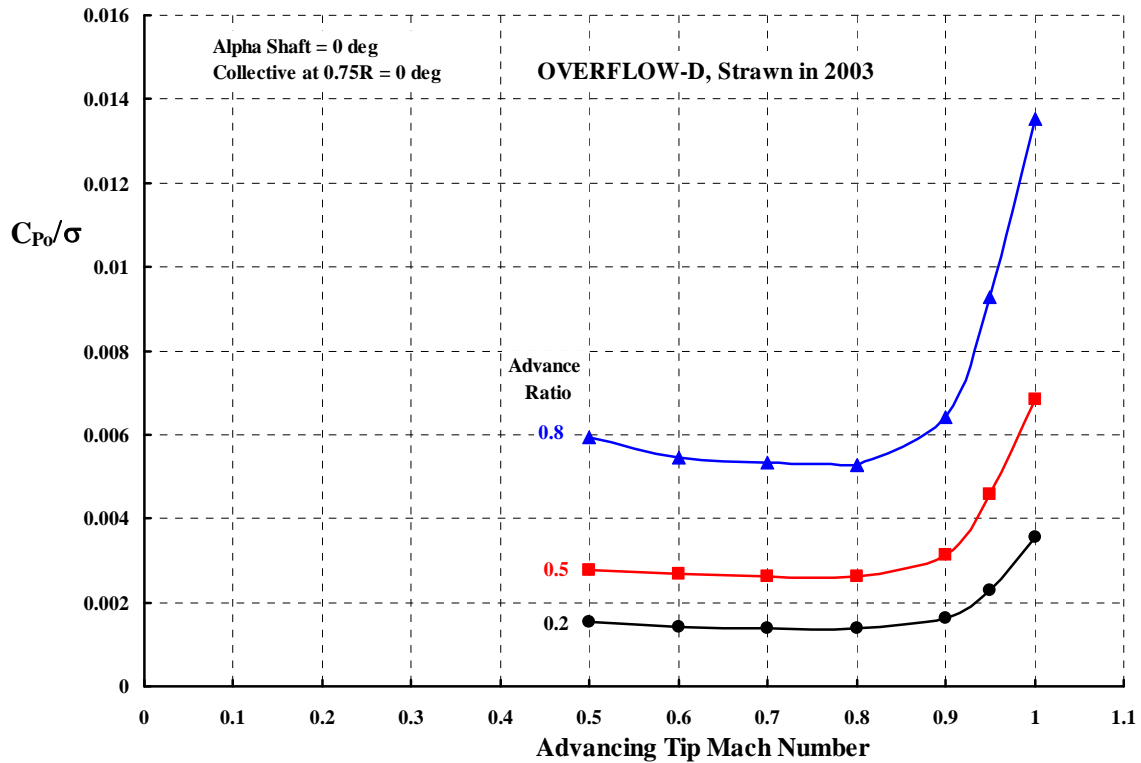
Ref: Final CFD Theory vs. Test Alpha=Collective=ZERO (Sept. 11, 2008).xls

Alpha shaft = 0, Collective, Cyclic = 0, $C_L/\sigma = 0$, C_Y/σ not recorded

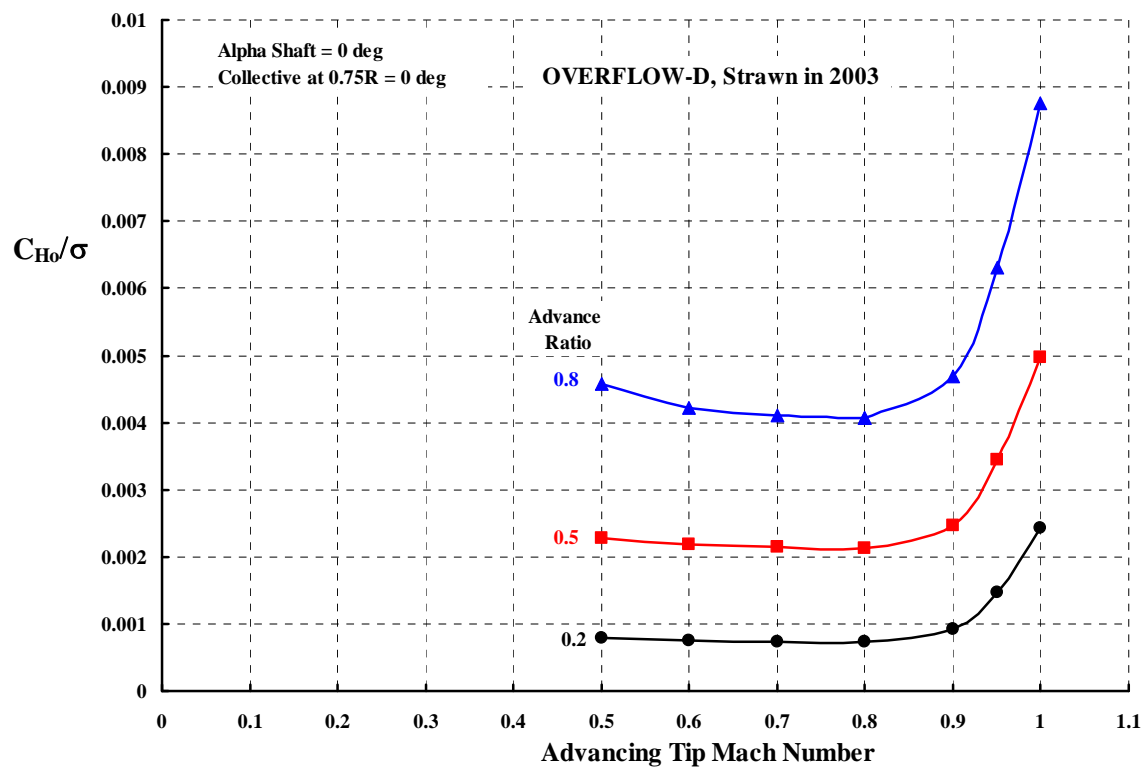
Advance Ratio	Advancing Tip Mach Number	Tip Speed (ft/sec)	Forward Speed (ft/sec)	Forward Speed (knots)	C_{Ho}/σ	C_{Qo}/σ	$C_{Po}/\sigma = C_{Qo}/\sigma + \mu C_{Ho}/\sigma$
0.00	0.50	562.664	0.0	0.0	0.000000	0.001282	0.001282
0.20	0.50	468.887	93.777	55	0.000788	0.001373	0.001531
0.40	0.50	401.903	160.761	95	0.001718	0.001502	0.002190
0.60	0.50	351.665	210.999	125	0.002912	0.001800	0.003547
0.80	0.50	312.591	250.073	148	0.004585	0.002263	0.005931
1.00	0.50	281.332	281.332	166	0.006195	0.002519	0.008714
1.20	0.50	255.756	306.908	182	0.008369	0.002880	0.012922
0.00	0.90	1,012.795	0.000	0.000	0.000000	0.001731	0.001731
0.20	0.90	843.996	168.799	100	0.000922	0.001428	0.001612
0.40	0.90	723.425	289.370	171	0.001887	0.001706	0.002461
0.60	0.90	632.997	379.798	225	0.003123	0.002126	0.004000
0.80	0.90	562.664	450.131	266	0.004681	0.002661	0.006406
1.00	0.90	506.398	506.398	300	0.006607	0.003290	0.009898
1.20	0.90	460.361	552.434	327	0.008990	0.004003	0.014791
0.20	0.50	468.887	93.777	55	0.000788	0.001373	0.001531
0.20	0.60	562.664	112.533	67	0.000746	0.001269	0.001419
0.20	0.70	656.441	131.288	78	0.000730	0.001244	0.001390
0.20	0.80	750.219	150.044	89	0.000727	0.001233	0.001379
0.20	0.90	843.996	168.799	100	0.000922	0.001428	0.001612
0.20	0.95	890.885	178.177	105	0.001462	0.002000	0.002292
0.20	1.00	937.773	187.555	111	0.002438	0.003061	0.003548

Roger Strawn Data From 2003

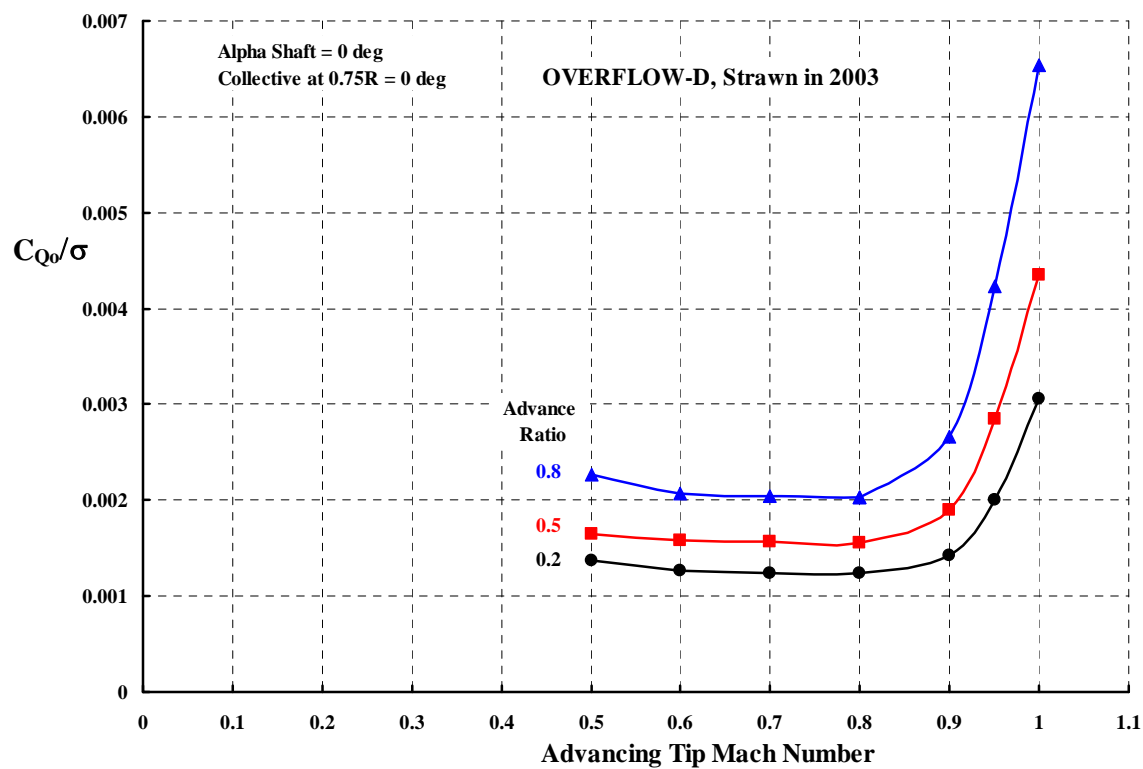
Advance Ratio	Advancing Tip Mach Number	Tip Speed (ft/sec)	Forward Speed (ft/sec)	Forward Speed (knots)	C_{Ho}/σ	C_{Qo}/σ	$C_{Po}/\sigma = C_{Qo}/\sigma + \mu C_{Ho}/\sigma$
0.50	0.50	375.109	187.555	111	0.002273	0.001649	0.002785
0.50	0.60	450.131	225.066	133	0.002193	0.001586	0.002682
0.50	0.70	525.153	262.577	155	0.002147	0.001562	0.002636
0.50	0.80	600.175	300.087	178	0.002121	0.001553	0.002613
0.50	0.90	675.197	337.598	200	0.002468	0.001900	0.003134
0.50	0.95	712.708	356.354	211	0.003438	0.002849	0.004569
0.50	1.00	750.219	375.109	222	0.004976	0.004356	0.006844
0.80	0.50	312.591	250.073	148	0.004585	0.002263	0.005931
0.80	0.60	375.109	300.087	178	0.004217	0.002072	0.005445
0.80	0.70	437.628	350.102	207	0.004115	0.002038	0.005330
0.80	0.80	500.146	400.117	237	0.004062	0.002036	0.005285
0.80	0.80	500.146	400.117	237	0.004062	0.002033	0.005282
0.80	0.90	562.664	450.131	266	0.004681	0.002661	0.006406
0.80	0.95	593.923	475.139	281	0.006314	0.004226	0.009277
0.80	1.00	625.182	500.146	296	0.008754	0.006537	0.013540



Roger Strawn Data From 2003



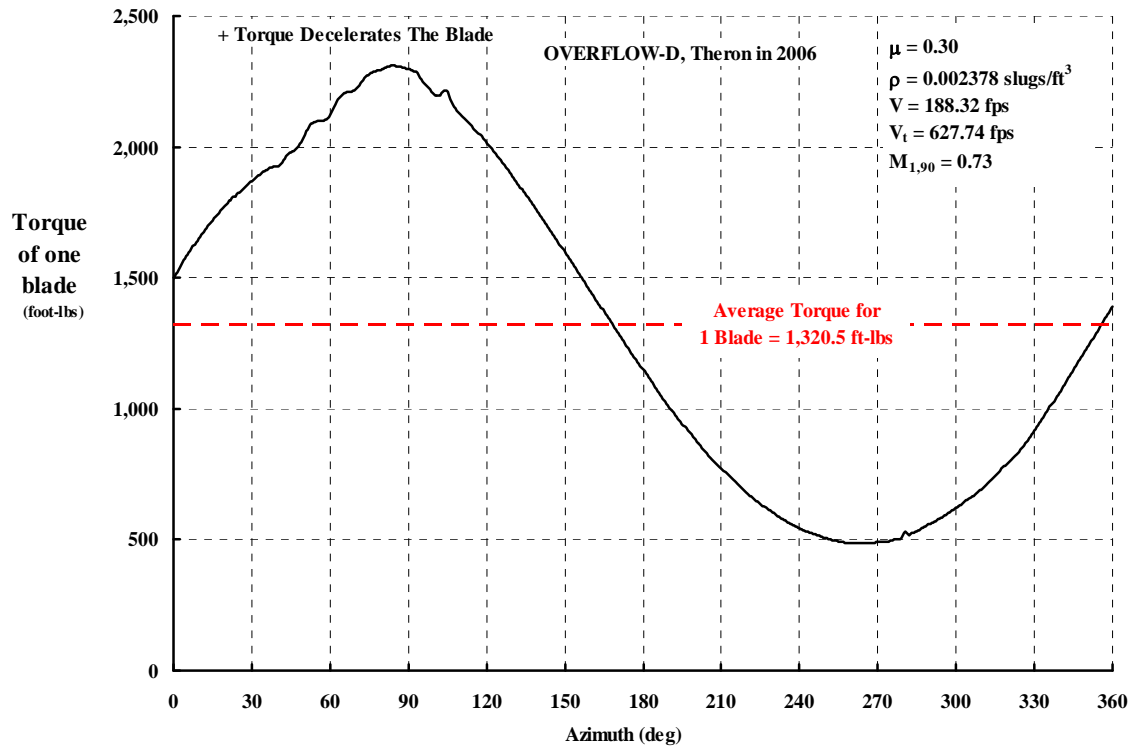
Roger Strawn Data From 2003



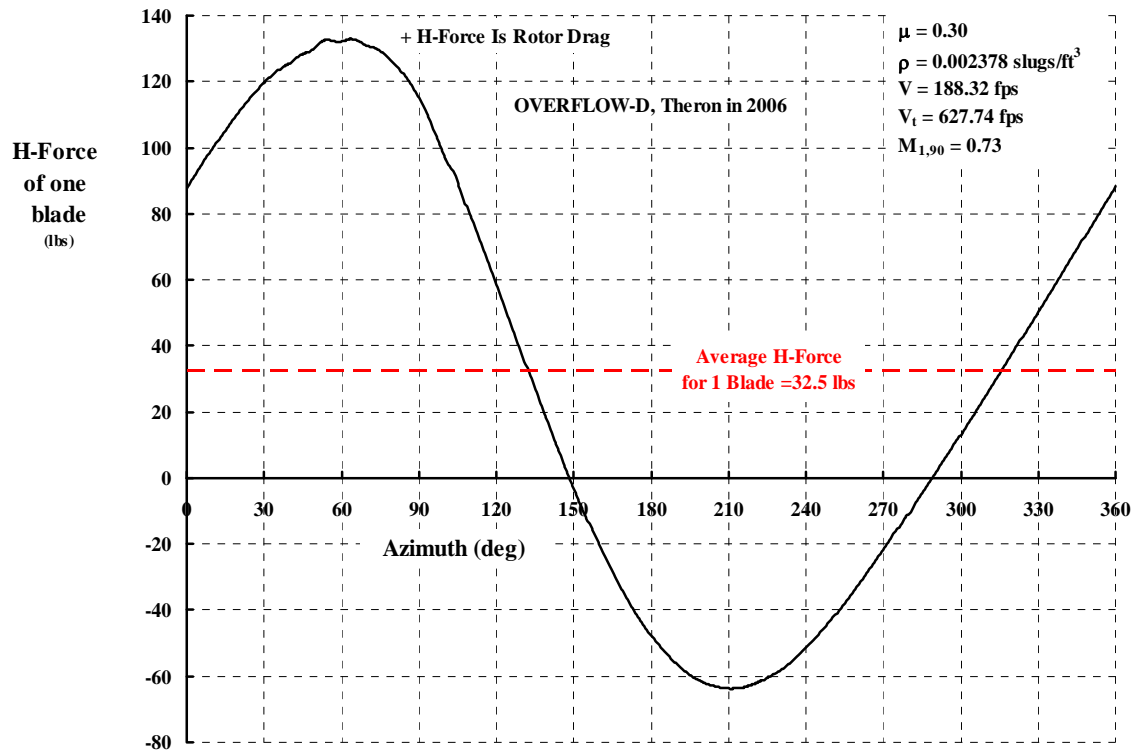
Roger Strawn Data From 2003

Jan Theron Data From 2006

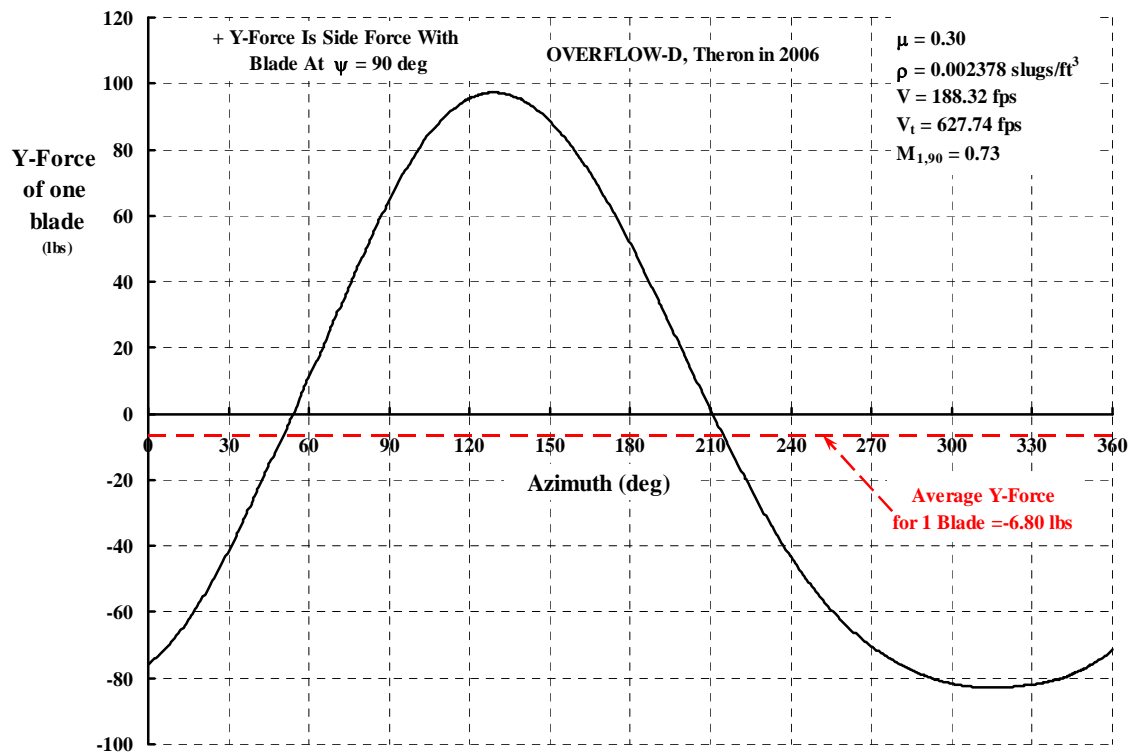
Advance Ratio	Advancing Tip Mach Number	Tip Speed (ft/sec)	Forward Speed (ft/sec)	Forward Speed (knots)	C_{Ho}/σ	C_{Yo}/σ	C_{Qo}/σ	$C_{Po}/\sigma = C_{Qo}/\sigma + \mu C_{Ho}/\sigma$
0.30	0.73	627.740	188.322	111	0.0009290	-0.0001944	0.0013482	0.0016269
0.40	0.83	662.751	265.100	157	0.0013015	-0.0002642	0.0014639	0.0019845
0.71	0.68	444.542	315.625	187	0.0023413	-0.0005180	0.0018327	0.0034951
1.05	0.54	294.469	309.192	183	0.0043145	-0.0007161	0.0026002	0.0071304



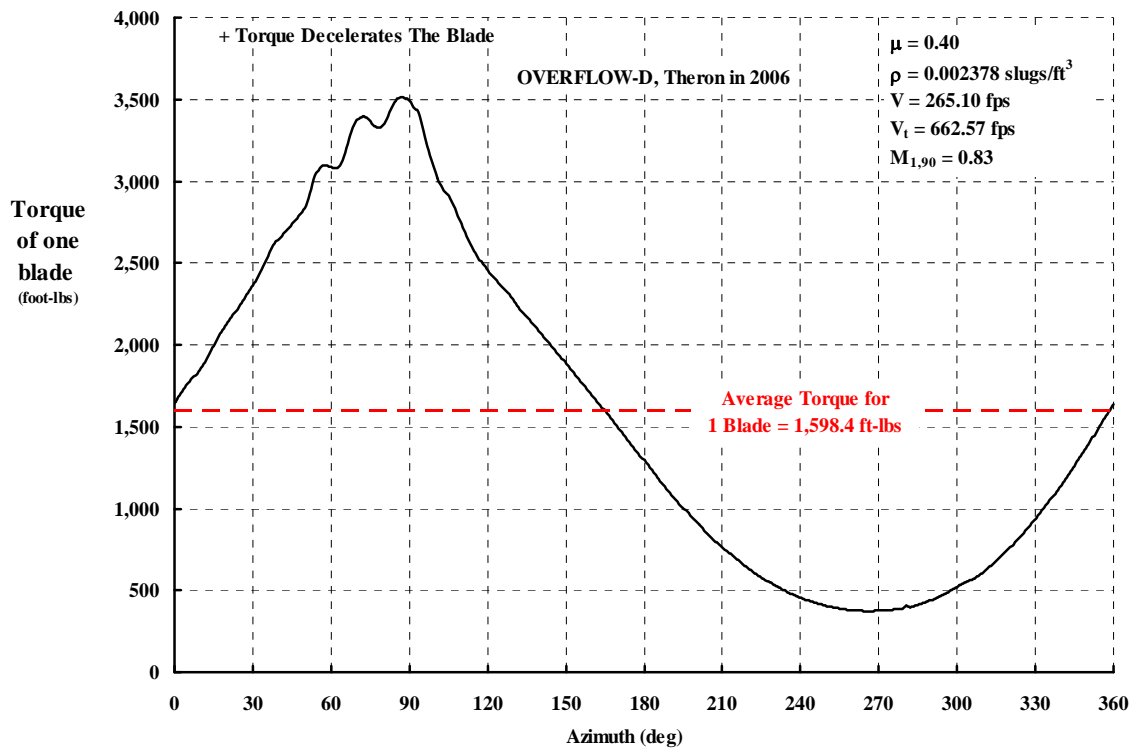
Jan Theron Data From 2006



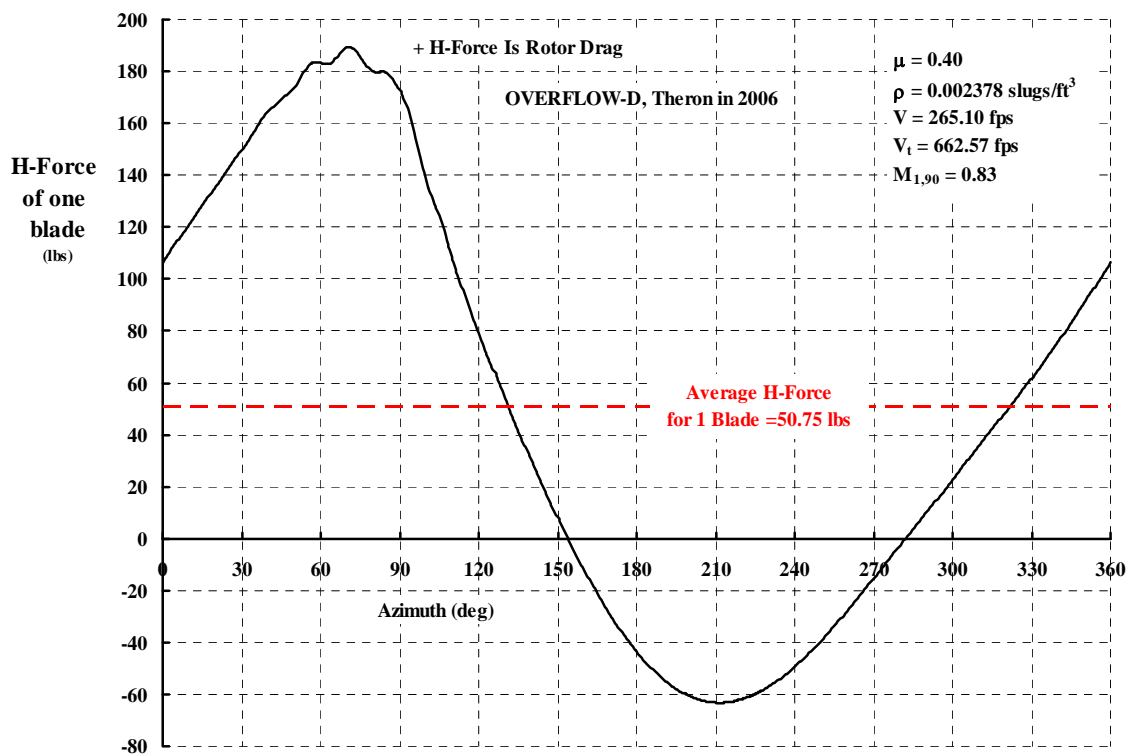
Jan Theron Data From 2006



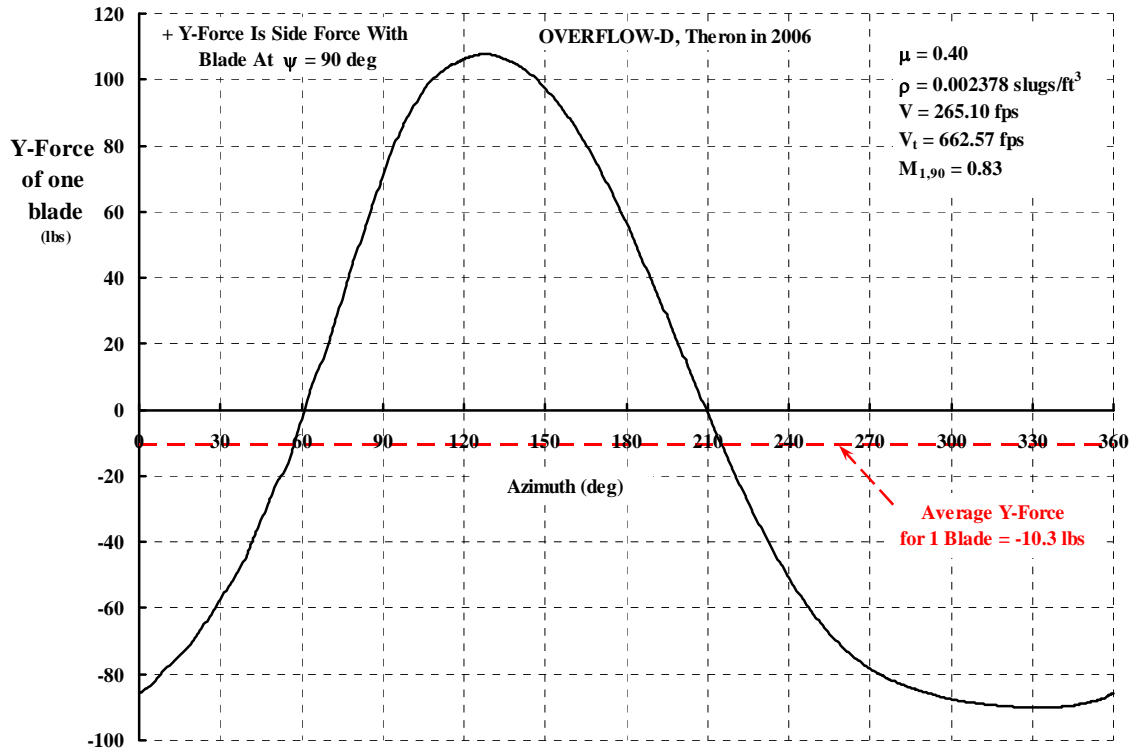
Jan Theron Data From 2006



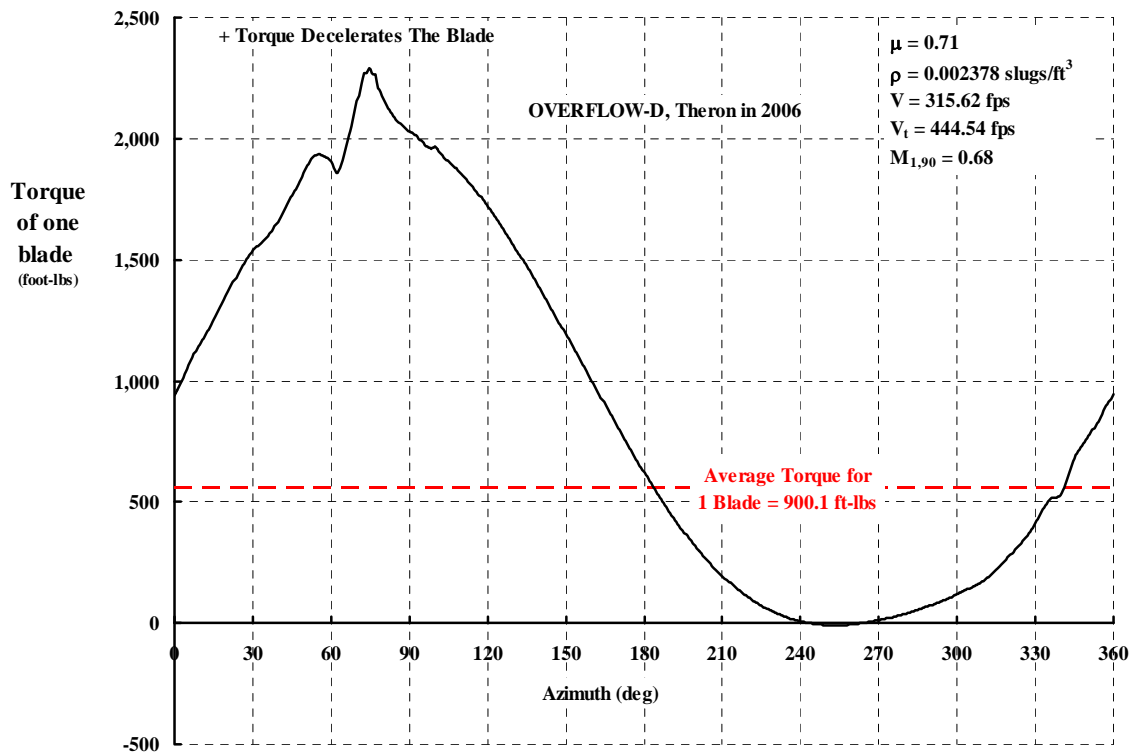
Jan Theron Data From 2006



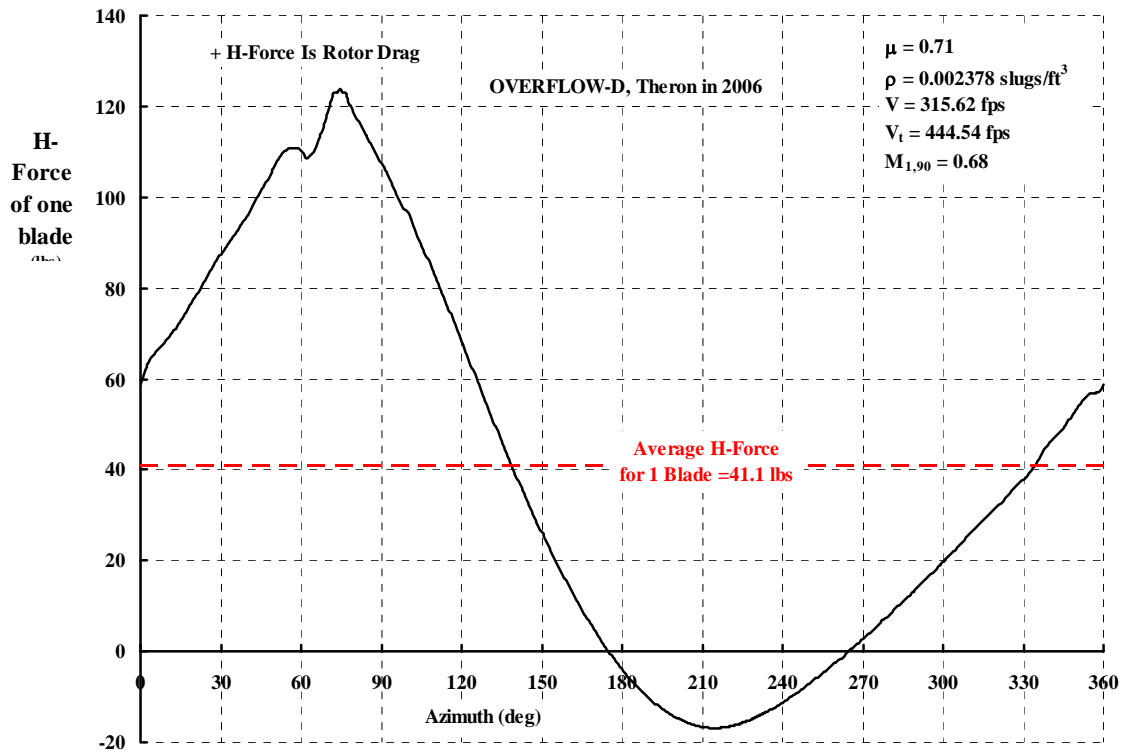
Jan Theron Data From 2006



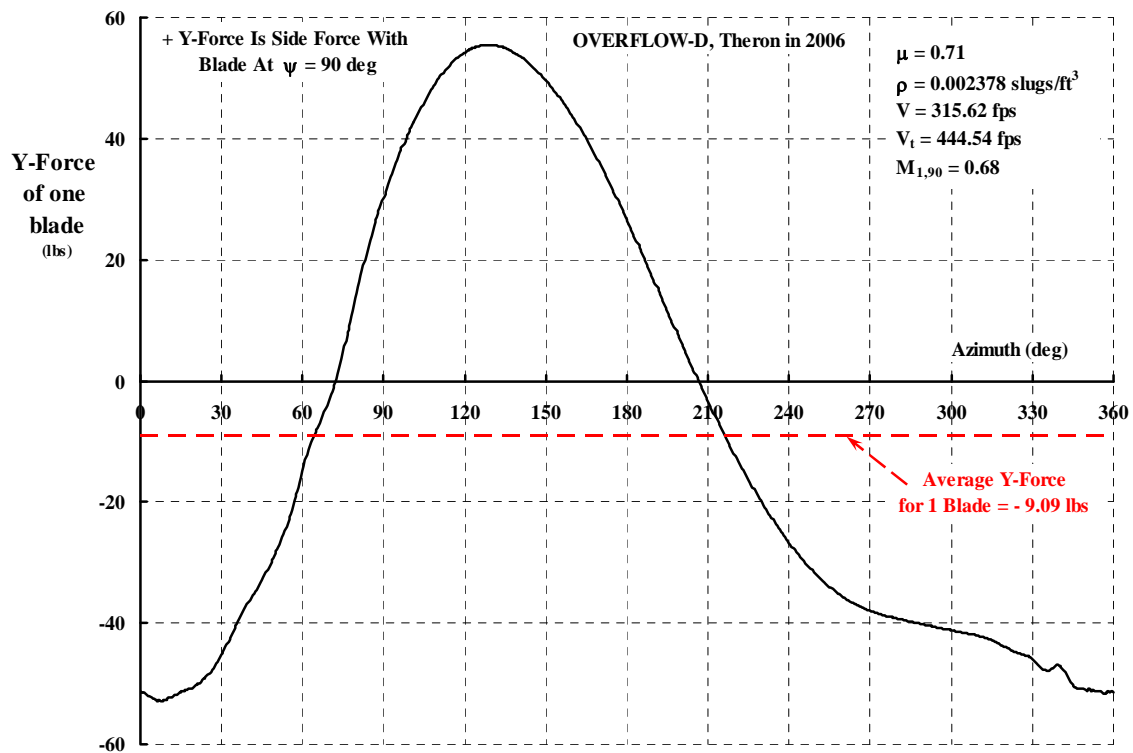
Jan Theron Data From 2006



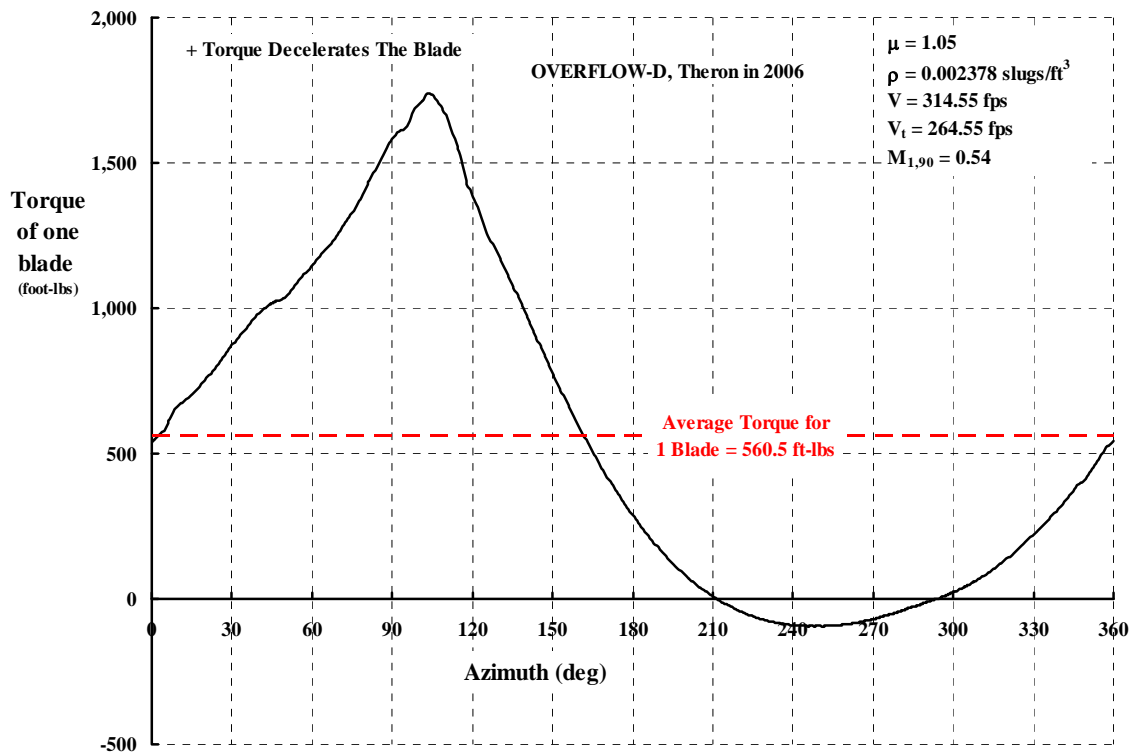
Jan Theron Data From 2006



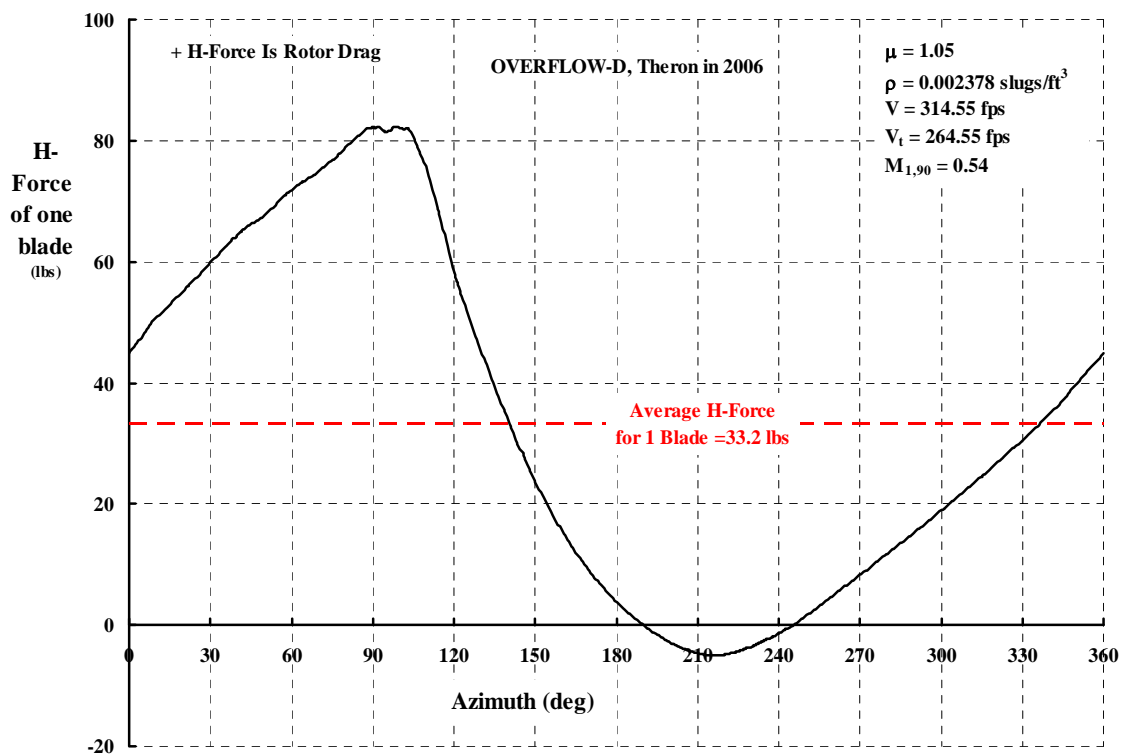
Jan Theron Data From 2006



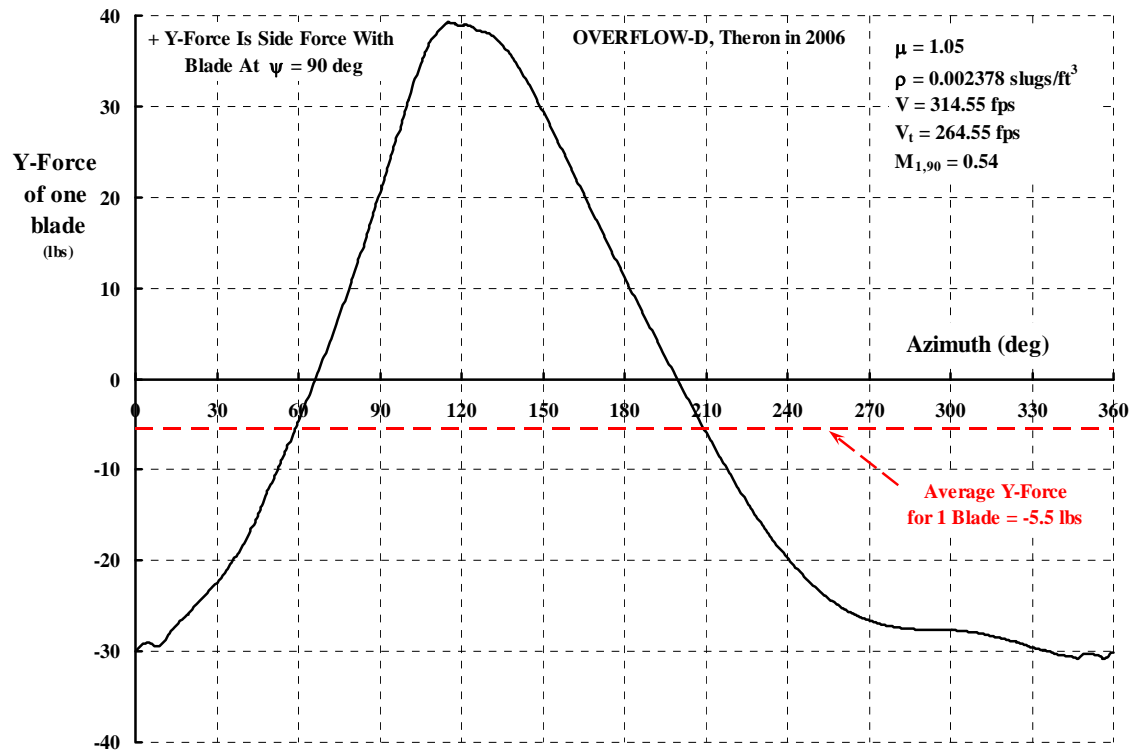
Jan Theron Data From 2006



Jan Theron Data From 2006



Jan Theron Data From 2006



Jan Theron Data From 2006

Angle of Attack (deg)	Mach Number	NACA 0012 Airfoil Cd	NACA 0012 Airfoil Cl	Angle of Attack (deg)	Mach Number	NACA 0012 Airfoil Cd	NACA 0012 Airfoil Cl
0	0.200	0.009892	na	7.5	0.600	0.038066	0.841420
0	0.400	0.008879	na	7.5	0.715	0.075148	0.578881
0	0.600	0.008425	0.000033	7.5	0.810	0.099146	0.451210
0	0.715	0.008514	0.000032				
0	0.750	0.008682	na	10	0.600	0.083921	0.761694
0	0.775	0.009862	na	10	0.715	0.114308	0.562418
0	0.810	0.020094	0.000035	10	0.810	0.136770	0.541233
0	0.830	0.032356	na				
5	0.600	0.015204	0.625851	180	0.200	0.013564	0.000161
5	0.715	0.041110	0.620255	180	0.400	0.012420	0.000251
5	0.810	0.066238	0.353989				

Jan Theron Data From 2006

11.14 UH-1 versus CAMRAD II

References: 1. USAAVLABS Technical Report 69-2, Wind Tunnel Investigation of Semirigid Full-Scale Rotors Operating at High Advance Ratios by Bruce Charles and Watson (Hank) Tanner January 1969
2. Harris EXCEL File: MASTER UH-1 versus CAMRAD II.xls

Airfoil	NACA 0012
Chord	1.75 ft
Diameter	34.00 ft
Twist	-1.42 deg Washout
Disc Area	908 sq. ft
Reference Area (2 blades)	59.5 sq. ft
Nominal Solidity	0.0656
Lock Number	3.62
Flap Moment of inertia	1,584 slug ft ²

Notes: 1. Wind axis data measured. Shaft axis data derived.
2. Shaft torque derived from wind tunnel balance forces and moments.
3. Coefficients based on rotor tip speed and total blade area ($\sigma A = 59.5$ sq. ft.)
4. Teetering, under slung hub with $z/R = 0.0256$
5. Pitch bearing at $r/R = 0.0578$
6. Hub precone angle of 2.75 degrees
7. Lateral cyclic to remove lateral flapping not provided.

Table of CAMRAD II Output

Advance Ratio	Collective at 0.75R (deg)	Shaft Angle of Attack (deg)	Long Cyclic (deg)	Lat Cyclic (deg)	CL/Solidity	CD/Solidity	CT/Solidity	CH/Solidity	CQ/Solidity	CDe/Solidity	Rotor Alone L/De
0.510	0.0	-4.0	-1.36	0.36	-0.021780	0.004560	-0.022050	0.003030	0.000891	0.006310	-3.45
0.510	3.0	-4.0	1.70	-0.12	-0.005760	0.003590	-0.006000	0.003180	0.001384	0.006300	-0.91
0.510	4.0	-4.0	2.70	-0.28	0.000670	0.002700	0.000480	0.002740	0.001734	0.006100	0.11
0.510	5.0	-4.0	3.69	-0.44	0.007130	0.002210	0.006960	0.002700	0.002080	0.006290	1.13
0.510	6.0	-4.0	4.69	-0.61	0.013340	0.001850	0.013180	0.002780	0.002480	0.006710	1.99
0.510	0.0	0.0	0.20	-0.07	0.001390	0.002480	0.001390	0.002480	0.001474	0.005370	0.26
0.510	1.0	0.0	1.19	-0.25	0.007630	0.002680	0.007630	0.002680	0.001457	0.005530	1.38
0.510	2.0	0.0	2.19	-0.40	0.013270	0.003460	0.013270	0.003460	0.001476	0.006360	2.09
0.510	3.0	0.0	3.20	-0.56	0.019050	0.003420	0.019050	0.003420	0.001648	0.006650	2.86
0.510	4.0	0.0	4.22	-0.68	0.025390	0.003440	0.025390	0.003440	0.001971	0.007310	3.47
0.510	0.0	4.0	1.76	-0.54	0.025610	0.004500	0.025860	0.002710	0.001100	0.006660	3.85
0.510	1.0	4.0	2.76	-0.68	0.031340	0.005110	0.031620	0.002910	0.000954	0.006980	4.49
0.510	2.0	4.0	3.79	-0.83	0.036790	0.005530	0.037080	0.002950	0.001040	0.007570	4.86
0.510	3.0	4.0	4.80	-0.97	0.042600	0.005950	0.042900	0.002960	0.001189	0.008280	5.14
0.510	2.0	0.0	2.19	-0.40	0.013270	0.003460	0.013270	0.003460	0.001476	0.006360	2.09
0.510	2.0	1.0	2.59	-0.52	0.019050	0.003190	0.019100	0.002860	0.001542	0.006220	3.06
0.510	2.0	2.0	2.97	-0.61	0.025370	0.003480	0.025470	0.002590	0.001441	0.006300	4.03
0.510	2.0	3.0	3.37	-0.72	0.031220	0.004400	0.031410	0.002760	0.001222	0.006800	4.59
0.510	2.0	4.0	3.77	-0.83	0.036490	0.005420	0.036780	0.002870	0.001028	0.007440	4.90
0.510	2.0	5.0	4.19	-0.93	0.042260	0.007160	0.042720	0.003460	0.000590	0.008320	5.08
0.510	2.0	6.0	4.58	-1.01	0.048290	0.008280	0.048870	0.003190	0.000360	0.008980	5.38
0.510	2.0	7.0	5.02	-1.10	0.054590	0.010510	0.055450	0.003780	-0.000311	0.009900	5.51

0.652	0.0	-4.0	-1.89	0.29	-0.026240	0.009970	-0.026870	0.008120	0.000311	0.010450	-2.51
0.652	6.0	-4.0	4.96	-0.67	-0.006990	0.007770	-0.007450	0.007270	0.001424	0.009950	-0.70
0.652	7.0	-4.0	6.03	-0.84	-0.001800	0.007200	-0.002130	0.007070	0.001918	0.010130	-0.18
0.652	8.0	-4.0	7.16	-1.00	0.001170	0.007010	0.000490	0.007060	0.002348	0.010600	0.11
0.652	9.0	-4.0	8.24	-1.09	0.006300	0.007250	0.005710	0.007670	0.002710	0.011400	0.55
0.652	10.0	-4.0	9.32	-1.15	0.012190	0.005930	0.011730	0.006770	0.003711	0.011610	1.05
0.654	0.0	0.0	0.15	-0.26	0.001630	0.005410	0.001010	0.005410	0.001428	0.007600	0.21
0.654	1.0	0.0	1.31	-0.38	0.004760	0.005510	0.004590	0.005510	0.001672	0.008060	0.59
0.654	2.0	0.0	2.43	-0.49	0.008020	0.005680	0.007850	0.005680	0.001329	0.007710	1.04
0.654	3.0	0.0	3.72	-0.63	0.006780	0.007390	0.006730	0.007390	0.001259	0.009310	0.73
0.654	4.0	0.0	4.82	-0.72	0.011490	0.005980	0.011490	0.005980	0.002023	0.009070	1.27
0.654	5.0	0.0	5.81	-0.84	0.019000	0.005570	0.018960	0.005570	0.002041	0.008690	2.19
0.654	6.0	0.0	6.91	-0.93	0.024500	0.005030	0.024500	0.005030	0.002600	0.009000	2.72
0.654	7.0	0.0	8.03	-1.06	0.028000	0.006140	0.027990	0.006140	0.002809	0.010440	2.68
0.654	8.0	0.0	9.13	-1.16	0.032300	0.005350	0.032300	0.005350	0.003422	0.010590	3.05
0.654	9.0	0.0	10.24	-1.22	0.036640	0.007690	0.036630	0.007690	0.003812	0.013520	2.71
0.652	0.0	4.0	2.29	-0.77	0.026560	0.009120	0.027130	0.007240	0.000429	0.009780	2.72
0.652	1.0	4.0	3.42	-0.91	0.030080	0.008720	0.030610	0.006600	0.000634	0.009690	3.10
0.652	2.0	4.0	4.52	-0.99	0.035230	0.010170	0.035850	0.007680	0.000792	0.011380	3.10
0.652	3.0	4.0	5.67	-1.08	0.038330	0.010000	0.038930	0.007300	0.001010	0.011540	3.32
0.652	4.0	4.0	6.78	-1.18	0.042080	0.009760	0.042660	0.006800	0.001380	0.011870	3.55
0.652	5.0	4.0	7.91	-1.31	0.045820	0.010470	0.046440	0.007240	0.001561	0.012850	3.57
0.652	6.0	4.0	9.02	-1.45	0.049850	0.010790	0.050480	0.007280	0.001877	0.013660	3.65
0.652	2.0	-4.0	0.36	0.00	-0.018570	0.009120	-0.019140	0.007800	0.000551	0.009960	-1.86
0.653	2.0	-3.0	0.88	-0.14	-0.012310	0.008400	-0.012690	0.007740	0.000844	0.009690	-1.27
0.654	2.0	-2.0	1.40	-0.28	-0.006130	0.006160	-0.006310	0.005950	0.001275	0.008110	-0.76
0.654	2.0	-1.0	1.94	-0.39	0.001000	0.004970	0.000550	0.004980	0.001638	0.007470	0.13
0.654	2.0	0.0	2.43	-0.49	0.008020	0.005680	0.007850	0.005680	0.001329	0.007710	1.04
0.654	2.0	1.0	2.97	-0.58	0.014870	0.005020	0.014950	0.004760	0.001858	0.007860	1.89
0.654	2.0	2.0	3.49	-0.68	0.021120	0.006190	0.021330	0.005450	0.001522	0.008520	2.48

0.653	2.0	3.0	4.01	-0.84	0.027800	0.006710	0.028110	0.005250	0.001338	0.008760	3.17
0.652	2.0	4.0	4.53	-1.01	0.035720	0.009540	0.036290	0.007030	0.000910	0.010930	3.27
0.652	2.0	5.0	5.06	-1.13	0.041690	0.012120	0.042580	0.008440	0.000355	0.012660	3.29
0.650	2.0	6.0	5.53	-1.32	0.049320	0.013700	0.050480	0.008470	0.000044	0.013770	3.58
0.649	2.0	7.0	6.06	-1.43	0.054720	0.014630	0.056100	0.007860	-0.000383	0.014050	3.89
0.648	2.0	8.0	6.59	-1.53	0.061040	0.016840	0.062790	0.008180	-0.000999	0.015310	3.99
0.646	2.0	9.0	7.02	-1.71	0.070270	0.017790	0.072190	0.006570	-0.001184	0.015980	4.40
0.644	2.0	10.0	7.45	-1.86	0.079000	0.021310	0.081500	0.007260	-0.002049	0.018170	4.35
0.757	2.0	0.0	2.50	-0.50	0.006180	0.005080	0.006170	0.005080	0.001850	0.007520	0.82
0.757	2.0	1.0	3.08	-0.63	0.012900	0.006530	0.013000	0.006310	0.001722	0.008810	1.46
0.757	2.0	2.0	3.72	-0.77	0.019310	0.006170	0.019510	0.005490	0.001518	0.008180	2.36
0.757	2.0	3.0	4.24	-0.96	0.028990	0.010260	0.029480	0.008730	0.000785	0.011300	2.57
0.757	2.0	4.0	4.91	-1.09	0.032630	0.008500	0.033140	0.006210	0.001036	0.009870	3.31
0.757	2.0	5.0	5.46	-1.25	0.042930	0.012480	0.043860	0.008690	0.000258	0.012820	3.35
0.757	2.0	6.0	6.11	-1.45	0.048070	0.012220	0.049090	0.007130	0.000461	0.012830	3.75
0.757	2.0	7.0	6.58	-1.53	0.056950	0.015620	0.058430	0.008570	-0.000421	0.015070	3.78
0.757	2.0	8.0	7.15	-1.67	0.063890	0.017640	0.065720	0.008580	-0.001064	0.016240	3.93
0.757	2.0	9.0	7.67	-1.85	0.075060	0.020500	0.077330	0.008510	-0.001735	0.018210	4.12
0.757	2.0	10.0	8.24	-1.95	0.082220	0.022370	0.084840	0.007760	-0.002369	0.019240	4.27
0.856	0.0	-4.0	-2.25	0.16	-0.033060	0.015270	-0.033980	0.012930	-0.000606	0.014570	-2.27
0.856	4.0	-4.0	2.45	-0.22	-0.027940	0.011410	-0.028660	0.009430	0.000957	0.012530	-2.23
0.856	5.0	-4.0	3.55	-0.38	-0.023600	0.011340	-0.024340	0.009660	0.000746	0.012210	-1.93
0.856	6.0	-4.0	4.73	-0.51	-0.021770	0.012710	-0.022600	0.011160	0.000353	0.013120	-1.66
0.856	7.0	-4.0	5.86	-0.58	-0.018260	0.012410	-0.019080	0.011110	0.000782	0.013320	-1.37
0.856	8.0	-4.0	7.07	-0.71	-0.018290	0.015100	-0.019290	0.013780	0.001010	0.016280	-1.12
0.856	9.0	-4.0	8.24	-0.86	-0.015070	0.014830	-0.016050	0.013750	0.000822	0.015790	-0.95
0.856	10.0	-4.0	9.43	-1.05	-0.013300	0.015990	-0.014330	0.015030	0.000776	0.016900	-0.79
0.856	11.0	-4.0	10.52	-1.16	-0.009980	0.017560	-0.011020	0.016830	0.000738	0.018420	-0.54
0.856	12.0	-4.0	11.63	-1.15	-0.007440	0.017140	-0.008380	0.016600	0.001549	0.018950	-0.39
0.856	0.0	0.0	0.17	-0.46	0.001410	0.008270	0.001270	0.008270	0.001300	0.009780	0.14

0.856	1.0	0.0	1.35	-0.55	0.001760	0.006070	0.001750	0.006070	0.001831	0.008210	0.21
0.856	2.0	0.0	2.56	-0.60	0.002640	0.006520	0.002590	0.006520	0.001872	0.008710	0.30
0.856	3.0	0.0	3.76	-0.66	0.003130	0.007240	0.003050	0.007240	0.002057	0.009650	0.32
0.856	4.0	0.0	4.95	-0.75	0.003430	0.008090	0.003390	0.008090	0.002153	0.010600	0.32
0.856	5.0	0.0	6.12	-0.83	0.005110	0.008840	0.005050	0.008840	0.002277	0.011500	0.44
0.856	6.0	0.0	7.29	-0.89	0.007010	0.010930	0.006950	0.010930	0.002377	0.013710	0.51
0.856	7.0	0.0	8.46	-0.99	0.009720	0.010040	0.009720	0.010040	0.002446	0.012900	0.75
0.856	8.0	0.0	9.60	-1.08	0.012630	0.009790	0.012610	0.009790	0.003020	0.013310	0.95
0.856	9.0	0.0	10.76	-1.20	0.014570	0.011650	0.014550	0.011650	0.003186	0.015370	0.95
0.856	10.0	0.0	11.84	-1.28	0.018820	0.010740	0.018810	0.010740	0.003918	0.015310	1.23
0.856	11.0	0.0	13.04	-1.28	0.018470	0.014250	0.018380	0.014250	0.003135	0.017910	1.03
0.856	12.0	0.0	14.20	-1.17	0.021560	0.016410	0.021450	0.016410	0.003077	0.020000	1.08
0.856	0.0	4.0	2.67	-1.14	0.034470	0.013220	0.035310	0.010780	0.000076	0.013310	2.59
0.856	1.0	4.0	3.90	-1.18	0.034260	0.013960	0.035150	0.011540	0.000218	0.014220	2.41
0.856	2.0	4.0	5.06	-1.31	0.035620	0.014310	0.036520	0.011790	0.000553	0.014960	2.38
0.856	3.0	4.0	6.26	-1.35	0.035460	0.012040	0.036180	0.009540	0.001196	0.013430	2.64
0.856	4.0	4.0	7.48	-1.40	0.035980	0.014450	0.036890	0.011900	0.000868	0.015460	2.33
0.856	5.0	4.0	8.71	-1.45	0.035670	0.013420	0.036510	0.010900	0.001461	0.015120	2.36
0.856	6.0	4.0	9.90	-1.50	0.037900	0.014140	0.038790	0.011460	0.001829	0.016270	2.33
0.856	7.0	4.0	11.06	-1.54	0.038840	0.013760	0.039710	0.011010	0.002094	0.016200	2.40
0.856	8.0	4.0	12.20	-1.61	0.041720	0.015470	0.042690	0.012520	0.002222	0.018060	2.31
0.856	9.0	4.0	13.28	-1.66	0.044970	0.016300	0.046000	0.013130	0.002389	0.019090	2.36
0.856	10.0	4.0	14.30	-1.59	0.049840	0.016210	0.050830	0.012690	0.003129	0.019860	2.51
0.856	11.0	4.0	15.47	-1.48	0.051730	0.017880	0.052840	0.014220	0.003319	0.021750	2.38
0.856	2.0	-4.0	0.10	0.01	-0.029280	0.011300	-0.030000	0.009240	0.000314	0.011670	-2.51
0.856	2.0	-3.0	0.68	-0.18	-0.020180	0.010820	-0.020720	0.009750	0.000520	0.011430	-1.77
0.856	2.0	-2.0	1.28	-0.32	-0.011240	0.007540	-0.011440	0.007140	0.001731	0.009560	-1.18
0.856	2.0	-1.0	1.91	-0.46	-0.004830	0.006870	-0.004680	0.006790	0.002483	0.009770	-0.49
0.856	2.0	0.0	2.56	-0.60	0.002640	0.006520	0.002590	0.006520	0.001872	0.008710	0.30
0.856	2.0	1.0	3.22	-0.74	0.009330	0.006010	0.009410	0.005850	0.002741	0.009210	1.01
0.856	2.0	2.0	3.85	-0.87	0.017390	0.008590	0.017660	0.007980	0.001797	0.010690	1.63

0.856	2.0	3.0	4.46	-1.11	0.026210	0.011900	0.026780	0.010520	0.000709	0.012730	2.06
0.856	2.0	4.0	5.06	-1.32	0.037260	0.016290	0.038290	0.013650	0.000335	0.016680	2.23
0.856	2.0	5.0	5.58	-1.54	0.048250	0.017830	0.049600	0.013560	-0.000102	0.017710	2.72
0.856	2.0	6.0	6.14	-1.68	0.058360	0.018210	0.059940	0.012010	-0.000435	0.017700	3.30
0.856	2.0	7.0	6.79	-1.77	0.066700	0.019920	0.068630	0.011650	-0.000980	0.018780	3.55
0.856	2.0	8.0	7.41	-1.89	0.075350	0.023050	0.077820	0.012340	-0.001631	0.021150	3.56
0.856	2.0	9.0	8.02	-2.01	0.082940	0.022810	0.085490	0.009560	-0.001898	0.020600	4.03
0.856	2.0	10.0	8.62	-2.15	0.092110	0.026500	0.095310	0.010100	-0.002737	0.023300	3.95
0.945	0.0	0.0	0.18	-0.49	0.000690	0.007860	0.000670	0.007860	0.001817	0.009790	0.07
0.945	1.0	0.0	1.40	-0.54	-0.000270	0.008040	-0.000180	0.008040	0.001726	0.009860	-0.03
0.945	2.0	-10.0	-3.75	0.79	-0.102060	0.030230	-0.105760	0.012050	-0.005006	0.024940	-4.09
0.945	2.0	-9.0	-3.18	0.70	-0.088170	0.028080	-0.091480	0.013940	-0.003933	0.023920	-3.69
0.945	2.0	-8.0	-2.51	0.58	-0.081340	0.028240	-0.084470	0.016640	-0.002959	0.025100	-3.24
0.945	2.0	-7.0	-1.90	0.42	-0.070000	0.024920	-0.072510	0.016210	-0.002209	0.022580	-3.10
0.945	2.0	-6.0	-1.30	0.28	-0.056180	0.018140	-0.057750	0.012170	-0.000874	0.017210	-3.26
0.945	2.0	-5.0	-0.67	0.19	-0.044080	0.014070	-0.045140	0.010180	-0.000005	0.014070	-3.13
0.945	2.0	-4.0	0.01	0.04	-0.035580	0.012500	-0.036360	0.009980	-0.000080	0.012410	-2.87
0.945	2.0	-3.0	0.63	-0.07	-0.026240	0.012340	-0.026850	0.010950	0.000681	0.013060	-2.01
0.945	2.0	-2.0	1.27	-0.27	-0.016530	0.009920	-0.016860	0.009340	0.001459	0.011470	-1.44
0.945	2.0	-1.0	1.93	-0.41	-0.009500	0.010130	-0.009640	0.009960	0.001576	0.011800	-0.81
0.945	2.0	0.0	2.61	-0.58	-0.001040	0.008930	-0.000650	0.008930	0.001904	0.010940	-0.10
0.945	2.0	1.0	3.30	-0.75	0.006770	0.009040	0.006930	0.008920	0.001615	0.010750	0.63
0.945	2.0	2.0	3.97	-0.86	0.014570	0.010350	0.014890	0.009840	0.001378	0.011810	1.23
0.945	2.0	3.0	4.64	-1.04	0.024360	0.011380	0.024920	0.010090	0.000958	0.012390	1.97
0.945	2.0	4.0	5.18	-1.10	0.037120	0.013870	0.037990	0.011240	0.001141	0.015070	2.46
0.945	2.0	5.0	5.83	-1.52	0.047480	0.017250	0.048790	0.013050	-0.000105	0.017140	2.77
0.945	2.0	6.0	6.44	-1.67	0.059310	0.018870	0.060960	0.012570	-0.000559	0.018280	3.24
0.945	2.0	7.0	7.03	-1.85	0.070820	0.023690	0.073180	0.014880	-0.001413	0.022200	3.19
0.945	2.0	8.0	7.65	-1.93	0.081540	0.022480	0.083870	0.010920	-0.001874	0.020500	3.98
0.945	2.0	9.0	8.20	-2.07	0.094830	0.024050	0.097430	0.008920	-0.001144	0.022840	4.15
0.945	2.0	10.0	8.88	-2.19	0.104360	0.026200	0.107320	0.007680	-0.001425	0.024690	4.23

1.093	0.0	0.0	0.21	-0.56	-0.000200	0.011510	-0.000180	0.011510	0.001554	0.012930	-0.02
1.093	0.5	0.0	0.84	-0.56	-0.002910	0.012160	-0.002790	0.012160	0.001581	0.013610	-0.21
1.093	1.0	0.0	1.49	-0.54	-0.006390	0.014080	-0.006380	0.014080	0.001164	0.015140	-0.42
1.093	1.5	0.0	2.11	-0.54	-0.007960	0.014390	-0.007950	0.014390	0.001295	0.015570	-0.51
1.093	2.0	0.0	2.74	-0.53	-0.009510	0.011930	-0.009480	0.011930	0.001398	0.013210	-0.72
1.093	2.5	0.0	3.40	-0.49	-0.011820	0.012390	-0.011780	0.012390	0.001587	0.013840	-0.85
1.093	3.0	0.0	4.03	-0.48	-0.014230	0.012440	-0.014220	0.012440	0.001281	0.013610	-1.05
1.093	3.5	0.0	4.63	-0.50	-0.015440	0.012860	-0.015420	0.012860	0.001362	0.014100	-1.10
1.093	4.0	0.0	5.28	-0.50	-0.017980	0.015240	-0.017950	0.015240	0.000941	0.016100	-1.12
1.093	4.5	0.0	5.89	-0.51	-0.018770	0.017180	-0.018730	0.017180	0.000277	0.017430	-1.08
1.093	5.0	0.0	6.50	-0.49	-0.020270	0.015900	-0.020270	0.015900	0.001011	0.016820	-1.21
1.093	5.5	0.0	7.12	-0.49	-0.020590	0.016180	-0.020590	0.016180	0.001075	0.017170	-1.20
1.093	6.0	0.0	7.71	-0.48	-0.020500	0.018400	-0.020500	0.018400	0.000672	0.019010	-1.08
1.093	6.5	0.0	8.29	-0.54	-0.020290	0.016940	-0.020290	0.016940	0.000727	0.017610	-1.15
1.093	7.0	0.0	8.88	-0.55	-0.019300	0.020510	-0.019280	0.020510	0.000232	0.020720	-0.93
1.093	7.5	0.0	9.47	-0.57	-0.019600	0.024030	-0.019600	0.024030	-0.000433	0.023630	-0.83
1.093	8.0	0.0	10.04	-0.64	-0.018500	0.023090	-0.018470	0.023090	-0.000170	0.022940	-0.81
1.093	8.5	0.0	10.61	-0.70	-0.016600	0.023100	-0.016590	0.023100	0.000143	0.023230	-0.71
1.093	9.0	0.0	11.17	-0.75	-0.014700	0.022470	-0.014690	0.022470	0.000078	0.022540	-0.65
1.093	9.5	0.0	11.71	-0.80	-0.012970	0.024460	-0.012950	0.024460	-0.000313	0.024180	-0.54
1.093	10.0	0.0	12.35	-0.51	-0.016880	0.025320	-0.016880	0.025320	-0.000128	0.025210	-0.67

11.15 UH-1 versus CHARM

No UH-1 points were computed by CHARM

11.16 UH-1 versus RCAS

References: 1. USAAVLABS Technical Report 69-2, Wind Tunnel Investigation of Semirigid Full-Scale Rotors Operating at High Advance Ratios by Bruce Charles and Watson (Hank) Tanner January 1969
2. Harris EXCEL File: MASTER UH-1 versus RCAS.xls
3. Harris EXCEL File: MASTER UH-1 versus RCAS-Part I.xls

Airfoil	N.A.C.A. 0012
Chord	1.75 ft
Diameter	34.00 ft
Twist	-1.42 deg Washout
Disc Area	908 sq. ft
Reference Area (2 blades)	59.5 sq. ft
Nominal Solidity	0.0656
Lock Number	3.62
Flap Moment of inertia	1,584 slug ft ²

Notes: 1. Wind axis data measured. Shaft axis data derived.
2. Shaft torque derived from wind tunnel balance forces and moments.
3. Coefficients based on rotor tip speed and total blade area ($\sigma A = 59.5$ sq. ft.)
4. Teetering, under slung hub with $z/R = 0.0256$
5. Pitch bearing at $r/R = 0.0578$
6. Hub precone angle of 2.75 degrees
7. Lateral cyclic to remove lateral flapping not provided.

Table of RCAS Output

Advance Ratio	Shaft Collective		Long Cyclic	Lat Cyclic	C_L/σ	C_D/σ	C_T/σ	C_H/σ	C_Y/σ	C_Q/σ	C_{De}/σ	Rotor Alone L/De
	at 0.75R	Angle of Attack										
(deg)	(deg)	(deg)	(deg)	(deg)								
0.510	0.0	-6.0	-2.09	0.72	-0.038082	0.006064	-0.038507	0.002050	-0.000073	-0.000111	0.005846	-6.51
0.510	2.0	-6.0	-0.14	0.39	-0.024467	0.004601	-0.024814	0.002018	0.000038	0.000330	0.005249	-4.66
0.510	4.0	-6.0	1.80	0.01	-0.010465	0.003032	-0.010724	0.001921	0.000090	0.000998	0.004990	-2.10
0.510	6.0	-6.0	3.73	-0.37	0.003953	0.001422	0.003782	0.001828	0.000103	0.001899	0.005149	0.77
0.510	8.0	-6.0	5.67	-0.69	0.018514	-0.000158	0.018430	0.001779	0.000080	0.003016	0.005761	3.21
0.510	10.0	-6.0	7.72	-0.92	0.032996	-0.001806	0.033004	0.001653	-0.000064	0.004403	0.006833	4.83
0.510	12.0	-6.0	9.83	-1.05	0.046882	-0.003588	0.047000	0.001332	-0.000198	0.006054	0.008292	5.65
0.510	0.0	-4.0	-1.33	0.46	-0.024743	0.003821	-0.024949	0.002086	0.000013	0.000724	0.005243	-4.72
0.510	2.0	-4.0	0.63	0.14	-0.011240	0.002819	-0.011409	0.002028	0.000049	0.001067	0.004914	-2.29
0.510	4.0	-4.0	2.58	-0.23	0.002617	0.001706	0.002491	0.001885	0.000025	0.001652	0.004949	0.53
0.510	6.0	-4.0	4.52	-0.59	0.016907	0.000530	0.016829	0.001708	-0.000042	0.002462	0.005360	3.15
0.510	8.0	-4.0	6.45	-0.92	0.031503	-0.000636	0.031470	0.001563	-0.000167	0.003484	0.006200	5.08
0.510	10.0	-4.0	8.45	-1.15	0.045747	-0.001866	0.045766	0.001330	-0.000315	0.004763	0.007481	6.12
0.510	12.0	-4.0	10.47	-1.32	0.060051	-0.003177	0.060127	0.001020	-0.000495	0.006313	0.009212	6.52
0.510	0.0	-2.0	-0.56	0.21	-0.011291	0.002466	-0.011371	0.002071	0.000027	0.001233	0.004886	-2.31
0.510	2.0	-2.0	1.40	-0.11	0.002088	0.001961	0.002019	0.002033	-0.000004	0.001464	0.004835	0.43
0.510	4.0	-2.0	3.36	-0.46	0.015890	0.001334	0.015834	0.001888	-0.000081	0.001942	0.005145	3.09
0.510	6.0	-2.0	5.30	-0.82	0.030127	0.000606	0.030087	0.001657	-0.000240	0.002639	0.005784	5.21
0.510	8.0	-2.0	7.24	-1.13	0.044489	-0.000147	0.044467	0.001406	-0.000443	0.003561	0.006841	6.50
0.510	10.0	-2.0	9.19	-1.39	0.058931	-0.000902	0.058927	0.001155	-0.000660	0.004729	0.008378	7.03
0.510	12.0	-2.0	11.24	-1.55	0.072562	-0.001861	0.072583	0.000673	-0.000928	0.006269	0.010442	6.95
0.510	0.0	0.0	0.24	-0.05	0.001858	0.002046	0.001858	0.002046	-0.000041	0.001393	0.004780	0.39
0.510	2.0	0.0	2.19	-0.36	0.015444	0.002032	0.015444	0.002032	-0.000126	0.001517	0.005009	3.08
0.510	4.0	0.0	4.14	-0.71	0.029266	0.001890	0.029266	0.001890	-0.000264	0.001857	0.005534	5.29
0.510	6.0	0.0	6.09	-1.05	0.043390	0.001612	0.043390	0.001612	-0.000485	0.002432	0.006385	6.80
0.510	8.0	0.0	8.03	-1.36	0.057712	0.001308	0.057712	0.001308	-0.000740	0.003238	0.007663	7.53
0.510	10.0	0.0	10.00	-1.60	0.071738	0.000912	0.071738	0.000912	-0.001053	0.004387	0.009521	7.54

0.510	12.0	0.0	12.36	-1.78	0.080193	0.000129	0.080193	0.000129	-0.001633	0.006274	0.012441	6.45
0.510	0.0	2.0	1.04	-0.31	0.015059	0.002539	0.015138	0.002012	-0.000208	0.001228	0.004950	3.04
0.510	2.0	2.0	2.97	-0.63	0.028796	0.003021	0.028884	0.002014	-0.000340	0.001222	0.005419	5.31
0.510	4.0	2.0	4.92	-0.96	0.042482	0.003357	0.042573	0.001873	-0.000536	0.001445	0.006192	6.86
0.510	6.0	2.0	6.87	-1.29	0.056529	0.003548	0.056619	0.001573	-0.000807	0.001919	0.007313	7.73
0.510	8.0	2.0	8.83	-1.58	0.070585	0.003613	0.070668	0.001148	-0.001129	0.002681	0.008873	7.95
0.510	10.0	2.0	10.94	-1.77	0.081944	0.003293	0.082009	0.000431	-0.001674	0.004115	0.011369	7.21
0.510	12.0	2.0	13.60	-1.98	0.085405	0.002420	0.085437	-0.000562	-0.002240	0.006274	0.014732	5.80
0.510	0.0	4.0	1.80	-0.56	0.028671	0.004001	0.028881	0.001991	-0.000436	0.000700	0.005374	5.33
0.510	2.0	4.0	3.74	-0.90	0.042184	0.004913	0.042424	0.001958	-0.000622	0.000597	0.006084	6.93
0.510	4.0	4.0	5.69	-1.21	0.055710	0.005722	0.055973	0.001822	-0.000866	0.000720	0.007135	7.81
0.510	6.0	4.0	7.64	-1.52	0.069486	0.006352	0.069760	0.001489	-0.001182	0.001135	0.008578	8.10
0.510	8.0	4.0	9.66	-1.77	0.082165	0.006527	0.082420	0.000780	-0.001628	0.002078	0.010605	7.75
0.510	10.0	4.0	12.02	-2.01	0.088835	0.005948	0.089033	-0.000263	-0.002299	0.003918	0.013637	6.51
0.510	12.0	4.0	14.61	-2.06	0.092994	0.005218	0.093132	-0.001282	-0.002648	0.006032	0.017055	5.45
0.510	0.0	6.0	2.56	-0.82	0.042093	0.006344	0.042526	0.001910	-0.000728	-0.000151	0.006049	6.96
0.510	2.0	6.0	4.50	-1.16	0.055541	0.007677	0.056039	0.001829	-0.000959	-0.000334	0.007021	7.91
0.510	4.0	6.0	6.46	-1.46	0.068787	0.008890	0.069339	0.001651	-0.001241	-0.000266	0.008368	8.22
0.510	6.0	6.0	8.45	-1.73	0.081503	0.009743	0.082075	0.001170	-0.001612	0.000232	0.010198	7.99
0.510	8.0	6.0	10.60	-1.95	0.091154	0.009731	0.091672	0.000149	-0.002164	0.001546	0.012764	7.14
0.510	10.0	6.0	13.01	-2.14	0.096625	0.009226	0.097060	-0.000925	-0.002741	0.003545	0.016182	5.97
0.510	12.0	6.0	15.62	-2.02	0.100427	0.008339	0.100749	-0.002205	-0.002878	0.005733	0.019588	5.13
0.510	4.0	8.0	7.25	-1.69	0.081083	0.012635	0.082052	0.001227	-0.001645	-0.001379	0.009928	8.17
0.510	6.0	8.0	9.30	-1.93	0.091832	0.013436	0.092808	0.000525	-0.002101	-0.000606	0.012248	7.50
0.510	8.0	8.0	11.59	-2.13	0.098812	0.013208	0.099688	-0.000672	-0.002687	0.001079	0.015326	6.45
0.510	4.0	10.0	8.06	-1.91	0.092253	0.016773	0.093764	0.000498	-0.002121	-0.002471	0.011925	7.74
0.510	6.0	10.0	10.25	-2.11	0.100274	0.017158	0.101730	-0.000515	-0.002636	-0.001245	0.014716	6.81
0.654	10.0	-8.0	6.81	-0.58	-0.003468	0.004259	-0.004027	0.003735	0.000339	0.001833	0.007062	-0.49
0.654	0.0	-6.0	-2.74	0.84	-0.043761	0.007477	-0.044303	0.002862	0.000057	-0.000555	0.006629	-6.60
0.654	2.0	-6.0	-0.63	0.55	-0.034324	0.006379	-0.034803	0.002756	0.000019	-0.000109	0.006212	-5.53
0.654	4.0	-6.0	1.50	0.19	-0.023924	0.005302	-0.024347	0.002772	0.000072	0.000438	0.005971	-4.01
0.654	6.0	-6.0	3.61	-0.16	-0.012671	0.004188	-0.013040	0.002841	0.000124	0.001165	0.005969	-2.12
0.654	8.0	-6.0	5.70	-0.53	-0.001049	0.003187	-0.001376	0.003060	0.000122	0.002036	0.006300	-0.17

0.654	10.0	-6.0	7.81	-0.84	0.010386	0.002362	0.010082	0.003435	0.000114	0.003047	0.007021	1.48
0.654	12.0	-6.0	9.91	-1.13	0.021817	0.001529	0.021538	0.003801	0.000040	0.004250	0.008027	2.72
0.654	0.0	-4.0	-1.76	0.50	-0.028682	0.005047	-0.028964	0.003034	0.000093	0.000588	0.005946	-4.82
0.654	2.0	-4.0	0.36	0.23	-0.019474	0.004328	-0.019729	0.002959	0.000016	0.000914	0.005726	-3.40
0.654	4.0	-4.0	2.49	-0.09	-0.009498	0.003595	-0.009726	0.002924	-0.000024	0.001372	0.005693	-1.67
0.654	6.0	-4.0	4.61	-0.45	0.001350	0.002815	0.001150	0.002903	-0.000053	0.002017	0.005899	0.23
0.654	8.0	-4.0	6.72	-0.79	0.012642	0.002077	0.012466	0.002954	-0.000120	0.002813	0.006378	1.98
0.654	10.0	-4.0	8.83	-1.10	0.023918	0.001570	0.023750	0.003235	-0.000172	0.003730	0.007272	3.29
0.654	12.0	-4.0	10.93	-1.38	0.035378	0.001085	0.035217	0.003550	-0.000268	0.004828	0.008467	4.18
0.654	0.0	-2.0	-0.77	0.18	-0.013364	0.003543	-0.013480	0.003074	0.000063	0.001295	0.005523	-2.42
0.654	2.0	-2.0	1.37	-0.11	-0.004615	0.003259	-0.004726	0.003096	-0.000026	0.001462	0.005495	-0.84
0.654	4.0	-2.0	3.49	-0.42	0.004921	0.002926	0.004816	0.003096	-0.000106	0.001805	0.005685	0.87
0.654	6.0	-2.0	5.61	-0.72	0.015605	0.002524	0.015507	0.003067	-0.000166	0.002335	0.006095	2.56
0.654	8.0	-2.0	7.74	-1.07	0.026564	0.002088	0.026475	0.003014	-0.000306	0.003042	0.006739	3.94
0.654	10.0	-2.0	9.86	-1.37	0.037635	0.001866	0.037547	0.003178	-0.000449	0.003873	0.007787	4.83
0.654	12.0	-2.0	11.97	-1.64	0.048823	0.001731	0.048733	0.003434	-0.000608	0.004867	0.009172	5.32
0.654	0.0	0.0	0.23	-0.17	0.001533	0.003053	0.001533	0.003053	-0.000061	0.001521	0.005379	0.28
0.654	0.0	0.0	0.23	-0.16	0.001619	0.003053	0.001619	0.003053	-0.000062	0.001521	0.005379	0.30
0.654	2.0	0.0	2.38	-0.46	0.010147	0.003158	0.010147	0.003158	-0.000159	0.001567	0.005555	1.83
0.654	4.0	0.0	4.49	-0.76	0.019411	0.003238	0.019411	0.003238	-0.000262	0.001755	0.005921	3.28
0.654	6.0	0.0	6.64	-0.98	0.029684	0.003233	0.029684	0.003233	-0.000334	0.002176	0.006560	4.52
0.654	8.0	0.0	8.78	-1.34	0.040408	0.003141	0.040408	0.003141	-0.000522	0.002766	0.007370	5.48
0.654	10.0	0.0	10.90	-1.64	0.051291	0.003241	0.051291	0.003241	-0.000714	0.003488	0.008573	5.98
0.654	12.0	0.0	13.02	-1.89	0.061937	0.003408	0.061937	0.003408	-0.000913	0.004441	0.010198	6.07
0.654	0.0	2.0	1.24	-0.50	0.016450	0.003576	0.016564	0.003000	-0.000291	0.001294	0.005554	2.96
0.654	2.0	2.0	3.37	-0.79	0.025309	0.004038	0.025435	0.003152	-0.000399	0.001213	0.005893	4.29
0.654	4.0	2.0	5.47	-1.09	0.034562	0.004550	0.034700	0.003341	-0.000525	0.001259	0.006475	5.34
0.654	6.0	2.0	7.65	-1.27	0.044202	0.004915	0.044347	0.003369	-0.000646	0.001566	0.007309	6.05
0.654	8.0	2.0	9.79	-1.61	0.054632	0.005202	0.054781	0.003293	-0.000845	0.002039	0.008319	6.57
0.654	10.0	2.0	11.94	-1.87	0.064708	0.005480	0.064860	0.003219	-0.001036	0.002791	0.009747	6.64
0.654	12.0	2.0	14.14	-2.08	0.073379	0.005819	0.073537	0.003254	-0.001253	0.003853	0.011710	6.27
0.654	4.0	3.0	5.97	-1.22	0.042099	0.005543	0.042331	0.003332	-0.000675	0.000861	0.006859	6.14
0.654	0.0	4.0	2.23	-0.83	0.031581	0.005123	0.031861	0.002907	-0.000575	0.000587	0.006021	5.25

0.654	2.0	4.0	4.35	-1.11	0.040718	0.005930	0.041032	0.003075	-0.000707	0.000380	0.006511	6.25
0.654	4.0	4.0	6.46	-1.37	0.049870	0.006809	0.050224	0.003313	-0.000858	0.000340	0.007329	6.80
0.654	6.0	4.0	8.65	-1.57	0.058708	0.007527	0.059090	0.003413	-0.001016	0.000529	0.008336	7.04
0.654	8.0	4.0	10.82	-1.85	0.068065	0.008041	0.068460	0.003273	-0.001198	0.001039	0.009629	7.07
0.654	10.0	4.0	13.01	-2.09	0.077050	0.008436	0.077451	0.003041	-0.001465	0.001918	0.011369	6.78
0.654	12.0	4.0	15.21	-2.28	0.085252	0.008830	0.085660	0.002862	-0.001982	0.003286	0.013854	6.15
0.654	0.0	5.0	2.73	-1.00	0.039162	0.006245	0.039558	0.002808	-0.000742	0.000071	0.006353	6.16
0.654	2.0	5.0	4.87	-1.30	0.048045	0.007162	0.048486	0.002947	-0.000899	-0.000166	0.006908	6.95
0.654	4.0	5.0	6.96	-1.51	0.057367	0.008256	0.057868	0.003225	-0.001051	-0.000259	0.007861	7.30
0.654	0.0	6.0	3.21	-1.15	0.046974	0.007639	0.047515	0.002687	-0.000928	-0.000570	0.006767	6.94
0.654	2.0	6.0	5.34	-1.42	0.056037	0.008745	0.056644	0.002839	-0.001052	-0.000863	0.007426	7.55
0.654	4.0	6.0	7.47	-1.64	0.064728	0.009873	0.065406	0.003053	-0.001258	-0.000920	0.008466	7.65
0.654	6.0	6.0	9.68	-1.85	0.072463	0.010768	0.073191	0.003134	-0.001462	-0.000691	0.009711	7.46
0.654	8.0	6.0	11.86	-2.09	0.080871	0.011453	0.081625	0.002937	-0.001741	-0.000049	0.011378	7.11
0.654	10.0	6.0	14.07	-2.32	0.089066	0.011929	0.089825	0.002554	-0.002237	0.001115	0.013634	6.53
0.654	12.0	6.0	16.30	-2.48	0.096336	0.012401	0.097104	0.002263	-0.002886	0.002703	0.016534	5.83
0.654	0.0	7.0	3.70	-1.31	0.054583	0.009242	0.055303	0.002521	-0.001133	-0.001306	0.007246	7.53
0.654	2.0	7.0	5.84	-1.61	0.063331	0.010401	0.064127	0.002605	-0.001297	-0.001575	0.007992	7.92
0.654	4.0	7.0	7.97	-1.77	0.071867	0.011631	0.072749	0.002785	-0.001468	-0.001614	0.009163	7.84
0.654	6.0	7.0	10.18	-1.99	0.079209	0.012580	0.080152	0.002833	-0.001705	-0.001321	0.010560	7.50
0.654	0.0	8.0	4.19	-1.45	0.062113	0.011047	0.063046	0.002295	-0.001340	-0.002121	0.007805	7.96
0.654	2.0	8.0	6.34	-1.74	0.070560	0.012240	0.071577	0.002301	-0.001494	-0.002330	0.008678	8.13
0.654	4.0	8.0	8.49	-1.93	0.078685	0.013463	0.079793	0.002381	-0.001698	-0.002305	0.009939	7.92
0.654	6.0	8.0	10.69	-2.13	0.085891	0.014493	0.087072	0.002399	-0.002015	-0.001923	0.011554	7.43
0.654	8.0	8.0	12.91	-2.36	0.093134	0.015280	0.094354	0.002170	-0.002512	-0.001023	0.013716	6.79
0.757	0.0	-6.0	-3.12	0.84	-0.049157	0.008683	-0.049795	0.003497	0.000223	-0.000916	0.007473	-6.58
0.757	2.0	-6.0	-0.90	0.58	-0.042999	0.007895	-0.043588	0.003358	0.000046	-0.000512	0.007219	-5.96
0.757	4.0	-6.0	1.29	0.27	-0.034511	0.007088	-0.035063	0.003441	0.000013	-0.000015	0.007067	-4.88
0.757	6.0	-6.0	3.47	-0.06	-0.024769	0.006269	-0.025289	0.003646	0.000030	0.000612	0.007078	-3.50
0.757	8.0	-6.0	5.64	-0.41	-0.014573	0.005649	-0.015084	0.004094	0.000060	0.001321	0.007394	-1.97
0.757	10.0	-6.0	7.75	-0.68	-0.003562	0.005366	-0.004103	0.004964	0.000233	0.002086	0.008121	-0.44
0.757	12.0	-6.0	9.96	-0.91	0.005960	0.005271	0.005377	0.005865	0.000283	0.002979	0.009206	0.65
0.757	0.0	-4.0	-2.01	0.47	-0.032496	0.006136	-0.032845	0.003855	0.000192	0.000429	0.006703	-4.85

0.757	2.0	-4.0	0.21	0.25	-0.026447	0.005600	-0.026774	0.003741	-0.000009	0.000761	0.006605	-4.00
0.757	4.0	-4.0	2.42	-0.02	-0.019123	0.005128	-0.019434	0.003781	-0.000097	0.001143	0.006637	-2.88
0.757	6.0	-4.0	4.61	-0.34	-0.009962	0.004604	-0.010259	0.003897	-0.000151	0.001681	0.006824	-1.46
0.757	8.0	-4.0	6.75	-0.71	0.000386	0.004127	0.000097	0.004144	-0.000240	0.002340	0.007218	0.05
0.757	10.0	-4.0	8.90	-0.91	0.010866	0.004066	0.010555	0.004814	0.000023	0.003040	0.008081	1.34
0.757	12.0	-4.0	11.12	-1.16	0.020303	0.004267	0.019956	0.005673	0.000056	0.003814	0.009304	2.18
0.757	0.0	-2.0	-0.90	0.12	-0.015387	0.004502	-0.015535	0.003962	0.000093	0.001305	0.006225	-2.47
0.757	2.0	-2.0	1.34	-0.12	-0.009929	0.004360	-0.010075	0.004011	-0.000066	0.001450	0.006275	-1.58
0.757	4.0	-2.0	3.56	-0.37	-0.003542	0.004255	-0.003688	0.004129	-0.000168	0.001691	0.006488	-0.55
0.757	6.0	-2.0	5.75	-0.69	0.005264	0.004097	0.005118	0.004278	-0.000248	0.002075	0.006837	0.77
0.757	8.0	-2.0	7.83	-1.06	0.016120	0.004002	0.015971	0.004562	-0.000352	0.002557	0.007379	2.18
0.757	10.0	-2.0	10.06	-1.14	0.025591	0.004102	0.025432	0.004992	-0.000071	0.003253	0.008398	3.05
0.757	12.0	-2.0	12.28	-1.40	0.034867	0.004575	0.034687	0.005789	-0.000118	0.003928	0.009763	3.57
0.757	0.0	0.0	0.23	-0.26	0.001356	0.003941	0.001356	0.003941	-0.000079	0.001595	0.006048	0.22
0.757	2.0	0.0	2.47	-0.49	0.006646	0.004165	0.006646	0.004165	-0.000186	0.001574	0.006243	1.06
0.757	4.0	0.0	4.70	-0.74	0.012434	0.004462	0.012434	0.004462	-0.000253	0.001617	0.006597	1.88
0.757	6.0	0.0	6.87	-1.06	0.020868	0.004717	0.020868	0.004717	-0.000309	0.001793	0.007085	2.95
0.757	8.0	0.0	8.82	-1.30	0.032906	0.005276	0.032906	0.005276	-0.000316	0.002113	0.008066	4.08
0.757	10.0	0.0	11.26	-1.34	0.040021	0.005392	0.040021	0.005392	-0.000097	0.002841	0.009144	4.38
0.757	12.0	0.0	13.49	-1.60	0.048665	0.006126	0.048665	0.006126	-0.000160	0.003453	0.010687	4.55
0.757	0.0	2.0	1.36	-0.62	0.018088	0.004503	0.018234	0.003869	-0.000345	0.001306	0.006227	2.90
0.757	2.0	2.0	3.58	-0.86	0.023691	0.005022	0.023852	0.004192	-0.000409	0.001133	0.006518	3.63
0.757	4.0	2.0	5.81	-1.11	0.029330	0.005712	0.029511	0.004685	-0.000438	0.000990	0.007019	4.18
0.757	6.0	2.0	7.97	-1.43	0.037208	0.006437	0.037410	0.005134	-0.000436	0.000946	0.007686	4.84
0.757	8.0	2.0	9.99	-1.38	0.047611	0.007568	0.047846	0.005901	-0.000416	0.001437	0.009465	5.03
0.757	10.0	2.0	12.41	-1.57	0.054547	0.007782	0.054785	0.005874	-0.000340	0.001971	0.010386	5.25
0.757	12.0	2.0	14.65	-1.81	0.062857	0.008541	0.063116	0.006342	-0.000654	0.002818	0.012262	5.13
0.757	0.0	4.0	2.46	-0.97	0.035221	0.006201	0.035568	0.003729	-0.000629	0.000411	0.006743	5.22
0.757	2.0	4.0	4.70	-1.21	0.040824	0.006925	0.041208	0.004061	-0.000666	0.000128	0.007094	5.75
0.757	4.0	4.0	6.92	-1.46	0.046465	0.007916	0.046904	0.004656	-0.000640	-0.000128	0.007748	6.00
0.757	6.0	4.0	8.99	-1.79	0.054697	0.009185	0.055205	0.005347	-0.000606	-0.000338	0.008738	6.26
0.757	8.0	4.0	11.19	-1.58	0.062107	0.010538	0.062691	0.006180	-0.000744	0.000301	0.010936	5.68
0.757	10.0	4.0	13.54	-1.83	0.069222	0.010913	0.069814	0.006058	-0.001002	0.000987	0.012217	5.67

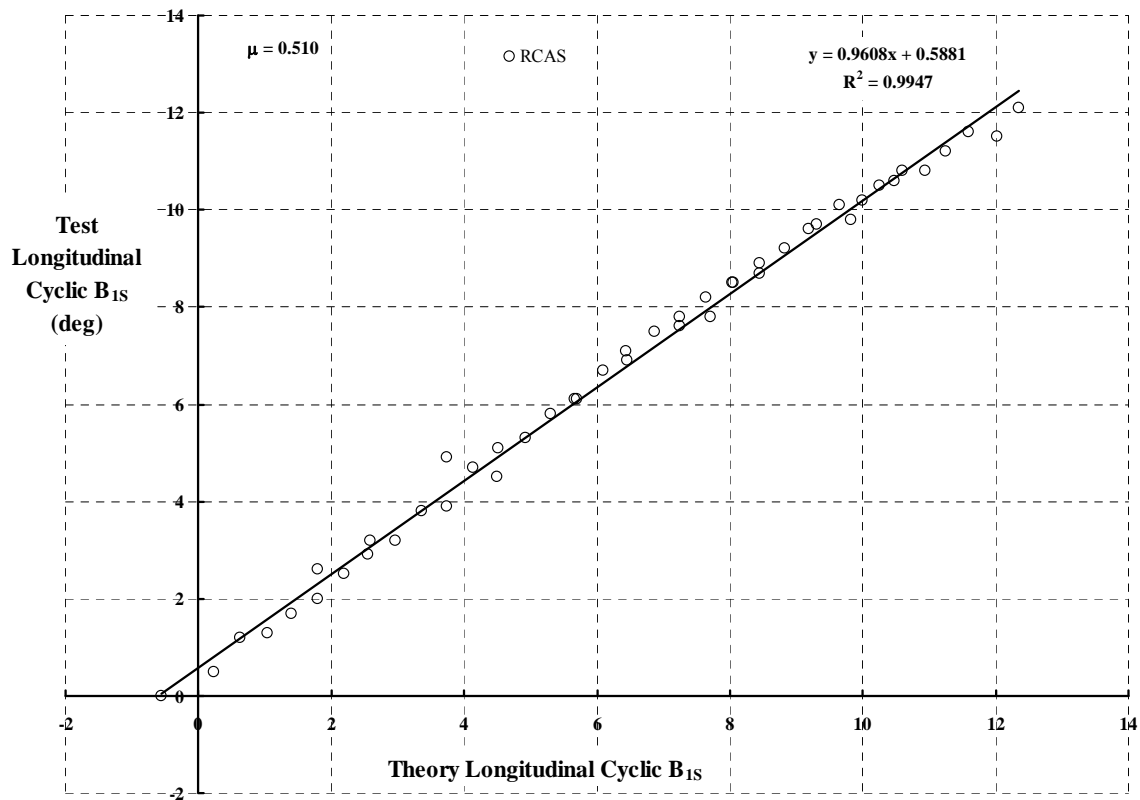
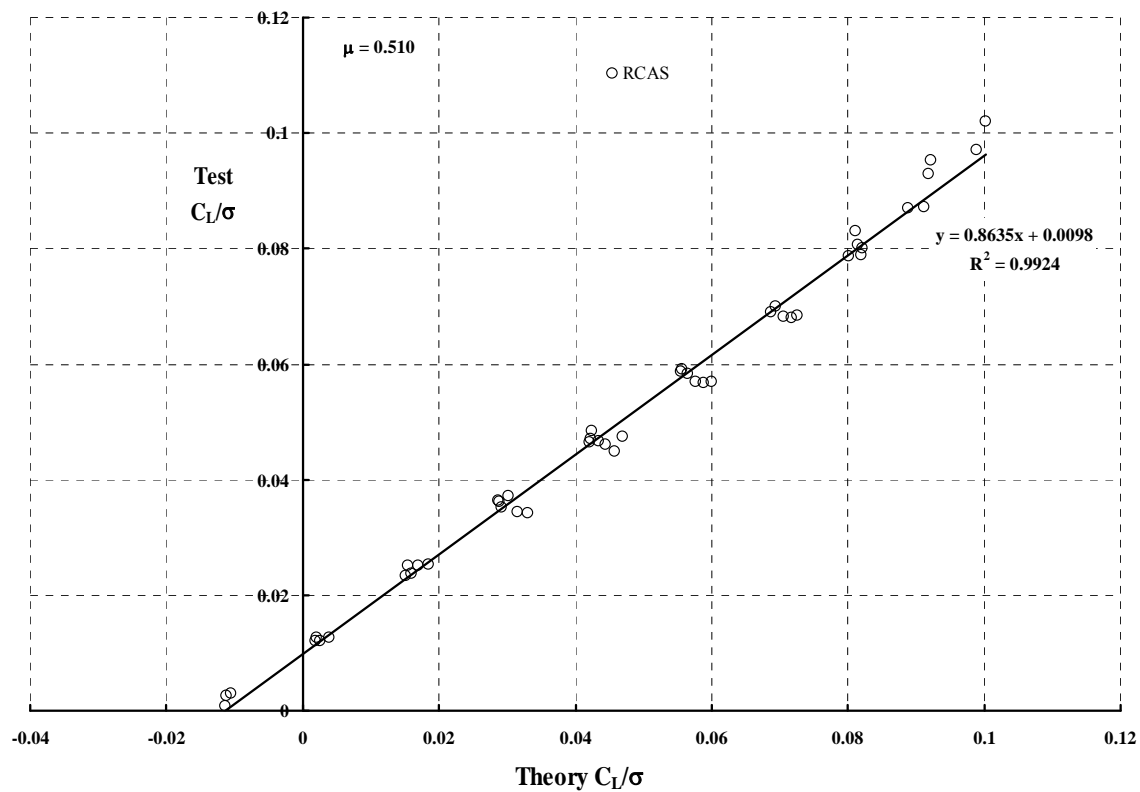
0.757	12.0	4.0	15.77	-2.04	0.077305	0.011649	0.077930	0.006228	-0.001534	0.002138	0.014474	5.34
0.757	0.0	6.0	3.58	-1.34	0.051996	0.008799	0.052631	0.003315	-0.000965	-0.000945	0.007550	6.89
0.757	2.0	6.0	5.81	-1.58	0.057603	0.009695	0.058301	0.003621	-0.000992	-0.001278	0.008007	7.19
0.757	4.0	6.0	8.03	-1.84	0.063305	0.010875	0.064095	0.004198	-0.000939	-0.001558	0.008818	7.18
0.757	6.0	6.0	9.97	-2.04	0.072902	0.012822	0.073843	0.005131	-0.001147	-0.001632	0.010666	6.83
0.757	8.0	6.0	12.35	-1.86	0.077010	0.013937	0.078045	0.005811	-0.001516	-0.000882	0.012772	6.03
0.757	10.0	6.0	14.67	-2.09	0.083321	0.014502	0.084381	0.005713	-0.001920	0.000024	0.014535	5.73
0.757	12.0	6.0	16.98	-2.36	0.088478	0.015041	0.089566	0.005710	-0.002630	0.001678	0.017257	5.13
0.757	0.0	8.0	4.68	-1.67	0.068700	0.012269	0.069739	0.002588	-0.001316	-0.002697	0.008706	7.89
0.757	2.0	8.0	6.92	-1.92	0.074350	0.013320	0.075480	0.002843	-0.001313	-0.003020	0.009332	7.97
0.856	10.0	-8.0	6.54	-0.34	-0.035154	0.011731	-0.036444	0.006724	0.000386	-0.000946	0.010625	-3.31
0.856	0.0	-6.0	-3.40	0.80	-0.055805	0.009929	-0.056537	0.004041	0.000448	-0.001211	0.008515	-6.55
0.856	2.0	-6.0	-1.11	0.59	-0.052663	0.009435	-0.053361	0.003879	0.000088	-0.000854	0.008438	-6.24
0.856	4.0	-6.0	1.13	0.32	-0.045996	0.008970	-0.046681	0.004113	-0.000061	-0.000462	0.008430	-5.46
0.856	6.0	-6.0	3.35	0.03	-0.037631	0.008502	-0.038313	0.004522	-0.000104	0.000027	0.008533	-4.41
0.856	8.0	-6.0	5.57	-0.28	-0.028707	0.008269	-0.029414	0.005223	-0.000069	0.000567	0.008932	-3.21
0.856	10.0	-6.0	7.78	-0.65	-0.019911	0.008650	-0.020706	0.006522	-0.000068	0.001053	0.009880	-2.02
0.856	12.0	-6.0	9.74	-0.92	-0.006751	0.009134	-0.007669	0.008378	0.000197	0.001682	0.011098	-0.61
0.856	8.0	-6.0	5.57	-0.28	-0.028768	0.008279	-0.029476	0.005226	-0.000071	0.000561	0.008934	-3.22
0.856	0.0	-4.0	-2.19	0.40	-0.037061	0.007283	-0.037479	0.004680	0.000312	0.000299	0.007633	-4.86
0.856	2.0	-4.0	0.10	0.24	-0.034577	0.006982	-0.034980	0.004553	-0.000053	0.000600	0.007683	-4.50
0.856	4.0	-4.0	2.36	-0.01	-0.029487	0.006785	-0.029889	0.004712	-0.000227	0.000900	0.007836	-3.76
0.856	6.0	-4.0	4.60	-0.29	-0.021893	0.006572	-0.022298	0.005029	-0.000313	0.001298	0.008088	-2.71
0.856	8.0	-4.0	6.82	-0.59	-0.013323	0.006439	-0.013740	0.005493	-0.000357	0.001789	0.008528	-1.56
0.856	10.0	-4.0	9.00	-1.00	-0.004341	0.006895	-0.004811	0.006575	-0.000463	0.002196	0.009460	-0.46
0.856	12.0	-4.0	10.95	-1.10	0.008900	0.007741	0.008339	0.008343	0.000166	0.002770	0.010977	0.81
0.856	0.0	-2.0	-0.99	0.02	-0.017826	0.005564	-0.018010	0.004939	0.000126	0.001295	0.007077	-2.52
0.856	2.0	-2.0	1.32	-0.16	-0.016003	0.005590	-0.016189	0.005028	-0.000129	0.001411	0.007238	-2.21
0.856	4.0	-2.0	3.60	-0.36	-0.012602	0.005742	-0.012795	0.005299	-0.000280	0.001543	0.007545	-1.67
0.856	6.0	-2.0	5.85	-0.63	-0.005768	0.005880	-0.005970	0.005675	-0.000334	0.001766	0.007943	-0.73
0.856	8.0	-2.0	8.07	-0.95	0.002562	0.006041	0.002350	0.006127	-0.000406	0.002086	0.008477	0.30
0.856	10.0	-2.0	10.12	-1.42	0.012984	0.006602	0.012745	0.007051	-0.000595	0.002346	0.009342	1.39
0.856	12.0	-2.0	12.15	-1.31	0.024805	0.007854	0.024516	0.008715	0.000192	0.002979	0.011335	2.19

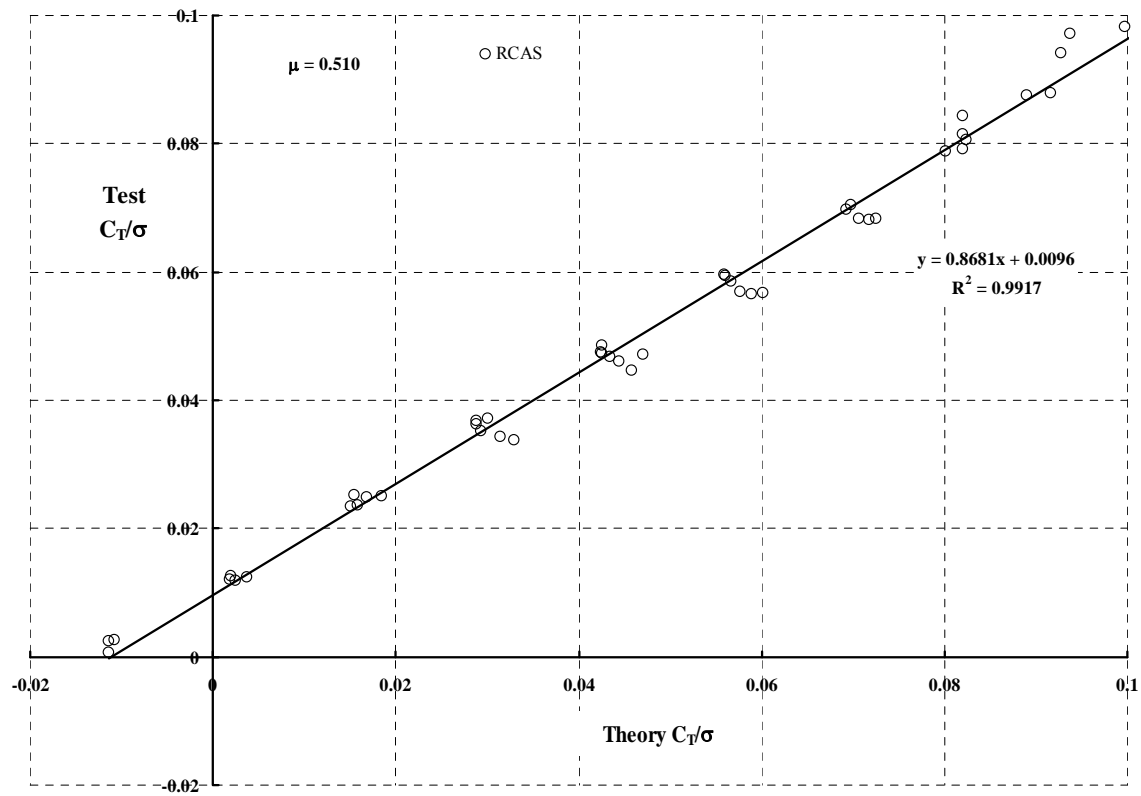
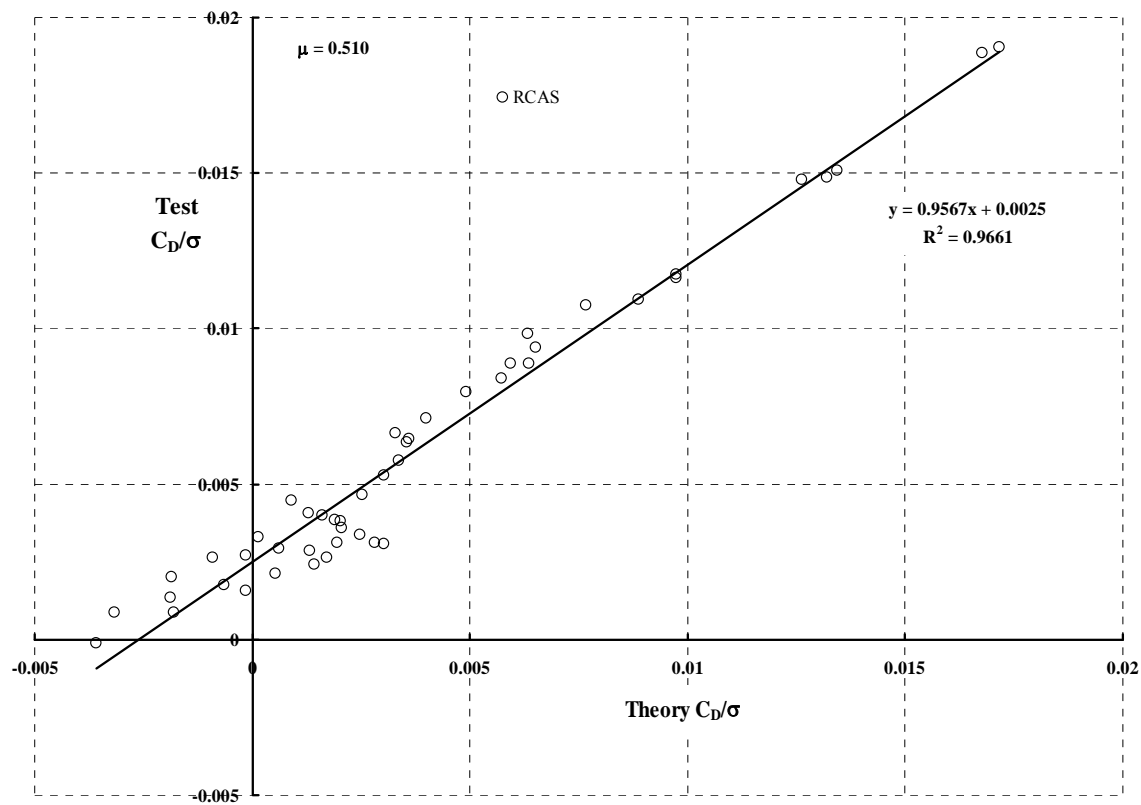
0.856	0.0	0.0	0.22	-0.38	0.001242	0.004941	0.001242	0.004941	-0.000105	0.001643	0.006861	0.18
0.856	2.0	0.0	2.53	-0.57	0.002800	0.005307	0.002800	0.005307	-0.000234	0.001547	0.007115	0.39
0.856	4.0	0.0	4.83	-0.76	0.004912	0.005863	0.004912	0.005863	-0.000295	0.001436	0.007541	0.65
0.856	6.0	0.0	7.09	-1.00	0.010643	0.006404	0.010643	0.006404	-0.000282	0.001408	0.008049	1.32
0.856	8.0	0.0	9.30	-1.36	0.018605	0.006959	0.018605	0.006959	-0.000299	0.001466	0.008672	2.15
0.856	10.0	0.0	11.11	-1.64	0.032169	0.008457	0.032169	0.008457	-0.000364	0.001659	0.010395	3.09
0.856	12.0	0.0	13.31	-1.58	0.041177	0.009413	0.041177	0.009413	0.000010	0.002499	0.012332	3.34
0.856	0.0	2.0	1.44	-0.78	0.020149	0.005535	0.020330	0.004828	-0.000412	0.001297	0.007050	2.86
0.856	2.0	2.0	3.74	-0.96	0.022081	0.006119	0.022281	0.005345	-0.000417	0.001032	0.007325	3.01
0.856	4.0	2.0	6.04	-1.15	0.024004	0.007045	0.024235	0.006203	-0.000378	0.000697	0.007859	3.05
0.856	6.0	2.0	8.32	-1.38	0.027973	0.008013	0.028236	0.007032	-0.000275	0.000421	0.008505	3.29
0.856	8.0	2.0	10.46	-1.78	0.036046	0.009000	0.036338	0.007736	-0.000295	0.000286	0.009333	3.86
0.856	10.0	2.0	12.05	-1.86	0.052756	0.011646	0.053130	0.009798	-0.000678	0.001058	0.012882	4.10
0.856	12.0	2.0	14.46	-1.80	0.057948	0.011921	0.058329	0.009891	-0.000622	0.001904	0.014145	4.10
0.856	0.0	4.0	2.64	-1.17	0.039176	0.007275	0.039588	0.004525	-0.000696	0.000291	0.007616	5.14
0.856	2.0	4.0	4.95	-1.36	0.041174	0.007963	0.041629	0.005071	-0.000631	-0.000079	0.007870	5.23
0.856	4.0	4.0	7.25	-1.55	0.043091	0.009105	0.043621	0.006077	-0.000498	-0.000516	0.008502	5.07
0.856	6.0	4.0	9.52	-1.79	0.046244	0.010361	0.046855	0.007110	-0.000396	-0.000855	0.009363	4.94
0.856	8.0	4.0	11.51	-2.16	0.055064	0.012160	0.055778	0.008289	-0.000660	-0.000932	0.011072	4.97
0.856	10.0	4.0	12.87	-2.02	0.073880	0.015787	0.074801	0.010595	-0.001185	0.000423	0.016281	4.54
0.856	12.0	4.0	15.62	-1.99	0.073971	0.015364	0.074862	0.010166	-0.001438	0.001083	0.016629	4.45
0.856	0.0	6.0	3.84	-1.54	0.058286	0.010002	0.059012	0.003855	-0.000975	-0.001262	0.008528	6.83
0.856	2.0	6.0	6.14	-1.74	0.060523	0.010769	0.061317	0.004384	-0.000863	-0.001657	0.008833	6.85
0.856	4.0	6.0	8.44	-1.94	0.062517	0.011937	0.063423	0.005337	-0.000726	-0.002014	0.009584	6.52
0.856	6.0	6.0	10.70	-2.21	0.065076	0.013290	0.066109	0.006415	-0.000755	-0.002171	0.010754	6.05
0.856	8.0	6.0	12.55	-2.43	0.073959	0.016152	0.075242	0.008333	-0.001401	-0.001608	0.014274	5.18
0.856	10.0	6.0	13.74	-1.98	0.092393	0.020479	0.094028	0.010709	-0.001670	-0.000465	0.019936	4.63
0.856	12.0	6.0	16.87	-2.27	0.085882	0.019157	0.087413	0.010075	-0.002467	0.000865	0.020167	4.26
0.856	0.0	8.0	5.03	-1.91	0.077240	0.013656	0.078389	0.002774	-0.001309	-0.003268	0.009839	7.85
0.856	4.0	8.0	9.63	-2.33	0.081371	0.015447	0.082729	0.003972	-0.001142	-0.003633	0.011203	7.26
0.943	0.0	0.0	0.23	-0.38	0.000874	0.005939	0.000874	0.005939	-0.000121	0.001664	0.007704	0.11
0.943	2.0	0.0	2.59	-0.51	-0.001353	0.006467	-0.001353	0.006467	-0.000271	0.001497	0.008054	-0.17
0.943	4.0	0.0	4.93	-0.65	-0.002878	0.007280	-0.002878	0.007280	-0.000344	0.001255	0.008611	-0.33

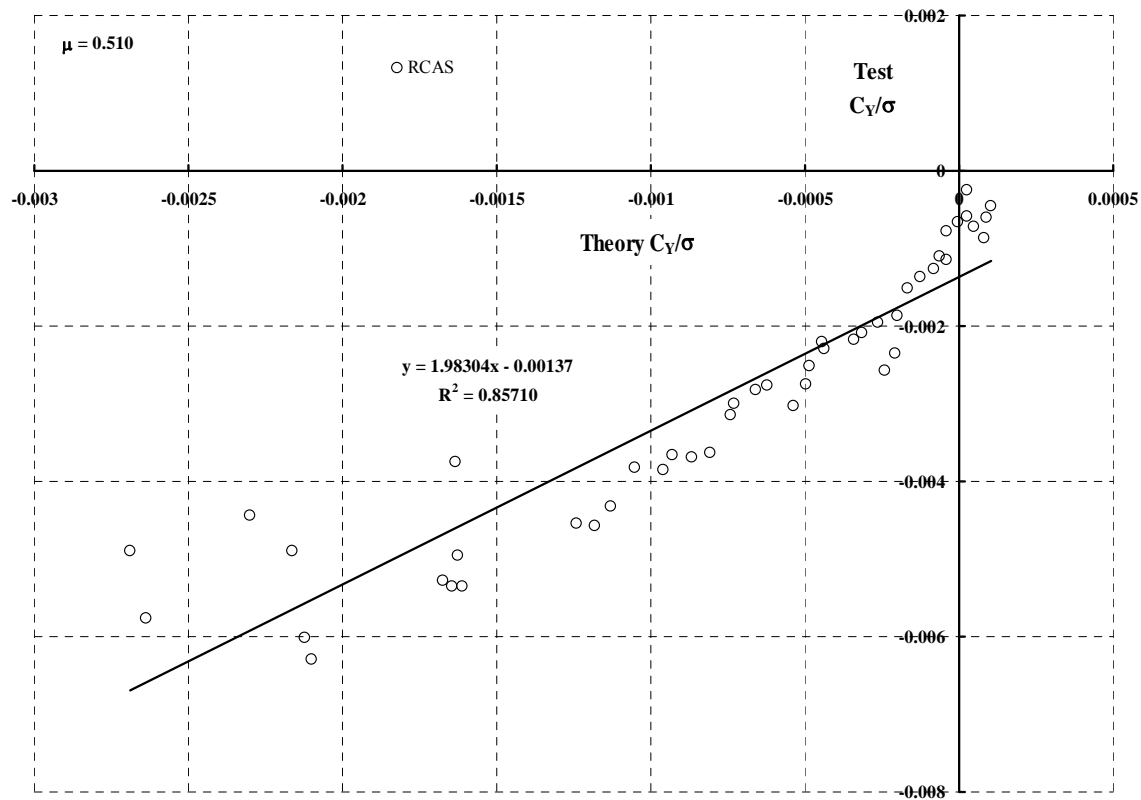
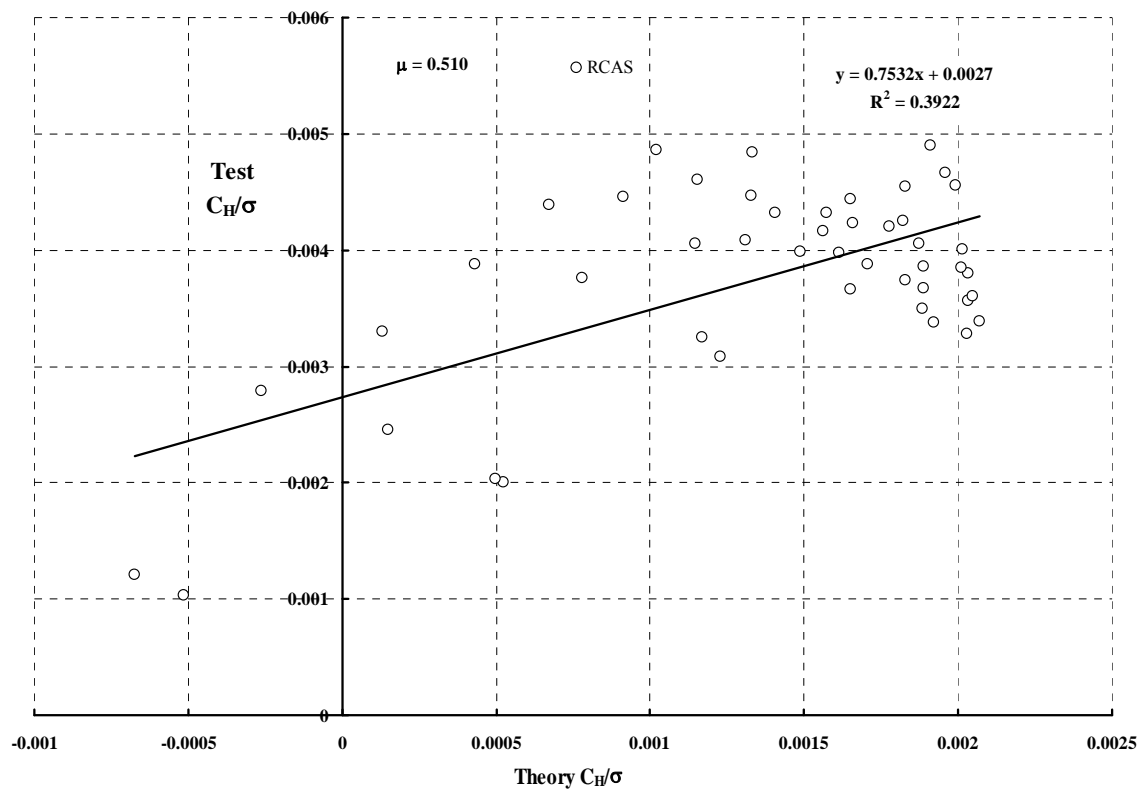
0.943	6.0	0.0	7.22	-0.86	0.000927	0.008129	0.000927	0.008129	-0.000294	0.001036	0.009227	0.10
0.943	8.0	0.0	9.43	-1.22	0.008098	0.009062	0.008098	0.009062	-0.000250	0.000831	0.009943	0.81
0.943	10.0	0.0	11.15	-1.49	0.022898	0.011272	0.022898	0.011272	-0.000023	0.000778	0.012097	1.89
0.943	12.0	0.0	13.43	-1.36	0.030001	0.012239	0.030001	0.012239	0.000438	0.001507	0.013837	2.17
0.943	8.0	1.0	10.04	-1.48	0.017537	0.009906	0.017707	0.009599	-0.000146	0.000239	0.010160	1.73
0.943	0.0	2.0	1.51	-0.80	0.022308	0.006537	0.022522	0.005754	-0.000446	0.001300	0.007915	2.82
0.943	2.0	2.0	3.85	-0.93	0.020622	0.007182	0.020860	0.006458	-0.000398	0.000979	0.008220	2.51
0.943	4.0	2.0	6.21	-1.08	0.018465	0.008294	0.018743	0.007645	-0.000315	0.000527	0.008852	2.09
0.943	6.0	2.0	8.51	-1.29	0.020127	0.009583	0.020449	0.008875	-0.000145	0.000027	0.009612	2.09
0.943	8.0	2.0	10.62	-1.71	0.027264	0.010997	0.027632	0.010039	-0.000125	-0.000353	0.010623	2.57
0.943	10.0	2.0	12.02	-1.70	0.047443	0.014569	0.047922	0.012905	-0.000137	0.000174	0.014754	3.22
0.943	12.0	2.0	14.64	-1.58	0.048206	0.014587	0.048686	0.012896	-0.000240	0.000816	0.015453	3.12
0.943	0.0	4.0	2.78	-1.23	0.043885	0.008286	0.044357	0.005205	-0.000730	0.000260	0.008562	5.13
0.943	2.0	4.0	5.12	-1.37	0.042328	0.008933	0.042848	0.005959	-0.000572	-0.000147	0.008777	4.82
0.943	4.0	4.0	7.47	-1.51	0.040578	0.010211	0.041192	0.007356	-0.000335	-0.000695	0.009475	4.28
0.943	6.0	4.0	9.77	-1.74	0.040797	0.011739	0.041516	0.008864	-0.000159	-0.001212	0.010454	3.90
0.943	8.0	4.0	11.68	-2.07	0.048745	0.014441	0.049633	0.011005	-0.000204	-0.001402	0.012954	3.76
0.943	10.0	4.0	12.86	-1.71	0.070005	0.018498	0.071124	0.013570	-0.000454	-0.000696	0.017761	3.94
0.943	12.0	4.0	15.85	-1.77	0.065703	0.018010	0.066799	0.013383	-0.001129	-0.000141	0.017861	3.68
0.943	2.0	5.0	5.75	-1.57	0.053346	0.010210	0.054033	0.005522	-0.000662	-0.000920	0.009235	5.78
0.943	4.0	5.0	8.09	-1.73	0.051699	0.011477	0.052503	0.006928	-0.000400	-0.001426	0.009965	5.19
0.943	6.0	5.0	10.37	-1.98	0.051816	0.013091	0.052760	0.008525	-0.000239	-0.001868	0.011111	4.66
0.943	0.0	6.0	4.03	-1.64	0.065490	0.011102	0.066292	0.004196	-0.001004	-0.001406	0.009612	6.81
0.943	2.0	6.0	6.37	-1.78	0.064314	0.011711	0.065186	0.004924	-0.000771	-0.001779	0.009825	6.55
0.943	4.0	6.0	8.71	-1.94	0.062796	0.012926	0.063803	0.006291	-0.000492	-0.002195	0.010598	5.93
0.943	6.0	6.0	10.99	-2.22	0.062453	0.014564	0.063633	0.007956	-0.000415	-0.002486	0.011928	5.24
0.943	8.0	6.0	12.74	-2.44	0.070974	0.018509	0.072520	0.010989	-0.001087	-0.001846	0.016552	4.29
0.943	10.0	6.0	13.95	-1.73	0.087643	0.022563	0.089521	0.013278	-0.001227	-0.001549	0.020920	4.19
0.943	12.0	6.0	17.09	-2.05	0.079841	0.021672	0.081669	0.013207	-0.002032	-0.000132	0.021531	3.71
0.943	2.0	7.0	7.00	-1.99	0.075222	0.013455	0.076301	0.004188	-0.000904	-0.002734	0.010557	7.13
0.943	4.0	7.0	9.33	-2.16	0.073812	0.014579	0.075039	0.005475	-0.000646	-0.003017	0.011381	6.49
0.943	2.0	8.0	7.62	-2.19	0.086057	0.015413	0.087365	0.003287	-0.001055	-0.003746	0.011442	7.52
0.943	4.0	8.0	9.96	-2.37	0.084622	0.016426	0.086084	0.004489	-0.000839	-0.003856	0.012338	6.86

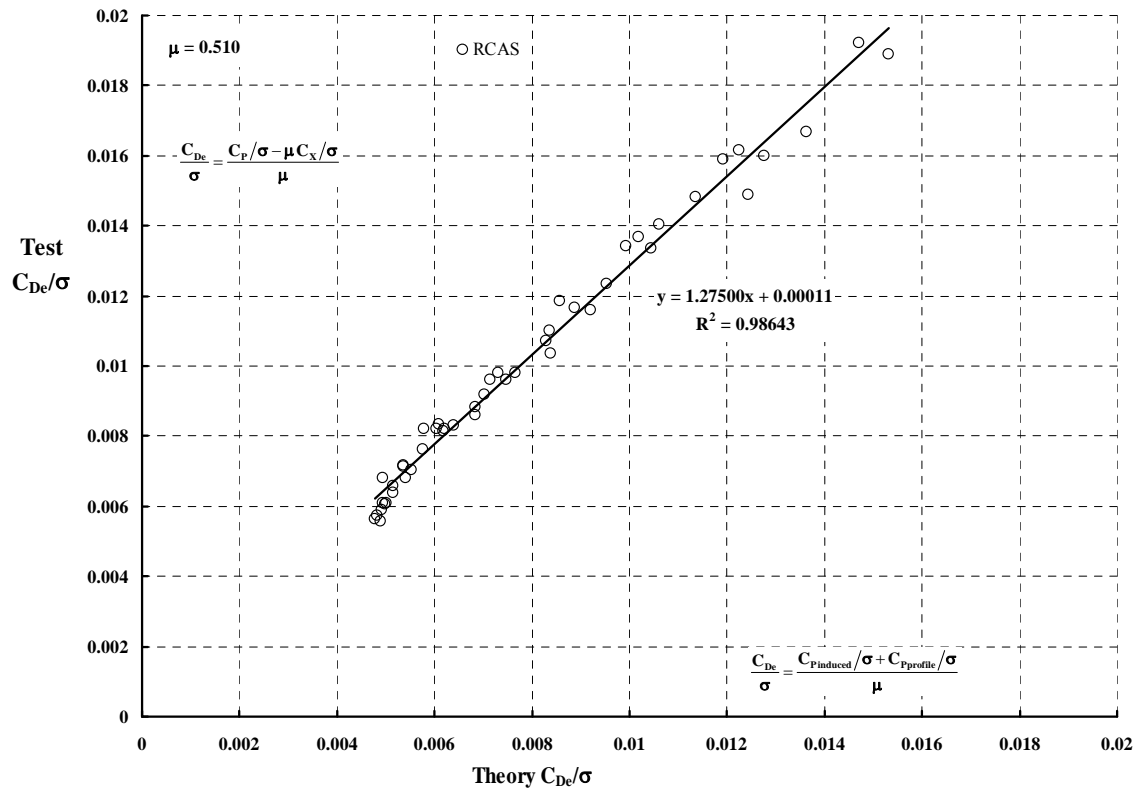
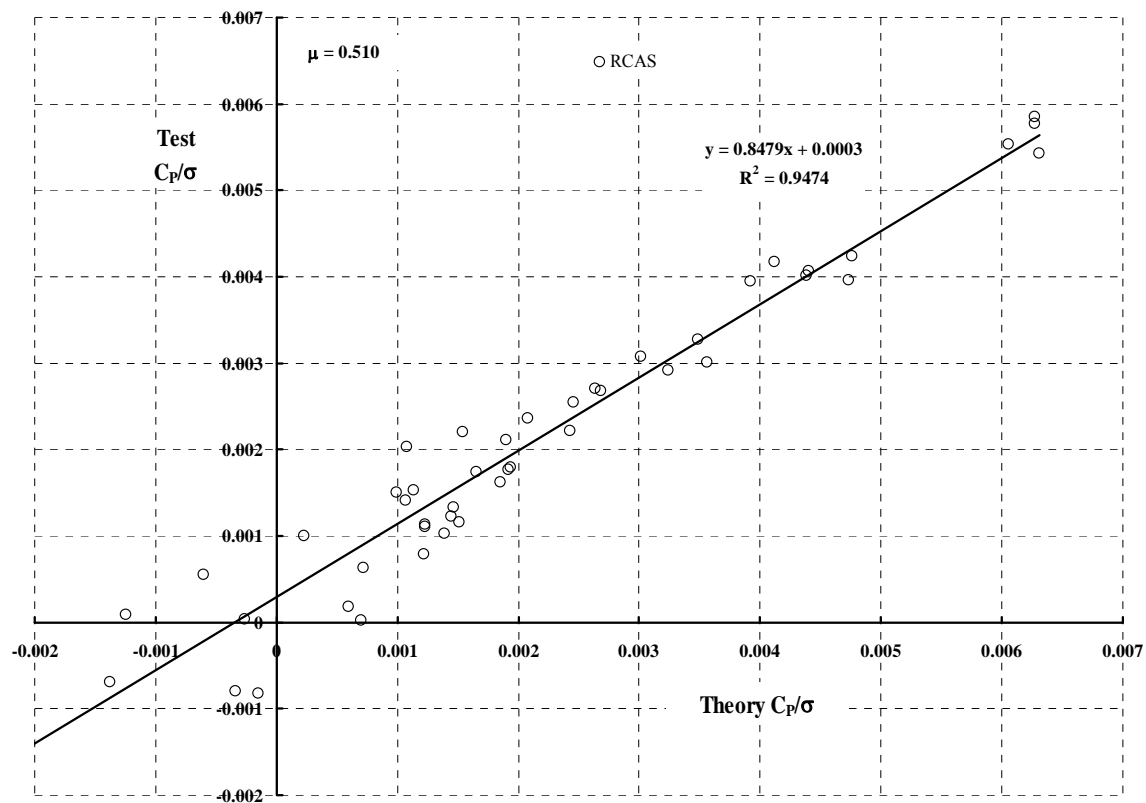
1.093	2.0	-1.0	2.02	-0.12	-0.024898	0.009011	-0.025052	0.008575	-0.000385	0.001270	0.010173	-2.45
1.093	0.0	0.0	0.25	-0.38	-0.000311	0.007934	-0.000311	0.007934	-0.000150	0.001638	0.009433	-0.03
1.093	1.0	0.0	1.46	-0.36	-0.005410	0.008315	-0.005410	0.008315	-0.000245	0.001488	0.009678	-0.56
1.093	2.0	0.0	2.69	-0.39	-0.010860	0.008853	-0.010860	0.008853	-0.000343	0.001283	0.010027	-1.08
1.093	2.0	0.0	2.68	-0.38	-0.010830	0.008853	-0.010830	0.008853	-0.000346	0.001282	0.010026	-1.08
1.093	3.0	0.0	3.90	-0.40	-0.015965	0.009509	-0.015965	0.009509	-0.000422	0.001023	0.010445	-1.53
1.093	4.0	0.0	5.10	-0.39	-0.019651	0.010272	-0.019651	0.010272	-0.000449	0.000704	0.010916	-1.80
1.093	4.0	0.0	5.11	-0.40	-0.020001	0.010270	-0.020001	0.010270	-0.000448	0.000709	0.010918	-1.83
1.093	5.0	0.0	6.27	-0.44	-0.020216	0.011015	-0.020216	0.011015	-0.000406	0.000391	0.011373	-1.78
1.093	6.0	0.0	7.42	-0.53	-0.018884	0.011783	-0.018884	0.011783	-0.000319	0.000067	0.011844	-1.59
1.093	6.0	0.0	7.42	-0.53	-0.018958	0.011780	-0.018958	0.011780	-0.000319	0.000069	0.011844	-1.60
1.093	7.0	0.0	8.56	-0.66	-0.016732	0.012596	-0.016732	0.012596	-0.000206	-0.000275	0.012344	-1.36
1.093	8.0	0.0	9.67	-0.87	-0.013509	0.013445	-0.013509	0.013445	-0.000144	-0.000621	0.012877	-1.05
1.093	10.0	0.0	11.31	-1.41	-0.000556	0.016916	-0.000556	0.016916	0.000329	-0.001257	0.015765	-0.04
1.093	12.0	0.0	13.24	-1.04	0.012351	0.020089	0.012351	0.020089	0.002061	-0.000474	0.019655	0.63
1.093	2.0	1.0	3.35	-0.64	0.003324	0.008934	0.003480	0.008875	-0.000335	0.001165	0.010000	0.33
1.093	6.0	1.0	8.11	-0.79	-0.007526	0.012165	-0.007312	0.012294	-0.000115	-0.000301	0.011889	-0.63
1.093	1.0	2.0	2.80	-0.90	0.022638	0.008733	0.022929	0.007938	-0.000435	0.001149	0.009785	2.31
1.093	0.0	2.0	1.59	-0.90	0.027506	0.008527	0.027787	0.007562	-0.000511	0.001277	0.009696	2.84
1.093	2.0	2.0	4.01	-0.91	0.017711	0.009288	0.018024	0.008664	-0.000353	0.000883	0.010096	1.75
1.093	4.0	2.0	6.42	-0.93	0.008071	0.010908	0.008447	0.010620	-0.000174	0.000111	0.011010	0.73
1.093	6.0	2.0	8.79	-1.05	0.004575	0.012748	0.005017	0.012581	0.000060	-0.000754	0.012058	0.38
1.093	8.0	2.0	10.95	-1.49	0.009634	0.014882	0.010148	0.014537	0.000144	-0.001636	0.013385	0.72
1.093	10.0	2.0	12.03	-1.67	0.031644	0.021571	0.032378	0.020454	0.001043	-0.000954	0.020699	1.53
1.093	12.0	2.0	14.40	-1.38	0.034805	0.022740	0.035577	0.021511	0.001671	-0.000520	0.022264	1.56
1.093	2.0	3.0	4.67	-1.16	0.031951	0.009917	0.032426	0.008231	-0.000368	0.000445	0.010323	3.09
1.093	1.0	4.0	4.12	-1.42	0.050706	0.010394	0.051308	0.006832	-0.000627	0.000099	0.010485	4.84
1.093	0.0	4.0	2.91	-1.42	0.055502	0.010298	0.056085	0.006401	-0.000778	0.000254	0.010530	5.27
1.093	2.0	4.0	5.33	-1.42	0.045950	0.010837	0.046594	0.007605	-0.000401	-0.000159	0.010692	4.30
1.093	4.0	4.0	7.75	-1.45	0.036293	0.012419	0.037071	0.009857	0.000027	-0.000916	0.011581	3.13
1.093	6.0	4.0	10.11	-1.60	0.030147	0.014511	0.031086	0.012373	0.000330	-0.001829	0.012837	2.35
1.093	8.0	4.0	12.05	-2.00	0.034251	0.018064	0.035428	0.015631	0.000140	-0.002443	0.015828	2.16
1.093	10.0	4.0	12.56	-1.47	0.064253	0.026588	0.065951	0.022041	0.001255	-0.000608	0.026032	2.47

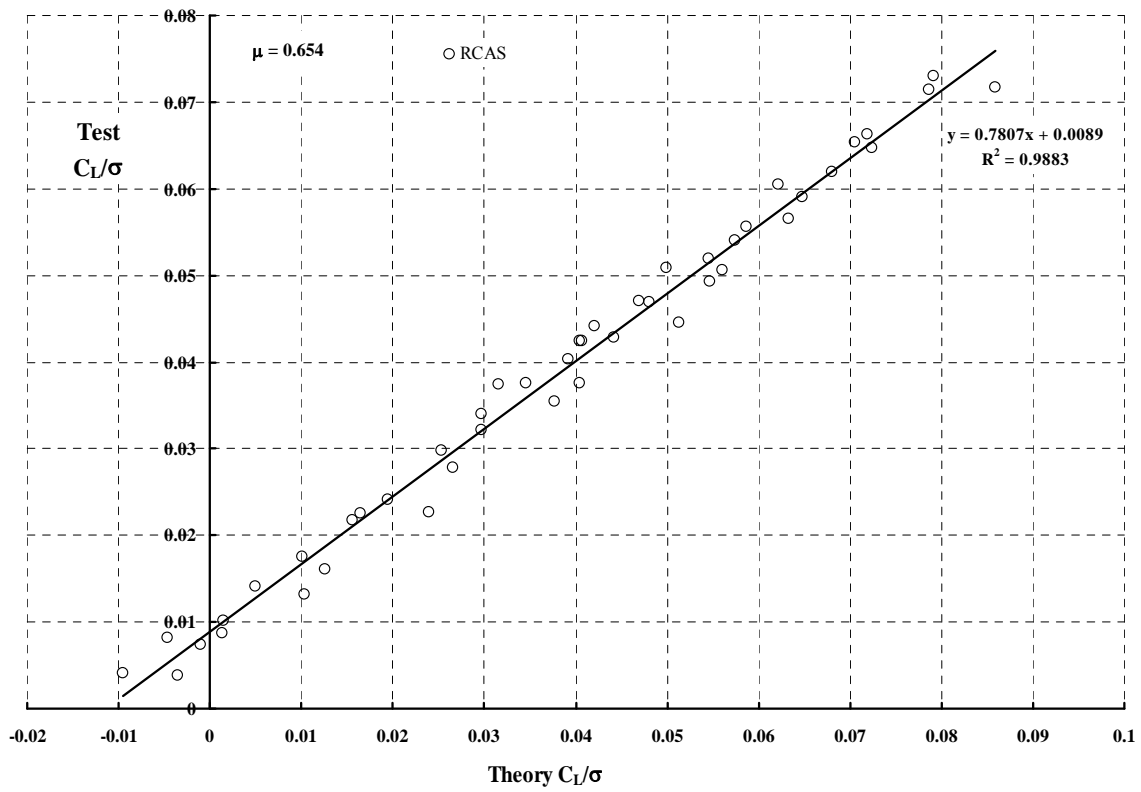
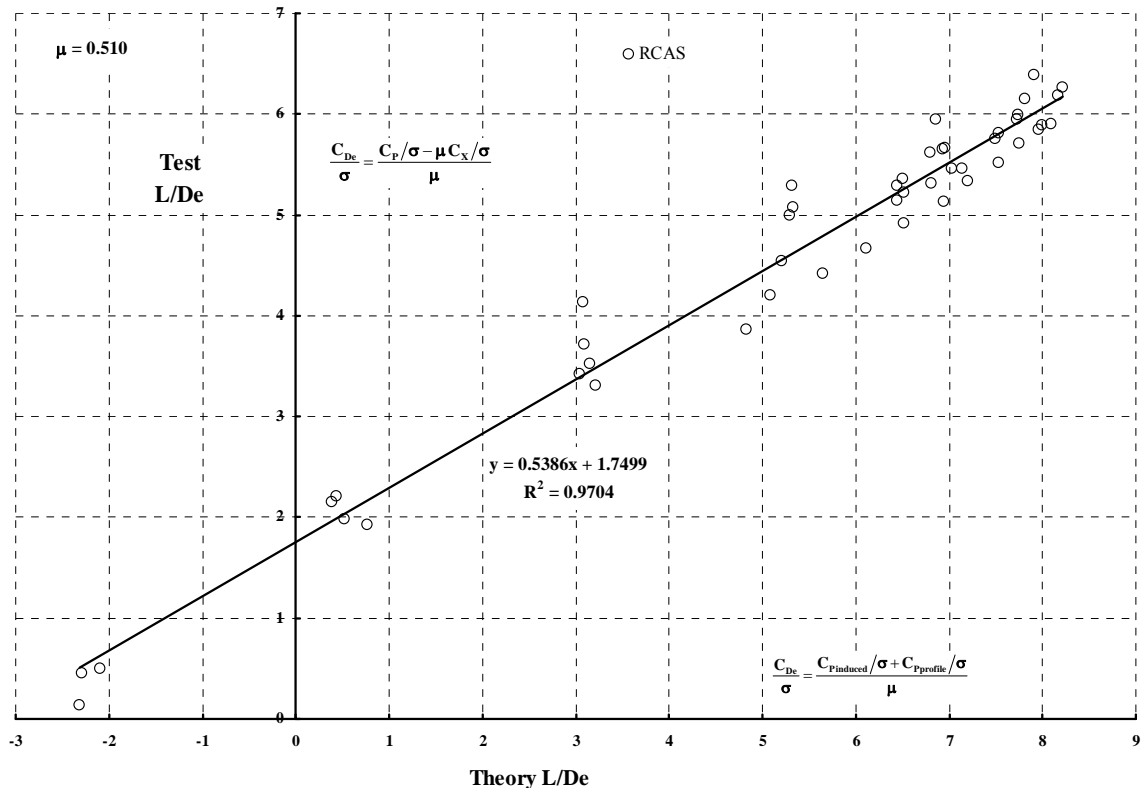
1.093	12.0	4.0	15.53	-1.61	0.056050	0.026266	0.057746	0.022292	0.000789	-0.000559	0.025755	2.18
1.093	2.0	5.0	5.98	-1.66	0.060427	0.012078	0.061250	0.006765	-0.000421	-0.000924	0.011233	5.38
1.093	1.0	6.0	5.43	-1.91	0.078629	0.013245	0.079582	0.004953	-0.000790	-0.001589	0.011791	6.67
1.093	3.0	6.0	7.85	-1.94	0.069520	0.014132	0.070616	0.006788	-0.000179	-0.002055	0.012252	5.67
1.093	0.0	6.0	4.23	-1.89	0.082837	0.013205	0.083764	0.004473	-0.001003	-0.001450	0.011877	6.97
1.093	2.0	6.0	6.64	-1.92	0.074164	0.013552	0.075175	0.005725	-0.000484	-0.001793	0.011910	6.23
1.093	4.0	6.0	9.06	-1.96	0.064829	0.014949	0.066036	0.008090	0.000119	-0.002383	0.012768	5.08
1.093	6.0	6.0	11.38	-2.17	0.058083	0.017184	0.059561	0.011019	0.000354	-0.003023	0.014418	4.03
1.093	8.0	6.0	13.13	-2.43	0.061575	0.022631	0.063604	0.016071	-0.000349	-0.002445	0.020394	3.02
1.093	10.0	6.0	13.45	-1.47	0.089065	0.030842	0.091801	0.021363	0.000885	-0.000733	0.030172	2.95
1.093	12.0	6.0	16.65	-1.71	0.076973	0.030105	0.079698	0.021894	0.000186	-0.000016	0.030091	2.56
1.093	2.0	7.0	7.30	-2.17	0.088045	0.015337	0.089258	0.004493	-0.000548	-0.002803	0.012772	6.89
1.093	4.0	7.0	9.71	-2.22	0.078996	0.016589	0.080429	0.006838	0.000070	-0.003221	0.013642	5.79

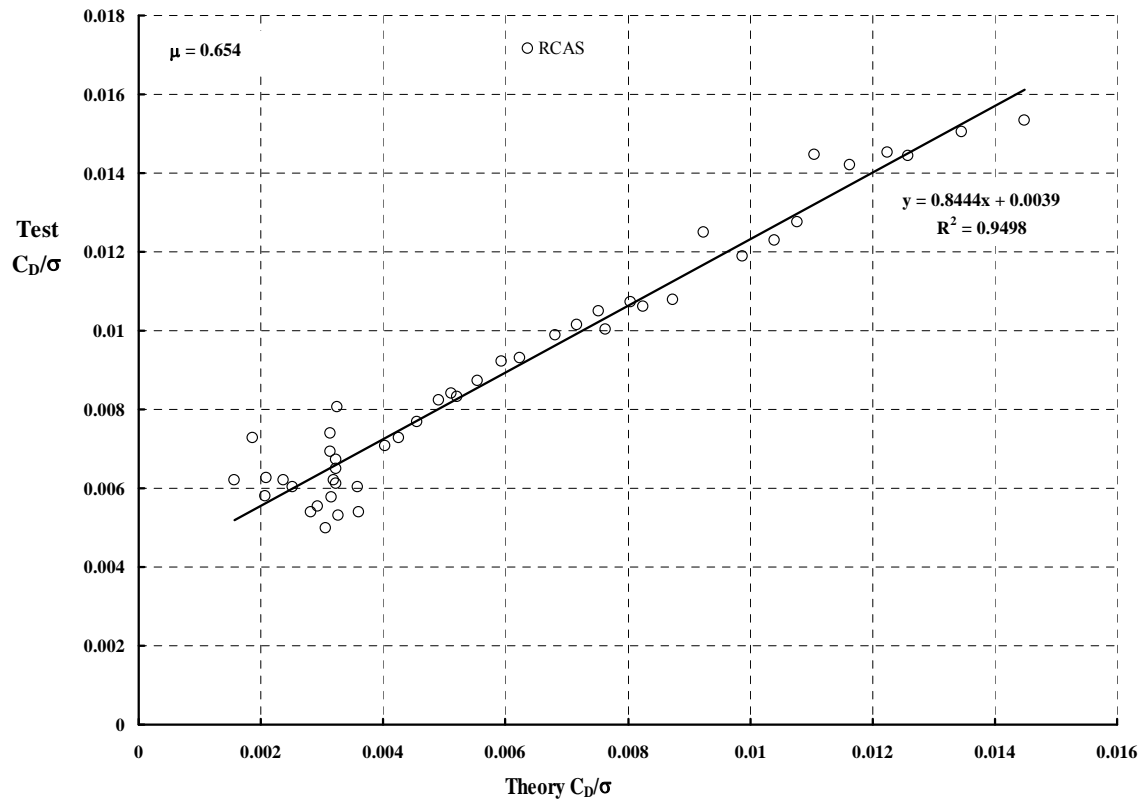
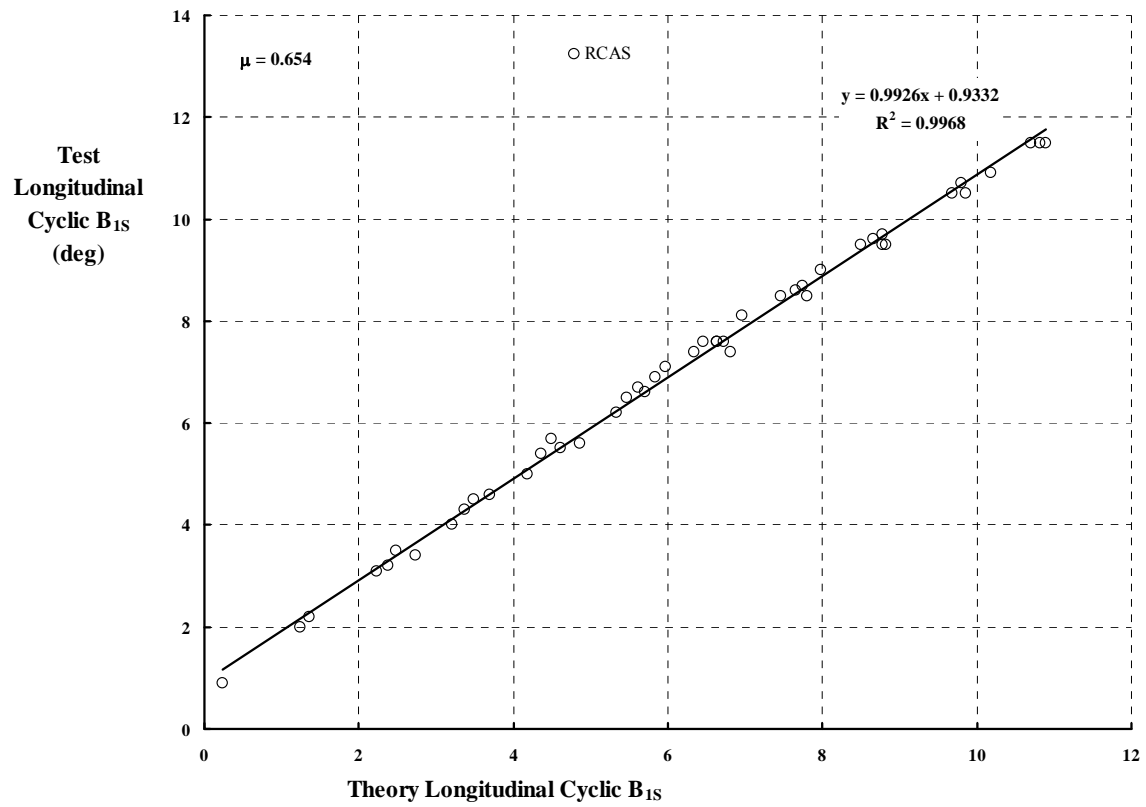


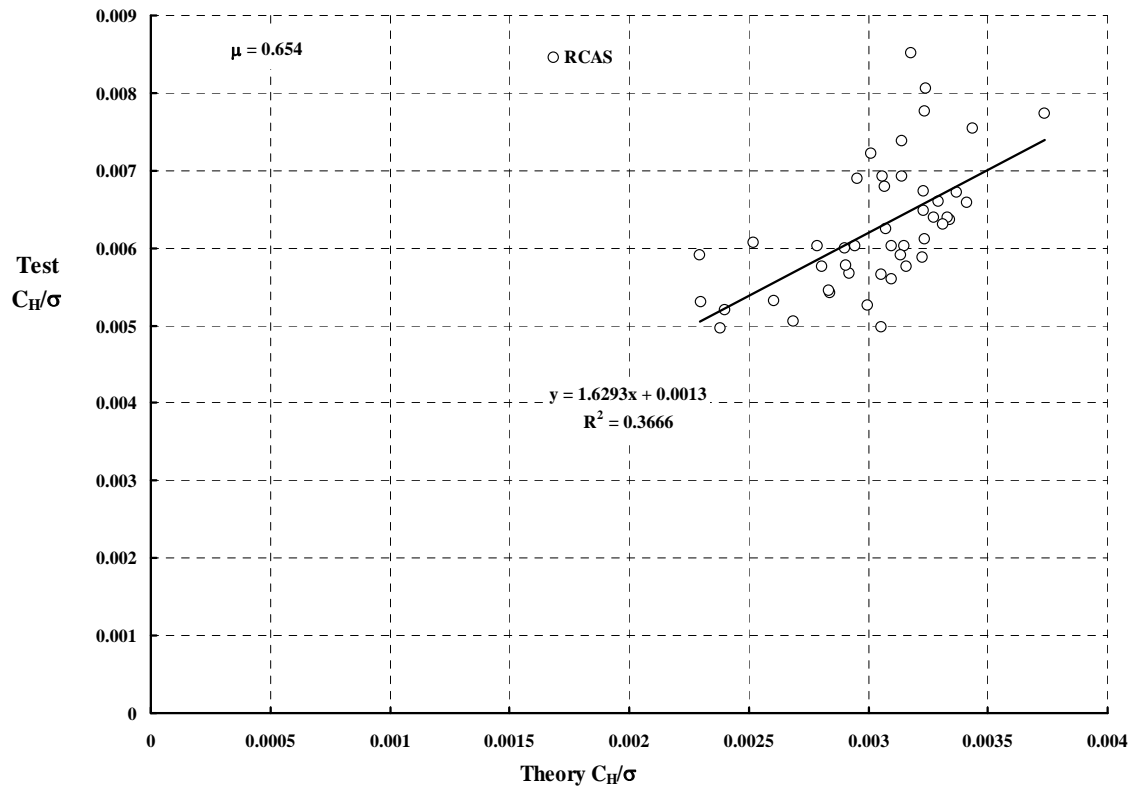
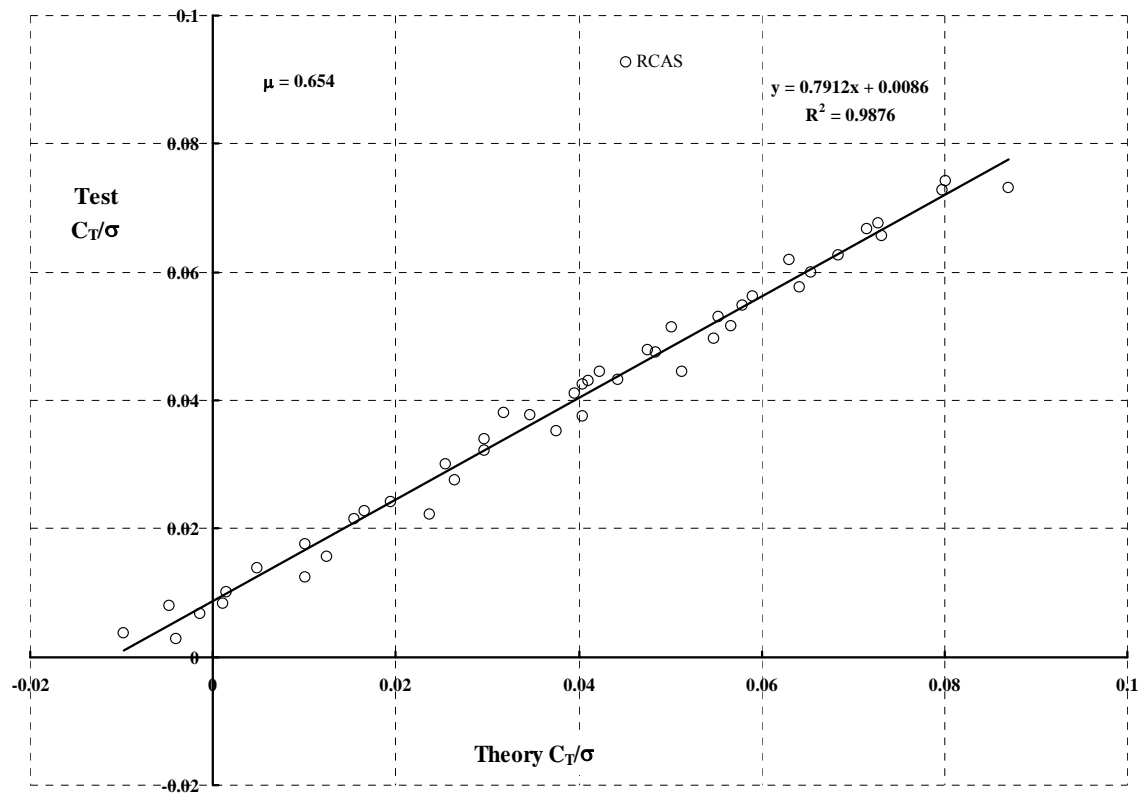


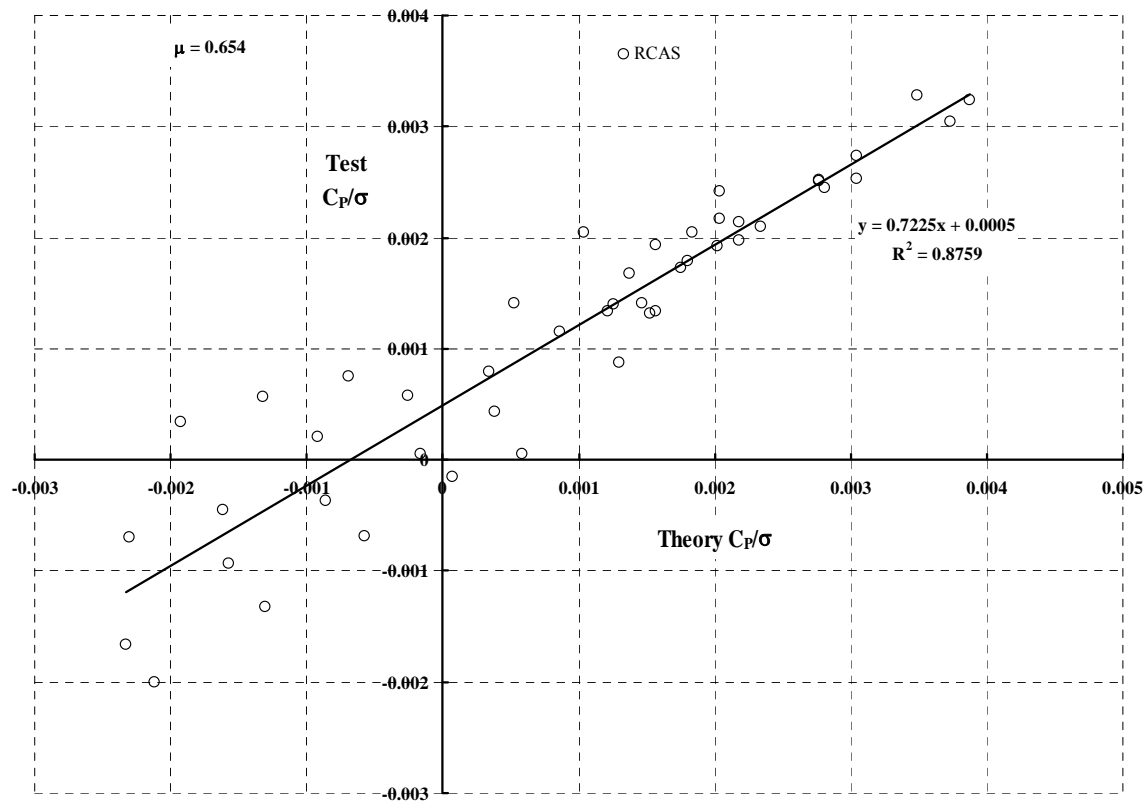
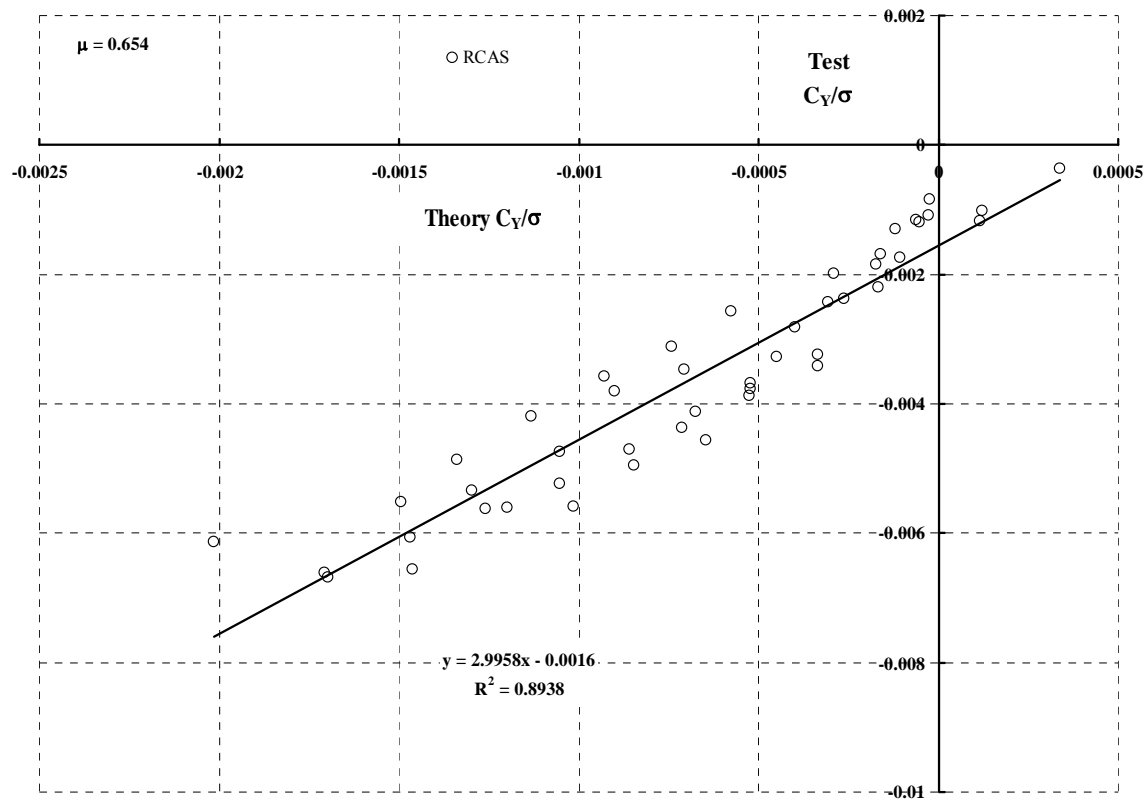


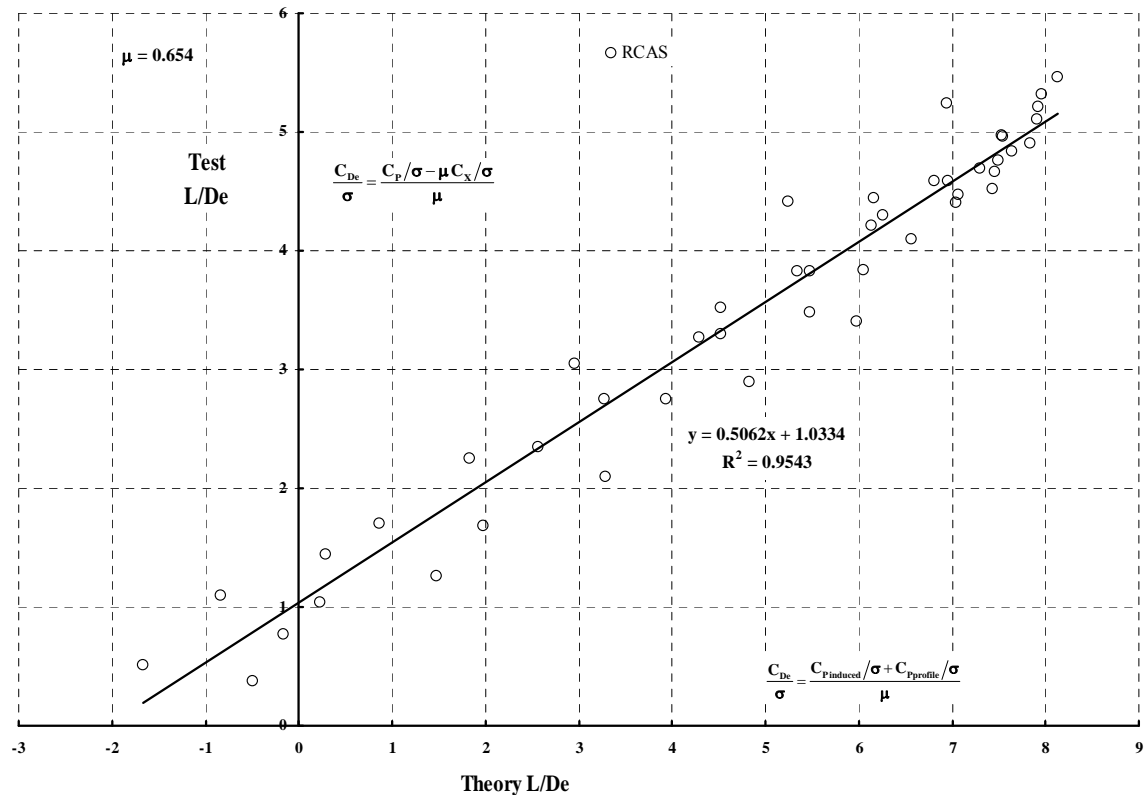
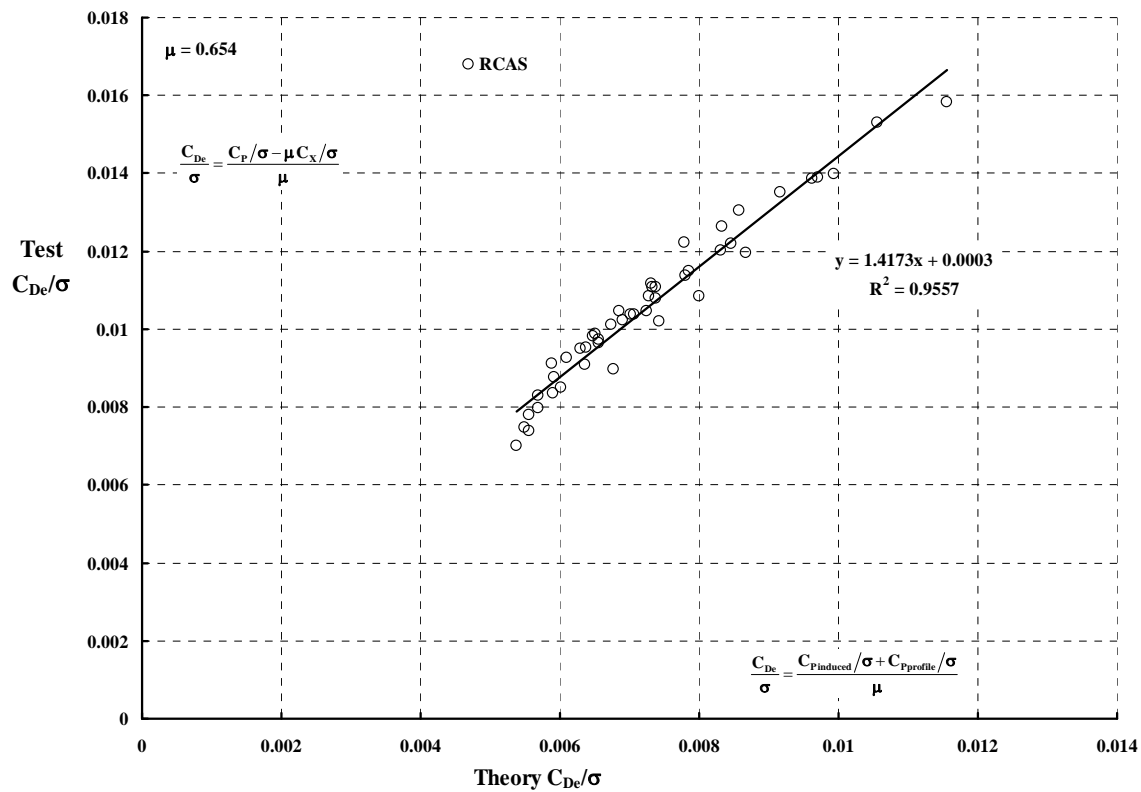


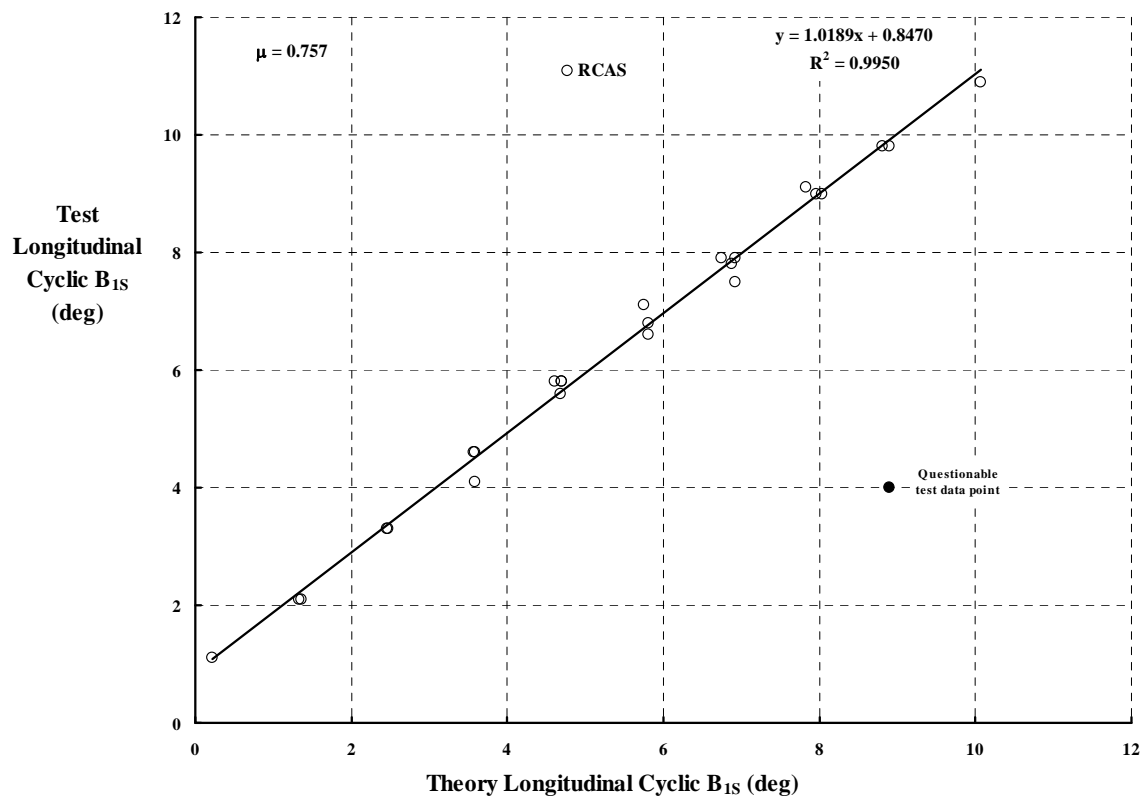
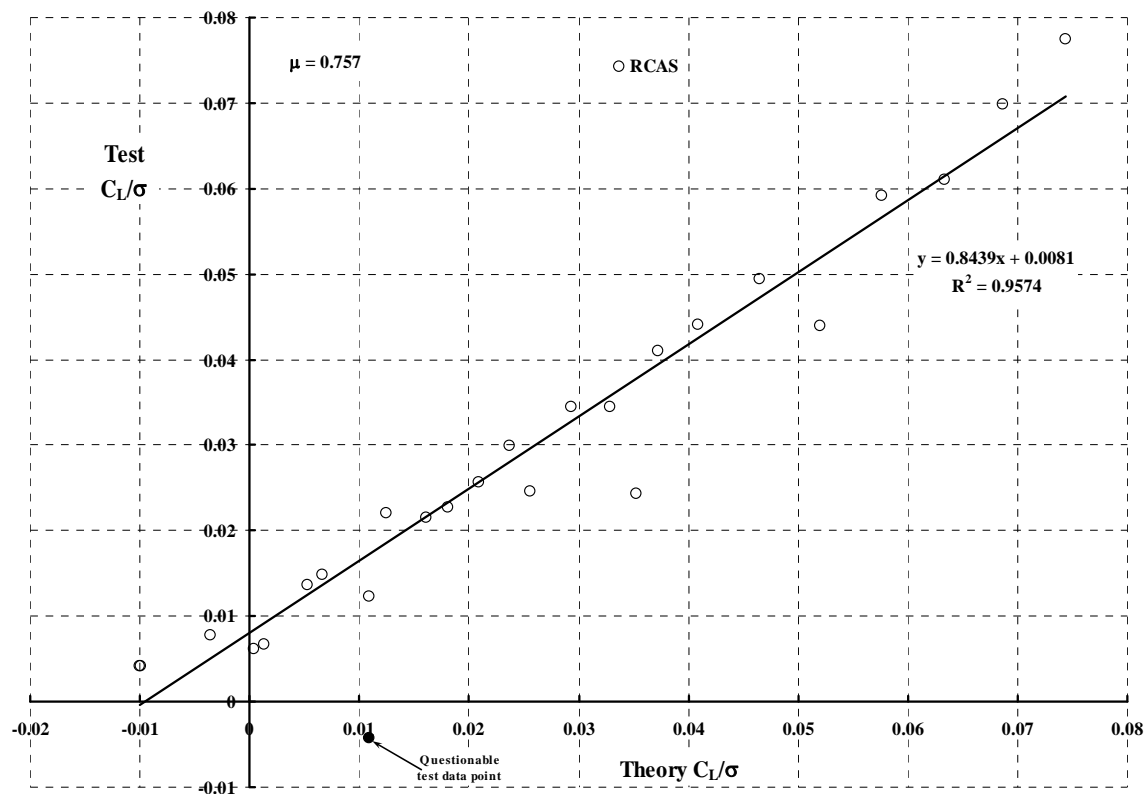


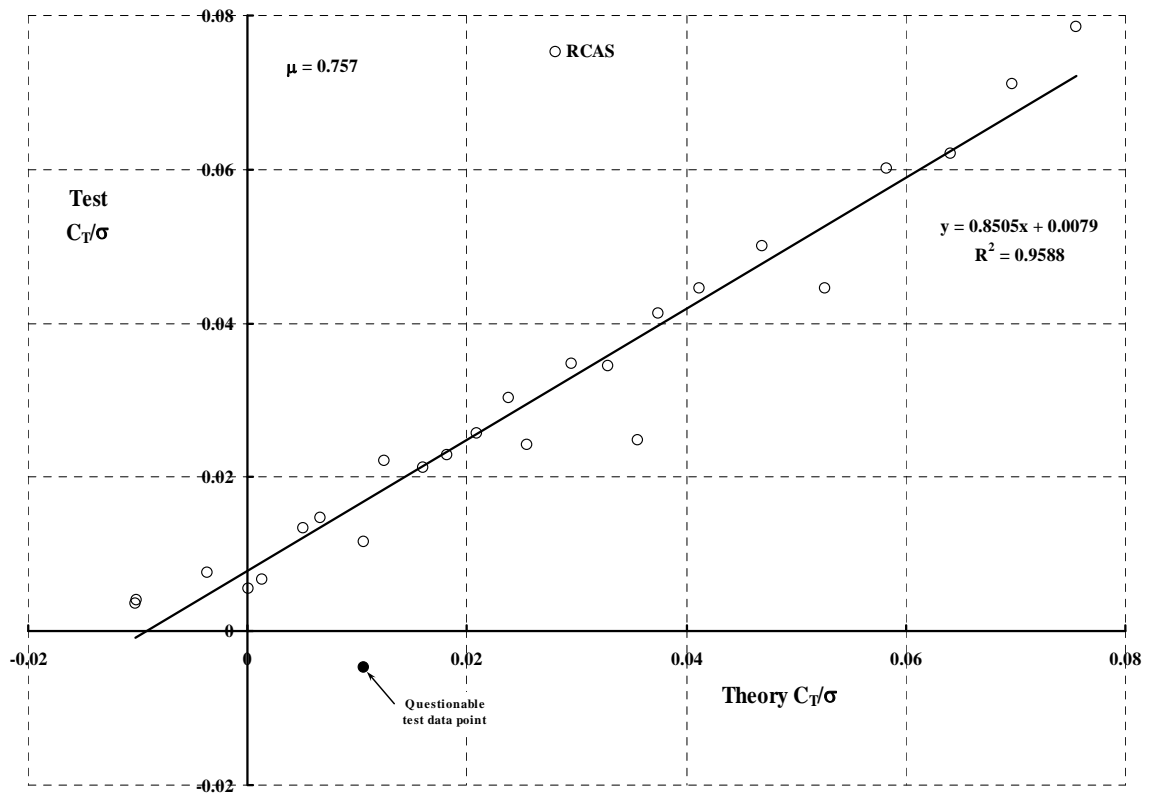
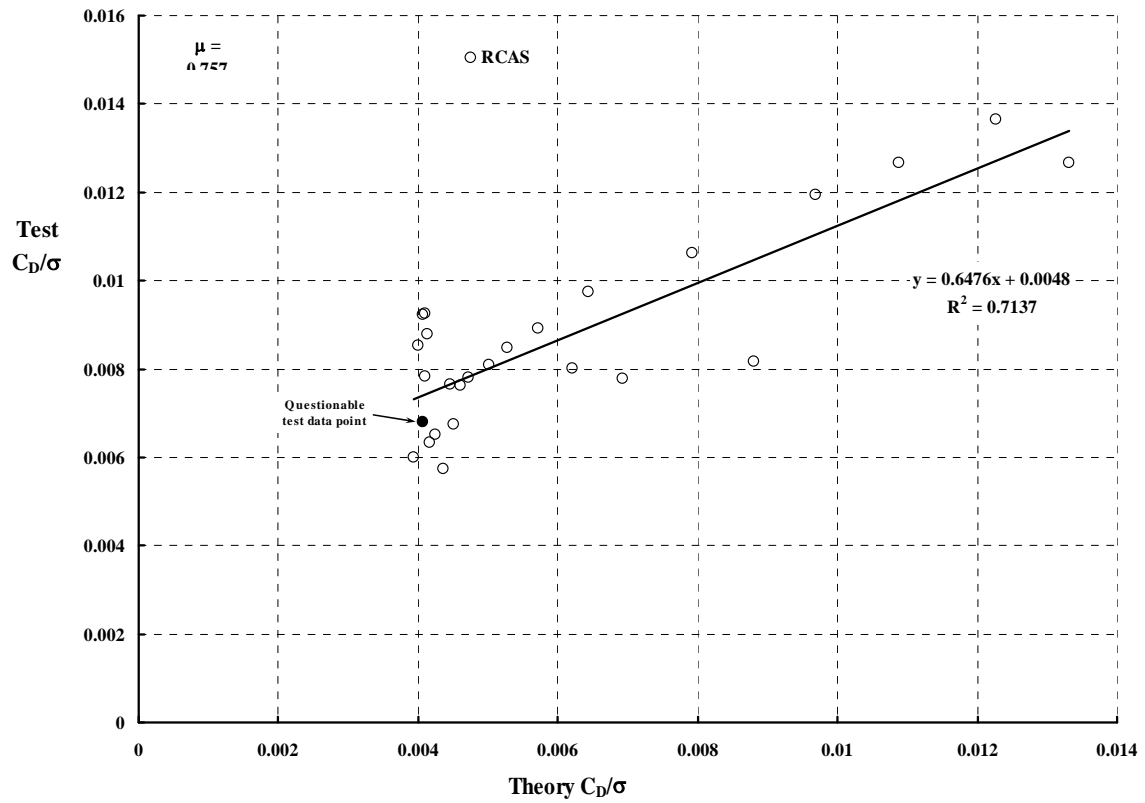


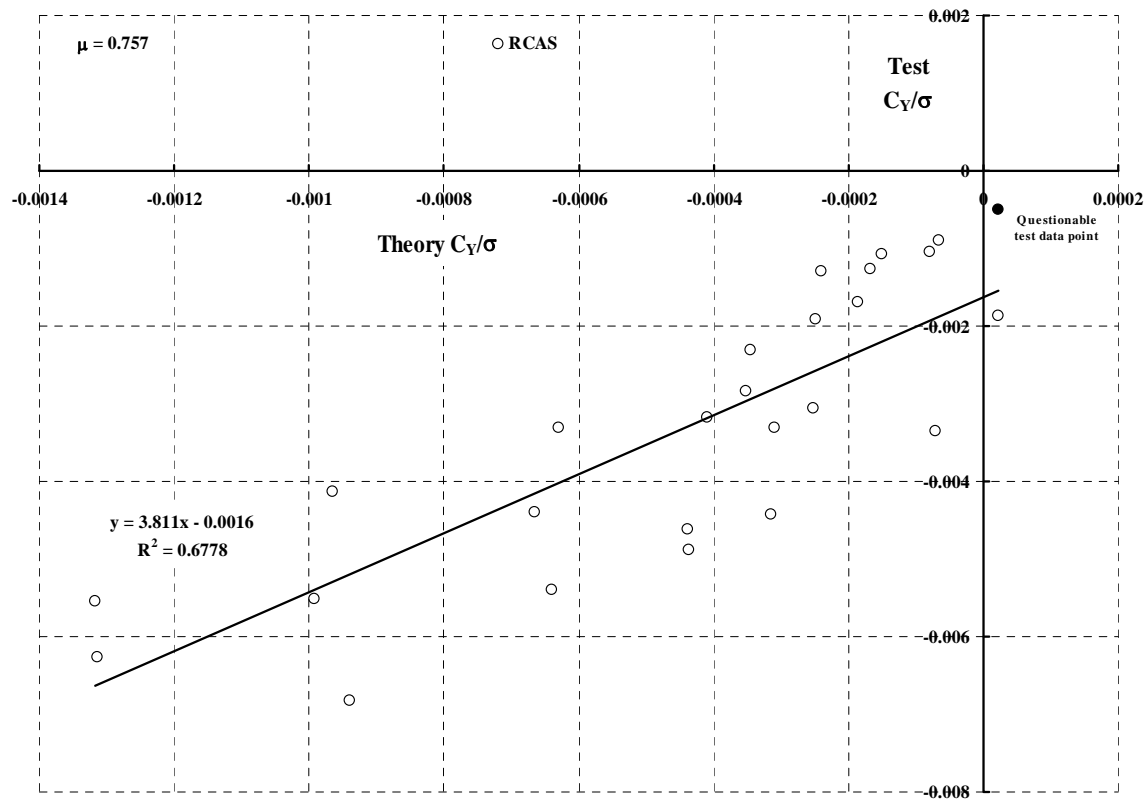
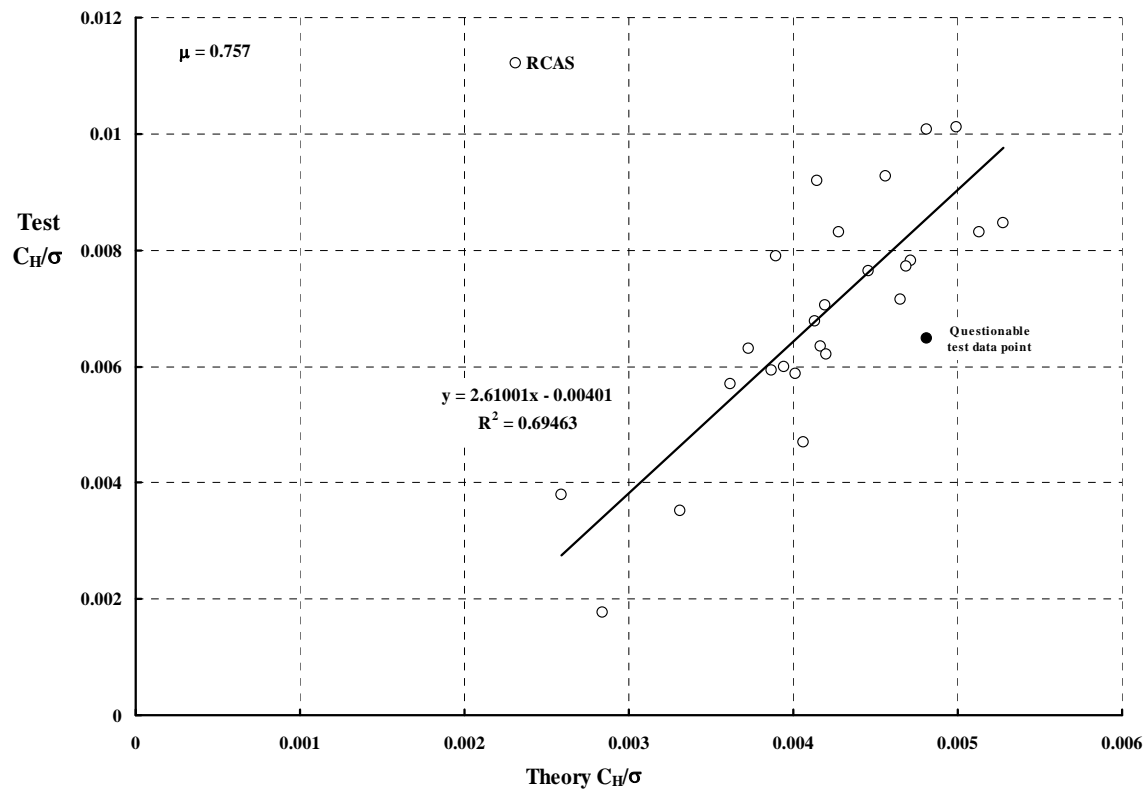


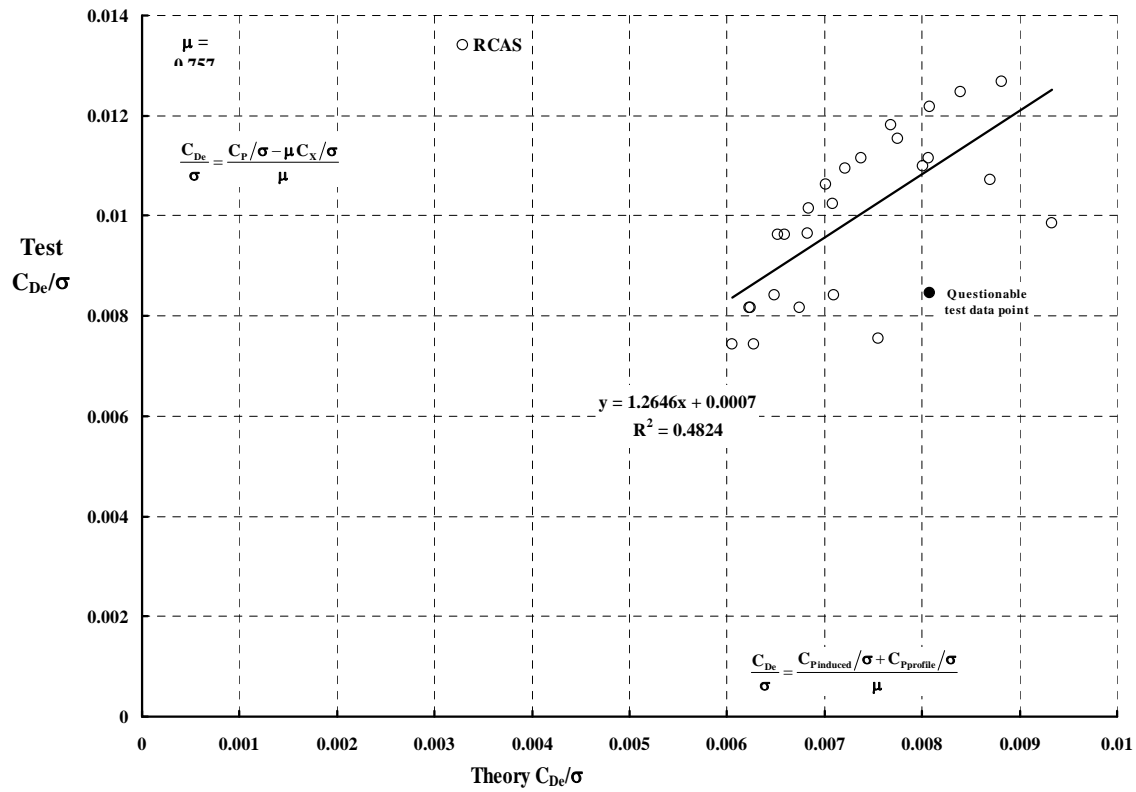
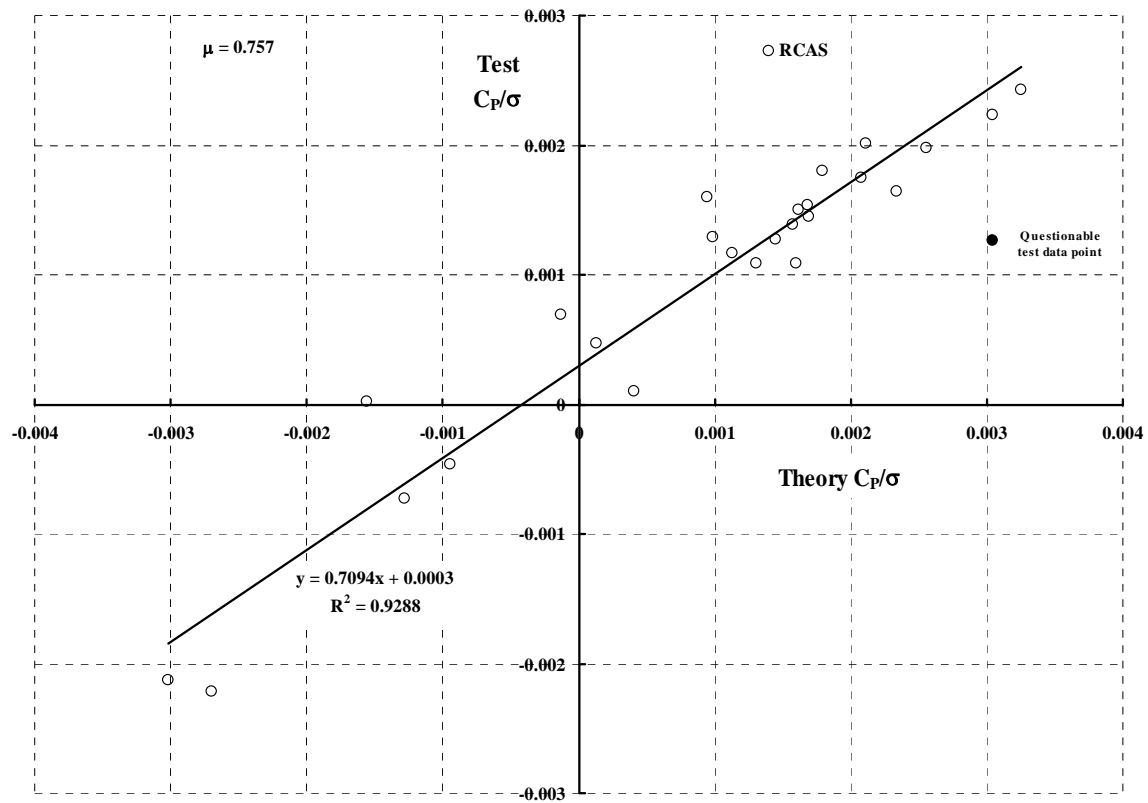


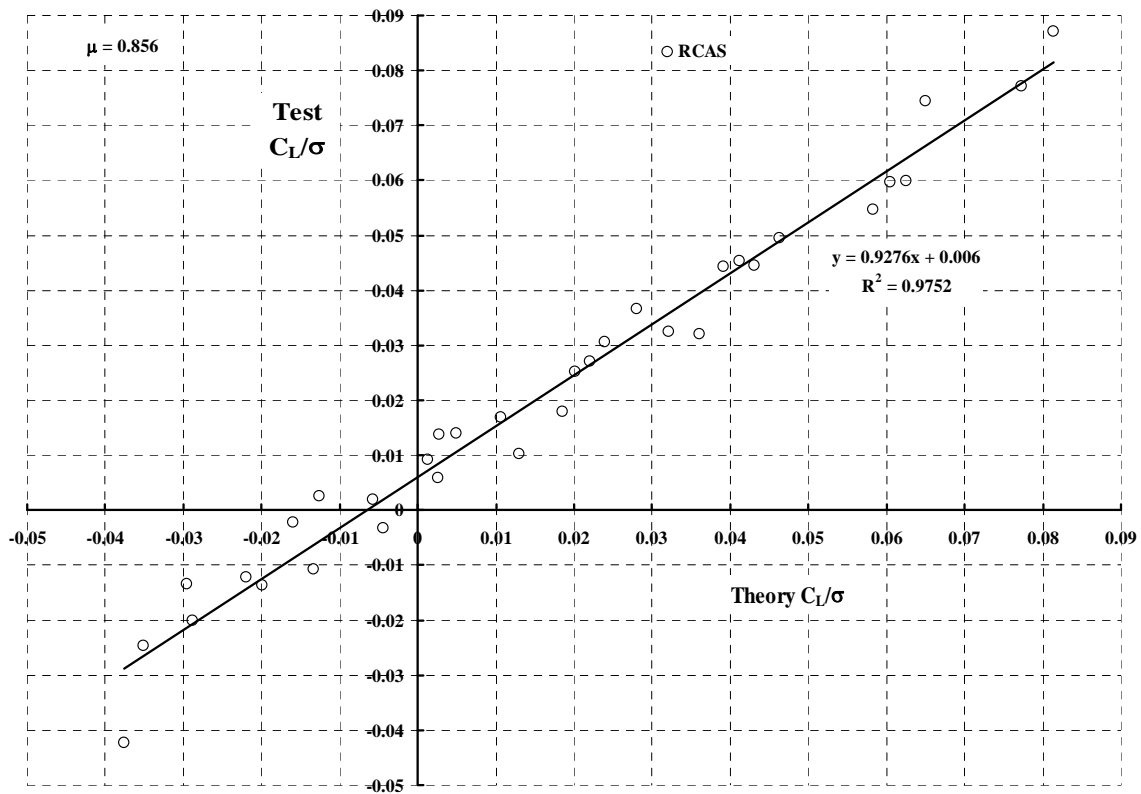
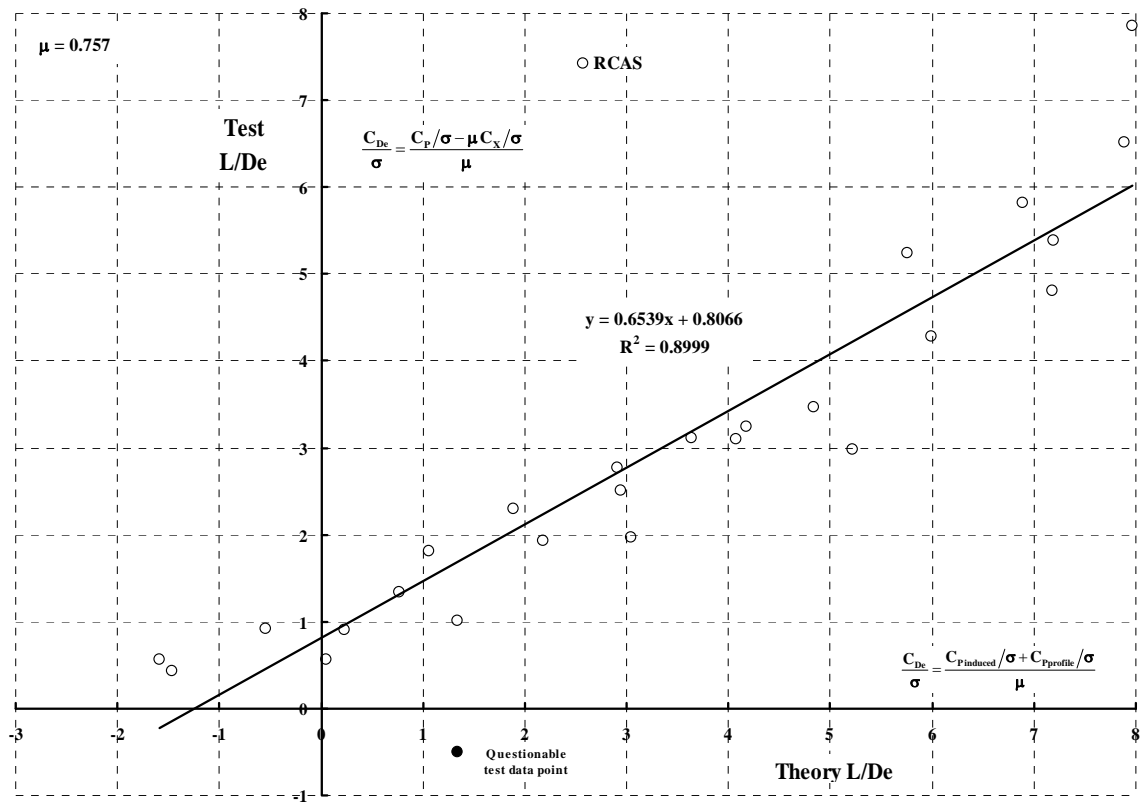


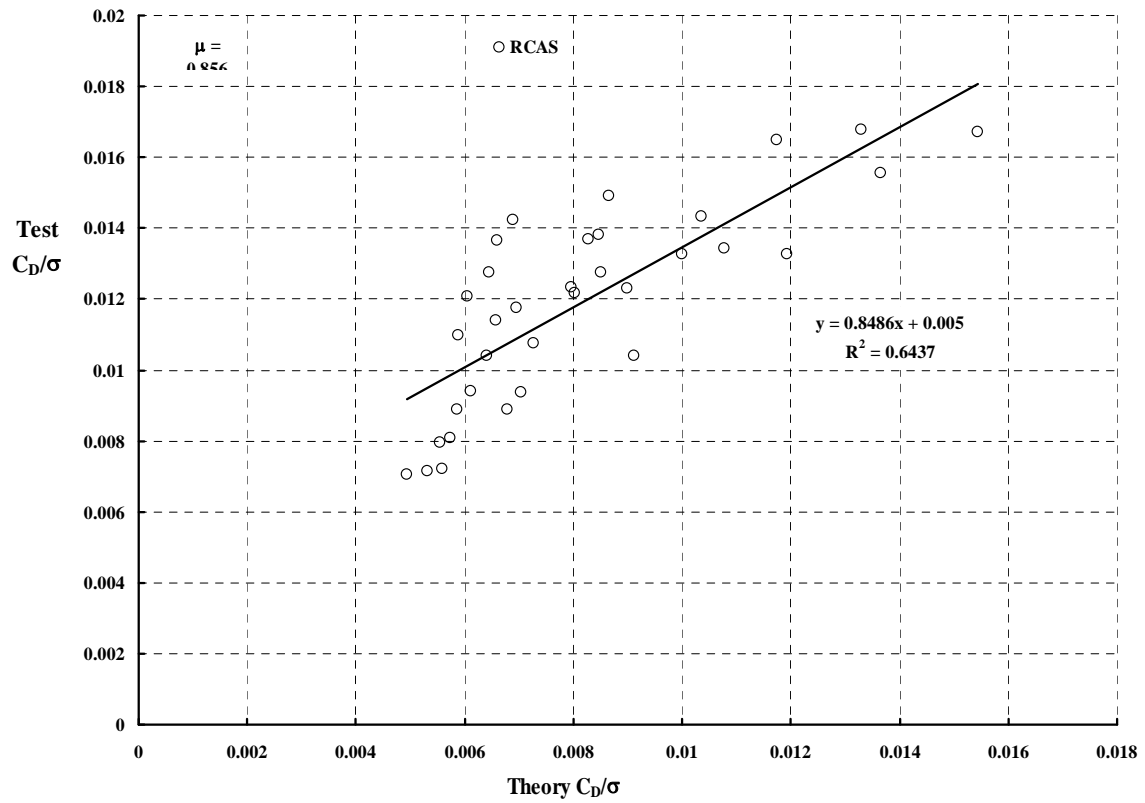
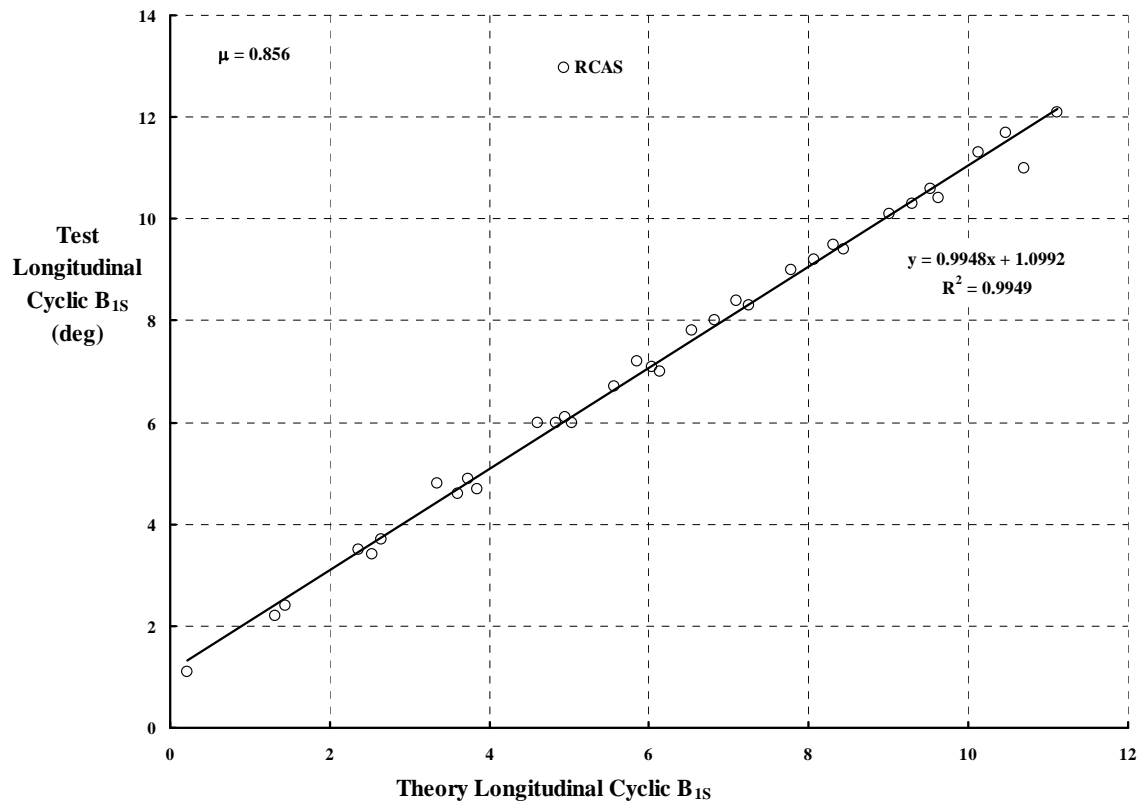


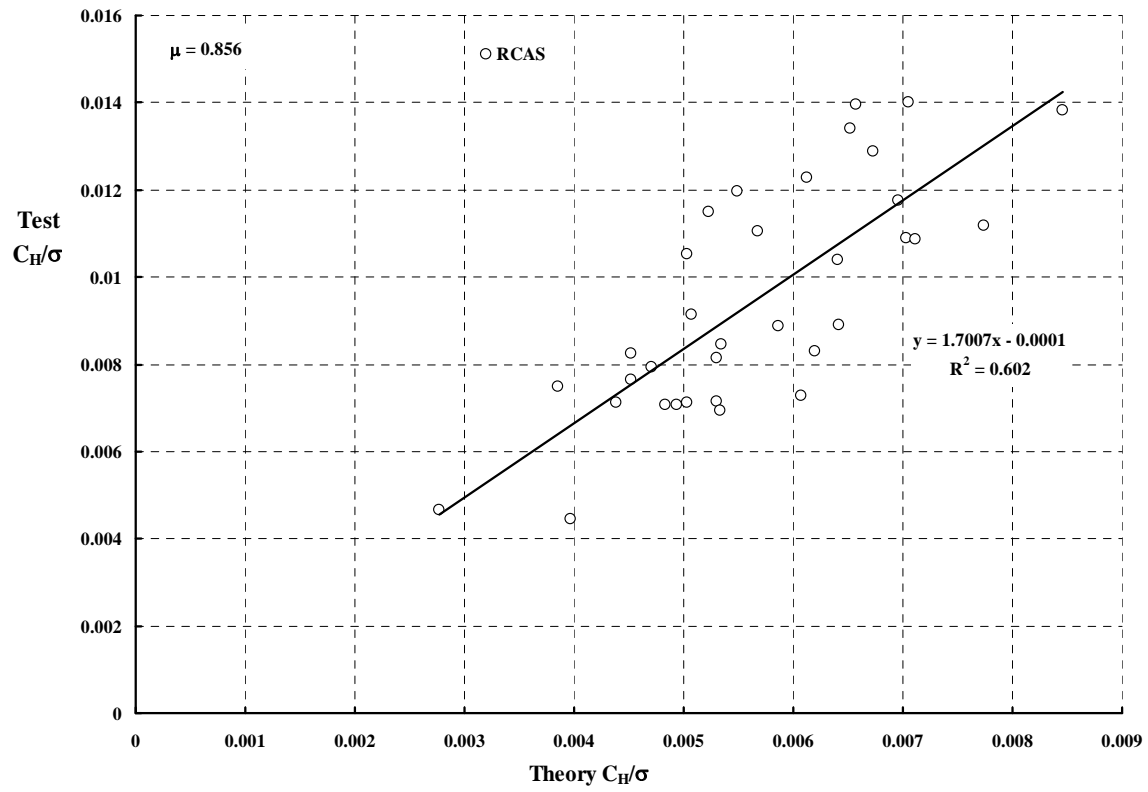
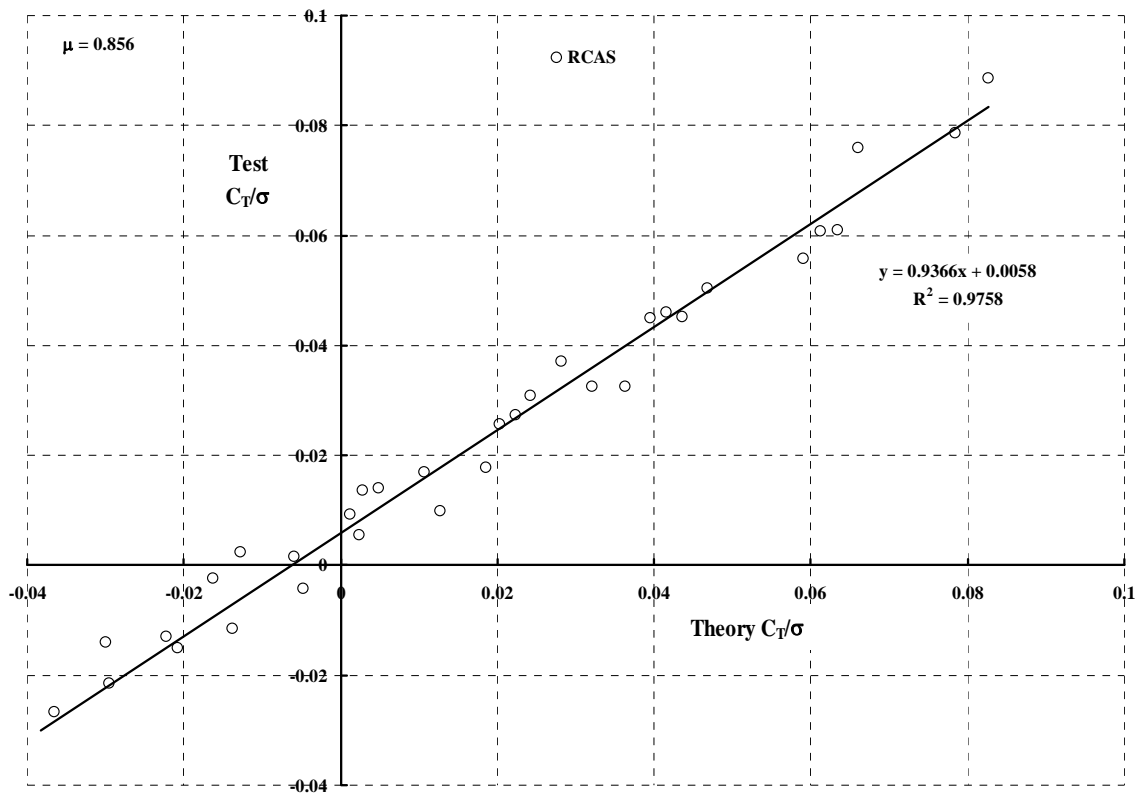


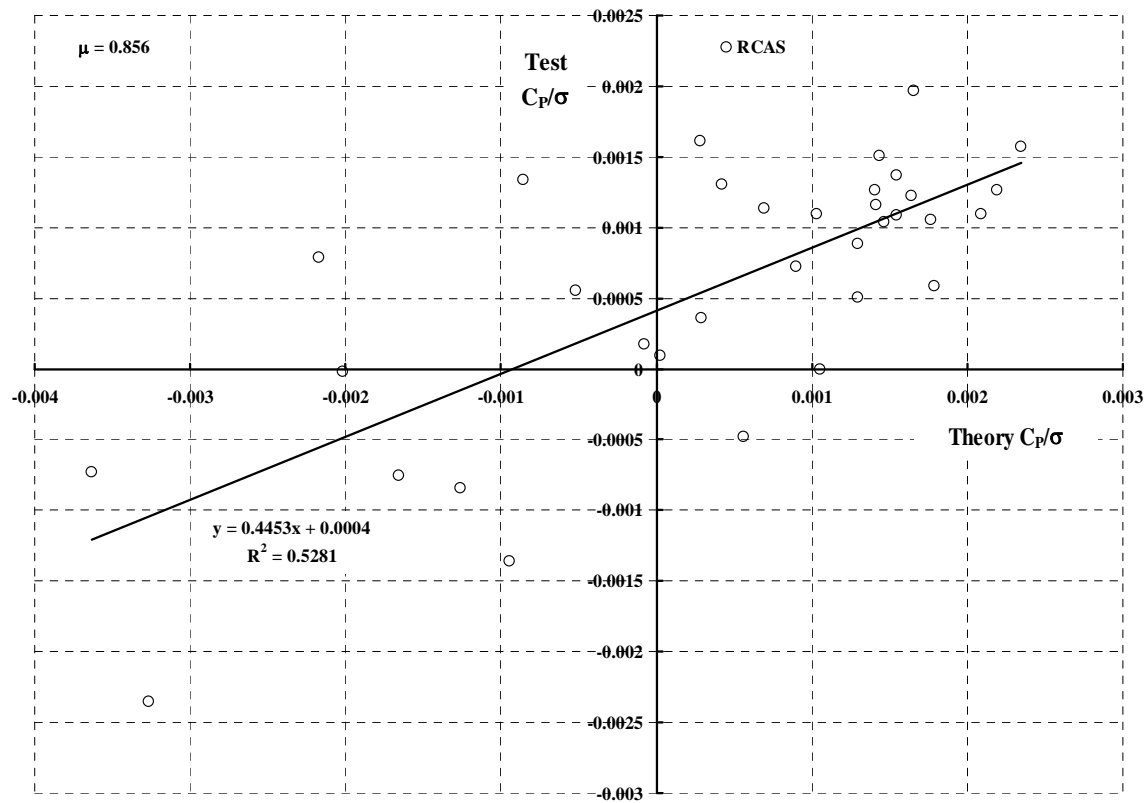
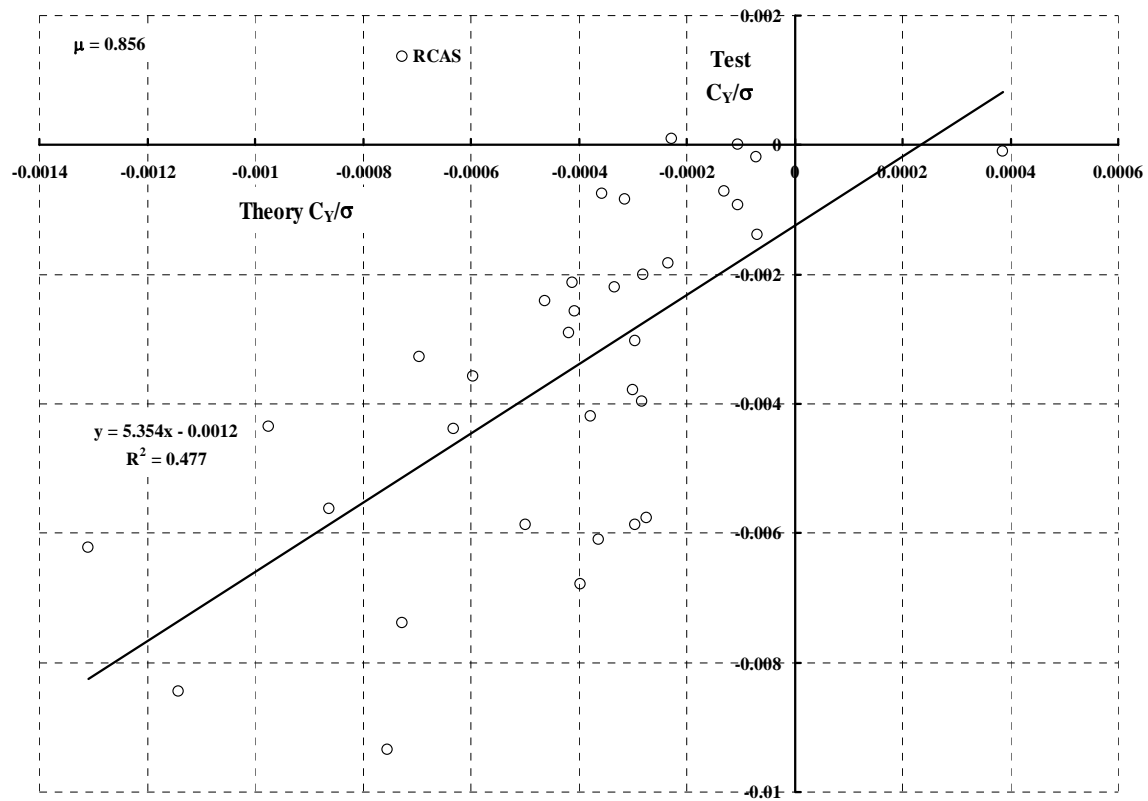


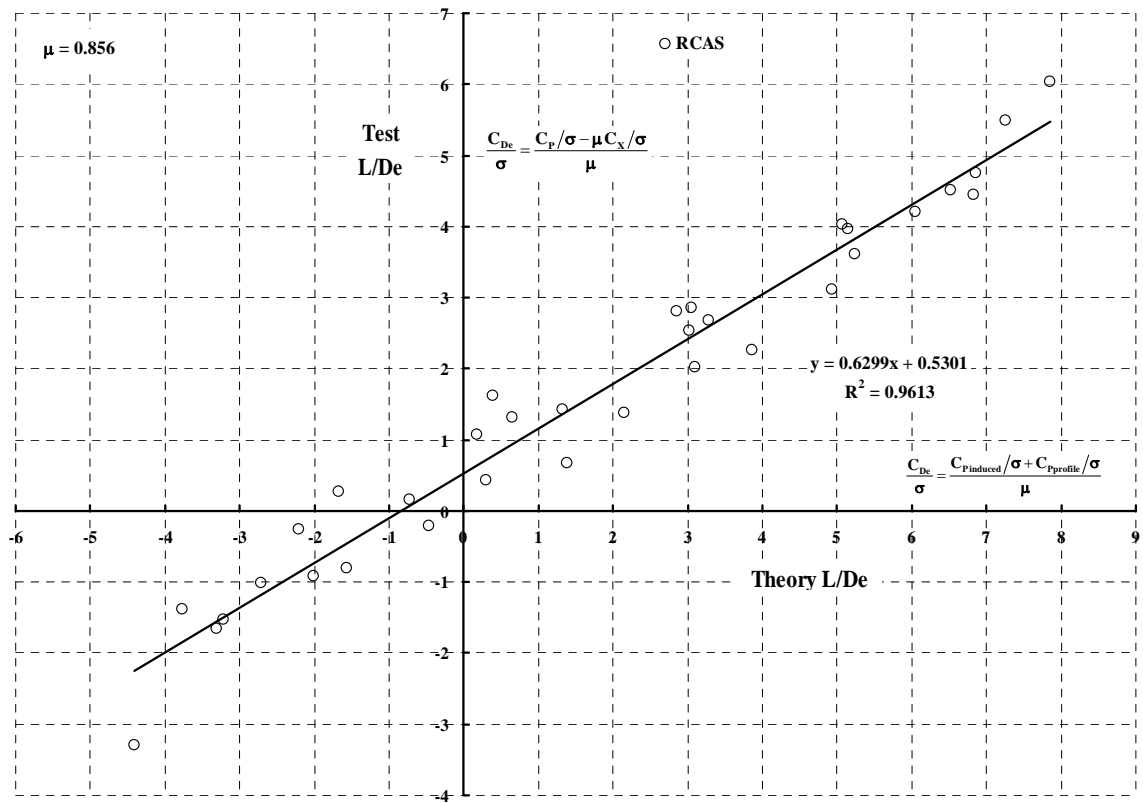
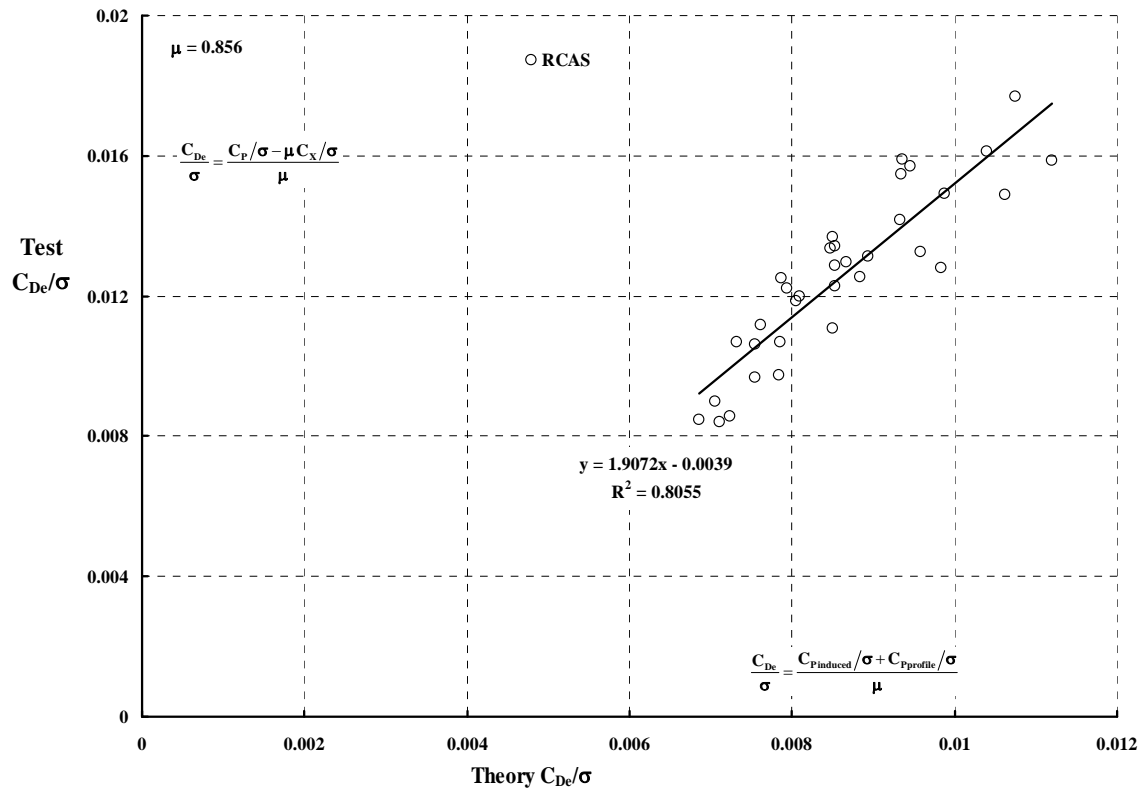


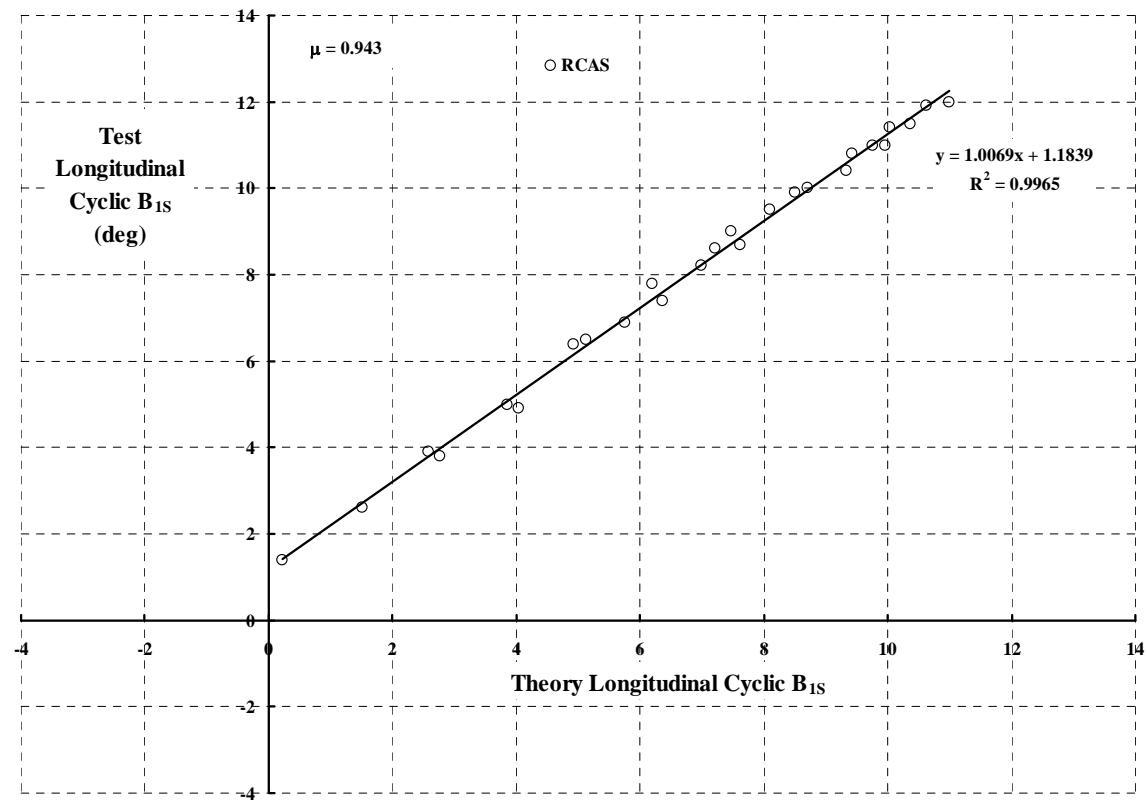
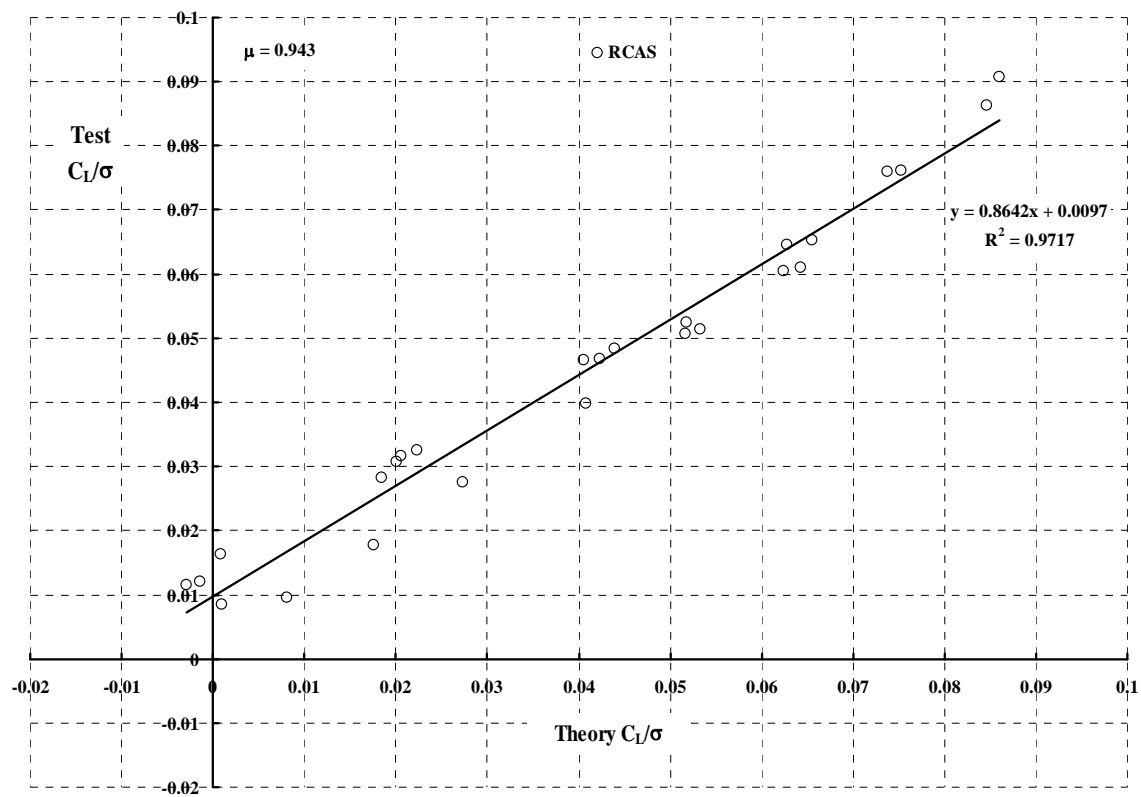


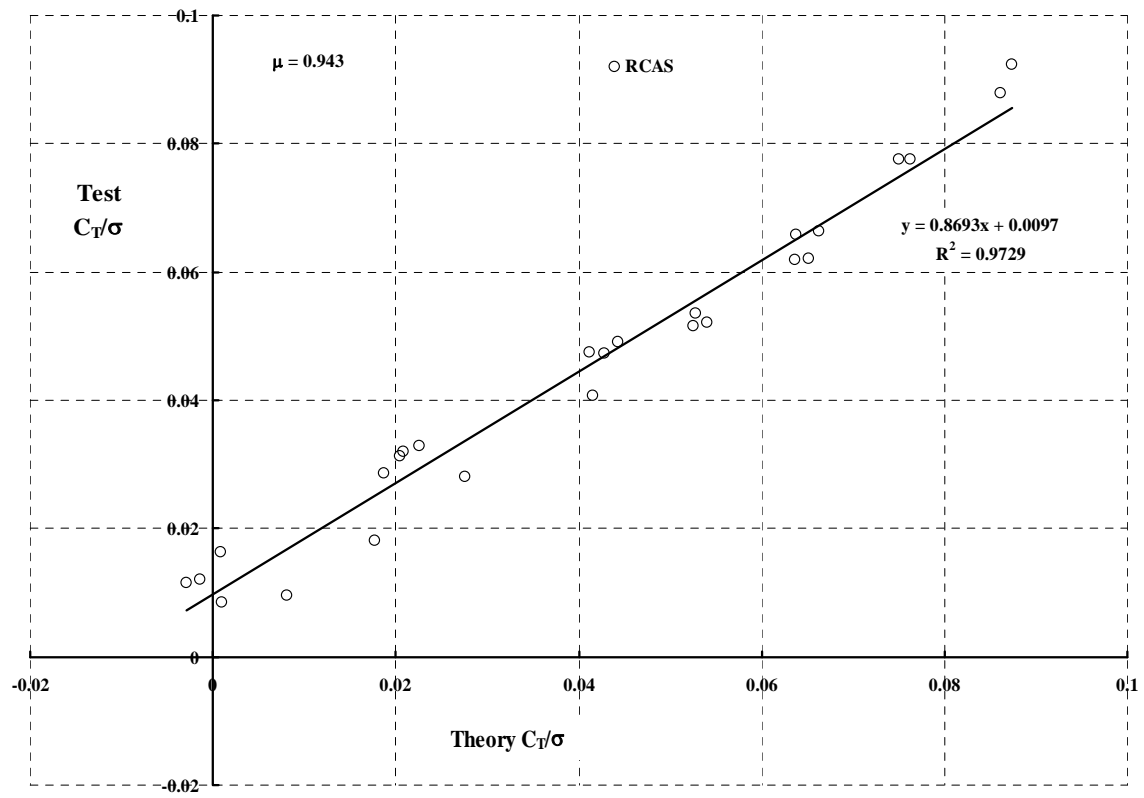
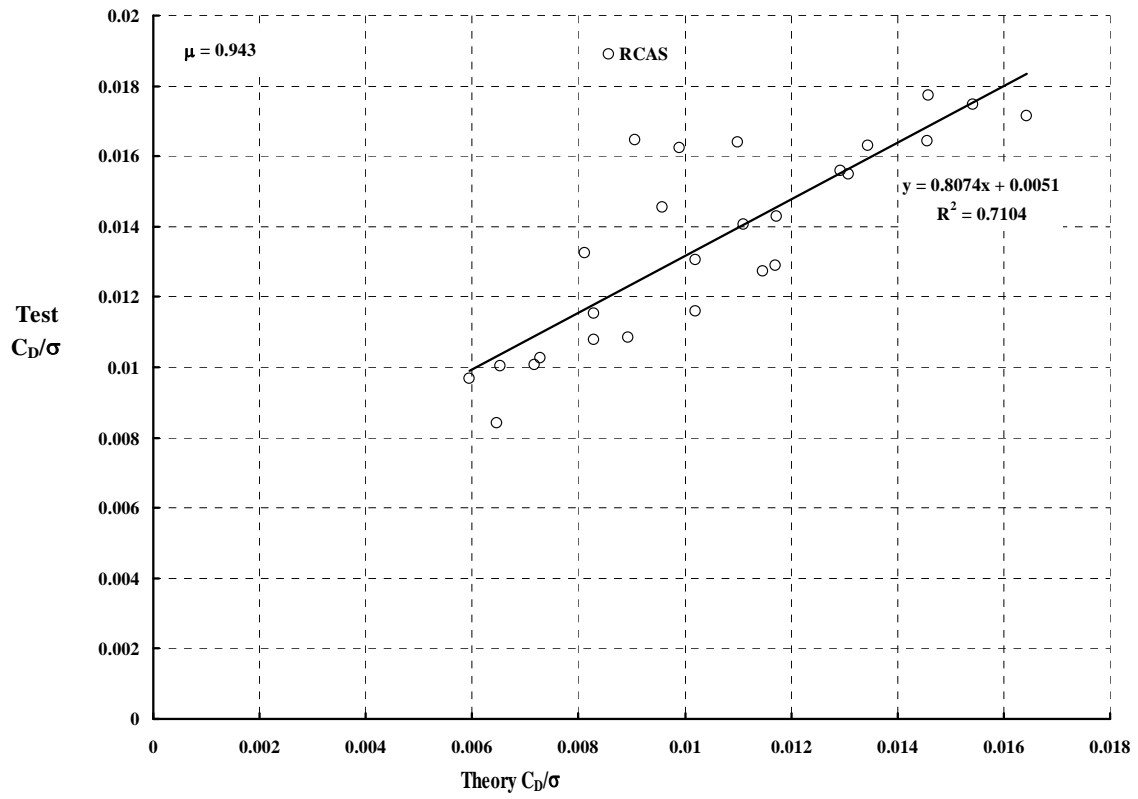


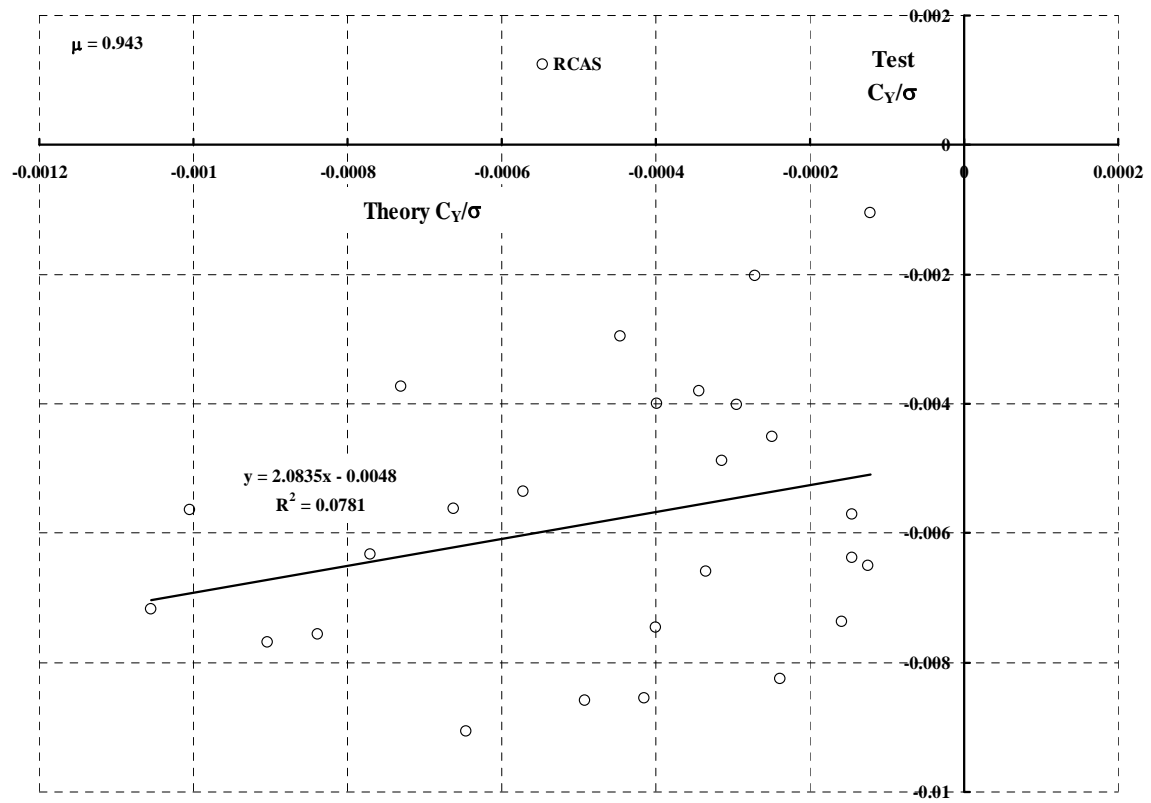
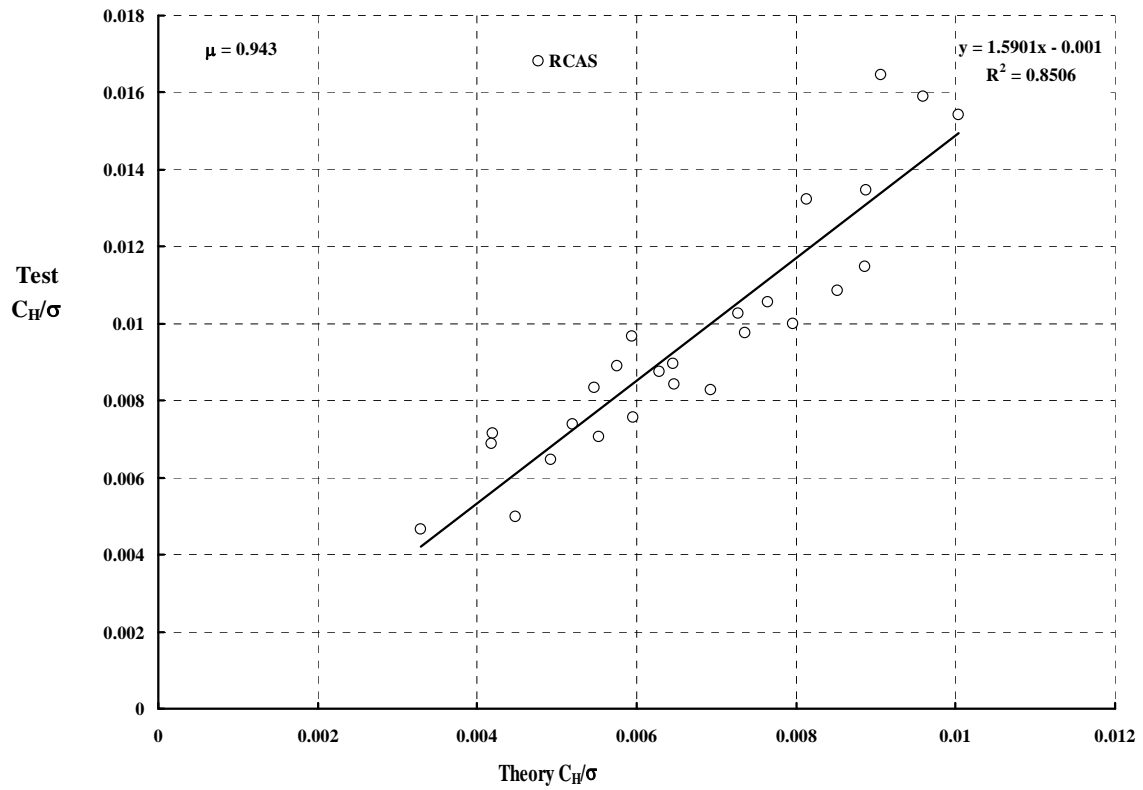


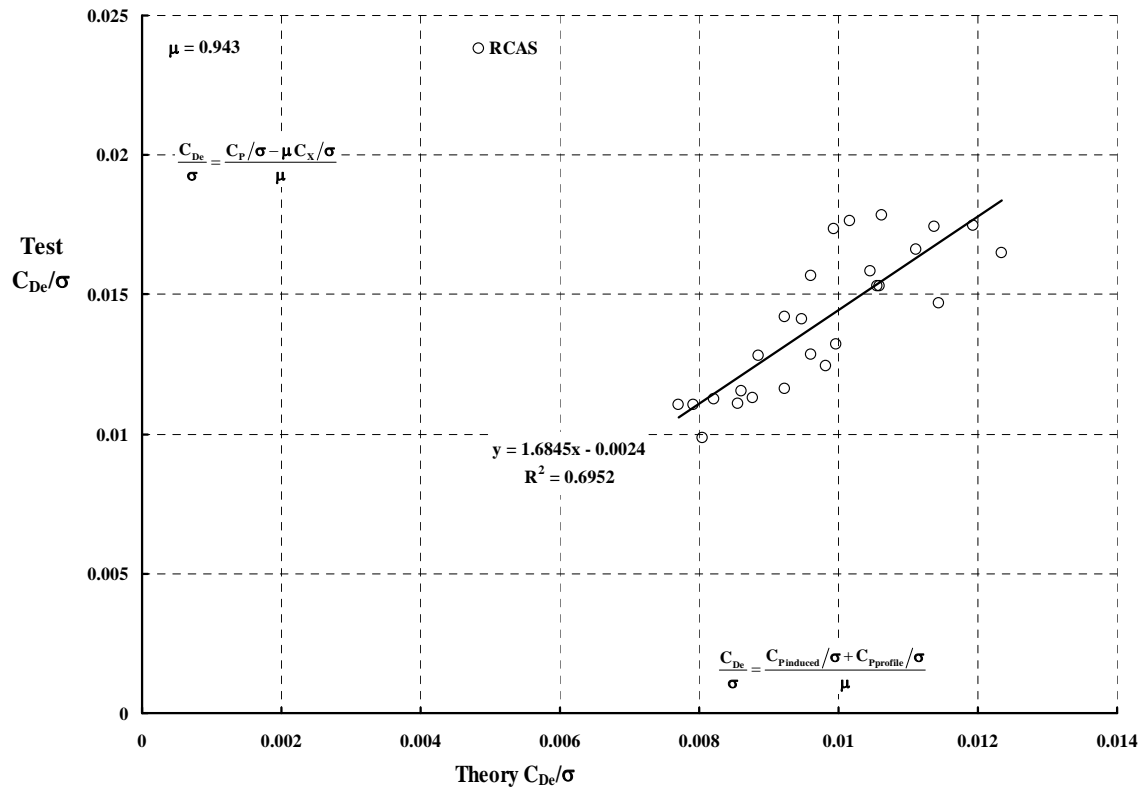
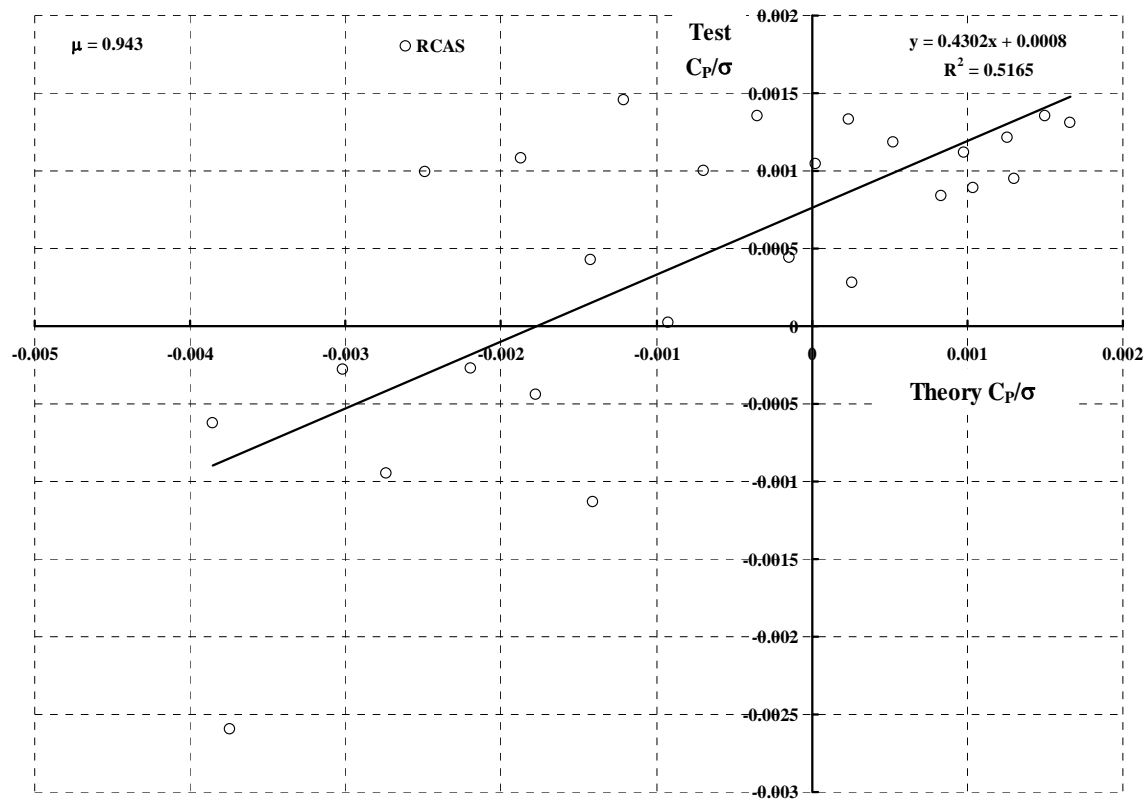


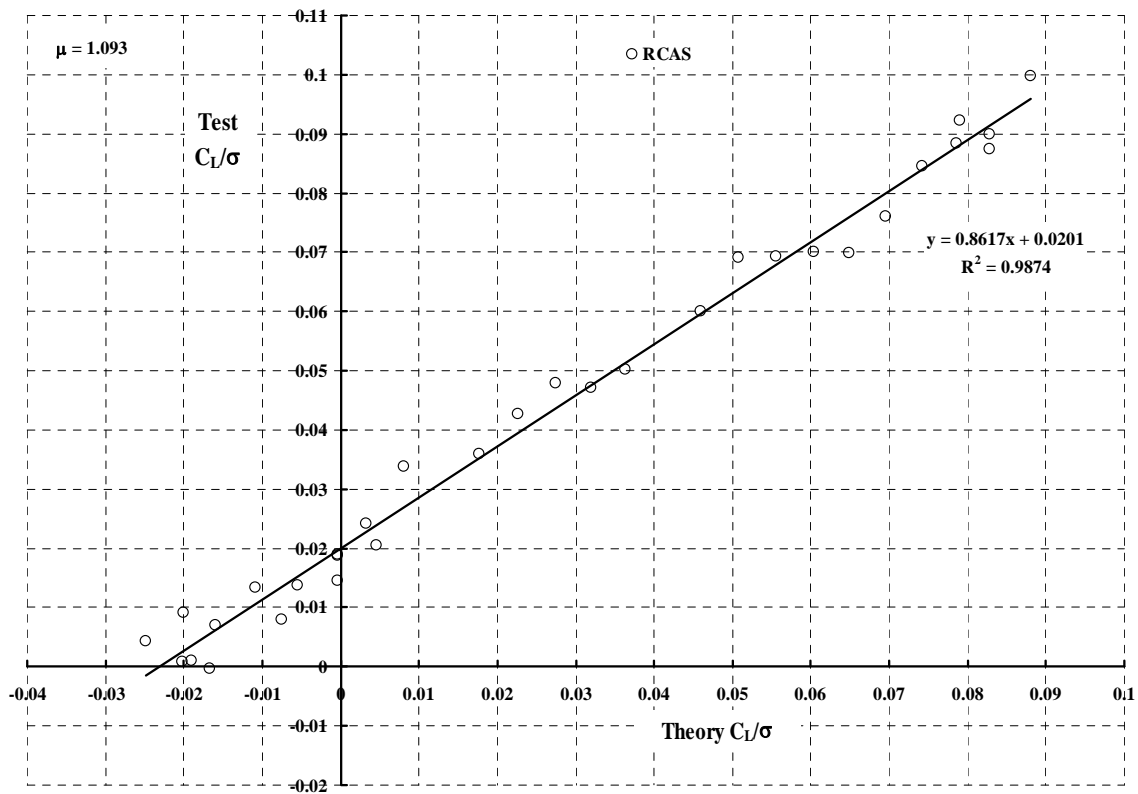
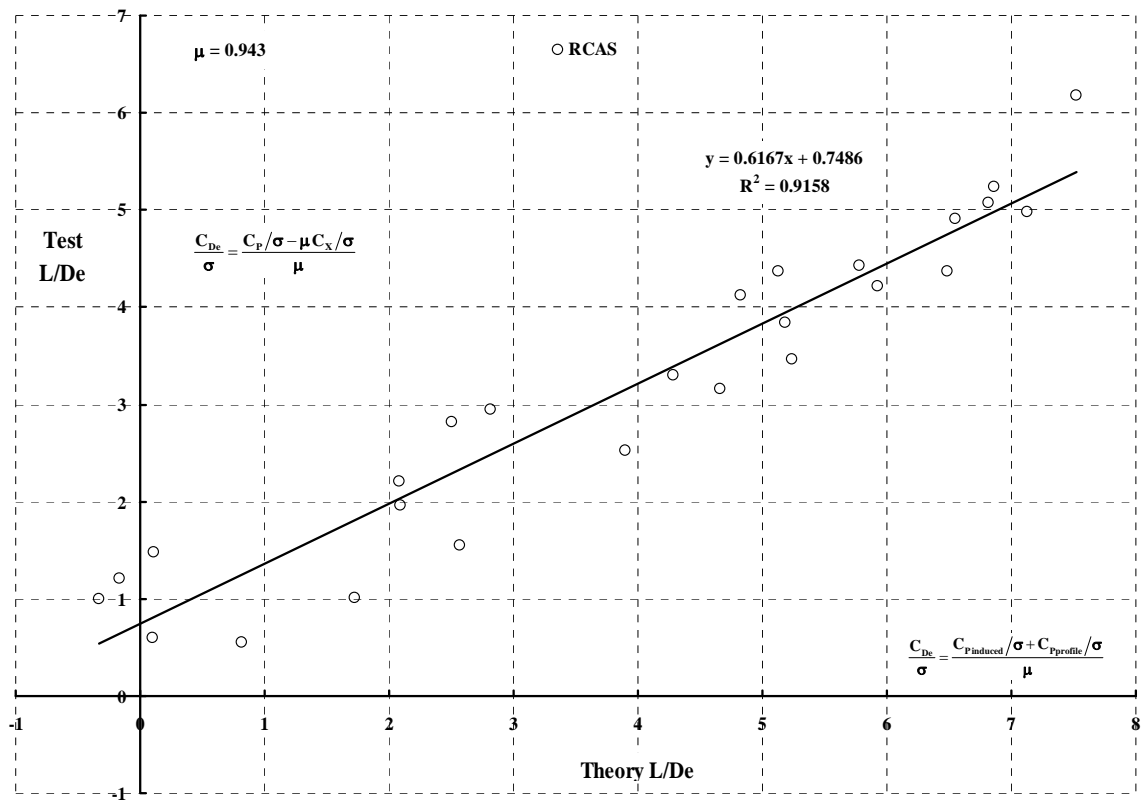


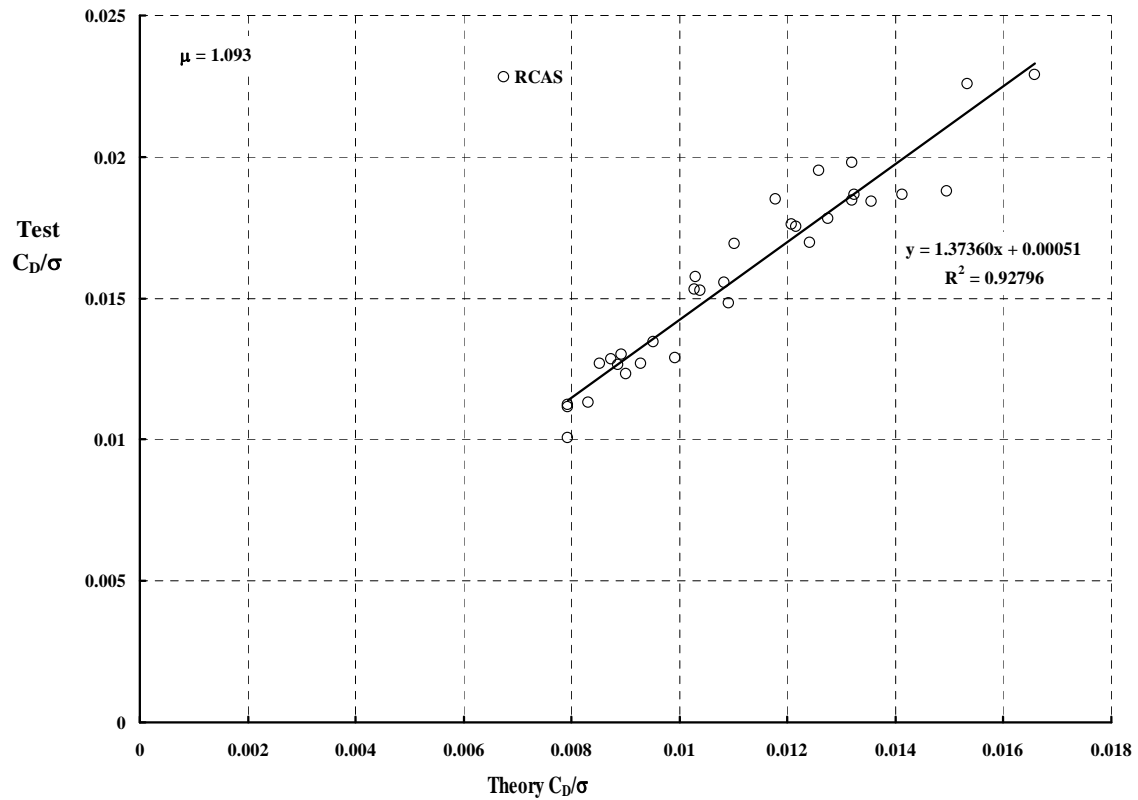
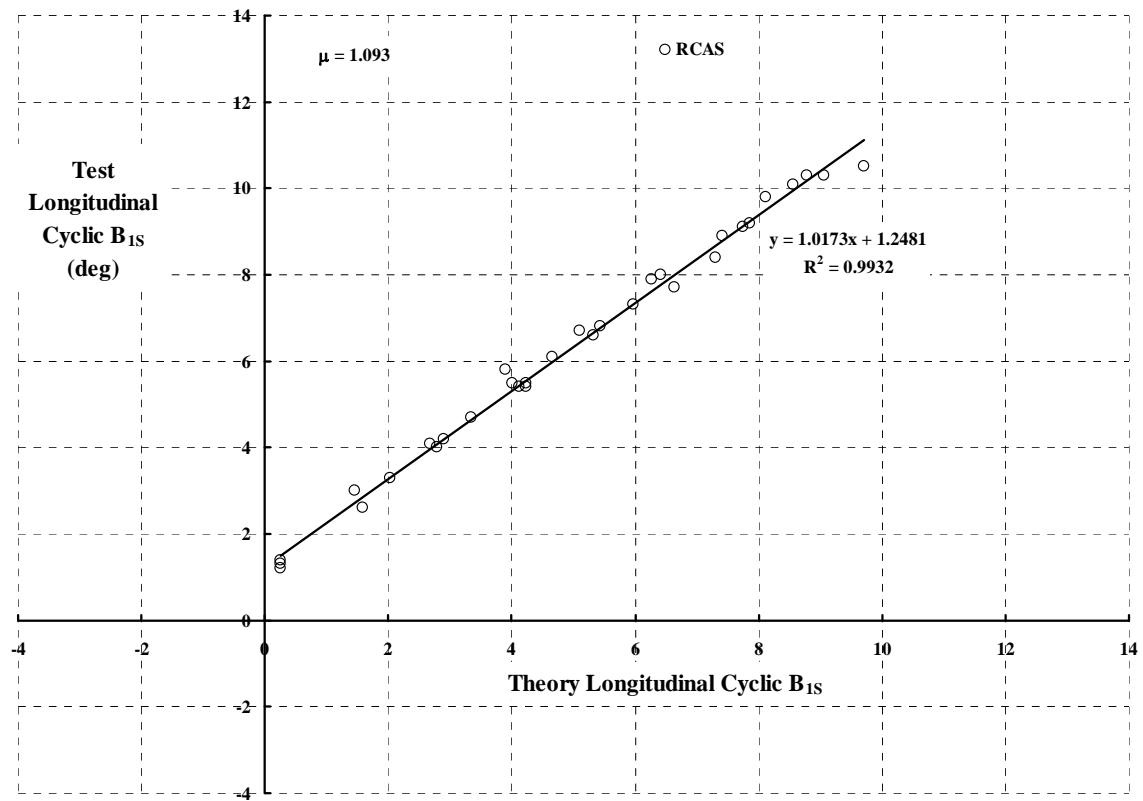


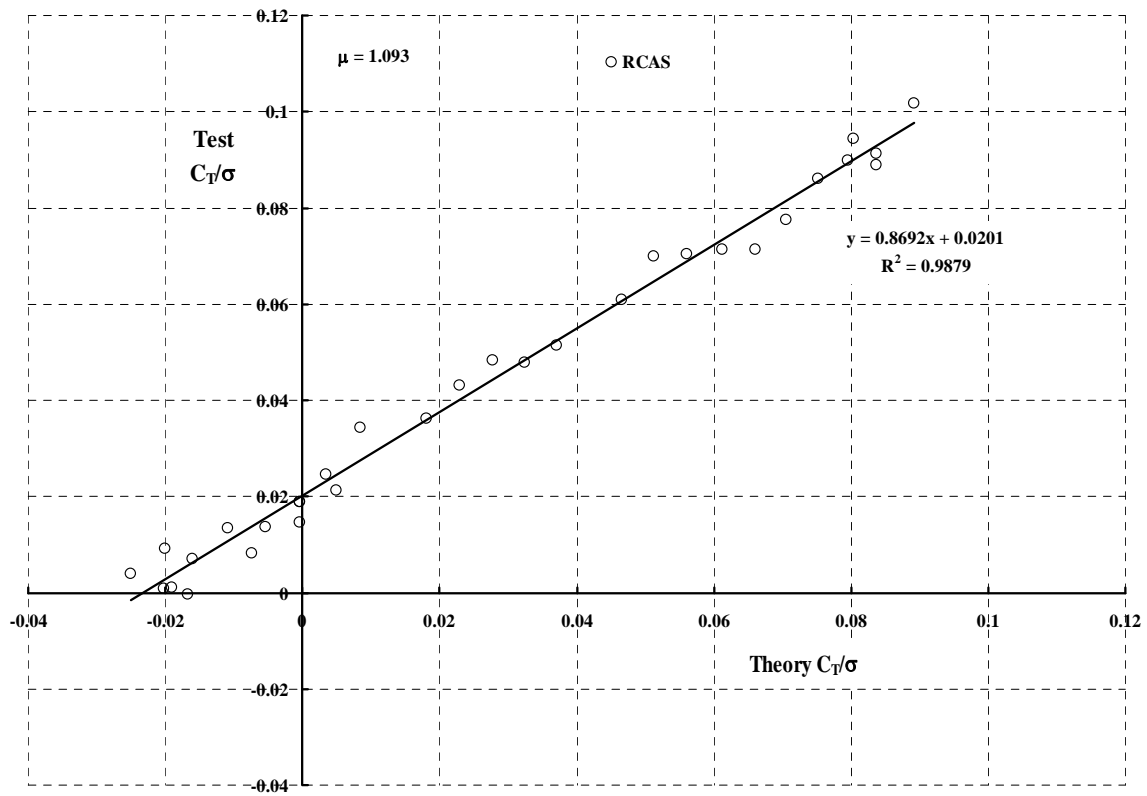
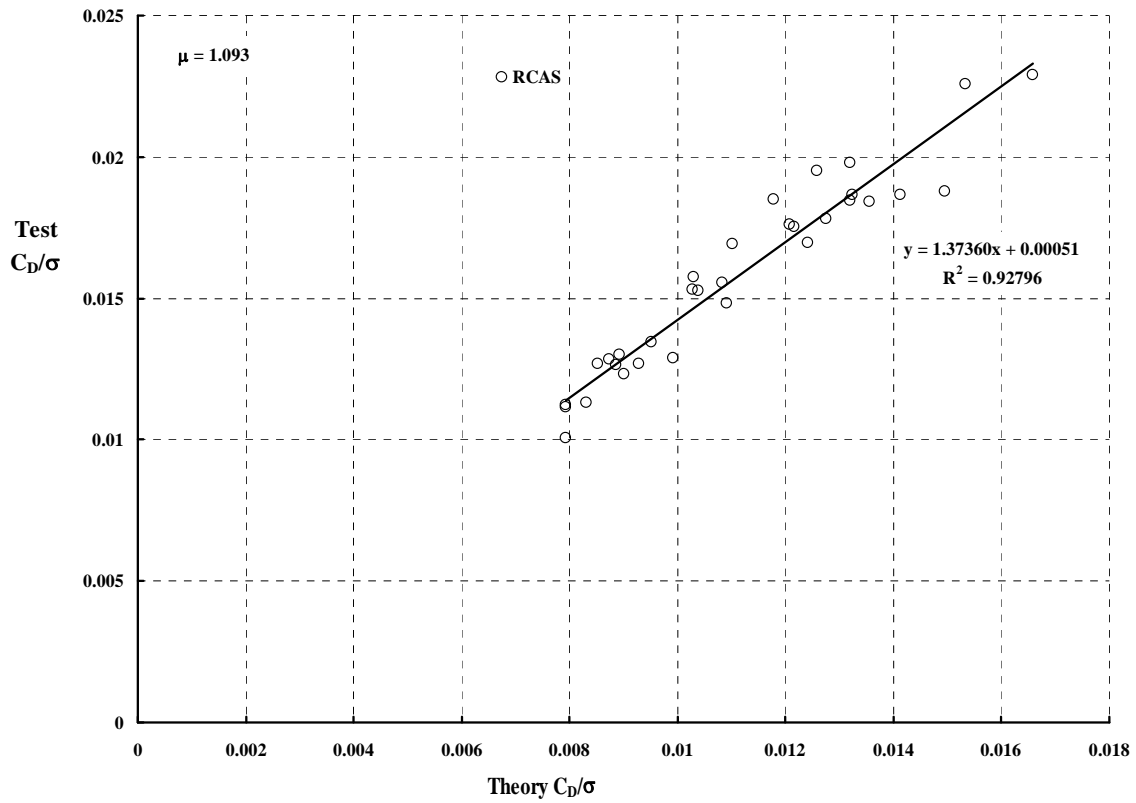


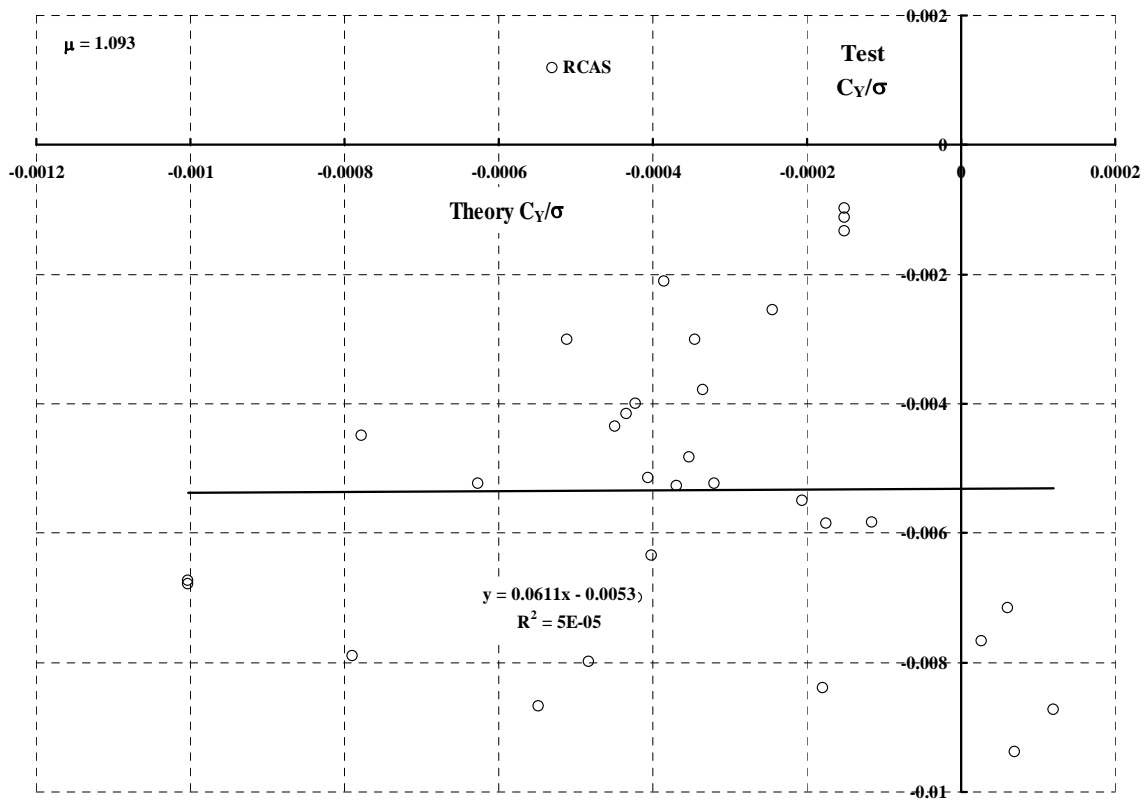
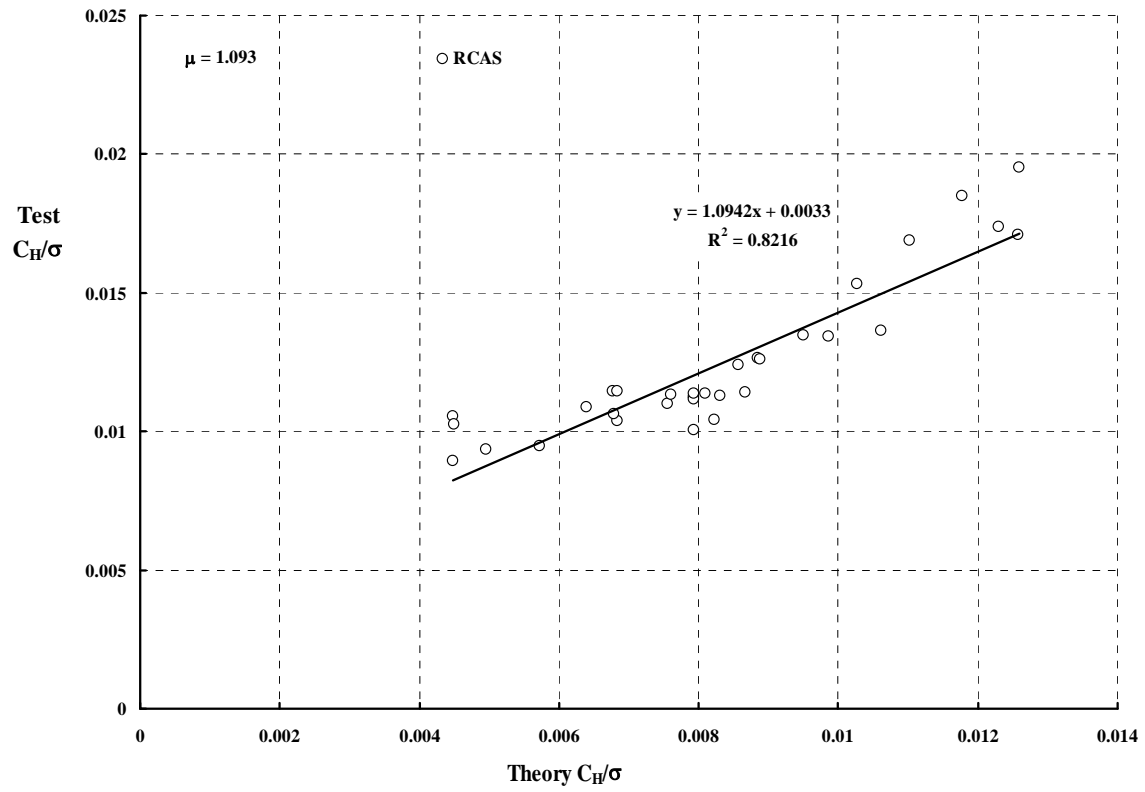


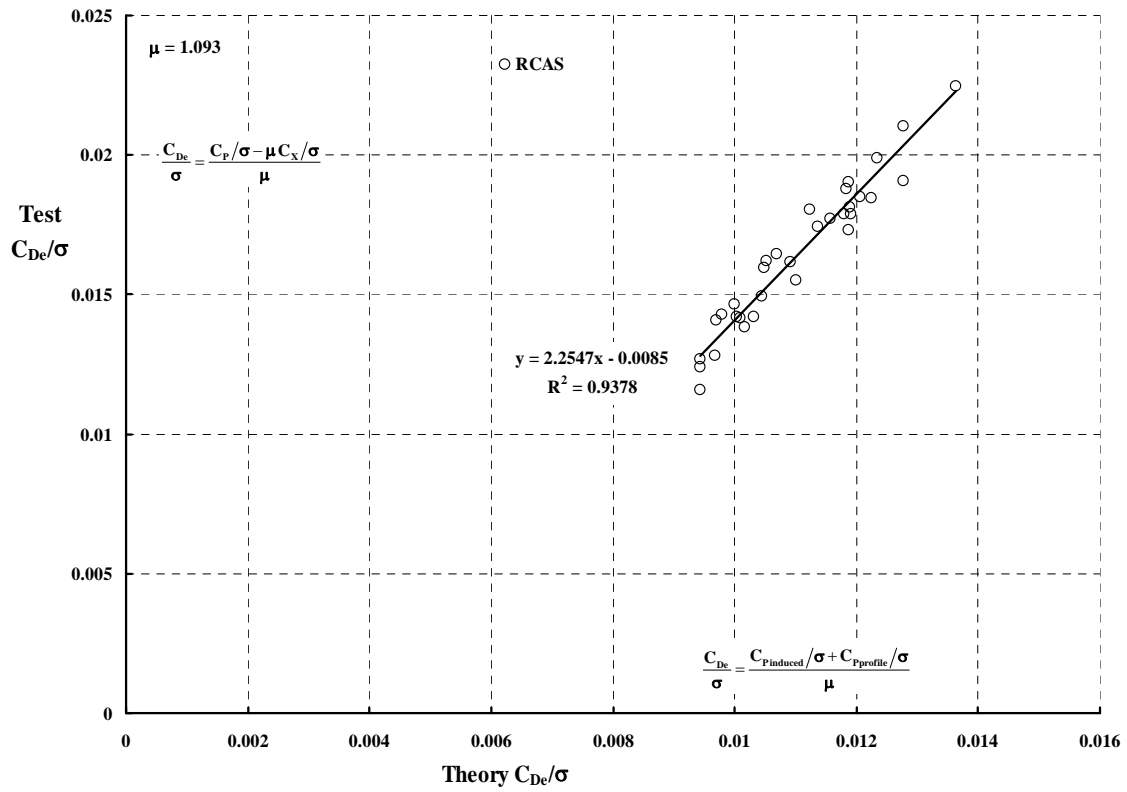
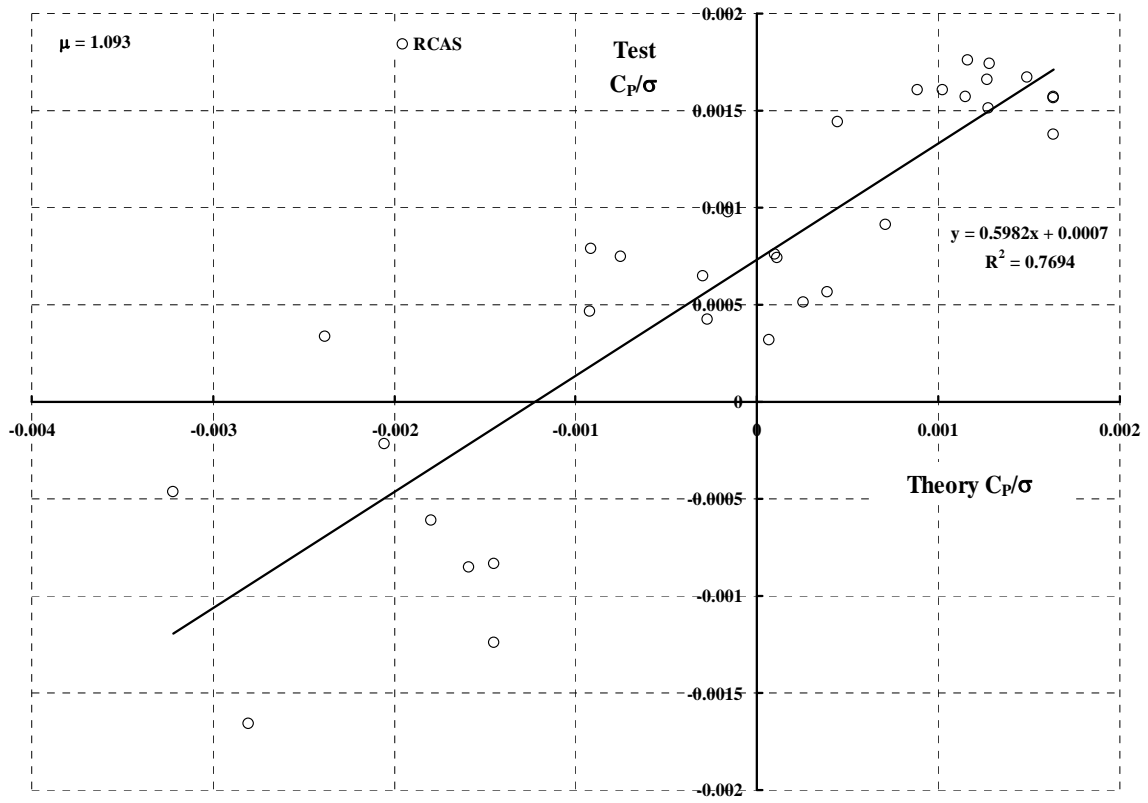


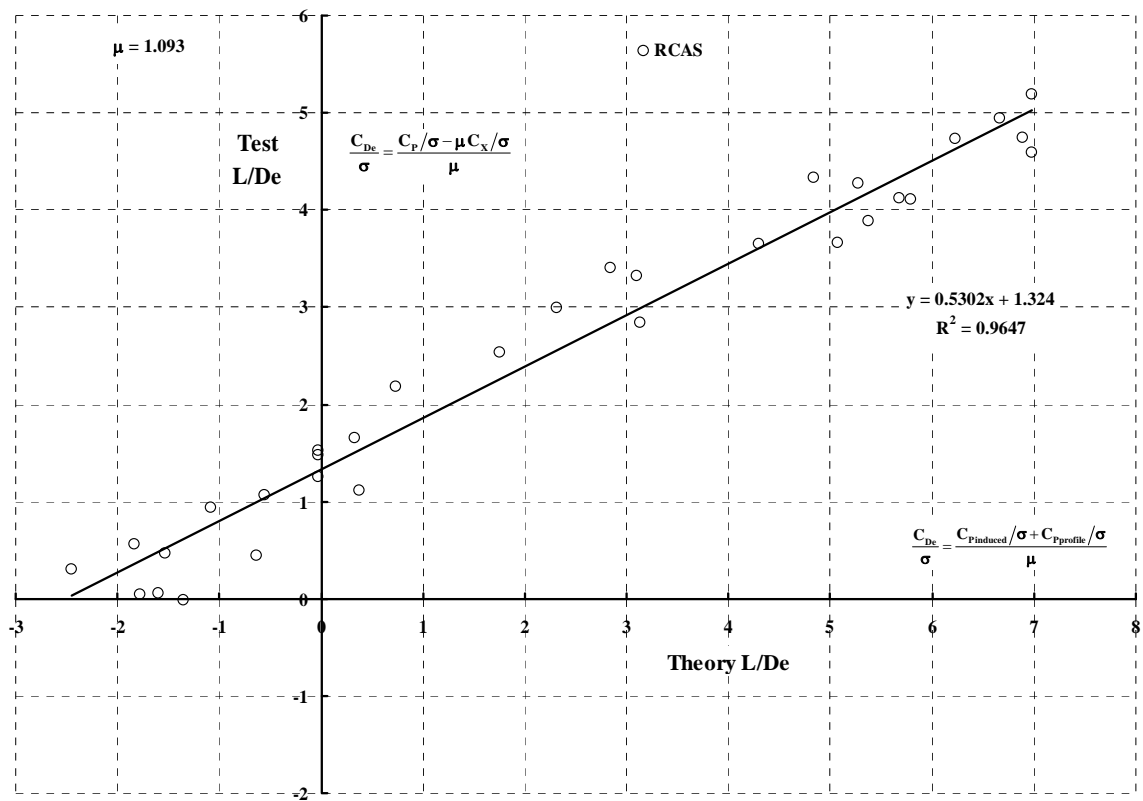






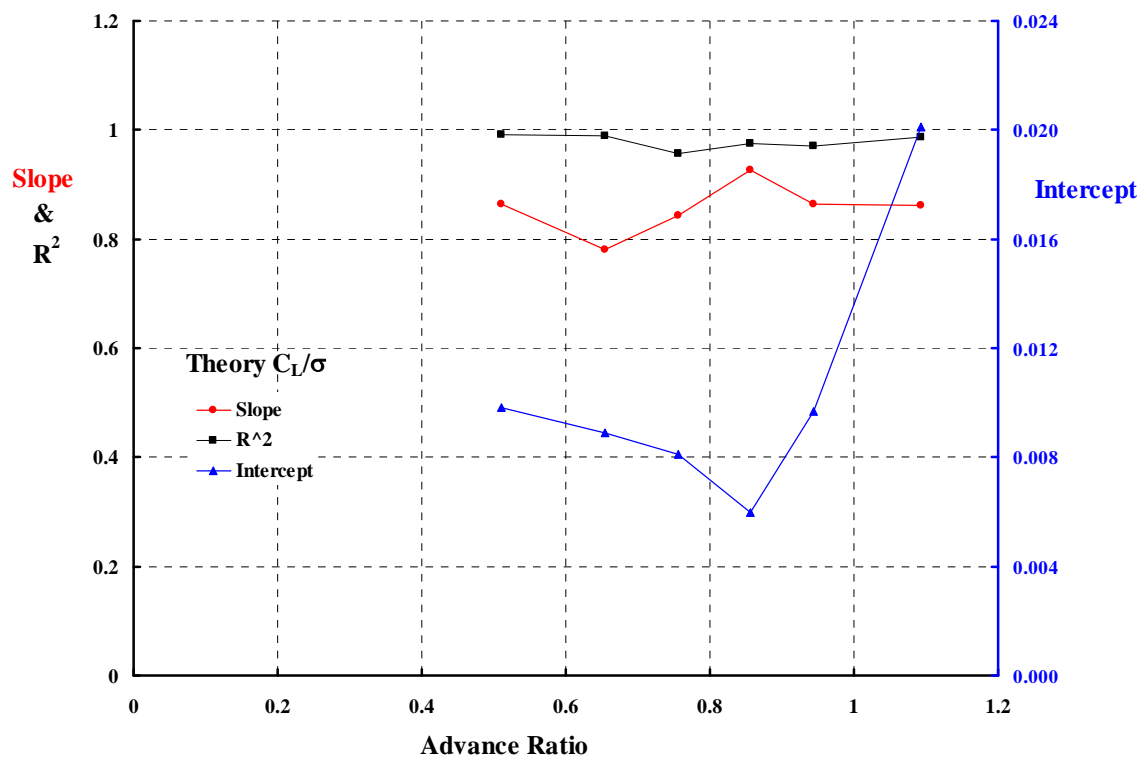


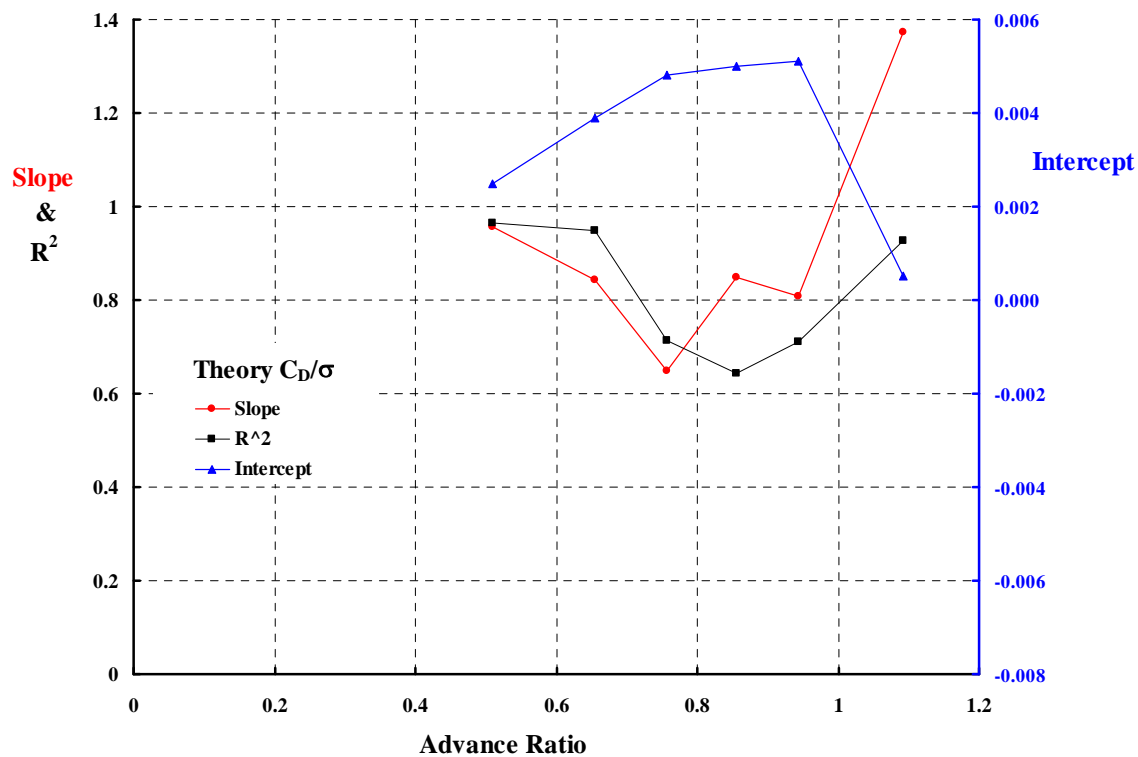
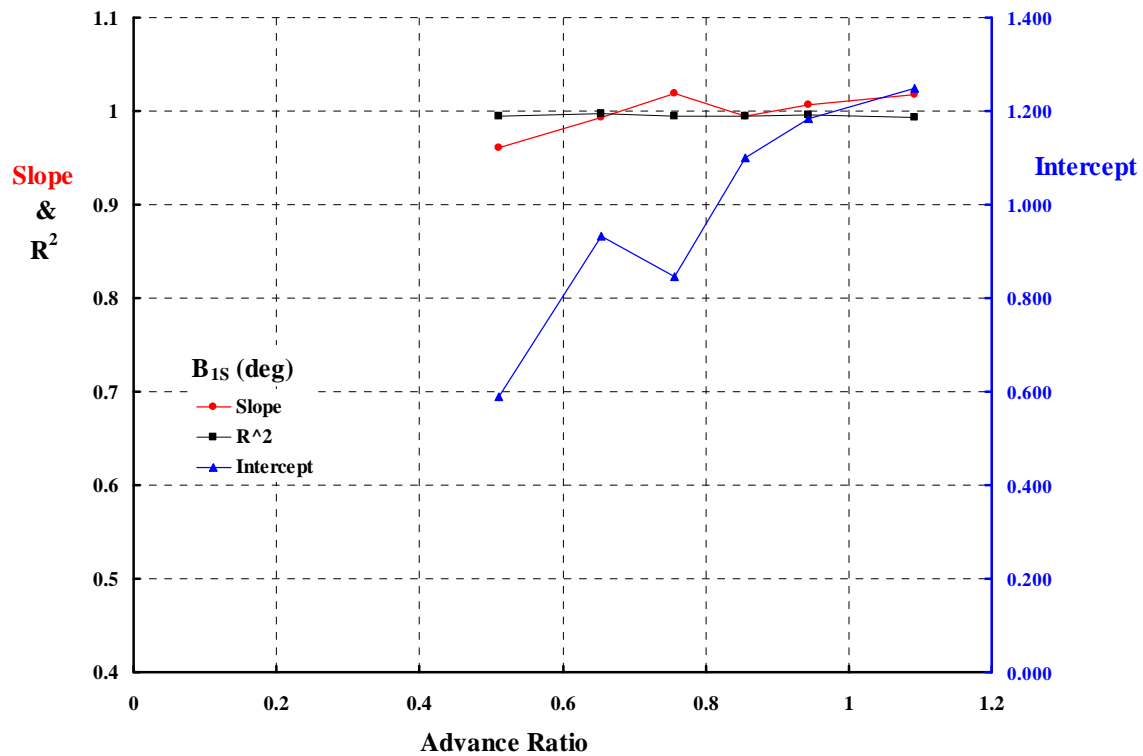


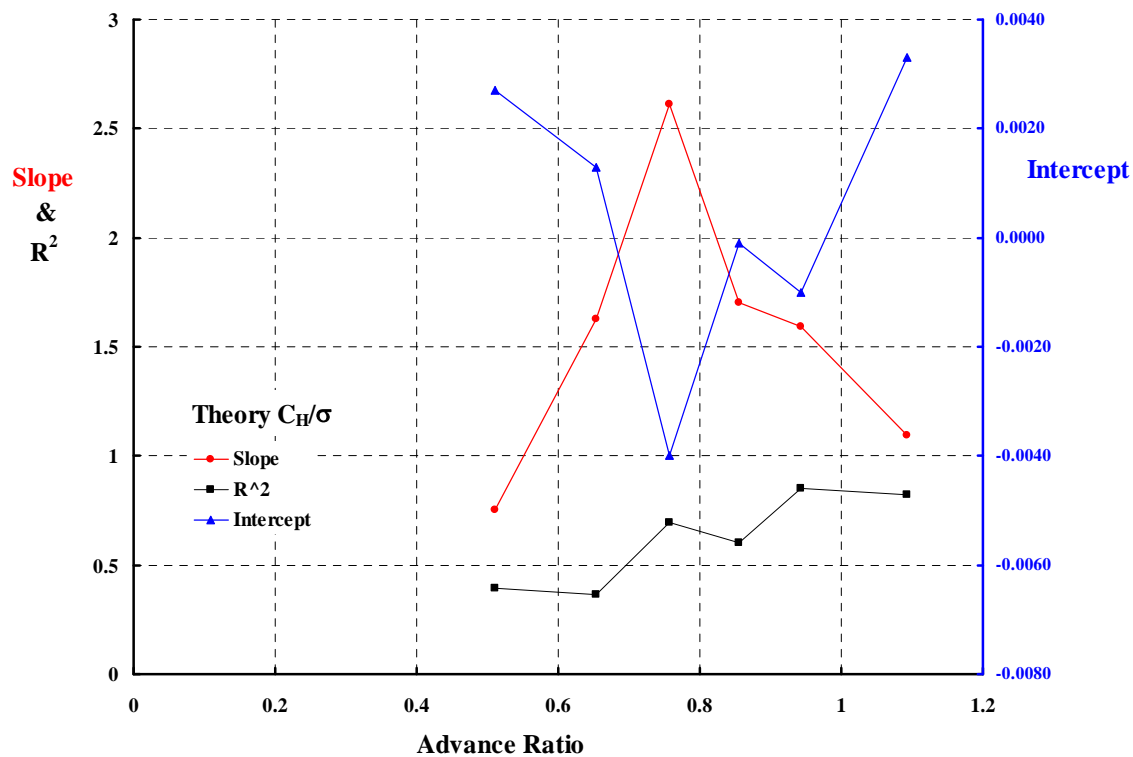
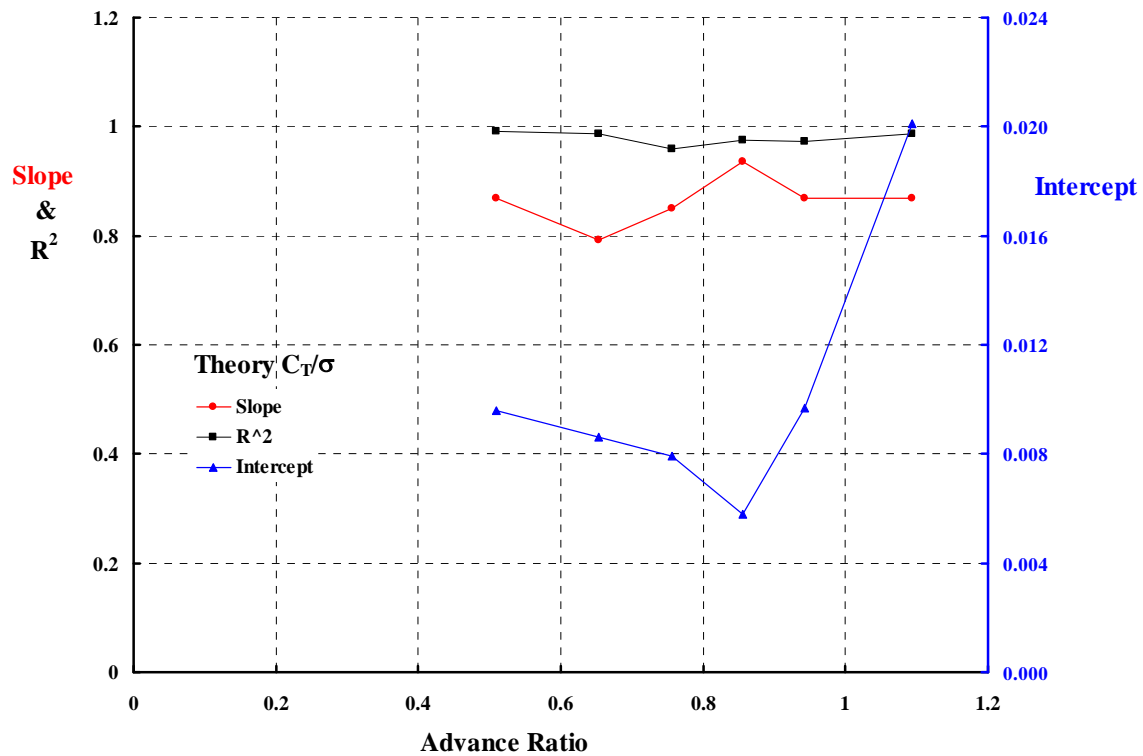


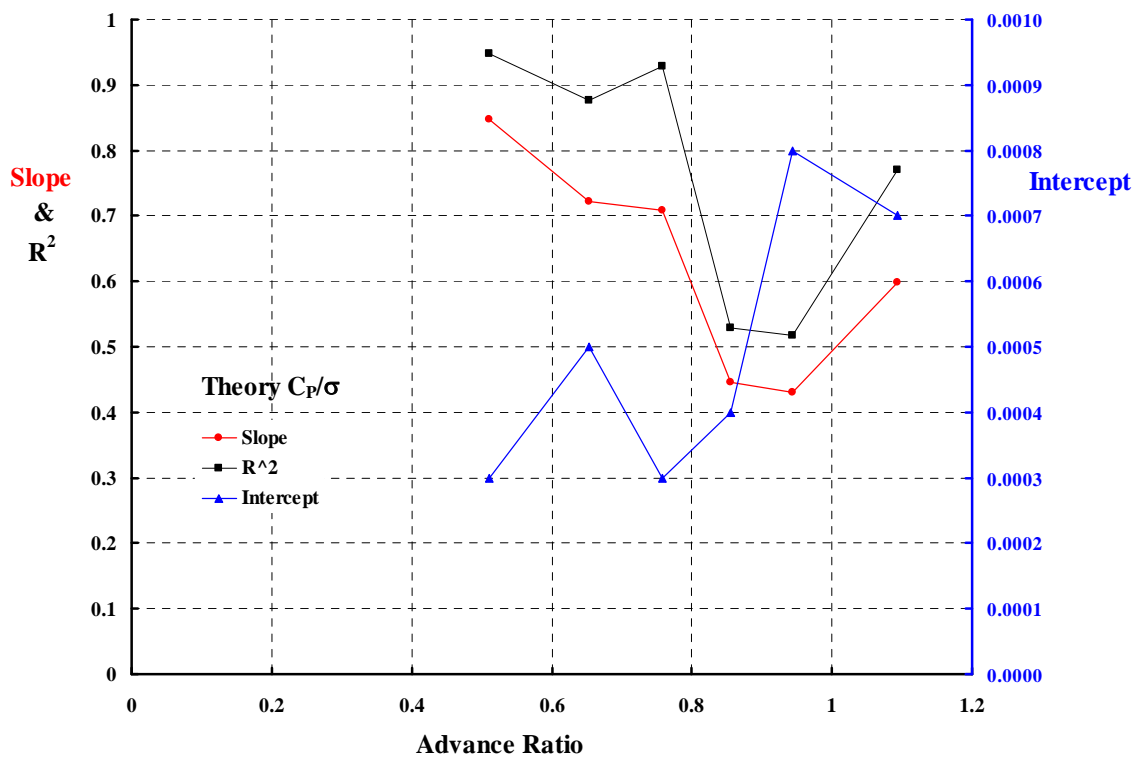
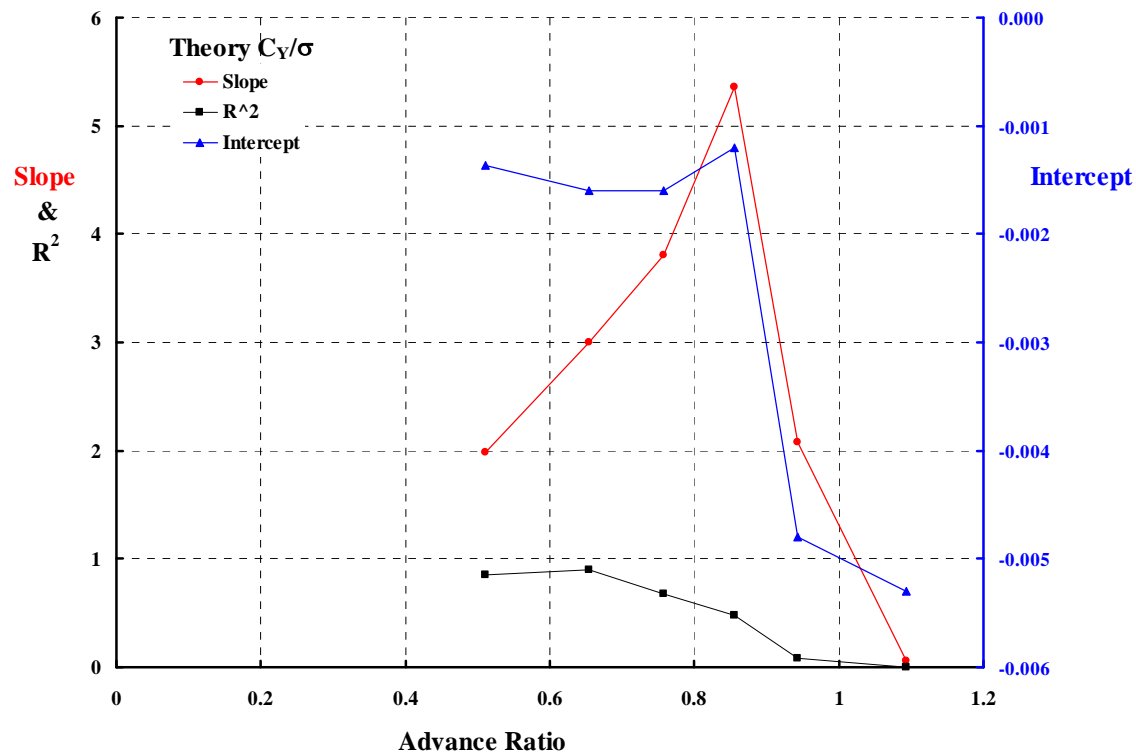
Longitudinal Cyclic				Lateral Cyclic		
Mu	SLOPE	Intercept	R ²	SLOPE	Intercept	R ²
0.510	0.9608	0.5881	0.9947	No test data		
0.654	0.9926	0.9332	0.9968	No test data		
0.757	1.0189	0.8470	0.9950	No test data		
0.856	0.9948	1.0992	0.9949	No test data		
0.943	1.0069	1.1839	0.9965	No test data		
1.093	1.0173	1.2481	0.9932	No test data		
Lift Coefficient				Drag Coefficient		
Mu	SLOPE	Intercept	R ²	SLOPE	Intercept	R ²
0.510	0.8635	0.0098	0.9924	0.9567	0.0025	0.9661
0.654	0.7807	0.0089	0.9883	0.8444	0.0039	0.9498
0.757	0.8439	0.0081	0.9574	0.6476	0.0048	0.7137
0.856	0.9276	0.0060	0.9752	0.8486	0.0050	0.6437
0.943	0.8642	0.0097	0.9717	0.8074	0.0051	0.7104
1.093	0.8617	0.0201	0.9874	1.3736	0.0005	0.9280
Thrust Coefficient				H-Force Coefficient		
Mu	SLOPE	Intercept	R ²	SLOPE	Intercept	R ²
0.510	0.8681	0.0096	0.9917	0.7532	0.0027	0.3922
0.654	0.7912	0.0086	0.9876	1.6293	0.0013	0.3666
0.757	0.8505	0.0079	0.9588	2.6100	-0.0040	0.6946
0.856	0.9366	0.0058	0.9758	1.7007	-0.0001	0.6020
0.943	0.8693	0.0097	0.9729	1.5901	-0.0010	0.8506
1.093	0.8692	0.0201	0.9879	1.0942	0.0033	0.8216
Y-Force Coefficient				Power Coefficient		
Mu	SLOPE	Intercept	R ²	SLOPE	Intercept	R ²
0.510	1.9830	-0.0014	0.8571	0.8479	0.0003	0.9474
0.654	2.9958	-0.0016	0.8938	0.7225	0.0005	0.8759
0.757	3.8110	-0.0016	0.6778	0.7094	0.0003	0.9288
0.856	5.3540	-0.0012	0.4770	0.4453	0.0004	0.5281
0.943	2.0835	-0.0048	0.0781	0.4302	0.0008	0.5165
1.093	0.0611	-0.0053	0.0001	0.5982	0.0007	0.7694

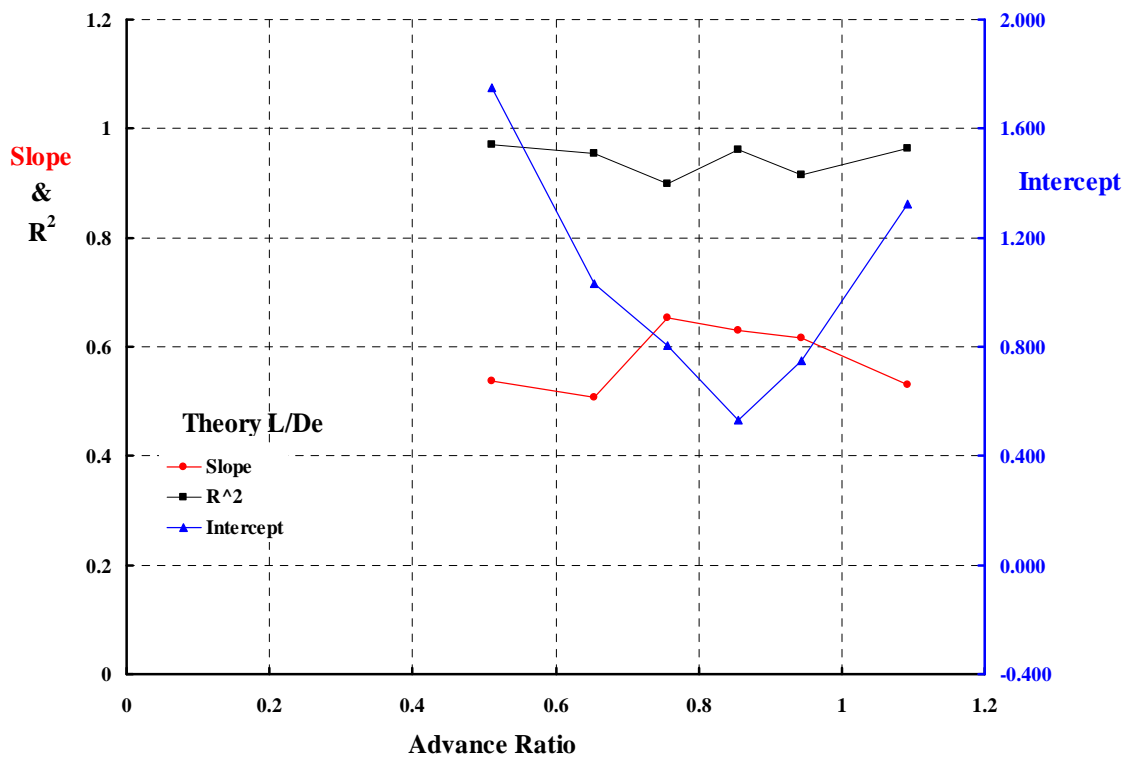
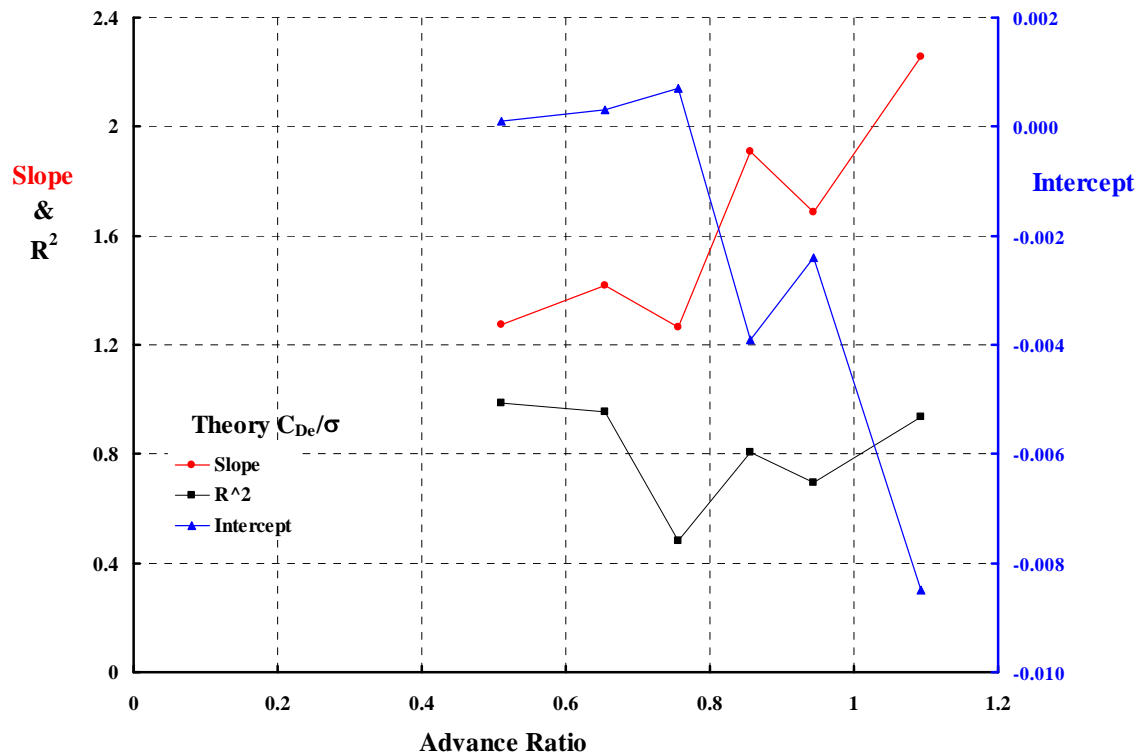
Mu	CDe			L/De		
	SLOPE	Intercept	R ²	SLOPE	Intercept	R ²
0.510	1.2750	0.0001	0.9864	0.5386	1.7499	0.9704
0.654	1.4173	0.0003	0.9557	0.5062	1.0334	0.9543
0.757	1.2646	0.0007	0.4824	0.6539	0.8066	0.8999
0.856	1.9072	-0.0039	0.8055	0.6299	0.5301	0.9613
0.943	1.6845	-0.0024	0.6952	0.6167	0.7486	0.9158
1.093	2.2547	-0.0085	0.9378	0.5302	1.3240	0.9647











11.17 UH-1 versus OVERFLOW-2 Coupled with CAMRAD II

No UH-1 points were computed by OVERFLOW-2 Coupled with CAMRAD II

11.18 PCA-2 versus CAMRAD II

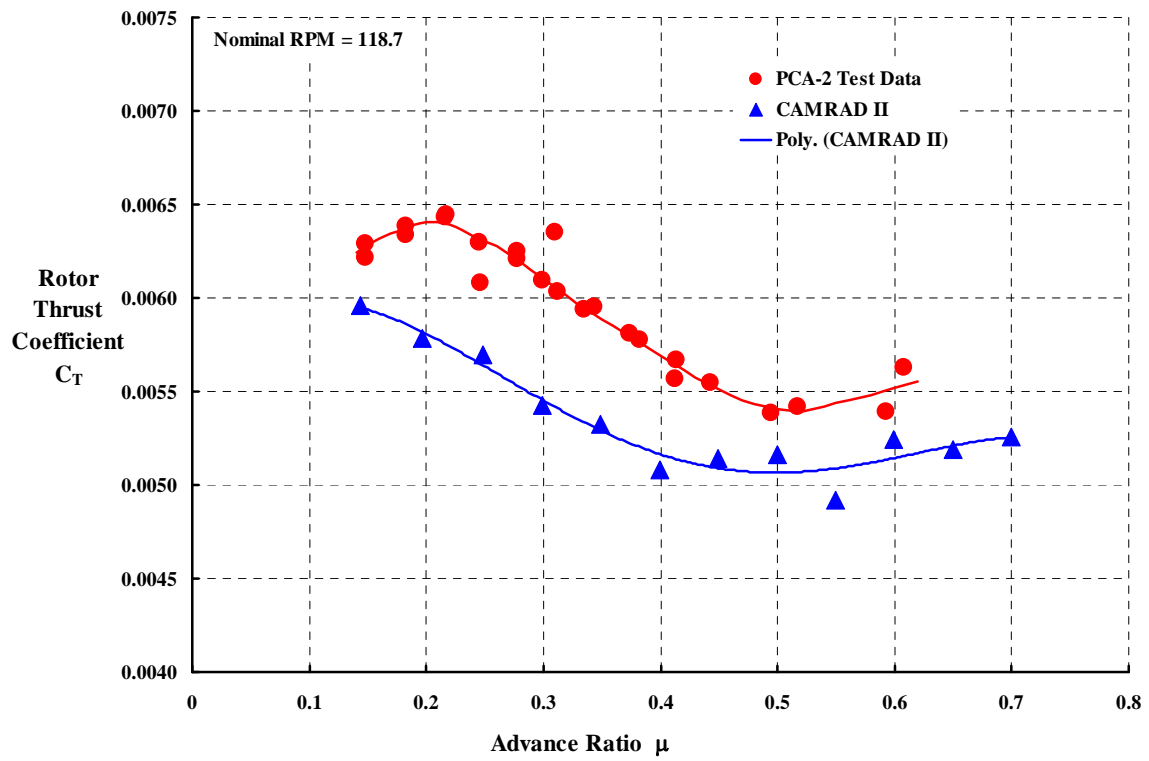
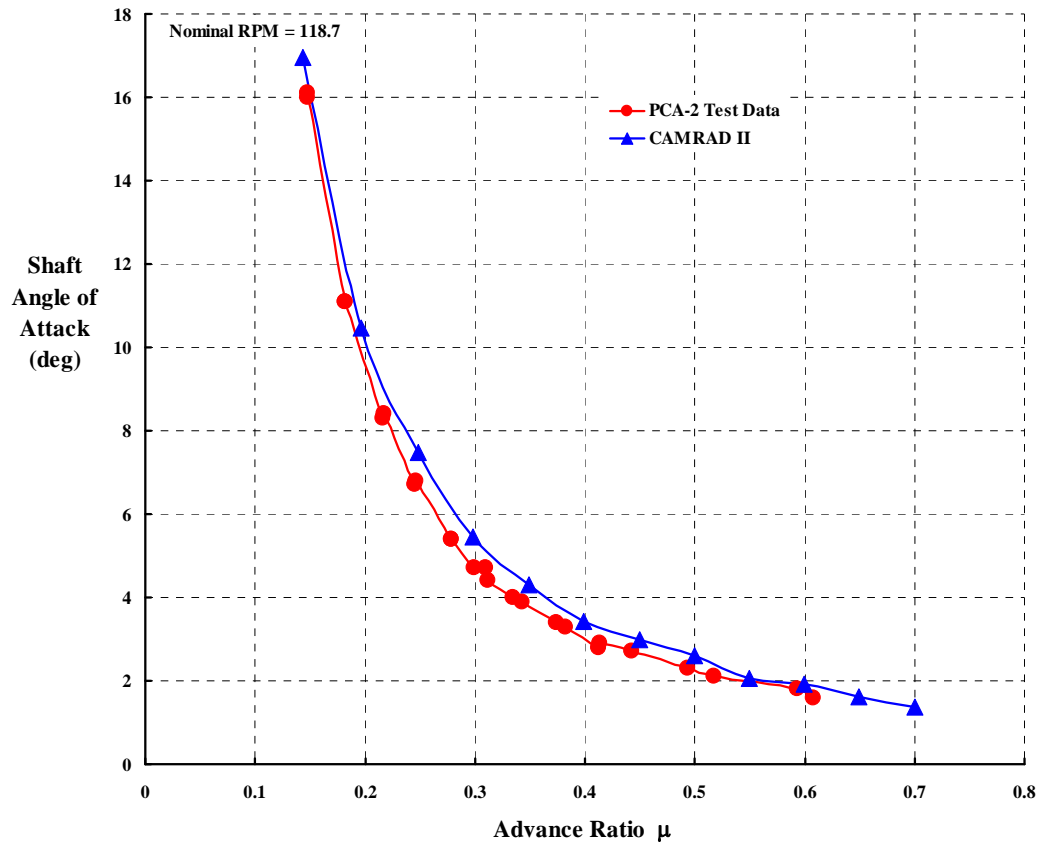
References: 1. N.A.C.A. Report No. 515, Full-Scale Wind-Tunnel Tests of a PCA-2 Autogiro Rotor by John B. Wheatley and Manley J. Hood, October 1934
2. Harris EXCEL File: PCA-2 versus CAMRAD II (PLUS Rotor Alone Test Data + Geometry & Properties).xls

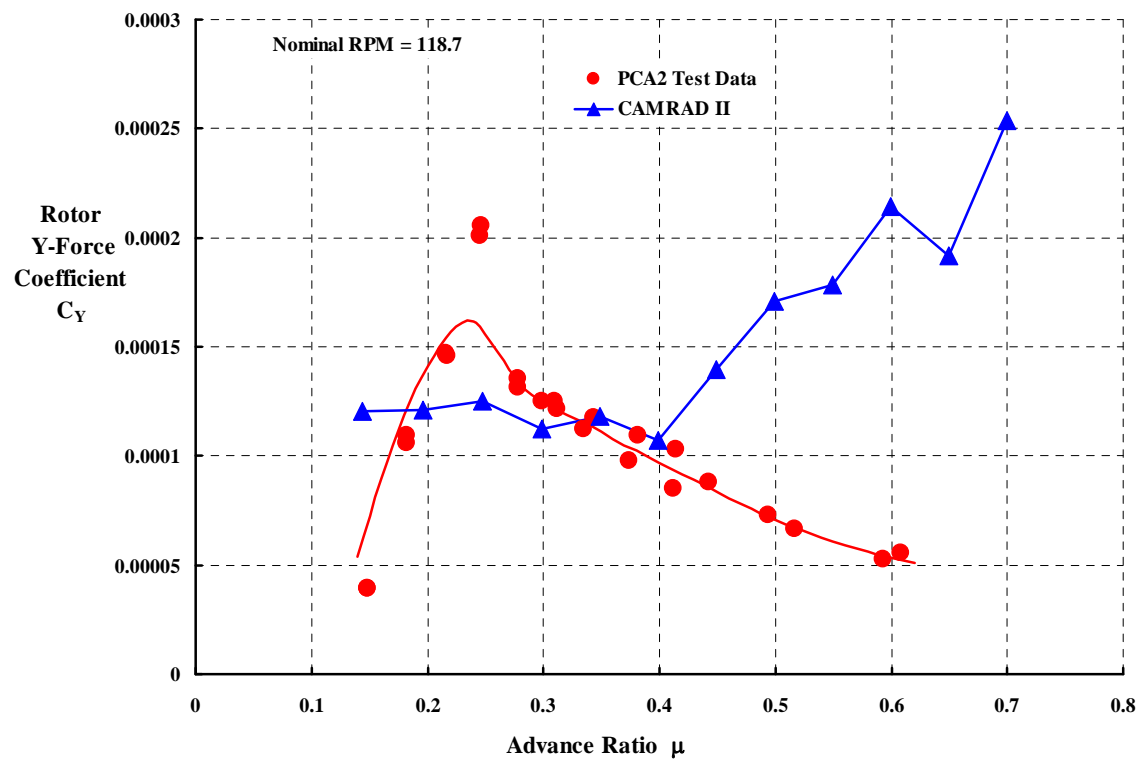
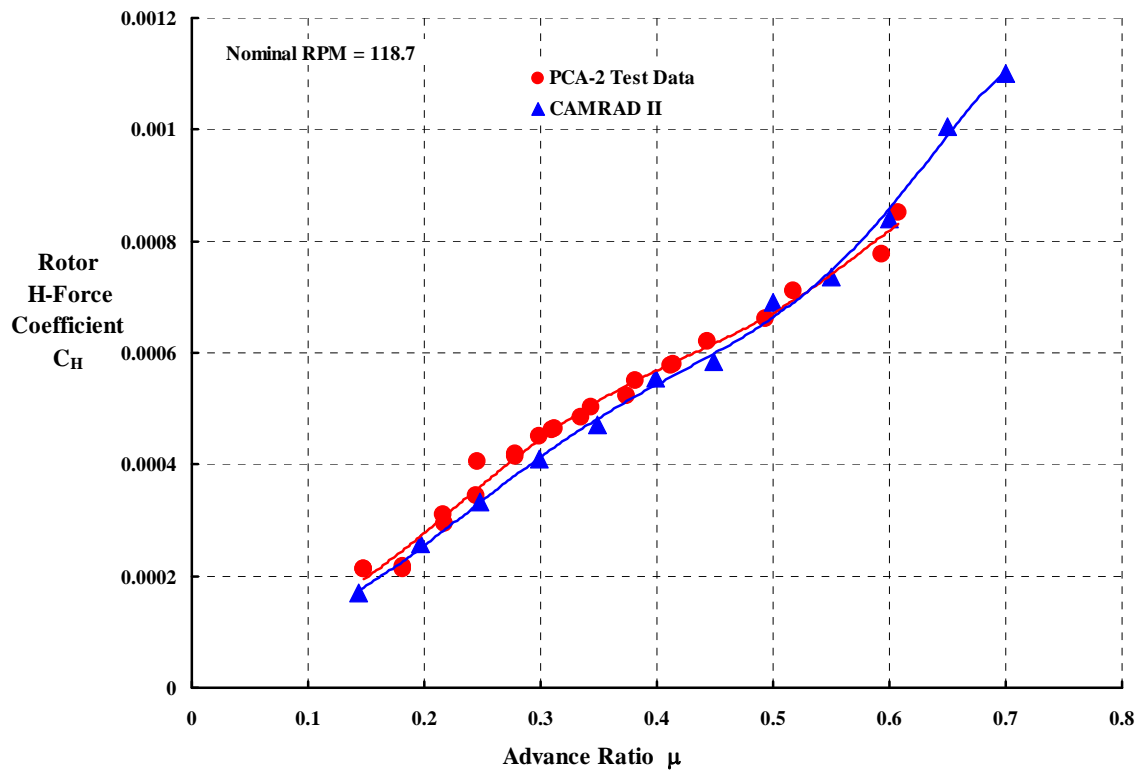
Airfoil	See Appendix 11.5, page 222
Chord	See Appendix 11.5, page 222
Diameter	45.00 ft
Twist	See Appendix 11.5, page 222
Disc Area	1,588 sq. ft
Reference Area (4 blades)	154.4 sq. ft
Nominal Solidity	0.0971
Lock Number	19.2
Flap Moment of inertia	334 slug ft ²
Weight Moment	780 lb-ft
Flap Hinge Radius	3.375 inches
Lag Hinge Radius	7.75 inches

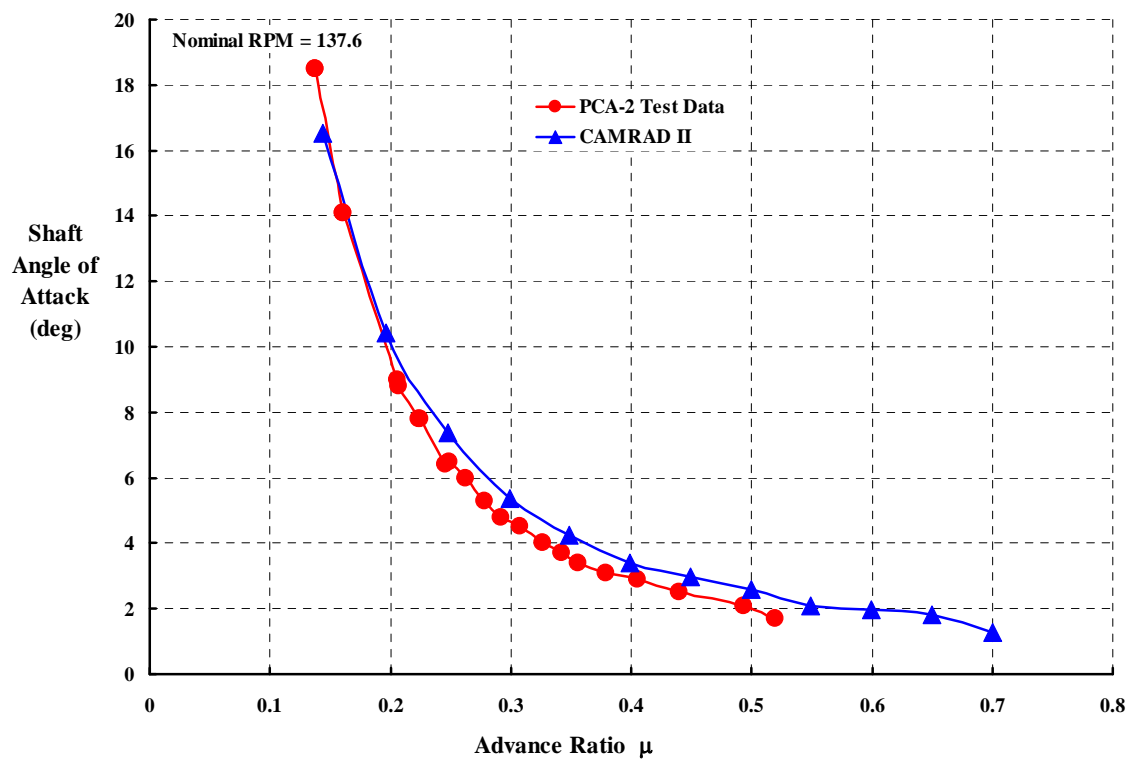
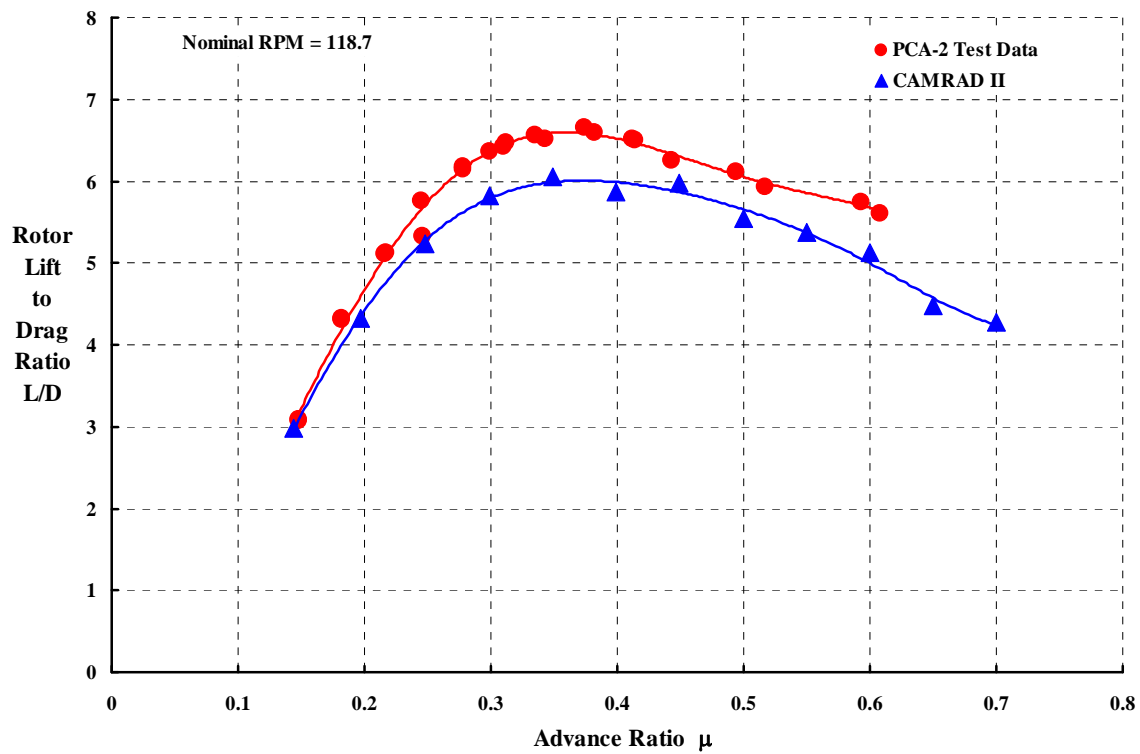
Notes: 1. Wind axis data measured. Shaft axis data derived.
2. Shaft torque equal zero for all data points because rotor unpowered.
3. Wind axis coefficients based on wind tunnel dynamic pressure and rotor disc area ($A = 1,590$ sq. ft.).
4. Derived shaft axis coefficients based on rotor tip speed and rotor disc area ($A = 1,590$ sq. ft.).
5. Data includes hub drag and drag of droop and blade to blade lag cables.
6. Articulated flap and lag hub but with no in-flight pitch change provisions.

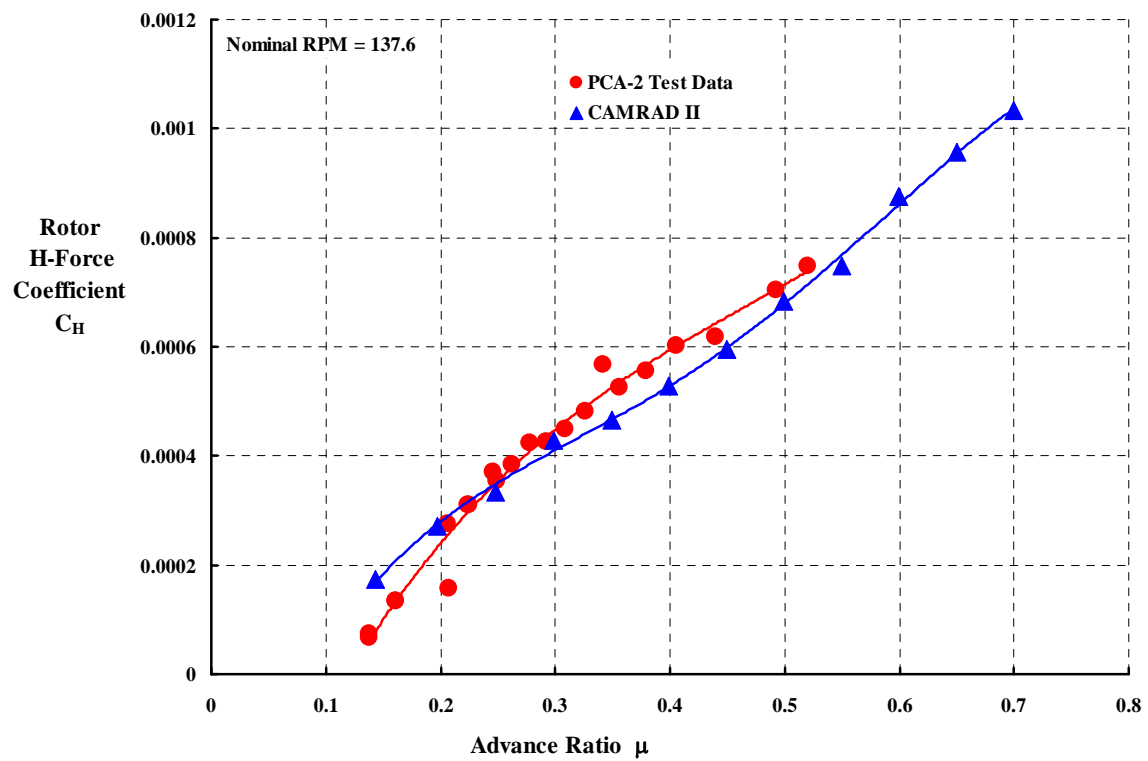
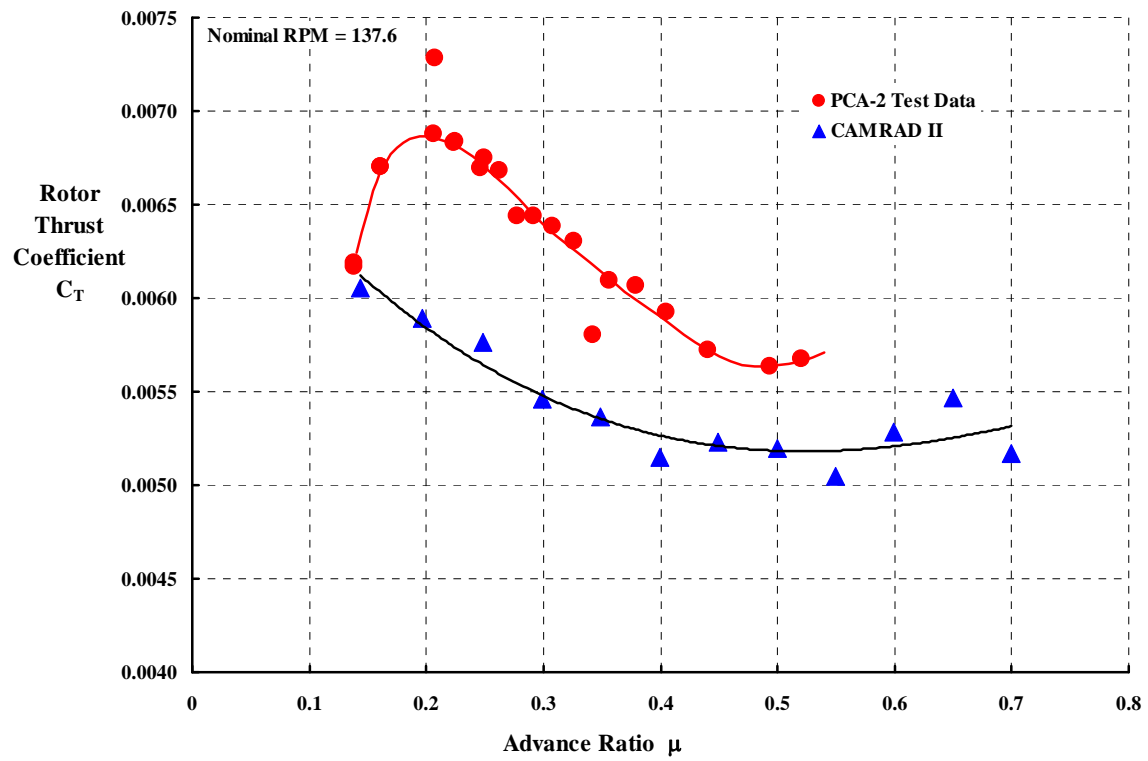
Advance Ratio	Shaft Angle of Attack (deg)	Airplane Lift Coeff.	Airplane Drag Coeff.	L / D	RPM	Airplane Rolling Moment Coeff.	Airplane Pitching Moment Coeff.	Airplane Lateral Force Coeff.	Rotor C _T	Rotor C _H	Rotor C _Y
0.1435	16.98	0.494326	0.166101	2.986	98.63	0.000310	-0.000191	0.010333	0.005862	0.000164	0.000116
0.1966	10.56	0.279403	0.065150	4.296	98.63	0.000136	0.000181	0.005568	0.005729	0.000257	0.000111
0.2478	7.53	0.176877	0.034163	5.183	98.63	0.000075	0.000212	0.003526	0.005617	0.000335	0.000110
0.2986	5.52	0.117805	0.020489	5.745	98.63	0.000060	0.000202	0.002249	0.005363	0.000408	0.000101
0.3490	4.41	0.085388	0.014319	5.962	98.63	0.000029	0.000202	0.001775	0.005279	0.000472	0.000109
0.3993	3.47	0.063016	0.010506	5.988	98.63	0.000013	0.000156	0.001175	0.005081	0.000533	0.000094
0.4494	3.08	0.050612	0.008575	5.904	98.63	0.000010	0.000169	0.001229	0.005161	0.000592	0.000124
0.4995	2.66	0.040677	0.007640	5.331	98.63	-0.000003	0.000174	0.001258	0.005119	0.000718	0.000157
0.5496	2.16	0.032842	0.006428	5.114	98.63	-0.000008	0.000160	0.001023	0.004996	0.000784	0.000155
0.5997	1.77	0.027555	0.005879	4.688	98.63	-0.000008	0.000106	0.000886	0.004986	0.000904	0.000159
0.6498	1.29	0.022296	0.005152	4.327	98.63	0.000033	0.000095	0.000839	0.004729	0.000982	0.000177
0.6999	1.08	0.019634	0.004833	3.981	98.63	0.000004	0.000113	0.000966	0.004824	0.001093	0.000237
0.1435	16.97	0.502316	0.168932	2.976	118.7	0.000342	0.000057	0.010706	0.005957	0.000169	0.000120
0.1967	10.46	0.282081	0.065175	4.318	118.7	0.000163	0.000262	0.006041	0.005782	0.000258	0.000121
0.2479	7.48	0.179419	0.034337	5.242	118.7	0.000094	0.000279	0.003998	0.005696	0.000334	0.000125
0.2986	5.45	0.119231	0.020489	5.821	118.7	0.000074	0.000251	0.002492	0.005426	0.000409	0.000112
0.3490	4.31	0.086116	0.014187	6.054	118.7	0.000057	0.000222	0.001931	0.005322	0.000470	0.000118
0.3993	3.43	0.063047	0.010711	5.874	118.7	0.000038	0.000187	0.001337	0.005083	0.000554	0.000107
0.4494	3.00	0.050442	0.008411	5.983	118.7	0.000028	0.000204	0.001380	0.005142	0.000584	0.000140
0.4995	2.61	0.041019	0.007399	5.544	118.7	0.000029	0.000180	0.001367	0.005160	0.000691	0.000171
0.5496	2.06	0.032368	0.006025	5.368	118.7	0.000012	0.000171	0.001180	0.004921	0.000735	0.000179
0.5997	1.93	0.028991	0.005651	5.124	118.7	-0.000005	0.000152	0.001191	0.005244	0.000840	0.000214
0.6497	1.63	0.024436	0.005461	4.479	118.7	0.000005	0.000155	0.000909	0.005187	0.001006	0.000192

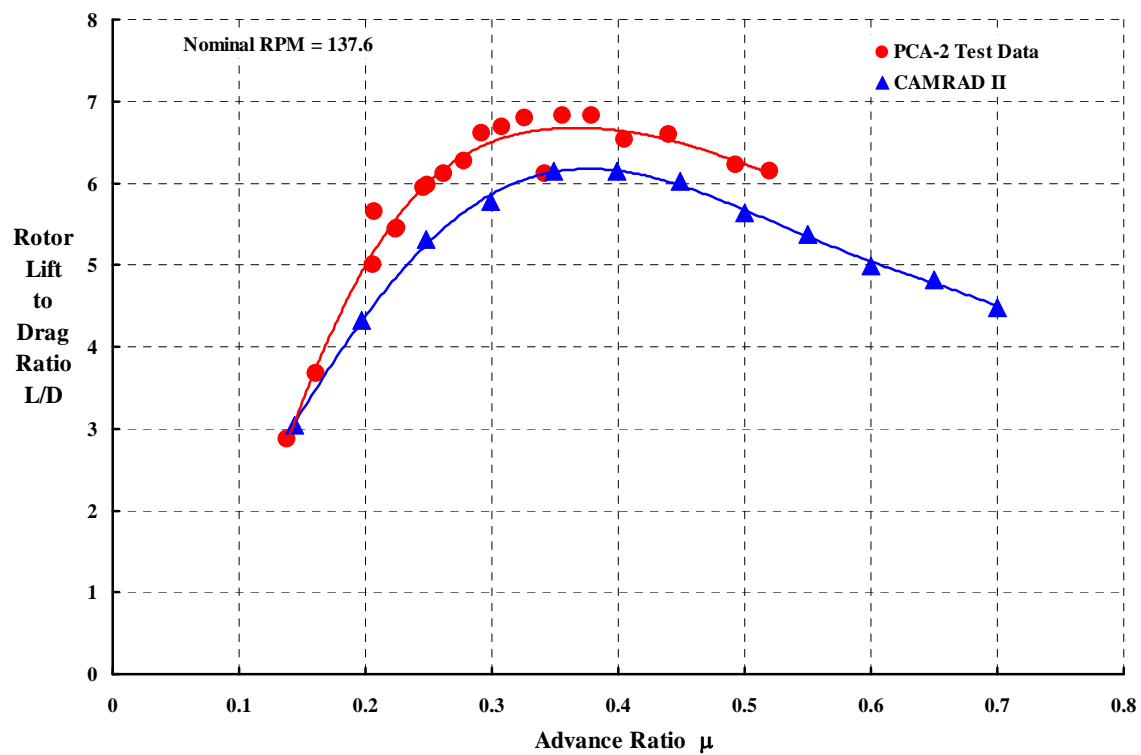
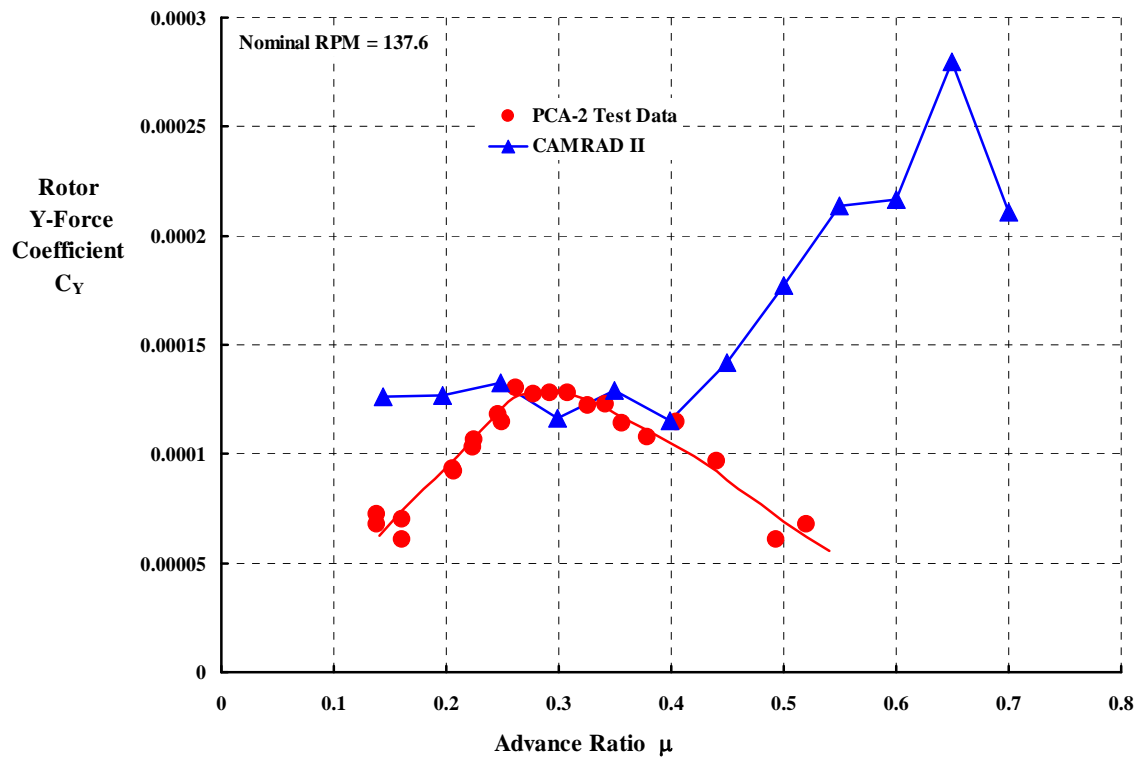
0.6998	1.38	0.021369	0.005008	4.271	118.7	-0.000006	0.000110	0.001036	0.005256	0.001100	0.000254
0.1438	16.54	0.511681	0.168126	3.05	137.6	0.000321	0.000253	0.011200	0.006054	0.000175	0.000126
0.1967	10.44	0.287443	0.066729	4.317	137.6	0.000181	0.000342	0.006339	0.005892	0.000271	0.000127
0.2479	7.36	0.181626	0.034224	5.307	137.6	0.000117	0.000317	0.004251	0.005763	0.000334	0.000133
0.2987	5.35	0.120000	0.020784	5.77	137.6	0.000112	0.000269	0.002590	0.005461	0.000428	0.000117
0.3490	4.26	0.086831	0.014101	6.148	137.6	0.000077	0.000223	0.002108	0.005365	0.000466	0.000129
0.3993	3.39	0.063909	0.010398	6.149	137.6	0.000039	0.000193	0.001442	0.005150	0.000528	0.000115
0.4494	2.97	0.051300	0.008533	6.025	137.6	0.000028	0.000202	0.001399	0.005228	0.000594	0.000142
0.4995	2.57	0.041302	0.007328	5.639	137.6	0.000026	0.000180	0.001416	0.005194	0.000683	0.000177
0.5496	2.10	0.033197	0.006169	5.379	137.6	0.000012	0.000181	0.001412	0.005046	0.000749	0.000214
0.5996	1.97	0.029218	0.005870	4.983	137.6	0.000034	0.000165	0.001203	0.005287	0.000875	0.000216
0.6497	1.81	0.025760	0.005344	4.826	137.6	0.000033	0.000146	0.001324	0.005467	0.000956	0.000280
0.6998	1.27	0.021027	0.004685	4.485	137.6	0.000011	0.000126	0.000860	0.005170	0.001033	0.000211
0.1438	16.52	0.516425	0.169777	3.046	147.9	0.000338	0.000316	0.011512	0.006110	0.000180	0.000130
0.1967	10.38	0.288981	0.066816	4.312	147.9	0.000191	0.000343	0.006578	0.005922	0.000273	0.000132
0.2479	7.35	0.182513	0.034661	5.269	147.9	0.000128	0.000339	0.004313	0.005793	0.000345	0.000135
0.2987	5.30	0.120677	0.020534	5.876	147.9	0.000100	0.000270	0.002611	0.005490	0.000419	0.000118
0.3490	4.23	0.087459	0.014184	6.17	147.9	0.000079	0.000237	0.002164	0.005403	0.000470	0.000133
0.3993	3.44	0.065334	0.010607	6.177	147.9	0.000066	0.000220	0.001446	0.005266	0.000533	0.000116
0.4494	2.91	0.051259	0.009104	5.636	147.9	0.000048	0.000192	0.001201	0.005227	0.000657	0.000122
0.4995	2.57	0.041501	0.007368	5.644	147.9	0.000038	0.000177	0.001426	0.005220	0.000688	0.000178
0.5496	2.06	0.033192	0.006260	5.307	147.9	0.000026	0.000160	0.001268	0.005046	0.000766	0.000192
0.5996	1.99	0.029903	0.005895	5.072	147.9	0.000028	0.000170	0.001173	0.005411	0.000874	0.000211
0.6497	1.71	0.025599	0.005539	4.627	147.9	0.000003	0.000154	0.001314	0.005431	0.001008	0.000278
0.6998	1.45	0.022245	0.005113	4.349	147.9	-0.000005	0.000110	0.001209	0.005470	0.001115	0.000296

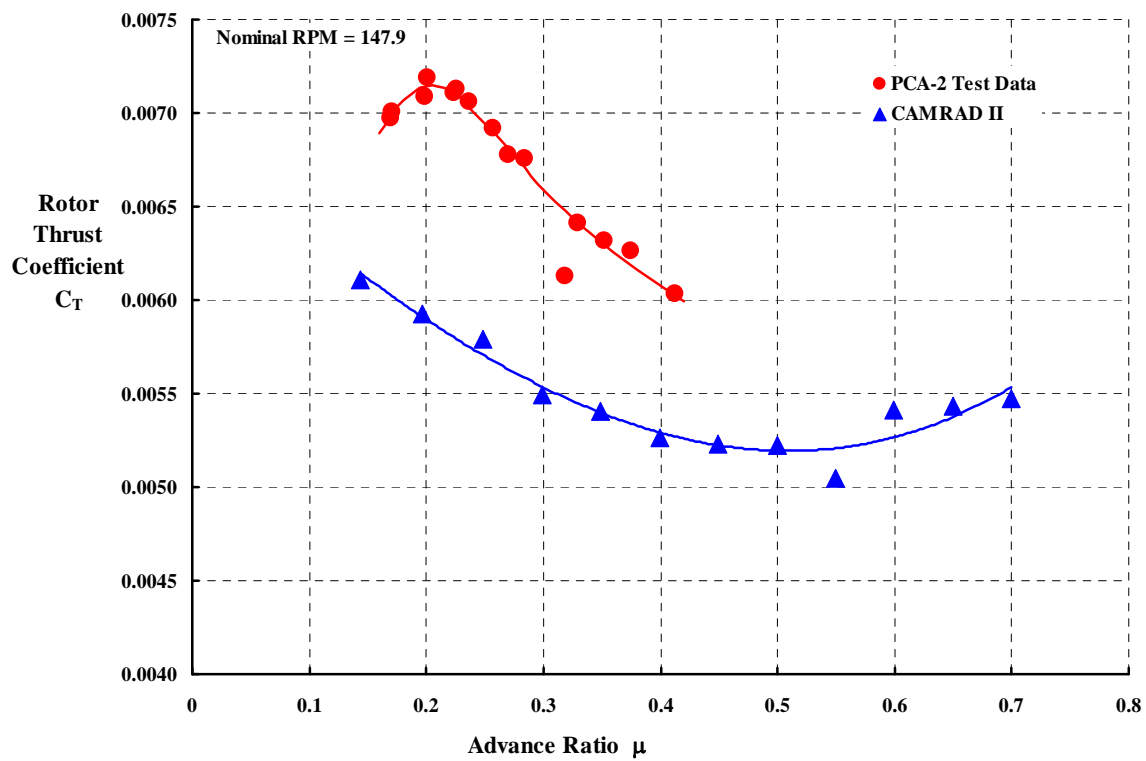
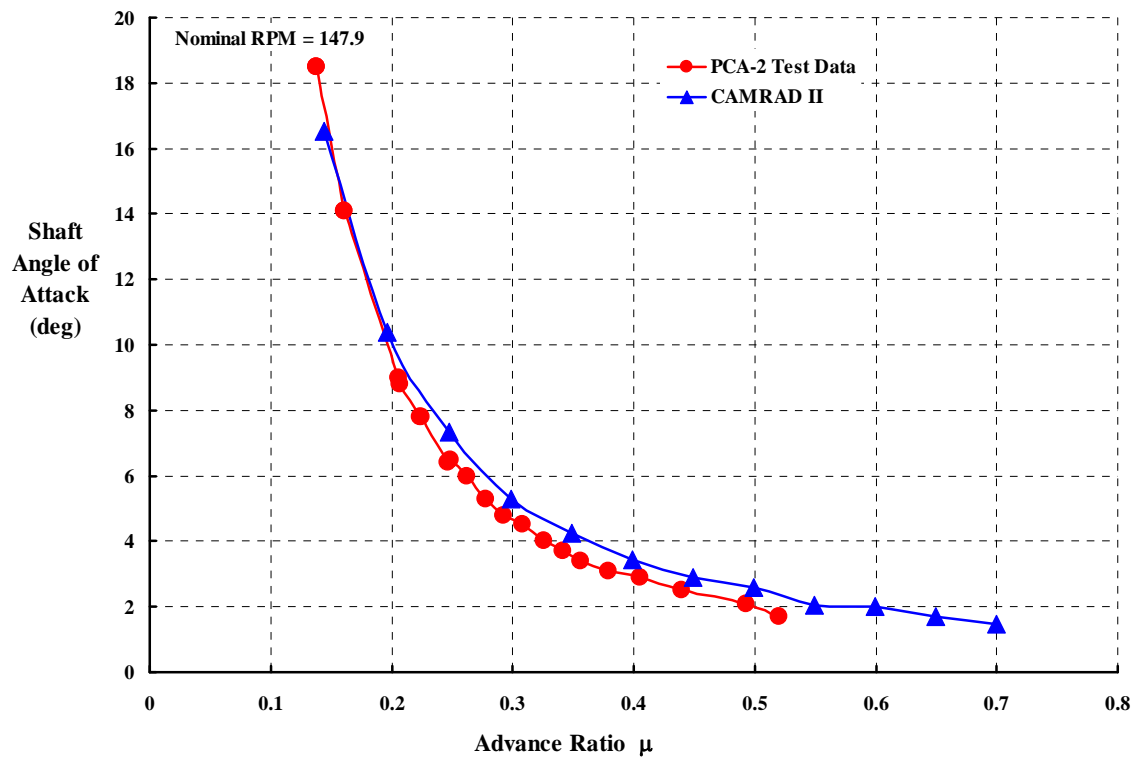


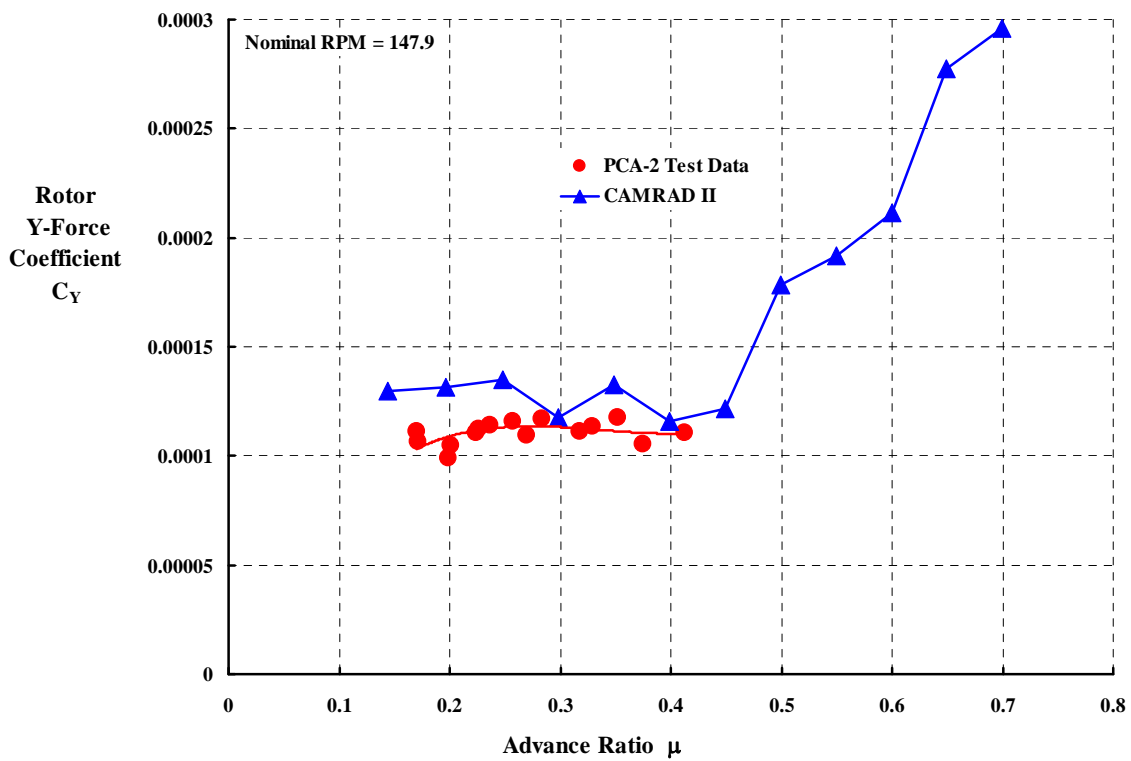
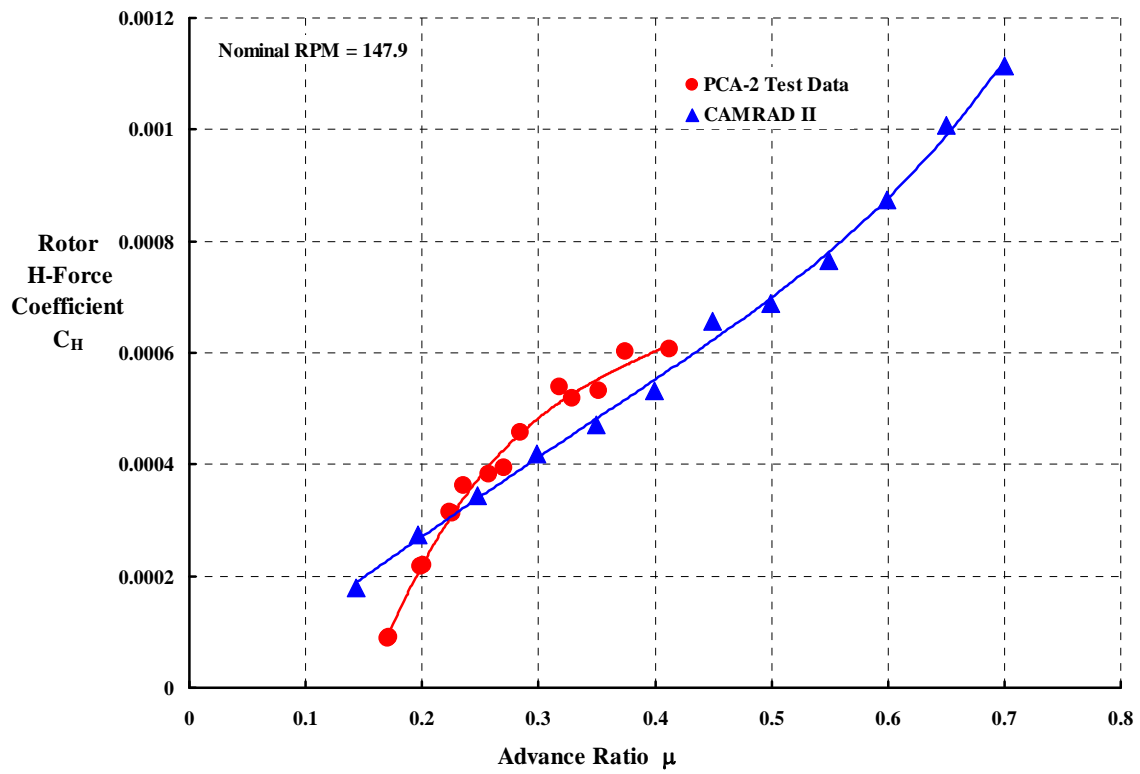


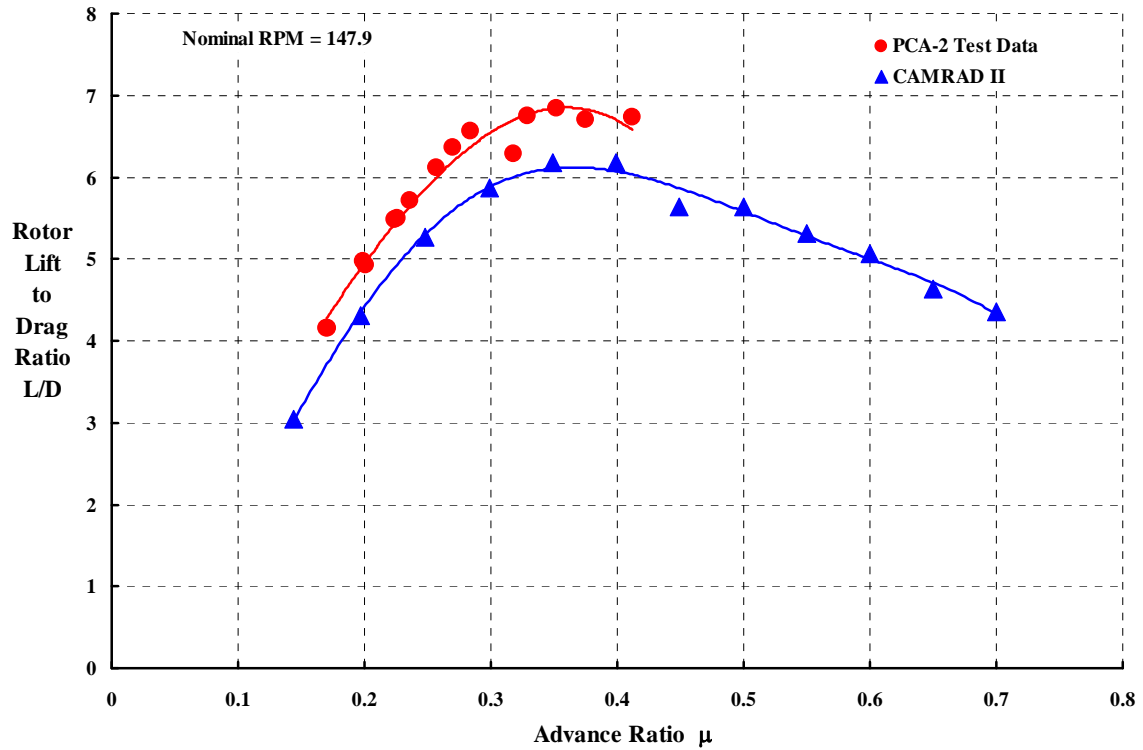












11.19 PCA-2 versus CHARM

No PCA-2 points were computed by CHARM

11.20 PCA-2 versus RCAS

No PCA-2 points were computed by RCAS

11.21 PCA-2 versus OVERFLOW-2 Coupled with CAMRAD II

No PCA-2 points were computed by OVERFLOW-2 or by OVERFLOW-2 coupled with CAMRAD II